ASIA-PACIFIC GROUP
ICOLD

4th Asia-Pacific Group Symposium
9th East Asian Area Dam Conference

Proceedings of International Symposium on

INNOVATIVE TECHNOLOGIES FOR DAMS AND RESERVOIRS TOWARD THE FUTURE GENERATIONS

September 26th to 30th, 2016, Sapporo, JAPAN

The Yubari-shuparo Dam

©TAISEI CORP.

The Apporo Dam

HOKKAIDO GOVERNMENT

The Kyogoku Power Station
(Upper reservoir & Kyogoku Dam)

© HEPCO

Organizers:
Asia-Pacific Group / ICOLD
Japan Commission on Large Dams

Partners:
Chinese National Committee on Large Dams
Korea National Committee on Large Dams

4th Asia-Pacific Group Symposium & 9th East Asian Area Dam Conference
September 26th to 30th, 2016, Sapporo, JAPAN

Proceedings of International Symposium on

INNOVATIVE TECHNOLOGIES
FOR
DAMS AND RESERVOIRS
TOWARD THE FUTURE GENERATIONS

Asia-Pacific Group / ICOLD
Japan Commission on Large Dams

Preface/ President, Japan Commission on Large Dams i
Message / Chairman of ICOLD Asia-Pacific Group ii
Symposium Committee members (JCOLD) iii

Contents

Plenary Session Page

Professor Tadashi YAMADA, Chuo University, Major disasters and the role of dams -Recent flood disasters in Japan p-1

Professor Yasuyuki SHIMIZU, Hokkaido University, The development of the Ishikari River basin and the role of its dam reservoirs p-11

Session (1) Innovative Technologies of Dam

Paper title Page
Authors, Country

Large-scale Dam Body Drilling by Tsuruda Dam Redevelopment Project 1-1
K. Kaji, K. Oobayashi, K. Miyahara, T. Fujisawa, H. Yoshida & N. Yasuda, Japan

Main Challenges and Innovations in Design and Construction of Chitgar Artificial Lake in the City of Tehran, Iran 1-7
A. Emam, M. Zolfagharian, V. Tabesh, A.A Efatmanesh & H. Alavi Deilami , Iran

Construction of Apporo Trapezoidal CSG Dam 1-13
S. Yoshimura, S. Takasugi, M. Konno, T. Fujisawa, H. Yoshida & N. Yasuda, Japan

Construction of a Coastal Levee at Hamamatsu City Coastline using Trapezoidal CSG Dam Technology 1-19
N. Itoh, T. Suzuki, S. Terada, T. Fujisawa, Y. Kinouchi & N. Yasuda, Japan

Study on Rapid Construction Technology for Surface Cover Board Joint of the Slab Joint of CFRD 1-25
M. Li & Z. H. Sun, China

The Underwater Excavation By The Shaft-Style Underwater Excavator T-iROBO UW, 1-31
N. Yachi, H. Miura & A. Ueyama, Japan

Development of Embankment Material Grading Control Continuous Management System Using Three-dimensional Image Processor 1-37
M. Fujiwara, W. Nakane, & I. Miyairi, M. Omata, T. Otake, I. Kobayashi, T. Hashizume & A. Nakamura, Japan

Seismic Evaluation of an Inclined Cored Rockfill Dam using Innovative Centrifuge Modeling 1-43
D.S. Park & N.R. Kim, Korea

Reduction of Ground Water Flow by Promoting Clogging Effect of Soil Particles 1-49
T. Tamai, T. Shiono, N. Sorimachi, T. Tsukada & F. Kawashima, Japan

Deformation Control and Porosity Detection Technologies for High Rockfill Dam 1-55
J. H. Lu, J. X. Tan& B. Tian, China

Construction of Gokayama Dam by the Cruising RCD Construction Method 1-59
R. Nishiyama, M. Yugeta, T. Toyomasu, H. Yotsumoto, T. Fujisawa, Y. Kinouchi & N. Yasuda, Japan

Development of a Crawler Type Soil Mixing Machine with Dryer Function 1-65
S. Yamada, T. Temmyo, T. Koshida, I. Sandanbata, H. Itoh & A. Yamagishi, Japan

Proposal of the Rationalization of Dam Construction Quality Control 1-71
H. Yoshida & M. Kusumi, Japan

The Applicability Analysis of Local Riverbed Aggregate for Hardfill Dam 1-77
J.S. Yoon, H.K. Lee, K.Y. Kim & K.T. Kim, Korea

A Study on the Development of Hybrid Dam Technologies 1-81
W.Y. Park, H.C. Park, J.S. Yoon & S.J. Gang, Korea

Intelligent Monitoring and Control System for Crack Prevention of Concrete Dam and Its Application 1-85
G.X. Zhang, S.H. Li, Y. Liu & L. Zhang, China

Decision Making Model for High Rock Fill Dam Construction during Flood Period based on Markov Process 1-91
L. Liu , Y.H. Zhou, C.J. Zhao & L. Song, China

Feedback Design of Temperature Control Measures for Concrete Dams Based on Real-time Temperature Monitoring and Simulation of Construction Process 1-97
Y.H. Zhou, H.W. Zhou, C.J. Zhao, H.M. Guo & C. Hu, China

Optimization of Construction Process for High Arch Dam Storehouse Surface Based on Virtual Prototype Technology 1-103
C.J. Zhao, C. Hu, Y.H. Zhou, L. Song & H.W. Zhou, China

The Application of RBF Neural Network on Optimization of temperature control Measures of Super-high arch dam Concrete Block 1-109
L. Wang, China

Georadar Application for Dam Safety Study (Case Study of Sutami Dam) 1-115
M. T. B. Raharjo, K. Windianita, F. Hidayat, R. V. Ruritan, Harianto, H.E. Setiawan, M. Ibrahim, N. Sadikin & D. Indrawan, Indonesia

Application of Fusegates As An Innovative Spillway Control System for Sarough (Al Ghadir) Reservoir Dam in West Azarbayjan Province of Iran 1-119
M. Ashrafi & B. Dasi, Iran

CSG (New Technology Development) on Ab-Pa Delay CSG Dam Construction on Iran 1-125
N. Jafari, B. Dasi & A. Akbarpour, Iran

Session (2) Extending Service Life of Dams

Paper title Page
Authors, Country

Extending Service Life of Dams by Improvement of Operation Regularity (IOR) (IRAN dams policy review) 2-1
S.M. Noorbakhsh, Iran

Decision Support System Development To Optimize Djuanda Dam Operation 2-7
A. Mardiyono, H.M. Sungguh & R. Mayasari, Indonesia

Investigation and Repair on Deteriorated Transverse joint of Kasabori Dam 2-13
H. Kawasaki & S. Iwasaki, Japan

The Upper-Pond Remedial Project of Lam Ta Khong Hydropower Plant for Reducing Long Term Deformation 2-19
N. Chaowalittrakul, S. Thongjaeneg & N. Raphitphan, Thailand

Vertical Multi-Holed Double-Pipe System: A New Sediment Suction Method Utilizing a Natural Head 2-25
A. Hisano, S. Oota & K. Maeda, Japan

Abrasion and Corrective Measures of a Sediment Bypass System at Asahi Dam 2-31
T. Nishikawa, Y. Yamane & Y. Omoto, Japan

Preliminary Study on High Arch Dam Reservoir Basin Deformation and Its Effect on Dam Operating Behavior 2-37
W. Minhao, D. Lincai & D. Xiaokai, China

Research on a Method on Effective Restoration of the Capacity for Severe Depositing Reservoirs 2-41
Z. Lianjun, R. Yanfen & L. Yuanfa, China

Preliminary Analysis On Sediment Flushing Efficiency From XiaoLangDi, Yellow River 2-47
L.Tao, L.Zhe, Y.Zhenfeng & L.Xinjie, China

Influence of Polyurea Impermeable System on the Effect of CFRP-strengthened Reinforced Concrete 2-53
L. Bingqi & Z. Yuchi & L. Xiaonan, China

Session (3) Dam Safety, Risk Management and Climate Change

Paper title Page
Authors, Country

Experimental Study on Seismic Response Behavior of Fill Dams Influenced by Dam's Shapes and Input Wave's Directions 3-1
Y. Hayashida, S. Mastukawa, I. Asano & H. Tagashira, Japan

Seismic Performance Evaluation of Embankment Dams by Physical Modeling toward Engineering Practice 3-7
N.R. Kim, Korea

Seismic Fragility Evaluation of Imha Dam based on Deformation 3-13
D.H. Shin, C.K. Kang, K.Y. Kim & K.W. Kim, Korea

Dynamic Characteristics of Dams Evaluated Using Earthquake Monitoring Data for Safety Assessment 3-19
M. Kashiwayanagi, H. Onishi, N. Osada & S. Hayakawa, Japan

Natural Disasters and Dam Safety Issues in Nepal 3-25
D. P. Sangroula, Nepal

Dam Safety Management In Indonesia 3-31
A. Zubaidi, H. A. Rahman & M. Anissa, Indonesia

Case Study on Extreme Flood Affected Minmyin Dam 3-35
U. Victor, Myanmar

Potential Impacts of Climate Change on Reservoir Flood Control in the Huong River Basin, Vietnam 3-41
D.V.Quan & K.Kuntiyawichai, Thailand

Actual Working Performance Assessment of Super-high Arch Dams 3-47
Y. Liu, G. Zhang, B. Zhu, F. Shang, Y. Liu & G. Zhang, China

Research on Mechanism of Slab Horizontal Breakage of High Concrete Faced Rockfill Dam Using a Structural Mechanics Method 3-53
G. Deng, Y. Zhang, X. Wang, Y. Wen & S. Yu & R. Chen, China

The Macro and Micro-Approaches for the Deformation Control of High Concrete Face Rockfill Dams 3-59
X.L. Chang, W. Zhou & G. Ma, China

Improvement of Deformation Prediction of Rock-fill Dam with GPS Measurement 3-65
H. Soda, S. Nigo & N. Sato, Japan

GPS Precise Positioning Technology Applied in the Project Deformation Measurement of Xiaowan Hydropower Station 3-71
C. Hao, A. Yongping & Z. Zhiyong, China

Application of Global Positioning System for Dam Deformation Monitoring 3-77
H. Arizono, H. Okumura, H. Onishi & N. Shimizu, Japan

Study on The Deformation Mechanism of an Ageing Dam Aiming at Future Deformation Prediction 3-83
H. Onishi, M. Kashiwayanagi & M. Yoda, Japan

Gate Operation Support Table of Ohno Flood Control Dam against Excess Flood Inflow 3-89
J. Kashiwai, T. Kubozono &T. Takada, Japan

Safety Technology Application and Development of the Management of the Chaersen Reservoir Dam 3-95
Y. Fan, China

Study on the Seismic Safety of Foundation Gallery of High Rockfill Dam Located on Deep Alluvium Deposit 3-101
C.X. Xing, H.Y. Long, & X. Kun, China

Determination of Dam Construction Schedule Robustness Metric Weight with Analytic Hierarchy Process 3-107
M.Q. Zhao, X.L. Wang & J. Yu & L. Bi, China

Numerical Simulation of Grouting for Dam Foundation 3-111
X.F. Ao, X.L. Wang, S.H. Deng & R.J. Li, China

Technical Feasibility Evaluation and Optimized Selection of Discharging and Energy Dissipation Scheme of High Dams 3-115
B. Pang & G. Wang, China

Rockfill Dam Construction Simulation based on CYCLONE and Stochastic Petri nets 3-121
J. Zhang, X. Wang & J. Yu, China

Schedule Risk Analysis of Roller Compacted Concrete Dam Based on Risk Driver Theory 3-127
J. Yu, B. Wu, X. Wang & M. Zhao, China

Study on Safety Assessment of Earth and Rock-fill Dam Based on Multi-level Fuzzy Evaluation 3-131
C. Hongjie & L. Ji, China

Effects of the Hydropower Station Operation on the Water Temperature in the Downstream 3-137
H. Xiang,Y. Fuhai & L. Sihua, China

Seepage Safety Assessment of Fill Dam using Safety Evaluation Chart 3-141
D. Shin, K. Kim & J. Lee, Korea

Study on Water Resources Security of Three Gorges Reservoir from the Non-traditional Security Perspective 3-147
X.H. Wen, J.Z. Zhou & X.E. Hu, China

Structure Design of Dam Section in Riverbed Parts for a Hydropower Station 3-153
Y. Xu, J. Wang & L. Yang, China

Numerical Investigation of Upper Gotvand Rockfill Dam's Settlement During Construction Stage and First Impounding Reservoir 3-159
A. K. Tooseh & H. Akbari, Iran

Investigation and Rehabilitation of Abnormal Seepage Monitoring System of Rockfill Dam 3-165
J. Lee, Korea

A Study on the Multi-criteria Decision Making using Hydrological Safety Evaluation Result 3-171
J.Y. Park, J.H. Kwon & T.H. Kim, Korea

Dam Management Strategies to Tackle Climate Change 3-175
A. Chantanumate & W. Kumnerdpet, Thailand

Geophysics Interpretation Unveil Cause of Dam Imperfection for Dam Improvement and Dam Safety Management: Bang Niao Dum Dam, Phuket, Thailand 3-181
C. Pedugsorn & N. Poomviset, Thailand

Increasing the Safety of Rock Fill Dams by Reducing the Possibility of Hydraulic Fracturing 3-187
D. Djarwadi, K.B. Suryolelono, B. Suhendro & H.C. Hardiyatmo, Indonesia

Impact of Climate Change to Safety of Pasak Jolasid Dam 3-193
E. Nanudorn & S. Sopanangkool, Thailand

Preface

We are very much honored to host the 4th Asia-Pacific Group Symposium and 9th East Asian Area Dam Conference in Sapporo, capital city of Hokkaido, a major northern island of Japan. The core event of this international gathering is a two-day symposium under the main theme of "Innovative Technologies for Dams and Reservoirs toward the Future Generations".

We invited two distinguished speakers for the Opening Ceremony of this symposium. The first key note speech by Professor Tadashi YAMADA, Chuo University, is on recent water-related disasters in Japan and risk management policies including roles of dam reservoirs. The second key note speech by Professor Yasuyuki SHIMIZU, Hokkaido University, is on the development and the flood disaster reduction of the basin of the Ishikari River which has the largest catchment area in Hokkaido island and forms the major plain field for inhabitation and economic activities.

For the main symposium, we have received as many as 68 papers from 8 countries related to themes listed below, in which 30 papers are presented in oral session and others in poster session. We really appreciate effort and eagerness of the authors.

Themes of the symposium

- Innovative Technologies of Dams
- Extending Service Life of Dams
- Dam Safety and Risk Management
- Climate Change and Dams

We believe these valuable papers would contribute to the development and the dissemination of dam technologies among Asia-Pacific countries.

N. Hashimoto

Noriaki HASHIMOTO
President, Japan Commission on Large Dams

Message from the Chairman of the Asia Pacific Group

Historically and undoubtedly, one of the most important developments of humankind has been "writing," where it is a different name of "recording." History says, wherever writing is prevailing, uncountable and brilliant advances exist.

In this regard, sharing our knowledge and experience by means of this proceedings on dam and water resources related issues with our members of EADC and APG countries is a truly meaningful activity we can do.

On behalf of the Asia and Australasia Zone of ICOLD, I would like to extend my deepest gratitude to not only the organizing committee of JCOLD for the 9th EADC but also APG member countries for their enthusiastic participations in each preparation step of the Symposium.

Especially, I have to say great thanks to all of authors, speakers and audiences of this Symposium for their academic and professional contributions to making advances in dam and water resources engineering.

As known well to all, this proceedings includes many valuable papers prepared by experienced and distinguished writers, thus will be referred by other dam engineers ever and ever.

Hopefully, I would like to see more and more another advances in "recording" and/or "writing" on innovative technologies for dams and reservoirs toward the future generations.

With warm regards,

Kyung-taek YUM
Chairman of Asia Pacific Group and Vice President of ICOLD

Symposium committee member (JCOLD)

Chairman, Tatsuo Hamaguchi
Vice-chairman, Masayuki Kusumi
Joji Harada
Masayuki Kashiwayanagi
Kentaro Kido
Kenji Maeda
Taketoshi Matsunaga
Kentaro Nishimura
Kazuyuki Nishiura
Hiroaki Noguchi
Shigeru Tsuruta
Tomoyuki Tsukada
Yuichi Yamane
Mitsuaki Yamaguchi
Akira Koganezawa
Tomoko Hoshiba
Shiho Yamane

Keynote Presentation Ⅰ

Major disasters and the role of dams -Recent flood disasters in Japan

Prof. Yamada Tadashi
Dept. of Civil and Environmental engineering,
Faculty of Science and Engineering, Chuo University

Major disasters and the role of dams ~Recent flood disasters in Japan

Yamada Tadashi
Dept. of Civil and Environmental engineering,
Faculty of Science and Engineering, Chuo University

Contents

1. Disaster risk management considering the uncertainty of physical process

- Background
- Flood risk management
- Uncertainties in rainfall-runoff process
- Rainfall-runoff analysis considering uncertainty
- Analysis of flood levee reliability considering uncertainty

2. The role of dams(1): 1947 Kathleen typhoon

- Reproducing calculation considering the uncertainty of spatial distribution
- Reproducing calculation considering the uncertainty of typhoon path
- The flood control effect of yanba dam

3. The role of dams(2): 2015 Kanto & Tohoku heavy rain

- Flood control by dam gate operation
- The flood control effect of dam group in the upstream of Kinugawa river basin

Contents

1. Disaster risk management considering the uncertainty of physical process

- Background
- Flood risk management
- Uncertainties in rainfall-runoff process
- Rainfall-runoff analysis considering uncertainty
- Analysis of flood levee reliability considering uncertainty

2. The role of dams(1): 1947 Kathleen typhoon

- Reproducing calculation considering the uncertainty of spatial distribution
- Reproducing calculation considering the uncertainty of typhoon path
- The flood control effect of yanba dam

3. The role of dams(2): 2015 Kanto & Tohoku heavy rain

- Flood control by dam gate operation
- The flood control effect of dam group in the upstream of Kinugawa river basin

Background

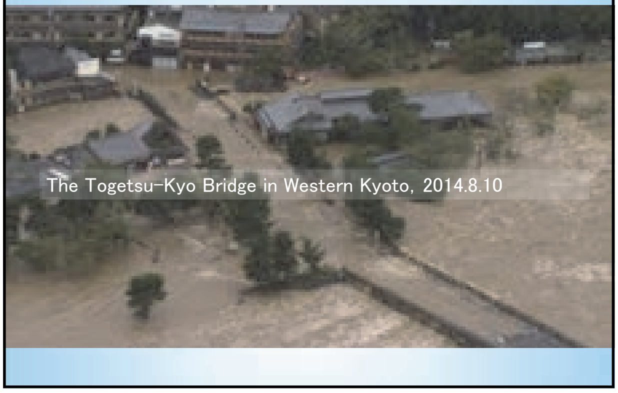
The Togetsu-Kyo Bridge in Western Kyoto, 2014.8.10

Flood Risk Management

In order to do the flood management, We have to understand the rainfall-runoff process.

◆Rainfall-runoff process

To understand the path from rainfall to the flow in river channel

2011 Heavy rain event in Niigata

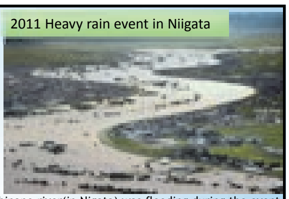
Shinano river(in Nigata) was flooding during the event
By Sankei news: 2011.07.30

Problem

◎We are trying to analysis and predict the rainfall-runoff system based on uncertainty information

◎We want to know the risk of flood events under those uncertainty information

Rainfall-runoff analysis based on stochastic process theory

The uncertainties in rainfall-runoff process

1) Rainfall=Probabilistic event , prob. distribution, extreme value problem

2) Rainfall=Temporal uncertainty

3) Rainfall=Spatial uncertainty

4) Uncertainty of runoff mechanism

5) Uncertainty of parameters in runoff model

6) Observation error

6) Due to the positions of observers
uncertainty(agnosticism)＝titubation(shaking actualy、the measurement is possible) or there are some of error, but we forced to use these.
indeterminacy＝God only knows(off the register)≒beyond human understanding≒the limit of experience≒ignorance≒unsure…agnosticism

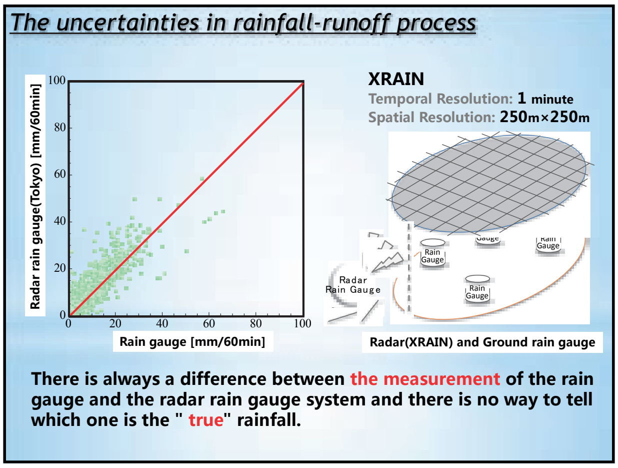

The uncertainties in rainfall-runoff process

XRAIN
Temporal Resolution: 1 minute
Spatial Resolution: 250m×250m

Radar(XRAIN) and Ground rain gauge

There is always a difference between the measurement of the rain gauge and the radar rain gauge system and there is no way to tell which one is the " true" rainfall.

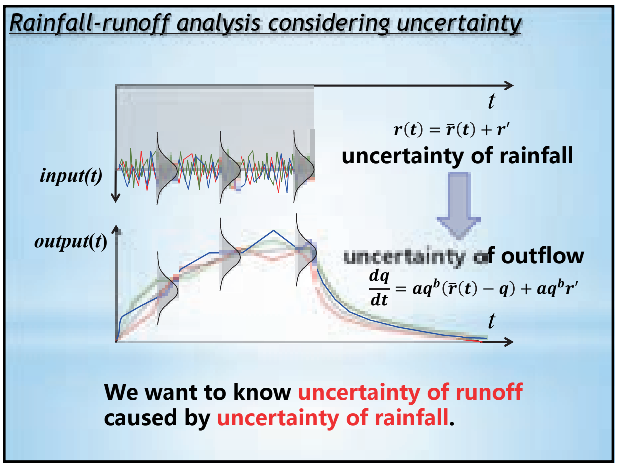

Rainfall-runoff analysis considering uncertainty

$r(t) = \bar{r}(t) + r'$

uncertainty of rainfall

uncertainty of outflow

$\frac{dq}{dt} = aq^b(\bar{r}(t) - q) + aq^b r'$

We want to know uncertainty of runoff caused by uncertainty of rainfall.

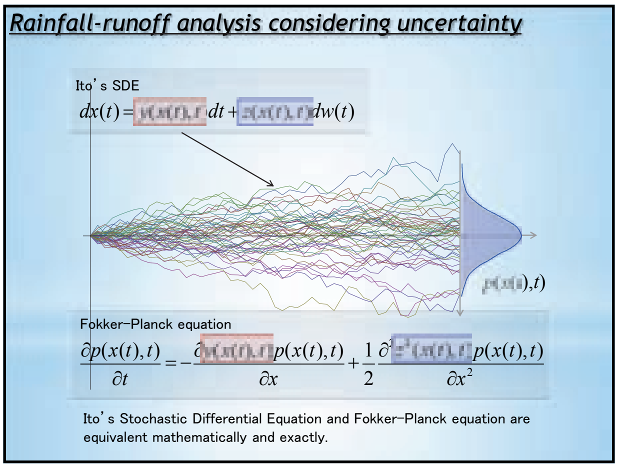

Rainfall-runoff analysis considering uncertainty

Ito' s SDE

$dx(t) = y(x(t),t)\,dt + z(x(t),t)\,dw(t)$

Fokker–Planck equation

$$\frac{\partial p(x(t),t)}{\partial t} = -\frac{\partial y(x(t),t)\,p(x(t),t)}{\partial x} + \frac{1}{2}\frac{\partial^2 z^2(x(t),t)\,p(x(t),t)}{\partial x^2}$$

Ito' s Stochastic Differential Equation and Fokker–Planck equation are equivalent mathematically and exactly.

Rainfall-runoff analysis considering uncertainty

Langevin equation

$$\frac{dx}{dt} = y(x) + \zeta'(x,t)$$

Step1:Devide the input into a random part and an average part

$$\frac{dq}{dt} = aq^b(\bar{r}(t) - q) + aq^b r'$$

Ito's stochastic differential equation

$$dx(t) = y(x(t),t)dt + z(x(t),t)dw$$

Step2:Write the equations in the Ito stochastic differential equation form

$$dq = aq^b(\bar{r}(t) - q)dt + \sigma\sqrt{T_L}dw$$

Fokker-Planck equation

$$\frac{\partial P(x,t)}{\partial t} = -\frac{\partial y(x)P(x,t)}{\partial x} + \frac{1}{2}\frac{\partial^2 z^2 P(x,t)}{\partial x^2}$$

Step3:Drive the governing equations of the probability density function

$$\frac{\partial P(q)}{\partial t} + \frac{\partial aq^b(\bar{r}(t) - q)P(q)}{\partial q} = \frac{1}{2}\frac{\partial^2 (aq^b\sigma\sqrt{T_L})^2 P(q)}{\partial q^2}$$

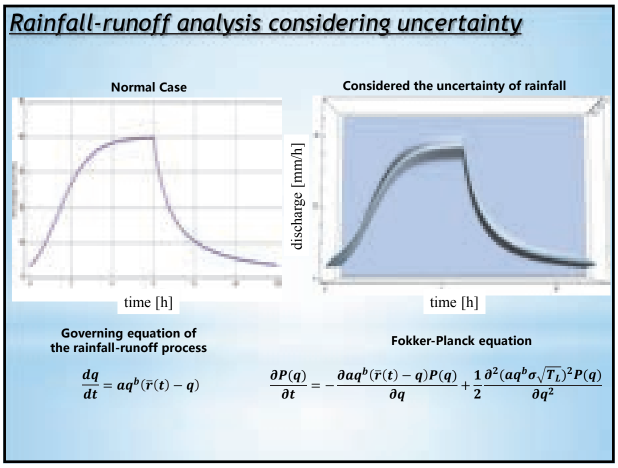

Rainfall-runoff analysis considering uncertainty

Normal Case

Considered the uncertainty of rainfall

Governing equation of the rainfall-runoff process

$$\frac{dq}{dt} = aq^b(\bar{r}(t) - q)$$

Fokker-Planck equation

$$\frac{\partial P(q)}{\partial t} = -\frac{\partial aq^b(\bar{r}(t) - q)P(q)}{\partial q} + \frac{1}{2}\frac{\partial^2 (aq^b\sigma\sqrt{T_L})^2 P(q)}{\partial q^2}$$

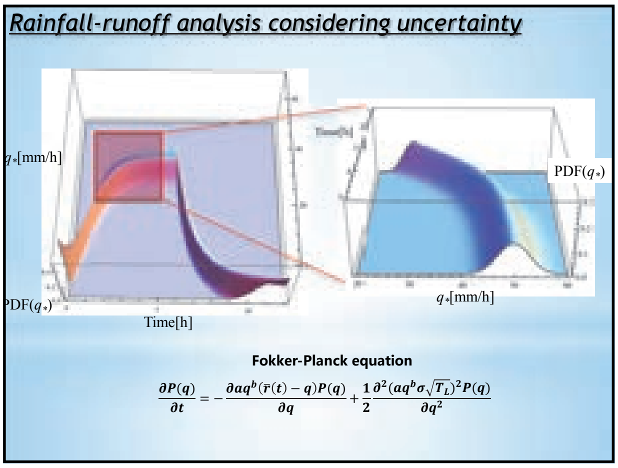

Rainfall-runoff analysis considering uncertainty

Fokker-Planck equation

$$\frac{\partial P(q)}{\partial t} = -\frac{\partial aq^b(\bar{r}(t) - q)P(q)}{\partial q} + \frac{1}{2}\frac{\partial^2 (aq^b\sigma\sqrt{T_L})^2 P(q)}{\partial q^2}$$

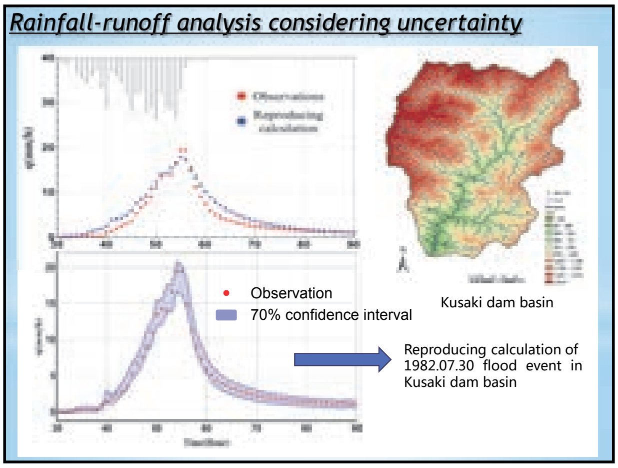

Rainfall-runoff analysis considering uncertainty

Reproducing calculation of 1982.07.30 flood event in Kusaki dam basin

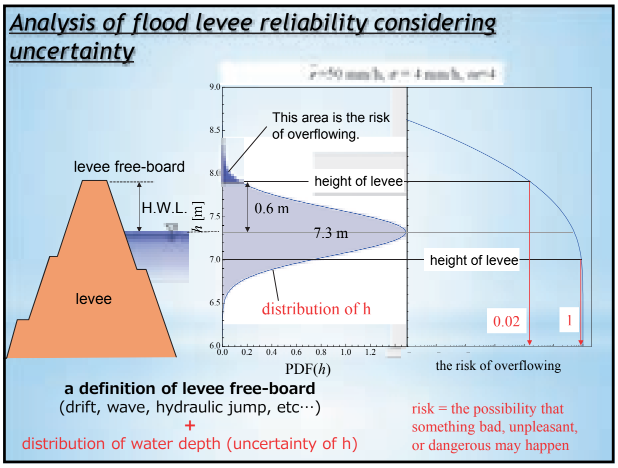

Analysis of flood levee reliability considering uncertainty

This area is the risk of overflowing.
levee free-board
height of levee
H.W.L.
0.6 m
7.3 m
height of levee
levee
distribution of h
0.02
1
h [m]
9.0
8.5
8.0
7.5
7.0
6.5
6.0
0.0
0.2
0.4
0.6
0.8
1.0
1.2
PDF(h)
the risk of overflowing

a definition of levee free-board
(drift, wave, hydraulic jump, etc···)
+
distribution of water depth (uncertainty of h)

risk = the possibility that something bad, unpleasant, or dangerous may happen

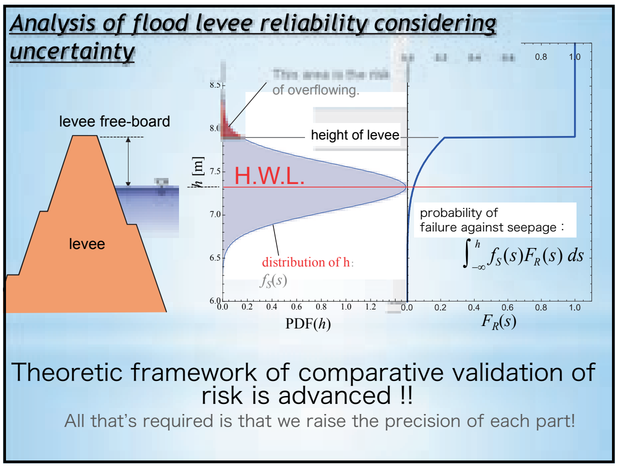

Analysis of flood levee reliability considering uncertainty

This area is the risk of overflowing.
levee free-board
height of levee
H.W.L.
levee
h [m]
8.5
8.0
7.5
7.0
6.5
6.0
distribution of h:
$f_S(s)$
probability of failure against seepage :
$\int_{-\infty}^{h} f_S(s)F_R(s)\,ds$
0.0
0.2
0.4
0.6
0.8
1.0
1.2
PDF(h)
$F_R(s)$

Theoretic framework of comparative validation of risk is advanced !!

All that's required is that we raise the precision of each part!

Contents

1. Disaster risk management considering the uncertainty of physical process

- Background
- Flood risk management
- Uncertainties in rainfall-runoff process
- Rainfall-runoff analysis considering uncertainty
- Analysis of flood levee reliability considering uncertainty

2. The role of dams(1): 1947 Kathleen typhoon

- Reproducing calculation considering the uncertainty of spatial distribution
- Reproducing calculation considering the uncertainty of typhoon path
- The flood control effect of yanba dam

3. The role of dams(2): 2015 Kanto & Tohoku heavy rain

- Flood control by dam gate operation
- The flood control effect of dam group in the upstream of Kinugawa river basin

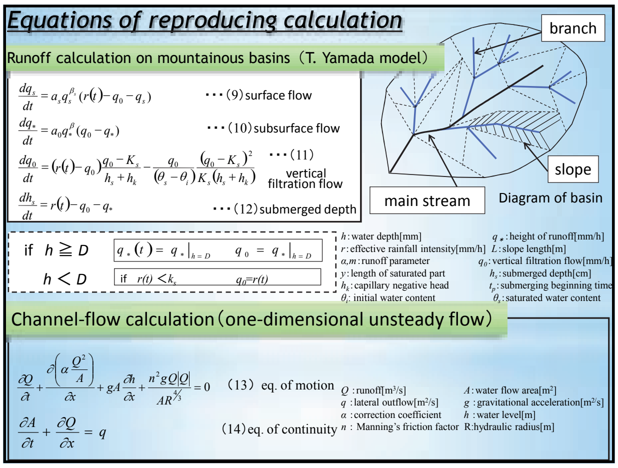

Equations of reproducing calculation

Runoff calculation on mountainous basins（T. Yamada model）

$$\frac{dq_s}{dt} = a_s q_s^{\beta_s}\left(r(t) - q_0 - q_s\right) \quad \cdots (9)\ \text{surface flow}$$

$$\frac{dq_*}{dt} = a_0 q_*^{\beta}\left(q_0 - q_*\right) \quad \cdots (10)\ \text{subsurface flow}$$

$$\frac{dq_0}{dt} = \left(r(t) - q_0\right)\frac{q_0 - K_s}{h_s + h_k} - \frac{q_0}{(\theta_s - \theta_i)}\frac{(q_0 - K_s)^2}{K_s(h_s + h_k)} \quad \cdots (11)\ \text{vertical filtration flow}$$

$$\frac{dh_s}{dt} = r(t) - q_0 - q_* \quad \cdots (12)\ \text{submerged depth}$$

if $h \geqq D$ $\quad q_*(t) = q_*|_{h=D} \quad q_0 = q_*|_{h=D}$

$h < D$ $\quad$ if $r(t) < k_s \quad q_0 = r(t)$

h: water depth[mm]
r: effective rainfall intensity[mm/h]
α, m: runoff parameter
y: length of saturated part
h_k: capillary negative head
θ_i: initial water content
q_*: height of runoff[mm/h]
L: slope length[m]
q_0: vertical filtration flow[mm/h]
h_s: submerged depth[cm]
t_p: submerging beginning time
θ_s: saturated water content

branch
slope
main stream
Diagram of basin

Channel-flow calculation（one-dimensional unsteady flow）

$$\frac{\partial Q}{\partial t} + \frac{\partial\left(\alpha \frac{Q^2}{A}\right)}{\partial x} + gA\frac{\partial h}{\partial x} + \frac{n^2 g Q|Q|}{AR^{4/3}} = 0 \quad (13)\ \text{eq. of motion}$$

$$\frac{\partial A}{\partial t} + \frac{\partial Q}{\partial x} = q \quad (14)\ \text{eq. of continuity}$$

Q: runoff[m³/s]
q: lateral outflow[m²/s]
α: correction coefficient
n: Manning's friction factor
A: water flow area[m²]
g: gravitational acceleration[m²/s]
h: water level[m]
R: hydraulic radius[m]

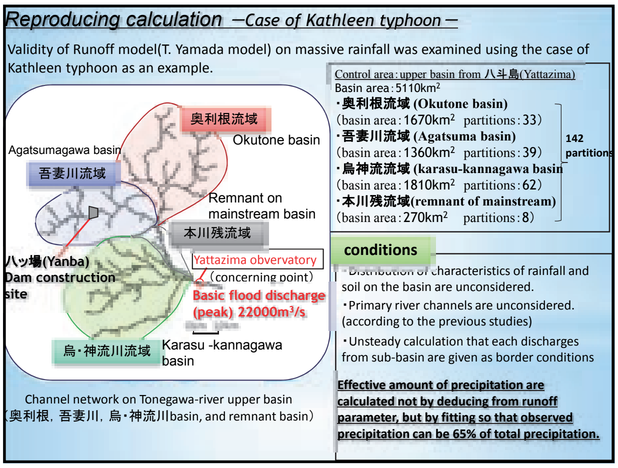

Reproducing calculation －Case of Kathleen typhoon－

Validity of Runoff model(T. Yamada model) on massive rainfall was examined using the case of Kathleen typhoon as an example.

奥利根流域
Okutone basin
Agatsumagawa basin
吾妻川流域
Remnant on mainstream basin
本川残流域
ハッ場(Yanba) Dam construction site
Yattazima obvervatory
（concerning point）
Basic flood discharge (peak) 22000m³/s
烏・神流川流域
Karasu -kannagawa basin

Channel network on Tonegawa-river upper basin
（奥利根，吾妻川，烏・神流川basin, and remnant basin）

Control area : upper basin from 八斗島(Yattazima)
Basin area : 5110km²
- **奥利根流域 (Okutone basin)**
（basin area : 1670km²　partitions : 33）
- **吾妻川流域 (Agatsuma basin)**
（basin area : 1360km²　partitions : 39）
- **烏神流流域 (karasu-kannagawa basin)**
（basin area : 1810km²　partitions : 62）
- **本川残流域(remnant of mainstream)**
（basin area : 270km²　partitions : 8）

142 partitions

conditions

- Distribution of characteristics of rainfall and soil on the basin are unconsidered.
- Primary river channels are unconsidered. (according to the previous studies)
- Unsteady calculation that each discharges from sub-basin are given as border conditions

Effective amount of precipitation are calculated not by deducing from runoff parameter, but by fitting so that observed precipitation can be 65% of total precipitation.

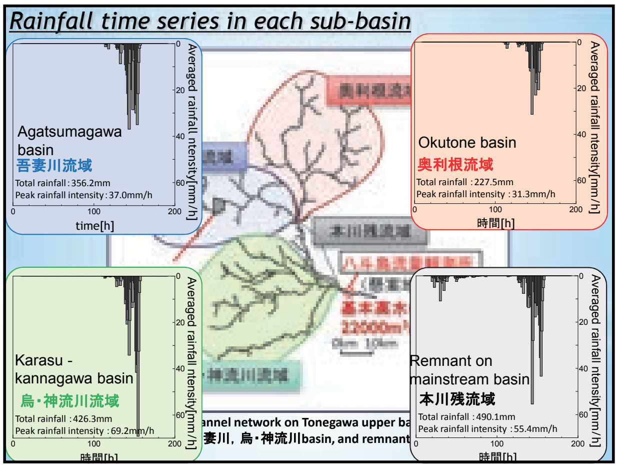

Rainfall time series in each sub-basin

annel network on Tonegawa upper ba
妻川，烏・神流川basin, and remnant

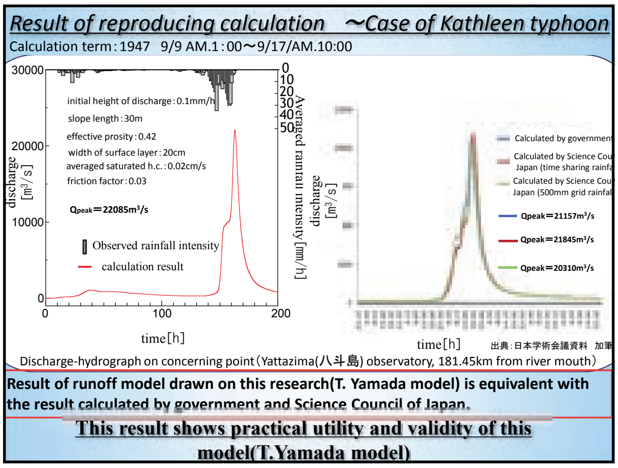

Result of reproducing calculation ～Case of Kathleen typhoon

Calculation term : 1947 9/9 AM.1 : 00～9/17/AM.10:00

Discharge-hydrograph on concerning point（Yattazima(八斗島) observatory, 181.45km from river mouth）

Result of runoff model drawn on this research(T. Yamada model) is equivalent with the result calculated by government and Science Council of Japan.

This result shows practical utility and validity of this model(T.Yamada model)

Contents

1．Disaster risk management considering the uncertainty of physical process

・Background
・Flood risk management
・Uncertainties in rainfall-runoff process
・Rainfall-runoff analysis considering uncertainty
・Analysis of flood levee reliability considering uncertainty

2. The role of dams(1): 1947 Kathleen typhoon

・Reproducing calculation considering the uncertainty of spatial distribution
・Reproducing calculation considering the uncertainty of typhoon path
・The flood control effect of yanba dam

3. The role of dams(2): 2015 Kanto & Tohoku heavy rain

・Flood control by dam gate operation
・ The flood control effect of dam group in the upstream of Kinugawa river basin

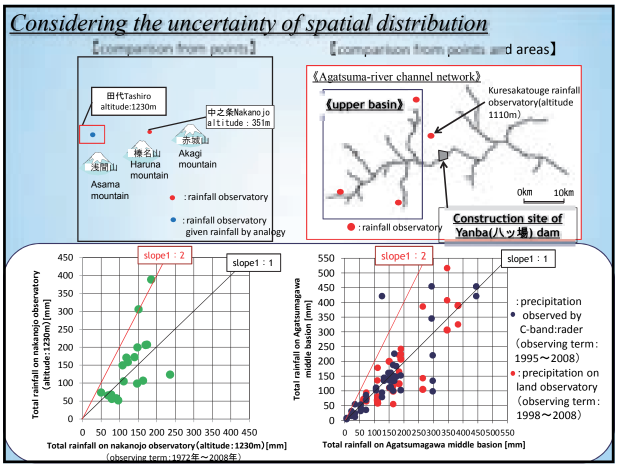

Considering the uncertainty of spatial distribution

【comparison from points】 【comparison from points and areas】

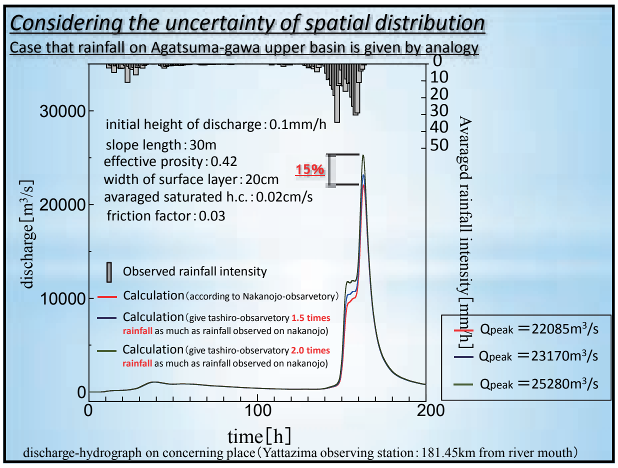

Considering the uncertainty of spatial distribution

Case that rainfall on Agatsuma-gawa upper basin is given by analogy

discharge-hydrograph on concerning place（Yattazima observing station : 181.45km from river mouth）

Contents

1．Disaster risk management considering the uncertainty of physical process

・Background
・Flood risk management
・Uncertainties in rainfall-runoff process
・Rainfall-runoff analysis considering uncertainty
・Analysis of flood levee reliability considering uncertainty

2. The role of dams(1): 1947 Kathleen typhoon

・Reproducing calculation considering the uncertainty of spatial distribution
・Reproducing calculation considering the uncertainty of typhoon path
・The flood control effect of yanba dam

3. The role of dams(2): 2015 Kanto & Tohoku heavy rain

・Flood control by dam gate operation
・ The flood control effect of dam group in the upstream of Kinugawa river basin

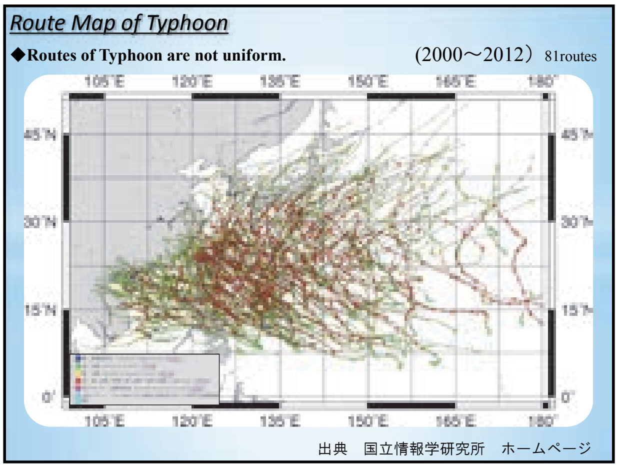

Route Map of Typhoon

◆Routes of Typhoon are not uniform. （2000～2012） 81routes

105°E
120°E
135°E
150°E
165°E
180°
45°N
30°N
15°N
0°

出典　国立情報学研究所　ホームページ

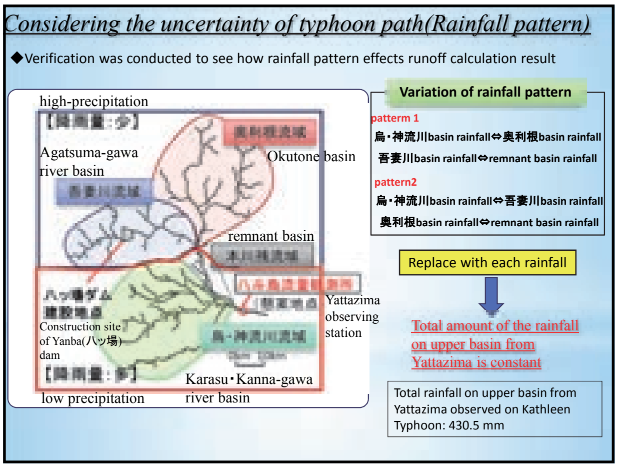

Considering the uncertainty of typhoon path(Rainfall pattern)

◆Verification was conducted to see how rainfall pattern effects runoff calculation result

high-precipitation
Agatsuma-gawa river basin
Okutone basin
remnant basin
Construction site of Yanba(八ッ場) dam
Yattazima observing station
Karasu･Kanna-gawa river basin
low precipitation

Variation of rainfall pattern

patterm 1

烏･神流川basin rainfall⇔奥利根basin rainfall

吾妻川basin rainfall⇔remnant basin rainfall

pattern2

烏･神流川basin rainfall⇔吾妻川basin rainfall

奥利根basin rainfall⇔remnant basin rainfall

Replace with each rainfall

Total amount of the rainfall on upper basin from Yattazima is constant

Total rainfall on upper basin from Yattazima observed on Kathleen Typhoon: 430.5 mm

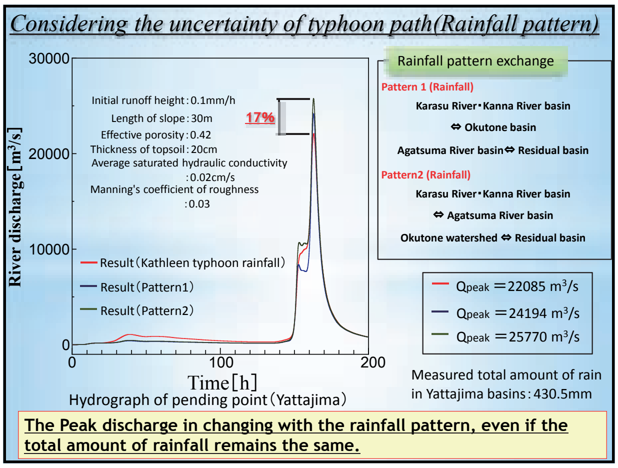

Considering the uncertainty of typhoon path(Rainfall pattern)

Initial runoff height：0.1mm/h
Length of slope：30m
Effective porosity：0.42
Thickness of topsoil：20cm
Average saturated hydraulic conductivity：0.02cm/s
Manning's coefficient of roughness：0.03

Hydrograph of pending point（Yattajima）

Rainfall pattern exchange

Pattern 1 (Rainfall)

Karasu River･Kanna River basin ⇔ Okutone basin

Agatsuma River basin⇔ Residual basin

Pattern2 (Rainfall)

Karasu River･Kanna River basin ⇔ Agatsuma River basin

Okutone watershed ⇔ Residual basin

$Q_{peak} = 22085\ m^3/s$

$Q_{peak} = 24194\ m^3/s$

$Q_{peak} = 25770\ m^3/s$

Measured total amount of rain in Yattajima basins：430.5mm

The Peak discharge in changing with the rainfall pattern, even if the total amount of rainfall remains the same.

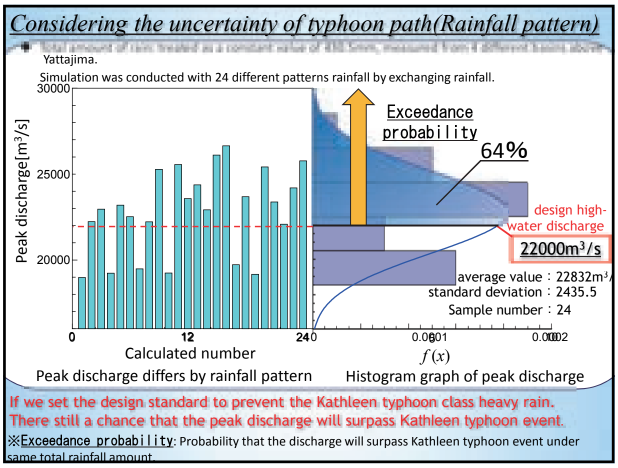

Considering the uncertainty of typhoon path(Rainfall pattern)

◆ Total amount of rain treated as a constant value of 430.5mm, measured from 4 different basins above Yattajima.

Simulation was conducted with 24 different patterns rainfall by exchanging rainfall.

average value：22832m³/
standard deviation：2435.5
Sample number：24

Peak discharge differs by rainfall pattern　　Histogram graph of peak discharge

If we set the design standard to prevent the Kathleen typhoon class heavy rain. There still a chance that the peak discharge will surpass Kathleen typhoon event.

※Exceedance probability: Probability that the discharge will surpass Kathleen typhoon event under same total rainfall amount.

Contents

1．Disaster risk management considering the uncertainty of physical process

- ･Background
- ･Flood risk management
- ･Uncertainties in rainfall-runoff process
- ･Rainfall-runoff analysis considering uncertainty
- ･Analysis of flood levee reliability considering uncertainty

2．The role of dams(1): 1947 Kathleen typhoon

- ･Reproducing calculation considering the uncertainty of spatial distribution
- ･Reproducing calculation considering the uncertainty of typhoon path
- ･The flood control effect of yanba dam

3．The role of dams(2): 2015 Kanto & Tohoku heavy rain

- ･Flood control by dam gate operation
- ･ The flood control effect of dam group in the upstream of Kinugawa river basin

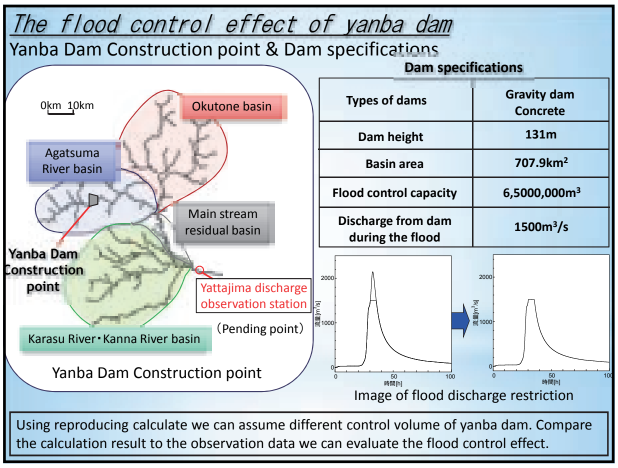

The flood control effect of yanba dam

Yanba Dam Construction point & Dam specifications

0km 10km
Okutone basin
Agatsuma River basin
Main stream residual basin
Yanba Dam Construction point
Yattajima discharge observation station
（Pending point）
Karasu River･Kanna River basin

Yanba Dam Construction point

Dam specifications

Types of dams	**Gravity dam Concrete**
Dam height	**131m**
Basin area	**707.9km²**
Flood control capacity	**6,5000,000m³**
Discharge from dam during the flood	**1500m³/s**

2000
1000
0
流量[m³/s]
0
50
100
時間[h]

Image of flood discharge restriction

Using reproducing calculate we can assume different control volume of yanba dam. Compare the calculation result to the observation data we can evaluate the flood control effect.

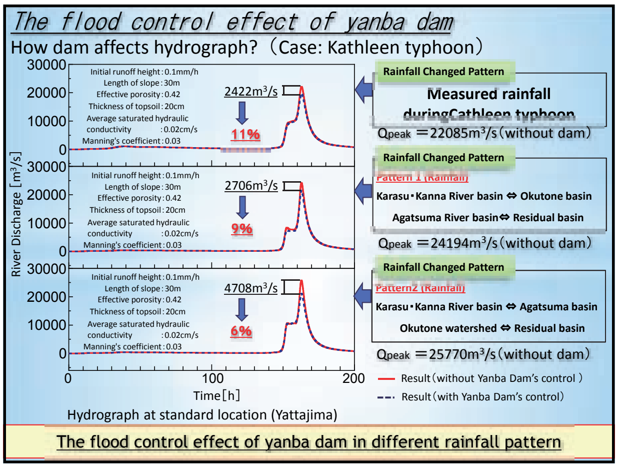

The flood control effect of yanba dam

How dam affects hydrograph?（Case: Kathleen typhoon）

Qpeak ＝22085m³/s（without dam）

Qpeak ＝24194m³/s（without dam）

Qpeak ＝25770m³/s（without dam）

Hydrograph at standard location (Yattajima)

The flood control effect of yanba dam in different rainfall pattern

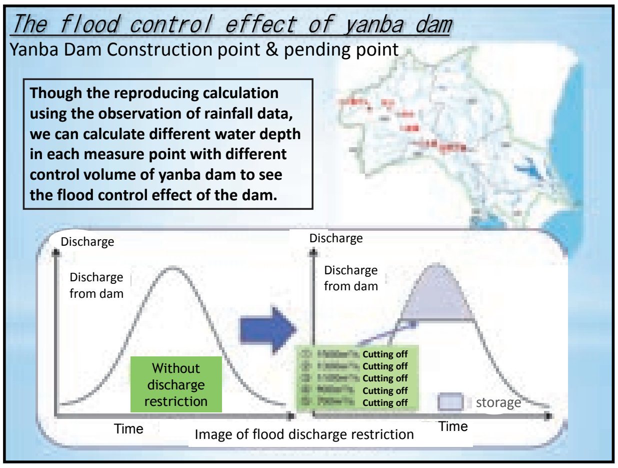

The flood control effect of yanba dam

Yanba Dam Construction point & pending point

Though the reproducing calculation using the observation of rainfall data, we can calculate different water depth in each measure point with different control volume of yanba dam to see the flood control effect of the dam.

Discharge
Discharge from dam
Without discharge restriction
Time
Discharge
Discharge from dam
Cutting off
Cutting off
Cutting off
Cutting off
Cutting off
storage
Time

Image of flood discharge restriction

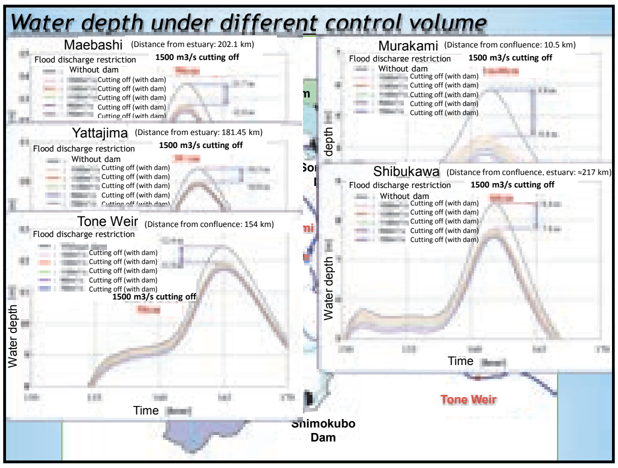

Water depth under different control volume

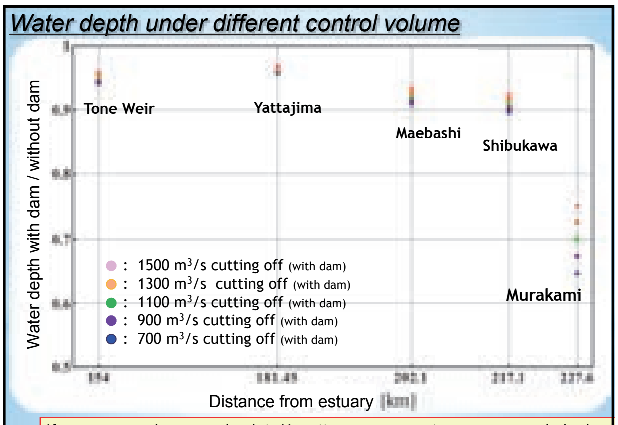

Water depth under different control volume

If we compare the water depth in Yattajima measure point, we can conclude that, The flood control effect of yanba dam makes the peak water depth 4%~5% lower.

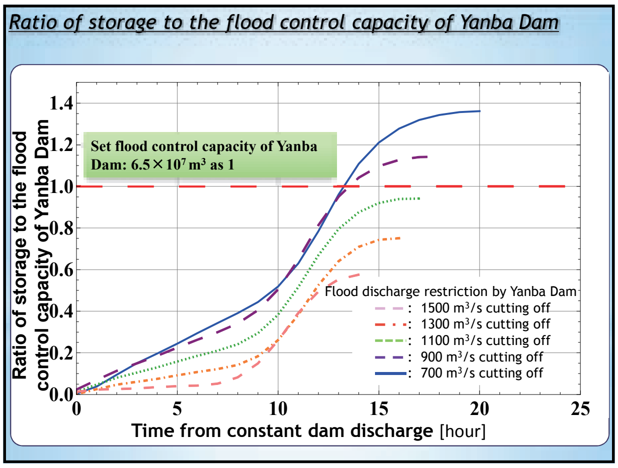

Ratio of storage to the flood control capacity of Yanba Dam

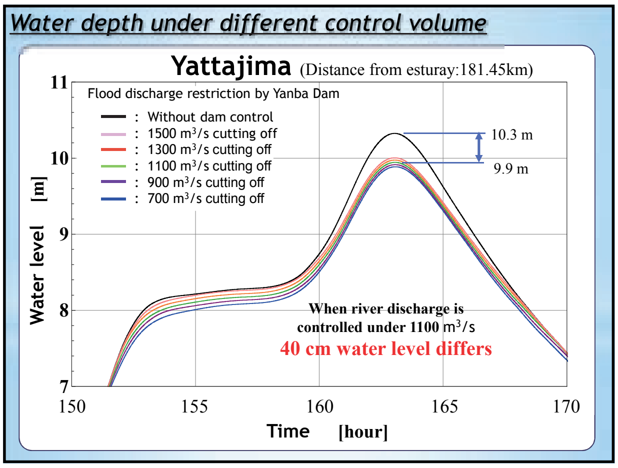

Water depth under different control volume

When river discharge is controlled under 1100 m³/s

40 cm water level differs

~ Application Example — For flood control capability of Yanba Dam —~

・If you have to verify the effect of Yanba Dam as a target the measured rainfall of Kathleen typhoon , showed that you can control the flow rate of about 2500m^3 / s (10%) with respect to the measured flow rate.

・If it is assumed that there was a Yanba Dam during the Kathleen typhoon , was verified for the flood control capacity of Yanba Dam. As a result, when you have a certain amount released a 1100m^3 / s , and the reservoir up to 90% of the maximum flood control capacity , it showed that it is the maximum possible use of the flood control capacity

・When Kathleen typhoon , comparing the case where there is a certain amount of discharge and when there is no dam , showed that there is reduction of 40cm water level in Yattajima stations at fixed amount discharge of 1100m^3 / s.

Contents

1. Disaster risk management considering the uncertainty of physical process

- ・Background
- ・Flood risk management
- ・Uncertainties in rainfall-runoff process
- ・Rainfall-runoff analysis considering uncertainty
- ・Analysis of flood levee reliability considering uncertainty

2. The role of dams(1): 1947 Kathleen typhoon

- ・Reproducing calculation considering the uncertainty of spatial distribution
- ・Reproducing calculation considering the uncertainty of typhoon path
- ・The flood control effect of yanba dam

3. The role of dams(2): 2015 Kanto & Tohoku heavy rain

- ・Flood control by dam gate operation
- ・The flood control effect of dam group in the upstream of Kinugawa river basin

---

Flood control by dam gate operation

Various functions of multi purpose dam reservoir

Flood control, water supply, irrigation, power generation

Flood control method by dam gate operation based on

○Rainfall prediction

○Runoff analysis

→ Predictive uncertainties

there is a risk to reduce reservoir level for water use.

○Runoff characteristics of a basin

Flood control by dam gate operation

The capacity distribution of multi purpose dam reservoir

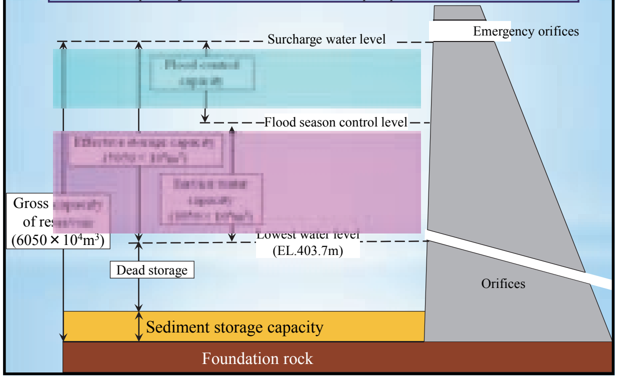

Flood control by dam gate operation

※ A new concept of dam gate operation

$$-\int_0^t (Q_{IN}-Q_{OUT})dt = V(Q_{IN}(t))$$

Total amount of anticipatory release

Total amount of inflow in recession period

By transforming this equation, it could be possible to calculate the anticipatory release quantity

$$Q_{OUT}=Q_{IN}+\frac{dV}{dQ_{IN}}\cdot\frac{dQ_{IN}}{dt}$$

Anticipatory release quantity is equals to quantity which obtained by this equation

---

Flood control by dam gate operation

※ Total Inflow in recession curve of hydrograph

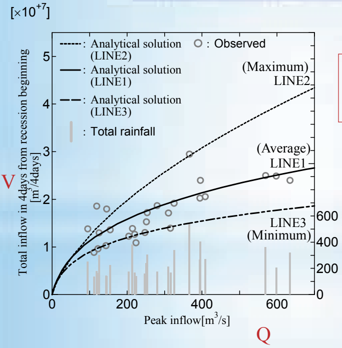

By fitting with the observed data , **dV/dQ** is fixed.

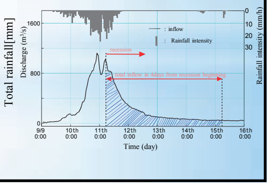

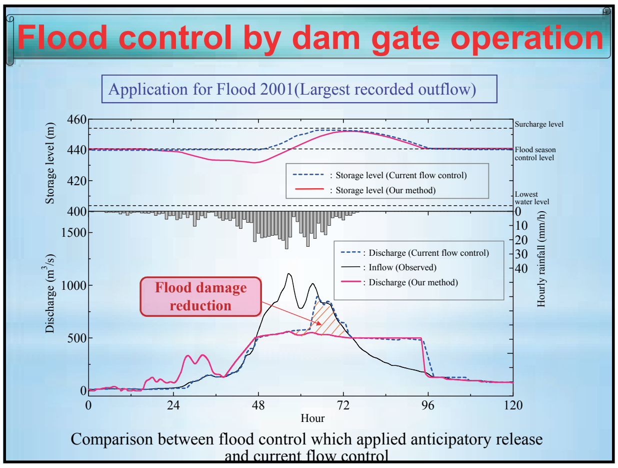

Flood control by dam gate operation

Application for Flood 2001(Largest recorded outflow)

Comparison between flood control which applied anticipatory release and current flow control

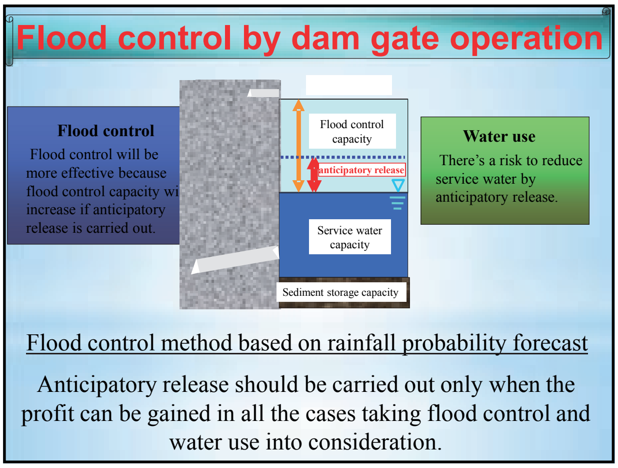

Flood control by dam gate operation

Flood control

Flood control will be more effective because flood control capacity wi increase if anticipatory release is carried out.

Water use

There's a risk to reduce service water by anticipatory release.

Flood control method based on rainfall probability forecast

Anticipatory release should be carried out only when the profit can be gained in all the cases taking flood control and water use into consideration.

The necessary information for decision making

Rainfall probability forecast

P_f%: Probability of total rainfall more than R [mm]

Minimum rainfall of the basin

The total rainfall exceeding minimum rainfall, R_M [mm] occurs with probability of P_M [%]

Runoff characteristics of the basin

When it rains more than R [mm] in total,

the runoff, totally V [m^3/s] flows into dam reservoir

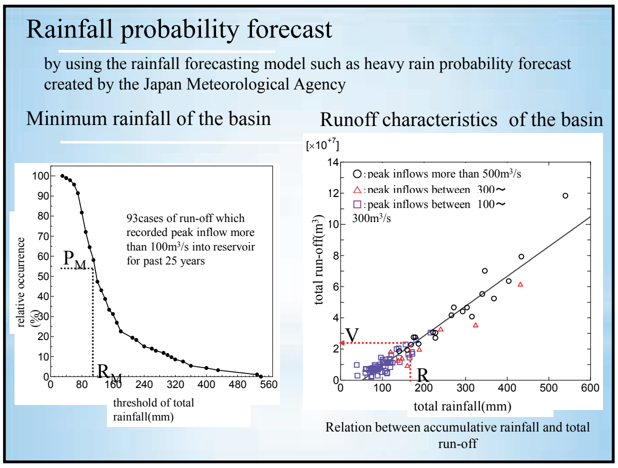

Rainfall probability forecast

by using the rainfall forecasting model such as heavy rain probability forecast created by the Japan Meteorological Agency

Minimum rainfall of the basin

Runoff characteristics of the basin

Relation between accumulative rainfall and total run-off

All cases of decision making for anticipatory release based on rainfall probability forecast

■ Case Ⅰ

Rainfall probability forecasts prove right.

■ Case Ⅱ

Rainfall probability forecasts prove wrong, but the prediction of minimum rainfall proves right.

■ Case Ⅲ

Both rainfall probability forecast and minimum rainfall prediction prove wrong.

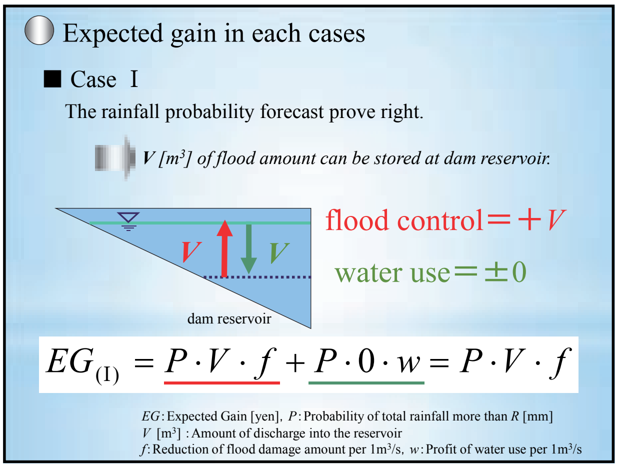

Expected gain in each cases

■ Case Ⅰ

The rainfall probability forecast prove right.

V [m^3] of flood amount can be stored at dam reservoir.

flood control ＝ $+V$

water use ＝ ± 0

$$EG_{(\mathrm{I})} = \underline{P \cdot V \cdot f} + \underline{P \cdot 0 \cdot w} = P \cdot V \cdot f$$

EG: Expected Gain [yen], P: Probability of total rainfall more than R [mm]
V [m^3] : Amount of discharge into the reservoir
f: Reduction of flood damage amount per 1m^3/s, w: Profit of water use per 1m^3/s

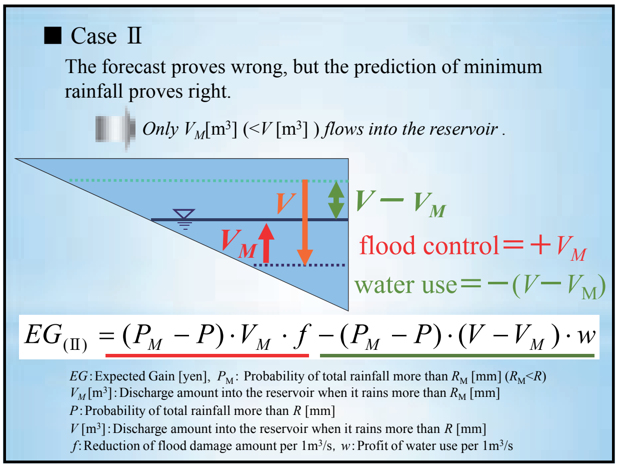

■ Case Ⅱ

The forecast proves wrong, but the prediction of minimum rainfall proves right.

Only V_M[m^3] (<V [m^3]) *flows into the reservoir .*

flood control$=+V_M$

water use$=-(V-V_M)$

$$EG_{(\mathrm{II})}=\underline{(P_M-P)\cdot V_M\cdot f}\underline{-(P_M-P)\cdot(V-V_M)\cdot w}$$

EG: Expected Gain [yen], P_M: Probability of total rainfall more than R_M [mm] ($R_M<R$)
V_M[m^3]: Discharge amount into the reservoir when it rains more than R_M [mm]
P: Probability of total rainfall more than R [mm]
V [m^3]: Discharge amount into the reservoir when it rains more than R [mm]
f: Reduction of flood damage amount per 1m^3/s, w: Profit of water use per 1m^3/s

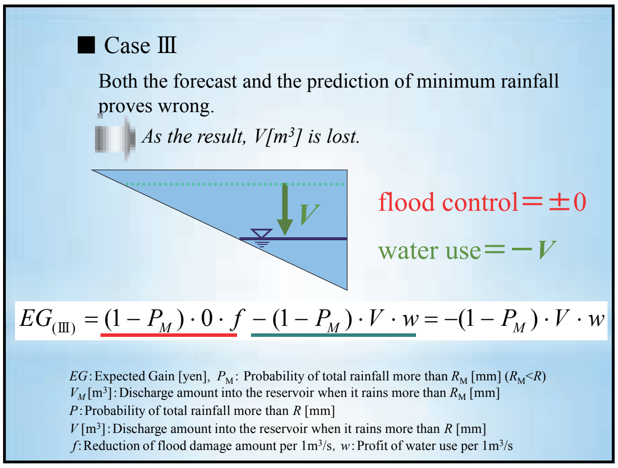

■ Case Ⅲ

Both the forecast and the prediction of minimum rainfall proves wrong.

As the result, $V[m^3]$ *is lost.*

flood control$=\pm 0$

water use$=-V$

$$EG_{(\mathrm{III})}=\underline{(1-P_M)\cdot 0\cdot f}\ \underline{-(1-P_M)\cdot V\cdot w}=-(1-P_M)\cdot V\cdot w$$

EG: Expected Gain [yen], P_M: Probability of total rainfall more than R_M [mm] ($R_M<R$)
V_M[m^3]: Discharge amount into the reservoir when it rains more than R_M [mm]
P: Probability of total rainfall more than R [mm]
V [m^3]: Discharge amount into the reservoir when it rains more than R [mm]
f: Reduction of flood damage amount per 1m^3/s, w: Profit of water use per 1m^3/s

Determination of the threshold to judge whether anticipatory release will be carried out

Total expected gain at all cases should be over 0.

$$\sum_{i=3} EG_{(i)}=EG_{(\mathrm{I})}+EG_{(\mathrm{II})}+EG_{(\mathrm{III})}>0$$

↓

$$\boxed{P>\frac{V\cdot w-P_M\cdot V_M\cdot(f+w)}{(V-V_M)\cdot(f+w)}}$$

EG: Expected Gain [yen], P_M: Probability of total rainfall more than R_M [mm] ($R_M<R$)
V_M[m^3]: Discharge amount into the reservoir when it rains more than R_M [mm]
P: Probability of total rainfall more than R [mm]
V [m^3]: Discharge amount into the reservoir when it rains more than R [mm]
f: Reduction of flood damage amount per 1m^3/s, w: Profit of water use per 1m^3/s

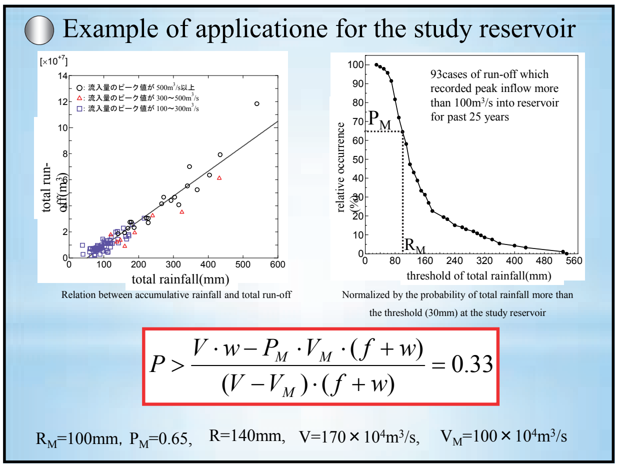

Example of applicatione for the study reservoir

Relation between accumulative rainfall and total run-off

Normalized by the probability of total rainfall more than the threshold (30mm) at the study reservoir

$$\boxed{P>\frac{V\cdot w-P_M\cdot V_M\cdot(f+w)}{(V-V_M)\cdot(f+w)}=0.33}$$

R_M=100mm, P_M=0.65, R=140mm, V=170 × 10^{4}m^3/s, V_M=100 × 10^{4}m^3/s

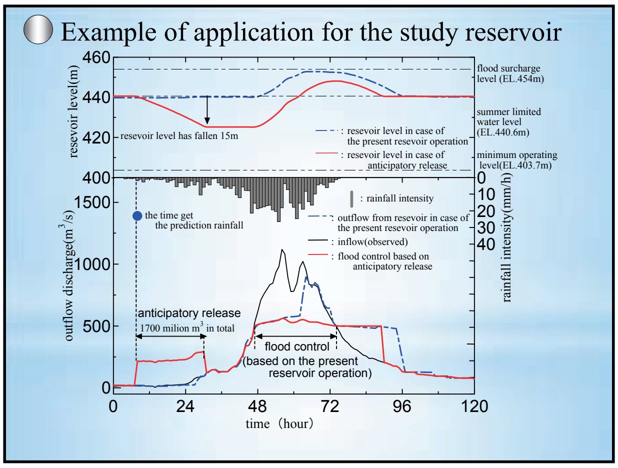

Example of application for the study reservoir

Contents

1. Disaster risk management considering the uncertainty of physical process

- Background
- Flood risk management
- Uncertainties in rainfall-runoff process
- Rainfall-runoff analysis considering uncertainty
- Analysis of flood levee reliability considering uncertainty

2. The role of dams(1): 1947 Kathleen typhoon

- Reproducing calculation considering the uncertainty of spatial distribution
- Reproducing calculation considering the uncertainty of typhoon path
- The flood control effect of yanba dam

3. The role of dams(2): 2015 Kanto & Tohoku heavy rain

- Flood control by dam gate operation
- The flood control effect of dam group in the upstream of Kinugawa river basin

The graph of flood control of Kawaji-dam at 2015 Kanto & Tohoku heavy rain

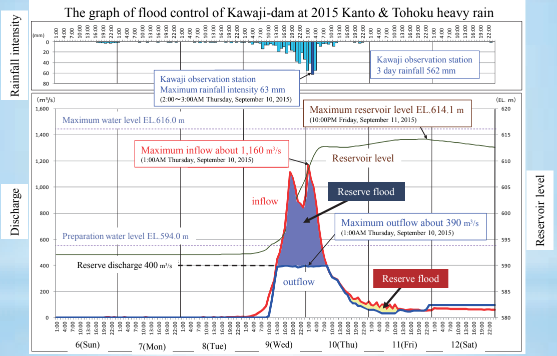

国土交通省関東地方整備局:『平成27年9月関東・東北豪雨災害に係る鬼怒川の洪水被害及び』

The graph of flood control of Kawamata-dam at 2015 Kanto & Tohoku heavy rain

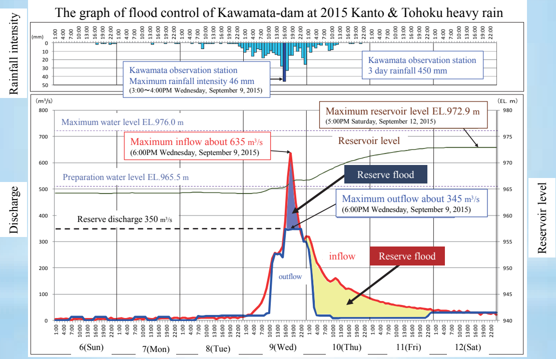

国土交通省関東地方整備局:『平成27年9月関東・東北豪雨災害に係る鬼怒川の洪水被害及び』

The graph of flood control of Ikari-dam at 2015 Kanto & Tohoku heavy rain

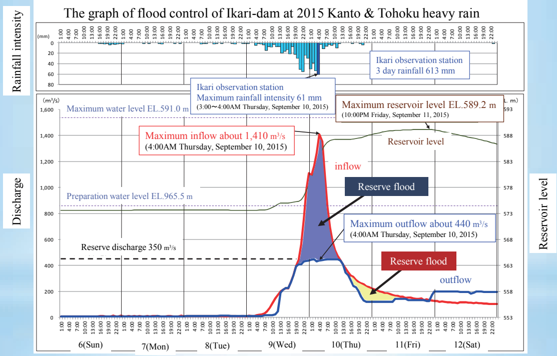

国土交通省関東地方整備局:『平成27年9月関東・東北豪雨災害に係る鬼怒川の洪水被害及び』

The graph of flood control of Yunishikawa-dam at 2015 Kanto & Tohoku heavy rain

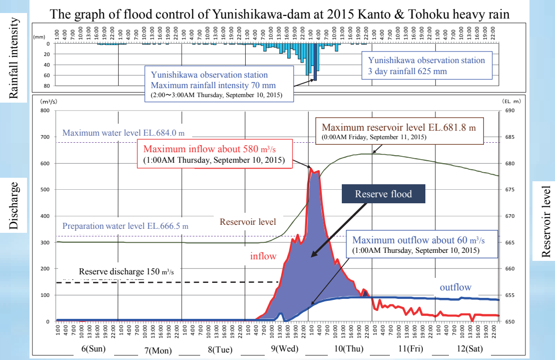

国土交通省関東地方整備局:『平成27年9月関東・東北豪雨災害に係る鬼怒川の洪水被害及び』

The flood control effect of the 4 dams in Kinugawa river

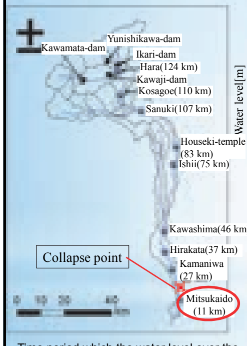
Yunishikawa-dam
Kawamata-dam
Ikari-dam
Hara(124 km)
Kawaji-dam
Kosagoe(110 km)
Sanuki(107 km)
Houseki-temple
(83 km)
Ishii(75 km)
Kawashima(46 km)
Hirakata(37 km)
Kamaniwa
(27 km)
Collapse point
Mitsukaido
(11 km)

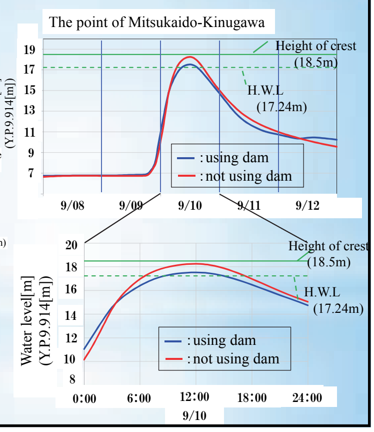

Time period which the water level over the high water level
With dams：About 6 hours
（observation data is 5 hours）
Without dams：About 11 hours

Thank you for listening

Keynote Presentation Ⅱ

The development of the Ishikari River basin
and the role of its dam reservoirs

Prof. Dr. Yasuyuki Shimizu
Laboratory of Hydraulic Research
Division of Field Engineering for the Environment
Faculty of Engineering, Hokkaido University

The 4th Asia-Pacific Group (APG) Symposium and 9th East Asian Dam Conference (EADC)

石狩川流域の開発とダム貯水池の役割

The development of the Ishikari River basin and the role of its dam reservoirs

北海道大学 大学院工学研究院
環境フィールド工学専攻 水工水文学研究室
教授 清水 康行

Prof. Dr. Yasuyuki Shimizu
Laboratory of Hydraulic Research
Division of Field Engineering for the Environment
Faculty of Engineering, Hokkaido University

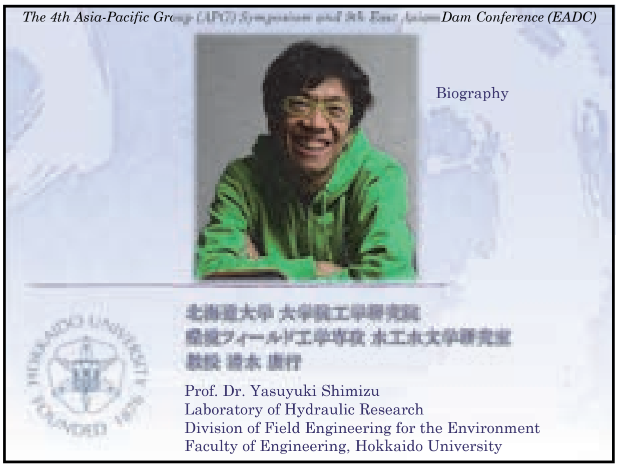

The 4th Asia-Pacific Group (APG) Symposium and 9th East Asian Dam Conference (EADC)

Biography

北海道大学 大学院工学研究院
環境フィールド工学専攻 水工水文学研究室
教授 清水 康行

Prof. Dr. Yasuyuki Shimizu
Laboratory of Hydraulic Research
Division of Field Engineering for the Environment
Faculty of Engineering, Hokkaido University

Topics

1. The Ishikari River Basin today and its importance
2. Development of the Ishikari River Basin and the effects of flood control projects there
3. Development of Sapporo city and the effects of dam reservoirs in the Toyohira River Basin
4. Towards sustainable development of the Ishikari River Basin

---

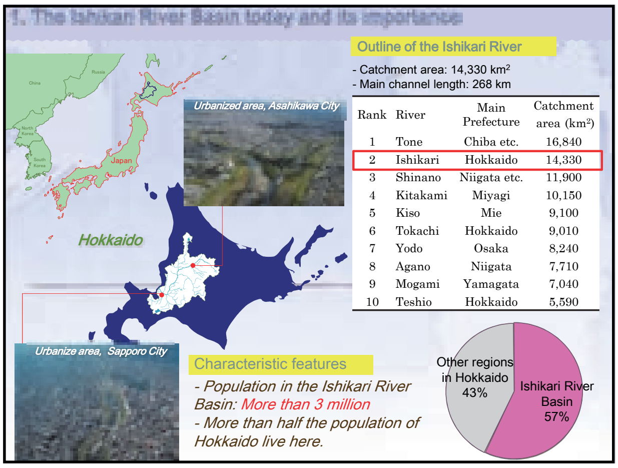

1. The Ishikari River Basin today and its importance

Outline of the Ishikari River

- Catchment area: 14,330 km^2
- Main channel length: 268 km

Rank	River	Main Prefecture	Catchment area (km^2)
1	Tone	Chiba etc.	16,840
2	Ishikari	Hokkaido	14,330
3	Shinano	Niigata etc.	11,900
4	Kitakami	Miyagi	10,150
5	Kiso	Mie	9,100
6	Tokachi	Hokkaido	9,010
7	Yodo	Osaka	8,240
8	Agano	Niigata	7,710
9	Mogami	Yamagata	7,040
10	Teshio	Hokkaido	5,590

Characteristic features

- Population in the Ishikari River Basin: More than 3 million
- More than half the population of Hokkaido live here.

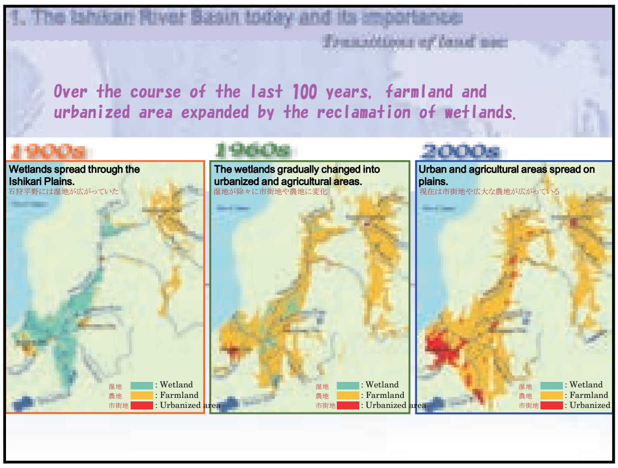

1. The Ishikari River Basin today and its importance

Transitions of land use

Over the course of the last 100 years, farmland and urbanized area expanded by the reclamation of wetlands.

1900s
Wetlands spread through the Ishikari Plains.
石狩平野には湿地が広がっていた

1960s
The wetlands gradually changed into urbanized and agricultural areas.
湿地が除々に市街地や農地に変化

2000s
Urban and agricultural areas spread on plains.
現在は市街地や広大な農地が広がっている

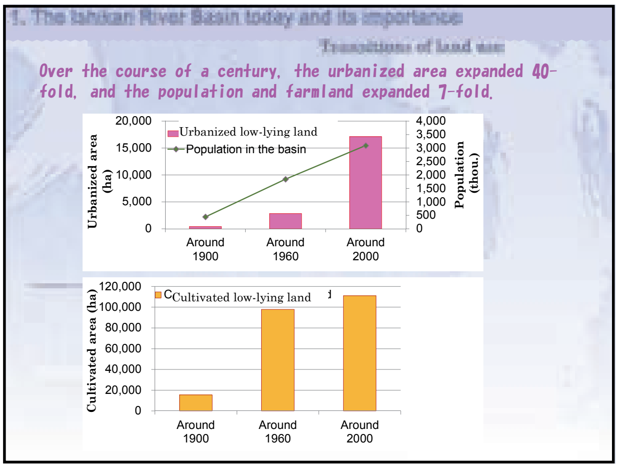

1. The Ishikari River Basin today and its importance

Transitions of land use

Over the course of a century, the urbanized area expanded 40-fold, and the population and farmland expanded 7-fold.

Topics

1. The Ishikari River Basin today and its importance
2. Development of the Ishikari River Basin and the effects of flood control projects there
3. Development of Sapporo city and the effects of dam reservoirs in the Toyohira River Basin
4. Towards sustainable development of the Ishikari River Basin

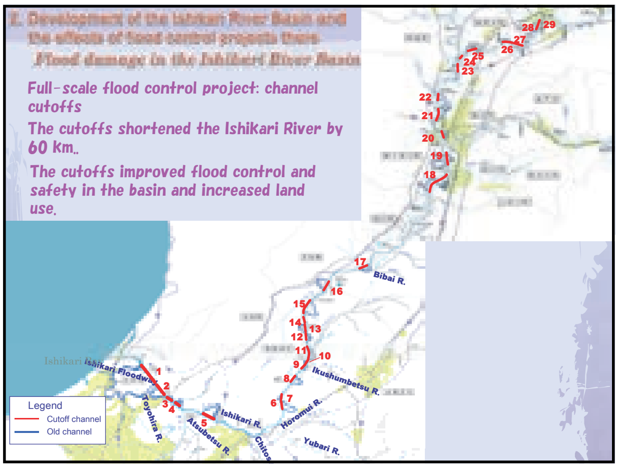

2. Development of the Ishikari River Basin and the effects of flood control projects there

Flood damage in the Ishikari River Basin

Full-scale flood control project: channel cutoffs

The cutoffs shortened the Ishikari River by 60 km..

The cutoffs improved flood control and safety in the basin and increased land use.

Legend
Cutoff channel
Old channel
Ishikari Bay
Ishikari Floodway
Toyohira R.
Atsubetsu R.
Ishikari R.
Chitose
Horomui R.
Yubari R.
Ikushumbetsu R.
Bibai R.
1
2
3
4
5
6
7
8
9
10
11
12
13
14
15
16
17
18
19
20
21
22
23
24
25
26
27
28
29

Oyafuru cutoff channel

(the first and the largest cutoff channel)

1918-1934

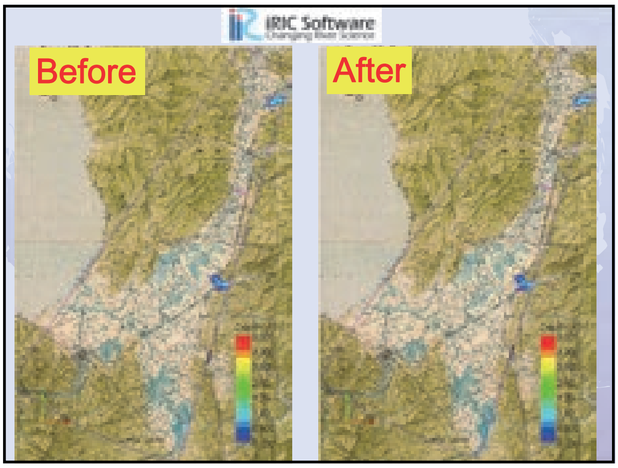

iRIC Software
Changing River Science
Before
After

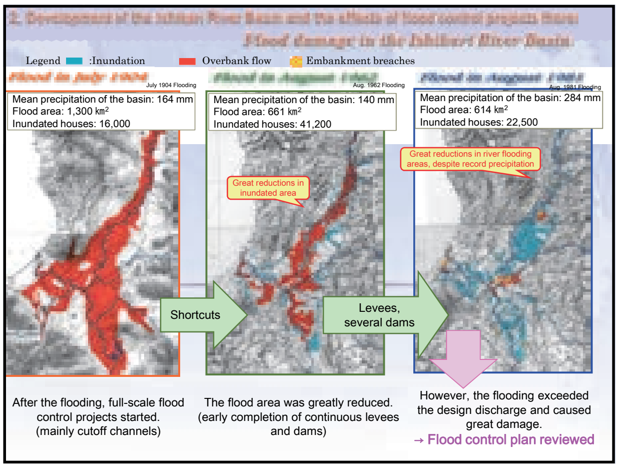

2. Development of the Ishikari River Basin and the effects of flood control projects there

Flood damage in the Ishikari River Basin

Legend 🟦 :Inundation 🟥 Overbank flow Embankment breaches
Flood in July 1904
July 1904 Flooding
Flood in August 1962
Aug. 1962 Flooding
Flood in August 1981
Aug. 1981 Flooding
Great reductions in inundated area
Great reductions in river flooding areas, despite record precipitation
Shortcuts
Levees, several dams

Mean precipitation of the basin: 164 mm
Flood area: 1,300 km²
Inundated houses: 16,000

Mean precipitation of the basin: 140 mm
Flood area: 661 km²
Inundated houses: 41,200

Mean precipitation of the basin: 284 mm
Flood area: 614 km²
Inundated houses: 22,500

After the flooding, full-scale flood control projects started. (mainly cutoff channels)

The flood area was greatly reduced. (early completion of continuous levees and dams)

However, the flooding exceeded the design discharge and caused great damage.
→ Flood control plan reviewed

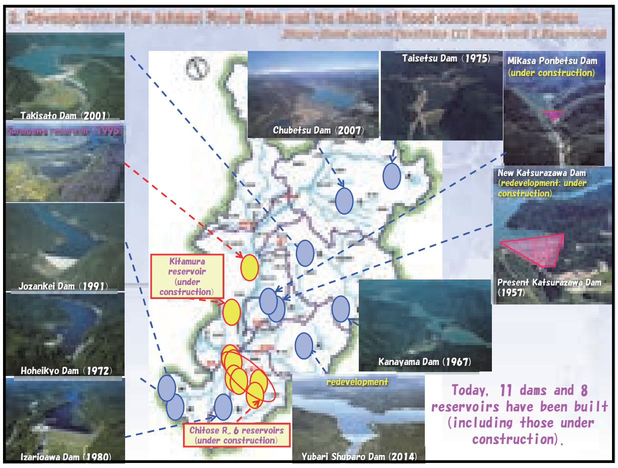

2. Development of the Ishikari River Basin and the effects of flood control projects there

Takisato Dam (2001)
Sunagawa reservoir (1995)
Jozankei Dam (1991)
Hoheikyo Dam (1972)
Izarigawa Dam (1980)
Chubetsu Dam (2007)
Taisetsu Dam (1975)
Mikasa Ponbetsu Dam (under construction)
New Katsurazawa Dam (redevelopment: under construction)
Present Katsurazawa Dam (1957)
Kanayama Dam (1967)
redevelopment
Yubari Shuparo Dam (2014)
Kitamura reservoir (under construction)
Chitose R., 6 reservoirs (under construction)

Today, 11 dams and 8 reservoirs have been built (including those under construction).

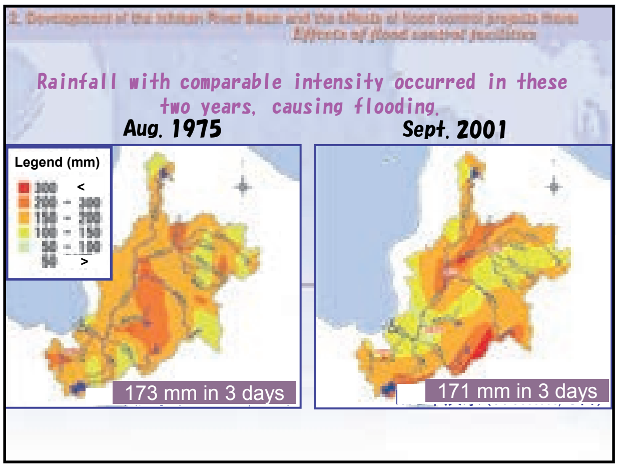

2. Development of the Ishikari River Basin and the effects of flood control projects there: Effects of flood control facilities

Rainfall with comparable intensity occurred in these two years, causing flooding.

Aug. 1975 **Sept. 2001**

Legend (mm)
300 <
200 – 300
150 – 200
100 – 150
50 – 100
50 >
173 mm in 3 days
171 mm in 3 days

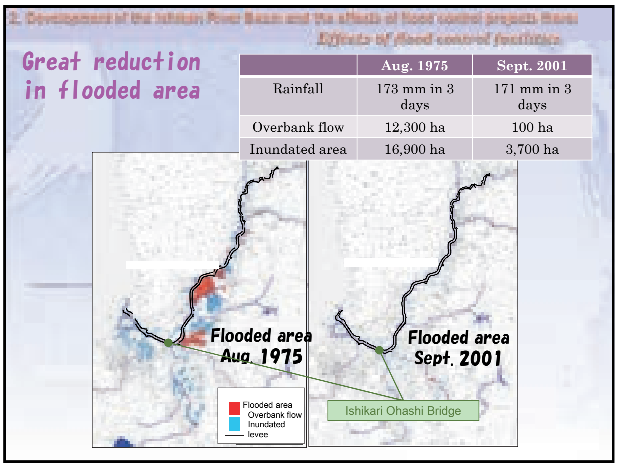

2. Development of the Ishikari River Basin and the effects of flood control projects there: Effects of flood control facilities

Great reduction in flooded area

	Aug. 1975	Sept. 2001
Rainfall	173 mm in 3 days	171 mm in 3 days
Overbank flow	12,300 ha	100 ha
Inundated area	16,900 ha	3,700 ha

Flooded area Aug. 1975
Flooded area Sept. 2001
Flooded area
Overbank flow
Inundated
levee
Ishikari Ohashi Bridge

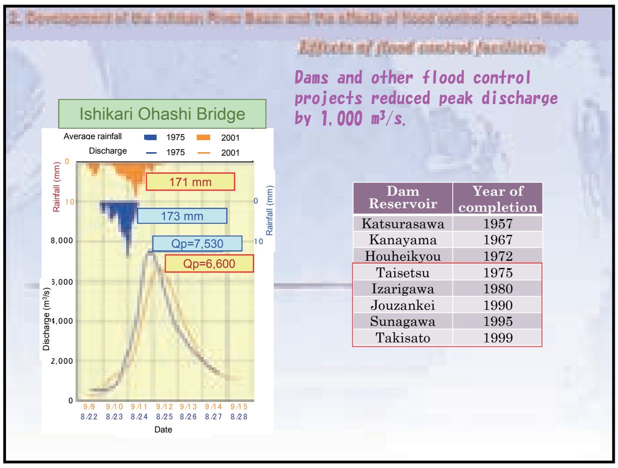

2. Development of the Ishikari River Basin and the effects of flood control projects there: Effects of flood control facilities

Dams and other flood control projects reduced peak discharge by 1,000 m^3/s.

Dam Reservoir	Year of completion
Katsurasawa	1957
Kanayama	1967
Houheikyou	1972
Taisetsu	1975
Izarigawa	1980
Jouzankei	1990
Sunagawa	1995
Takisato	1999

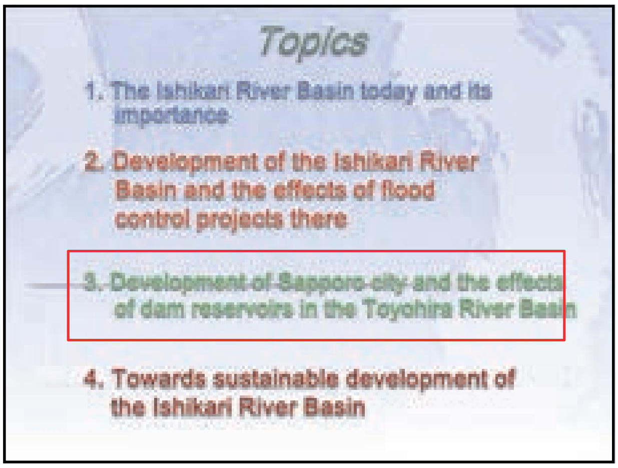

Topics

1. The Ishikari River Basin today and its importance
2. Development of the Ishikari River Basin and the effects of flood control projects there
3. Development of Sapporo city and the effects of dam reservoirs in the Toyohira River Basin
4. Towards sustainable development of the Ishikari River Basin

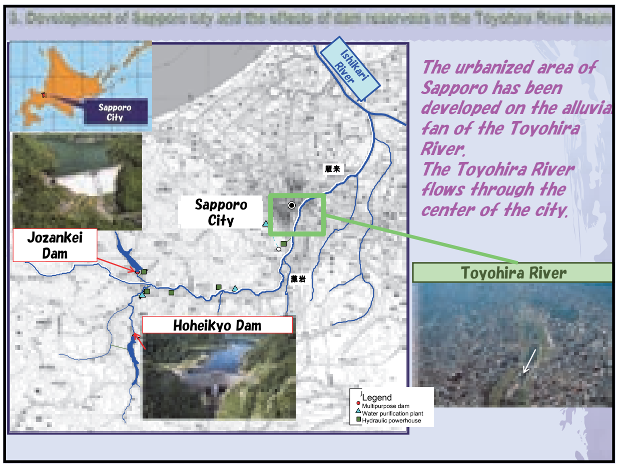

3. Development of Sapporo city and the effects of dam reservoirs in the Toyohira River Basin

The urbanized area of Sapporo has been developed on the alluvial fan of the Toyohira River.
The Toyohira River flows through the center of the city.

Sapporo City
Ishikari River
Sapporo City
雁来
藻岩
Jozankei Dam
Hoheikyo Dam
Toyohira River
Legend
Multipurpose dam
Water purification plant
Hydraulic powerhouse

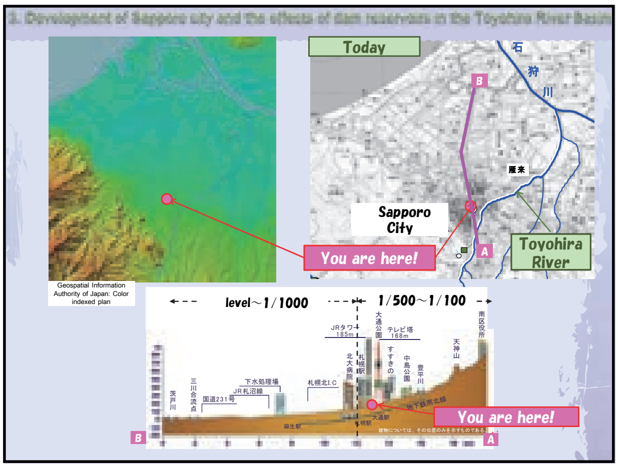

3. Development of Sapporo city and the effects of dam reservoirs in the Toyohira River Basin

Geospatial Information Authority of Japan: Color indexed plan

Today
石狩川
B
雁来
Sapporo City
You are here!
A
Toyohira River
level～1/1000
1/500～1/100
JRタワー 185m
大通公園
テレビ塔 168m
南区役所
天神山
すすきの
中島公園
豊平川
北大病院
札幌駅
札幌北I.C
下水処理場
JR札沼線
国道231号
三川合流点
茨戸川
麻生駅
札幌駅
大通駅
地下鉄南北線
建物については、その位置のみを示すものである。
You are here!
B
A

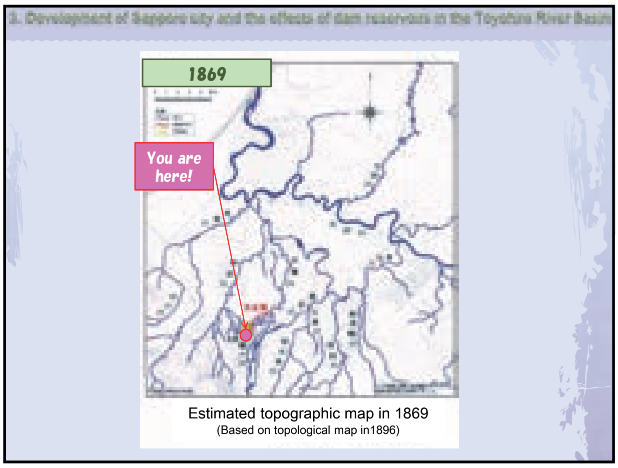

1. Development of Sapporo city and the effects of dam reservoirs in the Toyohira River Basin
1869
You are here!

Estimated topographic map in 1869
(Based on topological map in1896)

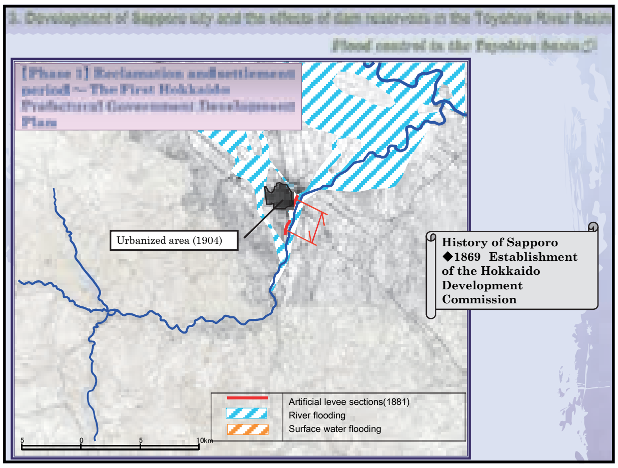

1. Development of Sapporo city and the effects of dam reservoirs in the Toyohira River Basin
Flood control in the Toyohira basin ②
[Phase 1] Reclamation and settlement period ~ The First Hokkaido Prefectural Government Development Plan
Urbanized area (1904)
5
0
5
10km

History of Sapporo
◆1869 Establishment of the Hokkaido Development Commission

Artificial levee sections(1881)
River flooding
Surface water flooding

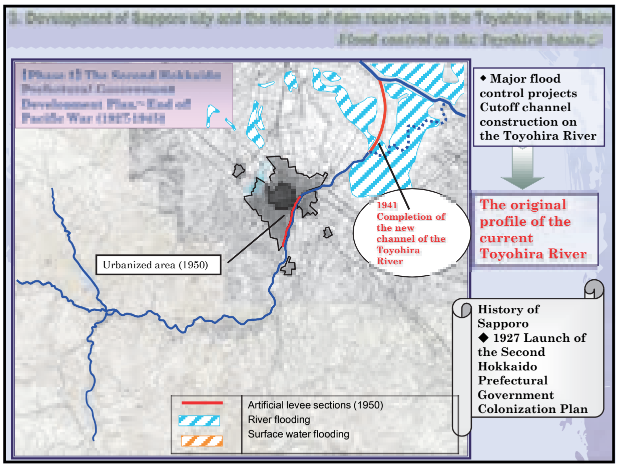

1. Development of Sapporo city and the effects of dam reservoirs in the Toyohira River Basin
Flood control in the Toyohira basin ②
[Phase 2] The Second Hokkaido Prefectural Government Development Plan ~ End of Pacific War (1927-1945)
Urbanized area (1950)
1941 Completion of the new channel of the Toyohira River

◆ Major flood control projects Cutoff channel construction on the Toyohira River

The original profile of the current Toyohira River

History of Sapporo
◆ 1927 Launch of the Second Hokkaido Prefectural Government Colonization Plan

Artificial levee sections (1950)
River flooding
Surface water flooding

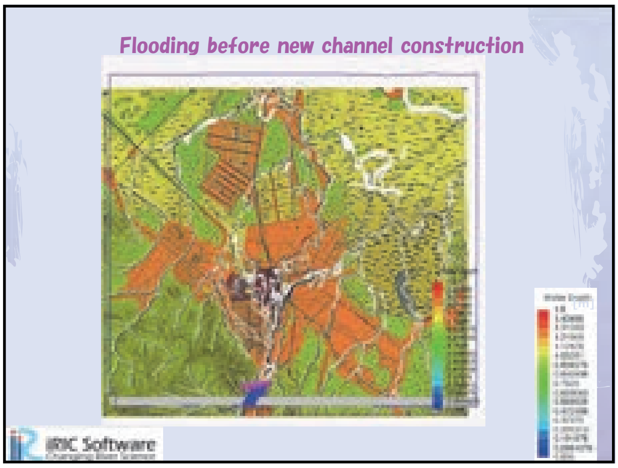

Flooding before new channel construction

iRIC Software

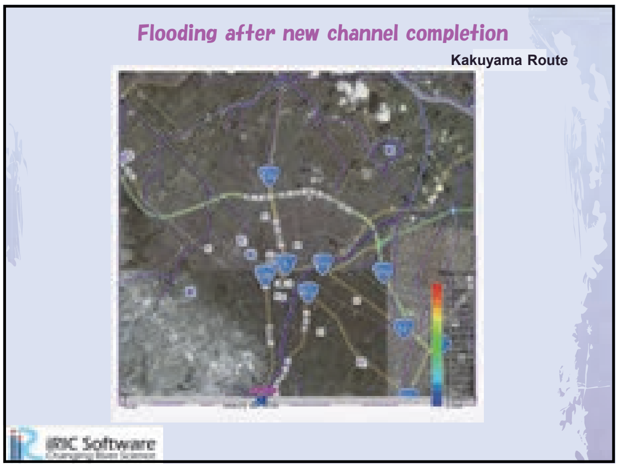

Flooding after new channel completion

Kakuyama Route

iRIC Software

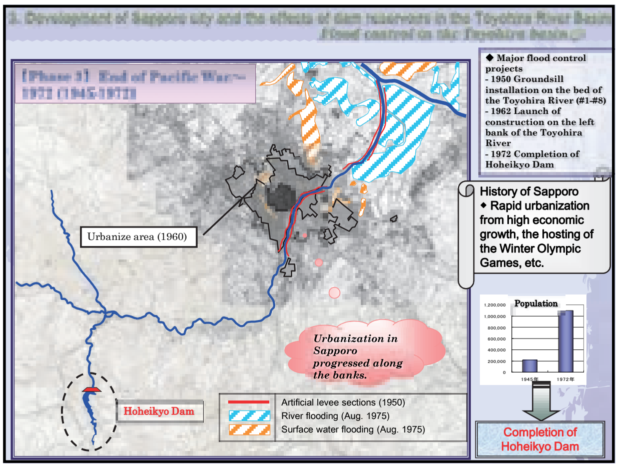

1. Development of Sapporo city and the effects of dam reservoirs in the Toyohira River Basin
Flood control in the Toyohira basin ②
[Phase 3] End of Pacific War ~ 1972 (1945-1972)
Urbanize area (1960)
Urbanization in Sapporo progressed along the banks.
Hoheikyo Dam
Population
1,200,000
1,000,000
800,000
600,000
400,000
200,000
0
1945年
1972年

◆ Major flood control projects
- 1950 Groundsill installation on the bed of the Toyohira River (#1-#8)
- 1962 Launch of construction on the left bank of the Toyohira River
- 1972 Completion of Hoheikyo Dam

History of Sapporo
◆ Rapid urbanization from high economic growth, the hosting of the Winter Olympic Games, etc.

Artificial levee sections (1950)
River flooding (Aug. 1975)
Surface water flooding (Aug. 1975)

Completion of Hoheikyo Dam

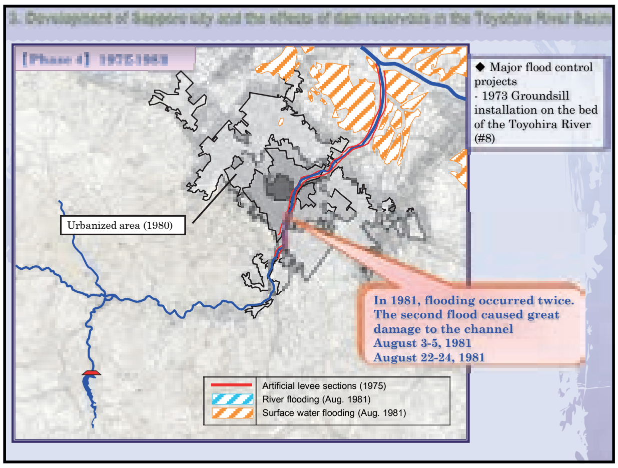

3. Development of Sapporo city and the effects of dam reservoirs in the Toyohira River Basin

【Phase 4】 1975-1981

◆ Major flood control projects
- 1973 Groundsill installation on the bed of the Toyohira River (#8)

Urbanized area (1980)

In 1981, flooding occurred twice. The second flood caused great damage to the channel
August 3-5, 1981
August 22-24, 1981

Artificial levee sections (1975)
River flooding (Aug. 1981)
Surface water flooding (Aug. 1981)

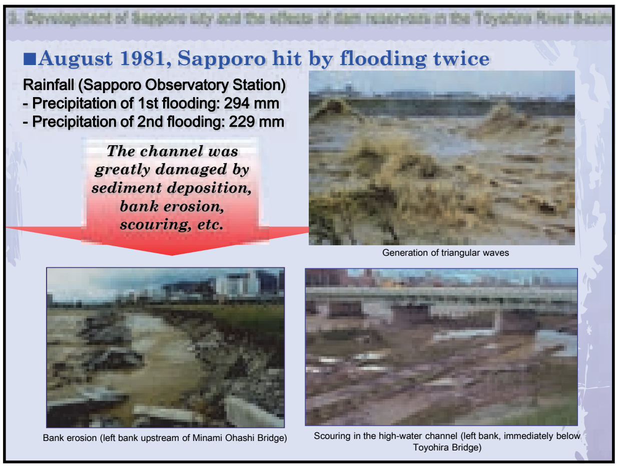

3. Development of Sapporo city and the effects of dam reservoirs in the Toyohira River Basin

■August 1981, Sapporo hit by flooding twice

Rainfall (Sapporo Observatory Station)
- Precipitation of 1st flooding: 294 mm
- Precipitation of 2nd flooding: 229 mm

The channel was greatly damaged by sediment deposition, bank erosion, scouring, etc.

Generation of triangular waves

Bank erosion (left bank upstream of Minami Ohashi Bridge)

Scouring in the high-water channel (left bank, immediately below Toyohira Bridge)

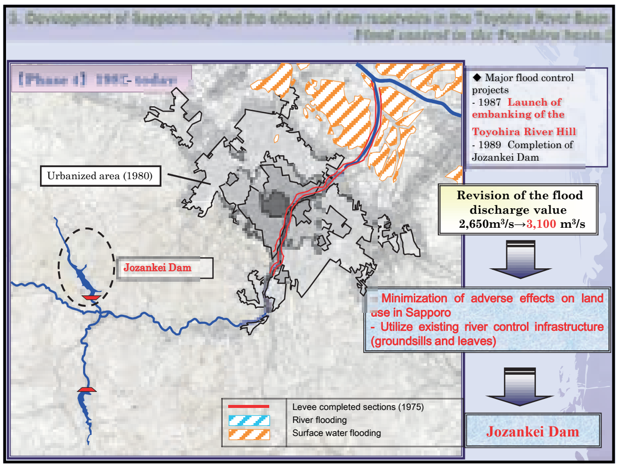

3. Development of Sapporo city and the effects of dam reservoirs in the Toyohira River Basin
Flood control in the Toyohira basin ②

【Phase 5】 1981- today

◆ Major flood control projects
- 1987 Launch of embanking of the Toyohira River Hill
- 1989 Completion of Jozankei Dam

Urbanized area (1980)
Jozankei Dam

Revision of the flood discharge value
2,650m³/s→3,100 m³/s

- Minimization of adverse effects on land use in Sapporo
- Utilize existing river control infrastructure (groundsills and leaves)

Jozankei Dam

Levee completed sections (1975)
River flooding
Surface water flooding

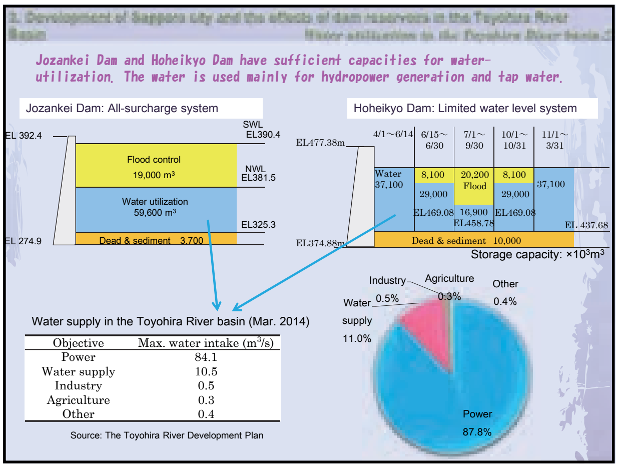

3. Development of Sapporo city and the effects of dam reservoirs in the Toyohira River Basin
Water utilization in the Toyohira River basin ①

Jozankei Dam and Hoheikyo Dam have sufficient capacities for water-utilization. The water is used mainly for hydropower generation and tap water.

Jozankei Dam: All-surcharge system

EL 392.4
SWL
EL390.4
Flood control
19,000 m³
NWL
EL381.5
Water utilization
59,600 m³
EL325.3
EL 274.9
Dead & sediment 3,700

Hoheikyo Dam: Limited water level system

EL477.38m
4/1～6/14
6/15～6/30
7/1～9/30
10/1～10/31
11/1～3/31
Water
37,100
8,100
20,200
Flood
8,100
37,100
29,000
29,000
EL469.08
16,900
EL458.78
EL469.08
EL 437.68
EL374.88m
Dead & sediment 10,000

Storage capacity: ×10³m³

Water supply in the Toyohira River basin (Mar. 2014)

Objective	Max. water intake (m³/s)
Power	84.1
Water supply	10.5
Industry	0.5
Agriculture	0.3
Other	0.4

Source: The Toyohira River Development Plan

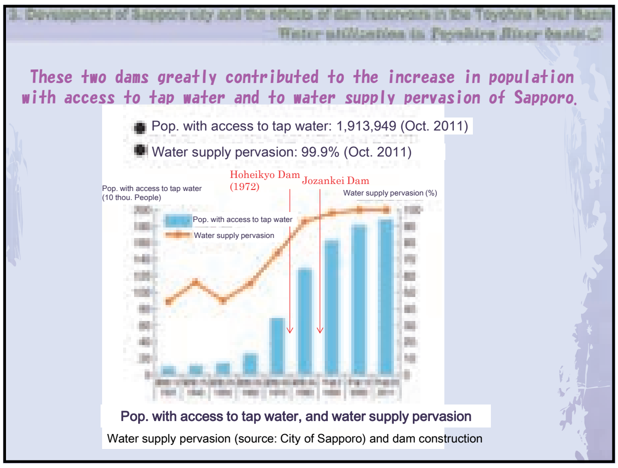

3. Development of Sapporo city and the effects of dam reservoirs in the Toyohira River Basin
Water utilization in Toyohira River basin ②

These two dams greatly contributed to the increase in population with access to tap water and to water supply pervasion of Sapporo.

- Pop. with access to tap water: 1,913,949 (Oct. 2011)
- Water supply pervasion: 99.9% (Oct. 2011)

Pop. with access to tap water, and water supply pervasion

Water supply pervasion (source: City of Sapporo) and dam construction

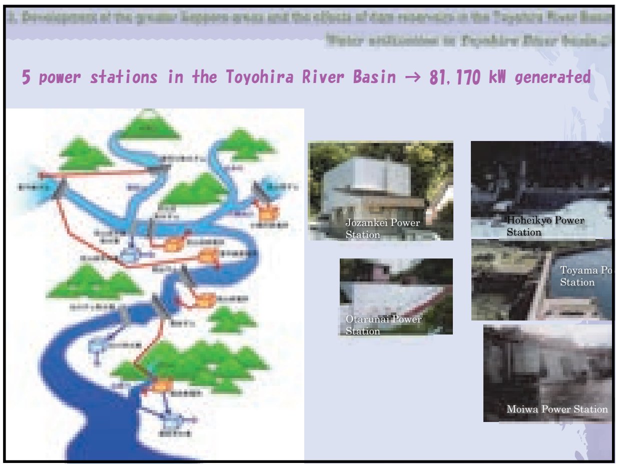

3. Development of the greater Sapporo areas and the effects of dam reservoirs in the Toyohira River Basin
Water utilization in Toyohira River basin ③

5 power stations in the Toyohira River Basin → 81,170 kW generated

Jozankei Power Station
Hoheikyo Power Station
Toyama Po
Station
Otarunai Power Station
Moiwa Power Station

3. Development of Sapporo city and the effects of dam reservoirs in the Toyohira River Basin

Flood control projects, such as channel cutoffs and dam construction

Effects on flood control

Effects on water utilization

Great contribution to the development of Sapporo

Topics

1. The Ishikari River Basin today and its importance
2. Development of the Ishikari River Basin and the effects of flood control projects there
3. Development of Sapporo city and the effects of dam reservoirs in the Toyohira River Basin
4. Towards sustainable development of the Ishikari River Basin

---

4. Towards sustainable development of the Ishikari River Basin

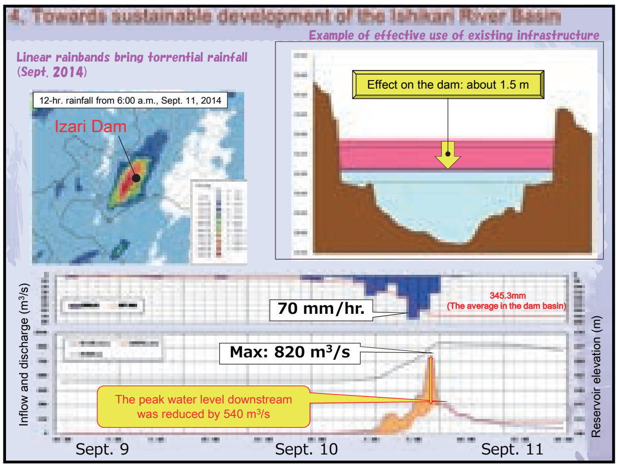

Example of effective use of existing infrastructure

Linear rainbands bring torrential rainfall (Sept. 2014)

12-hr. rainfall from 6:00 a.m., Sept. 11, 2014

Izari Dam

Effect on the dam: about 1.5 m

70 mm/hr.

345.3mm (The average in the dam basin)

Max: 820 m³/s

The peak water level downstream was reduced by 540 m³/s

---

4. Towards sustainable development of the Ishikari River Basin

Increases in typhoon frequency and scale (Aug. 2018)

Example of effective use of existing infrastructure

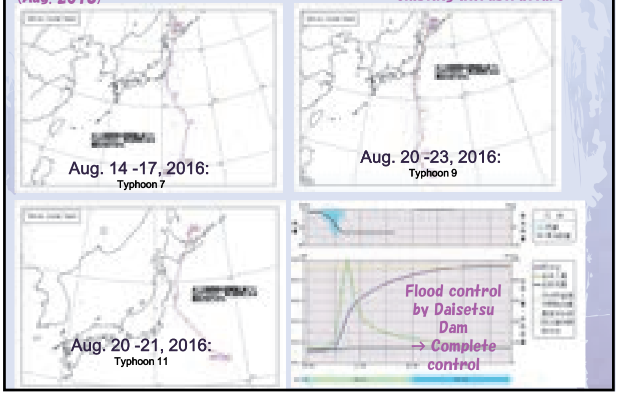

Flood control by Daisetsu Dam → Complete control

Thank you for your attention.

Papers

Session (1) Innovative Technologies of Dam

4th APG Symposium and 9th EADC on

INNOVATIVE TECHNOLOGIES FOR DAMS AND RESERVOIRS TOWARD THE FUTURE GENERATIONS

Large-scale Dam Body Drilling by Tsuruda Dam Redevelopment Project

K. Kaji, K. Oobayashi & K. Miyahara
Sendai River Office, Kyushu Regional Development Bureau, MLIT, Kagoshima, Japan
kaji-k8910@qsr.mlit.go.jp

T. Fujisawa, H. Yoshida & N. Yasuda
Japan Dam Engineering Center, Tokyo, Japan

ABSTRACT:
The Ministry of Land, Infrastructure, Transport and Tourism is now redeveloping Tsuruda Dam. The objective of the project is to improve its flood control function by increasing its flood control capacity and installing 3 additional large outlets for flood control. Remarkable features of the project are its large scale: 6m diameter holes and 4.8m diameter outlet. And the height of the dam crest above the holes is more than 60m.

This work had to be executed while ensuring Tsuruda Dam's flood control and water supply functions, requiring the construction of a cofferdam in the reservoir before drilling the dam body. Because underwater work at the large depth was necessary, we developed a new type of floating cofferdam.

This report introduces an outline of large-scale dam body drilling at Tsuruda Dam redevelopment project.

Keywords: dam body drilling, dam redevelopment, floating cofferdam, vibration velocity

1. OUTLINE

It is considered that the necessity of projects to redevelop existing dams will become greater in the future in light of their merits compared with a new dam construction project. Redevelopment can [1] manifest flood control and water supply effects much earlier, [2] minimize impacts on the natural and social environments, and [3] can achieve economic purposes.

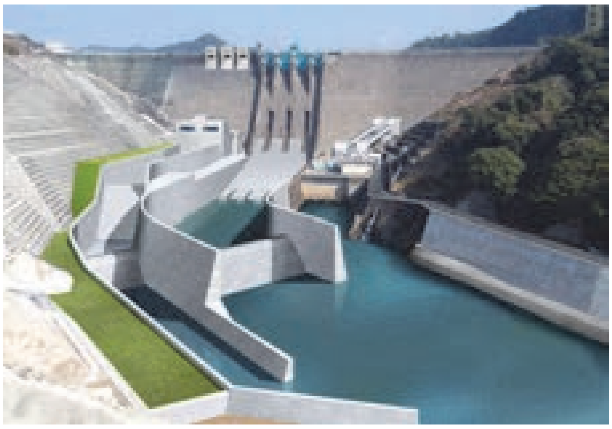

Figure 1. Conceptual drawing of completed redevelopment work（White colored parts are redeveloped.）

Tsuruda Dam is a 117.5m high concrete gravity dam completed in 1966. In 2006, record-breaking torrential rainfall occurred in its catchment, causing severe flood damage in the downstream basin, even though Tsuruda Dam made full use of its reservoir capacity to control the flood. The Ministry of Land, Infrastructure, Transport and Tourism is now redeveloping Tsuruda Dam. The objective of the project is to improve its flood control function by increasing its flood control capacity from 75 million m^3 to 98 million m^3, and at the same time, drilling the right side of the dam body to install 3 additional outlets for flood control (Fig. 1).

Remarkable features of this project are its large scale, the 6m diameter of the hole drilled and the 4.8m diameter outlet installed in the dam body. And the height of the dam crest above the holes is more than 60m.

At the design stage, we carried out detailed analytic study of the stress generated by the drilling of the dam body, and conducted a preliminary drilling test, too. During execution, we monitored vibration velocity to prevent the dam body drilling from harmfully effecting the dam body concrete. This work had to be executed while ensuring Tsuruda Dam's flood control and water supply functions, requiring the construction of a cofferdam in the reservoir before drilling the dam body. It is usually necessary to place pedestal concrete as the foundation on the reservoir side and to construct the cofferdam on top of the pedestal. But at Tsuruda Dam, because underwater construction work in deep water was necessary, we developed a new type of floating cofferdam. Cofferdam assembled in advance on the reservoir surface was towed to the dam body and installed there, eliminating the need for a pedestal concrete, reducing the quantity of deep underwater work and speeding up the work.

The redevelopment project of Tsuruda Dam includes, in addition to these works, improvement of the existing energy dissipation works, and the relocation of two penstocks on the left side of the dam body.

This report introduces an outline of the design and execution of large-scale dam body drilling at Tsuruda Dam redevelopment project.

2. DEVELOPMENT OF THE FLOATING COFFERDAM

2.1. Outline

Dam redevelopment projects in Japan are often executed while maintaining the dam’s flood control and water supply functions. To drill a dam body while it stores water, it is necessary to install a cofferdam upstream the dam body in advance, then drain the water from inside it to create a dry space on the reservoir side. At Tsuruda Dam, we developed a new type of floating cofferdam and used along with a conventional pedestal concrete type cofferdam, verifying the effectiveness of the new floating cofferdam.

2.2. Background to the technology development

In Japan, cofferdams installed inside reservoirs are usually either the bearing frame type or pedestal concrete type. A bearing frame type cofferdam is constructed by first installing a brace and the cofferdam’s bottom shutter in the water, then constructing the cofferdam on top of it by assembling shutters one level at a time. A pedestal concrete type is built by excavating the concrete footing and bedrock at the upstream side of the dam body, then installing the pedestal concrete. The cofferdam is constructed by assembling shutters one at a time above the pedestal concrete. In case of Tsuruda Dam, according to the initial plan, in order to ensure safety of the cofferdam from the large buoyancy acting on it, the pedestal concrete type was to be adopted for the cofferdams at all three outlets.

A pedestal concrete type cofferdam requires diving work to excavate the foundation bedrock in the reservoir, to remove the existing concrete footing, and to place the pedestal concrete. At Tsuruda Dam, the diving work must be done at a depth of more than 30m.To insure the safety of the divers, it is necessary to use special diving technology called saturation diving. And the existing concrete crushing work in deep underwater was very difficult. This presented problems related to the cost of the work, difficulty of execution, and work period. So as the cofferdam used for the No. 3 outlet which was installed furthest to the right of the three outlets, we adopted the newly developed floating cofferdam (Fig. 2).

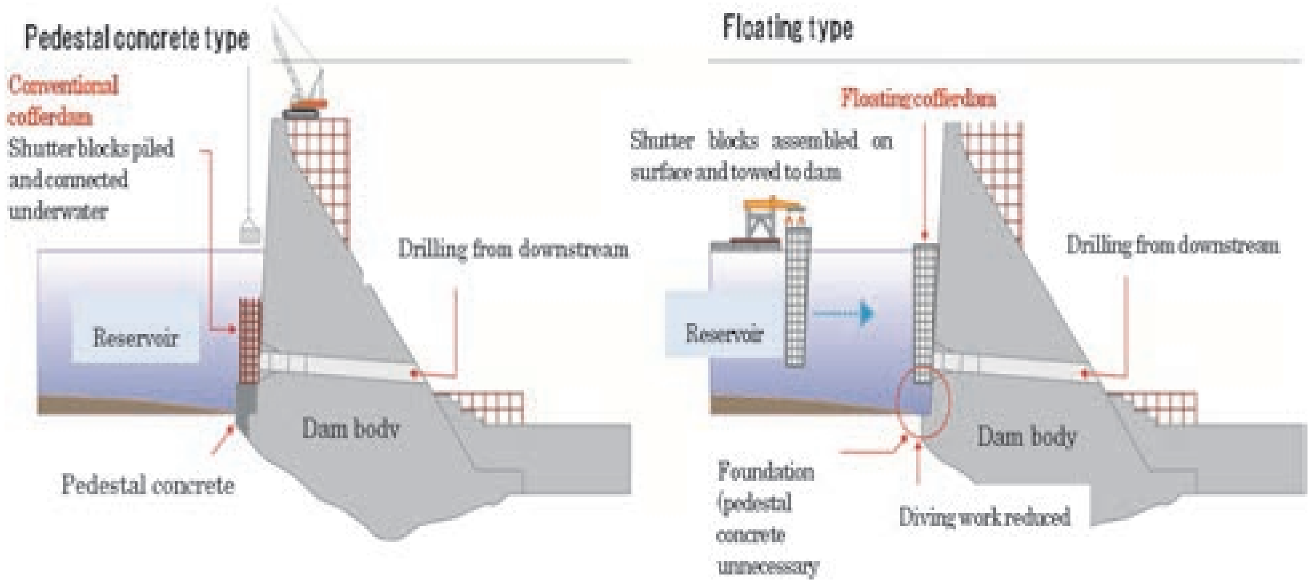
Pedestal concrete type
Conventional cofferdam
Shutter blocks piled and connected underwater
Drilling from downstream
Reservoir
Dam body
Pedestal concrete
Floating type
Floating cofferdam
Shutter blocks assembled on surface and towed to dam
Drilling from downstream
Reservoir
Dam body
Foundation (pedestal concrete unnecessary
Diving work reduced

Figure 2. Comparison of pedestal concrete type and floating type

2.3. Structure of the floating cofferdam

A floating cofferdam applies the ballast water technology of oil tankers. On the shutter blocks of a floating cofferdam, air-tight buoyancy chambers are formed by attaching steel plates (skin plates) on the inside and outside (Fig. 3). The quantity of water in the buoyancy chambers installed on each shutter block is adjusted, permitting control of buoyancy acting on the shutters and their attitude. The cofferdams are shaped asymmetrically, and if buoyancy is simply applied to the shutters, only one side is buoyant and it rotates, so its attitude cannot be maintained. Thus, when a shutter is installed, it is necessary to maintain a balance between self-weight and buoyancy by filling and draining the buoyancy chambers inside the shutter in a correct sequence. When water has been drained from inside the cofferdam, water pressure presses the watertight rubber installed on the shutters against the gate sheets installed in advance on the dam body, maintaining water-tightness. It is designed so that the friction resistance produced by water pressure and the floating prevention hardware installed above the shutters resists the buoyancy that acts on the cofferdam.

2.4. Execution

Shutter blocks manufactured at an on-site plant are assembled on the surface of the reservoir (Fig. 4).
The assembled cofferdam is towed to the installation location at the dam body where it is pulled against and installed on the dam body with a winch (Fig. 5).
After it is installed, water is drained from the cofferdam by pumps (Fig. 6).
Leakage from the cofferdam after draining was extremely small, at about 1 liter/minute (Fig. 7).

2.5. Effects of the floating cofferdam

The floating cofferdam reduced deep water work, because large scale equipment such as pedestal concrete or bearing frame of a conventional cofferdam were unnecessary. This resulted in safer execution, a shorter work period, and lower cost. When drilling multiple holes in a dam body, such as was done at Tsuruda Dam, it is necessary to dissemble and reassemble cofferdams just as it is with the conventional method. But in the case of a floating cofferdam, it is possible to tow it to the next execution location and easily install without disassembling the shutters. This method is, therefore, counted on to be applied to other dams in the future.

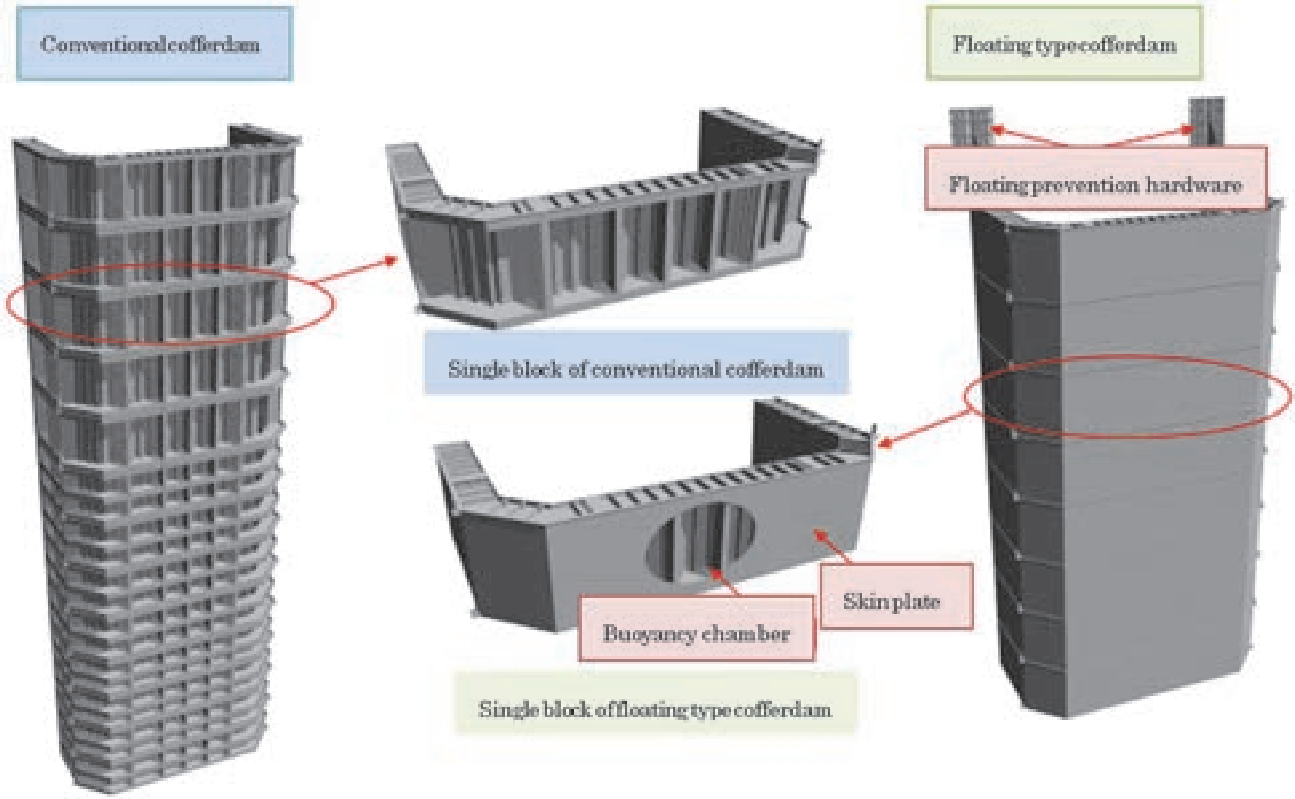
Conventional cofferdam
Floating type cofferdam
Floating prevention hardware
Single block of conventional cofferdam
Skin plate
Buoyancy chamber
Single block of floating type cofferdam

Figure 3. Comparison of conventional type and floating type cofferdams

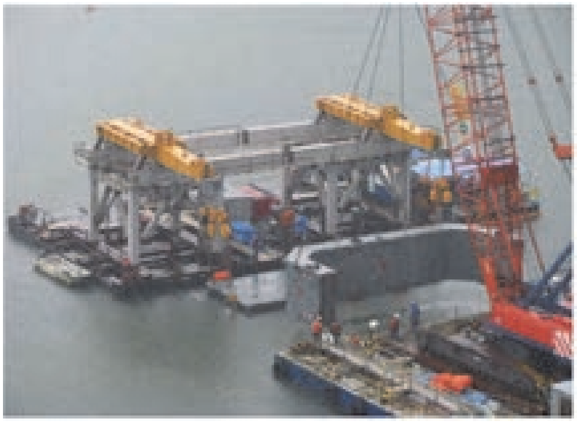

Figure 4. Assembly on the reservoir

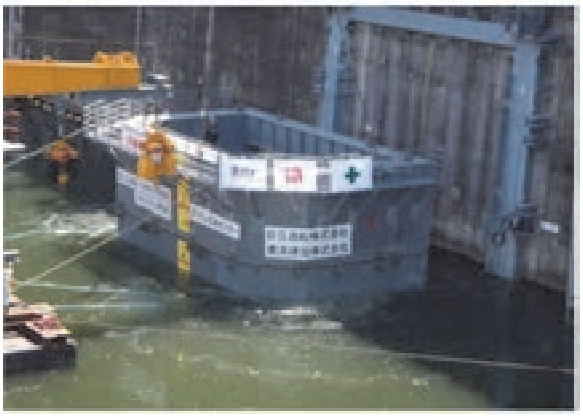

Figure 5. Towing to the dam body

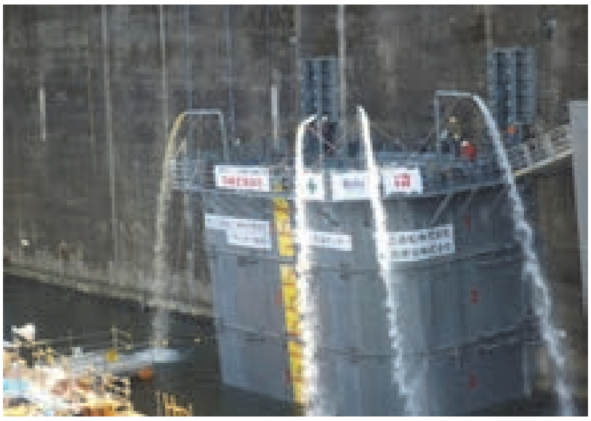

Figure 6. Drainage by pumps

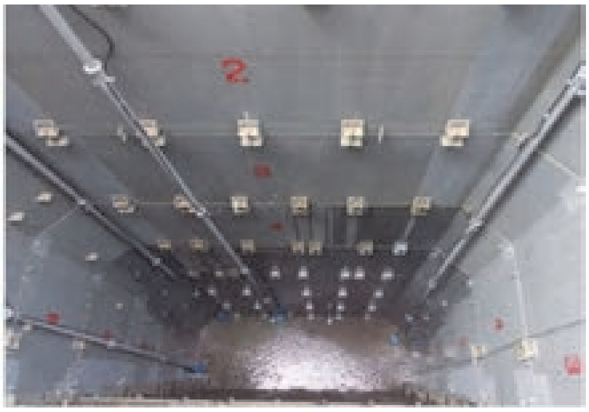

Figure 7. Inside the cofferdam after drainage

3. DRILLING THE DAM BODY

3.1. Outline of the drilling work

At Tsuruda Dam, 3 holes are drilled in the right side of the dam body. In Japan, there have been several cases of dam body drilling, but remarkable features of the Tsuruda Dam projects are its large scale: 6m diameter holes and 4.8m diameter outlet, and the more than 60m level difference between the bore holes and the dam crest.

If the hole diameter is smaller than 5m, which is 1/3 of the 15m width of 1 block, stress generated in the dam body concrete during drilling is not so large. But the hole diameter of Tsuruda Dam is 6m. And the height of the dam crest above the holes is more than 60m. In Japan, there has never been a case where holes were drilled with such large diameter so far below the dam crest. So the design work included a detailed analytical study of the tensile stress that will be generated in the concrete during drilling of the dam body. And a preliminary drilling test conducted in advance of the work confirmed that the drilling does not cause cracking. A control value was set for vibration velocity and during execution the vibration velocity was constantly monitored in order to prevent any harmful impacts on the dam body concrete.

3.2. Measures taken at the design stage

3.2.1 3D stress analysis

In order to confirm the tensile stress that will be generated in the concrete during drilling of the dam body, 3D finite element method based stress analysis was performed. The results confirmed that tensile stress produced in the crest of the hole during drilling will be below the concrete tensile strength. And stress analysis was also performed of the tensile stress that will be generated by fluctuation of the reservoir water level when the reservoir is in operation after completion of the redevelopment project. The results confirmed that it will be below the tensile strength of the concrete. These analyses were done using a model that abstracted only one block of the dam body. In fact, tooth-shaped keys were formed at the transverse joints between the blocks of the dam body, and to control the behaviour of both blocks, the actual tensile force produced was reduced to a level lower than the analysis value. It is estimated that the analysis value will be higher than the stress actually produced and on the safe side.

3.2.2 Shapes of the excavation sections

The shapes of the excavation section selected were rectangular. This selection was made because it will lower the maximum value of tensile stress by 25% than in the case of a circular section.

3.2.3 *Preliminary drilling test*

Among dam redevelopment projects already undertaken in Japan, the tensile stress generated during drilling of the dam body of Tsuruda Dam is the largest value. So before starting drilling, a trial drilling was done on the downstream slope of Tsuruda Dam at almost the same location as tensile stress is generated during drilling. The results of the trial drilling confirmed that tensile cracking will not occur, so final full-scale drilling work was started.

3.3. Measures taken during execution (measuring the vibration velocity)

In order to prevent harmful effects on dam body concrete by drilling work, 2 to 5 kine (1kine = 1cm/s) is normally set as the vibration velocity control value, during execution to perform the execution under the control value. For Tsuruda Dam, the control value of the vibration velocity was set at 2 kine. Before and during the work, the vibration velocity was measured at three stages from Phase 1 to Phase 3 shown below.

3.3.1 Phase1 : Measurement on the downstream surface of the dam body

Before drilling No. 3 outlet, which was the first drilled, a vibration velocity gauge was installed on the downstream slope of the dam body and used to measure the vibration velocity. The drill machine is a free cross-section excavator.

3.3.2 Phase 2: Measurement in the inspection gallery

On the left side of Tsuruda Dam, work to relocate 2 penstock is in progress. The No. 1 penstock will cross the inspection gallery inside the dam body. So when the hole for the No. 1 penstock was drilled, a vibration velocity gauge was installed on the side wall of the inspection gallery and used to measure the vibration velocity before pass through. This was done in order to confirm the suitability of concluding drilling at a location where the thickness of the concrete from the upstream surface of the dam body was 80cm.

3.3.3 *Phase3: Measurement on the upstream surface of the dam body*

When the bell mouth that will be installed on the upstream side of the dam body was drilled, a compact vibration velocity gauge was installed on the upstream surface of the dam body to measure the vibration velocity.
The measurements were done at all drilling locations.

3.4. Evaluating vibration velocity

The relationship of the distance from the drilling location and the measured maximum value of vibration velocity is shown in Fig. 8. This figure shows results of all measurements from Phase 1 to Phase 3 at Tsuruda Dam including the results of measurements made earlier at Yoroihata Dam. The measured vibration velocities are smaller than the control value of 2 kine, and it can be concluded that the vibration of dam body drilling by a free section excavator will not impact the existing dam concrete.

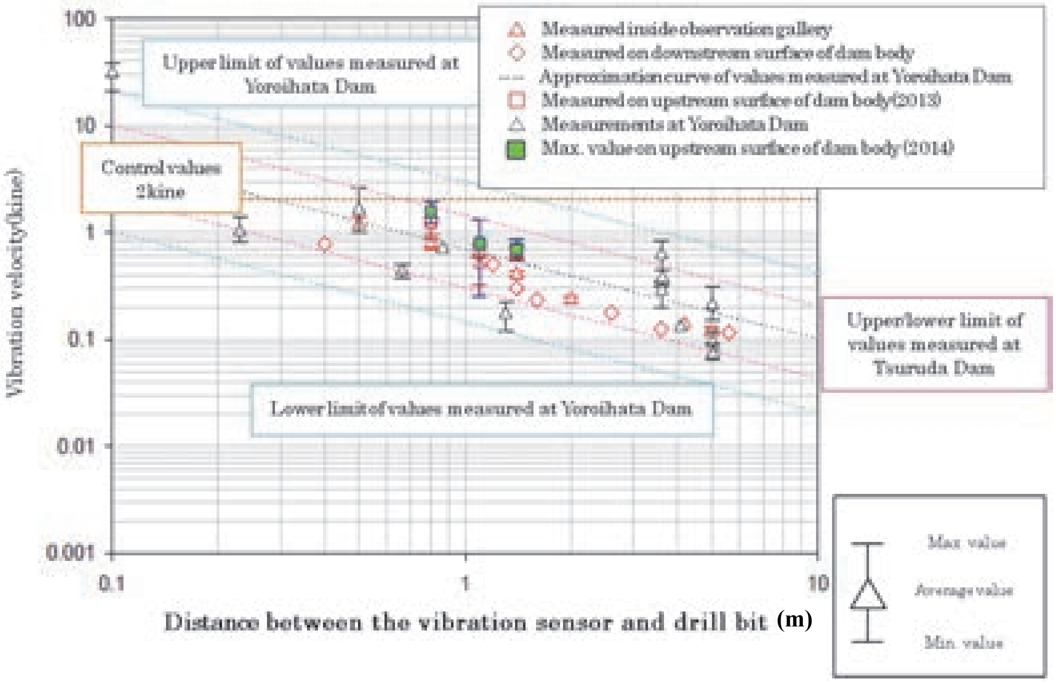

Figure 8. Distance from drilling location and vibration velocity

The following conclusions have been reached based on these results.

・When a free section excavator is used to drill a dam body, it generates low vibration velocity and actually has no harmful impact on the dam body concrete.

・When vibration velocity is measured, the distance between the blades and measuring location at vibration velocity of 0.1 kine or higher is good after it is smaller than 2m.

4. CONCLUSIONS

At Tsuruda Dam redevelopment project, we developed a new type of floating cofferdam. Leakage from the cofferdam after draining was extremely small. The floating cofferdam reduced deep water work. This resulted in safer execution, a shorter work period, and lower cost. When drilling multiple holes in a dam body, it is possible to tow it to the next execution location and easily install without disassembling the shutters. We hope the floating cofferdam will be applied to other dam redeveloping projects in the future.

We used a free section excavator to drill the dam body.

It generated low vibration velocity and actually had no harmful impact on the dam body concrete.

Large-scale dam body drilling of Tsuruda Dam started in 2011, and the three outlets and new energy dissipation works on the downstream side were completed in March 2016.

4th APG Symposium and 9th EADC on

INNOVATIVE TECHNOLOGIES FOR DAMS AND RESERVOIRS TOWARD THE FUTURE GENERATIONS

Main Challenges and Innovations in Design and Construction of Chitgar Artificial Lake in the City of Tehran, Iran

A. Emam
Managing Director of Engineering and Development Organization of the City of Tehran (EDOCT), Tehran Municipality, Iran, Aliemam1234@yahoo.com

M. Zolfagharian
Project Manager of Construction of Persian Gulf Martyrs (Chitgar) Lake, Tehran Municipality – Iran

V. Tabesh
General Director & Project Manager, Armature Pardis Engineering Company, Iran

A.A Efatmanesh
Site Executive Manager, Armature Pardis Engineering Company, Iran

H. Alavi Deilami
Deputy Project Manager, Sadd Tunnel Pars consulting Engineers, Iran

ABSTRACT:
Chitgar dam is a 12m high earthfill dam with the crest length of 730 m and dam body volume of 550,000 m3 which was constructed in 2013. The main aim of construction of this dam was to create an artificial lake in the northwest of the city of Tehran called as “Persian Gulf Martyrs’ (Chitgar) lake”. The lake spread over an area of 132 ha. And its circumference is about 5 km. With the volume of 6.9mcm maximum depth of 9.5 m and average depth of 5.3 m, Chitgar Lake is the largest artificial lake in the Middle East.
Design and construction of such a large reservoir faced with several challenges. The main challenges were: a) constructing a dam and its reservoir at a location which is 7kilometers far from river bed; b) controlling the quality of water in the lake and constructing a water treatment plant and recycling the water; c) water tightening of a large reservoir; and d) impact assessment of dam failure on the residential areas and Hakim Highway at downstream.

Keywords: Chitgar Lake, Quality of water, Tightening, Dam Failure

1. INTRODUCTION

Construction of “Persian Gulf Martyrs’ (Chitgar) lake” in a large city like Tehran with population of about 8 million has brought many environmental, social and economic achievements including the growth of recreational activities, job creation, regional air refreshing, attraction of migrating birds, friendship with nature and development of economic activities in the region.

Design and construction of this lake which lasted 30 months has faced many challenges. Coincidence of design and execution activities and employment of more than 30 engineering experts indicates the special complexity of the project.

The project of Chitgar artificial lake is located at northwest of Tehran and between two main highways. Being adjacent to south hillside of Alborz mountain ranges and Chitgar forest park, the attractiveness and charming scenery of the project has been increased. (See Figs. 1&2)

Figure 1. The pictures indicating the presence of residents and migrating birds

Figure 2. The Lake, Alborz mountain ranges and Chitgar forest park

The three main parts of project are classified as:
1. Kan diversion dam, 2.The water transmission system from Kan River into the lake, 3.Dam and reservoir

In the following figure these three parts are represented.

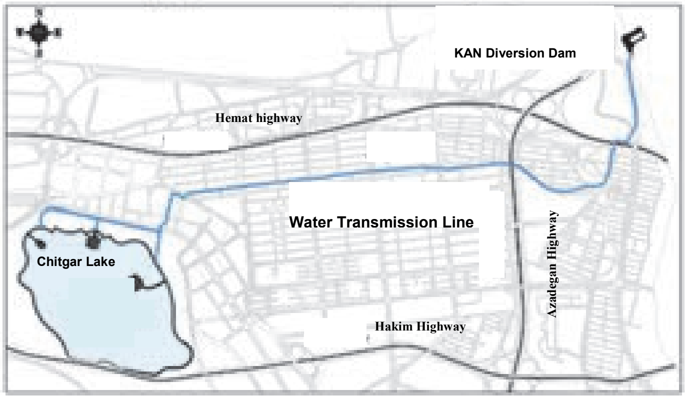

Figure 3. Kan diversion dam, Water transmission system, Reservoir

Kan diversion dam is a concrete structure constructed 7km far from the lake on Kan seasonal river and the goal is to raise the water level of river and divert the water into the lake. (Sadd Tunnel Pars Consulting Engineers, 2011)

The water transmission system from the Kan River into the lake includes a 3.5km concrete canal of 1.5m*1.1m and 3.5km GRP pipes with diameters of 600mm to 1200mm. The maximum flow rate of 1.2m^3/sec is transmitted into the lake from the river.

The reservoir of Chitgar Lake spreading over an area of 132ha and water volume of 6.9mcm is the main part of the project. The base and the surrounding earth dikes are water tightened by using geo-membrane. The lake encompasses three islands with total area of 3ha. Considering the topography of the region, the geometry of the lake and to create the required depth, a main dam with the height of 10.5m, the length of 735m, surrounding earth dikes of 4070m water tightened by geo-membrane and crest elevation of 1268.5m from sea level was constructed.

In this paper four challenges during design and construction of the project are presented.

2. PROBLEMS WITH CONSTRUCTION OF THE LAKE AT A DISTANCE OF 7km FROM KAN RIVER

One of the most especial characteristic of the project is to build the lake out of Kan River bed (the only water supply) in a distance of 7 km. This distance makes building the water transmission system inevitable. To economize the water transmission, the water conveyance was decided to be under gravity condition. Considering the surface and underground obstacles, traffic intersections and highways, drinking water pipes of west of Tehran, a 7 km route accompanied by 5 ponds, two siphons and 38 manholes was designed. The performance of designed rout crossing the abovementioned obstacles was terminated with extreme accuracy considering the point that underground drawings of obstacles were not accessible. One of the most important underground obstacles was existence of 4 concrete water pipes with 40 years old and diameter of 1200 mm. Considering the security issues, the design team of project finally performed an especial practical method to underpass securely the lake's pipe line in siphon way and through casing in a secure distance from the above structures. (See Fig. 4)

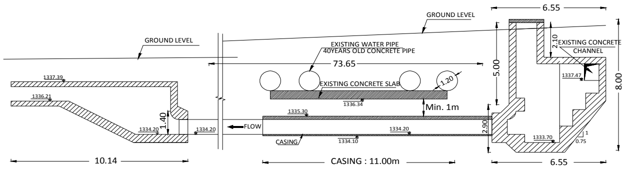

Figure 4. The water transmission line passing under the existing old pipes

Half of the rout of transmission system made of concrete canal and being constructed many years ago was repaired and reused, and the rest half was selected of GRP pipes to speed up the operations. This type of pipe was selected because it was cheaper than Polyethylene and steel pipe, more flexible than cast-iron and more tolerable against corrosion in comparison with steel and cast-iron pipes. The stiffness of pipes used in this project was 10000 pa and were able to tolerate 6 bar pressures.

3. WATER QUALITY CONTROL OF THE LAKE

The laboratory analysis on water of Kan River, as the only source of water supply for the lake, indicates that the phosphorus and nitrate levels are higher than the standard level identified for water of the lake. The reason is recognized as contamination of water in catchment area of Kan River due to rural, agricultural, animal husbandry, pilgrimage and tourism related activities.

Environmental experts reached the conclusion that the stagnation of water in the first 3 to 5 years does not cause eutrophication of the lake and no change in odour and colour of the water will be made. But after this period, the water quality condition may get worse. Therefore a treatment plant with a capacity of 400 litres per second and with a focus on reducing total phosphorus index was designed in north-east of the lake and in direction of transmission line. (Sadd Tunnel Pars Consulting Engineers, 2012). Nowadays, the executive operation of the plant is being done by 50 percent physical progress and will be finished in a year. After the construction and operation of the treatment plant was completed, the water of Kan River will cross the water treatment and its phosphorus and turbidity rate will be reduced before entering into the lake. At the time, when dewatering of the river is not done, by using recycling line and pumping station which is located at the lake spillway, water will be pumped from bottom outlet into refinery and after finishing treatment operation will re-enter into the lake. (See Figs. 5&6)

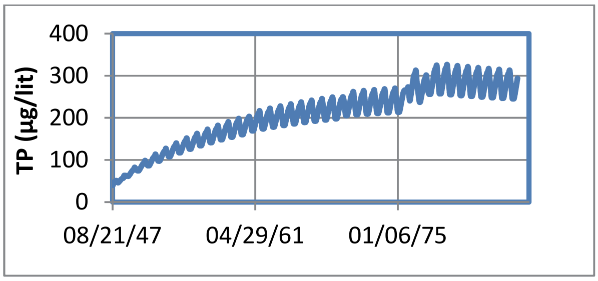

Figure 5. The concentration of phosphorus in the lake without treatment plant

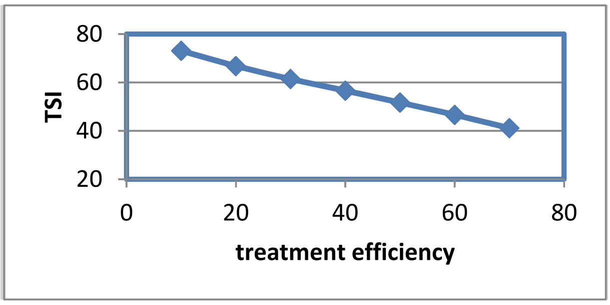

Figure 6.TSI index changes for different treatment efficiency

To increase safety factor in preserving water quality condition of lake, based on a study, it was proposed to release around one hundred thousand of baby fishes of Amoor, Phitophag and Bighead in the lake before construction of refinery. (Toos-Ab Company, 2013)

Grass carp-silver carp, big head carp and common carp (omnivorous), for each 1 kg of their body weight, consume 30 kg plants, 10 kg micro-organisms and 7-8 kg of aquatic organisms respectively and can help in purifying the water of lake.

In order to monitor the water quality changes of both the river and the lake as well as the presence effects of fishes and their growth process, several stations were determined for sampling and conducting relevant experiments which were monitored and analyzed periodically by experts.

The fisheries study suggests that the presence of fishes not only guarantee the desirable quality of water but also in the future, fishing can become a pleasant recreational activity to the visitors of the area.

Table 1. Changes in phosphorus concentrations of water of lake and corresponding TSI index for different refinery efficiency

TSI Index	Phosphorus Concentrations (μg/Lit)	Refinery Efficiency (%)
81	205	0
73	119	10
67	77	20
61	53	30
57	38	40
52	27	50
47	19	60
41	13	70

4. CREATING WATERTIGHT LINING

Considering the water shortage problem in a large city like Tehran and to prevent water waste through leakage, for making a watertight lining, different alternatives were investigated from technical and economical point of view of which clay blanket, injection in an alluvial aquifer, concrete lining, hydraulic asphalt concrete (HAC) and Geo-membrane can be proposed. (Sadd Tunnel Pars Consulting Engineers, 2011). The case of injection in an alluvial aquifer was rejected due to its high cost. The concrete lining case was rejected due to the possibility of leaks that may occur through cracks and also the sealing problems of concrete panels at the place of expansion joints. The clay blanket case was rejected for its high transportation cost, the possibility of muddying the water of lake and the lack of nearby borrow clay sources. Finally between HAC and Geo-membrane, HAC was selected the best alternative on the basis of value engineering.

Forming a special technical group to be responsible for preparing mixing concrete, making concrete test specimens and finding the required borrow sources, the problems such as unavailability of the required permeability rate, the long distance of borrow sources for making asphalt, the lack of appropriate equipment for implementation of asphalt on sloped area and finally the problems due to implementation of asphalt pavement in cold weather were observed.

Considering all abovementioned issues, Geo-membrane liner was selected as the practical alternative by the client.

The geo-membrane used as waterproof liner was supplied from one domestic supplier and three foreign suppliers. The liner's largest advantages was high-speed performance, however the lack of quality control tests can be named as disadvantages. To assure that the domestic test results are accurate and reliable, an international laboratory in Canada was selected to conduct check tests and endorse the outputs. The figure below depicts the section of geo-membrane.

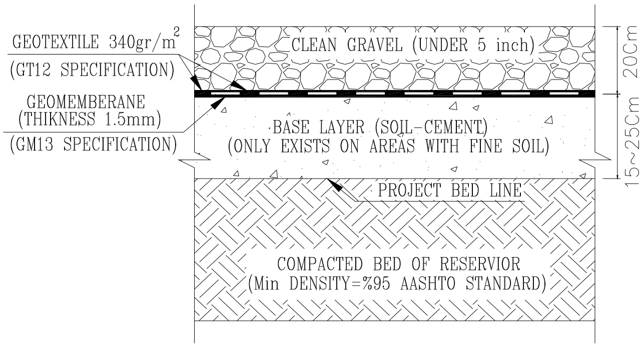

Figure 7. Section of watertight geo-membrane element

The explosive growth of the exchange rate at the time of construction caused the problem of rising prices and financing problems for the project. Despite all these problems, the quality control done by site supervision group on the basis of international standards, GM13 and GT12a, led to on-time and high- quality implementation of waterproof liner. The records from standpipe piezometer indicated that no leakage was taking place and thereby implementation of high quality liner was achievable.

After implementation was complete, there was the probability of Geo-membrane uplift in the wind velocity of 17 km/h. Also because of recreational usage of the lake, damage and perforation was possible in operational period. Therefore, 20 cm round corner rubble was implemented on Geo-membrane. Rubble advantages over other protective coatings such as concrete, was its lower cost and high-speed implementation. In order to prevent damage of Geo-membrane of surrounding earth walls, concrete and Malone cover can be used.

Using an enormous amount of geo-synthetic in construction of the lake, becoming the largest geo-synthetic event without precedent in Iran and the Middle East (133 hectares Geo-membrane and 265 hectares Geo- textile), compliance with international standards and integration of internal and external quality control data proved that the establishment of the lake was an effective step toward improving the quality of our country products, the country's quality management system and an opportunity for training technicians. (See Fig. 8)

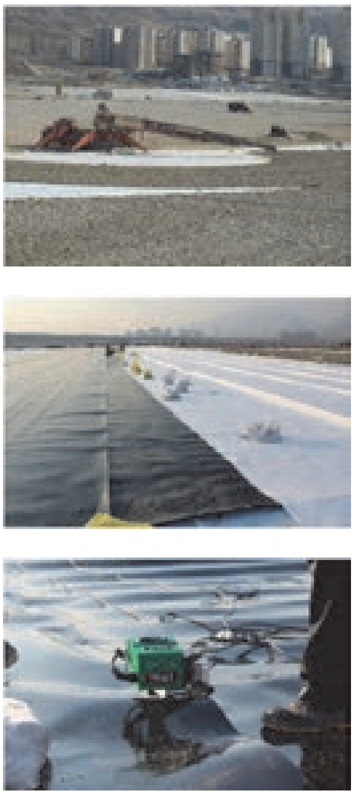

Figure 8. The Steps of implementation of geo-membrane and the surface protective layer

5. DAM-BREAK PROBLEMS

Two scenarios are taken into consideration for Chitgar dam-break and flood simulation. The first scenario is dam-break in a sunny day and is called piping failure. This happens due to scour phenomenon and thereby development of scour cavity in normal water elevation condition. In this case the flood magnitude due to dam-break is equivalent to normal water elevation volume. In the second scenario, the dam-break is commonly due to overtopping. In this case the flood magnitude is higher than the capacity of spillway and the reservoir outlets. In order to compute failure parameters, the dam break height assumed to equal the height of dam, the reservoir water volume in overtopping and piping failure conditions were considered 8.2mcm and 6.9mcm respectively. (Sadd Tunnel Pars Consulting Engineers, 2014)

In the following table the results of simulation studies for two scenarios are presented.

Table2. Results of simulation studies for two scenarios

Scenario	Parameter	Unit	first section after Chitgar dam (100m d/S of dam)	Section 11424/11 (700m d/S of dam)	Section at the border of hill and plain area (2300m d/S of dam)
Piping Failure	The entrance time of the first flood wave to d/s	Min	22	32	51
	Max flow rate	m3/Sec	1190.78	1187.53	1165.34
	Time of max flow rate	Min	84	85	93
	The exit time of the last flood wave	Min	316	318	326
Overtopping Failure	The entrance time of the first flood wave to d/s	Min	13	21	39
	Max flow rate	m3/Sec	1613.84	1607.50	1593.35
	Time of max flow rate	Min	86	89	93
	The exit time of the last flood wave	Min	277	289	294

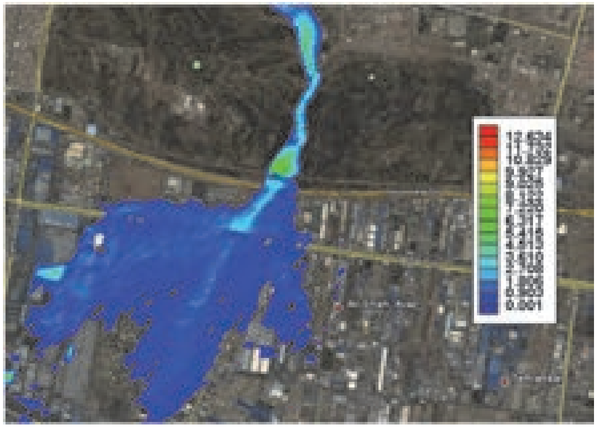

Figure 9. The water level changes plan after 150 minutes of start of overtopping

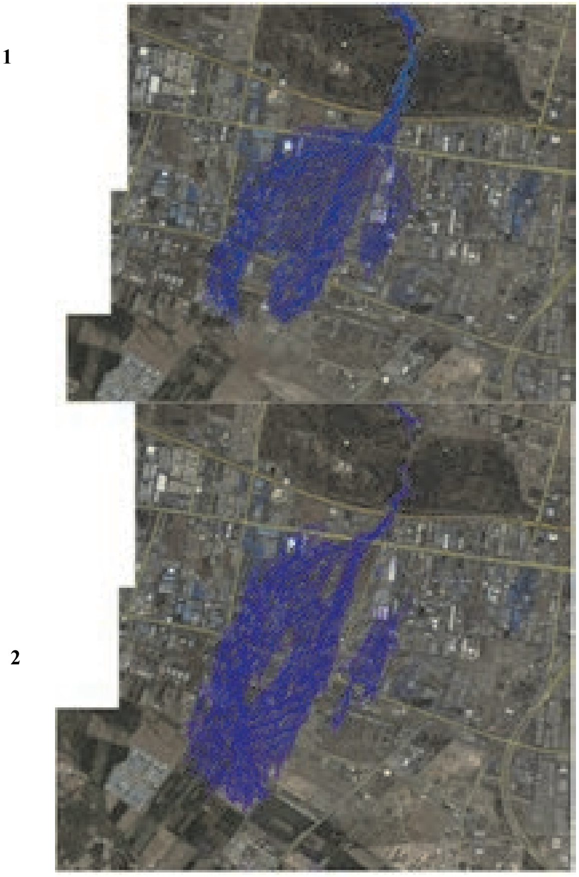

Figure 10. Inundation area of d/s face due to overtopping
1. After 220 minutes of start of dam-break
2. After 350 minutes of start of dam-break

Considering the results of simulation studies, the following procedures are represented for reducing failure risk of Chitgar dam:

. Providing monitoring system to measure leakage and dam body’s displacements in different directions
. Establishment of a program of surveillance from downstream, bottom outlet and spillway of dam and control of the possible damages
. Establishment of flood control system in upstream of the lake and its diversion to out of the area
. Identification of the muster points in downstream of dam and transferring the residents to these points at the time of dam break
. Implementation of flood warning system for downstream of dam

Among the abovementioned procedures, because prevention of entrance of upstream flows into the reservoir could prevent overtopping and dam failure, establishment of flood Control system in upstream of the lake and its diversion to out of the area can be proposed as a solution to design optimization of dam and reservoir and thereby reducing the risk of dam failure. To prevent dam failure due to piping event, 17 Drainage wells is embedded at the heel of downstream face, at the time of leakage from upstream to dam body, to collect and divert the additional flows toward a protected outlet. (Sadd Tunnel Pars Consulting Engineers, 2013)

ACKNOWLEDGEMENTS

As a member of Engineering and Development Organization of the City of Tehran (EDOCT) who participated in lake construction process as executor, we need to appreciate honourable Technical & civil Affairs deputy of Tehran municipality as the client of the project which provided us with sufficient data required for preparation of the paper.

REFERENCES

Sadd Tunnel Pars Consulting Engineers (2013): The detail study of Chitgar artificial lake, Report on maintenance and operation instructions, No.: CAL-STP-R-GEN-IN-DD-001
Sadd Tunnel Pars Consulting Engineers (2012): The detail study of Chitgar artificial lake, Studies on water quality of lake, No.: CAL-STP-R-GEN-EN-DD-001A
Toos-Ab Company (2013): Studies on promoting the quality of entrance water into the artificial lake
Sadd Tunnel Pars Consulting Engineers (2014): The feasibility study of Chitgar artificial lake, Report on dam-break studies, No.: CAL-STP-R-DAM-HY-BD-005A
Sadd Tunnel Pars Consulting Engineers (2011): The feasibility study of Chitgar artificial lake, Report on water resource studies, No.: CAL-STP-R-GEN-HY-BD-001A
Sadd Tunnel Pars Consulting Engineers (2011): The feasibility study of Chitgar artificial lake, Report on reservoir water tightening design, No.: CAL-STP-R-RES-ST-BD-001

Construction of Apporo Trapezoidal CSG Dam

S. Yoshimura & S. Takasugi
Apporo Dam Construction Office, Hokkaido Prefectural Government, Japan
okabe.yasunori@pref.hokkaido.lg.jp

M. Konno
Erosion Control Division, Bureau of Public Works, Hokkaido Prefectural Government, Japan

T. Fujisawa, H. Yoshida & N. Yasuda
Japan Dam Engineering Center, Tokyo, Japan

ABSTRACT:

The Apporo Dam is the second trapezoidal CSG dam in Hokkaido, following the Tobetsu Dam. At the Apporo Dam, the shale is used as the CSG material, which is the dam body material, and the dam is constructed on the foundation of the shale and shale-sandstone alternative layer. Shale has the characteristic which causes the slaking phenomenon when it is dried, so various technical studies were conducted to prepare for its use. For the concrete gravity dam, shale or mudstone cannot be used as the aggregates, so the aggregate for the Apporo Dam with original concrete gravity type was planned to purchase from quarry place.

Furthermore, the foundation surface of the dam is extremely uneven and bumpy, so the investigation was carried out to select the execution machinery. According to the extent and depth of undulation, the proper spreading and compaction machinery are used in the Apporo Dam. As existing Tobetsu Dam and Kim Dam with trapezoidal CSG type had an even foundation surface, large-size construction machine was chosen. So, this kind of investigation has an important role for the construction of the new Trapezoidal CSG dams.

Keywords: Apporo Dam, trapezoidal CSG dam, shale, slaking.

1. INTRODUCTION

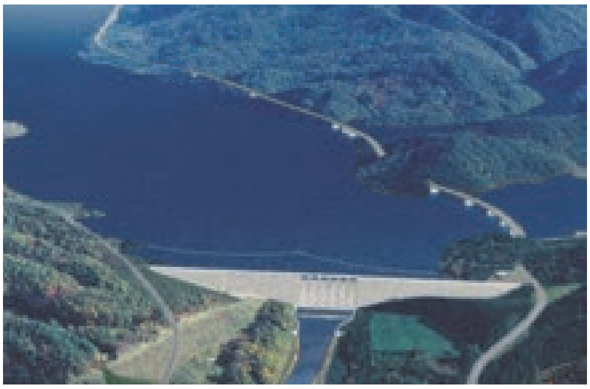

Figure 1. Drawing of completed Apporo Dam

The Apporo Dam is a multi-purpose dam under construction in Hokkaido as a trapezoidal CSG (Cemented Sand and Gravel) dam as shown in Table 1 and Fig. 1. Apporo Dam was initially planned as a concrete gravity dam, but when surveys and studies to adopt the new technology, the trapezoidal CSG dam, were undertaken, this new method was adopted in light of its economic and environmental superiority.

Placing the dam body material started on April 30, 2015, and about 50% of the dam volume has been completed on November 15, 2015.

Apporo Dam is not only constructed using shale, which shows slaking properties, as the CSG material for the dam body, but also constructed on foundation rock of shale. This paper reports on the investigation results concerning foundation rock and dam body material, which are prone to slaking. The standard cross section of the dam is illustrated in Fig. 2.

2. MAIN FEATURES OF A TRAPEZOIDAL CSG DAM

The type of trapezoidal CSG dam is developed in Japan to contribute to improving economic efficiency and reducing the environment impact (JDEC, 2012).

The trapezoidal CSG dam is shaped like a trapezoid, lowering stress produced inside the dam body. Highly durable concrete is placed on the surfaces of the dam body. The required performance of CSG is that its strength should be greater than produced stress inside the dam body with an appropriate design allowance.

Thus, CSG material has a wide range of applicable qualities, enabling the use of low quality material. On the other hand, the method of quality control to ensure the required strength is very important.
Furthermore, at a trapezoidal CSG dam, the adhesion of the foundation rock with the dam body plays an in important role in ensuring the sliding stability, requiring careful treatment of the rock contact surface and attentive CSG execution.

Table 1. Main feature of Apporo Dam

Type	Trapezoidal CSG
Height	47.2 m
Crest length	516 m
Volume	481,100 m^3
Catchment area	105.3 km^2
Ponding area	3.03 km^2
Total reservoir capacity	47,400,000 m^3
Effective reservoir capacity	43,100,000 m^3

3. THE FOUNDATION ROCK AND DAM BODY MATERIAL AT APPORO DAM

The foundation rock at Apporo Dam, is Neogene – Miocene sedimentary rock, with alternating layers of shale and sandstone but mainly shale. This rock is prone to the slaking phenomenon caused by repeated wetting and drying action (Figs. 1 and 2).

Table 2. Basic physical properties of CSG material

Physical properties	value
Surface dry density	2.2 – 2.3 g/cm3
Water absorption coeff.	10 -15 %

The dam body material is easily obtained near the dam site and sedimentary soft rock similar to the foundation rock distributed inside the reservoir (Figs. 3 and 4).

The properties of this material are shown in Table 2 and this kind of low quality material could not be used asaggregate for concrete.

4. TECHNICAL SOLUTIONS AT THE APPORO DAM

The following are the technical solutions faced regarding the foundation rock and CSG material of the Apporo Dam.

4.1 Technical solutions related to the foundation rock

In the foundation rock of the Apporo Dam, the rock contact surface after excavation was uneven (level differences from 30 to 80cm) as a result of cracks along bedding planes and cracks caused by weathering near the surface (Fig. 5).

It was, therefore, necessary to improve the reduced workability of the CSG caused by the unevenness on the rock contact surface. Additionally, the countermeasure against the slaking was also required.

The foundation rock of Apporo Dam could not be dried to prevent the slaking, so investigations were required to adopt shotcrete and to establish a rational execution method which can enable the certain contact between rock and dam body. These investigations were intended to ensure the required performance (slide resistance) of the rock contact part.

4.2 Technical solutions regarding the dam body material

CSG has features which allow change of the grain size distribution of the material. On the other hand, in order to ensure the stipulated CSG strength, it is important to clarify the variation of the grain size distribution of the CSG material.

The refining of the gradation of the CSG material by slaking impacts the variation of its gradation distribution. Therefore, quality control must consider the scale and configuration of the stockpile of CSG material, the stocking period, and other aspects of the execution process.

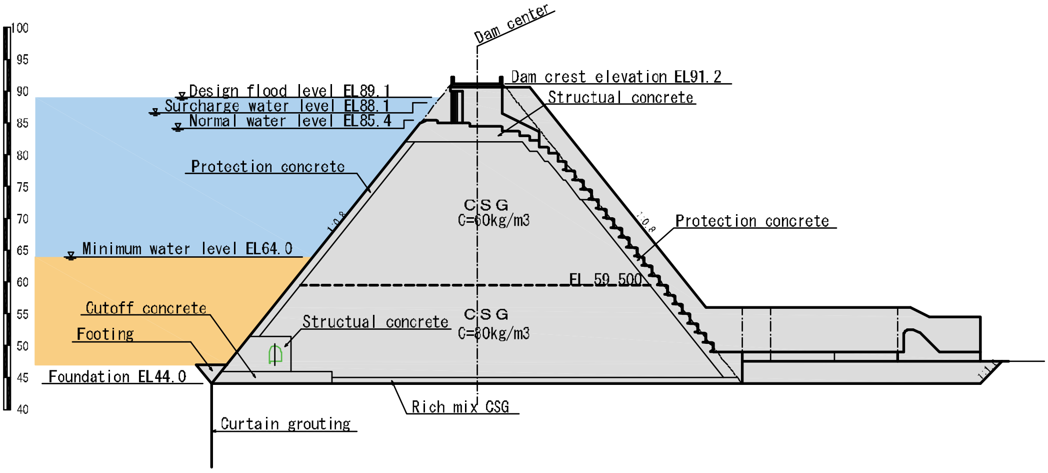
Dam center
Dam crest elevation EL91.2
Structual concrete
Design flood level EL89.1
Surcharge water level EL88.1
Normal water level EL85.4
Protection concrete
CSG
C=60kg/m3
1:0.8
1:0.8
Protection concrete
Minimum water level EL64.0
EL 59.500
Cutoff concrete
Footing
Structual concrete
CSG
C=80kg/m3
Foundation EL44.0
Rich mix CSG
Curtain grouting
100
95
90
85
80
75
70
65
60
55
50
45
40

Figure 2. Standard cross section of Apporo Dam

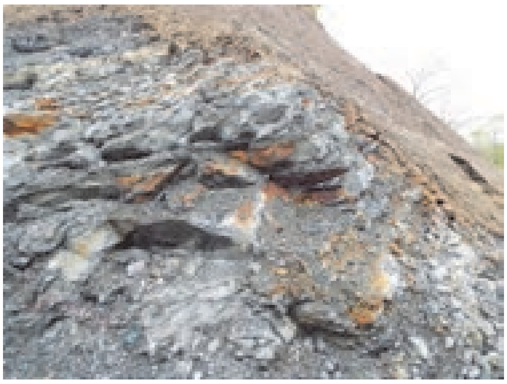

Figure 3. Foundation rock (fresh)

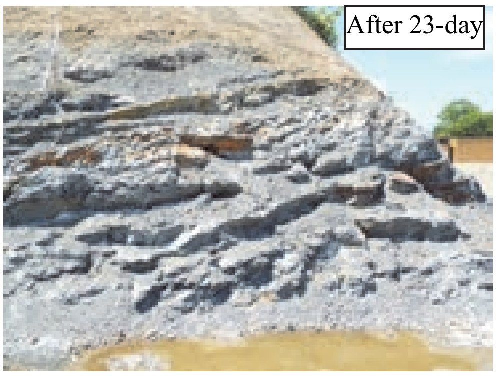

Figure 4. Slaking property of foundation rock after 23-day exposure

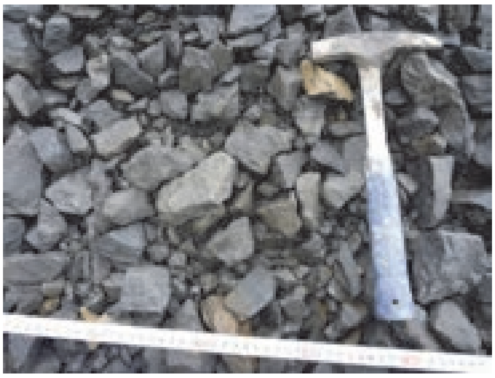

Figure 5. CSG raw materials (fresh)

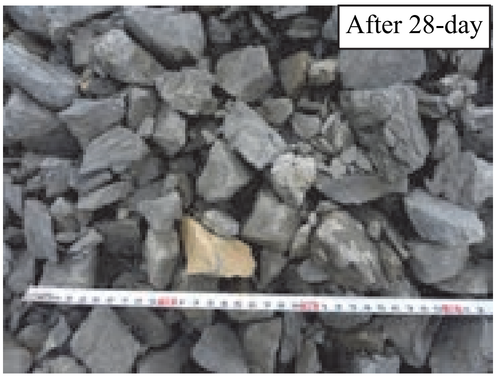

Figure 6. Slaking of CSG raw materials after 28-day exposure

The slaking increases the finer gradation fraction (0.075mm or smaller) of the CSG material, and this finer gradation material is caused to adhere to relatively large grain size material by rain water (Figs. 8 and 9). This prevents the uniformity of the mixed material with cement, causing anxiety about ensuring the required strength and scattering of its quality.

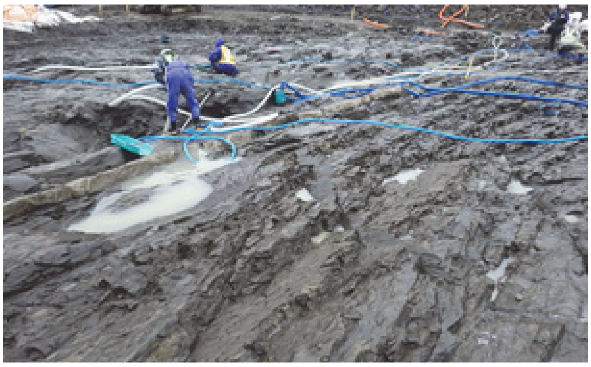

Figure 7. Unevenness of foundation rock

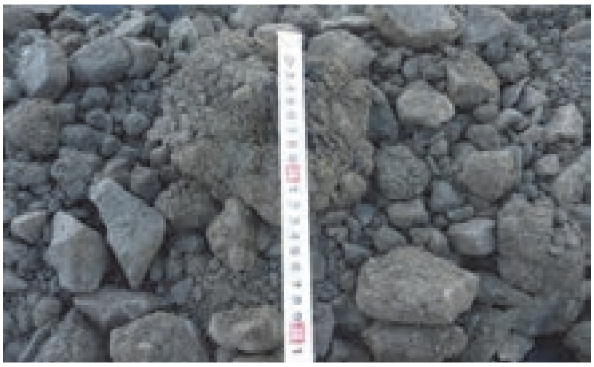

Figure 8. CSG materials just after crushing

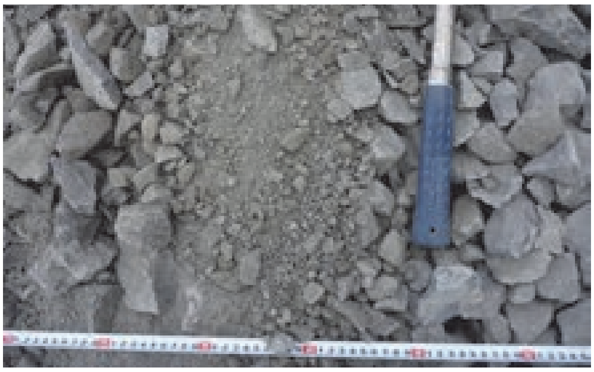

Figure 9. Aggregated CSG materials

5. TECHINCAL SOLUTIONS

There were several technical solutions on the slaking rock for the foundation and the dam body materials.

5.1 Confirming slaking of the foundation rock

In-situ testing under the following conditions was executed in order to clarify the progress rate of slaking of the foundation rock and to investigate a curing method between finishing excavation of the foundation rock and placing work of CSG (See Table 3).

When the foundation rock of Apporo Dam was left standing in natural condition, honeycomb cracking occurred in about 1 hour (Fig. 10). On the other hand, if it was maintained in wet condition, the slaking of the foundation rock did not occur.

Table 3. Investigation cases

Foundation rock (4 types)	Shale (Hard and weak), Alternation of Shale and Sand stone (Hard and weak)
Test conditions (3 cases)	Natural state, Wet state (water sprayed), Wet state (curing mat)

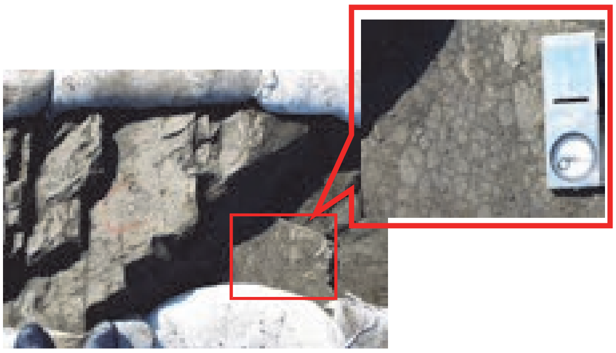

Figure 10. State of foundation rock (after 1-hour exposure)

5.2 Confirming the rock contact part execution method

To execute the rock contact part, the application of shotcrete in order to deal with the unevenness of the rock surface and the slaking by filling the concave parts with CSG reliably and improving the workability (convenience and execution speed while ensuring quality) was studied.

The existing trapezoidal CSG dams were executed by carefully performing manual work and using compact machines in order to fill concave parts with CSG reliably as shown in Fig. 11.

Though treating the unevenness of the rock surface by the same execution procedure would be extremely inefficient at Apporo Dam. Because of anxiety about the filling of concave parts with CSG, the improvement of efficiency by placing the CSG using a bulldozer and a large compactor were investigated with the spread mortar on the rock contact surface as a supplementary measure as shown in Figs. 12 and 13 (Study Committee, 2014).

Regarding the execution properties, the cement ratio of the mortar was varied to confirm the adhesion properties and mortar thickness on the foundation rock. The basic mortar mix was set considering specifications of the construction machinery, and the required performance of the rock contact part as the foundation of Trapezoidal CSG dam.

Furthermore, the test surface of rock contact part was excavated and visually observed, clarifying that the CSG reliably filled the concave parts of the rock contact part as shown in Fig.14.
The above also confirmed the suitability of shotcrete execution as shown in Fig.16.

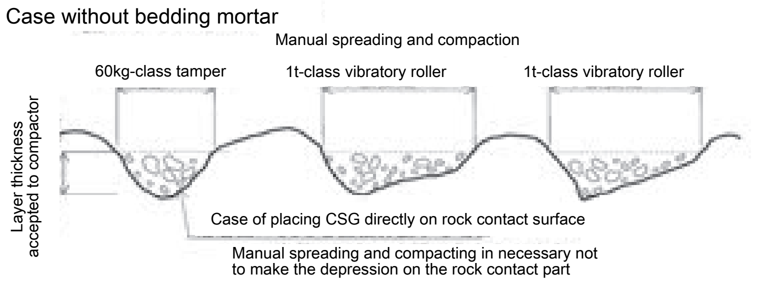
Case without bedding mortar
Manual spreading and compaction
60kg-class tamper
1t-class vibratory roller
1t-class vibratory roller
Layer thickness accepted to compactor
Case of placing CSG directly on rock contact surface
Manual spreading and compacting in necessary not to make the depression on the rock contact part

Figure 11. Conventional execution method of rock contact part

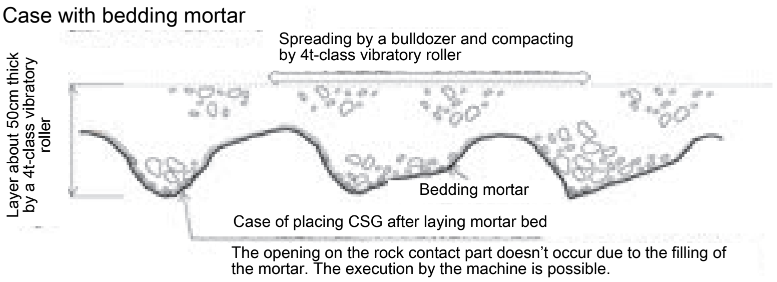
Case with bedding mortar
Spreading by a bulldozer and compacting by 4t-class vibratory roller
Layer about 50cm thick by a 4t-class vibratory roller
Bedding mortar
Case of placing CSG after laying mortar bed
The opening on the rock contact part doesn't occur due to the filling of the mortar. The execution by the machine is possible.

Figure 12. Improved execution method of rock contact part

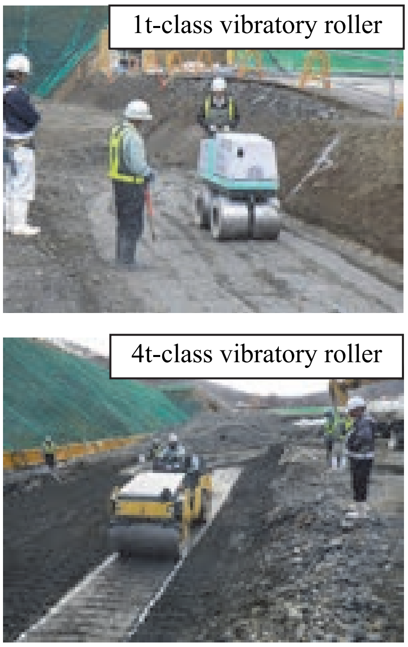
1t-class vibratory roller
4t-class vibratory roller

Figure 13. Execution of rock contact part

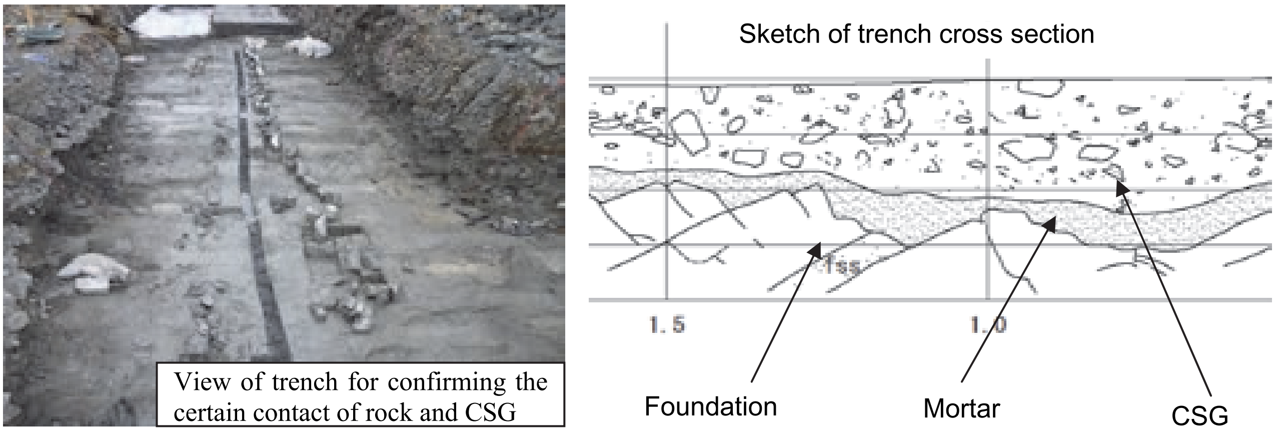
View of trench for confirming the certain contact of rock and CSG
Sketch of trench cross section
1.5
1.0
Foundation
Mortar
CSG

Figure 14. Filling of CSG to concave parts of foundation rock

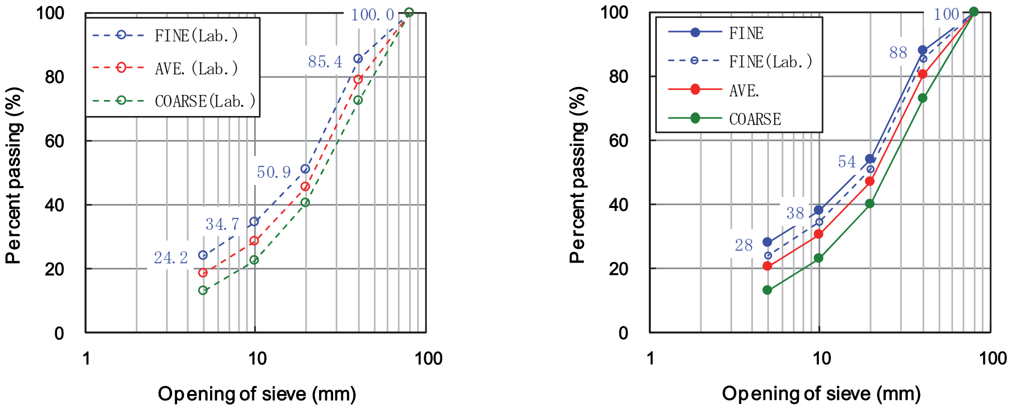

Figure 15. Quality control of grain size distribution range

Figure 16. Shotcrete with mortar

5.3 Impacts of slaking on dam body materials

To clarify affected depth of slaking during stocking of CSG material, a stockpile was built and used for an exposure test. The test results clarified that the refining of the CSG material by slaking occurs for about 100mm deep from the pile surface which is exposed to the effects of the outside air, but does not occur any deeper than that.

The percentage of CSG material in which occurs slaking will be only about 1% of all the stock volume. The results also show that the influence on change of the grain size distribution will be extremely small. But, in order to perform certain quality control, the range of the grain size distribution of the CSG material was widened to include finer grain particles as shown in Fig. 15.

It also confirmed the influence of the increase of the finer gradation fraction by slaking on scattering of the required CSG strength and CSG quality. Newly prepared material and material aggregated by adherence of finer gradation fraction on the surface of material were used to perform strength tests of CSG with the standard specimens. The grain size distributions of both materials tested were adjusted to have the same gradation.

As shown in Fig. 17, it has been clarified that equal strength has been obtained, and non-uniformity caused by aggregation during mixing will have no influence, and that the normal production method can be applied.

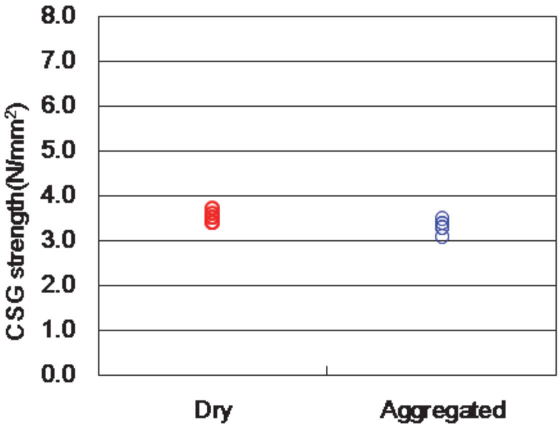

Figure 17. Comparison of CSG strengths with laboratory specimens

6. SUMMARY

Slaking of the foundation rock at the Apporo Dam can clearly be resolved by wet curing and spraying mortar.
In addition, the decline of workability on uneven parts was avoided by spraying mortar and using large construction machines.

And for the actual execution, based on the results of the above studies, an execution method and various machines suited for the degree of unevenness (level differences) have been adopted.

It was confirmed that the slaking of the dam body material will have extremely small influence both on the grain size distribution by refinement of the CSG material and on the aggregation by an increase of the finer gradation fraction. The results of these studies have been reflected in the CSG quality control methods.

7. CONCLUSIONS

The Apporo Dam was initially planned as a concrete gravity dam, but in 2003, surveys and studies to adopt the trapezoid CSG dam were started, and in light of its economic and environmental superiority, a decision was made to construct it as the second trapezoidal CSG dam in Hokkaido, following the Tobetsu Dam.

The type of trapezoidal CSG dam was developed to rationalize “design”, “execution”, and “materials” simultaneously, and technical development of this type of dam is continuing in an effort to achieve further rationalization.

The results from the Apporo Dam reported in this paper are results of efforts to overcome unprecedented problems, but the rationalized rock contact part execution method can be applied to other dams with similar unevenness of foundation rock. Consequently, using material susceptible to slaking as CSG material must have broadened the diversity of CSG materials.

The construction work of dam body started in October 2014, CSG placing started on April 30, 2015. 247,000m^3 of the total volume of 481,100m^3 including the CSG and ordinary concrete has been placed as of November 10, 2015.

REFERENCES

Japan Dam Engineering Center (JDEC) (2012), Engineering Manual for Design, Construction Quality Control of Trapezoidal CSG Dam, Japan Dam Engineering Center, June (in Japanese).

Study Committee on the Design and Construction of Trapezoidal CSG Dam (2014), CSG Notes, No. 4, Design and construction of Rock Contact Parts, Engineering for Dams, No. 330, pp.3-16, March (in Japanese).

Construction of a Coastal Levee at Hamamatsu City Coastline using Trapezoidal CSG Dam Technology

N. Itoh, T. Suzuki & S. Terada
Coastal construction Service Group, Hamamatsu Public Works Office, Shizuoka Prefecture, Japan
hamado-engan@pref.shizuoka.lg.jp

T. Fujisawa, Y. Kinouchi & N. Yasuda
Japan Dam Engineering Center, Tokyo, Japan

ABSTRACT:
In order to mitigate giant tsunami damage predicted to occur on the Hamamatsu City Coastline, a coastal levee higher than Level-1 Tsunami is being constructed about17.5 km from Lake Hamana to the mouth of the Tenryu River. Here, Level-1 Tsunami is a tidal wave which occurs as the result of an earthquake of magnitude (M) 8 with the return period of roughly 100 year-150 year cycle along Suruga-trough and Nankai-trough.

The planned coastal levee is located on a long sandy beach with a seaside protection forest parallel to it on the north side. Considering the conservation of valuable plants and animals, the seriously eroded shoreline, and the scenic appearance of the site, basically the ground level of the seaside protection forest is raised and CSG (Cemented Sand and Gravel) is placed at the center of the levee section and the outer sections are constructed as earth dikes. The planned coastal levee is required to have tenacity enabling it to withstand overflow of Tsunami but, strength equal to that of a concrete structure is not needed, so a CSG structure, which has been developed by dam engineering, is adopted for the internal portion of the levee.

Keywords: CSG, Coastal Levee, Hamamatsu City Coastline

1. INTRODUCTION

Terrace deposits and mudstone quarried at Mt. Akura in Hamamatsu City shown in Fig. 1 are used for the CSG material, but to achieve effective usage of material in the field, it is mixed with locally produced sand material from excavation work executed to construct the coastal levee.

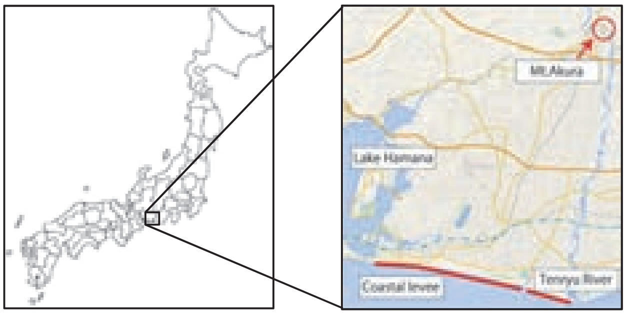

Figure 1. Locations of the coastal levee and Mt. Akura

To surely design and construct the CSG structure on sandy ground, the results of plate loading tests, standard penetration tests, and Swedish sounding tests performed before construction have been summarized and analyzed to develop a method of evaluating bearing capacity and the foundation elevation of the CSG structure, which can be performed simply at the site.

2. STRUCTURE OF THE COASTAL LEVEE

The following are the basic conditions required for the construction of the Hamamatsu Coastal Levee. First, the crest height of the coastal levee is basically T.P. +13.0m (Tokyo Bay mean sea level; Tokyo Peil, T.P.), which was determined from the height of Level-2 Tsunami as reference. The crest height is lower than that of Level-2 Tsunami. However, the levee body has been composed of CSG which is a tenacious structure to resist breaching against the overflow of sea water. CSG is made from cement, water, rocky materials, and has been developed as the new design and construction methods at dam engineering. CSG has the characteristics of the rapid construction period and the usage of materials obtained from the vicinity of the field with less restriction (Yoshizawa, et al. 2016).

Here, Level-2 Tsunami is a tidal wave which occurs as the result of a disastrous earthquake of Magnitude (M) 9

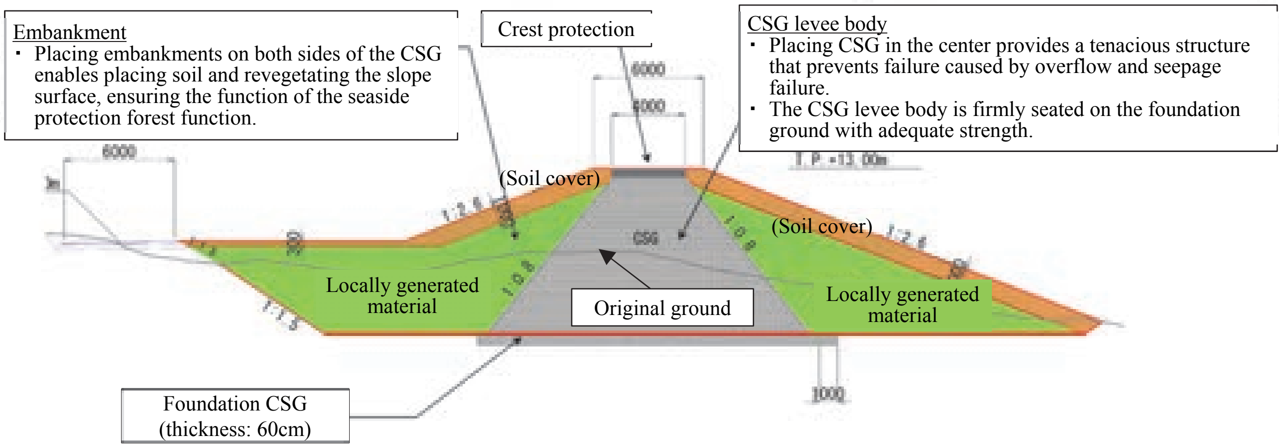
Embankment
・Placing embankments on both sides of the CSG enables placing soil and revegetating the slope surface, ensuring the function of the seaside protection forest function.
Crest protection
CSG levee body
・Placing CSG in the center provides a tenacious structure that prevents failure caused by overflow and seepage failure.
・The CSG levee body is firmly seated on the foundation ground with adequate strength.
6000
4000
6000
T.P.+13.00m
(Soil cover)
(Soil cover)
CSG
1:2.5
1:0.8
1:0.8
1:2.5
1:3
1:1.5
Locally generated material
Original ground
Locally generated material
Foundation CSG (thickness: 60cm)
1000

Figure 2. Typical cross section of the coastal levee

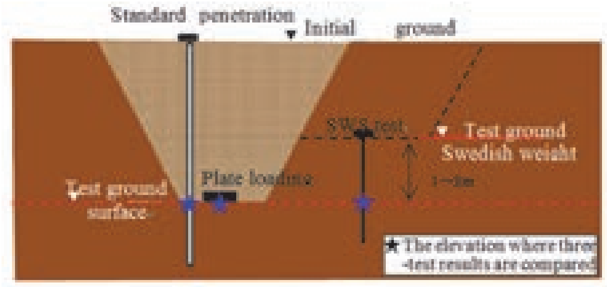
Standard penetration
Initial ground
SWS test
Test ground Swedish weight
Test ground surface
Plate loading
1~2m
★The elevation where three test results are compared

Figure 3. SPT test, Plate loading test and SWS test

Figure 4. View of SWS test

with a return period of several thousand years, and which can cause enormous damage when it occurs.

Secondly, the location of the coastal levee is a seaside forest reserve, which prevents the intrusion of blowing sand from the shoreline. Therefore, even after the levee is completed, it is necessary to restore the forest reserve to maintain its original protection function.

As the basic structure of the coastal levee, CSG with trapezoidal shape and wide levee base is located in the center, constructing embankments at each end to satisfy the above two conditions (see Fig.2). Finally, the coastal levee has the following special characteristics.

a) Forming a trapezoidal shape of CSG in the center lowers vertical reaction force of the structure base and reduces fluctuation of the basal reaction force by changeable load caused by earthquakes etc. Additionally, a highly rigid structure can be constructed on sandy ground. Furthermore, the trapezoidal shape basically helps it resist overturning.

b) CSG is, as a mixture of rocky material with cement and water, material with higher strength than foundation grounds and embankments made of earth materials, so a levee body composed of this material can resist the failure by seepage or overflow.

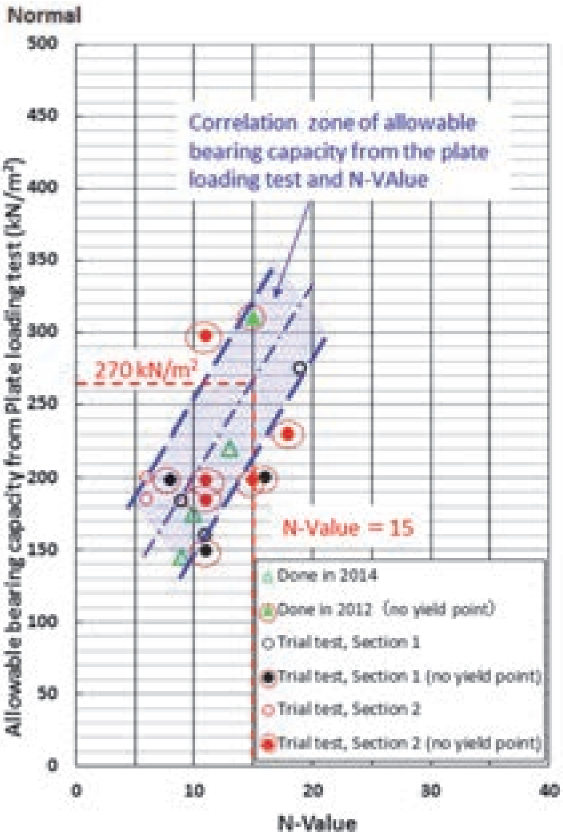

Figure 5. Relationship of N-value and bearing capacity from plate loading test

c) As a result of the above factors, the levee structure with extremely large yield strength against Level-2 Earthquake and Tsunami, which will come from Nankai megathrust earthquakes, can be constructed.

d) Once liquefaction or other deformation of the foundation ground is caused by an earthquake, the CSG dam body will also naturally be deformed. But the levee body is composed of CSG and embankment, so it will be not destroyed partially or completely by the succeeding tsunami. Therefore its reconstruction after the disaster will be performed relatively easy.

e) Embanking on both sides of the CSG part will enable the soil-covering and revegetating the surface of levee, enabling the maintenance of the original function of the seaside forest reserve.

3. BEARING CAPACITY OF FOUNDATION

3.1. Preliminary Survey

In order to directly confirm the bearing capacity of the ground, a plate loading test was carried out during a preliminary inspection and trial execution. A boring survey and Swedish weight sounding test were performed at the same time as the plate loading test, comparing the bearing capacity obtained from the plate loading test with the N-value.

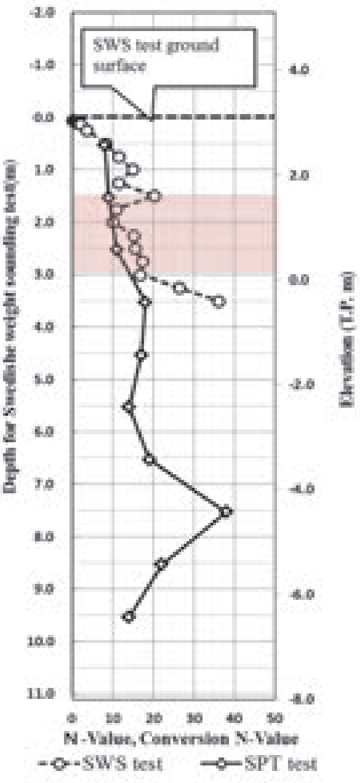

Figure 6. Relationship of SWS test results and N-values of standard penetration test

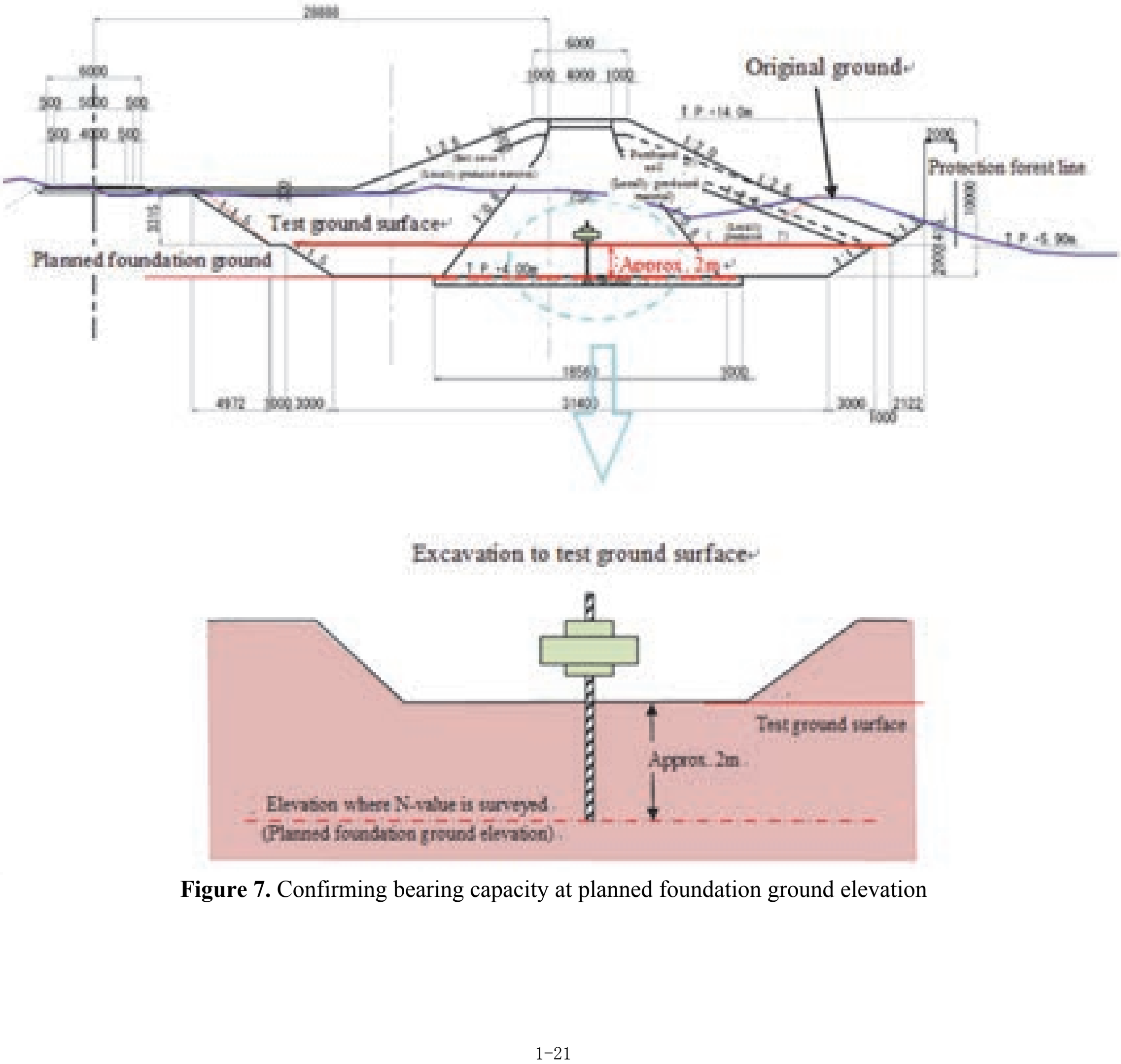
28000
6000
1000
4000
1000
6000
500
5000
500
500
4000
500
Original ground
T.P.+14.0m
Protection forest line
2000
10000
T.P.-5.90m
Test ground surface
Planned foundation ground
T.P.+4.00m
Approx. 2m
2315
2000
18560
2000
4972
1000
3000
21400
3000
2122
1000
Excavation to test ground surface
Test ground surface
Approx. 2m
Elevation where N-value is surveyed
(Planned foundation ground elevation)

Figure 7. Confirming bearing capacity at planned foundation ground elevation

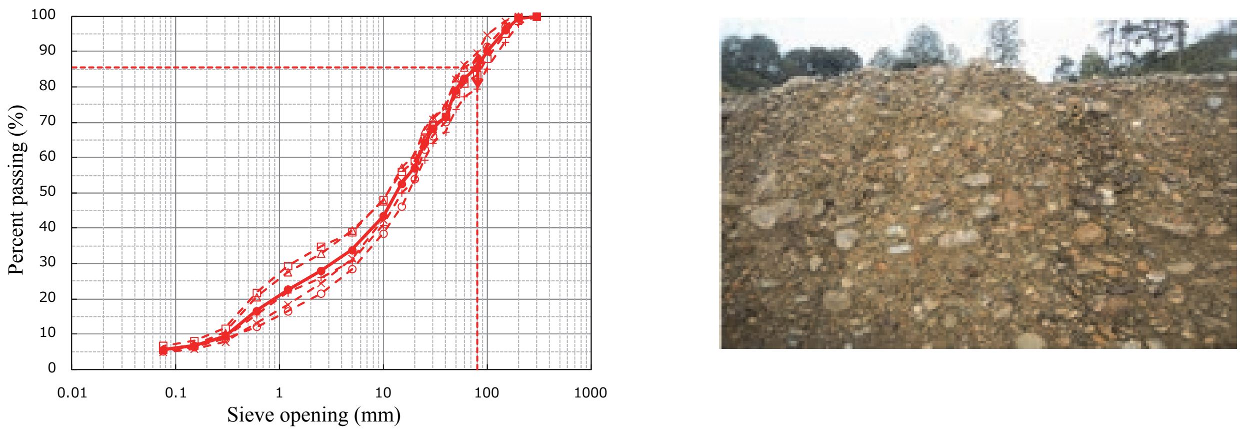

[1] Terrace deposits

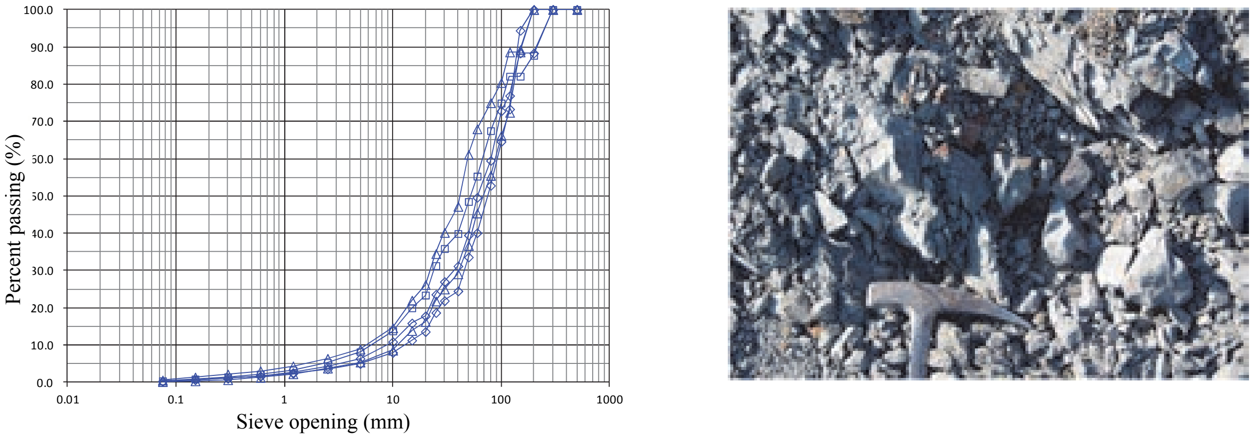

[2] Mudstone

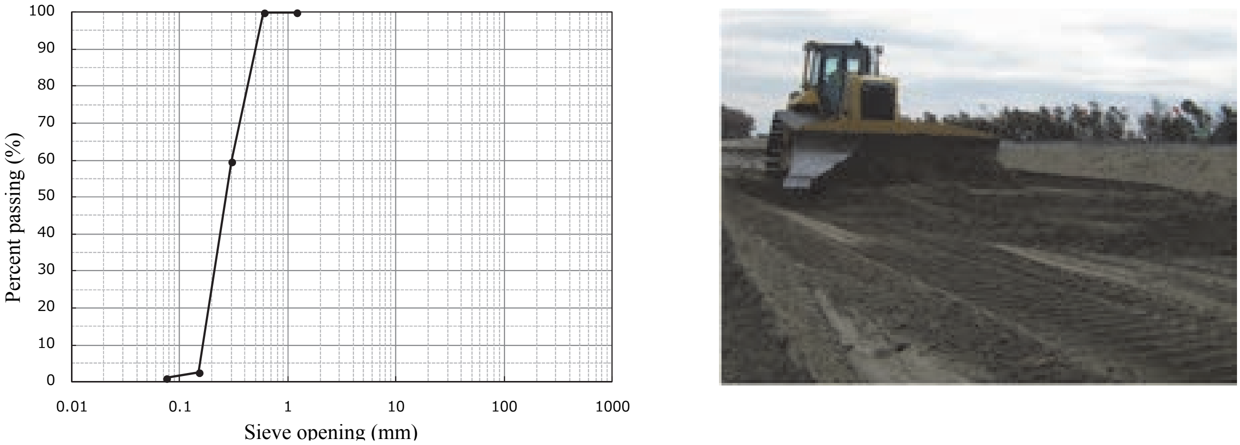

[3] Beach sand

Figure 8. CSG materials

Figs. 3 and 4 show the positional relationship of the tests and the test procedure is shown below.

1) A standard penetration test (SPT) is done on the initial ground surface (ground surface of the original topography) at the same time as the boring survey, to measure the N-value at each depth.

2) The original ground is excavated to perform the plate loading test. The plate loading test is carried out on each ground surface which is lowed every 1 m by stage in order to compare the result with the N-value measured by SPT.

3) The Swedish weight sounding test (SWS test) is done near the same location as the boring and plate loading

test. This test is also done in a same manner as the plate loading test.

Regarding the bearing capacity of the foundation ground, the relationship of the allowable bearing capacity obtained by the plate loading test performed in-situ with the N-value at the adjacent boring was arranged as shown in Fig. 5.

The allowable bearing capacity at N-value of 15, is 273 kN/m^2 as the median value in the correlation zone, so here, the allowable bearing capacity at N-value of 15 is set at 270kN/m^2 (normal condition) and 405 kN/m^2 (seismic condition). 405 kN/m^2 at seismic condition is 1.5 times as much as 270 kN/m^2 at normal condition.

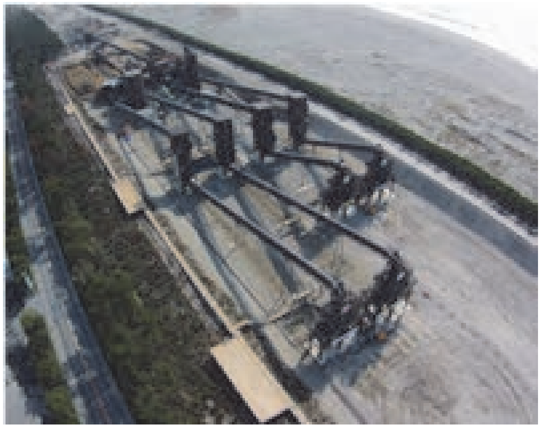

Figure 9. CSG mixing plant

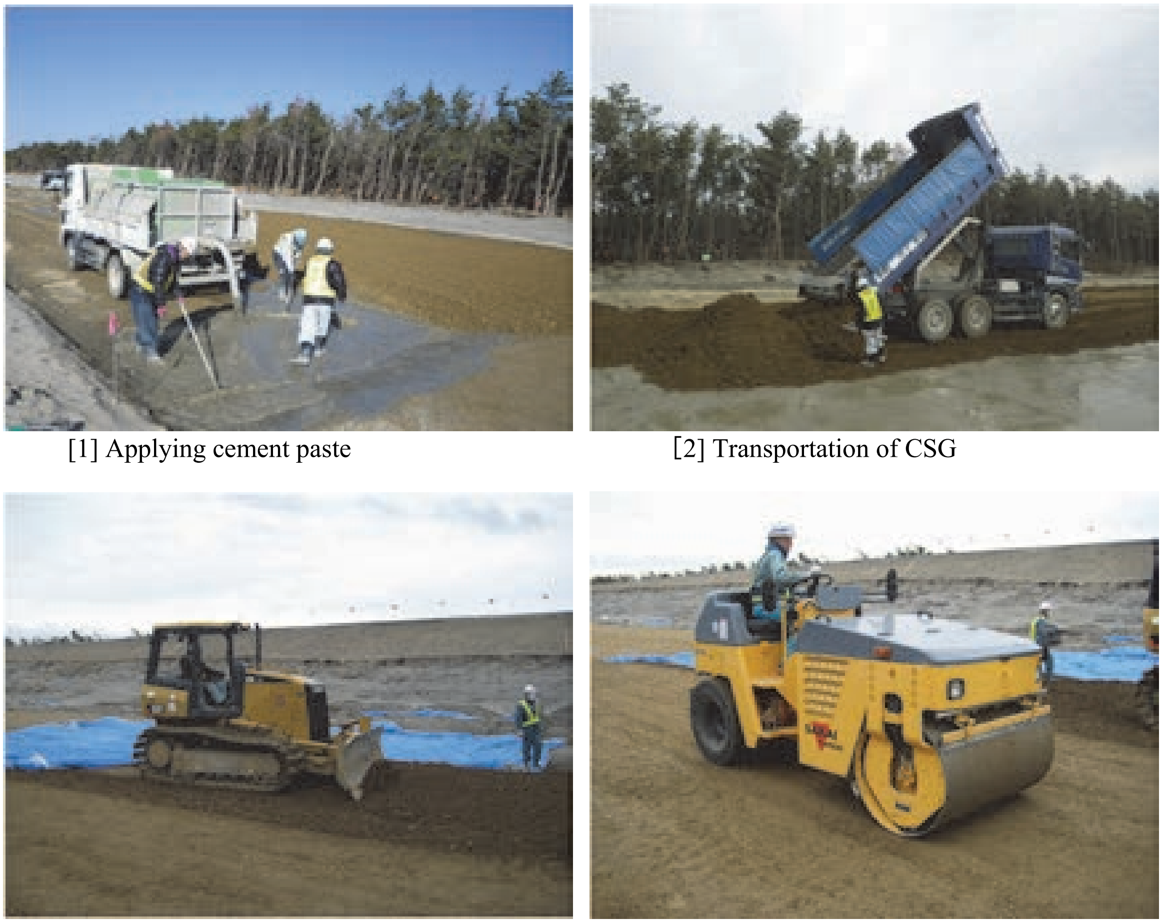

[1] Applying cement paste

[2] Transportation of CSG

[3] Spreading of CSG

[4] Roller compaction

Figure 10. Views of CSG execution

3.2. Survey during execution

During execution, the SWS-test was done at 25m long intervals along the axis of the levee, confirming that the required bearing capacity can be obtained.

The SWS-test was influenced by looseness near the ground surface, but it clarified by a preliminary survey that test results with the earth covering of 1 and 2m or thicker conform to the values of SPT as shown in of Fig. 6. Therefore as shown by Fig. 7, the SWS-test was done when the excavation had reached 2m above the planned foundation ground, and the excavation was continued till the required bearing capacity near the planned foundation ground elevation was confirmed.

4. CSG PRODUCTION AND CONSTRUCTION

As CSG material, terrace deposits and mudstone quarried at Mt. Akura have been used. Each sediments and mudstone is efficiently mixed with 20% or 40% of beach sands produced during excavation of the levee foundation.

The gradation of the terrace deposits and mudstone is shown in Fig. 8. The materials with 80mm of the maximum grain size are produced by the crushers. The mixtures of adjusted sediments and sands, or adjusted mudstone and sands having the specified weight ratio are blended by the CSG production equipment.

The CSG is produced by adding cement and water to the blended CSG material, and transported to the construction sections and placed at the site. The CSG is made at the mixing plant shown in Fig. 9, and supplied to multiple construction sections at one time. The mixing of CSG centralized in one plant so that the quality control of CSG is performed efficiently.

As stated above, placing of CSG placing is done simultaneously, in several construction areas. The construction procedure majorly consists of cement paste and transportation, spreading and compaction of CSG, as shown in Fig. 10 [1] to [4], respectively.

5. CONCLUSIONS

The CSG structure is constructed using material obtained from the vicinity of the levee, and unlike a concrete structure, using a low unit volume of cement. The CSG is made from cement, water, rocky materials, and has been developed as the new design and construction methods at dam engineering.

As a result, this type of levee ensures stability against external forces that include the predicted wave force or the overflow of the tsunami and the earthquake motion, and it enables the restoration of the seaside protection forest to protect the environment and landscape of the region.

Three of eight construction sections in the coastal levee were completed in March, 2016. The construction work has been carried out aiming the whole completion in March, 2020.

REFERENCES

Yoshizawa, Y., Itoh, N. and Hakamata, M. (2016): Construction of a coastal levee at Hamamatsu City Coastline, Engineering for dams, No. 354, pp.75-106, (in Japanese).

Study on Rapid Construction Technology for Surface Cover Board Joint of the Slab Joint of CFRD

M. Li & Z. H. Sun
China Institute of Water Resources & Hydropower Research, Beijing, China
limengwho@163.com

ABSTRACT:
This paper presents a rapid construction technology by using brushing polyurea to connect the surface cover board joint of the slab joint of CFRD. Through grinding surface and using special interface agent, good bonding between brushing polyurea and EPDM cover board can be guaranteed. The test result shows: compared with the method of using brushing polyurea on EPDM cover board, the method of using brushing polyurea combining PET nonwoven substrates has better stress condition, which can meet the requirements of the EPDM cover board joint deformation and anti-seepage. This technology has been used in the construction of slab joint seal for Liyuan CFRD, and achieved a satisfactory effect.

Key words: EPDM cover board, brushing polyurea, interface agent, joint

1. GENERAL INTRODUCTION

Concrete Face Rockfill Dam (Hereinafter referred to as CFRD) is one type of dam, which uses rockfill body as the main material and adopts the reinforced concrete face slab for upstream seepage control. From the beginning of Morena dam which was 54m and completed in 1895 to Today's Shuibuya and Bakun CFRD with the height of 200m, CFRD has been widely applied and gradually developed towards high dams and large scale projects due to the advantages of safety, economy and convenient construction. Compared with other types of dam, dam deformation of CFRD is large, which results in large opening, shearing and subsiding displacements of joints (especially peripheral joints). Joint seal for CFRD is an item of more difficulty technology. Joint seal has signality to the safe operation of CFRD.

Setting the protective cover board on water stop of joint surface is usually used in the design of slab joint seal for CFRD. At present, flexible waterproofing rolls are widely used as a protective cover board, which includes EPDM cover board, rubber plate, PVC waterproofing membrane and composite SB rubber plate. It is used more due to good age resistance and high and low temperature resistances of EPDM cover board.

The peripheral joint seam is complicated in concrete slab joint sealing construction. There are a number of T-type or L-type joints which shows for non planar space form. In the section of joint change, the joint of EPDM cover board must be made to measure according to the actual angle of joint on site, and then these joints are connected with straight segment EPDM cover board by vulcanization. According to technical specifications for joint seal of concrete face rockfill dam (DL/T5115-2000), the joints between the seepage protective cover plates on plastic filler surface have two types including butt joint by vulcanization and lapped joint, and lap length should be greater than 200mm. It is difficult to ensure the quality of butt joint by vulcanization in construction process on site, and the construction is long in period. Although the application of lapped joint has advantage of simple construction, but it is easy to damage in the joint area because of the frequent changes of the water level of pumped storage hydropower station in the cold region(Zhang, 2013). (See Fig. 1) Therefore, it is necessary to study rapid connecting method and construction technology on the joint of EPDM cover board on site.

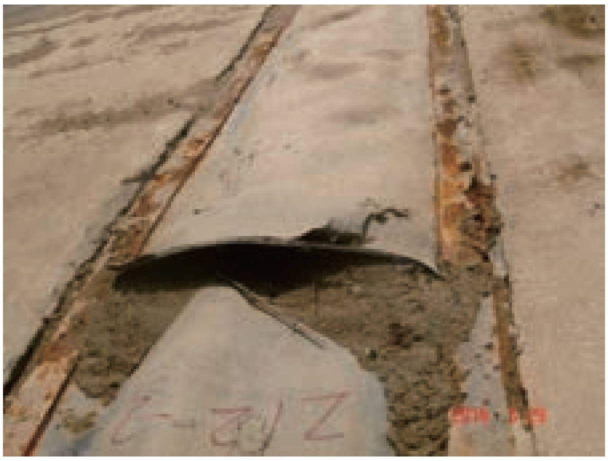

Figure1. Destruction of lapped joint of EPDM cover board

2. ADHESIVE MATERIAL AND CONSTRUCTION TECHNOLOGY OF EPDM COVER BOARD JOINT

Interconnect material for EPDM cover boards should have high strength, aging resistance, good flexibility (to adapt EPDM cover board deformation) and good bonding behavior. Brushing polyurea is a one-component material, whose main technical specifications are shown in Table1 (Sun, 2011). Brushing polyurea has a lot of advantages such as high strength, good aging resistance, large elongation rate, excellent abrasion resistance, strong impermeability, good frost resistance, combining PET nonwoven substrates inside the polyurea coating and easy construction. In order to guarantee the bonding strength between brushing polyurea and EPDM cover board, special interface agent was developed and used (the main technical specifications in Table2). The interface agent between brushing polyurea and EPDM cover board coheres well, and it is flexible when cured.

Table1. Main Mechanical Indexes of Brushing Polyurea

Items	Technical indexes
Tensile strength, MPa	⩾15
Break elongation rate, %	⩾300
Low temperature flexibility, ℃	⩽-45
Tear strength, kN/m	⩾40
Hardness, HA	⩾50
Adhesion (moist surface), MPa	⩾2.5
Color	French grey, adjustable

Table2. Main Performance Indexes of Interface Agent

Items	Standard authorized value
appearance	Yellow or translucent liquid, no impurities
Surface drying time, h	⩽ 12
Density, g/ml	1.0±0.1
Bonding strength, MPa	⩾1.0

The bonding construction process between brushing polyurea and EPDM cover board: first of all, polish EPDM cover board surface with buffing machine; next, clear the dust and brush interface agent on the surface; finally, brush brushing polyurea layered when the interface agent surface is dry. The curing time of brushing polyurea is 28 days.

3. BOND TEST OF EPDM COVER BOARD BUTT JOINT

3.1 Brushing polyurea combining PET nonwoven substrates

On the butt joint of EPDM cover board surface, brushing polyurea and adding a layer of PET nonwoven substrates inside the polyurea (hereinafter referred to as "polyurea with PET nonwoven substrates coating") (Yu, 2009). The width, thickness and length of polyurea with PET nonwoven substrates coating are respectively 50mm, 3mm, 400mm. The test experiment was conducted according to Geotextiles — Wide-width tensile test (executive standard: GB/T 15788-1995). The test process is shown in Fig.2, the test results are shown in Table3 and Fig.3.

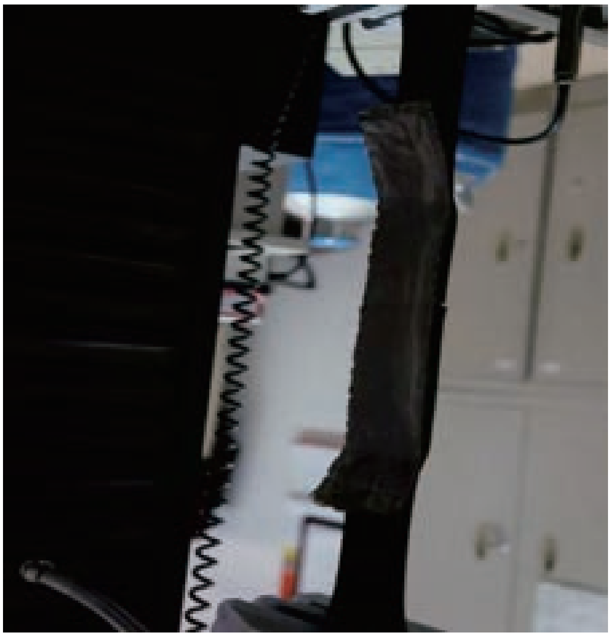

Figure.2 Failure processes of tensile test of butt joint of EPDM cover board (polyurea with PET nonwoven substrates coating)

Through the whole test process, we can see that polyurea with PET nonwoven substrates coating is brushed in the middle part of butt joint of EPDM cover board. Because the coating can distribute the load to both sides through PET nonwoven substrates, it can be seen that the deformation of polyurea with PET nonwoven substrates coating is very small under load and the obvious deformation of EPDM cover board appeared at the both ends of polyurea with PET nonwoven substrates coating. In the whole bond failure process, EPDM cover board at the both ends of polyurea with PET nonwoven substrates coating become thinner and thinner firstly due to tension, which cause the interface between polyurea with PET nonwoven substrates coating and EPDM cover board to be pulled apart from both ends, with EPDM cover board deformation developing gradually to the central, the interface between coating and EPDM cover board become separated until the deformation is close to the butt joint of EPDM cover board.

Through the test data shown in Table3 and Fig.3, it can be seen that test loading speed has a greater effect on tensile strength of the coating. The faster the loading speed is, the greater the tensile strength and elongation rate is. Failure trend and final failure mode is the same. It can be guaranteed that fracture will not occur in the interior of polyurea, if the polyurea with PET nonwoven substrates coating is 3mm thick.

Table 3. Test results of the butt joint (polyurea with PET nonwoven substrates coating)

Sequence number	Thickness of coating(mm)	Width (mm)	Maximum load(N)	Tensile strength (kN/m)	Elongation rate (%)	Stretching rate (mm/min)
1	2.96	50	620	12.4	146	200
2	2.80	50	460	9.18	86.5	20
3	2.86	50	470	9.40	67.8	20

Table 4. Test results of the butt joint (polyurea coating)

Sequence number	Thickness of coating(mm)	Width (mm)	Maximum load(N)	Tensile strength (kN/m)	Elongation rate (%)	Stretching rate (mm/min)
1	2.0	50	420	8.34	39.5	200
2	3.8	50	490	9.76	41.69	200
3	3.5	50	380	7.66	24.5	20

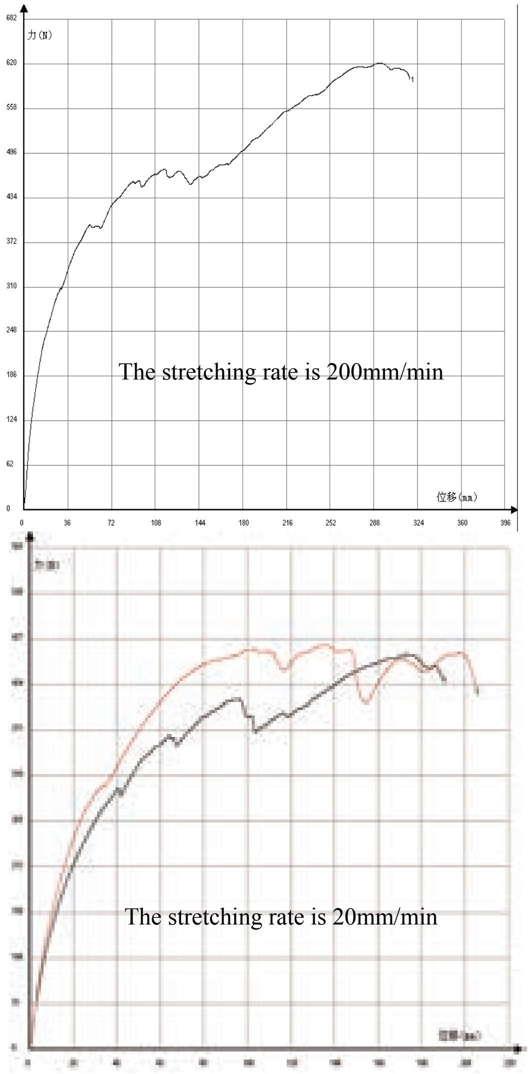

Figure.3 Tensile test results of the butt joint of EPDM cover board with polyurea with PET nonwoven substrates coating

3.2 Brush brushing polyurea

On the butt joint of EPDM cover board surface, brushing polyurea inside without PET nonwoven substrates (hereinafter referred to as "polyurea coating"). The width, thickness and length of polyurea coating is respectively 50mm, 2~3.8mm, 400mm. The test was conducted according to Geotextiles — Wide-width tensile test (executive standard: GB/T 15788-1995). The test process is shown in Fig.4, the test results are shown in Table4.

In this test, we only brushed polyurea coating on the butt joint of EPDM cover board. By the test data and test process shown in Table4 and Fig.3, we can see that the deformation occurred simultaneously in the middle of polyurea coating and both ends of EPDM cover board under the load. Because the force is concentrated in the middle of the polyurea coating and it can not be distributed to the whole area of polyurea coating through PET Substrate Nonwovens, the breakage first appeared in the middle of polyurea coating. The greater the thickness of polyurea coating is, the greater the tensile strength is, but the elongation rate remains broadly stable. It can be seen that the test loading speed has a greater effect on tensile strength of the polyurea coating. The faster the loading speed is, the greater the tensile strength and elongation rate is.

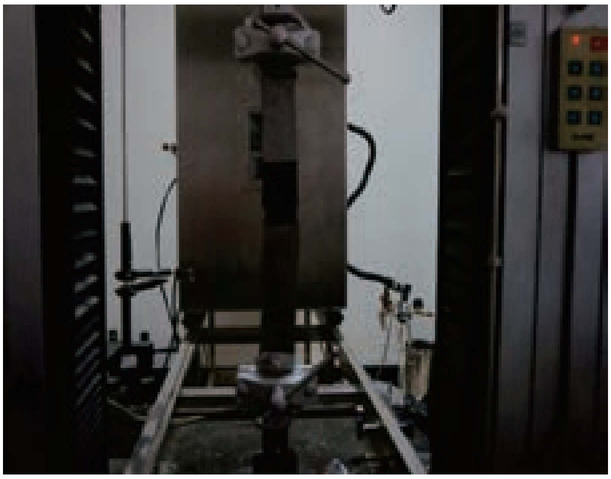

Figure.4 Tensile test results of butt joint of EPDM cover board (polyurea coating)

Comparing the results shown in Table3 and Table4, it can conclude that combining PET Substrate Nonwovens in the polyurea coating could reduce the stress concentration. Due to it, the tensile strength and elongation rate of the polyurea coating have risen considerably.

4. BOND TEST OF EPDM COVER BOARD LAPPED JOINT

On lapped joint of EPDM cover board surface, brushing polyurea and adding a layer of PET nonwoven substrates inside the polyurea. The width, thickness and length of polyurea with PET nonwoven substrates coating is respectively 50mm, 3mm and 350mm.

Table 5. Test results of the lapped joint (polyurea with PET nonwoven substrates coating)

sequence number	thickness (mm)	width (mm)	Maximum load(N)	Tensile strength (kN/m)	Elongation rate (%)	stretching rate (mm/min)
1	2.96	50	600	11.96	73.7	200
2	2.84	50	600	11.98	66.2	200

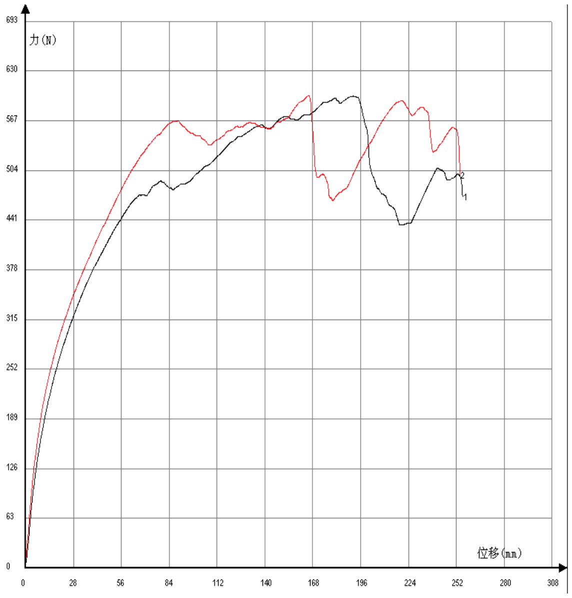

Figure.5 Tensile test results of lapped joint of EPDM cover board (Polyurea with PET nonwoven substrates coating)

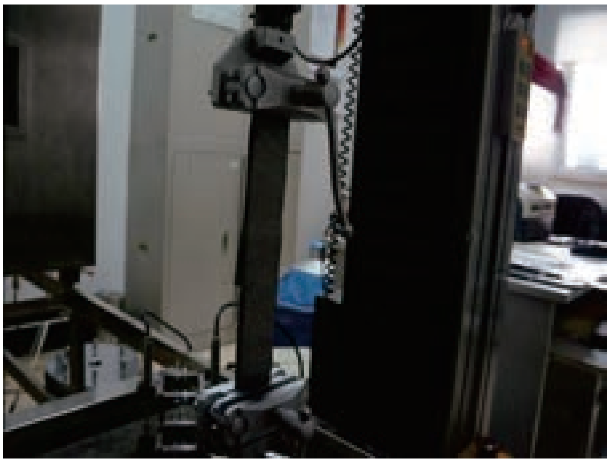

Figure.6 Tensile test of lapped joint of EPDM cover board (Polyurea with PET nonwoven substrates coating)

Through the whole test process, we can see that polyurea with PET nonwoven substrates coating is brushed on lapped joint of EPDM cover board surface. Because the coating can distribute the load to both sides through PET nonwoven substrates, it can be seen that the deformation of polyurea with PET nonwoven substrates coating is very small under load and the obvious deformation of EPDM cover board appeared at the both ends of polyurea with PET nonwoven substrates coating. In the whole bond failure process, EPDM cover board at the both ends of polyurea with PET nonwoven substrates coating become thinner and thinner firstly due to tension, which cause the interface between polyurea with PET nonwoven substrates coating and EPDM cover board to be pulled apart from both ends, with EPDM cover board deformation developing gradually to the central, the interface between coating and EPDM cover board become separated until the deformation is close to the butt joint of EPDM cover board.

Different connection types (lapped joint or butt joint) have no great influence on the bonding effect of EPDM cover board and polyurea with PET nonwoven substrates coating, and the both failure modes are from both sides to the center. It can be guaranteed that fracture will not occur in the interior of polyurea and good seepage control can be obtained in joint of EPDM cover board, if the polyurea with PET nonwoven substrates coating is 3mm thick.

5. PEELING TEST OF EPDM COVER BOARD AND BRUSHING POLYUREA

Brushing polyurea coating or polyurea with PET nonwoven substrates coating on the EPDM cover board surface, the width of coating is the same as EPDM cover board, 50mm. The bonding length is 100mm. The test was conducted according to Specification for test and measurement of geosynthetics (SL235-2012) & Test method of peeling strength. The tensile rate is set at 300mm/min.

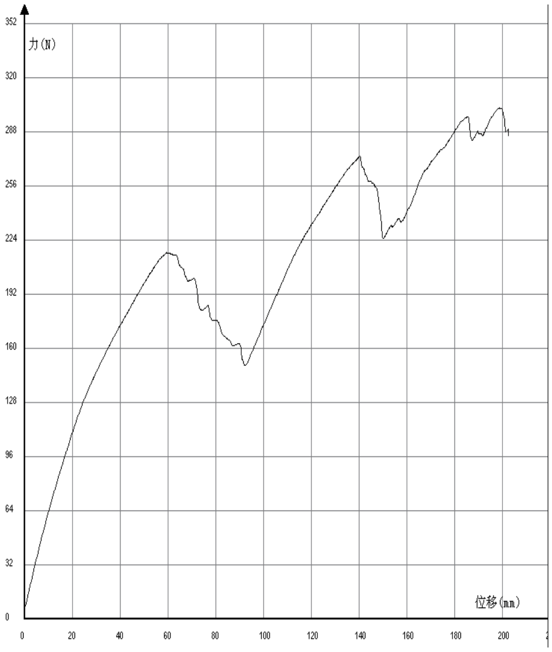

Figure.7 Test result for peeling strength of polyurea with PET nonwoven substrates coating- to-EPDM cover board

Table 6. Results of disbanding test

Specimen Type	Sequence Number	Thickness (mm)	Maximum load (N)	Peeling Strength (kN/m)	Remark
polyurea with PET nonwoven substrates coating	1	2.96	425	8.49	The bonding interface is torn.
	2	2.86	652	13.04	
	3	2.94	302	6.04	
Polyurea coating	1	3.5	536	10.7	The polyurea coating is snapped
	2	2.0	431	8.6	

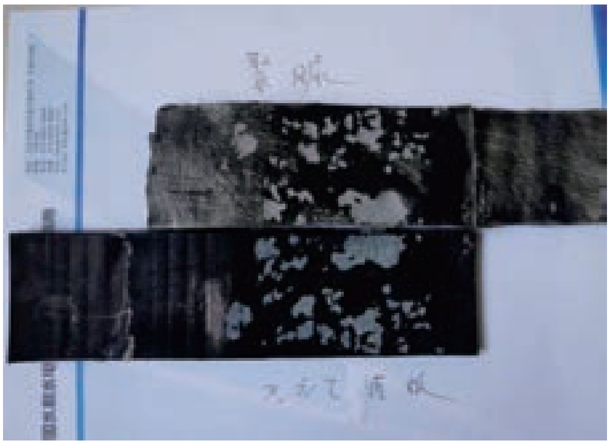

Figure.8 Surface Condition for peeling test of polyurea with PET nonwoven substrates coating- to-EPDM cover board

Through the test results of peeling strength, it is found that EPDM cover board brushed polyurea with PET nonwoven substrates coating on surface become elongate and thin with the peeling of polyurea with PET nonwoven substrates coating, and the peeling strength has nothing to do with the thickness of polyurea with PET nonwoven substrates coating and has some fluctuations. Meanwhile, according to the test results, we can also see that the minimum peeling strength is 6N/mm, and the bond strength is nonuniform distribution between polyurea with PET nonwoven substrates coating and EPDM cover board. While brushing polyurea coating directly on EPDM cover board surface, the test result shows that peeling strength is related to polyurea coating thickness and the bonding destruction happen inside the polyurea coating if the polyurea coating is thinner.

6. EPDM COVER BOARD JOINT CONNECING TECHNICAL TEST ON SITE

Design specifications of CFRD put forward two joint types of surface cover board including butt joint by vulcanization and lapped joint. In order to facilitate the construction and improve the construction speed, a technical field test was conducted to compare the method of using polyurea with PET nonwoven substrates coating on EPDM cover board joint and the method of butt joint by vulcanization in joint water stop construction process of Liyuan CFRD. GB EPDM composite cover board which was applied for the joint of CFRD of Liyuan hydropower station is 100cm wide and 10mm thick. The test result shows that the disadvantages with the use of method of butt joint by vulcanization lie in the difficulty in construction, long operation time and the difficulty in quality control **(**see Fig.9**)**. Instead, the other method has advantages of convenient construction, short operation time and good quality control **(**see Fig.10**)**.

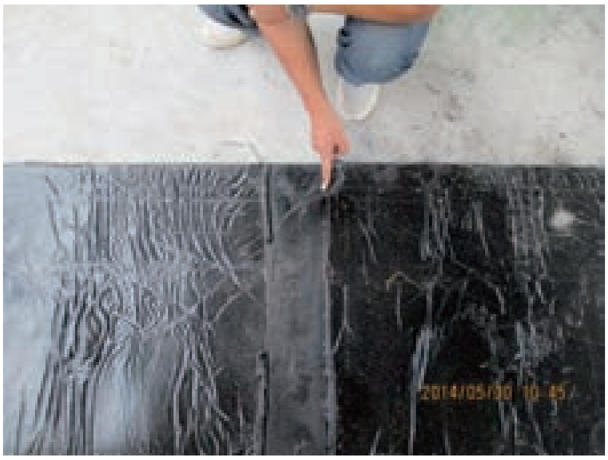

Figure.9 Butt joint of EPDM cover boards by vulcanization

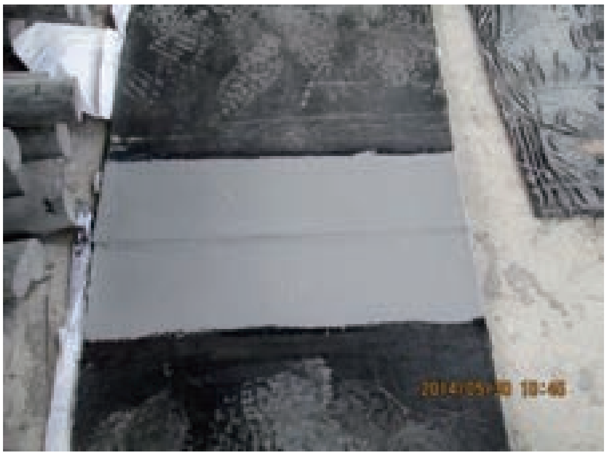

Figure.10 Lapped joint of EPDM cover boards with polyurea with PET nonwoven substrates coating

Through comparing the test results, the method of using polyurea with PET nonwoven substrates coating on EPDM cover board lapped joint was finally adopted in joint water stop construction process of Liyuan CFRD. The lapped length of EPDM cover board is 200mm. The practical construction technology is: first of all, polish EPDM cover board surface and clear the dust; next, brush special interface agent on the surface; Finally, brush 3mm thick polyurea with PET nonwoven substrates coating layered (brush polyurea coating 4 times in all, add a layer of PET Substrate Nonwovens after the second brushing) when the interface agent surface is dry, stretching 100mm long on either side of the lapped joint.

7. CONCLUSIONS

(1) Through polishing EPDM cover board surface and brushing special interface agent, the bond strength of brushing polyurea/ EPDM cover board is higher, which can meet the deformation and anti-seepage requirements in lapped joint of EPDM cover board.

(2) During tensile test, only brushing brushing polyurea in lapped joint or butt joint of EPDM cover board, it was found that the polyurea failed by tension fracture in the middle because of the phenomenon of stress concentration. Instead, polyurea with PET nonwoven substrates coating has better stress condition, which failed gradually from both ends to the center in the progress of tensile test, because PET Substrate Nonwovens can distribute the stress to the whole area.

(3) The method of brushing polyurea with PET nonwoven substrates coating on EPDM cover board joint has such advantages as convenient construction and good quality control. This technology has been used in the construction of slab joint seal for Liyuan CFRD, and achieved a satisfactory effect. It is worth promoting the application.

REFERENCES

Zhang, G.L. and Sun, Z.H. (2013): Protection and Cracks Treatment on Concrete Slabs of Pumped Storage Power Station in Cold Area. The 3rd international symposium on rockfill dams.

Sun, Z.H., Li, M. and Ni, Y. (2011): Application of SK flexible coating in repair of expansion joints and cracks on concrete structure, Dam & Safety, 1, pp. 48-52.

Yu, J.P. and Louis, D. (2009): Exposed waterproofing elastic coating used for high-speed railway bridge, China building waterproofing, 5, pp.7-9.

4^{th} APG Symposium and 9^{th} EADC on

INNOVATIVE TECHNOLOGIES FOR DAMS AND RESERVOIRS TOWARD THE FUTURE GENERATIONS

The Underwater Excavation
By The Shaft-Style Underwater Excavator T-iROBO UW

N. Yachi
Taisei Corp., Tokyo, Japan
yachi@ce.taisei.co.jp

H. Miura
Aktio Corp., Tokyo, Japan

A. Ueyama
Kyokuto Construction Corp.,Okinawa, Japan

ABSTRACT:
In order to solve the problems caused by deterioration and the inefficiency of the conventional method in redevelopment of existing dams, a shaft-style underwater construction machine (T-iROBO UW) was developed and utilized in the Amagase Dam Redevelopment Project in Uji City, Kyoto Prefecture. The machine is operated remotely to ascend, descend, rotate, to crash and gather the rock using a power shovel that is fixed to a shaft that goes down from the barge to the lake bottom, for underwater works. The underwater excavation is carried out while observing several monitors at the same time. One of the monitors shows landform of the lake bottom in 3D graphics, using the data obtained by investigation of sonar device. On the 3D graphics of landform, the movement of the power shovel is featured in animation, by measuring the angles of the arm of the power shovel. The ultrasonic camera is used to provide the operator a real-time image on the other monitor. It is also possible to replace attachments of the power shovel, and currently the underwater breaker, bucket, and pump are being used. This is a report of the development of T-iROBO UW and its performance.

Keywords: underwater excavation, remote operation, visualization of blurred underwater image, diver unnecessary, deep water

1. INTRODUCTION

In recent years, existing dams in Japan are deteriorating, and dams that were built more than 50 years ago are increasing. However, there are few sites suitable for dam construction, and it has become difficult to secure land for the construction of new dams. As a result, there is a growing need to redevelop existing dams and to use them efficiently for long periods of time. In the redevelopment of existing dams, it is preferred that work be carried out while maintaining the function of the dam, so underwater work performed while maintaining the level of water in the reservoir is increasing. In this case, a large-scale temporary pier and diver work at great depths is often necessary, which causes issues such as longer construction time, an increase in cost, and more hazardous work.

In order to solve the problems that arise in underwater construction and to execute the work safely and accurately, a shaft-style remote-controlled underwater construction machine, the T-iROBO UW (patent No.4792123), was developed and utilized in a dam redevelopment project. This paper is a case study of the utilization of the shaft-style remote-controlled underwater construction machine T-iROBO UW in the excavation of reservoir bedrock.

2. UNDERWATER EXCAVATION ISSUES IN DAM REDEVELOPMENT

In the redevelopment construction of existing dams, it is preferred that work be carried out while maintaining the function of the dam. Therefore, it is necessary to carry out the work while retaining the level of the water in the reservoir. Excavation at great depths, such as bedrock excavation, is particularly challenging.

In underwater construction, securing the construction yard is the most immediate challenge. In the past, the construction yard was secured by installing a coffering structure. (Fig.1.) However, when working at great depths the pier needs to be very high, requires time to install, and increases construction costs.

Furthermore, in underwater bedrock excavation, usually the methods such as casing rotation excavation method and percussion method that are using heavy machinery is used, the efficiency of the construction is low. Because this conventional construction method precludes observation of the excavation site, excavation must be carried out while constantly checking vertical accuracy on the pier, which also makes precision work in close proximity to underwater structures impossible. Furthermore, the placement large amounts of heavy machinery results in many blind spots on the pier, so this method has a constant risk of accidents, such as caught-between accidents. In this method, divers are used to check excavation conditions and progress and for precision work in close proximity to underwater structures. However, diver work has a high level of potential danger, and in projects like this case study, which required work at a depth of close to 40m, air diving allows only a short period of time for work, and equipment for saturation diving incurs an enormous expense.

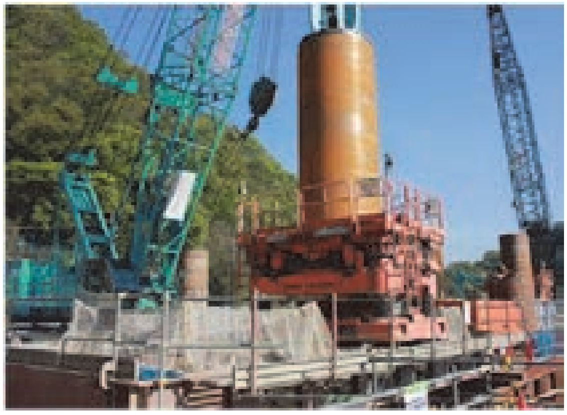

Figure 1. The conventional way of securing construction yard by installing a coffering structure (casing rotation excavation method)

3. DEVELOPMENT OF T-IROBO UW

3.1 Development Focal Points

To solve the problems mentioned above, the development of an excavator that could be controlled remotely to excavate bedrock was undertaken.

First of all, in order to implement excavation accurately underwater, it was important to determine how to obtain the location information (coordinates) of the construction machine, which would be underwater and invisible to the naked eye. Therefore, a method was adopted in which a construction machine is attached to a shaft and lowered beneath the water and location information for the underwater construction machine is obtained by giving location information to the top end of the shaft and measuring the inclination of the shaft and the position of the machine upon it.

In addition, a visualization apparatus to give information to the operator and a machine guidance system was developed in order to enable the remote control of the underwater construction machine.

A hydraulic excavator that can be fitted with a variety of attachments was selected to serve as the base machine in order to handle the various requirements of the underwater work, which is not limited to excavation. Moreover, the hydraulic excavator consists of 3 joints which enable smooth movements, making it optimal for displaying the functions of a variety of attachments.

3.2 Composition

A shaft-style remote-controlled underwater construction machine (T-iROBO UW) was manufactured based on the development focal points mentioned above. T-iROBO UW (Fig.2.) is fixed to a shaft that goes down from a barge to the lakebed, and an underwater auger is equipped to the end of the shaft to fix it on the lake bedrock. Since the underwater construction machine is a hydraulic excavator that attaches to the shaft, it can be operated to ascend, descend, and rotate on the shaft.

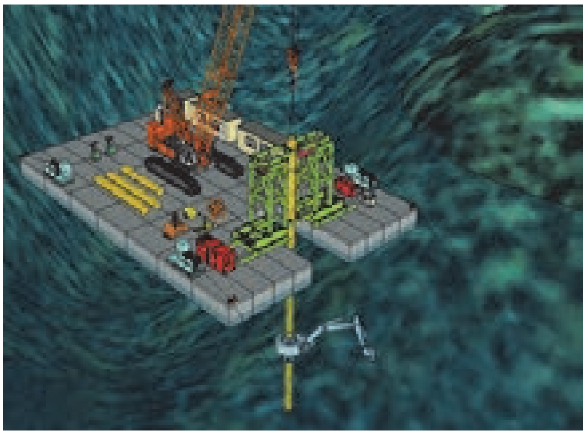

Figure 2. The key map of T-iROBO UW

A control room for the remote operation of the construction machine, an electric power generator, and a crawler crane were installed on the barge.

The underwater excavator is controlled remotely with a joystick and pedals, the same as a normal excavator used on land. The visualization apparatus and machine guidance are deployed from the monitor. Underwater sound waves are picked up using a hydrophone.

3.3 Features

T-iROBO UW has numerous features, including the ability to carry out the excavation with a high level of accuracy, versatility, and enhanced safety. The following is a detailed description of the features of the T-iROBO UW.

3.3.1 Shaft-style Excavator

Adopting a shaft-style system made it possible to obtain accurate location information for the underwater construction machine. Real-time location information can be gathered by setting the target on the top end of the shaft and tracking it automatically. As the distance between the shaft and the underwater construction machine is measured beforehand, and the real-time position of the underwater construction machine is obtained from a protractor and encoder attached to the boom, it is possible to easily obtain location information for the main body of the machine and the extremities of the attachments based on the location information of the top end of the shaft. With a conventional underwater construction machine, it was difficult to get location information on a centimeter-scale basis, and diver work was necessary, resulting in there being a limit to the depth at which construction work could be carried out. In regard to this matter, with the specifications of the T-iROBO used in this project operation at a depth of 50m was possible. If some parts are changed, the design allows for underwater operation at a depth of up to 100m.

The adoption of the shaft-style system allows for the machine to be easily fixed on steep slopes and for a counterweight to be secured. The stability of the underwater construction machine is ensured by inserting a separately-developed underwater auger, which is equipped to the end of the shaft, approximately 1m into the bedrock fixing the shaft securely between the barge and the bedrock.

3.3.2. Remote Control via Computerized Construction Apparatus

The computerized construction apparatus (the underwater construction visualization apparatus and sound receiver) is one of the most important functions performed during underwater construction.

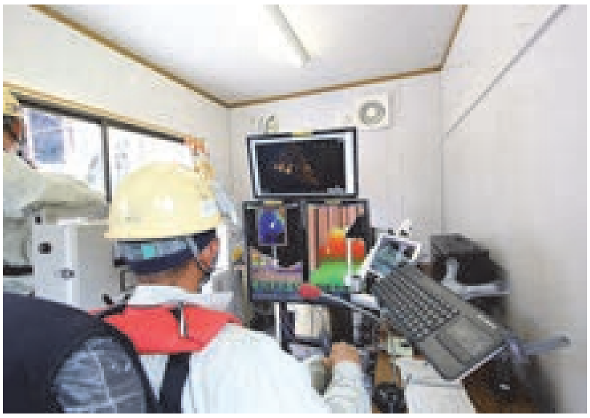

Figure 3. The remote control room

The topography data sounded by the multi-fan beam is projected in 3D on the monitor in the remote control room. (Fig.3.) Simultaneously, an animation of the main body of the underwater construction machine based on the data obtained by each measuring instrument is projected on the same monitor. (Fig.4.) It is possible to display the real-time position of the main body of the construction machine, so the operator can control the machine while looking at its position.
If there is any existing structure under the water, by inputting the information in advance, the operator can see the structure as though they were actually looking at it in real time.

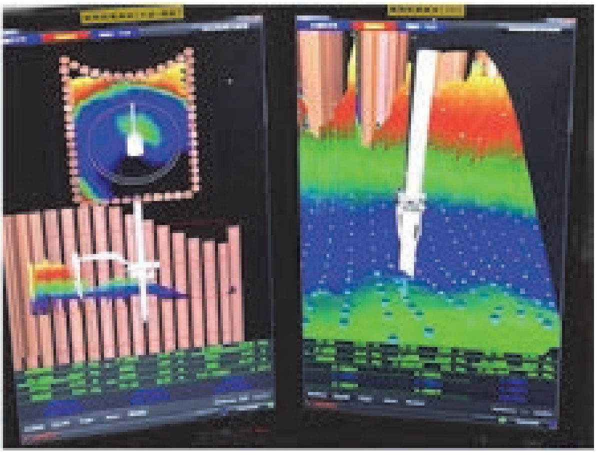

Figure 4. The animation of the main body of the underwater construction machine projected on the monitor

The topography data is updated when sounding is carried out, so it does not change in real-time during excavation. However, the coordinates of extremities of the attachments, such as the breaker and bucket, can be attained in real time, so the operator can check them and decide when to finish crushing and excavating the bedrock.

To support these functions, an underwater camera and hydrophone were installed. It is difficult to display the lakebed with an optical camera due to the great depth and turbidity of the water, so an ultrasound camera was chosen. The video taken by the ultrasound camera enabled the operator to see the location and distance of existing structures and obstacles with their own eyes, allowing them to carry out excavation without accidental collision.

Speakers were installed in the remote control room so that the operator could listen to the sound from the hydrophone while working. The hydrophone clearly picks up the sound of the rocks being broken and the bucket collecting sand and earth as well as the sound of the hydraulics. By obtaining aural information in addition to visual information, it was possible to convincingly replicate the feeling of sitting in the operator's chair that you would have when operating machinery on land in the control room.

3.3.3 Versatility at Various Types of Construction

As the base machine is a highly versatile hydraulic excavator, it is possible to mount it with most of the attachments that you would use in onshore construction. In this project it was used for excavation, but it is also suitable for a variety of other construction work, such as concrete demolition and removal of obstructions and extraneous matter.

3.3.4 Machine Operator

No special training is required for the operation of this machine. It can be operated by anyone with qualifications to operate an onshore machine. In the operation of an onshore backhoe, ground vibrations are felt directly by the operator during excavation, which places a burden on their body. However, the operator's seat for this machine is on the barge, meaning no vibrations are felt, reducing the burden on the operator's body. It is also easy to take breaks, and the operator's work environment is vastly improved.

For these reasons, it is also helpful as a countermeasure against the increased age of workers and the lack of skilled workers, which have become societal issues in recent years.

3.3.5 Improvement of Safety

The T-iROBO UW is operated via remote control, meaning that it requires no workers aside from one operator and no divers, allowing for the guarantee of a high level of safety. Just by virtue of being operated underwater, the burden of safety management against caught-in and caught-between accidents is dramatically reduced.

4. CONSTRUCTION RESULTS

4.1 Construction Outline

The T-iROBO UW was introduced for the inflow section (Fig.5.) construction work on the Amagase Dam redevelopment project in Uji, Kyoto. There was approximately 5000m³ of underwater excavation, and of that the T-iROBO UW was used for approximately 1300m³ of bedrock excavation. The horizontal area excavated was approximately 21 x 8m, with the circumference surrounded by steel pipe sheet piles and a maximum depth of 38m. This underwater construction machine has an operating radius of 10m, however as excavation close the shaft is not possible, it was shifted 3 - 4 times in order to cover the entire horizontal area.

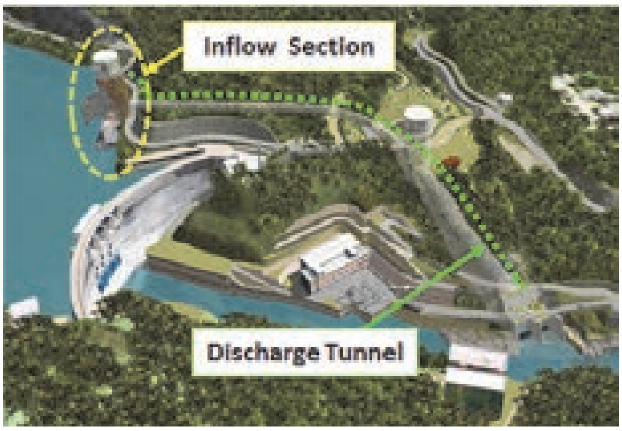

Figure 5. Amagase Dam Redevelopment Project (The inflow section)

4.2 Construction Method

The barge is moved to the designated position according to the location survey. When the position of the barge is decided, the shaft is assembled using a crawler crane. A single standard shaft is 9m, with 4m and 2m shafts for adjustment. The numbers of adjustment shafts necessary for the shaft to reach the lakebed are added to the standard shaft. When the lakebed is reached, the auger is turned on, sunk soundly into the bedrock, and fixed.

Next, the underwater construction machine is suspended and attached to the top of the shaft. The underwater construction machine is first fitted with a 3m shaft, so it can carry out construction work while being attached to the shaft. After attachment, the underwater excavation machine is launched and sunk via remote control.

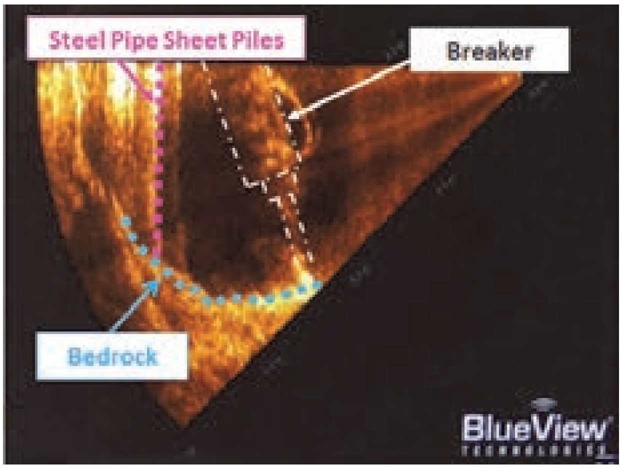

Figure 6. The real time video taken by ultrasonic camera

The operator checks the elevation of the underwater excavation machine on the monitor and stops it at the designated depth, then uses a multi-fan beam to sound the topography of the lake bed and project it in 3D. The operator carries out excavation work while looking at this 3D topography data and real-time video taken by an ultrasonic camera.

Fig.6 shows the monitor equipped at the remote control room which provides the operator real time information obtained by an ultrasonic camera. On the screen, the breaker, bedrock, steel pipe sheet pile is projected, and the operator carries out the excavation by steering the point of the breaker towards the bedrock.

Excavation begins by using a breaker to crush the rock, then switching the attachment to a bucket to collect the rock. This switching operation can be carried out with the ease of an onshore operation by lifting the underwater construction machine to the surface of the water and placing the boom on the barge. When excavation is complete, the underwater construction machine is lifted and placed temporarily on the barge. The numbers of shafts are detached to not touch the lakebed, the barge is moved to the next position, and the excavation recommences. The surplus rock crushed and collected by the underwater construction machine is dredged using a bucket attached to a crawler crane.

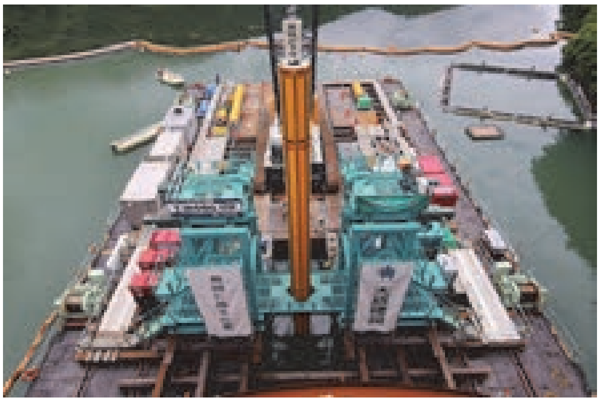

Figure 7. The whole view of T-iROBO

4.3 Construction Results

This construction work took 6.5 months from assembly to excavation and disassembly. The average area excavated per day was 25m³ (including movement of the shaft and dredging work by the floating crane) with a total of 10 shaft shifts requiring 3-4 hours and 5 shaft shifts to switch to dredging requiring 6-8 hours. All construction works were implemented more or less to schedule.

Using conventional methods this project would require approximately 10.1 months. It was possible to reduce the necessary construction time by 40% to 6.5 months. Furthermore, conventional methods would require the installation and removal of temporary piers, requiring approximately 10 additional months. It was also possible to reduce construction costs by 40% when compared with the cost of conventional methods, ascertaining this method’s validity.

4.4 Precision of Construction

When placing the underwater construction machine at the site of construction, calibration was carried out onshore, and underwater excavation commenced after ascertaining that the margin of error between the coordinates of the underwater construction machine displayed on the monitor in the remote control room and the coordinates measured by the actual machine was less than 5cm. The final result of the excavation was able to sufficiently satisfy standards.

5. CONCLUSION

The T-iROBO UW (Fig.7. and 8.) was introduced for the first time in the Amagase Dam redevelopment project, and operation was carried out according to plan with no complications. In the future, the T-iROBO UW can contribute to the improvement of functions and the prolonging of the life of existing infrastructure with a reduction in the length of construction time, construction costs, and the amount of dangerous work involved in projects such as dam renewal that require construction work at great depths.

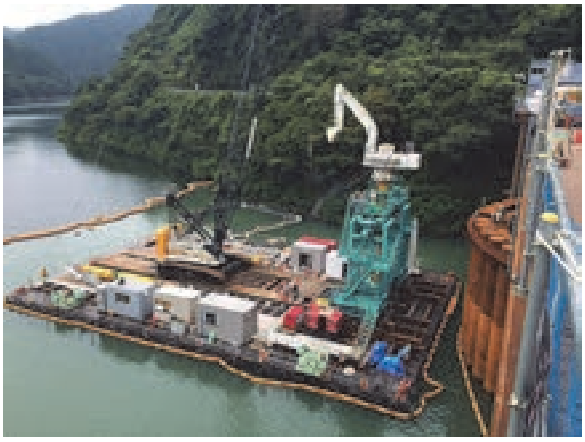

Figure 8. The whole view of T-iROBO

Development of Embankment Material Grading Control Continuous Management System Using Three-dimensional Image Processor

M. Fujiwara, W. Nakane, & I. Miyairi, M. Omata, T. Otake
Obayashi Corporation, Tokyo, Japan
fujiwara.munekazu@obayashi.co.jp

I. Kobayashi, T. Hashizume, A. Nakamura
Nagano Prefecture, Nagano Construction Office, Asakawa Improvement Office, Japan

ABSTRACT:
In dam construction, grading control of embankment material is of vital importance in quality control. The conventional practice is to take samples and carry out sieve analyses at regular intervals, which is both labor- and time-consuming. When constructing a trapezoidal dam with cemented sand and gravel, it is standard practice to produce embankment material by mixing locally available earth material such as riverbed deposits and excavated material with cement and water. In order to achieve the required strength of embankment material, therefore, grading control checks need to be made to ensure that its strength is kept within the allowable range. The authors have developed a new continuous grading management system using three-dimensional image processing technology. The newly developed system makes real-time monitoring of grading possible by irradiating line laser light onto the material on the conveyor, calculating the volume of particles of each size from the image data continuously acquired with a digital camera and thereby determining particle size distribution. The usefulness of the system has been verified by using it for a countermeasure against landslide in which cemented sand and gravel embankment material was used. This paper introduces the new system and reports the field verification results.

Keywords: *three-dimensional image analysis, liner laser, real-time management, particle size distribution, CSG method*

1. INTRODUCTION

In recent years, productivity improvement and labor-saving efforts in dam construction projects have brought about dramatic changes in construction methods. With the evolution of construction methods from the block construction method to the RCD (Roller Compacted Dam-concrete) method and then to the cruising RCD method, the resulting rationalization and mechanization of construction have greatly contributed to the achievement of a shorter construction period and a lower construction cost.

Efforts to improve construction materials have led to the development of trapezoidal CSG (cemented sand and gravel) dams so that concrete dams can be built mostly by use of heavy construction equipment. Improvements have been made in the area of fill dams, too, through the improvement of construction equipment performance, the development of larger construction equipment, and the mechanization of finishing works of excavation and treatment of rock-embankment contact zone. The increasing use of information and communication technology (ICT) has also accelerated construction rationalization through labor saving and automation.

With the progress of construction efficiency improvement and mechanization, new technologies are being introduced in the area of construction management, too.

By improving the image processing technology (Fujisaki et al. 2013; Eda et al. 2014) which has made a remarkable progress in recent years to the extent of being put to practical use in various applications, the authors have developed a continuous grading management system using a three-dimensional image processing system, which is a completely new type of grading management system designed for higher-accuracy real-time management of grading control (hereinafter referred to as the "new system"). The newly developed method aims to manage particle size measurement and control on the basis of the image volume ratio instead of the image area ratio as in the conventional management method. This paper briefly describes the new system and reports the results of the field tests conducted to verify the usefulness of the new system used for the CSG countermeasure against landslide at Asakawa Dam.

2. OVERVIEW OF THE NEW SYSTEM

2.1. Background of development

Embankment material called CSG commonly used for the construction of the main structures of dams is produced by mixing locally available earth material with cement and water without making grading adjustments or washing. Grading control, therefore, is important in order to attain the required strength of CSG mixes. To this end, sieve analysis is carried out manually every one or two hours to check whether the particle size of CSG is within the diamond-shaped area on the strength–unit water content chart. In order to achieve speedy high-volume placement of CSG mixes, it is necessary to develop a technique for real-time management of quality control.

To achieve this goal, a new method for continuous CSG grading management by use of a three-dimensional image processing system has been developed. The system is capable of automatic measurement of CSG grading by applying the image processing technology (see Fig.1) used in various applications such as completion inspection of automotive parts. The system was in-situ test in the CSG embankment work at Asakawa Dam.

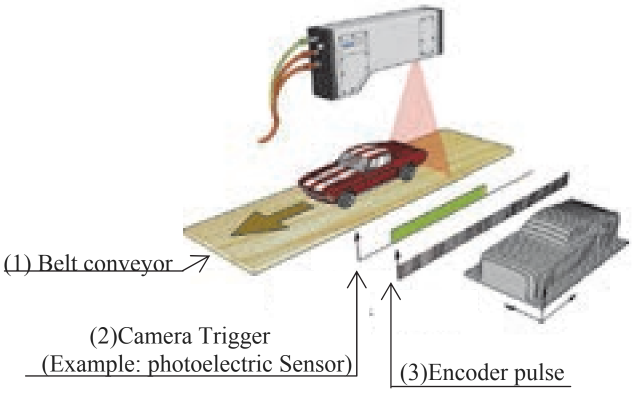

Figure 1. Line laser camera used in a production line

2.2. Image processing technology: challenges and solutions

Processing of digital image data involves processing the image data obtained from an input device such as a camera or a scanner to extract desired image information. To do that, a number of problems had to be solved:

① Since clear images are needed, there is a need for photography techniques, including lighting and shooting techniques, that make it possible to obtain clearly defined images of each particle.

② There is a need for an image processing technology to remove unnecessary image elements (dirt) from the recorded images.

③ There is a need for an image processing (edge processing) technology that makes it possible to recognize, from image data, each of a number of particles in contact with one another as an individual particle.

④ The number of particles recorded in a single image is too small for grading measurement.

In order to separate individual particles from a conglomerate of particles in recorded image data, it is necessary to perform edge processing (e.g. binarization with a Laplacian filter, wavelet transform) of two-dimensional image data. It was known, however, that real-time grading control by that method was not possible because the computing capability required was not available.

As the first step, therefore, a study was conducted to determine how the test sample can be mechanically dispersed so as to shorten image processing time and improve the accuracy of analysis. The previously developed method of dropping the sample was tested, but the method turned out to be inadequate because of problems such as low image quality (poor focusing), inadequate dispersion of fine particles and long image acquisition time. It was necessary, therefore, to come up with a completely different approach to sample dispersion. As a result, it was decided to disperse the sample by use of the velocity difference between the belt feeder and the belt conveyor.

The image processing method was determined by searching for a method that does not require edge processing as part of two-dimensional image processing. For real-time grading measurement of CSG, the author turned attention to a three-dimensional (3D) line laser camera (3D smart camera) system used for such applications as the completion inspection of automotive parts. In view of the fact that the 3D line laser camera system is capable of instantaneously measuring the volume of CSG by continuously acquiring three-dimensional surface profile data, the authors decided to use the system, thinking that it would probably make real-time grading management possible.

2.3. Preliminary experiments with 3D line laser camera

An experiment using a 3D line laser camera system was conducted by using the setup shown in Fig. 2.

The experiment was conducted by using the optical cutting method in which three-dimensional measurement can be made by combining a two-dimensional digital camera and a line laser system.

Fig.1 illustrates the principle of three-dimensional imaging. As shown, line laser is irradiated to the sample (in the illustration, the automobile) on the moving table (for example, a belt conveyor), and the image of the laser light striking the surface of the sample is recorded with a diagonally positioned two-dimensional digital camera.

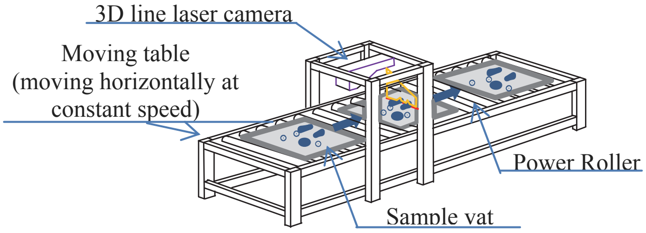

Figure 2. Preliminary experiment apparatus using 3D line laser camera

The images thus obtained are turned into profile data and converted to three-dimensional data on the computer. The locus of points lit up by the laser light is recorded, and three-dimensional images are generated from continuously recorded images. In short, the principle is the same as mathematical integration for volume calculation. High-speed image analysis is made possible by extracting only height information from the profile data in the camera and reducing the extracted information to single-line data.

In the three-case experiment using the apparatus mentioned above, the degree of dispersion and arrangement of CSG samples on the moving table were varied. Although the results in the three cases should have been identical, the measurement results showed errors but they were within 1.5% (Table 1). Thus, it has been shown that the measuring system excels in reproducibility (see Fig. 3).

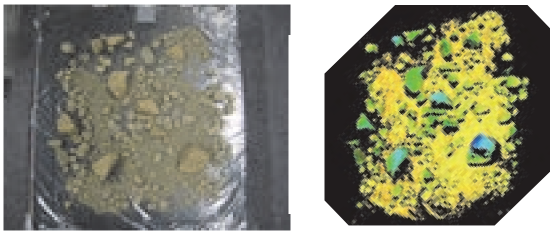

CSG sample on the moving table　　Distance image

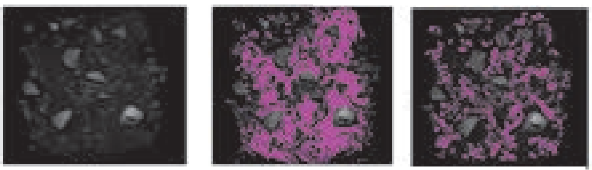

3D image of CSG sample　<5mm　5～10mm

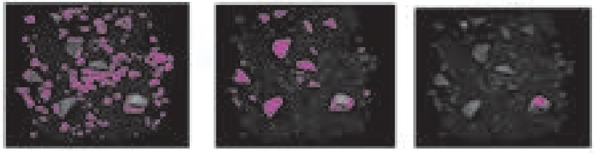

10～20mm　20～40mm　40～80mm

Image fractionated for each particle

Figure 3. Images from preliminary experiment conducted by using 3D line laser camera

Table1. Results of preliminary experiment using 3D line laser camera (particle size content based on image analysis)

Particle size	<5mm	5-10mm	19-20mm	20-40mm	>40mm
case1	24.17	10.52	8.75	4.06	0.24
case2	25.71	10.93	8.59	3.39	0.27
case3	24.50	10.66	8.83	3.74	0.42
max−min(%)	1.54	0.41	0.24	0.33	0.18

3. SYSTEM CONFIGURATION

In view of the results of the preliminary experiment, a particle size measuring system for in-site test was developed. As shown in Fig. 4, the new system consists of a feeding hopper, a belt feeder, a belt conveyor and a 3D line laser camera (see Figs.4 and 5).

3.1.1. Dispersion device

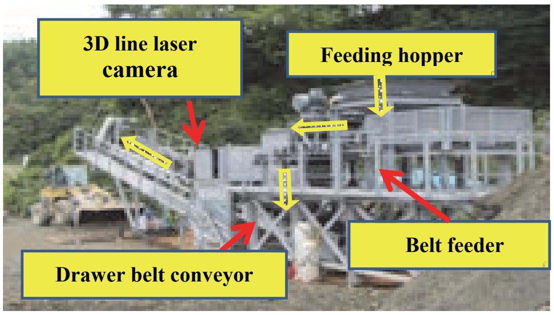

Figure 4. General view of the system

The velocity difference between the belt feeder and the belt conveyor was used as a dispersion method by which to recognize individual particles more accurately at the image processing stage. The effectiveness of the dispersion device was checked in advance, and the belt feeder speed and the belt conveyor speed were set to 1 m/min and 75 m/min, respectively. As a result, the CSG mix fed by the belt feeder onto the belt conveyor in the form of a 10-centimeter-thick layer was dispersed to a thickness (theoretical) of 1.3 mm.

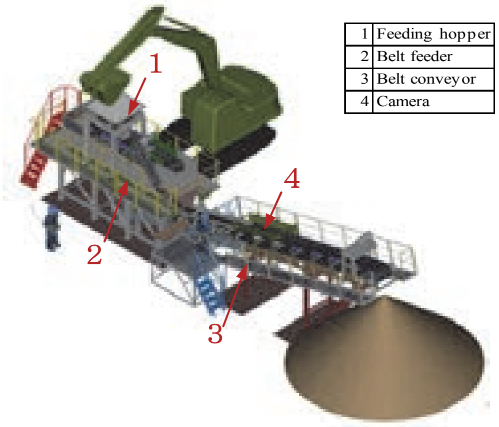

view of dispersing device

3.1.2. 3D Line laser camera system

As an image acquisition device, a 3D line laser camera designed for the optical cutting method was used. The camera was set so as to acquire 800 profiles (3D profiles of the CSG mix moving on the belt conveyor) per second. This means that if the belt conveyor speed is 75 m/min, 0.16-centimeter-wide profiles are acquired (Fig. 6). The camera was installed in a darkroom so that the reflected light can be seen clearly.

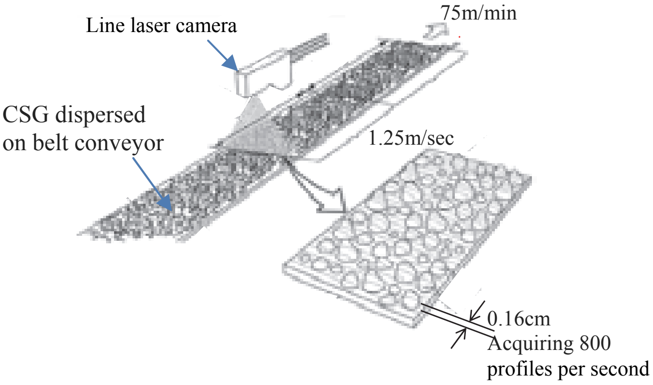
Line laser camera
75m/min
CSG dispersed on belt conveyor
1.25m/sec
0.16cm
Acquiring 800 profiles per second

Figure 6. Optical cutting method using line laser camera

equipment were kept apart, and impact bars were installed to the belt conveyor so as to keep the distance between the conveyor surface and the camera unchanged and keep the surface flat.

3.2. Overview of system performance verification

3.2.1. Material used

The material used for the system performance verification was the same as the CSG mix used for the countermeasure against landslide at Asakawa Dam. The material was smaller-than-80-mm andesite (Neogene volcanic rock) particles obtained by using a mobile screen.

3.2.2. Verification method

Fig.7 illustrates the flow of the verification process.

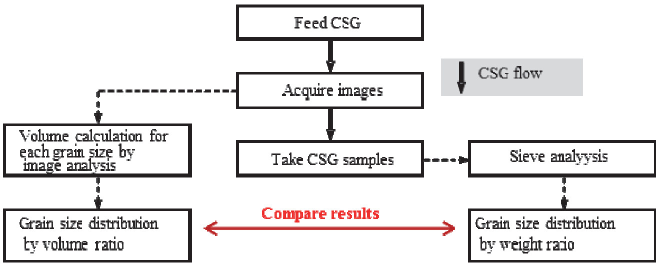
Feed CSG
CSG flow
Acquire images
Volume calculation for each grain size by image analysis
Take CSG samples
Sieve analyysis
Compare results
Grain size distribution by volume ratio
Grain size distribution by weight raio

Figure 7. Field verification flow**Figure 5.** Schematic

To evaluate the influence of differences in the condition of the CSG mix, samples were taken at different locations and verification tests were conducted on different days. Ten samples were measured on each day, and a total of 30 samples were used. Thirty kilograms or more of each sample was used, and, by using all samples collected (about one minute), comparisons were made between the particle size distribution calculated through image processing (a volume ratio based on the height from the belt conveyor surface determined by analyzing the entire image was taken to be the particle size ratio) and the particle size distribution determined through sieve analysis (simplified manual sieve analysis) (see Figs. 8 and 9).

3.3. Field verification result

3.3.1. Grading comparison: image processing vs. sieve analysis

Fig.10 shows the test results of comparison of grading by image processing and sieve analysis. The Case 1 to Case 3 results show the averages of the values obtained from a total of 10 samples in each case. The solid lines show sieve analysis results, and the dotted lines represent volume ratios determined through image processing.

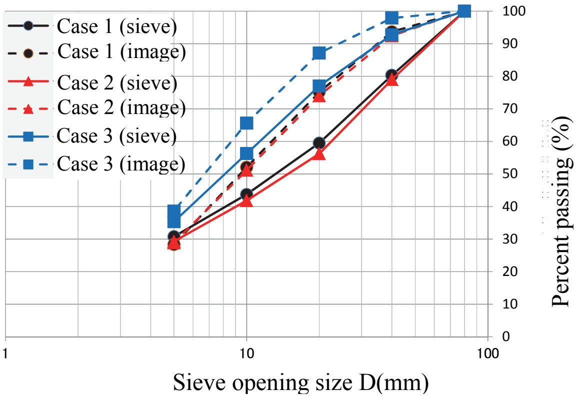

Figure10. Comparison of particle size distribution determined through image processing and sieve analysis

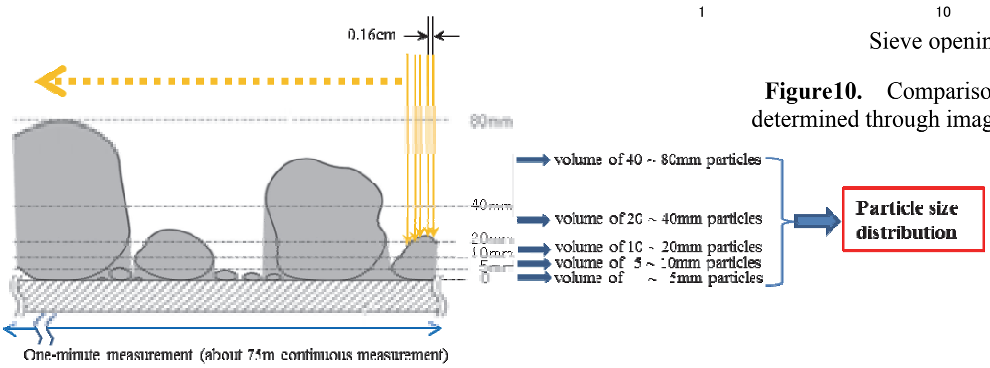
Laser beam
0.16cm
80mm
40mm
20mm
10mm
5mm
0
volume of 40 ~ 80mm particles
volume of 20 ~ 40mm particles
volume of 10 ~ 20mm particles
volume of 5 ~ 10mm particles
volume of ~ 5mm particles
Particle size distribution
One-minute measurement (about 75m continuous measurement)

Figure 8. Schematic view of particle size distribution by volume ratio through image processing

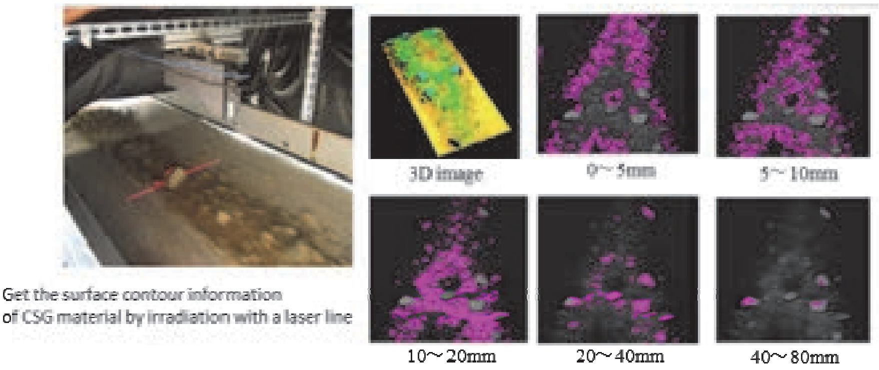
3D image
0~5mm
5~10mm
Get the surface contour information of CSG material by irradiation with a laser line
10~20mm
20~40mm
40~80mm

Figure 9. Slice images showing particles of different sizes acquired with the line laser camera

The particle sizes determined through image processing were obtained by calculating the volume ratio, by equating the distance (height) from the belt conveyor surface with the sieve opening size (5, 10, 20 and 40 mm) used in sieve analysis, from the three-dimensional model obtained through image processing and converting the volume ratio to particle size distribution.

As shown in Fig. 10, the volume ratios obtained through image processing differed considerably from the weight ratios determined through sieve analysis.

The authors thought of the possibility that the density differences among different particle sizes caused the differences mentioned above. Comparison was made, therefore, with the weight ratios obtained by calculating the weight per unit image volume for each particle size category and using the weight thus determined as a coefficient to be multiplied by the volume ratio. The comparison revealed, however, that the differences remained unchanged.

3.3.2. Volume ratio correction based on optimum threshold

The authors then thought that the particle size differences shown in Fig. 10 were attributable to oblateness of CSG particles and decided to make threshold-based corrections when classifying three-dimensional models obtained through image processing.

The reason why the authors thought so is that particle size differences will naturally result if the height from the belt conveyor surface is assumed to be equal to particle size because image acquisition was made when the particles were in a stable condition. To be more specific, the authors thought that if the particles are oblate in shape as shown in Fig. 11, the intermediate edge length *b* should be used as the particle size of the circumscribed rectangular parallelepiped, but actually the shortest edge length *c* was used to determine particle size distribution.

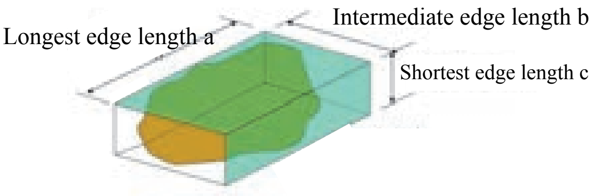

Figure 11. Circumscribed rectangular parallelepiped

Hence, the authors decided to find the threshold that makes the relation "volume ratio = weight ratio" hold true. Although the 30 samples used in the verification experiment had different thresholds, it was decided to use common values (thresholds) obtained through statistical processing. The optimum thresholds used for the verification experiment were 0, 5, 8.5, 14 and 27 mm, while the particle size thresholds used for the sieve analysis were 0, 5, 10, 20 and 40 mm. Fig. 12 compares the volume ratios calculated by using the optimum thresholds and the weight ratios determined through the sieve analysis. As shown, the curves, which showed significant differences in shape in Fig. 12, now show smaller differences.

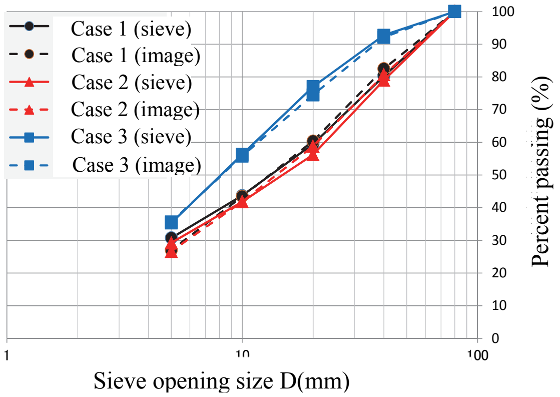

Figure12. Relationship between the optimum threshold-based volume ratio and the weight ratio

Fig.13 shows the cumulative percentages of different particle sizes determined through sieve analysis (weight ratio) and through image processing (volume ratio). The differences were within about ±5%.

The optimum thresholds were calculated as follows. The volume ratio was calculated in steps of 0.5 mm in the height from the belt conveyor surface. Then, a threshold histogram corresponding to the sieve analysis results (weight ratio) was produced, and an optimal value close to the median was taken as the optimum threshold.

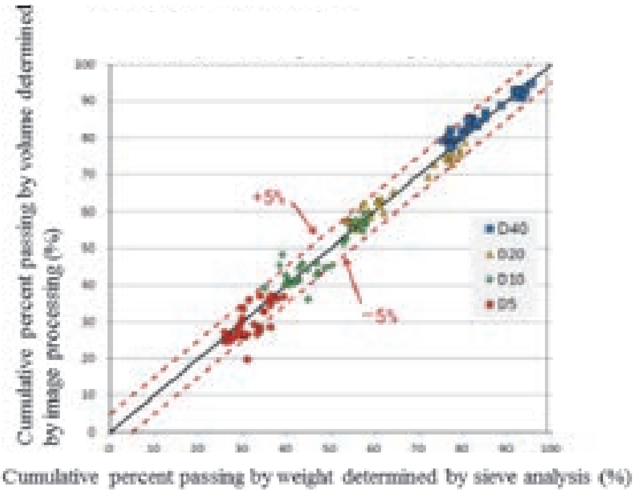

Figure 13. Comparison of particle size distributions: sieve analysis (weight ratio) vs. image processing (volume ratio) (Cumulative percent passing: sieve analysis vs. image processing (Cases 1 to 3))

4. FUTURE OPERATIONAL

There has been growing demand in recent years for labor saving in public works projects because of the shortage of construction workers, as well as for the reduction of cost and environmental stress. In the area of quality control, too, there is a growing need to make redoubled efforts to make automatic instrumentation and real-time management possible.

To meet these needs, the authors have developed a new method for continuous particle size measurement of CSG mixes by use of a three-dimensional image processing system so as to automate particle size measurement and reflect measurement results in construction work in real time.

The newly developed technology makes high-accuracy measurement possible by performing the simple and easy-to-understand task of calculating the volume of mechanically dispersed earth material by use of a commercially available camera and processing the obtained results statistically.

Since the profile of irradiated line laser light is recorded with a 3D line laser camera, measurement results are not affected by such factors as background color, lighting conditions, the color and shade of the subject, and sticking dirt.Particle size measuring systems using conventional image processing technology are not capable of real-time measurement because edge processing is time-consuming. The new system performs all processing tasks from 3D surface profile data acquisition to the conversion from particle size–volume data based on optimum thresholds and the calculation of particle size distribution (weight ratio) in several seconds.

The authors believe that the technology can be applied to not only the CSG method but also other construction methods that use mixtures of ordinary earth materials and cement.

The new system has made it possible to monitor particle size control, which at present can only be performed after placement, in real time. The method of facilitating the management of the moisture content of embankment material by using such instruments as nuclear gauges has already been put to practical use. The authors believe that since particle size and moisture content can be controlled in real time, it is now possible to automatically adjust the quantities of cement and water to be added to the mix being used according to the measured weight of the material on the belt conveyor. It is hoped that the newly developed method is utilized to make fully automated production of cement-based mixes possible.

5. CONCLUSIONS

The knowledge gained from the development of the new system and the field test conducted at Asakawa Dam in connection with countermeasure against landslide using CSG:

(1) Application to various sites and materials made possible by simple image acquisition settings.

Measurements can be obtained simply by dispersing the CSG mix by use of a belt feeder (1 m/min) and a high-speed belt conveyor (75 m/min).

(2) Speedy data acquisition without using sophisticated analysis program (image analysis based on the volume ratio instead of the area ratio).

It is now possible to acquire data in one minute and output particle size distribution measurement results in real time.

(3) Continuous 100% measurement

The new system determines particle size distribution from the volume of all CSG mix put into the testing apparatus. The quantity of samples analyzed, therefore, is always greater than the minimum quantity of samples that need to be taken. As a result, measurement results are free from the influence of uneven sampling and sample quantity, and measuring accuracy is improved (the system is capable of measuring 100 kg or more per minute of CSG mixes).

(4) Simple calibration

In preparation for measurement by use of the new system, image volume is determined in steps of 0.5 mm in the height from the belt conveyor surface from the three-dimensional surface profile of the CSG mix passing in the specified time period (one minute), and the obtained values are compared with the measured values (particle size data) obtained in advance through sieve analysis. The heights thus determined as the values closest to the particle size distribution are regarded as optimum thresholds. In about one day prior to system operation, optimum threshold heights can be determined by carrying out calibration for about 30 samples. Since the differences between the measurement results obtained from the new system and the measurement results obtained through sieve analysis are within about 5%, the proposed method can be used as a particle size measuring method in place of sieve analysis.

(5) Quality control through real-time particle size measurement.

The new system is capable of converting one-minute measurement results in a short period of time (about one minute) for comparison with the specified range. Particle size management can be performed in real time instead of in an ex post facto manner. If particle size distribution is likely to deviate from the specified range, the quality control manager is automatically notified in real time so that corrective action can be taken in a timely manner.

ACKNOWLEDGEMENT

The authors would like to express their heartfelt appreciation to the members of the Nagano Construction Office (Asakawa Dam) of the Nagano Prefectural Government for the materials and test yard generously made available in connection with the field tests conducted for the purposes of the development of the new system.

REFERENCES

Fujisaki, K., Kuronuma, I., Kawano, K. and Takei, A. (2013): Fluctuation monitoring system for pparticle size distribution of CSG materials using digital image analysis, Journal of Japan Society of Dam Engineers, 23(1), 19–26 (in Japanese).

Eda, M., Arai, H., Katayama, S. and Yoshida, H. (2014): Development of the continuous pparticle size distribution analysis system by digital Image analysis, Journal of Japan Society of Dam Engineers, 24(2), 84–93 (in Japanese).

4th APG Symposium and 9th EADC on

INNOVATIVE TECHNOLOGIES FOR DAMS AND RESERVOIRS TOWARD THE FUTURE GENERATIONS

Seismic Evaluation of an Inclined Cored Rockfill Dam using Innovative Centrifuge Modeling

D.S. PARK & N.R. KIM
K-water Institute, Daejeon, Republic of Korea
fulgent@kwater.or.kr

ABSTRACT:
The purpose of this study is to evaluate seismic safety of an inclined cored aging rockfill dam (H of 131m) under strong seismicity using innovative dynamic centrifuge modeling. Because of uncertainty, two cases for the dam were modeled - reasonably competent rockfill model and less competent rockfill model by adjusting the density or stiffness of model rockfill material. A series of laboratory tests for three main materials used for dynamic centrifuge modeling were conducted. Applying geometry similitude, stiffness matching technique, and generalized scaling laws, the tests were conducted successfully. Measured peak base motion reached up to about 1.0g. As a result, upstream slope with less compaction can be relatively more vulnerable to deform than downstream slope. Excess pore pressure was not generated significantly within clay and filter layer. Displacement for the model with R_D = 85% was much greater than the model with R_D = 95%. Some longitudinal tension cracks and upstream side decent slope sliding were observed for less competent rockfill. In either case, freeboard was remained safe. Amplification ratio of peak acceleration from crest to base was about 1.7. The results will produce complementary technical aspects for seismic safety in accordance with numerical modeling.

Keywords: seismic, dynamic model, fill dam, earthquake, centrifuge

1. INTRODUCTION

The dynamic safety of an aging fill dam, located in an area of high seismicity, is of utmost importance. The purpose of this study is to evaluate seismic safety of an inclined cored aging rockfill dam under very high PGA (peak ground acceleration) using innovative dynamic centrifuge modeling.

Centrifuge modeling technique has advantages in seismic evaluation of large embankment (Baziar et al. 2009, Kim et al. 2011, Kutter and James 1989, Kutter 1984). It can apply various type of earthquake motions and different intensities. It can provide optimum and more convincing results after comparing with detailed numerical analysis. It may also provide the optimal reinforcing method of the dam through validation of seismic dam performance before and after seismic reinforcement, if required. The idea of using centrifuge as a physical modeling is to produce a realistic stress distribution in controlled experiments with well-defined boundary conditions and material properties. Identical stress field between model and prototype is particularly important because strength, stiffness, dilatancy, void ratio of soil have nonlinear dependences on effective stress. Thus, modeling accuracy is enhanced by stress similarity (Garnier 2006, ISSMGE TC2 2007, Taylor 1995).

Dynamic centrifuge modeling in this study aims to study only for the strong shaking induced deformation and stability of the dam. In this study, geometry similitude with the same upstream and downstream slope angles was taken for similitude. Innovative generalized scaling relations suggested by Iai et al. (Iai et al. 2005) were adopted to accommodate relatively massive dam structure in a model with reduced scale. The materials used for core and shell layer were reasonably scaled down to represent similar mechanical behavior of the prototype dam materials. Because of uncertainty, two cases for the dam were modeled - reasonably competent rockfill model and less competent rockfill model by adjusting the density or stiffness of model rockfill material. Measured dynamic performance of the AG dams during centrifuge modeling provides us with unique observations for inclined cored rockfill embankment shaken by inexperienced substantially large shaking, accounting for the effect of the degree of density of shell. Important observation and finding are summarized as a result of state-of-the-art dynamic centrifuge modelling for an inclined cored rockfill dam.

2. DYNAMIC CENTRIFUGE MODEL

2.1. Outline

An AG dam is a 131m high dam (marked as AGM) as shown in Fig. 1 and Fig. 2. The dam has been in operation since 1967. The potentially active fault segment passes within 250 m of the left abutment of the saddle dam, which the dam must be able to withstand it safely (EDCOP and T&T 2012). The PGA (peak ground acceleration) of MCE (maximum credible earthquake) level recently determined is remarkably high as 0.94g (Pöyry Energy Ltd., 2015).

Figure 1. Upstream and downstream slope of AG dam

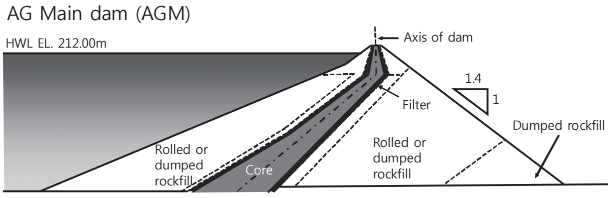
AG Main dam (AGM)
HWL EL. 212.00m
Axis of dam
1.4
1
Filter
Dumped rockfill
Rolled or dumped rockfill
Core
Rolled or dumped rockfill

Figure 2. A typical cross-section of the AG main dam

2.2. Geo-centrifuge Facility

For dynamic centrifuge modeling with a high peak acceleration as 0.94 g, a state-of-the-art large-scale centrifuge facility was adopted at K-water Center for Centrifuge Modeling (KCCM) (Fig. 3). K-water centrifuge has an 800g-tons payload capacity, 8.0m platform radius, 2.0m(L) × 2.0m(W) × 2.0m(H) large platform dimension. For seismic evaluation, a large scale uniaxial servo hydraulic in-flight earthquake simulator has been equipped with 1.6m(L) × 0.8m(W) experimental platform. The earthquake simulator can simulate maximum 22g horizontal base motion in sinusoidal waveform to shake 1500 kg payload. The maximum shaking acceleration level is 60g without payload mass.

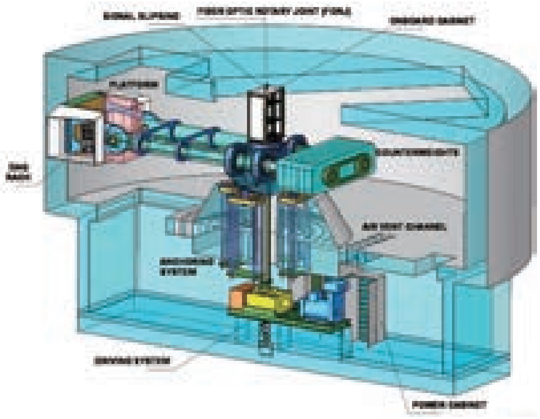
SIGNAL SLIPRING
FIBER OPTIC ROTARY JOINT (FORJ)
ONBOARD CABINET
PLATFORM
COUNTERWEIGHTS
AIR VENT CHANNEL
DRIVING SYSTEM
POWER CABINET

Figure 3. K-water geo-centrifuge facility

2.3. Design of Centrifuge Model

The design of dynamic centrifuge modeling for AG dam was carefully planned to have the same geometry shape as the prototype. For the geometry of AG dam, the upstream slope is much flattened comparing to the downstream slope. Main control variable was the compaction degree of rockfill due to uncertainty of in-situ embankment density. Thus, we designed two cases for the dam models with reasonably competent rockfill and less competent rockfill by adjusting the density or stiffness of model shell material (Table 1). In Table 1, AGM1 test was done as a dummy test for shaker calibration. It was intended for the verification of design parameters of test series and calibration of earthquake simulator.

Table 1. Test series for centrifuge modeling of AG dam

ID	Contents
AGM1	dummy test for shaker calibration
AGM2	with competent rockfill
AGM3	with less competent rockfill

For the dynamic centrifuge modeling of AG dam, the key points to observe were seismic amplification, earthquake induced settlement, deformation, and excess pore pressure response within the core and shell.

Instrumentation layout is composed of multiple accelerometers, pore pressure transducers, and displacement transducers. Since the model core and shell layer is significantly compacted to reach the target relative compaction, some embedded miniature accelerometers and pore pressure transducers are expected to be mal-functioning, out of order, or damaged. Thus, a pair of sensors was installed at the same depths in parallel (Line 1 and 2 in Fig. 4).

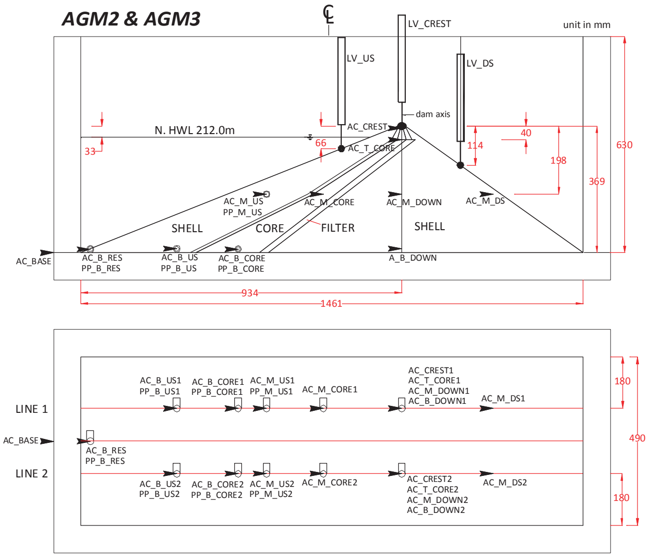
AGM2 & AGM3
℄
LV_CREST
unit in mm
LV_US
LV_DS
dam axis
N. HWL 212.0m
AC_CREST
AC_T_CORE
33
66
40
114
198
369
630
AC_M_US
PP_M_US
AC_M_CORE
AC_M_DOWN
AC_M_DS
SHELL
CORE
FILTER
SHELL
AC_BASE
AC_B_RES
PP_B_RES
AC_B_US
PP_B_US
AC_B_CORE
PP_B_CORE
A_B_DOWN
934
1461
LINE 1
AC_B_US1
PP_B_US1
AC_B_CORE1
PP_B_CORE1
AC_M_US1
PP_M_US1
AC_M_CORE1
AC_CREST1
AC_T_CORE1
AC_M_DOWN1
AC_B_DOWN1
AC_M_DS1
180
AC_BASE
AC_B_RES
PP_B_RES
490
LINE 2
AC_B_US2
PP_B_US2
AC_B_CORE2
PP_B_CORE2
AC_M_US2
PP_M_US2
AC_M_CORE2
AC_CREST2
AC_T_CORE2
AC_M_DOWN2
AC_B_DOWN2
AC_M_DS2
180

Figure 4. Dimension and sensor layout, unit in mm

Adopted design drawings for dynamic centrifuge modeling is shown in Fig. 4. Accelerometer is denoted as "AC", pore pressure transducer as "PP", and displacement measuring LVDT as "LV" in the first two letters of each label. A high speed video camera was installed to capture every detail of a model dam during strong shaking. A rectangular type of rigid container box was used for modeling with the inner dimension of 1.461m (L) * 0.49m (W) * 0.63m (H).

A series of laboratory tests for three main materials (core, filter, and shell) used for dynamic centrifuge modeling were conducted. For core material, sieve analysis and hydrometer test were done together for gradation curve plotting. Atterberg limit tests and specific gravity test were also done for clay core. To determine the optimum water content, maximum dry unit weight of soil and relative density, standard compaction tests were executed for both core and shell materials. Fine sand was used for the construction of filter and transition zone. Sieve analysis was done for fine sand.

Since the stiffness of the shell in physical modeling is critical to match similitude with in-situ prototype, a special large-scale resonant column test for the shell material was conducted to fit the stiffness of model shell using adjustment of relative compaction during construction. The description of K-water large-scale resonant column test apparatus is seen in Ha and Kim (Ha and Kim, 2013).

The following Table 2 exhibits main results of material properties used in the centrifuge modeling. Based on the compaction test result, OMC (optimum moisture content) were determined as 18.2% and 6.3% for clay core and shell, respectively.

Table 2. Material condition applied for AG dam models.

Zone	Item	AGM2	AGM3
Core	$\gamma_{d,max}$ (kN/m^3)	16.22	16.22
	w (%)	18.2	18.2
	R_D (%)	95	95
	γ_t (kN/m^3)	18.21	18.21
	W (kg)	26.53	26.53
Shell	$\gamma_{d,max}$ (kN/m^3)	21.89	21.89
	w (%)	6.3	6.3
	R_D (%)	95	85
	γ_t (kN/m^3)	22.11	19.78
	W (kg)	254.31	227.54

Note, $\gamma_{d,max}$ = maximum dry unit weight of soil, w = water content, R_D = relative compaction, γ_t = total unit weight of soil, and W = total weight of modeling material.

In out model, 30g centrifugal acceleration was also chosen to apply such an extremely high peak ground acceleration of 0.94g in prototype scale, considering the maximum capacity of earthquake simulator.

Regarding the scaling, generalized scaling relations for dynamic centrifuge tests suggested by Iai et al. (2005) were applied because of massive prototype structure. Iai et al. (2005) derived scaling factors for cases that ordinary scaling principles for centrifuge test cannot be directly applied because of either the limitations of testing machine or the largeness of prototype structure by combining scaling principles for 1g shaking table tests and Ng dynamic centrifuge tests. The proposed models in this study represent virtual prototypes of 1/11 scaled AG main dam.

Dam model construction was divided into multiple stages. Inclined cored rockfill dam models including zones of core, filter, and shell were prepared with the same geometry shape as prototype. The weight of each material was calculated based on preliminary compaction test results. For clay material preparation, real core material collected from existing earth-cored dams in Korea was instead used because it was not permitted to take out core material from AG dam. Shell material was obtained by sieving subgrade layer gravels. The maximum diameter was set up to 20 mm for the shell.

To reasonably simulate dam construction density, we used 95% of relative compaction for AGM2. For AGM3, much lower relative compaction of shell (= 85%) was applied just for comparison.

Before dynamic shaking of AG dam model, we needed to stabilize the model dam due to increase of gravitational force on the model dam. Water was not impounded at the initial static spin-up. After stabilizing the model dam body at 30g, all sensors were initialized again and reservoir water was impounded up to NHWL (Normal High Water Level), which is a target reservoir water level. To mimic consolidation and steady state seepage conditions, the model stayed for a couple hours at 30g with water. During this period, seepage induced pore pressure response was carefully monitored until converging.

Then dynamic shaking was applied with a previously calibrated strong motion directly. To achieve this method, the earthquake simulator must be calibrated before test with dummy testing model. During shaking motion, acceleration, pore pressure, displacement as well as high speed video were recorded more than 1000 samples/s/ch.

As an input earthquake motion, Rudbar-T motion (PGA = 0.94g, significant duration = 33s, predominant period = 0.19s, predominant frequency = 5.3 Hz) was edited for physical modeling purpose, considering the realistic capacity of the shaker (Fig. 5). Though the earthquake simulator at K-water Institute is one of the biggest in-flight shakers in the world, it should be noted that there need to be a reasonable compensation to account for dynamic characteristics of the system of model and safety measures of the machine. Thus, the cut-off frequencies of input motion are 20 and 400~600 Hz at high g-level in consideration of resonant frequency of the system, ambient noise level, and mechanical challenge to generate very high frequency content).

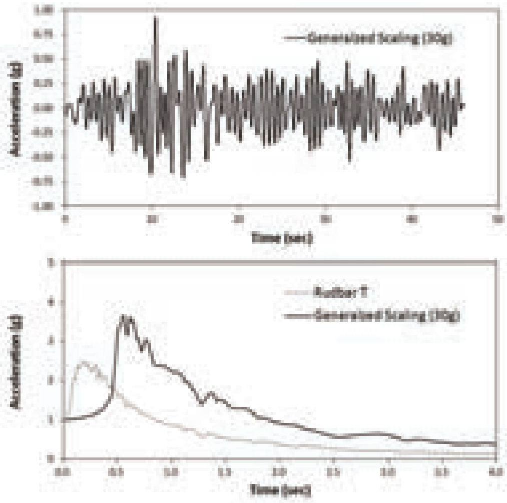

Figure 5. Target input motion applied for dynamic shaking for the dam model.

3. RESULTS

Data reduction was performed for a lot of dynamic event data obtained from measurement of accelerometers, pore pressure transducers, and LVDTs. The results of dynamic centrifuge modeling for AG main dam are briefly summarized as the Table 3. In the Table, a_{max} is the peak acceleration measured, T_p is predominant period obtained from ARS (acceleration response sprectrum), I_a is Arias Intensity, US means upstream slope, and DS means downstream slope.

Table 3. A summary of acceleration amplification and displacement induced by dynamic shaking

Model		AGM2	AGM3
Shell R_D (%)		95	85
a_{max} (g)	Base	1.010	1.041
	Crest	1.769	1.762
	Ratio	1.8	1.7
T_p (s)	Base	0.653	0.634
	Crest	1.351	1.379
	Ratio	2.1	2.2
I_a (m/s)	Base	0.423	0.338
	Crest	0.847	1.730
	Ratio	2.0	5.1
Settlement (cm / %H)	Crest	46-55 (0.36-0.43)	91-95 (0.71-0.74)
	US	18-39 (0.14-0.31)	216-295 (1.7-2.3)
	DS	26-28 (0.20-0.22)	86-108 (0.67-0.85)
Remark		Moderate US sliding	

3.1. AGM2

As a result of AGM2 modeling, the model dam was reasonably safe under the measured peak acceleration of the base of 1.010 g (taking datum as AC_B_DOWN1), which exceeds the target peak acceleration, 0.94 g. Relative compaction of shell material was 95% considering the configuration of well-compacted rockfill during construction. There was no significant slope sliding or considerable permanent displacement. The crest acceleration measured was recorded up to 1.769 g, which is about 1.75 times the base peak acceleration (Table 3, Fig. 7). Shaking amplification from the base up to the middle portion was not so higher (e.g., a_{peak} at AC_M_US1 = 1.169 g), but most amplified motion is observed around the upper top area. Arias Intensity (I_a) becomes also greater at the crest (at about twice the base I_a). Predominant period at the crest (= 1.35 s) computed by response spectra analyses becomes longer comparing to the base motion (= 0.65 s) (Table 3 and Fig. 8). It means that the upper part near the crest becomes relatively weaker in terms of dynamic stiffness.

Crest settlement was recorded up to 46 – 55cm. It corresponds to 0.43% of model dam height in maximum. Settlements of upstream and downstream slopes are decently less than those of crest (Table 3 and Fig. 9). Horizontal permanent displacement was to be measured by laser displacement sensors, but they did not work at 30 G of centrifugal field.

It was interesting to investigate pore pressure response during strong shaking within shell and core layers. Many pore pressure transducers above the phreatic line were not measured any meaningful values. The maximum r_u (excess pore pressure ratio) reached merely up to 44% near the contact area of core and container, and most sensors showed much less values. It means that strong motion does not induce significant excess pore pressure within well-compacted plastic clay core. If we can assume clay core is reasonably in sound condition in-situ, highly strong dynamic shaking does not significantly affect the generation of excess pores pressure of shell either. Because shell material is a kind of free draining material, excess pore pressure is quickly dissipated.

3.2. AGM3

The AGM3 model simulates the AG Main dam with less competent shell material, which has lower relative density and stiffness. Relative compaction of shell material was 85%, which falls in a highly conservative assumption. Identical input motion was applied as AGM2. Earthquake shaking was conducted up to about 1.0g peak acceleration level in prototype scale.

The crest acceleration was measured up to 1.762 g, which is about 1.7 times the base peak acceleration (Table 3 and Fig. 7). In view of peak acceleration, amplification from the base to the middle of the embankment remains relatively stable (1.041g at AC_B_DOWN1 to 1.018g at AC_M_CORE1), but the most amplification occurred at the upper crest region. In terms of Arias Intensity (I_a), amplified crest I_a is 1.73 m/s (5.1 times greater) whereas the base I_a is 0.338 m/s. Predominant period from the base to the crest is also shifted to longer period (0.63 s to 1.38 s) (Table 3 and Fig. 8).

In overall, though some longitudinal tension cracks and comparable permanent displacement were observed around the crest, upstream slope and downstream slope, the embankment was not severely damaged to cause an uncontrolled reservoir water release (Fig. 6). Settlement and/or displacement level seemed still acceptable, but the amount of deformation was far greater than AGM2 model with competent rockfill. From the photos, longitudinal cracks near the dam crest and curved LVDT extension rod were observed.

Obviously displacement for AGM3 (R_D = 85%) is much greater than AGM2 (R_D = 95%). Crest settlement was recorded up to 91 - 95cm (0.71 – 0.74% H). Settlements of downstream slope were about 86 – 108cm (0.67 – 0.85% of H). Settlements of upstream slopes were about 2.16 to 2.95m (1.7 – 2.3% H), which implies deformation or sliding of slope induced by strong shaking (Fig. 9).

It is of particular interest to observe significantly larger deformation on the mild upstream slope (1 : 2.5) than the much steeper downstream slope (1 : 1.4). Based on the visual inspection and data analysis, sliding deformation possibly occurred on the upstream side (Fig. 6). It indicates that the saturated less compacted upstream shell can be much more vulnerable to strong shaking than the steeper downstream slope possibly due to the effect of pore pressure. It appears apparent that the deformation concentrates on the upper crest region of the dam model, and this is consistent with observed case studies from strong earthquake shaking. Though there was comparable deformation for AGM3 model, inclined core layer remains to be valid as a water barrier.

Analysis of pore pressure response showed that the maximum estimated r_u (excess pore pressure ratio) reached merely up to 12% at PP_B_US2 sensor, and most sensors showed much less values. It means that strong motion does not induce significant excess pore pressure even for the embankment of relative compaction of 85% shell. If we can assume clay core is reasonably in sound condition in-situ, highly strong dynamic shaking does not significantly affect the generation of excess pores pressure. Because shell material is a kind of free draining material, excess pore pressure is quickly dissipated. Note that many pore pressure sensors were not measured on the downstream side of shell or filter layer, which implicates phreatic line was reasonably formed along the inclined core layer and it worked well for steady state seepage.

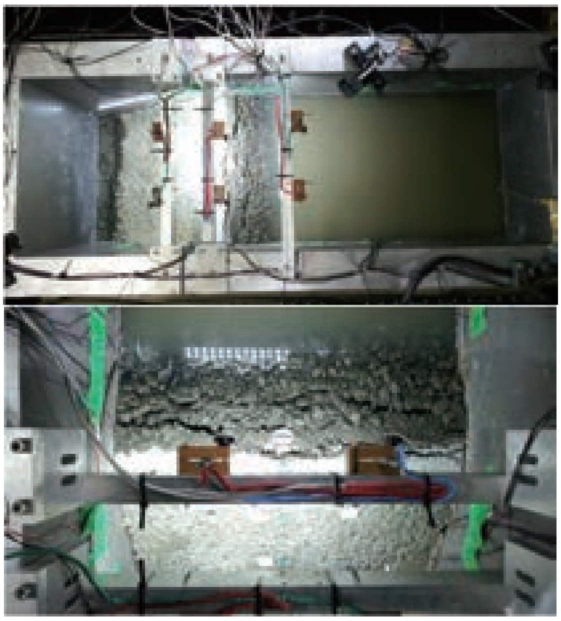

Figure 6. Deformation after strong shaking for AGM3

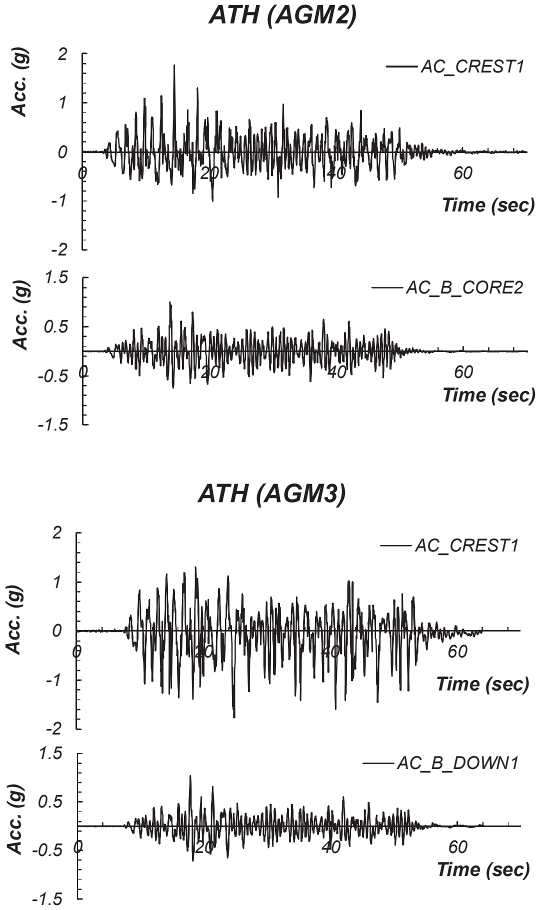

Figure 7. Recorded acceleration time histories and amplification of motion

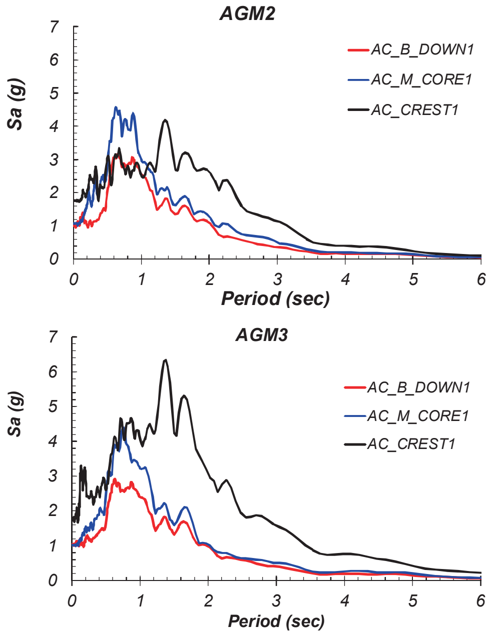

Figure 8. Measured acceleration response spectra

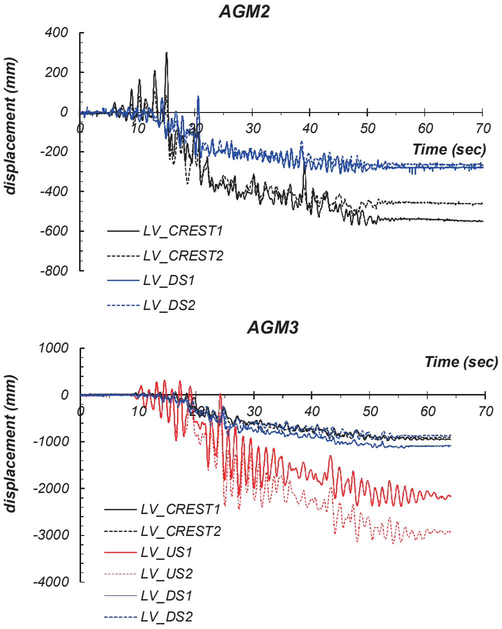

Figure 9. Recorded settlement time histories

4. CONCLUSION

Applying geometry similitude, stiffness matching technique, and generalized scaling laws, dynamic centrifuge modelling was conducted successfully for an inclined cored rockfill dam. Measured peak base motion reached up to about 1.0g, which is higher than the target g-level (0.94g). Through the centrifuge tests, the following observations and findings are obtained.

In overall, the model dams were a lot resistant to the strong shaking under the PGA of about 1g. Amplification ratio of peak acceleration from crest to base was about 1.7 for main dam models. Excess pore pressure was not generated significantly within clay and filter layer. Though the maximum excess pore pressure ratio measured was up to about 44~54% near the interface of core and base rock or container, but in most cases, the values were a lot lower. Obviously displacement for the model with R_D = 85% was much greater than the model with R_D = 95%. But, in either case, still freeboard was remained safe. Some longitudinal tension cracks and upstream side decent slope sliding were observed for less competent rockfill. Though downstream slope angle is much steeper than upstream slope, dynamically induced deformation shows that upstream slope with less compaction can be relatively more vulnerable to deform than downstream slope. The results will produce complementary technical aspects for seismic safety in accordance with numerical modeling.

ACKNOWLEDGEMENT

The dynamic centrifuge modelling was conducted by the agreement with Pöyry Energy Ltd., Thailand (2015) as a part of Angat Dam Rehabilitation Study, which was prepared for Angat Hydropower Corporation (AHC). The data report was reviewed by Dr. Shin, Dong-Hoon at K-water, Stefan Ehlers at Pöyry. Mr. Gu, Bang-Seo and Mr. Ahn, Tae-Sung at K-water helped model construction work. All their helps are greatly appreciated. Any opinions, findings, conclusions, or recommendations expressed herein are the authors' and do not necessarily reflect the views of Pöyry or AHC.

REFERENCES

Baziar, M., Salemi, S. and Merrifield, C. (2009): Dynamic centrifuge model tests on asphalt-concrete core dams, Géotechnique, 59:9, pp. 763-771.

Kim, M.-K., Lee, S.-H., Choo, Y. W. and Kim, D.-S. (2011): Seismic behaviors of earth-core and concrete-faced rock-fill dams by dynamic centrifuge tests, Soil Dynamics and Earthquake Engineering, 31:11, pp. 1579-1593.

Kutter, B.L. and James, R. (1989): Dynamic centrifuge model tests on clay embankments, Géotechnique, 39:1, pp. 91-106.

Kutter, B.L. (1984): Earthquake deformation of centrifuge model banks, Journal of Geotechnical Engineering, 110:12, pp. 1697-1714.

Garnier, J. (2006): Development of centrifuge modelling in geotechnics, K-water International Seminar on Geo-Centrifuge, Daejeon, South Korea.

ISSMGE TC2 (2007): Catalogue of scaling laws and similitude questions in centrifuge modelling, Physical Modelling in Geotechnics.

Taylor, R.N. (1995): Centrifuges in modeling: principles and scale effects, Geotechnical Centrifuge Technology, Taylor, R.N. ed., Blackie Academic & Professional.

Iai, S., Tobita, T. and Nakahara, T. (2005): Generalised scaling relations for dynamic centrifuge tests, Géotechnique, 55:5, pp. 355-362.

EDCOP and T&T (Engineering and Development Corporation of the Philippines and Tonkin & Taylor International Ltd.) (2012): Study of Angat Dam and Dyke Safety, final report, A report prepared for PSALM (Power Sector Assets and Liabilities Management Corporation and MWSS (Metropolitan Waterworks and Sewerage System).

Pöyry Energy Ltd. (2015): Angat dam rehabilitation study.

Ha, I.-S. and Kim, N.-R. (2013): Dynamic deformation properties of coarse granular materials with respect to gradation characteristics, Journal of the Korean Geotechnical Society, 29:8, pp. 5-14.

Reduction of Ground Water Flow by Promoting Clogging Effect of Soil Particles

T. Tamai
TEPCO Power Grid, Tokyo, Japan
tamai.takeshi@tepco.co.jp

T. Shiono, N. Sorimachi, T. Tsukada & F. Kawashima
Tokyo Electric Power Company Holdings, Tokyo, Japan

ABSTRACT:
Grouting was conducted to reduce groundwater flow in the bedrock of a reservoir of a pumped storage power plant, located in the site where the ground water level is low. We conducted grouting around the bottom of the reservoir, due to difficulty of forming the grout curtain reaching the low permeable layer of the bedrock. To reduce the permeability of bed rock with the smaller volume of grout, we invented a method to promote clogging effect artificially by spreading soil particles into reservoir water. The soil particles were obtained from the residual horticultural soil after being screened, collected near the reservoir, in order to reduce the cost. This paper summarizes the results and evaluation of laboratory tests, field tests and application of the invented method.

Keywords: soil particles, clogging, groundwater flow, reservoir, grouting

1. OUTLINE OF CLOGGING PROMOTION METHOD

Grouting was conducted at Yashio dam reservoir, the upper reservoir of the Shiobara pumped storage power plant of Tokyo Electric Power Company with a maximum output of 900 MW, in order to reduce relatively large amount of water leakage seeping into the bedrock of the reservoir. Curtain grouting was abandoned because of the high permeability rock existed so deep under the bed rock that it was difficult to extend the curtain grouting to low permeable rock layer. Therefore, instead of curtain grouting, we planned to apply grouting at the bottom of the reservoir, encircling from both banks, as shown in Fig. 1(a) and 1(b) (Kawashima, F., et al. 2010).

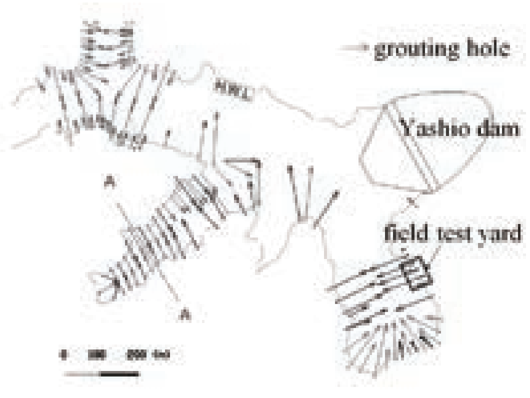

Figure 1(a). Design of the grouting (Plan)

However, since the grouting area was large, we considered relatively wide spacing between each grouting hole, for rough grouting. In addition, we made a study on an auxiliary method to promote clogging artificially by spreading fine soil particles in the reservoir (hereinafter referred to as the clogging promotion method).

Since large amount of soil particles were expected to be used by the clogging promotion method, materials were to be obtained at lowest cost possible. Surveys were made to seek for applicable materials around the site, since few soil particles were available near the site. (Asphalt facing was adopted at Yashio Dam because few core materials were available in the vicinity.) Surveys revealed that screened soil particles were discarded at a horticultural soil plant (known as Kanumatsuchi), located 40 km from the dam site. Kanumatsuchi is sandy, volcanic cohesive soil.

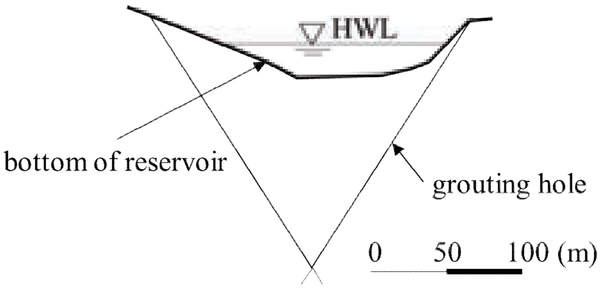

Figure 1(b). Design of the grouting (A-A cross section)

The density of screened soil particle is 2.5 g/cm^3, including twenty percent of particles smaller than five micro meters, and did not contain toxic substances. These characteristics are suitable for the material of promoting clogging method. In addition, stable supply of 20 to 30 m^3/day was ensured.

2. FIELD TEST OF CLOGGING PROMOTION METHOD

2.1. Field test of clogging promotion method

Soil particles were mixed with water and turned into slurry, transported by a barge, and spread into the reservoir. As for the concentration of soil particle slurry, a flow time of ten seconds or less had to be achieved in order to pump through pipes, referring to the performance of cement milk used for grouting. In addition, the ratio of soil particles to water (S:W) was applied at 1:2, so as to minimize the capacity of the barge for transporting soil particle slurry. The applied ratio of S:W = 1:2 proved to achieve the flow time of ten seconds or less, after mixing the slurry for approximately ten minutes.

The field verification tests were conducted for clogging promotion method. The method settles out the soil particles naturally. The verification tests were conducted in the area encircled by net, to prevent soil particles from diffusing throughout the reservoir, as shown Fig.2.

To keep turbidity of the reservoir by soil particles as long as possible, for effective clogging, input rate of slurry was examined. Input rate of slurry was measured at the point when slurry is distributed uniformly inside the net (hereinafter referred to as standard turbidity). Turbidity was measured at a water depth of approximately six meters. Fig. 2 shows the method of spreading soil particles in the reservoir.

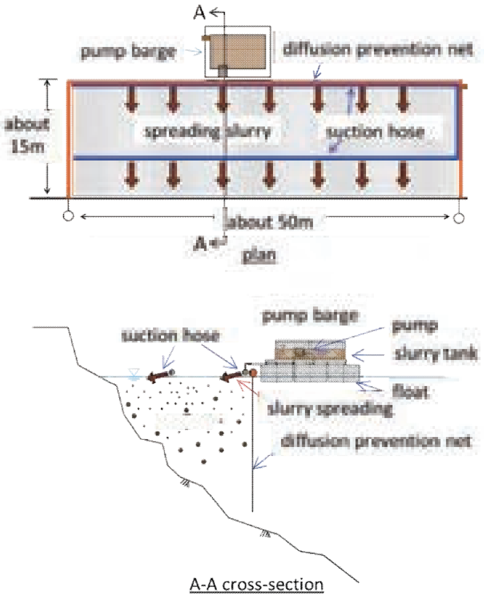
A
pump barge
diffusion prevention net
about 15m
spreading slurry
suction hose
about 50m
A
plan
suction hose
pump barge
pump
slurry tank
float
slurry spreading
diffusion prevention net
A-A cross-section

Figure 2. Outline of spreading soil particles

2.2. Study of standard turbidity

Fig. 3 shows the time history of turbidity, varying with standard turbidity, and integrated turbidity (turbidity multiplied by time).

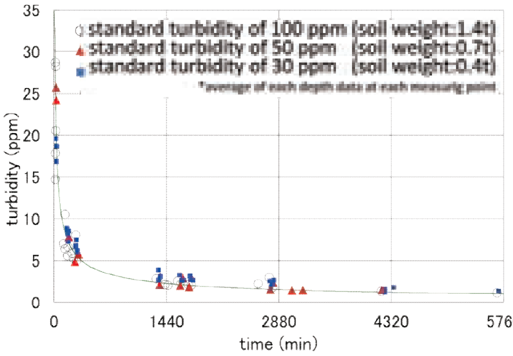

standard turbidity (ppm)	integrated turbidity (ppm·day)			
	0-24hr	24-48hr	48-72hr	72-96hr
100	6	2	2	1
50	5.2	2	2	1
30	5.2	2	2	1

Figure 3. Result of field tests (time history of turbidity of each initial turbidity case)

Immediately after the input, turbidity varied according to standard turbidity, however, turbidities in all cases became nearly equal after approximately two hours. In addition, turbidity decreasing curves were all similar in shape, and integrated turbidity had little or no difference. Based on the results, standard turbidity of 30 ppm was adopted. On the other hand, laboratory tests were conducted to verify the reason why standard turbidity had no influence on turbidity decreasing curves, using the equipment shown in Fig. 4.

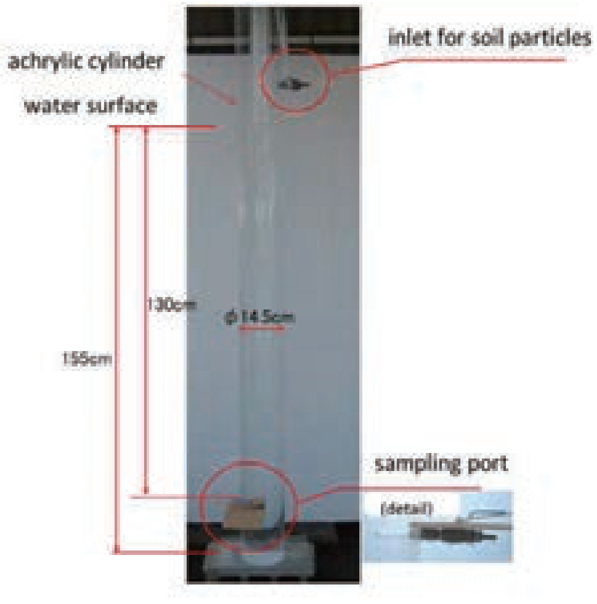
achrylic cylinder
water surface
inlet for soil particles
130cm
φ14.5cm
155cm
sampling port
(detail)

Figure 4. Outline of the equipment of laboratory test (particle settling test)

Tests were conducted at standard turbidities of 1000, 500, 100 and 30 ppm. Visual inspection of soil particles' settlement confirmed that settlement of relatively large soil particles creates a wake flow, which draws in small particles subsequently. It was therefore assumed that wake flow have outstanding effect, and that maintaining turbidity is difficult where large particles are included. Based on the above results and economic efficiency, standard turbidity of 30 ppm was adopted.

3. VERIFICATION OF CLOGGING IN CRACKS

Tests using parallel plates, for simulating cracks, were conducted to verify two aspects of the clogging using soil particles. One is the influence of the width of the crack, and the other is the influence of back pressure. The influence of back pressure was examined since the reservoir of a pumped storage power plant have rapid drawdown, causing back pressure, which may wash out the clogged particles. Fig. 5(a) and 5(b) shows the description of test equipment.

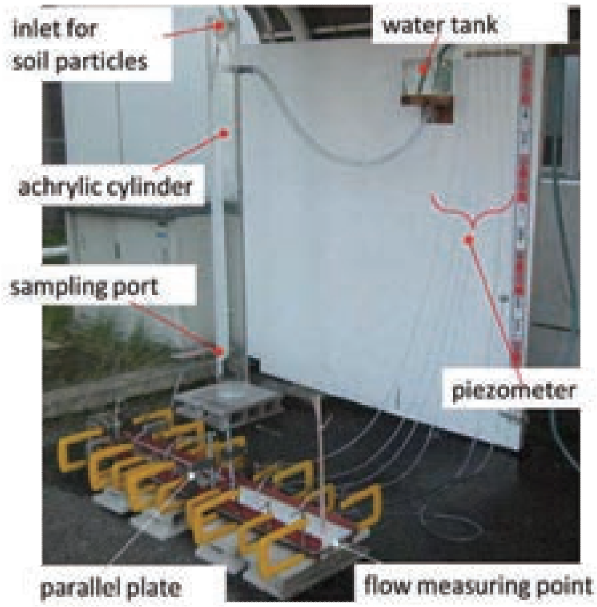

Figure 5(a). Equipment of laboratory tests

Table 1. Condition of laboratory tests in each case

		The velocity ratio of each case against the velocity of the case 2		
		0.75	1	1.5
area/slit	1mm^2 (a=1 × b=1mm)	CASE 1 number of slit : 12 sectional area of slit : 12mm^2 initial flow: 600ml/min.	CASE 2 number of slit : 9 sectional area of slit : 9mm^2 initial flow: 600ml/min.	CASE 3 number of slit : 6 sectional area of slit : 6mm^2 initial flow: 600ml/min.
	2mm^2 (a=1 × b=2mm)		CASE 4 number of slit : 5 sectional area of slit : 10mm^2 initial flow: 670ml/min.	CASE 5 number of slit : 3 sectional area of slit : 6mm^2 initial flow: 600ml/min.
	4mm^2 (a=2 × b=2mm)			CASE 6 number of slit : 3 sectional area of slit : 12mm^2 initial flow:1200ml/min.

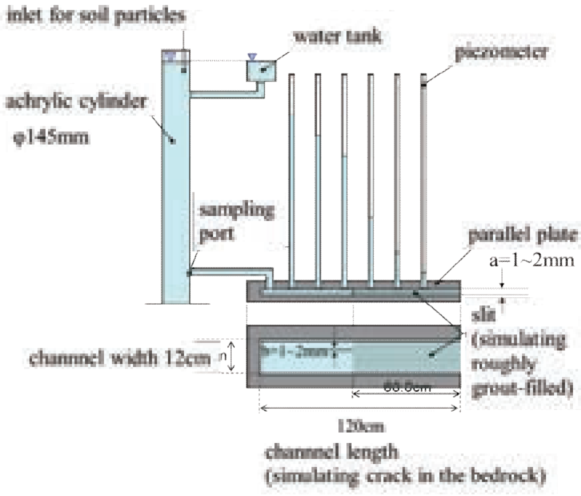

Figure 5(b). Outline of the equipment of laboratory tests

3.1. Verification of short-term clogging

Table 1 shows the test cases to verify the parameters affecting clogging (crack width and flow velocity). As shown in Fig. 5(b), slit zone was installed at the downstream side of the parallel plates, to simulate cracks being roughly filled with grouting. The flow velocity at the parallel plates in case 6 is equivalent to the suction strength of four to five (suction flow velocity of approximately 6 to 10 cm/sec), while in other cases three (suction flow velocity of approximately 4 cm/sec). The suction strength was measured in field submersible surveys, where suction strength indicates the degree of suction flow velocity. Suction strength was measured by watching the movement of colored water sucked into the inlet hole. The relationship between movement of colored water and suction velocity were confirmed by field tests. The input of the soil was set to 10.3 g each time, to be equivalent to the input per unit area of previous field test, in case of natural settlement method. In Table 1, flow velocities are shown as the ratio to the velocity of case 2 (111.1 cm/sec).

Fig. 6 shows the result of case 1. In case 1, by inputting slurry four times, flow decreased from 600 ml/min to 240 ml/min, approximately 60% of the initial flow, after 2.5 hours. Water head shows that clogging occurred at the transition point from parallel plates to slit zone. From the observation, the clogging was first induced by relatively large particles, followed by fine particles gradually filling the remained space.

Fig. 7 shows the particle size distributions of the clogged soils for each cases. Comparing to original slurry (i.e., input slurry), clogged particle grading is decreased in smaller than 20 micro meter and increased from 20 to 60 micro meter. Table 2 shows the results of short-term tests. The results indicates the tendency that clogging is induced by relatively small slit and low velocity. On the other hand, clogging will not be induced with large opening of parallel plates and high velocity, as shown in case 6.

It was verified that clogging developed by large particles first, followed by particles of 20 to 60 micro meter, resulting in reducing the flow.

3.2. Verification of long-term clogging

Long-term clogging tests were conducted to verify the influence of inputting slurry over a long period of time, on the reduction of flow, and, the influence of back pressure on clogging. Long-term tests were conducted in case 1 and case 6, basically under the same condition with short-term clogging tests. The differences are the number of times of input (42 times per cycle for long-term clogging test), and the process of applying back pressure after each cycle. The objective of applying back pressure is to simulate the condition when the water level is drawing down rapidly in the upper reservoir, due to power generation.

Fig. 8 shows the test results of case 6 (long-term). Clogging was observed at all locations of slits, as the slurry have been inputted. In addition, flow decreased greatly accordingly. After third cycle, the flow have decreased by 99%. On the other hand, increase of flow was observed after applying back pressure. Approximately 60 to 70 % of the flow, compared to the previous flow cycle, was restored. However, though some of the fine particles deposited at the parallel plates were washed out, particles clogged inside the narrow slits were not washed out by back pressure, as shown in Fig. 9.

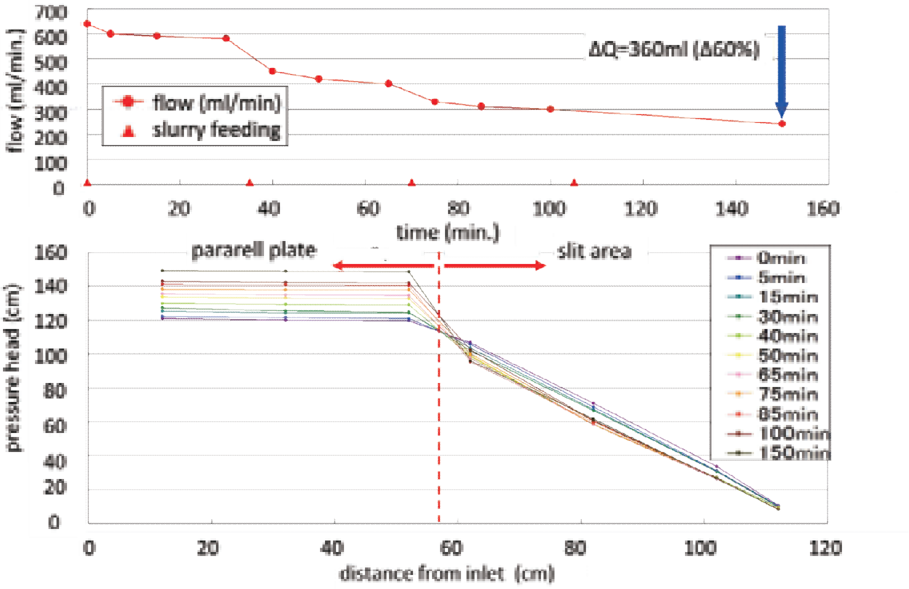

Figure 6. Flow and pressure head in case 1

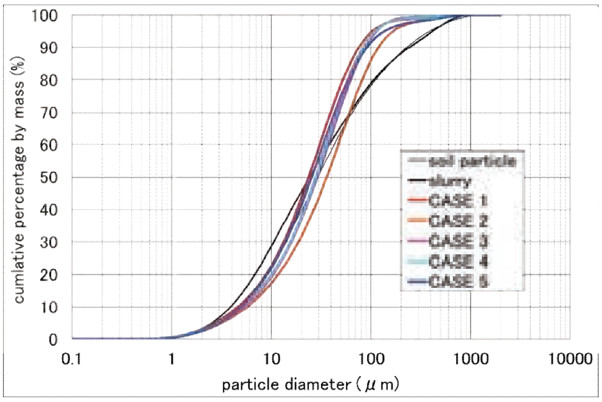

Figure 7. Particle size distribution after clogging tests (short term test)

Table 2. Results of clogging tests in each case

		The velocity ratio of each case against the velocity of the case 2					
		0.75		1		1.5	
area/slit	1mm^2 (1 × 1mm)	CASE 1		CASE 2		CASE 3	
		clogging ○	reduction rate of flow 54～63%	clogging ○	reduction rate of flow 52～53%	clogging ○	reduction rate of flow 44～46%
	2mm^2 (1 × 2mm)			CASE 4		CASE 5	
				clogging ○	reduction rate of flow 34～37%	clogging ○	reduction rate of flow 5～21%
	4mm^2 (2 × 2mm)					CASE 6	
						clogging ×	reduction rate of flow –

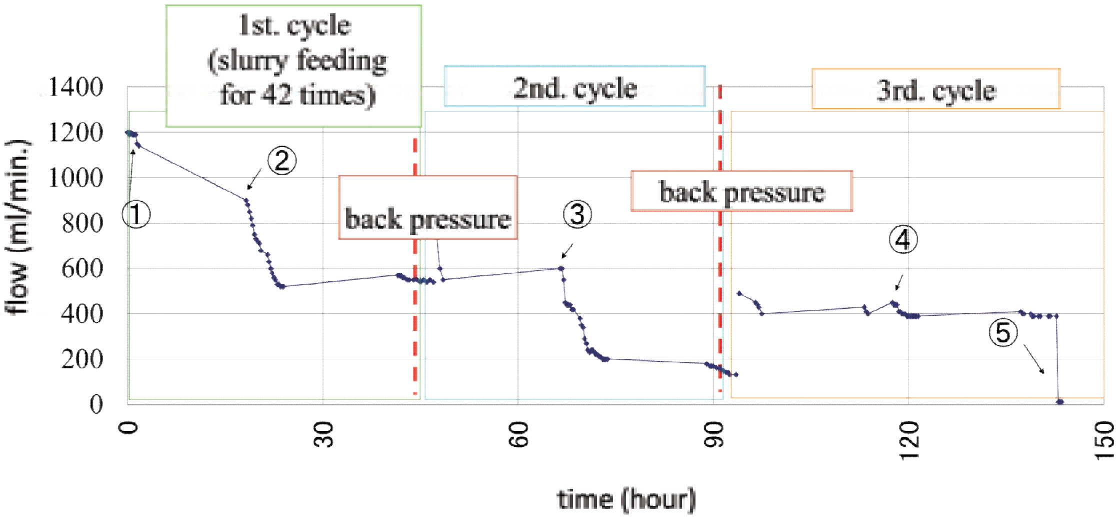

①one of three slits was clogged

②two of three slits were clogged

③three slits were clogged

④one of three slit was opened

⑤three slits were clogged

Figure 8. Result of clogging tests (Case 6)

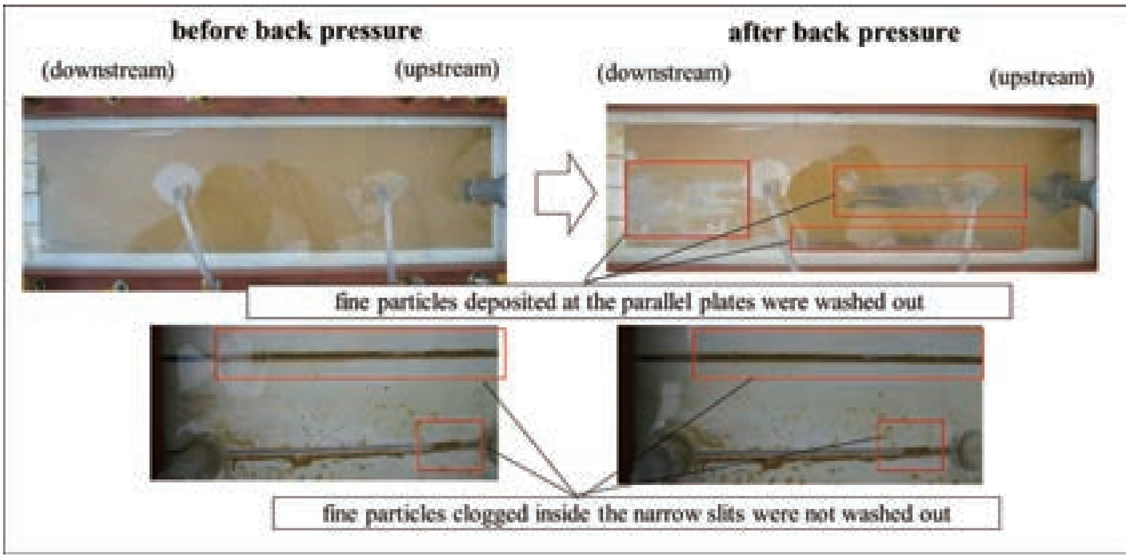
before back pressure
(downstream)
(upstream)
after back pressure
(downstream)
(upstream)
fine particles deposited at the parallel plates were washed out
fine particles clogged inside the narrow slits were not washed out

Figure 9. Situation after clogging tests (Case 6)

Fig. 10 shows the particle size distributions of the clogged soils. Compared to the short-term tests, particles that clogged in the long-term tests contained more fine particles, which indicates that fine particles will also be effective for clogging in long-term.

As a result, clogging promotion method was determined to be effective for reducing water leakage of the reservoir, since the soil particles will be clogged solidly in narrow spaces by inputting repeatedly, and would not be washed out by back pressure.

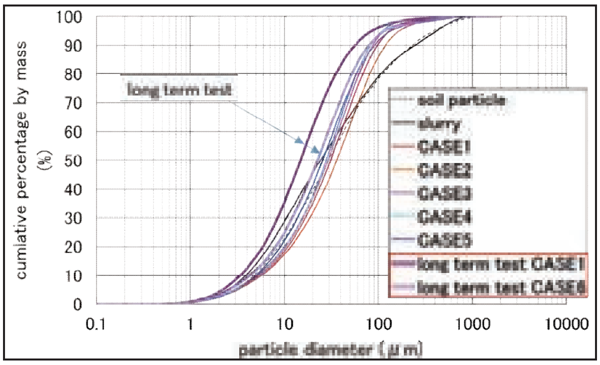

Figure 10. Particle size distribution after clogging tests (long term test)

4. EFFECTS OF THE METHOD IN FIELD TEST

In order to verify the effects of the clogging promotion method, field test was implemented at the south side of the reservoir, as shown in Fig. 11, where relatively numerous inlet holes were found in preliminary investigations of slopes by divers. The test site was encircled by a net to prevent soil particles from diffusing throughout the reservoir. In the field test , soil particles were input for four weeks. Input was repeated in the first two weeks at standard turbidities of 100, 50 and 30 ppm to grasp the tendency of turbidity reduction. In the second two weeks, relations between input, integrated turbidity and suction strength were identified. Particles were input at standard turbidities of 30 and 100 ppm in the third and fourth weeks, respectively. The total input of soil particles was 10.2 t and the integrated turbidity was 100 ppm-day.

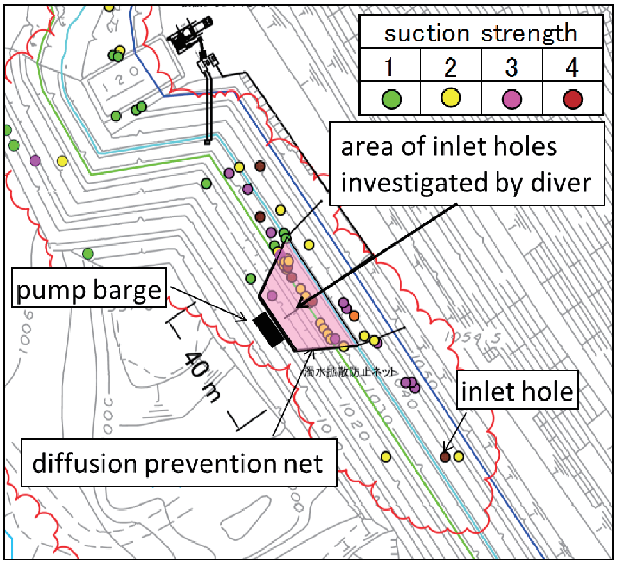

Figure 11. Area of inlet holes investigation

The effectiveness of the clogging promotion method was determined based on the increased or decreased number of inlet holes with different suction strength. Submersible investigations of inlet holes were made before field test, and, approximately once a week thereafter. Fig. 12 shows the results of submersible investigations. Inlet holes with a suction strength of 2 to 4, which were found in the preliminary investigation, was reduced. Inlet holes with a suction strength of 0 increased from none to 10, after the tests. The results therefore verified that the clogging promotion method was effective to some extent.

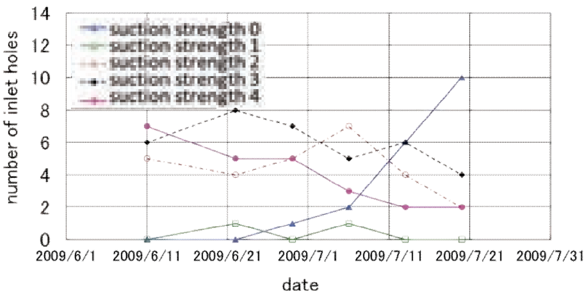

suction strength	flow velocity (cm/sec)
0	0.0
1	1.0
2	2.5
3	4.0
4	6.0

Figure 12. Result of inlet holes investigation

5. CONCLUSION

A study was made on the applicability of the clogging promotion method as an auxiliary method for grouting, which uses low-cost materials available in the vicinity of the reservoir site. Field and laboratory tests were conducted to decide slurry density for the clogging promotion method and to confirm the clogging effect. In addition, influence of back pressure were examined by laboratory tests. From the results we estimated that this method is applicable to the actual site. Therefore, the clogging promotion method was conducted in the actual leakage-prevention works as an auxiliary method for grouting, and proved to be effective to some extent. We are planning to make a report about further verification of the effect and durability of the clogging method in the near future.

ACKNOWLEDGEMENT

We would express our sincere thanks to Professor Emeritus Makoto Nishigaki, Okayama University, Tatsuo Ohmachi, Professor Emeritus, Tokyo Institute of Technology and Advisor to Japan Dam Engineering Center (JDEC), Dr. Norihisa Matsumoto, Advisor to JDEC, Mr. Joji Yanagawa, President, JDEC and Mr. Mitsuaki Mizuno, former director of Japan Water Agency for their kind guidance.

REFERENCES

Kawashima, F. and Tsukada, T. (2010): A Study for the behavior of groundwater flow along the open fissures with high dip angles, ICOLD symposium 2010, CD.

4^{th} APG Symposium and 9^{th} EADC on

INNOVATIVE TECHNOLOGIES FOR DAMS AND RESERVOIRS TOWARD THE FUTURE GENERATIONS

Deformation Control and Porosity Detection Technologies for High Rockfill Dam

J. H. Lu, J. X. Tan& B. Tian
Changjiang Institute of Survey, Planning, Design and Research, Wuhan, China
95352680@qq.com

ABSTRACT:

Rockfill dams in China, built during 1960s and 1970s, have common defects of high porosity and non-convergent deformation which leads to repeated damage of impervious system. There is still no effective approaches to control deformation for rockfill dams with large height and serious deformation. Controllable filling grouting was developed to reduce rockfill dam's porosity and increase its ability to resist deformation. Meanwhile, packaged drilling technologies for rockfill dam was developed. The hard problem of controlling rockfill dam's deformation is solved by above technologies. Porosity detection for finished high rockfill dam is a difficult problem, although currently there are various methods. Therefore, the improved nuclear moisture-density detecting method for deep inclined rock layer was developed to detect porosity for the whole body of high rockfill dam.The dangerous deformation of Mopan Rockfill Dam in Guangxi Province is still not controlled after several reinforcements. The controllable grouting technology was successfully applied in reinforcing process of this dam. Detection results showed that injected grouting materials were distributed evenly and porosity was reduced from 42% to 22.5%. Now this dam's deformation is convergent. Above reinforcement and detection technologies have remarkable innovation and important promotional value.

Keywords: deformation control of rockfill dam, porosity detection, controllable filling grouting

1. INTRODUCTION

The earliest rockfill dams are supposed to appear during the Gold Rush in western United States in the 1750s and they are generally wooden facerockfill dams with steep dam slopes. Rockfill dams built during earlier times in China are mainly constructed through approaches such as artificialfilling; cast blasting filling and so on. Xibeikou Dam, 95 meter high and built in 1985, is a typical modern concrete face rockfill dam. Presently, China has over 4,000 rockfill dams, of which more than 1,500 are defective ones(NiuXinqiang. and XuLinxiang,2002). In the 1960s and 1970s, many rockfill dams were built in China and a large proportion of them became defective. Examples include Hongfeng Dam, Shibianyu Dam and so on. Moban Rockfill Dam in Guangxi, China was also built in this time period. Limited by historical conditions and engineering levels, earlier rockfill dams built in China mostly possess features such as large porosity, deformation and severe leakage of dam body, threatening safety of the dams. Even for rockfill dams built in recent years, there were large deformation, leakage and other problems happening before. Examples include Majiagou Dam in Chongqing, Zhushuqiao Dam in Hunan, Baiyun Dam in Hunan and so on.

According to study on home and abroad situation, several methods are now being taken for rehabilitation of defective rockfill dams, including partially replacing and rebuilding, vibroflotation, and partially grouting. Grouting is usually used for lower rockfill dams or surface layer of rockfill dams. Currently, Anti-leakage treatment is widely implemented both at home and abroad for defective rockfill dam rehabilitation. However, due to lack of proper control of dam body deformation, anti-leakage system may meet subsequent damages caused by development of dam body deformation. Therefore, in order to ensure safety of the dam which has its dam body deformation still developing; the principal task is to control dam body deformation and then comes reinforcement of its anti-leakage system.

Mopan Reservoir in Guangxi, China was built in the 1970s. Dam crest of the concrete face rockfill dam is 203 meter long, maximum dam height 61 meter, upstream dam slope 1:0.649, and downstream dam slope from 1:1.4 to 1:2. The dam was artificiallyfilled,whose porosity was 45%(Porosity is a ratio of the pore volume and the rockfill volume in the dam body.). Since completion of this dam, dam body deformation had never stopped and been growing serious. Although rounds of historical reinforcing activities had been carried out for the dam, the dam body deformation was still under development due to high altitude and large deformation of the dam body, and difficulty in technology implementation. After the year of 2005, the dam body deformation further developed and endangered the whole dam.

Considering the fact that there is no effective way to control dam body deformation for high and endangered rockfill dams both at home and abroad, we settled down to study dam body deformation controlling methods for rockfill dams, conduct many field tests and theoretical analysis and acquired creative techniques in dam body deformation control for rockfill dams (Tan Jiexiong, Lu Jianhua,2010).

2. STUDY ON GROUTING TECHNOLOGY

2.1. Objectives of Study

Rockfill dams usually have less homogeneous, diameter diversified and complex filling materials. So our commonly used an-leakage reinforcing method cannot resolve the problem completely, as its resistance to deformation is relatively low. In order to control dam body deformation of rockfill dams, we come up with a controllable filling grouting technology aiming at reducing dam body porosity, improving adaptive performance of rockfill dam to deformation, and increasing resistance to deformation of dam body and durability of anti-leakage system. Controllable filling grouting materials are easy to operate and control. The grouting material could be injected into dam body evenly, having sound bonding strength and ensuring stability of grouting material. In view of above goals, we also studied several key aspects and techniques in grouting for rockfill dams about grouting material, grouting control, drilling and detecting after grouping.

2.2. Study on Performance of Grouting Material

Regarding basic characteristics of rockfill dams with high porosity, we systematically analyzed performances of the grouting material and property of the seriflux. The ideal grouting material could be used in rockfill dam with high porosity, be controllable and easy to operate, have proper strength and even distribution in dam body. Performance of the grouting material depends on its yield strength, viscosity, weight and some other parameters. Basiccomponents for grouting materials include cement, clay, bentonite, coal ash, water glass, water reducer and so on. And grouting materials can be divided into cement slurry, cement-sand mixture, stabilizing cement slurry, stabilizing mixed slurry, stabilizing cream slurry and so on. When appropriate grouting materials and mix proportion was finalized, the injected mixture would cease diffusing after entering dam body for a certain distance. Correspondingly, loss of grouting materials could reduce dramatically and formed solid body has high strength and even distribution.

2.3. Study on Drilling Technologies on Rockfill Dams

Temporary drilling technology may lead to drill stuck, drill burning out, unstability of pore wall, pore collapse and loss of pore washing liquor. It is hard to form drilling hole in rockfill dams, especially deep inclined hole. Our studied drilling technique is characterized byadvantages of high quality of drilling holes,low loss of drilling tools, high working efficiency and so on. Through theoritical research and onsite test, creative points are summerized as follows.

2.3.1. Technology of internal rotating diamond wheel to break the core drilling

When drilling on a rockfill dam, small diameter-diamond-geological drilling machine (e.g. XY-2PC) is used. The drill is core-breaking diamond drill without extracting the core. Traditional core-breaking bit cone is moved from the diamond drill to the reamer, which can increase drilling tool's life and increase working efficiency.

2.3.2. Technology of gradient correction of deep inclined hole

When drilling deep inclined hole on rockfill dam, the gradient is difficult to control and easy to decline. We made some changes to the drilling tool, that is, installing reamer on the drill and the drill stern. Corebarrel is lengthened to 5 meter and guide tubes are installed every 10 meter along the drill stern. Meanwhile, KXP-1 inclinometer is used to correct the gradient and ensure the deep inclined hole run in the right direction.

2.3.3. Technology of drilling cooling for rockfill dams

Drilling hole washing for rockfill dam adopts a method combined with clear water and clay slurry. Water (clay) is injected inside and at the entrance of the drilling hole. Water input at the entrance is more than inside the hole. Water meter is insalled on inflow pipe at the entrance and water pressure is displayed to monitor washing status inside the hole. Inflow rate of washing liquid need to be adjusted according to onsite condition in order not to burn out the drill.

The above mentioned set of drilling technologies for rockfill dams is excelling by its high quality of drilling holes,low loss of drilling tools, high working efficiency features, and bring solution to technical problem for drilling on high rockfill dams.

3. STUDY ON GROUTING PROCESSES

Grouting processes for rockfill dams with high porosity is quite difficult to master, especially for grouting in deep inclined hole. Grouting pressure is a critical parameter for grouting in rockfill dam, and a key factor affecting diffusing capability and cementation quality of the seriflux. Through engineering practice and research, grouting pressure can be decided properly in consideration of row order, hole order and hole depth. Appropriate length of grouting section may improve grouting quality and working efficiency. So it is important to select length of grouting section based on row order and hole order respectively and determine ending criteria for rockfill dams with high porosity. Ciriterias for pressure limiting, flow limiting, interval and cementing stay when grouting in empty area of rockfill dams are also to be studied.

Common grouting method may not achieve satisfying effect and be less likely to meet requirements for large scale construction, because its low working efficiency and asymmetry of the grouting materials. We studied a new grouting technique called hole mouth stirring grouting, which can keep the filling materials and cement slurry mixed evenly and inject them into the hole continuously, stably and efficiently. The process is automatically performed by our self-developed hole mouth sand-mixing device. The device joints with the drill pipe, rotating together with the pipe. Surroundingsandbody can be fully stirred under jet flow from the stirring blades. The grouting process composed of seriflux jet, stirring blade and connector and some other parts, can increase grouting efficiency by over 100% compared with traditional way and can ensure sound grouting quality.

4. STUDY ON DENSITY DETECTING TECHNOLOGY OF ROCKFILL DAMS

Nowadays, extra mass method, nuclear method, surface wave method and some others are applied to detect lamellar or low rockfill dam porosity during construction. But as for those already built rockfill dams, higher than 60 meter and with complex internal filling materials, it is difficult to detect the compactness and the detecting method is still under research both at home and abroad. We updated the original detecting method of deep nuclear moisture-density by configuring FD3019 deep nuclear density meter and DR501 deep nuclear moisture-density meter in deep inclined hole of the dam body, and detecting in situ density and water content at the same measuring point. The updated method is flexible to operate and capable of acquiring stable datas.

5. APPLICATION OF THE STUDIED TECHNOLOGIES

5.1. Layout of the Grouting Holes

Based on our study results, we applied the technologies to onsite test and reinforcement for Mopan Dam. Grouting started on September 2009, ended on February 2010. The total cost was 32 million RMB.The drilling holes were laid out along the dam crest, which made controllable grouting possible. Firstly, stable seriflux was injected into the two rows of holes near the downstream slope, forming a closed grouting region together with upstream concrete surface. And then, grouting holes were evenly laid out with the main rockfill dam body. Grouting holes distributed along the dam crest. The two rows of stable seriflux grouting holes(F1 and F2) are vertical, with hole and row intervals both to 1 meter. For better groutingresults, there were 8 rows of holes along the dam crest(from E1 to E8), with hole interval 1.5 meter and row interval 1 meter. Please see Fig.1 for layout of the drilling holes and Fig.2 for reservoir storage after dam grouting.

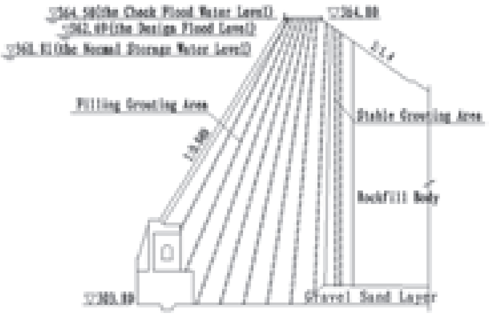
▽364.50(the Check Flood Water Level)
▽362.69(the Design Flood Level)
▽361.11(the Normal Storage Water Level)
▽364.80
Filling Grouting Area
1:0.80
Stable Grouting Area
Rockfill Body
▽303.80
Gravel Sand Layer

Figure 1. Layout of drilling holes at Mopan Rockfill Dam

Figure 2. Reservoir storage after dam grouting

5.2. Grouting Materials for Dam Body

Basic materials for the seriflux are cement, coal ash, betonies, water, water reducer and so on. The cement is ordinary Portland cement with its strength no less than 42.5 degree. Fineness of the coal ash is less than the cement's and no bigger than 5 to 30μm. As for betonies, content of minus 0.08mm particle is no less than 90%, liquid limit bigger than 40% and plasticity index bigger than 40. Admixture is water glass. The clay onsite has high sand content and low viscosity, unsuitable for grouting use.

5.2.1.Stable Seriflux Grouting.

Design indexes for stable seriflux are strength of solid body no less than 5 MPa(28 days) and plasticity viscosity within 0.15 to 0.25 Pa.s. Through laboratory tials and onsite grouting tests, we finally chose the mixing proportion of G-3. Please see Table 1. for the mixing proportion of stable seriflux, and Table 2. for grouting pressures and length of sections. The ending criteria is when design grouting pressure reached and seriflux consuming rate was no bigger than 1 to 3 liter per minute, grouting would last for another 5 minutes and then stopped for this section.

Table 1. Mixing proportion of stable seriflux

No.	Cement （kg）	Coal ash （kg）	Bentonite （kg）	Density of sefiflux(g/cm^3)
G-1	250.0	75.0	120.0	1.527
G-2	250.0	75.0	160.0	1.557
G-3	250.0	75.0	200.0	1.586

Table 2. Grouting sections and grouting pressures

Item	Hole □	Hole □	Hole □
Pressure （MPa）	0～0.05	0.05～0.1	0.1～0.2
Length of section（m）	2m for the entrance section, and 3m below	3m at the entrance, and 5 m below	3m at the entrance, and 5 m below

5.2.2.Cement Slurry Injecting.

Dam body grouting seriflux is divided into three classes, with water-cement ratio of the cement slurry at 1:1, 0.8:1 and 0.6:1 respectively. After tests, we chose 0.6:1. Please see Table 3. for dosage of the materials and Table 4. for grouting pressures and length of sections. Hole I and Hole II used cement-sand mixture for grouting, with its strength no less than M7.5. Hole III used 0.6:1 cement slurry for grouting. The ending criteria is when the injection rate under set pressure was no bigger than 1 litre per minute, grouting would last for another 5 minutes and then stopped.

Table 3. Mixing proportion of cement slurry

Water-cement ratio	Cement（kg）	Water (L)	Density （g/cm^3）	Content of cement (kg/L)
1:1	113.6	113.6	1.50	0.76
0.8:1	133.9	107.1	1.59	0.89
0.6:1	182.9	91.5	1.80	1.22

Table 4. Grouting sections and pressures

Item	1st section	2nd section	3rd section	4th section and following
Length of section（m）	2	3	5	5
Pressure （MPa）	0.05	0.05	0.05	0.1

5.3. Dam body grouting

Hole I and II used cement-sand mix for grouting by hole mouth stirring method. The grouting materials flew into the hole by gravity without external pressure. For Hole III, thick cement slurry with water-cement ratio at 0.6:1 was injected, and the grouting pressure was within 0.1 to 0.2 MPa.

Relevant criterias for interval, clotting stay, admixture, pressure limit, flow limit and so on when grouting in the rockfill dam body, were determined through tests. Our tested criterias are as follow, (1)interval: Hole I applied when dosage of cement-sand mix equal or greater than 750 kilogram per minute; Hole II applied when equal or greater than 600 kilogram per minute; the invertal is 8 hours. (2)clotting stay: when dosage of cement-sand mix was equal or greater than 1000 kilogram per minute, the stay was 3 three days. (3)admixture: 3% water glass was used for grouting during the interval.

Through above-mentioned adjustment, it was found that enclosing effect of the stable seriflux grouting holes was fine. There was no loss nor leakage of the seriflux. Diffusing radius for single hole grouting was between 1.5 meter and 2.5 meter. The grouting materials distributed evenly within the dam body. Grouting for the rockfill dam was sucessfully completed, with a total grouting amount of 32,000 cubic meters.

After grouting for the rockfill dam body finished, we gave treatments to anti-leakage defects at joints between different dam sections and dam foundation, to form a complete and closed anti-leakage system for Mopan Rockfill Dam.

6.QUALITY TESTS

In order to get a clear awareness of dam body performance after grouting, we used deep nuclear water-density meter to detect porosity within the rockfill dam body. There were 9 testing holes and 2 inclined holes at the dam crest, and the total length of the testing holes was 440 meter. Layer detection was carried out every 0.5 meter from upside down along the drilling holes. Detecting results showed that the grouting materials distributed evenly within the dam body, the porosity reduced from 42% to 22.5%, dam body deformation was effectively controlled.The concrete seepage control panel was reconstruction after the completion of the dam grouting.MopanReservoir has been running safely at high water level for three years since reinforcing till now.

7.CONCLUSION

Based on comprehensive and systematical study on reinforcing technology and experience for defective reservoirs from both home and abroad, we proposed a new rockfill dam grouting technology focusing on controlling dam body deformation with several innovative points. The solution was confirmed feasible after implementation. Expert group reached a common conclusion that our study results had made innovation and breakthrough in many aspects, promoted development of reinforcing technology of rockfill dams, and it can be applied in the similar reinforcement engineering.

REFERENCES

NiuXinqiang. and XuLinxiang. (2002):Leakage Control Design of Zhushuqiao Concrete Face Rockfill Dam, People’s Changjiang River, 11, pp. 1-3.

Tan Jiexiong, Lu Jianhua. (2010): Research and Application of Reinforcing Technologies for Rockfill Dams, People’s Changjiang River, 15 ,pp. 38-42.

Construction of Gokayama Dam by the Cruising RCD Construction Method

R. Nishiyama, M. Yugeta, T. Toyomasu & H. Yotsumoto
Gokayama Dam Construction Office, Fukuoka Prefectural Government, Japan
nishiyama-r8711@pref.fukuoka.lg.jp

T. Fujisawa, Y. Kinouchi & N. Yasuda
Japan Dam Engineering Center, Tokyo, Japan

ABSTRACT:
RCD (Roller Compacted Dam-Concrete) construction method was developed as a rationalizing dam concrete placing method and has been used to speed up the construction works of concrete gravity dams. The cruising RCD construction method adopted to construct Gokayama Dam has been developed to aim for even more rationalizing dam concrete placing, and which improves construction work efficiency by advancing the placing procedure of the internal RCD, so it enables the continuous placement of dam concrete and enables placement of concrete more speedily.

In Gokayama Dam, the slumping concrete is placed in the outer concrete and RCD is place in the inner concrete. Originally, the RCD is not placed unless the placement of slumping concrete is finished in one lift. The cruising RCD construction method is that the placement of RCD starts from one side of the dam site, while the slumping concrete is placed at the other side of the dam site. In that case, the RCD is placed at the next lift. Simultaneously, the RCD and slumping concrete are placed at different two lifts. The placement of RCD antecedent to that of the slumping concrete enables this execution, unlike the conventional RCD construction method in which the slumping concrete is placed antecedent to that of RCD.

Keywords: Concrete gravity dam, Gokayama Dam, Cruising RCD construction method

1. INTRODUCTION

Gokayama Dam is a 102.5m-high concrete gravity type and is now under construction on the Naka River by Fukuoka Prefecture, Japan.

The purposes of the dam are flood control, maintenance of normal function of the river flow, water supply for public use and emergency supply during droughts.

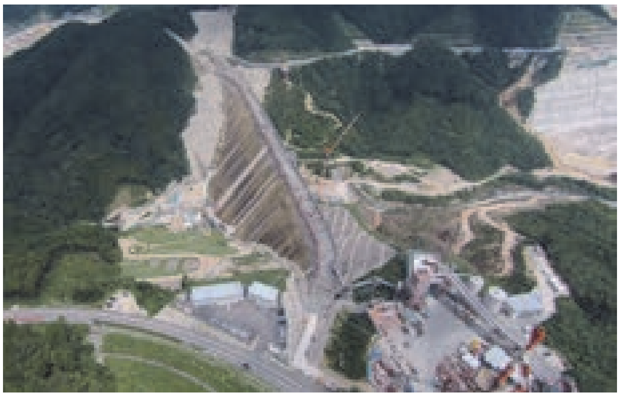

Figure 1. View of dam body placement
(View of placement work on July 31, 2015, EL401.5m, 88 lifts)

Table 1. The main features of dam and reservoir

Type	Concrete gravity
Height	102.5m
Crest lenght	556.0m
Volume	935,000m^3
Catchment area	18.9km^2
Reservoir area	1.3km^3
Total reservoir capacity	40,200,000m^3
Effective reservoir capacity	39,700,000m^3
Flood control capacity	8,000,000m^3
Water use capacity	15,100,000m^3

The originally adopted conventional RCD construction method was placed by the so called cruising RCD construction method due to shortening the construction period. This construction method was technically proposed by the contracted construction company and was the fourth time in Japan. Fig. 1 is a construction view of Gokayama Dam, and Table 1 shows the main features of dam and reservoir.

Table 2 shows the construction equipment used for Gokayama dam, and the layout of the construction equipment, respectively. At Gokayama Dam, an

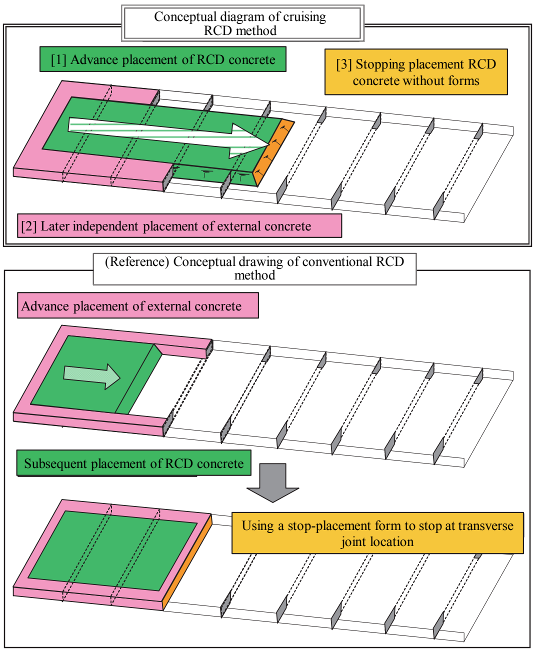
Conceptual diagram of cruising RCD method
[1] Advance placement of RCD concrete
[3] Stopping placement RCD concrete without forms
[2] Later independent placement of external concrete
(Reference) Conceptual drawing of conventional RCD method
Advance placement of external concrete
Subsequent placement of RCD concrete
Using a stop-placement form to stop at transverse joint location

Figure 2. Conceptual drawing of the cruising RCD construction method

Table 2. Execution Equipment

Equipment		Equipment specifications
Placing equipment	Concrete production plant	2-shaft forced circulating mixer 3.0m^3×2×1 (Batcher top improved type)
	Cement storage equipment	1,000t (Fly-ash replacement rate of 20%)×1 600t (Fly-ash replacement rate of 30%)×1
	Concrete transport equipment	18t fixed cable crane×1 (5.5m^3) 6.5t fixed cable crane×1 (2.5m^3) SP-TOM×1 (diameter 700)
	On-site concrete transport equipment	40t dump truck (to transport RCD) ×3 10t crawler dump (to transport slumping concrete) ×4 9.0m^3 ground hopper×1
Aggregate handling equipment	Production equipment	Production capacity: 500t/h (wet production)
	Storage equipment	Coarse: 9 bins, Fine: 4 bins (4-day supply at average daily use during maximum placement month
	Transport equipment	W1,050mm belt conveyor
	Adjustment bins	Coarse: 3 bins, Fine: 1 bin (5-day supply)
	Others	Heating and cooling equipment

SP-TOM (Spiral Pipe Transportation Method) is installed on the left bank abutment in order to transport large quantities of concrete. Fig. 3 is a view of the installation of the SP-TOM.

The maximum quantity of transported concrete is 220m^3/h due to the concrete production capacity of the batcher plant.

2. EXECUTION OF THE DAM BODY BY THE CRUISING RCD CONSTRUCTION METHOD

2.1 Characteristics of the Cruising RCD Construction Method

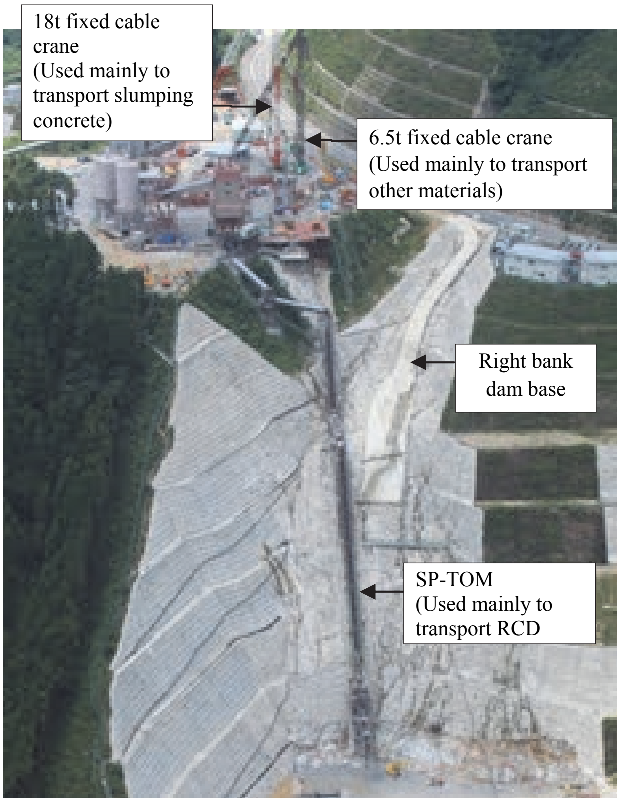
18t fixed cable crane
(Used mainly to transport slumping concrete)
6.5t fixed cable crane
(Used mainly to transport other materials)
Right bank dam base
SP-TOM
(Used mainly to transport RCD

Figure 3. View of layout of concrete placement equipment

The cruising RCD construction method is developed in Japan to achieve greater rationalization of execution. It has the following three characteristics.

1) The preceding placement of the inner RCD.

2) The outer slumping concrete is independently placed afterwards.

3) Placing of RCD can be stopped at any time without using a metal form.

Fig. 2 shows the concept of this execution method (JDEC 2012). The various execution specifications of the basic technologies for the execution method implemented at Gokayama Dam are shown in Table 3 (Kamouchi et al. 2015a).

2.2 Development of new technologies and innovations to maintain high speed execution

The execution technologies of the cruising RCD construction method newly implemented at Gokayama Dam are described below along with their effectiveness.

1) Adoption of a flat plate compactor (FPC) to compact the slope edges of RCD.

2) Realization of 2-lift continuous execution

Table 3. Execution Specifications of Basic Technologies at Gokayama Dam

Item	Results of confirmation trial execution	Execution specifications decided
Compacting edge slopes of RCD	The RI method and core sample confirmed that the densities of the edge slope and normal parts are equal.	(1) Compacted using FPC. (2) Crest 15sec+slope 15sec of compaction time
Treatment of RCD joint surfaces (soft treatment)	Good quality treatment was achieved by doing it about 2 hours after completing 0.7MPa (50 to 100l/min.) roller compaction (cumulative temperature of 70°C･h according to outside air temperature).	(1) Done about 2 hours after completion of roller compaction (cumulative temperature of 70°C･h according to outside air temperature) (2) Treatment water pressure is 0.7MPa (water quantity 50 to 100l/min.)
Integrating RCD with outer concrete	Good reliable integration was confirmed by a sampled core even at a joint 720 hours after edge slope compaction. Even compressive testing did not break the joint surface.	Outer concrete joints possible until 720 hours after slope compaction. But, mortar is spread on edge slope surface before placement external concrete.
Jointing to 1:0.8 edge slope of RCD	The joint surface of a core sampled from a joint is firmly integrated, and even the compressive test results show no breakage of the joint surface and strength equal to normal parts.	(1) Spreading mortar on edge slope (2) Not concentrating large pebbles near edge slope (3) Manually cutting and trimming thin edge at crest. (4) Reliably compacting to edge with a vibrating roller
Driving dump trucks on fresh concrete	Plastic planking was placed immediately after roller compaction was completed, and a 10t dump truck drove over it 20 round trips, but the concrete surface was undamaged, confirming there are no problems.	(1) Six hours after completing roller compaction (cumulative temperature of 130°C･h according to outside air temperature), protecting it with plastic planking. (2) After six hours, it is unprotected, but curb sections are protected by plastic planking etc.
Edge treatment of sloped placement stops	Treatment height of 15cm, 4.0 hours after completion of roller compaction (cumulative temperature of 83.3°C･h of exterior air temperature) obtained good result.	After roller compaction, edges are treated to height of 15cm with the target set as cumulative outside air temperature between 80 and 100°C･h.

3) Development of other new technologies

2.2.1. Adoption of the flat plate compactor (FPC) to compact slope edges of RCD

Slope edge compaction, which is an important aspect of preceding placement of RCD, was carried outusing a 2-surface constraining type compactor at existing 3 dams.

Before the use of this type of compactor, the slope edge must be formed carefully by using a slope bucket after spreading RCD with a bulldozer, in order that the gradient of the slope edge fit the fixed compaction plate shape. So, this compactor could simultaneously vibrate both crest and slope surfaces. However, this careful forming (scraping) increases the execution work, and makes it necessary to ensure adequate distance between the downstream surface form and the backhoe arm, which tended to expand the width of the outer slumping concrete.

So at Gokayama Dam, the FPC (see Fig. 4) was developed to eliminate the preliminary slope trimming and simplify the compaction work of the slope edge. The single plate of FPC compacted each surface －the crest and slopes, respectively. This compactor saved labor required for slope edge compaction, improving workability (Kamouchi et al. 2015b).

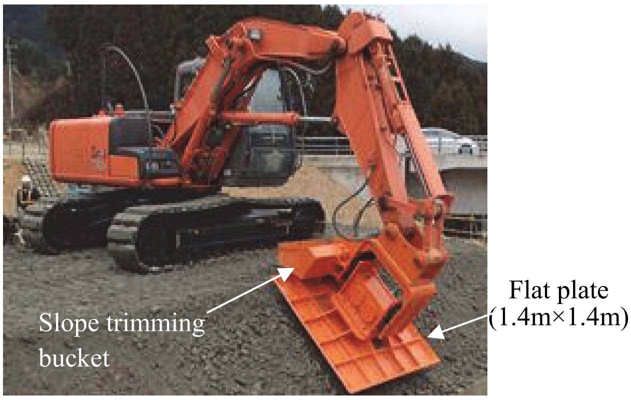

Figure 4. FPC (Flat Plate Compactor)

Furthermore, the FPC enables compaction according to the natural state of the slope after spreading of RCD, and is capable of dealing with the change of the lift thickness. As a result, finishing sloped joint necessary to move heavy machines could be formed unrestrictedly and efficiently. The FPC also allows partial compaction of RCD according to conditions.

2.2.2. Achievement of 2-lift continuous execution

At existing three dams constructed by the cruising RCD construction method, "1-lift placement" execution was adopted: starting placement of the following one lift after completing previous one lift. This 1-lift placement is restricted from the layout of concrete transport equipment and transport conditions (see Fig. 2).

Table 4. Comparison of 1-lift execution with 2-lift continuous execution

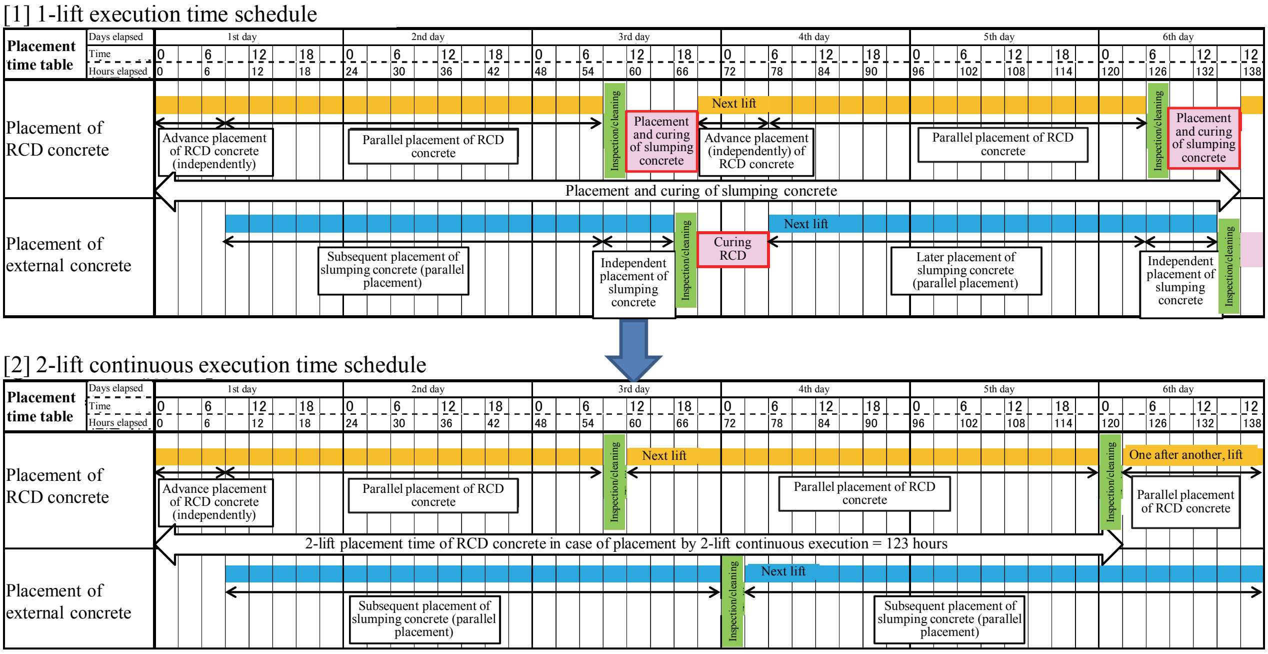

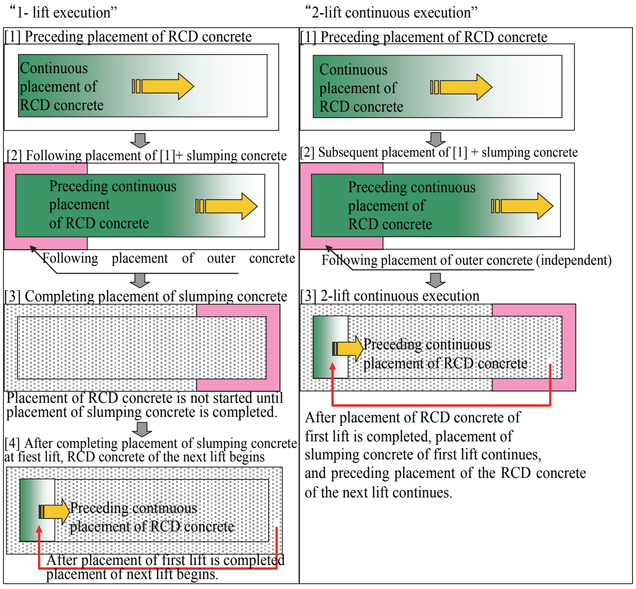
"1- lift execution"
"2-lift continuous execution"
[1] Preceding placement of RCD concrete
Continuous placement of RCD concrete
[1] Preceding placement of RCD concrete
Continuous placement of RCD concrete
[2] Following placement of [1]+ slumping concrete
Preceding continuous placement of RCD concrete
Following placement of outer concrete
[2] Subsequent placement of [1] + slumping concrete
Preceding continuous placement of RCD concrete
Following placement of outer concrete (independent)
[3] Completing placement of slumping concrete
Placement of RCD concrete is not started until placement of slumping concrete is completed.
[3] 2-lift continuous execution
Preceding continuous placement of RCD concrete
After placement of RCD concrete of first lift is completed, placement of slumping concrete of first lift continues, and preceding placement of the RCD concrete of the next lift continues.
[4] After completing placement of slumping concrete at fiest lift, RCD concrete of the next lift begins
Preceding continuous placement of RCD concrete
After placement of first lift is completed placement of next lift begins.

Figure 5. Differences between 1-lift execution and 2-lift continuous execution

In response to such previous cases, at Gokayama Dam, the layout of construction facilities was planned from the beginning considering 2-lift continuous execution. For the first time in Japan, 2-lift continuous execution was performed at 61 lifts of dam body during about 10 months.

Differences between 1-lift execution and 2-lift continuous execution are shown in Table 4 and Fig. 5 (Nishiyama, et al. 2015a). 2-lift continuous execution enables placement of slumping concrete for a concerned lift and the preceding placement of the RCD for the next lift simultaneously. The shortening of waiting time comes to the large speed-up of the execution.

It is necessary for the 2-lift continuous execution to plan in the early stage the layout of the construction facilities capable of transporting concrete of different mixtures to the different placement locations simultaneously.

At Gokayama Dam, this 2-lift execution was made possible by combining the immovable supply equipment, SP-TOM (Spiral Pipe Transportation System) with an 18t fixed cable crane.

It was necessary for the installation of the cable crane of slumping concrete transportation to consider its relationship with the layout of the inspection gallery as is needed the placement of slumping concrete.

As stated above, at dams which have a plan to adopt the cruising RCD construction method in the future, it is important to plan in early planning stage a concrete transport system that enables 2-lift continuous execution.

2.2.3. Developing other new technologies

At Gokayama Dam, the efforts to develop other new technologies such as the following were made to further rationalize the execution.

1) RCD in rock contact part

Slumping concrete has been conventionally placed in rock contact part in order to ensure reliable filling of concrete and water tightness in uneven surfaces of the foundation bedrock. This procedure has practically reduced the efficiency of the construction work.

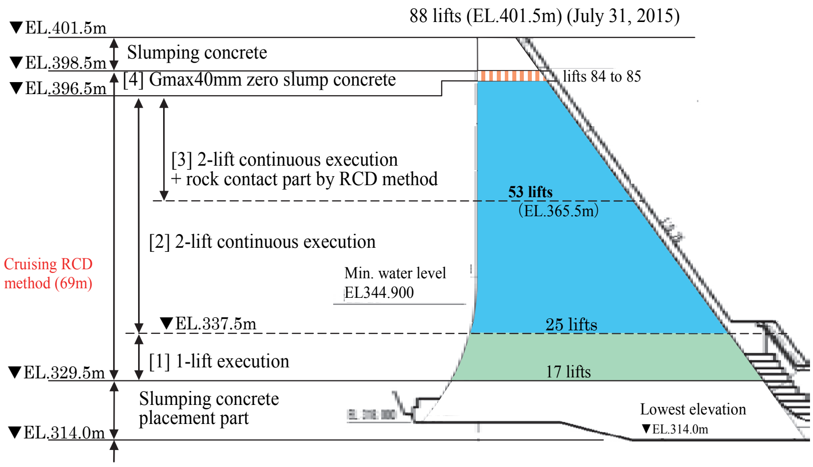
88 lifts (EL.401.5m) (July 31, 2015)
▼EL.401.5m
▼EL.398.5m
▼EL.396.5m
Slumping concrete
[4] Gmax40mm zero slump concrete
lifts 84 to 85
[3] 2-lift continuous execution
+ rock contact part by RCD method
53 lifts
(EL.365.5m)
[2] 2-lift continuous execution
Cruising RCD
method (69m)
Min. water level
EL344.900
▼EL.337.5m
25 lifts
[1] 1-lift execution
▼EL.329.5m
17 lifts
Slumping concrete
placement part
Lowest elevation
▼EL.314.0m
▼EL.314.0m

Figure 6. Placement sections by cruising RCD construction method (placement section [1] - [4]) at Gokayama Dam

Table 5. Placement sections by cruising RCD construction method at Gokayama Dam

Category	Lifts	Execution range	Outline of execution	Average placement rate (m/Month)
Placement section [1]	17 to 24	EL.329.5m to EL.337.5m	1 lift execution	4.7 m/Month (1.5 Months)
Placement section [2]	25 to 52	EL.337.5m to EL.365.5m	2-lift continuous execution	6.0 m/Month (10 Months)
Placement section [3]	53 to 83	EL.365.5m to EL.390.5m	2-lift continuous execution + rock contact part by RCD method	
Placement section [4]	84 to 85	EL.396.5m to EL.398.5m	Execution by RCD method using Gmax40mm zero slump concrete	4.0 m/Month

So, at Gokayama Dam, the rich blend RCD mix with 40mm of G_{max} (the maximum grain size of aggregates used) and an execution method using this mix were developed. This method improved work efficiency significantly and increased construction speed on rock contact parts.

The rich blend RCD mix with 40mm of G_{max} shows no segregation of aggregates and good construction property as the conventional slumping concrete does.

2) Execution of the RCD construction method in narrow parts near the dam crest

Originally, in the narrow range of construction width less than about 15m near the dam crest, the execution was switched to ELCM (Extended Layer Construction Method) due to complication from the passing each other of dump trucks, bulldozers, and backhoes etc. at conventional RCD construction method .

As the cancelation of complication of the construction work and the maintenance of placing speed, the cruising RCD construction method using the inner zero-slump concrete with 40mm of G_{max} was also executed instead of ELCM at the narrow area near the dam crest. This was confirmed to provide both good workability and quality.

3. EXECUTION RESULTS OF THE DAM BODY

At Gokayama Dam, placement of the dam body began on February 17, 2014, and full-scale placement by the cruising RCD construction method started on June 16 (17 lifts, EL329.5m). By July 30, 2015, placement had advanced to 88 lifts at EL.401.5m. This was about 91% volume of the dam body.

The cruising RCD construction method at Gokayama Dam was, as explained in Chapter 3, divided into 4 sections—[1] [2] [3] [4]—shown in Table 5 and Fig. 6 (Nishiyama, et al. 2015b).

Fig. 7 shows the placement rates of the conventional RCD construction method at comparatively large-scale dams, and performance of the cruising RCD construction method at Gokayama Dam and other two existing dams (Nishiyama, et al. 2015b).

According to Gokayama Dam in Fig. 7, in contrast to a placement rate of 4.7m/month by 1-lift execution in placement section [1], the placement rate of 2-lift continuous execution (placement sections [2] – [3]) was improved to an average of 6.0m/month. This was a result of shortened waiting time until the start of placement of next lift. During 10 months (sections [2] - [3]), a monthly average volume of about 60,000m^3 was maintained.

The numbers [1] to [4] shown in balloons of Fig. 7 correspond to those enclosed in boxes in Table 5 and in the drawing in Fig. 6.

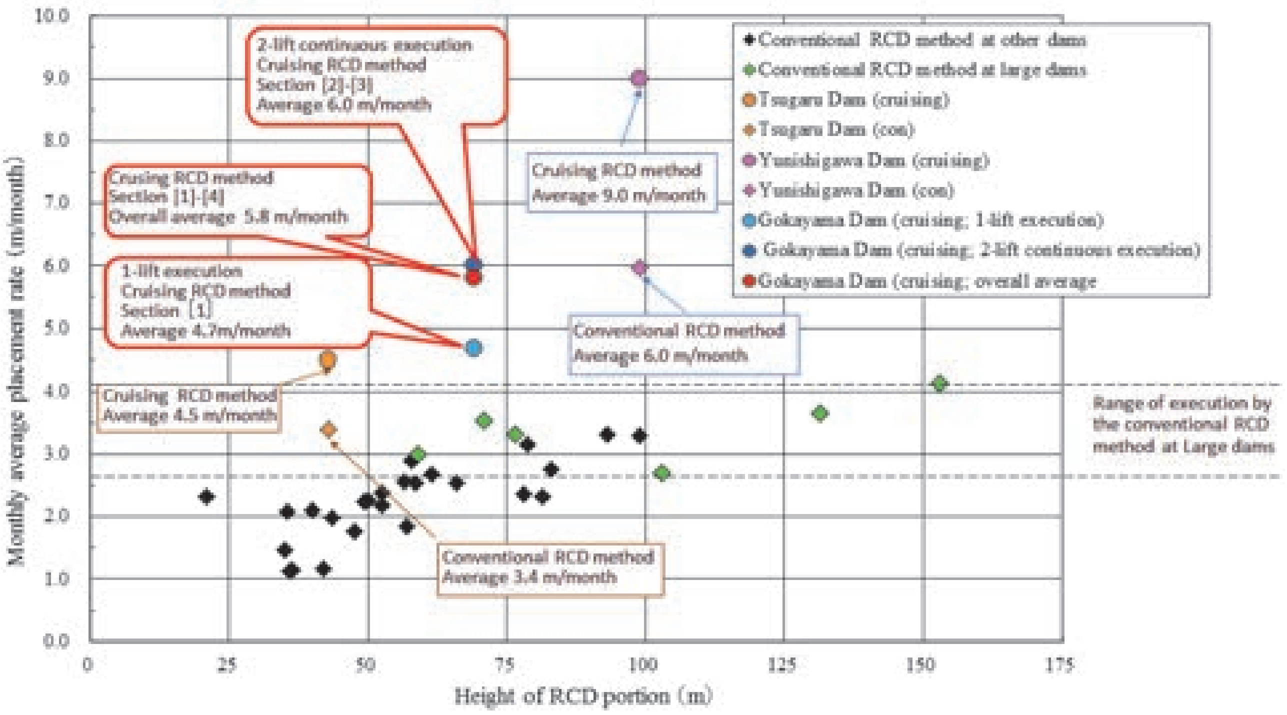

Figure 7. Placement rate at Gokayama Dam

4. CONCLUSIONS

As explained above, at Gokayama Dam, continuous placement by the cruising RCD construction method and applying other newly developed technologies were executed at totally 69 lifts. Its placement rate was an average of 5.8m/month for the 12.5 month placement period by the cruising RCD construction method, and for 10 month among this period, it was 6.0m/month (raising height of placed concrete per month) at sections [2] and [3]. As a result, 1.3 m/mon. of concreting speed is improved comparing with that at section [1].

At dams where the cruising RCD construction method will be adopted in the future, it will be important to plan a layout of the construction facilities that will allow the efficient and continuous transports of different concrete mix without any mutual interference.

In conclusion, the execution of Gokayama Dam by the cruising RCD construction method was finished on July 12, 2015, and the whole completion of dam will be at the end of 2017.

REFERENCES

Japan Dam Engineering Center (JDEC) (2012): Revised Edition, Technical memorandum of Cruising RCD construction method, February (in Japanese).

Kamouchi, A., et al. (2015a): Application of the cruising RCD construction method to dam body work at Gokayama Dam —Part 1—, Engineering for Dams, No. 340, pp. 80 - 106, January (in Japanese).

Kamouchi, A., et al. (2015b): Application of the cruising RCD construction method to dam body work at Gokayama Dam —Part 2—, Engineering for Dams, No. 342, pp. 83 - 119, March (in Japanese).

Nishiyama, T., et al. (2015a): Application of the cruising RCD construction method dam body work at Gokayama Dam —Part 3—, Engineering for Dams, No. 347, pp. 44 - 73, August (in Japanese).

Nishiyama, T., et al. (2015b): Application of the cruising RCD construction method to dam body work at Gokayama Dam —Part 4—, Engineering for Dams, No. 349, pp. 58 - 84, October (in Japanese)

Development of a Crawler Type Soil Mixing Machine with Dryer Function

S. Yamada, T. Temmyo, T. Koshida, I. Sandanbata, H. Itoh & A. Yamagishi
Hazama Ando Corporation, Tokyo, Japan
yamada.satoshi@ad-hzm.co.jp

ABSTRACT:
This paper describes a newly developed soil mixing machine with dryer function. Regarding the core embankment of rock-fill dams, fine-grained soil and coarse-grained gravel must be mixed uniformly and efficiently in the stockpile. When the fine-grained soil is relatively wet, compared to optimum water content, blended soil becomes difficult to be mixed uniformly because fine-grained soil tends to become what is called “clay lumps”. Therefore reducing water content of fine-grained and wet soils is an important issue for the improvement of core quality.

In this background, we developed a machine called “Mantis”, which can blend fine-grained soil and coarse-grained material efficiently even though the mix has a very high content of fines and water. We used a crawler type soil mixing machine, called “Stabilizer” which was improved with a fan for sending hot air produced with engine’s exhausted heat. Finally, we carried out a trial blending test at the stock yard. We found that the processed material was well mixed and its water content was reduced.

Keywords: Fill dam, Core material, Fine-grained Soil, High water content, Stabilizer

1. GENERAL INSTRUCTIONS

Regarding the core embankment of rock-fill dams, when single material does not comply with the specifications, we use two types of material and mix them. Then fine-grained soil and coarse-grained gravel must be mixed uniformly and efficiently in the stockpile. Generally, each material is piled by layers and then mixed by bulldozer. This method is called “Slice cut”.

When the fine-grained soil has high content of water, fine-grained soil becomes difficult to be mixed uniformly, because it becomes what is called “clay lumps”. “Clay lumps” has a diameter between 5 cm and 15 cm and affects the impermeable quality and performance of core. "Clay lumps" portion has excessive content of water. Even if leaving such kind of material under the sun for a long time, the water ratio does not change easily.

In this background, we developed a machine which can blend fine-grained soil and coarse-grained material efficiently even when the mix has a very high content of fines and water. The base machine is “Stabilizer”, employed currently in dam construction with the same problem in core material (Japan Dam Foundation 2009). We named the developed machine “Mantis” because it resembled the insect. Mantis was developed considering carbon dioxide emissions reduction and cost. It has the following features:

(1) Structure is simple because heat sources is engine’s exhausted heat.
(2) Using engine’s exhausted heat is environmentally friendly because it does not increase carbon dioxide emission.
(3) Running cost is low because it uses engine’s exhausted heat.
(4) Because the base machine is stabilizer, it can mix soil well.

To check the functions mentioned above, we carried out trial blending by using the developed machine as shown in Fig. 1.

2. TRIAL BLENDING

2.1. Summary of the trial

On-site trial was conducted in the stock yard of the zoned earth fill dam project. In the stock piles of the stock yard, fine-grained soil and coarse-grained soil were stacked in layers. Fine-grained soil is consist of volcanic ash cohesive soil, natural water content and optimum water content are approximately 90% and 63% respectively, and fine fraction content is approximately 85%. Coarse-grained soil is consist of weathered rock and gravelly soil, natural water content is approximately 10%, and fine fraction content is approximately 12%.

Two cases were conducted in the trial blending: Case 1 was using “Mantis” without drier function and Case 2 was using “Mantis” with drier function. In each case, “Mantis” was operated on the stock piles with 15m length. During the trial blending, we obtained the data every 5times of traveling, namely at 0, 5, 10, and 20 times. Before starting the trial blending, the “Mantis” without using dry function mixed fine-grained soil and coarse-grained soil by a single traveling. Schematic image of the trial blending is shown in Fig. 2.

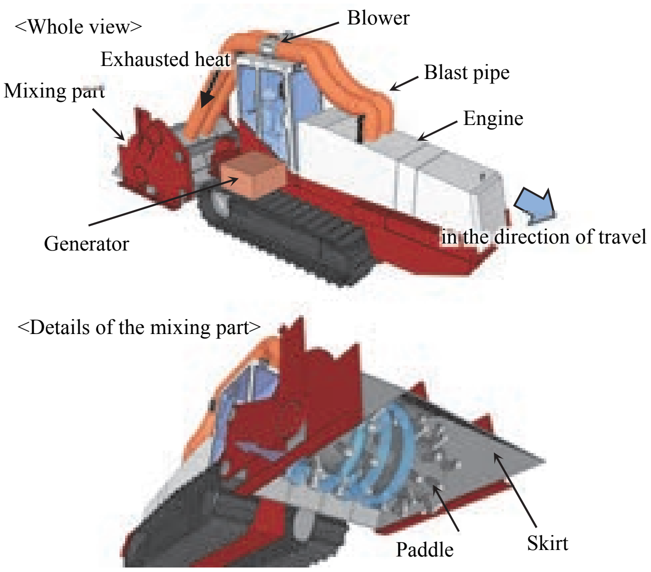
<Whole view>
Blower
Exhausted heat
Mixing part
Blast pipe
Engine
Generator
in the direction of travel
<Details of the mixing part>
Paddle
Skirt

Figure 1. Images of “Mantis”

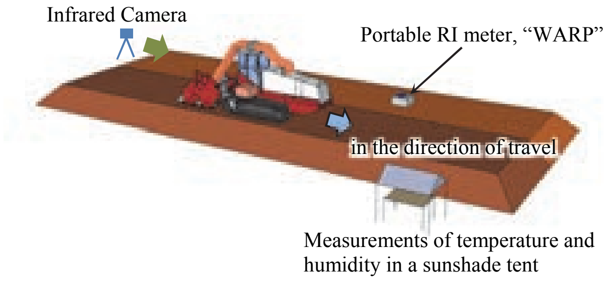
Infrared Camera
Portable RI meter, “WARP”
in the direction of travel
Measurements of temperature and humidity in a sunshade tent

Figure 2. Schematic image of the trial blending

2.2. Specifications of the Stabilizer

The side view of the Stabilizer and the specification are respectively shown in Fig. 3 and Table 1.

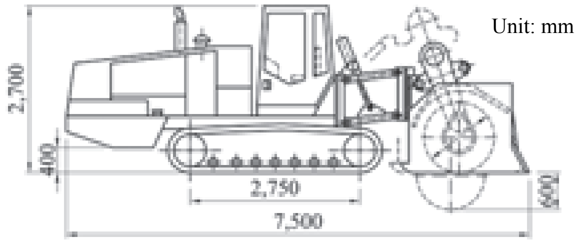
Unit: mm
2,700
400
2,750
7,500
600

Figure 3. Side view of the Stabilizer

Table 1. Specification of the Stabilizer

Type	STB210C (Toyo Stabi Co., Ltd.)
Length	7.5 m
Width	2.85 m
Height	2.7 m
Mixing width	1.8 m
Mixing depth	0.5 m (Max 0.6 m)
Rated power	151.5 kW(206 PS)、2,200 rpm
Speed of rotation	60～100 rpm (Max 135 rpm)
Running speed (Reference)	Operation : Approx. 2 km/h Moving : Approx.10km/h

2.3. Controlled Data and Equipment

Data types and its specification are shown in this sub-section.

2.3.1. Temperature and Humidity

Atmospheric temperature and humidity were measured with a thermometer and hygrometer indicator. Intentionally, measurement was conducted inside a sunshade tent in order to prevent direct sunlight effects.

The specifications and the picture of this indicator are shown in Table 2 and Fig. 4, respectively.

Table 2. The specification of thermometer and hygrometer indicator

Name	thermometer and hygrometer indicator
Type	LR5001 (HIOKI Co., Ltd)
Range	-40.0 °C∼+ 85.0 °C
Accuracy	±0.5 °C

Figure 4. Thermometer and hygrometer indicator

2.3.2. Water Content of Soils (RI Method)

Water content of soil was measured by Simplified Radio Isotope Moisture Meter (Portable RI meter, “WARP”). This new equipment is able to measure water content of soil easily compared to the conventional RI equipment; additionally it is small and light.

Measurements were conducted after smoothing the soil surface, and then data of water content were taken after 0, 5, 10, and 20 times of traveling by “Mantis”. We took the average of 3 data points as a representative data of water content. Specifications of “WARP” and its figure are shown in Table 3 and Fig. 5, respectively.

Table 3. Specification of Radio Isotope moisture meter (Portable RI meter, "WARP")

Type	Neutron Disperse Type (Soil & Rock Co., Ltd)
Detector	^{3}He Proportional counter
Radiation source	Californium 252 1.11MBq
Range	Water content : 0～100%
Measurement depth	10 cm
Measuring time	1 min
Service temperature	0～50 °C

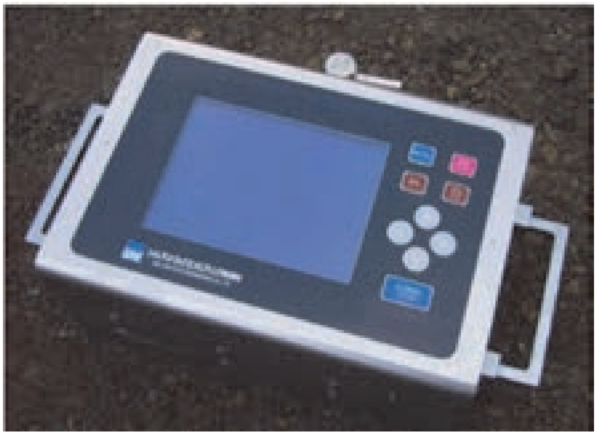

Figure 5. Portable RI meter, "WARP"

2.3.3. Surface Temperature of Soils and "Mantis"

In order to check the effect or the heating system, the surface temperature of soils and "Mantis" was measured by infrared camera.

Specifications of the infrared camera and its figure are shown in Table 4 and Fig. 6, respectively.

Table 4. Specification of infrared camera

Name	Thermo-shot
Type	F-30S (Japan Abionics Co., Ltd)
Range	- 20～100 °C.
Accuracy	± 2 °C.

Figure 6. Infrared Camera

2.3.4. Observation of soils sticking to the mixing paddle

Cohesive soil is easy to stick to the mixing paddle, and reduces the efficiency. In order to check the ability of anti-accretion by "Mantis", mixing paddle was observed by digital camera at each operating time.

2.4. Photographs of Trial Blending

Trial blending was carried out at the rock fill dam project site in Fukushima on the 13th October 2015. Photographs of the trial blending are shown in Fig. 7 to Fig. 9.

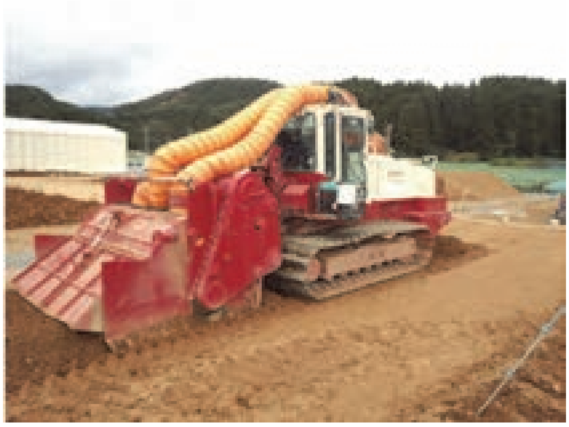

Figure 7. Operating "Mantis" (close range view)

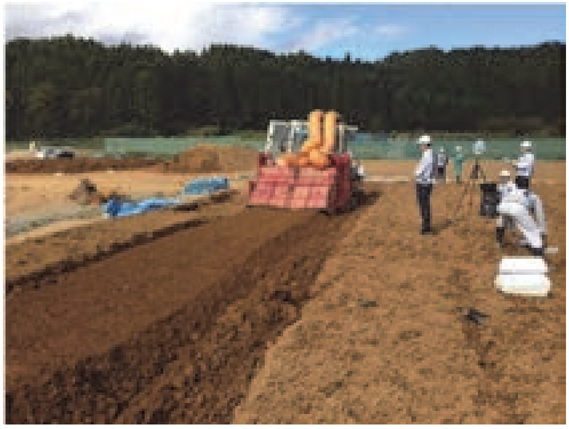

Figure 8. Operating "Mantis" (distant view)

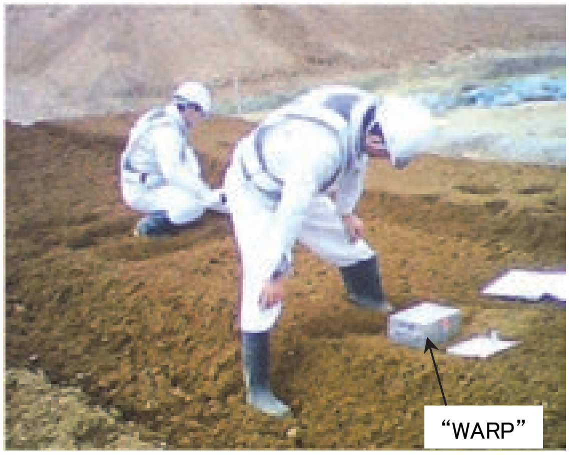

Figure 9. Measurement of water content by "WARP"

3. RESULTS

3.1. Temperature and Humidity

During Case 1 (without using drier function), weather was fine, temperature was between 17 and 20 °C around 10:30 AM., and the humidity was approximately 60 %. However, during Case 2 (using drier function) weather was changing suddenly, with some drizzle and strong wind. Temperature dropped and was between 15 and 18 °C (11:18-11:33 A.M.). Ambient temperature and humidity at the trial site is shown in Fig. 10.

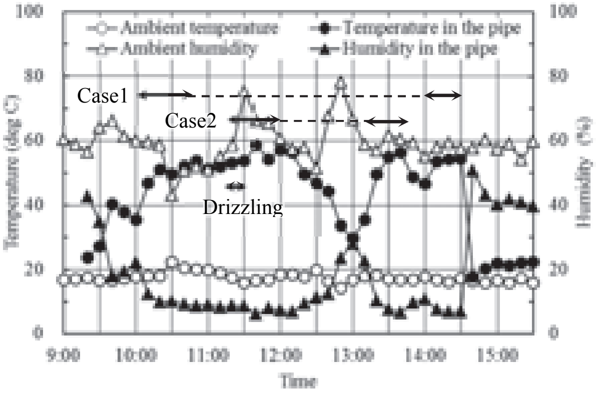

Figure 10. Atmospheric temperature and humidity

3.2. Thermo-graphic Images by Infrared Camera

Infrared camera and digital camera were set in parallel. Thermo-graphic and visible images could be compared during the trial.

The surface temperatures obtained from thermo-graphic image in the side (Fig. 11) were 97.3 °C at engine part, 47.0 °C at blast pipe entrance point, 42.9 °C at blast pipe intermediate point and 41.7 °C at blast pipe discharge point. It is found that the temperature in the blast pipe is gradually falling down toward the mixing part.

The surface temperatures obtained from thermo-graphic image in the mixing part (Fig. 12) were between 20 and 23 °C at skirt of mixing part and from 18.9 to 19.7 °C at surface of the soil.

Since ambient temperature was between 15 and 18 °C, we could estimate that an increment of 2 - 4 °C was caused by heat supplied to the soil by “Mantis”.

3.3. Water Content of Soils

Results of water content of soils by portable RI meter, “WARP” are shown in Table 5 and Fig. 13 respectively. Water decreasing rate defines that subtracting the water content at the running times “0” from “N”.

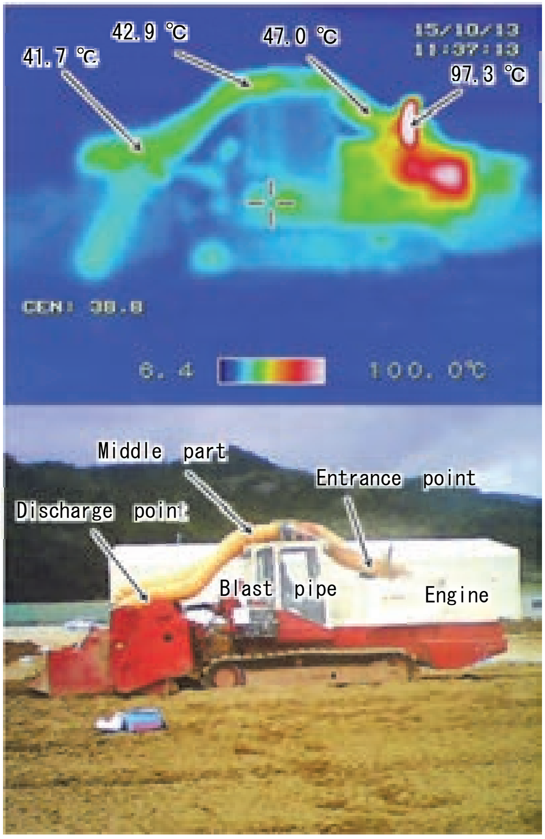

Figure 11. Thermo-graphic image (Whole side)

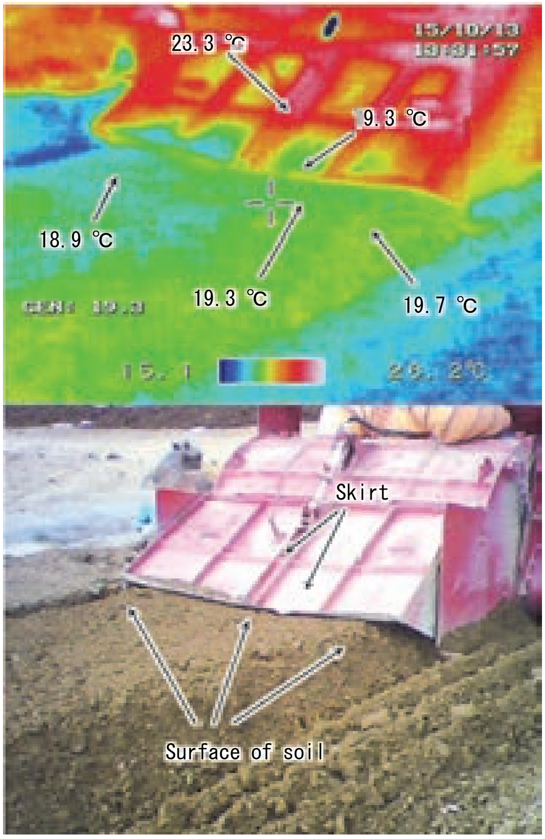

Figure 12. Thermo-graphic image (Mixing Part)

Results show that water degreasing rate at 10 times of running in Case 1 (without using drier function) is 7.8%, and Case 2 (using drier function) is 11.7%. The difference between Case 1 and Case 2 is 3.9%. On the other hand, water decreasing rate at 20 times of running in Case 1 is 12.5%, and Case 2 is 15.4%. The difference between Case 1 and Case 2 is 2.8%.

We found that introducing the stabilizer to blend the soil material in the stockpile was very effective. However, introducing drier function to the stabilizer was more effective to reduce the water content of soils by supplying heat to the soil.

Table 5. Results of water content by "WARP"

Numpers of times of traveling	Water content W1 (%)		Reduction of moisture content W2 (%)		Difference W3 (%)
	Case 1	Case 2	Case 1	Case 2	
0	29.9	35.8	0.0	0.0	0.0
5	23.6	31.2	-6.4	-4.6	-1.8
10	22.1	24.1	-7.8	-11.7	3.9
20	17.4	20.4	-12.5	-15.4	2.8

W1: Average of data at 3 points
W2: W1 minus W1 (at 0 times)
W3: W2 (without dry function minus with dry function)

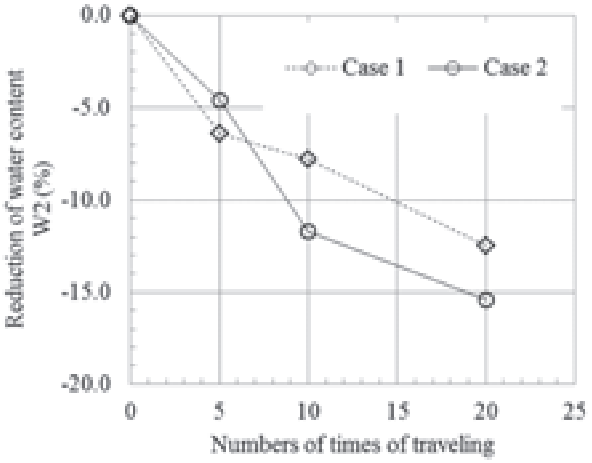

Figure 13. Reduction of water content

3.4. Observation of the Mixing Paddle

Observation of Case 1 and Case 2 could not find a relevant differential. Both of them show almost no soil was sticking to the paddle. It was considered that the water content of soil was relatively low and therefore difficult to stick the paddle.

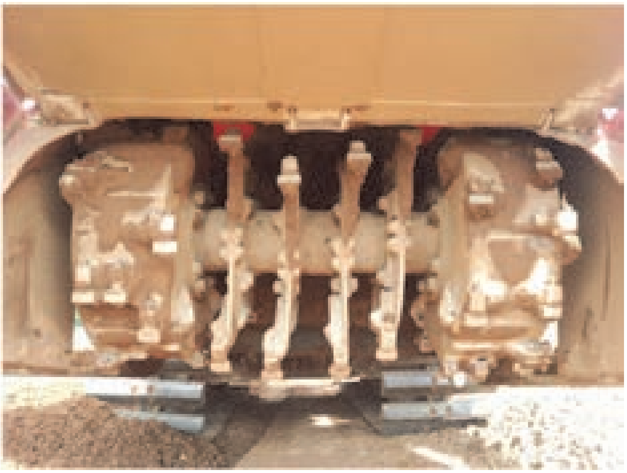

(1) Case 1 (without using drier function)

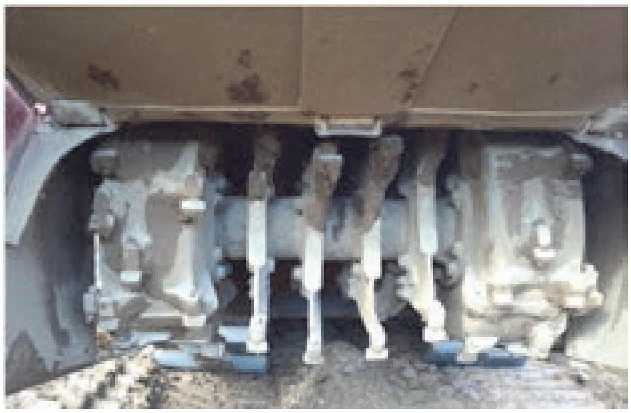

(2) Case 2 (using drier function)

Figure 14. Observation of the Mixing Paddle

4. CONCLUSION

In order to dry soil environmentally friendly and economically, we developed "Mantis" by renovating the conventional stabilizer.

Thermo-graphic at the trial showed the blow air temperature was reached to more than 40 °C, and supply heat from 2 to 4 °C to the soil when ambient temperature was from 15 to 18 °C.

Water degreasing rate increased in from 3% to 4% by using dry function when running time was from 10 to 20 times.

Results showed that new developed "Mantis" could dry wet soils effectively for core materials of fill dams.

REFERENCES

Japan Dam Foundation Committee on Construction Technology . (2009): Construction of Fill Dam, Japan Dam Foundation, in Japanese.

4th APG Symposium and 9th EADC on

INNOVATIVE TECHNOLOGIES FOR DAMS AND RESERVOIRS TOWARD THE FUTURE GENERATIONS

Proposal of the Rationalization of Dam Construction Quality Control

H. Yoshida
Chairman, Dam Construction Technology Research Group, Japan Society of Dam Engineers
Vice President, Japan Dam Engineering Center, Japan
yoshida@jdec.or.jp

M. Kusumi
Member, Dam Construction Technology Research Group, Japan Society of Dam Engineers
Counselor Dam Engineer Section Civil Engineering Division, Taisei Corporation, Japan

ABSTRACT:
The Dam Construction Technology Research Group of the Japan Society of Dam Engineers studied rationalization of the quality control of the dam construction work. We surveyed many cases of quality control of dam construction executed in recent years and conducted a study based on execution data concerning the possibility of rationalizing quality control. Based on the results of this study, we proposed the rationalization of quality control of future dam construction work.

Key words: Quality control, test methods, test frequency, rationalization of quality control, new technologies

1. INTRODUCTION

Dam technologists from industry, government and academia in Japan have established the Japan Society of Dam Engineers, which has conducted a variety of activities including survey research of dam engineering and spreading information to the public. The Construction Technology Research Group of the Japan Society of Dam Engineers has conducted a survey study of the rationalization of quality control test of dam body construction work. This paper summarizes the results of its studies. (Construction Technology Research Group of the Japan Society of Dam Engineers. 2013）

The test items and test frequencies in quality control of present-day dam construction work are often decided based on the construction experience of the precedent dams. So they are almost the same regardless of the dam volume or the construction method or the completion year.

The essential purpose of concrete strength test is to confirm that strength satisfies the standard values. However, it takes time to obtain the results of tests, and in the end, all that is achieved is that it’s possible to manage the trends in fluctuation of strength over time following the construction work. And concrete strength test is done intermittently, so continuous control of concrete strength is not performed.

On the other hand, in Japan, Information and Communication Technology (ICT) executions and automatic measurements are often applied to dam construction work. (Yamaguchi. Y, et al. 2012), Their use permits quality control and execution control to be performed continuously and that enhances reliability not possible in the past. (Computerized Construction romotion Committee. 2008)

Based on the above-mentioned situation, we decided to inspect quality control method of the conventional dam construction work. We believe that the time has come to develop and introduce more rational quality control methods of dam construction work.

2. PROBLEMS AND PRESENT STATE OF QUALITY CONTROL

The Research Group first analyzed the state of quality control of dam construction work.

2.1. Problem in the quality control of the concrete dam

We analyzed test items and test frequency at gravity concrete dams, mainly those completed after 1964 (33 dams). The results identified the following items as problems to the quality control of concrete dams.
[1] Regarding test items and test frequency, there are no differences according to construction method (Block method, Roller Compacted Dam Concrete Method (RCD) or Extended Layer Construction Method (ELCM)) or dam volume, or completion year. And at all dams, a constant test frequency was applied from the

start to the end of dam construction work. In the future, appropriate quality control test items and test frequency should be selected according to the materials, the construction method, dam volume. We must return to the original quality control: watching quality variation trends to take improvement measures as needed.

[2] Much attention has been paid to concrete strength test and other laboratory quality control test. In the future, priority should be on quality control integrated throughout the entire execution process: quality control of materials from quarrying to aggregate production, execution control during placing of concrete, and curing management.

[3]When multiple mixes of concrete are used simultaneously, the quality of each mix is separately controlled, resulting in a massive rise in the number of test samples used to control by age. If a certain quantity of data can be obtained to confirm correlation, it will enable rationalization through prioritized control of a representative mix and omission of control of other mixes, which in turn will reduce the number of tests.

[4] In case of scale malfunction or cement adherence to the scales during concrete production, the weight may be shown incorrectly, so it is important to check the scales.

2.2. Problem in the quality control of the embankment dam

We analyzed the test items and test frequency in quality control of core material at embankment dams (21 dams) constructed during and after the 1960s, when construction machinery increased in size and hydraulic control technologies were developed. As a result, as at concrete dams, it was not possible to confirm differences in the test items and test frequency according to dam volume and completion year. Constant test frequency was applied from the start to the end of dam construction works.

The following items were cited as proposed improvements.

[1] The test frequency of the quality control is set by layer units, calendar units, or embankment quantity units. Imbalance of the coarseness and minuteness occurs for the quality control because of a way of the setting of the test frequency. Appropriate test frequency should be reviewed according to the dam volume and construction speed.

[2] At embankment dams, essentially, the material is changed during execution in order to effectively use natural materials. In many cases where material is changed on the way, quality control test is done at the originally decided fixed frequency. When the material is changed on the way, it is necessary to take measures such as increasing the test frequency until quality has stabilized.

Fig. 1 is an example of a history of core material dry density, showing great change in dry density caused by change of material. When material is changed on the way, until stability of quality is confirmed, careful quality control test must be performed.

[3] As methods of on-site density test, in many cases, the joint use of the sand replacement method and Radio Isotope method (RI method) is prescribed. The RI method is simpler and faster than the sand replacement method, and if the correlation of the two can be confirmed, we should use the RI method mainly and should use the sand replacement method secondarily.

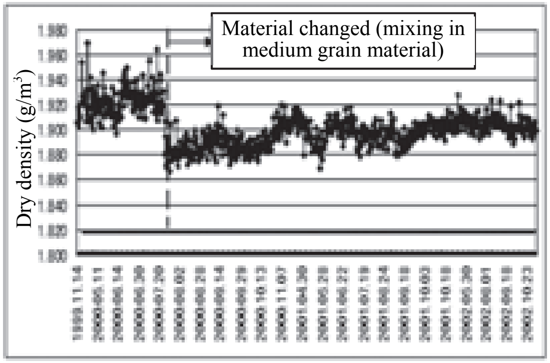

Figure 1. Core material dry density history

Fig. 2 is an example of the correlation of the sand replacement method with the RI method applied during on-site density test. Relatively good correlation of the two methods is seen, and the RI method obtains smaller values.

In this case we should perform quality control using the RI method mainly. The RI method can perform the quality control of the safer side and the correlation with sand replacement method is high.

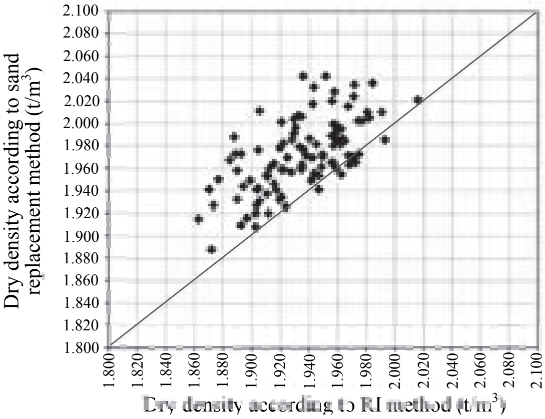

Figure 2. Correlation of sand replacement method and RI method for on-site density test

On-site density test data is point data on embankment, so it is not verified that quality is ensured for an entire embankment. The RI method can be tested more easily than the sand replacement method, and quality control should be varied by increasing the RI test frequency. It is necessary to make efforts to introduce new technologies or new testing methods to quality control, by developing new testing methods that permit clarification of area data or continuous data.

[4] To control quality of cores, it is important to ensure density and coefficient of permeability, but it takes time

for the results of these quality control tests to be manifested, and data are organized after execution. When materials are stock-piled, stabilized quality should be ensured by priority execution of quality control before the materials are brought to the dam site.

3. QUALITY CONTROL TEST FREQUENCY

3.1. Case of a concrete dams

Fig. 3 is an example of a 91 day strength histogram of a concrete dam. The histogram shows shape that is almost a normal distribution.

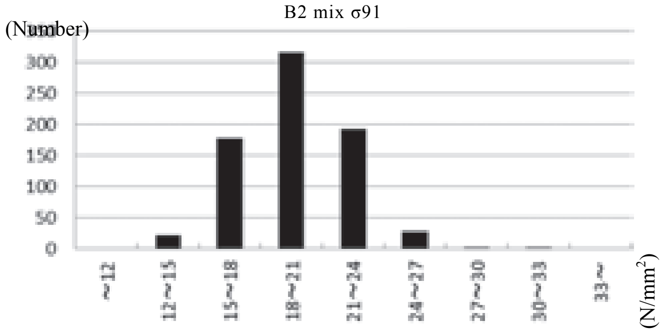

Number	737
Average	19.77
Standard differential	2.54
Coefficient of variation (%)	12.9
Maximum	31.9
Minimum	13.1

Figure 3. Example of results of concrete strength test (Dam A)

Next, we analyzed the impacts on statistical results of average values, maximum values, minimum values, standard differential, and coefficient of variation in a case where the test frequency was lowered at a constant percentage.

Fig. 4 shows the results of analysis of change of the standard differential and coefficient of variation in the case where test frequency was reduced regularly by 1/2, 1/3, and 1/4 at placing period (first phase, intermediate phase, final phase) at 5 concrete dams.

The results were almost identical even if the data declined along with the standard differential and coefficient of variation. At dams other than dam B, in the final phase, both the standard differential and coefficient of variation clearly tended to decline, indicating that the quality had stabilized.

We similarly analyzed the average, maximum, and minimum values, but even in the results showing decline of the data, the trends were almost identical. This shows that test frequency can be reduced while quality has stabilized.

From the above test results, the following proposals are made concerning rationalization of quality control of concrete dam construction work.

[1] For quality control of concrete, further increase of testing frequency or setting harsh control standard values when the material quality is not stabilized will be studied. When the test results have stabilized, revision will be done by reducing test frequency or adopting a simple test method.

[2] Quality control of concrete materials will be considered seriously. In particular, if material is changed midway, testing frequency will be reviewed according to the state of progress or state of execution on the site, doing supplementary testing etc.

[3] When, during concrete strength testing, confirmatory testing by mix or by age has confirmed that strength dispersion is small and there is correlation, then we should revise the reduction of the number of test specimens by mix or by age.

[4] The use of Global positioning system (GPS) or other ICT technology will be encouraged and areal or continuous control will be done to ensure reliability or traceability of execution.

3.2. Case of embankment dams

Fig. 5 shows the histogram distribution in a case where quality control data is methodically reduced to 1/2 for dry density, degree of compaction (sand replacement method, RI method) or coefficient of permeability of an embankment dam, and the results of analysis of statistical quantities such as maximum value, minimum value, average value, standard differential, and coefficient of variance.

This result is identical to the distribution shape of the original histogram, showing that the statistical values are also almost equal.

From the above test results, the following proposals are made concerning rationalization of quality control of embankment dam construction work.

[1] Frequency of quality control should be divided into early execution and stable period.

[2] Intensively incorporating the RI method or other simple test method. Using GPS or other ICT method to control roller compaction frequency or placing thickness, and performing areal and continuous control to increase the reliability of execution. (Ministry of Land, Infrastructure, Transport and Tourism. 2012)

[3] Fig. 6 is a flow chart of the embankment dam quality control test rationalization proposal. It is almost identical to the concrete dam case.

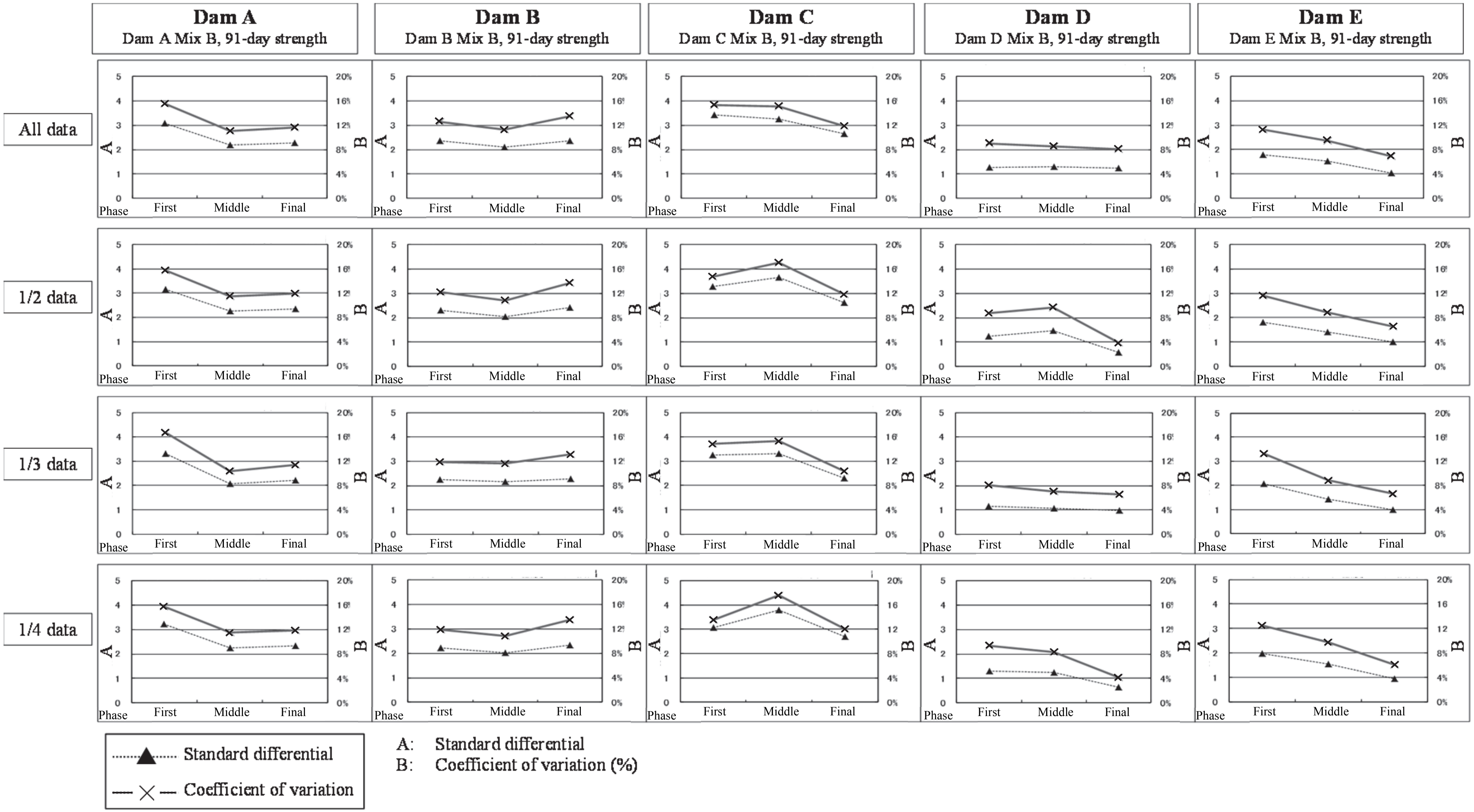

Figure 4. Comparison of the statistic in case of all data and reduced data

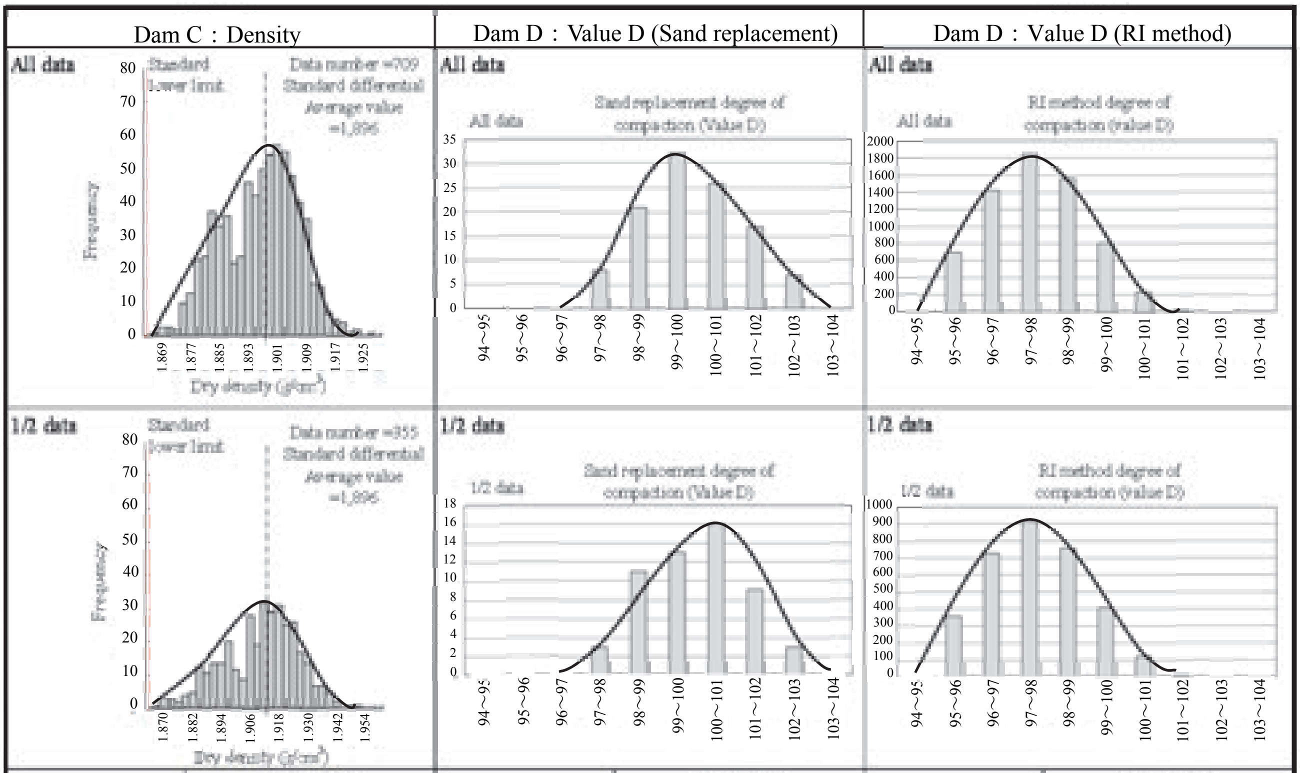

Item	Dry density (On-site density test, sand replacement)		Item	Compaction (On-site density test, sand replacement)		Item	Compaction (On-site density test, RI method)	
	All data	1/2 data		All data	1/2 data		All data	1/2 data
Sample number	709	355	Sample number	111	55	Sample number	6,586	3,293
Max. value (t/m³)	1.927	1.922	Max. value (t/m³)	102.9	102.8	Max. value (t/m³)	101.9	101.6
Min. value (t/m³)	1.866	1.866	Min. value (t/m³)	67.2	97.7	Min. value (t/m³)	95	93.5
Average value (t/m³)	1.896	1.896	Average value (t/m³)	99.9	100	Average value (t/m³)	97.6	97.5
Standard differential	0.011	0.01	Standard differential	1.3	1.3	Standard differential	1.3	1.4
Coefficent of variance	0.006	0.005	Coefficent of variance	0.013	0.013	Coefficent of variance	0.013	0.014

Figure 5. Comparison of histogram distribution shape with statistical quantities for case where 1/2 of test frequency is thinned

4. CONCLUSIONS

Judging from the above, proposals to rationalize quality control of concrete dams and embankment dams can be summarized as follows.

1] It is necessary to perform dynamic quality control: constantly monitoring data fluctuation trends and when the necessary quality cannot be confirmed, quickly making improvements at the material procurement, production, storage, or execution stages.

2] It is necessary to perform "continuous revision of quality control": instead of following uniform quality control items, testing and measurement frequency from the start of execution to its completion, changing quality control frequency and priorities while observing quality fluctuation trends.

3] It is necessary to rationalize quality control of dam construction work by introducing new technologies and new testing methods that can clarify continuous data instead of fragmentary point data while using ICT.

REFERENCES

Construction Technology Research Group of the Japan Society of Dam Engineers. (2013): Proposed rationalization of quality control dam construction work, Dam Engineering 23 (2), 121 – 163.

Yamaguchi.Y, Sato.H, Hashimoto.H (2012): Research on rationalization of rockfill dam execution control methods introducing ICT execution, Annual report of the PWRI.

Computerized Construction Promotion Committee. (2008): Computerized construction promotion strategies.

Ministry of Land, Infrastructure, Transport and Tourism. (2012): Embankment compaction control techniques using TS-GNSS

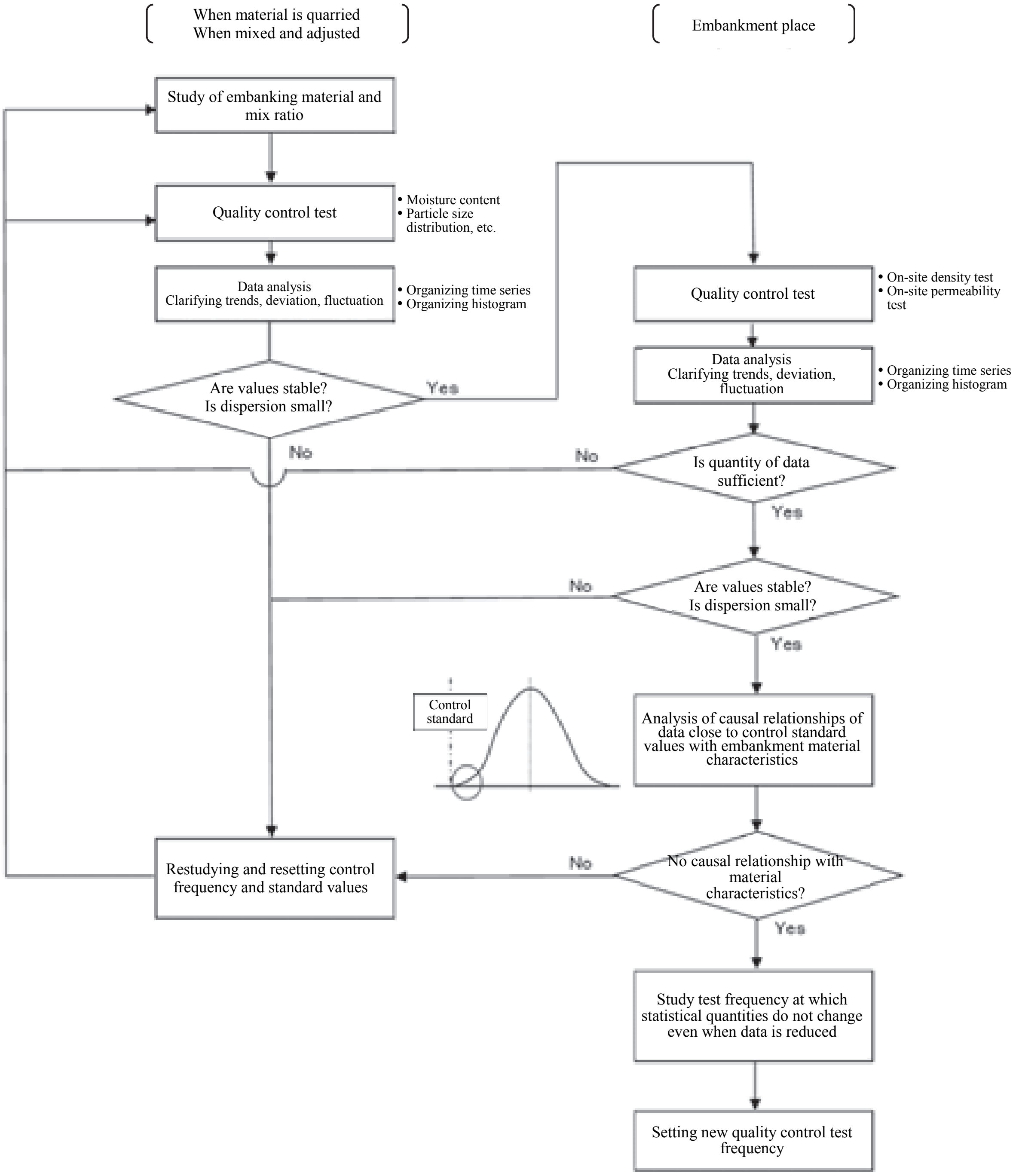
When material is quarried
When mixed and adjusted
Embankment place
Study of embanking material and mix ratio
Quality control test
• Moisture content
• Particle size distribution, etc.
Data analysis
Clarifying trends, deviation, fluctuation
• Organizing time series
• Organizing histogram
Are values stable? Is dispersion small?
Yes
No
Quality control test
• On-site density test
• On-site permeability test
Data analysis
Clarifying trends, deviation, fluctuation
• Organizing time series
• Organizing histogram
No
Is quantity of data sufficient?
Yes
No
Are values stable? Is dispersion small?
Yes
Control standard
Analysis of causal relationships of data close to control standard values with embankment material characteristics
Restudying and resetting control frequency and standard values
No
No causal relationship with material characteristics?
Yes
Study test frequency at which statistical quantities do not change even when data is reduced
Setting new quality control test frequency

Studying active introduction of a simple test method such as the RI method as the test method

Figure 6. Rationalization of Quality Control Testing of an Embankment Dam (Proposed)

The Applicability Analysis of Local Riverbed Aggregate for Hardfill Dam

J.S.Yoon
Manager & K-water, Deajeon, Republic of Korea
yoonjs@kwater.or.kr

H.K.Lee
General Manager & Dongbu Engineering, Seoul, Korea

K.Y.Kim
Principal Researcher & K-water, Deajeon, Republic of Korea

K.T.Kim
Clerk & K-water, Deajeon, Republic of Korea

ABSTRACT:
The Hardfill is construction method of dam by compacting the mixture which consists of water, cement and riverbed aggregate. Riverbed aggregate is from submerged area of the dam and sorted with minimal process. Hence, the most important factor of mixing design is the grain-size distribution of local riverbed aggregate. The objective of this study lies in evaluating the applicability of bed aggregates for Hardfill dams that are observed in upper rivers in Korea where it's possible to develop small- and mid-sized dams. To this end, a grain-size distribution analysis of bed aggregates for laboratory mixture tests sampled in the upper rivers was performed herein, along with a geometric statistical analysis of grain-size curves estimated with the same bed aggregates. Also, the authors comparatively used and studied other similar approaches employed in Korean and overseas dam design practices and cases from Japan's CSG Research Society, Korea's Hwabuk Dam (constructed as a pilot project with the CSG technique), the U.S. Portland Cement Association and the U.S. Army Corps of Engineers (EM 1110-2-2006) to estimate with at least 90% in confidence level the upper and lower boundaries for the grain-size distribution of bed aggregates applied for the laboratory mixture tests.

Keywords: Hardfill dam, grain-size distribution, riverbed (or bed) aggregate, geometric statistical analysis, laboratory mixture test

1. BACKGROUND

Globally changing dam development environment, which has been accompanied with, particularly, ongoing climate change, challenging environmental stresses, shrinking public investments, etc., has raised a need to develop dam development techniques with which it would be possible to save construction costs and minimize environmental impacts. The conceptual birth of Hardfill dams dates back to early 1992 when P. Londe introduced them to address the reality where sites geologically optimal for dam development are becoming rare. Since then, tens of Hardfill dams have been constructed and operated in Japan, China, Turkey, etc. Particularly in Japan where relatively many cases of studies and projects have been underway, they are termed as "Cemented Sand and Gravel" (CSG) dams.

Actually, the Hardfill method has been recognized as a brand-new technique engineered to save construction costs and ensure environmental preservation and equipped with the structural stability of concrete dams and the good constructability of fill dams.

With the Hardfill method, it's possible to dramatically simplify series of work processes, including the procurement of aggregates, mechanical stabilization of grain sizes, mixture, placement, etc., since along with onsite excavated soil bed sand and gravel materials easily to procure around a dam site are used to blend with a mixture of cement and water without being screened except that large-size gravels are removed from them. Hence, the Hardfill method has been recognized and employed as a relatively proven technique in overseas design practices although there is almost no case in Korea where the same method has ever been used to construct a main dam, which is why there is a need to put in place relevant design standards and criteria and construction techniques of Korea's own. Accordingly, the objective of this study is to evaluate the applicability of bed aggregates for Hardfill dams that are present in major rivers in Korea. To this end, the authors surveyed and analyzed bed aggregates in the target rivers.

2. METHODOLOGY

First, the authors studied with similar Korean and overseas cases where the Hardfill method was employed to construct a dam, including the following cases, and other relevant data before proceeding to analyze the grain-size distribution of bed aggregates in major rivers in Korea:

- CSG Research Society (Japan): Case of aggregate grain sizes where the grain-size distribution of aggregates for the CSG method as proposed by the CSG Research Society was analyzed
- Hwabuk Dam (Korea, 2005): Case of mix design where bed aggregates available around a dam site were used to construct its coffer dams with the CSG method(K-water, 2008)
- CSG Research Society (Japan): Case of the mechanical stabilization of grain sizes for laboratory tests
- Standard RCC: Case from the U.S. Portland Cement Association(PCA, 2000)

Also, the authors surveyed data about the grain-size distribution of bed aggregates for each of major river systems in Korea whose catchment area is at a small or middle level, and then statistically analyzed them to draw out a grain-size distribution curve at each confidence level and estimate the upper-limit, median and lower-limit grain-size distribution of aggregates for laboratory mixture tests.

3. STAUS OF RIVERS IN KOREA

7 major river systems in Korea as surveyed herein include the Han river system, the Nak-dong river system, the Kum river system, the Man-kyung river system, the Sap-kyo river system, the Seom-jin river system, and the Hyung-san river system(MOLIT, 2002~ 2009), which are respectively shown in Tables 1 to 7 and Figs. 1 to 7.

3.1. HAN RIVER SYSTEM

Table 1. Han river system

River	Catchment area(km^2)	Length(km)
O-dae river	451.50	57.80
Sok-sa river	120.00	31.37
Nae-rin river	186.70	60.76
Seo river	167.07	27.50
Han-jeon river	30.54	10.37
Su-ip river	318.99	44.25
Gye river	283.62	38.84

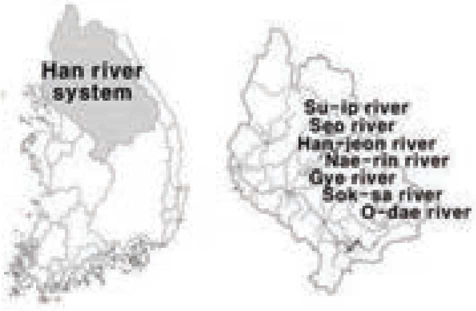
Han river system
Su-ip river
Seo river
Han-jeon river
Nae-rin river
Gye river
Sok-sa river
O-dae river

Figure 1. Han river system

3.2. NAK-DONG RIVER SYSTEM

Table 2. Nak-dong river system

River	Catchment area (km^2)	Length (km)
Ja-ho river	327.80	46.70
Nam river	160.02	22.20
Ban-byeon river	780.31	75.70
Seo river	364.64	32.00
Chung-do river	336.98	41.00
Ssang-gye river	501.36	43.80

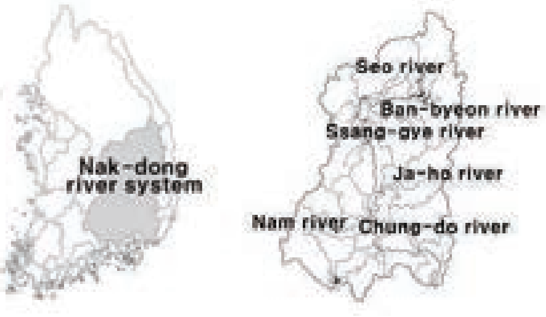
Nak-dong river system
Seo river
Ban-byeon river
Ssang-gye river
Ja-ho river
Nam river
Chung-do river

Figure 2. Nak-dong river system

3.3. KUM RIVER SYSTEM

Table 3. Kum river system

River	Catchment area (km^2)	Length (km)
Kum river	303.40	35.55
Jang-gye river	114.08	16.55
Jang-su river	16.12	5.85
Mi-ho river	287.32	39.07
Cho river	183.18	27.50

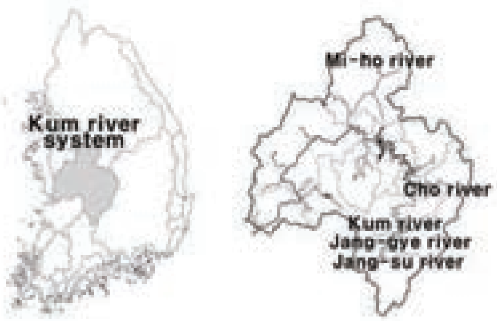
Kum river system
Mi-ho river
Cho river
Kum river
Jang-gye river
Jang-su river

Figure 3. Kum river system

3.4. MAN-KYUNG RIVER SYSTEM

Table 4. Man-kyung river system

River	Catchment area (km^2)	Length (km)
Man-kyung river	1,527.10	77.40
Jeon-ju river	272.60	37.00
So-yang river	152.4	24.50

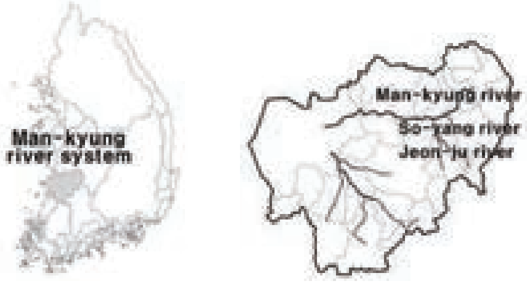
Man-kyung river system
Man-kyung river
So-yang river
Jeon-ju river

Figure 4. Man-kyung river system

3.5. SAP-KYO RIVER SYSTEM

Table 5. Sap-kyo river system

River	Catchment area (km^2)	Length (km)
Gok-kyo river	396.84	25.33
Mu-han river	382.71	40.66

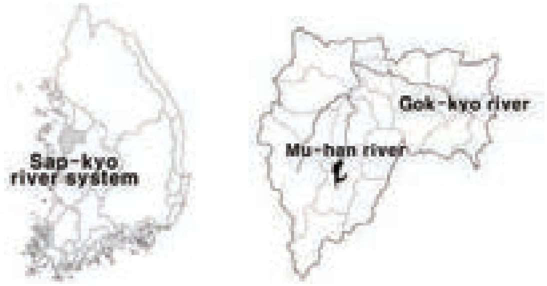
Sap-kyo river system
Gok-kyo river
Mu-han river

Figure 5. Sap-kyo river system

3.6. SEOM-JIN RIVER SYSTEM

Table 6. Seom-jin river system

River	Catchment area (km^2)	Length (km)
Yo river	273.80	42.10

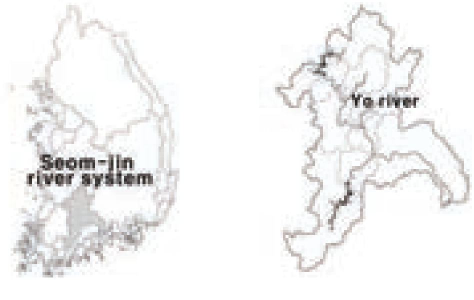
Seom-jin river system
Yo river

Figure 6. Seom-jin river system

3.7. HYUNG-SAN RIVER SYSTEM

Table 7. Hyung-san river system

River	Catchment area (km^2)	Length (km)
Hyung-san river	22.16	7.28

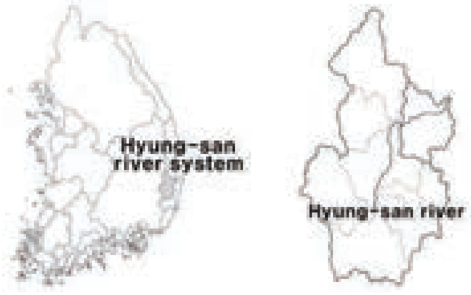
Hyung-san river system
Hyung-san river

Figure 7. Hyung-san river system

4. CASE STUDY

The authors studied comparable cases from Japan's CSG Research Society, Korea's Hwabuk Dam and standard RCC dams to estimate the upper and lower limits for the grain-size distribution of aggregates as shown in Figure 8:

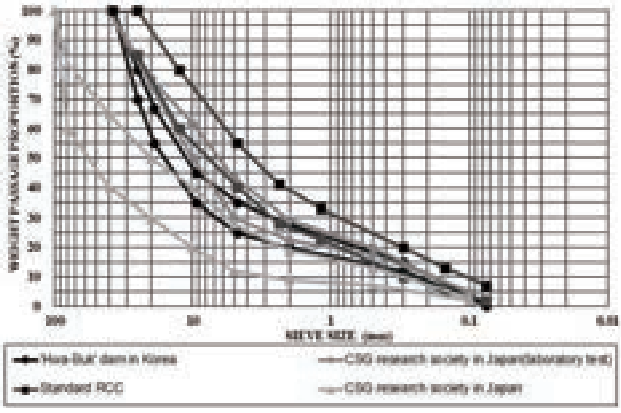

Figure 8. Grain-size distribution of aggregates as shown in similar Korean and overseas cases

Generally, unit cement requirement is significantly higher for standard RCC dams than for Hardfill dams, which is why fine fractions account for the relatively substantial portion of aggregates in the former ones as indicated in the figure.

5. GRAIN-SIZE DISTRIBUTION OF BED AGGREGATES BY RIVER SYSTEM

The authors analyzed the grain-size distribution of bed aggregates observed in some of the major river systems whose catchment area stands at a small or middle level. Table 8 shows bed aggregate data used for the foregoing analysis, and Figure 9 indicates grain-size distribution curves, which were compared against the corresponding curves applied in comparable Korean and overseas cases with Hardfill dams to evaluate the rough range of the grain-size distribution curves:

Table 8. Data of water systems

Water system	Number of data
Han river	23
Nak-dong river	25
Kum river	19
Man-kyung river	30
Sap-kyo river	7
Seom-jin river	7
Hyung-san river	4
Total	115

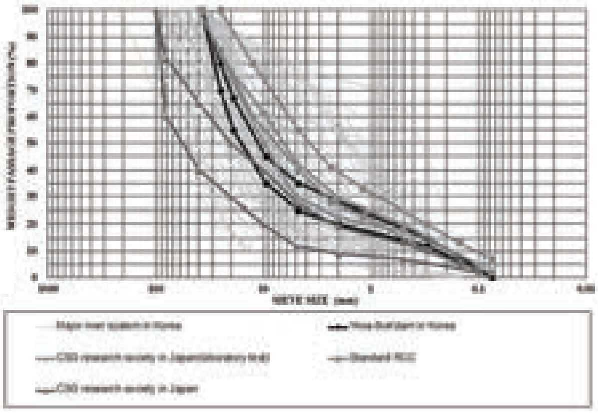

Figure 9. Grain-size distribution curves for bed aggregates

6. STATISTICAL ANALYSIS OF GRAIN-SIZE DISTRIBUTION OF BED AGGREGATES IN KOREA

Bed aggregates used for a statistical analysis performed herein show a substantial level of deviation and variance in terms of their grain-size distribution, so that their arithmetic mean and standard deviation alone couldn't reasonably account for the grain-size distribution. This is why a geometric statistical analysis was conducted herein with their geometric mean and standard deviation. For a grain-size distribution analysis of bed aggregates, results and findings from a geometric statistical analysis of grain-size data covering the major rivers in Korea were used along with relevant Korean and overseas cases from Japan's CSG Research Society, Korea's Hwabuk Dam (constructed as a pilot project with the CSG technique), the U.S. Portland Cement Association and the U.S. Army Corps of Engineers (EM 1110-2-2006) (USACE, 2000), and the USCS (Unified Soil Classification System).

Out of 230 populations, data with $D_{95}\leq 20$mm or $F_{\#200}\geq 5\%$ were excluded in the geometric statistical analysis since their corresponding applicability for Hardfill dams was considered as low. Also, a mechanical stabilization of grain sizes was made considering that the maximum grain size of aggregates for compaction tests was 37.5mm (KSF 2306) so that a confidence level of 90% or higher might be achieved. Figure 10 shows the grain-size distribution at each confidence interval, along with the upper, middle and lower limits of the grain-size distribution applied herein for laboratory mixture tests.

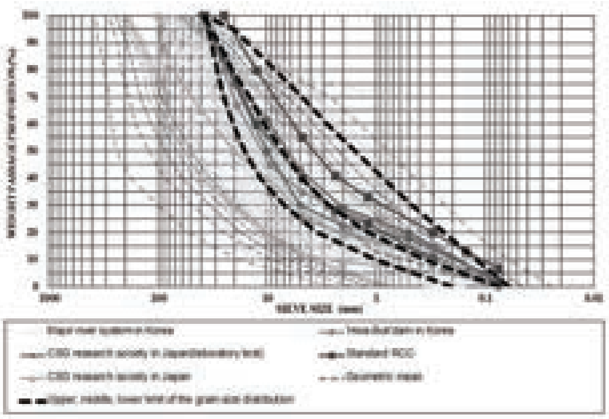

Figure 10. Statistical analysis of the grain-size distribution of bed aggregates

The upper, middle and lower limits for the grain-size distribution of bed aggregates for laboratory mixture tests were determined herein as follows:

- Upper: $D_{95}\leq 20$mm and $F_{\#200}\geq 5\%$ with a confidence level of 90% achieved
- Middle: Geometric statistical mean
- Lower: Maximum grain-size requirement (i.e., 37.5mm) met at a confidence level of 99%

7. FUTURE PLAN

The ultimate goal of this study is to put in place Korea's own construction standards for Hardfill dams. But the study yet remains at its early stage where aggregates are selected for laboratory mixture tests. In the future study, accordingly, the authors will proceed to perform the laboratory mixture tests and onsite test construction works, ensure design application for real-size dams, and develop relevant design standards.

REFERENCES

K-water, Korea Water Resources Corporation (2008): Criteria of mixing design and laboratory test CSG, pp. 11-12.

PCA, Portland Cement Association (2000): Guide for developing RCC specifications and commentary, pp. 6-7.

MOLIT, Ministry of Land, Infrastructure and Transport in Korea: Basic Plan for River Maintenance (2002~2012)

USACE, US Army Corps of Engineers (2000): Roller-Compacted Concrete (EM 1110-2-2006), pp. 3-4~3-12

4^{th} APG Symposium and 9^{th} EADC on

INNOVATIVE TECHNOLOGIES FOR DAMS AND RESERVOIRS TOWARD THE FUTURE GENERATIONS

A Study on the Development of Hybrid Dam Technologies

W.Y.Park
Assistant Manager & K-water, Daejeon, Republic of Korea
Pwy3428@kwater.or.kr

H.C.Park
Managing Director & Dohwa Engineering, Seoul, Korea

J.S.Yoon
Manager & K-water, Daejeon, Republic of Korea

S.J.Gang
Director Manager & K-water, Daejeon, Republic of Korea

ABSTRACT :
Globally changing dam development environment, which has been accompanied with, particularly, ongoing climate change, challenging environmental stresses, shrinking public investments, etc., has raised a need to develop dam development techniques with which it would be possible to save construction costs and minimize environmental impacts.
Against this backdrop, such four different dam types as hardfill Dam, ACRD, PCPT and RCCR in which advanced, converged dam engineering techniques are melted were selected herein as the next-generation promising ones that can be introduced to Korea.
Furthermore, the study will work on the research and development of Korea's own national construction standards(including dam design standards and standard dam specifications) through developing optimal engineering and construction techniques, which will be applied to small- and medium-size dams as pilot projects for their further advancement.

Keywords: Hybrid Dam, Hardfill, ACRD, RCCR, PCPT

1. KOREA'S TRENDS IN DAM CONSTRUCTION TECHNIQUES

1.1. Trending shift in dam types

Modern types of dams constructed in the early 20th century are mainly occupied by concrete dams. However, the subsequent development of relevant techniques and technologies has enabled the mechanical construction of dams, which was why most of large-scale dams constructed in the 1960's and thereafter were of fill dam type.

Fill dams have evolved themselves from earthfill dams through rockfill dams(in the mid 20th century) to CFRDs(Concrete Faced Rockfill Dams).(see Fig. 1.). However, materials used to construct the fill dams make them relatively lower in terms of stability against levee body overflow than concrete dams. Furthermore, it's also impossible for the fill dams to have a spillway installed within their levee body; the spillway should separately be installed in the fill dams, which indicates that they are unfavorable in terms of economic feasibility compared to the concrete dams.

Hence, efforts to save construction costs through developing concrete dams(e.g., RCDs(Roller Compacted Dams), RCC(Roller Compacted Concrete dams, etc.) whose mechanical construction is allowed with large machinery as used in fill dams have been made:

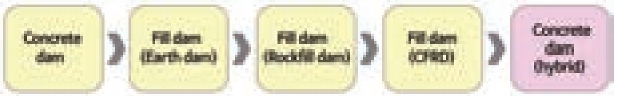

Figure 1. Trends in dam types

1.2. Status of dam construction techniques

In 1920, various dam types and techniques were introduced and applied, which enabled the accumulation of dam construction experiences and techniques and successfully ensured preventive flood control and reliable water supply with the construction of multipurpose dams.

Constructed as a Rockfill dam in 1973, Soyang R. Dam is the first dam that was ever built through mechanical construction with large-scale excavation and hauling equipment.

In the case of Andong Dam which was constructed as a core-centered rockfill dam in 1976, it played a role in expanding the applicability of rockfill materials; it had originally been so designed that clay materials might be used, which plan was so changed later that the same materials would be replaced by granite soil.

The year 1988 saw the first-stage completion of Peace Dam that was of CFRD type. Chungju Dam(constructed in 1985) is another example of concrete dams. With Daecheong Dam(ER/PG) constructed as a hybrid dam in 1980, it became possible to work on the joint between concrete and Rockfill dam parts.

The first example of RCD recently constructed with the RCD method with which it's possible to shorten the construction period and save construction costs is Hantan R. Dam, and the first example of dam constructed with the ELCM(Extended Layer Construction Method) is Bohyeon-san Dam where the existing block placing method is so expanded along the dam axis that multiple blocks might be placed on at one time to install later joints within the placed zone after or during a stage of placement.

As for now, however, dam types introduced and applied in Korea are so limited that there may be neither example of arch dams, hollow dams or buttress dams; the level of Korea's dam construction techniques still remain on the track of following overseas advanced ones that have already been proven as such.

2. BACKGROUND

Recently, there have been growing interests in the development of economically effective, efficient hybrid dams into which various techniques are converged. Against this background, various dam types were studied with a focus on the five topics (i.e., economic feasibility & constructability, sustainability, maintenance, hydropower and landscape improvement) to decide the four different types of dam engineering techniques, including the Hardfill Dam method, the ACRD(Asphalt Concrete core Rockfill Dam) method, the PCPT(Precast Concrete Post Tension) method and the RCCR(Roller Compacted Concrete and Rockfill) method, as the next-generation promising ones that should be introduced to develop and construct dams in Korea.

3. OBJECTIVE&CONTENTS

3.1. Objective

The objective of this study lies in putting in place and advancing the selected four different types of dam engineering techniques through surveying various Korean and overseas advanced techniques, setting the direction of dam development and analyzing dam development environment to construct hybrid dams that can fit with Korea's own dam development conditions, and in acquiring their optimally converged techniques which would enable the development & construction of dams highly favorable in terms of economic feasibility, constructability and landscape.

3.2. Contents

3.2.1. Hardfill Dam method

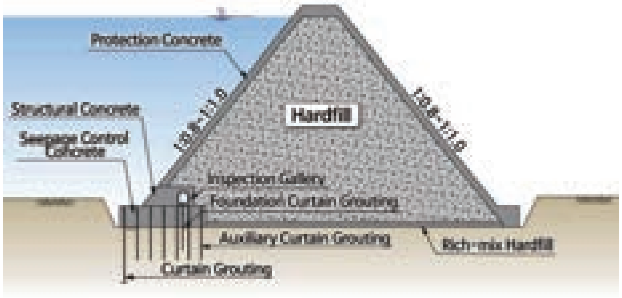

Figure 2. Schematic diagram for the Hardfill Dam method

The Hardfill Dam method is a method in which aggregates procured onsite, including riverbed sand and gravel materials and tunnel-blasted rock materials, are mixed with cement and water before they are compacted with a vibratory roller.(see Fig. 2.). The conceptual birth of Hardfill dams dates back to early 1992 when P. Londe introduced them for the first time in the history of dam development. Since then, tens of Hardfill dams have been constructed and operated all over the world. Particularly in Japan where relatively many cases of studies and projects have been underway, they are termed as "Cemented Sand and Gravel" (CSG) dams.

Table 1. Examples of Hardfill Dam applications

Country	Examples of Hardfill Dam applications
Japan	▪TOBETSU Dam(H=52.0m), OKUKUBI Dam(H=39.0m) ▪The Hardfill Dam method was applied for various locations and uses, including cofferdams, temporary channels, slope protection works, counterweight fill works, etc.
China	▪Cindere Dam, which was constructed as a large dam in Turkey in 2008 (H=107.0m) ▪Applied for small- and medium-size cofferdams in 2004
Korea	▪Partially applied for cofferdams (of Gunwi Dam) ▪Applied for an intake weir (of a small hydropower dam by K-water in Afghanistan)

Hardfill dams are characterized by 1) stability against overturning and sliding to allow good adaptability to foundation ground, 2) convenient procurement of embankment materials and simplicity in producing them, 3) good constructability thanks to simplified work processes and equipment requirements, and 4) less environmental impacts thanks to no need to develop a large-scale quarry since onsite available materials are used

3.2.2. ACRD method

In ACRDs (Asphalt Concrete core Rockfill Dams which are among fill dams, asphalt concrete is used as central core materials.(see Fig. 3.). They were developed in Germany in 1962. There are reportedly more than 120 dams around the world that were constructed with this ACRD, which is characterized by a high level of economic feasibility, constructability, safety and environment-friendliness. Also, the same method allows the saving of construction costs and the minimization of environmental impacts:

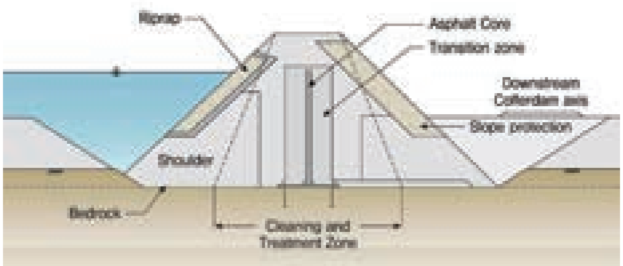

Figure 3. Schematic diagram for the ACRD method

A case study covering overseas examples of ACRD applications indicates that the method has been employed in many cases where it's difficulty to apply the existing engineering methods as shown in Table 2:

Table 2. Examples of ACRD applications

Country	Dam (HxL,m)	Remark
China	Yele (124.5x411.0)	▪Constructed in seismically hazardous regions
Canada	Nemiscau-1 (15.0x336.0)	▪Constructed as part of efforts to acquire construction experiences with this ACRD method
Iran	Shur (80.0x450.0)	▪Constructed in seismically hazardous regions
Austria	Eberlasie (28.0x480.0)	▪Constructed on heterogeneous compressible alluvial ground with 28m in height
Norway	Storglomantn (124.5x411.0)	▪Use of low-quality Rockfill ▪Stable AC core
Tibet	Xiabandi (124.5x411.0)	▪Constructed in seismically hazardous regions ▪Foundation rock mass(below 150m in subsurface depth)

This ACRD method allows 1) self-remedy of cracks and ready response to displacement (accompanied with earthquakes and settlement), 2) reduction of levee body's width and adjustment of asphalt mix, which concerns economic feasibility, 3) freedom from the impacts of meteorological conditions and good core responsiveness to erosion, and 4) convenient maintenance; there has been no case of leakage in dams constructed with the same method.

3.2.3. PCPT method

The PCPT (Precast Concrete Post Tension) method that represents a combination of PC (Precast Concrete) and PT (Post Tension) is a method in which precast (PC) dam body segments are directly assembled underwater to be connected via PT cables while cast-in-place RCC, etc. are applied on downstream and side faces.(see Fig. 4.).

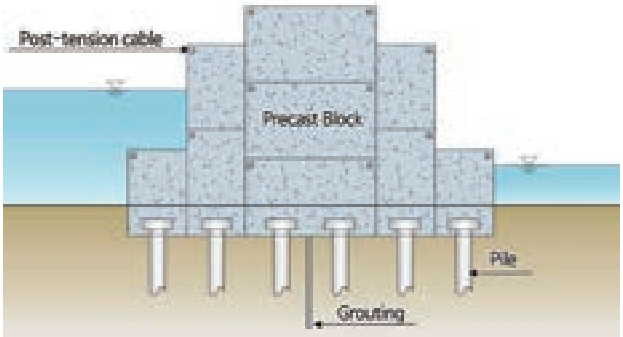

Figure 4. Schematic diagram for the PCPT method

A case study covering construction examples of PCPT applications indicates that the PC technique has been used in small- and medium-size canal dams while the PT technique has mainly been employed to improve the seismic performance of existing dams, but that there is no case with the PCPT technique, a combination of the two ones.

With this PCPT method, it's possible to 1) minimize quantity requirements for coffering works, 2) ensure safety against flood at a stage of construction, 3) improve the structural stability of levee body, and 4) shorten the construction period substantially.

3.2.4.RCCR method

The RCCR (Roller Compacted Concrete and Rockfill) method is a method in which the upper and lower parts of levee body correspond to concrete and fill dams, respectively: (see Fig. 5.).

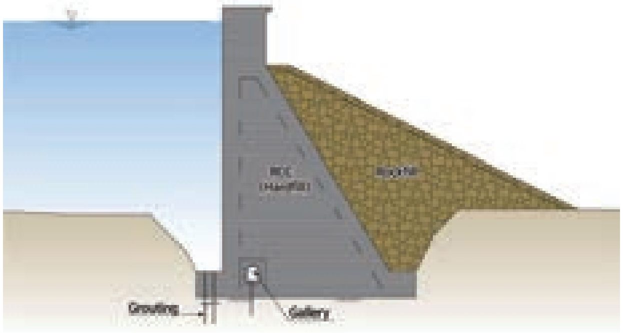

Figure 5. Schematic diagram for the RCCR method

This RCCR method allows 1)the construction of Rockfill and RCC zones with the same earthwork equipment, 2) the sectional reduction of the concrete-dam part, which concerns economic feasibility, 3) the use of the lower fill-dam part as a construction road, which concerns constructability, and 4) the application of riprap rubble stone on the frontal section of the concrete-dam part and its afforestation to improve landscape.

4. DIRECTION OF STUDY

4.1. Development of Optimal Mix Technique

The study will be directed toward developing a method to identify optimal design mix with the performance of laboratory tests based on the distributional characteristics of aggregates in each of target areas, which come from relevant data containing aggregate reserves, river master plans, etc. For its relevance, in turn, the method will comparatively be evaluated against Korean and overseas design standards on laboratory tests to identify optimal design mix.

4.2. Development of Optimal Engineering Technique

The study will be directed toward through surveying & acquiring Korean and overseas dam design standards and guidelines to compare among them in terms of their features and differences, and finally to identify what should be introduced into the former ones.

In the study to develop an optimal engineering technique, various general status (containing topographical, environmental and geological status and foundation conditions) will be surveyed and reviewed covering sites proposed for Bonghwa Dam and Wonjucheon Dam whose development is planned. Also, dam stability will be evaluated through making a decision about dam size, temporary facilities & structures, waterstop method, etc. and based on the results & findings of internal and external numeric analyses, which will be followed by the estimation of construction costs as per the whole construction schedule, and finally the economic feasibility analysis of the target engineering technique this study is committed to.

4.3. Development of Optimal Construction Technique

An optimal B/P (batch plant) to produce materials should be selected considering the physical properties of aggregates, daily construction requirement, site conditions, environmental & meteorological characteristics, etc. In the case of an C/P (crusher plant), relevant overseas cases will be so reviewed as to enable the development of Korea’s own model of C/P. For silos to store materials, in principle, it will be so planned as to use a stock yard as such silos; provided that, however, any measures are needed to provide against potential stormwater, such silo types as seat type, roof type and storage type will be considered to review their applicability. Also, an onsite test construction plan will be formulated to compare the results of the study against those of laboratory tests, and thereby check for their relevance.

4.4. Development of Optimal Quality Management Technique

Quality management aims, mainly, at managing the strength of placed materials. For their onsite strength management, their density management (e.g., making of test specimen at a stage of placing, performance of core tests on placed faces, etc.) is required; tests with standard specimens should be considered as references.

5. FUTURE PLAN

Such advanced engineering techniques as Hardfill Dam and ACRD have been recognized as proven ones in overseas design practices. Hence, the study will perform laboratory tests and onsite test construction works with the foregoing techniques from which the results and findings will be used to develop optimal mix technique, engineering technique, construction technique and quality management technique for their applicability for the dams to be constructed, and ultimately Korea’s own national construction standards (including dam design standards and standard dam specifications).

In the case of such converged engineering techniques as PCPT and RCCR, there has been no example of construction with any of the foregoing techniques. Hence, the study will work on the research and development of optimal engineering technique, construction technique and quality management technique to ensure their applicability.

REFERENCES

Norwegian Geotechnical Institute(1993) : Asphaltic concrete cores for embankment dams, pp. 13-27

K-water Institute, Dam Safety Research Institute(2004) : Trapezoid CSG Dam, pp. 2-13

K-water(2008) : Study on Optimal Design & Construction Techniques to Improve the Internal Stability of CSG Dams, pp. 4-36

Vlad Alicescu, Jean Pierre Tournier and Pierre Vannobel(2010) : Design and construction of Nemiscau-1 Dam, the first Asphalt Core Rockfill Dam in North-America, Canadian Dam Association Bulletin, 21:1, pp. 9-18

Japan Dam Engineering Center(2012) : Design, Construction and Quality Management of Trapezoid CSG Dam, pp. 1.1-1.9

Intelligent Monitoring and Control System for Crack Prevention of Concrete Dam and Its Application

G.X.Zhang, S.H.Li, Y.Liu & L.Zhang
China Institute of Water Resources and Hydropower Research, Beijing, China
Zhanggx@iwhr.com

ABSTRACT:
This intelligent monitoring and control system was developed for the purpose of preventing the cracks and improving the quality of mass concrete constructions. It is composed of four parts, including perception, interconnection, analysis and decision-making, and control. The system has realized the automatic perception, transmission, and sharing of temperature control information, and intelligent control in related key sections throughout the processes of raw material precooling, concrete mixing, concrete transportation, concrete placemen, concrete vibration, concrete water cooling, and concrete surface maintenance. Meanwhile, the system has realized the management of all factors and the entire process of temperature control and crack prevention by means of a kind of rebuilt networking combination which is based on Zigbee and internet technique. This system has been applied in four large China's concrete dams. Engineering applications show that the system can help improve the management level and prevent cracks during concrete construction.

Keywords: concrete dam, temperature control, crack prevention, intelligent monitoring and control

1. INTRODUCTION

Multiple super-high concrete dams, including Ertan, Xiaowan, Laxiwa, Goupitan, Longtan, Jinping-I and Xiluodu, have been completed in China, with Baihetan, Wudongde and Maji dams still under construction. All these dams, once completed, will play a significant role in relieving strains on power resources and tinkering shortage of water resources of our country, further achieving remarkable social and economic benefits.

Crack control has long been among the difficulties in the construction of mass concrete dams. Theoretical researches and engineering practices of temperature control and crack prevention can be dated back to as early as 1930s. Decades of development has gradually established themselves as a comparatively well-developed theoretic system that accommodates structured measures for concrete temperature control and crack prevention, including improvement of concrete crack resistance, joint spacing, reduction of pouring temperature, pipe cooling and surface heat preservation. Despite the achievements, no dam without crack remains an objective fact. Concrete cracks may occur as a result of complex reasons, such as structure, material and construction while another important reason lies in the failure to acquire timely, accurate, true and systematic information which results in insufficient temperature control measures and management. Meanwhile, in the artificial control mode, large deviation from the design occurs as construction quality is frequently influenced by the literacy of site engineering personnel, creating four major problems in temperature control construction, namely, excessive temperature difference, temperature drop, rate of temperature drop and temperature gradient. All of the said consequently result in concrete cracks.

To address the issue of temperature control and crack prevention for super-high arch dams, academician Zhu Bofang proposed the concept of digital hydropower station in 2006, that is, optimized, visualized and networked planning, design, research, construction and management of hydropower stations. He also developed the first domestic digital temperature control system – concrete temperature and stress control decision-making supporting system, which was later applied in the Zhougongzhai Project. The system allows whole-process simulation analysis of the whole dam on the basis of the actual construction conditions and temperature control measures. In this mode, temperature and stress of all blocks of the dam body and actual effects of various temperature control measures are captured in a timely manner, and the temperature and stress states in the operation period after completion can be predicted. In 2007, Zhu came up with the idea of "digital monitoring" The idea integrates traditional instrument monitoring with whole-process digital simulation analysis throughout the engineering construction period, the initial storage period and the operation period. In this way, it enables whole-process real-time monitoring on such key factors as dam temperature, deformation, stress and the like, effectively overcoming the defects of instrument monitoring like dispersion in space and interruption in time. In 2009, "digital monitoring" was applied in Jinping-I and Xiluodu Projeccts. The system allows real-time assessment on dam behaviors, reduces accident risks and offers decision-making support for dynamic design of the construction period.

Academicians Zhong Denghua and Ma Hongqi proposed the concept of “digital dam” by integrating “informatization” with “digitization”. The concept was applied in the Nuozhadu Project. On the basis of GPS, GPRS and PDA technologies, the system achieves whole-process, elaborate and real-time online monitoring on roller-compaction parameters including times and tracks of compaction, roller speed, exciting force and compaction depth. It provides a new approach for quality control in the construction of high core rock-fill dams and is well ready to be promoted to roller-compaction concrete dams.

Artificial intelligence and automation on the basis of informatization and digitization achieve some intelligent steps affecting quality in the construction process. In water conservancy engineering, Zhang Guoxin et al. raised an idea to transform from “digital dam” to “intelligent dam”. They pointed out that intelligent technologies can be used in processes like pouring temperature, placement surface temperature control, pipe cooling and concrete preservation. “In terms of an intelligent dam, communication and control technologies are applied to achieve real-time information perception, automatic analysis and performance control of a conventional concrete dam through its whole life span” , as was proposed by Li Qingbin, who managed to establish a comprehensive framework for personalized management and analysis and control over dam performances on the basis of Zigbee, automatic monitoring and cloud computation in 2014.

Soaring development of technologies including informatization, digitization, numerical simulation and big data has presented opportunities for intelligent temperature control and crack prevention of dams. The author, in addressing problems in mass concrete temperature construction and digital monitoring, presented a “Nine-Three-One Temperature Control Mode”. “Nine” refers to a guiding principle formed by nine words (in Chinese) which means “earlier protection and cooling by smaller temperature difference with longer time”; “Three” refers to three-stages cooling at “first stage, middle stage and second stage”; “One” refers to one monitoring or “intelligent monitoring”. Joint efforts of the “Nine-Three-One” temperature control mode and intelligent control effectively solve the problem of failure to acquire timely, accurate, true and systematic information and take excessive temperature difference, temperature drop, rate of temperature drop and temperature gradient under control, radically achieving the goal of concrete temperature control and crack prevention.

2. OVERALL STRUCTURE OF INTELLIGENT CONTROL SYSTEM

Similar to artificial intelligence, an intelligent Monitoring system is composed of such four parts as perception, interconnection, analysis & decision-making, and control. “Perception” means (automatic and manual) acquisition of various key factors; “Interconnection” aims to achieve multilevel network communications, and close link, interflow and sharing between various remote and heterogeneous terminals, and software and hardware resources by means of informatization. Control consists of artificial intervention and intelligent control. The former refers to human intervention based on commands of early warning, alarm and feedback of diversified solutions and measures that are formed on the basis of intelligent analysis, judgement and decision-making. The latter refers to automatic and intelligent control of microenvironment indicators covering temperature, humidity and wind speed, concrete preservation and pipe cooling regulation. “Analysis & decision-making”, as the core of the system, enable the formation of a decision after a process covering learning, memorization, analysis, judgement, inversion and prediction. “Perception”, “Interconnection” and “Control” depend on and supplement each other so as to form a unified whole of intelligent monitoring encompassing “analysis & decision-making”, as shown in Fig. 1.

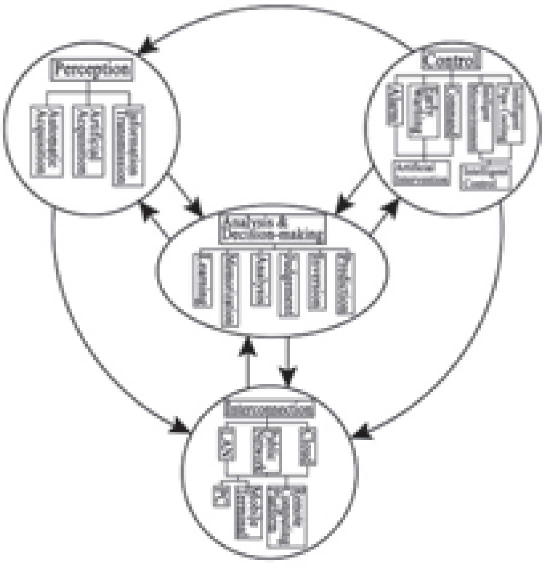

Figure 1. Structure of Intelligent Monitoring on Mass Concrete

Fig. 2 shows the schematic diagram of the site structure of the intelligent monitoring system for concrete crack prevention. In various concrete construction links, sensors are distributed at the mixing plant, concreting displacement surface, interior and surface of concrete. Sub-control stations are arranged in the dam area as required for collecting relevant information and giving commands. Intelligent control is applied to any parameter that allows automatic control. All sub-control stations achieve information exchange with the master control room by means of wireless transmission, thus forming a complete monitoring system.

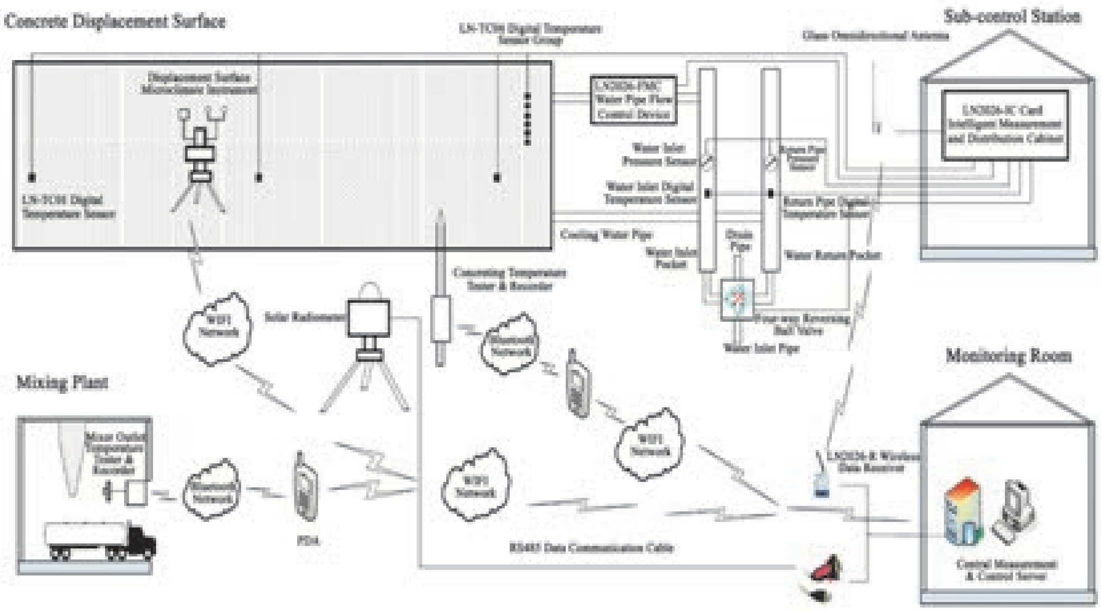
Concrete Displacement Surface
LN-TC08 Digital Temperature Sensor Group
Sub-control Station
Glass Omnidirectional Antenna
Displacement Surface Microclimate Instrument
LN2026-FMC Water Pipe Flow Control Device
LN2026-IC Card Intelligent Measurement and Distribution Cabinet
Water Inlet Pressure Sensor
Return Pipe Pressure Sensor
Water Inlet Digital Temperature Sensor
Return Pipe Digital Temperature Sensor
LN-TC08 Digital Temperature Sensor
Cooling Water Pipe
Water Inlet Pocket
Drain Pipe
Water Return Pocket
Concreting Temperature Tester & Recorder
Four-way Reversing Ball Valve
WIFI Network
Solar Radiometer
Bluetooth Network
Water Inlet Pipe
Monitoring Room
Mixing Plant
Mixer Outlet Temperature Tester & Recorder
WIFI Network
LN2026-R Wireless Data Receiver
Bluetooth Network
WIFI Network
PDA
RS485 Data Communication Cable
Central Measurement & Control Server

Figure 2. Schematic Diagram of Site Structure of Intelligent Monitoring System

3. PERCEPTION

"Perception" means real-time acquisition of information at various links. Key links for temperature control include concrete mixing plant, concrete mixer outlet, concrete transportation and placement, concrete vibration, pipe cooling and placement surface protection. All these links allow the arrangement of digital temperature measuring equipment like (fixed-type or handheld) digital thermometers or infrared thermometers. Analysis reveals 22 parameters requiring real-time perception (Refer to Fig. 3) so as to monitor factors affecting temperature control and state of concrete in the whole construction process. Most observed parameters allow automatic observation with fixed-type devices. Some others require semi-automatic observation with handheld digital thermometers.

An intelligent perception package accommodating digital thermometer, temperature gradiometer, placement surface microclimate installation, aggregate infrared thermometer and mixer outlet, placement and pouring temperature testers is developed for all-factor and whole-process perception indicators. The placement surface microclimate observer can detect temperature, humidity and wind speed and direction simultaneously. It is aimed at real-time monitoring of placement surface environment. In pipe cooling process, not only the temperature of water and concrete but also the pressure, direction and flow of water at outlet and inlet need to be observed. Some factors influencing temperature control cannot be directly perceived by instruments and require manual acquisition and entry, such as geometrical information, location, opening time and closing time of the concrete tank. Some information is modelled in the system as design data while others need be input along with construction progress.

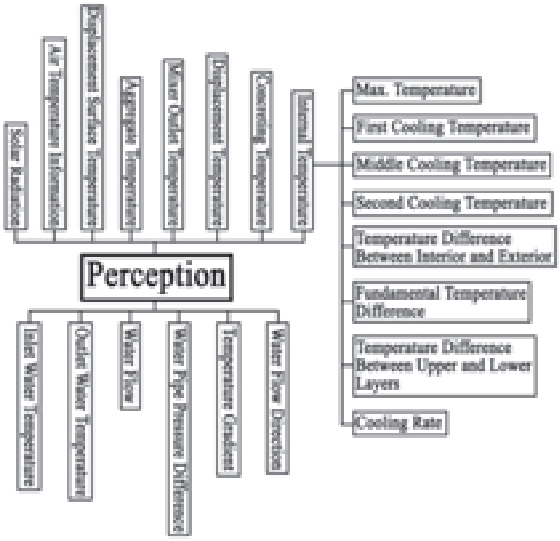
Solar Radiation
Air Temperature Information
Displacement Surface Temperature
Aggregate Temperature
Mixer Outlet Temperature
Displacement Temperature
Concreting Temperature
Internal Temperature
Max. Temperature
First Cooling Temperature
Middle Cooling Temperature
Second Cooling Temperature
Temperature Difference Between Interior and Exterior
Fundamental Temperature Difference
Temperature Difference Between Upper and Lower Layers
Cooling Rate
Perception
Inlet Water Temperature
Outlet Water Temperature
Water Flow
Water Pipe Pressure Difference
Temperature Gradient
Water Flow Direction

Figure 3. Perception Parameters of Intelligent Monitoring System

4. INTERCONNECTION

On the basis of multiple ITs (Bluetooth, GPS, ZigBee, cloud technology, Internet and Internet of Things) and through development of relevant equipment and layout of sub-control stations and master control room, "Interconnection" establishes real-time communications between construction equipment, between temperature measuring devices, between temperature measuring devices and sub-control stations and between sub-stations and master control room. It can achieve real-time acquisition, sharing, analysis, control and feedback of various temperature control data of concrete from raw material, concrete mixing, concrete placement surface control till concrete internal life cycle (interconnection structure is shown in Fig. 4).

Equipment enabling interconnection mainly includes sensors, controllers, mobile terminals, construction equipment, water supply equipment, fixed terminals and display equipment. Technologies mainly cover cloud interconnection, Bluetooth, ZigBee, Wi-Fi and GPS. Interconnection between equipment and sub-control stations or master control room is mainly achieved through LAN, the same between sub-control stations and master control room through LAN or WAN, and remote access to database through public WAN.

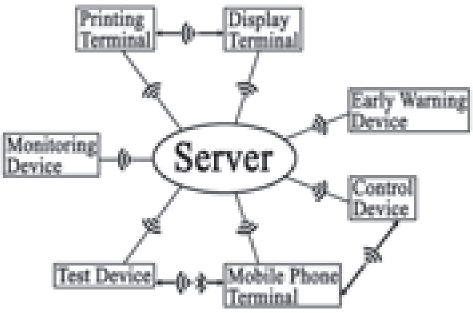

Figure 4. Interconnection Architecture of Intelligent Monitoring System (Revised)

5. ANALYSIS & DECISION-MAKING

As the core of the whole system, "analysis & decision-making" is a process in which directly or indirectly acquired perception parameters consequently form decision-making information through learning, memorization, analysis, judgement, inversion and prediction. It mainly includes the SAPTIS (Simulation Analysis Program for Temperature and Stress) model, ideal temperature control curve model, temperature and flow prediction and forecast model, temperature control effect assessment model, surface heat preservation prediction model and crack risk prediction and early warning model (Refer to Fig. 5).

(1) The simulation analysis software SAPTIS [18], as a whole-process and multi-field coupling simulation analysis system for concrete structure developed by the author's team through efforts of 30 years, bears these characteristics as "9321". "9" refers to the nine processes it can simulate. They are climate change process, bedrock excavation process, backfill support process, concreting and hardening process, temperature control process, grouting and anchoring process, time-dependent deformation process, water infiltration process and long-term operation process; "3" refers to three-filed coupling between water, heat and force; "2" refers to two nonlinearities, namely, elastoplasticity nonlinearity and damage nonlinearity; "1" refers to one iteration, i.e., open-close iteration of various cracks. The software can simulate temperature filed, seepage field and stress field of various links in the entire process from foundation excavation, construction till operation and make numerical assessment on whole and local working conditions of the dam[17].

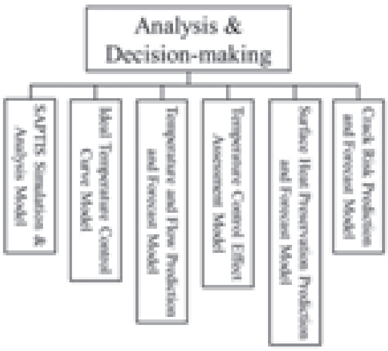
Analysis & Decision-making
SAPTIS Simulation & Analysis Model
Ideal Temperature Control Curve Model
Temperature and Flow Prediction and Forecast Model
Temperature Control Effect Assessment Model
Surface Heat Preservation Prediction and Forecast Model
Crack Risk Prediction and Forecast Model

Figure 5. Structure of Analysis & Decision-making

(2) The ideal temperature control curve model creates personalized temperature control curves for different projects, different concrete zonings or even each silo of concrete. The idea is developed on the basis of characteristics of different dam types and different zonings of a dam body under certain temperature control criteria. It also takes into consideration factors including temperature difference classification, temperature reduction rate and spatial gradient control following the principle of minimal temperature stress.

(3) The temperature and flow prediction and forecast model can predict future temperature change and give water supply control parameters. The model takes the influence of such factors as internal heat, surface heat dissipation, heat transfer between adjacent blocks and heat removal from water supply into account. It conducts self-learning and self-correction by taking advantage of monitoring data.

(4) The temperature control effect assessment model enables intuitive, real-time and comprehensively quantitative assessment on quality of temperature control construction by designing 8 tables and 12 figures.

(5) The surface temperature prediction model conducts real-time search of exposed surface of the dam based on its actual concreting progress. It links it with information like weather forecast, measured air temperature and internal temperature of concrete to calculate long-term and short-term stresses of the exposed surface through stress simulation and superimpose them. Finally, it provides suggestions on whether heat preservation is required and depth of the heat preservation layer based on the stress analysis result and parameter performances of the heat preservation materials in actual application.

(6) Crack risk prediction and early warning model predicts future temperature, stress and crack risks in a timely manner, triggers real-time early warning and offers measures and suggestions through real-time tracking, inversion and simulation analysis in the entire process from dam concreting to operation.

6. CONTROL

"Control" classified as manual intervention and intelligent control is mainly composed of 5 subsystems (Fig. 6). Such subsystems as early warning release, intervention feedback and decision-making require manual intervention.

On the basis of the real-time site monitoring data acquired, subsystems of early warning release and intervention feedback carry out automatic computation through the analysis & decision-making module. They automatically send out alarm or early warning against any parameter out of limit, which are eventually transferred to the terminals of construction personnel who initiate manual intervention accordingly. The decision-making support subsystem realizes periodic summary by means of weekly report, monthly report, quarterly report, progressive report or site training.

The intelligent control system mainly includes intelligent water pipe cooling subsystem, intelligent microenvironment subsystem and intelligent preservation subsystem. The intelligent water pipe cooling subsystem allows automatic control of water direction, flow and temperature through automatic control equipment. This subsystem follows the requirements for ideal temperature control construction, bases itself on a unified information platform and measured data, and applies the calibrated and verified prediction and analysis model. The intelligent microenvironment subsystem automatically controls microenvironment devices (such as sprayer) in the silo based on the real-time measured temperature and humidity. Thus, microenvironment of the displacement surface satisfies site concreting requirements. The intelligent concrete curing subsystem automatically controls equipment for flowing water curing based on real-time measured internal and surface temperature of concrete.

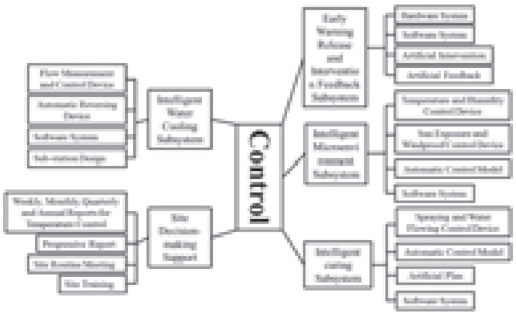
Control
Flow Measurement and Control Device
Automatic Reversing Device
Software System
Sub-station Design
Intelligent Water Cooling Subsystem
Weekly, Monthly, Quarterly and Annual Reports for Temperature Control
Progressive Report
Site Routine Meeting
Site Training
Site Decision-making Support
Early Warning Release and Interventio n Feedback Subsystem
Hardware System
Software System
Artificial Intervention
Artificial Feedback
Intelligent Microenvi ronment Subsystem
Temperature and Humidity Control Device
Sun Exposure and Windproof Control Device
Automatic Control Model
Software System
Intelligent curing Subsystem
Spraying and Water Flowing Control Device
Automatic Control Model
Artificial Plan
Software System

Figure 6. Control Structure

7. ENGINEERING APPLICATION

Ever since 2009, some functions of the intelligent monitoring system have been successfully applied in projects like Jinping-I, Xiluodu and Ludila. Now, the system is fully implemented in the Fengman and the Huangdeng projects.

Fig.7 shows the result of intelligent water cooling, which includes flow, measured temperature, targeted temperature and predicted temperature. As is revealed in the figure, the measured temperature is basically consistent with targeted temperature and predicted temperature. Fig. 8 shows site layout of monitoring devices and Fig. 9 software interface.

Lastly, engineering practices indicate that no temperature crack is found in Jinping-I anchor dam, the number of cracks of the monitored sections of the Ludila gravity dam is obviously smaller than that of the unmonitored sections and no crack is found in the monitored sections of the Zangmu gravity dam.

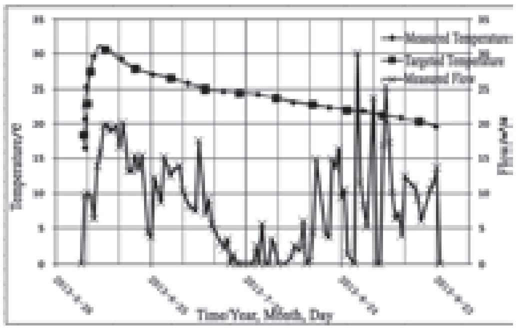

Figure 7. Intelligent Water Cooling Result

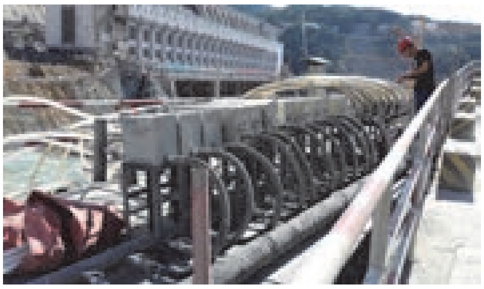

Figure 8. Site Layout of Monitoring Devices

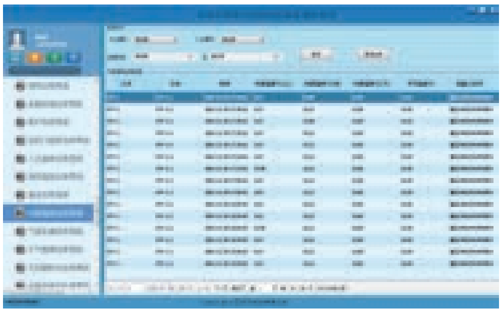

Figure 9. Temperature data in Software

8. CONCLUSION

Development of information, digital and intelligent technologies have created conditions for intelligent temperature control and crack prevention. In various links of concrete temperature control, such as raw material pre-cooling, concrete mixing, concrete transportation, concrete displacement, concrete vibration, concrete water cooling and concrete surface protection, application of digital technology, Internet technology and automatic control technology with simulation, analysis, early warning and decision-making as the core effectively avoids deviation incurred from traditional construction and uncertainty from human factors.

The “perception” technology based on digital transmission technology allows real-time and accurate acquisition of effective information of various links, such as temperature, flow, wind speed and pressure; The Internet technology based on LAN and WAN enables interconnection and data sharing between perceiving instruments, construction machines, control devices, mobile terminals and fixed terminals on construction site, which achieves seamless management thanks to wired, wireless, remote and local accesses. Intelligent control of material pre-cooling and mixing, surface environment, water cooling realizes whole-process high precision control of temperature in various links.

Core of the intelligent control lies in analysis & decision-making, which, by applying the deterministic simulation analysis method and the statistical analysis model and setting feasibility of stress optimized measures as its target, dynamically determines the cooling curve of each silo of concrete and adjusts temperature control parameters of various links accordingly. Through repeated comparisons between predicted target temperature and measured target temperature, it adjusts temperature control parameters constantly for optimized max. Temperature, temperature difference and temperature change rate so as to reach the goal of stress control and crack prevention.

The intelligent control has been successfully applied in two arch dams like Jinping and Xiluodu and another two gravity dams like Ludila and Zangmu, with sound effect. Practices indicate that several temperature control models of the analysis & decision-making part, as key technologies, remains to be constantly improved and optimized when applied in specific projects.

ACKNOWLEDGEMENTS
This work was financially supported by Special Projects of 973 Project of China (2013CB035904、2013CB036406), 12th Five -Year Plan Technology Support Project of China (SQ2013BAJY4138B02) and National Natural Science Foundation of China (51579252).

REFERENCE

China Society for hydropower engineering(2015):Almanac of China’s Water Power(2013) [M].. Beiijng: China electric power pres.

Zhang Guoxin, Liu Yi, Li Songhui,et al(2014): Research and practice of nine three one temperature control mode[J], Journal of Hydroelectric Engineering,33(2): 179-184.(in Chinese)

Thermal stress and temperature control of mass concrete[M](1999). Beijing: China electric power press,

Liu Yi, Zhang Guoxin(2014):Discussion on key points of temperature control and crack prevention dam[J],Water Resources and Hydropower Engineering,45(1): 77-89. (in Chinese).

Zhu Bofang,Zhang Guoxin, Xu Ping,et al(2008): Decision making support system for temperature and stress control of high concrete dams in construction period[J], Journal of Hydraulic Engineering,39 (1): 1-6.(in Chinese).

Zhu Bofang(2008): Numerical monitoring of concrete dams[J], Water Resources and Hydropower Engineering, 39 (2)15-18.(in Chinese).

Zhu Bofang, Zhang Guoxin, Jia Jinsheng,et al(2009): Numerical monitoring of concrete dams - a new way for improving the safety control of concrete dams[J], Journal of Hydroelectric Engineering,28(1):130-136.(in Chinese)

Liu Yi,Zhang Guoxin,Wang Jimin,et al(2012):Numerical monitoring methods and system for construction of super high arch dam and its engineering practice[J],Water Resources and Hydropower Engineering, 43 (3): 33-37.(in Chinese) .

Zhang Guoxin, Zhang lei, Liu Yi, etc(2014), The True Working Performance Inversion Simulation Analysis of Jinping Level-I Arch Dam[C],Key technical issues and research progress in hydropower development. Zhengzhou: The yellow river water conservancy press,.77-83.

Ma Hongqi, Zhong Denghua, Zhang Zongliang, et al(2011): Key technologies of real-time construction control for major hydraulic and hydroelectric projects[J],Engineering Sciences,13(12): 20-27. (in Chinese)

Zhong D H， Liu D H, Cui B(2011): Real-time compaction quality monitoring of high core rock fill dam[J],Sci China Tech Sci,,54:1906-1913.(in Chinese)

Ma Hongqi(2012):Key Technologies on Construction Quality Control of Rock fill Dam with Core Wall Filled by Clay Soil Mixed with Gravel in NuoZhadu Hydropower Station Project[J]. Water Power, 12-15.（in Chinese）.

Zhang Guoxin, Liu Youzhi, Liu Yi(2012) :"Digital dam" to "intelligent dam"—Progress of temperature control research on high dam[C], Technical progress in construction and management of dams, The yellow river water conservancy press,74-84

Li Qingbin(2014) :Demonstration on intelligent dam[J]. Journal of Hydroelectric Engineering,33(1):139-146.(in Chinese)

Zhang Guoxin,Liu Yi,Li Songhui.et al(2014).Intelligent monitoring and control and control system for temperature control and crack prevention of concrete dam and its engineering application[J], Water Resources and Hydropower Engineering, 45(1): 96-102.(in Chinese)

Tan Kaiyan, Chen Junqi, et. Al(2012):Research on the automatic data acquisition system of mass concrete water pipe cooling and its application[C], , Technical progress in construction and management of dams. Zhengzhou: Zhengzhou: The yellow river water conservancy press,502-507

Zhang Guoxin(2013):Development and application of SAPTIS— software of multi-field simulation and nonlinear analysis of complex structure(Part 1)[J], Water Resources and Hydropower Engineering, 44(1): 31-44. (in Chinese)

4th APG Symposium and 9th EADC on

INNOVATIVE TECHNOLOGIES FOR DAMS AND RESERVOIRS TOWARD THE FUTURE GENERATIONS

Decision Making Model for High Rock Fill Dam Construction during Flood Period based on Markov Process

L. Liu , Y.H. Zhou, C.J. Zhao & L. Song
College of Hydraulic and Environmental Engineering, Three Gorges University, Hubei, China
amelielau@whu.edu.cn

L. Liu
State Key Lab. of hydropower project construction and management of Hubei Province, Three Gorges University, Hubei, China

C.J. Zhao
Experimental Teaching and Demonstration Center of Water Conservancy and Environmental, China Three Gorges University, Yichang, China

ABSTRACT:

Time variation of retaining water risk and uncertainty of filling progress increase the difficulties in making decision for high rock fill dam construction during flood period. Accordingly, the water retaining risk of high rock fill dam is calculated by stochastic simulation, and then classified into three risk degree which can indicates decision states. With the objective of minimizing the cost of the entire construction process in flood season, the critical factors such as flood flow, filling schedule and cost of decisions are taken into account, then a decision making model is established based on Markov Processes for high rock fill dam construction during flood period. Base on this model, the flood prevention strategies, cost functions and transfer probability for each risk degree are analysed. After testing the Markov property, the optimal strategy for each state in current time and a sequential risk decision path in this process can be predicted by strategy iteration method. A study case shows that the model can describe the decision-making process of high rock-fill dam construction during flood period, is provided for manager by getting a full grasp with actual construction state timely and adjusting schedule and cost rapidly and accurately.

Keywords: High rock fill dam, Risk decision making, Flood prevention, Construction, Markov process

1. INTRODUCTION

With the dam construction centre transferring to southwest and northwest region in china, a series of 200m level high rock fill dams have been under construction. These projects are mostly located in high mountains and gorges, in which flood level and flow change greatly during the long construction period. To ensure the safe and economical flood prevention in process of dam construction, different flood prevention schemes such as cofferdam retaining, dam body retaining, overflowing and so on are chosen accordingly at different stages(Zhang et al. 2014). Flood prevention of high rock fill dam throughout the whole procedure of construction, so the decision-making and schedule (time) as well as the filling height (space) are affected one another when the dam is higher than cofferdam. That means more uncertain factors should be taken into account and more complicated decisions should be made for high rock fill dam construction in flood season compared with other types of dams. Therefore, it is very important to seek scientific and dynamic decision-making method for controlling the real-time risk effectively, ensure the safe and economical construction of the high rock fill dam during flood period.

The decision making for flood prevention of high rock fill dam demines the safety and schedule in the mid and later stage of dam construction. If the filling height exceeds the flood control standard in pre-flood, dam section is used for retaining water; If it does not reach the height, some protection measures for overflowing(Hu et al.2014)or accelerating filling to the water retaining height(Liu et al. 2013) should be taken in advance. Previous studies and practices were focus on the relationship between construction diversion and benefit (Fan et al. 2008, Rasekh et al. 2010), the method is proposed to determine the utility function of decision maker and a multi-objective decision model based on the utility function is established; Evaluation method of construction diversion scheme according to expectations and risk tolerance is given (Zhong et al. 2002). The above research provides theory and practice reference for decision-making of flood prevention. Furthermore, a mathematical model to estimate the water containment risk for high rock fill dams during interim seasonal flood is established for non-overtopped dam (Zhang et al. 2014). Construction period of the high rock fill dam was divided into 4 stages, and AHP method was used to calculate the risk of sub project and established risk assessment model based on improved catastrophe evaluation method (Li et al. 2014); Considering interaction between schedule and risk, the adaptive control theory into high rock fill dam construction process was introduced and dynamic water retaining risk control model was established (Liu et al. 2015). Decision behaviour of a single-agent extended to multi-agent, and negotiation mechanism to decision making is introduced for flood prevention based on the difference of risk preference and evolution utility among the agents (Xue et al.2014).

Previous studies focused on evaluating and selecting flood prevention schemes for a single or some key notes during the construction process. However, the dam appearance, flood flow, the risk level and the decision making costs which change dynamically are affected by time sequencing with the constant progress in filling dam. It is not accurately reflecting the characteristics of predicted decisions if the affected factors are not considered relevant to time in whole dam construction process. This paper regards decision making for high rock fill dam flood prevention as a sequential decision problem based on time variability of water containment risk during flood season. The critical factors including flood flow, filling schedule and cost of decisions are taken into account. Then a decision making model is established based on Markov Processes for high rock fill dam construction during flood period. After testing the Markov property, the optimal strategy for each state in current time and a sequential risk decision path in this process can be predicted by strategy iteration method. Finally, a case study shows the effectiveness and feasibility of this model.

2. WATER RETAINING RISK ANALYSIS AND DECISIONS COST ANALYSIS

2.1. Water retaining risk simulation

Flood risk of high rock-fill dam construction in flood season is one of the key factors in decision of construction diversion scheme. In the beginning of flood season, water retaining risk of high rock fill dam is defined a kind of probability, that water level of the dam in next month exceeds the planned water retaining elevation in this month schedule, while the filling height of dam is beyond cofferdam height. The risk can be represented as the following Eq. 1.

$$P_f(n) = prob[H_{n+1} \geq G_n \mid D_{n+1}] = \int_{G(n)}^{G^*} f(H \mid D)\mathrm{d}H \qquad (1)$$

where P_f is the water retaining risk of high rock fill dam construction during flood period; D_{n+1} is prediction of flood discharge of next month; H_{n+1} is the possible highest water level by stochastic simulation; G_n is the planned water retaining elevation by the end of this month; G^* is the design elevation of the high rock fill dam; $f(H|D)$ is the water level probability density of next month under the condition of D.

It is difficult to solve the water level distribution function directly, so the Monte-Carlo stochastic is adopted. The P-III pattern distribution is taken as the flood series (flood volume) distribution determined by the monthly hydrological data in dam area. The discharge capacity coefficient follows triangular distribution assuming it is affected only by roughness of discharge structures. The water retaining elevation of dam can be obtained according to construction schedule. Water retaining dynamic risk rate simulation process of high rock fill dam is as follows:

(1) Beginning to calculate at the end of the month before the flood season;

(2) Determining the flood series distribution parameters of next month and the simulation times M of MC method;

(3) Generating random numbers of flood process and simulating it of next month;

(4) Generating random numbers of discharge capacity coefficient and fitting a curve of it;

(5) The possible highest water of dam H_{n+1} can be obtained by flood regulating calculation based on the simulated flood process and discharge curve, combined with water level-capacity relationship;

(6) Comparing H_{n+1} and G_n;

(7) By repeated simulation calculation , the statistic counts of H_{n+1} that exceeds G_n is denoted as M_R. The water retaining risk rate in the n-th month is: $P_f(n) = M_R / M$;

(8) Going to step 2 and calculate the water retaining risk rate next month $P_f(n+1)$ until G_n is equal to G^*.

2.2. Cost of decisions calculation

When the filling height of rock fill dam is higher than the elevation of cofferdam, flood prevention mainly takes three kinds of decision during construction: accelerating filling of temporary section for retaining water, protection measures against overflowing the dam surface and implementation of the original construction schedule. The cost function of decision is L_k (k=1,2,3). To minimize the impact of other stochastic factors to the cost, function object is only focus on one decision maker that is constructor without considering multiple decision makers.

(1) Accelerating filling of temporary section for retaining water： Filling intensity increases before the flood to decrease the risk by additional resources and cost. The cost function L_1 is shown in Eq. 2：

$$L_1 = -C_q(n, \Delta h) - C_p(n, \Delta h) \qquad (2)$$

where C_q is additional cost for accelerating filling, such as the consumption of manpower and machinery for night working.C_p is the opportunity cost in condition of limited resources.L_1 is related to decision-making point t and rising height Δh in that month.

(2) Protection measures against overflowing the dam surface：When the dam height is below the standard of

temporary flood protection during dam construction process, the measures against overflowing the dam surface can be taken. In such case, dam placement needs to stop combined the erosion prevention approaches for flowing surface. The whole or part of rock fill dam face is usually protected by reinforcing cage, mortar and dry laid stones, as well as leaves the flood discharge gap or sets the overflow. Water storage time for power generation is delayed and the benefit of power generation is decreased due to the works suspension. The cost function L_2 is shown in Eq. 3:

$$L_2 = -\sum_{i=1}^{3} C_i(n) \tag{3}$$

where C_1 is protection expense of cofferdam and dam by multiplying the quantities and their integrated unit prices of reinforcing cages, mortar and dry laid stones;C_2 is the clearing-up expense; C_3 is the duration cost mainly consist power generation; $C_3 = -phW\Delta t$ .where p is electricity prices, h is the daily valid time for generating, W is the installed generating capacity, Δt is the lost time on a daily basis.

(3) Implementation of the original construction schedule: When the rising height this month can meet the requirement of flood risk control, flood prevention scheme can be used by retaining water according original construction schedule. Although this decision saves the cost of accelerating filling or overflowing, once the risk happens, decision makers need to take the losses for overtopping. The cost function L_3 is shown in Eq.4:

$$L_3 = -\sum_{i=1}^{3} P_f(n) C_{fi}(n) \tag{4}$$

where C_{fi} is the loss when dam encounters the over-level flood at t without taking erosion prevention for flowing surface and warning measure, which covers the dam surface cleaning and repairing cost C_{f1}, social and economic property C_{f2} in submerged region (if dam-break flood is formed), as well as the duration loss C_{f3}. C_{f1}, C_{f3} has the same calculation basis as C_1 and C_3. C_{f2} is shown in Eq.5:

$$C_{f2} = C_j + (1+k)\sum_{i=1}^{m} \beta_i V_i \tag{5}$$

where C_j is the disaster rescue expense; k is indirect loss coefficient; β_i is rate of loss per hectare at the i-th submerged region;V_i is the submerged area at the i-th submerged region.

3. RISK DECISION MAKING MODEL BASED ON MARKOV PROCESS

To achieve dynamic risk-controlling and balanced resource allocation, Markov Process model (MPM) is taken into prevention decisions of high fill-rock dam dynamically and by order during flood period. Markov Process is a mathematical model to describe the state transition of complex system. The characteristic is that current decision state is only related to state or action of previous one, but independent of the earlier ones, therefore, a series of decision-making process in future may be predicted by current status and occurrence trend. Accordingly, temporary construction resource scheduling and decision are carried out before the first flood season.

Decision maker determines the flood prevention scheme in next stage by hydrological forecasting and present construction progress. In addition, decision vector of multiple stages also can be deduced by current dam progress as well as implementing effect of last decision-making. Above all, prevention decision for high rock-fill dam construction during flood period can be regarded as a Markov decision process. The calculation procedure of decision-making during flood period based MPM is as shown in Fig.1.

3.1.The model structure and parameters

After decomposing the process of flood prevention into n decision points number (month as time interval) from t_0 to t in flood season, a discrete time dynamic decision making mathematics model is established by the following 5 parameters$\{X, P, A, R, V\}$.

(1) $X(t_n)=i(i=1,2,\ldots, m)$ is water retaining risk levels of high rock fill dam classified by the value of $P_f(t)$,which stands for the dam risk state set in construction process during flood season.

(2) Flood prevention actions set is $A_i=(a_k)(k=1,2,3)$, a_k is the method respectively includes :

1) Accelerating filling of temporary section for retaining water;

2) Protection measures against overflowing the dam surface;

3) Implementation of the original construction schedule. Flood protection in different state can form strategy vector $\Pi(i)$, $\Pi(i) \in A(i)$.

(3) The transition probability matrix is $P=[P_{ij}]$, in which $P_{ij}=P\{X(t_n)=j|X(t_{n-1})=i,\ A(i)\ \}(i,j=1,2,\ldots,m)$ represents the transition probability from state i to j by performing action $A(i)$ at $t_n(n=0,1\ldots)$,and can be estimated by either a direct subjective assessment or statistical procedures.

(4) Return function is $R(i,\ \Pi(i)\ )=L_k$,which means expected benefits or costs got by decision makers when they take strategy $\Pi(i)$ from the state i to j. The factors affect return function are water retaining risk, schedule (power generation) income or loss, loss of overflow dam, protection measures costs and so on.

(5) The current and future decision returns are both considered in the decision-making of flood prevention scheme. $V^{\Pi}(n)$ is the objective function total cost in state i at n-th time by given strategy $\Pi(i)$.

3.2. Test of Markov Property

Testing the Markov property of flood controlling decision stochastic process during dam construction is a necessary precondition for the application of MPM. In generally, the Markov decision process of discrete sequences can be tested by statistic χ^2 – distribution. The state set has *m* possible risk states, and N_{ij} stands for the frequency from risk state *i* to *j* in time. The sum of the column *j* values of transfer frequency matrix divided by the sum of all rows and columns is called "marginal probability" and denoted by P_j^*, the transition probability from state *i to j* is P_{ij} represented by the Eq. 6.

$$P_j^* = \frac{\sum_{i=1}^{m} N_{ij}}{\sum_{i=1}^{m}\sum_{j=1}^{m} N_{ij}}, and \ P_{ij} = \frac{N_{ij}}{\sum_{j=1}^{m} N_{ij}} \tag{6}$$

Statistic $\chi^2 = 2\sum_{i=1}^{m}\sum_{j=1}^{m} N_{ij} \, | \ln \frac{P_{ij}}{P_j^*} |$ is defined by χ^2 distribution with $(n-1)^2$ degree of freedom, and confidence interval is equals to *B*. If $\chi^2 > \chi_B^2((m-1)^2)$ by looking up tables, this stochastic process is considered having Markov property.

3.3. Iterative Calculation Process

Discount formula and iteration method (Yan, et al. 1995) can be used to find the optimal strategy because risk state set $X(t_n)$ and strategy Π are finite sets, by comparing the total expected return of each strategy .In iterative calculation process, V^{Π} is calculated explicitly, then the following Eq. 7 and Eq. 8 are introduced to improve the predictive strategies.

$$Q^{\Pi}(i) = R(i,\Pi(i)) + \gamma \sum_{j \in X(t_n)} P_{ij}^{a} V^{\Pi}(j) \tag{7}$$

$$\Pi^{'}(i) = \arg \ \ min \ Q^{\Pi}(i) \tag{8}$$

where Q^{Π} is the action function, which means expected return by taking action *a* in state *i* while strategy Π in other states. γ is the discount factor $(0 < \gamma < 1)$.

Due to the limited number of strategies, the algorithm can converge in a finite number of iterations to the optimal strategy. Steps are as follows:

(1) Initial strategy: Choosing the flood control strategy of high rock fill dam in the original construction plan as initial strategy Π, and starting with Π.
(2) Evaluation strategy: Computing the value of function V^{Π} for strategy Π by solving a linear equation group, which is Eq. 9.with the set of *m* equations in *m* unknowns.

$$V^{\Pi}(i) = R(i,\Pi(i)) + \gamma \sum_{j \in X(t_n)} P_{ij}^{\Pi} V^{\Pi}(j) \tag{9}$$

(3) Improvement strategy: Using equation (7) (8), resolving ties arbitrarily, but giving preference to the currently selected action.
(4) Convergence test: If $\Pi^{'}$ is the same as Π, going to step 5. Otherwise, setting $\Pi=\Pi^{'}$ and going to step 2.
(5) Returning an optimal strategy Π^* at this time.

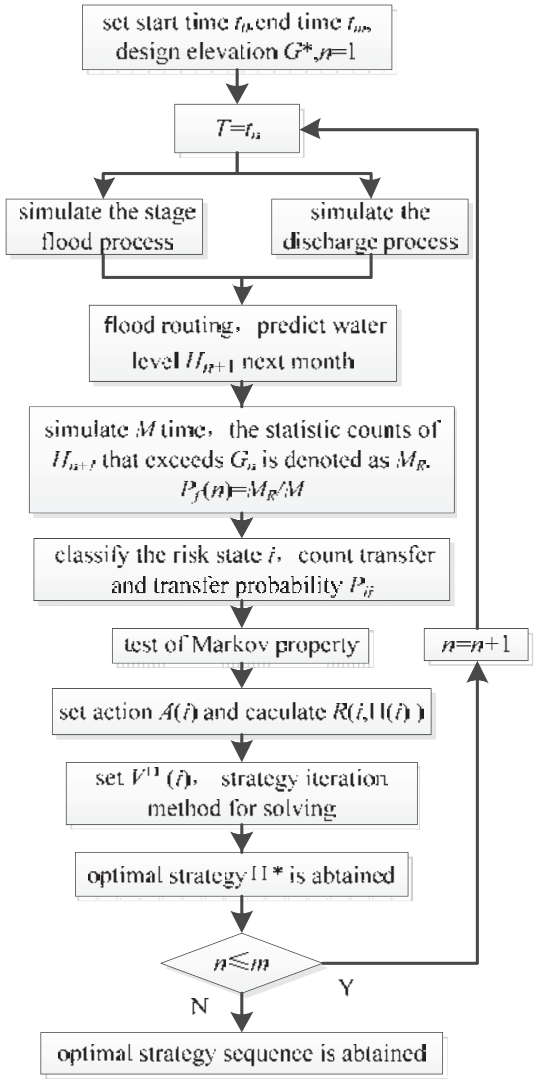
set start time t_n,end time t_m, design elevation G^*,n=1
T=t_n
simulate the stage flood process
simulate the discharge process
flood routing, predict water level H_{n+1} next month
simulate M time, the statistic counts of H_{n+1} that exceeds G_n is denoted as M_R. $P_f(n)$=M_R/M
classify the risk state i, count transfer and transfer probability P_{ij}
test of Markov property
n=n+1
set action $A(i)$ and caculate $R(i,\Pi(i))$
set $V^{\Pi}(i)$, strategy iteration method for solving
optimal strategy Π* is abtained
n≤m
Y
N
optimal strategy sequence is abtained

Figure 1. Flow chart of decision-making during flood period based MPM

4. CASE STUDY

4.1. Background

The water retaining dam of TK hydropower station was a faced rock fill dam with the elevation of 171.00m and the maximum height of 162.0m.Based on construction diversion scheme and scheduling, earth-rock overflow cofferdams were built in both downstream and upstream. The retaining water standard of cofferdam is ten- year cycle flood in dry seasons (From October to April) of which design flow is 2420m^3/s. The overflow water standard is twenty-year cycle flood of which design flow is 10400m^3/s, combined discharge of diversion tunnel. According to schedules, the dam temporary section can retain or overflow water after cofferdam overflowing in one flood season. Diversion schemes of the dam of TK station during construction are shown in Table1:

Table 1. Diversion Schemes of TK Hydropower Station during Construction

Construction stage	Diversion standard		Schemes	Filling height/m
	P/%	Q/$m^3.s^{-1}$		
Oct in 2nd year – Mar in 3rd year	10	2420	Water retaining by cofferdam	30
Mar in 3rd year – Sept in 3rd year	5	10400	Overflowing by cofferdam and dam	30~37
Oct in 3rd year - Mar in 5th year	0.5	17500	Water retaining and overflowing by dam body	140
Apr in 5th year-design elevation	0.2	20300	Water retaining by dam body	171
	0.1	22500		

4.2. Risk calculation result

The source of retaining water risk analysis parameters are as follows respectively: hydrological statistical parameters of peak flow follows P-□ distribution, of which distribution mean, variation coefficient and skewness coefficient obtained by the stage design flood at this station; Discharge capacity coefficient follows triangular distribution with lower limit a= 0.011, mode b=0.015 and upper limit c=0.020 based on the characteristics of diversion system; Through the stochastic simulation of inflow flood and discharge ,as well as flood regulating calculation, the possible highest water level in different month can be obtained. The statistic counts of highest water level H_{n+1} that exceeds G_n divided by the number of simulation is water retaining risk of high rock fill dam in a month. Calculation results of water retaining risk from March in 3rd year to September in 4th year during construction period are as shown in Table 2.

Table 2. Calculation results of water retaining risk in different month

Month	G_n /m	P_f/%
Oct. in the 3rd year	56	0.345
Nov. in the 3rd year	65	0.55
Dec. in the 3rd year	68	0.21
Jan. in the 4th year	75	0.11
Jun. in the 4th year	98	0.167
Jul. in the 4th year	98	0.11
Aug. in the 4th year	98	0.133
Sep. in the 4th year	98	0.62

4.3.Optimal strategy in a month

The risk calculated by the simulation is classified three levels equates three states by risk size: less than 0.2% as low risk, more than 0.2% and less than 0.6% as medium risk, more than 0.6% as high risk. Frequency matrix N_{ij} and transfer probability matrix P_{ij} are obtained as Eq. 10 by transfer frequency statistics from one state to another.

$$(N_{ij})_{3\times3}=\begin{pmatrix}0&3&1\\1&2&1\\3&1&0\end{pmatrix},\ (P_{ij})_{3\times3}=\begin{pmatrix}0&3/4&1/4\\1/4&2/4&1/4\\3/4&1/4&0\end{pmatrix} \qquad (10)$$

The marginal probability and the statistics $\chi^2=10.874$ are calculated thereafter. The Significance level $B=0.05$ is given to get the quantil $\chi_B^2((m-1)^2)=\chi_B^2(4)=9.488<10.874$ by table look-up; therefore the risk sequence satisfies the Markov property. After Markov text, transfer probability matrix P=[P_{ij}] is built. The return function R $(i,\Pi(i))$ (cost of flood prevention) and expected cost q_i for different strategies in each risk level state this month are obtained based on formula (2)- (4),as shown in Table 3.

Table 3. Transfer probability of risk state & expected cost of strategies

State	a_k	P_{ij}			R $(i,\Pi(i))$/ thousand yuan			q_i/ thousand yuan
Low	a_1	0.65	0.20	0.15	-860	-730	-298	-749.7
	a_2	0.35	0.35	0.30	-730	-540	-190	-501.5
	a_3	0.65	0.15	0.20	-500	-760	-1120	-663
Med-ium	a_1	0.50	0.30	0.20	-910	-850	-360	-782
	a_2	0.75	0.15	0.05	-650	-600	-330	-594
	a_3	0.90	0.06	0.04	-430	-770	-1060	-475.6
High	a_1	0.50	0.40	0.01	-1100	-840	-450	-931
	a_2	0.70	0.15	0.15	-530	-410	-210	-464
	a_3	0.85	0.10	0.05	-400	-760	-1020	-467

The value of discount factor γ can be equal to 0.9， A set of flood prevention actions $\Pi_0(1)=(a_2,a_3,a_2)$ with minimum cost in each current state is taken as the initial strategy. The result of improvement strategy is shown in Table 4 by using strategy iteration method.

Table 4. Iteration process of improvement strategy

Iteration count	$\Pi(i)$	$V^{\Pi}(i)$		
0	(a_2,a_3,a_2)	-4845.4	-4815.8	-4817
1	(a_2,a_2,a_2)	-4664.3	-4568.2	-4646.5
2	(a_2,a_2,a_2)	-4664.3	-4568.2	-4646.5

As the Table 4 shows, optimal strategy for flood prevention in different risk level state is achieved though only two iterations. This means overflowing is the optimal strategy for flood prevention at this point to ensure the minimum cost no matter what the state of risk.

4.4.Sequential decision prediction

The optimal strategies in any state for every decision point sequentially can be achieved by the approach above. The set of optimal strategies is stored in an offline strategy sheet. The water retaining risks in Table 2 are classified corresponding risk states, and thenthe sequential risk decision prediction for the high rock fill dam during flood period will be figured out by checking that sheet. The comparison between original decisions and sequential risk decision prediction as indicated in Table 5.

Table 5. Comparison between original decisions and sequential risk decision prediction

n	Month	Original decisions	Optimal strategy by MPM	Sequential decision prediction
1	Oct. in the 3rd year	a_3	(a_3, a_3, a_2)	a_3
2	Nov. in the 3rd year	a_3	(a_3, a_3, a_3)	a_3
3	Dec. in the 3rd year	a_3	(a_3, a_3, a_2)	a_3
4	Jan. in the 4th year	a_3	(a_3, a_3, a_3)	a_3
5	Jun. in the 4th year	$\boldsymbol{a_3}$	(a_1, a_1, a_2)	$\boldsymbol{a_1}$
6	Jul. in the 4th year	a_2	(a_2, a_2, a_2)	a_2
7	Aug. in the 4th year	$\boldsymbol{a_3}$	(a_2, a_2, a_2)	$\boldsymbol{a_2}$
8	Sep. in the 4th year	$\boldsymbol{a_3}$	(a_3, a_3, a_1)	$\boldsymbol{a_1}$

As can be seen from Table 5, the prevention decisions result predicted by MPM is the same as one of the original plan from October to December, in which the flood flow is lower. The selected decisions during this period are temporary section for retaining water in original filling schedule of the dam rather than other decisions. However, there are changes in June, August and September in the 4th year. For reducing more flood prevention cost in the dam construction process, overflowing the dam surface has replaced accelerating filling in June, retaining water in original filling schedule has replaced overflowing and accelerating filling in August and September respectively. In the actual project, the dam construction of TK station was scheduled the filling height from 30*m*-37*m* to 44*m* between June and September in the 4th year, which is just compatible with the accelerating strategies calculated by MPM during that period.

5. CONCULSION

Markov Process model (MPM) is taken into prevention decisions of high fill-rock dam construction dynamically and by order during flood period. It can predict decisions according to the current state that will provide the guidance for determining the standard and scheme of interim flood protection, as well as arrangements for construction schedule of high rock fill dam. However, emergency and temporary characteristics of flood prevention require the real-time and accuracy of decision making, and the execution results from prediction in the early stage will feed back the risk states in later stage. To resolve this issue, the model must own the ability to interact with the external environment. The final realization of prediction–regulation– revision- feedback decision making mechanism is still a problem which needs to be solved in follow-up research.

ACKNOWLEDGEMENT

This research was supported by National Natural Science Foundation of China (SN: 51509143，51279137), the Open Foundation of Key Laboratory of Hydropower Engineering Construction and Management of Hubei Province (SN: 2014KSD10). The authors thank the reviewers for useful comments and suggestions that helped to improve the paper.

REFERENCES

Zhang Chao and Hu Zhigen.(2014): Water Containment Risk Estimation during Interim Flooding for High Rock-Fill Dams, Advanced in Water Science , 25:6, pp. 873-879.

Liu Lian and Hu Zhigen.(2013):Negotiation Decision Evolutionary Analysis of High Rock Fill Dam Construction during Flood Period on Time-Varying, Journal of Hydraulic Engineering , 44:11,pp.1359-1365.

Fan Xie and Hu Zhigen.(2008):Multi-objective Decision Model for Construction Diversion Schemes based on Utility. Engineering Sciences,10:7,pp.137-140,157.

Rasekh, A , Afshar, A and Afshar, M. (2010): Risk-Cost Optimization of Hydraulic Structures: Methodology and Case Study, Water Resources Management, 24:11, pp. 2833 -2851.

Zhong Denghua, Mao Zhaihan and Liu Donghai.(2002): Multi-criterion Comprehensive Appraisal Method for Construction Diversion Schemes, Water Resources and Hydropower Engineering,33:5,pp.17-20,63.

Li Zongkun,Ge Wei and Wang Juan.(2014):Improved Catastrophe Theory Evaluation Method and Its Application to Earth-Rock Dam Risk Evaluation during Construction. Journal of Hydraulic Engineering, 45:10, pp.1256-1260.

Li Zongkun, Zhang Yadong and Guan Hongyan. (2014): Dynamic Risk Analysis of High Rock fill Dam during Construction period , Water Resouces and Power, 32:10, pp.138-141,172.

Liu Lian and Hu Zhigen.(2015): Water Retaining Risk Dynamic Control Model for High Rock-Fill Dams under Construction in Flood Season, Journal of Hydroelectric Engineering ,35:2,pp.1-8.

Xue Jinping, Hu Zhigen and Liu Quan.(2014):Method of Multi-Attribute Group Negotiation Decision of Construction Diversion Schemes , System Engineering-Theory&Practise , 34:5,pp.1324-1329.

Yan Ying,Cheng Shixue,Cheng Kai(1995):Stochastic Model of Operation Research, Renmin University of China Press.

Feedback Design of Temperature Control Measures for Concrete Dams Based on Real-time Temperature Monitoring and Simulation of Construction Process

Y.H. Zhou, H.W. Zhou, C.J. Zhao, H.M. Guo & C. Hu
College of Hydraulic and Environmental Engineering, China Three Gorges University, Yichang, China
zhyh@ctgu.edu.cn

Y.H. Zhou & H.W. Zhou
Hubei Key Laboratory of Construction and Management in Hydropower Engineering, China Three Gorges University, China

Y.H. Zhou & C.J. Zhao
Collaborative Innovation Centre for Geo-Hazards and Eco-Environment in Three Gorges Area, Hubei Province, Yichang, China

ABSTRACT:
Crack prevention is a significant issue in the construction process of concrete dams. The vast majority of concrete cracks are related to temperature variation process and hence temperature control is a primary method of crack prevention. In this paper, an integrated concept, named feedback design (FD) of temperature control measures, which incorporates temperature real-time monitoring, temperature field simulation and construction process simulation as a large system is first put forward for temperature control scheme optimization. Temperature variation process is obtained from distributed temperature sensors embedded in typical concrete blocks. Thermal parameters of concrete materials are obtained based on temperature monitoring data. Meanwhile, accurate construction environmental parameters are obtained through dam construction process simulation. Afterwards, temperature fields of dam blocks are simulated by incorporating initial temperature control measures, material inversion parameters and construction environmental parameters from last step. Then, effects of initial temperature control measures are assessed by comparing the simulation results with temperature design standards to determine revised measures if the standards are not satisfied. If there are revised measures, repeating the simulation process until temperature design standards are satisfied. The FD approach was applied to Xiluodu arch dam located in southwest of China, which has been proven efficacious.

Keywords: Concrete dam, Temperature control, Real-time monitoring, Feedback design, Construction simulation

1. GENERAL INSTRUCTIONS

During the construction of a concrete dam, large quantities of concrete are employed to form a monolithic mass concrete structure (Zhu 2012). Heat generated by the hydration of cement leads to a rising temperature in the dam body, and, owing to its massiveness, several years are required for a concrete dam to attain a stable temperature after a peak temperature is reached. Such variations in the temperature of concrete dams usually lead to cracks, which greatly impacts the safety and normal operation of concrete dams.

To prevent such type of cracking, years of practices and in-depth research have been conducted on revealing mechanism of temperature cracking and effects of various temperature control measures (Zhang et al. 2014; Zhu 2006; Cao et al. 2012; Su et al. 2014). However, the crack problem is not vanishing consequently. It is still a puzzling problem for engineers. For instance, during design and construction of Xiaowan double-curvature arch dam in China, strict measures have been incorporated in materials and construction technologies to prevent cracking according to experimentation and simulation results, but 16 cracks were found in 6 monoliths in the initial stage of construction (Zhu 2015; Lin et al. 2015).

Previous studies and practices have clearly demonstrated that the accuracy of concrete thermal and environmental parameters involved in initial conditions and boundary conditions are remarkably contributing to the simulation results of temperature and stress fields (Qu et al. 2012). Moreover, in most practical cases, real boundary conditions of each concrete block might be significantly different from on which the temperature and stress simulations are based. Accordingly, more valuable simulation results should be based on more accurate material parameters and construction process parameters (Wang et al. 2008, 2011). Besides that, as the temperature control effect is the most concerned factor during the construction process, monitoring data should be fully utilized for predicting risk zone and guiding engineers to take measures as early as possible to prevent cracks (Ha et al. 2014).

In this paper, an integrated concept, named FD of temperature control measures, which incorporates concrete temperature real-time monitoring, temperature field simulation and construction process simulation as a large system is first proposed for temperature control scheme dynamical optimization during the construction period of concrete dams. It has been proven reliable and valuable in the application of Xiluodu arch dam.

2. FRAMEWORK OF THE FD CONCEPT

Various temperature control measures have been widely used in the construction process of concrete dams for crack prevention, although the degrees to which the different measures influence the temperature and temperature stress fields are not equivalent. Optimizing the temperature control scheme of a concrete dam in the construction process is critical for achieving an effective combination of these measures in the construction organization design and management of the dam.

The FD concept of temperature control measures is fulfilled along the following steps: (1) Monitoring the concrete temperature variation process and collecting data through distributed temperature sensors embedded in concrete blocks; (2) Reconstructing temperature fields and back-analyzing the thermodynamic parameters of construction materials according to the collected temperature data; (3) Simulating the dam construction process by incorporating construction scheme parameters with quality restriction to obtain accurate parameters of construction schedule for determination of accurate constructing environmental parameters; (4) Simulating temperature and stress fields within dam concrete by incorporating initial temperature control measures, material parameters from step (2), environmental parameters from step (3) and construction schedule from step (3) to predict distribution and other details of temperature fields and stress fields; (5) Assessing effects of initial temperature control measures by comparison with results from step (4) and temperature design standards to determine revised measures if design standards are not satisfied; (6) If there are revised measures, repeating step (4) to step (5) until temperature design standards are satisfied.

Works from step (1) to step (6) are repeated in each concrete block to propose individuated control measures for respective concrete blocks. The flow chart of temperature control scheme optimization based on the concept is shown in Fig.1.

3. KEY TECHNOLOGIES AND METHODS

3.1. Principle of optical fiber based temperature monitoring

Distributed temperature sensing (DTS) is a technique which allows for measuring of temperature along optical fibers (Jong et al. 2015). Fiber-optic DTS system is an automatic monitoring system which composed of laser light source, sensor fiber and monitoring instrument. In the system, fiber is not only a kind of sensing medium but also a kind of transmission medium. When laser pulse travels through the optical fiber, Raman scattering happens at every point in the optical fiber. Because scattering lights is isotropic, only partial scattering lights return along the optical fiber. If we set the start time as the laser pulse going into the optical fiber, the scattering echo signal that the input terminal receives at time t, indicates a distance of L from scattering point to the input terminal. And the laser pulses in optical fibers have travelled $2L$. The distance L can be expressed as $L = ct/2n$, where c is the light speed in vacuum, n is the refractive index of optical fiber.

When the light travels through the optical fiber, the incident light's photons are scattered by the inelastic collision with optical photons in the fiber. The scattered light can be sorted as Stokes light and anti-Stokes light. Keeping the external parameters and the optical fiber parameters unchanged, there is functional relation between the temperature T at the monitoring position and the anti-Stokes light's optical power, which can be written as:

$$T = \frac{hcv}{k\left[\ln a - \ln\left(\frac{las}{ls}\right)\right]} \tag{1}$$

where las is the anti-Stokes light's optical power; ls is the Stokes light's optical power; a is the temperature correlation coefficient; h is the Planck coefficient ($J \cdot s$); c is the light speed in vacuum (m/s); v is the Raman shift amount (m^{-1}); k is the Boltzmann constant (J/K); and T is the Kelvin rating (K).

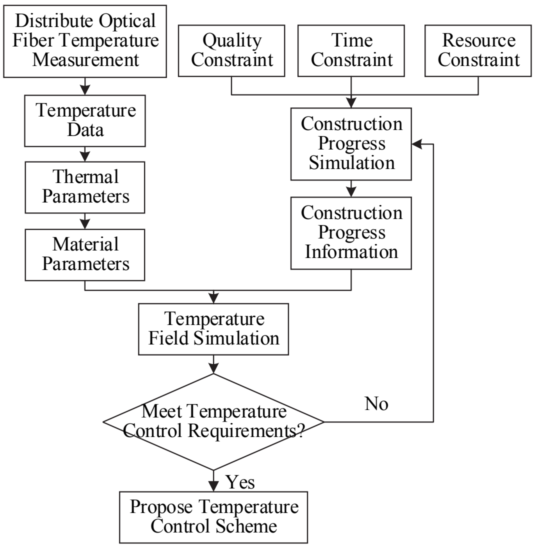
Distribute Optical Fiber Temperature Measurement
Quality Constraint
Time Constraint
Resource Constraint
Temperature Data
Construction Progress Simulation
Thermal Parameters
Construction Progress Information
Material Parameters
Temperature Field Simulation
Meet Temperature Control Requirements?
No
Yes
Propose Temperature Control Scheme

Figure 1. Flow chart of temperature control scheme optimization

3.2. Temperature field simulation

3.2.1. Intelligent inversion method of thermal parameters
Incorporating genetic algorithm, intelligent optimization algorithm of neural network and finite element

simulation method, an intelligent inversion method of thermal parameters for mass concrete is proposed in this paper.

After determining the thermal parameters for inversion, possible combinations ($\boldsymbol{x} = \{x_1, x_2, \cdots, x_n\}$) of several groups of the parameters are constructed with orthogonal design method and several value sets of the parameters for inversion are built. Calculated temperature values ($T_i(t_j)$) of multiple typical nodes are obtained using temperature field simulation method. In order to make the difference between temperature values of the typical nodes calculated based on the inversed thermal parameters and actual monitoring temperature values of the corresponding nodes minimum, a constructed objective function is proposed as follows：

$$e_i = \sum_{i=1}^{i}\sum_{j=1}^{j} |(T_i(t_j) - T_i^*(t_j))| \tag{2}$$

where e_i is the *i*-th set of thermal parameters for inversion; $T_i(t_j)$ is the temperature calculation value of the *i*-th typical node of Quasi mass concrete at the time t_j ; $T_i^*(t_j)$ is the actual measured temperature in the *i*-th typical node at the time t_j ; *i* is the total number of typical nodes; *j* is the total number of times.

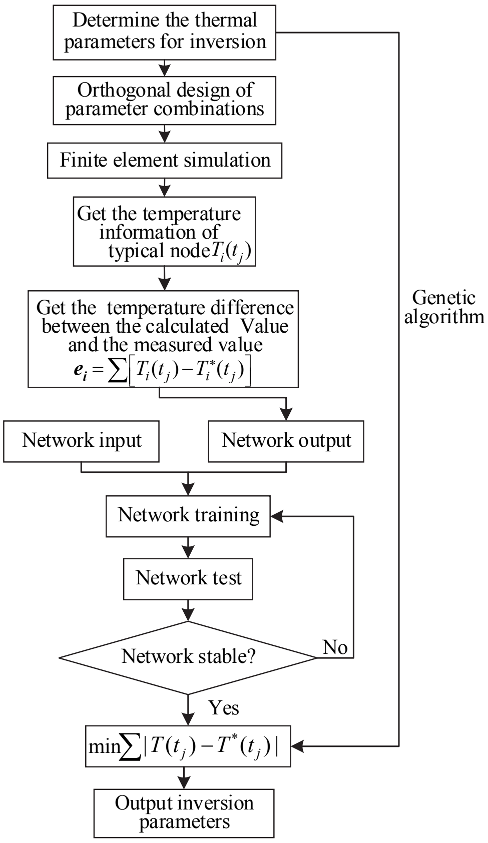
Determine the thermal parameters for inversion
Orthogonal design of parameter combinations
Finite element simulation
Get the temperature information of typical node$T_i(t_j)$
Get the temperature difference between the calculated Value and the measured value
$e_i = \sum \boxed{T_i(t_j) - T_i^*(t_j)}$
Network input
Network output
Network training
Network test
Network stable?
No
Yes
$\min\sum|T(t_j) - T^*(t_j)|$
Output inversion parameters
Genetic algorithm

Figure 2. Flow chart of intelligent inversion of thermal parameters

Each set of the parameters for inversion $\boldsymbol{x}_i$ and each group of objective function values e_i can make up a learning sample. Training and testing of the neural network are carried on by taking the inversion parameter sets $\boldsymbol{x}_i$ as input sample sets and e_i as output sample sets to get a neural reasonable network model. This neural network model is used to describe the nonlinear relationship between the concrete thermal parameters and the concrete temperature field. When the objective function value in the formula (2) is minimum, the corresponding set of parameters is the optimal solution of the parameters.

3.2.2. Calculation theory of temperature field

The equation of heat conduction considering the effect of water-pipe cooling can be expressed as [1]

$$\frac{\partial T}{\partial \tau} = a\left(\frac{\partial^2 T}{\partial x^2} + \frac{\partial^2 T}{\partial y^2} + \frac{\partial^2 T}{\partial z^2}\right) + \frac{Q}{c\rho} \tag{3}$$

where T is the concrete temperature (°C); τ is the time (h); a is the thermal diffusivity coefficient of concrete, given as $a = \lambda/c\rho$ (m^2/h); Q is the heat generation rate per volume (kJ/(m^3·h)); λ is the thermal conductivity coefficient (kJ/(m·h·°C)); c is the specific heat (kJ/(kg·°C)); and ρ is the material density (kg/m^3).

The initial condition is given in terms of standard Cartesian coordinates and time as follows.

$$T(x, y, z, 0) = T_0(x, y, z) \tag{4}$$

Three boundary conditions must be considered during calculation of the temperature field. The first boundary condition is that the surface temperature is a function of time, which is given as

$$T_s(\tau) = f(\tau) \tag{5}$$

The second boundary condition is that the heat flux across the surface is a known function of time, and is given as

$$-\lambda \frac{\partial T}{\partial n} = f(\tau) \tag{6}$$

The adiabatic boundary condition $\partial T / \partial n$ =0 can be obtained by substituting $f(\tau)$=0 into Eq. (4).

The third boundary condition is that the concrete surface is in contact with the air, which can be expressed as follows.

$$-\lambda \frac{\partial T}{\partial n} = \beta(T_s - T_a) \tag{7}$$

where $T_0(x,y,z)$ is the initial temperature; T_s is the surface temperature; n is the surface external normal direction; β is the surface conductance (kJ/ ($m^2 \cdot h \cdot °C$)); and T_a is the air temperature.

3.3. Construction process simulation

3.3.1. Analysis of concrete dam construction simulation system

Concrete dam construction system can be decomposed into three subsystems: concrete production system, concrete transportation system, and storehouse pouring system. The construction simulation system belongs to discrete type system. In order to study the dynamic change process of concrete construction state over time, dam blocks are used to divide the pouring stage. That is to say, pouring of each block can be taken as one time period during the simulation process. And the construction state of the dam at the end of each stage is measured and described. The whole process is quantitatively described by the mathematical logic relation among state variables, decision variables and construction constraints. State variables include some construction parameters such as concrete volume, start time and finish time of concrete pouring. Decision variables mainly include concrete pouring machine and concrete blocks. Constraints include intermittent time, height difference between adjacent blocks, initial setting time of concrete, and preparation time of concrete block surface. With constant change of the state variables and decision variables, the dam block pouring sequence is arranged by the main program according to the dam construction layout and various constraints. Indicators of dam construction process, such as block division detail, resource utilization, running situation of construction road, month's construction strength, and mechanical strength, are recorded at any time. On the basis of that, construction process of the dam is finally determined.

3.3.2. Design of concrete dam construction simulation model

The overall simulation model of concrete dam construction process is mainly includes three parts, which are data pre-treatment part, construction process simulation part and results analysis part. Data pre-treatment module is mainly focused on standardized information processing and collection of relevant boundary conditions, solution parameters and dam body parameters based on the data structure and inerratic expression of the simulation model to help engineers and technicians complete related parameters setting, adjustment and input in a proper way. Vast amounts of construction parameters can be managed by the pre-treatment module with the database as information carrier. Parameters input is realized by filling in the form. And the primary reasonableness test of the parameters is executed. During the simulation process, calculation data such as concrete pouring sequence and hour strength of concrete production are obtained. Generally, thousands of pouring sequence records are included in the simulation results. According to these data, construction system parameters such as total construction time, monthly dam construction intensity and schedule, construction machinery intensity and utilization, supply intensity of concrete material feeding line and proportion statistics of old concrete. This part of function is realized in the construction simulation results analysis module. In order to better deal with the above parameters, visualization method is generally used to visualize the construction parameters. At the same time, in order to facilitate the query, the interactive query technique based on visualization is introduced to provide convenience for the analyses of construction scheme features.

4. ENGINEERING APPLICATION

4.1. Brief introduction to dam site

The proposed method was applied to Xiluodu arch dam for temperature control and crack prevention during the construction period (Zhou et al. 2011, 2012, 2013). The project is located on the Jinsha River, in the Leibo County of Sichuan province. The Xiluodu hydropower station is mainly consists of a double-curvature arch dam with 285.5 meters high, overflow structures, diversion buildings, underground powerhouse, and logway. The crest elevation and the minimum height of the foundation face of the dam are 610 m and 324.5 m, respectively. It's the third high arch dam in China. The dam with crest width of 14 m, bottom thickness of 60 m, a maximum central angle 95.58°, arch axis arc length of 681.51 m, a thickness-height ratio of 0.216 and an arc height ratio of 2.451 endures 600 m of water pressure under its normal operation state. The dam is divided into 31 dam monoliths and 4 typical dam monoliths (5#, 15#, 16#, and 23#) are selected to be monitored by DTS system. The construction of the dam was started in March 2009, and the concrete construction process was finished in March 2014.

4.2. Layout of DTS system and monitoring results

From pouring of first concrete block of the typical dam sections, temperature of each concrete block was real-time online measured by distributed optical fiber embedding in the concrete. Spatial resolution, sample frequency and sample interval of DTS system were set as 1.0 m, 2h/t, and 1.0 m, respectively. This setup ensures the distributed optical fiber sensing network obtain a temperature measurement value per meter.

DTS temperature measurement host has high requirements to the environment as its normal operation is mainly influenced by air temperature, dust, vibration, humidity, frequent power outages or voltage instability, and local optical fiber damage. In the Xiluodu arch dam, temperature measurement host and optical fiber lead were first laid in corridors of the dam to fulfill the above requirements.

The application has demonstrated that sub-corridors used for deformation monitoring in the dam can provide suitable environment for the host running. On the basis of monitoring sub-corridors, transportation corridors, and basic corridors, a stable whole dam section DTS monitoring system was built.

Synergistic effect of concrete pouring and fiber optic cable laying construction at the site should be considered. Under the premise of no construction mechanical damage, temperature measuring optical fiber cable was embedded in the concrete block before its initial set by fully use of cable crane, crane, concrete spreading machine, and concrete vibratory machine. In the fiber optic cable laying construction project of Xiluodu arch dam, a variety of fiber layout types were first developed, such as pressure-vibration method, double-strand method, bracket method, and spiral method.

Taking the Xiluodu 5# dam monolith of 25th pouring block (5#-25) for example, temperature variation process lines of typical monitoring points are shown in figure 3.

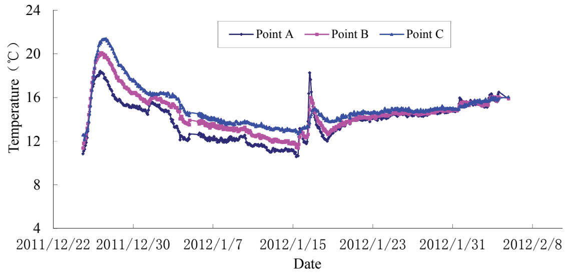

Figure 3. Temperature variation process lines of three typical monitoring points in 25th pouring block of 5# dam monolith

4.3. Thermal parameters inversion results

Concrete temperature is affected by a variety of factors. Experimental thermal parameters cannot reflect the actual situation. In order to accurately simulate the temperature field, five parameters are selected for inversion in this study. They are heat conductivity coefficient, surface heat transfer coefficient, adiabatic temperature rise, temperature rising rate and equivalent surface heat release coefficient of cooling water pipe. According to the intelligent inversion method of thermal parameters proposed in this paper, inversion results are shown in Table 1.

Table 1. Intelligent inversion results

Parameter	λ /KJ/(m·d·℃)	β /KJ/(m^2·d·℃)	θ /℃
Value	158.77	687.04	31.13
Parameter	n	β' /KJ/(m^2·d·℃)	\ \
Value	1.35	61347.7	\

4.4. Construction process simulation results

Based on the construction simulation model of concrete dam proposed in this paper, the whole concrete pouring process of Xiluodu arch dam was simulated by taking concrete block as basic unit. Main entities in the construction system are consist of cable crane, concrete spreading machine, vibrating car, and concrete blocks. Construction environmental parameters, such as monthly concrete pouring strength, concrete construction duration and concrete pouring sequence, are obtained through the construction simulation process. Dam placement appearance at the end of 2011 is shown in Fig. 4.

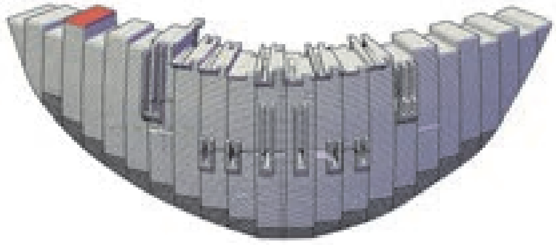

Figure 4. Construction progress of the dam at the end of 2011

4.5. Temperature field simulation results

Taking several blocks of the 15# dam monolith as example. The computational model are built as shown in Fig. 5. Eight-node hexahedral isoparametric elements are employed in the numerical model. The direction along which the river flows represents the positive x-axis direction and the vertical upward direction represents the positive z-axis direction. The remaining positive y-axis direction is placed to form a standard right-hand Cartesian coordinate system.

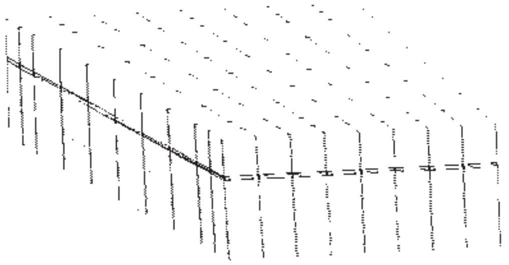

Figure 5. 3-D Finite element model

Then, temperature fields of the selected dam blocks are simulated by incorporating initial temperature control measures, material inversion parameters and the simulated construction parameters. Temperature distribution of the blocks are obtained through simulation before real construction of these blocks. And after the construction of them, real temperature variance law are obtained through real time monitoring with DTS. Taking two typical points located in the centre of the dam monolith as examples, the temperature variance lines from simulation before construction and real values from monitoring are shown in Figs. 6 and 7. It’s obvious that the simulation results are in well accordance with the monitoring values. The results demonstrate that the simulation model is correct and the proposed FD concept is reliable and can be used to forecast the temperature fields of the concrete blocks which are planned to pouring. By doing that, temperature control measures are finally designed.

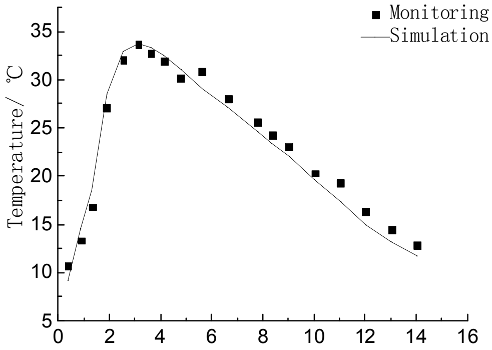

Figure 6. Temperature variance lines of typical point 1# by monitoring and simulation

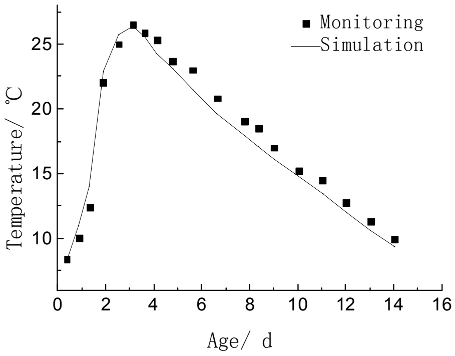

Figure 7. Temperature variance lines of typical point 2# by monitoring and simulation

5. CONCLUSIONS

An integrated concept, named feedback design (FD) of temperature control measures, was first proposed for temperature control scheme optimization in this study. The concept is incorporates concrete temperature real-time monitoring, temperature field simulation and construction process simulation as a large system. The method was applied to Xiluodu arch dam located in southwest of China. The application results demonstrate that the simulation model is correct and the proposed FD concept is reliable and efficacious. It can be used to forecast the temperature fields of the concrete blocks before the real construction process.

ACKNOWLEDGEMENT

This research was supported by National Natural Science Foundation of China (SN: 51479103), the Open Foundation of Key Laboratory of Hydropower Engineering Construction and Management of Hubei Province (SN: 2014KSD06). The authors thank the reviewers for useful comments and suggestions that helped to improve the paper.

REFERENCES

Zhu, B.F. (2012): Thermal Stresses and Temperature Control of Mass Concrete, China WaterPower Press, Beijing.

Zhang, G.X., Liu, Y., and Li, S.H. (2014): Research and practice of Nine-Three-One temperature control mode, Journal of Hydroelectric Engineering, 33:2, pp. 179-184.

Zhu, B.F. (2006): Current situation and prospect of temperature control and cracking prevention technology for concrete dam, Journal of Hydraulic Engineering, 12, pp. 1424-1432.

Cao, F.J., Fang, G.H., Ma, X.G., and Hu, Z.N. (2012): Simulation analysis of crack cause of concrete overflow dam for Hadashan Hydro Project by 3-D FEM, 3, pp. 48-54.

Su, H.Z., Li, J.Y., and Wen, Z.P. (2014): Evaluation of Various Temperature Control Schemes for Crack Prevention in RCC Arch Dams During Construction, Arabian Journal for Science and Engineering, 39:5, pp. 3559-3569.

Zhu, B.F. (2015): Discussion on the causes of crack formation during construction of Xiaowan Arch Dams, Water Resources and Hydropower Engineering, 46:4, pp. 1-5.

Lin, P., Zhou W.Y., and Liu, H.Y. (2015): Experimental Study on Cracking, Reinforcement, and Overall Stability of the Xiaowan Super-High Arch Dam, Rock Mechanics and Rock Engineering, 48:2, pp. 819-841.

Qu, L.X., Huang, Y.Y., Zhou, Y.H., Gong, J.W., Zhou, S.W., Li, J.H., and Tang, G.Q. (2012): Experiment of real-time on-line monitoring on surface of pouring concrete and transverse joint based on distributed fibers in hot season, Engineering Journal of Wuhan University, 45:4, pp. 423-426.

Qu, L.X., Zhou, Y.H., Huang, Y.Y., Gong, J.W., Zhou, S.W., Li, J.H., and Chen, W.F. (2012): Multi-objective fuzzy synthetic evaluation of temperature status of concrete dam, Journal of Hohai University(Natural Sciences), 40:6, pp. 641-647.

Wang, Z.H., Zhu, Y.M., and Li, F. (2008): Back Analysis of Concrete Thermal Parameters and Study of Feedback Based on Genetic Algorithm, Journal of Wuhan University of Technology (Transportation Science & Engineering), 32:4, pp. 599-602.

Wang, Z.H., Zhang, G.X., and Liu, Y. (2011): Test and Inverse Analysis for Temperature Control Parameters of Concrete with Cooling Pipe, Journal of Sichuan University (Engineering Science Edition), 43:3, pp. :56-60.

Ha, J.H., Jung, Y.S., and Cho, Y.G. (2014): Thermal crack control in mass concrete structure using an automated curing system, Automation in Construction, 45, pp. 16-24.

Jong, S.A.P., Slingerland, J.D., van de Giesen, N.C. (2015): Fiber optic distributed temperature sensing for the determination of air temperature, Atmospheric Measurement Techniques, 8:1, pp. 335-339.

Huang, Y.Y., Zhou, Y.H., Jiang, K., Wang, L.J., Zhou, J.B., and Li, J.H. (2011): Monitoring of vertical temperature of 3 m concrete pouring deck with distributed fiber, Large Dam & Safety, 5, pp. 47-49.

Zhou, Y.H., Zhou, J.B., Huang, Y.Y., Zhou, S.W., and Li, J.H. (2012): Monitoring of Temperature Gradient on Concrete Surface by Distributed Optical Fiber and Feedback Analysis, Journal of Yangtze River Scientific Research Institute, 29:9, pp. 42-45.

Zheng, X.H., Zhou, Y.H., Huang, Y.Y., Li, J.H., Tian, K.P., and Wei, X.B. (2013): Feedback Analysis of the Insulation Effect of Insulation Pads on Pouring Cube Surface Based on Distributed Optical Fiber, China Rural Water and Hydropower, 8, pp. 112-115.

Optimization of Construction Process for High Arch Dam Storehouse Surface Based on Virtual Prototype Technology

C.J. Zhao, C. Hu, Y.H. Zhou, L. Song & H.W. Zhou
College of hydraulic & environmental engineering, China Three Gorges University, Yichang, China
chunju.zhao@163.com

C.J. Zhao, C. Hu, Y.H. Zhou, L. Song & H.W. Zhou
Hubei Key Laboratory of Construction and Management in Hydropower Engineering, China Three Gorges University, China

C.J. Zhao & Y.H. Zhou
Collaborative Innovation Centre for Geo-Hazards and Eco-Environment in Three Gorges Area, Hubei Province, Yichang, China

ABSTRACT:

In this paper, a visual prototyping simulation system for high arch dams is established to visualizing the vivid construction process of concrete placement based on virtual prototyping technology. The basic idea is as follows: 1) After classifying all kinds of objects in the concrete pouring system of high arch dams according to structure, machinery layout, materials, personnel and equipment, N-dimensional models of the objects are built based on openness, normative and scalability principles; 2) A physical space state transition model of concrete placement surface and a space motion simulation model of construction equipment are established. 3）A collision detection method is first proposed. By simulating motion of each object in the concrete pouring system according to the construction procedure, collisions are recorded and adjusted based on adjustment mechanism; 4) Integrating database technology, virtual reality platform and the methods mentioned above, a virtual prototype analysis system for concrete pouring system of high arch dams is established, which can execute construction progress simulation with three-dimensional virtual scene, as well as collision and adjustment during pouring process. The system has been implemented in a real project, and the results prove that the system is reliable and effective.

Keywords: arch dam，construction process, virtual prototyping, optimization, storehouse surface

1. INTRODUCTION

Construction resources of high arch dam in the storehouse surface are limited by spatial. It is difficult to arrange the resources and procedure as the narrow space, which is easily lead the interference in construction and may reduce work efficiency. Therefore, it is significant to make a scientific schedule before construction.

Previous studies have demonstrated that a reasonable plan is critical for the smooth implement of construction. By rehearsing and optimizing the plan before execution, then applying the optimization results to guide the real construction process.

Virtual prototyping (VP) is a method in the process of product development. It involves using computer aided design, computer automated design and computer aided engineering software to validate a design before committing to making a physical prototype. In recent years, VP has been applied in civil engineering and demonstrated it can improve work efficiency and reduce cost and rework (Huang et al. 2007). Some scholars in Hong Kong Polytech Univ. have applied VP in lifecycle management of buildings, construction process, safety management, resources and schedule optimization (GuoLi and Li 2013, Li et al. 2009, Li et al. 2008, Huang et al. 2007, Choi and Chan 2004, GuoLi and Skitmore 2010). Song and Kim has optimized the construction schedule of high-rise building by analyse its construction technology and progress based on VP and BIM (Song Yang and Kim 2012, Kim et al. 2013). Agrama has applied this method in high-rise building construction process simulation and optimization (Agrama 2014). In the field of bridge construction, Li and Sampaio have tried this technology to optimization the construction procedure and resources allocation in large-scale bridge construction (Sampaio and Martins 2014, Li et al. 2012). Xue Yang and Sijie Zhang have introduced this method combine with real-time monitoring and feedback in the architecture construction field, which can control and predict the process (Yang and Ergan 2014, Zhang et al. 2013). From above researches, it can infer that VP is a powerful technology in assisting AEC (Architecture, Engineering and Construction), which can provide multi-dimensional information including schedule, quality, cost, safety etc. By analysing the characters of AEC, the basic unit (floors) is highly similarity, the construction progress is a repeated process, the kind of machine is rare and the construction constrain is simple. However, the construction process of high arch dam is more complicated than AEC, the spatial is limited and intensity is high. Therefore, failure in planning impacts safety, quality and productivity adversely. It is critical to figure out a scientific construction scheme which can avoid unexpected clashes or pitfalls and optimize the construction schedule with resources allocation for construction of high arch dam. In view of these practical applications, a Dam Construction Virtual Prototyping (DCVP) is developed in this paper. The DCVP is a construction process simulator developed based on virtual reality platform, integrated with dam construction N-dimensional (N-D) information management, 3D models of building components, construction equipment, temporary works as well as labours force, the motion simulator, collision detection and adjustment. The proposed system can analyse the plan dynamic and aid planner to review the construction process with detailed information. In this paper, the second section presents the framework of DCVP. The third section describes the overall approach of DCVP. In the fourth section, a case study is presented. The last section discusses and concludes the further development of DCVP.

2. FRAMEWORK OF DCVP

The framework of DCVP is shown in Fig. 1. It mainly contains four subsystems, data collection and analyse, data management, virtual display, plan optimization and decision-making system. The data collection and analysis is the foundation of the whole system. It contains all information including 3d models of construction objects, equipment, resources, and scene. Also all properties of the models are abstracted into different classification like identification, material, structure, appendix, schedule, cost and so on, which is called N-D model. Then all information mentioned above are stored in different database, where mainly contains three databases, construction program, N-D information, construction model. Then, by employing a virtual reality platform, the construction process can be presented, which including collision detection and adjustment, information management, resources management, human-computer interaction. Finally, the result of construction is output, the detail data of process can be applied in progress analysis, quality analysis, cost analysis, efficiency analysis and so on.

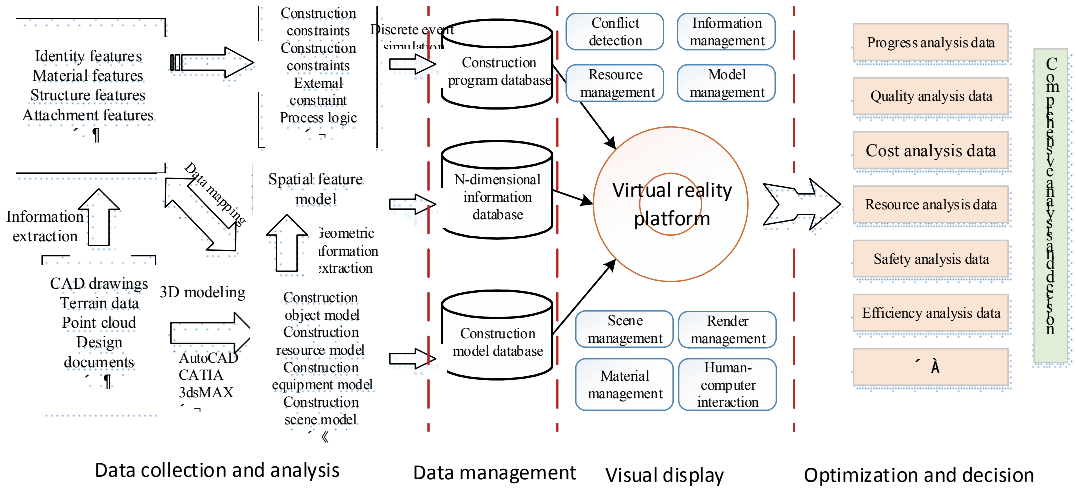
Identity features
Material features
Structure features
Attachment features
Information extraction
CAD drawings
Terrain data
Point cloud
Design documents
Data mapping
3D modeling
AutoCAD
CATIA
3dsMAX
Construction constraints
Construction constraints
External constraint
Process logic
Discrete event simulation
Spatial feature model
Geometric information extraction
Construction object model
Construction resource model
Construction equipment model
Construction scene model
Construction program database
N-dimensional information database
Construction model database
Conflict detection
Information management
Resource management
Model management
Virtual reality platform
Scene management
Render management
Material management
Human-computer interaction
Progress analysis data
Quality analysis data
Cost analysis data
Resource analysis data
Safety analysis data
Efficiency analysis data
Comprehensive analysis and decision
Data collection and analysis
Data management
Visual display
Optimization and decision

Figure 1. The framework of DCVP

3. DAM CONSTRUCTION VIRTUAL PROTOTYPING – OVERALL APPROACH

3.1. N-D modelling

One of the main concerns of engineers for project planning is which approaches and methodologies to be adopted during the real construction execution. The more detailed information, the better for decision-making. Therefore, the first step is to establish N-D model. N-D model is oriented to lifecycle management. As construction involving many constructors and a long period. The method and efficiency of construction information management have a direct impact on the whole process. With all parties concerning with overall construction information, reference the concept of building information model, integrating different types of information called N-D model is established. The data structure containing a variety of information data for all parties in project. The information runs through the entire project life and the information flow can be abstracted as the following model in Fig. 2. According to the model, each construction part is closely linked, each of them has its own properties. Property is the expression of construction features in different dimensions.

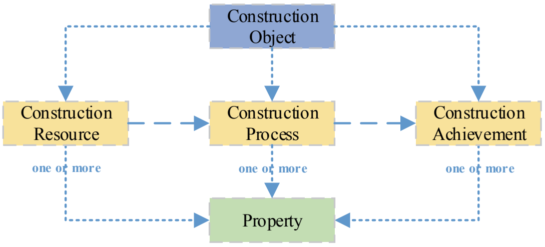
Construction Object
Construction Resource
Construction Process
Construction Achievement
one or more
one or more
one or more
Property

Figure 2. Construction Information Classification

The system demanding is to analysing schedule, cost, quality, safety and other object, by analysing the data of the DCVP.

The data is quite scatter. Thus, the demanding and data must connect in a certain way. The DCVP integrated all kind of information in project. Then a four-levels structure modelling is applied, as shown in Fig.3. By classify the features top-level application, such as "quality, schedule, cost, security, environment and energy etc.". The index of each object is decomposed. Then these index are further broken into class attribute relationship, identity characteristics, material composition, mechanical parameters, costs and other information. The corresponding information representing model based on the decomposition of each index can be established. Then the characteristics are broken into meta-data and stored into its corresponding database.

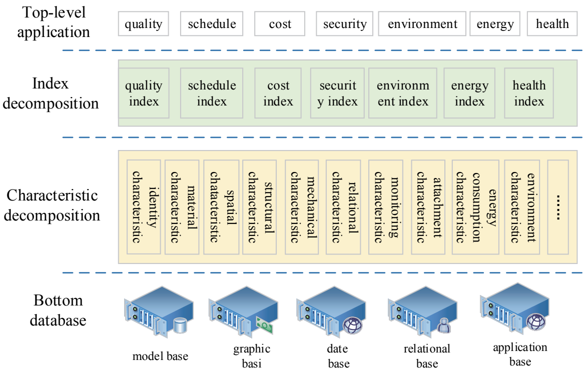
Top-level application
quality
schedule
cost
security
environment
energy
health
Index decomposition
quality index
schedule index
cost index
security index
environment index
energy index
health index
Characteristic decomposition
identity characteristic
material characteristic
spatial characteristic
structural characteristic
mechanical characteristic
relational characteristic
monitoring characteristic
attachment characteristic
energy consumption characteristic
environment characteristic
……
Bottom database
model base
graphic basi
date base
relational base
application base

Figure 3. The composition of N-D model

3.2. Equipment spatial motion simulation

3.2.1. Spatial operation mechanism

With more and more efficient construction machinery being adopted in engineering, the jobs in the storehouse surface become multifarious, in which many different kinds of machineries are required to cooperate. Therefore, the selection, operation and efficiency of the construction equipment have a great effect on the smooth process of storehouse surface construction. In this paper, the major construction equipment motion on storehouse surface has been analysed. The motion simulation method has been established by the means of on-site inspection, data collection and mathematical modelling, which has been proved effective in the modelling.

When describe the equipment moves in space, the position transfer can be expressed in a single continuous function of time (t) that

$$p(t) = [x(t) \quad y(t) \quad z(t)] \tag{1}$$

And the corresponding angle of rotation about the x axis, the y axis or the z axis can be expressed:

$$o(t) = \left[o_x(t) \quad o_y(t) \quad o_z(t) \right] \tag{2}$$

The dimensional operation of construction equipment contains both translational operation and rotational operation, so vector $r(t) = \begin{bmatrix} p(t) \\ o(t) \end{bmatrix}$ is defined to express the location and direction of the equipment at same time. When the construction equipment moving, the time will advance from t_1 to t_2, and the locational vector will change from $r(t_1)$ to $r(t_2)$. In this function, $R_{3\times3}$ is to express the related rotation, and $P_{3\times1}$ to express the translation. So the dimensional operation of construction equipment can be expressed by the counterchange matrix:

$$T = \begin{bmatrix} R_{3\times3} & P_{3\times1} \\ 0_{1\times3} & 1 \end{bmatrix} \tag{3}$$

3.2.2. Equipment path analysis

The main equipment in construction are cable cranes, tower cranes, lateral unloading cars, dozers and vibrators. Take cable crane for example to demonstrate spatial motion simulation process. The concrete bucket carries concrete from production system to storehouse surface. The typical path is shown in Fig. 4.

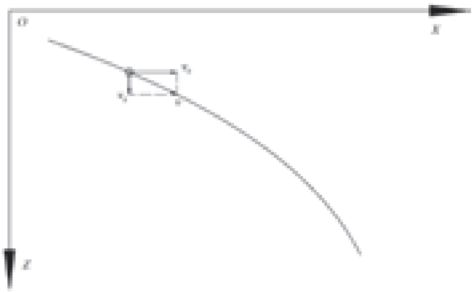

Figure 4. Typical bucket path

The speed of bucket consists horizontal speed v_h and vertical speed v_v, where $\boldsymbol{v} = \boldsymbol{v}_h + \boldsymbol{v}_v$. Then its acceleration value can be described as $\boldsymbol{a}_h = d\boldsymbol{v}_h/dt$, $\boldsymbol{a}_v = d\boldsymbol{v}_v/dt$. From the cable crane operation guide, the motion in each direction contains three stages, accelerate motion, uniform motion and decelerate motion. So can be expressed:

$$\begin{cases} x = \dfrac{1}{2}a_h(t-t_1)^2 (t_1 \le t \le t_{11}) \\ x = \dfrac{1}{2}a_h t_{11}{}^2 + v_h(t-t_{11})(t_{11} \le t \le t_{12}) \\ x = \dfrac{1}{2}a_h t_{11}{}^2 + v_h t_{12} + v_h(t-t_{12}) - \dfrac{1}{2}a_h(t-t_{12})^2 (t_{12} \le t \le t_2) \end{cases} \tag{4}$$

$$\begin{cases} z = \dfrac{1}{2}a_v(t-t_1)^2 (t_1 \le t \le t_{31}) \\ z = \dfrac{1}{2}a_v t_{31}{}^2 + v_v(t-t_{31})(t_{31} \le t \le t_{32}) \\ z = \dfrac{1}{2}a_v t_{31}{}^2 + v_v t_{32} + v_v(t-t_{32}) - \dfrac{1}{2}a_v(t-t_{32})^2 (t_{32} \le t \le t_3) \end{cases} \tag{5}$$

Five typcical position were chosen to simulate the crane buckets path, the results is similary to actual situation, as shown in Fig. 5. Other equipments path can not present in this paper as the limitated space.

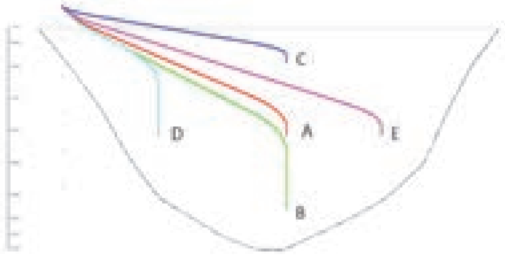

Figure 5. Typical cable crane bucket path

3.3. Construction collision detection and adjustment

3.3.1. Entity spatial expression

There are different kinds of entities on a storehouse surface, and each entity has its own function and property. Based on the object oriented method, the entities are divided into the following categories:

Table 1. Types of entities

Type	Example
Equipment	Cable crane, tower crane, truck etc.
Personnel	Commander, bar engineer, coordinator etc.
Material	Concrete, steel, cooling pipe, template etc.
Object	Dam block, prefab, steel frame etc.

Each entity occupies some spatial in the construction system. The occupied space of each entity can be expressed by three layers, which are efficiency space, safety space and physical space, as shown in Fig. 6. The occupied space can be described with three elements, as shown in Table 2.

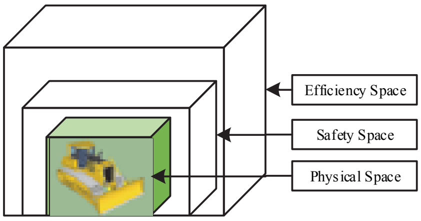
Efficiency Space
Safety Space
Physical Space

Figure 6. Entity Occupied Space

Table 2. Entity spatial expression

Name	Explanation
Geometric parameter	Geometric size, like length, width, height, dimeter, etc.
Location parameter	Coordination
Location direction	Cardinal direction

Some entities are dynamically changing with time and space in the construction system. And the relationship between two entities can be expressed as:

$$R(E_1, E_2) = R(Orientation, Distance) \tag{6}$$

Where E_1 and E_2 represent two entities; *Orientation* express the orientation of E_2 relative to E_1; *Distance* express the distance of E_2 relative to E_1.

The location of the relationship between entities is mainly composed by the following description:

（*Up, Below, Inside, Behind, Front, Left, Right, Cross*）

3.3.2. Collision detection in storehouse

By analysing the operation of the storehouse construction equipment, the time-space collision in the construction process are divided into the following categories:

Table 3. Types of collisions

Collision Type	Explanation
Collison 1	Among cable cranes
Collision 2	Among bucket and surface machine
Collision 3	Between bucket and dam body
Collision 4	Between bucket and temporary structure
Collision 5	Between bucket and other hoists
Collision 6	Among machines in the storehouse
Collision 7	Between machines and dam structure

By the means of Bounding Box (BB), the above mentioned collisions can be tested well. While the constructing method of BB has been ignored in this paper. The construction state are changes along with the change of entity's state. The entity state is classified into active entity and passive entity. Active entity refers to object's location and state changes with time, while passive entity's state would not change with time. In consequence, the collision can be simplified into two categories 1) the collision among active entities, and 2) the collision among active entities and passive entities.

The process of collision detection advance with the change of entity's state in storehouse. And the change of entity's state is evolved from the series of regularly process flow as well. On the basis of every entity's moving state and pattern, virtual construction process can be carried out. And the flow just as the following Fig. 7.

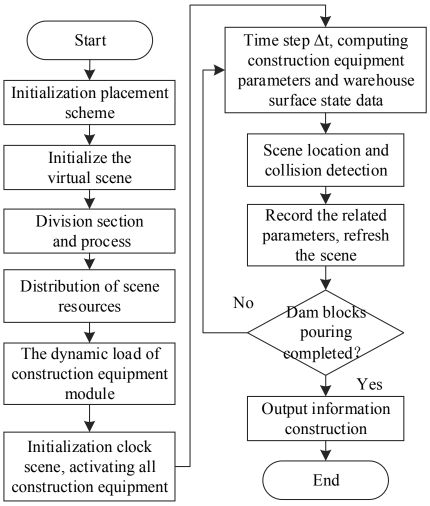
Start
Initialization placement scheme
Initialize the virtual scene
Division section and process
Distribution of scene resources
The dynamic load of construction equipment module
Initialization clock scene, activating all construction equipment
Time step Δt, computing construction equipment parameters and warehouse surface state data
Scene location and collision detection
Record the related parameters, refresh the scene
No
Dam blocks pouring completed?
Yes
Output information construction
End

Figure 7. The flow of construction simulation

In collision detection process, all of the active entities are assigned into Dynamic Entity List (DEL), nevertheless, the passive entities are assigned into Static Entity List (SEL). Analysing the ply of the entity's bounding box, some entities have both root node and child node. So the collision detection can be partitioned into three stages that the detection between both root nodes, the detection between root node and child node and the detection between both child nodes. In the virtual construct scene, the entities' state can be tested by the following pseudo-code with time Δt.

```
void DVCP-Collision(DynamicEntityList, StaticEntityList)
{
    DEL ← dynamicEntityList
    SEL ← staticEntityList
    CEL ← collidedstaticEntitylist(SEL, SEL)
    CEL ← RootRootDetection(DEL, SEL)
    CEL ← RootSubrootDetection(DEL, CEL)
    CEL ← subRootsubRootDetection(DEL, CEL)
return CEL
}
```

Initially, the DEL and SEL can be created from entities' state. The first step is to get the Collision Entity List (CEL) by detecting the crossed elements in the SEL. And then, using cross detection to test both active entity and passive entity, note the record in the CEL. According to the CEL, cross detection should be applied to test the collision between root note and child note, and the collision between both child notes should be detected as well. In the end a final CEL will be generated and return to the system.

3.3.3. Collision influence evaluation and adjustment

The collision in the storehouse refers to more than two entities activate overlaps at the same and same place. Different overlaps lead to different effects in construction process. Therefore, the effects collision influence can be evaluated with the following indexes.

(1) The space area of collision (S_c). Two entities have intersection in space when collisions take place, and the degree of collision can be measured intuitively by the calculated area of intersection.

(2) The space ratio of collision (S_r). The space ratio means the ratio between the space area of collision and the original entity, because the entity of Collision gets different damage in the collision, this index can reflect influence extent between the two collisions.

(3) The continuance of collision (D_c). The continuance means the overlap time of two entities in the space, reflect the influence of working procedure, if the continuance is long, and it maybe influence the project schedule.

(4) The duration ratio of collision (D_s). The duration ratio means the ratio between the continuance and the set time, and determine the adjustment will be necessary or not according to this index.

With the above indexes, the collision influence for project can be divided into the following types:

(1) Significant Effect. Significant effect usually caused by the breakdown of key equipment during construction. Key equipment can't work normally, so the construction can't be carried out. For example, the cable crane breaks down due to collision, and there is no alternate equipment, the placing of concrete can't be carried out.

(2) Great Effect. Great effect caused by some troubles of construction equipment due to collision, but it can be solved by analysing and eliminating the troubles in a certain time, but it may be delay the project schedule more or less as the long solving time.

(3) General Effect. Suspend the construction for a short time because of collision, but it can be solved by some simple processing, and it influences the project for a short time.

(4) Slight Effect. Collision leads to the put-off of construction date of the following activities, but the normal construction can be assuring by simple adjustment or delay of the process, and it has no effect on the whole schedule.

(5) No Effect. Although there is collision, the degree is subtle and it has no effect on construction entities and schedule.

From above indexes, the collision not only effect the time, but also effect the space. Therefore, the adjustment strategy can be carried from time and space.

Timing strategy mainly include two types: Waiting (as shown in Fig.8) adjustment and procedure adjustment. Space adjustment refers to change the original path to avoid collision. The priority object is active entity.

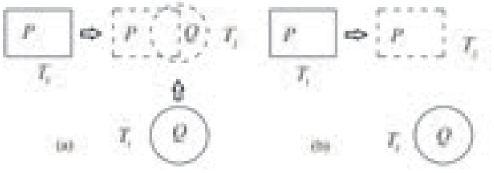

Figure 8. Waiting method

4. CASE STUDY

A real-life construction project is presented to demonstrate the applicability of the dam construction virtual prototyping approach. The purpose of this study is to assist planner to optimize construction process, reduce collision, and improve machine efficiency.

The project is located in the southwest of China. The max dam height is 285.5m. The dam body is divided into more than 2000 storehouses. One of a construction storehouse (as shown in figure 8, the red one) is taken to simulate the process. The block located in 7# section layer 38, height 512.0~518.0m. The volume is 3069 m^3, area is about 1023m^2. The horizontal distance from surface to feeder plate is about 450m, vertical is about 120m. In initial plan, 5 cable cranes, 5 lateral unloading cars, 2 scrapers and 2 vibrators is assigned.

After deduction of scene simulation, the total pouring time is 26.2h. The operation parameters of every cable crane is counted and listed in Table 4. The times of each kind of collision is counted, as listed in Table 5.

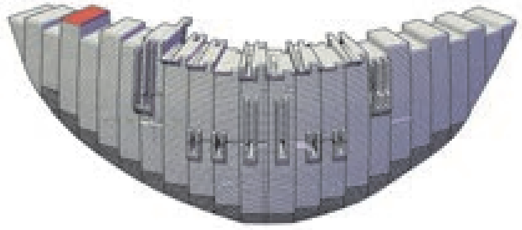

Figure 9. The simulated storehouse

Table 4. The working time with 5 cable cranes (min)

Cable crane	Times	Volume	Working time	Total time	Efficiency
1#	18	162.0	762.08	1572	48.48%
2#	81	729.0	995.67	1572	63.33%
3#	83	747.0	959.83	1572	61.06%
4#	81	729.0	808.67	1572	51.44%
5#	78	702.0	1008.18	1572	64.13%

Table 5. The Statistics of collision

The type of Collision	Collision Records	Solution
Collision 1	45	Avoid
Collision 2	23	Avoid
Collision 3	0	Null
Collision 4	3	Avoid
Collision 5	0	Null
Collision 6	8	Avoid
Collision 7	19	Avoid

The statistic results demonstrate that collisions are mainly caused by cable crane, which also reduce the efficiency. By analysis the layout of cable crane, crane 2#~4# are located upward of block, crane 1# and 5# may effect by middle cranes. Thus, a new plan is carried out by reducing the cable crane number, and simulate again. the work time of each cable crane is listed in Table 6.

Table 6. The working time with 4 cable cranes (min)

Cable crane	Times	Volume	Working time	Total time	Efficiency
2#	86	774.0	1079.3	1396	77.31%
3#	89	801.0	1112.9	1396	79.72%
4#	87	783.0	1044.5	1396	74.82%
5#	79	711.0	890.1	1396	63.76%

From above table it can know that the construction time has reduced to 23.23h. And the efficiency of each crane has improved. It can illustrate that the appropriate configuration of machine can improve the working efficiency and short the time. Also demonstrate DCVP can help to optimize the plan.

5. CONCLUSION

A Dam Construction Virtual Prototyping (DCVP) approach was proposed in this paper for the storehouse surface construction process modelling and simulating. The framework enables planners to rehearse and simulate construction process virtually prior to the implantation of a real project. The example illustrated the DCVP can assist planners to design a precise construction schedule and avoid any potential unproductive activities. The rapid prototyping of DCVP system can be enhanced by improving the existing process and resources optimization, constructability and safety evaluation.

ACKNOWLEDGEMENT

This research was supported by National Natural Science Foundation of China (SN: 51379109), the Open Foundation of Key Laboratory of Hydropower Engineering Construction and Management of Hubei Province (SN: 2014KSD04).

REFERENCES

Huang (2007) A virtual prototyping system for simulating construction processes. Automation in Construction, 16, 576-585.

Agrama, F. A. (2014) Multi-objective genetic optimization for scheduling a multi-storey building. Automation in Construction, 44, 119-128.

Choi, S. H. & A. M. M. Chan (2004) A virtual prototyping system for rapid product development. Computer-Aided Design, 36, 401-412.

Guo, H. L., H. Li & M. Skitmore (2010) Life-Cycle Management of Construction Projects Based on Virtual Prototyping Technology. JOURNAL OF MANAGEMENT IN ENGINEERING, 1, 41-47.

Guo, H. L., H. Li & V. Li (2013) VP-based safety management in large-scale construction projects: A conceptual framework. Automation in Construction, 34, 16-24.

Kim, H., K. Anderson, S. Lee & J. Hildreth (2013) Generating construction schedules through automatic data extraction using open BIM (building information modeling) technology. Automation in Construction, 35, 285-295.

Li, H., N. Chan, T. Huang, H. L. Guo, W. Lu & M. Skitmore (2009) Optimizing construction planning schedules by virtual prototyping enabled resource analysis. Automation in Construction, 18, 912-918.

Li, H., N. K. Y. Chan, T. Huang, M. Skitmore & J. Yang (2012) Virtual prototyping for planning bridge construction. Automation in Construction, 27, 1-10.

Li, H., T. Huang, C. W. Kong, H. L. Guo, A. Baldwin, N. Chan & J. Wong (2008) Integrating design and construction through virtual prototyping. Automation in Construction, 17, 915-922.

Sampaio, A. Z. & O. P. Martins (2014) The application of virtual reality technology in the construction of bridge: The cantilever and incremental launching methods. Automation in Construction, 37, 58-67.

Song, S., J. Yang & N. Kim (2012) Development of a BIM-based structural framework optimization and simulation system for building construction. Computers in Industry, 63, 895-912.

Yang, X. & S. Ergan (2014) Evaluation of visualization techniques for use by facility operators during monitoring tasks. Automation in Construction, 44, 103-118.

Zhang, S., J. Teizer, J. Lee, C. M. Eastman & M. Venugopal (2013) Building Information Modeling (BIM) and Safety: Automatic Safety Checking of Construction Models and Schedules. Automation in Construction, 29, 183-195.

The Application of RBF Neural Network on Optimization of temperature control Measures of Super-high arch dam Concrete Block

L. wang
China Three Gorges Corporation, Yichang, China
wang_lei11@ctgpc.com.cn

ABSTRACT:
With the advancement of water resources development strategy, China has entered into the stage of super-high arch dam construction. The higher strength requirements of extra-super-high arch dam make the requirements of temperature control and crack prevention stricter than before. It is of great significance for temperature control and crack prevention of extra-super-high arch dam to optimize the temperature control measures in the first stage of water temperature control after pouring concrete. However, the optimization of temperature control measures is a complicated nonlinear process and it is difficult to establish optimization model. As information technology develops rapidly, artificial neural network theory shows great superiority to deal with the problem of strong coupling, serious nonlinearity relationship. Under such context, this paper puts forward a method based on radial basis function (RBF) neural network to explore the optimization of temperature control measures in the first stage of water temperature control.

Keywords: Super-high arch dam, the first stage of water temperature control, temperature control measures, RBF neural network; optimization

1. GENERAL INSTRUCTIONS

With the advancement of water resources development strategy and its transfer to the Southwest, China has entered the stage of construction of super-high arch dams. For example, both Baihetan and Wudongde, the constructing hydropower projects along the downstream reach of the Jinsha River, adopt super-high arch dams.

Super-high arch dams have higher requirements for crack control（Guoxin Zhang, Yongping Ai, Youzhi Liu, etc.(2010)）. During the practice of construction, the temperature control measures including the aggregate pre-cooling, spray water on the surface of the concrete block, the post-cooling water are generally applied to control the peak value of temperature when pouring concrete block（Bofang Zhu.(1999); Bofang Zhu and Shufang Mai.(2006); Yueming Zhu and Jianbin Zhang.(2002)）. However, because the conditions of construction site are complicated, and it is a much more complicated nonlinear process when combining the peak value of temperature when pouring concrete block and the temperature control measures（Zhongming Wang,Boyuan Yang,Yunjun Li,etc.(2006)）, it is still possible that the highest temperature of the concrete block may exceed the allowable temperature of design.

As a result, this paper applied RBF neural network which possesses arbitrary nonlinear mapping ability, established the optimization model of temperature control measures through MATLAB, and elaborated the feasibility and practicability of the RBF neural network on optimization of temperature control measures when pouring concrete block by the analysis of the constructed super-high arch dam in Xiluodu of the Jinsha River basin.

2. THE RATIONALES OF RBF NEURAL NETWORK AND MATLAB REALIZATION OF OPTIMIZATION MODEL

2. 1. RATIONALES

Radial Basis Function (“RBF”) neural network is a three-layer feedforward neural network structure which has only one hidden layer. FIg. 1 shows a RBF neural network that is an “n-h-m” structure possessing “n” inputs, “h” hidden notes and “m” outputs. $\mathbf{x}=(x_1,x_2,\dots,x_n)^T\in\mathbf{R}^n$ is network input space vector, $\mathbf{W}\in\mathbf{R}^{h\times m}$ is weight matrix between the hidden layer and the output layer, $\mathbf{b}=\left[b_0,b_1,\dots,b_m\right]^T$ is output offset vector, $\mathbf{y}=\left[y_1,y_2,\dots,y_m\right]^T$ is output vector, and $\phi_i\left(*\right)$ is kernel function of RBF neural network. c_i, a hidden note in FIg. 1, is the data center of the ith hidden note. Then, $\sum$ of notes in output layer indicates linear mapping from the hidden layer to the output layer, and $\lVert * \rVert$（Haikun Wei.(2005)）means Euclidean Norm.

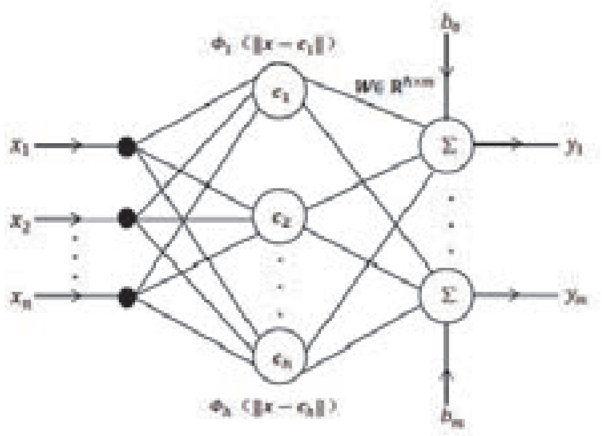

Figure 1. Structure of RBF neural network

RBF neural network treats radial basis function as kernel function. The kernel function of common use is Gaussian Function, i.e.

$$\phi_i(t)=e^{-\frac{t^2}{\delta_i^2}} \tag{1}$$

δ_i in (1) is called expansion constant or spread of such basis function. Obviously, the smaller δ_i is, the smaller the spread of radial basis function is, the more selectivity the basis function possesses.

Therefore, in FIg.1, the kth output of RBF neural network can be showed as:

$$y_k=\sum_{i=1}^{h} w_i\phi_i\left(\|\mathbf{x}-\mathbf{c}_i\|\right)+b_k \tag{2}$$

2.2. MATLAB REALIZATION OF RBF NEURAL NETWORK MODEL

In order to output precise RBF neural network, the network is required to:

i) design rational input-output pattern through the analysis of actual conditions:
ii) build training sample set and testing sample set which are consistent with actual conditions:
iii) satisfy the given requirement of output accuracy by network training of built sample set.

When RBF neural network consistent with the above requirements is built, such network is competent to make precise output according to new input data. The specific process is:

Step 1 Select appropriate input layer note and output layer note.

Step 2 Normalize data. When inputting sample, data normalization will be requisite to wipe off influence of dimension. This paper adopt mapminmax function of intro Matlab to proceed with data normalization,

[Y,ps]=mapminmax(X,YMIN,YMAX)

There into, X is a training sample needed to be normalized, Y is a training sample after being normalized under certain standardization, “ps” records mapping of such standardization, and [YMIN，YMAX] indicates the section of normalization. In this paper, such section is [0,1].

Step 3 Set up and train the network. Confirm the value of the spread of radial basis function, and call newrbe function to set up RBF neural network,

net=newrbe(P,T,spread)

There into, P is input vector, T is target vector, and spread means the expansion speed of radial basis function. The process of setting up a RBF neural network is a training process, and the built network is trained network as well

Step 4 Test the network. Call sim function to test the network, and then compare the output results after reverse normalization with actual values

Step 5 Normalize reversely the Data. Reverse normalization is necessary to forecast true values of data after normalization. This paper adopts mapminmax function of intro Matlab to proceed with reverse normalization,

X=mapminmax('reverse',Y,ps)

Step 6 Adjust the network. Through error analysis between actual output values and measured values, if huge error emerges, it will be necessary to reselect of samples, reset expansion constant, and readjust the structure of such network according to actual conditions

Step 7 Apply the network and evaluate the results（Di Lian,Yaoying Huang,Xiaohui Zheng,etc.(2014)）.

2.3. The procedures of optimizing the temperature control measures of RBF neural network

When optimizing temperature control measures in the first stage of temperature control through water, we analyze reversely the temperature control measures according to the peak value of concrete block and environmental air temperature substantially by RBF neural network model in order to pick out the most advantageous group of temperature control measures for guiding construction. The above procedure is divided into the following steps:

Step 1 Set up temperature control measures model. This paper chooses the peak value of concrete block and environmental air temperature as network input, and the pouring temperature, arrangement of water pipes, flow of cooling water, and temperature of cooling water as network output, then train the optimization model via collecting engineering data of actual measurement

Step 2 Optimize the temperature control measures. Determine ideal peak value of concrete block temperature in accordance with design requirements and engineering experience, and input into trained optimization model the peak value of concrete block temperature and data of environmental air temperature, then preliminarily acquire the respective information of pouring temperature, arrangement of water pipes, flow and temperature of cooling water.

Step 3 Set up a model forecasting the peak temperature of concrete block. Choose the pouring temperature, environmental air temperature, arrangement of water pipes, flow and temperature of cooling water, and thickness of concrete block as input variables, and choose the peak temperature of concrete block as output variable, then set up a forecast model with higher accuracy by means of engineering data of actual measurement

Step 4 Test the reliability of the optimization model. Use the data of step 2 about pouring temperature, environmental air temperature, arrangement of water pipes, and flow and temperature of cooling water as a model to input into the forecast model of step 3, and compare the calculated peak temperature with designed peak temperature of concrete block to verify the veracity of the optimization model.

3. ANALYSIS OF ENGINEERING PROJECTS

3.1. Optimization of temperature control measures

This paper recognizes the built super-high arch dam of Xiluodu along the Jinsha River basin as object of study, of which the height of dam crest is 611 meters, and the highest dam is 285.5 meters. The dam has been divided into 31 dam sections, and the temperature of concrete block has been detected in real time by means of burying distributed optical fiber in four typical dam sections.

During practice of construction, because the conditions of maintaining the concrete block differ in high temperature season and low temperature season, the samples are divided into two periods, one is the high temperature season from May to October, and the other is the low temperature season from November to April in order to assure the reliability and accuracy of optimization model （Jianbin Zhou,Yi Wang,Xiaopeng He,etc.(2013)）. This paper collects 100 groups of data samples from the high and low temperature season to make network training. Table 1 shows partial training samples:

Table 1. Training samples of high and low temperature season

T_{max} /℃	T /℃	T_0 /℃	T_1 /℃	Q L/min	r /m
High temperature season					
25.69	26.9	10.8	11	20	0.8754
25.47	27.9	10.7	10	53	0.8754
26.38	25.9	11.1	8	58	0.7148
26.85	29.8	11.7	8	48	0.8754
26.61	29.4	11.1	8	70	0.7148
26.73	32.5	11.4	8	56	0.7148
26.48	27.1	10.9	8	67	0.7148
26.64	25.9	10.6	8	58	0.7148
27.17	26.8	11.0	9	20	0.7148
25.58	26.3	11.0	9	33	0.8754
Low temperature season					
25.18	14	10.9	11	29	0.8754
25.36	14	10.6	8	17	0.8754
24.53	11.6	13.9	8	32	0.8754
25.47	12.4	10.3	8	61	0.8754
24.62	12	10.5	8	23	0.8754
24.48	9.2	10.3	9	28	0.8754
24.7	9.4	10.4	9	30	0.8754
24.64	9.6	10.5	9	20	0.8754
23.85	10	10.5	9	25	0.8754
24.47	8.3	10.5	9	30	0.8754

Note: There into, T_{max} means the peak value of temperature; T stands for environmental air temperature; T_0 means pouring temperature; T_1 means temperature of cooling water; Q stands for flow of cooling water; r is equivalent radius of cooling water pipes. Then, the arrangement of water pipes has been normalized, and treated equivalently according to the principle of equal areas. The calculating formula of equivalent radius is $r=\sqrt{1.07L_1L_2/\pi}=0.5836\sqrt{L_1L_2}$, and L_1 is horizontal spacing, L_2 is vertical spacing.

Through analysis of the samples in Table 1, it is obvious that the peak value of concrete block temperature fluctuates from 25 ℃ to 29 ℃ in high temperature season, and fluctuates from 24 ℃ to 26 ℃ in low temperature season. Since the object in the first stage of controlling temperature by cooling of Xiluodu is to make the peak value of concrete block temperature lower than 27℃, 26℃, 26.5℃and 27℃ are input as model in high temperature season, then the environmental air temperature chooses 27℃, the average of measured data; 25 ℃ 、 25.5 ℃ 、 26 ℃ are input as model in low temperature season, then the environmental air temperature chooses 13℃, the average of measured data. Table 2 and 3 show the combination of temperature control measures in high and low temperature season:.

Table 2. The combination of temperature control measures in high temperature season

Input		Output			
T_{max} /℃	T /℃	T_0 /℃	T_1 /℃	Q L/min	r /m
26	27	10.55	8	33	0.8754
26.5	27	11.1	8	45	0.7148
27	27	11.3	9	29	0.8754

Table 3. The combination of temperature control measures in low temperature season

Input		Output			
T_{max} /℃	T /℃	T_0 /℃	T_1 /℃	Q L/min	r /m
25	13	9.6	14	20	0.8754
25.5	13	11.1	13	30	0.8754
26	13	12.2	12	43	0.8754

3.2. The Reliability Test of Combination of Optimized Temperature Control Measures

The author chooses the pouring temperature, environmental air temperature, arrangement of water pipes, flow and temperature of cooling water, and thickness of concrete block as input variables, and selects the peak temperature of concrete block as output variable to build a model forecasting the peak values of temperature according to collected engineering data of actual measurement. Table 4 shows partial samples:

Table 4. Training samples of high and low temperature season

	T_0 /℃	T /℃	T_1 /℃	Q L/min	r/m	d /m	T_{max} /℃
High temperature season	11.5	25.4	8	33	0.8754	3	25.38
	12.2	29.6	8	28	0.7148	3	25.85
	11.7	23.07	8	27	0.7148	3	26.87
	12.0	26.4	8	30	0.8754	3	27.69
	11.3	22.9	8	33	0.7148	3	23.47
	11.9	22.9	8	28	0.7148	3	22.21
	11.7	28.2	8	30	0.7148	3	24.11
	11.5	28.9	8	28	0.7148	3	25.67
	11.8	29.8	8	30	0.7148	3	27.51
	11.7	24	8	30	0.7148	3	26.09
	10.2	25.5	8	30	0.8754	3	26.61
	11.25	27.82	8	32	0.8754	3	27.06
	11.2	25.3	8	30	0.8754	3	25.47
	11.6	25.23	9	40	0.8754	3	26.11
	10.7	26.7	8	28	0.8754	3	23.56
Low Temperature Season	10.5	10	9	25	0.8754	3	23.85
	11.1	10.1	9	43	0.8754	3	25.96
	11.0	12.7	8	62	0.8754	3	24.24
	11.3	11.2	8	20	0.8754	3	24.16
	11.3	8.2	8	45	0.8754	3	25.21
	10.5	12	8	23	0.8754	3	22.62
	11.1	7.4	9	15	0.8754	3	24.97
	11.4	12.4	9	45	0.8754	3	30.1
	11.4	16.9	9	15	0.8754	1.5	23.76
	11.5	11.6	9	54	0.8754	3	29.61
	11.5	13.6	9	40	0.8754	3	27.52
	10.3	9.2	9	28	0.8754	3	24.48
	11.4	12.3	8	65	0.8754	3	26.52
	10.4	9.4	9	30	0.8754	1.5	24.7
	10.5	9.6	9	20	0.8754	3	24.64

Note: There into, the arrangement of water pipes has been normalized, and treated equivalently according to the principle of equal areas. The calculating formula of equivalent radius is $r = \sqrt{1.07 L_1 L_2 / \pi} = 0.5836\sqrt{L_1 L_2}$, and L_1 is horizontal spacing, L_2 is vertical spacing.

Then we train the RBF neural network by making use of samples in high and low temperature season and test samples to proceed with simulation prediction. FIg.2 and FIg.3 show the analysis of absolute error of prediction:

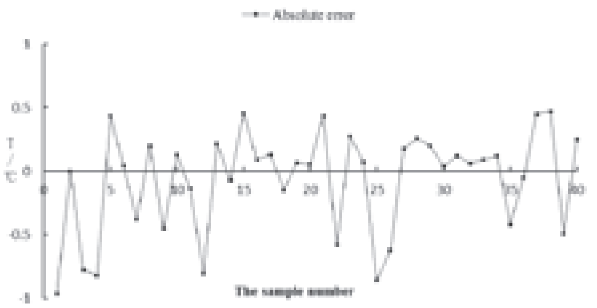

Figure 2. Prediction of high temperature season

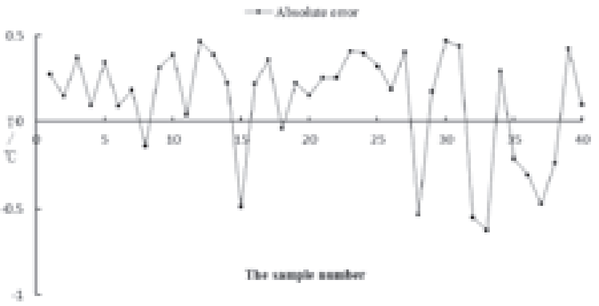

Figure 3. Prediction of low temperature season

There into, the biggest error approximates 0.96℃ in prediction of high temperature season, and 0.62℃ in prediction of low temperature season. That indicates the accuracy of built prediction model of peak temperature is high and it can be used to test the reliability of optimization model.

The author selects the combination of temperature control measures in FIg.2 to be tested, and chooses reasonable data of pouring temperature, temperature and flow of cooling water and arrangement of water pipes to be input in the forecast model for calculation, then compare the peak temperature in concrete block with the input value, the result is indicated in Table 5:

Table 5. The test of combination of temperature control measures

Input		Output				Consequence	
T_{max} /℃	T /℃	T_0 /℃	T_1 /℃	Q L/min	r /m	T'_{max} /℃	T' /℃
26	27	10.55	8	33	0.8754	26.12	0.12
26.5	27	11.1	8	45	0.7148	26.59	0.09
27	27	11.3	9	29	0.8754	26.89	-0.11

Note: There into, T'_{max} means the forecasting peak value of temperature, and T' means the absolute error of temperature.

It can be inferred from Table 5 that the optimized combination of temperature control measures of built RBF neural network performs better for controlling the peak temperature of concrete block and possesses higher accuracy. Therefore, such combination can be adopted as preliminary optimized temperature control measures.

4. SUMMARY AND PROSPECT

This paper combines the optimization model of temperature control measures with the forecast model of peak temperature based on the RBF neural network, and conducts associated optimization of temperature control measures under multiple factors. Using Xiluodu as a practical example, the results indicates that the above method is convenient in operation and highly accurate in calculation, and can provide guidance for controlling temperature of on-site super-high arch dams. If much more factors can be taken account into the process of setting up an optimization model, such as cement hydration thermal, febricity of concrete block, etc., and the associated optimization of temperature control measures under multiple factors can be conducted in the whole process of water cooling, and even the whole construction period of a dam, the application value of such model will be further improved.

REFERENCES

Guoxin Zhang, Yongping Ai, Youzhi Liu, etc.(2010): Discussion on temperature control and crack prevention for super-high dams, Journal of hydroelectric engineering,29:5,pp.125-131.

Bofang Zhu.(1999): Mass Concrete Temperature Stress and Temperature Control, China Electric Power Press.

Bofang Zhu and Shufang Mai.(2006):Permanent compound plate of thermal and water insulation for concrete dams, Water Resources and Hydropower Engineering,37:4,pp.13-18.

Yueming Zhu and Jianbin Zhang.(2002):Study on appliction of water cooling pipe measures to RCCDs' thermal control during continuous construction in high-temperature seasons, Journal of hydroelectric engineering,N0.11,pp.55-59.

Zhongming Wang,Boyuan Yang,Yunjun Li,etc.(2006):Forecast and control of temperature of massive concrete based on an improved BP model,Journal of Hefei University of Technology,29:3,pp.330-333.

Haikun Wei.(2005): The theory and method of neural network structure design, Beijing national defence industry press.

Di Lian,Yaoying Huang,Xiaohui Zheng,etc.(2014):Research on Optimization of First Stage Cooling Measures of Concrete Casting Warehouse, China Rural Water and Hydropower,No.11,pp.90-97.

Jianbin Zhou,Yi Wang,Xiaopeng He,etc.(2013):Rapid Prediction of the Highest Temperature of Concrete Block,Water Power,39:12,pp.46-48.

Georadar Application for Dam Safety Study (Case Study of Sutami Dam)

M. T. B. Raharjo, K. Windianita, F. Hidayat, R. V. Ruritan & Harianto
Jasa Tirta I Public Corporation, Malang, Indonesia
megateguh89@gmail.com

H.E. Setiawan, M. Ibrahim, N. Sadikin & D. Indrawan
Research and Development Center of Water Resources - The Ministry of Public Works and Housing, Bandung, Indonesia

ABSTRACT:
Sutami dam, a rockfill dam with core, is located in the Brantas River, East Java, Indonesia. Sutami dam construction was conducted from 1961 to 1972. As an effect of water pressure during reservoir operation, dam will continue to deform. It is very important to understand dam deformation behavior in order to ensure that the deformation does not affect to the dam safety. Sutami dam is an aged dam, having a high level of risk. In 2014 it revealed longitudinal cracks on its crest with a width varying between 0.3 to 0.5 cm. To understand the causes and mechanisms of cracking, we conducted a study of cracks and deformation behavior of Sutami dam body by using Ground Penetrating Radar (GPR) or georadar for further treatment of the cracks. Based on the interpretation of georadar investigation results, it revealed that longitudinal cracks that occur at Sutami dam crest are approximately 120 m length with depth of 1.5 to 2.0 m from the surface.

Keywords: Cracks, dam, deformation, georadar

1. INTRODUCTION

1.1. Background

Sutami dam is a rockfill dam with core, located in the Brantas River, in East Java, Indonesia. Sutami dam construction conducted from 1961 to 1972. As an effect of water pressure during reservoir operation, dam will continue to deform. The deformation behavior is very important to know in order to ensure that the deformation which occurs does not affect to the dam safety. Sutami dam is an aged dam, having a high level of risk with a longitudinal cracks occur in the crest dam in 2014 (Fig. 1). So it is necessary to study the crack and deformation behavior of the dam body. It is needed to avoid further damage and provide appropriate treatment.

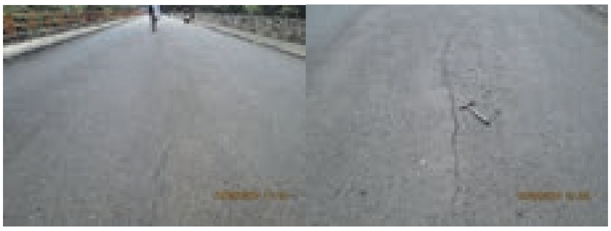

Figure 1. The longitudinal cracks on the dam crest with 0.3 to 0.5 cm width

One method to study cracks in dam that are not destructive is by using Ground Penetrating Radar (GPR) or georadar. Georadar is a geophysical method that was developed as a tool to study the geological of shallow subsurface in detail. The principle use in this method is not much different from the seismic reflection method.

1.2. Problem Identification

Identification of the problems encountered in this study are:
a. Longitudinal cracks occured in the dam crest of Sutami dam.
b. The pattern and depth of the cracks that occurred is unknown.
c. The effect of cracks to dam safetyin Sutami dam is unknown.

1.3. Purpose

The purpose of this study are:
a. Studying the pattern of cracks on the dam crest in Sutami dam, causes and treatment suggestions.
b. Determining the influence of cracks to the dam safety of Sutami dam.

2. METHOD

Ground Penetrating Radar (GPR) is a geophysical method that uses radar pulses to image the subsurface. This nondestructive method uses electromagnetic radiation in the microwave band (UHF/VHF frequencies) of the radio spectrum, and detects the reflected signals from subsurface structures. GPR can have applications in a variety of media, including rock, soil, fresh water, structures, etc. We can use GPR to detect subsurface objects, changes in material properties, and voids and cracks (Daniels, 2004).

GPR uses high-frequency (usually polarized) radio waves, usually in the range 10 MHz to 1 GHz. A GPR transmitter emits electromagnetic energy into the ground. When the energy encounters a buried object or a boundary between materials having different permittivities, it may be reflected or refracted or scattered back to the surface. A receiving antenna can then record the variations in the return signal. The principles involved are similar to seismology, except GPR methods implement electromagnetic energy rather than acoustic energy, and energy may be reflected at boundaries where subsurface electrical properties change rather than subsurface mechanical properties as is the case with seismic energy. How the tool works can be seen in Fig. 2.

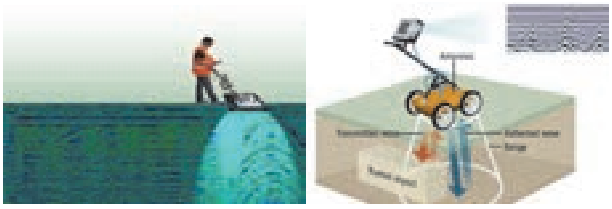

Figure 2. The working of georadar
(source:http://monteprama.blogspot.co.id)

Equipments such as "Subsurface Interface Radar" consists of georadar unit GSSI Inc. SIR System (USA), an antenna 100 MHz or other frequency selection (there are 6 types of frequency). The way to move the antenna on the surface soil can be done by manually drawn on a path which is relatively short and for relatively long path or we can use wheeled vehicle when path trajectory possible. Each path will be measured (scanned), using 100 MHz antenna with measuring capabilities up to a depth of 30 m and a 270 MHz antenna with measuring capabilities up to a depth of 15 m.

Stages of implementation activities of georadar measurement at Sutami dam are as follows:

a. Georadar measurement will be conducted by dividing the work area into two kinds of path include transverse and longitudinal path consisting of 4 longitudinal path and 58 transverse path. Sketch of the track can be seen in Fig. 3
b. Determination of the distance between the points will be reviewed at each path. On the longitudinal path measurement taken, there was one meter distances between points from a start point. In the transverse path measurement, there was two meters distances between points. After the location of the points that will be measured at each path is obtained, the points are marked in order to facilitate the measurements.
c. After the above steps are determined, the next step is georadar installation. GPR antenna used is 270 MHz.
d. Implementation of georadar measurement in crest dam (Fig. 4).

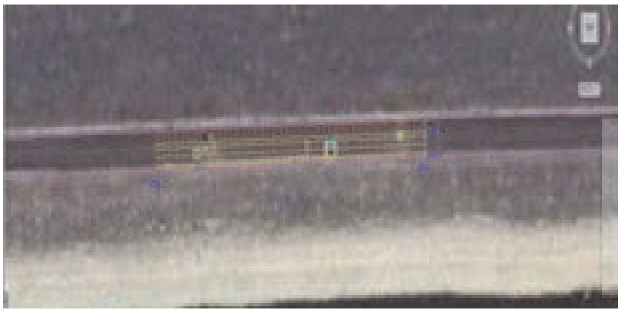

Figure 3. Location map of georadar measurement path in Sutami dam

Figure 4. Implementation of georadar measurement in Sutami dam

3. RESULT AND DISCUSION

3.1. Georadar Intepretation of Longitudinal Path

Longitudinal path of georadar measurement in Sutami dam consists of D1-D5-D5', D2-D6-D6', D7-D7-D3' and D4-D8-D8'. The illustrated diagrams of the georadar measurement result described the land subsidence in subsurface in some area and also some of weak zone that indicated by black areas. Georadar measurement results on the longitudinal path D1-D5-D5' and D2-D6-D6', respectively as shown in Fig. 5 below.

a. D1-D5, D5-D5' Path
   D1-D5 path has a length of 42.5 m from ground zero (0), measurements were carried out along the path close to the upstream. Results radargram dividing the two (2) part of the embankment dam and a core zone at a depth of about 1.8 m. On the horizontal distance from 0 to 22.5 m and 42.5 m visible embankment dam has a relatively higher density than the core zone (bright parts). Light colored section looks do not have

continuity of, this was expected because the area is a mixture of rock and soil material. Georadar can be detected up to a depth of 3.5 m, where from 2 m to the bottom, it looks more homogeneous densities. Paths D1-D5 showed area decreased (arrow dashed white line) at a distance of 20 m up to 22.5 m of point 0 at a depth of 1 m upstream, a weak zone (dashed white circle) was also detected in a distance of 30 m up to 32.5 m.

D5-D5' path at a distance of about 72.5 m shows some weak zone (dark part), at a distance of 12.5 m to 17.5 m to ranging from 63 m from the point D5. The decline seen at a distance of 37.5 to 40 m with a depth of 0.5 m and at a distance of 68.5 m to 71.5 m with a depth of 0.5 m upstream. The core area has a relative continuity of temperature and density were almost same.

b. D2-D6, D6-D6' Path

D2-D6 path with a length of approximately 42.5 m from ground zero (0), the measurement is done along the paths to the 2nd from the upstream, or 2 m of path D1-D5-D5 'in the downstream direction. Results radargram dividing the two (2) part of the embankment dam and a core zone at a depth of about 2 m. Results radargram depict multiple densities below the surface, extending from point 0 to 25m has a higher density than the surrounding areas (light colors). Georadar can be detected up to a depth of 3.5 m, 2 m with densities down to look more homogenous.

D6-D6' path with a length of approximately 72.5 m showed a weak zone (dark part), at a distance of 66 m from the point D6. Decrease (arrows dashed white line) is seen at a distance of 20 m to 35 m, with a depth of 0.5 m. The core area has a relative continuity of temperature and density were almost same.

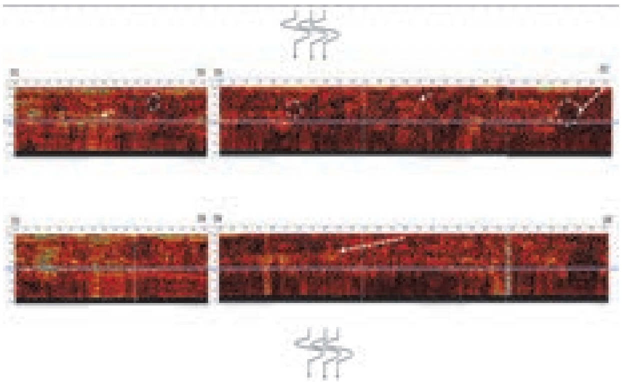

Figure 5. Longitudinal path measurement result (D1-D5-D5' and D2-D6-D6')

3.2. Georadar Intepretation of Transverse Path

Transverse path of georadar measurement result consists of E1 up to E58. The illustrated diagrams of the georadar measurement result described the land subsidence in subsurface in some area and also some of weak zone that indicated by black areas. Interpretation of Georadar measurement results on the longitudinal path E7 and E9 respectively as shown in Fig. 6 below:

a. E7 Path

Radargram on E7 shows the core zone and the embankment dam, apart at a depth of about 1.8 m. In the area of the embankment dam, radargram discontinuities showed many layers and multiple layers have a higher density (bright color) and there are also low density (dark red). While in the core zone, the dominance of the lining is still constantly. Indicated the existence of the fault line (dashed arrow lines in blue) at a distance of about 3 m from the point 0 to the upstream direction, from the surface to a depth of 1.5 m. Radargram in the core area still shows the dominance of continuous layers.

b. E9 Path

Radargram on path E9 shows the core zone and the embankment dam, apart at a depth of about 1.8 m. In the area of the embankment dam, radargram discontinuities showed many layers and multiple layers have a higher density (bright color) and there are also low density (dark red). Indicated the existence of a weak zone (dotted white circle) at a distance of 4.5-5 m at a depth of 0.6-1.8 m. Radargram in the core area still shows the dominance of continuous layers.

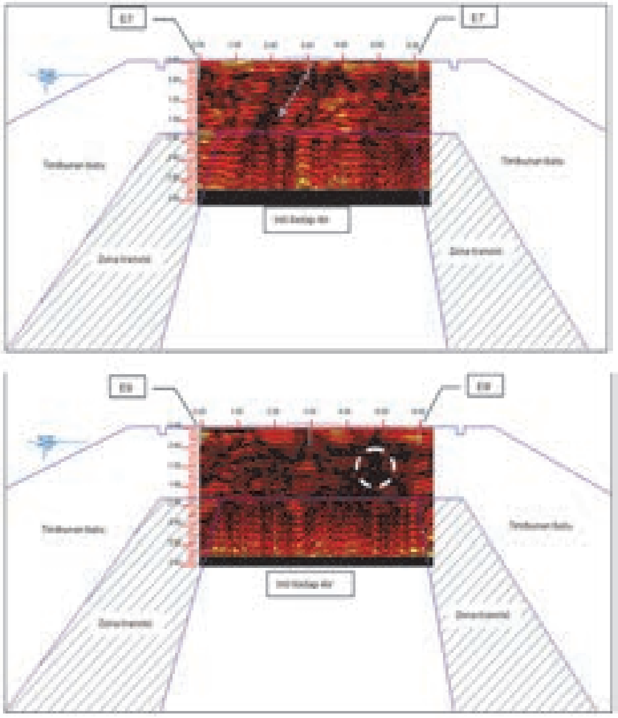

Figure 6. Transverse path measurement result (E7 and E9)

3.3. Deformation Behavior

Crest Settlement point at Sutami Dam is located in the middle section of the road (Fig. 7), initial reading of crest settlement point is unknown. In 1996 conducted measurement at existing settlement point in order to obtain an elevation used as a a datum for comparison with furthermore measurements. From Fig. 8 known that the maximum deformation that occurred at the Sutami crest dam is 0.044 m or 44 mm. On the upstream slope in cracks area a decline in rip-rap are not indicated, it is also on the downstream slope which is above the water surface. but at the crest area of the dam nearby the crack there a difference deformation between downstream and upstream area.

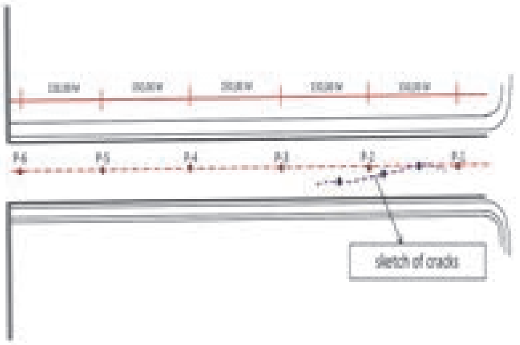

Figure 7. Location of crest settlement point at Sutami dam

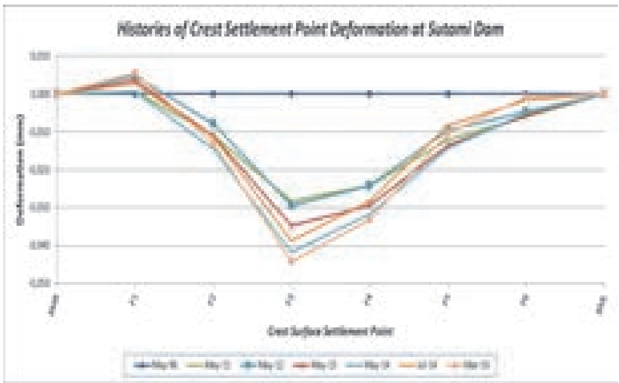

Figure 8. Deformation of crest Sutami dam

4. CONCLUSION

Based on the interpretation of georadar investigations in Sutami dam, we can conclude that:

a. The top layer subsidence and weak zone in dam crest subsurface that identified by georadar suspected to be the cause of cracks.
b. Longitudinal cracks that occur at crest of Sutami dam is approximately 120 m width with a depth of 1.5 to 2.0 m from the surface.
c. Crack patterns in crest of Sutami dam are different subsidence between upstream side and downstream side. The downstream subsidence is bigger than the uspstream. This is probably due to the reservoir operation as supported by dinamics analysis result.
d. Georadar measurement result cannot be used independently because it must be supported by dam safety instrumentation analysis and evaluation such as dial gauge, surface settlement point, etc. The opinion of the dam experts who conducted visual inspection at the dam is also needed.

REFERENCES

Daniels DJ (ed.) (2004): Ground Penetrating Radar (2nd ed.). Knoval (Institution of Engineering and Technology). pp. 1–4.

Jasa Tirta I, Perum & Puslitbang SDA (2014): Laporan Akhir: Studi Retakan Pada Puncak Bendungan Dengan Alat Georadar Dan Studi Respon Dinamik Akibat Gempa Bendungan Sutami, Jawa Timur.

Jasa Tirta I, Perum (2014): Laporan Analisis dan Evaluasi Keamanan Tubuh Bendungan Di Wilayah Kerja Perum Jasa Tirta I Triwulan III 2014.

Application Of Fuse gates As An Innovative Spillway Control System For Sarough (Al Ghadir) Reservoir Dam In West Reservoir Dam In West Azarbayjan Province Of Iran

M. Ashrafi & B. Dasi
Planning and development deputy manager of West Azerbaijan Regional Water Authority,orumieh,Iran
ashrafi1353@yahoo.com

M. Ashrafi
University of Shahid bahonar, Kerman, Iran

B. Dasi
University of Tehran, Tehran, Iran

ABSTRACT:
Ab VaTosseaPaydar has been the first company who has implemented the Fuse gate System for Sarough Reservoir in the West Azerbaijan Province in Iran. Developed and marketed by Hydroplus, France, the Fuse gates are a cost effective means of providing increased reservoir storage capacity and spillway discharge potential for spillway. Through this application, the reservoir capacity is increased by 40 mcm, which corresponds to 30%.Fusegates are free-standing units installed side-by-side on a spillway sill to form a watertight barrier. During extreme flood events, the Fuse gates are designed to tip over and discharge the flows incrementally, thus preventing the dam to be overtopped.

Keywords: Fuse gate System, flood control, storage capacity, discharge coefficient, spillway

1. INTRODUCTION

Sarough dam (Al Ghadir dam) is located on the Sarough River in the West Azerbaijan Province, 17.5 km north of Takab City. Completed in 2012, it is used for irrigation and water supply. The dam is composed of a rock & earth fill embankment having a central clay core with a maximum height of 67.5 m above the bed rock. Its crest length is 418 m and impounds a reservoir storage volume of 40 mcm.A total of six labyrinth crested Fusegates (Narrow Moderate Head type), each 3,50m high and 3,50m wide have been accommodated on the 26m wide broad crested weir at the Sarough dam spillway. The weir is divided in 3 spans by two 2,50m wide piers. The Fusegates will form a watertight barrier raising the permanent pool up to the level of their overspilling crest at El.1841,30m. Fusegates have been selected as a spillway control system because of the particular hydrology of the site. Indeed, this duration is not sufficient to face mechanical faults, power loss or disoperation of classic mechanical gates.TheFusegates were invented in 1989 by hydroplus company as a safe and robust non-mechanical spillway control system.

Ab VaTosseaPaydar has been the first company to implement the Fusegate System in Iran, which is a patented technology developed by Hydroplus of France.Fusegated spillways have been constructed on a number of dams throughout the world, and physical model studies have been conducted in laboratories in many countries.

2.THE FUSEGATE SYSTEM AT SAROUGH DAM

2.1.Concept

The Fusegate System is an innovative and cost effective non-mechanical spillway control system providing increased reservoir storage and spillway discharge capacity. As of today, Fusegate System has been installed in more than 70 dams in 27 different countries around the world.

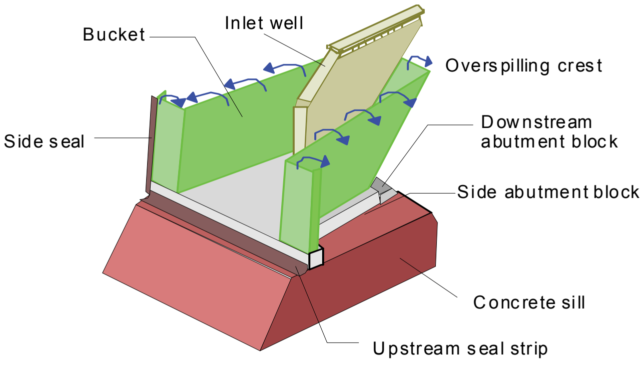

Figure 1. Typical 3D view of a labyrinth Fusegate

2.2. Features of the Fusegate System

The Fusegate System is based on the following concept: Fusegates are free-standing units installed side-by-side on a spillway sill to form a watertight barrier.

They bear against small abutment blocks set in the sill to prevent them from sliding before they are required to rotate (under extreme flood conditions).

There is a chamber in the base of each Fusegate, with drain holes to discharge incidental inflows (due to leaking seals for example).

An inlet well on the upstream side of the Fusegate crest discharges water into the chamber when the headwater reaches a predetermined level. (Well lips on individual Fusegates are actually set at different levels).

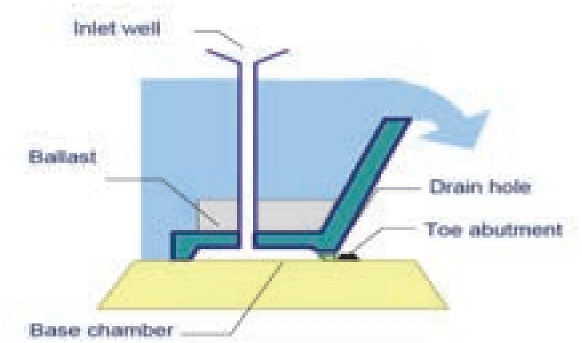

Figure 2. View of a labyrinth Fusegate (normal)

During very large floods, water entering the chamber over the inlet well causes an uplift pressure to develop in the chamber.

The uplift pressure, combined with the hydrostatic pressure (acting from left to right on the diagram below) is sufficient to overcome the restraining forces and the imbalance causes rotation of the unit off the spillway. The Fusegate is then washed away clear of the spillway by the flood.

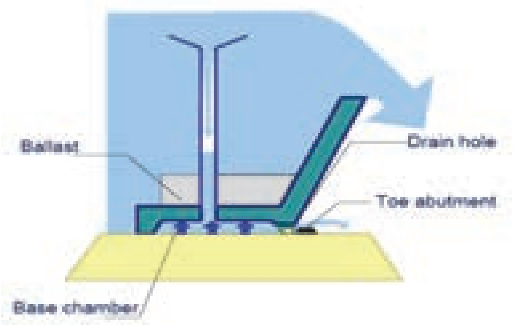

Figure 3. View of a labyrinth Fusegate (large floods l)

If the water level continues to rise after the first breach, more Fusegates can rotate, all according to pre-determined upstream water levels until eventually there are no more units remaining and the spillway is free to pass the original maximum design flood. Until rotation of the first Fusegate, (for floods of extremely low risk of occurrence), the user has the benefit of the additional storage.

Each Fusegate has a different overturning level, precisely determined by the height of the water inlet and its own unique stability.

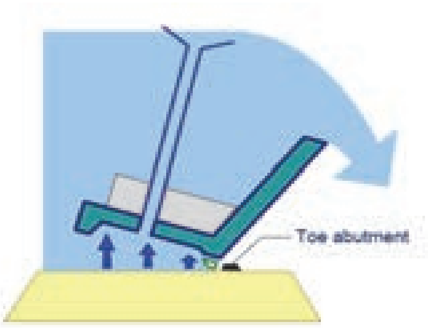

Figure 4.view of a labyrinth Fusegate (overturning)

2.3. Types of Fusegates

2.3.1. Labyrinth-crested Fusegates
Labyrinth-crested Fusegates are made of steel or concrete depending on the size and economy. The Fusegates' height can vary from 1 to 6.5 metres, depending on the spillway layout and hydrology at the dam. This type of Fusegate is selected when the head of water above the overspilling crest of the Fusegate corresponds to a height ranging from 40% to 80% of the Fusegate's height.

2.3.2. Straight-crested Fusegates
These Fusegates are streamlined in order to achieve an optimum discharge coefficient. Concrete Fusegates can be cast-in-place or pre-cast depending on the size. Straight-crested Fusegates can discharge a water head equivalent to 3 times of their height. The well shaft is can be made in steel or concrete.

3. STABILITYCRITERIAANDANALYSID

3.1. Stability analysis

Although the principles discussed here apply to all Fusegate types, the following discussion will be confined to labyrinth-crested Fusegates (see next figure) and will deal with stability against overturning and sliding.Stability against sliding is ensured simply by the downstream toe abutments built into the spillway sill. They are designed to withstand the horizontal loads from the Fusegates.Analysis of Fusegate stability against overturning involves determining the moments on the abutments from all the forces acting on the Fusegate.

The overturning moment involves the following forces:

- hydrostatic pressure from the reservoir water, acting on the upstream side of the Fusegate

- uplift pressure in the chamber and under the Fusegate base (when water spills into the inlet well, the uplift pressure rises rapidly and causes the Fusegate to overturn).

The stabilizing moment involves:

- the dead weight of the Fusegate.

- the weight of concrete ballasts (if any).

- the weight of the water on the bucket floor (applying a downward pressure on the Fusegate).

- back-pressure from tailwater against the downstream face of the Fusegate.

A detailed analysis of the stability is given hereafter.To simplify the following equations, the hydrostatic pressure on the inlet wells is not taken into account.

With the reservoir level above Fusegate base designated by h:

If h ≤H, resultant of upstream pressure :

$$F_{us} = 1/2\ \rho w\ g\ W\ h^2 \tag{1}$$

Moment of upstream pressure:

$$Mus = 1/6\ \rho w\ g\ W\ h3 \tag{2}$$

Where:

H = Fusegate height,

W = Fusegate width,

ρw = density of water,

g = acceleration caused by gravity.

If h > H,

$$Fus = 1/2\ \rho w\ g\ W\ H2 + \rho w\ g\ W\ H\ (h - H) = 1/2\ \rho w\ g\ W\ H\ (2h - H) \tag{3}$$

$$Mus = 1/6\ \rho w\ g\ W\ H3 + 1/2\ \rho w\ g\ W\ H2(h - H) = 1/6\ \rho w\ g\ W\ H2\ (3h - 2H) \tag{4}$$

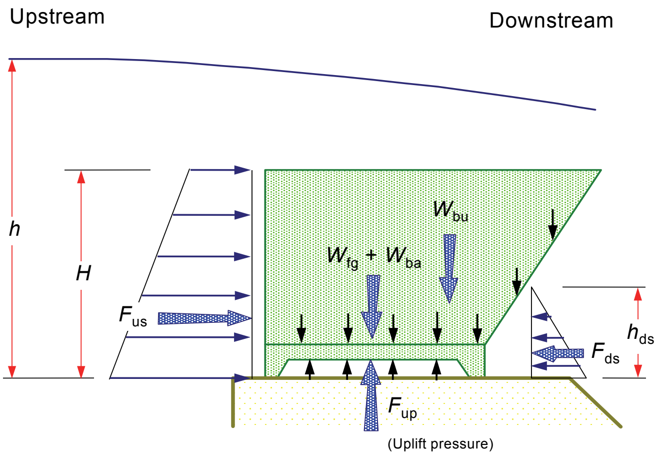

Figure 5 .Ballasted Fusegate height

Where,

Empty Fusegate weight: W_{fg}

Moment of empty Fusegate weight: $M_{fg} = W_{fg} .Y_{fg}$

Ballast weight: W_{ba}

Moment of ballast weight: $M_{ba} = W_{ba} .Y_{ba}$

Where Y_{fg} and Y_{ba} are the horizontal distances of the centers of gravity of the Fusegate and ballast from the abutments respectively.

Uplift pressure in the chamber and under the base:

Knowledge of the uplift pressure distribution in the chamber and below the Fusegate base in normal and critical conditions is essential for a proper understanding of the Fusegate stability. The provision of an inlet well admitting water into the chamber at a precise headwater level means that the Fusegate will have an ample stability margin until the chamber fills, and after that it will rotate reliably when the design headwater level is reached.

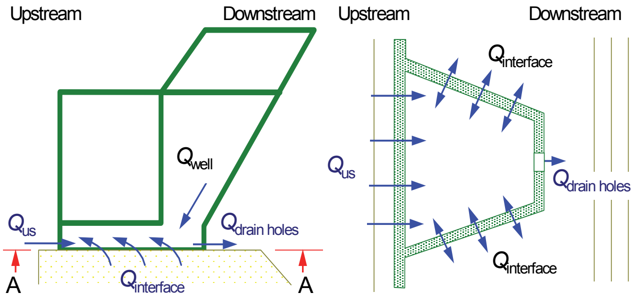

Figure 6 .Input and output of the Fusegates

4.PARAMETERS OF THE SAROUG SPILLWAY SILL

The Sarough spillway sill will consist of a broad crested weir, total 26 m long, divided into 3 spans of 7m long each by 2 piers of 2,5m width (i.e. 26m=3x7m+2,5mX2). Its crest is set at El.1837,80m, with a maximum permissible deviation of +/-2mm over its entire surface.

The installation of Fusegates requires the spillway platform to be equipped with small toe abutments at its downstream (two per Fusegate) to prevent the Fusegates from sliding.

5. GEOMETRICAL FEATURES OF THE FUSEGATE SYSTEM

The main geometrical features of Fusegates developed for Sarough dam are presented hereafter:

Fusegate type:Labyrinth crested

Fusegate number:6

Fusegate height:	3,50m
Fusegate actual width:	3,47m
Fusegate nominal width:	3,50m
Fusegated spillway length:	21,00m
Fusegatelength :	3,52m
Fusegate bottom level:	El.1837.80m
Fusegate top level :	El.1841.30m

6. TIPPING SCHEME

Tipping level is the water level to be reached in the reservoir to cause the tilting of the Fusegates. This level is taken far enough at upstream of the spillway so that the water approach speed can be considered negligible. The tipping level of each Fusegate is as indicated here after:

Table 1. Tipping sequences and tipping levels

Tipping sequence	Fusegates involved	Tipping level (m)	Tipping level compared to the Fusegate crest (m)	Tipping level compared to the spillway sill crest (m)
1	F1	1843.30	2.00	5.50
2	F2	1843.34	2.04	5.54
3	F3	1843.38	2.08	5.58
4	F4	1843.41	2.11	5.61
5	F5	1843.44	2.14	5.64
6	F6	1843.46	2.16	5.66

It will be noted that the difference in level between two consecutive tipping is below the usual tipping accuracy; it means that the Fusegates might not tip in the predetermined order. However, only the number of Fusegates required to tip-off to pass to corresponding flood will tip. Next figure shows the Fusegate location.

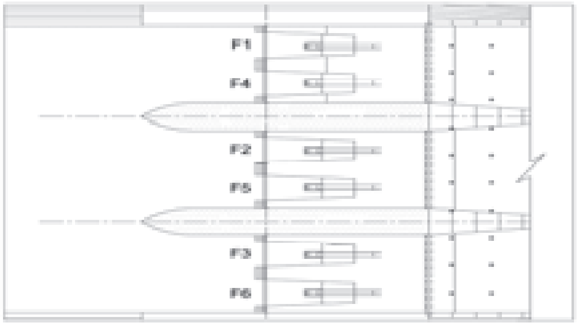

Figure 7 . Fuse gate location

7. HYDRAULIC STUDIES

7.1. Hydraulic parameters of the spillway sill

The discharge over the spillway sill (once the Fusegates have tipped) per unit length can be calculated by the following formula:

$$Q(m^3/s) = \sqrt{2\ g}\quad C_d\quad h'^{\frac{3}{2}} \qquad (5)$$

Where:

h’: upstream head above the sill (h’ = h + H).

H: Fusegate height.

h: upstream head above the Fusegate crest.

C_d is the spillway discharge coefficient, which depends on the spillway shape and on the upstream conditions. It has been assumed that the discharge coefficient C_d is equal to 0.43.

7.2.Hydraulic parameters of Fusegates

The hydraulic characteristics of the labyrinth Fusegate crest have been determined through model test carried out in reputable laboratories in Europe and in the United States. For the Sarough project a particular model of Fusegate has been developed to meet specific site conditions. The values mentioned in this report have been verified through a reduced hydraulic model test at Hydroplus's laboratory in Marolles, France, and are consistent with the values obtained from standard models.

The discharge over the labyrinth crest per unit length measured along the spillway sill can be calculated by the following formula:

If $h < 0.27$ m
If $h > 0.27$ m

$$Q(m^3/s) = \sqrt{2 \quad g} \quad \mu \quad h^{\frac{3}{2}} \tag{6}$$

Where,
h = upstream head above the Fusegate's overspilling crest

μ, A, B and k are constants which depend on physical parameters of the Fusegate and on physical conditions of the flow.

These constants have been determined through model tests carried out in reputable laboratories in Europe and in the United States.

7.3. Contraction effect due to the piers, abutments and Fusegates

The progressive overturning of Fusegates involves openings through the Fusegate barrier. Such openings will create a contraction of the flow, which can be taken into account by using, for each of the openings, a reduced length (effective length).

$$L_e = L \quad 2\left(NK_p + K_a + k_f\right) h \tag{7}$$

Where:
N: number of piers

K_p: piers contraction coefficient

K_a: abutment contraction coefficient

K_f: Fusegate contraction coefficient

At Sarough dam, the values of these coefficients are estimated as follows:

Kp: 0 (round-nosed piers)

Ka: 0 (no abutments).

Kf: 0.05 (no adjacent Fusegates).

7.4. Flood routing results of the Fusegated spillway

The flood rooting calculations are performed considering that the reservoir level is at El. 1841.30 m (i.e. Full supply level) at the beginning of the flood.

The results of the flood routing simulations are given in the following table:

Table 2. Summary results of flood routing with different periods

Designation	Inflow (m^3/s)	Outflow (m^3/s)	Water level (m)	Number of Fuse gates tipped
Maximum flood before 1st tipping	270	222	1843.30	0/6
Maximum flood before 2nd tipping	295	268	1843.34	1/6
Maximum flood before 3rd tipping	343	328	1843.38	2/6
Maximum flood before 4th tipping	384	374	1843.41	3/6
Maximum flood before 5th tipping	443	434	1843.44	4/6
Maximum flood before 6th tipping	487	478	1844.46	5/6
10 000 years flood (design flood)	614	580	1843.75	6/6

This configuration allows for a freeboard of 0.75m in the case of Design flood. The flood routing hydrograph of the design flood is given hereafter.

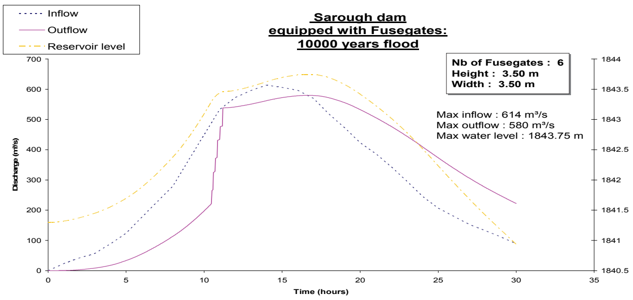

Figure 8 . The 10000-year return period flood hydrograph

8. CONCLUSION

The application of the Fusegate System at Sarough dam helps to increase the Full Supply Level by 3.50m. The 100-year flood will be passed through the spillway without any Fusegate tipping as a labyrinth-crested weir is created by Fusegates. Taking into account the short 6 hour duration of the design flood, the Fusegates System offers maximum protection against the failure of the dam thus the downstream population, since there is no room for mechanical faults, power loss or disoperation of classic mechanical gates. Although there is no possibility for any of the Fusegates not to operate as designed (unless in the case of sabotage involving blockage of inlet wells/chambers), malfunctioning of one or two Fusegates will not create a hazard for the dam as the next pair of Fusegates would tip with slightly higher tipping elevations. The Fusegates have valuable safety features inherent to the concept and not shared by other spillway control systems:

- they tip-off automatically, responding to physical forces acting upon them.
- they are entirely self-operating and do not require any source of power or human intervention to operate.
- only minimal maintenance is required compared to other mechanical gates.
- The fabrication could be done locally, and thus benefiting the local economy,
- They are very fast to fabricate and to install.

ACKNOWLEDGEMENT

We would like thank Mr. Karimi, General Director, West Azerbaijan Water Board Authority and Mr. SajadBarshandeh, Planning and Development Deputy Manager, West Azerbaijan Water Board for their support and attention to implement the Fusegate technology for the first time in Iran at Al Ghadir dam (Sarough dam), and we look forward to using this technology in future projects with all Water Board Authorities across the country.

REFERENCES

Lemperiere. F. and Bessiere. C. (1992):HYDROPLUS submersible Fusegates for surface spillways. Modification of dams to accommodate major floods.USCOLD, Fort Worth, Dallas, Texas.

Hay. N. and Taylor. G. (1970): Performance and design of labyrinth weirs. Journal of Hydraulic Div., 96(11): 2237-2357.

Falvey. H. and Treille. P. (1995):Hydraulics and design of Fusegates.Journal of Hydraulic Engineering, July 1995: 512-518.

Taylor. G.M. Mahooty. D. and Rayssiguier. J.(2001): Historic dam, modern upgrade.USSD conference, Denver July 2001

AïtAlla. A. (1996):The Role of Fuse gates in Dam Safety. Hydropower & Dams. Volume Three: Issue Six, 1996. Hasan. T. Kocahan. Russell Wyckoff. And Martin Wosnik .(2009): Spillway inadequacy remediation in US. International water power & dam construction, November 2009

Ab va tosseapaydar.co.(2010):sarugh dam detailed hydraulic studies . April 2010

Ab va tosseapaydar. Co.(2010):sarugh dam detailed stability report, April 2010

CSG(New Technology Development) ON AB-PA Delay CSG Dam Construction ON IRAN

N. Jafari & B.Dasi & A. Akbarpour
Project manager of AB-PA CSG Delay Dam from AbVaTosseapaydar Consultant Engineer,Tehran,Iran
naderjafari@ymail.com

N. Jafri
University of Sharif, Tehran, Iran

B. Dasi
University of Tehran, Tehran, Iran

ABSTRACT:
Dashtestan County with Borazjan city central, Approximately 80 Km North of Boushehr Province With long Coastline on Persian Gulf Located in East South of Iran. The Dashtestan County is the important Centre of Agricultural Development especially is the main Economy County with various Kind of Dates farms. But the DashtestanCounty during time of Rain, yearly has beendistressed by the heavy floods and catastrophic natural Disasters and had stacked the huge damages on the social disruption and even loss of people life (dead).

AbvaTosseapaydar Consultant Engineer for first time by detail field investigation along the flood catchments and with consideration all the site, geology, hydraulic, barrow area, decided, to delay the flood .Stream by CSG material dam over the last catchment of main Ardo ,catchments which is flowing the maximum flood discharge which is endangers the lives of Humans and other species on county with name of AB PA CSG delay dam.

The CSG material dam is new technology aimed, to lesser the cost, management is easy to equipped, short schedule on construction, by river bed materials even over poor foundation.

Keywords: CSG Delay Dam, Flood Control , Agriculture Development, Dates farms

1. INTRODUCTION

The purpose of this paper, is to present the investigate procedure on flood behavior of three main basin catchments characteristics of Ardo area and effects of that occurred yearly, across the Dashtestan, county especially directed huge damage over the Borazjan city and local community groups on the way of flood stream or other structures. The results of this investigation done by consultant engineer, just showed scope of floods in Ardo catchments for reduction of damages, delay and given the strategy for flood control activities and plans development in area, with local site conditions respectively, by use of detailed technical analysis and historic information for managing the flood risks and even improvement and uses of surplus water discharge in downstream area for development.

So in steps of explorations in Ardo area, we studied the physiography region faction, climate factor, Hydrologic and geological survey represented by, district and official recordeddates. And barrow area material and morphology system for optional utilization of the available for engineering requirements reliable estimates of magnitude and frequency of floods to optimizing the mitigation on the flood consequence and wealth of knowledge to protect the public and water management even in developing country which are facing with hazards shortages of water.

Finally,in accordance to resultant of achieving data, through Ardo, investigation. It has been decided to construct the three totally tabloid projects, for flood control after approval of client respectively as, consider below mentioned.

1.1.C.S.G material delay Dam.

1.2.Flood protection by construction of Homogeneous Dam.

1.3.Retention pond (circular pond).

at present regarding to approval of Bushehr water board authority, priority among the chosen three catchment area, projects, the best location path of the flood stream, On terminative out flow of catchment selected with name of AB-PA, as delay Dam with C.S.G material .

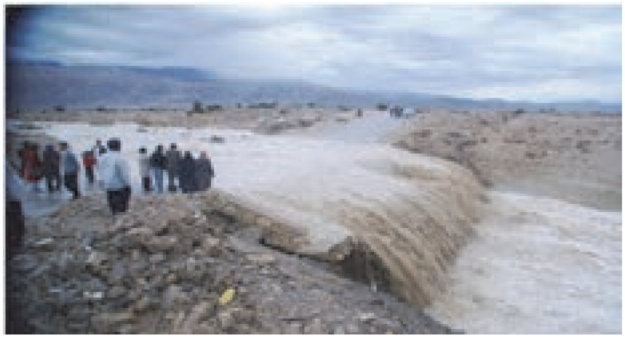

Figure 1.view of floods on Borazjan

2.WHY C.S.G MATERIAL DELAY DAM TYPE SELECTED

The field work, for AB-PA site barrow area investigation, located 20 km away from the site and comprised the 9 mechanical excavation test pits and profiling of various soil layers general divided in three sections materials with depth of about 2 m (fine clay material, sands and rock material) to identify suitable embankment materials But the final results of test pits, biases on the quality control of soil type, shows due to presence of huge amount of gypsum with liquidation particles and completely and highly weathered was the critical hazard zone on Gachsaran formation. so it has been rejected to be used.

- The other argument was the access road for material transportation is so impossible among the villages along the traffic board road
- So, by all the above mentioned reasons, for an earth embankment sufficient quantities of neither semi, or imperious and shell materials could be sourced of else who in the area.
- Therefore the only way to achieve the material for AB-PA embankment was the rock materials from the left abutment and from the unlimited alluvium material over the bed river gravel with mean depth of 1.5m with high efficiency and good quality of sand – gravel and rock around the 0-100 grading size which are easily obtained near the dam site for mixing by simple devices and Transpiration, for compaction after adding cement and water with the optimized consideration units, by JDEC instruction. And the Japanese engineering manual for design and other procedure involve with this technology, considering all shortage on AB-PA site study.
- This the important part of investigation done by consultant to have the modern technology literature of dam to be constructing with trapezoidal C.S.G material with great advantages.

Based on bellow mentioned views.

- The AB-PAC.S.G material dam, is reduce risks due to natural disasters like earthquake (No risk of seismic activity- Irreversible
- No any irreversible on social environment changes and protecting ecosystems in future.
- The AB-PA river is almost seasonally, therefore no need of any diversion system and the flood steady can over flow the body of dam within the time constriction and also, no any erosion sensitivity or damages occur due to passage of floods over the constructed body.
- The AB-PA trapezoidal C.S.G dam is constructed over the inhomogeneous, bed rock and abutment (weak rocks formation) as, we explained, above this C.S.G dam is constructed for the first time in Bushehre, on south province of IRAN with high temperature so the execution of C.S.G dam can be done in any climate conditions.
- The C.S.G material is prepare through simplified processing, from river alluvial deposition on the site is made by mixing cement, water, and easy to transport over the axis of dam, without any sorting or grading adjustment, or washing, the mixed will be placed on the foundation by use of heavy machinery (tracks bulldozer, vibration rollers) and then spreading / leveling in the designee layer, for compaction (ordered in JDEC manual test compaction)
- Additionally the most advantages considered in AB-PAC.S.G dam are
- The dam volume of material is minimized
- No any land use change
- No any environmental effects
- No any social pollution
- Short, low cost on construction and time schedule.
- Safe by over topping the flood with in construction.

3. SITESELECTION OF AB-PA C.S.G, MATERIAL DELAY DAM

- The consultant engineer for AB-PA delay dam, considered the guide lines and other stakeholders, on investigative process for site selection in accordance with professional standards included.below mentioned subtitles
- Topography and morphology study of catchment for optimizing the least of volume of fill placed of dam and sidelong structural.
- For as much as the AB-PA catchment is passing through the marl stones formation, with high erosion rate so, in this particular geology situation, due frequent flection of flood on AB-PA reservoir.

  So for avoidance of geological erosion we selected the dam foundation on Gory lime stone rock.
- The foundation and abutments of AB-PA delay dam, as the geological and geotechnical condition, showed the nature strength, thickness and permeability of bed rock are a set of after decisive factors in selection of the dam type
- No need of any major accesses road, so it reduce the cost of project

4.BASICALLY SPECIFICATION OF AB-PA C.S.G DAM

Location: the AB-PAC.S.G delay dam is located on 20km distance on east of Borazjan city, Built over the ARGHOUN river on 6km west of AB-PA village with geographic coordinates 536825E , 3224668w with the main access road of Borazjan to AB-PA village.

Purpose: the main purpose of AB-PA C.S.G delay dam used:

- To control the Arghoun river floods, for reducing or preventing the detrimental of flood waters.
- Reducing the damages property and endangers the lives of people and economic activities.
- Retain the extra water on dam reservoir as a benefit of AB-PA villager use for Agricultural development and other.
- The most important, strategy of developing of C.S.G dam, to be built over the rivers of country with all advantages in water board industry.

Table1.The Specification of AB-PA Dam (on brief)

Dam body	
Owner	Boushehr water board authority
Dam type	Trapezoidal C.S.G dam
Body material to be used	C.S.G (cemented, sand, gravel)
The max, height of dam from the river bed	23.0 m
The crest length of C.S.G dam	154.0 m
Dam crest with	6 m
Storage capacity	1.3 m.c.m
Flood control system	
Type of spill way	Open free shut spill way
Location	Over the crest of C.S.G dam
The width of spill way	15.0 m
The max discharge over the spill way	68.0 m^3/sec.
Water intake system	
Culvert(unexposed steel pipe withe)	

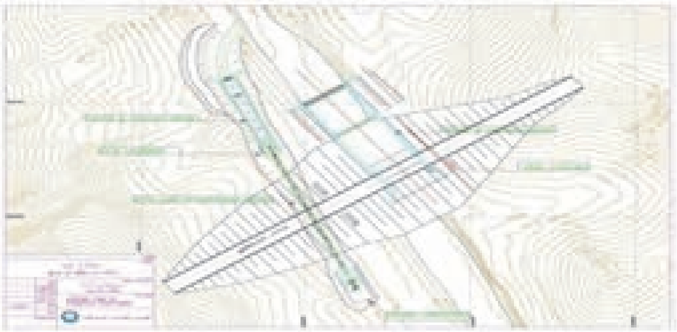

Figure 2. The AB-PA C.S.G dam location and its structures

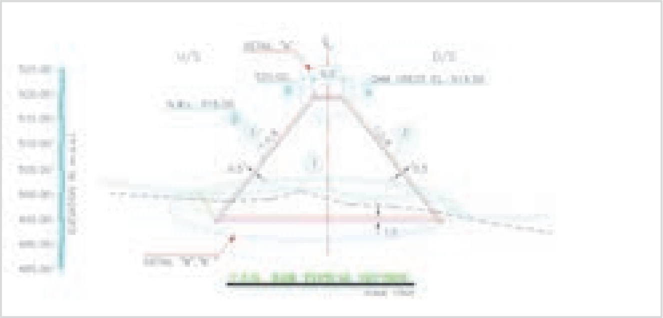

Figure 3. The cross section of C.S.G

5.GEOLOGICAL & GEOTECHNICAL INVESTIGATION OF AB-PA C.S.G DAM

These part of investigation field works of the AB-PA site, was the second field works of consultant engineer, to provide the impression of the engineering and geological aspect. Of the proposed site, for the achieving the necessary data and mapping, to evaluate whether the foundation of the dam and its structures are adequate to safely construct.

So, the field of investigation included surface and subsurface explorations had been done in accordance to the below steps.

- Geophysical explorations (site geologic maps and reports.
- Material exploration and testing reports
- Geotechnical study
- Reservoir rim conditions and land slide history (in case of storage a part of flood)
- Laboratory specimen test.

Geophysical explorations

The flood catchment of Arghoun or AB-PA C.S.G dam area is located in the margin of flooded Zagros Mountains. The main geology of axis of dam abutments and reservoir, downstream area of AB-PA C.S.G dam are made up the Mishan formation (LI), (MA), composed of goory limestone, thegrey and green marl stone units.

The axis is almost symmetric in geometry shape, but lithology point of view is inhomogeneous.

There is no sign of any fault or broken zone left abutment composed of strong goory lime LI stone and river bed and right abutment with 70 to 30 degree inclination, consist of strong goory lime stone.

It is also identified; the best material available is almost alluviums with 2-3 m thickness aggregates as a principle C.S.G material with various grain sizes.

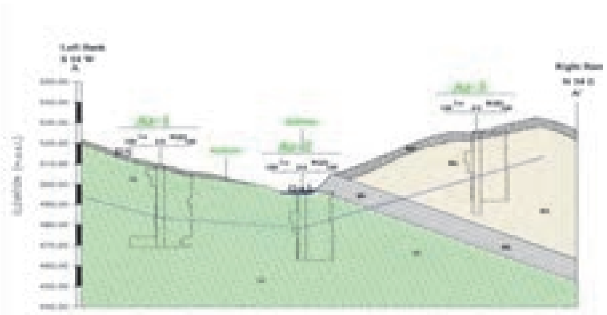

Figure 4. Geological section along axis dam

6. GEOTECHNICAL SITE INVESTIGATION

To provide a generalized set of guidelines with regard to the design and production, of C.S.G material, as a modern technology dam construction and transportation, the role of geotechnical investigation in surface and subsurface of AB-PA C.S.G dam area, was important phase of exploration on (soil and rock) with various in – situ tests, have been done.

Depending on the final design height and length of AB-PA C.S.G dam and geologic conditions in the area and complexity of embankment, foundation, water intake system direction and other structures.

The guide lines program for exploration consist of (test pits for C.S.G material use on row alluvium) drilling, coring field testing in site-laboratory physics, done in accordance to the following table list sets for the program.

Table 2. Parameter of Type of Rocks

Type of Rocks	Parameter index	Mean value
Lime stone	Dry density (gr-cm^3)	2.60
	Saturated density (gr-cm^3)	2.62
	Moisture content (%)	1
	Moisture absorption rate (%)	2
	Porosity rate (%)	3
Marlstone	Dry density (gr-cm^3)	2.46
	Softhearted density (gr-cm^3)	2.59
	Moisture content (%)	4
	(water absorption rate (%)	16
	Porosity rate (%)	13

Table 3. Geomechanical parameters of AB-PA C.S.G Dam

Type rock	C (MPA)	ϕ (degree)
Lime stone	0.6	32
Marl stone	0.25	22
Geo- parameter	Lime stone	Marl stone
Compressive string ht of rock original (mpa)	Dense (7)	Weak (2)
Mean rate RQO	Good (17)	Mean well (13)
The re space discontinuity of rook (m)	Medium to high (10-15)	Medium to low (8-10)
The joint condition	Fluted-weathered to slightly weathered (1-20)	Fluted – slightly weathered (1-20)
The ground water condition	Wet to moist (7-10)	Wet to moist 7
The discontinuity correction	Good	
The corrected Rock quality	65-70	40-45
Type of rock	Parameters	Mean value
Limestone	The in comprehensible compressible of rock original (Mpa)	45-55
	Deformation modulus (Gpa)	3.8
	Pervasion rate	0.25
Marlstone	The incomprehensible compressible of rock original (mpa)	10-15
	Deformation modulus (Gpa)	0.5
	Pervasion rate	0.3

7.DESIGN OF AB-PA C.S.G RELATED DAM

The ABPA C.S.G dam design is the most adequate trapezoidal cross sectional body shape, conformity, with the new material properties of C.S.G with aim of, lower cost and with less impact on the environment, by the help of field investigation and stability analysis, in accordance to short listed tabloid data mentioned below.

Table 4. Resistivity parameter of C.S.G material

Type of material	E (gpx)	C (mpa)	Q	f΄c (mpa)
The C.S.G material	4	0.7	30	2.5
Lime stone	4	0.6	32	-
Marl stone	0.5	0.25	22	-

Table 5. Combination of impressments

Condition	Combination of impressment	The effective loads
Empty reservoir after construction	Normal	The weight of dam body + sediment force
Floods	Unusual	The weight of dam body+ the sediment force +the water press an load the uplift waters press an
Earthquake	Unusual	The weight of dam body +the sediment load +inertial force

Table 6.the safety factors and the allowable stress required

The combinations loads	The min safety factor for sliding (stability)	The resultant forces passing the rough foundation	The allowable shear stress on foundation	The allowable tension pressure of material (c.s.g)	The allowable tensile tension of C.S.G
Normal	2	1.3 middle	≤ Allowable	0.3f`c = 750kpa	0
Unusual	1.7	1.2 middle	≤ Allowable	0.5f`c = 1.25mpa	R/3=200kpa

F`c unconfined compressive strength of C.S.G material =2.5Mpa

R =the tensile strength of C.S.G = 0.6mpa

In this relation round F`c is considered with psi unit $R=0.51(F`c)^{0.88}$

Table 7. The analysis resultant for Max section of

Loading	The s.f of sliding	The passage resultant forces through the foundation	The Max tension (kpa)	The min tension (kpa)
Empty reservoir		1.3 meddle	316	309
Earthquake		1.3 meddle	382	243

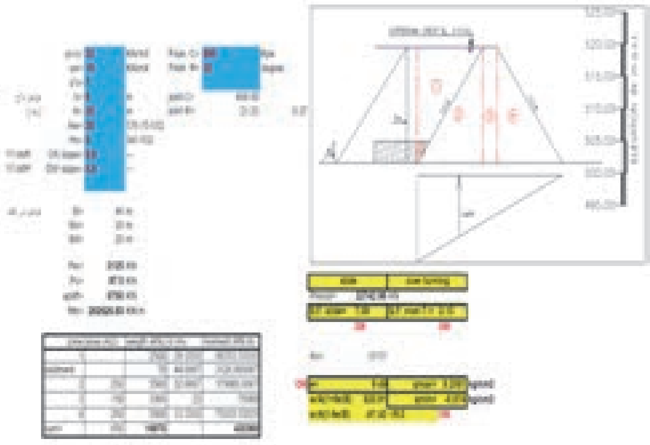

Figure 5. Sliding & overturning stability of AB-PA dam

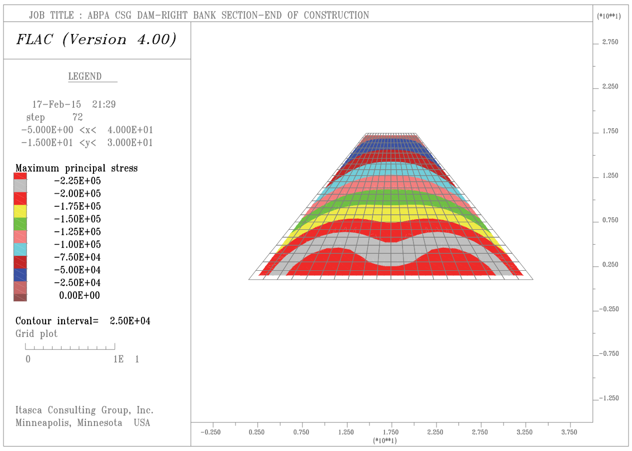

Figure 6. The min stress of the C.S.G material end of constriction

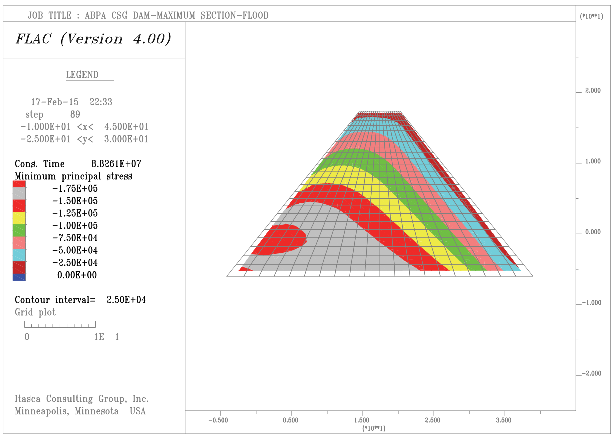

Figure 7. The max stress of the C.S.G material end of constriction

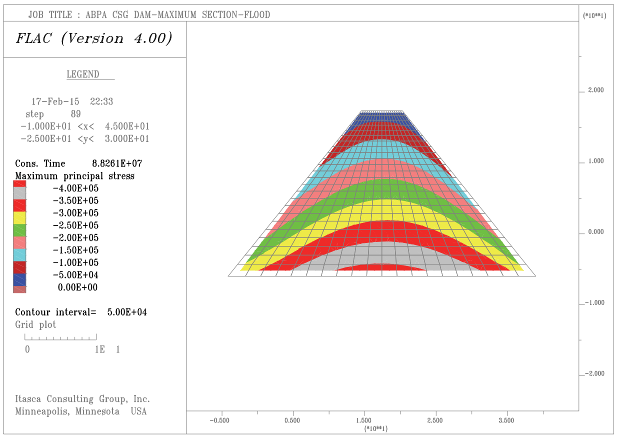

Figure 8. The max stress of the C.S.G material on flood

8. CONCLUSION

AS we know, the floods are the most common and costly widespread of all natural disasters which carry significant risks to people's lives and environment and the major cause of death and health impacts.

In this paper, beside the flood strategy explanation, there is great opportunity by guide lines and technical support of JDEC, to study the Ardo flood catchments characteristics of modern technology of the trapezoid-shaped C.S.G dam, as a delay control structure construction in IRAN for first time.

The results benefits of our investigation are summarized in the following conclusions.

1- Compared with other dams, stress generated in a dam body of a trapezoid-shaped, because of its slopes gradient, the maximum stress is decreased

2-The C.S.G dam appeared elasto–plasticity

3-The C.S.G has a safety margin, against unexpected serious earthquake, or heavy floods, because of wide range of plasticity.

4-The C.S.G dam can spill the floods overtopping the body, on construction time.

5-it can be construct over the weak foundation

6-the time C.S.G dam construction is short

7-The C.S.G dam can be developing as a large and multipurpose over any rivers with economic benefits

ACKNOWLEDGEMENT

We The AB-PA C.S.G delay dam is new technology and consumed huge amount of field works and investigation, so, we are highly indebted to Bushehr water board authority, as a employer and AB & TOSSEA PAYDAR, consultant engineer, for their support, and express our thanks and appreciation to: Mr.Ko Sakai– Jica expert in IRAN and Dr. Tatsuo Hamaguchi vice president of newjec.co.jp, for their guidance, as, well as, providing necessary information and visit of our engineers from C.S.G dam on japan.

REFERENCES

AB & TOSSEA PAYDAR consultant engineer covering final reports on:
- Geologic & geotechnical and borrow area, laboratory tests
- Design concept of foundation and the trapezoid – shaped of AP-PA C.S.G dam
- Design concept of spillway and water intake structures. (2013-2014).

Tatsuo.O.(2012):Engineering manual for design, construction and Quality control of trapezoidal C.S.G dam. JDEC.

JDEC.(2012):the engineering manual for design, construction and quality control of trapezoidal CSG Dam.

Ali. N. and Hasan. Z.(2014):the Farsi translated (eng. manual for design, construction and quality control of trapezoidal CSG Dam) .

Papers

Session (2) Extending Service Life of Dams

4th APG Symposium and 9th EADC on

INNOVATIVE TECHNOLOGIES FOR DAMS AND RESERVOIRS TOWARD THE FUTURE GENERATIONS

Extending Service Life of Dams by Improvement of Operation Regularity (IOR) (IRAN dams policy review)

S.M. Noorbakhsh
Head of Water and Wastewater Structures Operation, Ministry of Energy, Tehran, Iran
mahdi.noorbakhsh@gmail.com

ABSTRACT :
There are many factors that can be helpful for extending service life of dams. Some of them are related to design and construction phase and the others are linked to operation. Some of the actions that can extend the service life of dams after construction are: establishment of maintenance systems, employing qualified person, review and continuous improvement of technical instructions, periodic assessment of equipment performance, using new methods and operational management and also application and replacement of equipment by new technologies. All of these actions and considerations can be categorized and named as Improvement of Operation Regularity (IOR).

The most important component of an IOR program is to increase authority and administration on operation units. On the other hand, the core of extending service life of any infrastructure during operation time is the authority and mechanism to oblige operation units to follow continuous improvement programs.

Outsourcing the operation and maintenance activities and continuous evaluation and ranking of water facilities from the operation viewpoint, are the most important strategies that has been established by Iran government for IOR. Based on these two main approaches, extending the service life of dams is expected during a medium term period.

Keywords: Privatization, Outsourcing, Iran Dams, Operation Regulation, Supervision

1. INTRODUCTION

Infrastructures such as dams, bridges and power plants in some countries have been in service for several generations because of their value for public economy. Obviously, extending service life of such structures more than 100 years which often is an arbitrarily presumed service life of infrastructure is beneficial. Service life is the period of time during which the structure like dam is capable of carrying out its intended function at a satisfactory performance level with routine maintenance incorporated (Ang, A. And Tang, W. (1975)).

Service life of each structural component may vary and can be treated differently. These actions may include replacement or major repair of components or materials. So estimation and prediction of remaining service life can be helpful in timely and low-cost maintenance. Predicting remaining service life of structural components can be done in different ways such as CBM and risk-based prediction. For example risk analysis is used to predict the probabilities of the occurrence of future events as a result of taking or not taking an action.

As we move from design phase toward operation, options for extending lifespan will diminish as shown in Fig. 1. For instance approaches such as considering alternative facilities and using better material will become impossible after design and construction phase.

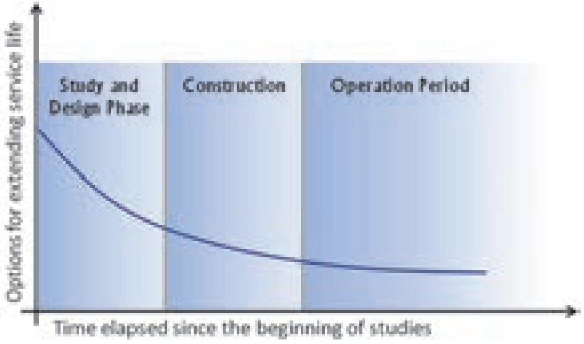
Options for extending service life
Study and Design Phase
Construction
Operation Period
Time elapsed since the beginning of studies

Figure 1. Limiting options for extending service life of dams as moving from design phase toward operation

Since most of the dams are constructed all over the world and also considerations for extending service life are usually more cost effective during operation period, it is very important to study and focus on strategies that are effective after construction.

Definition and implementation of proper regulation for O&M activities, is the key point for achieving predicted service life. Such regulation must include all essential components for sustainable servicing. These components should clearly identify who, how and with what quality should perform the required activities. Since there are different ways to mange facilities, it should seek to promote and improve existing regulation. So we named series of actions to supplement current situation and extending service life of structures as Improvement Operation Regularity or IOR for brevity.

An effective IOR program must be associated with a systematic supervision to achieve predicted service life of dams and its extension. It should be noted that using qualified and skilled manpower for implementation of operation and maintenance activities is the most important component of regulation and supervision that should be take in account during related policymaking. In the following sections two main approaches in IOR program and their components, outsourcing and supervision, will be discussed.

2. OUTSOURCING

Outsourcing is said to be helpful for firms in order to perform well in their core functions and mitigate shortage of skill or expertise in the areas where they want to outsource. Outsourcing can offer greater budget flexibility and control. Outsourcing lets organizations pay for only the services they need, when they need them. It also reduces the need to hire and train specialized staff, brings in fresh engineering expertise, and reduces capital and operating expenses (Overby, S. (2007)).

Outsourcing operation and maintenance activities can be done in different ways, but all outsourcing models should include some basic components. First of all, there should be a process to identify and approve qualification of service provider companies. In the second step all the requested services during contract time, must be clearly defined. In order to facilitate the preparation of outsourcing contracts and determining amount of it, a reference price list for operation and maintenance activities can be very helpful (Olive, B. (2004)).

The third basic component of outsourcing model is a system for evaluation of contractor (service provider) services. The result of this action can help to encourage diligent contractor or restricting unfit one based on predefined instruction. The aim of this instruction is to deal with violations that can lead to low quality in services or damages to equipments and structures. Necessary components of outsourcing are shown in Fig. 2. It should be noted that some other secondary items can be included in this chart. In the following sections, more details about these basic components are presented.

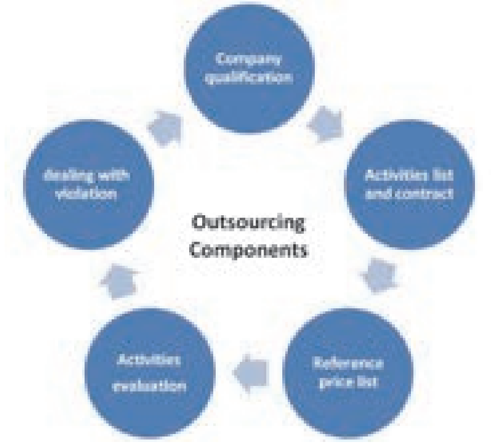
Company qualification
Activities list and contract
Reference price list
Activities evaluation
dealing with violation
Outsourcing Components

Figure 2. Basic components of an outsourcing

2.1. Identify and qualification of service provider

The aim of identification and qualification of service provider is preparing a list of licensed companies for dam's owner or who is responsible for operation and maintenance. In addition there must be some regulations that confine operation and maintenance activities just to these companies. To do so, two main subjects should be defined clearly: the criteria for qualification and the level of activities that are transferable to each qualified company.

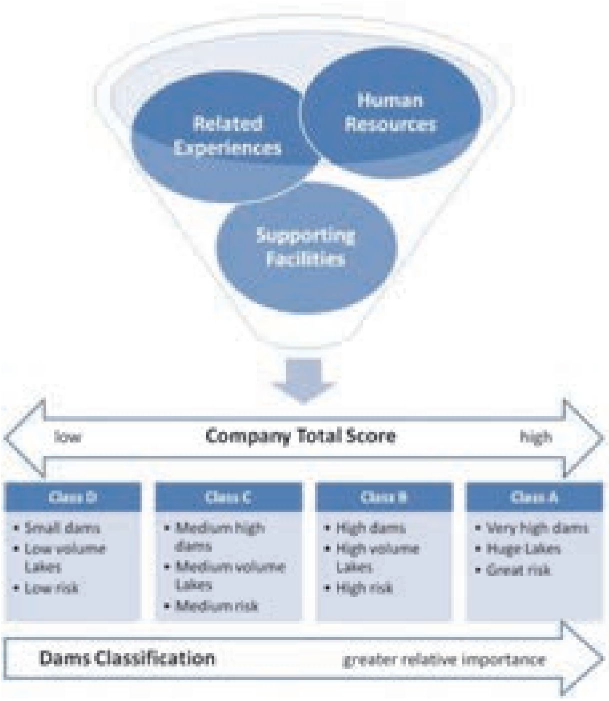
Related Experiences
Human Resources
Supporting Facilities
low
Company Total Score
high
Class D
• Small dams
• Low volume Lakes
• Low risk
Class C
• Medium high dams
• Medium volume Lakes
• Medium risk
Class B
• High dams
• High volume Lakes
• High risk
Class A
• Very high dams
• Huge Lakes
• Great risk
Dams Classification
greater relative importance

Figure 3. Qualification of applicant companies and transferring activities based on total score and dams classification

Since every dam based on its characteristics and relative importance needs different level of care, in first step there should be a classification of dams. This classification can be a combination of components such as dam height, lake volume, servicing maintenance and the properties and lives at risk. Operation of dams with greater level of relative importance will entrust to more eligible companies.

There are many factors that should be considered for company that is applicant for operation of dam. Within these factors three main features are more important: human resources, related experiences and supporting facilities and equipment. By rating each of these components and weighting of them, the total score of applicant company will be defined. This rating reflects the company's ability to perform requested services.

2.2. Contract format and details

There are different types of activities in dam operation and maintenance that should be identified before contract. This is an important step for preparing a comprehensive and clear agreement. These activities can be classified in four main categories: safety control, operation, maintenance and general related services. In addition each activity in the list should accompany with time, equipment, human resource and expertise. It should be noted that there are some differences between various dams in required activities.

Responsibilities of service provider should be clarified in contract. For example there are three main types of maintenance, namely:

- routine or normal maintenance which includes all work necessary to keep the systems functioning;
- special maintenance including repairs of damage caused by major disasters, such as floods, earthquakes and typhoons;
- deferred maintenance including any work necessary to regain the lost flow capacity in canals, reservoirs and structures when compared to the original design.

Within above predefined classes, it seems the third one is out of contractor capacities and should be determined in contract. Also the necessary equipment needed for doing O&M actions and number of person and their expertise should be defined clearly in contract. Clarifying these issues can ensure proper operation and preventing conflicts in responsibilities. The required components of a comprehensive contract are outlined in Fig. 4.

2.3. Reference price list for operation activities

One of the most challenging issues in outsourcing O&M activities is the financial aspects and total price of contract. After defining responsibilities of a company in an outsourcing contract, as described in previous section, estimation of total cost is the next step. Preparing a general price list for O&M activities in dam can be very helpful to achieve a good estimation. For this mean it is suggested to gather all O&M records in different dams and classify these activities to reveal a base price for each activity.

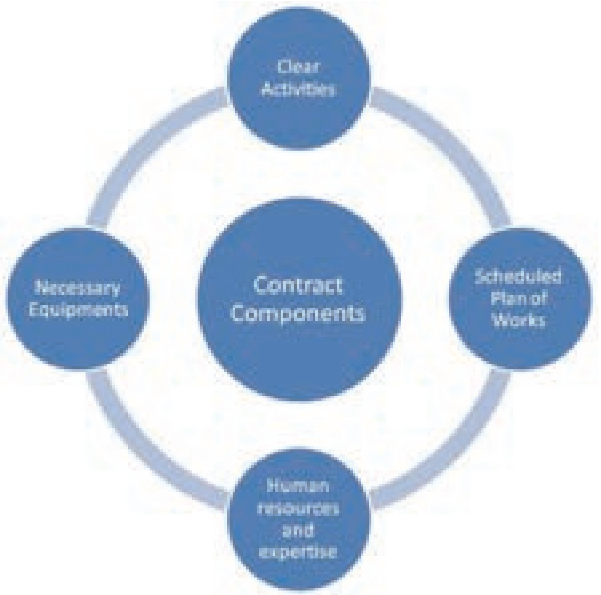

Figure 4. Necessary components of a comprehensive contract for dam operation

Apparently some of activities for specific dam aren't common enough to be included in the general price list. In such cases the price can be defined by asking active companies on that field. By the way the majority of contract price is measurable by preparing general price list and the remaining part can be determined by Inquiries or negotiation. It should be noted that it is necessary to define some coefficients for working in different regions or specific situation.

2.4. Contractor evaluation and dealing with violation

The main goal of evaluation of company who is responsible for operation and maintenance of specific dam is to encourage diligent contractor or restricting unfit one based on predefined instruction. Prerequisite for such evaluation is comprehensive and clear contract with measurable responsibilities.

The quantity and quality of scheduled works must be evaluated randomly based on predefined measures. Completing checklists and preparing periodic performance reports by contractor can help to this evaluation. Finally the result of company evaluation can affect the total score in qualification step as a decreasing or increasing factor.

Since operation of dam is a critical activity and it deals with the lives and property of people, violation is not accepted and may lead to permanent exclusion. So it should be an instruction that all the penalties for any violation described clearly to highlight and emphasis on importance of accepted responsibilities. A service provider company must know which manners are against rules and procedures and what is the consequences of ignoring them.

3. SUPERVISION

As a supplementary system for outsourcing O&M of dams, supervision has a great role in implementation of policies and getting feedback to reveal shortages and system weaknesses. The aim of supervision is to measure distance between existing condition of operation and desired (or predefined) situations.

Supervision result stated in quantitative way instead of descriptive terms as far as possible (ICOLD, Bulletin No. 158). Undoubtedly a proper supervision can result in modification of approaches and methods and finally lead to extension of dam's service life. It should be noted that there are some differences between evaluations of contractor works and dam operation supervision; because the first one focus on contract detail but the latter targets all the necessary components for proper operation. On the other hand, evaluation of contractor is part of supervision.

3.1. Measures

The most important component of a comprehensive supervision is incorporated measures. These measures should focus on the quality of operation and maintenance activities. Some important measures are presented in Table 1. Also each measure must have three main specifications.

First, it should be related to O&M activities, because the aim is evaluation of dam from operation aspects and other measures like material quality is not our subject. For this mean all measures should be clearly defined and sensible for everybody.

All measures should be also easily measureable with minimal equipment and time, which is the second important feature of them. For example, remaining lifetime of structures cannot be measured simply and need too much time and special tests.

The last substantial property of measures is the ability of improve them during operation time; on the other hand, in supervision process, there should be opportunities for improvement of operation conditions. For example, human resource measure is capable to upgrade during annual supervision process, but there is no way to solve the problems that have arisen since design and construction time.

3.2. Procedure

Supervision must be done by qualified person. As mentioned in previous section, all the measures should be clearly defined and scoring methods must be determined. To get the best results and to avoid argument, these methods must be described in detail and be illustrated with examples and pictures if possible. To do so it is recommended to prepare unified checklists for each section and train person in field.

Supervision process must be repeated periodically. The period of O&M condition evaluation depends on relative importance of dam or total score. Dams in class A (as described in sec. 2.1) need supervision more frequently. Dams with lower scores in previous evaluation have similar situation.

Table 1. Some important measures for operation supervision

Measure	Description
Human Resources	Number of person and their expertise for operation
Instruction	Necessary instructions and guidelines for O&M
Energy	Energy consumption in return for services
Healthy	Situation of equipment and structures in comparison with predicted life
Recovery	Continuous improvement using new technologies and methods
Safety	Preparing to deal with emergency situation by preparing EAP instruction and updating instrumentation
Resilience	Ability of equipments and structures to bear different conditions during acceptable time

Final result of supervision must be recorded in central database with details and must be available through secure web pages to related managers and policymakers. The result of supervision is a score (for example from 1000 points) which is calculated through a combination of measures.

3.3. Outputs

Supervision result which will be stated as a total score for each dam, can answer many key questions about operation, as follows:

- How much distance is there between current situation and standard or predefined conditions?
- What are the most important weaknesses in

operation performance that should be addressed?
- Which activities must be done and what strategies should be followed to improve operation conditions efficiently and rapidly?

By repeating the process of supervision and comparing the results, other helpful facts will be revealed such as:

- Has operation conditions improved during evaluation period?
- Which operation measures have been improved or downgraded in a specific dam?
- Have the measures that have been low in previous evaluation, improved enough?

By gathering and processing the result of supervision of all dams, valuable information will be obtained for decision-makers and managers. They can decide about future approaches and prepare national or regional instructions or guidelines and follow needed legislation. They can also track the consequences of policies and approaches.

4. IRAN DAMS CONDITION

Based on ICOLD definition, there are more than 220 large dams under operation in IRAN. The first modern Iran dam, Golpayegen, which is an embankment type has been constructed 59 years ago (see Fig. 5). This dam 50 years after building was rehabilitated for extending service life because the dead volume (reservoir under bottom outlet) had been filled with sediments. This operation was carried out by raising the level of bottom outlet. It is predicted that the service life of Golpayegan dam has increased at least for 30 another years (Ghaderi S. (2009)).

Figure 5. Golpayegan dam, first modern constructed dam in Iran with 57m height

Also there are about 100 large dams under construction which will be operated soon. In contrast with normal useful life of dams, as shown in Fig. 6, most of the dams in Iran are young (Noorbakhsh S.M. (2016)). So by choosing right approaches and policies there is opportunity to operate dams in best conditions and to extend their service life. Using other countries experiences can help to obtain such goal.

There are some issues and problems in dam operation that convinced Iran politicians and managers to move toward outsourcing. Most of troubles were result of governmental management. Some of these problems are:

- Lack of human resources and qualified person in operation section,
- Motivational and punitive tools are limited,
- Implementation of new ideas and technologies is not easy,
- No competition to provide better services.

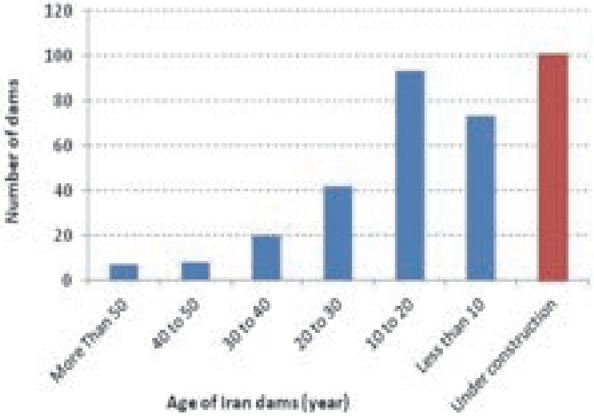

Figure 6. Age of Iran dams [6]

In fact, the above issues are the main reasons for outsourcing or privatization. Establishment of such model has been started for Iran dams since 2012 by preparing instructions.

5. CONCLUSION

Outsourcing O&M activities can extend service life of dam by employing capabilities of private section. Qualified human resources, using new technologies and methods, light body and efficient systems are the most important specifications of them in contrast with government (public) sector.

Increasing the quality of services while reducing costs is the result of competition between service providers. Such result can be as a result of using new ideas and methods. Apparently better services leads to extend dam’s service life.

A good outsourcing regulation must be accompanied with proper supervision. The result of supervision is very helpful tool for assessment quality of outsourcing. These result must be quantitative values based on predefined measures. On the other hand, supervision guarantee an IOR program implementation.

ACKNOWLEDGEMENT

The completion of this paper could not have been possible without the participation and assistance of so many people whose names may not all be enumerated. Their contribution are sincerely appreciated and gratefully acknowledged. However the person I would like to express his deep appreciation and indebtedness particularly is Mr M. Sadeghi, water systems engineer, Ministry of Energy.

REFERENCES

Ang, A. And Tang, W. (1975): Probability concepts in engineering planning and design: Volume I – Basic principles, Wiley, NewYork

Overby, S. (2007): ABC: An Introduction to Outsourcing, CIO.com.

Olive, B. (2004): Outsourcing Growing, Despite Controversy, Power: 148(4), 19–20.

Dam Surveillance Guide, International Commission on Large Dams, Bulletin 158.

Ghaderi S. (2009): Golpayegan dam rehabilitation Report, 3rd national confrence on civil engineeing, Tehran, Iran.

Noorbakhsh S.M. (2016): Iran Dams Repot , Iran Water Resource Manegement Co., Ministry of Energy.

Decision Support System Development To Optimize Djuanda Dam Operation

A. Mardiyono
Head of Division II of Jasa Tirta II Public Corporation, INDONESIA
antonmardiyono@yahoo.com

H.M. Sungguh
Director of Jasa Tirta II Public Corporation, INDONESIA

R. Mayasari
Head of Water Allocation Bureau of Jasa Tirta II Public Corporation, INDONESIA

ABSTRACT:
Djuanda dam as the biggest multi-purposes dam in country with impounding capacity of 3 x 10^9 m^3 and installed capacity of 187.5 MW of Hydroelectric Power Plant (HPP) is intended to meet a reliable supply of 240.000 ha irrigation area and 900 Million m^3/year DMI water for urban residents. Djuanda Reservoir plays strategic supply availability role since increasing the provision of irrigation and DMI water services. The achievement of the goals will depend on the raw water availability and its continuity, which will challenge the Dam operation. Decision Support System (DSS) is a system assisting executive on managing assumptions, alternatives, and opinions to decision makers in making a decision which there are complex situation. The Citarum Water Resources (WR)-DSS development is envisioned to consist of hydrological and GIS database; analytical models such as rainfall-runoff, water allocation and quality models; and optimized monitoring activities for acquisition of hydrological and water quality data. The DSS will be applied in the IWRM system of the basin, and utilized to optimize its IWRM. The Citarum WR-DSS will address the challenge to optimize Djuanda dam operation, to secure the irrigation and DMI water availability and sustain the dams function.

Key words : Multi-Purposes Dam, Complex Situation, Citarum WR-DSS

1. INTRODUCTION

Citarum River, the biggest river in West Java Province, characterizes by three large dams formed a cascade system to serve multiple users and is considered as the most strategic river basin in Indonesia. Citarum cascade hydropower consists of Saguling dam at the uppermost, Cirata dam in the middle that has the biggest installed capacity of 1000 MW and became operational in 1988, Djuanda dam at the lowest part of the system. Djuanda dam which has the biggest reservoir acts as buffer for the upper two reservoirs with exceptional purpose to supply the Djuanda irrigation system, the largest contiguous irrigation system in Indonesia, domestic, municipal and industry raw water supply beside generating hydro-electricity as the main purpose of the upper two reservoirs (Fig.1). Ir. H. Djuanda (Djuanda) dam including hydro power plant (HPP) and irrigation infrastructures has been commenced in 1958 and in fully operational since 1967, which the total irrigation area served under the Djuanda reservoir is 240,000 ha. It is the largest contiguous irrigation system in Indonesia and is a major rice production area. The Citarum cascade reservoirs have a combined effective volume of 3,276 x 10^6 m^3 which is approximately 57% of annual mean run off of Citarum, indicating that the system was not designed to provide carry-over storage during year-long periods. Using non-shared optimised reservoir operation, the total water released of the Citarum cascade reservoirs can reach 5,531 x 10^6 m^3, which is nearly 100% of water resources potential has been controlled. The water resources potential in the Citarum river is around 6 x 10^9 m^3 annually. The biggest consumer so far is irrigation which uses up about 87% of total regulated water from Djuanda reservoir and other rivers in the system.

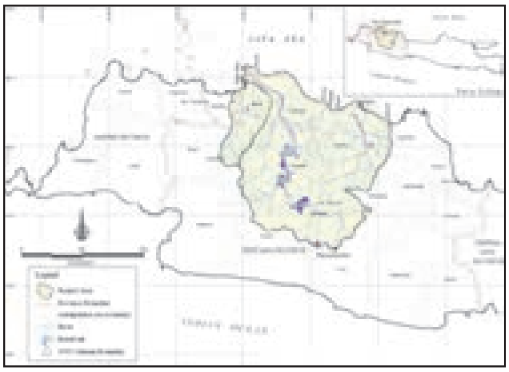

Figure 1. Jurisdiction area of PJT II

The demand of the system can be generalized into three parts: (i) irrigation water supply to the North, East, and West Tarum areas, (ii) raw water supply to drinking water treatment plants for the districts and municipalities in the corridor of the canals including Jakarta, and (iii) to industrial zone along the corridor from Jakarta to Cirebon, including the region around Purwakarta. These demands can partially be satisfied by rivers which are intersecting the main canals. The balance has to come from the Citarum, which are the greatest part of the intake requirements at the diversion weirs has to come from the Djuanda reservoir.

2. PRESENT COMPLEX CONDITION OF CITARUM RIVER BASIN

2.1. Impacts of Climate Change

Djuanda hydropower has been in operation since 1967, followed by Saguling in 1986 and Cirata in 1988. In the latest period of operation, the hydrologic flow regime is changing. This may infer to hydrologic effects of land use changes. However, this is not only the reason of investigations to modify Citarum hydropower operation. Shifting of seasons, longer dry seasons and shorter but more intense wet seasons that have been valued as the impacts of climate change are likely future rainfall pattern in Java (ADB Technical Assistant Team, 2010). A further catalyst to starting to explore climate change was the recent decline in inflows to the inflow in Citarum reservoirs cascade system (Fig.2). The records showed a significant reduction (the mean annual flow has not been reached within 10 years of operation and the higher fluctuation between maximum and minimum annual flow).

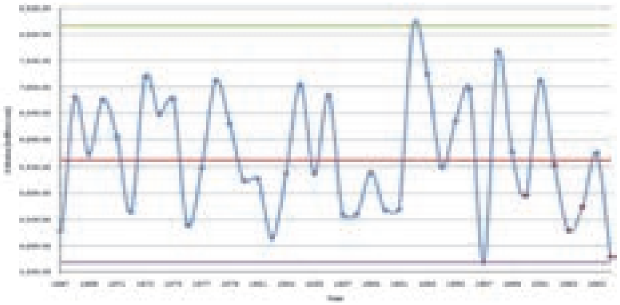

Figure 2. Annual volume of Citarum during 1967-2010 period of Dam operation

However, the uncharacteristic heavy rainfall intensity occurred in beginning of 2010 that results flood at the several low land of west java province, particularly along the Citarum river alignment. Fig.3 below shows the significant increment of monthly real Saguling inflow comparing to the pattern either normal or wet during January till June 2010, as a result of increased rainfall intensity mentioned above (Biro Pengelolaan dan Pengendalian Data dan Alokasi Air, 2014).

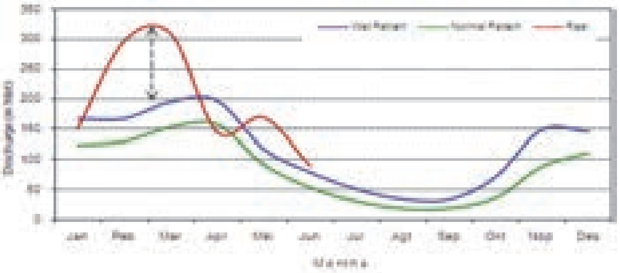

Figure 3. 2010 Saguling Dam inflow, showing comparison between wet / dry pattern and real inflow

By understanding the figures mentioned above, it could be understood that shifting of seasons was occurred. Peak of wet season was shifted and followed by the raising rainfall intensity extremely, as indication of climate change that is likely future rainfall pattern in Java. At Citarum cascade reservoirs and HPPs operation, this raised the question internally of “How would our storages and operations cope if this was to occur to our inflows?”

2.2. Shortage Future Water Balance to Meet Increasing of Water Demand

It is evident that there is substantial unmet demand for treated water supply especially in urban Jakarta and rapidly-developing areas east of the Jakarta city through which the West Tarum Canal of Djuanda system. The predicted demands for the five identified urban district area are summarized in Table 1 below. A reliable supply of drinking water for urban residents is one of the primary requirements for full and productive economic participation. The city of Jakarta and its strategic surrounding areas are unable to provide their constituents with acceptable access to a reticulated water supply. While there are several reasons for this deficiency, supply availability is one of the major contributing factors. Djuanda Reservoir plays strategic role since has the capacity to supply more than 80% substantial quantities of raw water to Jakarta and its strategic surrounding areas.

Table 1. Predicted water demands for urban district surrounding West Tarum Canal Area

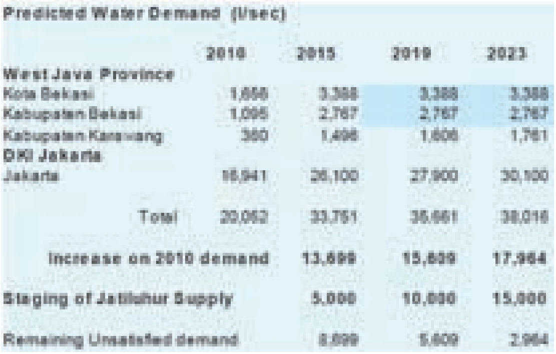

Predicted Water Demand (l/sec)	2010	2015	2019	2023
West Java Province				
Kota Bekasi	1,656	3,388	3,388	3,388
Kabupaten Bekasi	1,095	2,767	2,767	2,767
Kabupaten Karawang	360	1,496	1,606	1,761
DKI Jakarta				
Jakarta	16,941	26,100	27,900	30,100
Total	20,052	33,751	35,661	38,016
Increase on 2010 demand		13,699	15,609	17,964
Staging of Jatiluhur Supply		5,000	10,000	15,000
Remaining Unsatisfied demand		8,699	5,609	2,964

2.3. Water Quality Deterioration

The overpopulated fish cultivation in the reservoirs burdens the organic matter deposition in the bottom of reservoir. Floating net fisheries in early 1990s has been practiced in Djuanda reservoir and has been increasing since then. The effect of the activity was foreseen to make worse the water quality condition within the reservoir. The impact of high pollutants loading performed an excess of distracted gases (i.e. H^2S and CO_2-aggressive). It causes the electrical and mechanical equipment such as turbine blades, valves, electronic cards, and termination unit of controlling equipment become corroded and need to be replaced oftener (see Fig.4 below). The deteriorated environmental of Djuanda reservoir has mainly affecting the HPP performance, especially in equipment failures and increased operation and maintenance annual cost (PT Dua Ribu Satu Pangripta & PJT-2, 2007).

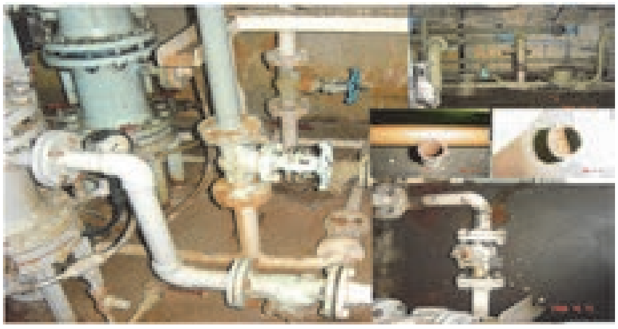

Figure 4. The rotten and corrosion of HEPP equipment and infrastructure

3. GENERAL STRATEGIC PLANNING

Adaptations to climate change are a variety of initiatives and measures aimed at reducing the vulnerability of natural and human systems in the face of current or expected climate change effects. Adaptation will be necessary to cope with impacts resulting from global warming that are already inevitable because of past emissions. There are many potential adaptive responses, ranging from purely technological measures (e.g., engineering infrastructures, storage, sea defenses), to behavioral responses (e.g., water saving, efficiency and water productivity, altered food and recreational choices), to managerial (e.g., integrated water resources management, altered farm practices), and to policy (e.g., planning regulations). In the water sector the adaptation strategies range from water storage to more extensive rainwater harvesting, conservation measures, water reuse, irrigation efficiency and desalination (KWater Team, 2008).

The methodology to develop normal system operations in a multipurpose reservoir as describe in Fig.5 include development of optimal end-of-month storage which maximize the expected value of selected primary objective function for the system, subject to satisfying other system objectives based on the specification of target performance levels. The domestic, municipal, and industry water demands (DMI) and irrigation water requirement as calculated from the previous procedure become an input to the reservoir operation model and synchronized with hydro-power to evaluate reservoir rule curves. Based on this model, an annual operational plan for Citarum cascade reservoirs is made using expected demands, statistical inflows based on dry, wet, normal years (each month). In this plan, the total energy of the system is maximized subject to a number of conditions : (1) The demands at Djuanda reservoir should at least be met, (2) The upper and lower rule curves for the reservoirs should be observed as much as possible, (3) At the end of the year (or planning period) certain reservoir levels should be met, and (4) order to prevent individual reservoir levels from changing to much from month to month, the relative net storage of each reservoir with respect to the total net storage in the system should be kept constant (Biro Bina Operasi dan Konservasi, 2008).

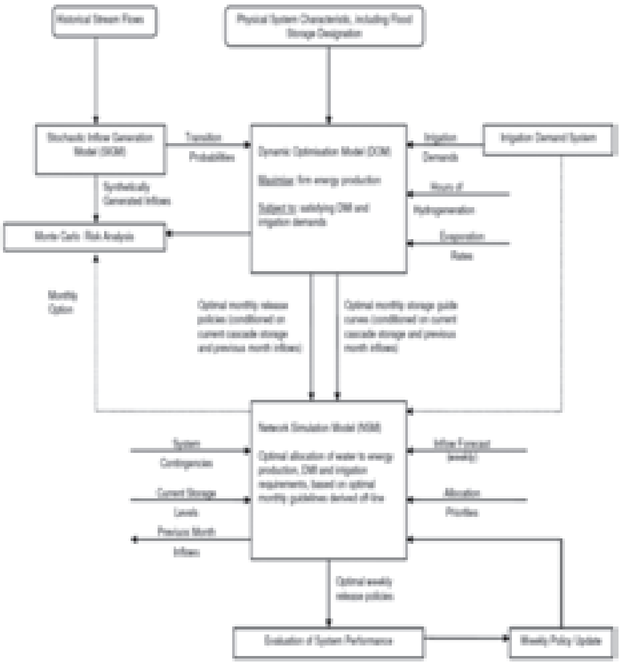
Historical Stream Flows
Physical System Characteristic, including Flood Storage Designation
Stochastic Inflow Generation Model (SIGM)
Transition Probabilities
Dynamic Optimisation Model (DOM)
Maximise: firm energy production
Subject to: satisfying DMI and irrigation demands
Irrigation Demands
Irrigation Demand System
Hours of Hydrogeneration
Evaporation Rates
Synthetically Generated Inflows
Monte Carlo Risk Analysis
Monthly Option
Optimal monthly release policies (conditioned on current cascade storage and previous month inflows)
Optimal monthly storage guide curves (conditioned on current cascade storage and previous month inflows)
Network Simulation Model (NSM)
Optimal allocation of water to energy production, DMI and irrigation requirements, based on optimal monthly guidelines derived off-line
System Contingencies
Current Storage Levels
Previous Month Inflows
Inflow Forecast (weekly)
Allocation Priorities
Optimal weekly release policies
Evaluation of System Performance
Weekly Policy Update

Figure 5. Hierarchical approach for developing optimal normal reservoir operation policies

4. DECISION SUPPORT SYSTEM (DSS) DEVELOPMENT

4.1. Concept the DSS in Citarum River Basin

DSS is a system assisting executive on managing assumptions, alternatives and opinions to decision makers in making a decision which there are complex situations. The DSS is expected to serve as a standardized framework on which all current monitoring, modeling and conservation practices can be integrated and analyzed by the river basin manager. Its intended that the DSS be suitably comprehensive and will provide support to all river managers without need for future operation and expansion of the DSS to other river basins under local supervision.

The DSS to be developed will be a structured collection of databases including hydrological and spatial databases and analytical tools such as rainfall-runoff model, water allocation model and water quality models. The component of DSS be integrated and communicate directly with one another as follows; (1) GIS-Database will serve as a central database for data sharing throughout the whole basin, (2) Hydrological Database will store rainfall, water level, flow, ground water level and water quality, (3) Rainfall Runoff model will be used to predict stream flows for short, mid and long term periods, (4) Water allocation Model will be used to analyses water resources allocation in the basin and adjacent basins, and (5) Water quality Models will be used to predict water quality for the rivers, canals, and reservoirs (KWater Team, 2008).

Other features of the DSS to be developed are the user interface, a database and model integration system and a communication module that will allow access to the data from the internet and sharing of information between agencies and stakeholders. An overview of the structure of the DSS is shown in Fig.6. The DSS provides support for data collection, processing, analysis, decision making and implementation.

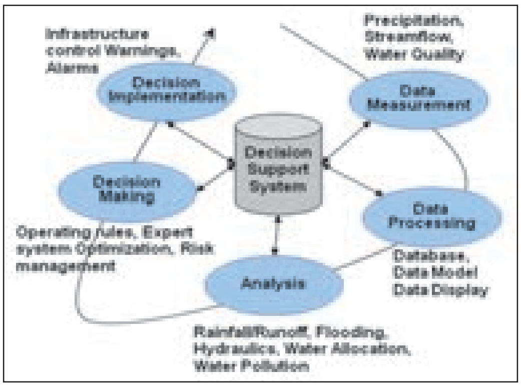
Infrastructure control Warnings, Alarms
Precipitation, Streamflow, Water Quality
Decision Implementation
Data Measurement
Decision Support System
Decision Making
Data Processing
Operating rules, Expert system Optimization, Risk management
Database, Data Model Data Display
Analysis
Rainfall/Runoff, Flooding, Hydraulics, Water Allocation, Water Pollution

Figure 6. Overview of Decision Support System Structure

Main function of the DSS are :

- Planning and evaluation; Monitoring, planning, and evaluation for integrated water resources management in citarum river basin to support the basin managers.
- Operation; Water resources management; Establish short-term water supply plan, Balance seasonal water demands between users through reservoir and stream flow management, Integrated river-reservoirs system operational planning.
- Management; Hydrological and GIS Data Management (Data collection, archiving, management and validation, data sharing and dissemination among agencies and stakeholders), Water Resources Management (Quantity spatial and temporal runoff amounts, improve the efficiency of basin reservoir system management, drought contingency planning and water right analysis), Water quality management (simulation of steady state water quality in stream, reservoir water quality management, propose water quality improvement alternatives.

4.2. DSS Components

The DSS will consist of module for water allocation, water quality, and rainfall-runoff modelling besides the GIS database. The potential software options to be utilized for modelling were identified on the basis of situation analysis in Indonesia. Final selection for the key DSS components based on a quantitative analysis of the available options on the criteria of design parameters. The DSS will consist of GIS based integrated database interacting with data management system and the users through a convenient Graphic User Interface (GUI). A hydrological and water quality database will be tagged on the spatial database to construct the GIS database. Three core modules, the analysis module, the pre-processing and the post processing module will comprise the data processing engines of the DSS.

The Dashboard Features.

The "first page" of convenient Graphic User Interface (GUI) is designed through the dashboard of the system as illustrated by Fig.7. Kind of mentioned modules were accommodated and in line with the requirements of the users. The dashboard informs kind of visual data such as reservoir water level, reservoir release water discharge, and water discharge from the Curug main barrage. In the side bar, module of spatial data, location, water distribution scheme, data management, data editing, data series, module link, and setting are provided.

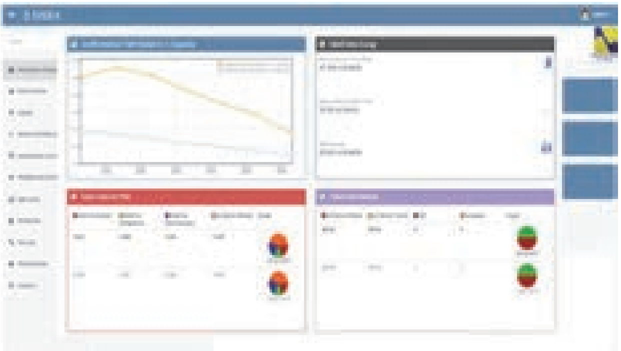

Figure 7. Dashboard of DSS

Spatial and Tabular Data

Spatial data menu show information geographic layer files (point, line and polygon) that will be proceed by the users to results thematic-geographical maps. The layers will show tabular information while clicked on which inform more detail data dealing with required layers. Fig.8 show spatial and tabular (hydrology) data of Cirata Dam as a part of cascade dams system in Citarum river basin.

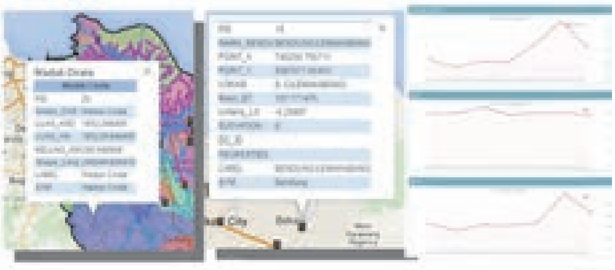

Figure 8. Spatial and Tabular Data of DSS

Water Allocation Module.

This module accommodate the users to analyse downstream water allocation that should be released from the dam to 5ulfill the multi proposes requirements. The module is included the water allocation schematic, that also completed with the tabular information as shown in figure 9. The module inform the daily water balance of Citarum cascade dams; Saguling, Cirata and Djuanda Dam.

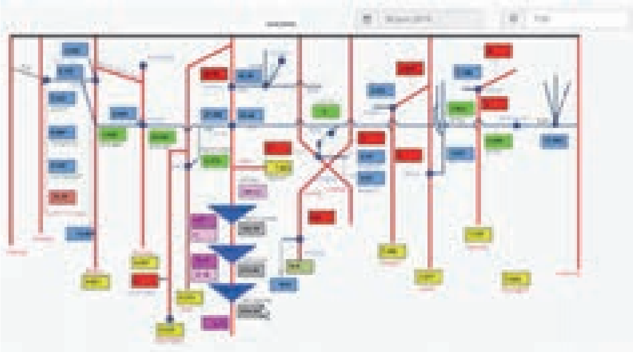

Figure 9. Djuanda Dam Water Allocation Schematic and Module

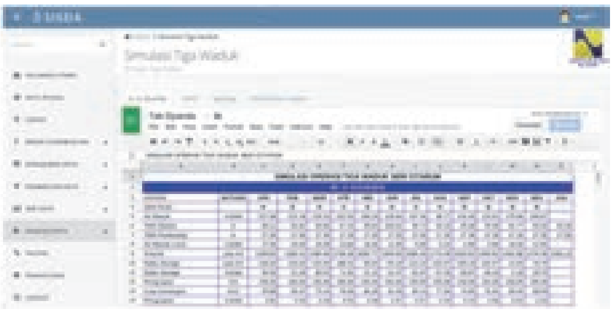

Figure 10. Djuanda Dam Operation Data and Simulation Module

Analytical and Management Data Module.

The daily dam operation, decision and policy is determined based on the proper and provided data from the site which already verified by the engineers. Dealing with the verifying process, the data could be execute, visualized and displayed by the DSS through this module. The data which dealing with the daily dam operation such as inflow and outflow dam discharge, power plant production simulation, water quality condition, etc., are presented and interfacing (Fig.10) the users to results proper decision of dam operation, in order to optimize the operation.

5. CONCLUSION

Decision Support System (DSS) is a system assisting executive on managing assumptions, alternatives, and opinions to decision makers in making a decision which there are complex situation. The Citarum Water Resources (WR)-DSS development is envisioned to consist of hydrological and GIS database; analytical models such as rainfall-runoff, water allocation and quality models; and optimized monitoring activities for acquisition of hydrological and water quality data. The activities include collecting, validating, archiving, managing and disseminating relevant data. The DSS will be applied in the IWRM system of Citarum river basin, and utilized by the main stakeholders in order to optimize its IWRM. Automatically, The Citarum WR-DSS will address the challenge to optimize Djuanda dam operation, to secure the irrigation and DMI water availability and sustain the dams function.

REFERENCES

ADB Technical Assistant Team (2010). Report on Data and decision Support System. Jakarta, Indonesia.

Biro Pengelolaan dan Pengendalian Data dan Alokasi Air (2014). Pengembangan Water Resources - Decision Support System. PJT-2, Purwakarta, Indonesia.

PT Dua Ribu Satu Pangripta & PJT-2 (2006-2007). Studi KJA Waduk Ir.H. Djuanda Tahap I&II, Purwakarta, Indonesia.

Biro Bina Operasi dan Konservasi (2008). Program Pemantauan Kualitas Air Waduk Ir.H. Djuanda. PJT-2, Purwakarta, Indonesia.

KWater Team (2008). Development of a Water Quality Management System for the West Tarum Canal of Citarum River Basin in West Java Province, Indonesia. Purwakarta, Indonesia.

4th APG Symposium and 9th EADC on

INNOVATIVE TECHNOLOGIES FOR DAMS AND RESERVOIRS TOWARD THE FUTURE GENERATIONS

Investigation and Repair on Deteriorated Transverse joint of Kasabori Dam

H. Kawasaki
Japan Dam engineering Center, Tokyo, Japan
kawasaki@jdec.or.jp

S. Iwasaki
Sanjo Regional Bureau, Niigata Prefecture, Japan

ABSTRACT:
Kasabori dam is a concrete gravity dam with height of 74.5m completed in 1964 by Niigata prefectural government in a snowy region, for the purposes of flood control and hydropower. It was redeveloped in 1973-79 and again in 2011-17 to upgrade its flood control function. The present work, which started in 2014, includes heightening the dam by 4m, placing concrete on its downstream surface to increase its thickness by 2m, renewing its two gates, and extending its spillway.
However, a visual inspection confirmed a serious increase of water leakage around the J2 transverse joint, and the extension of cracks along J2 since the first repair in 1973-79. Thus, before the main work, repair work started in 2014 and, cutting down around J2 by line drilling was performed after lowering the reservoir level. After water-stop installation and steel-bar reinforcement, the concrete was placed, and the J2 repair work was finished by June 2015. Experientially, there were some difficulties coping with the transverse joint trouble (Kawasaki, H., et al. 2014). In this paper, we introduce the investigation process and the repair work on the traverse joint, and try to explain the mechanism of deterioration by earthquakes and heavy freezing-thawing.

Keywords: Transverse joint, Leakage, Crack, Cutting face, Repair

1. OUTLINE

Kasabori dam is a concrete gravity dam with height of 74.5m completed in 1964 where is in mid of Niigata prefecture, for the purposes of flood control and hydropower. Since flood damage continued, the first redevelopment project was carried out from 1973 to 1979 to upgrade the flood control function. Its main works were the installation of one more crest gate and a spillway. In addition, the J2 transverse joint was repaired to decrease its water leakage. Figs. 1 and 2 show their situation.

The present redevelopment project was started after the serious flood damage by heavy rain in July 2011. The Kasabori dam project is intended to ensure its flood control function by increasing the dam height by 4m, placing concrete on the downstream surface to increase its thickness by 2m, renewing two gates, and extending its spillway (Figs. 3~6). The main work started in 2014, and the project is due to continue until 2017.

Repair work started in 2014, and cutting down around J2 by line drilling was performed after lowering the reservoir level. To cut and remove the area impacted by the crack around J2, the concrete cut volume was amounted about 50m^3, which is a big-scale cutting. Then, after installing the PVC water-stop, the reinforcing bar, and joint bar to unify the old and new body (Fig. 7), the new concrete was placed. And the J2 repair work was finished by June, 2015. At the same time, the grouting under J2 was carried out to reduce permeability and fill the voids under the dam base.

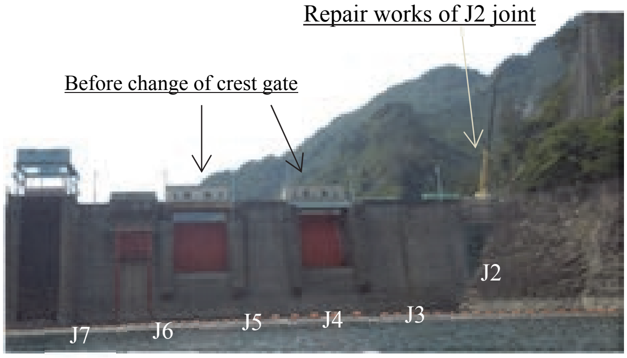

Figure 1. Upstream view of Kasabori dam on 2015.5.28

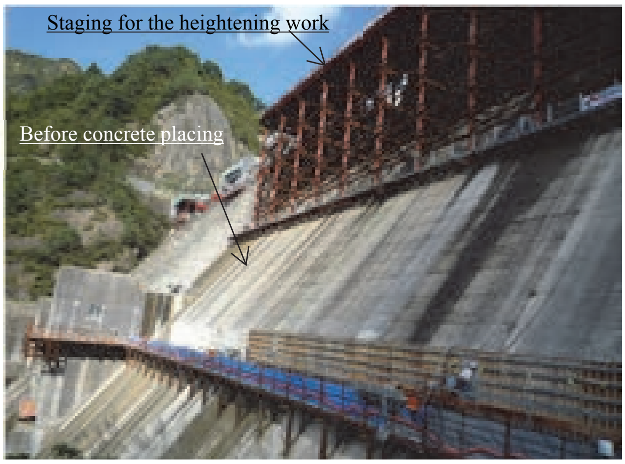

Figure 2. Kasabori dam under construction on 2015.10.05

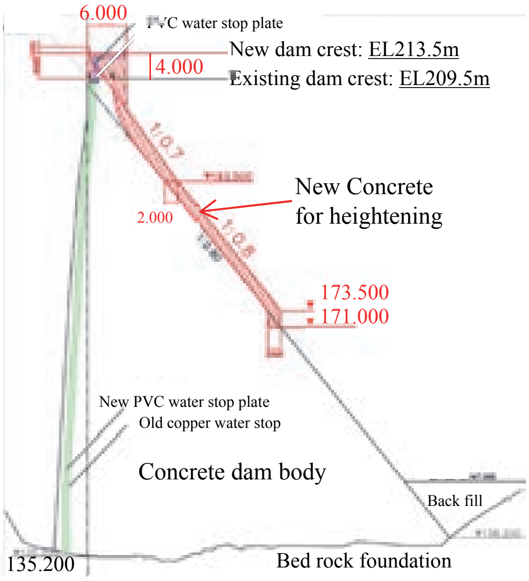
6.000
PVC water stop plate
4.000
New dam crest: EL213.5m
Existing dam crest: EL209.5m
1:0.7
New Concrete
for heightening
2.000
1:0.8
173.500
171.000
New PVC water stop plate
Old copper water stop
Concrete dam body
Back fill
135.200
Bed rock foundation

Figure 3. Cross-section of Block No.4
(Non-overflow section)

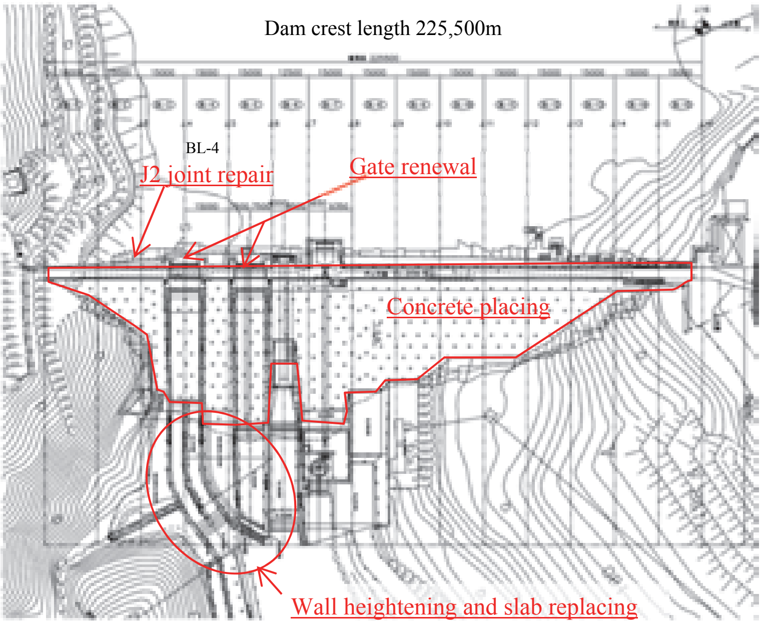
Dam crest length 225,500m
BL-4
J2 joint repair
Gate renewal
Concrete placing
Wall heightening and slab replacing

Figure 4. Ground plan of Kasabori dam

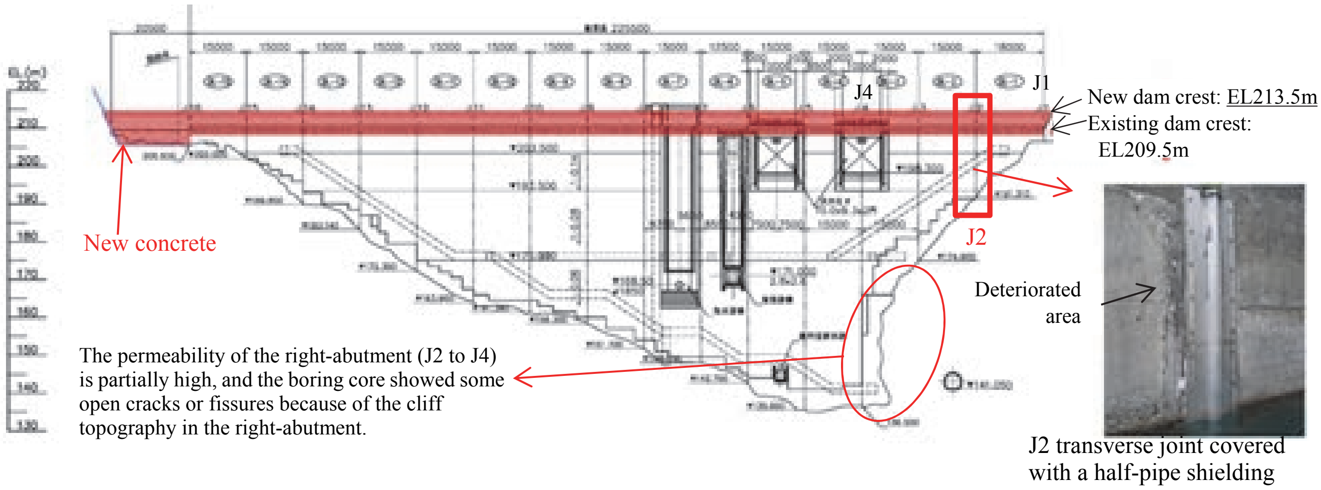
EL (m)
220
210
200
190
180
170
160
150
140
130
J4
J1
New dam crest: EL213.5m
Existing dam crest:
EL209.5m
New concrete
J2
Deteriorated
area

The permeability of the right-abutment (J2 to J4) is partially high, and the boring core showed some open cracks or fissures because of the cliff topography in the right-abutment.

J2 transverse joint covered with a half-pipe shielding

Figure 5. Upstream view of Kasabori dam (meshed zone shows the concrete placing zone)

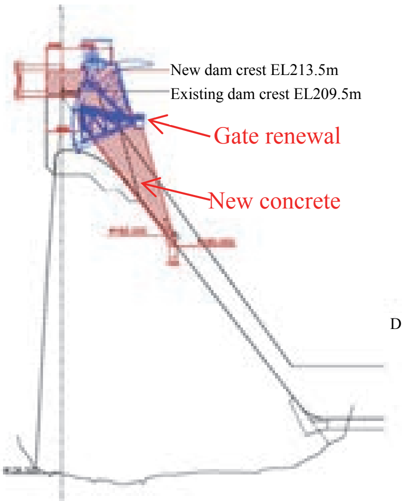
New dam crest EL213.5m
Existing dam crest EL209.5m
Gate renewal
New concrete

Figure 6. Cross-section of Block No.5
(overflow section)

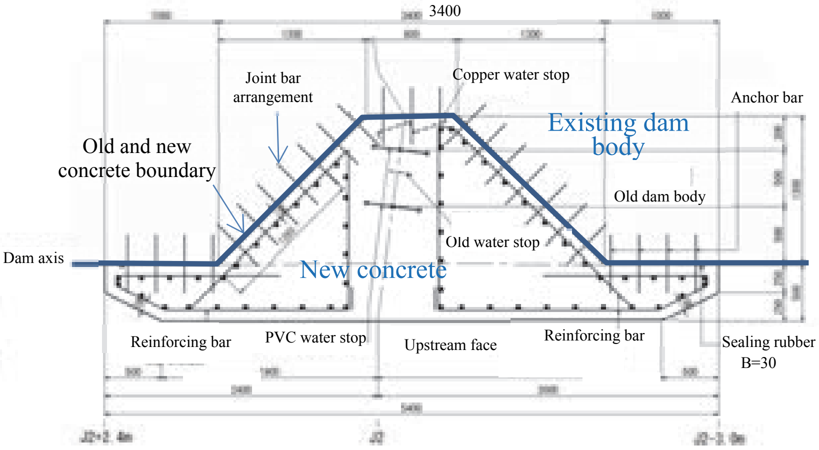
3400
Joint bar
arrangement
Copper water stop
Anchor bar
Existing dam
body
Old and new
concrete boundary
Old dam body
Old water stop
Dam axis
New concrete
Reinforcing bar
PVC water stop
Upstream face
Reinforcing bar
Sealing rubber
B=30
J2

Figure 7. Repair plan of J2 transverse joint

2. WATER-PASSAGEWAY INVESTIGATION

Visual integrity investigations were conducted in 2012 and 2013 in advance of the redevelopment work. The results confirmed that on the surface of the dam body and its inspection gallery, deterioration such as water leakage, joint opening, cracks, exfoliations, and surface erosions had severely progressed. Since the dam is located in a heavy snowfall region, these phenomena were judged to have been facilitated by frost damage. Above all, the biggest crack was extended vertically and downstream along the J2 transverse joint in the dam right-abutment.

The deterioration condition of J2 upstream face is shown in Fig. 8. Although the water stop work was carried out by installing half-pipe shielding of stainless steel during the first redevelopment (ended in 1979), at present, big cracks have extended to the left along the half-pipe shielding, which was the locations of the water passageways (Fig. 9).

In the downstream face of J2, water leakage at a maximum of 500 l/min was measured in April 2013 when the reservoir level rose. Then, coloured water was injected from the bore hole, confirming that the crack along J2 is the main water passageway. Moreover, a suction opening was found by an underwater diving search at the upstream face near J2, and a drilling and endoscope survey confirmed that the cracks on the upstream face originated at J2 with the inner part. Based on the above water-passageway survey at J2 and its adjacent blocks, the following three points were confirmed as a main water leakage route (See Fig. 10)

(1) When the reservoir level was about EL195.0m, the water leakage in the downstream was not confirmed.

(2) When the reservoir level was EL201.5-203.5m, the water exuded from the joint of EL194-196 m.

(3) When the reservoir level was EL204.5-206.5m, the water leaked from the joint of EL199.0m (See Fig. 11).

Eventually, it was estimated that the water passageway is mainly "Open crack along J2 over EL200m => Estimated crack line through the dam body in Fig. 9 => J2 joint and inspection gallery => the J2 downstream end between EL199~196m". Thus, it was decided to thoroughly cut and remove the deteriorated concrete around J2, and to reconstruct the transverse joint.

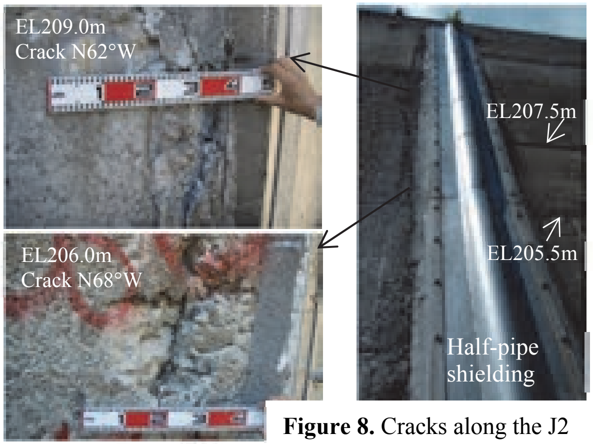
EL209.0m
Crack N62°W
EL206.0m
Crack N68°W
EL207.5m
EL205.5m
Half-pipe shielding

Figure 8. Cracks along the J2

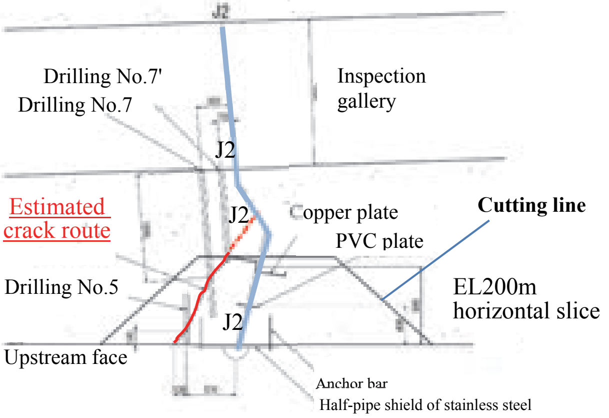
J2
Drilling No.7'
Drilling No.7
Inspection gallery
J2
Estimated crack route
J2
Copper plate
PVC plate
Cutting line
Drilling No.5
EL200m horizontal slice
J2
Upstream face
Anchor bar
Half-pipe shield of stainless steel

Figure 9. Crack survey plan by drilling near the J2 at EL200m

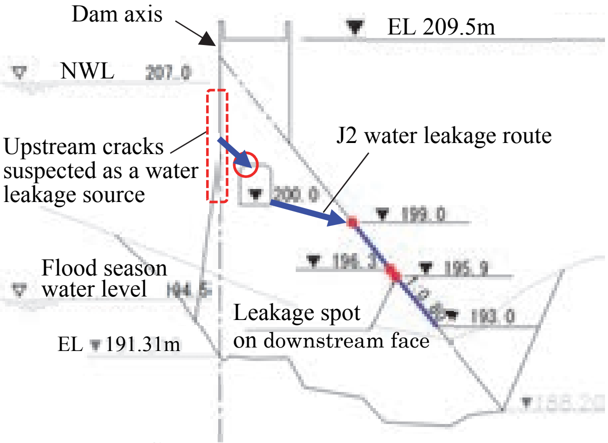
Dam axis
EL 209.5m
NWL 207.0
Upstream cracks suspected as a water leakage source
J2 water leakage route
200.0
199.0
196.3
195.9
Flood season water level 194.5
Leakage spot on downstream face
193.0
EL 191.31m
188.20

Figure 10. Cross-section of J2 and a water leakage route

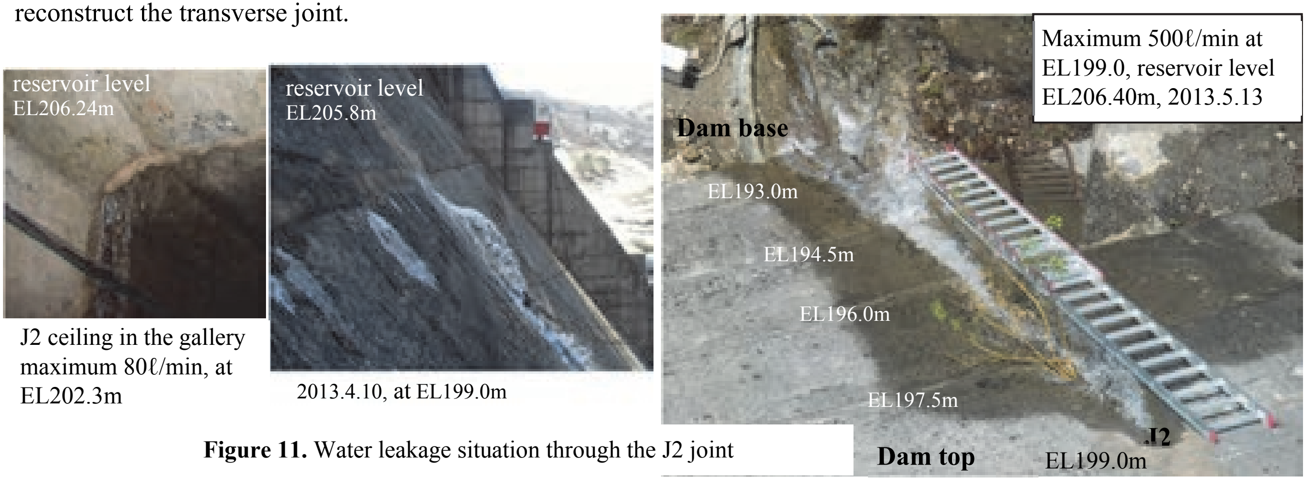
reservoir level EL206.24m
reservoir level EL205.8m
Dam base
EL193.0m
EL194.5m
EL196.0m
EL197.5m
J2
Dam top
EL199.0m

J2 ceiling in the gallery maximum 80ℓ/min, at EL202.3m

2013.4.10, at EL199.0m

Maximum 500ℓ/min at EL199.0, reservoir level EL206.40m, 2013.5.13

Figure 11. Water leakage situation through the J2 joint

3. REPAIR OF THE TRANSVERSE JOINT

Repair work was implemented by cutting and removing the dam concrete of the upstream face along the J2 transverse joint vertically to the dam bottom, and by reconstructing J2 by the next flood season (June, 2015). In addition, grouting work to improve the highly permeable zone of the bedrock under J2 and contiguity blocks was implemented.

These works were started in November, 2014 after lowering the reservoir water level, and ended in June, 2015. The cutting situation and extended cracks along J2 are shown in Fig. 12.

3.1 Cutting and face observation

The horizontal plane of the J2 cutting was determined to remove all the crack-influenced concrete. In the depth direction, it was cut to the surface of the bedrock in which the loosening was found. The cutting work was implemented for five months to March on 2014. On both sides of J2, cutting ranges were 3.5m x 1.3~ 0.9m in the horizontal plane, and it was 18m in height from the dam crest to the base rock (concrete cut volume: about 50m^3).

The concrete body was cut carefully after the outer edge cutting by line drilling and wire saw work. It was removed out every 0.75m in depth and cutting face was smoothed at 1~3m of depth. The distribution status of cracks was confirmed by the cutting face observation. Fig. 13 is the horizontal section showing the crack route through J2. The observation result is shown below.

3.1.1 Horizontal direction

The main crack passed through the left end of the copper water stop from inside J2, and it extended toward the upstream face. It is presumed that the water passageway occurred along the main crack. In the dam bottom, the main crack pierced through the concrete footing adjacent to the upstream side. It was shown that the crack progressed to the upstream side.

3.1.2 Vertical direction

The above main cracks continued downward along the left side of the half pipe shielding. The crack tended to incline towards the left (valley side) on the topographic slope. Further, the cracks were extended at the lower elevation, and reached the surface of the bedrock below the dam bottom. In addition, in the vertical cutting face, the crack shifted to the left side at the lower elevation.

3.1.3 The extension direction of the crack

It can be said that the main crack progressed upstream from downstream. It is assumed that the shearing that occurred in J2 initiated the crack, and extended it to the upstream face through the left end of the copper water stop. At the dam bottom, the main crack pierced the footing upstream, and below, it also extended to the surface of the bedrock.

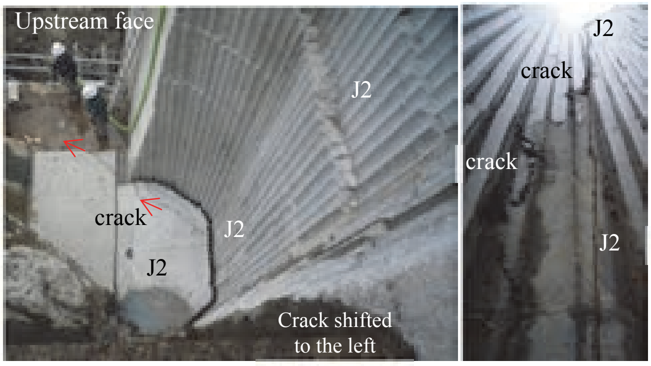

Figure 12. Cutting face and cracks at EL195.0m, 2015.2.26

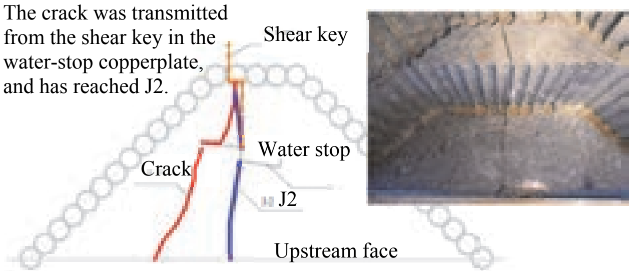

The crack was transmitted from the shear key in the water-stop copperplate, and has reached J2.

EL203.5m: Cutting face sketch

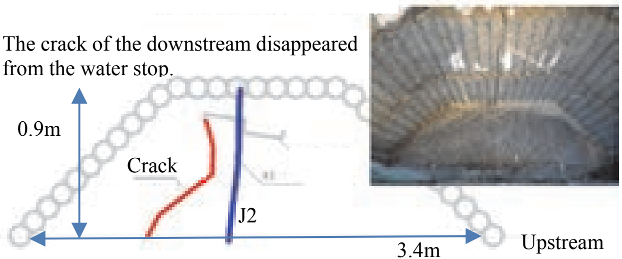

The crack of the downstream disappeared from the water stop.

EL201.5m: Cutting face sketch

The crack is extended from the water stop to the downstream, and the crack was barely distributed inside the cutting width.

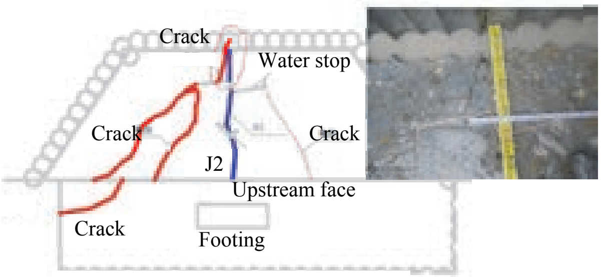

EL197.5m: Cutting face sketch

The concrete crack is going through the water-stop edge to J2. The crack is mostly contained in the exposed rock foundation, and the right side of cutting face is reached at the rock foundation.

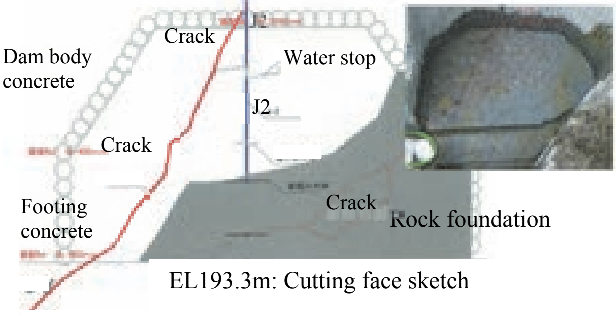

EL193.3m: Cutting face sketch

Figure 13. Cutting face observation along the J2

3.2 Reconstruction of the J2 transverse joint

A water stop and reinforcing bars were installed on the bedrock, and the concrete of the transverse joint and the footing was placed from March to June, 2015. The work process is described below (see Figs. 14 and 15).

3.2.1 Transporting the concrete
The concrete (ready mixed concrete) was transferred into the bucket from the concrete mixer truck, and was carried to the placing site by the rough terrain crane. Placing concrete was performed per 1.5m lift.

3.2.2 Adhesion of the existing and new concrete
In order to attain the unification of the existing and new concrete, while performing sufficient chipping of the existing dam concrete, the joint bars were arranged in the bonding plane. Moreover, reinforcing bars were arranged in the new concrete to increase its strength.

3.2.3 Water stop installation
Since a copper water stop might facilitate crack around the transverse joint, a flexible double vinyl chloride water stop was newly installed in the transverse joint.

3.2.4 Treatment of the crack section
In order to end the possibility of crack extension from inside the transverse joint, the crack section of the cut end was excavated in the shape of a trapezoid, and was filled up with highly adhesive repairing material (polymer cement).

3.3 Grouting to the rock foundation

A boring survey found some high permeability zones under the Blocks No.2 and No.3 near J2. So, grouting with fan-shaped layout was implemented from the inside of the inspection gallery to the bedrock to decrease the permeability. In addition, open cracks or fissures caused by the cliff topography were found in the boring cores of the bedrock, so grouting should be useful by reducing loosening. Some check borings will be conducted after the all grouting works in this year to confirm the permeability reduction and the void filling.

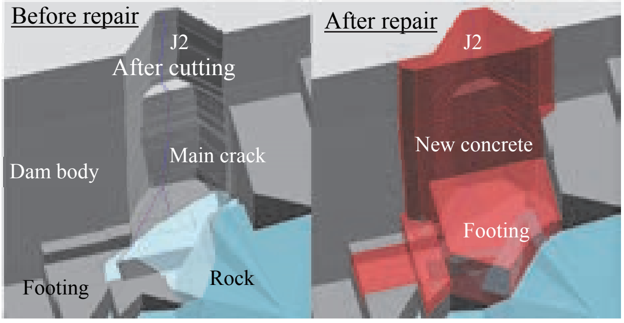

Figure 14. Image of the J2 joint repair

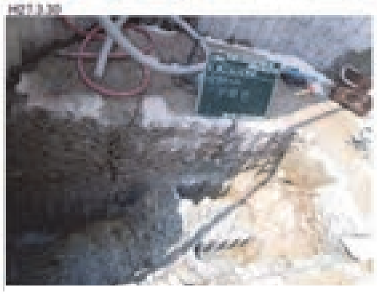

Deep cut in the rock foundation

Water-stop setting in the rock foundation

Crack break by the steel half pipe at EL193.3m

1st lift before concrete placing (EL193.3)

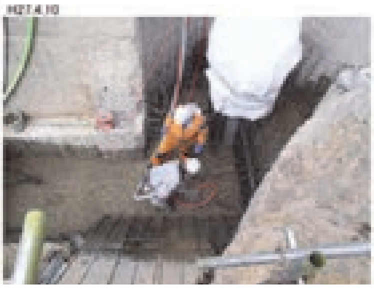

2nd lift before concrete placing (EL194.0)

3rd lift before concrete placing (EL194.75)

Joint bar setting to the old concrete body

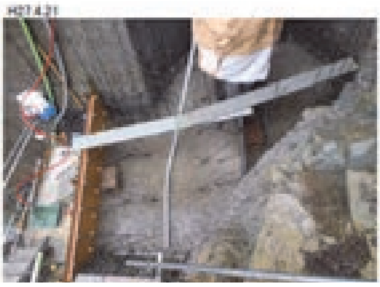

4th lift before concrete placing (EL195.5)

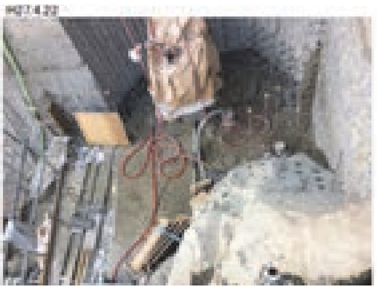

4th lift after concrete placing (EL196.25)

Figure 15. Reconstruction works of the J2 joint

4. CRACK DEVELOPIMG MECHANISM

From the cutting face observation, it was confirmed the main crack from the J2 joint was extending to the valley side of the upstream face through the left end of the copper water stop. On the other hand, the Blocks No.2~ 4 of the dam body rides on the steep slope of the cliff, and the slope face inclines steeply to the valley and downstream. For this reason, the crack direction might correspond with the topographic incline.

The largest external force that induced the above crack was presumably the Niigata Earthquake in 1964 (June 16, 1964, see Fig. 16), which generated quite strong shaking with seismic intensity of 5 on the JMA (Japan Metrological Agency) scale in this vicinity. Although placing concrete at the Kasabori dam ended in October, 1964, the earthquake struck in the middle of high elevation concrete placing in June, 1964. Since the dam concrete, which had not reached sufficient strength suffered from the very strong ground motion, it is easy to imagine that many invisible cracks and other damages might have occurred inside the dam body near J2 and other transverse joints at that time.

After the dam completion, water leakage at J2 of a maximum of 500 l/minute was observed in 1976. Although the leakage was decreased greatly by the J2 repair in 1974-79, the total leakage of the inspection gallery increased again to 100~150 l/min after 2000.

On October 23, 2004, the Mid Niigata Earthquake struck the Kasabori dam, causing extremely strong shaking, which recorded 622 cm/s^2 at the dam crest. Then, while the leakage from the inspection gallery decreased sharply, the leakage from the J2 downstream face increased remarkably. It seems, therefore, that the cracks to the downstream face were enlarged and the water-passageway was changed, by this earthquake.

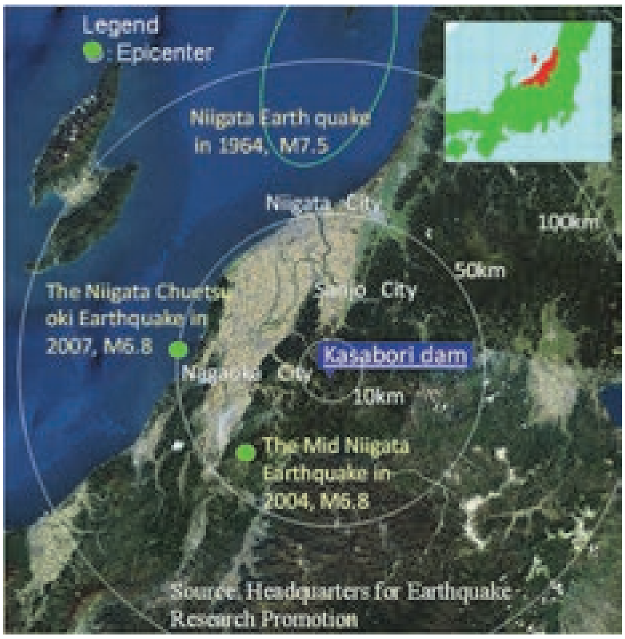
Legend
● : Epicenter
Niigata Earth quake in 1964, M7.5
Niigata City
100km
50km
Sanjo City
The Niigata Chuetsu oki Earthquake in 2007, M6.8
Kasabori dam
Nagaoka City
10km
The Mid Niigata Earthquake in 2004, M6.8

Source: Headquarters for Earthquake Research Promotion

Figure 16. Kasabori dam and the past major earthquakes

5. CONCLUSION

The conclusions are described below.

(1) From the cutting face observation of J2 and around, it was confirmed that the main crack from J2 was extending to the valley side of the upstream face.

(2) All the cracks around J2 were confirmed to be inside the cutting width, and it was judged that the cracked area influenced by the J2 behaviour was mostly removed.

(3) Since the boundary of the old and new concrete is vertical, it was necessary to increase its adhesion. So, on the boundary face, chipping of old concrete, setting the joint bar to the adhesion face, and setting reinforcing bars to reinforce the new concrete, etc. were implemented.

(4) The copper water stop was removed and double flexible vinyl chloride water stops were installed. In addition, the opening crack around the back of the water stop was cut off deeply, and filled with polymer cement.

(5) High permeability zones with open cracks or fissures were found in the bedrock under the Block No.4 and NO.3 by the cliff topography. Thus, the grouting work was performed to reduce the permeability and loosening.

(6) The original cause of the leakage in the J2 joint was presumed to be the big impacts of the Niigata Earthquake in 1964, and the heavy freezing-thawing facilitated the concrete deterioration, and the Mid Niigata Earthquake in 2004 gave the damage around J2.

The following are future subjects to be checked.

a. Checking the effect of the dewatering works: During full impoundment in 2017, the water stop effect of the J2 repair will be confirmed.

b. J2 repair from the inspection gallery: The inspection gallery (near EL 201m) is very close (about 1m) to the cutting area. So, it is necessary to complete the water leakage repair from the inspection gallery after the check during impounding has been done.

Finally, the main work for dam heightening will starts in April, 2016. The concrete will be placed on the downstream face. Since the horizontal thickness of the new concrete is as thin as 2m, advanced countermeasures against temperature cracks are due to be performed.

ACKNOWLEDGEMENT

I sincerely appreciate the cooperation given by the staff members of Niigata prefecture and KAJIMA Corporation for this paper on the Kasabori dam redevelopment project.

REFERENCES

Kawasaki, H., Itoh, H., Yaegashi, H., (2014): Repair of aged deterioration and visual inspection of the Tohno dam ten years later, the 8th EADC Symposium, 2-2

The Upper-Pond Remedial Project of Lam Ta Khong Hydropower Plant for Reducing Long Term Deformation

N.CHAOWALITTRAKUL, S.THONGJAENG&N.RAPHITPHAN
Dam Safety Review Section, Dam Safety Department, Civil Maintenance Division,
Electricity Generating Authority of Thailand, Thailand
Nampol.c@egat.co.th

ABSTRACT:

Lam Ta Khong hydropower plant is a pumped-storage hydropower plant which consists of the Upper-Pond in order to store the water which pumped up from Lam Ta Khong reservoir. The Upper-Pond is a rock-filled dam with asphalt facing. After the operation period, the dam monitoring showed the high rate of displacement on the dam crest and downstream slope.

The safety assessment of the Upper-Pond was done in 2011. It was concluded that the material of downstream side contains high volume of claystone which has high degree of degradation. However, the result of the analysis showed that the Upper-Pond was still safe but if we neglect this problem, the factor of safety would be decreased and the upper-pond will not be safe in the near future. Therefore, the remedial design criteria were implemented by using a geo-synthetic clay liner with textured HDPE (GCL with textured HDPE) covered on the downstream side of the Upper-Pond in order to protect claystone from rain. After remedial work has been completed in 2013, there is downward trend in term of displacement rate. The result shows that the design criteria of remedial project are effective and can maximize the service life of the upper pond.

Keywords: Displacement, Geo-Membrane, Claystone

1. INTRODUCTION

Lam Ta Khong hydropower plant is a pumped-storage hydropower plant located in northeastern Thailand. There is the Upper-Pond in order to store the water which pumped up from reservoir as shown in Fig. 1.

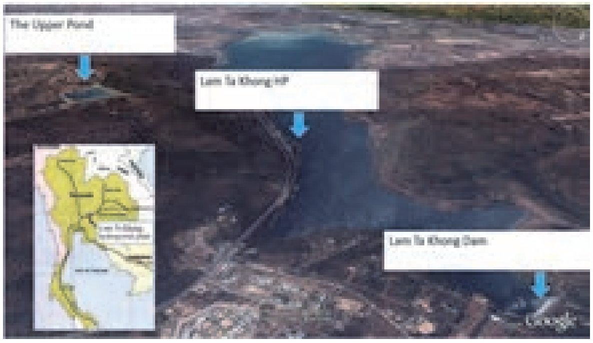

Figure 1. The location of Lam Ta Khong hydropower plant

The Upper-Pond is a rock-filled dam with asphalt facing. During the impounding in the Upper-Pond, the leakage was founded. After lowering water level, a damaged area was identified. Investigation on the damage led to the cause of the incident. In summary, deformation in claystone foundation causes the leakage of asphaltic facing. Therefore, impervious membrane, high density polypropylene (HDPE), was installed on the upstream face to be a seepage barrier. Subsequently, the leakage was not found anymore.

The general description of the Upper-Pond and the typical section of the Upper-Pond are shown in Fig. 2 and Table 1, respectively.

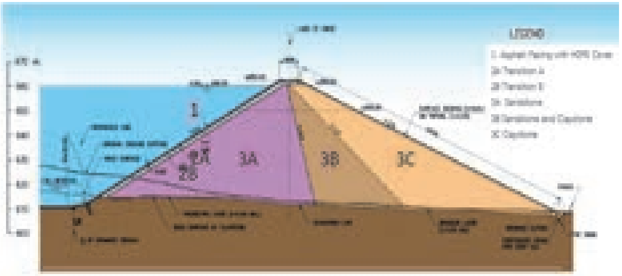

Figure 2. Typical section of the Upper-Pond

Table 1. The general description of the Upper-Pond

Type of Dam	Rock-filled dam with asphalt facing.
Height	50 m.
Crest Elevation	+662.00 m.MSL.
Crest Length	2,170 m.
Reservoir Surface Area	0.34 sq.km.
Normal Height Water Level	9.9 MCM
Design Earthquake	0.05g

1.1. Settlement and displacement characteristics

In order to monitor the settlement and displacement of the Upper-Pond, surface settlement and displacement points were installed along the dam crest as shown in Fig. 3.

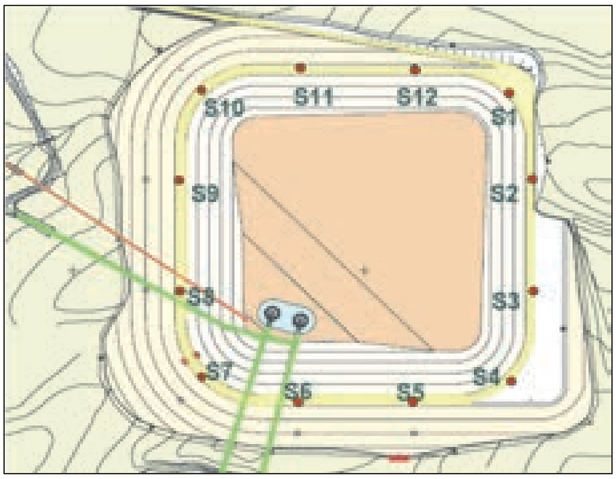

Figure 3. Layout of the surface settlement and displacement points

The result indicated that settlement and displacement appeared to be slightly higher than usual.

As a result, EGAT in cooperation with Kasetsart University (KU) initiated dam safety assessment project to evaluate the safety condition of the Upper-Pond. The remedial design finished in 2011.

1.2. The safety assessment of the Upper-Pond

The safety assessment of the Upper-Pond was started and finished in October 2010 and May 2011 respectively. There were various types of testing such as standard penetration testing (SPT), large direct shear test, conventional triaxial test and resistivity survey. The result of these testing was used as parameters in numerical analyses.

According to results of the testing and the finite element model, they ensure that the claystone in random zone (3C) has high degradation rate, particularly when it directly contacts with rain. In addition, the results of numerical analysis concluded that the stability of the Upper-Pond was still safe but if we neglect this problem and let the high degree degradation of claystone occur, the safety factor would be decreased and the Upper-Pond will not be safe in the near future (GERD 2010).

Therefore, the remedial design criteria were implemented by using the impervious membrane, covering on the downstream side of the Upper-Pond in order to protect claystone from rain.

2. THE UPPER-POND REMEDIAL DESIGN

The objective of the remedial design was to design an impervious membrane, covering on the random zone at downstream in order to protect the random zone (3C) which made from claystone (Nampol 2014). The component of the Upper-Pond remedial design is shown in Fig. 4.

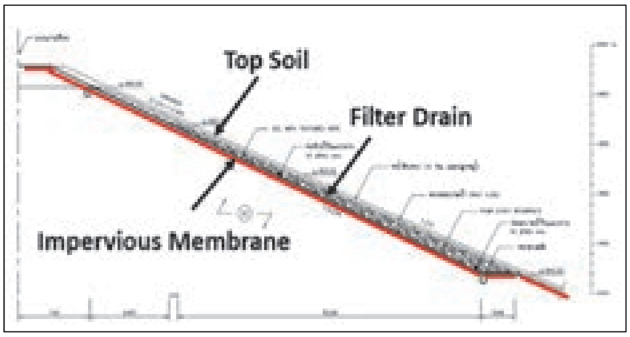

Figure 4. Typical section of the Upper-Pond

2.1. Geo-synthetic Clay Liner (GCL) with textured HDPE

GCL was selected to be an impervious membrane. There are many advantages of GCL as follows:

- GCL is difficult to deteriorate because bentonite, which is the component of GCL, is a natural mineral.
- GCL has a self-sealing properties.
- GCL is easy to install.

However, a slip surface failure was still considered, a special layer was designed to increase the friction angle by using a HDPE. The HDPE sheet was added in the GCL sheet as shown in Fig. 5.

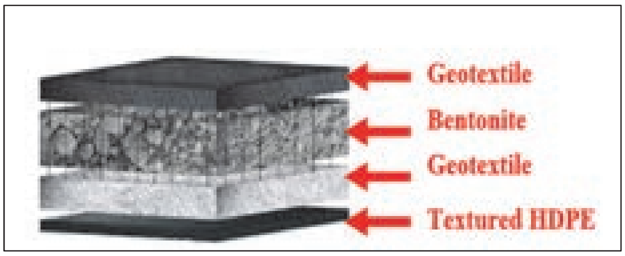

Figure 5. The component of GCL with textured HDPE

2.2. Filter drain

After the impervious membrane have already been installed, water pressures and hydraulic gradients behind and around the impervious membrane are likely to increase. Therefore, the filter drain was designed in order to release the pore water pressure, occurring from rain and increase the stability of downstream side.

The filter drain consists of sand and rock. The main factor that play an important role of design is a permeability. The technical specification required permeability more than 10^{-3} cm/s.

2.3. Top Soil

Top soil with 0.3-meter thickness was designed to place on the downstream slope for surface seeding to ensure good scenery in harmony with surrounding nature. Furthermore, surface seeding can protect the top soil from surface erosion.

3. THE UPPER-POND REMEDIAL PROJECT

The Upper-Pond remedial project was started on January 2012 and completed in December 2013. The remedial project area is 186,510 m^2 as shown in Fig. 6.

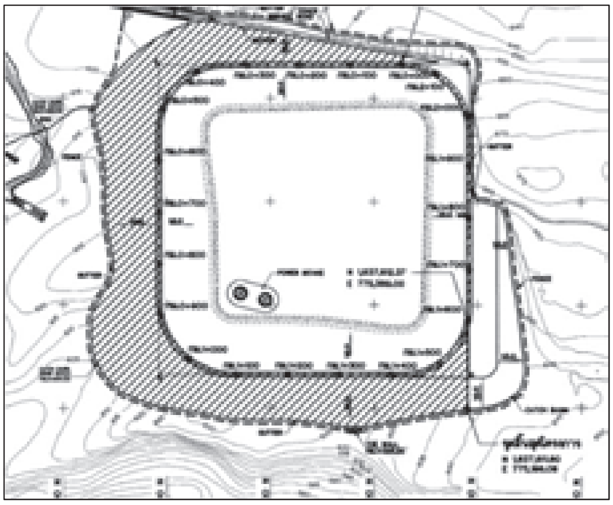

Figure 6. The remedial project area

3.1. Remedial Procedure

3.1.1. Surface excavation

The main objective of surface excavation is to prepare the surface area on the downstream slope in order to place GCL with textured HDPE and fill with filter drain and top soil. Due to the length of downstream, GCLs with textured HDPE are required to cover the whole area. This is a reason why the trench was designed for anchorage between upper and lower sheet of GCL as shown in Fig. 7 and 8. Besides, the benching was designed to be working area for machine under excavated anchored trench.

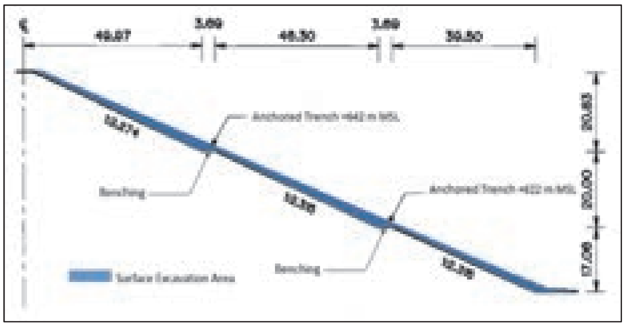
49.07
3.00
48.30
3.00
30.50
Anchored Trench +642 m MSL
Benching
Anchored Trench +622 m MSL
Benching
Surface Excavation Area
20.83
20.00
17.06

Figure 7. The location of anchored trench

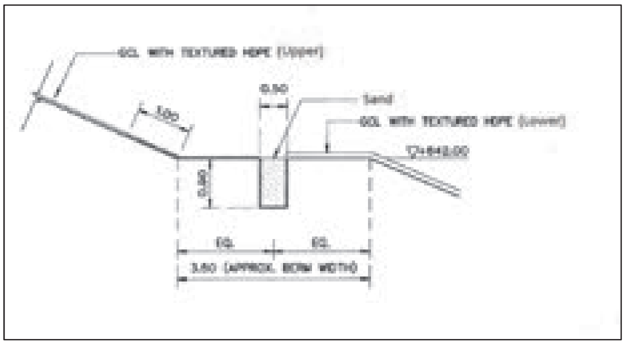
GCL WITH TEXTURED HDPE (Upper)
0.50
Sand
GCL WITH TEXTURED HDPE (Lower)
3.00
▽+642.00
0.80
EQ.
EQ.
3.60 (APPROX. BERM WIDTH)

Figure 8. The section detail of anchored trench

The surface excavation was commenced on May 2012 and finished in January 2013 as shown in Fig. 9and 10.

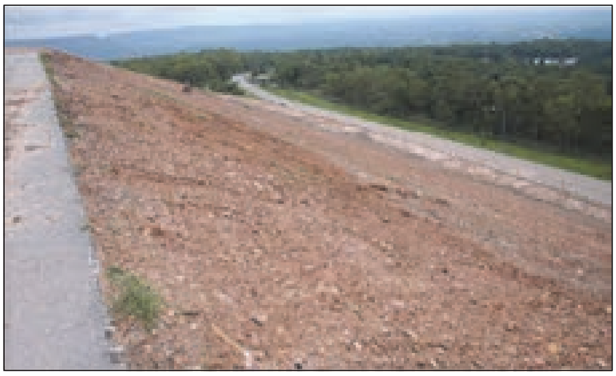

Figure 9. The surface excavation

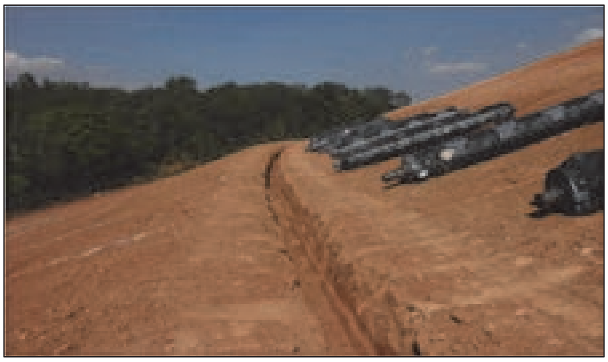

Figure 10. The anchored trench

3.1.2. GCL with textured HDPE Installation

The GCL with textured HDPE was installed by placing on the downstream slope of the Upper-Pond as shown in Fig. 11. In general, the GCL with textured HDPE cannot resist the ultra violet radiation; therefore, the filter drain need to be filled above the GCL with textured HDPE immediately.

In accordance with the GCL standard guideline, it recommends that overlapping should not be less than 0.30 m. Nevertheless, the displacement is still concern; as a result, the designer decided to use 1.0 m. overlapping length.

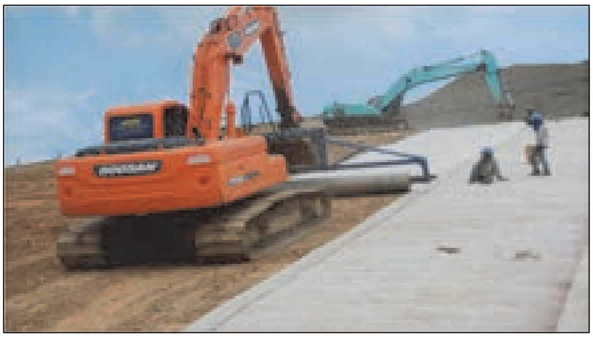

Figure 11. The GCL with textured HDPE installation procedure

3.1.3. Filter drain and top soil

Filter drain, which consists of sand and rock, was designed to release pore water pressure on the downstream side. Fig. 12 shows the filling of the filter drain.

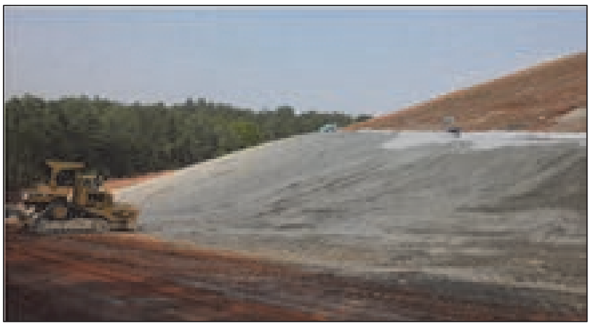

Figure 12. Filling the filter drain.

Top soil layer is placed beyond the filter drain in order to do surface seeding as shown in Fig. 13.

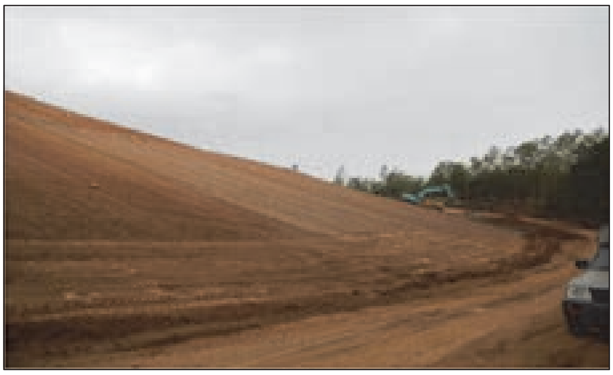

Figure 13. Filling the top soil layer

3.2 Instrumentation

Additional instruments were installed as follows:

3.2.1. Surface settlement and displacement

After the surface excavation was finished, the surface settlement and displacement points were removed. Therefore, the new settlement and displacement points were installed in new location as shown in Fig. 14. However, the new location is not much far from the former location in order to compare the settlement and displacement rate between before and after remediation.

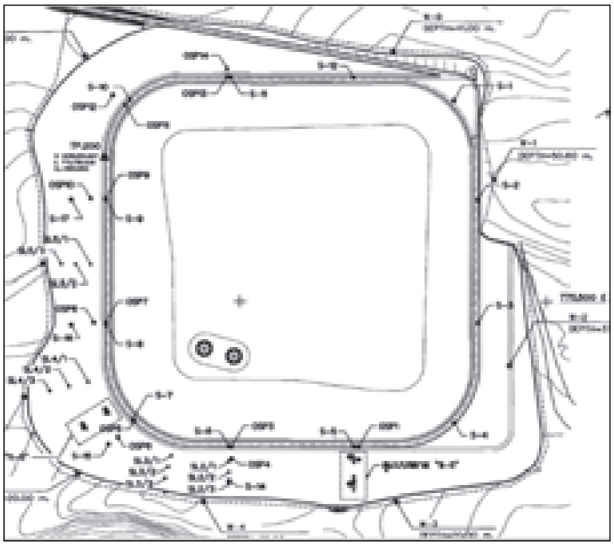

Figure 14. The location of new settlement and displacement points

3.2.2. Magnetic Extensometer

Previously, the Upper-Pond had only surface settlement and displacement points. Thus, the magnetic extensometers were chosen to install at Sta.0+950 and Sta.1+125 to monitor the internal settlement of the Upper-Pond.

3.2.3. Shape Accel Array (SAA) Inclinometer

SAA inclinometers were selected to use in this project in order to monitor the internal displacement in the

Upper-Pond. The shape accel array (SAA) inclinometers were installed at Sta.0+950 and Sta.1+250 nearby the magnetic extensometers. The advantages of SAA are shown below:

- The measurement is highly accurate, including the full height of area of interest.
- Real-time displacement data collection.
- 3 direction of displacement can be observed.

4. POST-REMEDIATION SETTLEMENT AND DISPLACEMENT OF THE UPPER-POND

After the remedial work was completed in 2013, the settlement and displacement monitoring have already started. Recently, all of instruments are used to assess the dam safety condition of the Upper-Pond.

According to the data from the instrument, it reveals that the surface settlement and displacement rate after remedial work have a downward trend as shown in Fig. 15.

Magnetic extensometer and SAA inclinometer do not show the unusual characteristic of the Upper-Pond.

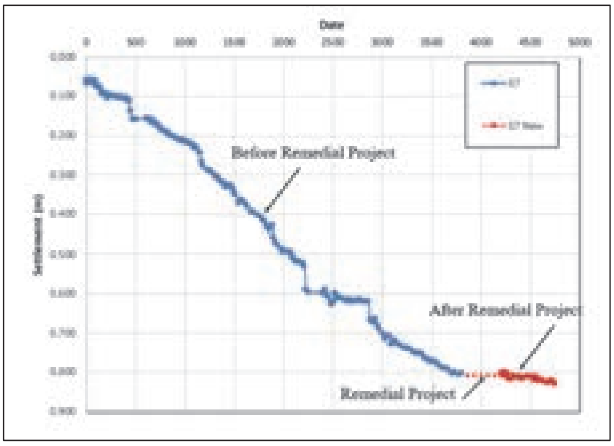

a) Surface settlement of the Upper-Pond

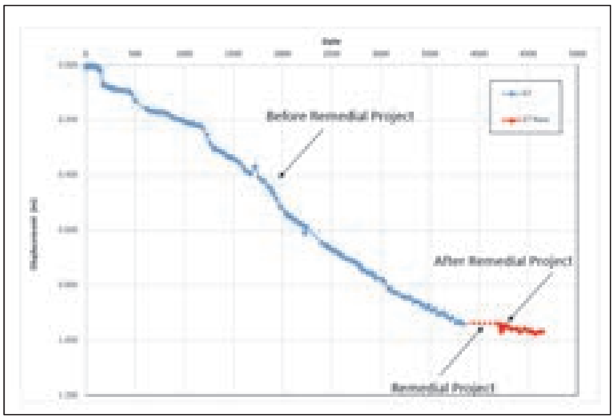

b) Surface displacement of the Upper-Pond

Figure 15. Post-remediation settlement and displacement of the Upper-Pond

5. CONCLUSION

According to the collected data, settlement and displacement of the Upper-Pond have increased over time since the first time of operation. The safety assessment of the Upper-Pond project can be concluded that the shell material of downstream side contains high volume of claystone which has high degree of degradation in rainy season. However, the result of stability analysis showed that the Upper-Pond was still safe but if we neglect this problem and let the high degree degradation of claystone occur, the safety of factor would be decreased and the Upper-Pond will not be safe in the near future. As a result, the remedial design criteria were implemented by using the GCL with textured HDPE as the impervious membrane, covering on the downstream side of the Upper-Pond.

After remedial work has been completed in 2013, there is a downward trend in term of deformation rate. The result shows that the design criteria of remedial project are effective and can maximize the service life of the Upper-Pond. Nevertheless, EGAT has regularly monitored the settlement and displacement characteristics of the Upper-Pond in order to assess the safety condition of the Upper-Pond after renovation.

ACKNOWLEDGEMENT

The authors would like to express their gratitude to Mr.Pakorn Kijsomporn, Head of Dam Safety Department, Mr.Danai Wattanadilokkul, Civil Engineer Level 10, Dam Safety Department and Mr.Potcharapol Brohmsubha, Civil Engineer Level 5, Dam Safety Department for excellent guidance and strong support.

REFERENCES

Electric Power Development Co., LTD (EPDC). 2002: Lam Ta Khong pumped storage project contract No. EGAT 47/8-32-5021. Technical Report Volume 1: Electricity Generating Authority of Thailand, EGAT.

Geotechnical Engineering Research and Development (GERD) 2010. Completion report stability analysis of the LTK Project. Bangkok, KU.

Geosynthetic Institute, 2013: Design considerations for Geosynthetic Clay Liners (GCLs) in various applications.

Nampol Chaowalittrakul 2015: The Analysis of the Displacement of the Upper-Pond of Lam Ta Khong Hydropower Plant and Its remedial design, 3th Long Term Behavior of Dam conference. Nanjing, China.

4th APG Symposium and 9th EADC on

INNOVATIVE TECHNOLOGIES FOR DAMS AND RESERVOIRS TOWARD THE FUTURE GENERATIONS

Vertical Multi-Holed Double-Pipe System: A New Sediment Suction Method Utilizing a Natural Head

A. Hisano & S. Oota
Chigasaki Research Institute, Electric Power Development Co., Ltd.(J-power), Japan
akihiro_hisano@jpower.co.jp

K. Maeda
Electric Power Development Co., Ltd.(J-power), Japan

ABSTRACT:
At present, the sediment removal method using a suction pipe is the subject of research as an effective method for discharge of accumulated sediment in dam reservoirs. Vertical Multi-Holed Double-Pipe System is one of these methods and has been researched by the authors for the application to an actual reservoir. This system is expected to reduce the cost of removing sediment accumulated repeatedly around a local place such as the neighborhood of the intake. This paper explores the following topics: methods and results of the laboratory tests of the system; the hydraulic design method based on the laboratory tests; and the estimation of sediment concentration in the discharge flow.

Keywords: sediment removal, suction pipe, vertical multi-holed double-pipe system

1. INTRODUCTION

At present, the hydro-suction sediment removal system is researched as an effective method for discharge of accumulated sediment in dam reservoirs. The method is to discharge sediment to the lower reaches of the dam utilizing the natural head between the reservoir water level and the outlet of the pipe.

This paper presents a new hydro-suction sediment removal system called “Vertical Multi-Holed Double-Pipe System (Maeda, K., et al. 2015).” The purpose of this system is periodical sediment removal at a local area such as the neighborhood of a water intake facility. The vertical multi-holed double pipe is composed of an outer pipe and an inner pipe, which enable the system to suck sediment continuously by negative pressure occurred between the two pipes.

This paper investigates the following three topics. First, laboratory tests using a small model and quasi-full-scale model were carried out in order to estimate the suction ability. Secondly, the hydraulic design method was established from the test results. Finally, the estimation method for sediment concentration in the pipe based on the flow and pressure was established.

2. OUTLINE OF VERTICAL MULTI-HOLED DOUBLE-PIPE SYSTEM

Conceptual figures of installation of Vertical Multi-Holed Double Pipe System and its hydraulic mechanism are shown in Fig. 1 and Fig. 2, respectively. The system is composed of an outer pipe and inner pipe. The outer pipe is equipped with suction holes on its side, while the inner pipe is equipped with suction holes with gates on its side. This structure has a clearance between the outer and inner pipes, which makes it possible to suck the sediment continuously even if the pipes are buried in sediment. The sediment removal area by this system is not very large because the pipe is fixed on the dam body. However, this system is expected to reduce the cost of removing sediment accumulated repeatedly around a local place such as the neighborhood of the intake.

The system is installed on the dam body. First, the pipe flow reaches steady state in a few minutes after the valve is opened. Next, the system begins to suck the sediment after the higher and lower suction holes on the inner pipe are opened. After the start of sediment discharge, the system is expected to suck sediment through the suction holes using the water head difference. After discharge of the sediment is completed, its surface becomes hemiconical shaped centered by the vertical pipe. The slope gradient is determined by the underwater angle of repose.

3. LABORATORY TEST USING A SMALL MODEL AND ESTABLISHMENT OF THE HYDRAULIC DESIGN METHOD

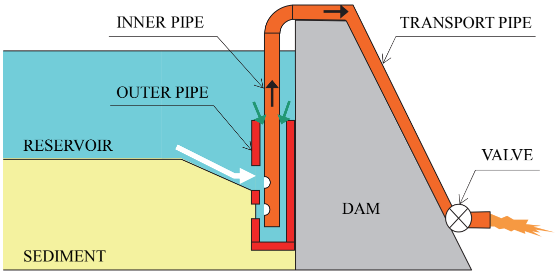
INNER PIPE
TRANSPORT PIPE
OUTER PIPE
RESERVOIR
VALVE
DAM
SEDIMENT

Figure 1. Conceptual figures of installation of the Vertical Multi-Holed Double Pipe System.

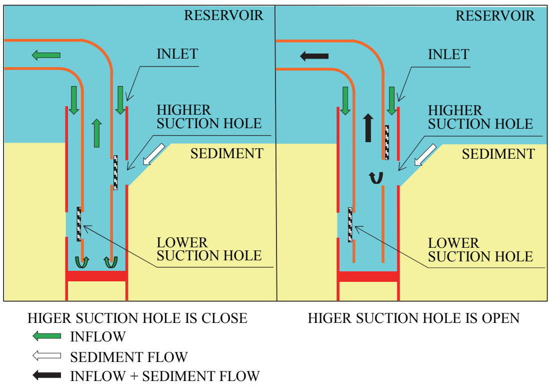
RESERVOIR
INLET
HIGHER SUCTION HOLE
SEDIMENT
LOWER SUCTION HOLE
RESERVOIR
INLET
HIGHER SUCTION HOLE
SEDIMENT
LOWER SUCTION HOLE
HIGER SUCTION HOLE IS CLOSE
HIGER SUCTION HOLE IS OPEN
INFLOW
SEDIMENT FLOW
INFLOW + SEDIMENT FLOW

Figure 2. Hydraulic mechanism of Vertical Multi-Holed Double Pipe System.

3.1. Conditions of the laboratory test

The authors carried out the laboratory test using a small model in order to estimate the suction ability. The profile of the experimental facilities and the installed positions of the pressure meters are shown in Fig. 3. The measured values of pressure meter were used for verification of the hydraulic design method. The tank used for the laboratory test was 5 m in length, 2.6 m in width, and 2.6 m in height. The authors installed the small model of the system in the tank, and buried it in the sediment whose thickness was 1.4 m. The sediment removal laboratory test was carried out keeping the head about 4.4 m. The items of measurement and observation during sediment discharge were as follows: 1) suction pipe pressure by the pressure meter; 2) suction pipe flow by the electromagnetic flow meter; 3) sediment concentration at the outlet of the suction pipe by sampling of water; and 4) observation of the flow in the suction pipe by video camera. After sediment discharge, the quantity of discharge sediment was estimated by measuring the surface of the remaining sediment. The diameter of the inner pipe was fixed as 0.2 m. The diameters of the outer pipe and the suction holes were varied as shown in Table 1. The suction abilities of the system in each case were estimated.

3.2. Results of the laboratory test

The results are shown in Table 2. The findings obtained from the laboratory test are as follows:

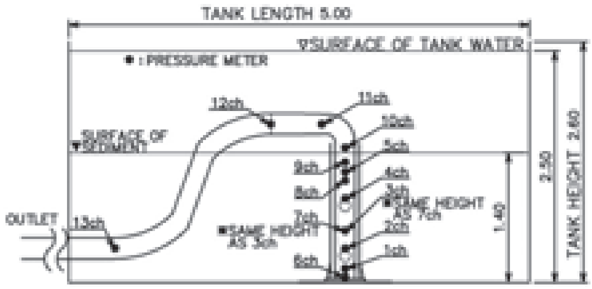
TANK LENGTH 5.00
SURFACE OF TANK WATER
● : PRESSURE METER
12ch
11ch
10ch
SURFACE OF SEDIMENT
5ch
9ch
4ch
8ch
3ch
SAME HEIGHT AS 7ch
OUTLET
13ch
7ch
SAME HEIGHT AS 3ch
2ch
1ch
6ch
1.40
2.50
TANK HEIGHT 2.60

1 ~ 5 ch. : THE INNER PIPE
6 ~ 9 ch. : THE OUTER PIPE
10 ~ 13 ch. : THE TRANSPORT PIPE

Figure 3. Profile of the experimental facilities and installed positions of the pressure meters (m).

Table 1. Diameter conditions

Case	Inner pipe(m)	Outer pipe(m)	Suction holes(m)
1	0.2	0.3	0.12
2	0.2	0.4	0.12
3	0.2	0.4	0.20

Table 2. Results of the laboratory test

Case	Average flow (L/sec)	Suction ability (m^3/h)	Max sediment concentration (%)
1	54.1	13.2	17.4
2	63.0	8.5	4.0
3	58.0	9.5	17.4

- When the diameter of the inner pipe is the same, the velocity head around the suction holes and the sediment suction ability are greater when the diameter of the outer pipe is smaller than when the diameter is larger (from the comparison between Case 1 and Case 2).
- When the diameters of both the inner and the outer pipes are fixed, the sediment suction ability is greater when the diameter and the suction area of the suction holes are larger than when they are smaller (from the comparison between Case 2 and Case 3).

3.3. Establishment of the hydraulic design method

For the purpose of hydraulic design for the full-scale facilities of Vertical Multi-Holed Double-Pipe System, the hydraulic design method for sediment transportation was established and verified by the results of the pressure meters, which is based on Bernoulli's equation (Eq. 1).

$$H = \frac{1}{2g}\left(\frac{Q}{A}\right)^2 + \frac{p}{\rho g} + z + \sum h_L \,, \tag{1}$$

where,

H: Total head (m)
g: Gravity acceleration (m/s^2)
Q: Pipe flow (m^3/s)
A: Pipe section area (m^2)
p: Pipe pressure (Pa)
ρ: Flow density (kg/m^3)
z: elevation head (m)
h_L: Head loss (m)

The forth term of the right-hand side in Eq. 1 was headloss, composed of shape loss and friction loss. Friction loss h_f is shown in Eq. 2. When the pipe flow contains sediment, the value of h_f increases because friction loss coefficient λ increases as shown in Eq. 3.

$$h_f = \lambda \frac{1}{2g}\left(\frac{Q}{A}\right)^2 \frac{L}{D}, \tag{2}$$

$$\lambda = \lambda_w + \lambda_s = \lambda_w\left(1 + \phi C\right), \tag{3}$$

where,

h_f: Friction loss (m)
λ: friction loss coefficient
L: Pipe length (m)
D: Pipe diameter (m)
λ_w: Friction loss coefficient in flow
λ_s: Additional friction loss coefficient in sediment flow
ϕ: Pressure loss coefficient
C: Sediment concentration (%)

Pressure loss coefficient ϕ was determined by Kazenskij's equation (Eq. 4), in which particle size distribution can be taken into consideration (Kazanskij, I. 1978). The other loss is estimated based on the references(Anderson, A.G., et al. 1948, Okano, M., et al. 2004).

$$\phi = 180 D^{0.5} V^{-3}\left(\overline{Fr_{xj}{}^{1.5}}\right)^{0.5}, \tag{4}$$

Where,

$\overline{Fr_{xj}{}^{1.5}} = \sum \left(Fr_{xj}\right)^{1.5} X_n \big/ 100$
Fr_{xj}: Froude number based on diameter and settling velocity
X_n: Weight percentage based on particle size distribution
V: Mean velocity

The calculated (solid line) and measured (closed circle) values of the pressure head in the pipe are shown in Fig. 4. The lower suction hole is installed between 2 ch and 7 ch. As the cross-section area of the pipe varies, the calculated value of the pressure head also varies greatly along this section. Except for the above-mentioned section and that the calculated pressure head at 11 ch was a little higher than the measured value, the calculated higher values of the pressure head coincided with the measured values. On the whole, it was confirmed that the hydraulic design method could reproduce the pressure head along the pipe.

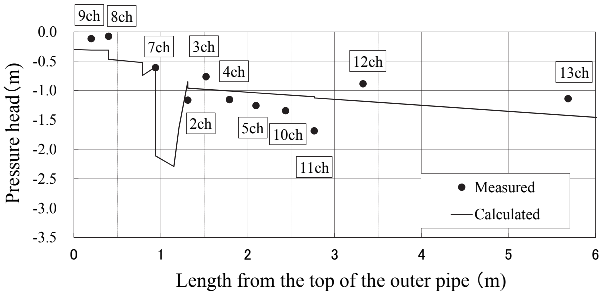

Figure 4. Comparison of measured and calculated values.

4. LABORATORY TEST USING A QUASI-FULL-SCALE MODEL AND ESTIMATION OF SEDIMENT CONCENTRATION

4.1. Conditions of the laboratory test

Aiming to apply the system to an actual reservoir, the authors carried out a laboratory test using a quasi-full-scale model based on the results of the laboratory test using a small model. As the thickness of the sediment layer in actual dams is about 5.0 m, the scale of the quasi-full-scale model is from about 1/3 to 1/2 for the model that is installed at an actual dam. The profile of the quasi-full-scale model and installed position of measurements are shown in Fig. 5. The facility specifications of the quasi-full-scale model are shown in Table 3.

In order to avoid pipe blockage depending on increasing sediment concentration in the suction pipe, the quasi-full-scale model has another pipe called the "water supply pipe." The pipe can supply the water from the surface of the water tank to the suction pipe. Therefore, the water supply pipe is used to reduce the sediment concentration in the pipe when the sediment concentration in the pipe is excessive.

Mixed-particle-size sand was used as the sediment material for the laboratory test. The 50% particle diameter is about 0.4 mm. The particle size distribution curve is shown in Fig. 6. The water tank used for the laboratory test was 6.0 m in length, 4.7 m in width, and 5.0 m in height. The authors installed the quasi-full-scale model of the system in the tank and buried it in the sediment whose thickness is 2.2 m. The sediment removal laboratory test was carried out keeping the head about 4.4 m. The items of measurement and observation during sediment discharge are as follows: 1) suction pipe pressure by the pressure meter; 2) suction pipe flow by the ultrasonic flowmeter; 3) sediment concentration at the outlet of the suction pipe by sampling of water; and 4) observation of the flow in the suction pipe by video camera. After sediment discharge, the quantity of discharge sediment was estimated by measuring the surface of the remaining sediment.

4.2. Results of the laboratory test

The results of the test are shown in Fig. 7: suction pipe flow including water supply pipe flow; water supply pipe flow; sediment concentration at the outlet of the suction pipe; and sediment thickness around the suction pipe. After opening the higher suction hole, the sediment

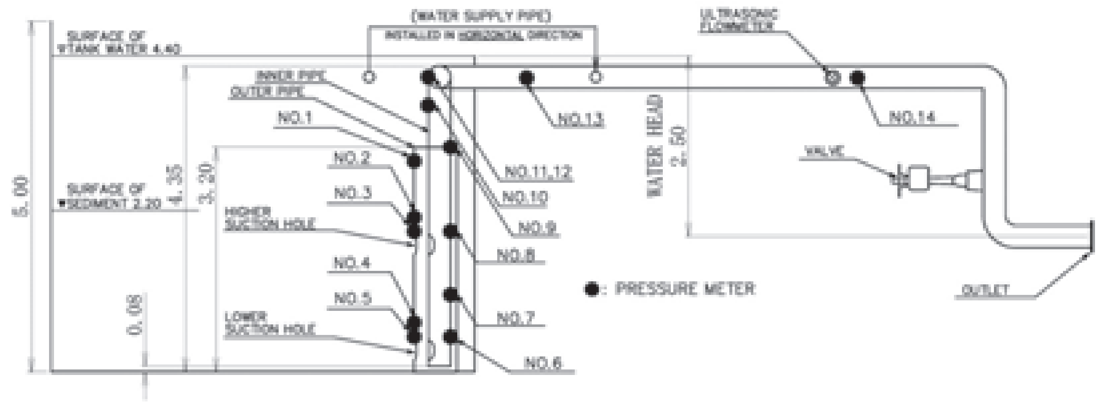
(WATER SUPPLY PIPE)
INSTALLED IN HORIZONTAL DIRECTION
ULTRASONIC FLOWMETER
SURFACE OF TANK WATER 4.40
INNER PIPE
OUTER PIPE
NO.1
NO.2
NO.3
HIGHER SUCTION HOLE
NO.4
NO.5
LOWER SUCTION HOLE
SURFACE OF SEDIMENT 2.20
5.00
4.35
3.20
0.08
NO.13
NO.14
NO.11,12
NO.10
NO.9
NO.8
NO.7
NO.6
WATER HEAD 2.50
VALVE
●: PRESSURE METER
OUTLET

Figure 5. Profile of the quasi-full-scale model and installed position of measurements (m).

Table 3. Facility specifications of the quasi-full-scale model

Inner pipe	Diameter	0.30 m
	Height	4.35 m
Outer pipe	Diameter	0.60 m
	Height	3.20 m
Suction holes	Diameter	0.28 m
	Higher height	1.36 m
	Lower height	0.17 m
Water supply pipe	Diameter	0.15 m
	Length	4.0 m
Transport pipe	Diameter	0.30 m
	Total length	10.8 m

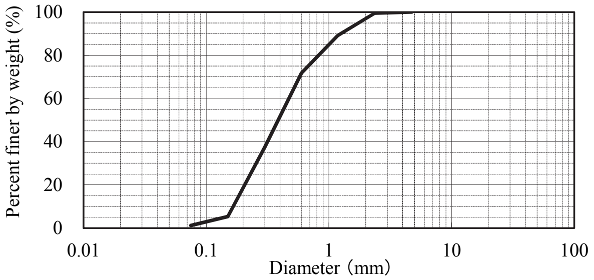

Figure 6. Particle size distribution curve of sediment material.

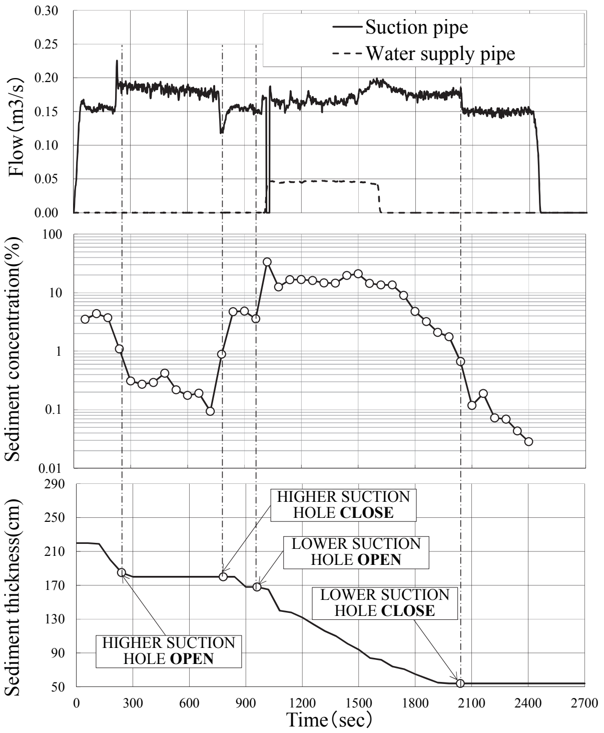

Figure 7. Results of the laboratory test using a quasi-full-scale model.

concentration of the discharge flow and the sediment thickness were not greatly changed in spite of increasing the suction pipe flow. Because the sediment level of the laboratory test was a little higher than the higher suction hole, the hole did not suck much sediment. However, after opening the lower suction hole, the suction pipe flow changed greatly. Because the sediment level of the laboratory test was higher than the lower suction hole, the hole could suck much sediment. Therefore, the suction pipe was almost blocked in response to the rapid increase in sediment concentration in the suction pipe. The sediment concentration of the discharge flow at this time was 33.6%, and the sediment accumulated at the bottom of the horizontal part of the transport pipe. After starting supply from the water supply pipe, the sediment concentration of the discharge flow was reduced to about 10% and the suction pipe flow became steady. After that, the sediment concentration of the discharge flow gradually decreased. The sediment of the laboratory test was continuously sucked until the lower suction hole was closed. The shape of discharge sediment measured at the surface of the remaining sediment is shown in Fig. 8. After discharge of the sediment is completed, its surface becomes hemiconical shaped centered by the vertical pipe. The slope gradient is determined by the underwater angle of repose. At traverse line Ⅳ, the sediment above 0.33 m was sucked. The quantity of sucked sediment was about 15 m^3. The time was 40 minutes until the end of discharge.

4.3. Verification of the hydraulic design method

Based on the results of the quasi-full-scale laboratory test, the hydraulic design method was verified. The calculated value of the pressure head at the transport pipe, which is used to measure the sediment concentration of the

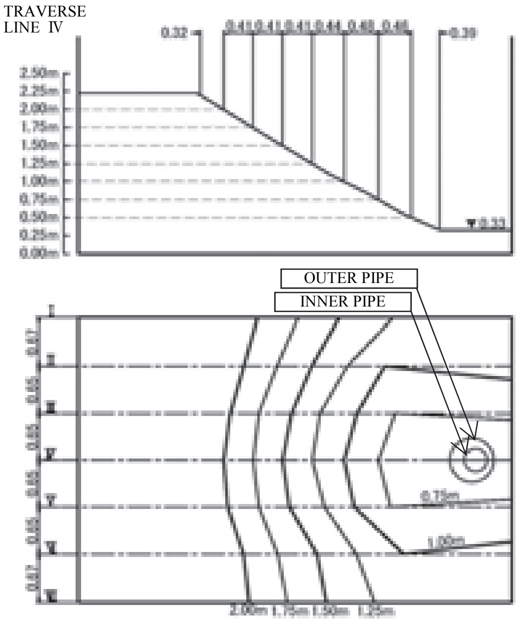
TRAVERSE
LINE Ⅳ
0.32
0.41
0.41
0.41
0.44
0.48
0.46
0.39
2.50m
2.25m
2.00m
1.75m
1.50m
1.25m
1.00m
0.75m
0.50m
0.25m
0.00m
0.33
OUTER PIPE
INNER PIPE
Ⅰ
Ⅱ
Ⅲ
Ⅳ
Ⅴ
Ⅵ
Ⅶ
0.75m
1.00m
2.00m 1.75m 1.50m 1.25m

Figure 8. Shape of discharge sediment.

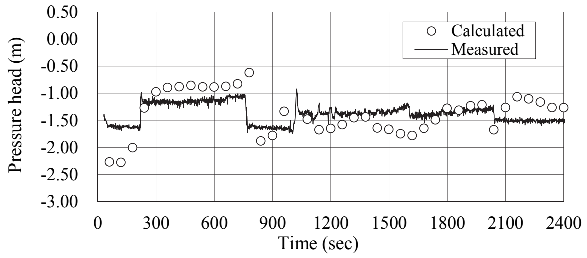

Figure 9. Comparison of measured and calculated values.

discharge flow and the suction pipe flow, and the measured value (11ch) of the pressure head at the transport pipe are shown in Fig. 9. As shown in Fig. 9, the calculated value of the pressure head coincided with the measured value on the whole. Therefore, it was verified that the hydraulic design method can be applied to quasi-full-scale facilities using Vertical Multi-Holed Double-Pipe System.

4.4. Hydraulic design of verification test facilities using the hydraulic design method

The hydraulic design procedure for verification test facilities is shown in Fig. 10. The parameters used for hydraulic design method are shown in Table 4. Basic specification of the verification test facilities was determined using the method. When the method is applied to assumed facilities, it is possible to judge whether it can suck the target sediment or not based on the particle size of the target sediment. In addition to the following parameters used by the method, this method used the parameters shown in Table 4: total head; diameter of the inner and outer pipe; diameter of the suction hole; transportation distance; suction pipe flow; and sediment concentration in the suction pipe.

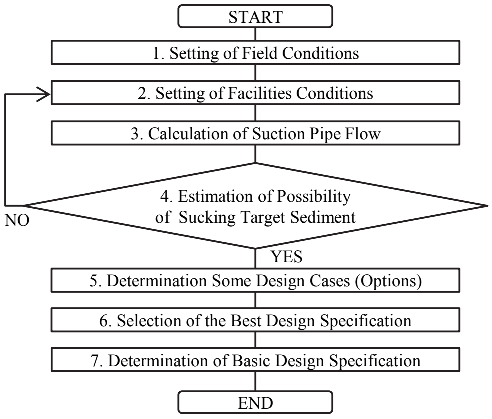
START
1. Setting of Field Conditions
2. Setting of Facilities Conditions
3. Calculation of Suction Pipe Flow
4. Estimation of Possibility of Sucking Target Sediment
NO
YES
5. Determination Some Design Cases (Options)
6. Selection of the Best Design Specification
7. Determination of Basic Design Specification
END

Figure 10. Hydraulic design procedure.

Table 4. Parameters used for the hydraulic design method

Inflow loss coefficient at suction holes (Estimated from results of lab test)		0.1
Shape losses	Inlet	1.0
	Section changed sharply	0.3
	Curve at suction hole	1.0
	Curve at elbow of transport pipe	θ = 90° [3)]
Roughness degree of suction pipe		0.013(Steel) 0.0105(Acryl, VP)
Friction loss in sediment flow (α :Correction coefficient)		$Fr_{xi}^{1.5}$=0.50 α =1.65

Table 5. Consideration cases

Item	Case 1	Case 2	Case 3
Total head	2.0 m	3.0 m	4.0 m
Inner pipe diameter	I. 500 mm II. 400 mm III. 300 mm	I. 500 mm II. 400 mm III. 300 mm	I. 500 mm II. 400 mm III. 300 mm
Outer pipe diameter	Inner pipe diameter +300 mm		
Sediment concentration	0%, 5%, 10%		

First, field conditions such as particle size of the target sediment, total head, and so on are set as design criteria. Then, the conditions of the facilities such as diameter of the pipes are set as the design case. Next, suction pipe flow is calculated using the method based on the design criteria. After calculation, the possibility of sucking the target sediment is estimated based on comparison of calculated flow velocity and target sediment diameter. If the assumed facilities can suck the target sediment based on calculated flow velocity, the design case is adopted as an option for the basic specification. The same procedure is carried out for different design cases. The basic design specification is finally selected from the adopted options.

The authors plan to carry out the verification test of Vertical Multi-Holed Double-Pipe System in actual dams. In order to determine the basic specification of the verification test facilities, 9 sets of conditions of facilities were estimated based on the hydraulic design method. The remaining 5 of 9 sets were adopted as design options. Finally, Case 2-II in Table 5 was adopted based on economical considerations.

4.5. Estimation of sediment concentration at the outlet

When the system is applied to an actual dam, it is necessary to avoid excessive sediment supply to the lower reaches of dam. Therefore, the system is expected to have a function to open and close the suction holes automatically in response to the sediment concentration in the discharge flow. This paper briefly presents the method of estimating sediment concentration of the discharge flow based on laboratory test results using a quasi-full-scale model.

In order to realize this function, the authors established a method for real-time estimation of sediment concentration in the suction pipe. This method is based on the relationship between estimated sediment concentration of the discharge flow and measured pressure of the head and pipe flow, derived from the equation of pipe friction proposed by Turian et al (Raffi, M.T., et al. 1977). When Turian's equation is used, it is necessary to estimate the sediment transport type (Noda, K. 1986) to select the parameters of the equation. Sediment concentration in the discharge flow both measured and estimated by Eq. 5 (Noda, K. 1986, Zandi, I., et al. 1967, Newitt, D.M., et al. 1955, Rubey, W.W. 1933) are shown in Fig. 11.

$$C = \left(\frac{1}{a} \frac{\lambda^{s}}{\lambda_{w}^{b} \cdot C_{D}^{c} \cdot \left[V^{2} / gD(S-1) \right]^{d}} \right)^{1/e}, \qquad (5)$$

where,

a,b,c,d,e:	Coefficients based on sediment transport type
C_D:	Drag coefficient
S:	Specific gravity of sediment particle

The estimation was carried out when the pipe flow was steady. As shown in Fig. 11, the estimated value of sediment concentration of the discharge flow coincided with the measured value. Therefore, the authors consider that it is possible to estimate sediment concentration in the discharge flow by using Eq. 5.

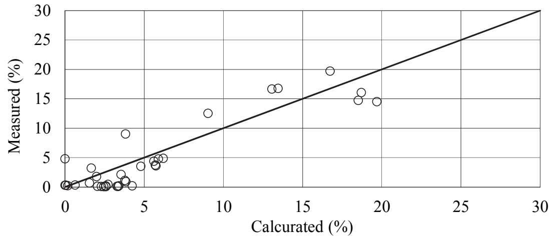

Figure 11. Comparison of measured and calculated values of sediment concentration of the discharge flow.

5. CONCLUSIONS

The followings are the conclusions of this paper:

1. The basic sediment suction ability of the system was estimated by carrying out a laboratory test using a small model. In addition, the hydraulic mechanism of the system was revealed by using hydraulic design method that could calculate the pressure head based on the results of the laboratory test using a small model.

2. The sediment suction ability of the system was estimated by carrying out a laboratory test using a quasi-full-scale model. In addition, the problem of suction pipe blockage was resolved by supplying water, which reduced the sediment concentration in the pipe from the water supply pipe.

3. By applying the hydraulic design method to the results of the laboratory test using a quasi-full-scale model, it was confirmed that the hydraulic design method was valid for quasi-full-scale facilities.

4. The basic specification of verification test facilities was determined by using the hydraulic design method.

5. The estimation method of sediment concentration at the outlets of the suction pipe was presented.

It was found that Vertical Multi-Holed Double-Pipe System was feasible through the laboratory tests with the small model and the quasi-full scale model. In order to confirm further applicability of the system to actual sites, the authors plan to carry out a verification test of the system at an actual dam.

REFERENCES

Maeda, K., Shoji, Y. and Oota, S. (2015): Sediment discharge tests of Vertical Multi-Holes Double-Pipes system and development of estimation method of discharge sediment concentration, Advances in River Engineering, Vol.21, pp. 83-88, in Japanese.

Kazanskij, I. (1978): Scale-up Effects in Hydraulic Transport Theory and Practice, Hydrotransport 5, B3, pp. 47-49.

Anderson, A.G. and Straub, L. (1948): Hydraulics of conduit bends, St. Anthony Falls Hydraulic Laboratory, Bulletin No.1.

Okano, M., Matano, F., Katayama, H., Tajima, Y., Nakagawa, H. (2004): Studies on Dreging in a Reservoir using Multi-Hole Suction Pipe, Journal of Japan Society of Dam Engineers, Vol.14 (4), pp. 237-249, in Japanese.

Raffi, M.T. and Tran-Fu, Y. (1977): Flow of slurries in pipelines, AIChE Journal, Vol.23 (3), pp. 232-243.

Noda, K. (1986): Sediment Transport in Pipelines, Lecture Notes of the 22th Summer Seminar on Hydraulic Engineering, Corse A, pp. 1-16, in Japanese.

Zandi, I. and Govatos, G. (1967): Heterogeneous Solid Transportation in Pipelines, Journal of Hydraulics Division, ASCE, Vol.93, pp. 145-159.

Newitt, D.M., Richerdson, J.F., Abbot, M. and Turtle, R.B. (1955): Hydraulic conveying of solids in horizontal pipes, Trans. Inst. Chem. Engrs., Vol.33/2, pp. 93-103.

Rubey, W.W. (1933): Settling velocity of gravel, sand, and silt particles, American Journal of Science, Vol.25, pp. 325-338.

Abrasion and Corrective Measures of a Sediment Bypass System at Asahi Dam

T. Nishikawa & Y. Yamane
The Kansai Electric Power Co., Inc., Osaka, Japan
nishikawa.toru @ b4.kepco.co.jp

Y. Omoto
Newjec Inc., Osaka, Japan

ABSTRACT:
At the Asahi Dam of Kansai Electric Power Co., Inc., a sediment bypass system was built and in operation in 1998 to take a fundamental measure to mitigate impacts by prolonged water turbidity and sedimentation ascribable to collapse of mountain slopes in the upstream caused by a great flood in 1990. The effectiveness of the bypass system has been verified and reported in the past. In the meantime, the tunnel invert has been worn notably by a significant sediment transport at high velocity and how to improve the efficiency of periodical maintenance is an issue.
This paper describes the abrasion of the tunnel invert of the sediment bypass system at the Asahi Dam that has been in operation for approximately 15 years, and evaluates possible tunnel maintenance methods using the life-cycle cost based on monitored data of abrasion.

Keywords: sediment, bypass system, abrasion, life-cycle cost

1. OUTLINE OF ASAHI DAM

The Asahi Dam is on the lower regulating reservoir of the Oku-yoshino Power Plant, which is a pure pumped-storage power plant and has been in operation since 1978. The location of the power plant is shown in Fig. 1 and the specifications are listed in Table 1.

Osaka
Tokyo
Asahi dam

Figure 1. Location of Asahi Dam

Table 1. Technical features of Asahi Dam

Catchment area	$39.2km^2$	
Design flood	$1{,}200m^3/s$	
Power plant	Max. output	1,206MW
	Max. discharge	$288m^3/s$
	Effective head	505m
Dam	Type	Arch dam
	Height	86.1m
	Crest length	199.41m
Reservoir	Gross storage	$15.47 \times 10^6m^3$
	Effective Storage	$12.63 \times 10^6m^3$
	Available depth	32m

2. PLAN AND DESIGN OF SEDIMENT BYPASS SYSTEM

At the Asahi Dam, a sediment bypass system was built and in operation in 1998 to take a fundamental measure to mitigate impacts by prolonged water turbidity and sedimentation ascribable to collapse of mountain slopes in the upstream caused by a great flood in 1990.

The sediment bypass system at the Asahi Dam was designed to divert bed load and suspended load besides wash load for the purposes of mitigating both prolonged turbidity and sedimentation. The capacity of the bypass tunnel is designed as $140m^3/sec$, which can practically diminish the number of prolonged turbidity days induced by a flood peak of $200m^3/s$, which equals to the discharge of the return period of 1-year, and also can sluice almost all of bed load transported by the design flood of $1{,}200m^3/s$.

Technical features of the bypass system is shown in Table 2 and Fig. 2. Based on a uniform flow calculation, the cross-section of the bypass tunnel was designed so that the tunnel could pass the flow with the water depth of 80% of the tunnel height. D-shape cross section was adopted because of cost effectiveness and ease of maintenance. The entrance of the tunnel was composed of a diversion weir and an orifice intake, by which the volume of river water and sediment into the tunnel could be naturally regulated.

Table 2. Technical features of sediment bypass system

Diversion weir	Height	13.5m
	Crest length	45.0m
Orifice intake	Height	14.5m
	Width	3.8m
	Length	18.5m
	Type	Reinforced concrete and steel lining
	Gate	1
Bypass tunnel	Length	2,350m
	Height x Width	3.8m x 3.8m
	Shape	D-shape
	Gradient	Approx. 1/35
	Max. discharge	140m^3
Outlet	Width	8.0 ~ 5.0m
	Length	15.0m
	Type	Reinforced concrete

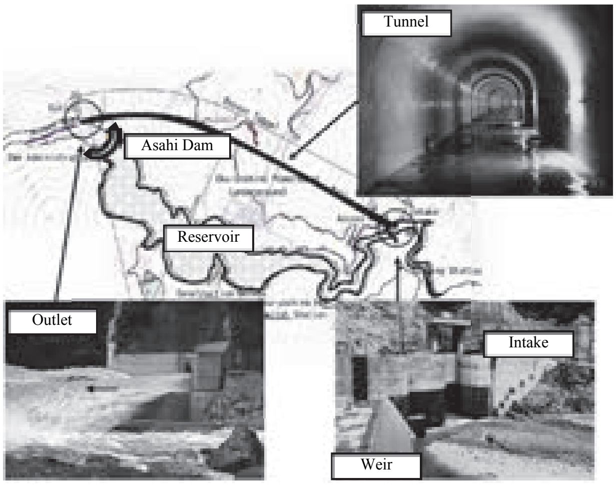

Figure 2. Plan view of the bypass system at Asahi Dam

3. PERFORMANCE AND EFFECT OF SEDIMENT BYPASS SYSTEM

3.1. Performance of Sediment Bypass System

Fig. 3 shows annual total inflow into the reservoir and bypass tunnel since the start of operation. 50% to 80% of total inflow were flowed downstream via the bypass tunnel every year. As shown in Fig. 4, a peak flow of 895m^3/s, which is the highest flow since the start of operation, was recorded at the Asahi Dam in September 2011.

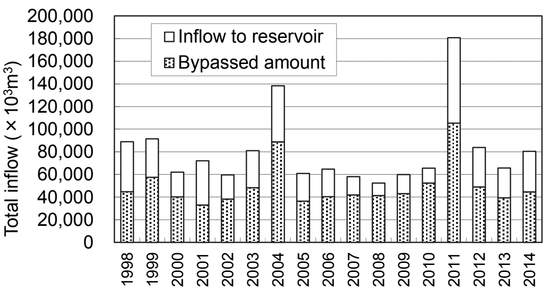

Figure 3. Annual total inflow to the reservoir

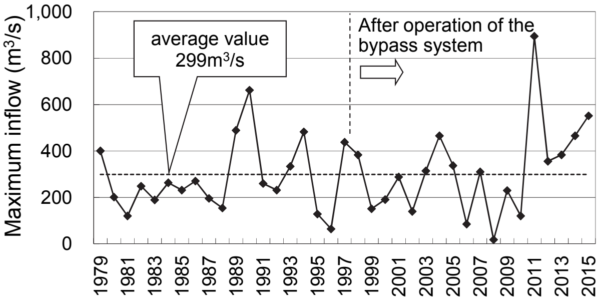

Figure 4. Maximum inflow at the Asahi Dam

3.2. Effects of Sediment Bypass System

The data on suspended solids concentration (SS) have been collected once a day at the two gauging stations: 4.3km upstream and 1.6km downstream of the Asahi Dam. Water in the reservoir was turbid for 50 to 130 days during a year on average depending on scale of floods before the sediment bypass operation. The average number of days of prolonged turbidity was reduced to about 10 days after the start of operation. It shows the bypass system was effective for mitigating water turbidity on a long-term basis.

Also, with regard to deduction of sedimentation in the reservoir, it was estimated that 80% of the total sediment, which would have deposited in case that there was not the bypass system, would be bypassed downstream. The estimate was made by calculating the volume of bed load that reached the diversion weir using a bed load equation (Ashida-Michiue Formula) and assuming that the total volume would be bypassed. Details of effects reducing sedimentation would be referred to relevant reports i.e. Harada, M., et al. 1997, Kataoka, K. 2000, Doi, H. 2005 and Fukuroi, H. 2012.

Fig. 5 shows changes in sedimentation volume (bed elevation) and Fig. 6 shows changes in bed material grain size distribution in downstream course. They indicate that changes owe to the operation of the bypass system.

The changes in downstream sedimentation volume (bed elevation) show that bed elevations in downstream channels had repeatedly increased or decreased and basically stabilized but that sedimentation volume increased to approximately 200,000 m^3 due to landslides caused by a flood of 2011.

Significant changes were made in bed material grain size distribution in downstream course. Fine grained fractions have been increased since the commencement of bypass operation. It is thus found that sediment was supplied to the downstream of the reservoir by the bypass system and the river condition is getting close to that before the construction of the dam.

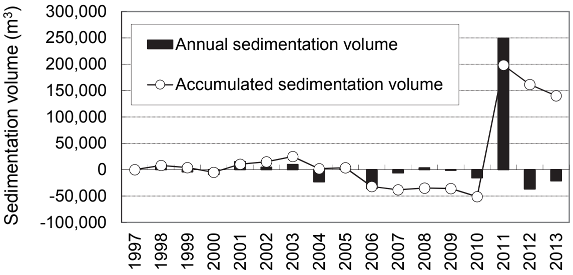

Figure 5. Changes in sedimentation volume in the downstream course

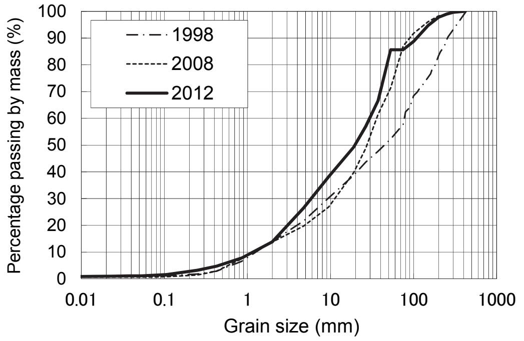

Figure 6. Changes in bed material gain size distribution in the downstream course

4. ABRASION OF SEDIMENT BYPASS

When designing the bypass tunnel, a study on concrete strength and abrasion allowance at invert section was made in order to determine its specification and allowance considering scale of repair.

Based on the study for the design, the following measures were applied. (1) an intake where severe abrasion was evidently expected to occur was reinforced with steel plates; (2) the invert section of the tunnel was constructed by high strength concrete of 36N/mm^2 except the part of the downstream end where the invert was constructed by higher strength concrete of 70N/mm^2.

It has been known through repeated repair during 15 years of operation that the distribution of abrasion tends to show a particular pattern. In addition, knowledge important to the control of abrasion was also obtained based on the results of monitoring of reinforcing materials in trial constructions. These were used to develop efficient measures to control the abrasion of the bypass tunnel.

4.1. Prediction of Abrasion in the Design Phase

In the area upstream of the Asahi Dam, granites are distributed and granite boulders have deposited on the river bed. The bed materials at the bypass intake had a mean grain diameter of 50 mm and a maximum diameter of 300 mm. It was assumed that the sediment of the size flowed through the tunnel.

For predicting abrasion in the design phase, an Ishibashi's formula shown below (Ishibashi, T. 1983) was used.

$$V = C_1 \times E_t \times C_2 \times W_t \qquad (1)$$

Where, V is the volume of abrasion (damage) (m^3), C_1 is the coefficient of damage by impact (m^2/N), C_2 is the coefficient of abrasion due to friction (m^2/N), E_t is the total kinetic energy of gravel acting on the channel bed (N x m), and W_t is the total work done by abrasive force. (N x m).

The mean thicknesses of annual abrasion of concrete and steel were estimated at 40 to 50 mm/year and 0.2 mm/year, respectively, which were repairable level considering period of maintenance. As a result, the tunnel invert was therefore lined with concrete (design strength: 36 N/mm^2 and lining thickness: 40 cm).

4.2. Actual Abrasion and Abrasion Pattern

Described below are the results of monitoring of actual abrasion at the intake lined with steel-plate and at other section constructed by concrete since the commencement of bypass system operation.

4.2.1. Steel plates at intake

The intake of the bypass tunnel was lined with steel plates because the severest abrasion was expected. Damage was made predominantly on the right bank side in the steel-plate-applied area where the slope is changed from sharp to moderate (Fig. 7) and sediment likely flowed on the right bank side. Repair has been made three times in this area since the commencement of operation. After the flood of 2011, repair was made again in a wider area mainly on the right bank side too. Frequency of repair has, however, been much less than in the tunnel section.

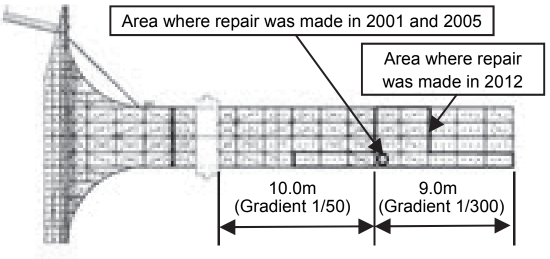
Area where repair was made in 2001 and 2005
Area where repair was made in 2012
10.0m
(Gradient 1/50)
9.0m
(Gradient 1/300)

Figure 7. Areas repaired with steel plates at the intake

4.2.2. Tunnel section

Abrasion on concrete section was observed nearly throughout the invert in the tunnel section. Repair was made periodically using higher-strength concrete (design strength: 70 N/mm^2) instead of concrete of 36N/mm^2. From a viewpoint of tunnel structure, fracture of reinforcement in the invert was allowed, however, the invert was repaired before the rock was exposed to prevent adverse effects on the sidewalls and arch section. In actual, repair was made on a priority basis before the fracture of reinforcement over a length of approximately 100 m from the intake which was an important part to tunnel structure. Sidewalls were worn slightly in areas at low elevations. In the arch, long-term cracking and exposure of reinforcement were observed in some areas. Because it was unlikely that sediment of the grain size contributing to abrasion reached the arch, these phenomena were attributed to the effects of ordinary deterioration.

As abrasion in the invert was predominant, the past records of distribution and volume of abrasion in the invert were focused and summarized. The cumulative abrasion since the commencement of bypass operation is shown using contours to verify the tendency of planar distribution of abrasion (Fig. 8). The cumulative abrasion is calculated by annual measurement results. The depth of abrasion is locally larger near the tunnel outlet than near the tunnel intake. In the transverse direction, abrasion was predominant on the right bank side at the intake and on the left bank side at the outlet. The maximum cumulative abrasion depth on the left bank side at the outlet was largest at 1,272 mm. The tendency shows that the sediment does not flow uniformly in the cross section but flows in a certain pattern due to the tunnel alignment that bends leftward from the midpoint. In other words, bed load concentrate on the right bank side at the intake and then on the left bank side downstream of the bend owing to the secondary flow created by bending, resulting in increase in abrasion volume. Abrasion depth was larger at the outlet than at the intake also because secondary flow was more likely to develop in the bend than at the intake and consequently the points of passing sediment flow were concentrated more.

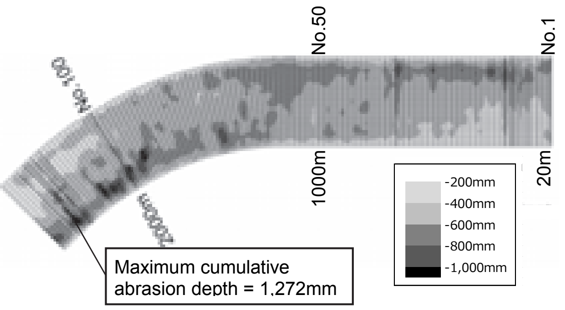

Figure 8. Cumulative abrasion in the tunnel invert (sum of abrasion between the commencement of bypass operation and November 2011)

The results of measurement of the volume of sediment that passed the bypass tunnel, volume of abrasion in the tunnel invert and the volume of materials used for repair are shown in Fig. 9 in order to quantitatively evaluate abrasion. The changes in abrasion volume affected by the volume of sediment passing the bypass tunnel were indicated by the relation between annual volume of abrasion and sediment load in the bypass tunnel (annual abrasion volume (m^3/year)/sediment load in the bypass tunnel (m^3/year) (Fig. 10). The volume of abrasion tends to increase nearly in proportion to the volume of sediment that passed the bypass tunnel. The volume of abrasion was highest in 2011 when the maximum flow was recorded. The percentage of high-strength concrete increased on the invert surface of the bypass tunnel owing to periodical repair (Fig. 11). Fig. 10 shows that the volume of abrasion relative to the volume of sediment decreased from 2003 when the percentage of high-strength concrete exceeded 70% and in subsequent years. In addition, the planar distribution of abrasion was not affected by the volume of passing sediment, and abrasion was predominant in the convex bend.

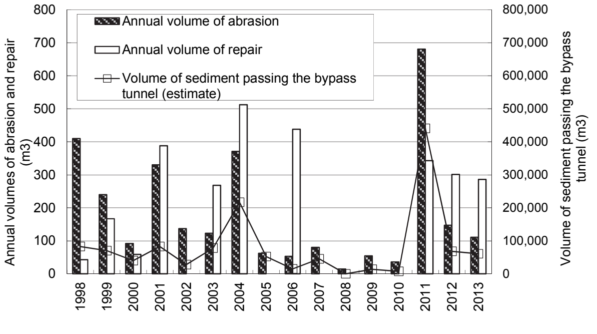

Figure 9. Annual volumes of abrasion and repair

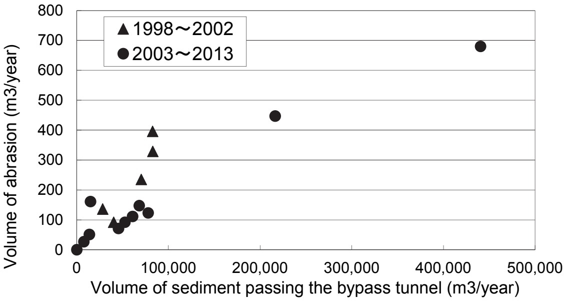

Figure 10. Relationship between the volumes of abrasion and sediment passing the bypass tunnel

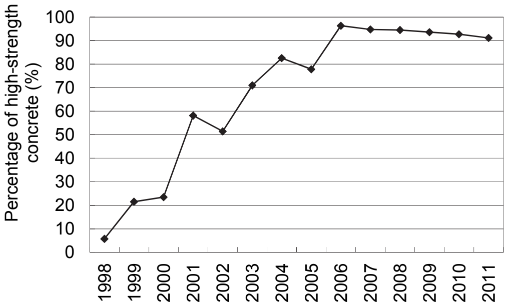

Figure 11. Percentage of high-strength concrete

4.3. Trial Construction

Other materials than concrete have also been applied in the invert on a trial basis in order to confirm effectiveness of the original design since 1999. Fig. 12 shows how they were placed. As reinforcing materials, higher-strength precast panels, steel plates and stones which had a good record as materials highly resistant to abrasion, and resins with a low modulus of elasticity were selected. The abrasion resistance of respective materials was tested and monitored through actual bypassing. Nearly all of the materials were greatly worn or delaminated in a few years after its construction. It was found that abrasion was likely to progress from the joint of the material, and created a weak point and that the reinforcing material was delaminated rapidly at once owing to the impact of gravel or for other reasons. In 2013, an abrasion-resistant protective material made of rubber, which has been applied in many sabo dams, was placed as one of trial materials additionally.

The condition was verified ten months after its installation. As a result, it was found that the volume of abrasion was greater in the bypass tunnel than in sabo dams as the mean abrasion volume was 0.7 to 1.1 mm/year in the bypass tunnel while actual mean abrasion volume in sabo dams was 0.1 to 0.3 mm/year.

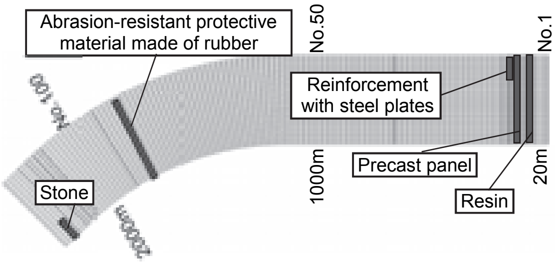
Abrasion-resistant protective material made of rubber
No.50
No.1
No.100
Reinforcement with steel plates
Precast panel
Stone
1000m
20m
Resin
2000m

Figure12. Locations of materials applied in trial construction

5. DISCUSSIONS ON OPTIMUM MATERIAL AGAINST ABRASION

High-strength concrete (70N/mm^2) has been adopted to resist abrasion because of the availability of repair materials and ease of construction. In order to improve the efficiency of repair cost, new repair materials were examined based on the results of trial construction. The materials compared with one another are described in detail in Table 3. The materials were applied in locations with high volume of abrasion. In other locations, high-strength concrete was applied for repair as conventionally practiced. The annual volume of abrasion of each repair material was expressed as a ratio to the annual volume of abrasion of high-strength concrete based on the results of trial construction and published data. Unit costs are expressed by relative value to a unit cost for high-strength concrete based on the actual results and published costs. Table 4 shows the area and the percentage to the total area of invert which corresponds to various amounts of annual abrasion volumes of high-strength concrete. The service life of high-strength concrete was obtained by dividing a marginal volume of abrasion of 200 mm by the annual volume of abrasion.

Table 3. Annual volume of abrasion and unit cost of repair materials

No.	Repair material	Annual volume of abrasion	Unit cost
1	High-strength concrete	1.0000	1.0
2	Resin (t=15mm)	0.2430	2.5
3	Precast panels (t=50mm)	0.2500	4.0
4	Reinforcing steel plates (t=16mm)	0.0028	6.4
5	Abrasion-resistant rubber protectors (t=50mm)	0.0075	8.5
6	Stones (t=150mm)	0.1000	22.6

Table 4. Annual volume of abrasion of high-strength concrete in invert (2006 to 2011) and service life

Annual volume of abrasion (mm)	Area (m^2)	Ratio to total area of invert (%)	Service life (years)
160 or higher	0.0	0	1
150 or higher	4.0	0.05	
140 or higher	14.0	0.16	
130 or higher	21.0	0.24	
120 or higher	27.0	0.30	
110 or higher	35.0	0.39	
100 or higher	40.0	0.45	
90 or higher	56.0	0.63	2
80 or higher	81.5	0.91	
70 or higher	128.1	1.44	
60 or higher	200.7	2.25	3
50 or higher	375.3	4.20	
40 or higher	704.8	7.89	4
30 or higher	1,539.2	17.24	5
20 or higher	3,190.6	35.73	7
Less than 20	5,739.4	64.27	10

Life-cycle cost of each materials were calculated by the formula shown as below (Eq. 2). Fig. 13 shows the relationship between the location where the repair material was applied and life-cycle cost. For comparing the life-cycle cost, the study period was set at 50 years and the social discount rate was set at 4.0%. If the concerned facility has a residual value at the end of the 50-year period, the residual value was deducted.

$$LCC = \sum_{t=0}^{49} \left\{ \frac{C_c}{(1+r_s)^t} \right\} - R_v \tag{2}$$

Where, LCC is life-cycle cost, C_c is construction cost in the t th year, t is passed years, r_s is social discount rate and R_v is residual value at the end of the 50-year period.

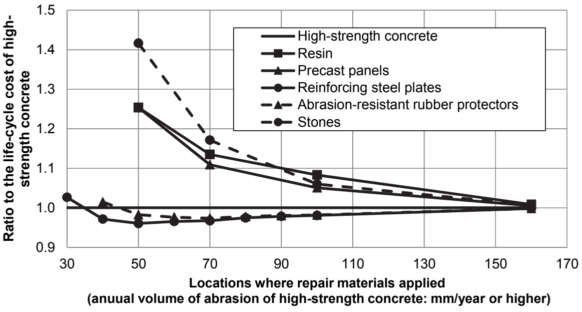

Figure 13. Relationship between the location of repair and life-cycle cost

Fig. 13 shows that the life-cycle cost in cases where resin, precast panels and stones were used were higher than in the case where higher-strength concrete was applied throughout the invert. The life-cycle cost of the case which reinforcing steel plates and abrasion-resistant rubber protectors were used were at a minimum level in case that the material were applied at the location with annual volume of abrasion of high-strength concrete were 50~70mm/year. Applying the materials at a location with smaller annual volume of abrasion led to the increase of the area where the material should be applied, and increased the life-cycle cost. When the materials were applied in locations with large annual volume of abrasion, life-cycle cost also increased because the area of high-strength concrete that requires frequent repair increased although the area where the material was applied decreased. Life-cycle cost was the lowest in the case where reinforcing steel plates were applied in locations with an annual volume of abrasion of 50 mm or higher. Life-cycle cost was reduced compared to the case where high-strength concrete was applied throughout the invert by approximately 4% in 50 years. Thus, the effect of cost reduction was very small. In the case where abrasion-resistant rubber protectors were adopted, the life-cycle cost was estimated approximately 3% below the high-strength concrete case.

Reinforcing steel plates were selected as the most economical repair material based on the results of comparison in life-cycle cost. Reinforcing steel plates, however, have several drawbacks. Uplifting or delamination occurred for unknown reasons in trial construction. There is a possibility of abrasion advancing from the point of uplifting. Such defects, once they occur, involve large-scale repair work. The life-cycle cost shown in Fig. 13 takes no effects of steel plate delamination into consideration. If the effects are considered, life-cycle cost is likely to exceed the cost in the case where high-strength concrete is applied throughout the invert. It was assumed that a certain percentage of reinforcing steel plates are delaminated every five years according to the results of the trial construction, and life-cycle cost including the cost of repair of delaminated steel plates were compared (Fig. 14). It was found that life-cycle cost of reinforcing steel plates exceeded the cost in the case where high-strength concrete was applied throughout the invert when the percentage of delaminated plates exceeded 12%. As the area where reinforcing steel plates were applied in this study (Fig. 15) involve uncertainty, making repairs in a large area bundling scattered locations where reinforcing steel plates should be applied is practical, and then applying reinforcing steel plates is no longer advantageous in terms of cost because high unit cost is required.

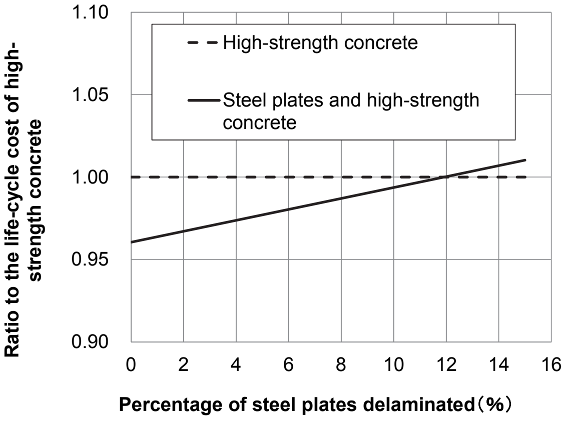

Figure 14. Relationship between the percentage of steel plates delaminated and life-cycle cost

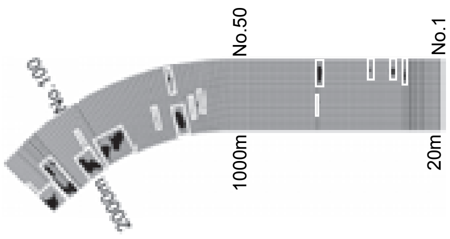

Shown in black: Locations with an annual volume of abrasion of 50 mm/year or higher
Shown in white: Locations where reinforcing steel plates were applied

Figure 15. Locations where reinforcing steel plates were applied

In view of the above discussions, the repair method using high-strength concrete as currently practiced is considered efficient and valid because it requires no large-scale equipment, unlike the method employing reinforcing steel plates, and because it is applicable to the points of repair of varying shapes that are scattered in the invert.

6. CONCLUSIONS

This paper described the distribution and volume of abrasion in a bypass tunnel. The results of trial construction could serve as basic data for determining types of repair materials and the frequency of repair as they showed the importance of treatment at the joint, a weak point in abrasion control, and that the bypass tunnel had larger volume of abrasion than sabo dams and was placed under a severe condition. As the result of life-cycle cost evaluation, it was found that the repair method using high-strength concrete as currently practiced is considered efficient and valid.

ACKNOWLEDGEMENT

We would like to express our sincere gratitude to Dr. Tetsuya Sumi, a professor of Disaster Prevention Research Institute, Kyoto University, he supported us to evaluate the abrasion of the bypass system and the life-cycle cost of the repair materials.

REFERENCES

Harada, M., Terada, M., Kokubo, J. (1997): Planning and hydraulic design of bypass tunnel for sluicing sediments past Asahi reservoir. 19th ICOLD Congress.

Kataoka, K. (2000): An overview of sediment bypassing operation in Asahi reservoir, Proceedings of International Workshop and Symposium on Reservoir Sedimentation Management, Japan.

Doi, H. (2005): Reservoir sedimentation management at the Dashidaira and Asahi Dams. International Workshop on Sediment Management for Hydro Projects.

Fukuroi, H. (2012): Damage from Typhoon Talas to Civil Engineering Structures for Hydropower Stations and the Effect of the Sediment Bypass System at Asahi Dam. 24th ICOLD Congress.

Ishibashi, T. (1983): A hydraulic study on protection for erosion of sediment flush equipment of dams. Journal of Hydraulic, No.334.

Preliminary Study on High Arch Dam Reservoir Bedrock Deformation and Its Effect on Dam Operating Behavior

W.Minhao
Power Construction Corporation of China, China
duxiaokai2003@163.com

D.Lincai&D.Xiaokai
China Renewable Energy Engineering Institute, China

ABSTRACT:
It is found that the reservoir bedrock shows a warping deformation with subsidence in front of the dam and a little uplift behind the dam, according to monitoring data of high arch dam reservoir bedrock deformation. Therefore, in order to study the deformation of high arch dam reservoir bedrock and its effect on dam operating behavior, corresponding affect factors were studied firstly. Furthermore, x hydropower project wide range numerical model is built, including reservoir area, rock base and dam. The research reveals the general law of reservoir bedrock deformation. Moreover, it is proposed that the deformation caused by reservoir bedrock should be taken into consideration when evaluating dam operating behavior.

Key Words: high arch dam, reservoir bedrock deformation, monitoring, modulus inversion

1. INTRODUCTION

The engineering experience suggests that the maximum radial replacement of arch dam is always one of the most significant indexes to evaluate arch dam operating behaviour (P.Jiazheng,2000). However, the effect of reservoir bedrock is always ignored in the general analysis on high arch dam operating behavior. In the early 1980s, some engineers have noticed such problems caused by high arch dam reservoir bedrock deformation and some exploratory researches have been carried out as well. It has been noticed that numerical calculation results of arch dam deformation are very different from monitoring data in practical projects. The monitoring data in storage stage demonstrates that dam would show upstream deformation under the effect of water, temperature, reservoir bedrock deformation and specified dam structures. X hydropower station are taken into analysis as follows. X arch dam is 294.5m high, the normal water level is 1240m and the total reservoir storage is 15 billion m^3. During the storage stage, the arch dam radius deformation shows that great difference exists among calculation results and monitoring values

2. INFLUENCE FACTORS OF HIGH ARCH DAM RESERVOIR BEDROCK DEFORMATION

The influence factors of high arch dam reservoir bedrock deformation contain water body size, geological condition, reservoir bedrock type and its influence area (L.Zan,2004). Since the geological condition is too complex, the reservoir bedrock type and its simulation range, water pressure are mainly studied in this paper.

(1) Reservoir bedrock type: the effect of different reservoir bedrock type, such as linear type river channel (Fig.1a), branch-off type river channel (Fig.1b) and sudden-enlargement type river channel (Fig.1c).

(2) Reservoir bedrock influence range: the impact of width, depth and length of reservoir bedrock on reservoir bedrock deformation, as well as the impact of different extended length towards downstream.

(3) Water pressure: the influence of water pressure on the reservoir bedrock deformation under different water levels with certain reservoir bedrock type, geological condition and reservoir bedrock influence range.

The study found that the subsidence reaches the maximum in the middle of the river channel, and the value declines gradually along two sides and with the depth increase. Meanwhile, the subsidence is relatively small in the downstream. The maximum subsidence of linear type, branch-off type and sudden-enlargement type river channel appears at the middle of the channel, bifurcation part and the center of water gravity respectively. With the increase of the upstream range of reservoir bedrock (5km → 30km), the deformation distribution on longitudinal profile vertical to river channel tends to convergence. The difference between the amounts of deformation of reservoir bedrock tends to convergence as well with the increases of bedrock depth (3km→10km). The downstream range has less impact on the reservoir bedrock deformation. At the same time, the subsidence of reservoir bedrock increases with the rise of upstream water level.

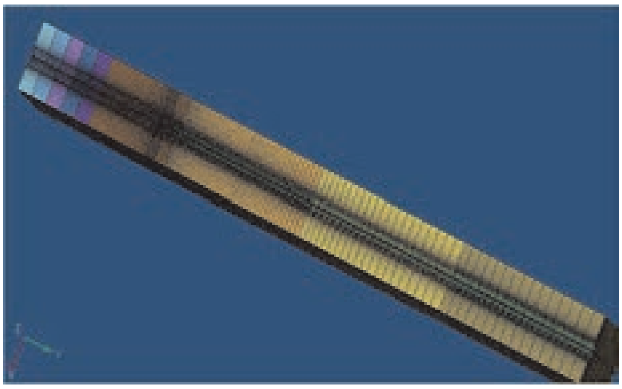

a. linear type river channel

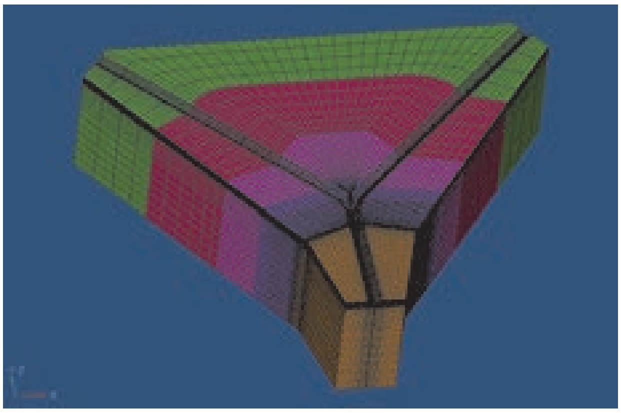

b. branch-off type river channel

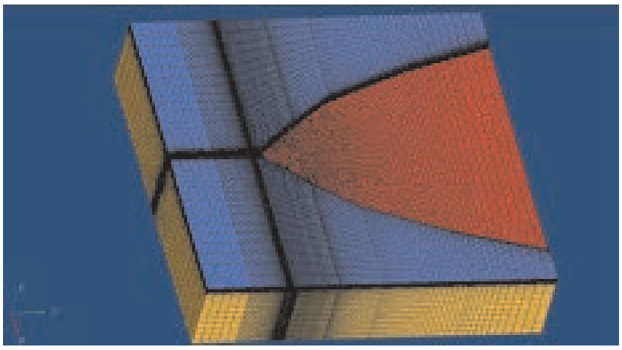

c. sudden-enlargement type river channel

Figure 1. Reservoir bedrock type of high arch dams with large storage

In terms of those influence factors, such as reservoir type, bedrock depth, the extended length of upstream and downstream and different water levels, the improved entropy method can be applied to build weight calculating model. Weights of above factors are 0.37, 0.17, 0.11, 0.55 and 0.30 respectively.

3. ANALYSIS OF X RESERVOIR BEDROCK DEFORMATION AND EFFECTS

The X hydropower station is a branch-off type reservoir.

3.1. Monitoring deformation rules of X reservoir bedrock

The benchmark network for deformation monitoring of X reservoir bedrock is shown in Fig.2. The monitoring scope ranges from 1km upstream to 4km downstream, with a total observation line of 33km.

The whole deformation monitoring network of reservoir bedrock has 33 benchmarks of which 15 dots are arranged upstream and 18 dots are arranged downstream. According to the measured benchmark results, X reservoir bedrock shows warping deformation, with subsidence upstream and a little uplift downstream. Monitoring subsidence ranges from -1.6mm to 35mm, where the maximum is 1km upstream from dam site while the minimum is 4km downstream. As shown in Fig.3, the reservoir bedrock in dam area has a slight rotation toward the upstream.

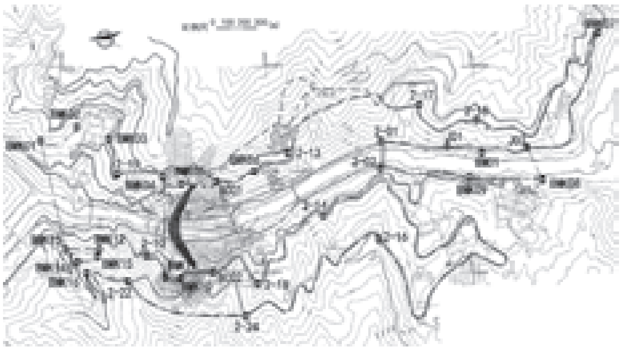

Figure 2. Benchmark network of X reservoir bedrock deformation monitoring

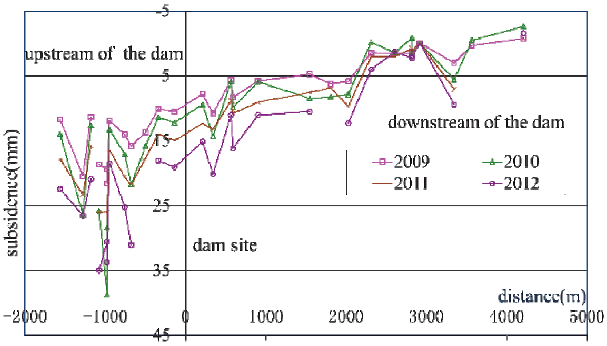

Figure 3. Subsidence distribution of X reservoir basin along the river

3.2. Numerical analysis and deformation modulus inversion

Fig.4 shows the FEM model of X reservoir bedrock. Combining the research results of modeling scope for branch-off type river channel, it includes generalized geological layers of near dam and reservoir area and main geological structure such as fault zone F1、F2 and fault F7. The FEM model boundary of X reservoir bedrock is 44km upstream, 21km downstream, 40km along the left bank, 50km along the right bank and 10km in depth. The model has 934740 elements and 958636 nodes in all.

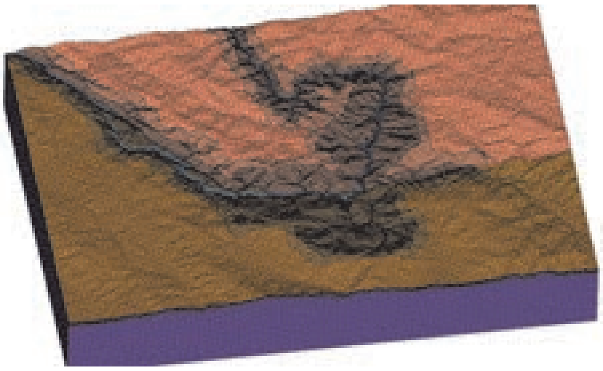

Figure 4. Numerical analysis model of X reservoir bedrock

Based on monitoring data of benchmarks around dam site in X reservoir area, the optimizing objective function for inversion is conducted by the square root of the average square error of monitoring and calculated displacement of benchmark as follows.

$$S = \frac{1}{K}\sum_{j=1}^{K}\sqrt{\frac{1}{N}\sum_{i=1}^{N}(\delta_{ic} - \delta_{im})^2} \qquad (1)$$

Where δ_{ic} are the calculated value of nodes at benchmark points in the reservoir model, δ_{im} are the monitoring value of benchmark points in the reservoir, N is the number of benchmarks, K is the number of repeated measurements. When the value of S reaches minimum, corresponding parameters of the FEM model represents the true material parameters of X reservoir bedrock.

3.3. Elastic modulus inversion of X arch dam

Based on the deformation analysis of reservoir bedrock, FEM model of X near dam area is established. Elastic modulus of X dam is inverted to study the influence of reservoir deformation on X high arch dam (G.Chongshi,2006). In order to simulate the complicated geological conditions in X near dam area accurately, the near dam FEM model includes 779914 elements and 821914 nodes totally, where 530173 elements belong to the dam body.

3.3.1. Component separation model of X dam deformation influence factors

According to the time and space analysis of X arch dam horizontal displacement monitoring data, main affect factors of dam deformation are water pressure, temperature and time-dependent components. Namely, the displacement consists of water pressure component, temperature component and time-dependent component.

$$\delta = \delta_H + \delta_T + \delta_\theta \qquad (2)$$

Where δ represents dam displacement, δ_H , δ_T and δ_θ are water pressure component, temperature component, time-dependent component respectively.

Therefore, the water pressure component, temperature component and time-dependent component can be gradually separated. Analysis showed that among all components of X dam radial displacement, water pressure component occupies the largest proportion, and dam downstream displacement arises along with the rising water level. Meanwhile, temperature change also have some influences on dam radial displacement, increasing temperature causes the dam deformation towards the upstream and decreasing temperature causes the dam deformation towards downstream. Moreover, the dam deformation has a certain time-dependent component which indicates that dam deformation has the trend towards to downstream.

3.3.2. The modulus inversion of X dam

Considering the impact of X reservoir bedrock deformation, dam deformation under water pressure is calculated. On the basis, dam elastic modulus is inverted with the previously separated water pressure component. Inversion results are shown in Table 1. Concrete elastic modulus of X dam A, B, and C district are 27.96GPa, 27.18GPa, 26.19GPa respectively. The analysis was consistent with the actual design of the dam.

Table 1. The concrete elastic modulus inversion results of X dam

material	μ	E_0 (GPa)	f'	c'(MPa)	E afeter inversion *in*(GPa)
A District	0.18	25.89	1.4	1.6	27.96
B District	0.18	25.17	1.4	1.6	27.18
C District	0.18	24.25	1.4	1.6	26.19

3.4. Effects of reservoir bedrock deformation

X arch dam horizontal displacement along river under reservoir bedrock deformation (1240m water level) is shown in Fig.5. Considering the reservoir bedrock deformation, X dam has a toppling deformation towards upstream and the deformation is relatively larger in the riverbed dam block. Preliminary calculation results demonstrate that the upstream displacement of crown cantilever 22# dam crest is 18.46mm, the displacement towards to the upstream of the inverted plumb point in the bedrock is 12.01mm. Therefore, relative to the base point in the bedrock, the displacement to the upstream of 22# dam crest is 6.45mm. However, the current study only focuses on the effects of the reservoir bedrock deformation on the dam deformation, the influence of reservoir bedrock deformation on stress and overall stability of the dam will be analyzed in the future.

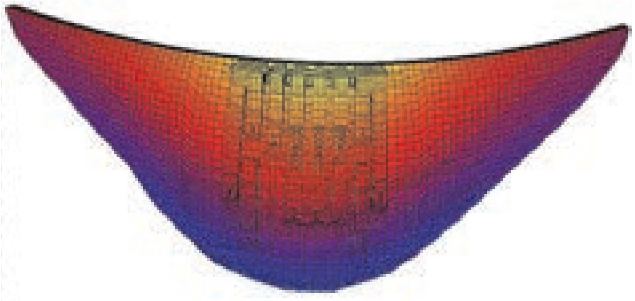

Figure 5. Dam horizontal displacement along river distribution (m)

4. CONCLUSIONS

In this paper, combined with X dam, a preliminary study of high arch dam reservoir bedrock deformation and its effect on dam operating behavior were carried out. The conclusions are as follows.

(1) The reservoir bedrock deformation of high dam projects and its influence on the dams have attracted more and more attention from hydropower engineers, and more studies need to be done in the future.

(2) Influence factors of reservoir bedrock deformation have been explored, such as reservoir bedrock types, reservoir bedrock range and water pressure. And weighted model has been established based on the improved entropy method to calculate the impact weight of each factor. Influence laws of each factor on the numerical analysis of high arch dam reservoir bedrock deformation have been revealed.

(3) X reservoir bedrock deformation modulus and dam concrete elastic modulus have been inversed using monitoring data of reservoir bedrock subsidence and dam horizontal displacement. And the inversion values of comprehensive elastic modulus has a certain reduce when considering reservoir bedrock deformation effect.

(4) Research results can be used to analyze the “doubtful deformation points” exist in those running hydropower projects. At the same time, for high dam with large reservoir, due to the subsidence and deformation caused by reservoir water pressure on the reservoir bedrock, it is recommended that reservoir bedrock deformation should be taken into account when analyzing and evaluating dam operating behavior.

(5) Arch dam is a statically indeterminate structure. The effect of reservoir bedrock deformation is not only a simple problem of the whole rigid body deformation of dam and its foundation. Reservoir bedrock deformation is influenced by reservoir type, geological conditions, reservoir water pressure, etc. The problem is extremely complicated. At home and abroad, there are a certain amount of super high arch dams with storage capacity of more than 10 billion m^3. The further research of corresponding problems should be carried out to study the criterion of the existence of reservoir deformation. Meanwhile, general laws of high arch dam reservoir bedrock deformation should be summarized and refined considering geological conditions, water pressure and different reservoir bedrock types.

REFERENCES

PAN Jiazheng, HE Jing.(2000): Large dams in China - a fifty-year review, China Water Power Press,China.

LI Zan, CHEN Fei, ZHENG Jianbo, et al.(2004) :Study on key problems of super high arch dam, China Electric Power Press,China.

GU Chongshi, WU Zhongru. (2006):Safety monitoring of dams and dam foundations – theories & methods and their application, Hohai University Press,China.

Research on a Method on Effective Restoration of the Capacity for Severe Depositing Reservoirs

Z.Lianjun,R.Yanfen＆L.Yuanfa
Yellow River Institute of Hydraulic Research, Key Laboratory of Yellow River Sediment Research, Zhengzhou, China,
zhaolianjun88@163.com

ABSTRACT:
The impacts of sedimentation in reservoirs and the importance of removing the sedimentation to restore the effective storage of reservoirs were analyzed in this paper firstly. Compared with those common desilting measures for reservoir restoration, we demonstrated that the self-suction sediment transport piping system, a kind of efficient restoring method for reservoir capacity, was effective and low-cost. Recently, some researchers made further study on this method and pointed out that this restoring technique for reservoir capacity has an advantage of transporting more sediment with less water volume and lower energy. Furthermore, some key technologies of this new method still need a further study and a physical model should be carried, to promote the development of this technique.

Keywords: Reservoir Sediment; Effective Capacity; Effective restoration; self-suction sediment transport piping system

1. THE IMPORTANCE OF RESTORING THE EFFECTIVE CAPACITY OF RESERVOIRS

The lack of effective sediment-transporting design in numerous small- and middle-sized reservoirs in China has led to severe sedimentation after years of operation. As a result, the effective capacity of reservoirs reduced severely, which led to the benefit reduction of flood control, irrigation, water supply and electricity generation etc. Especially in recent years, with the abnormal weather, continuous drought and flood disaster in most areas, reservoir sedimentation has greatly influenced the normal function of reservoir. Especially in the middle reaches of the Yellow River, where the Yellow River flows through the Loess Plateau, many small- and middle-sized reservoirs have suffered severe reservoir sedimentation. In some areas, the depositing rate even goes higher than the dam construction rate. some reservoirs have been totally scrapped. What's worse, because of the lack of new constructing reservoirs for replacement, a lot of reservoirs which were severely deposited are still in use. When a rainstorm happens, those reservoirs are in danger of dam break. Statistical data show that the reservoirs' capacity was reduced almost 200 thousand m^3 per day in Shanxi province. This amount is equal to the loss of the capacity of a middle-sized reservoir each year. The lost capacity has reached the number of 1.5 billion m^3 so far, and the number still increases with the rate of 40−60 million m^3 each year. The severe sedimentation seriously affects the reservoirs' economic benefits and restricts the sustained and healthy development of local economy. Fig. 1 shows the sedimentation scene in Beichaji reservoir in Gansu province, Fig. 2 shows the sedimentation scene in Xiaohuashan reservoir in Shanxi province, the sedimentation problem significantly reduces the reservoir benefits and regulation function.

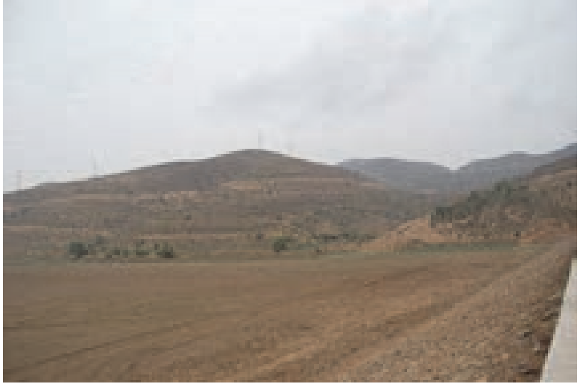

Figure 1. The sedimentation scene in Beichaji reservoir, Gansu province

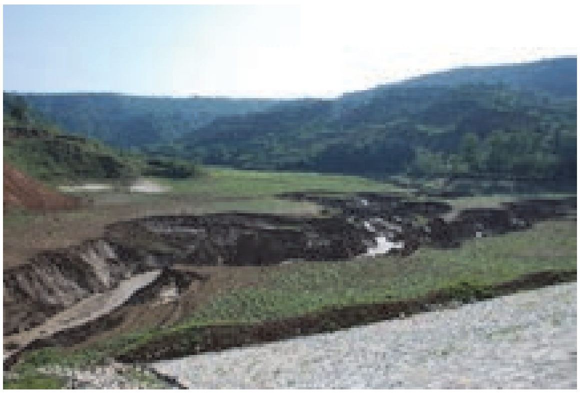

Figure 2. The sedimentation scene in Xiaohuashan reservoir, Shanxi province

The sedimentation problems not only reduce the effective capacity and normal function of reservoirs, but also increase pressures on flood defense and safe operation of reservoir. Moreover, the water quality in reservoir areas can also be badly affected by the pollutants attached to sediment, thus the ecological environments become worse. Therefore, it is imperative to take effective measures to desilt the sediment for keeping long-term function of those reservoirs.

2 TRADITIONAL DESILTING MEASURES OF RESERVOIR SEDIMENT

Dredging was the most traditional measure used in ports, reservoirs and land reclamation. With the constraint of the cost, now dredging was only used in the minority of reservoirs. Instead, empty-reservoir desilting, density current desilting and other technologies were widely used in the majority of reservoirs. What's more, suction piping experiments both in China and abroad showed that this new method for desilting is also effective.

2.1. Empty-reservoir desilting

Empty-reservoir desilting is mainly used in the reservoirs in mountainous regions where slope of river is big enough. The reservoir’s operating schedule is based on the condition of runoff. The sediment silt in the reservoir firstly in drought season. When flood comes, all the hydraulic outlet open and reservoir is scoured. The characteristics of empty-reservoir desilting is that the releasing sediment concentration is high. The scouring intensity hydrograph is spike morphology, front of which is formed by rainfall erosion and erosion intensity is effected by water level fluctuation. What’s more, erosion intensity of post-maximum is effected by the amount of sediment and degree of its consolidation. Inflow magnitude plays a major role in deciding erosion intensity and duration.

2.2 Density current desilting

The basic reason for density current formation is the difference of the specific gravity of clear water and muddy water. When the muddy water comes into the reservoir area, it goes down to the bottom while the clear water in the top. Then the density current forms and flows to the dam. If the hydraulic outlets are open in time, the sediment can be discharged out of the reservoir. As energy loss of density current is low while the sediment transporting capacity is large, if the effective measure is taken, there will be a large sediment releasing rate. For some small reservoirs, the amount of sediment releasing is even larger than that flowing into the reservoirs, which means the sediment transporting ratio can even be larger than 1. When the discharge of the reservoir outflow is more than that of the inflow, water discharge of density current increases along the distance, and sediment transporting capacity of which also increases. As a result, the sediment transporting ratio rises up. Additionally, Sediment concentration and diameter gradation of density current also influence on desilting efficiency. If median particle diameter is small, the sediment will not deposit in a short time after the density current forms, so the desilting time should be extended. Fig. 3 shows Heisonglin reservoir in Shaanxi province which density current desilting is successful applied. Fig. 4 shows the water and sediment releasing process of density current in Xiaolangdi reservoir in Henan Province.

Figure 3. Heisonglin reservoir in Shanxi province

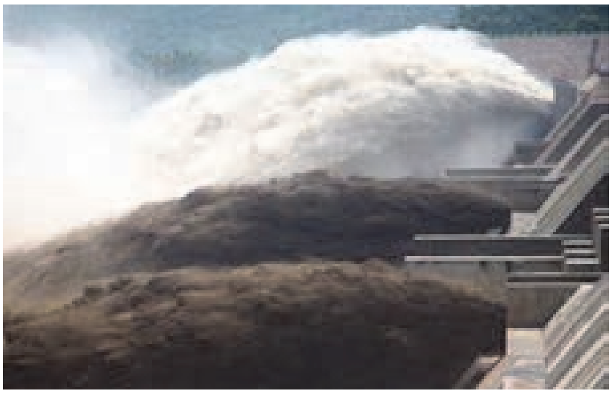

Figure 4. Water and sediment releasing process of density current in Xiaolangdi reservoir

2.3 Mechanical dredging

Mechanical dredging is one kind of desilting technique by using different kind of pipeline dredgers, it can be divided as mud bucket dredger, pipeline dredger and suction dredger according to different working principles. At present, mechanical dredging is used in the desilting control of rivers and lakes. Recently in some foreign reservoirs, mechanical dredging methods have been put into test, but it was limited with its high cost.

3 A METHOD ON EFFECTIVE RESTORATION OF RESERVOIR CAPACITY-- SELF-SUCTION SEDIMENT TRANSPORT PIPING SYSTEM

Self-suction sediment transport piping system uses the head difference of upstream and downstream of the dam as power, uses boats to control the suction-head for absorbing mud. Furthermore, connected pipes are used to transport mud absorbed out of the reservoirs. Fig. 5 shows the sketch of self-suction sediment transport piping system. Energy dissipation of this system is small and cost of desilting is low, which give this system a brighter future for application.

The idea of self-suction sediment transport piping system was put forward by a Frenchman, M. HeDing. In the 1970s, this method was first used in reservoirs in Africa that were deposited seriously and couldn't be desilted by reducing water level and releasing water discharge, such as BaoJi tile reservoir, Sidi muhammad reservoir, Wu foda reservoir in Algeria and Joseph guest taffy reservoir in Morocco.

The dam of Wu foda reservoir is 90m high and sediment thickness reaches 50m, two of the four desilting tunnels are used as flush gallery. The amount of sediment discharge capacity can be three million m^3 every year and is more than the inlet amount when the diameter of suction pipe is 400 millimetres and the length of it is 1-2km with 4000 hours' working time a year of this desilting system (Ye Zhiqiang 1988). Workers on water conservancy in our country once used self-suction sediment transport piping technique to do some desilting experiments in middle and small reservoirs in Shanxi, Gansu and Shaanxi Province.

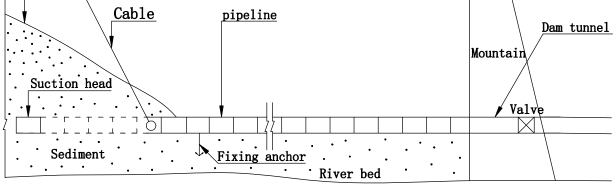

Figure 5 Schematic diagram of self-suction sediment transport piping system.

Tianjiawan reservoir is a small-size reservoir with dam height of 29.5m. Researchers in the Water Conservancy Science Research Institute in Jiangxi Province conducted a self-suction sediment transport piping experiment in Tianjiawan reservoir. Desilting equipment consisted of a suction pipe and an operation boat, and sediment can be discharged out of the reservoir by desilting pipe connecting with irrigation pipe. The sediment concentration reached 800kg/m^3.

Beichaji reservoir is another small-sized reservoir located in Jingning County in Gansu Province. In 1978, a self-suction sediment transport piping experiment was taken with a desilting system consisted of an operation boat, a drag-head and a mud conveying steel pipe with the diameter of 410 millimeters. The sediment concentration reached 484.25kg/m^3 and the sediment transport rate was 550t/h. In 1984, the amount of sediment discharge capacity was 135 thousand tons and was more than the inlet amount with only 392.5 hours' working time that year.

Xiaohuashan reservoir is also a small-sized reservoir located in Hua County in Shanxi Province and its effective storage is 1.392 million m^3. Many desilting measures were taken to solve the serious deposition problems, such as density current desilting, empty-reservoir desilting and artificial dredging and so on. However, in 1976, the residual effective storage was only 0.558 million m^3. From 1976, the self-suction sediment transporting piping experiment had been taken. From 1981 to 1986, the inlet sediment amount was 368.4 thousand tons while the discharged amount in outlets was 478.3 thousand tons, the ratio of sediment releasing was 129.88%.

Danghe reservoir is a middle-sized reservoir located in Dunhuang City in Gansu Province and its effective storage is 44.6 million m^3. In 1993, a self-suction sediment transport piping system was used in this reservoir, which was first used in middle-sized reservoir on the basis of test results in small reservoirs in Gansu Province. The diameter of desilting pipe was 400 millimetres, the releasing rate of sediment was 216t/h, the sediment concentration reached 220~1100kg/m^3 and the amount of sediment releasing in outlets was 690 thousand tons per year.

Moreover, such experiments were done in Xintian reservoir in Gansu Province, Quhe reservoir in Linfen city, Hongqi reservoir in Pinglu city, Hushan reservoir in Fanzhi City, Xiaohe reservoir in Taigu city in Shanxi province, Youhe reservoir in Weinan city in Shanxi province. In the 1980s, with the social and economic development and adjustment, those experiments lost the financial support from the government. Those self-suction sediment transport piping systems were abandoned. Now, measures such as increasing the height of dam and empty- reservoir desilting have to be taken in these reservoirs to maintain the normal operation of reservoirs, which increase the reinforcement fees and reduce the comprehensive benefits.

4 RESEARCH AND PROSPECTS ON EFFECTIVE RESTORATION OF THE CAPACITY FOR SEVERE DEPOSITING RESERVOIRS

In 2006, Yellow River Conservancy Commission organized a seminar named “key technology and equipment for sediment treatment” near Xiaolangdi Reservoir (Liao Yiwei et al. 2006). At the meeting, GaoHang from Yellow River Institute of Hydraulic Research published a paper titled “Research on pipe desilting technology and equipment in Xiaolangdi Reservoir”, HuangZiqiang from Yellow River Conservancy Commission published a paper titled “The Possibility of high water level sediment ejection and transport in Xiaolangdi Reservoir”, and LianJijian from Tianjin University published a paper titled “Research on deep water efficient sediment ejection technology in reservoirs” and so on. All these papers discussed pipe desilting technology from different aspects. It showed that this desilting technology had high desilting efficiency and large desilting range. Besides, compared with mechanical dredging, this desilting technology was more economical with low operating cost, simple structures and convenient to control etc.

In 2009, in the report of “comparative study of sediment starting and transporting scheme in Xiaolangdi Reservoir” (Jiang Enhui et al. 2009), researchers in Yellow River Institute of Hydraulic Research on the basis of sedimentation conditions and layout of the structures designed self-suction sediment transport piping large scheme and small scheme. In the large scheme, pipe diameter was 4 meters, desilting range was 25 kilometers in front of dam and the amount of annual sediment discharge capacity was 0.3 billion. While in the small scheme, pipe diameter was 2 meters, desilting range was 5 kilometers in front of dam and the amount of annual sediment discharge capacity was 0.06 billion. The desilting cost was ¥1 (RMB) per ton. Fig. 6 showed the resistance test in self-suction sediment transport piping model.

In the research project, detailed study was conducted on the position for pipeline passing dam, constructing method, pipe type selection, pipe-laying method and drag-head type selection. The result showed that it was feasible for using self-suction sediment transport piping system in Xiaolangdi Reservoir. Aiming at studying depositing problems in Dakupan reservoir, researchers from Water conservancy and civil engineering institute of Xinjiang Agricultural University conducted some physical model experiments and the results proved that using self-suction sediment transport piping system had an advantage of large desilting amount, low water consumption and low energy consumption (Zhang Li et al. 2010).

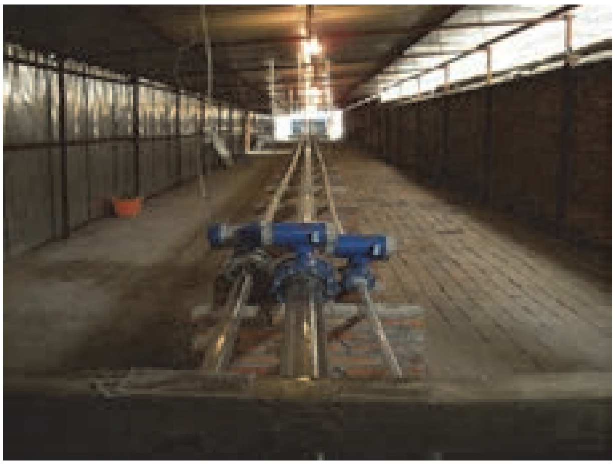

Figure 6 Resistance test in self-suction sediment transport piping model(1)

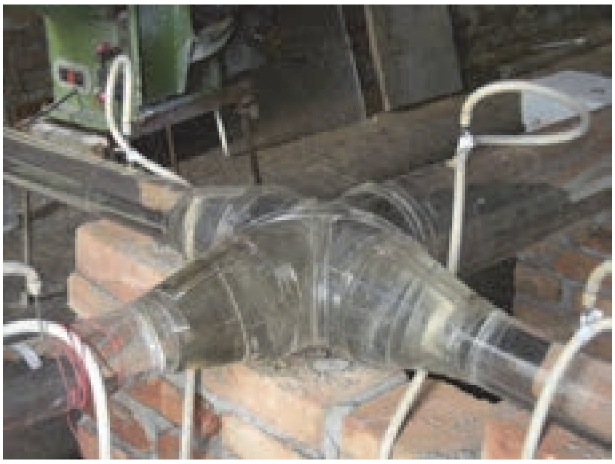

Figure 7 Resistance test in self-suction sediment transport piping model(2)

Self-suction sediment transport piping system has been successfully used in small- and middle-sized reservoirs. For large reservoirs which have large water depth, large desilting scale and complex crossing dam technology, further study should be done in controlling boat, drag-head type design, pipe connector design, pipeline disassembling and laying construction technology, pipeline crossing dam scheme design, pipeline crossing tunnel underwater connection construction technology. What’s more, self-suction sediment transport piping scheme should be put into test continually, to promote the development and improvement of this method.

5 CONCLUSION

(1) The reservoirs’ sedimentation not only reduces the effective storage and benefits, but also increases pressures on flood defence and ecological environment. So how to extend the life of those depositing reservoirs for long term becomes a priority.

(2) Among many desilting measures, the self-suction

sediment transport piping system use head difference between upstream and downstream of the dam as power and use pipeline to transport sediment out of the reservoir. This technique has an advantage of low energy consumption and low unit price, which is an effective technique for restoration of capacity.

(3) In the 1970s, the self-suction sediment transport piping system was applied in small- and middle-sized reservoirs both at home and abroad. If this technique can be used correctly, both the inlet sediment and the previous deposition can be discharged. However, influenced by policy change and other factors, the reservoir management department don’t have enough expenditure to maintain the normal operation of this desilting system, all these systems were abandoned from the 1980s.
(4) From the year 2006, some scholars have paid attention to the self-suction sediment transport piping technique again and study the key technology. they pointed out that this efficient desilting system has an advantage of large desilting amount, low water consumption and low energy consumption.
(5) Considering that the self-suction sediment transport piping technique was successfully used in small- and middle-sized reservoirs before, it may feasible for large reservoirs. Before that some key technology of this technique still need to be further studied and pilot scale test should also be carried to promote the development and improvement of this technique.

Foundation item: Natural Science Foundation of China(50339020,51379086,51309109), Ministry of Water Resources' special funds for scientific research on public causes (201501003)

REFERENCES

Ye Zhiqiang. 1988: A new reservoir desilting technique -Hydraulic pumping desilting equipment[J]. Water Conservancy & Electric Power Machinery, (3):26-28.0.

Hydraulic suction device experimental group in Tianjiawan reservoir.1976: preliminary experimental study on hydraulic suction device[R]. Taiyuan: Shanxi Hydraulic Research Institute.

A corpus of reservoirs desilting experiments research results in Gansu Province[R]. 1987: Lanzhou City: Gansu Hydraulic Research Institute.

Shanxi Hydraulic Research Institute, Shanxi Hua County water conservancy and water resources protection agency, Hua County Guapo reservoir management station.1987: Summary of hydraulic suction desilting experiment in Xiaohuashan reservoir[R]. Xian City.

Liao Yiwei, Xue Songgui, Shang Hongqi. 2006: Collected Works of sediment treatment key technology and equipment seminar in Xiaolangdi Reservoir[M]. Zhenzhou City: Publishing House of Yellow River water conservancy.

Jiang Enhui, Gao Hang, Li Yuanfa etc. 2009: Comparative study of sediment starting and transport scheme in Xiaolangdi Reservoir[R]. Zhenzhou City: Yellow River Institute of Hydraulic Research.

Zhang Li, Xia Xinli, Chen Chenglin etc. 2010: Experimental study on self-pressure Pipe Desilting of Reservoir with large bottom area[J]. Water Power, 36(4)：92-94.

Preliminary Analysis On Sediment Flushing Efficiency From XiaoLangDi, Yellow River

L.Tao[1,2,3], L.Zhe[4] , Y.Zhenfeng[1,3] L.Xinjie[1,3]

1 Yellow River Institute of Hydraulic Research,YRCC, China，2 State Key Lab oratory of Water Resources and Hydropower Engineering Science, Wuhan University, China，3 Key Laboratory of Yellow River Sediment Research,MWR, China litao@hky.yrcc.gov.cn,4Yellow River Xiaolangdi water resource investment co., LTD, MWR,China,

ABSTRACT:

It has an important role of XiaolangDi Reservoir on the Yellow River water-sediment Regulation System. In this paper, analysis on sediment flushing in conditions of backwater of open channel flow and density current plunging from the existing domestic and abroad reservoirs has been carried out, with discussing on present situation and the hot point that forecasts sediment flushing in XiaolangDi Reservoir. At last, a preliminary solution has been given. In future, water and sediment data surveyed need to be strengthened in the reservoir. By means of mathematical model and physical model, studying the law on water and sediment transport in different sections and different flow regimes, calculation accuracy of reservoir flushing prediction would have been improved. A new direction on forecasting sediment flushing in XiaolangDi Reservoir has been put forward in the paper.

Keywords: XiaoLangDi Reservoir, backwater of free flow, density current plunging, Sediment Flushing

1. INTRODUCTION

The reservoir Sediment Flushing is quite an important part of the reservoir sedimentation, which have great practical significance. By use of reservoir sedimentation and desilting laws, through the reservoir scheduling, the so-called ‘Storing water and discharging muddy water’ method comes from some successful experience of some reservoirs in the practice. Plenty of reservoir sedimentation slow down, or even no longer occurs sedimentation. And using the reservoir density difference between sandy rivers flow and water flow, the efficiency of reservoir sand flushing will be improved and precious water resource could be made full use of, which have the important value and practical significance of the people's livelihood.

Reservoir sediment discharge is the parameters of the reservoir sediment flushing ability. While the reservoir sediment flushing capacity are correspondent with river boundary, tributary distribution, flow regime and drainage buildings distribution etc. General boundary conditions is about channel wide among the narrow, with bending and tributaries confluence like branches distribution. A part of reservoir volume could not be ignored with water level variation, when water and sediment exchange is limited. Reservoir boundary diversity increases with flow regime diversity of the Xiaolangdi reservoir, which produce a variety of flow regimes under the same water level. Above the end of the reservoir backwater, it mostly belongs to free open channel flow, with backwater of free open channel flow in alluvial delta. But in front of the delta slope section, there are density current. Among them, the multistage water drop exist and flow regime and changes much, laws on water and sediment changing is extremely complex. Prediction accuracy of reservoir flushing would be improved with its laws.

As some key points for prediction of reservoir flushing ratio, like position of the reservoir, reservoir flushing law on backwater of open channel and open channel flow, play an irreplaceable role in analysis and research on flow regime in reservoir and judging river sedimentation. Previous work has been done much, and many meaningful results have been achieved.

Analysing the domestic and foreign precious study on gravity current plunging conditions, backwater and normal open channel flow desilting, this paper discusses the current situation and the key point of the Xiaolangdi reservoir density current prediction, and puts forward a preliminary solution.

2. RESERVOIR SEDIMENT FLUSHING CONDITIONS OF NODE ANALYSIS

2.1. Sediment flushing in open channel

The open channel flow has the strongest ability for sediment transport, backwater flow followed, and density current last. The water depth of open channel flow is small, and it has large velocity, so the water flow carrying sediment capacity is big. Water depth of backwater is larger, and its velocity is small, so water flow carrying sediment capacity is smaller. Density flow belongs to subcritical flow, inertia force plays a leading role with the saturated sediment transportation, and the minimum water carrying capacity.

The backwater of free flow obey unbalanced sediment, suspended load sediment in the water and caused sedimentation riverbed sediment exchange or flushing, related to flow, sediment concentration and bed material composition.

Backwater of free flow sediment mainly depends on reservoir volume and outbound traffic of the contrast between the relationship, is mainly carried out three kinds of forefathers' research, one kind is strong theoretical, Han Qiwei (1984), as to directly according to the unbalanced sediment formula, get the simple formula of outbound sediment concentration to siltation percentage after a row of fly:

$$\eta = \sum_{e=1}^{m} \frac{p_{e0} q}{\alpha \omega_e L} \left(1 - e^{\frac{-\alpha \omega_e L}{q}} \right) \qquad (1)$$

This formula has theoretical significance with its parameters being difficult to be used.

Another kind is has a certain theoretical meaning, indirectly, considering the influence of unbalanced sediment by empirical formula, such as Brune (1953) in the renting rate of reservoir Sediment Flushing conditions of the empirical curve, which is also joined some surveyed data of China.

The rest are mostly based on the observed data of reservoir experience relationship. From Eq.2 about reservoir backwater deposition calculation, it can be seen that with the decrease of the water volume, the increase of output discharge, open channel flow of backwater increases accordingly.

$$\eta = a \lg Z + b \qquad （2）$$

Above the Eq.2, η is the ratio between output and input sediment, Z for the backwater index, $Z = VQ_{input} / Q_{output}^2$, V for water volume (m^3) during the calculating time, a =−0. 8232, b =4. 5087。 Yellow River Institute of Hydraulic Research, Zhang Qishun, institute of hydraulic and science research of Shanxi province and Tsinghua University, Jiao EnZe established input and output sediment transport rate equation based on the observed data of the reservoir and appropriately simplified the formula to forecast the flushing efficiency of open channel flow. This shows that sediment distribution in the input section also has great influence on the sediment characteristics of backwater section in open channel flow. But the reservoir conditions differs heavily, in addition to the above empirical formula is not very comprehensive on considering factors, or main and secondary factors are not entirely clear, with using little surveyed data, so it is difficult to be widely used commonly. Therefore, reference experience relationship between the line graphs can be found in every relation diagram, and also highlighted the observed data at the same time, which indicated the corresponding reservoirs, in order to offer the reference when the user chooses.

There are a few class experience coefficients of different methods for different reservoir. Curves made by Brune, Tu Qihua, Zhang Qishun are not a single value curve, but a set of curves.Hanqiwei’s research points out the mainly depending on a parameter of backwater and sediment. Curves made by Brune, TuqiHua, Zhang Qishun have a certain theoretical basis, which is not a single value curve, but a set of curves for different reservoirs. It is better for people to conform to the actual by the best combination of experience in the practical work.

2.2. Plunging of density current

Study on density current plunging is divided into two kinds, one kind is the "box" model, using small scale flume experiment, research and carrying a certain volume of brine muddy water shape formation density flow movement situation, and to establish a validated mathematical model, calculation, such as Huppert & Simpson (1980), Dade & Huppert (1995) and Hogg & Huppert (2001), Lee and Yu (1997) using long 20 m, width 0.2 m, 0.6 m deep sink, suspended sediment for kaolin to test and mathematical model calculation, close to the test results; As another kind of prototype experimental study, using natural river reservoir being built on collecting relevant data, to analysis and research, acquired a lot of rules, such as Eril Emda reservoir in Algeria, Guanting reservoir,Sanmenxia reservoir, Xiaolangdi reservoir, Danjiangkou reservoir in China, lake Mead in America.

As dive into the research methods of hydraulics, mainly divides into three aspects, one aspect is the use of revised the Fr number judgement, such as Fan Jiahua flume experiment are used to get the revised the Fr number 0.78, in Harleman (1961) based on the work, Wunderlich and Elder (1973) argue that dive point location is determined by the modified the Fr number formula is also given; Savage and Brimberg (1975) for Schijf and Schnfeld (1953) gives a dimensional motion equations are derived, considering the bottom slope and the influence of the interface and the bottom resistance, corrected the Fr number;Hebbert etal. (1979) to simplify the water cross section for the triangular section rather than the conventional rectangular cross section, the triangle at the bottom of the half Angle as a parameter, momentum and mass conservation equation are used to get the downstream section corrected the Fr number and the section depth and dive into the water depth to determine the ratio of the relationship between dive into the water depth.

One aspect is the use of hydraulic factors of judgment, namely uniform deep water and actual depth contrast. Such as Singh and Shah (1971) in tilted salt density flow experiment was carried out in the sink to get into some depth, then similar formulae is derived from the momentum equation form, Wunderlich and Elder (1973) hypothesis into the Fr is 0.5, get into some depth, Akiyama and Stefan generalized model (1981) using dive point, under the condition of uniform flow momentum integral equation of get into some depth under small slope.

Table 1. Fr at plunging point

Literature	Fr at plunging point
Ford and Johnson (1980)	0,1 to 0,7
Itakura and Kishi (1979)	0,54 to 0,69
Singh and Shah (1971)	0,30 to 0,80
Kan and Tamai (1981)	0,45 to 0,92
Fukuoka and Fukushima (1980)	0,40 to 0,72
Farrell and Stefan (1986)	0,66 to 0,70
Akiyama et al. (1987)	0,56 to 0,89
Fan Guhua	0.78

On the other hand is to use other methods are derived.Basson from the perspective of rivers, the minimum power, put forward the formation and the condition of continuous transport density flow;Rooseboom (1975) from the water and muddy water density difference pressure difference point of view, put forward the conditions for density current, density flow pressure is greater than the turbulent pressure;Akiyama et al. (1987) to verify the occurrence of uniform density flow density flow when the power is less than or equal to the river incoming power. Wang Wanzhan (2008) concluded that their research results show that the main factors affecting the formation of density flow is, into the river upstream and downstream slope and density difference.

These dive consider into points distance is close to import or distance into the upstream near the hydraulic factors under the condition of known judgment and prediction. In Xiaolangdi reservoir in practical reservoir scheduling, subject to the natural conditions and technical level, the hydraulic conditions of point test has always been a difficult problem.

For density current into point prediction, predecessors have carried out extensive research, at the beginning of the reservoirs, regardless of the channel type reservoirs and lakes type reservoir, reservoir volume is big, general in density flow form and sand reservoir, and because the streamwise above deposition is less, incoming water and sediment conditions can be used as a dive into the water discharge conditions for prediction and calculation; In late stop sand for long and narrow channel type reservoir, due to large reservoir sedimentation, reservoir submerge point upstream water and sediment conditions and the interaction of the complex boundary conditions, diving points complicated water and sediment conditions change, the present stage is not to predict, need further prototype observation, using mathematical model and physical model study, data analysis and other methods.

3. ANALYSIS ON SEDIMENT FLUSHING FORECAST IN XIAOLANGDI RESERVOIR

Between 2001 ~ 2003, the location of the Xiaolangdi reservoir density flow occurred basic fixed, about 77.28 km from the dam (HH43) ~ 60 km (HH36), narrow upper reaches the river deep dive point, less water and riverbed sediment exchange, a large amount of sediment deposition in into some place, some walked in the form of density flow silting, the rest of the sediment in the form of density flow running to the front of the dam. From 2004 to 2009, a number of reservoirs and the water-sediment regulation practice, as is in Li tao et al. (2006,2011),based on the single reservoir, library and space docking methods such as mold density flow in Xiaolangdi reservoir, so as to make full use of the density flow sand flushing to save water to reduce the reservoir sedimentation. Reservoir, therefore, the water-sediment regulation plan preparation, scheduling goal is to continuously improve the reservoir row of fly for reservoir sedimentation reduction, and increase the lower reaches of the Yellow River beach flow.

Concerned the water-sediment regulation of artificial density flow, is in the middle without flooding, through joint scheduling Wan Jiazhai, Sanmenxia and Xiaolangdi reservoir, make full use of Wan Jiazhai, Sanmenxia reservoir above water, wash in the Sanmenxia reservoir area of flood sediment deposition and accumulation period at the end of the Xiaolangdi reservoir sediment, shape the density current in Xiaolangdi reservoir area and desilting outbound, realization of Xiaolangdi reservoir Sediment Flushing and adjust the target in the form of reservoir deposition. Shape the variable density flow reservoir of water sediment flow, to drain the reservoir sediment, reducing reservoir sedimentation, and make the purpose of reservoir sediment drainage loading outbound smoothly into the sea. From 2004 to 2009, based on the main stream reservoir group of scheduling, artificial joint density flow model has been underway for six times, desilting is detailed in Table 2.

We can see from Table 2,2004-2009,concerned the water-sediment regulation period, Sanmenxia reservoir

Sediment Flushing 296.6 million t, Xiaolangdi outbound sediment, a total of 087.2 million t, row of fly by an average of 29.4%.But concerned density flow line vary widely, fly as high as 61.8% in 2008, accounting for 52.5% of the 6 times concerned density current discharge; For 2005 years, 2009 years older than only 4.42% and 6.61%, respectively, especially concerned the water-sediment regulation in 2009, density flow running distance is the shortest, incoming sediment 054.5 million t to Xiaolangdi reservoir outbound sediment 003.6 million t, row of fly is only 6.61%, is only about 1/5 of the average line of fly.

Table 2. Flushing characteristics during water-sediment regulation of Xiaolangdi reservoir by density flow before flood period

year		2004	2005	2006
Period		7.7～7.14	6.27～7.2	6.25～6.29
duration(d)		8	6	5
Average discharge（m^3/s）		689.6	776.9	1254.5
Sediment content（kg/m^3）		54.4	95.8	58.8
Sediment volume（billion/10 t）	Sanmenxia	0.385	0.452	0.23
	Xiaolangdi	0.055	0.02	0.069
flushing ratio（％）		14.29	4.42	30
year		2007	2008	2009
Period		6.26～7.2	6.27～7.3	6.30～7.3
duration(d)		7	6	4
Average discharge（m^3/s）		1568.7	1324	1062.7
Sediment content（kg/m^3）		50.2	71.2	122.8
sediment volume（billion/10 t）	Sanmenxia	0.613	0.741	0.545
	Xiaolangdi	0.234	0.458	0.036
flushing ratio（％）		38.17	61.8	6.61

Xiaolangdi reservoir density flow shape, there are three kinds of the sediment sources: one is occurred in the middle reaches of the Yellow River small flood, Tongguan to sand to improve the density flow line above most good fly; Second is sediment deposition in the Sanmenxia reservoir in flood season, this part, including WanJiazhai reservoir sediment by Tongguan water filling water flushing and Sanmenxia reservoir of the chang, enter the Xiaolangdi reservoir, is the main sand density flow and sand; Three is from the Xiaolangdi reservoir slope section of scouring sediment itself, rely on or in the early years of the Sanmenxia reservoir in the water-sediment regulation big flow process, warp, scouring accumulation in Xiaolangdi reservoir on some of the more fine sediment desilting outbound in density flow way.

From calendar year plan preparation and practice, from the Yellow River water-sediment regulation of Xiaolangdi reservoir area water sand transport complex and changeful, row involving reservoir fly not accurately predict reservoir backwater of free flow period of erosion or deposition and backwater flow period of sedimentation and gravity current plunging forecast period of water and sediment conditions, the corresponding power for the section water sediment exchange law knowledge level, such as it still needs further research.

To sum up, the Xiaolangdi reservoir discharge fly prediction is the key to grasp the change rule of the complicated water flow conditions of sand, and predict the reservoir at the present stage of fly are preliminary, qualitative prediction is relatively easy, and quantitative forecast still cannot meet the production requirements. Must strengthen the reservoir water sand factor test, the use of the mathematical model and physical model two kinds of methods, research different libraries section, different flow of water and sediment transport law, to improve the predictive accuracy of Xiaolangdi reservoir row of fly.

4. CONCLUSIONS AND RECOMMENDATIONS

From previous studies at home and abroad, the key technologies for reservoir Sediment Flushing, whether the reservoir flow period of water and sediment transport and Sediment Flushing, or gravity current plunging the discriminant conditions, are mostly stay in experience, mostly as a macroscopic and long period of time (years), as a short duration, high precision of predictionneed to be further studied, with complex reservoir boundary conditions and the existence of numerous tributaries of Xiaolangdi reservoir. Accurate prediction of Xiaolangdi reservoir flushing sediment quantity still has a long way, reservoir water and sediment factor tests must be strengthened in the future, using the mathematical model and physical model, and different segment and water and sediment inflow movement must be studied to promote the accuracy of calculation, thus improving the ability to predict reservoir flushing sediment.

ACKNOWLEDGEMENT

The study is supported by national nature science foundation of China（No.51309110、51179072、51509100）, Non-profit Industry Financial Program of MWR (No.201401023) and Yellow River Institute of Hydraulic Research Central level, scientific research institutes for basic R & D operating expenses of special funds (compact number:HKY-JBYW-2014-01). We thank anonymous reviewers for their patience and time for

reviewing this article.

REFERENCES

Han qiwei ，Shen Xiying. （1984）:Reservoir capacity of the cone of the deposition and deposition process and backwater desilting relationship [J]. Journal of sediment research, 2, 35-51.

Brune，G.M. （1953）: Trap Efficiency of Reservoirs [J].Trans.AGU, 34 :(3), 10.

China water conservancy society of professional committee of silt editor. （1989）:Sediment handbook [M]. Beijing: China environmental science press.9, 330-400.

Institute of water conservancy and science of Shanxi province co-editor of institute of sediment research of water conservancy engineering department of Tsinghua University. (1979) reservoir sediment [M]. Beijing: water conservancy electric power press, 2:76-82.

Fan Jiahua. (1960) Density flow experimental study [J]. Water science progress. 9 (2):275-303.

Fan Guhua. (1986): Density flows in a reservoir [J]. Wat. Int...11 (3):107-116.

Zhang Qishun, etc. (1982): sketch of scour and deposition in reservoir and the calculation of its process [J]. Journal of sediment research. 1:1-12.

Savage, S.B. and Brimberg, J. (1975): Analysis of Plunging Phenomena in Water Reservoirs [J]. *Hydro. Res., Int. Ass. Hyd. Res.*, 13: (2), 187-204.

Singh, B. and Shah, C.R. (1971): Plunging Phenomenon of Density Currents in Reservoirs [J].*La Houille Blanche*.26 (1), 59-64.

Ford，D.E.，Johnson，M.C.，and Monismith，S. G. (1980): Density inflows to Degray Lake Arkansas [J].2rd Int.Symp.on Stratified Flows，IAHR.Trondheim，Norway.

Akiyama and Stephan, J. and Stefan, H.G. (1987): Onset of Underflow in Slightly Diverging Channels [J]. *Hydr. Engrg., Am. Soc. Civ. Engrs*, 113: (7), 825-844.

Basson, G.R. and Rooseboom, A. (1998): Dealing with Reservoir Sedimentation [J]. South African Water Research Commission Publication,11-20.

Wang Wanzhan. (2006): Different flow and study abroad overview [C]. Reservoir density flow problems seminar. Zhengzhou: the Yellow River water conservancy press. 10, 76-81

Li tao, Zhang Junhua, etc. (2006): review on reservoir density flow [J]. China's rural water conservancy and hydropower. 9:21-24.

Li tao, Zhang Junhua shu-kui Chen, Ma Huaibao. (2011): Conditions of Xiaolangdi reservoir density flow into study [J]. China's rural water conservancy and hydropower. 10.

4th APG Symposium and 9th EADC on

INNOVATIVE TECHNOLOGIES FOR DAMS AND RESERVOIRS TOWARD THE FUTURE GENERATIONS

Influence of Polyurea Impermeable System on the Effect of CFRP-strengthened Reinforced Concrete

L.Bingqi & Z.Yuchi
China Institute of Water Resources and Hydropower Research, Beijing, China
libq@iwhr.com

L.Xiaonan
Beijing University of Chemical Technology, Beijing, China

ABSTRACT:
We propose a comprehensive method combined anti-seepage hydraulic structure and CFRP-strengthened reinforcement in this paper. By means of model experiment and Finite Element Method (FEM), the influence of polyurea impermeable system on the mechanical property of CFRP-strengthened concrete is studied. Firstly, the comparative experiments are conducted, and the results show that the interfacial bonding property can be enhanced with polyurea impermeable body contained. Secondly, the bilinear bond-slip model on the framework of ABAQUS is also proposed aimed at the non-linear finite element analysis, on the conditions of whether or not containing the polyurea impermeable body. The numerical results agree well with experimental data, if the polyurea impermeable body contained. The polyurea impermeable body can strengthen the load carrying capacity, and improve the interfacial fracture energy, which can be elucidated by the numerical results and experimental data.

Keywords: polyurea impermeable system; CFRP Sheet; debonding; bonding property; FEM analysis

1. INTRODUCTION

It is usually appear the problems of anti-seepage and reinforcement in hydraulic structures. The traditional methods of hydraulic concrete strengthening conclude steel-bonded reinforcement method, pre-stress strengthening, increased cross-section reinforcement method, steel-reinforced law outsourcing and so on. Comparing with existing concrete strengthening methods, CFRP-strengthened concrete has a lot of advantages, such as convenient for operation, anti-corrosion, high strength and low dead-weight. Currently, the bonding exterior CFRP-strengthened concrete method is commonly used, such as Teng et al.(2002) and ACI. The CFRP-strengthened concrete method bonds FRP to surface of concrete with adhesive materials, which make concrete structure and CFRP be a unified whole and ensure that two parts work together. Adhesive materials include primer, leveling material and dipping resin. As shown in Fig.1, the functions of primer are strengthening concrete surface adhesion and improving the bond strength between concrete and leveling material or dipping resin. The function of leveling material is making surface evenness of concrete meets the requirement by the way that filling the hole and crack in the concrete, which would ensure high bond strength between primer and dipping resin. The primary adhesive material that is applied to bond carbon fiber sheets is dipping resin, which would bond carbon fiber sheets and concrete datum tightly.

KOBATAKE Yoshiro et al. (1996), Dolan B E et al. (1998) and YUE QingRui (2000) had demonstrated that the performance of CFRP-strengthened concrete is determined by adhesive property between carbon fiber sheets and concrete datum, which is affected by many factors. Sang-Kyun Woo et al. (2010) has researched on some factors like length, width and layer of CFRP and concrete intensity. According to Dai J G et al. (2003), the properties of adhesive materials play a major role in determining bond performance. In this paper, we propose a new bond structure as shown in Fig.1. Add the flexible polyurea impermeable body to the layer between concrete and carbon fiber sheets. Huang WeiBo et al. (2003) proved that the polyurea has good adhesion with concrete and other properties such as high curing speed, deformation ability, environmental friendly, low modulus of elasticity and high elongation. Due to the above advantages, this method overcomes many disadvantages of traditional bond structure like the CFRP easy to strip, fracture. Meanwhile, it effectively avoids the leakage of concrete structure.

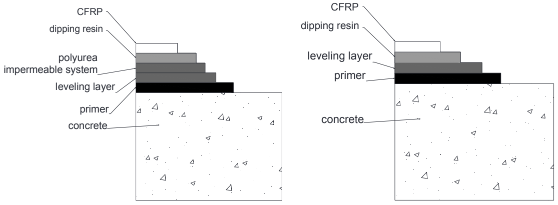

(a) contain polyurea impermeable body (b) remove polyurea impermeable body

Figure 1. Carbon fiber reinforced concrete

This research compares model experiment with FEM, and analyses the adhesive properties of interfaces between

CFPR and concrete that polyurea impermeable body is contained or not. Furthermore, the adhesive properties include ultimate bearing capacity and debonding energy.

2. EXPERIMENTAL MODEL

Taking comparative experiments study on bond strength between carbon fiber sheets and concrete by mean of in-plane shear method at room temperature (around 25 degree centigrade). The first working condition contains polyurea impermeable body, by contrast, the second condition doesn’t contain. Each of two conditions includes 5 test specimens.

2.1. Material Property

In this experiment, adopting C30 concrete and measuring concrete compressive strength in accordance with “Standard for test method of mechanical properties on ordinary concrete”(GB/T 50081-2002). The debonding fracture in CFRP-strengthened concrete mainly occurs on the concrete surface. Oehlers D J et al. (1990) proposed that debonding fracture is mainly caused by shearing strength in 1990. Concrete shearing strength determines the shearing failure capacity under shear stress. Guo ZhenHai (1999) adopted Eq.(1):

$$\tau_f = 0.39 f_{cu}^{0.57} \tag{1}$$

Where τ_f is the shearing strength of concrete, f_{cu} is the cube compressive strength of concrete.

Table 1 list the compressive strength and shearing strength which is calculated by Eq. (1)

Adhesive material properties in this study are shown in Table 2. Normal bonding strength between primer and concrete datum is 3.1MPa, elongation of polyurea is about 300%, and adhesive strength between polyurea and primer is 3.4MPa. However, adhesive strength between dipping resin and polyurea impermeable body is 3.8MPa. Mass per unit area and design thickness of carbon fiber sheets are 600g/m^2 and 0.333mm, respectively. Furthermore, mechanical properties of carbon fiber sheets are shown in Table 3.

2.2. Experimental Method

We take in-plane shear method in the experiment and specimen is made of precast concrete which cross section is 300mm*300mm and 800mm long. Experimental mechanics model as shown in Fig.2 takes displacement load method and loading rate is controlled by hydraulic jack. Force sensors measure force and displacement sensors installed at the bottom of specimen to obtain relative displacement of carbon fiber sheets through electronic data of force and displacement automatically measured. Also, we obtain deformation of carbon fiber sheets from strain gauge on the top of them. Furthermore, force, relative displacement and deformation of carbon fiber sheets are measured in the experiment

2.3. Results and Discussion

2.3.1. Interface debonding fracture energy

We can obtain local adhesive stress τ through the difference Eq.(2) :

$$\tau = E_f t_f \frac{d\varepsilon_f}{dx} \tag{2}$$

Where ε_f is strain for CFRP which is measured by strain gauge located on the top of CFRP.

Micro-segment S between two adjacent strain gauges is taken force analysis. The hypothesis is that shear stress is uniform pressure distribution along the segment.

Maximum adhesive stress $\tau_{\max}$ is obtained from whole force analysis of the micro-segment.

$$\tau_{\max} = \Delta\varepsilon_f E_f A_f / (s \bullet b_f) \tag{3}$$

Table 1. Mechanical Properties of Concrete

Test value	Condition 1					Condition 2				
specimen	1-1	1-2	1-3	1-4	1-5	2-1	2-2	2-3	2-4	2-5
Compressive strength/MPa	32.8	34.2	33	31.8	32	31.7	32.2	34	32.5	33.4
Shearing strength/MPa	2.85	2.92	2.86	2.80	2.81	2.8	2.82	2.91	2.84	2.88

Table 2. Mechanical Properties of Resin Materials

Performance index	primer	polyurea impermeable body	Digging resin
Tensile strength/MPa	—	23.3	36
Elasticity modulus/MPa	—	28	2910
Compressive strength/MPa	—	—	75
Normal bonding strength/MPa	3.1	3.4	3.8

Table 3. Mechanical Properties of Carbon Fiber Sheets

Performance index	Tensile strength	Elasticity modulus	standard
value	4260 MPa	254GPa	Technical specification for strengthening concrete structures with carbon fiber reinforced polymer laminate（CECS146）

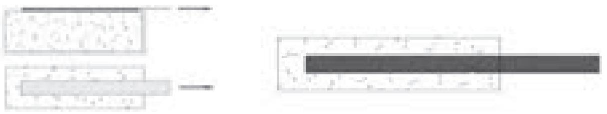

Figure 2. Experimental mechanics model

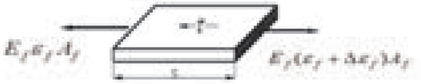

Figure 3. Force analysis of micro-segment

Where $\Delta\varepsilon_f$ is the difference between adjacent strains gauges under peak load condition. E_f is the elasticity modulus of carbon fiber sheets, MPa. A_f is the cross section of carbon fiber sheets, mm² S is the interval distance of strain gauges, mm. b_f is the width of carbon fiber sheets,mm.

According to study of Taljsten B (1994) on fracture mechanics, under the condition of enough CFRP adhesive length, the interface debonding fracture energy G_f is:

$$G_f = \frac{p_u^2}{2 \cdot b_f^2 \cdot E_f \cdot t_f} \tag{4}$$

Where G_f is interface debonding fracture energy, N·mm^{-1}. p_u is debonding bearing capacity, KN. b_f is width of carbon fiber sheets, mm. t_f is the thickness of carbon fiber sheets, mm.

Effective anchoring length L_e is calculated by Eq. (5):

$$L_e = p_u / \left(\tau \cdot b_f\right) \tag{5}$$

The result from the experiment and calculation based on above Eqs. (3),(4),(5) are summarized in Table 4.

(1) Ultimate capacity and interface debonding fracture energy of condition 1 are better than condition 2. (2) Maximum adhesive stress of working condition 1 is lower than condition 2.The reason of (1) is polyurea impermeable body between carbon fiber sheet and concrete datum transmits the shear stress effective, and will enhance the capacity of interface. Smaller interface shear stiffness due to flexible and high strength of polyurea impermeable body improves the interface debonding fracture energy. The reason of (2) is polyurea impermeable body pulls down the whole shear stiffness of adhesive materials, which can avoid the phenomenon of stress concentration in carbon fiber sheets. Maximum adhesive stress declined and effective anchoring length increased between carbon fiber sheet and concrete when containing polyurea impermeable body

Table 4. List of experiment results

Specimen number	p_u /KN		G_f /N·mm^{-1}		$\tau_{\max}$ /MPa		L_e /mm			
	value	average	value	average	value	average	value	average	Failure mode	failure surface
1-1	137.20	132.35	11.13	10.40	3.19	3.25	430.09	409.12	Carbon fiber sheets	
1-2	132.98		10.45		3.27		406.67		Carbon fiber sheets	
1-3	117.64		8.18		3.46		340.00		debonding	Primer surface
1-4	141.59		11.85		3.08		459.71		Carbon fiber sheets	
1-5	63.06*		2.35*		2.12*		297.45*		invalid	
2-1	43.96	45.72	1.14	1.24	5.68	5.02	77.39	94.30	debonding	Dipping resin
2-2	42.22		1.05		5.94		71.08		debonding	Concrete surface
2-3	46.89		1.30		4.35		107.79		debonding	Dipping resin
2-4	49.82		1.47		4.12		120.92		debonding	Dipping resin
2-5	34.03*		0.68*		2.53*		134.51*		invalid	

2.3.2. Load-displacement curve

Experiment data obtained from in-plane shear test is shown in fig.4

Carbon fiber sheets bond with concrete through adhesive materials when containing polyurea impermeable body. Load-displacement curve is shown in Fig.4(a), load and displacement present linear elastic relation in the situation of small load, and interface adhesive stress increase along with the increase of load. Load-displacement curve presents nonlinearity when load reaches a critical point. Interfaces among concrete, adhesive materials and carbon fiber sheets appear micro-crack, stress redistribution occurred in the interface between carbon fiber sheet and concrete at the same time.

Along with the increase of load, carbon fiber sheets ruptured when tensile stress reaches strength of extension.

The load-displacement curve shown in Fig.4(b) is under the condition without containing polyurea impermeable body. Adhesive interface appears micro-crack even load is small. Along with the increase of load, interface adhesive shear stress will soften gradually. Interface debonding extend to head quickly when load reaches ultimate load, and brittle debonding fracture is happened in the interface.

2.3.3. CFRP strain distribution

As shown in Fig.5, CFRP strain distribution curve in the situation of peak load is obtained from CFRP-strengthened concrete structure experiment.

We can conclude from Fig.5(a) that closer to loading end, larger the strain of CFRP. Strain in the carbon fiber sheet transmit steadily and uniform stress distribution in it. Under the condition without containing polyurea impermeable body as shown in Fig.5(b), strain couldn’t transmit effectively through carbon fiber sheet, and adhesive shear stress distribution is scattered. Because of stress concentration, CFRP and concrete can’t work together. As a result, strength of CFRP out of function.

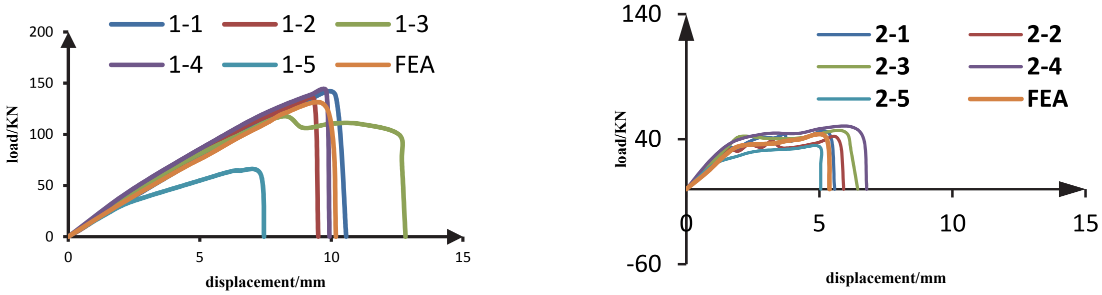

(a) contain polyurea impermeable body (b) remove polyurea impermeable body

Figure 4. Load-displacement curves

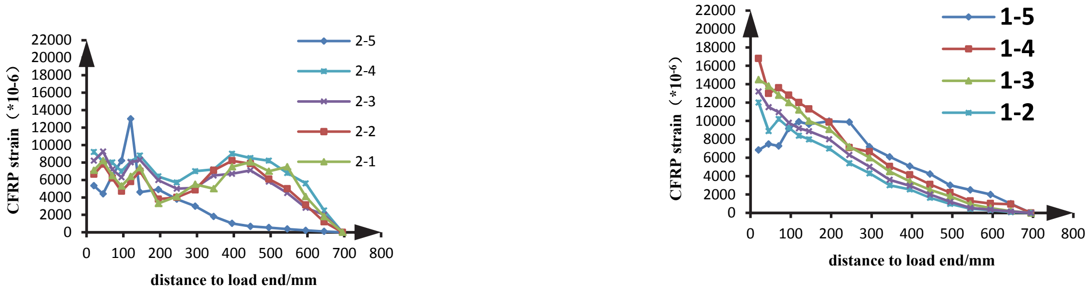

(a) contain polyurea impermeable body (b) remove polyurea impermeable body

Figure 5. CFRP distribution

3. FEM ANALYSIS

Nonlinear elastic FEM analysis is taken to CFRP-reinforced concrete using ABAQUS. Based on abundant element type and material model, under the conditions that whether polyurea impermeable body is contained or not, and building different FEM models and material constitutive models to concrete, CFRP and adhesive materials.

3.1. FEM Model

In the analysis, as shown in Fig. 6., concrete and CFRP take C3D8R and CFRP as element type, respectively. Furthermore, rebar is set as Timoshenko beam element (B32). In order to simulate fracture, crush of adhesive materials and bond slip of interface, as shown in Fig. 6(b), it takes cohesive element (COHD8) as adhesive material between CFRP and concrete. Reinforce beam element is embedded into concrete element, coupling DOF, making rebar and concrete work together.

3.2. Material Constitutive

Lee, Jeeho et al (1998) and Lubliner J et al (1989) adopted elastic and plastic fracture-damage model will be used in simulating concrete behviour, and introduces damage index to concrete model. Discounting elastic stiffness matrix of concrete matches the character of concrete that unload stiffness decreasing along with the increase of damage. The behavior of crack can be controlled by experimenter and better simulating the behavior of concrete under cycling load. As shown in Fig.8 is the material constitutive curve. Xie Jian et al (2001).

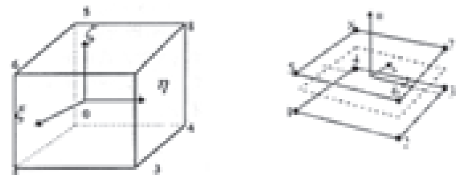

(a)solid element with 8 notes (b)cohesive element with 8 notes

Figure 6. Finite element types

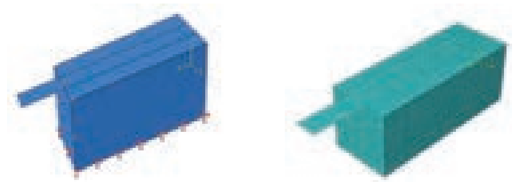

Figure 7. FEA models

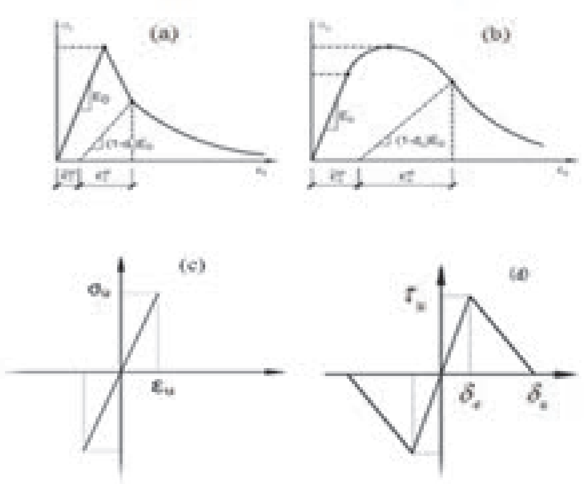

Figure 8. Material constitutive rules

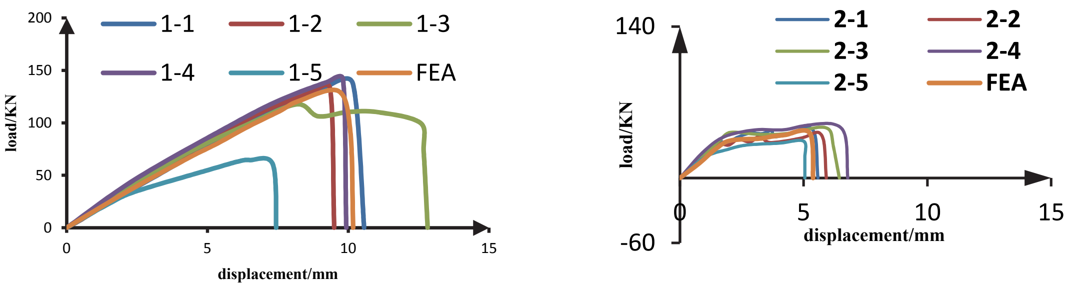

(a) contain polyurea impermeable body (b) remove polyurea impermeable body

Figure 9. Load-displacement curves

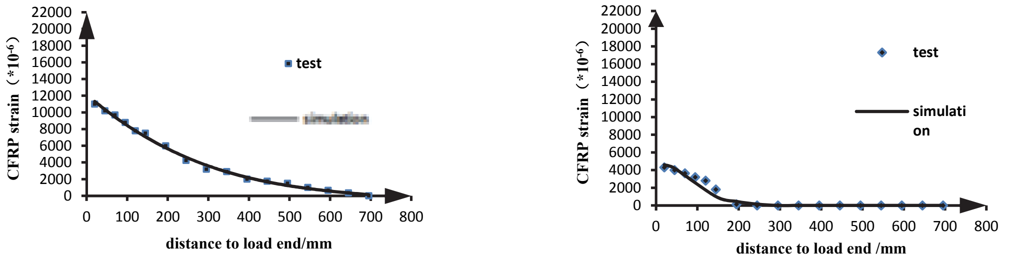

(a) contain polyurea impermeable body (b) remove polyurea impermeable body

Figure 10. Strain distribution of CFRP

Table 5. The statistical results of $\delta_u, \delta_e, \tau_u$

condetion	τ_u /MPa	δ_e /mm	δ_u /mm
1（average）	3.72	2.54	4.85
2（average）	2.64	0.06	0.78

Table 6. Results comparison between test and FEA

condition	P_u/KN			G_f/N·mm-1		
	Average of test	simulation	Average of test /simulation	Average of test	simulation	Average of test /simulation
1	132.35	130.14	1.02	10.40	9.32	1.12
2	45.72	41.39	1.10	1.24	1.09	1.14
1/ 2	2.89	3.14	/	8.39	8.76	/

(2001) demonstrated that carbon fiber sheet in CFRP-strengthened concrete technology wouldn't exceed tensile strength. However, stress-strain curve of CFRP keeps well elastic before damage, as shown in Fig.8(c).
Bond-slip model between CFRP and concrete uses bilinear relation curve as shown in Fig.8(d). δ_u, δ_e, τ_u of adhesive material are obtained from tensile test and bond strength test. We take average values in table 5 as the properties of materials.

3.3. Results

3.3.1. Load-displacement Curve

Load-displacement curves obtained from simulation and experiment are compared in Fig.9.
Results from simulation or experiment keep better consistency whenever containing polyurea impermeable body or not. However, the bilinear bond-slip constitutive model could simulate the adhesive relation between CFRP and concrete, meanwhile, it can predict ultimate capacity of CFRP-strengthened concrete and extension of interface.

3.3.2. CFRP strain distribution

6mm displacement load to specimen is applied in in-plane shear test. Strain distribution curve is shown in Fig10. Results from simulation or experiment keep better consistency whenever containing polyurea impermeable body or not.

3.3.3. Comparative results

Debonding capacity and interface debonding fracture energy of simulation are listed in Fig.6. For condition 1, ratios for maximum load and interface debonding fracture energy between test and simulation are 1.02 and 1.12, respectively. For condition 2, the ratios are 1.10 and 1.14.This shows that the bilinear bond-slip constitutive model could simulate the adhesive relation between CFRP and concrete. Comparing the ultimate capacity and interface debonding fracture energy between tow conditions through test and simulation, we can conclude that polyurea impermeable body highly increases ultimate capacity and interface debonding fracture energy of CFRP-strengthened concrete.

4. CONCLUSIONS

(1) Properties of adhesive materials have a big influence on bond strength and failure mode between CFRP and concrete. In this paper, we propose adhesive materials containing polyurea impermeable body, which is a flexible material has low stiffness and high strength.
(2) Polyurea impermeable body could reduce whole shear stiffness of adhesive materials, and improve bond strength between CFRP and concrete. Furthermore, the body can enhance ultimate shear strength, debonding capacity and interface bonding fracture energy. In this paper, comparing the results from simulation and test, proving that condition containing polyurea impermeable body could highly increase bonding strength and interface bonding fracture energy, and test presents 2.89 and 8.39 times than condition doesn't contain polyurea impermeable body.
(3) Strain distribution of CFRP shows that polyurea impermeable body could improve bond quality between CFRP and concrete, make shear stress transmit effectively and fully make use of CFRP's strength.
(4) Results from simulation or experiment keep better consistency whenever containing polyurea impermeable body or not. This shows that the bilinear bond-slip constitutive model could simulate the adhesive relation between CFRP and concret.

REFERENCE:

Teng J G. FRP (2002): Strengthened RC Structures [J]. Frontiers in Physics, 266.

American Concrete Institute. Building Code Requirements for Reinforced Concrete[s].ACI

KOBATAKE Yoshiro, KIMURA Kohzo, KATSUMATA Hideo. (1996)A Retrofitting Method For Reinforced Concrete Structures Using Carbon Fiber [J]. Japanese architectural society technical report, (2):62-67.

Dolan B E, Hamilton H R, Dolan C W. (1998) Strengthening with bonded FRP laminate [J].Concrete International, 20(6):51-55.

YUE QingRui. (2000) Present Status of Research and Application of Strengthening and Repairing Technology with Carbon Fiber Reinforced Plastic(CFRP) and its outlook in China [J]. Industrial Construction, 30(10):23-26.

Sang-Kyun Woo, Yun Lee. (2010) Experimental study on interfacial behavior of CFRP-bonded concrete[J]. KSCE Journal of Civil Engineering, 14(3):385-393.

Dai J G, Ueda T. (2003) Local bond stress slip relations for FRP sheets-concrete interfaces, Proc.6th International Symposium on FRP Reinforcement for Concrete Structures World Scientific Publications, Singapore, 143-152.

Huang WeiBo, Yang YuRun, Wang BaoZhu. (1999) Spray Polyurea Elastomer Technology [J]. Polyurethane Industry, 44(4):7-11.

Oehlers D J, Moran J P. (1990) Premature failure of externally plated reinforced concrete beams[J]. Journal of Structural Engineering, 116(4):978-995.

GuoZhenHai, Principle of reinforced concrete.Tsinghua University Press, Beijing

Täljsten B. (1994)Plate bonding strengthening of existing concrete structures with epoxy bonded plates of steel or fiber reinforced plastics [J].

Lee, Jeeho, Fenves, Gregory L. (1998) Plastic-Damage Model for Cyclic Loading of Concrete Structures [J]. Journal of Engineering Mechanics, 124(8):892-900.

Lubliner J, Oliver J, Oller S, et al. (1989)A plastic-damage model for concrete[J]. International Journal of solids and structures, 25(3): 299-326.

Xie Jiang, Zhao Tong, Liu MingGuo et al. (2001) Experimental Study on the Mechanical Properties of Continuous Carbon Fiber Sheet [J]. New Carbon Materials, 16(1):63-66

Papers

Session (3) Dam Safety, Risk Management and Climate Change

Experimental Study on Seismic Response Behavior of Fill Dams Influenced by Dam's Shapes and Input Wave's Directions

Y. Hayashida, S. MASUKAWA, I. ASANO & H. TAGASHIRA
National Institute for Rural Engineering, National Agriculture and Food Research Organization, Tsukuba, Japan.
fill@affrc.go.jp

ABSTRACT:
The characteristics of the seismic behaviour of fill-type dams were examined by shaking table tests, in which three shapes of dam models, namely, symmetric about both a maximum cross section and a dam axis, symmetric about only a dam axis, and asymmetric about both a maximum cross section and a dam axis, were shaken separately in the stream direction and in the dam axis direction, and then the effects of the dam's shape and the direction of the input wave on the seismic response behaviour were verified. From the results of the experiment, the point at which the maximum acceleration values were recorded during the shaking in the stream and the dam axis directions was found to be right above the deepest part of the dam's valley. It was clarified that the response orthogonal to the shaking direction could arise depending on the shapes of the dam, the direction, and the dominant frequencies of the input waves. In particular, in the case of shaking in the dam axis direction, the point at which no response could be incited appeared on the crest of the dam depending on the shape of the dam and the dominant frequencies of input waves.

Keywords: Fill dam, Seismic response, Shaking table test, Shape of dam, Direction of input wave

1. INTRODUCTION

After the Southern Hyogo Prefecture Earthquake in 1995, huge earthquakes have been occurred frequently in Japan, for example the Mid Niigata Prefecture Earthquake in 2004, the Iwate-Miyagi Nairiku Earthquake in 2008, the 2011 off the Pacific coast of Tohoku Earthquake and so on.

No fill dam designed by seismic coefficient method was utterly destroyed caused by such huge earthquake motion. However, damages such as settlement and longitudinal cracks at crest were observed (Kohgo,Y. 2016; Masukawa,S., et.al. 2000, 2002, 2005, 2009, 2012 and 2014). It is supposed that these damages are caused by the complicated three dimensional seismic behaviour of dam body. So it is considered that the complicated three dimensional seismic behaviour of dam body in higher seismic mode will be important factor to manage the safety of existing dams.

In this study, the characteristics of the seismic behaviour of fill type dams were examined by shaking table tests, in which three dam models with different shapes were shaken separately in the stream direction and in the dam axis direction, and then the effects of the dam's shapes and the direction of the input wave on the seismic response behaviour were verified.

2. TEST METHOD

2.1. Property of Dam Models

Three types of dam model which have different shapes are tested to evaluate the effect of dam's shapes to their seismic behaviour. A model consists of the dam body made of silicon rubber and abutment made of metal frames and wood board. Schematics of dam models are shown in Fig. 1.

The shape of Model A is symmetric about both a maximum cross section and a dam axis. The shape of Model B is symmetric about only a dam axis and the shape of Model C is asymmetric about both a maximum cross section and a dam axis. All models have same height, length of crest and slope gradient, their height are 300 mm, their lengths of crest are 1200 mm and their slope gradients are 1: 2.5. Accelerometers are set on the appointed place shown in Fig. 1 to record the acceleration during tests. Arrows on Fig. 1 show the direction of positive acceleration value.

2.2. Test condition

This study intends to verify the change of seismic behaviour according to shaking direction and frequency of input wave.

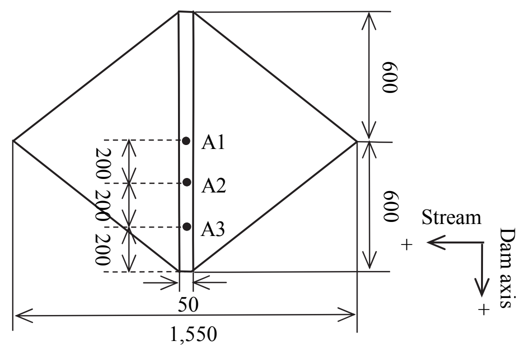

(a) Model A

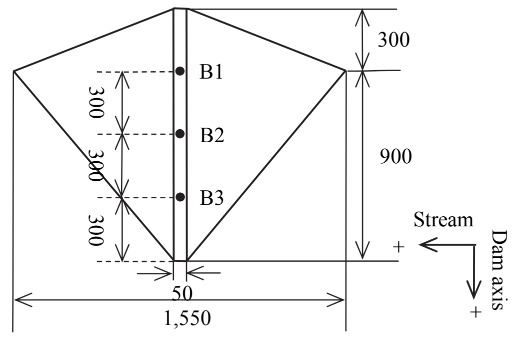

(b) Model B

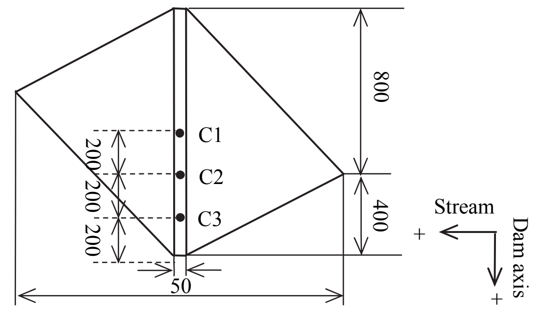

(c) Model C

● : Accelerometer Unit : mm

Figure 1. Shape of models

Shaking directions are stream and dam axis direction, the former is called as Case 1, and the latter is called as Case 2. Input waves used in tests are sine waves whose frequency are swept from 0.6 Hz to 14.0 Hz and their amplitude are 1.0 m/s^2. However, the shaking table test device used in test cannot sweep the frequency from 0.6 Hz to 14.0 Hz thoroughly because of the limitation of data volume in a test. So two waves are adopted as input waves. Wave 1 sweeps the frequency from 0.6 Hz to 9.3 Hz, and Wave 2 sweeps the frequency from 4.7 Hz to 14.0 Hz. Amplitude of each wave is 1.0 m/s^2.

Table 1 shows the specification of the experiment cases. Fig. 2 shows results of acceleration records measured at the shaking table in an experiment. As shown in Fig. 2, it is found that amplitudes of input waves are almost 1.0m/s^2 and the shaking table test device represented the prescribed amplitude value of input waves.

Table 1. Specifications of experiment cases

	Experiment case	Frequency (Hz)	Amplitude (m/s^2)	Shaking direction
Frequency sweep	Case 1	0.6 ～9.3 (WAVE 1) 4.7～14.0 (WAVE 2)	1.0	Stream
	Case 2	0.6 ～9.3 (WAVE 1) 4.7～14.0 (WAVE 2)	1.0	Dam axis

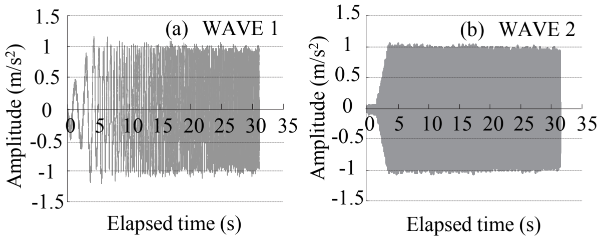

Figure 2. Input waves

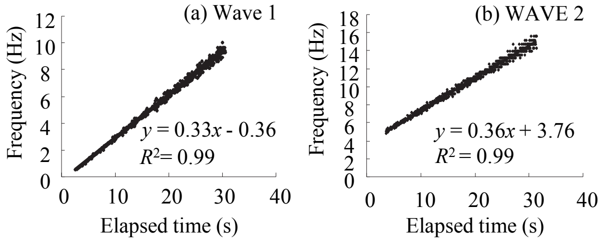

Figure 3. Frequencies of input waves changing with elapsed time

Fig. 3 shows the relation between frequencies of acceleration records measured at the shaking table and elapsed time. As shown in Fig. 3, frequency of both waves increase lineally between prescribed frequency ranges, in WAVE 1 at a rate of 0.33 Hz/s and in WAVE 2 at a rate of 0.36 Hz/s. From these results, it is confirmed that shaking table device can reproduce the required amplitude and frequency of input waves.

3. TEST RESULTS AND CONSIDERATION

3.1. Acceleration Response

The direction and maximum value of acceleration response are focused on. The maximum values of acceleration response (absolute values) measured in the test are shown in Table 2. Acceleration loci on the horizontal plane (stream and dam axis plane) are shown in Fig. 4. Herein, results of Wave 1 (frequency is from 0.6 Hz to 9.3 Hz) and Wave 2 (frequency is from 4.7 Hz to 14.0 Hz) are merged into a graph, so each graph shows the acceleration loci at the frequency swept from 0.6 Hz to 14.0 Hz. Two direction arrow in each graph shows shaking direction.

As shown in Fig. 4 (a), all points of Model A response to only shaking direction in both cases. As shown in Fig. 4 (b), all points of Model B response to only shaking direction in Case 1. But, in Case 2, B1 and B2 response to shaking direction (dam axis) and its orthogonal direction (stream) like drawing a ellipse on the horizontal plane. At B1 which is right above the deepest part of the valley, the maximum absolute value of acceleration response to shaking direction (dam axis) is 6.9 m/s^2 and that to its orthogonal direction (stream) is 3.0 m/s^2 (see Table 2). At B2 which is on the centre of crest, the maximum value of acceleration response to shaking direction (dam axis) is 6.5 m/s^2 and that to its orthogonal direction (stream) is 3.7 m/s^2. Thus, in Model B, it is found that the acceleration response orthogonal to the shaking direction will arise and the acceleration loci will show the ellipse shape on the horizontal plane when dam body is shaken to dam axis direction.

As shown in Fig. 4 (c), C1 which is right above the deepest part of the valley and on the centre of crest shows different behaviour from other points of Model A and Model B in Case1. The maximum value of acceleration response to shaking direction (stream) is 10.3 m/s^2 and then the value of acceleration response to its orthogonal direction (dam axis) shows -1.2 m/s^2 simultaneously. The minimum value of acceleration response to orthogonal direction (dam axis) is -2.0 m/s^2 and then the value of acceleration response to shaking direction shows 3.1 m/s^2 simultaneously. Thus, in Model C, C1 which is right above the deepest part of the valley and on the centre of crest will response to not only the shaking direction but also the direction orthogonal to input wave when the shaking direction is stream. In Case 2, C1 and C2 show the acceleration response orthogonal to shaking direction (stream). At C1, the minimum value of acceleration response to shaking direction (dam axis) is -9.3 m/s^2 and then the value of acceleration response to its orthogonal direction shows -1.2 m/s^2. At C2 the maximum value of acceleration response to shaking direction is 5.8m/s^2 and the value of acceleration response to orthogonal direction shows -1.1 m/s^2 simultaneously. The dominant response directions of C1 and C2 are opposite.

Table 2. Measured maximum acceleration values (Absolute values)

	Case 1 (Stream direction)			Case 2 (Dam axis direction)		
	Stream (m/s^2)	Dam axis (m/s^2)	Vertical (m/s^2)	Stream (m/s^2)	Dam axis (m/s^2)	Vertical (m/s^2)
A1	11.8	0.7	1.1	0.6	9.7	2.4
A2	5.5	1.4	0.6	0.5	5.3	3.9
A3	3.1	0.3	0.3	0.5	2.9	1.4
B1	8.6	0.7	0.6	3.0	6.9	4.4
B2	5.7	1.0	0.7	3.7	6.5	4.1
B3	4.2	0.7	0.3	0.6	2.3	1.2
C1	10.3	2.0	0.9	2.1	9.3	0.8
C2	4.3	1.3	0.9	2.4	5.8	3.8
C3	2.4	0.5	0.4	0.7	2.5	0.9

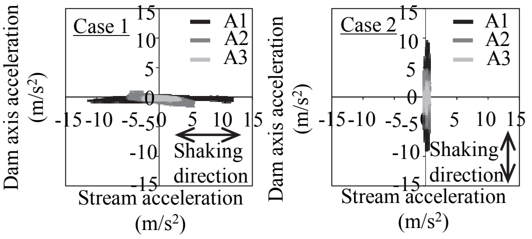

(a) Model A

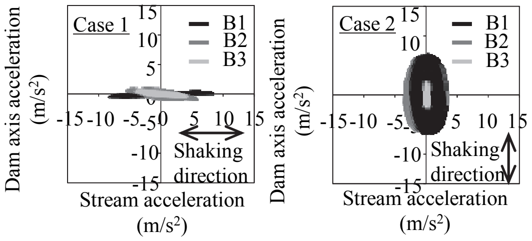

(b) Model B

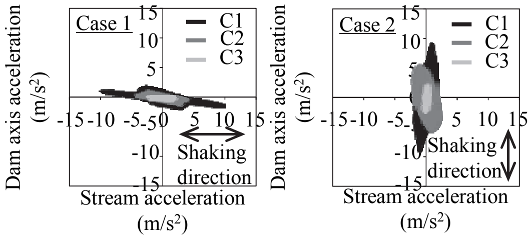

(c) Model C

Figure 4. Loci of measured acceleration in stream and dam axis plane

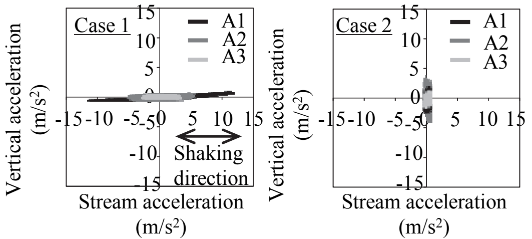

(a) Model A

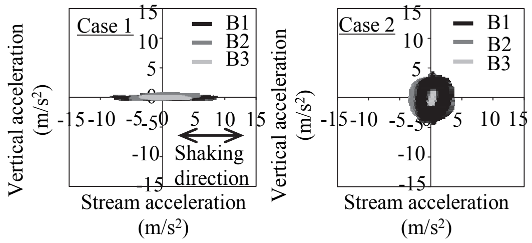

(b) Model B

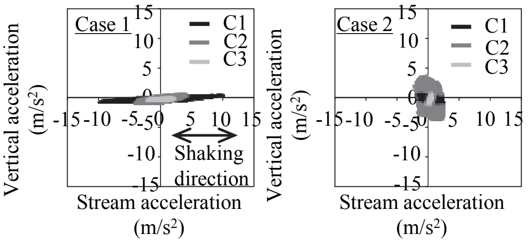

(c) Model C

Figure 5. Loci of measured acceleration in stream and vertical plan

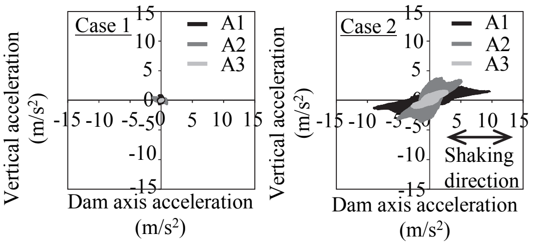

(a) Model A

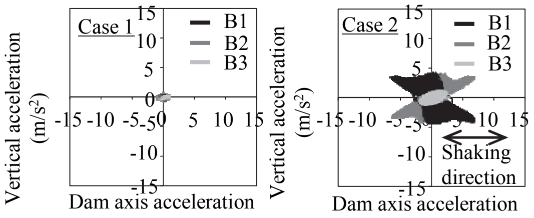

(b) Model B

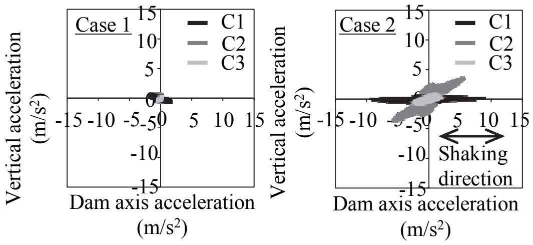

(c) Model C

Figure 6. Loci of measured acceleration in dam axis and vertical plane

The acceleration loci of each model on stream and vertical plane and dam axis and vertical plane are shown in Fig. 5 and Fig. 6 respectively. In a graph without two direction arrow, shaking direction is perpendicular to the plain. All points of three models show little response to the vertical direction in Case1, but show remarkable response to the vertical direction in Case 2. In the case of Model A, the maximum value of acceleration response to the vertical direction are 2.4 m/s^2 at A1 which is right above the deepest part of the valley and on the centre of crest, 3.9 m/s^2 at A2 and 1.4 m/s^2 at A3 which is near to abutment. Thus, remarkable response to the vertical direction arise at all points of Model A. In the case of Model B, the maximum absolute values of acceleration response to the vertical direction are 4.4 m/s^2 at B1 and 4.1 m/s^2 at B2. The dominant response directions of B1 and B2 are opposite (see Fig. 6 (b) Case 2). In the case of Model C, the acceleration response to vertical direction at C1 and C3 are not remarkable but the maximum absolute value of acceleration response to vertical direction at C2 is 3.8 m/s^2.

From these results, it is found that the tendencies of acceleration response will be different at each point on dam's crest. When shaking direction is stream, points which is right above the deepest part of the valley (A1, B1 and C1) show the maximum value of acceleration response. Here, the value which is normalized the acceleration response value at each point by the amplitude of input wave is defined as response ratio. Maximum response ratios at A1, B1 and C1 are 11.8, 8.6 and 10.3 respectively (see Table 2). In Model A and Model C, the point which is right above the deepest position of valley corresponds to the centre of crest. But in Model B, the point which is right above the deepest part of the valley is near to abutment. Then, it is supposed that the value of response ratio at B1 is smaller than that at A1 and C1 because B1 is more strongly influenced by the abutment than the others.

When the shaking direction is dam axis (Case 2), points which are right above the deepest part of the valley (A1, B1 and C1) show the maximum value of acceleration response. This tendency corresponds to that in Case 1. Maximum response ratio at A1, B1 and C1 are 9.7, 6.9 and 9.3 respectively. However, in Model B, B2 which is the centre of crest shows comparatively high response ration 6.5 which is almost same as B1. In Case 2, it is supposed that all models show the remarkable response perpendicular to the direction of input wave because deformation of dam body toward dam axis is restricted by the abutment and then dam bodies show the complicated three dimensional behaviour.

It is concluded that the point at which the maximum acceleration values were recorded during the shaking in the stream and the dam axis directions is right above the deepest part of the valley. It is clarified that the response orthogonal to the shaking direction could arise depending on the shapes of the dam, the direction of the input waves. Especially, when the shaking direction is dam axis, dam body will show the complicated three dimensional behaviour.

3.2. Relationships between Acceleration Response and Frequency

Fourier spectra analysed from the three components of acceleration response at each point of models by Fast Fourier Transform (FFT) are shown in Fig. 7, Fig. 8 and Fig. 9. Here, Fourier spectra analysed form the data of WAVE 1 and WAVE 2 are merged into a graph. In these figures, solid arrow shows 1st predominant frequency and broken arrow shows 2nd predominant frequency. Double arrow shows inflection point at which Fourier spectrum changes decrease to increase and its frequency value is shown too. Dominant frequencies at each point are shown in Table 3.

As shown in Fig. 7 (a), Fig. 8 (a) and Fig. 9 (a), in Case 1, all points except C1 response to only stream direction through targeted range of frequency. Dominant frequency at A1, B1 and C1 which are right above the deepest part of the valley show the maximum acceleration response value are 6.3 Hz, 6.1 Hz and 6.0 Hz respectively and these values are almost same (see Table 3). The shapes of Fourier spectra at A1 and C1 seems almost same and show a single peak remarkably. But the shape of Fourier spectrum at B1 is different from the others and show the double peak among targeted range, 1st predominant frequency is 6.1 Hz, 2nd predominant frequency is 11.5 Hz and frequency of inflection point at which Fourier spectrum changes decrease to increase is 8.6 Hz (see Table 3 and Fig. 8(a)).

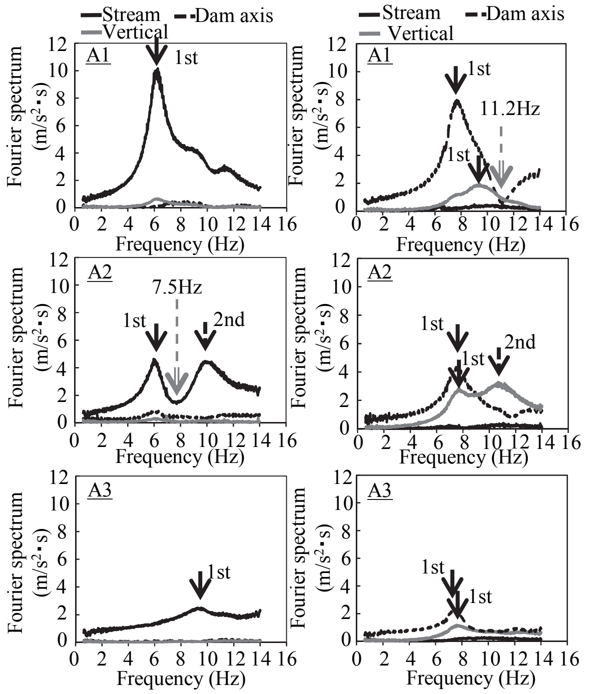

(a) Case1 (Stream direction) (b) Case 2 (Dam axis direction)

Figure 7. Fourier spectra of the amplitudes at each point in Model A

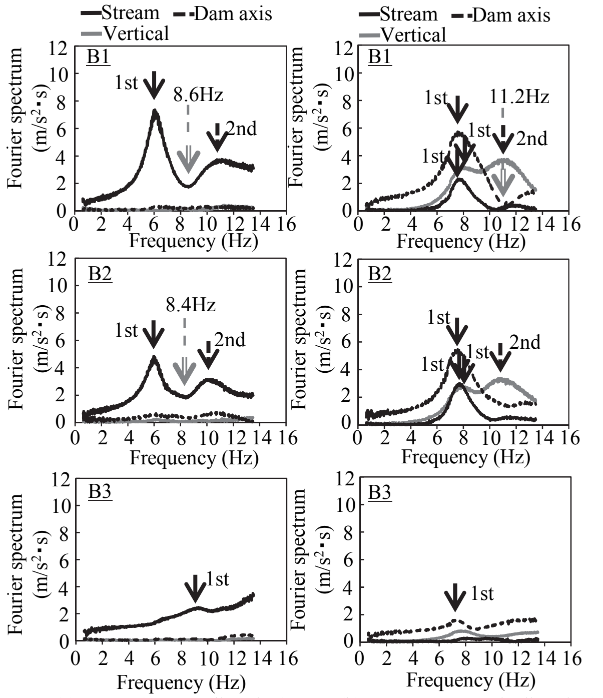

(a) Case1 (Stream direction) (b) Case 2 (Dam axis direction)

Figure 8. Fourier spectra of the amplitudes at each point in Model B

A1 and C1 are just above the deepest part of the valley and on the centre of crest, so they are less influenced by the abutment. On the other hands, B1 is just above the deepest part of the valley but near to abutment and B2 is on the centre of crest but depth is lower, so these points are affected by the restriction of abutment. The shapes of Fourier spectra at A2, B2 and C2 show the double peak same as B1 and B2. So, it is considered that shape of Fourier spectrum at the point which is less influenced by abutment shows remarkable single peak, but shape of Fourier spectrum at the point which is affect by the restriction of abutment shows double peaks or no remarkable peak.

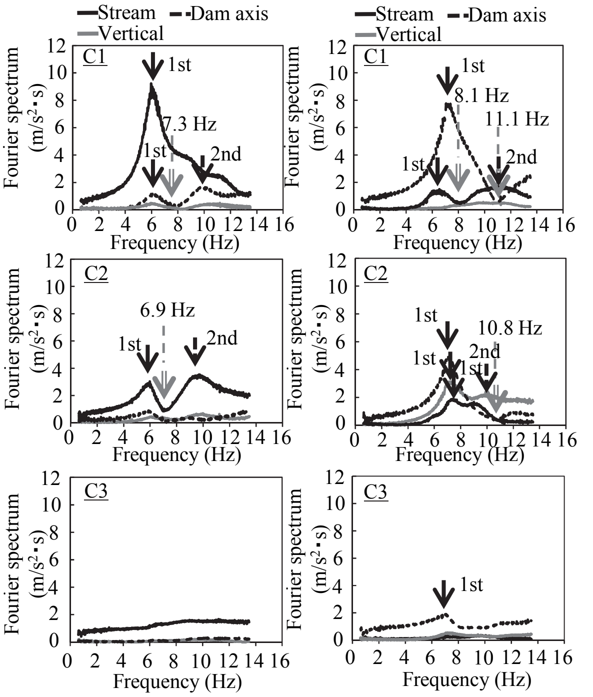

(a) Case1 (Stream direction) (b) Case 2 (Dam axis direction)

Figure 9. Fourier spectra of the amplitudes at each point in Model C

Table 3. Measured dominant frequencies of each model

	Case 1			Case 2		
	Stream	Dam axis	Vertical	Stream	Dam axis	Vertical
A1	6.3	-	-	-	7.6	9.4
A2	6.0 (9.9)	-	-	-	7.6	7.7 (10.7)
A3	9.2	-	-	-	7.5	7.6
B1	6.1 (11.5)	-	-	7.6	7.6	8.2 (11.3)
B2	6.0 (10.0)	-	-	7.7	7.6	8.0 (10.8)
B3	9.3	-	-	-	7.2	-
C1	6.0	6.2 (9.7)	-	6.5 (11.1)	7.8	-
C2	6.0 (9.7)	-	-	7.4	7.0	7.1 (10.0)
C3	-	-	-	-	7.0	-

Unit: Hz, ( ): secondary predominant frequency, - : undetected

As shown in Fig. 7 (b), Fig. 8 (b) and Fig. 9 (b), in Case 2, the points at which the maximum Fourier spectrum are recognized is right above the deepest part of the valley (A1, B1 and C1) and the 1st predominant frequencies at A1, B1 and C1 are 7.6 Hz, 7.6 Hz and 7.8Hz respectively and these values are almost same (see Table 3). In Model B and Model C, the maximum response to the direction orthogonal to input wave on the horizontal plane arise at B2 and C2 and the dominant frequency of stream direction at their points are 7.7 Hz and 7.4 Hz respectively (see Table 3) . As shown in these figures, it is recognized that the response to the shaking direction (dam axis) at A1, B1 and C1 which show the maximum Fourier spectrum are none on the frequency at about 11.2 Hz shown by double arrows. Especially, at A1 and B1, no response to orthogonal direction on horizontal plane (stream) are recognized on this frequency. So it is considered that these points are nodes of horizontal vibration on this frequency. Thus it is confirmed that response property at the points on crest will change according to the frequency of input wave and the seismic behaviour of dam body shows the complicated three dimensional behaviour on a specific frequency. In Case 2, the vertical response orthogonal to input wave direction arise remarkably at A2, B1, B2 and C2, these values exceed the horizontal response on the 2nd predominant frequency of the vertical direction (A2: 10.7 Hz, B1: 11.3 Hz, B2: 10.8 Hz and C2: 10.0 Hz, see Table 3).

From these results, it is found that response toward the orthogonal direction to the shaking direction will arise in the complex shape of dam body such as Model C when shaking direction is stream. It is verified that complicated three dimensional response will arise in not only the complex shape of dam body like Model B and Model C but also the simple shape of dam body such as Model A when the shaking direction is dam axis on a specific frequency.

4. CONCLUSIONS

In this study, the characteristics of the seismic behaviour of fill type dams were examined by shaking table tests, in which three dam models with different shapes were shaken separately in the stream direction and in the dam axis direction, and then the effects of the dam's shapes and the direction of the input wave on the seismic response behaviour were verified.

From test results, it is concluded that the points at which the maximum acceleration values were recorded during the shaking in the stream and the dam axis directions are right above the deepest part of the dam's valley. It is clarified that the response orthogonal to the shaking direction could arise depending on the shapes of dam body, the direction and the dominant frequency of input waves. Especially, when the shaking direction is dam axis, dam body shows the complicated three dimensional behaviour. In particular, in the case of shaking in the dam axis direction, the point at which no response could be incited appeared on the crest of the dam depending on the shape of the dam body and the frequency of the input waves. So it is important to pay attention about the relation between seismic modes of dam body and dominant frequency of input wave when the data recorded by seismometers installed in real dams are analysed and the cause of dam's damage is examined

REFERENCES

Kohgo, Y. (2006): Damage of embankment dams for irrigation due to the Mid Niigata Prefecture Eathquake in 2004, Technical Report of the National Institute for Rural Engineering, No. 205, pp. 37-44. (in Japanese)

Masukawa, S., Yasunaka, M., Asano, I. and Tagashira, H. (2000) : Effects of valley shape on seismic responses of fill dams, Proceeding of the 12th World Conference on Earthquake Engineering, No.0095.

Masukawa, S., Kohgo, Y., Asano, I. and Hayashida, Y. (2002) : Seismic behavior of fill dams by observing earthquake records, Bulletin of the the National Institute for Rural Engineering, No. 41, pp. 19-59. (in Japanese)

Masukawa, S. and Nakanishi, N. (2005) : Seismic behavior of large dams for irrigation by seismic observation records at Off Miyagi Earthquake (2003.5.26), Bulletin of the the National Institute for Rural Engineering, No. 44, pp. 105-138. (in Japanese)

Masukawa, S., Asano, I., Tagashira, H. and Hayashida, H. (2009): Damage and seismic behavior of large dams for irrigation, Jour. JSIDRE, 77:7, pp. 541-544. (in Japanese)

Masukawa, S., Tagashira, H., Kuroda, S. and Hayashida, H. (2012): Damages of embankment dams for irrigation due to the 2011 off the Pacific coast of Tohoku Earthquake, Technical Report of the National Institute for Rural Engineering, No. 213, pp. 217-242. (in Japanese)

Masukawa, S., Kuroda, S., Hayashida, H and Tagashira, H. (2014): Input seismic motion of dams for irrigation by large-scale earthquakes for 10 years of the early 21st century, Technical Report of the National Institute for Rural Engineering, No. 215, pp. 185-217. (in Japanese)

4th APG Symposium and 9th EADC on

INNOVATIVE TECHNOLOGIES FOR DAMS AND RESERVOIRS TOWARD THE FUTURE GENERATIONS

Seismic Performance Evaluation of Embankment Dams by Physical Modeling toward Engineering Practice

N.R. Kim
K-water Institute, Daejoen, Korea
namryong@kwater.or.kr

ABSTRACT:
Recently, strong earthquakes damaged embankment dams worldwide. Damages in embankment dams can threat safety of entire system and can be evolved to breach. The safety of embankments subjected to extreme disaster should be verified in design or maintenance stages and numerical simulations are commonly used in engineering practice. Reduced scale physical modelling is also carried out for the same purpose when the uncertainties in global behaviour of the system is involved. Physical modelling using geotechnical centrifuge have been applied to investigate seismic response of embankment dams for mostly research purpose. However, the application to large dams in engineering practice is sometime difficult because of limitation of equipment and scaling principles. This paper introduces generalized scaling principles which can be applied for seismic test of large embankment dams using geotechnical centrifuge. The scaling principles can be utilized when the centrifugal acceleration cannot be applied following the modelling scale. These scaling relations can be derived from dimensional analysis and validated by comparing with previous research. A series of tests is carried out to verify the principles varying acceleration level, loading frequency and other major factors. Finally, the experimental design strategies for appropriate physical model test considering these scaling principles will be discussed.

Keywords: embankment dam, earthquake, physical modelling, geotechnical centrifuge

1. INTRODUCTIONS

In last decades, number of embankment dams in the world have been damaged or even breached due to strong earthquake ground motion and these events highlight the importance of seismic design and evaluation of seismic performance of the systems. Damages in the embankment such as excessive settlement, cracks in impervious zone, movement or failure of slopes, liquefaction can deteriorate the safety performance and sometimes drive into tragic consequences. Therefore, the seismic response and performance of dams subjected to strong earthquake must be evaluated especially for the dams located in severe seismic zone and countermeasures must be prepared.

Various methods are employed in order to evaluate safety performance or validate design parameters of large earth systems. Numerical methods such as finite element analysis using commercial software packages are widely adopted in engineering practice since the engineers can easily model entire structure and simulate various loading conditions, and seismic response and behaviour of entire system can be also calculated by time integration algorithm. While we are able to model complicated structural and material characteristics, and to simulate various and more realistic loading conditions by numerical simulation with great advances of technology, reduced scale physical modelling is still useful and conducted in both research and practice. It is carried out in order to simulate complex model such as boundary conditions or effect of interfaces between different materials, and to consider more precise material characteristics, validate the result of numerical simulation.

Physical modelling using a centrifuge is widely applied in various geotechnical problems and provides appropriate scaling of self-weight stress conditions in large geotechnical systems (Gaudin et al. 2009; Schofield 1980; Taylor 1995). When the reduced scale model is accelerated within a centrifuge, the self-weight of the soil can be raised to in-situ conditions such that the entire behaviour of the model can be identical to full scale geotechnical systems; hence it can reliably represent performance behaviour of prototype structures. Based on this advantage, physical modelling technology using a centrifuge has been applied in various geotechnical engineering fields, especially in earthquake related problems.

There have been several cases of physical modelling of embankment dams to evaluate seismic response characteristics such as amplification, deformation and/or settlement, liquefaction susceptibility, slope stability, etc. With development of in-flight shaking table for centrifuge, various seismic tests for embankment dams were conducted by number of researchers, especially for the embankments sitting on the liquefiable foundation (Ng et al., 2004; Sharp & Adalier, 2006; Peiris et al., 2008). More recently, seismic response and amplification characteristics of earth core rock-fill dam and concrete faced rock-fill dams were investigated by a series of centrifuge tests (Kim et al., 2011).

The prototype dams of previous research are relatively small. In reality, failure of large dam has bigger risk to public safety so most of cases which geotechnical engineers are asked to evaluate the seismic performance by physical modelling deal with large dams. However, there are often conflicts between the modelling scale and centrifugal acceleration for test due to various limitations, hence special modelling strategy is required to model and simulate large dam for seismic safety evaluation.

In this paper, general principles of geotechnical centrifuge technology as well as the principles for seismic test of large embankment dams are introduced. The scaling factors for limited conditions could be derived from basic soil mechanics and validated comparing with generalized scaling relations. Seismic test using geotechnical centrifuge and earthquake simulator are carried out to verify the principles varying test and loading conditions. Finally, the experimental design strategies for appropriate physical model test considering these scaling principles are suggested.

2. CENTRIFUGE MODELING OF DAMS

2.1. Principles of geotechnical centrifuge modelling

Scaled model for centrifuge test is generally built using the same material following the same geometrical arrangement, and the experiments must be designed based on similarity laws derived from the fundamental equations governing the phenomena to be investigated. The basic scaling law for the geotechnical centrifuge testing is derived to ensure stress similarity between the model and corresponding prototype. When an acceleration of *N* times Earth gravity (*g*) is applied to a material with density ρ, the vertical stress, σ_v at depth h_m in the model is given by:

$$\sigma_{vm} = \rho \cdot Ng \cdot h_m \qquad (1)$$

In the full scale prototype, indicated by the subscript *p*, the vertical stress is expressed by:

$$\sigma_{vp} = \rho \cdot g \cdot h_p \qquad (2)$$

From the fundamental idea of the centrifuge modelling, the vertical stress in the model and the prototype is identical hence the scale factor for linear dimensions is 1:*N*. Basic scaling factors for physical quantities in centrifuge testing are derived based on dimensional analysis using this linear dimension scale. Since the mechanical properties of geomaterials used for general centrifuge models are identical with the prototype materials, those physical quantities can be easily derived. The scaling factors for basic quantities in centrifuge modelling can be found in Taylor (1995) and Garnier *et al.*, (2007).

2.2. Scaled modelling of large dams - limitations

Let us assume that we carry out a seismic centrifuge test for 100m high and 300m long embankment dam applying 0.4g peak ground acceleration (PGA) motion. If we build a model in a 1.5m long and 0.75m high container, the scale is 1:200 so we operate the centrifuge at 200g and apply 80g horizontal ground motion to simulate appropriate self-weight stress and dynamic loading conditions according to scaling principles. However, large centrifuges in the world are seldom operated to such a high acceleration and there are only few shaking tables with such a large platform area. Furthermore, most of in-flight shaking tables can be operated lower than 50g centrifugal acceleration (Iai *et al.*, 2005), and maximum shaking acceleration is generally smaller than 40g. Therefore, it is impossible to carry out physical model test of this large dam using on basic scaling principles, while there are needs and requirements from engineering practice to assess seismic safety of large dams subjected to extreme earthquake loads.

If we test the model despite of these limitations, we generally operate the centrifuge equipment up to maximum allowable acceleration level for shaking table operation. If the centrifugal acceleration applied to the model above is 50g for example, the model can be regarded as simulating 25m high embankment dam so it is a different case from original prototype hence the response will be also different. Therefore, it is difficult to directly estimate the seismic response or safety conditions of prototype structure so we need to find and validate alternative modeling strategy based on solid dimensional analysis. A special scaling principle for large structures for seismic centrifuge tests is suggested.

3. MODELING OF LARGE STRUCTURE – GENERALIZED SCALING RELATIONS

Iai *et al.* (2005) suggested generalized scaling relations, a special scaling principles which can be applied where ordinary scaling principles for centrifuge test cannot be directly applied because of either the testing machine or the largeness of prototype structure. The technique basically combines scaling principles for 1*g* shaking table test and *Ng* dynamic centrifuge test. In this method, if we define the scale between virtual intermediate prototype and model as η and that between virtual prototype and full scale prototype as μ, every scale factor for physical quantities in a test is derived by combination of η and μ. Generalized scaling factors of major physical quantities for dynamic centrifuge modeling are given in Table 1.

Table 1. Generalized scaling relations for major quantities

Quantity	Conventional (Ng)	Generalized (Partitioned)
Length	N	$\mu\eta$
Density	1	μ_ρ
Time (dynamic)	N	$(\mu\mu_\varepsilon)^{0.5}\eta$
Frequency	$1/N$	$(\mu\mu_\varepsilon)^{-0.5}/\eta$
Acceleration	$1/N$	$1/\eta$
Displacement	N	$\mu\mu_\varepsilon\eta$
Stress	1	$\mu\mu_\rho$
Strain	1	μ_ε
Stiffness	1	$\mu\mu_\rho/\mu_\varepsilon$

In general, the scaling factor for frequency used for scaling of earthquake motion in 1g shaking table test is defined as

$$\mu_f = (\mu\mu_\varepsilon)^{-0.5} \tag{3}$$

where μ_ε is a scaling factor for strain. In general cases, it is used as $\mu^{0.5}$ and it can be expressed as $\mu^{2\beta}$ more precisely (Iai, 1989; Iai & Sugano, 1999). The scaling factor of frequency for centrifuge test is

$$\eta_f = \eta^{-1} \tag{4}$$

hence the generalized scaling factor for frequency or period can be expressed as

$$f_{\mathrm{GS}} = (\mu_f \eta_f)\, f_{\eta g} = (\mu^{-0.75}\eta^{-1})\, f_{\eta g} \tag{5}$$

$$T_{\mathrm{GS}} = \mu^{0.75}\eta\, T_{\eta g} \tag{6}$$

The appropriateness of this scaling factor for dynamic centrifuge tests of large embankment dams can be verified considering the effect of centrifugal acceleration on stress/stiffness distribution in the model and resultant response characteristics of general earth structures, and it was concluded that this approach can be rationally applied.

4. VERIFICATION OF SCALING APPROACHES

4.1. Geotechnical centrifuge

The test was carried out using the geotechnical centrifuge at K-water Institute which is one of the largest centrifuges in the world. The platform radius of this centrifuge is 8.0m and the payload dimension is 2m×2m×2m. This large equipment provides advantages in physical modeling; relatively uniform acceleration field can be achieved from large platform radius and large testing model can reduce errors or uncertainties from testing results (Taylor, 1995). The centrifuge is shown in Fig. 1.

The earthquake simulator is used to generate input shaking motion. The payload dimension is 1.8m(L)×0.8m(W) and it allows maximum 1.44m long testing model to be equipped which is the biggest for centrifuge test. The shaking table can be operated under maximum 100g centrifugal acceleration and the maximum horizontal shaking acceleration is 22g for 1,500kg payload mass. It can simulate not only sinusoidal shaking motions but recorded earthquake motions, and the operational frequency range for reliable response is from 20 to 350Hz.

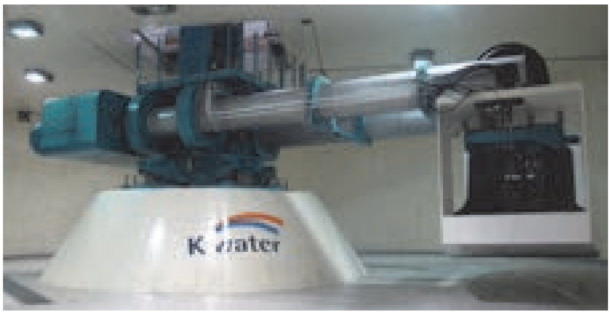

Figure 1. 800g-ton geotechnical centrifuge at K-water

4.2. Verification by modified modelling of models

Modelling of models (Ko, 1988) is widely applied to validate a centrifuge modelling technique. The main idea is to conduct tests using different scale models for a prototype at corresponding g-level, and compare the results considering the scaling factors so that the appropriateness of the modeling technique can be verified. In this study, modified modelling of models method was employed, which uses a model to be tested at different g-level. In dynamic test, the structural response varies with applied acceleration levels so the effect of testing condition can be evaluated and the appropriateness of the modeling or scaling method can be verified by analyzing the response characteristics.

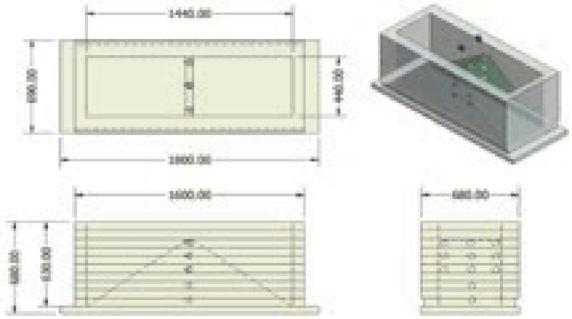

Figure 2. Design of testing model

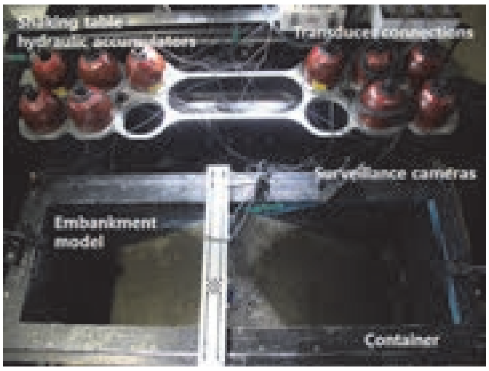

Figure 3. Dynamic centrifuge testing setup

Fig. 2 shows the design of embankment dam model used to verify the applicability of the scaling principles. The simplified model was designed as a uniform earth structure with 1:1.4 slopes on both sides. The length and the height of the model are 1440mm and 496mm, and these were determined considering the size of container. Because of the purpose of these tests, the model was specially designed to have fundamental natural frequency within the range that the earthquake simulators can generate sinusoidal excitation, while the global seismic response of the embankment is similar with those from shear-beam model approach by Dakoulas & Gazetas (1985). Hence the geometry of the model is simplified as much as possible and the slope had to be steep to have flexible behaviour.

The model was constructed using gravelly sand material. The maximum grain size is limited to 15mm and the material is classified as well-graded sand (SW). Thirteen accelerometers were installed in the center of the model to measure the response at each depth, 0*H*, 0.25*H*, 0.5*H*, 0.75*H*, and 1*H*, so the frequency response subjected to an input motion could be calculated from the measured data. The testing model installed at the centrifuge in-flight earthquake simulator is shown in Fig. 3.

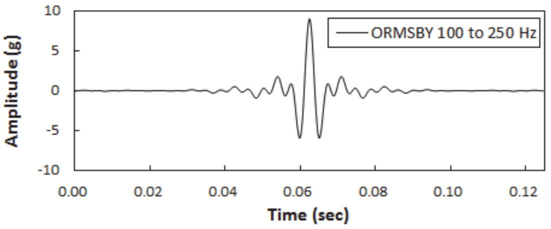

(a) Time history

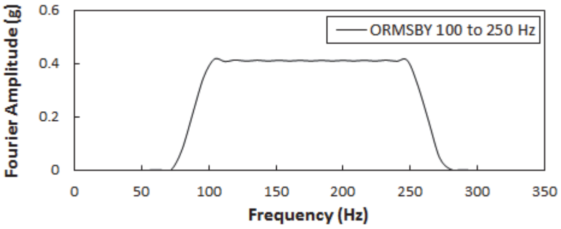

(b) Frequency characteristics

Figure 4. Ormsby wavelet for modelling

The seismic tests were conducted under 15 and 30*g* centrifugal acceleration conditions. Ormsby wavelet were applied in the base as input motion and the peak ground acceleration (PGA) was limited to 0.2*g* in prototype scale; $3g_{\text{shaking}}$ at $15g_{\text{centrifuge}}$ and $6g_{\text{shaking}}$ at $30g_{\text{centrifuge}}$. The frequency response of Ormsby wavelet (Ryan, 1994) is similar with band limited with noise so that the response of the structure directly shows the frequency response of the structure itself. Hence, it has an advantage in system identification of the structural system. The waveform and frequency characteristics of the input motion are given in Fig. 4.

4.3. Results and discussions

Fig. 5 shows the acceleration time history measured at the base and crest of the embankment model. In this result, Ormsby wavelet signal which has equivalent frequency amplitudes from 100 to 250Hz has been applied at the base (*Z*=0) and it could be observed that the motion is amplified as it goes up to crest.

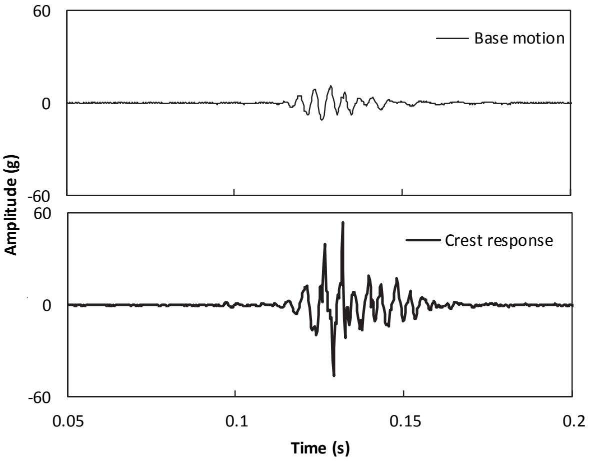

Figure 5. Base motion and crest response

The power spectrum of acceleration history measured at the crest can be regarded as the frequency response due to the frequency characteristic of input signal hence the fundamental mode natural frequency of the embankment at each g-level could be easily calculated and they are shown in Fig 6. In these results, the 1st mode fundamental frequencies (f_r) calculated from 15 and 30g conditions are 200 and 232Hz respectively. From Eq. 5, we can calculate the theoretical ratio between these two frequencies by assuming the ratio of centrifugal accelerations is 2. Table 2 summarizes the key results from experiments and the error between these two frequencies is about 2.5%. When we assume that the model represents a 1/200 scale of virtual prototype embankment dam, the natural period of the prototype is about 0.52 to 0.54 sec which are reasonable value for a 100m high embankment.

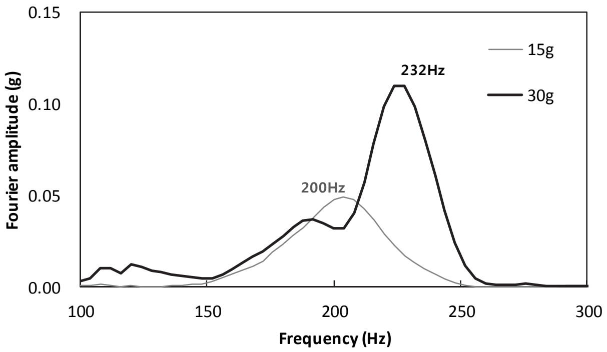

Figure 6. Base motion and crest response

Table 2. Summary of testing results

g_{cent}	f_r (Hz)	Theoretical Freq. ratio	Experimental ratio	T_p (sec)
15	200	1.189 ($2^{0.25}$)	1.16 (2.5% error)	0.52
30	232			0.54

4.4. Application to a large embankment dam

The applicability of the modelling method has been examined by a test for seismic performance evaluation of a large embankment dam (ECRD) in Korea. The dam inaugurated in 1965 is 45m high and 300m long in up-/down-stream direction and it was built as an earth core rockfill dam (ECRD). The testing model was designed by 1:135 scale. To apply generalized scaling relations, the g-level was decided as 45g so μ=3 and η=45 in Eqs. (5) and (6). The purpose of this experiment is to validate the scaling principles by means of determine the frequency characteristics of the structure, the model was simplified to only core and shell zone was considered in the design. Number of transducers (e.g. accelerometers, displacement transducers) were installed to measure the response and displacement, and the details are given in Fig. 7. In this case, to types of earthquake records were selected as input motions, i.e. Ofunato for short period motion and Hachinohe for long period motion, and various PGA were applied to investigate the effect of intensity.

Fig. 8 shows examples of base acceleration and crest response measured during the test applying Hachinohe input motion. It shows a good example of how the ground motion amplifies in the dam body, and the amplification ratio was about 1.7 for 0.12g peak ground motion (in prototype scale).

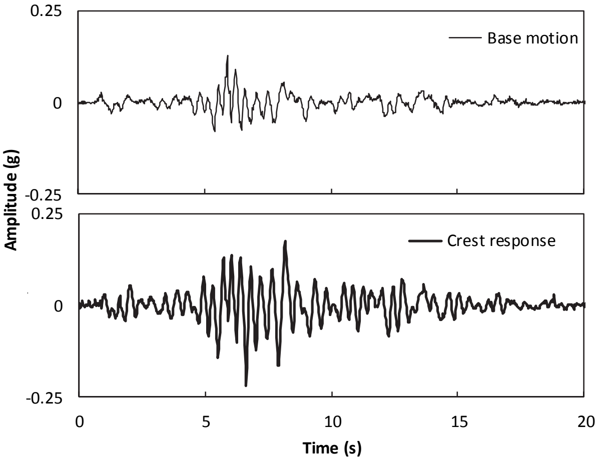

Figure 8. Acceleration history (Hachinohe input motion)

The fundamental period of the structure should be evaluated to validate the method, and it was reported that using ratio of response spectra between base motion and crest response gives reliable results (Ha, 2011; Okamoto, 1984). Fig. 9 shows the ratios of response spectra for two different input motions and these two results were quite similar. The fundamental natural period estimated by this test is around 0.6 sec. From the database of seismic response measurement and analysis from Japan and Korea, the fundamental period of 50m high embankment dam ranges from 0.3 to 0.5 sec (Ha, 2011). Considering the modelling condition, especially the difference of construction material and valley effect caused by boundary condition of the test, it can be concluded that the fundamental period from this test is reliable and the applicability of this modelling method has been verified.

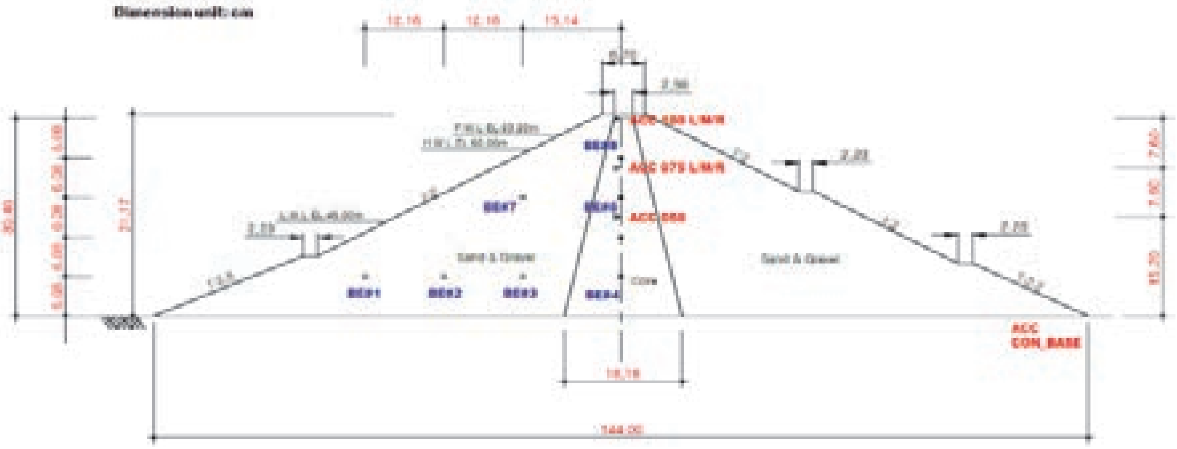

Figure 7. Design of an ECRD testing model for seismic test

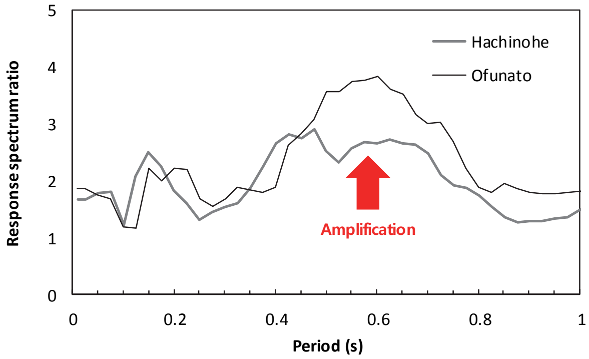

Figure 9. Ratio of response spectra

5. CONCLUSIONS

The strategy and principles for physical modelling of large embankment dams for experimental evaluation of seismic performance evaluation are introduced. The scaling principles are derived using stress-stiffness relations of geomaterials and validated by a series of centrifuge tests. Even though appropriate modelling for dynamic centrifuge test of large embankment dam is not available due to the limitations of testing equipment, the test can be designed by two stage modeming method so called generalize scaling relations and the behaviour of prototype dam can be estimated. To validate this modelling method, a simplified embankment dam model was prepared and seismic tests using geotechnical centrifuge have been conducted at two different acceleration states. The frequency responses were similar with general behaviours of embankment dams, and the dominant frequencies at each acceleration level validated the applicability of the method.

REFERENCES

Gaudin, C., White, D. J., Boylan, N., Breen, J., Brown, T., De Catania, S. and Hortin, P. (2009): A wireless high-speed data acquisition system for geotechnical centrifuge model testing, Meas Sci Technol, 20:9, pp. 1–11.

Schofield, A. N. (1980): Cambridge geotechnical centrifuge operation, Géotechnique, 20: 3, pp. 227–268.

Taylor, R. N. (1995): Geotechnical centrifuge technology, Blackie Academic, London, UK.

Ng, C.W.W., Li, X.S., Van Laak, P.A. and Hou, D.Y.J. (2004): Centrifuge modeling of loose fill embankment subjected to uni-axial and bi-axial earthquake, Soil Dyn Earthq Eng, 24:4, pp. 305–318.

Sharp, M.K. and Adalier, K. (2006): Seismic response of earth dam with varying depth of liquefiable foundation layer, Soil Dyn Earthq Eng, 26:11, pp. 1028-1037.

Peiris, L.M.N., Madabhush, S.P.G. and Schofield, A.N. Schofield (2008): Centrifuge modeling of rock-fill embankments on deep loose saturated sand deposits subjected to earthquakes, J Geotech Geoenviron, 134:9, pp. 1364-1374.

Kim, M. K., Lee, S. H., Choo, Y. W. and Kim, D. S. (2011): Seismic behaviors of earth-core and concrete-faced rockfill dams by dynamic centrifuge tests, Soil Dyn Earthq Eng, 31:11, pp. 1579–1593.

Garnier, J., Gaudin, C., Springman, S. M., Culligan, P. J., Goodings, D. J., Konig, D., Kutter, B., Phillips, R., Randolph, M.F. and Thorel, L. (2007): Catalogue of Scaling Laws and Similitude Questions in Geotechnical Centrifuge Modelling, International Journal of Physical Modelling in Geotechnics, 3, pp. 1–23.

Iai, S., Tobita, T. and Nakahara, T. (2005): Generalized scaling relations for dynamic centrifuge tests, Géotechnique, 55:5, pp. 355-362.

Ko, H.Y. (1988): Summary of the state-of-the-art in centrifuge model testing, Centrifuges in Soil Mechanics, Craig, James and Schofield Eds. Balkema. Rotterdam. pp. 11-18.

Iai, S. (1989): Similitude for shaking table tests on soil-structure-fluid model in 1g gravitational field, Soils Found, 29:1, pp. 105-118.

Iai, S. and Sugano, T. (1999): Soil-structure interaction studies through shaking-table tests, Proc. 2nd Int. Conf. on Earthquake Geotech. Engrg, Lisbon, pp. 927-940.

Dakoulas, P. and Gazetas, G. (1985): A class of inhomogeneous shear models for seismic response of dams and embankments, Soil Dyn Earthq Eng, 4:4, pp. 166-182.

Ryan, H. (1994): Ricker, Ormsby, Klauder, Butterworth - A Choice of Wavelets, CSEG Recorder. 19:7. 8-9.

Ha, I.S. (2011): Evaluation for Fundamental Periods of Domestic Rockfill Dams with Micro-earthquake Records, Journal of the Korean Geoenvironmental Society, 12:6, 53-60.

Okamoto S. (1984): Introduction to Earthquake Engineering. 2nd Edition. University of Tokyo Press. 466-477.

4th APG Symposium and 9th EADC on

INNOVATIVE TECHNOLOGIES FOR DAMS AND RESERVOIRS TOWARD THE FUTURE GENERATIONS

Seismic Fragility Evaluation of Imha Dam Based on Deformation

D.H. Shin, C.K. Kang, K.Y. Kim & K.W. Kim
K-water Institute Infrastructure Research Center, Daejeon, South Korea
cute_lion@daum.net

ABSTRACT:
Fragility assessments can be used to develop strategies to strengthen or retrofit structures to reduce their vulnerability or to predict the probability of structural damages induced by external loads such as earthquake motion. Especially, seismic fragility analyses, which provide measures of the safety margin of the structural system for the specified seismic hazard levels, is considered to be the central concept of risk assessment methods. In the present study, a seismic fragility analysis method for rockfill dams is proposed and seismic response analyses are conducted based on deformations of a rockfill dam by using QUAKE/W with nearfield and far-field earthquake waves collected from the world. In order to construct fragility curves of the dam, the relative crest deformations (settlements) of the dam, which are calculated from the Newmark sliding block analysis method, are used as a seismic risk evaluation indicator. The seismic fragility assessment is applied to the Imha multipurpose dam (centre core rockfill dam) in Korea. The analysis results imply that Imha Dam be more vulnerable to the far-field seismic waves than the near field earthquakes, which seems to be due to the difference in periodicity characteristics of the seismic waves according to the epicentral distance and the dam's natural period. Thus, it is explicitly confirmed that seismic fragility assessment can be a tool for robust safety evaluation of existing dams and decision-making on necessity of emergency action required to be made or not.

Keywords: Fill dam, Seismic fragility, Probabilistic analyses, Newmark sliding block method, Fragility curve

1. INTRODUCTION

Since the end of 1970s, a number of methodologies for fragility analysis have been proposed to assess the static and dynamic behaviour of various structures such as bridges, buildings, dams and so on. Nowadays, fragility assessment is considered as a very useful tool for rational safety evaluation of existing water infrastructures and decision-making by using a probabilistic framework taking into account uncertainties that may affect dam performance (Tekie, et al. 2003), and also may be used to develop strategies to strengthen or retrofit structures to reduce their vulnerability or to predict the probability of structural damages induced by external loads such as earthquake motion (Reinhorn, A.M. et al. 2001). Especially, seismic fragility analyses, which provide measures of the safety margin of the structural system for the specified seismic hazard levels, is considered to be the central concept of risk assessment methods (Lagaros, N.D. 2008). In Canada, the approach for assessing fragility of dams is adopted to estimate their seismic vulnerabilities and to rank the dams according to their vulnerabilities (Liu, L. et al. 2008). Moreover, a case of seismic fragility analysis taking into account both uncertainties of dam material parameters and ground motions was reported in the literature (Wang, D. et al. 2013).

In the present study, a seismic fragility analysis method for rockfill dams is proposed and seismic response analyses are conducted based on deformations of a rockfill dam by using QUAKE/W and SLOPE/W (Geo-Slope Ltd. 2010) with nearfield and far-field earthquake waves collected from the world. The seismic fragility analyses were conducted based on the fragility curves of the study dam. In order to construct fragility curves of the dam, the relative crest deformations (settlements) of the dam, which are calculated from the Newmark sliding block analysis method, were used as a seismic risk evaluation indicator (Abramson et. al., 2002). The seismic fragility assessment is applied to the Imha multipurpose dam (centre core rockfill dam) in Korea.

2. FRAGILITY ANALYSIS

Seismic fragility analysis requires the calculation of exceedance probabilities of limit state, and currently, the seismic hazard is normally represented by peak ground acceleration (PGA), spectral acceleration (Sa), or spectral displacement (Sd), rather than Modified Mercalli Intensity(MMI). Thus, in the present study, the PGA was used as a hazard parameter, and fragility curves were constructed as a function of PGA as below.

$$\mathrm{P}(damage \geq LS|PGA) = \left\{\frac{\ln(PGA) - \mu}{\sigma}\right\}$$
$$= \int_0^{PGA} \frac{1}{PGA \times \sigma \times \sqrt{2\pi}} \times exp\left[-\frac{1}{2}\left(\frac{\ln(PGA) - \mu}{\sigma}\right)^2\right] d(PGA) \tag{1}$$

Where, LS is the limit state of the dam by earthquake motion, σ the mean, and μ standard deviation of PGA values.

3. DEVELOPMENT OF FRAGILITY CURVES FOR IMHA MULTIPURPOSE DAM

3.1. Development procedure of seismic fragility curves

As mentioned above, seismic safety of existing water infrastructures can be evaluated by fragility assessment using seismic fragility curves, which require calculation of limit-state probabilities for a series of limit-states of monotonically increasing severity such as peak ground acceleration (PGA) of earthquake motion.

In this study, the construction procedure of fragility curve is as shown in Fig. 1.

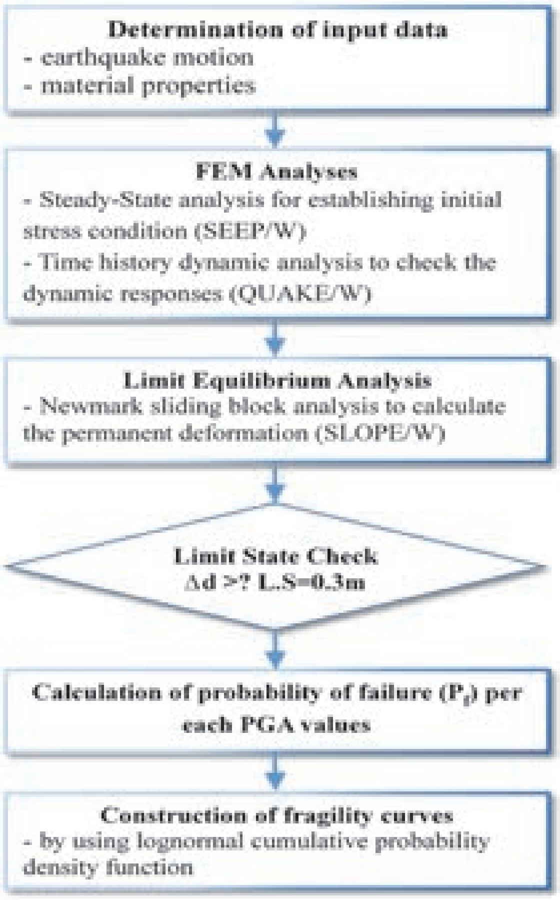
Determination of input data
- earthquake motion
- material properties
FEM Analyses
- Steady-State analysis for establishing initial stress condition (SEEP/W)
- Time history dynamic analysis to check the dynamic responses (QUAKE/W)
Limit Equilibrium Analysis
- Newmark sliding block analysis to calculate the permanent deformation (SLOPE/W)
Limit State Check
Δd >? L.S=0.3m
Calculation of probability of failure (P_f) per each PGA values
Construction of fragility curves
- by using lognormal cumulative probability density function

Figure 1. Flow chart of seismic fragility analysis

3.2. The study dam

Imha multipurpose dam is the 73m tall centre-cored rockfill dam with length of 515m and total reservoir storage of 595 million m^3, and operated by Korea Water Resources Corporation. The typical cross-section and its aerial view are shown in Figs. 2 and 3, respectively.

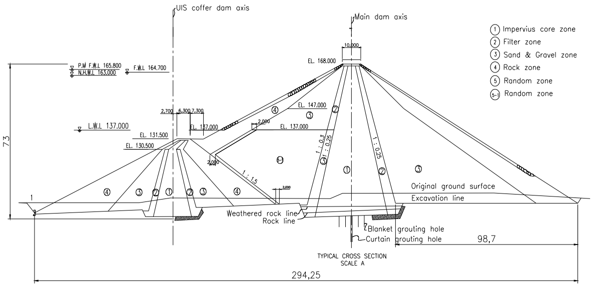
UIS coffer dam axis
Main dam axis
① Impervius core zone
② Filter zone
③ Sand & Gravel zone
④ Rock zone
⑤ Random zone
(5-1) Random zone
P.M F.W.L 165.800
N.H.W.L 163.000
F.W.L 164.700
EL. 168.000
10,000
EL. 147.000
EL. 137.000
2,000
L.W.L 137.000
EL. 131.500
EL. 130.500
2,700
6,300
7,300
73
1 : 0.3
1 : 0.25
1 : 0.25
1 : 1.5
Original ground surface
Excavation line
Weathered rock line
Rock line
Blanket grouting hole
Curtain grouting hole
98,7
TYPICAL CROSS SECTION
SCALE A
294,25

Figure 2. Typical cross-section of Imha Dam

Figure 3. Aerial View of Imha Dam

3.3. Input earthquake motions

For more rational seismic fragility analysis of dam, it is usually recommended to use site specific earthquake motions, which were recorded near or at the dam site, or selected seismic ground motion sets that include uncertainties due to epicentral distance, dominant frequency and lasting time, types of faulting mechanism and so on.

Since Korea's earthquake observation began in 1978, no earthquake with a magnitude of over 5.5 has occurred. The strongest earthquake was the 5.3 one that hit Euiju in North Korea in 1980. See Fig. 4. In the year observations began, Hongseong, South Chungcheong Province was hit by a 5.2 earthquake. Four more earthquakes with a magnitude of 5 or more have happened on the peninsula up until last year, but no one has been killed. But, the 50 years of data is too short a time period to properly study earthquakes. In addition, data of ground motions collected from those earthquakes are quite limited.

Thus, two types of earthquake waves were used to perform seismic fragility analyses; nearfield and far-field seismic data collected from earthquake records, where nearfield data are considered to be ones occurred within 10 km from dam site, while the others are out of 10km.

In order to calculate the failure probabilities at each level of PGA, every seismic data of 30 nearfield and 30 far-field real seismic data, of which seismicity are all over 6.0 in Modified Mercalli Intensity, was scaled up by 10 PGAs ranging from 0.05g to 2.0g.

The response spectra of earthquake accelerations occurred near- and far-field are shown in Figs. 5 and 6, respectively. In case of nearfield data, epicentral distances range from 0 to 9.8km, while that of far-field data are of 10.6km~96.8km.

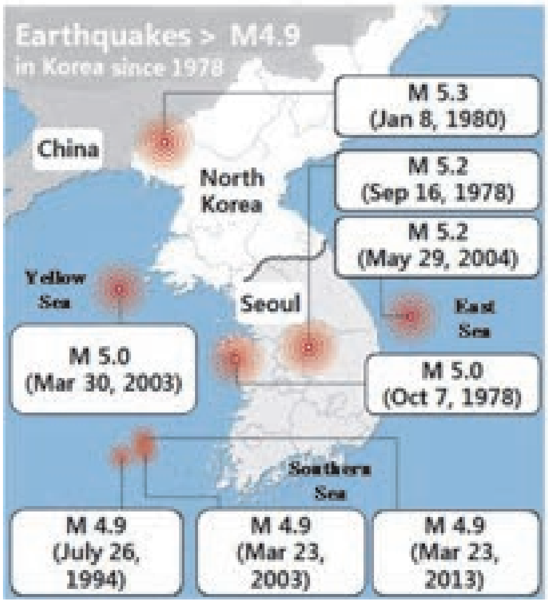
Earthquakes > M4.9
in Korea since 1978
China
North Korea
Yellow Sea
Seoul
East Sea
Southern Sea
M 5.3 (Jan 8, 1980)
M 5.2 (Sep 16, 1978)
M 5.2 (May 29, 2004)
M 5.0 (Mar 30, 2003)
M 5.0 (Oct 7, 1978)
M 4.9 (July 26, 1994)
M 4.9 (Mar 23, 2003)
M 4.9 (Mar 23, 2013)

Figure 4. Earthquakes > M 4.9 since 1978 in Korea

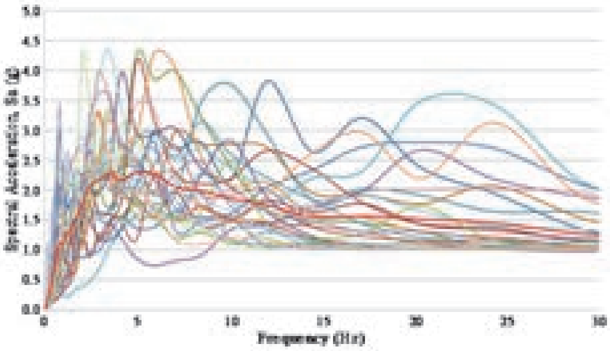

Figure 5. Response spectra of nearfield ground motions

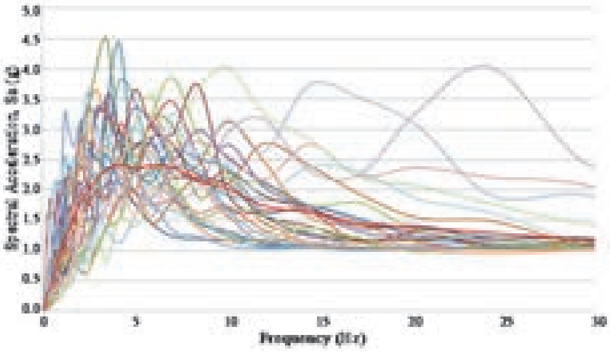

Figure 6. Response spectra of far-field ground motions

3.4. Material properties

Seismic fragility of dam is affected by uncertainties of material parameters and seismic loads. Thus, although those uncertainties in both sides should be considered, for the sake of simplicity of analysis, this study does not include the uncertainties of dam materials.

The material properties used in the analyses are presented in Table 1. The materials parameters were selected from the design report of Imha dam and the characteristics functions, which represent the seepage behaviour of materials of each zone and dynamic responses, are taken from the sample functions of SEEP/W and QUAKE/W.

3.5. Check for limit states

One of the key issues in seismic fragility analysis is what the limit states are and how to define them. Since the deformation such as crest settlement and/or horizontal displacement induced by earthquake motion is the most important factor that represents safety of the dam. It can be easily understood that if excessive crest settlements lager than the design free board occur by an earthquake, then the dam can be overtopped and consequently collapsed at the end. In this regard, we decided to use the relative settlement of dam as a seismic damage evaluation index.

For this case, what's needed is to check the design standard on performance level of dam. According to the design standard of dams in Korea, deformation of a dam by earthquake motion should not exceed 30cm of deformation at crest (MOLIT, 2011).

Thus, based on this limit state function in terms of relative crest settlements by earthquake motion, we can calculate the failure probabilities for each PGA value.

$$\text{Probability of Failure, } P_f = \mathrm{P}(Settlement \geq LS|PGA) = \frac{(Number\ of\ occurence\ exceeding\ the\ limit\ state\ at\ each\ PGA)}{Total\ number\ of\ seismic\ analyses} \quad (2)$$

3.6 Calculation of permanent deformations induced by earthquake

To calculate the failure probability, P_f depending on PGA, dynamic analyses based on finite element method and Newmark's sliding block method was applied by using SEEP/W, QUAKE/W and SLOPE/W.

Fig. 7 shows the typical cross section of Imha dam including foundation.

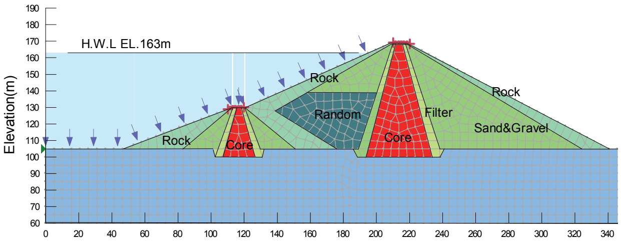
Elevation(m)
190
180
170
160
150
140
130
120
110
100
90
80
70
60
H.W.L EL.163m
Rock
Random
Rock
Core
Filter
Core
Rock
Sand&Gravel
0
20
40
60
80
100
120
140
160
180
200
220
240
260
280
300
320
340

Figure 7. Typical cross section of Imha dam

Table 1. Material properties of Imha multipurpose dam

Zone	USCS PI(%)	r_t (kN/m^3)	c (kPa)	Φ (°)	k_{sat} (cm/s)	ν	Θ, Fn	Θ_{sat} (m^3/m^3)	$\Theta_{residual}$ (m^3/m^3)	k	Gmax, Fn	G/Gmax-γ Fn	Model
Core	PI=13.3% OMC=14.94 Dr=98.7%	19.9	50.0	31.2	1.36x10^{-6} Qualification Test Result	0.43	sample clay	0.5	0.1	Fredlund & Xing	Hardin & Drnevich (1972)	Vucetic & Dobry 1991 PI=15	Mohr-Coulomb, Equivalent-linear
Filter	Dr=87%	19.3	-	37.0	2.0x10^{-3} Field Test Result	0.35	sample silt	0.43	0.04	Fredlund & Xing	Seed & Idriss (1970)	EPRI 1993 Sand 6-15m	Mohr-Coulomb, Equivalent-linear
Sand & gravel	Max. size of 20cm Dr=76.9%	20.8	-	38.0	3.0x10^{-3} Field Permeability Test	0.33	sample sand	0.35	0.01	Fredlund & Xing	Seed & Idriss (1970)	Rollins et al. 1998 Gravel	Mohr-Coulomb, Equivalent-linear
Rock zone	-	18.8	-	42	1.0x10^{-1}	0.32	sample gravel	0.25	0.0	Fredlund & Xing	Seed & Idriss (1970)	Rollins et al. 1998 Gravel	Mohr-Coulomb, Equivalent-linear
Random zone	Strengthens below 600mm, over Dr=70%	20.8	-	37	Field Permeability Test	0.33	sample sand	0.35	0.01	Fredlund & Xing	Seed & Idriss (1970)	Rollins et al. 1998 Gravel	Mohr-Coulomb, Equivalent-linear
Foundation	-	21.0	-	-	1.0x10^{-6}	0.20	-	0.25	-	Fredlund & Xing	Seed & Idriss (1970)	-	Linear elastic

Fig. 8 shows the deformed shape of Imha dam during earthquake, and Fig. 9 represents the response acceleration spectra.

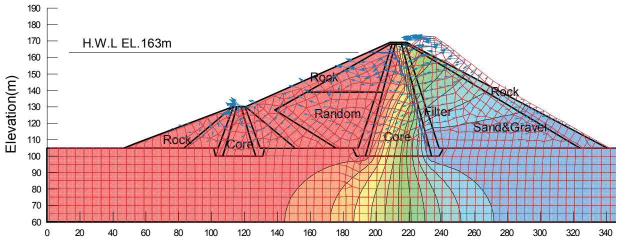

Figure 8. Deformed shape of Imha dam during earthquake

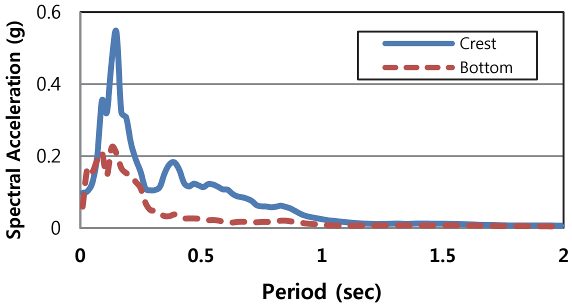

Figure 9. Response spectra of acceleration at crest and bottom of Imha dam

The Newmark sliding block analysis precisely considers the acceleration time history of the sliding block within the slope (Newmark, 1965). Such acceleration history, which represents the realistic ground motion model expected in the relevant ground, is compared with breakdown acceleration, this in order to determine the permanent plastic deformation.

The Newmark technique is based on the following assumptions.

1) Existence of a well-defined slip surface.
2) Material is rigid and perfectly plastic.
3) Decline of shear strength during the seismic motion is at a negligible degree.
4) Permanent plastic deformation occurs when dynamic stress exceeds shearing resistance force.

Fig. 10 describes the procedure of estimation of permanent settlements induced by earthquake using Newmark sliding block method.

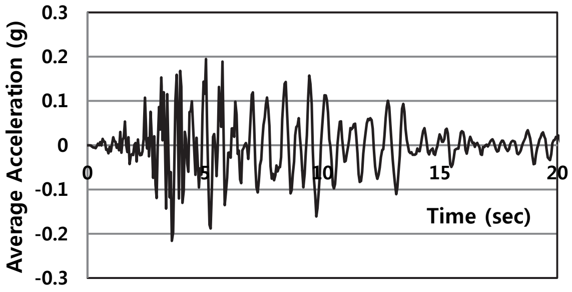

(a) Average acceleration along the slip circle

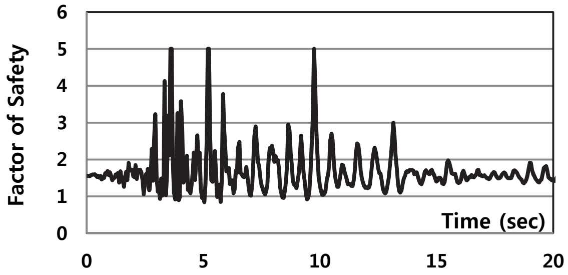

(b) Factor of safety during earthquake

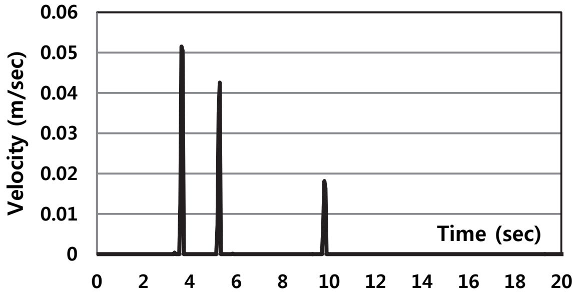

(c) Velocity vs. time

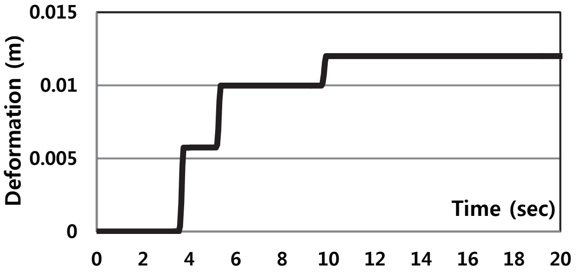

(d) Permanent settlements

Figure 10. Example of estimation of permanent settlements induced by earthquake using Newmark sliding block method

3.7. Seismic fragility curves

By incorporating the estimation results of permanent settlements through the seismic analyses including seepage analyses, and the equations (1) and (2), the seismic fragility curves for Imha dam are constructed as shown in Figs. 11 and 12 for nearfield and far-field earthquakes, respectively, and Table 2.

Table 2. Probabilities of failure versus PGA

	PGA(g)	Probability of Failure (P_f)
Nearfield earthquakes	0.05	0.00
	0.1	0.03
	0.2	0.27
	0.3	0.47
	0.4	0.63
	0.5	0.73
	0.75	0.80
	1.0	0.87
	1.5	0.93
	2.0	0.97
Far-field earthquakes	0.05	0.00
	0.1	0.07
	0.2	0.37
	0.3	0.50
	0.4	0.67
	0.5	0.80
	0.75	0.90
	1.0	1.00
	1.5	1.00
	2.0	1.00

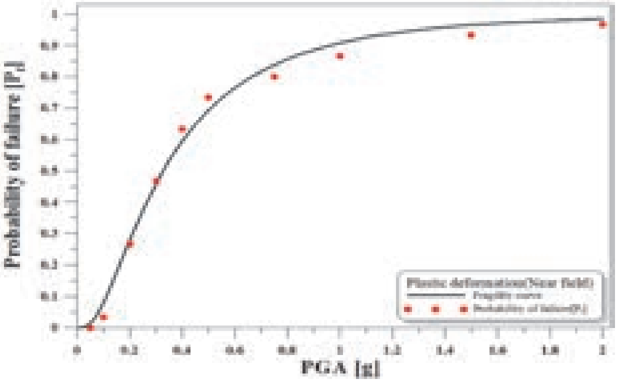

Figure 11. Seismic fragility curve of Imha dam for near field earthquake

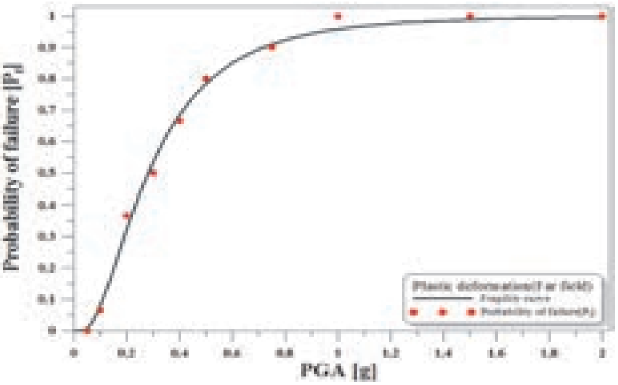

Figure 12. Seismic fragility curve of Imha dam for far-field earthquake

From the two seismic fragility curves in Figs. 11 and 12, it seems that Imha dam can be more vulnerable to far-field earthquakes than nearfield ones. However, as mentioned already above, seismic fragility of dam depends on various uncertainties such as type and dimension of dam, characteristics of earthquake (epicentral distance, occurrence mechanism, dominant frequency, etc.), variations in dam materials, current status of dam, and so on. In fact, therefore it should be noted that it is very difficult to conclusively determine which ones are less vulnerable. Thus it is strongly recommended to conduct more comprehensive studies on these issues in the future.

4. APPLICATION OF SEISMIC FRAGILITY CURVES TO SAFETY MANAGEMENT OF IMHA DAM

One of the objectives to develop seismic fragility curves is to provide safety information of dam structures. Indeed, Liu et al.(2008) reported an example that seismic fragility analyses were successfully carried out for 133 of total 933 dams in Canada and their results were used to rank the dams according to their apparent vulnerability, by decision-making authorities to ensure that owners of the high risk dams respond with detailed assessments and/or remedial actions for those dams.

In this regard, it is considered that seismic fragility curves can be correlated to the current safety status. For example, in cases that the dam is full of reservoir water up to high water level and shaken by a strong earthquake near the dam site, then we can estimate the seismic fragilities based on the scenarios anticipated to be realistically happened.

Table 3 shows the failure probabilities of Imha dam at reservoir water level, EL.163m subject to nearfield or far-field earthquake of which PGAs range from 0.05 to 2.0 g.

Table 3. Stability evaluation chart versus seismic fragility evaluation

PGA(g) / Initial Water Level(m)	0.05	0.1	0.2	0.3	0.4	0.5	0.75	1.0	1.5	2.0
163m (Normal Pool Level)-Near	0.013	0.081	0.281	0.460	0.595	0.693	0.838	0.908	0.965	0.984
163m (Normal Pool Level)-Far	0.009	0.080	0.322	0.536	0.685	0.784	0.910	0.958	0.989	0.996

5. CONCLUSION

1. A seismic fragility analysis method for rockfill dam is proposed, and seismic response analyses are conducted based on deformations of Imha multipurpose dam by using QUAKE/W. The analysis results reveal that Imha dam is more vulnerable to far-field earthquakes than nearfield ones. However, seismic fragility of dam depends on various uncertainties such as type and dimension of dam, characteristics of earthquake (epicentral distance, occurrence mechanism, dominant frequency, etc.), variations in dam materials, current status of dam, and so on. Thus it is strongly recommended to conduct more comprehensive studies on these issues in the future.

2. Seismic fragility curves can be applied to estimate the current safety status of dams and also to rank the dams for determining their priority in terms of technology and economy. Therefore, it is explicitly confirmed that seismic fragility assessment can be a tool for robust safety evaluation of existing dams and decision-making on necessity of emergency action required to be made or not.

ACKNOWLEDGEMENT
This research was supported by a grant (15SCIP-B065985-03) from Smart Civil Infrastructure Research Program funded by Ministry of Land, Infrastructure and Transport (MOLIT) of Korea government and Korea Agency for Infrastructure Technology Advancement (KAIA).

REFERENCES

Tekie, P.B. and Ellinggood, B.R. (2003), “Seismic fragility assessment of concrete gravity dams,” Earthquake Engineering and Structural Dynamics, 23(14), pp.221-224.

Reinhorn, A.M., Vorvera, R.B. and Ayala, A.G. (2001), “Spectral evaluation of seismic fragility of structures,” Structural Safety and Reliability (ICOSSAR 2001).

Lagaros, N.D. (2008), “Probabilistic fragility analysis: A tool for assessing design rules of RC buildings,”, Earthquake Engineering and Engineering Vibration, V0l.7, pp.45-56.

Liu, C.N. and Wu, C.C. (2008), Mapping susceptibility of rainfall-triggered shallow landslides using a probabilistic approach, Environmental Geology, v.55, n.4, pp.907-915.

Wang, D.B., Liu, H.L., Yu, T. and Yang, G. (2013), “Seismic fragility analysis for earth-rockfill dams based on deformation,” Chinese Journal of Geotechnical Engineering, Vo.35 No.5, pp.814-819.

Abramson L.W., Lee T.S., Sharma S, Boyce G.M. (2002), Slope stability and stabilization methods, John Wiley & Sons.

GEO-SLOPE International Ltd. (2010), Dynamic modeling with QUAKE/W 2007: An engineering methodology, 2010.

GEO-SLOPE International Ltd. (2010), SLOPE/W 2007 - An engineering methodology 2010.

Ministry of Land, Infrastructures and Transportation (2011), Design Standards and Commentary for Dams, prepared by Korea Water Resources Association.

Newmark N.M. (1965), Effects of earthquakes on dams and embankments, Geotechnique. 1965; 15(2):139-160.

Dynamic Characteristics of Dams Evaluated Using Earthquake Monitoring Data for Safety Assessment

M. Kashiwayanagi & H. Onishi
Chigasaki Research Institute, Electric Power Development Co. Ltd., Japan
masayuki_kashiwayanagi@jpower.co.jp

N. Osada &S. Hayakawa
JP Design Co.,Ltd, Japan

ABSTRACT:
Earthquake monitoring is normally conducted in high dams in Japan. The acceleration monitored is less utilized and is only accumulated to confirm the maximum values for further inspection. Detailed analysis of dam behaviour during an earthquake helps to identify the mechanical properties of the dam which could reflect its current soundness. This paper focuses on the effective utilization of earthquake monitoring data for the safety management of dams. Data on concrete gravity dams, arch dams and rockfill dams are examined so as to elaborate the management criteria in terms of the response characteristics and the predominant frequency. Such dynamic characteristics of concrete dams are formulated with influential factors, which are finally identified as the dam height, dam-reservoir interaction and mechanical properties of the transverse joints. In addition, the applicability of microtremor measurement is verified for another method of identifying the predominant frequency of dams through the in-situ measurement of an arch dam. It is concluded that the dynamic characteristics of the dam examined can be utilized as management indices to reveal an abnormal situation or degradation of the dam by detecting their deviations.

Keywords: Earthquake monitoring, Dynamic characteristic, Predominant frequency, Formulation, Management index

1. OUTLINE

Earthquake monitoring is conducted for the safety assessment of dams as well as monitoring of displacement, leakage etc. Seismometers are usually arranged to monitor the acceleration behaviour of dams due to earthquake impacts at the lowest gallery or the foundation and at the crest of each type of dam. Depending on the degree of earthquake response acceleration of the dam, a detailed inspection of the dam is occasionally necessary after an earthquake. Because of the difficulty in treating the earthquake monitoring data at the administration office of the dam, the maximum value of the acceleration response is only identified when the acceleration is not beyond the criteria for inspection. Many earthquake monitoring data on dams are accumulated and left for further analysis.

The earthquake behaviour of a dam is a structural response to a fluctuating load which depends on the mechanical properties of the dam and involves the interaction of the dam-foundation-reservoir system. Analysis of dam behaviour during an earthquake helps to identify the current mechanical properties of the dam and to understand the structural characteristics of the dam-foundation-reservoir system. Such results contribute to enhancing the numerical analysis method for dams during large earthquakes.

This paper focuses on the effective utilization of earthquake monitoring data for the safety management of dams. The acceleration response of dams owned by J-Power are analysed in order to prepare management criteria for the management personnel at the dam administration office. The dynamic characteristics of acceleration and the predominant frequency of dams are studied using the acceleration data during earthquakes. In addition, the factor of the predominant frequency of the arch dam is examined.

2. DAMS FOR EARTHQUAKE MONITORING

The basic characteristics and the locations of the dam studies in this paper are shown in Fig. 1 and Table 1. The acceleration behaviour of dams during earthquakes has been monitored at the lowest location and the crest at the highest section of the dam using seismometers. The downstream rock foundation instead of the lowest location of the dam is sometimes selected as the monitoring location.

Table 1. Earthquake monitoring in dams of J-Power

Dams	(1)	(2)	(3)	(4)
Nukabira	PG	76	1956	1987
Tagokura	PG	145	1959	1994
Sakuma	PG	155.5	1956	1981
Kazaya	PG	101	1960	2007
Ikehara	VA	111	1964	1987
Sakamoto	VA	103	1962	2007
Kuttari	ER	27.5	1987	1994
Ouchi	ER	102	1989	1985
Tadami	ER	30	1990	1990
Kassa	ER	90	1978	1977
Misakubo	ER	111	1969	1969
Kuzuryu	ER	128	1968	1968
Miboro	ER	131	1961	1969
Yanase	ER	115	1965	1965

(1) Type of dams, PG : Concrete gravity, VA : Concrete arch, ER: Rockfill (2) Dam height (m) (3) Year of Completion (4) Earthquake monitoring has been done since the year.

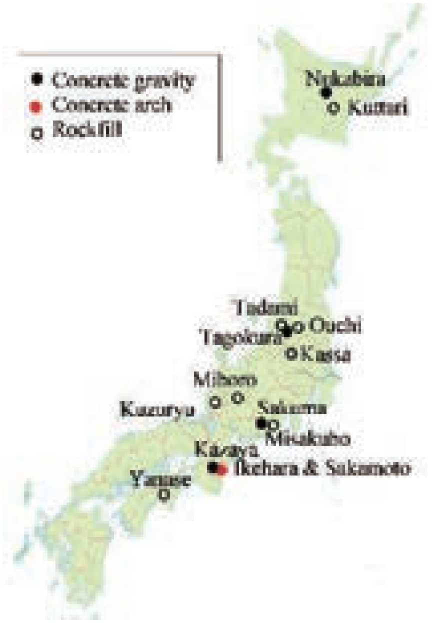

Figure 1. Large dams in J-Power

3. DYNAMIC CHARACTERISTICS OF DAMS

3.1. Response ratio

The acceleration behaviour of dams is frequently significant in the direction perpendicular to the dam axis of concrete gravity dams and rockfill dams and in the normal direction of the dam axis of arch dams due to the characteristics of these three-dimensional configurations. The acceleration data monitored in these significant directions are examined below. The response ratio is defined here as the ratio of the maximum accelerations at the crest and the lowest location of the dam. Both maximum values are not monitored rigorously at the same instant but are monitored almost simultaneously. It is considered that the maximum acceleration at the dam crest is excited by the maximum acceleration at the lowest location of the dam.

The acceleration response characteristics of the dams shown in Table 1 are illustrated in Fig. 2. The acceleration response characteristics of the lowest location and the crest of each dam show linear relations which are equivalent to the constant response ratios in the monitored range of acceleration. When a non-linear relation of these acceleration response or significantly different behaviour from a certain moment is found after an earthquake, damage to the dam or the dam foundation may be suspected due to the earthquake. However no facts described above are found in Fig. 2. It is suggested that non-linear characteristics of rockfill material cause the decline in the response ratio in the higher-acceleration range of as rockfill dam. The slight tendency of such phenomenon is found in Ouchi Dam shown in Fig. 2 (c).

The response ratios of the dams are summarized in terms of the height of the monitored locations in Fig. 3. Stronger dependency of the response ratio on the height of the monitored locations is found in concrete dams both of the gravity and the arch type, but not in rockfill dams. To further investigate this tendency, Eq. 1, by which the monitored acceleration at the crest is converted to acceleration of a dam of 100 m high, is introduced, assuming that the acceleration behaviour of the concrete dams is proportional to the dam height. The converted acceleration response is referred to as equivalent response acceleration in this paper.

$$A_{Ni} = \alpha \cdot A_i \cdot 100/H' \qquad (1)$$

Where, A_{Ni} : Equivalent acceleration response corresponding to the height difference of 100 m, A_i: Monitored acceleration response, H': height difference, α: Constant

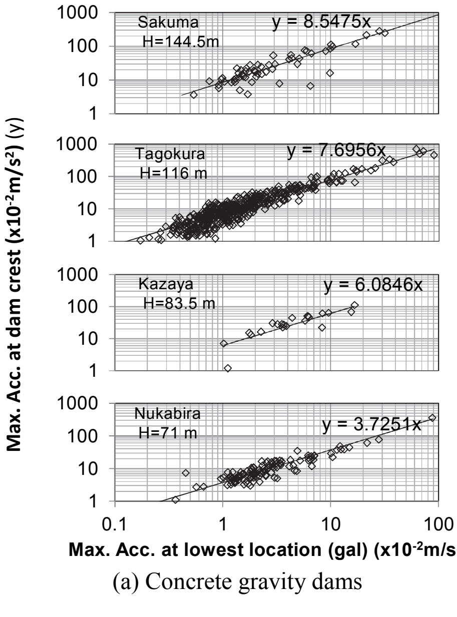

(a) Concrete gravity dams

Figure 2. Response ratio of dams

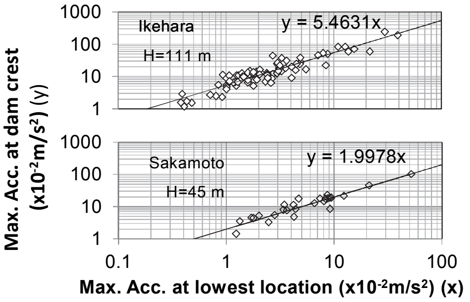

(b) Concrete arch dams

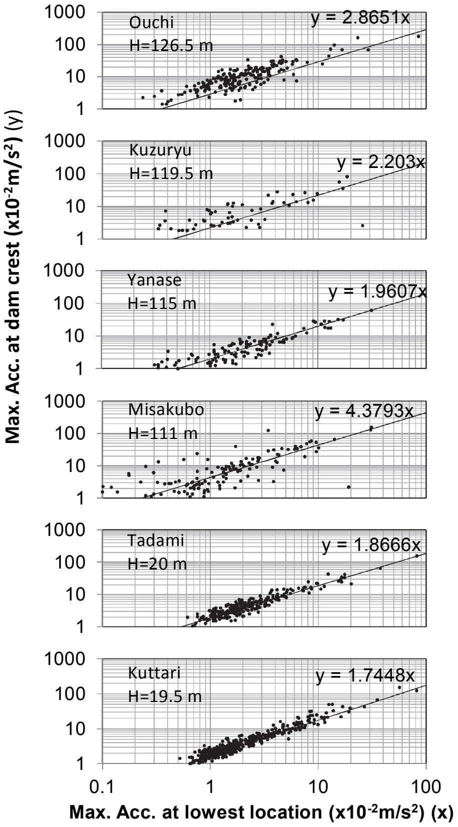

(c) Rockfill dams

Figure 2. Response ratio of dams

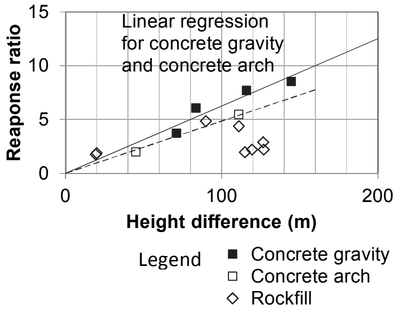

Figure 3. Summary of response ratio of dams

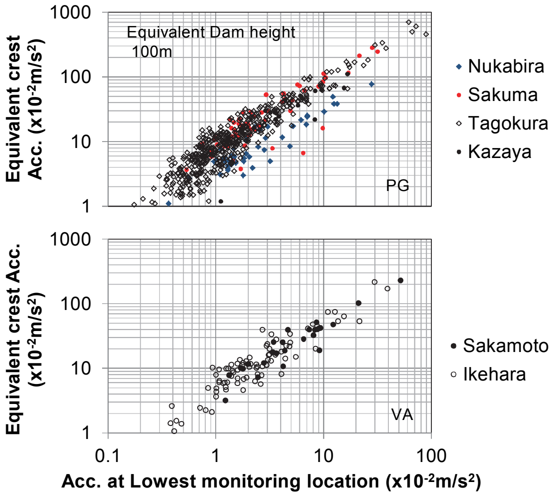

Figure 4. Equivalent response ratio of concrete dams

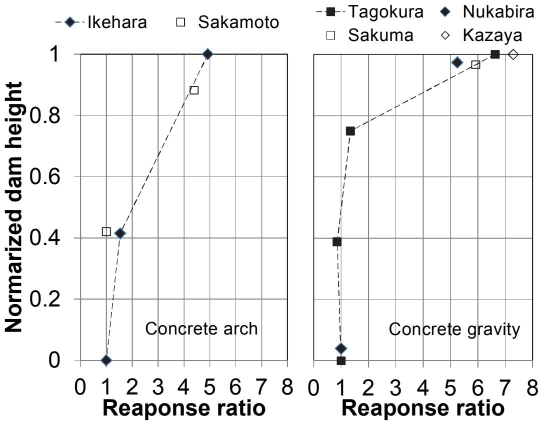

Figure 5. Response distribution of concrete dams

By applying Eq. 1 to the monitored acceleration response of the dam crest, the equivalent acceleration responses are plotted in terms of the dam types in Fig. 4. The converted data are closely plotted and show a closer tendency in the higher-acceleration range. This means that the acceleration response of the concrete dams significantly depends on the height of the dam or the monitoring location.

The distribution of the equivalent acceleration responses of concrete dams are examined as shown in Fig. 5. Both gravity dams and arch dams show specific distributions. These are roughly characterized by a sharp increase in the vicinity of the dam crest for a gravity dam and the a gradual increase along the dam height for an arch dam. The sectional shape is a major reason for the resulting specific response characteristics of each dam type, which are linear reduction of the sectional area of a gravity dam and the roughly constant section of an arch dam.

3.2. Predominant frequency

The predominant frequency of dams can be identified using several methods, which are broadly categorized into monitoring data analysis and numerical analysis. The transfer function which is estimated by the Fourier spectrum ratio at a certain two locations, is frequently utilized for monitoring data analysis. A numerical analysis method such as eigen frequency analysis and dynamic response analysis, requires an adequate calculation model involving the material properties of the dam at a certain moment, interactive behaviour due to the dam foundation and the reservoir, boundary conditions, etc. The material properties of the concrete dam inherently vary in respect to the concrete age, which corresponds to the moment of analysis. The methods of interaction between the dam and the reservoir affect the results of the analysis. However these conditions for numerical analysis are difficult to select, thus incurring difficulties in identifying the predominant frequency of the dam by numerical analysis.

Earthquake monitoring data are analysed to identify the predominant frequency of each dam type using the transfer function between the crest and the lowest location of the dam. The result in respect to the normalised water depth is shown in Fig. 6 for each dam type. Regression curves, estimated using the method by Kondo (Kondo et al., 2015), are added to the concrete dam cases. The predominant frequency of concrete dams clearly depends on the water depth and decrease according to the increase in water depth. It shows the mass effect of water fluctuating with the dam due to interaction of the dam and the reservoir during an earthquake. These predominant frequencies are scattered in a certain range at the same water depth. It shows something else in addition to the water interaction affecting the predominant frequency of the concrete dams. The rockfill dam shows a relatively constant tendency against the water depth, which means that the water interaction has less influence on the dam behaviour of a rockfill dam.

In the next section, the factors that affect the dynamic behaviour of an arch dam are examined in detail in terms of the characteristics of predominant frequency.

4. STUDY ON PREDOMINANT FREQUENCY OF A CONCRETE ARCH DAM

The predominant frequency of concrete dams is a fundamental parameter that reveals the dynamic properties of a dam at the time of monitoring. The diagnosis method for concrete dams has been studied by taking advantage of such characteristics of the predominant period (Sasaki et al., 2012). Factors affecting the dynamic characteristics of the dam can be selected from below:

(1) Elastic modulus of the dam concrete
(2) Mechanical characteristics of the transverse joints
(3) Reservoir water interaction
(4) Ambient temperature

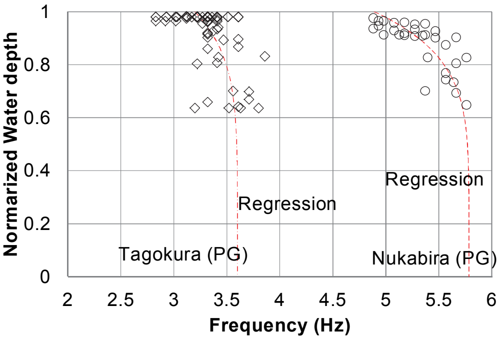

(a) Concrete gravity (PG)

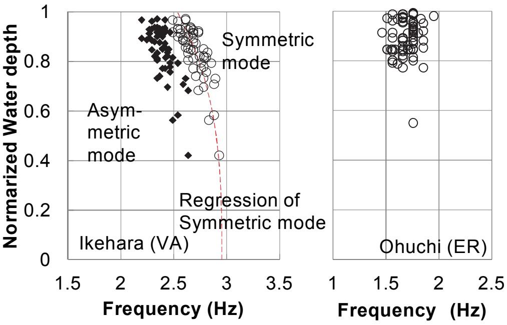

(b) Concrete arch (VA) and rockfill (ER)

Figure 6. Predominant frequency of dams estimated using earthquake monitoring data

The ambient temperature (item (4)) makes the volumetric change of the dam monolith, which induces alteration of the mechanical characteristics of the transverse joints (item (2)) by movement of the monoliths of the concrete gravity dam. Though the transverse joints of the arch dam are usually close due to the hydrostatic pressure on the upstream surface, the arch action of an arch dam may be affected by the condition of the transverse joints due to ambient temperature fluctuation. As cited above, the reservoir water interaction (item (3)) gives an additional load of hydrodynamic pressure on the dam and results in a shift in the predominant frequency due to the dam-reservoir interaction. It is well known that the physical properties of dam concrete continuously increase (item (1)) in terms of not only strength but also elastic modulus over a certain number of years due to hydration reaction. Imaoka et al.(2014) reported such results on the concrete of an arch dam by testing the cored concrete. The impacts of these factors can be observed as the shift in the predominant frequency of concrete dams.

To take the impacts due to items (2), (3) and (4) into account, Eq. 2 is introduced in this paper, referring to Kondo et al.(2015). The impact due to item (4) is examined hereinafter.

$$f_1(h,\theta) = c_0 + c_1(h/H)^{\beta} + \frac{c_2}{\sqrt{\theta^{*}-\theta}} + \mathrm{e} \qquad (2)$$

Where, $f_1(h,\theta)$: predominant frequency, h : water depth of the reservoir, H : full depth of the reservoir, β :

Parameter, θ : ambient temperature, θ^* : ambient temperature corresponding to zero opening of the transverse joint (40℃ is adopted.), c_0, c_1, c_2 : constant, e : residual

The examination of Eq. 2 is conducted by regression analysis based on the monitored predominant frequency of an arch dam, as shown in Fig. 6(b). As a result, parameter β is set as 3.0 and the average temperature over 30 days with a lag of 30 days is used for the ambient temperature. Multiple regression analysis for the predominant frequency of the arch dam provides a high regression coefficient of 0.81 and each constant of c_0, c_1 and c_2. The correlations between the monitored values and water depth or ambient temperature are shown in Fig. 7(a) and Fig. 7(b), respectively.

A parameter β of 6.0 was adopted for concrete gravity dams (Kondo et al., 2015). In this case, the influence of the parameter is limited to shallower-water-depth region. The regression curve with a smaller β which is applied to an arch dam, affect the shift in the predominant frequency to deeper-water region. These characteristics of the shift in the predominant frequency indicate good agreement with the vertical distribution of the response acceleration of the concrete dams as shown in Fig. 5. The concrete gravity dam shows significant response in a limited area of the crest vicinity, in which great impact is observed on the shift of predominant frequency. The arch dam shows a gradual increase in acceleration response from the middle to the crest. Its profile matches the profile of the shifted predominant frequencies of the arch dam. This phenomenon is interpreted to be caused by the difference of the degree of the dam-reservoir interaction between a concrete gravity dam and an arch dam.
The scatter appearance of the predominant frequency due to temperature fluctuation, shown in Fig. 7(b), indicates good quantitative correlation with the estimated frequency by Eq. 2. The influence of the temperature on predominant frequency is originally formulated for concrete gravity dams by Eq. 2, where the shear characteristic of transverse joints is incorporated in the manner of a simple mass-spring model instead of the opening of transverse joints due to temperature fluctuation. Because the transverse joints of the arch dam are subject to compression force due to hydrostatic pressure and the resulting arch action in the dam axis direction, little opening of the transverse joints is expected. However the alteration of the shear characteristic is certainly happened in the transverse joints of arch dams as well as concrete gravity dams due to temperature fluctuation. It is considered that the situation in Fig. 7(b) verifies indirectly the influence of temperature fluctuation on the shear characteristic of transverse joints.

As for another method to identify the predominant frequency of structures, microtremor measurement as well as the analytical method described in Section 3.2 is sometimes applied. Microtremor measurement requires simple devices, i.e., a servo-type velocity meter and data logger, which can be transported manually. The applicability of these methods is examined hereinafter. Dam-reservoir interaction is considered for eigen value analysis and dynamic time history analysis using added mass and FEM interaction analysis, respectively. The results of these methods are shown in Fig. 8.
A significantly great decline in predominant frequency in the higher-water-level region is found through analytical methods than through earthquake monitoring. This tendency is clearer in eigen frequency analysis. The deviation in estimated frequency of each analytical method is caused by the difference in hydrodynamic pressure distributions, even though dam-reservoir interaction is considered in both analytical methods. The excessive decline found through analytical methods in the high-water-level region should be addressed.

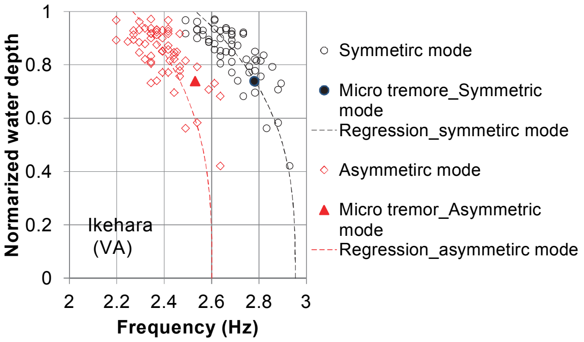

(a) Water depth

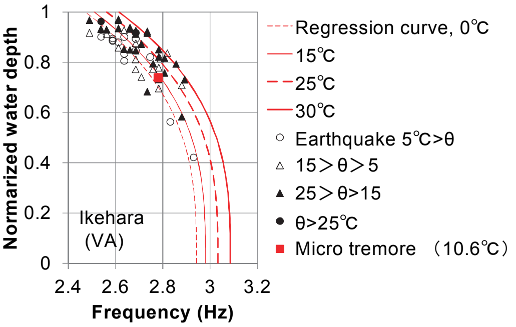

(b) Ambient temperature (for symmetric mode)

Figure 7. Dependence of predominant frequency of an arch dam

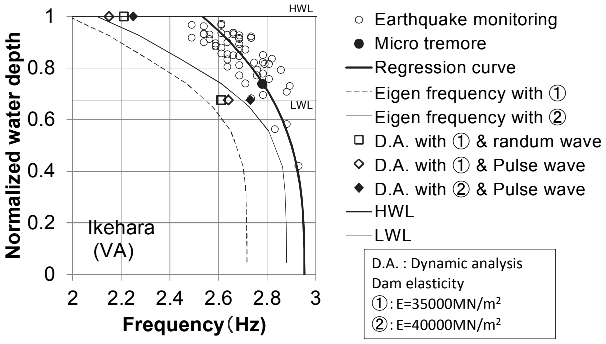

Figure 8. Comparison of estimation method of predominant period (Symmetric mode)

The analytical methods provide closer estimation to the monitored values in the case of an elastic modulus of 40000MN/mm^2. The current static modulus of an arch dam which more than five decades has passed is estimated to be 44000MN/mm^2 and 40000MN/mm^2 for a specimen extracted from the dam recently and a specimen molded at the construction site and cured in the laboratory, respectively. The analytical evaluation shall be equivalent to the monitored evaluations and the regression curve by Eq. 2 in the lower-water-depth region when the dynamic modulus is applied, considering the dynamic condition under earthquakes.

The temperature fluctuates in the range of 30 degrees centigrade at the arch dam site studied. The temperature fluctuation influence corresponds to a variation in the elastic modulus of approximately 5000MN/m^2 in terms of variation of the predominant period (refer to Fig. 7(b) and Fig. 8). The alteration of the shear characteristic of the transverse joints due to temperature fluctuation could be replaced by modification of elastic modulus of the dam. In other words, considerable dependence on ambient temperature is expected in the behavior of a dam during an earthquake at the time. This fact should be kept in mind regarding assessment of safety of dams against large earthquakes.

The frequency estimated by the data of microtremor measurement shows good agreement with the data of earthquake monitoring. Noise due to traffic, operation of a powerhouse situated near the dam, etc. could affect the measurements. However, little impact on the identification of the predominant frequency of the dam was found through the in-situ measurements. An example of the measurement conducted at Ikehara Dam is shown in Fig. 9. This feature enables easier continuous measurements, which can depict more clearly the influence of dam-reservoir interaction and temperature fluctuation on the frequency of arch dams.

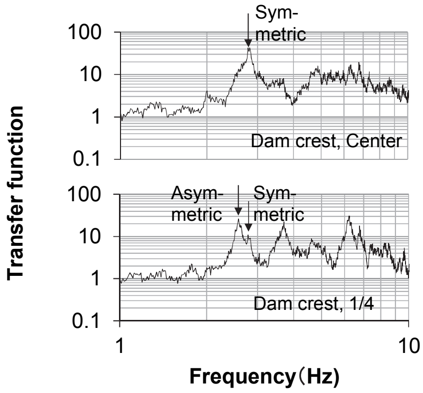

Figure 9. Example of micro tremor measurement at Ikehara dam

5. CONCLUSIONS

Earthquake monitoring data on dams are examined to evaluate the dynamic characteristics of the acceleration response and the predominant frequency for accessing the soundness and the current properties of dams. The conclusions are summarized below.

(1) The response acceleration at the dam crest during an earthquake has the characteristics of a linear relation and an independent response ratio to the bottom acceleration of the dam. Because of the dependence on the dam height of the response ratio of concrete dams, the acceleration response ratio is unified in terms of normalized dam height. Little tendency is found in the response ratios of rockfill dams, which each show a unique figure and a little non-linearity of acceleration response where the crest acceleration is greater.

(2) The vertical distribution of the response acceleration is figured identically in a concrete gravity dam and an arch dam using the equivalent response acceleration in respect to the dam height.

(3) The predominant frequency of concrete dams has a clear dependence on reservoir water depth and ambient temperature, while the predominant frequency of rockfill dams is almost constant without dependence on reservoir water depth and ambient temperature. The dependence on reservoir water depth and ambient temperature is caused by the dam-reservoir interaction during an earthquake and mechanical property alteration of transverse joints due to temperature fluctuation.

(4) Additionally considering the ageing of the elastic modulus of the dam concrete, the characteristic of the predominant frequency of arch dams is well formulated in terms of reservoir water depth and ambient temperature at the time. The applicability of microtremor measurement is verified for the method of identifying the predominant frequency of dams through in-situ measurement of an arch dam.

(5) The dynamic characteristics of dams examined in this paper can be utilized as management indices to reveal an abnormal situation or degradation of a dam by detecting their deviation. In this context, it is essential to accumulate data on all aspects relating to dam operation and its behavior and to periodically examine on these data.

REFERENCES

Kondo, M., Kobori, T., Kajima, T., Sasaki, T. (2015): Multiple regression analysis of natural frequency changes observed at concrete gravity dams, Journal of Dam Engineering, 25:1, pp. 16-28 (in Japanese)

Sasaki, T., Kondo, M., Kobori, T., Kajima, T., Odate, W. (2012): Applicability of micro tremor measurement on diagnosys of concrete gravity dams, Engineering for Dams, 313, pp. 18-30 (in Japanese)

Imaoka, T., Washio, T., Yasuda, Y. (2014): Mechanical propeteis of dam concrete aged at 50 years of Samamoto dam and Ikehara dam, Electric Power Civil Enginnering, 374, PP. 91-95 (in Japanese)

4th APG Symposium and 9th EADC on

INNOVATIVE TECHNOLOGIES FOR DAMS AND RESERVOIRS TOWARD THE FUTURE GENERATIONS

Natural Disasters and Dam Safety Issues in Nepal

D. P. Sangroula, Dr. Eng.
Professor, Department of Civil Engineering, Pulchowk Campus, Institute of Engineering, Tribhuvan University, Nepal.
dsangroula@ioe.edu.np

ABSTRACT:
The fragile geology of the Himalayas creates many structural stability problems in Nepal. Landslides are one of the major hazards, primarily caused by intense rainfall but also by earthquakes. The panic-stricken situation created in the aftermath of 25 April and 12 May 2015 earthquakes has further illustrated this fact. Substantial damage is also caused by water-induced disasters like floods. Earthquakes, landslides, floods and fragile geology result in structural failure or collapse, foundation failure, debris flows and large water volume flows, all and any of which can have direct impacts on hydropower plants. Considering continuing incidences of dam failures around the world and high potential to natural hazards in the Himalaya region, it is high time to highlight the need and importance of dam safety management. The likelihood of increases in weather extremes in future therefore gives great concern that the number or scale of weather-related disasters will also increase. Despite the fact that reservoirs are one of the major man made hazard, risk assessment legislation and dam safety rules and regulations do not yet apply in Nepal. There is no such legislation that imposes a system of safety checks on reservoir construction and operation in Nepal.

Keywords: Earthquake, Glacier lake outburst flood, Land slide dam outburst flood, Disasters and dam safety management.

1. BACKGROUND

Nepal, a mountainous landlocked country in the central Himalayas, is in one of the most fragile eco-regions of the world and is prone to natural and human-induced disasters. Dynamic geological conditions, great elevation differences, steep sloping terrain, soft soil cover, steep river gradient, climate change and decreasing vegetation cover, combined with high intensity seasonal rainfall makes the country very susceptible to natural disasters. These include earthquakes, rock and ice avalanches, landslides, mudslides, debris flows and glacial lake outburst floods (GLOFs), all of which can wreak havoc on infrastructure and communities. Large-scale landslides can damage river valleys leading to impoundment of upstream river flow and the inundation of river-side communities and infrastructure. Should a landslide dam fail, severe flooding (Landslide Dam Outburst Floods, LDOFs) can ensue with catastrophic consequences, like GLOFs, for many tens of kilometers downstream.

Nepal intends to develop its grossly under-developed hydropower for both internal consumption and export and has an ambitious pipeline of projects. Over the last few years, and as recently as 2 August 2014, 25 April 2015 and 12 May, 2015 many hydropower installations in Nepal have been affected badly by natural disasters resulting in very significant economic losses, amounting to millions of US dollars. It is widely believed that Nepal is currently not well prepared to manage such disasters. Recent incidents have demonstrated the lack of a national level preparedness and actions plans for disaster risk management in Nepal is general.

As the world becomes increasingly vulnerable to natural disaster, the greatest numbers of people are at risk level in the poorer nations of the developing world like Nepal. It is the challenges for disaster managers, planners, legislators, designers, development workers and donors to effectively mitigate and keep the people safe in the events of disaster. Natural hazards cannot be avoided, but timely, accurate prediction of hydro-climate extremes helps societies to prepare for and mitigate disasters and to reduce losses in infrastructures and productive activities. Early warning system and forecasts provide lead time, which together with public awareness , education and preparedness, can allow people to act quickly in response to hazard information, thereby increasing human safety and reducing the human and economic losses from natural disasters (WB, 2012).

2. NATURAL DISASTERS, HAZARD AND VULNERABILITIES ON HYDROPOWER PROJECTS

Generally there are three types of hydropower projects in operation in Nepal. They are storage type, peaking type of run-of-river (PRoR) and purely run-of- river (RoR). The 60 MW Kulekhani Hydropower project is only the storage type of hydropower project in Nepal and rest of hydropower projects are PRoR and RoR types. Not all the dams posses similar potential hazards if they fail or collapse so, it is necessary to distinguish between high potentially hazardous dams with less potentially hazardous dams. Potentially hazardous dams are those that, due to their size and/or location, could pose a threat to life, property or the environment if they were to fail. This does not necessarily mean that they are expected to fail. Failures of dams and any other hydraulic structures and their consequences in Nepal are very much linked to the rivers in which they are located. Hazards and vulnerabilities on the rivers directly related to their origin. There are basically three grades of rivers in the country.

Rivers that are originated from glacier on ice capped mountains above the snow line are categorized as the First Grade Rivers in Nepal. These rivers are perennial and carry sufficient flows in all seasons. Karnali, Gandaki and Koshi rivers as well as their tributaries which originate from glaciers are categorized as the first Grade Rivers. Landslides and Landslide-Dammed Outburst Floods (LDOFs) Glacial Lake Outburst Floods (GLOFs), river and surface water floods, debris flows, mudslides, Ice Dam Outburst Floods (IDOFs) pose hazards to any structures located along these river systems. Second Grades Rivers are originated from Mahabharata Hills. Mahabharata Hills fall below the snow line that lies at about 5000 meters altitude. They also do not dry up in the low flow period as they meet spring and shallow underground water tables. Landslides and landslide-Dammed Outburst Floods (LDOFs), river and surface water floods, debris flows, mudslides, cause vulnerability on any structures located along these river systems.

There are several types, events and scale of natural disaster (scale of impacts) in the Himalayan Region. Natural hazards (event trigger) and their flooding events and scale of impacts proposed by Reynolds (2014) are given in Table 1. This table shows that event trigger such as earthquake and cloudburst or exceptionally prolonged heavy rainfall can have severe consequences. Risk of dam failure and disaster risk management should be evaluated by considering all event trigger for each component for storage as well as run-of-river (ROR).

Table 1. Types of natural disasters (Reynolds, 2014)

Event trigger	Flooding events	Scale
Earthquake	Landslides and landslide-Dammed Outburst Floods (LDOFs)	Regional depending on the magnitude of the earthquake; multiple river catchments, thousands of km^2
Cloudburst or exceptionally prolonged heavy rainfall	Landslide-Dam and Glacial Lake Outburst Floods (GLOFs), river and surface water floods, debris flows, mudslides	Regional depending on the volume, rate and duration of precipitation; multiple river catchments, thousands of km^2
Rock-/ice-avalanche	Landslide-Dam, Glacial Lake Outburst Floods	Single catchment, run- out distances hundreds of km^2
Ice-dam failure	Ice Dam outburst Flood	Single catchment, run- out distance can exceed 1,000 km.

2.1. Earthquake

The 25 April 2015 Nepal earthquake also known as the Gorkha earthquake killed more than 9,000 people and injured more than 21,000. It was the worst natural disaster to strike Nepal since 1934. The earthquake triggered an avalanche on Mount Everest, killing 21, making April 25, 2015 the deadliest day on the mountain in history. The earthquake triggered another huge avalanche in the Langtang valley, where 250 people were reported missing. Hundreds of thousands of people were made homeless with entire villages flattened, across many districts of the country. A major aftershock occurred on 12 May 2015. The epicenter was near the Chinese border between the capital of Kathmandu and Mt. Everest. More than 200 people were killed and more than 2,500 were injured by this aftershock.

Kulekhani and some other hydropower projects were suffered from the earthquake. Cracks have appeared in the direction of the Kulekhani dam axis in the asphalt pavement and upstream shoulder for about 200m section in the middle part of the crest. The width of the crack is about 1 cm at the maximum (see Figure 1). Though the crack appeared at the core top and the dam crest settled by 15cm to 25cm by the earthquake, they are regarded as not serious with respect to the immediate safety of the dam. The dam still has a sufficient freeboard required in the design, 2.5m for the extraordinary flood of 1,380m^3/s and 3.3m for the probable maximum flood of 2,720m^3/s (JICA, 2015)

Fortunately, no substantial damage or deformation appeared on the dam, which would have endangered the immediate safety of the dam and could have caused substantial damage with serious consequences downstream. JICA (2015) reported that frequent monitoring of dam movement must be made to ensure the dam safety when raising the reservoir in the coming rainy season. A risk management and action plan must be prepared beforehand with prudent precautions.

On April 26, 2015 at 12:54pm an aftershock measuring 6.9Mw struck with epicenter at Sindhupalchowk about 10km from Upper Bhote Koshi Hydro Electric Project site. The earthquake triggered massive rock falls from the mountains. The penstock suffered major hits from the rock falls, which caused a major rupture of the pipe (see Fig. 1) at the 8th girder just above the second Anchor block. The rupture allowed uncontrolled release of the accumulated water inside the top reach of the penstock and headrace tunnel. The resulting deluge caused severe erosion and debris flows, damaged project facilities and flooded the powerhouse completely up to the "Erection Bay" or machine hall level. The electrical panels in the erection bay and control room were partially submerged in water for some time. The main generators, turbines and all equipment below the erection bay level were submerged in water. The main power transformers and emergency diesel generator was hit by water and debris and were partially buried by the debris flow.

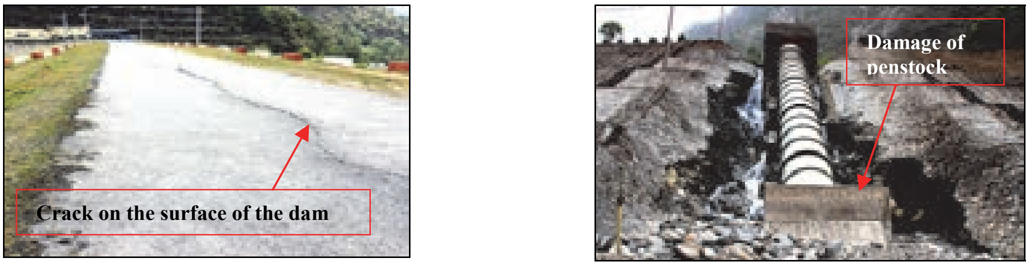

Figure 1. Crack on the crest of Kulekhani dam damage of penstock of Bhotekoshi Hydropower Project (courtesy of Neupane Hara Raj and Bikram Sthapit).

A Post Disaster Need Assessment (PDNA) has been completed by June 15, 2015 by the Government of Nepal (GoN) with support of donor community. For the electricity sector, it covered hydropower generation facilities owned by the Nepal Electricity Authority (NEA) and Independent Power Producers (IPPs).The report has identified that around 115 MW hydropower generation facilities out of the 787 MW total installed capacity in the country (grid and off-grid) were been severely damaged, and 60 MW were partially damaged. The earthquake damages has highlighted the needs for updating and enhancing the dams and hydropower power projects safety design standard and operation & maintenance (O&M) practice in a more comprehensive manner.

2.2. GLOFs

Rising temperature that causes retreat of mountain glaciers is one of the main factors responsible for the formation and expansion of glacier lakes (Mool, 2001).Almost all glaciers in the Himalayas have been retreating since the Little Ice Age (1400-1650AD) and on average they have retreated about 1 km. Such a retreat provides a large space for retaining melt water that leads to the formation of glacier lakes. The supporting dams of these lakes generally consist of loose moraines, which are not strong enough to resist the growing hydrostatic pressure on them caused by rising water level in the lakes, which makes them vulnerable to collapse. The collapse of such lakes may result in the instantaneous release of the stored lake water that may create devastating floods. Such floods are termed as Glacier Lake Outburst Floods (GLOF).

Potential intensification of monsoons combined with enhancement of GLOF risks also contributes to enhanced risk of flooding and landslides which can have serious impact on hydropower projects. Extreme events such as GLOFs have potential effects on water resources project because the massive force of a GLOF is often capable of destroying all infrastructures along the river valley in a very short period. This happened in the Dig Tsho GLOF in 1985 that completely swept away the Namche Hydropower Plant in the Khumbu region costing approximately 45 million Nepalese rupees (Thomas and Rai, 2005). For effective GLOF risk management, it is essential to define components and their relevant issues so that appropriate strategies can be employed. In many areas, the impact of climate change on the glacier systems upstream of the hydropower scheme must be taken into consideration if they are not to suffer the same fate as that of Dig Tsho.

It is a big challenge to identify those GLOF lakes which pose significant hazards from those which might not pose any such hazards. The National Adaptation Program of Action (NAPA) to Climate Change, (2010) and the Climate Change Policy, (2011) specifically highlight the GLOF issue. Monitoring of potential GLOF lakes that pose significant hazards, implementation of structural measures, establishment of early warning system and forecasting and preparedness in downstream communities are some of the recommended program activities contained in the NAPA and Climate Change Policy, 2011.

2.3. LDOFs AND FLASH FLOODs

Due to rugged topography, very high relief and intense precipitation during the monsoon period, the hilly regions of Nepal are very susceptible to landslides. Formation of temporary lakes due to landslide damming is a common phenomenon in high mountain areas where there are very narrow river channels and steep mountain slopes. Eleven disastrous floods caused by breaching of landslide dams have been reported in Nepal between 1967 and 1989 (Khanal, 1996). The 144 MW Kali Gandaki A (the biggest in Nepal so far) Hydroelectric Project faced significant landslide issues.

A large landslide debris dam was deposited by a large landslide at bordering region of Mankha and Ramche VDCs of Sindhupalchowk District at around 02:30 AM, Saturday morning of 2 August 2014. The landslide destroyed dozens of houses and deposited large volume of debris material at the existing waterway of Sunkoshi River. The massive Kanlay hill crumbed to the ground killing more than 156 people. This landslide in Sunkoshi River, which is one of the major tributaries of Koshi River, blocked the river flow for more than 13 hours and created a reservoir about 4 km long and 50 m deep. The massive landslide caused an abrupt interruption in the flow of Sunkoshi River, and impacted five hydropower projects: (1) 2.5 MW Sanima, (2) 10 MW Sunkoshi, (3) 45 MW Bhotekoshi, (4) 6 MW Chaku and (5) 3 MW Bhairabkunda Hydropower Projects (NHA, 2015). Two gates of the Sun Koshi Hydropower Dam were also washed away (see Fig. 2) and the power house of the Sanima Hydropower project was inundated.

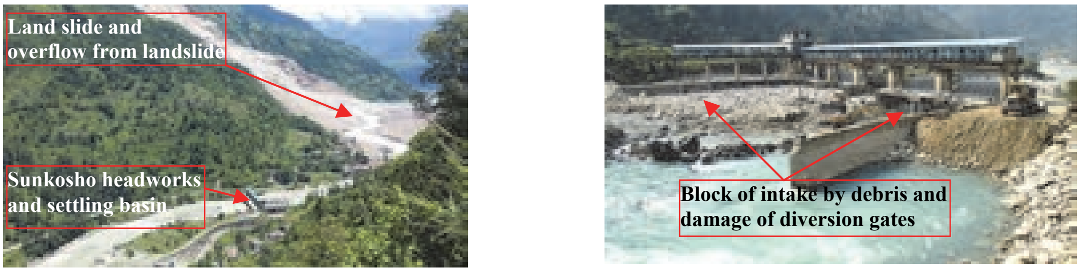
Land slide and overflow from landslide
Sunkosho headworks and settling basin
Block of intake by debris and damage of diversion gates

Figure 2. Landslide on Sunkoshi River and Sunkoshi headworks

High intensity rainfall events are often localized and have important implications for flash floods. These intense rainfall events, sometimes called cloudbursts, can occur in remote area as a result of topographic variations and are generally unreported because of inaccessibility and isolation. Flash floods are one of the most devastating natural disasters because of their rapid occurrence, short lead time for warning and often large volumes of water and debris load transported with high energy. Flash floods can be of different types. Intense rain fall floods (IRF), Glacier Lake Out-burst Flood (GLOF), Landslide Dam Out-burst Flood (LDOF) and flash flood due to rapid melting of snow and ice are the common types of flash floods encountered by the people of Nepal. Failure of man-made dams and other water-retaining structures can also lead to flash floods. Thousands of people, their lives, livelihood, and homes, along with expensive infrastructure are at great risk from flash floods in Nepal every year. The threat to downstream people is likely to increase in the face of climate and environmental change.

3. SAFETIES AND SUSTAINABLE HYDROPOWER DEVELOPMENT

The water resources are one of the principal opportunities for future economic development of the country. As based on hydrological data available up to 1993, the then Director General of Department of Hydrology and Meteorology (DHM) Mr. K.S. Yogacharya had derived the annual runoff from the total drained areas to be about 225 billion m^3 (Yogacharya, 1996). Also as mentioned by the ministry of Water Resources in the country's report to the first International Summit on “Sustainable use of water for energy”, some 225 billion m^3 of surface water flows through the Nepalese territory annually (WWC and IHA, 2003). This gives a specific runoff of about 0.12 million m^3/km^2/year, being about four times the world average. As reported by Water and Energy Commission Secretariat (WECS, 2011), the potential of 114 projects with a combined capacity of 46,610 MW have been identified as economically feasible. Unfortunately, the total power plant capacity of the country by mid-2015 is about 787 MW, which is about 1.5 % of economically feasible projects.

In addition to these existing plants, some hydropower projects are scheduled to be commissioned. Among others, these include the largest project under construction in the public sector, with domestic funding, is the NEA-owned 456 MW Upper Tamakoshi Project. Recently a Power Trade Agreement (PTA) has been signed between Nepal and India. Power Trade Agreement has also been signed between SAARC country during SAARC submit in (10-11 Nov, 2014) Kathmandu. A Power Development Agreement (PDA) has been signed between the Nepal Investment Board (NIB) and GMR Energy India for the development of 900 MW Upper Karnali. Similarly, PDA has also been signed with Satluj Jal Vidhut Nigam Limited (SJVNL) of India for the development of 900 MW Arun –III.

The proposed 260 m high dam Budhi-Gandaki storage project with installed capacity 1,200 MW and 140 m high dam Tanahu Hydropower project with installed capacity 140 MW are in the final design stage. Some other projects are very close to the construction phase. However, safety and sustainability related to sedimentation issues are not given as high priority as it is supposed to be. The proposed Tanahu Hydropower Project is located at about 4 km upstream from the Byas Municipality and the proposed Budhi Gandaki Hydropower Project is located at about 40 km upstream from the Bharatpur Sub-metropolitan city. The designers and planners have not been focusing seriously on sustainability and dam safety management issues for these proposed projects.

Moreover, the institutional framework and capacity of the GoN agencies is still weak in preparing and reviewing feasibility study, design, bidding documents, etc. of large-scale hydropower projects, which has resulted in long delays in reviewing and approving technical documents submitted by private developers. At the same time, the safety and sustainability of the hydropower schemes needs to be carefully reviewed. Considering the current management condition of existing dams/hydro power projects and quite a number of large-scale hydropower development projects under preparation, there are strong needs for enhancing the institutional framework and capacity for dam safety and quality assurance covering all relevant ministries and agencies in Nepal.

Dams are generally designed and built to operate safety through their long services and also the probability of dam failure is also very small. However, the consequences of dam failure are extremely severe. There have been approximately 2000 failures of constructed dams throughout the world since the twelfth century, and many thousands more failures of natural dams. During the 100 years, there have been about 200 significant failures of constructed dams, in which more than 11,000 people died: 6800 lives were lost in three failures alone: Vaiont Dam, Italy, 1963 (2600); South Fork Pennsylvania, 1889 (2200); and Machhu II, India 1974 (2000+) (Costa, 1985). Financial losses associated with dam failures are probably inestimable (Costa, 1985). Since, the risk of failure of hydropower projects can never completely be eliminated, it is important to carry out the dam safety management (DSM) from the very initial stage of hydropower development cycle with the objective of minimizing the potential risk of dam failure during planning, design, operation and maintenance stages. Although, there is a huge potential for development of hydropower in the Nepal, sustainability and dam safety issues are among the most challenging.

4. ASSESSMENT OF GAPS IN DISASTER RISK MANAGEMENT

Considering continuing incidences of dam failures around the world and high potential to natural hazards in the Himalaya region like Nepal, it is high time to highlight the need and importance of dam safety management. Despite the fact that reservoirs are one of the major man made hazard, risk assessment legislation and dam safety rules and regulations do not yet apply in Nepal. There is no legislation that imposes a system of safety checks on reservoir construction and operation in Nepal. The National Disaster Relief Act does not address the risk of disaster in relation to hydropower development. National Strategy for Disaster Risk Management, 2009 has mentioned about the hazard related to hydropower, however, failed to specify the disaster risk management. There is no national provision for hydropower project emergency preparedness plan. So far no guidelines have been developed in Nepal for early warning system in case of dam failure, although early warning systems in case of flooding and GLOF are in practices (NDR, 2013). The power sector has many institutions. In the case of tackling natural disasters, more agencies become involved. Lack of cooperation and coordination between various agencies has led to duplication of relief works during disasters.

The Department of Electricity Development (DOED) guideline does not stipulate standards for many important technical parameters. Furthermore, it does not incorporate the latest worldwide experiences in the relevant fields. A dam safety review protocol also does not currently exist in Nepal. Although no standard norms have been developed for inspection of dam, inspection around the headworks for RoR and PRoR projects in Nepal seems satisfactory. Regular maintenance works due to erosion on civil and mechanical components of headworks, repairs on gates and other hydraulic structures are taking place on a regular basis (Sangroula, 2015). There are facilities to observe seepage and leakage in some existing hydropower projects but fail to have cracking, movement/deformation and other structural defect tests. Hence, special equipments have to be installed at the dam/headworks for this purpose, especially for the storage projects.

5. CONCLUSIONS AND RECOMMENDATIONS

The hydropower development is the backbone of a country's development. However, the safety and sustainability issues are one of the major challenges in their development. For sustainability of any hydropower projects, life cycle management approach should be adopted rather than linear approach which is currently in practice. In relation to dam safety at the national level, the Government needs to develop legislation and policy on dam safety to fulfill its national and, where relevant, its international obligations. A properly established legal and governmental framework provides for the regulation of dams, reservoirs and related operational activities that can prevent any dam breaches and other inundation risks. It will also help to set clear assignment of responsibilities.

An independent regulatory body to assure the safety of dams is also lacking in Nepal. It is recommend to establish a scientific and technical group to develop the concepts and methodologies for integrated dam and valley risk management. The following objectives could be chosen in order to inspire the work:

1. To improve the engineering capability for dam break flow analysis and prediction on real complex situations.
2. To develop methodologies and guidelines for dam break flood risk management in Nepal as a first step towards a new integrated flood safety system based on structural and non-structural measures, including public participation.
3. To implement new advanced information technologies applied to hydraulic engineering analysis and land-use and safety management techniques.
4. To create a new concept for operational crisis control and integrated dam safety management, and also to contribute to improvement of the Nepalese dam safety regulation and land-use management in risk- prone areas.

REFERENCES

Costa, J. E. (1985): Floods from dam failure. USGS. Cascades Volcano Observatory, Vancouver, Washington.

JICA. (2015): Inspection report on Kulekhani dam and hydropower stations. Kathmandu, Nepal.

Mool, P.K. (2001): Inventory of Glaciers, Glacial Lakes and Glacial Lake outburst floods monitoring and early warning systems in the Hindu Kush Himalayan Region. Kathmandu: ICIMOD.

NDE. (2013): Nepal Disaster Report, Ministry of Home Affairs, Government of Nepal: Disaster Preparedness Network Nepal.

NHA. (2015): Assessment of disaster riskmanagement in the hydropower sector in Nepal, report submiited to World Bank, Nepal Hydropower Association, Kathmandu.

Reynolds, J.M. (2014): Natural disaster preparedness for hydropower development in high mountain environments. Reynolds International Ltd. Mold, UK.

Sangroula, D. P. (2015): Assessment of vulnerability of the power sector to natural risks including climate change and needs for improved hydromet services in Nepal, report submiited to World Bank.

Thomas, K. J. and Rai, S.C. (2005): An overview of glaciers, glaciers retreat, and subsequent impacts in Nepal, India and China. World Wildlife Fund Nepal.

WB. (2012): The Role of Hydrometeorological services in disaster risk management. Proceedings from the joint workshop co-organised by: the World Bank (WB), the United Nations International Strategy for Disaster Reduction, and the World Meteorological Organisation.

WECS. (2011): Water resources of Nepal in the context of climate change. Government of Nepal, Water and Energy Commission Secretariat, Kathmandu, Nepal.

WWC and IHA (World Water Council and International Hydropower Association). (2003): Proceeding of First International summit on sustainable use of water for energy. 3rd World Water Forum, Kyoto, Japan.

Yogacharya, K. S. (1996): Assessment of Water Resources of Nepal and Its Economic Value. Workshop on the Value of Water in the Economic Development of Nepal, 10 June 1996, Dhulikhel, Nepal.

Dam Safety Management In Indonesia

A. Zubaidi, Rahman H. A. & Anissa M.
Dam Safety Unit, Ministry of Public Work and Housing, Indonesia
azubaidi32@yahoo.co.id

ABSTRACT:
In order to maintain the function of the dam and technically keeping the dam safety, it is needed a proper dam safety role in Indonesia. With the number of dams in Indonesia until 2016 that reached 214 dams based on Minister Regulation No. 27/2015 on Dams criteria, Dam Safety Unit as technical committee of dam safety has taken several steps to improve the dam safety management such as facilitation of design, initial impounding, operating, design of rehabilitation, and decommissioning permit. Moreover, in several times ago has been conducted review of some Indonesia's existing dam safety guidelines based on the current condition in Indonesia as well as the development of world science.

Keywords: Dam safety, Dam safety unit, Dam safety management

1. INTRODUCTION

Indonesia is a tropical country which has 2 (two) seasons: dry and rainy seasons. The dams will provide huge reservoir to store excess water during the rainy season, to control the flood and also to be used in dry season.

Besides having many benefits, dams construction also keep potential hazards that can endanger the lives at the downstream. The dams failure can cause major flooding and damage in the downstream area.

In accordance with Minister Regulation No. 27 / PRT / M / 2015 on Dams, dam safety role is intended to realize the orderly development and utilization of dams so be worthy of a technical or non-technical aspects from the design stage, construction, and operation in order to prevent or reduce the potential failure risk of the dams construction. Below is one example of dam failure in Indonesia caused by poor manage, such us Situ Gintung Dam (Fig.1).

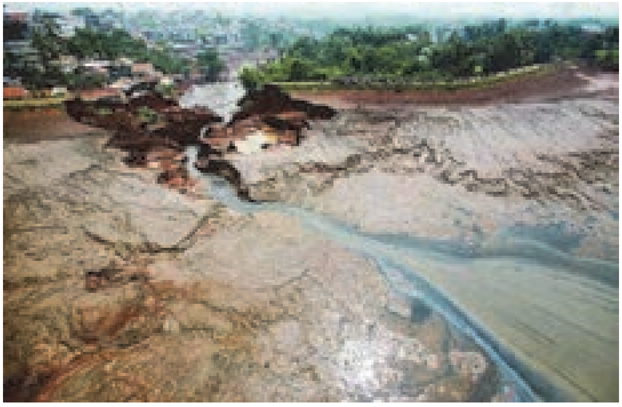

Figure 1. Situ Gintung Dam Failure

2. DAM SAFETY CONCEPTION

Dam safety conception is intended to protect the dam safety from dam failure possibility, as well as protecting lives, property, and public infrastructures in affected areas by potential hazards due to dam failure (Zainuddin, 2015). In order to manage the dams safety, dam construction in Indonesia should be based on a dam safety concept that consists of:

a. Structural safety against structural failure, hydraulic, and seepage.
b. Operation, maintenance, and monitoring.
c. Emergency action preparedness.

First of all in dam safety concept was started in dam design. The appropriate design is a must in this phase to make structural safety. Since design is an important factor, the good constructions also have an important role as well. If these activities were done well, the failure risk of dam could be minimize.

However, a risk can be minimized, but never totally eliminated. It is therefore necessary to recognize as soon as possible a damage, a defect in structural safety, or an external threat to safety so that the measures to master the danger that occurred can be taken. In order to achieve this, regular checks of the condition and the behavior of the dam as well as periodical safety evaluation are needed.

In case of an identified threat to the dam the situation of danger is managed according to the emergency concept. The concept consist of a strategy and preparation studies. They include determination of the potentially submerged area in case of dam break, the organizational measurements for ensuring the evacuation of the population.

The brief explanation about dam safety concept (Fig.2) is described below.

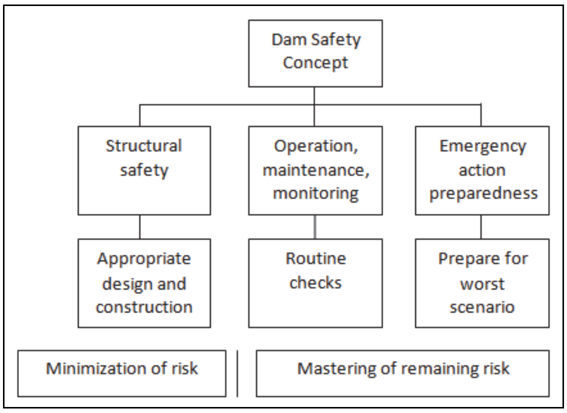
Dam Safety Concept
Structural safety
Operation, maintenance, monitoring
Emergency action preparedness
Appropriate design and construction
Routine checks
Prepare for worst scenario
Minimization of risk
Mastering of remaining risk

Figure 2. Dam Safety Concept in Indonesia

The scope of this regulation involves dam construction and management along the reservoirs. The provision of dam safety construction and management in Indonesia apply to the following criterias:

a. Dam with 15 (fifteen) meters height or more, measured from the deepest foundation;
b. Dam with 10 (ten) meters height up to 15 (fifteen) meters, measured from the deepest foundation with the following provisions:
    - The length of the dam crest at least 500 (five hundred) meters;
    - The capacity of the reservoir at least 500,000 (five hundred thousand) cubic meters; or
    - Maximum flood discharge at least 1,000 (one thousand) cubic meters per second; or
c. Dams with special difficulty on the foundation or dams designed with new technology and / or dams that have high hazard classification.

In order to review the safety of the dams, the dams construction in Indonesia must obtain a license or approval, including:

1. Design.
   This permission / approval is intended to obtain technical design aspect. In this process also can be obtained the construction approval if the documents requirement attached.
2. The construction in preparation for reservoir initial impounding.
3. The reservoir initial impounding in preparation for the dam operation.
4. Decommissioning of the dam functions.
   This permission / approval is filed if dams have been completed its life time.

In conducting of dam safety management, dam owners have following obligations including:

a. Collecting and archiving dam data and documents in accordance with applicable regulations
b. Monitoring the dam condition, include:
    1) Procuring, installing and maintaining instruments related to dam safety.
    2) Take measurements / reading instrument, record, store and evaluate the data regularly.
    3) Arrange for each dam has always been monitored by dam management unit.
    4) To do:
        - Routine Inspection (daily, weekly, monthly)
        - Periodical ordinary inspection (6-monthly, annual)
        - Major inspection and dam safety evaluation at least once in 5 years
        - Extraordinary or special inspection.
    5) Hydromechanical and electrical test regularly, at least once per year on equipment related to dam safety.
    6) Report the results of the 6-monthly and annual monitoring, as well as the evaluation results of the inspections.
c. Maintaining the dam, which includes routine and periodic maintenance. And if the condition of the dam is damaged, required to make improvements so the dams are always in a safe condition to operate.
d. Having emergency action plan. To anticipate the possibility of emergency conditions, the dam owner must prepare a system for handling emergency conditions that are always ready to handle the worst conditions, include: emergency sign system, organization and trained staff, equipment and materials for the handling of the emergency and the emergency action plan guidelines.
e. In conducting the dam operation, must consider the safety of upstream and downstream areas.
f. And others.

3. DAM SAFETY ORGANIZATION

As stated in Minister Regulation No. 27/PRT/M/2015 about Dam, Minister of Public Works and Housing was assisted by dam safety organization consisting of Dam Safety Commission and Dam Safety Unit.

In some cases, if the dam development requires further technical consideration about dam safety particularly those associated with:

a. Dams Height with 75 meters or more from the deepest foundation with minimum reservoir capacity is 100 MCM;
b. Dams with complex engineering difficulties; or
c. Dams with new technology based on Dam Safety Commission recommendation;

3.1. Dam Safety Commission

Dam Safety Commission (DSC) provides recommendation and suggestion to the minister in charge of dam safety activities and responsible to the minister.

Based on regulation no.27/2015 about Dam, the tasks of dam safety commission are as follow:

a. Giving the recommendation to the minister in order to giving design approval, initial impounding permit,

operation permit, design of rehabilitation approval, and decommissioning permit.
b. Giving the recommendation to the minister who organize human envelopment sector in first filling tailing permit and operation permit for tailing dam
c. Giving technical advice
d. Evaluating Dam Safety Unit activities
e. Regulated dam inspection

Dam safety commission member consists of representative of government and state-owned company as the owner of the dam, professional association and another government agency related to dam appointed by minister. The chairman of dam safety commission is Director General of Water Resources.

3.2. Dam Safety Unit

Based on structural organization, Dam Safety Unit (DSU) is under Directorate General of Water Resources, Ministry of Public Work and Housing. The main duty of dam safety unit is to provide support about dam safety to Dam Safety Commission.

Based on regulation no.27/2015 about Dams, the tasks of Dam Safety Unit are as follow:
a. Collecting and managing dams data
b. Study development and management of dams
c. Regulated dam inspection
d. Giving technical advice
e. Monitoring the construction of the dam safety aspects
f. Inventory and registration of dams
g. Managing archives of dams

4. DAM SAFETY LISENCE

There are some steps to do to have dam safety license in every phase of dam development. After the construction finished, there are another dam safety license for rehabilitation or removal of the dam. As mentioned above, that the members of DSC come from various institution based on their competency. So, the discussion about dam safety could be as detailed as could be for making sure the dam is safe.

Here the explanation about the process of dam safety license. In figure 4, dam safety license start with sending application from the dam owner to the Minister c.q. Director General of Water Resources as the chairman of Dam Safety Commission. The report about dam should be sent to DSU to have first assessment. After that, the DSC, DSU and dam owner inspect the dam site and discussed it. After inspection, the DSU reviewing the inspection result whether the reports are appropriate or not. If everything is going fine, then DSU, DSC, dam owner, consultant and/or contractor will take DSC technical meeting. In this meeting, it discussed about dam safety based on regulation, standard, guideline and manual in technical consideration. After the dam owner complete the suggestions at the technical meeting, then the process continue to plenum meeting. The DSC members who attend the plenum meeting vary from some other institution, such as environmental, electricity, and geological agency, which are related to dam safety. If all the process is finished, the DSC would give recommendation to the minister. Then the minister will issue the license of dam safety. The documents which are sent to dam safety unit in order to get dam safety license in every phase of dam development and management will be brief explained below.

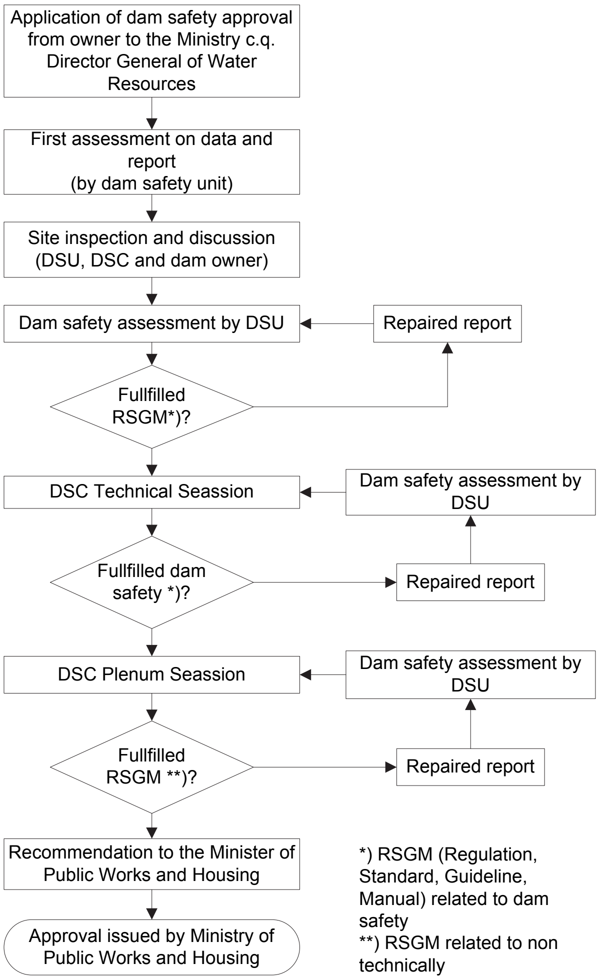
Application of dam safety approval from owner to the Ministry c.q. Director General of Water Resources
First assessment on data and report (by dam safety unit)
Site inspection and discussion (DSU, DSC and dam owner)
Dam safety assessment by DSU
Repaired report
Fullfilled RSGM*)?
DSC Technical Seassion
Dam safety assessment by DSU
Fullfilled dam safety *)?
Repaired report
DSC Plenum Seassion
Dam safety assessment by DSU
Fullfilled RSGM **)?
Repaired report
Recommendation to the Minister of Public Works and Housing
Approval issued by Ministry of Public Works and Housing
*) RSGM (Regulation, Standard, Guideline, Manual) related to dam safety
**) RSGM related to non technically

Figure 3. Dam Safety License Flowchart

5. DAM SAFETY IMPLEMENTATION

Until 2016, has been carried out the certification process of new and existing dams with the following caption:
- Approval of the design : 59 dams
- Approval of design changes : 3 dams
- Approval of the construction : 18 dams
- Approval of the initial impounding of the reservoir : 30 dams
- Approval of the operation : 21 dams

For dams that has not got the approval yet, in particularly the existing dams those were built before Minister Regulation of No. 27/2015 issued, the owners or the managements of the dams were currently processing the completeness of the documents required in obtaining of relevant approvals.

In addition to the certification of the dams, reported from Sinotech Engineering Consultant (2014), in the year of 2009 - 2013, Dam Safety Unit as the dam implementation technical unit have made new guidelines as well as updating the existing guidelines to follow international standards and the latest technological developments. They are:

1. New guidelines
   Dam Assets Management
2. Preparation for new guidelines
   Decommission of Dam
3. Updating guidelines, such as:
   - Registration and inventory of dam
   - Operation procedure for dam safety commission
   - Filling of reservoir
   - Dam safety inspection and evaluation
   - Dam safety evaluation and review
   - General criteria of eartfill dam design
   - Operation, maintenance, and surveillance of dam
   - Calculation of flood capacity of reservoir and spillway
   - Tailing dam
   - Construction of eartfill and rockfill dam
   - Reservoir sedimentation management

6. CONCLUSION

In order to improve the dam safety in Indonesia and to protect the people in the downstream were required enforcement of the regulations as well as updating the existing international guidelines become available as a basic standard.

REFERENCES

Zainuddin. (2015): Dam Safety Conception, pp. 43-58, Dam Safety Unit, Jakarta.

Minister of Public Work and Housing Regulation No.27/PRT/M/2015 about Dam, pp. 5-6, 61-64, Ministry of Public Work and Housing, Jakarta.

Sinotech Engineering Consultants, Ltd. (2014): Technical Assistance Service for Supporting The Implementation of Dam Safety Assurance and Institutional Improvement, pp. 1-6, Ministry of Public Work, Jakarta.

Case Study on Extreme Flood Affected Minmyin Dam

U.Victor
IMember, Central Committee, Myanmar National Committee on Large Dams, Myanmar
victor .con4@gmail.com

ABSTRACT:

On 18th July 2015, an extreme flood affected on Minmyin Dam and consequently dam overtopping occurred. Fortunately the dam was safe, although some gullies and slip happened on the downstream face of dam.

Keywords: extreme flood, dam overtopping, gullies, slip

1. GENERAL LAYOUT OF THE MINMYIN DAM

Minmyin Dam is located in Kantbalu Township, Sagaing Division. It is about 120 miles north of Mandalay. Minmyin Dam is an earthen dam utilizing mainly for irrigation though a 50 kW micro hydropower is installed.

The dam is situated on the Minmyin River, which is a secondary tributary of the Ayeyawady River. Minmyin is flowing into the reservoir which is formed by Kintat Diversion Dam on the Mu River. Mu is the primary tributary of the Ayeyawady.

Table 1. Some Salient Features of the Minmyin Dam

No.	Description	Unit	Quantity
1	Catchment area	square mile	64
2	Average annual rainfall	inches	42
3	Average annual inflow	acre-feet	14,620
4	Dam height	feet	88
5	Dam length	feet	2,350
6	Full tank capacity	acre-feet	19,010
7	Dead storage capacity	acre-feet	3,740
8	Size of conduit	feet	`6 x 4
9	Conduit design discharge	cubic feet/sec	60
10	Width of spillway	feet	80
11	Spillway design discharge	cubic feet/sec	8,731
12	Irrigable area	acre	2,000

According to the Table 1, the storage coefficient is 1.3. It means the storage capacity is more than the average annual inflow. The Spillway design discharge 8,731 cubic feet/sec is based on 1,000-yr return period flood.

curtailment of seepage and to retain earth in deep excavation.

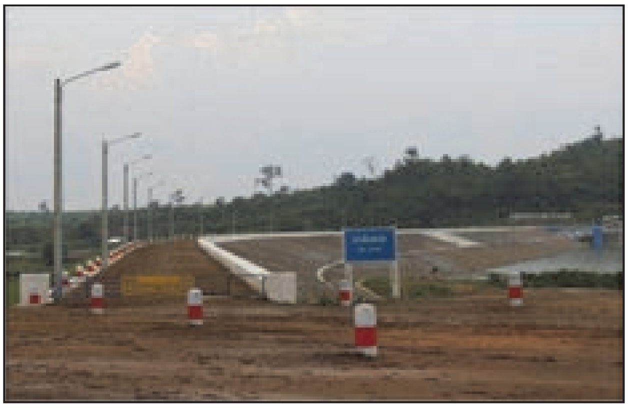

Figure 1. Completion of Dam

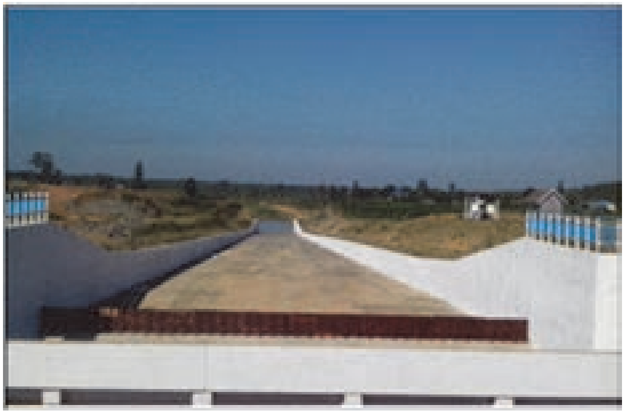

Figure 2. Completion of Spillway

The Minmyin Dam Project was started in 2010-2011 and completed in 2015-2016. The completed dam and spillway are shown in figs.1. and 2. Concerning with irrigable area, only 250 acres of land could be irrigated in the end of 2014 and the whole irrigable area in 2015-2016.

The impoundment of reservoir was started in June 2013. For the whole year round in 2013, the water level did not achieve to full tank level and also the same in 2014. Because of the partially completed irrigable area, it couldn't follow the rule curve of the reservoir operation. So that high water balance was resulted before an incident of extreme flood. Water balance recorded on May 25, 2015 was 11,640 acre-feet at R.L.669.15 ft.

2. DESIGN HYDROLOGIC DATA

Table 2. Flood Estimation for 1,000-yr, 10,000-yr and P.M.F.

No.	(1)	(2)	(3)	(4)	(5)	(6)
1	1,000	11	28,092	8,371	687.980	21,960
2	10,000	17	45,036	14,696	692.727	35,245
3	P.M.F.	29	75,212	-	-	-

(1) Return Period (year), (2) Rainfall (inches), (3) Peak Discharge (ft.^{3}/sec) (4) Routed Discharge (ft.^{3}/sec), (5) Flood R.L. (ft.) (6) Flood Volume (acre-ft.)

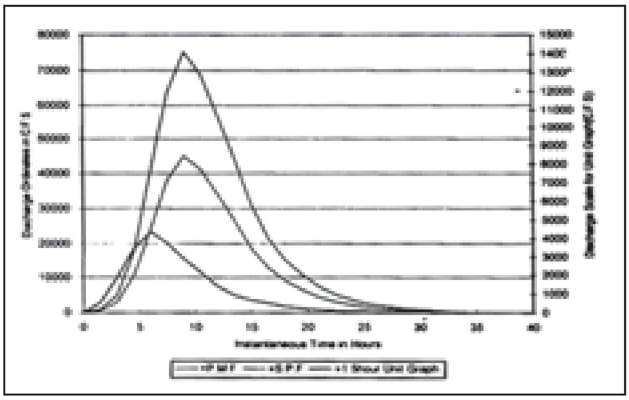

Figure 3. Adopted P.M.F. & S.P.F. Hydrographs

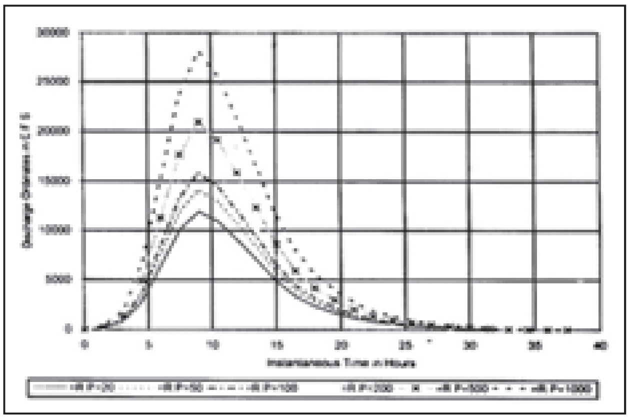

Figure 4. Adopted Design Flood Hydrographs

Design hydrologic data shown in Table 2. are getting from adopted hydrographs of Figs.3. and 4.

Size of the spillway and high flood level in the reservoir are determined by the 1,000-yr return period design hydrograph.

3. THE MAIN CAUSE OF EXTREME FLOOD ON MINMYIN DAM

From July 1, 2015 a series of typhoon LINFA, CHAN-HOM, NANGKA and finally HALOLA occurred in the Pacific Ocean successively. In connection with some low-pressure cells from India and a series of typhoon from the Pacific Ocean, a Low pressure Trough line was formed on July 5, 2015 between South China Sea and India across over Myanmar.

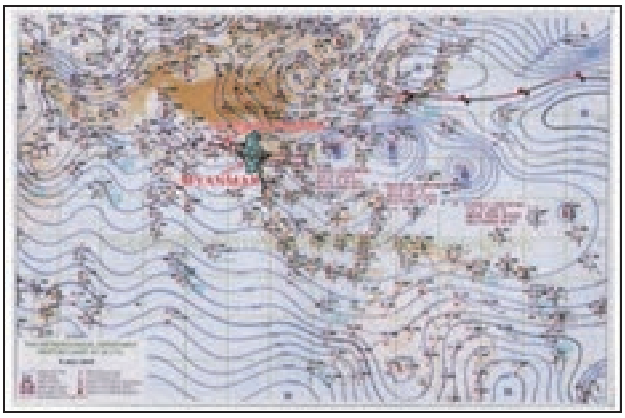

Figure 5. Low Pressure Trough Line over Myanmar

Due to this Low pressure Trough line shown in Fig.5. heavy rains poured down in Upper Myanmar, especially in Sagaing Division and Chin State and it caused severe inundation. Rainfall measurements at the dam site were recorded from July 7, 2015. The record of rainfall measurements is shown in Table 3.

Table 3. Rainfall Measurements at Dam Site

No.	Date	Unit	Measurement
1	7-7-2015	inch	0.94
2	8-7-2015	-	-
3	9-7.2015	inch	0.59
4	10-7-2015	inch	0.41
5	11-7-2015	inch	0.59
6	12-7-2015	inches	1.69
7	13-7-2015	-	-
8	14-7-2015	inches	2.24
9	15-7-2015	inch	0.20
10	16-7-2015	inches	2.09
11	17-7-2015	inches	2.54
12	18-7-2015	inches	10.66
13	19-7-2015	inches	8.22
	Total	inches	30.17

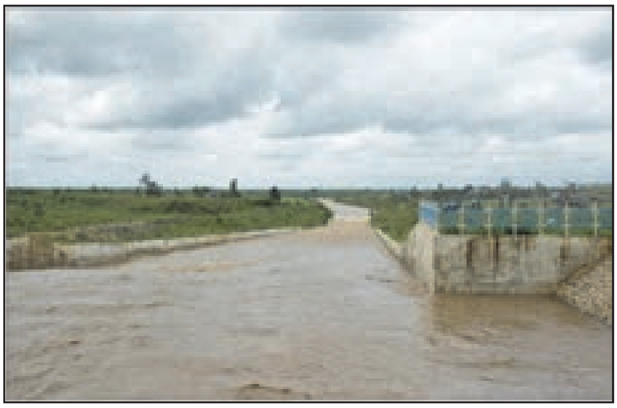

Figure 6. Flow Over Spillway

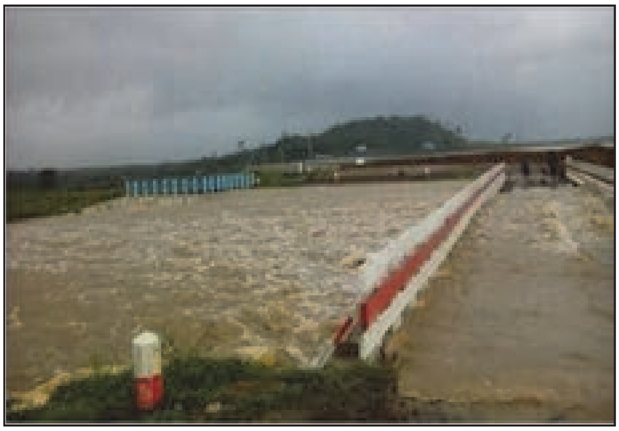

Figure 7. Submergence of Spillway-bridge

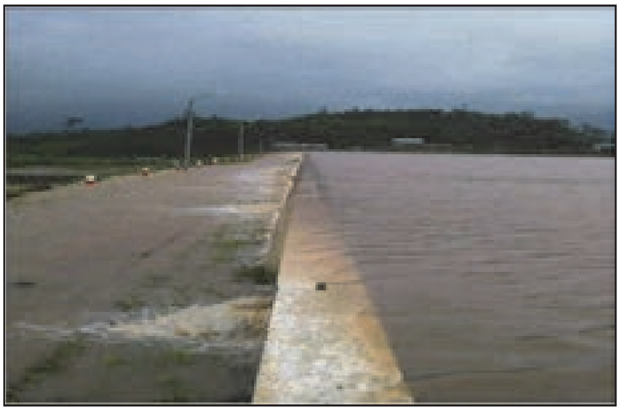

Figure 8. Spillway over Parapet

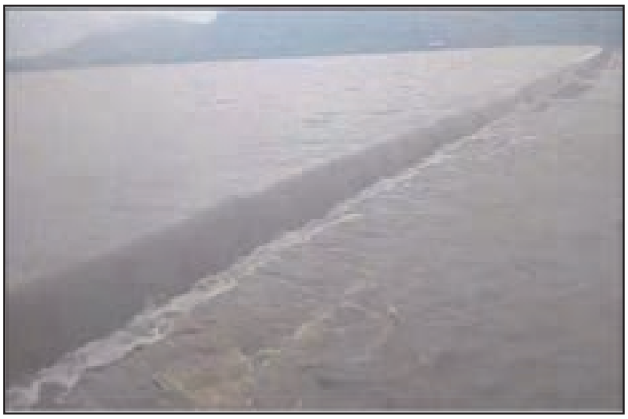

Figure 9. Dam Overtopping

According to Table 3. heavy rains started from July 7, 2015 at the dam site and in the catchment area. Consequence of high water balance in reservoir and heavy rainfall, water level was rising up rapidly in the reservoir and spilling over spillway happened for the first time on July 16, 2015 at 03:00 hr. Spillway crest level is R.L. 677 ft. which in equal to full tank level. Dam crest level is R.L.690 ft. and crest of the parapet is R.L. 692 ft.

The flow capacity over spillway was tremendous and it was beyond the design value and finally dam overtopping happened on July 18, 2015 at 08:00 hr. Subsequently submergence of spillway-bridge occurred at 09:00 hr. Flow over spillway is shown in Fig.6. Submergence of Spillway-bridge is shown in Fig.7. Spill over parapet is shown in Fig.8. Dam overtopping is shown in Fig.9.

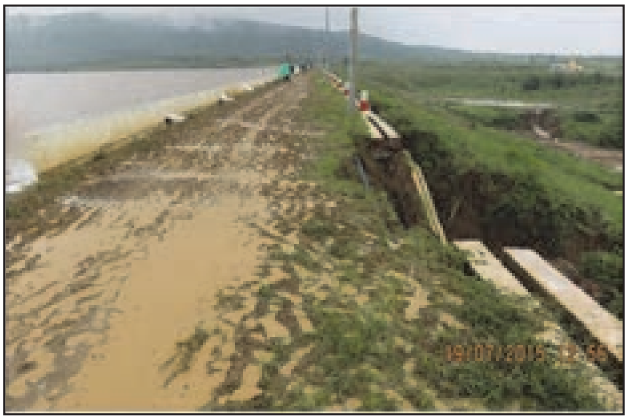

Figure 10. Dam Crest Erosion

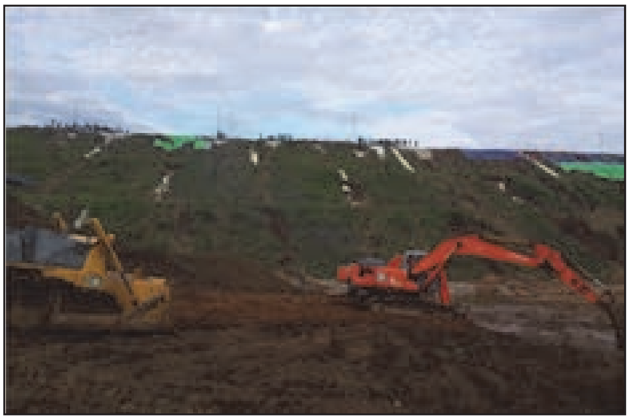

Figure 11. Dam Downstream Face Erosion

Duration of dam overtopping was about 5 hrs. It began from 08:00 hr. to 13:00 hr. on July 18, 2015. After the dam overtopping incident, some erosion happened on the dam crest and on the downstream face of dam. Slip happened at the downstream toe of dam. Dam crest erosion is shown in Fig.10. Dam downstream face erosion is shown in Fig.11.

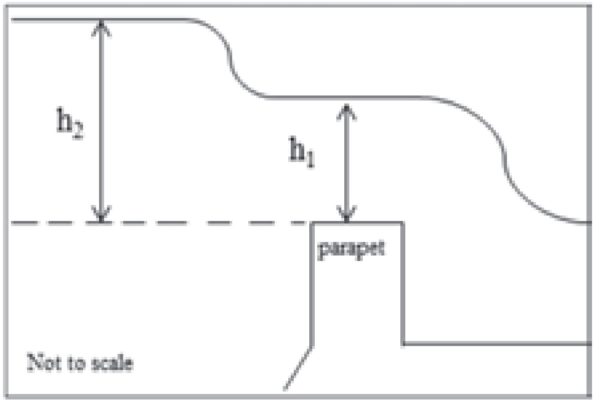

Figure 12. Flow Profile over Parapet

The inflow flood water level reached a peak at 09:20 hr.

Maximum water level recorded was R.L 692.3 ft. It means 0.3 ft. over 1.5 ft. wide parapet. But actually the flow profile over parapet is as shown in Fig.12. and according to the information, the highest water level in the reservoir could be confirmed as R.L.692.6 ft. Discharge calculations are made on this highest water level.

Parapet crest is R.L 692 ft. and so that the maximum height above parapet would be 0.6 ft. It is assumed that flow was evenly distributed over parapet and without considering dam settlement. The calculated peak discharge over parapet is 3,276.5 cubic feet/sec. Dam length is 2350 ft. Spillway crest is R.L. 677 ft. and height over spillway crest is 15.6 ft. Calculated peak discharge over spillway is 14,787.6 cubic feet/sec.

Before dam overtopping, rate of water level rising in the reservoir was very high on July 18, 2015. The recorded water level at 02:00 hr. was R.L.684.2 ft. and at 09:00 hr. was R.L.692 ft. Level difference was 7.8 ft. in duration of 7 hrs. So that rate of water level rising was 1.1 ft. per hour in average. The reason for rapid water level rising is due to steep riverbed slope or intense rainfall nearer to the dam in catchment area. The riverbed slope is noted as 0.006.

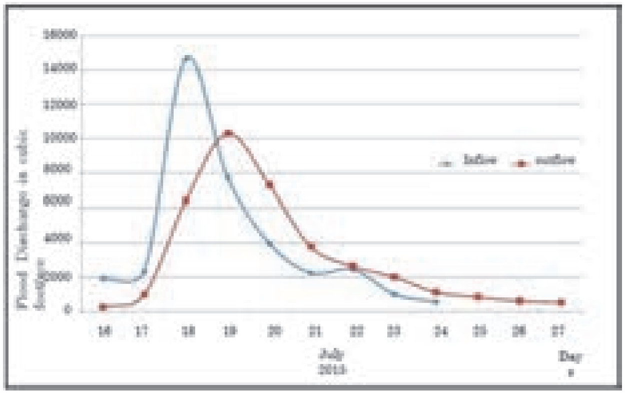

Figure 13. Inflow / Outflow Hydrographs

According to the hydrographs shown in Fig.13, it is observed that the inflow flood volume was about 73,381 acre-feet and the outflow flood volume was 73,210 acre-feet. It is also observed that the flood volume flowing over dam parapet was 463 acre-feet. Generally the ratio of inflow flood volume over catchment area is equivalent to depth of rainfall in catchment area and it is discovered as 21.5 inches. It is found that the total rainfall in Table 3. is greater than the depth, but if it is taken the intense rainfall of the last four days, it is 23.51 inches and almost equivalent.

4. DEFECTS ON DAM

After the incident, even though dam overtopping happened, dam was safe. But some defects observed on dam were as follows:-

- Gullies at the toe of the parapet,
- Gullies at R.D.800 ft., 1,200 ft. and 1,600 ft. of the downstream face of dam,
- (9) nos. of slope drains were damaged,
- Crest drain was damaged at R.D 1,600 ft. and 2,200 ft.,
- 150 ft. wide slip of dam toe at R.D. 1,200 ft. due to the drain scour,
- Eroded material deposited on rock toe,
- No differential settlement was observed,
- No bulging was observed on downstream face of dam,
- Spillway seemed in good condition.

5. LIST OF VILLAGES IN THE DOWNSTREAM AREA OF DAM

Table 4. List of Villages

No.	Village	Population
1	Shan Kon	727
2	Hin Phu Taw	292
3	Inma	467
4	Chaungma	77
5	Pe Kon (Taung)	1,000
6	Shan Su	152
7	Ma Gyi Inn	655
	Total	3,370

If dam failure occurred, these people would be directly affected and unprecedented flood due to dam break would cause damages to the villages listed in Table.4. and also to the Kintat Diversion Dam on the Mu River.

6. SOME COMMENTS ON INCIDENT

The following points are some comments on this incident:-

- Higher water balance in reservoir before extreme flood,
- Extraordinary rainfall in the catchment,
- Flood inflow volume is much greater than the average annual inflow and the storage capacity,
- Observed spillway discharge is less than the peak 1,000-yr design discharge, but much greater than routed 1,000-yr design discharge,
- Observed spillway discharge is almost equivalent to 10,000 yr-routed discharge,
- Observed flood highest water level is almost equivalent to 10,000-yr return period,
- Observed flood volume is double to 10,000-yr return period that leads to dam overtopping,
- Shorter duration of overtopping saved dam from failure,
- Rate of water level rising was very fast due to steep bed slope of river,
- Rainfall = Depth, it means calculated flood volume proved justified,
- Grass turfing, crest drain and thick kankar retard scouring to some extent, but scouring occurred when flow was concentrated at the end of overtopping,
- Scour at the toe of the parapet is due to insufficient compaction in kankar laying,
- Slip at the downstream dam toe must be filled back promptly,
- Parapet is excluded in dam height consideration, but 2.0 ft. parapet rendered absorption of flood in this incident though some leakage from gaps between parapets,
- Taking freeboard as 2.0 ft. above H.F.L. (High Flood Level) is a higher risk factor,
- Wrong decision can lead to failure in such incident,
- Climate change has effected on dams in Myanmar.

7. RECOMMENDATIONS

Concerning with the incident of dam overtopping, some points are recommended as follows:-

- Emphasize on safe dam design,
- Importance of Emergency Preparedness Plan,
- Practice of proper reservoir operation,
- Compliance with standards and specifications.

REFERENCES

Hydrological data of the Minmyin Dam, (2009) Page 2-3, Hydrology Branch, Irrigation Department.

Dam design data of the Minmyin Dam, (2010) Page 1-12, Design Branch, Irrigation Department.

Weather Chart, Thai Meteorological Department Website.

Damage Report of the Minmyin Dam, (2015) Page 1-30, Construction Circle (4), Irrigation Department.

Potential Impacts of Climate Change on Reservoir Flood Control in the Huong River Basin, Vietnam

D.V.Quan & K.Kuntiyawichai
Department of Civil Engineering, Faculty of Engineering, Khon Kaen University, Thailand
infohquan@gmail.com

ABSTRACT:

The assessment of flood risk in the river basin area under the impacts of climate change is necessary for sustainable flood management strategies at national level. In this sense, the research aims to investigate the potential impacts of climate change on reservoir flood control in the Huong River Basin, Vietnam. The Representative Concentration Pathways (RCPs) climate change scenario, RCP 8.5, from the HadGEM3-RA was selected for this study. To assess the level of flood risk posed to the study area, a coupling of hydrologic model (HEC – HMS) and hydrodynamic model (HEC – RAS) would provide much needed understanding. The key results demonstrated that the weather would be warmer in the future with the average temperature increasing from 0.2°C to 0.8°C, and the annual rainfall would also increase from 4.8% to 6.0%. It can be observed that water levels and runoff can potentially increase in the future from +0.1 m to +0.3 m and 10% to 30%, respectively. Moreover, the proposed reservoir operation was examined by incorporating the warning stages in order to reduce flood peaks downstream during the rainy season. The main findings of this study can be a good example for future planning of flood control reservoir systems in Vietnam.

Keywords: Climate change, Reservoir operation, Bias correction, HEC-HMS, HEC-RAS

1. INTRODUCTION

The potential impacts of climate change are likely to be experienced through changes in flood frequency and magnitude, which can adversely affect the downstream reservoir flood control system (Wu et al., 2014). In fact, reservoir operation is among the most efficient non-structural measures for flood mitigation and vulnerability control. Therefore, it is necessary to understand the impacts of climate change on reservoir operation in order to minimize the negative effects on downstream areas. In recent years, floods have taken place and resulted in economic depression and losses of the entire Huong River Basin, Vietnam. It is well known fact that the existing reservoirs, namely Huong Dien and Binh Dien, and the new developed Ta Trach reservoir, would significantly affect the hydrological and hydraulic regimes of the downstream of the river basin. According to the above mentioned reasons, this research aims to introduce a feasible rule in operating the reservoirs in relation to climate change in order to minimize the flood impacts at the lower part of the Huong River Basin. Within the context of flood risk assessment, the potential impacts of climate change on reservoir flood control in the Huong River Basin was carried out. To increase the details over the Huong River Basin, the procedures of bias correction, which relies on a transformation algorithm for adjusting a Regional Climate Model (RCM), was considered. Correspondingly, a quantile-mapping of the Distribution-Based Scaling (DBS) approach was used to correct the biases of RCM outputs using two gamma distributions with the 95th percentile cut-off values. Moreover, the evaluation of hydrological processes was accomplished by using a coupling of the hydrologic model (HEC – HMS) and hydrodynamic model (HEC – RAS). The main findings from this study will provide an insight to climate change and its potential impacts on dams and reservoirs, which is of importance to open up a discussion on future flood control efforts in the Huong River Basin and other areas in Vietnam.

2. STUDY AREA

The study area is focused on the Huong River Basin located in Thua Thien Hue Province, Vietnam (see Fig. 1). Geographically, the river basin has a total area of 2,830 km^2 in which nearly 80% of the total area is the mountainous area with its height varies between 200 m and 1,850 m above mean sea level (m+MSL). The river basin comprises of three major reservoirs, i.e. Ta Trach, Huong Dien, and Binh Dien, which are situated at the tributaries of the Ta Trach, Bo, and Huu Trach Rivers, respectively. The Ta Trach and Huu Trach tributaries meet each other at the Tuan confluence and connect to the Bo River at Sinh confluence before discharging to the Tam Giang – Cau Hai Lagoon. Due to sea level rising problems from the downstream of the Huong River Basin, the Thao Long barrage was constructed in order to protect saltwater intrusion, which could significantly affect to irrigation and agricultural sectors.

Climatologically, this area has a mean annual temperature between 21°C and 26°C with an average annual rainfall estimated between 2,500 mm to 3,500 mm. Along the coastline to the hilly area, the temperature has decreased gradually whereas the rainfall has increased. There are two main seasons in the river basin, namely dry season starting from January to August and rainy season extending from September to December. As the Huong River Basin located in the directly-affected zone of North-Western Pacific Ocean typhoon centre, it is therefore highly affected by major destructive natural disasters such as tropical cyclones, sea level rising, and flooding.

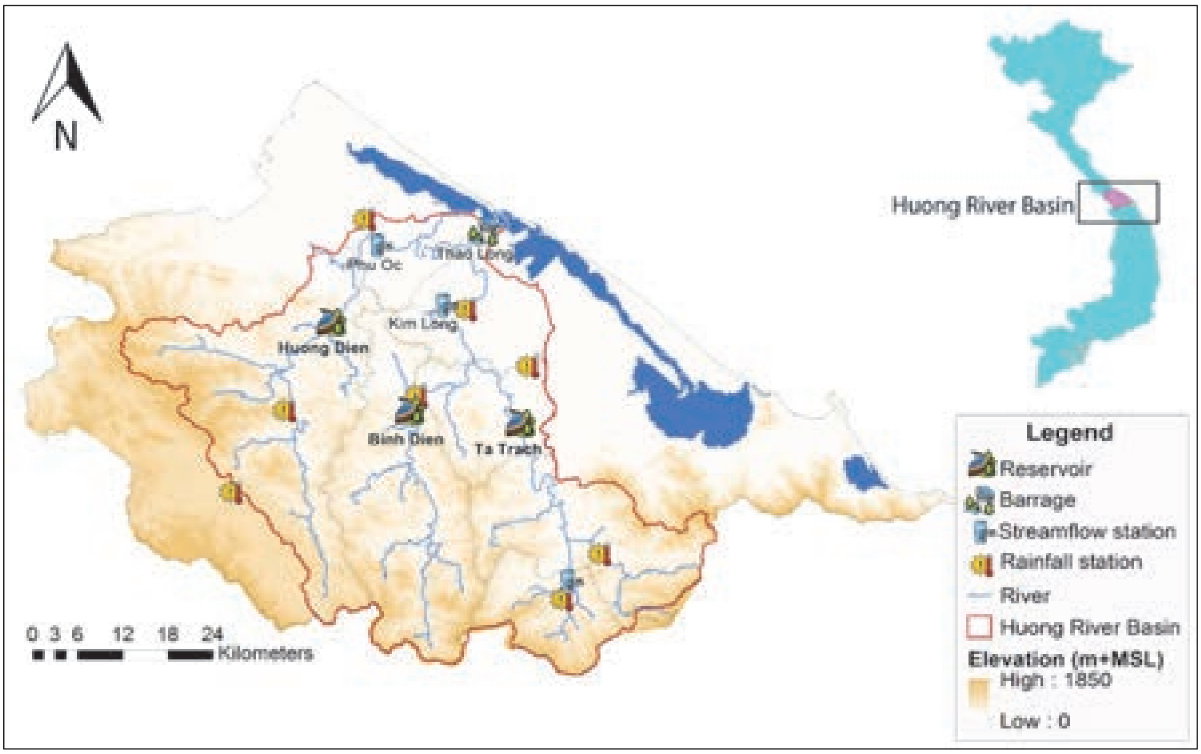

Figure 1. The Huong River Basin, Vietnam.

3. DATA AND METHODS

3.1. Data Collection

The meteorological data including the daily rainfall and temperature from 1977 to 2012, and discharge and water level from 2009 to 2014 were derived from the Thua Thien Hue Hydro-Meteorology and Forecasting Centre (TTH – HMFC), Vietnam. The spatial geo-referenced data, i.e. Digital Elevation Model (DEM) with 10 m x 10 m of geometrical resolution, was also obtained from the TTH – HMFC. In order to represent river basin characteristics of the study area, both 2014 land use and soil type were taken from the Resources and Environment Department (RED) of Thua Thien Hue Province.

A newly developed RCM from the Hadley Centre Global Environmental Model, version 3 (HadGEM3-RA) projections for 150 years from 1950 to 2100 was derived from the Met Office Hadley Centre, England. HadGEM3-RA has a horizontal grid resolution of 0.44° x 0.44° and complying with the protocol of the Coordinated Regional Climate Downscaling Experiment (CORDEX) for Asia (Giorgi et al., 2009). The Representative Concentration Pathways (RCPs) scenario (RCP 8.5) is characterized by high greenhouse gases (GHGs) concentration (Riahi et al., 2011), which was considered in assessing climate change to the river basin area.

3.2. Bias Correction

The basic principle to develop effective statistical bias correction is an establishment of statistical relationship or transfer function between observed data and global outputs (Li et al., 2010). A quantile-mapping approach is widely used nowadays such as Jeon et al., 2016, Rabiei & Haberlandt, 2015, which was introduced to map the distribution of daily rainfall and temperature from GCM/RCM variables onto that of gridded observed data. This method is an application of the probability integral transformation approach as described in Eq. 1.

$$P_c = F_o^{-1}\left(F_m(P_m)\right) \qquad (1)$$

where, P_c is corrected bias data, F_m is Cumulative Distribution Function (CDF) of RCM, P_m is RCM data, and F_o^{-1} is inverse of the CDF as known that quantile function.

The Distribution-Based Scaling (DBS) quantile-mapping version (Wei et al., 2010) was applied in this study for downscaling RCM outputs. In terms of rainfall, DBS assumes that frequency distribution of intensities can be accurately approximated using two gamma distributions, i.e. low and intermediate rainfall intensities (up to the 95% quantile), and extreme intensities (above the 95% quantile). It is well understood that temperature is more symmetrically distributed in comparison to rainfall. In this sense, a normal distribution of mean (μ) and standard deviation (σ) were integrated in downscaling temperature. The period from 1977 to 2001 was considered as baseline period and was also defined as calibration period whereas the period from 2002 to 2005 was considered as validation period. The transient projections were divided into three decades, i.e. 2020s (from 2016 to 2040), 2050s (from 2046 to 2070), and 2080s (from 2076 to 2100).

3.3. Investigation of Rainfall-Runoff Processes

In an attempt to perform the rainfall-runoff processes in the river basin, the Hydrologic Engineering Center – Hydrologic Modelling System (HEC – HMS) model was applied. In principle, the model is based on the river basin characteristics, meteorological data, and control specifications to calculate hydrographs for the river basin. The HEC – HMS model represents the behaviour of the river basin through four main components, i.e. model of runoff volume, model of direct runoff, model of baseflow, and model of channel flow (USACE-HMS, 2000).

The Soil Conservation Service – Curve Number loss method was used for the event-based study because it is a common method which relies on only one curve number parameter. The Snyder Unit Hydrograph transform method was applied to calculate runoff by utilizing a standard unit hydrograph for each sub-basin. The recession baseflow and Muskingum routing methods were also considered in this study to calculate the actual subsurface flow from sub-basins and segments of the river, respectively. In addition, these methods were selected based on the findings of the recent study by Quan & Kittiwet (2015) in the same river basin.

For evaluating the river basin characteristics, three stations, namely Phu Oc, Binh Dien, and Ta Trach, were selected. Due to the limitation of observed flow in the Bo River, the observed water level at Phu Oc station during the period of 2009 to 2010 was used for calibration, and the period of 2011 to 2012 was used for validation. At Binh Dien station, the observed inflow from 2010 to 2011 was used for calibration while the year 2012 was used for validation. It is important to note that the new developed Ta Trach reservoir was operated in the middle of 2014, thus, there was very limited streamflow data at this station. As a result, the observed inflow data from the periods of September to October and November to December 2014 were used for calibration and validation, respectively.

3.4. Investigation of Hydraulic Behaviour of River Systems

Investigation of hydraulic behaviour of river systems can be determined by using the Hydrologic Engineering Center – River Analysis System (HEC – RAS) model. The HEC – RAS model has been used in a widely range of areas such as dam break scenarios, floodplain delineation, flood forecasting, and flow routing (Sharkey, 2014). The model comprises of four river analysis components such as sediment transport, water quality, steady flow, and unsteady flow (USACE-RAS, 2010).

Regarding flood simulations, the unsteady flow analysis was applied in this study. As described in the HEC – RAS User's manual, the physical laws of the unsteady flow are governed by the principles of conservation of mass and momentum. The conservation of mass is given by the continuity equation in which the net rate of flow into the control volume is equal to the rate of change of storage inside the control volume. The conservation of momentum is given by the dynamic equation which describes the balances of gravity, friction, pressure, and inertia (Lopes et al., 2004). The Manning's *n* values were adjusted for each reach according to the river basin characteristics along the river. The released flows from Ta Trach, Huong Dien, and Binh Dien reservoirs were specified as the upstream boundary conditions and the water levels at Thuan An outlet was employed as the downstream boundary condition. Furthermore, the selected gauging stations, i.e. Kim Long and Phu Oc stations, were used to evaluate the relationship between the observed and simulated datasets. The observed water level from 2009 to 2010 was used for calibration and from 2011 to 2012 was used for validation process.

3.5. Model Evaluation

Two common statistical criteria were used for judging the goodness-of-fit of the calibrated model, i.e. determination coefficient (R^2) and Nash – Sutcliffe coefficient (E_{NS}) as shown in Eq. 2 and Eq. 3, respectively.

$$R^2 = \left[\frac{\sum_{i=1}^{n}(X_{obs}-\bar{X})(Y_{sim}-\bar{Y})}{\sqrt{\sum_{i=1}^{n}(X_{obs}-\bar{X})^2\sum_{i=1}^{n}(Y_{sim}-\bar{Y})^2}}\right]^2 \qquad (2)$$

$$E_{NS} = 1 - \frac{\sum_{i=1}^{n}(X_{obs}-Y_{sim})^2}{\sum_{i=1}^{n}(X_{obs}-\bar{X})^2} \qquad (3)$$

where, X_{obs} is observed variable, $\bar{X}$ is mean of observed variable, Y_{sim} is simulated variable, $\bar{Y}$ is mean of simulated variable, and *n* is number of variable.

4. RESULTS AND DISCUSSIONS

4.1. Evaluation of the RCM Model Performance

The historical climate data from the period of 1977 to 2005 of the HadGEM3-RA model were used and mapped with the observed data by using the DBS approach. The results showed that a large difference of rainfall frequency between observed data and RCM were reduced considerably during the calibration and validation processes. At the Hue station, the statistical values E_{NS} range from 0.78 to 0.86, and the R^2 values also vary between 0.80 and 0.89, which indicates a good performance in downscaling of rainfall. From the evaluation results of temperature downscaling, the E_{NS} values range from 0.93 to 0.95, and the R^2 values vary from 0.94 to 0.95. It is well recognized that temperature has a better correlation compared to rainfall in RCM. In addition, the obtained statistical results also confirmed the reliability of the DBS approach in improving resolutions of the RCM model for this study area.

4.2. Projections for Future Emission Scenarios

The projection for future mean annual rainfall indicates a moderate trend based on the RCP 8.5 scenario in the Huong River Basin (Fig. 2). The results proved that the rainfall tends to increase in the dry season (January to May) from 5% to 15%, and it is expected to increase during the rainy season (October to December) by approximately 2% to 5%. The results also show that the mean annual rainfall will also increase from 4.8% to 6.0% in comparison to the baseline period (1977 to 2001).

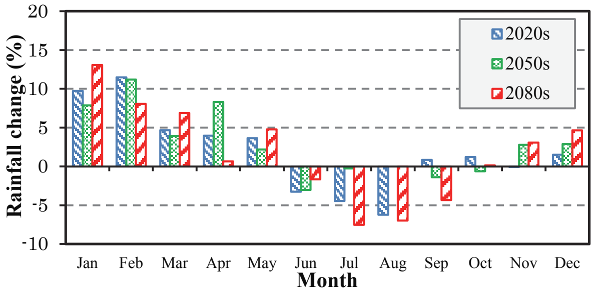

Figure 2. Mean monthly rainfall changes under RCP 8.5 scenario between the decades 2020s and 2080s.

In terms of temperature, the results suggest that the weather would be warmer in the future under the RCP 8.5 scenario (Fig. 3). During the periods from March to April, August, and November to December, the temperature tends to increase by 0.5°C to 2.0°C whereas it shows a decreasing trend in January, June, and the period of September to October, with a range between 0.5°C to 2.5°C. Based on the results from this investigation, the mean annual temperature is expected to be increased from 0.2°C to 0.8°C during the decades of 2020s to 2080s in comparison to the baseline period.

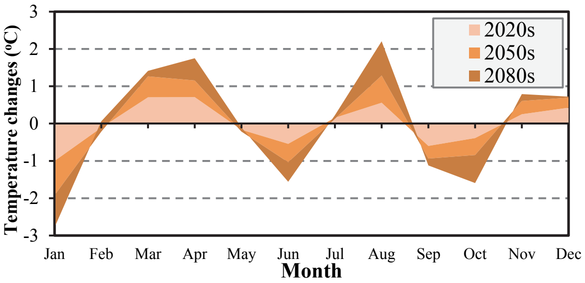

Figure 3. Mean monthly temperature changes under RCP 8.5 scenario between the decades 2020s and 2080s.

4.3. HEC-HMS Model Calibration and Validation

The evaluation process was applied to all three gauging stations, i.e. Ta Trach, Binh Dien, and Phu Oc, in order to prove the reliability and stability of HEC – HMS model. Fig. 4 illustrates the calibration and validation results of HEC – HMS model which presents the proper fit of peak flow and time to peak at Ta Trach station.

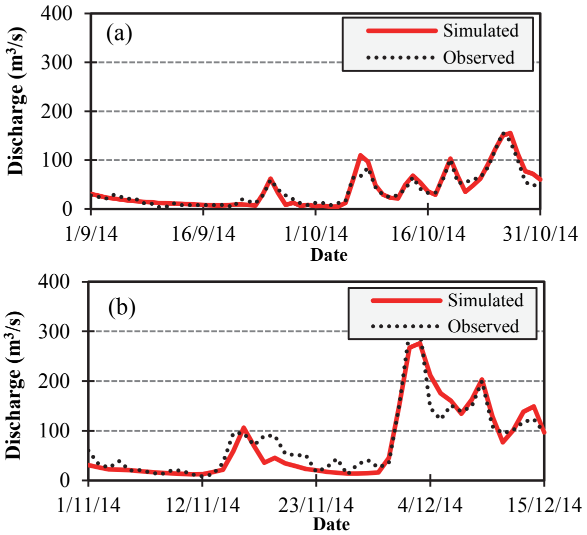

Figure 4. HEC – HMS modelling results between observed and simulated discharges (a) calibration period; and (b) validation period, at Ta Trach station.

More importantly, the model performance statistics were also determined for all three calibrated stations. The results for calibration and validation processes indicates that the HEC-HMS model provides a satisfactory representation of the flow with R^2 values ranging from 0.84 to 0.94 and E_{NS} values varying from 0.77 to 0.92. Therefore, it can be concluded that the HEC – HMS model performed well in simulating runoff response to rainfall in the study area.

4.4. HEC-RAS Model for Investigating Hydraulic Behaviour of River Systems

With respect to HEC-RAS model simulations, the simulated water level is in good agreement with the observed one which indicates good simulation performance at both Phu Oc and Kim Long stations as illustrated in Fig. 5. Based on the calibration and validation results of HEC-RAS model, the statistical indices of all calibrated stations showed acceptable levels of model fit, i.e. R^2 values ranging from 0.67 to 0.73 and E_{NS} values varying from 0.64 to 0.74 at Phu Oc station, whereas the R^2 values fluctuating from 0.78 to 0.79 and E_{NS} values ranging from 0.74 to 0.77 at Kim Long station. Referring to the acceptable (obtained) statistical indices, it can be claimed that the HEC – RAS model is suitable for investigating and simulating hydraulic behaviour of river systems in the study area.

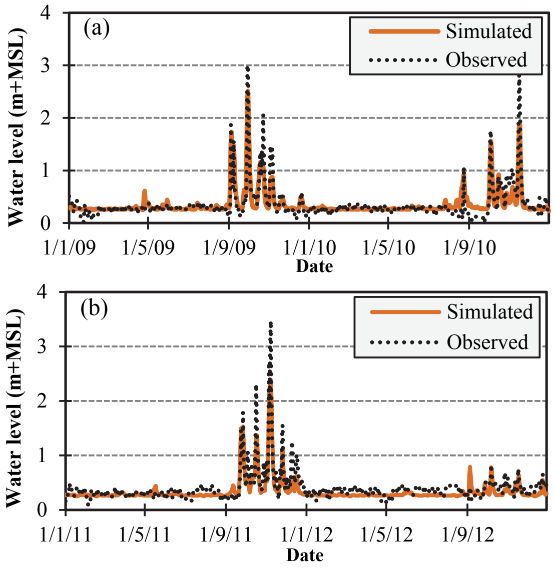

Figure 5. HEC – RAS modelling results between observed and simulated water levels (a) calibration period; and (b) validation period, at Kim Long station.

4.5. Flood Simulation under Future Climate Change Conditions

As a representative of a high carbon dioxide concentration, the RCP 8.5 scenario was selected for flood simulations under future climate change scenarios. The results showed the increase in water level and discharge at both Phu Oc and Kim Long stations under the impacts of climate change. In details, the water level seems to increase from +0.1 m to +0.3 m and discharge will also increase from 10% to 30% in the future. Based on the RCP 8.5 scenario, the rainfall will increase from 5% to 15%, 5% to 20%, and 5% to 25% at Ta Trach, Huong Dien, and Binh Dien reservoirs, respectively. The obtained results are really similar to the finding of IUCN Vietnam (2005) which stated that the rainfall will increase more than 20% in the dry season at the upstream of the Huong River Basin.

4.6. Reservoir Operation

During the dry season, the Ta Trach, Huong Dien, and Binh Dien reservoirs control the flows with the rates of 33 m^3/s, 20.5 m^3/s, and 25 m^3/s, respectively. By considering the impacts of climate change, the results suggested that more water from the reservoirs should be released during the dry season (January to May) as a result of increasing rainfall intensity at the upstream and water demand at the downstream. In addition, the gates of Thao Long barrage are suggested to be closed in order to prevent saltwater intrusion due to sea level rise. Due to the limitation of data, the determination of the effectiveness of flood control reservoirs during the dry season is restricted in this assessment and it is recommended to take the aforementioned issue into consideration in further studies. Regarding the rainy season, the reservoirs should be operated by incorporating with the warning stages in order to reduce flood peaks at the downstream. Based on the information from the TTH – HMFC, the warning stages is defined at three levels, namely Alarm I, II, and III, as shown in Table 1.

Table 1. Warning threshold levels

Station	Warning stages (m+MSL)		
	Alarm I	**Alarm II**	**Alarm III**
Phu Oc	1.5	3.0	4.5
Kim Long	1.0	2.0	3.5

In proposing a proper rule for reservoir operation in the rainy season, the following instructions can be considered. When the flood is coming, the reservoirs need to release by the amount of water which is smaller than the inflow, in association with the warning stages at Phu Oc (for Huong Dien reservoir) and Kim Long (for Binh Dien and Ta Trach reservoirs) as presented in Table 2.

Table 2. Regulations of reservoirs for the rainy season

Reservoir	Huong Dien	Binh Dien	Ta Trach
Flood control elevation	+56 m	+80.6 m	+25 m
Water level (WL) ≤ Alarm I	Discharge $196.2\left(\frac{m^3}{s}\right)$ but smaller than inflow	Discharge $70\left(\frac{m^3}{s}\right)$ but smaller than inflow	Discharge $82\left(\frac{m^3}{s}\right)$ but smaller than inflow
Alarm I ≤ WL ≤ Alarm III	Outflow ≤ Inflow	Outflow ≤ Inflow	Outflow ≤ Inflow
Water in reservoir is greater than:	(+58 m), discharge $7{,}878.2\left(\frac{m^3}{s}\right)$	(+85 m), discharge $7{,}061\left(\frac{m^3}{s}\right)$	(+46.97 m), discharge $7{,}483.5\left(\frac{m^3}{s}\right)$

When the flood is over, the reservoir level should be lowered to the flood control level so that the reservoirs can provide sufficient capacity for the next upcoming flood. It is also important to note that all gates of Thao Long barrage should totally be open in order to enable the maximum flow to be released during the flood receding period.

5. CONCLUSIONS

The assessment of potential impacts of climate change on reservoir flood control was conducted for the Huong River Basin. The results showed that the HadGEM3-RA model provided a realistic finding in estimating the potential impacts of climate change in this study area. In addition, the hydrologic model HEC – HMS and hydrodynamic model HEC – RAS were suitable to be applied for the case of the Huong River Basin. The results also demonstrated that the weather would be warmer in the future from 0.2°C to 0.8°C and annual rainfall would also increase from 4.8% to 6.0%. The water levels and discharges are also likely to increase from +0.1 m to +0.3 m and 10% to 30%, respectively. Moreover, the findings also highlighted that the rainfall would be increased in the upstream during the dry season from 5% to 25%, therefore, it is necessary to increase the released flow from the reservoirs during the period of January to May. The proposed reservoir operation together with the warning stages during the rainy season was also suggested. Finally, the overall outcomes of this research can be used as a guideline for adaptation measures against the impacts of climate change, and future planning for flood control reservoir systems in Vietnam.

ACKNOWLEDGEMENTS

The authors gratefully acknowledge the generous financial support received for various stages of this research by Khon Kaen University, Thailand.

REFERENCES

Wu, C., Huang, G., Yu, H., Chen, Z., and Ma, J. (2014). Impact of Climate Change on Reservoir Flood Control in the Upstream Area of the Beijiang River Basin, South China. American Meteorological Society. doi: 10.1175/JHM-D-13-0181.1

Giorgi, F., Jones, C., and Asrar, G. R. (2009). Addressing climate information needs at the regional level: The CORDEX framework. World Meteorological Organization (WMO) Bulletin(58), 175-183.

Riahi, K., Rao, S., Krey, V., Cho, C., Chirkov, V., Fischer, G., and Rafaj, P. (2011). RCP 8.5—A scenario of comparatively high greenhouse gas emissions. . Climatic Change(109), 33-57. doi: 10.1007/s10584-011-0149-y

Li, H., Sheffield, J., and Wood, E. F. (2010). Bias correction of monthly precipitation and temperature fields from Intergovernmental Panel on Climate Change AR4 models using equidistant quantile matching. Journal of Geophysical Research, 115(D10101). doi: 10.1029/2009JD012882

Jeon, S., Paciorek, C. J., and Wehner, M. F. (2016). Quantile-based bias correction and uncertainty quantification of extreme event attribution statements. Weather and Climate Extremes. doi: 10.1016/j.wace.2016.02.001

Rabiei, E., and Haberlandt, U. (2015). Applying bias correction for merging rain gauge and radar data. Journal of Hydrology, 522, 544-557. doi: 10.1016/j.jhydrol.2015.01.020

Wei, Y., Johan. A., Phil, G., Jonas O., Jorgen, R., and Fredrik W. (2010). Distribution- based scaling to improve usability of regional climate model projection s for hydrological climate change impacts studies. Hydrology Research, 41, 3-4.

USACE-HMS. (2000). Hydrologic Modeling System HEC-HMS A. D. Feldman (Ed.) Technical Refencence Mannual (pp. 155).

Quan, V. D., and Kittiwet, K. (2015). An assessment of potential climate change impacts on flood risk in Central Vietnam. European Scientific Journal, 1, 667-680.

Sharkey, J. K. (2014). Investigating Instabilities with HEC-RAS Unsteady Flow Modeling for Regulated Rivers at Low Flow Stages. (Master), University of Tennessee - Knoxvill.

USACE-RAS. (2010). HEC-RAS, River Annalysis System Hydraulic Reference Mannual Vol. 4.1. W. B. Gary (Ed.) (pp. 411).

Lopes, L. F. G., Do Carmo, J. S. A., Vitor Cortes, R. M., and Oliveira, D. (2004). Hydrodynamics and water quality modelling in a regulated river segment: application on the instream flow definition. Ecological Modelling, 173(2–3), 197-218. doi: 10.1016/j.ecolmodel.2003.07.009

IUCN Vietnam (2005). Environmental Flows: Rapid Environmental Flow Assessment for the Huong River Basin, Central Vietnam. IUCN Vietnam, Ha Noi, Vietnam (pp. 82).

4th APG Symposium and 9th EADC on

INNOVATIVE TECHNOLOGIES FOR DAMS AND RESERVOIRS TOWARD THE FUTURE GENERATIONS

Actual Working Performance Assessment of Super-high Arch Dams

Y. Liu, G. Zhang, B. Zhu & F. Shang
Department of Structures and Materials, China Institute of Water Resources and Hydropower Research, Beijing
liuyi@iwhr.com

Y. Liu & G. Zhang
State Key Laboratory of Simulation and Regulation of Water Cycle in River Basin, Beijing, China

ABSTRACT:
China is addressing the significant challenge posed by the construction of several 300 m high arch dams for the effective use of hydropower resources. Limited experience has been gained globally in the construction of super-high arch dams. Moreover, the present design codes are based on past experiences with arch dams with significantly lower height. Stress computation consists of many analytical simplifications. In addition, numerous questions may be raised regarding the reliability of this computation for application to super-high arch dams. This study presents an integrated analytical approach to simulate the actual working performance of super-high arch dams. This approach emphasizes the significance of the analytical descriptions on four actual factors, namely, actual material, actual structure, actual load, and actual process. Furthermore, the effectiveness of the actual working performance simulation has been proven by updated engineering practice.

Keywords: super high arch dam, actual performance assessment, multi-filed analysis

1. INTRODUCTION

A series of large hydropower projects, including large arch dams up to 300 m in height, have recently been designed and constructed in China (Zhang, 2004). Limited experience has been gained globally in the construction of super-high arch dams. Moreover, the conventional design and safety assessment method for arch dams are based on past experiences with arch dams having significantly lower height. According to the classical specifications in US (Bureau of Reclamation, 1977) and updated records in China (DL/T 5346-2006), several simplifications are introduced in the analysis of the arch dams.

First, the present design codes recommend the use of the multi-arch-beam and equivalent finite element methods (Zhu, et al., 1992) to calculate the stress state of arch dams under certain specific conditions. These conditions are analytically isolated from one another. In addition, the actual time-dependent state of the dam cannot be described from construction stage to operational stage, and all unfavorable states during the concrete casting, arch closure, initial impounding, and operational stages can hardly be covered. In this work, actual working performance is defined as the displacement / temperature / stress / seepage state of the dam during the whole period, including the concrete casting, arch closure, initial impounding and operational stages.

Second, thermal stress in arch dams during the construction and service stages after completion are computed independently. Zero stress state is generally recognized as the initial state of the service stage. It is assumed the residual thermal stress produced by construction process is always too small to affect the service performance of arch dams. However, recent engineering practice for super-high arch dams may prove that this assumption is false (Li, et al. 2014).

In the design code, an empirical formula is recommended for the calculation of reservoir water temperature distribution, but the applicability of such calculation was cast into doubt by recent monitoring data for super-high arch dams. In addition, the effect of solar radiation was also found significant to the thermal stress development in the arch dam (Jin, et al., 2012).

Third, the effect of the construction process on gravity stress is neglected. Gravity load is added either to only the beams of an arch dam or to the whole dam. The former method is an unrealistic construction process, in which transverse joints are never grouted, whereas the latter approach assumes that no transverse joints exist in arch dams. In fact, the real stress state in an arch dam could not be determined without a reasonable description of the contact states of transverse joints (Azmi, et al., 2002).

Fourth, the seepage effects on the dam structure and on the foundation are individually analyzed. A simplified uplift pressure formula is generally applied for dam structure. This formula can hardly coincide with the real water head distribution at the dam base. For the foundation, agreement can hardly be achieved when surface pressure on the reservoir basin is considered, such that this effect is often simply ignored. In addition, the effect of the impounding process has seldom been considered.

Finally, parameters from the small size of wet-sieving concrete specimen were used in the analysis because of the limitation of molds and test equipment. Studies have shown that significant differences in test results can be found between the wet-sieving concrete and the fully graded concrete that is actually used for dam construction (Song, et al., 2007). The use of parameters from wet-sieving specimens induces a risk of overestimation in the dam safety assessment.

Accordingly, conventional design methods attempt to consider these effects implicitly by introducing several safety factors to cover these simplifications. However, many questions might still be raised regarding the reliability of this approach when applied to the design and safety assessment of the super-high arch dams. These uncertainties surpass the concerns that have arisen from past experiences with conventional dams. Thus, the actual working performance of arch dams under real mechanical and environmental boundary conditions starting from the construction period must be studied.

Over the past two decades, numerous studies have assessed the actual working performance of arch dams. Wittke (1990) analyzed the dam structure-foundation system by considering both seepage force and buoyancy force. Tan and Chopra (1995) analyzed the seismic behavior of an arch dam including dam-water-foundation rock interaction. Yu et al. (2005) studied the stability of the dam abutments of a gravity-arch dam in China with 3D elasto-plastic finite-element method. Sheibany and Ghaemian (2006) analyzed the effects of environmental action on thermal stress Karaj arch dam. Léger and Leclerc (2007) studied the effect of nonlinear temperature difference, which was found to be significant to the crack occurrence in an arch dam after construction. Zhang et al. (2008) attempted to compute the over load safety factor by considering the actual process and temperature load. The analytical results emphasized that the contact nonlinearity of transverse joints is among the most important factors. Jin et al. (2011) conducted a comparative study procedure for the safety evaluation of high arch dams. Baris Sevim et al. (2012) analytically studied the seismic performance of the highest arch dam in Turkey with ambient vibration test results. Santillán, D. et al. (2014) tried to model the thermal response of arch dam with spatial and temporal discretization for solar radiation treatment.

However, most previous studies focused on only one or two aspects. In fact, the actual working performance of the arch dams are influenced by an integrated effect of these factors during their service lives, including such characteristics as the construction process, impounding procedure, residual thermal stress by mass concrete construction, and material characteristics (Zhang, et al. 2008). Nonetheless, these analytical results can hardly represent the actual working performance of arch dams.

Therefore, this study aims to simulate the actual working performance of super-high arch dams and attempts to answer the question of how to evaluate the safety of a super-high arch dam designed on the basis of current specifications. In this work, an integrated analytical approach is proposed to consider all actual factors that influence the performance of an arch dam. The significance of this approach is to be verified against updated engineering practices.

2. INTEGRATED ANALYTICAL APPROACH FOR SIMULATING THE ACTUAL WORKING PERFORMANCE OF A SUPER-HIGH ARCH DAM

2.1. Basic Computational Scheme

A variety of methods have been proposed for the safety assessment of an arch dam. These methods include model tests, empirical comparison, and numerical simulation. Model tests simplify the failure process and evaluate the overload factor of an arch dam. However, the results are difficult to reproduce and cost a large amount of money and time. Furthermore, many discussions give rise to questions regarding the similarity between the model and the actual dam-foundation system. Empirical comparison, such as Lombardi’s method, is based on past construction and operation experience of some “safe” arch dams. Such method only provides a relative safety evaluation. The reliability is uncertain for super-high arch dams.

By contrast, numerical simulation, such as finite element method, is based on the related mechanics theory. This theory can describe all kinds of structural details and analytical processes and can provide the detailed distribution of stress and deformation inside an arch dam. These obvious advantages have attracted considerable research attention and led to the increasingly wider application of this method in the engineering practice of arch dam construction. In this work, the finite element method is adopted to assess the actual working performance of super-high arch dams.

Four types of actual factors are considered: actual material, actual structure, actual loads, and actual process. Actual material parameters refer to hydration heat, time-dependent modulus, autogenous volume change and creep of the hydraulic concrete, and parameters for foundation on the basis of back analysis. In this work, the difference between fully graded concrete and wet-sieving concrete is considered. The actual structure includes transverse joints in the dam, faults, defects in the foundation, and the waterproof-drainage system.

2.2. Modeling of the actual material properties

2.2.1. Mechanical properties of fully graded concrete

Fully graded concrete is generally used for dam construction. The maximum aggregate size can be larger than 100 mm for the fourth grade concrete. Strictly speaking, the 450 mm × 450 mm × 900 mm specimen has to be casted to study fully graded concrete. However, the limitation of molds and test equipment resulted in the frequent use of much smaller specimens with the size of 150 mm × 150 mm × 350 mm. Coarse aggregate, with size larger than 40 mm, has to be screened out before casting. The material parameters for dam concrete in conventional analysis were generally based on this type of wet-sieving specimen.

In fact, the size of the coarse aggregate and specimen significantly affects the material test results of concrete. In addition, wet-sieving stage before casting results in a significant change in concrete mix portion and slurry content. In this work, testing results of the construction material are applied to each arch dam with respect to the characteristics of local aggregates and cementitious binder.

2.2.2. Thermal properties of fully graded concrete

The thermal properties of fully graded concrete has to be considered to simulate the effect of cementitious hydration and environmental temperature. In this work, the thermal parameters of concrete include adiabatic temperature rise, specific heat, thermal conductivity, thermal diffusivity, and coefficient of surface heat dissipation. These parameters can be obtained through inverse analysis while monitoring temperature data during the construction stage.

The mix portions of concrete for the recent construction of super-high arch dams notably include a large amount of fly ash, which comprises over 30% of cement. This aspect significantly changes the hydration process in a dam. Temperature rise would be reduced at the initial stage. However, a greater level of heat release could be expected in the later stages.

To consider this effect, a six-parameter model of adiabatic temperature rise for the dam concrete with large amount of fly ash is proposed. The formulation is as follows:

$$Q(\tau)=Q_1\left(1-e^{-\alpha_1\tau^{\beta_1}}\right)+Q_2\left(1-e^{-\alpha_2\tau^{\beta_2}}\right) \qquad (1)$$

where $Q_1\left(1-e^{-\alpha_1\tau^{\beta_1}}\right)$ stands for the adiabatic temperature rise due to the hydration of the cement while $Q_2\left(1-e^{-\alpha_2\tau^{\beta_2}}\right)$ stands for that of the fly ash.

2.2.3. Mechanical, thermal, and seepage properties of dam foundation

In this work, the foundation is simulated as an elastic-plastic material with a Mohr–Coulomb yielding surface. The natural permeability should be considered to calculate the seepage state in the foundation and its influence on dam working performance. The seepage effect of drainage holes will be discussed in the latter part of this paper. The foundation is simulated as a simple medium to transfer heat without any source in the thermal analysis. All mechanical and thermal parameters can be selected in accordance with current design and safety assessment.

2.2.4. Back analysis for actual material parameters

The design material parameters are generally fixed on the basis of engineer experience and material test data. In fact, the considerable difference between the design material parameters and the actual material parameters can hardly be ignored for super-high arch dams. Therefore, back analysis of temperature, displacement, and seepage fields have to be conducted for actual mechanical, thermal parameters, and foundation permeability characteristics, respectively. With these actual material parameters, the temperature, deformation, seepage, and stress state of the dam-foundation system can be accurately determined.

In this work, thermal parameters are analyzed according to the measured upstream water temperature, measured inner temperature of the dam, and measured atmosphere temperature. Mechanical parameters are analyzed according to the monitored settlement and horizontal deformation. During construction, settlement data are used for back analysis of the modulus. During impounding, plumb-line data are used. Permeability characteristics are analyzed according to the upstream water level, seepage pressure in front and at the back of the waterproof curtains, and leakage quantity in varied drainage galleries.

Mechanical back analysis is taken as an example. First, a typical period is used for analysis. Second, representative points of the arch dam are set as targets. Moreover, analytical displacements approach the monitored data by adjusting the modulus of the foundation and dam body. The mean square error between analytical displacement and monitored data are set as target function.

2.3. Modeling of the actual structure in a dam - foundation system

2.3.1. Modeling of contact state in a construction joint

During the construction of an arch dam, transverse joints are set with certain intervals along the arch axis to reduce thermal stress during hydration stage of the cementitious material in the dam.

Tensile stress can generally not be transferred through transverse joints, whereas compressive stress and shear stress are capable. The construction and impounding processes cause real stress states in transverse joints to be extremely complicated. At the initial stage of construction, the joint surfaces bear compressive stress because of temperature rise and gravity effect. Along with the decrease in temperature, the compressive stress will gradually decrease until the joint opens. After grouting and impounding, transverse joints may return to the compressive state, whereas the contact might be lost at the part close to the upstream surface. Seasonal temperature variation may also influence the open-closure state of the joints and the stress state in the nearby concrete.

To simulate the actual working performance of an arch dam, the real stress state of the joints must be included in the analysis. The interfacial elements with no volume are typically used to describe the open-closure of transverse joints. However, convergences could pose a serious problem when thousands of transverse joints in an arch dam are computed simultaneously. Zhang et al. (2008) developed a three-dimensional interfacial element that can simulate the nonlinear contact states of all transverse joints during construction and impounding.

2.3.2. Modeling of the seepage state in the foundation

Waterproof curtain and drainage hole are often used to reduce seepage pressure in the dam site to enhance the anti-sliding stability of hydraulic structures. Although many related studies have been conducted, seepage field analysis in a dam-foundation system remains a problem, especially in simulating the effect of a drainage hole. The diameter of a drainage hole cross section in the foundation is approximately 0.1 m–0.2 m. To simulate the water head in a drainage hole with reasonable accuracy, the size of the finite element near the hole should be set to be as small as the hole diameter. However, the usual size of the foundation elements is approximately 5 m–20 m for pure mechanical analysis. Hence, a large number of finite elements have to be used in the coupling analysis of seepage and mechanics.

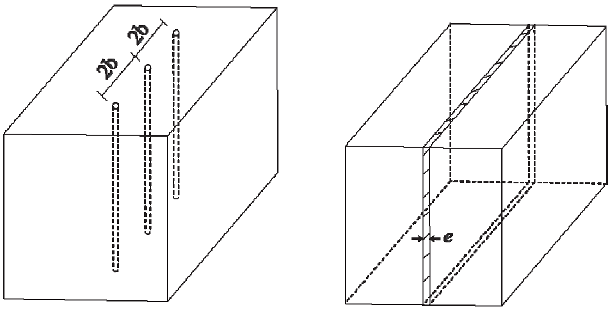

(a) (b)

Figure. 1. Equivalence of the drainage hole in the foundation
(a) Drainage holes in the foundation
(b) Equivalent seeping layer

To solve this problem, Zhu et al. (2013) proposed a method that equates a group of drainage holes as seeping layer inside a conventional solid element with the usual size. Figure 1 shows that a group of drainage holes are built in the dam foundation. These holes 2b have a hole diameter of 2rw. An equivalent seeping layer with the same depth is then used to simulate this drainage effect. The thickness of this layer is set as e=2rw. The horizontal coefficient of permeability kh is set to be the same as that of the natural foundation. Moreover, the vertical coefficient of permeability kz should be computed to have the same drainage effect of the original holes in the pure seepage analysis in advance. The parameter kz is then adopted for the coupling analysis of seepage and mechanics.

2.4. Analytical approach to consider the actual loads and actual process

2.4.1. Gravity load: Effect of construction process

A real arch dam is initially cast into discrete monoliths. The arch is then completed by grouting. Therefore, the gravity of each monolith is first sustained by itself before grouting during the construction process. Owing to the large volume, a super-high arch dam also has to be casted layer by layer, i.e., when the concrete is casted to a certain elevation (Hi), the transverse joints in the layer from Hi-1 to Hi is grouted. Subsequently, new concrete monoliths (Hi+1) will be casted. The newly added gravity load can be transferred through the grouted joints. Hence, gravity stress distribution in the dam is significantly influenced by the construction process and contact states of the transverse joints. In this work, the engineering measure of grouting all transverse joints in one layer (e.g., from Hi to Hi+1) is defined as one arch closure. N arch closures indicate that the arch beam is divided into N+1 layers to be casted.

Hence, analytical gravity load has to be added to the finite elements in accordance with the construction process. Transverse joint elements in the layer from Hi to Hi+1 that have not been grouted are set in “dead” state, i.e., no stress can be transferred. After being grouted, the transverse joint elements in the layer from Hi-1 to Hi become “active.” The stress states of these elements are first refreshed to zero state, which is followed by the constitutive modeling. This method is discussed above. Accordingly, the finite elements for the monoliths that have not been casted are set as “dead” ones, i.e., extremely small stiffness and zero density. When new monoliths (Hi+1) have been casted, the related finite elements turn “active” with the refreshed initial stress state and are then computed according to the current gravity load. Meanwhile, stress states in the finite elements below height Hi, including transverse joint elements, have to be recalculated.

2.4.2. Water load: Effect of the impounding process

Impoundment typically starts before dam completion to save on the building cost of super-high dams. In this manner, the hydropower station could start operation as early as possible. Therefore, the surface pressure of water is not added to the dam structure all at once.

This effect is therefore considered in the approach discussed in above. When the water level increases to elevation Hi, the water face load is applied to finite elements below this height. Transverse joints below Hi are “active” to transfer stress. Hence, water pressure can be sustained by both the arch and beam in the dam structure. After new transverse joints (from Hi to Hi+1) become “active,” the water level can increases Hi+1 at a certain time according to the impounding process.

2.4.3. Water load: seepage in the foundation

Seepage will occur in the whole dam-foundation system because of the large difference in water head between upstream and downstream. Owing to the extremely low permeability of the dam concrete, the water head will rapidly decrease near the surface of the dam structure. Hence, this effect can be rationally considered by adding the conventional water pressure on the dam surface.

However, the discussion becomes more complex for the foundation. First, seepage in the foundation will provide buoyance force to the dam structure. This force is harmful to dam stability against sliding. Waterproof curtain and drainage holes are typically used to reduce this effect. Second, seepage in the foundation will also reduce water pressure on the reservoir basin. In addition, water load is generally concentrated on the water proof curtain.

In this work, seepage state is first analyzed with equivalent method, as discussed in above. Then, seepage force can be calculated in each finite element and coupled with mechanical analysis. The impounding process can also be easily considered through this approach. The effect of the stress state on seepage state in the foundation is not considered for simplicity.

2.4.4. Temperature load

Temperature load is one of the key factors that affect stress states in the mass concrete structure of an arch dam. During the hydration stage of the initial 3 d–5 d after casting, the temperature inside the concrete rises to a maximum value and then drops when cooling water is used. Before closure grouting, thermal stresses in different monoliths do not influence one another.

Grouting work is designed to be taken when thermal deformation can hardly change inside each monolith. After the grouting of transverse joints, the thermal stress inside the dam is thought to be mainly governed by the atmosphere and reservoir water until attaining a quasi-stable field.

Therefore, continuous simulation of the working performance of the dam from the construction stage to the service stage is needed. In addition, nonlinear temperature difference has to be considered in simulating the crack potential at the dam surface caused by the sudden appearance of extreme atmosphere temperature.

3. APPLICATION FOR ENGINEERING PRACTICE

Jinping-1 arch dam is located on the river band of Yalong River, which is at the cross point of two counties of Yi Autonomous Prefecture of Liangshan, Muli, and Yanyuan in Sichuan Province, China. This structure is currently the highest arch dam worldwide, which has a maximum height of 305 m. Concrete casting started on October 23, 2009. The first group of generators started to work on August 30, 2013. Water level reached E.L. 1840 m on October 14, 2013. The dam concrete casting was completed on December 23, 2013.

The problem of arch grouting time selection is also encountered, similar to the case of Laxiwa. The transverse joints above E.L.1858 m were not grouted when water level reached E.L.1840 m in October 2013. According to the design plan, the water level should drop to E.L.1800 m in February 2014. Two options were proposed at this moment. One option is grouting with water level at E.L.1840 m. Another option is identified to be the original one, in which grouting is at much lower water level, E.L. 1800 m. The former option will accelerate the construction process. This option is preferable economically. However, dam safety became a dominating factor. The proposed actual performance assessment is applied here to help make a decision.

Fig. 2 shows the finite element discretization. Here, five different rock zones (class II, class III1, class III2, class IV1, class IV2, class V1) and complex faults (f2, f18, f5, f8, f42-9, f13, f14, and X) are considered in the model. In addition, the foundation treatment, such as shear transfer piles, backfill, and grouting, and detailed dam structures, such as fillets, holes, and gate piers, are simulated.

Back analysis was the performed by using the monitored data. The time duration between June 5 and July 20, 2013 is gathered for analysis, while water level increased from E.L.1700 m to E.L. 1800 m. During this period, the time duration was short with a rapid increase in water level, i.e., dam displacement is mainly governed by water pressure. Taking the mean square deviation of analytical horizontal displacement and monitored data as target function and ratio between analytical modulus and design modulus as variable, we could obtain the actual modulus with optimization analysis.

Two proposed plans are analytically compared on the basis of the finite element model and actual material parameters. If the first plan is adopted, i.e., accelerated grouting plan, tension stress would appear in transverse joints when water level falls to E.L.1800 m on Feb. 2014. Grouted joints will be forced to open. Typical joint opening states are shown in Fig. 3.

On the other hand, if the second plan is applied, i.e., grouting work is carried out when water level reaches E.L.1800 m, the opening of most transverse joints to be grouted are larger than 0.5 mm. Easier but better grouting work can be expected. Closure of all transverse joints is analytically predicted with the increase of water level after grouting. The integrity of the arch dam can be guaranteed. Therefore, actual performance assessment supports the original plan.

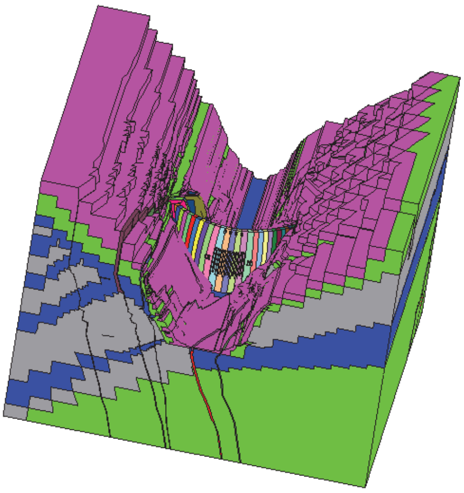

(a) global view of the analytical model

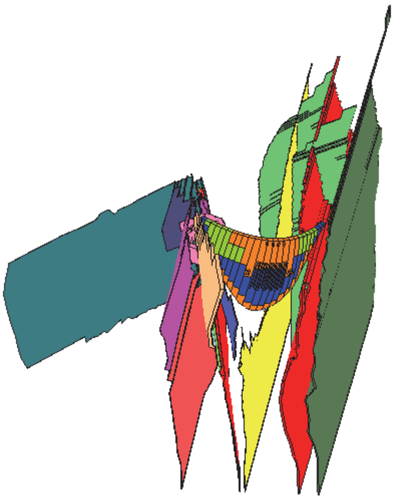

(b) dam body and main geometrical structure

Fig. 2. Finite element model for Jinping-I arch dam-foundation system

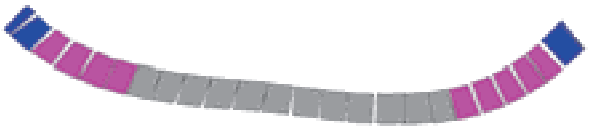

(a) E.L. 1856m

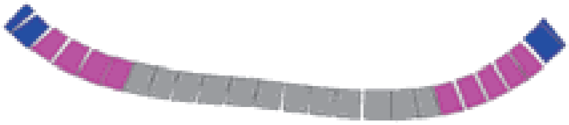

(b) E.L. 1863m

Figure. 3. The analytical opening of transverse joints after grouting at typical elevation when the water level drops to 1800m on Feb. 2014 according to the 1st plan.

4. CONCLUSION

China is addressing the significant challenge posed by the construction of several 300 m high arch dams for the effective use of hydropower resources. The limited experience in the construction of these super-high arch dams has given rise to many questions on the reliabilities of the current design specification and conventional safety assessment methods. This study presents an integrated analytical approach to simulate the actual working performance of the super high arch dams. Four significant factors have to be considered in the actual working performance assessment, namely, actual material, actual structure, actual loads, and actual process. The four factors are dependent on one another, as well as exhibit coupling effects that form the real stress states in the super high arch dam. This approach has been implemented on the computational platform, SAPTIS, which was developed by the authors in IWHR. The case study shows that the actual working performance assessment is effective for engineering practice.

REFERENCES

Zhang C (2004), “Challenge of High Dam Construction to Computational Mechanics”. Proceedings of the Sixth World Congress on Computational Mechanics in conjunction with the Second Asian-Pacific Congress on Computational Mechanics. Edited by Yao Z., Yuan, M. and Zhong W. Beijing: Tsinghua University Press & Springer, 2004.

Zhu B F, Rao B and Jia J S, et al. (1992), “Shape Optimization of Arch Dams for Static and Dynamic Loads”, Journal of Structural Engineering, 1992, Vol.118 (11), pp.2996-3015.

Li QB, Liang GH and Hu Y.(2014) “Numerical Analysis on Temperature Rise of a Concrete Arch Dam after Sealing Based on Measured Data”. Mathematical Problems in Engineering. Volume 2014, Article ID 602818. 12pages.2014.

Jin F, Chen Z, Wang J, Yang J.(2010) “Practical procedure for predicting non-uniform temperature on the exposed face of arch dams”. Applied Thermal Engineering, 2010,

Azmi, M and Paultre P. (2002), “Three-dimensional analysis of concrete dams including contraction joint non-linearity”, Engineering Structures, 2002, Vol.24 (6), pp.757-771.

Song YP and Wang HL (2007), “Endochronic damage constitutive model for fully-graded aggregate mass concrete” Frontiers of Architecture and Civil Engineering in China. 1(3):274-280, 2007.

Wittke W. (1990) “Rock mechanics - theory and applications with case histories”. Berlin: Springer-Verlag, 1990.

Tan H. and Chopra AK (1995) “Earthquake analysis of arch dams including dam-water-foundation rock interaction.” Earthquake Engineering & Structural Dynamics. 24(11):1453-1474. 1995.

Yu X., Zhou YF. and Peng SZ. (2005) “Stability analyses of dam abutments by 3D elasto-plastic finite-element method: a case study of Houhe gravity-arch dam in China”. International Journal of Rock Mechanics and Mining Sciences. 42(3):415-430. 2005.

Sheibany F. and Ghaemian M. (2006) “Effects of Environmental Action on Thermal Stress Analysis of Karaj Concrete Arch Dam.” Journal of Engineering Mechanics. 132(2006):532-544.

Léger P and Leclerc M.(2007) “Hydrostatic, Temperature, Time-Displacement Model for Concrete Dams”. Journal of Engineering Mechanics, 2007, 133(3):267-277.

Zhang G X, Liu Y, and Zhou Q J. (2008) “Study on real working performance and overload safety factor of high arch-dam.” Science in China, Series E: Technological Sciences, 2008, 51(sup): 48-59.

Jin F, Hu W, Pan J, Yang J, Wang J, Zhang C.(2011) “Comparative study procedure for the safety evaluation of high arch dams”. Computers and Geotechnics. 38(3), 2011, pp 306–317.

Sevim, B., Altunişik, A.C. and Bayraktar, A,(2012) “Earthquake behavior of Berke arch dam using ambient vibration test results”, Journal of Performance of Constructed Facilities, 26(6), 2012, pp 780-792.

Santillán, D., Salete, E., Vicente, D., and Toledo, M. (2014). ”Treatment of Solar Radiation by Spatial and Temporal Discretization for Modeling the Thermal Response of Arch Dams.” Journal. of Engineering. Mechenics., 140(11), 05014001.

Zhu B F. (2013). “Thermal Stresses and Temperature Control of Mass Concrete”. London: Butterworth- Heinemann Ltd. 2013.

Research on Mechanism of Slab Horizontal Breakage of High Concrete Faced Rockfill Dam Using a Structural Mechanics Method

G. DENG
China Institute of Water Resources and Hydropower Research, China
dgang@iwhr.com

Y. ZHANG, X. WANG, Y. WEN & S. YU
China Institute of Water Resources and Hydropower Research, China

R. CHEN
Shenzhen Graduate School, Harbin Institute of Technology, China

ABSTRACT:
Cross-sectional deformation mechanism of face slab of concrete faced rockfill dam (CFRD) and the conceptualization method were investigated. The relationship between deformation pattern and slope-direction stress of face slab were explored. The high slope-direction face slab stress is mainly attributed to the drag effect of dam deformation on face slab along slope direction plus the local bending deflection of face slab. Large creep deformation of dam body and the induced slope-direction deformation of face slab may result in global high compressive slope-direction stresses. Large compressive deformation of rockfill below the slab due to reservoir water pressure and the induced deflection of face slab may result in local high bending stress in slope direction. The global compressive stress and local bending stress in slope-direction, plus the stress enlargement by horizontal compression due to special terrain and the existing bending deflection were revealed to be the main cause of the horizontal extrusion breakage of face slab. The breakage may occur in construction joints of the first and the second stage face slab where local structural defect exists. A case of CFRD with the height of 185m was taken to investigate this mechanism.

Keywords: Concrete Faced Rockfill Dam (CFRD), Deformation Pattern, Conceptualization, Extrusion Breakage, Creep Deformation

1. INTRODUCTION

Extrusion breakage of face slab is a special phenomenon that occurs as the height of concrete faced rockfill dam (CFRD) increases. Vertical breakage of face slab was found firstly which is initiated from the upper vertical joints of CFRD in a narrow valley and is concentrated near river bed. Vertical breakage is mainly attributed to the displacement of dam body toward valley center induced by long-term deformation and the resultant high horizontal stress (Deng et al., 2008). Horizontal extrusion breakage of face slab was observed only in the last several years which was all initiated from the horizontal staged construction joints of face slab. Horizontal shear and extrusion breakage was observed at horizontal joints of Zipingpu CFRD after Wenchuan Earthquake on May 12nd 2008 (Guan et al., 2008). Extrusion breakage of horizontal construction joints was observed in more than 10 blocks of the first and the second stage face slab of the CFRD (main dam) of Sanbanxi Hydropower Station during reservoir filling. Horizontal extrusion breakage may be companied with extrusion breakage of vertical joints and diagonal cracks of face slab. Based on the analysis of in situ monitoring data, Wang et al. (2009) stated that the extrusion breakage at horizontal joints of face slab was directly induced by irregular L-shaping of surrounding blocks of face slab, horizontally building construction joints by mistake, fairly large deformation of upstream rockfill, rapid rising of reservoir water level and others. However, Yang (2010) believed that the direct reasons were related to over-stressing on joint face of horizontal joints and structural defect of Sanbanxi CFRD as well as too large deformation rate of dam body induced by the first rapid rising of reservoir water level. In Hu’s (2009) opinion, the extrusion breakage of face slab of Sanbanxi CFRD was mainly attributed to the imprecise and nonstandard construction at the crest of the first stage face slab and the rapid reservoir filing. Xu et al. (2011) stated that the main reasons leading to the extrusion breakage of face slab of Sanbanxi CFRD were the fairly low deformation modulus of rockfill near face slab and the sloping bank terrain of valley accommodating the dam. A variety of opinions cover various factors leading to extrusion deformation of face slab along slope direction and stress concentration.

The objectives of this study are to further reveal the relation between various factors and extrusion breakage of face slab, and to analyse its mechanism. Cross-sectional deformation mechanism of face slab of CFRD and its conceptualization method were investigated in this study. The relationship between deformation and slope-direction stress of face slab, and the generation mechanism of slope-direction stress of face slab were explored. The effect of external factors including time and reservoir water level on slope-direction stress of face slab was revealed. A case study of Sanbanxi CFRD was carried out to analyze various components of slope-direction stress of face slab and hence investigate the mechanism of horizontal breakage of face slab of CFRD. It was found that the rather high slope-direction stress of face slab is mainly attributed to long-term deformation of dam body and the induced slope-direction compression of face slab. Local surface slope-direction stress of face slab is further increased by local bending deflection of face slab due to reservoir water pressure, which may induce horizontal breakage. High horizontal stress of face slab due to special terrain also contributes to the serious extrusion of face slab along slope direction and eventually horizontal breakage occurs in the weak zone induced by construction, i.e., construction joints of the first and the second stage face slab. This study also demonstrates that the slope-direction stress of face slab is slightly affected by overall bending deflection of face slab due to reservoir water pressure but significantly affected by local bending of face slab induced by non-uniform deflection.

2. EXTRUSION BREAKAGE OF FACE SLAB OF SANBANXI CFRD

The studied case in this paper is the main dam of Sanbanxi Hydropower Station in China. Its height is 185.5 m and both upstream and downstream slopes are 1:1.4. From upstream to downstream the dam body is divided into cushion zone (IIA), transition zone (IIIA), upstream rockfill zone (IIIB), downstream rockfill zone and downstream block stone slope protection zone (IIICA and IIICB), special cushion zone under perimeter joint (IIB). Upstream clay blanket zone (IA) and weighted zone (IB) were set up under the 370 m elevation of upstream face slab (HydroChina ZhongNan Engineering Corporation, 2008; Dam Safety Supervision Centre, National Power Administration Committee of PRC, 2009). A typical cross section of the dam body is shown in Fig. 1.

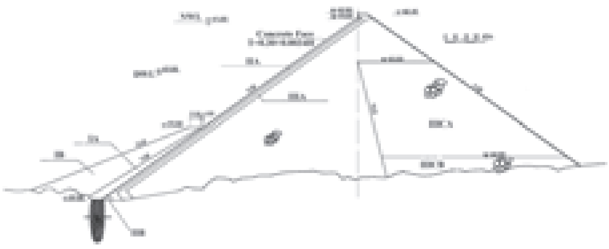

Figure 1. A typical cross section of Sanbanxi CFRD (HydroChina Zhongnan Engineering Corporation, 2008)

The thickness of the crest of face slab of main dam is 0.3 m and increases downwards. The thickness reaches 0.913 m at the bottom of dam. Uniform thick (i.e., 42.9 cm) blocks were built in the compression zone of the third stage face slab. 13 vertical compressive joints spaced in 16 m were set up at the middle of face slab. 13 and 11 vertical tensile joints spaced in 8 m were set up at the left and right banks, respectively. Apart from the face slab portion of right MB10 in which permanent horizontal joints were set up at the 383.543 m elevation, only horizontal construction joints were set up in other portions of face slab. Low-heat and micro-expansion fiber concrete of C30 were used in the face slab of main dam. Uniform two-layer and two-way reinforcement was used in the concrete (Dam Safety Supervision Centre, National Power Administration Committee of PRC, 2009).

The construction of dam body was divided into 5 stages. The construction began on November 15th 2003. On April 13th 2004, the elevation of dam body for temporary flood protection reached 390.00 m. In August 2005, the elevation of dam body reached 478.00 m. The construction of face slab was divided into 3 stages. The first construction stage of face slab (below 385.00 elevation) began on October 26th 2004 and ended on January 29th 2005. The second stage lasted from October 26th to December 19th 2005 and the corresponding elevation of dam body increased from 385.00 m to 440.00 m. The third stage began on April 22nd and ended on July 1st 2006 and the corresponding elevation of dam body increased from 440.00 m to 478.00 m. In December 2006, wave protection wall and structures at the top of dam were completed (HydroChina ZhongNan Engineering Corporation, 2008; HydroChina Guiyang Engineering Corporation, 2007).

The filling of Sanbanxi Reservoir began in Jan. 2006. The initial water level was 329.00 m and reached 429.00 m in June 2006. Then the level was kept at 430.00 m. When the water level began to increase again on June 5th 2007, leakage first increased suddenly, and then decreased a little with the drawdown of water level. At the same time, some joint meters, steel bar gauges and strain gauges near the construction joints of the first stage and second stage face slab of main dam showed a sudden increase in compression deformation, abnormal readings or data interruption in July 2007. In Aug. 2007, the temperature of some of the above-mentioned steel bars and strain bars became the same with that of reservoir water at the same elevation. The inclinometer located in face slab was in a blocked status at the 384 m elevation. (HydroChina Zhongnan Engineering Corporation, 2008; Dam Safety Supervision Centre, National Power Administration Committee of PRC, 2009; Li et al., 2009; Zhu et al., 2009).

Underwater inspection in Jan. 2008 showed that breakage occurred in many portions of face slab ranging from the left MB3 to right MB8 at the elevations from 382m to 388m (Dam Safety Supervision Centre, National Power Administration Committee of PRC, 2009). The largest width of breakage was 4 m and the maximum depth was 40 cm (HydroChina Zhongnan Engineering Corporation, 2008). Heave of skin reinforcement was observed at the portion of face slab near construction joints. Most concrete damage in surface layer of face slab occurred below the 385 m elevation. The depth of damage varied greatly due to the varying thickness of concrete prevention layer. On the other hand, the integrity of concrete and reinforcement at the bottom layer of face slab was almost not altered (Dam Safety Supervision Centre, National Power Administration Committee of PRC, 2009).

3. CONCEPTUALIZATION OF CROSS-SECTIONAL DEFORMATION PATTERN OF FACE SLAB AND ITS EFFECT ON SLOPE-DIRECTION STRESS

3.1. Cross-sectional deformation pattern of face slab

The stress and deformation of face slab is assumed to satisfy thin plate theory. It is also assumed that at the internal section of any block of face slab, stress and deformation are uniform along the width direction. Therefore, at the cross section of dam body, the displacement of any point at face slab of CFRD can be abstracted as the sum of components along two orthogonal directions, e.g., the displacement along upstream slope direction dw and the one vertical to upstream slope direction dv, or the horizontal displacement dy and the vertical displacement dh. Displacements of different points at face slab are generally different. For any portion (or full length) of face slab, its deformation can be decomposed into rigid motion, compression/extension along slope direction and normal bending deflection, as shown in Fig. 2. If breakage and plastic deformation of face slab are not taken into account, and elastic stress-deformation relation of face slab is assumed, stress of face slab can be superimposed.

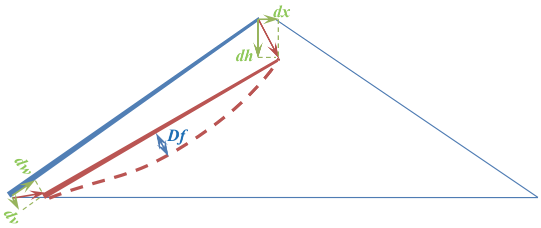

Figure 2. Decomposition of deformation pattern of face slab of CFRD

3.2. Tensile/compressive deformation induced by endpoint displacements of face slab

It is assumed that any portion of face slab under investigation is located at a height of H' and the upstream slope ratio is 1:n (n = 1.4 or 1.3 generally for CFRD and higher value for face sandy gravel dam). As a consequence, the slope angle of this portion of face slab is $\theta = \mathrm{arctg}(1/n)$ and the initial length of this portion of face slab is $L' = H'/\sin\theta \quad - A'$. For a given portion of face slab, A' is a constant including the lengths of toe plate (if any), peripheral joint, horizontal joint and wave protection wall. By assuming that tensile/compressive deformation of the portion of face slab for analysis is uniform along the length direction, the average tensile/compressive strain can be obtained from the displacements at two endpoints.

The displacements at two endpoints of a portion of face slab can be represented by the displacement along length direction (dw_1) and the displacement along normal direction (dv_1) at the bottom of the portion of face slab, and the vertical displacement (dx_2) and the vertical displacement dh_2 at the upper endpoint of the portion of face slab.

The strain of face slab induced by lower endpoint displacement of face slab, ε_{1-1}, and that induced by upper endpoint displacement of face slab, ε_{1-2}, can be computed by the following two equations (positive strain denotes compression and negative for tension in this paper):

$$\varepsilon_{1-1} = \frac{\Delta L'_1}{L'} = \frac{L' - \sqrt{(L' - dw_1)^2 + (dv_1)^2}}{L'} \qquad (1)$$

$$\varepsilon_{1-2} = \frac{\Delta L'_2}{L'} = \frac{L'}{L'} - \frac{\sqrt{(L' - dh_2 \sin\theta + dx_2 \cos\theta)^2 + (dx_2 \sin\theta + dh_2 \cos\theta)^2}}{L'} \qquad (2)$$

Rigid body displacement and rigid body rotation induced by endpoint displacements can be automatically eliminated by superimposition of the above two equations.

3.3. Tensile/compressive deformation and bending deflection deformation induced by deflection of face slab

Similar to tensile/compression deformation, it is assumed that the curvature of the portion of face slab for analysis along the length direction is identical. Hence, the deflection curve of face slab can be simplified as a circular arc with a constant radius of R' and a radius angle of α' and the maximum deflection of face slab is denoted as D_f. The tensile strain of face slab induced by the deflection of face slab can be computed as

$$\varepsilon_{2-1} = \frac{L' - 2R' \arcsin\left(\frac{L'}{2R'}\right)}{L'} \qquad (3)$$

The strain corresponding to bending deformation induced by the deflection of face slab is:

up surface, $\varepsilon_{2-2-u} = \frac{t}{2R'}$ (4)

bottom surface of slab, $\varepsilon_{2-2-d} = -\frac{t}{2R'}$ (5)

where *t* is the thickness of face slab.

3.4. Superimposition of stress and deformation of face slab

The stress and deformation of face slab induced by various patterns can be superimposed and it is assumed that face slab is uniformly distributed within the region of analysis. Hence, the average strain of face slab can be computed by:

up surface, $\varepsilon_u = \varepsilon_{1-1} + \varepsilon_{1-2} + \varepsilon_{2-1} + \varepsilon_{2-2-u}$ (6)

bottom surface, $\varepsilon_d = \varepsilon_{1-1} + \varepsilon_{1-2} + \varepsilon_{2-1} + \varepsilon_{2-2-d}$(7)

The strain depends on the length and the thickness of face slab, the endpoint displacements and the deflection between the two endpoints of the portion of face slab. From mathematical viewpoint, the length of face slab affects both tensile/compressive deformation and bending deflection. The larger the length of face slab is, the little the effect of endpoint displacement and deflection on the strain of face slab is. The thickness of face slab only affects bending deflection and this effect becomes more significant as the thickness of face slab increases. Endpoint displacement only causes tensile/compressive deformation and the components along orthogonal directions produce different effects on the strain of face slab. The deflection of face slab results in not only tensile deformation but also bending deflection. The larger the deflection is, the larger both tensile deformation and bending deflection are.

4. MECHANISM OF SLOPE-DIRECTION STRESS OF FACE SLAB AND INDUCED HORIZONTAL BREAKAGE OF FACE SLAB

4.1. Analysis of average slope-direction stress of face slab

Following the above conceptualization of deformation pattern of face slab and its effect on slope-direction stress and strain, face slab stress of Sanbanxi CFRD induced by endpoint displacements of face slab can be computed if only overall tensile/compressive deformation along the entire length of face slab is considered. The computed stress induced by lower and upper endpoint displacements of face slab is shown in Figs. 3, respectively. For the computation, the Young's modulus of concrete is 30 GPa and the effect of stress along other directions on slope-direction stress is not taken into account. According to sign convention specified in geotechnical engineering, compressive stress is positive and tensile stress is negative.

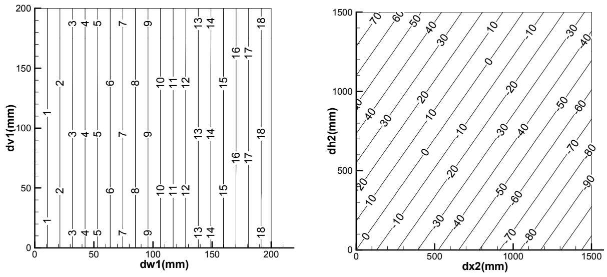

Lower ending point Upper ending point

Figure 3. Face slab stress of Sanbanxi CFRD induced by the lower and upper endpoint displacements of face slab (MPa)

For Sanbanxi CFRD, if overall bending deformation occurs along the entire length of face slab (i.e. along the dam height of 185.8 m), the relationship between deflection and curvature radius of face slab is shown in Fig. 4. It is found that the curvature radius is still higher than 7.4 km even the deflection of face slab reaches 1.5 m. The actual incremental deflection of face slab after construction of the third stage face slab of Sanbanxi CFRD was less than 0.15 m and hence the curvature radius of induced bending deflection was 100 km. In other words, the actual bending deflection induced by overall deflection of face slab was tiny. The relationship between global tensile deformation and curvature radius induced by face slab deflection is shown in Fig. 5. The relationship between global bending stress and curvature radius induced by deflection of face slab with different thicknesses is shown in Fig. 6. At a given curvature radius, the induced surface stress is higher when face slab is thicker. In other words, the induced surface stress at the bottom of face slab is higher than that at the top of face slab. Therefore, if tensile damage (i.e., crack) occurs in the face slab without double reinforcement under tension induced by bending of face slab, the development of crack might be automatically terminated as the tensile crack goes deeper into face slab (i.e., the effective thickness of face slab decreases) and the bending-induced tensile stress decreases gradually.

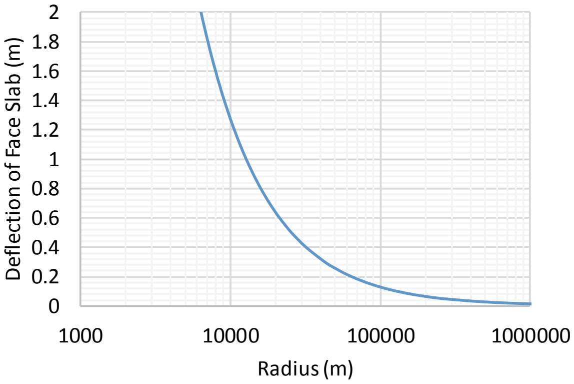

Figure 4. Relationship between deflection and curvature radius for face slab of Sanbanxi CFRD

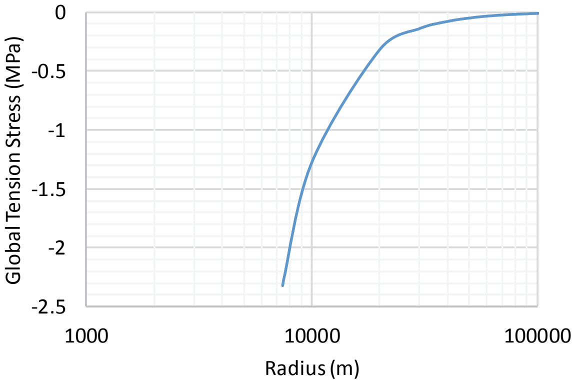

Figure 5. Relationship between stress and curvature radius for face slab of Sanbanxi CFRD

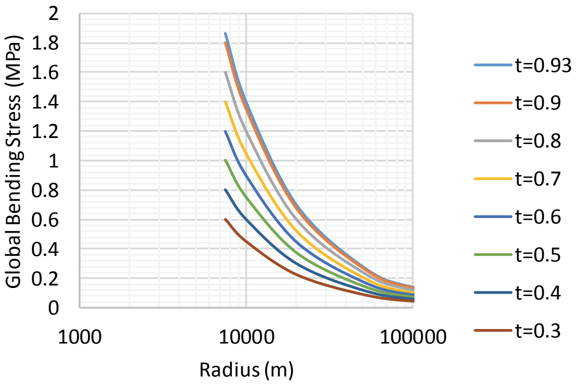

Figure 6. Relationship between surface stress and curvature radius for face slab of Sanbanxi CFRD

It can be seen from the above analysis that within the range of endpoint displacement and deflection of face slab in practice, the values of tensile strain and bending strain induced by deflection of face slab are far lower than those induced by endpoint displacement. At the same time, tensile/compressive strain induced by the lower endpoint displacement of face slab is far lower than that induced by the upper endpoint displacement of face slab. Therefore, in terms of average value, the slope-direction stress of face slab is mainly determined by the upper endpoint displacement of face slab. In practice, the upper endpoint of face slab is attributed to a combined effect of creep deformation of dam body under self-weight after construction, settlement and horizontal displacement of dam body due to reservoir water pressure, and stress transfer and resultant deformation of face slab induced by frictional effect from dam body deformation. In other words, the above three factors codetermine the slope-direction stress of face slab. From the whole, the dominant factor for induced face slab stress is the tensile/compression deformation of face slab along slope direction caused by drag effect of dam body deformation. Since overall bending deflection is far smaller than the tensile/compressive deformation along slope direction, slope-direction stress and strain are kept at a slightly eccentric tensile/compressive state.

According to the Safety Monitoring Data Analysis Report of Main and Auxiliary Dams of Sanbanxi Hydropower Station (Dam Safety Supervision Centre, National Power Administration Committee of PRC, 2009), the maximum settlement at the top of Sanbanxi CFRD reached 38.67 cm after October 2005 and the settlement at the top of face slab should be higher. At the same time, the maximum recorded horizontal displacement at the top of face slab reached 6.15 cm after December 2005. The tension of joints at the bottom of face slab at a large cross section was fairly small. After construction of the third face slab, the maximum deflection of face slab reached 16.8 cm and the induced overall tensile stress and bending stress were fairly small. It could be estimated that the overall average slope-direction stress induced by endpoint displacement of face slab was about 15MPa. It was obvious that the slope-direction stress at some locations of face slab should be larger than 15 MPa and vice versa. The above analysis is consistent with the distribution of measured slope-direction stress of face slab on July 24th 2007.

4.2. Sensitivity analysis of the length of bending deformation of face slab

From the whole, slope-direction stress of face slab is mainly induced by tension/compression along the slope direction and hence overall bending deflection is relatively not prominent. In practice, however, deflection curve induced by normal displacement of face slab often contains multiple radii of curvature similar to multi vibration modes in a vibration. The length of face slab corresponding to bending deformation significantly affects curvature radius. At the same time, at a given curvature radius, surface bending stress is affected by the thickness of face slab. Therefore, both thickness and length of face slab produce a significant effect on slope-direction stress of face slab. In practice, the dam body elevation difference corresponding to the length of face slab is used as an index for analysis, which is better for expression and analysis. In other words, dam body elevation difference and the elevation at which bending deformation occurs significantly affect slope-direction stress of face slab.

Fig. 7 shows the computed curvature radius and tension stress of face slab at various values of dam elevation difference and deflection, respectively. It is found that within the length of face slab corresponding to a rather small elevation difference of dam body, there exists a possibility that over tension or bending caused by deflection deformation may result in tensile crack or extrusion failure.

According to the above analysis, from the whole, components of face slab strain, ε_{1-1}, ε_{1-2}, ε_{2-1} and

ε_{2-2-u} as well as ε_{2-2-d} were not obviously related to the fluctuation of reservoir water level. However, apart from the strain component existing in the process of construction of dam body, in fact measured face slab strain generally includes not only the component associated with time (the part significantly related to time as isolated from face slab strain) but also the component associated with water level (the part significantly related to reservoir water level as isolated from face slab strain). Therefore, the component of face slab strain associated with time mainly arises from tension/compression of face slab caused by creep deformation of dam body, whereas the component associated with water level arises from local bending of face slab.

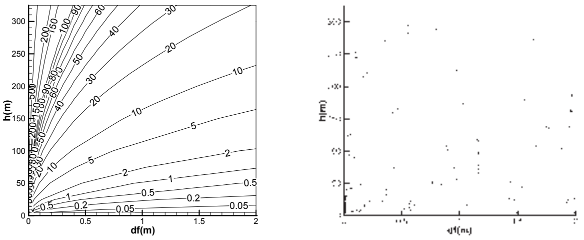

Curvature radius (km) Tension stress (MPa)

Figure 6. Curvature radius and tension stress of face slab at various values of dam length/height and deflection (km)

5. CONCLUSIONS

It can be seen from the above analysis, slope-direction stress is mainly sourced from creep deformation of dam body which is the main cause of horizontal extrusion breakage. Slope-direction stress of face slab on surface is increased by the local bending deflection of face slab due to reservoir water pressure. This is the fundamental and secondary reason of the slab failure.

The following measures should be adopted to prevent horizontal breakage of face slab by controlling compression along slope direction and local bending deflection of face slab:

(1) To reduce the face slab compression along slope direction: controlling the creep deformation of dam body by improving compaction degree of dam body and reducing post-construction deformation of dam body; keeping away from the peak creep deformation of dam body by extending pre-settlement duration before slab pouring; improve the adaptability of dam body to creep deformation by setting up permanent horizontal joints in face slab and improving flexibility of face slab along slope direction.

(2) To control local bending deflection of face slab: ensuring homogeneity of cushion layer beneath face slab to prevent uneven deflection of face slab; preventing local slope deficiency in cushion layer beneath face slab and local defect during face slab construction; increasing horizontal modulus of cushion layer.

ACKNOWLEDGEMENT

The authors acknowledge the support of National Key Technology Support Program (grant 2013BAB06B02), the Research Fund of the State Key Laboratory of Simulation and Regulation of Water Cycle in River Basin, China Institute of Water Resources and Hydropower Research (grant 2014RC02).

REFERENCES

DENG Gang, XU Zeping, LV Shengxi, LU Yumin.(2008): Analysis on long term stress and deformation of high concrete face rockf ill dam in narrow valley (in Chinese). Journal of Hydraulic Engineering. 39(6): 639-646

GUAN Zhicheng, SONG Yangang, CAI Dewen.(2008) Safety assessment and investigation on damage from disaster of “5.12” Wenchuan Earthquake for Zipingpu Concrete Faced Rockfill Dam(in Chinese). Water Resources and Hydropower Engineering, 39(9):36-43

HU Yongping. (2009): Damage cause and rehabilitation of the face slab of Sanbanxi high rock fill dam (in Chinese). Dam and Safety. (3): 75-77

HYDRO CHINA Zhongnan Engineering Corporation Limited. (2008): Self-inspection report of Design for the Completion Safety Appraisal of Sanbanxi Hydropower Station on Qingshui River [R] (in Chinese).

HYDRO CHINA Guiyang Engineering Corporation Limited. (2007): Self-inspection report of Supervision for the Completion Safety Appraisal of Sanbanxi Hydropower Station on Qingshui River [R] (in Chinese).

Large Dam Safety Supervision Center, State Electricity Regulatory Commission, SERC. (2009): Completion safety appraisal Report for Sanbanxi Hydropower Station [R] (in Chinese).

Large Dam Safety Supervision Center, State Electricity Regulatory Commission, SERC. (2009): Analysis on the Safety Monitoring Data of Main Dam and Auxiliary Dam of Sanbanxi Hydropower Station Prepared for Completion Safety Appraisal [R] (in Chinese).

LI Tao, WANG Yu-jie and ZHU Jinjie. (2009): Analysis on the Seepage Monitoring Data of Sanbanxi Face Slab Rock-fill Dam (in Chinese). Dam and Safety. (6): 41-45

National Energy Administration of the People’s Republic of China. (2009): Electric Power Industry Standard of People’s Republic of China: Design Code for hydraulic Concrete Structures (DL/T 5057-2009)(in Chinese). China Electric Power Press, Beijing

WANG Yu-jie, ZHU Jin-jie and LI Tao. (2009): Analysis on Cause Reason for Face-slab Damage of Sanbanxi Face-slab Rock-fill Dam (in Chinese). Dam and Safety. (6): 19-28

XU Zeping, DENG Gang, ZHAO Chun. (2011): Analysis on the operating performance of Sanbanxi CFRD. Dams and Reservoirs under Changing Challenges - Proceedings of 79th Annual meeting of ICOLD. Lucerne: 91-98

YANG Guoxiang. (2010): Causes for Cracks on Sanbanxi Concrete Face Rock-fill Dam (in Chinese). Hydropower Automation and Dam Monitoring. 34(6): 49-52

ZHU Jin-jie, LI Tao and DU Xuezhen. 2009. Analysis on Stress and Strain Before and After the Face-slab Damage of Sanbanxi Dam (in Chinese). Dam and Safety. (6): 46-48

The Macro and Micro-Approaches for the Deformation Control of High Concrete Face Rockfill Dams

X.L. Chang, W. Zhou & G. Ma
State Key Laboratory of Water Resources and Hydropower Engineering Science, Wuhan University, 430072, Wuhan, China
changxl@whu.edu.cn

ABSTRACT:
In the last 30 years, more than 150 concrete face rockfill dams (CFRDs) have been built for their obvious advantages. The deformation prediction and control of rockfill is a key issue in the high CFRDs construction, especially for 200-m-level dams. The post-construction and uncoordinated deformations may lead to concrete slab cracking and failure of sealing joint, which severely degrade the impermeability of concrete slab and affect the safety operation of the CFRD. In this paper, the deformation prediction and control methods are investigated from three aspects. Firstly, a brief introduction of four constructed high CFRDs was given, and the monitoring data were analyzed emphatically. Secondly, the practical control methods were discussed in detail, and some practical suggestions were provided for the later engineering design. Finally, the size effect of rockfill materials was studied to obtain more accurate constitutive parameters for deformation predicting, which plays an important guiding role in designing deformation control methods. The influence of size effect of particle strength on the scale effect was studied using the combined finite-discrete element method (FDEM), and the numerical results showed that the particle strength decreased with the increase of the maximum particle size.

Key words: Concrete face rockfill dam, deformation control, scale effect, particle strength, mesoscopic mechanism

1. INTRODUCTION

Concrete face rockfill dams (CFRDs) have been quickly adopted because of their safety, economy and adaptability to topography and geologic conditions. The impermeable layer of a CFRD is usually the concrete slab and the associated watertight joints between the concrete panels and the plinth. The concrete slab covers the upstream slope of the CFRD and is connected to a plinth by a flexible watertight joint. To maintain the impervious barrier and sealed joints, the rockfill must not experience excessive or uncoordinated deformations.

The deformation of rockfill material can be ascribed to various factors, such as the initial porosity or degree of compaction, properties of the parent rock, rockfill gradation, water content, and granule shape. For 100-m-level CFRDs, the deformation, especially the post-construction deformation of the rockfill, is negligible due to the lower height of the dam. Consequently, the slab damage is not prominent. However, for 200-m-level CFRDs, the impact of post-construction and uncoordinated deformation on the slab cannot be neglected (Clements 1984; Cooke 1984，1993， 1997,2000; Cooke and Sherard 1985, 1987; Fitzpatrick 1985; Hunter and Fell, 2003; Myoung et al. 2008).

Generally speaking, the development of CFRDs coincides with the evolution of dam deformation control methods. Early rockfill dams were composed of loose dumped rockfill, and most of those dams were not high because of the uncontrollable nature of the rockfill. The Cethana (110 m height) and Foz de Areia (160 m height) dams are considered two landmark projects (Fitzpatrick et al. 1982; Parkin 1985; Pinto et al. 1985). Although the two dams adopted the same rolling technique (rolling four times using a 10 t-level vibratory roller with similar rolling thickness and watering amount), their settlements are very different: the settlement of the Cethana Dam is only 56 cm (0.51% of the dam height), while the settlement of the Areia dam is up to 387 cm (2.4% of the dam height). The differences between the two dams are mainly the dam height and the valley’s aspect ratio, the main reason for high deformation for Foz de Areia dam is the low uniformity coefficient of the basalt rockfill (Hunter and Fell, 2003). The porosity and compactness of the rockfill obtained by the 10 t-level vibratory roller show a good match for these dams with different heights. However, when extended to a CFRD with a height of 160 m, considerable deformation is inevitable, as demonstrated by the latter two dams, which exceed 160 m. More specifically, the Aguamilpa Dam, with a 187 m height, built in 1993 and the Tianshengqiao Dam, with a 178 m height, built in 2000 both showed significant deformation and slab cracking (Zhang 2004).

After construction of the Tianshengqiao CFRD, three 200-m-high CFRDs in Hongjiadu, Sanbanxi and Shuibuya were built by learning from the experience of the Areia and Tianshengqiao dams. Comprehensive experiments and computational analyses were performed to control the post-construction, and uncoordinated deformation and systematic control techniques can be summarized (Zhou 2006). All three dams have been completed, and the maximum settlements are all controlled within 1% of the dam height. The post-construction deformation is also stable.

Based on the lessons learned from the completed CFRDs, this paper analyzes and discusses the selection of parent rock, rockfill zoning, compaction standards, and construction procedures. This work is organized as follows: first, a brief introduction is presented to describe the four completed 200-m-high CFRDs in China. The measured deformation data of these four CFRDs are presented in the next two sections. In the second section, a comprehensive discussion of the deformation control methods is presented. In the third section, numerical experimentation of scale effect was carried out to reveal the generation mechanism of scale effect from the meso-scopic level. Finally, the conclusion summarizes the control methods and offers suggestions.

2. THE 200-M-HIGH CFRDS IN CHINA

Since China began to build CFRDs in 1985, they have been widely adopted because of their excellent security, economy and flexibility. According to incomplete statistics, China has already built or is building more than 150 CFRDs, among which approximately 40 are over 100 m high and 4 are over 150 m high, viz., Tianshengqiao, Hongjiadu, Sanbanxi and Shuibuya. The 200-m-high CFRDs of the world are summarized in references (Yang 2007; Xu 2008).

The Tianshengqiao CFRD is located in the Nanpanjiang River in China, approximately 240km from Guiyang City. This CFRD is 178 m high, the upstream dam slope is 1:1.4, and the downstream-integrated dam slope is also 1:1.4. This CFRD's crest is 12 m wide and 1,104 m long, and the filling materials are approximately 18 million m^3, of which 4.8 million m^3 are soft rock materials, accounting for 27% of the total filling and used in secondary rockfill zone. Construction began in 1995 and was completed in 2000.

The Hongjiadu CFRD, lying in the downstream of the Liuchong River, which is the north headstream of the Wujiang River, is located at the junction of Qianxi County and Zhijin County in Guizhou Province and is 154 km from the northwest of the provincial capital, Guiyang City. The CFRD is 179.5 m high, and its construction began in March 2002 and was completed in 2005.

The Sanbanxi CFRD is located in the upstream of the Yuan River in Jinping County, Guizhou Province. The CFRD is 185.50 m high, the crest is 10.00 m wide and 423.3 m long, and the upstream and downstream dam slopes are both 1:1.4. Construction began in July 2003 and was completed in January 2007.

The Shuibuya dam, the highest CFRD in the world, is 233 m high and 675 m long at its crest. Construction of the dam began in March 2003 and was completed in October 2006. The reservoir was filled in several stages from October 2006 to November 2008. The rockfill zoning and construction process of the Shuibuya CFRD have already been described in detail by Zhou (2010, 2011).

3. DEFORMATION CONTROL METHODS FOR HIGH CONCRETE FACE ROCKFILL DAMS

The deformation control methods are discussed in detail in the following sections as follows: the selection of the parent rock, compaction standards, rockfill zoning, the impact rolling technique of rockfill, the pre-settlement of rockfill and construction procedures.

3.1. Physical Characteristics of Parent Rock

For high CFRDs, the filling material should be hard rock with good compaction properties and high shear strength, such as limestone or granite. Soft rocks, such as mudstone and shale, with a lower mechanical strength and deformation modulus, are easily collapsed and weathered, even muddy. Therefore, soft rocks used as rockfill materials may cause problems such as a low compression modulus, large dam deformation, and low permeability. Overall, the correct selection of the parent rock is an important basis for the dam's deformation control. Part of the rockfill material for the Tianshengqiao CFRD was soft rocks with a mixture of sandstone and mudstone. Excessive dam deformation and subsequent slab extrusion breakage are attributed to the low compressive modulus of the rockfill material.

After the construction of the Tianshengqiao CFRD, the Shuibuya, Hongjiadu, and Sanbanxi CFRDs mainly used hard rock (the uniaxial saturated compressive strength of which is greater than 60 MPa) or medium hard rock (the uniaxial saturated compressive strength of which is greater than 30 MPa) as the parent rock (Table 1). This type of rockfill has a higher strength and deformation modulus compared with rockfill composed of soft rock fragments.

3.2. Compaction Standards of Rockfill

The compaction standard of rockfill is the key factor for controlling the deformation of CFRDs. The compaction standard is usually defined in an empirical manner based on the project grade, dam height, shape of valley and quality of the parent rock. The CFRD compaction standards commonly used in China are the dry density or porosity ratio and compaction construction parameters. A collection of compaction standards of 200-m-high CFRDs built worldwide is shown in Table 1.

The main rockfill zone of the Aguamilpa Dam is filled with gravel with good gradation and a low porosity of 15.25%. The porosity of the transition rockfill zone is less than 20%. The deformation modulus of the rockfill was estimated based on the prototype monitoring value (Myoung et al. 2008). The deformation modulus of the downstream rockfill zone (43-47 MPa) is only 18% to 20% of the main rockfill zone (221-260 MPa) and is approximately 30% to 36% of the transition zone

(130-145 MPa). The significant difference in the deformation modulus between upstream and downstream rockfill is probably the main reason for the concrete slab cracks at or near the uppermost horizontal construction joint across the face of the dam. At an elevation of 180.0 m, there was a subsequent sharp increase in leakage for nearly one year after the first water impoundment. During the construction period, however, there was no significant deformation difference between the upstream and downstream, which indicates that the deformation of the rockfill also has a significant relationship with time in addition to the initial porosity ratio.

Table 1. The characteristics of rockfill for 200-m-high concrete face rockfill dams in the world

Name	Rockfill zoning	Lithology of rockfill	Hardness	Porosity (%)	Dry density (g/cm^3)	Maximum size	Uniformity coefficient	Curvature coefficient
Shuibuya	Main rockfill zone (III B)	Limestone	Hard rock	19.6	2.18	800	23.4	1.38
	Second rockfill zone (III C)	Limestone	Hard rock	20.7	2.15	800	27.4	1.61
	Downstream rockfill zone (III D)	Limestone	Hard rock	20.7	2.15	1200	35.4	1.20
Sanbanxi	Main rockfill zone (III B)	Tuff	Hard rock	19.33	2.17	800	27.3	1.62
	Second rockfill zone(III CA)	Tuff	Hard rock	19.48	2.15	-	-	-
	Downstream rockfill zone (III CB)	Tuff	Hard rock	20.07	2.15	-	-	-
Hongjiadu	Main rockfill zone (III B)	Limestone	Hard rock	20.02	2.18	600	30.73	1.51
	Specific rockfill zone (III BB)	Limestone	Hard rock	19.69	2.19	300	36.11	1.43
	Second rockfill zone (III C)	Limestone	Hard rock	22.26	2.18	600	53.8	2.07
	Downstream rockfill zone (III E)	Limestone	Hard rock	22.26	2.12	--	-	-
Tianshengqiao	Main rockfill zone (III B)	Limestone	Hard rock	23	2.1	600	28.45	1.43
	Second rockfill zone (III C)	Sand-mud mixture	Soft rock	22	2.15	--	-	-
	Downstream rockfill zone (III D)	Limestone	Hard rock	24	2.05	-	-	-

The main rockfill and downstream rockfill zones of the Tianshengqiao CFRD are composed of limestone rock fragments with a porosity of 23% to 24%. A mudstone mixture with a porosity of 22% was used in the construction of the secondary rockfill zone. Compared with the Aguamilpa CFRD, the porosity of the Tianshengqiao CFRD is on the high side. There was significant settlement deformation during the construction and operation period of the Tianshengqiao CFRD because of its loose compaction standard.

In the previous CFRD's construction, the compaction standards of the main rockfill zone are much stricter than the secondary and downstream rockfill zones, and Aguamilpa and Tianshengqiao CFRDs are typical cases. Table 1 shows that in the Sanbanxi, Hongjiadu and Shuibuya CFRDs, the porosity of each rockfill zone is approximately 20%. Moreover, the difference of the porosity between the main and secondary rockfill zones is no more than 1.1%. These high CFRDs are currently running well, and no destructive slab cracks have been found.

To sum up the experience of 200-m-level high dams, the porosity of the rockfill zone should be less than 20%. To take full advantage of excavation materials, the secondary rockfill zone can be set. However, for the main and secondary rockfill zones, the porosity and deformation modulus should be basically the same to ensure that the deformation is as small as possible after water impoundment, thereby reducing the possibility of slab and sealing equipment destruction.

3.3. Pre-settlement of Rockfill

For high CFRDs, rockfill pre-settlement is usually necessary, which means the construction of the concrete slab is postponed until the time-dependent deformation of the rockfill is stabilized. Based on this method, the time-dependent deformation of rockfill will not cause the concrete slabs to develop structural cracks. Table 2 presents the pre-settlement time of several high CFRDs. The pre-settlement time of the Hongjiadu, Sanbanxi and Shuibuya CFRDs were 3 ~ 7 months before the slab construction.

For the Tianshengqiao CFRD, the concrete slab was built within a month after the dam's completion. Due to the absence of pre-settlement, the separation phenomenon occurred between the top of the slab and the rockfill during construction. At the same time, the top of the temporary section showed 15 ~ 20-cm-wide cracks, and the number of cracks observed was approximately 30. However, the Hongjiadu and Shuibuya CFRDs adopted the pre-settlement measure before the construction of the slab. Therefore, the time-dependent deformation was almost finished before construction of the slab, and the adverse effects of the time-dependent deformation on the slab were effectively reduced.

Table 2. The pre-settlement time (month) of typical high concrete face rockfill dams in China

Name	Before construction of the first stage concrete face slab	Before construction of the second stage concrete face slab	Before construction of the third stage concrete face slab
Shuibuya	6	3	3
Sanbanxi	6	6	5
Hongjiadu	7	3	3
Tianshengqiao	0	0	0

By analyzing the experiences of the Hongjiadu and Shuibuya CFRDs, this paper summarizes the two control standards of pre-settlement for high CFRDs. One is that the pre-settlement time should be long enough for the rockfill to settle below the top elevation of the slab, and 3 ~ 7 months is commonly used in the high CFRDs in China. Another is that the settlement rate of rockfill lying below the slab should be stabilized before the construction of each phase of slab, and monthly settlement should be no more than 2 ~ 5 mm.

4. THE SCALE OF ROCKFILL MATERIALS

4.1. Numerical Samples

In order to eliminate the effect of different compactness on macroscopic strength and deformation characteristics, four cubical samples (as shown in Fig. 1) of different size are prepared (the relative density is 90%). It can be considered that the macroscopic mechanical properties shown by the samples of different size result from the size effect of particles themselves. The volume fraction of samples is defined as the percentage that the particle volumes of equivalent diameter less than a certain value account for the total particle volumes. The volume fraction of sample linearly varies from the minimum particle size to maximum particle size.

Several input parameters are required in the numerical simulations. Some parameters can be determined directly by regular physical mechanical tests, such as particle density, elastic modulus and Poisson ratio. Besides, there are some other parameters like friction angle between particles, normal and tangential contract stiffness. Table 3 shows the parameters that used in this work.

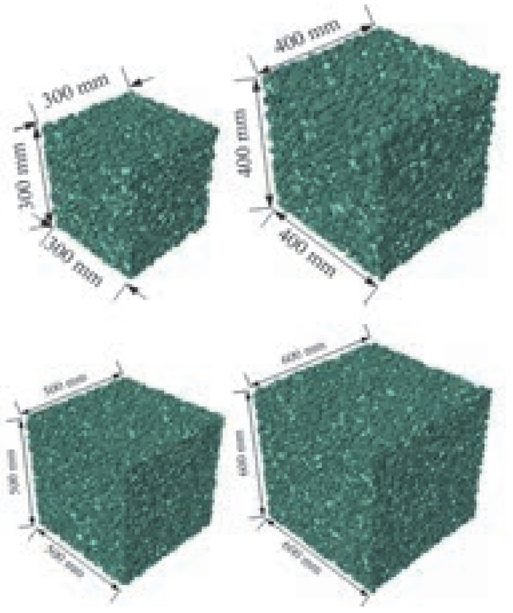

Figure 1. Numerical samples of different sizes

Table 3. Calculation parameters used in the simulations

Calculation parameters		Value
FEM	Density (kg/m^3)	2700.0
	Elastic modulus for mother stone of particles(GPa)	40.0
	Passion ratio of the mother stone	0.2
DEM	Friction coefficient of particles $\tan\varphi_u$	0.5
	Abnormal contact stiffness(N/m^3)	40×10^9
	Ratio of stiffness K_s/K_n	0.4
	Friction coefficient between particles and boundary	0.0

4.2. Size Effect of Particle Strength

The crushing characteristics of particle aggregate are based on the survival probability model with Weibull distributions in this paper.

$$P(d) = \exp\left(-\left(\frac{d}{d^0}\right)^3 \left(\frac{\sigma}{\sigma^0}\right)^m \right) \tag{1}$$

where σ is the stress acting on particles; m is a parameter of Weibull probability distributions, which reflects the rate of divergence of particle strength; d^0 is the particle size corresponding to the 37% survival probability and σ^0 is the characteristic stress acting on it.

Two aggregates of rockfill particles are considered and they are obtained by blasting on the same material field, and the two aggregates are expressed respectively by r_a, r_b and their survival probability model is assumed as P(d_a)=P(d_b), and because the two aggregates of rockfill particles are blasting from the same mother rock so that they possess the same microcrack density. The parameters of the two aggregates for Weibull distribution should also meet the following:

$$\left.\begin{array}{l} d_a^0 = d_b^0 \\ \sigma_a^0 = \sigma_b^0 \\ m_a = m_b \\ d_a^3 \sigma_a^m = d_b^3 \sigma_b^m \end{array}\right\} \tag{2}$$

The stress acting on the particle whose diameter is d_b is assumed as σ_b in the aggregate of particles r_b. In the aggregate of particles r_a, when the stress σ_a acting on the particle whose diameter is d_a meets the Eq. 3, both of them have the same survival probability.

$$\sigma_a = \sigma_b \left(\frac{d_b}{d_a} \right)^{\frac{3}{m}} \propto d_a^{-\frac{3}{m}} \tag{3}$$

The size effect of particle strength is reflected by Eq. 3. The crushing tests of a single particle are carried out and the use of power type to describe the relation between crushing load F and diameter d_a of particle is provided:

$$F_a = \eta d_a^{\lambda} \tag{4}$$

where η, λ are the fitting parameters of the model.

The stress σ_a of eq. 5 is proportional to the ratio of crushing load F_a and cross sectional area of particle which is proportional to the square of particle diameter d_a, namely:

$$\sigma_a \propto \frac{F_a}{d_a^{\ 2}} \tag{5}$$

Eq. 6 can be obtained by combining Eqs. 3, 4 and 5：

$$\left. \begin{aligned} & \sigma_a \propto \eta d_a^{\lambda-2} \\ & \lambda = 2 - \frac{3}{m} \end{aligned} \right\} \tag{6}$$

The value range of parameters λ is from 1.2 to 1.8 in rockfill materials, and the corresponding parameters of Weibull distribution is between 4 and 15.

4.3. The Macroscopic Mechanics Responses

Confining pressures of 0.8 and 1.6 MPa are considered in the numerical experiments. 40 numerical experiments are conducted with different values of λ. Limited by space, only part of the results under the confining pressures of 1.6 MPa is presented and analyzed.

The curves of peak internal friction angle along with the change of sample size are shown in Figs. 2. The figures show that size effect is not existed in particle strength when parameter λ=2 and the four samples simultaneously own the same relative density and diameter ratio, so the same macro-mechanical characters are expressed by the numerical samples of different size; the peak internal friction angle decreases with the increase of the maximum particle size as parameter λ<1.8. The smaller the parameter λ is, the more obvious size effect of particle strength is. For example, when parameter λ=2, the peak internal friction of 600 mm samples is just 0.13% smaller than the 300 mm diameter samples, but the peak internal friction of 600 mm samples is 2.1% smaller than the 300 mm diameter samples as parameter λ=1.2.

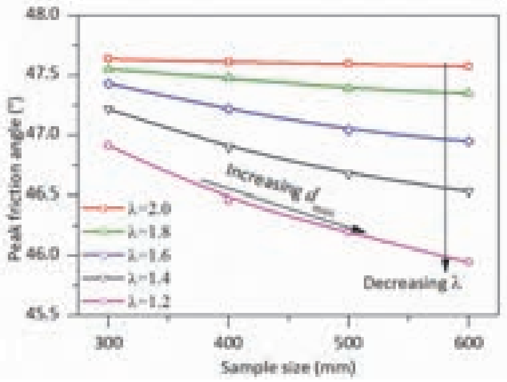

Figure 2. Curves of peak internal friction angle of different size effect parameter of particle strength versus sample size

5. CONCLUSION

This paper mainly analyzed the deformation monitoring data of several 200-m-high CFRDs. To reduce post-construction deformation and avoid uncoordinated deformation, several deformation control measures have been adopted for high CFRDs in China, such as selecting hard parent rock and applying high compaction standards for rockfill and rockfill zoning. The successful application of the impact rolling technique in the Hongjiadu CFRD provides another choice of rolling technique. Several recently developed CFRDs in China have adopted this technique. The pre-settlement method can effectively reduce the influence of time-dependent deformation on the stress of the slab. Reasonable construction procedures can effectively diminish the non-uniform deformation of the dam to prevent slab cracks. The simulation results show the peak internal friction angle decreases with the decrease of the size effect parameter of particle strength. The peak internal friction angle decreases with the increase of the maximum particle size under the same parameter λ.

REFERENCES

Clements, R.P.(1984): Post-construction deformation of rockfill dams, Journal of Geotechnical Engineering, 110:7, pp. 821-840.

Cooke, J.B. (1984):Progress in rockfill dams, Journal of Geotechnical Engineering, 110:10, pp. 1383–1414.

Cooke, J.B., and Sherard, J.L. (1985): Concrete Face Rockfill Dams: Design, Construction, and Performance, Proceedings of the 2nd Symposium, ASCE, New York. pp. 1–658.

Cooke, J.B., and Sherard, J.L. (1987): Concrete face rockfill dam: II Design, Journal of Geotechnical Engineering, 113:10, pp. 1113–1132.

Cooke, J.B. (1993): Rockfill and the rockfill dam, Proc., Int. Symposium on High Earth-Rockfill Dams, Chinese Society for Hydro-electric Engineering, Beijing, pp. 1–24.

Cooke, J.B. (1997): The concrete face rockfill dam, Non-Soil Water Barriers for Embankment Dams, 17th Annual USCOLD Lecture Series, United States Committee on Large Dams, San Diego, pp. 117–132.

Cooke, J.B. (2000): The high CFRD dam, Proc., Int. Symp. on Concrete Face Rockfill Dams, International Commission on Large Dams, Paris, pp. 1–4.

Fitzpatrick M.D., Liggins T.B. and Barnett R.H.W. (1982): Ten years surveillance of Cethana dam, In Proceedings of the

14th ICOLD Congress, Q55(R30), Rio de Janeiro, IWP & DC, pp. 847–865.

Fitzpatrick, M.D., Cole, B.A., Kinstler, F.L., and Knoop, B.P. (1985): Design of concrete-faced rockfill dams, Proc., Symp. on Concrete Face Rockfill Dams-Design, Construction and Performance, ASCE, New York, pp. 410–434.

Hunter, G and Fell, R. (2003): Rockfill modulus and settlement of concrete face rockfill dams, Journal of Geotechnical and Geoenvironmental Engineering, 129:10, pp. 909-917.

Christophe, D., Erick, M., François, D., Pierre-Yves, H. and Wei, H. (2011): Effect of sample size on the behavior of granular materials, ASTM geotechnical testing journal, 34:3, pp. 186-197.

Keming, C., Zhongping, and Caichangguang. (2007): Design research for very high CFRD, In Proceedings of the Workshop on High Dam Know-how, pp. 18–35.

Massarsch, K. R. and Fellenius, B. H. (2002): Vibratory compaction of coarse-grained soils, Canadian Geotechnical Journal, 39:3, pp. 695-709.

Marsal, R. J. (1967): Large scale testing of rockfill materials. Journal of the Soil Mechanics and Foundations Division, 93:2, pp. 27-43.

Myoung-Soo, W. and You-Seong, K. (2008): A case study on the post-construction deformation of concrete face rockfill dams, Canadian Geotechnical Journal, 45:6, pp. 845-852 .

Parkin, A.K. (1985): Settlement rate behavior of some rockfill dams in Australia, In Proceedings of the 11th ICSMFE, Vol. 4, pp. 7–10.

Pinto, N.L.D.S., Marques Filho, P.L., and Maurer, E. (1985): Foz do Areia dam-design, construction, and behavior, Proc., Symp. on Concrete Face Rockfill Dams: Design, Construction and Performance, ASCE, New York, pp. 173–191.

Xu, Z.P. and Deng, G. (2008): Development of high CFRD and key technologies for building super-high CFRD, Journal of Hydraulic Engineering, 39:10, pp. 1226–1234.

Yang, Z.Y.and Zhou, J.P. (2007): Construction and technique prospective on super-high concrete face rockfill dams in china, Water Power, 33:1, pp. 64–68.

Zhang, B.Y., Wang, J.G. and Shi, R.F. (2004): Time-dependent deformation in high concrete-faced rockfill dam and separation between concrete face slab and cushion layer, Computers and Geotechnics, 31:7, pp. 269-280.

Zhou, W and Chang, X.L. (2006): Three dimension FEM numerical simulating of the rockfill creep of high concrete face rockfill dam, Rock and Soil Mechanics, 27:8, pp. 1389–1392.

Zhou, W, Chang, X.L., Zhou, C.B. and Liu, X.H. (2010): Creep analysis of high concrete-faced rockfill dam, International Journal for Numerical Methods in Biomedical Engineering, 26:11, pp. 1477-1492.

Zhou, W., Hua, J.J., Chang, X.L. and Zhou, C.B. (2011): Settlement analysis of the Shuibuya concrete-face rockfill dam. Computers and Geotechnics, 38:2, pp. 269-280.

4th APG Symposium and 9th EADC on

INNOVATIVE TECHNOLOGIES FOR DAMS AND RESERVOIRS TOWARD THE FUTURE GENERATIONS

Improvement of Deformation Prediction of Rock-fill Dam with GPS Measurement

H. Soda, S. Nigo & N. Sato
Water Resources Engineering Department, Japan Water Agency, Japan
hideki_soda@water.go.jp

ABSTRACT:

Accurate and continuous data accumulation of deformation measurement of dam body is important for proper dam safety management. Regarding the improvement of the accuracy of rock-fill dam deformation survey, there are problems that the measurement frequency is low and the accuracy may be affected by slight differences in measurement techniques and by observer. In recent years, Global Positioning System (GPS) measurement system which enables us to measure the exterior deformation of rock-fill dam bodies continuously, accurately and three-dimensionally have been developed and is experimentally introduced in about 20 dams in Japan. The authors, based on the approximate expressions corresponding to the long-term settlement of the embankment, have proposed approximate expressions of settlement and the horizontal displacement by using the GPS measurement data in Tokuyama Dam. As a result, predicted deformation by using the approximate expressions well matched to the value measured by GPS measurement system. Based on the research results in Tokuyama dam, it is possible to monitor other dams by proposing approximate expressions using the same method that utilizes the features of the GPS of high precision and continuous observation data.

Keywords: fill dams, GPS measurement, exterior deformation, approximate expressions

1. INTRODUCTION

Aging of structures constructed during the rapid growth period of Japan has recently been much talked about, and implementation or review of reinforcement or reconstruction of social infrastructures is conducted in response to such apparent situation. It is important to understand the current condition of the structures in order to properly maintain those facilities and conduct appropriate reinforcement or reconstruction work. The Japan Water Agency (JWA) has been operating many dams, include over 50 years old. Authors has accumulated measuring result of eight rock-fill dams JWA manages, and regularly conducts cross-sectional safety checks and evaluation of dam body behavior of all of them.

In safety management of an embankment dam, measurement of external deformation of dam body is one of the most important items along with seepage measurement. To check those items, it is necessary to keep monitoring the dam body during its service years.

In addition, immediately after such a catastrophe as an earthquake and a large-scale flood, Dam owners will promptly need to ensure that the safety of the dam body and the prerequisite functions of the dam are properly maintained together with other regular inspections and observations.

So, the measurement of external deformation requires the long-term monitoring, appropriate level of precision, incessant and correct measurement, and easy maintenance. And furthermore, it has to be carried out as promptly as possible even under unfavorable conditions like the disasters.

Conducting the external deformation measurement continuously with high level of precision, involving three achievement should be payed:

1) Comprehension of dam body deformation behavior in detail;
2) High precision forecast of the possible deformation in the future;
3) Evaluation based on the forecast;

There are increasing number of cases where GPS measurement, which is often used to measure slopes, is also used for deformation measurement as part of the policy to refine dam body measurement. GPS measurement is capable of making continuous, highly accurate and three-dimensional measurement. When it is applied to dam body measurement, it is expected to produce various positive effects, including the capability of making measurement more accurate than the conventional methods and early detection of displacement caused by, for example, an earthquake.

With this concept, JWA has been developing a new high-precision deformation measurement method with the use of GPS at a few dams. The authors wanted to make an index for safety management by using the reliable measurement result using the GPS measurement.

The authors, based on the approximate expressions corresponding to the long-term settlement of the embankment, have proposed approximate expressions of settlement and the horizontal displacement by using the GPS measurement data of Tokuyama Dam. As a result, predicted deformation by using the approximate expressions well matched to the value measured by GPS measurement system. Based on the research results in Tokuyama dam, it is possible to monitor other dams by proposing approximate expressions using the same method that utilizes the features of the GPS of high precision and continuous observation data.

2. SETTLEMENT AND THE HORIZONTAL DISPLACEMENT OF ROCK-FILL DAM

2.1. Settlement and the horizontal displacement of Rock-fill Dam

Causes of behavior of rock-fill dams are analyzed as in Table 1. Although rainfall, one of the identified causes, affects the amount of water permeation, such influence does not indicate dam behavior. Therefore it is necessary to appropriately remove rainfall factor as a causal factor in question. Hence, it is not included in the table.

Table 1. Causes of behavior of rock-fill dams

		Behavior of the Dam			
		deformation	Settlement	Pressure of foundation	Seepage
Causes of behavior	Temperature	-	-	-	-
	Water level	L, E	S, P	L, E	M, VE
	Rainfall	-	-	-	L
	Consoridation	M, VP	L, VP	-	L,VP
	Clogging			M, VP	
	Earthquake	P	P	P	P

L,M,S: Amount of infuluence. Large, Medium, Small
V,P,E: Type of behavior V: visco, P: plastic, E: elastic

The relationship between the number of days and deformation of the dam is analyzed on the basis of those causes as in Fig. 1 and 2. The decimal logarithm is taken for horizontal axes. 13 rock-fill dams over 100m height are plotted in these figures.

Fig.1 shows relationship between the number of days after their completion and settlement of 13 dams at crest. It is generally understood that the amount of settlement varies depending on dam height, materials, compaction method, and dam shape. In after the lapse of 200 to 300 days after completion of the dam, settlement at the crest has a linear relationship with the logarithm of number of days. As Matsumoto N., et al. 1991 showed.
Fig. 2 shows relationship between the number of days after their initial filling and the amount of horizontal displacement at the crest. As in the case of the settlement, the amount of horizontal displacement greatly varies depending on dam height, materials and compaction method. Although changes occur depending on water level changes, it is presumed that the behavior after the lapse of 300 days has an almost linear relationship with the logarithm of the number of days.

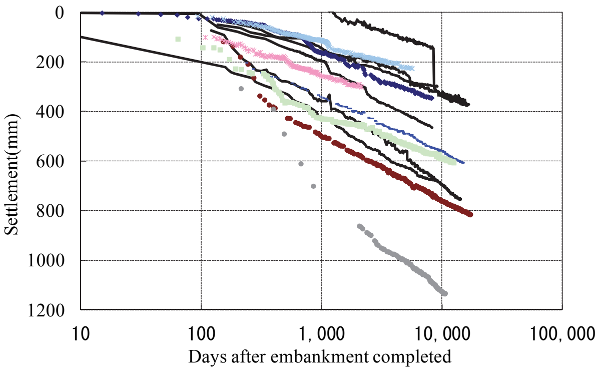

Figure 1. Settlement of rock-fill dams

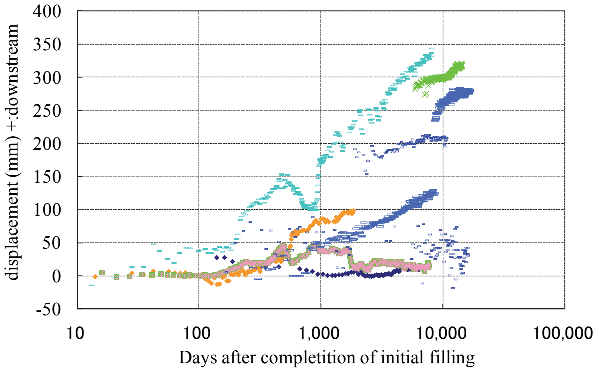

Figure 2. Horizontal displacement of rock-fill dam

2.2 Analysis of Settlement and the Horizontal Displacement of a Rock-fill Dam

According to large-scale testing of rock-fill materials by Marsal, etc., the relationship between the number of days and the amount of settlement when rock materials are compacted shows a time and compression relationship similar to primary and secondary consolidation of cohesive soil. In the experiment results, no fracture occurred in secondary compression, and a linear settlement due to compression is shown relative to the logarithms of the number of days.
Settlement of the rock-fill dam body is characterized by the amount of settlement having a linear relationship with the logarithms of the number of elapsed days. Since this behavior agrees with the test result of Marsal, 1967. etc., it is presumed that the behavior of secondary compression unique to the rock-fill materials comes to emerge in the process of settlement of the dam body. Since it is impossible to list any external force imposed on the dam body other than its dead weight, the amount of settlement of the dam body is logically judged to be caused by creep of the materials.

The components of horizontal deformation of the rock-fill dam, corresponding to temporal changes, are discussed here. Horizontal displacement shows an almost linear relationship with the logarithms of the number of elapsed days. Assuming that part of horizontal displacement is caused by creep that resists hydraulic pressure or by the horizontal components of settlement by the weight, it is considered reasonable that horizontal displacement has a linear relationship with the logarithms of the number of elapsed days as in the case of settlement.

Now deformation in response to horizontal displacement is discussed. Since the allowable range of water level changes is mostly limited at many dams, the influence of water level changes on hydraulic pressure always applied to the dam is considered small. It is also understood that water level changes that occur in ordinary operation will not greatly exceed the range of external force that was experienced in the past. As discussed above, it is logically feasible to think that occurrence of horizontal displacement relative to water level changes has a linear relationship with water level changes.

3. REVIEW ON APPROXIMATE EXPRESSIONS OF SETTLEMENT AND THE HORIZONTAL DISPLACEMENT

3.1.Review on Approximate Expressions for Settlement and the Horizontal Displacement of A Rock-fill Dam

As discussed in 2.1, long-term settlement shows a linear behavior relative to the logarithms of the number of days. This suggests it is feasible to develop an empirical approximation equation. However, the conventional practice of dam body observation with electro-optical measurement had been less frequent. A long period of time was therefore necessary to develop the appropriate approximation equation.

When horizontal displacement occurs, it generally occurs in three mixed ways: 1) the deformation caused by creep as in the case of settlement, 2) the elastic behavior relative to hydraulic pressure changes, and 3) settlement by impoundment in the upstream side rock zone. However, since measurement with electro-optical surveying had been generally conducted once a week even during initial filling and the dam's water level changed much greater while tracking horizontal displacement appropriately by such measurement, it was difficult to conduct future prediction or evaluation. This was the reason why qualitative evaluation had been a primary method of behavior evaluation.

If such viscous and elastic behavior can be separated, it should be able to add a quantitative index to future dam behavior evaluation. The authors attempted to separate viscous behavior from elastic behavior by making detailed observation of the settlement behavior and horizontal displacement behavior of the dam using the results of accurate continuous measurement based on GPS measurement.

3.2. Subject Dam of Evaluation

The Tokuyama Dam owned by the JWA was chosen as the subject of analysis. Fig. 3 shows plan of this dam. More than 5 years passed since completion of initial filling of the Tokuyama Dam in 2008, GPS measurement has been conducted since the beginning of the initial filling, it is reasonable to consider that the dam behavior has entered into a stabilized state.

Initial elastic deformation and its subsequent change to elastic deformation have been observed by GPS measurement system (Yamaguchi Y., et al. (2005)), (J.S.D.E(2014)). This system uses “Trend-model” as error-correction method to correct random noise (Shimizu N., et al. (2014)) and fixed-point observation method to correct tropospheric delay (Nakashima S., et al. (2014)).
Fig. 4 and 5 shows changes in horizontal displacement and settlement of the Tokuyama Dam over time. Correlation between the reservoir level and horizontal displacement of the Tokuyama Dam are shown in Fig. 6.

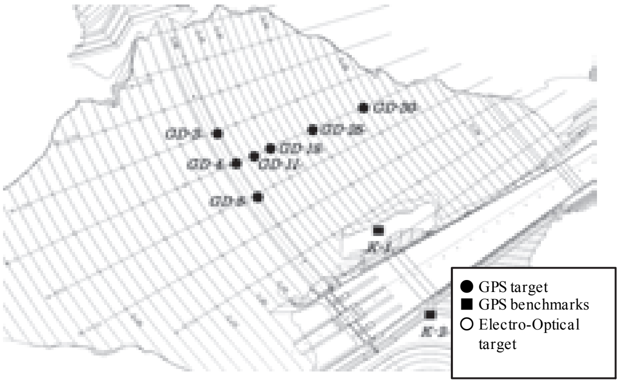

Figure 3. The plan of The Tokuyama Dam

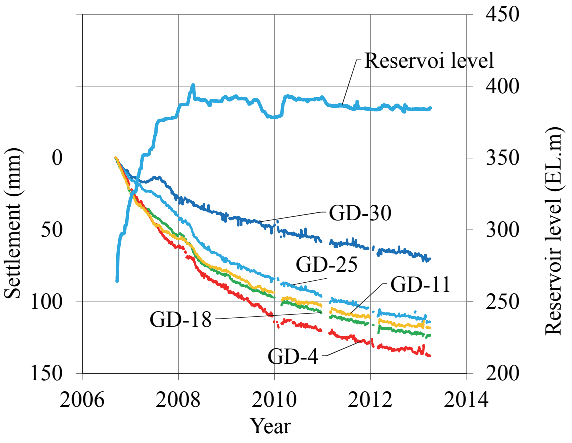

Figure 4. Changes in settlement of the Tokuyama Dam

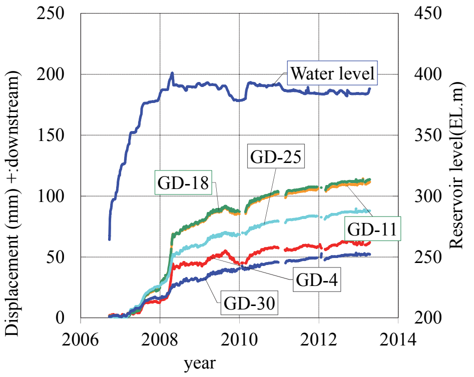

Figure 5. Changes in the horizontal displacement of the Tokuyama Dam

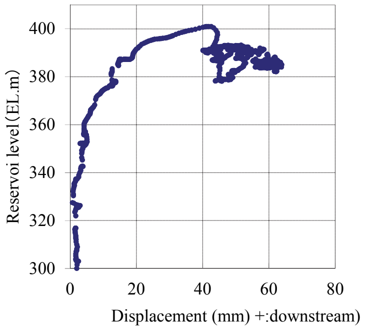

Figure 6. Correlation between the reservoir level and the horizontal displacement of the Tokuyama Dam

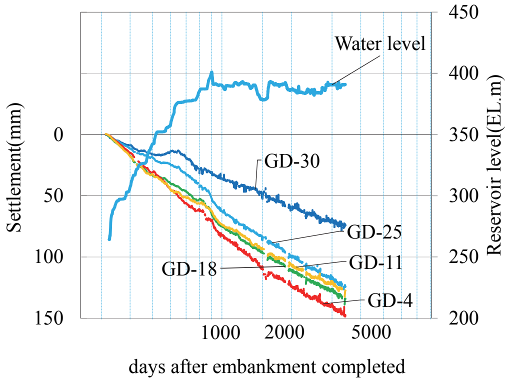

Figure 7. Relationship between settlement and logarithms of number of days

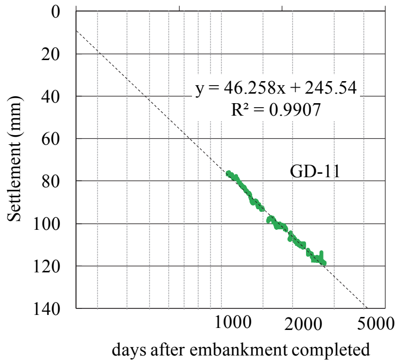

Figure 8. Approximation equation for GD-11

3.3. Evaluation Method of Settlement

Considering the fact that settlement shows linear behavior in its relation to the logarithms of the number of days, a linear approximation equation should be created for the logarithms of the number of days. Fig. 7 shows relationship between settlement and logarithms of number of days after embankment completed, settlement change linear relationship.

The behavior in 1,000 days after the change occurred to the water level showed a linear behavior relative to the logarithms of the number of days.

Fig. 8 shows the approximation equation for GD-11 based on the above review. The calculation result of the approximation equation almost agrees with the actual measurement of settlement, shows Eq.1

$$\delta v = 46.258 \ln (t) + 245.54 \qquad [1]$$

Where

δv: settlement (mm), t: days after completion

3.4. Evaluation Method of Horizontal Displacement

The authors assumed that horizontal displacement would be expressed as the superposition of the compressive deformation in the horizontal direction caused by hydraulic pressure and the elastic deformation caused by water level changes. The evaluation procedure is shown as follows:

(a) Fig.9 shows relationship between days since completion of initial filling and the horizontal displacement. In order to get an entire picture of horizontal displacement, a period that is considered to have linearity was set with the logarithmic of date as in case of settlement. In setting the period, the range that allows evaluation of long-term behavior, which is the purpose of review, was taken into consideration.

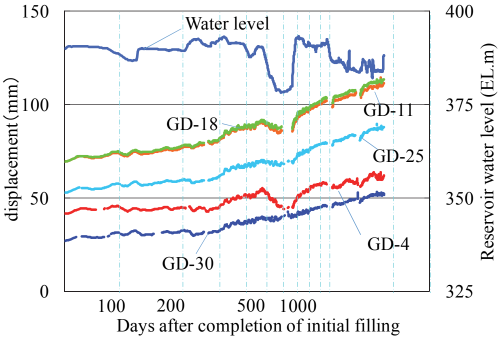

Figure. 9 Relationship between days since completion of initial filling and the horizontal displacement

(b) In the period selected in (a), the amount of horizontal displacement at the time of the same water level was selected and logarithmically approximated to the time axis, as in Fig. 10.

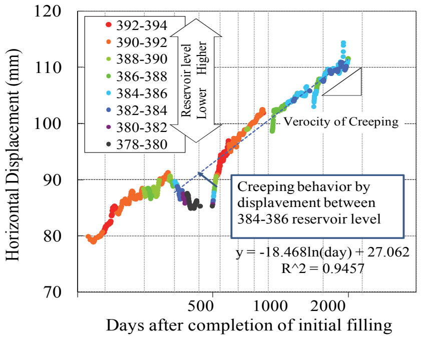

Figure 10. Change of the horizontal displacement with time under the same water level condition (GD-11)

(c) Deformation calculated from the logarithmic approximation equation determined in (b) was deducted from the actual deformation, and the relation with the water level was clarified as in Fig. 11.

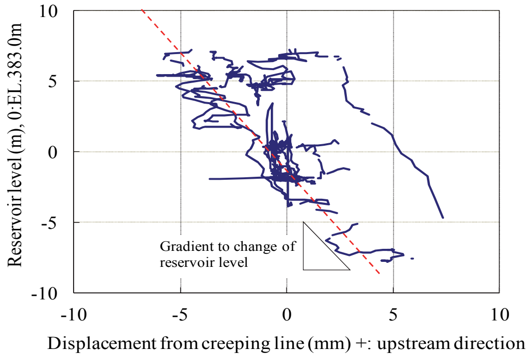

Figure 11. Relationship between the horizontal displacement with temporal change deducted and the water level (GD-11)

1) Setting of the period for assumption of horizontal displacement

The relationship between the number of days since completion of initial filling and the amount of deformation is plotted as in Fig. 9 in order to determine long-term deformation. As indicated by this figure, the amount of horizontal displacement seems to have a linear relationship with the logarithms of the number of days around after the lapse of 200 days.

As shown in Fig. 11, a linear relationship is established for the amount of settlement after the lapse of 100 days. It is therefore presumed that the amount of horizontal displacement would come to have a linear relationship with the time logarithm after the lapse of a certain length of time after experiencing the maximum value of stress as in the case of settlement.

Based on these results, the data obtained after the lapse of 200 days since completion of initial filling were organized for a better understanding.

2) Selection of horizontal displacement at the time of the same water level and logarithmic approximation

The amount of deformation at GD-11 in the period selected in 1) is arranged by the water level, and those values are plotted in different colors as in Fig. 10. Among the water levels shown in Fig. 10, logarithmic approximation was conducted for EL. 382 m to EL. 384 m, which is the range of water levels where the data of the longest period were obtained. The determination coefficient in this case (R^2) is 0.945, which indicates a good correlation.

3) Deduction of deformation speed calculated from logarithmic approximation

The deformation speed obtained from the logarithmic approximation conducted in 2) was deducted from the actually measured deformation to clarify the relationship with the water level as shown in Fig. 11. The reference water level is set to EL. 383.0 m. As shown by Fig. 11, as a result of deduction of the deformation speed, the water level and deformation seem to always draw a locus with a constant gradient. Based on this relationship, displacement of 12 mm is assumed relative to a water level difference of 18 m, and the relationship of 0.67 x 10^{-3} was obtained.

Based on the above relationship, the approximation equation determined for GD-11 of the Tokuyama Dam is Eq. 2.

$$\delta_h = -18.468 \ln(t) + 27.062 + 0.67(h_w - 383) \qquad [2]$$

Where
δh: horizontal displacement (mm; the downstream side is negative)
t: number of days since completion of initial filling (EL. m)
hw: reservoir level at the prediction date (EL. m)

These empirical approximation equations were computed at other GPS measurement points installed at the Tokuyama Dam, and the results did not suggest any points where approximation was impossible.

The superimposition of the measured value of horizontal displacement of the dam body at GD-11 with the predicted value by Eq. 1 is plotted in Fig. 12. This graph shows a good agreement between measurement and prediction.

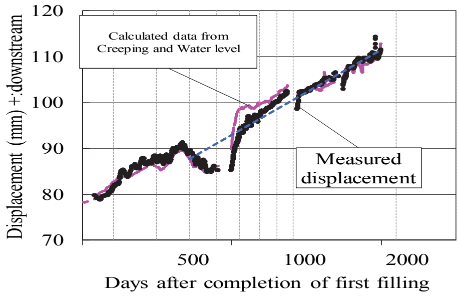

Figure 12. Measurement and prediction of the horizontal displacement (GD-11)

3.5. Applicability of Approximation Equations

It is considered that comparison with the current condition based on the approximation equations prepared based on the range of past data could lead to determine how the present condition has changed from the past. It was assumed that the elapsed time and the water level condition being input to the approximation equations obtained up to 3.4 would enable us to make a simple health check of the dam.

Fig.13 and 14 shows calculated values by approximation equation on 3.3.Eq. 1. and 3.4. Eq. 2. Figures compare values of the calculated and the measured. The data of either settlement or horizontal displacement show a good agreement between the measurement and approximation equations calculation results. When these approximation equations are established in advance and the present and past data are compared, we should be able to establish a simple judgment criterion for the dam stability.

4. CONCLUSION

The authors proposed techniques to measure and evaluate deformation behavior using GPS measurement as part of the process of quantification of behavior evaluation of a rock-fill dam, which had been empirically conducted, based on the existing data. The authors focused on settlement and upstream and downstream deformation and studied a technique to develop approximate equations based on the past data.

The authors attempted to decompose the data into elastic behavior associated with water level changes and viscous behavior relative to the time lapse as a preliminary review for prediction of the amounts of settlement and horizontal displacement of dam body based on the data obtained with GPS measurement. The approximation equations established based on the results of those operations was extrapolated for comparison with the present data. As a result, continuous and highly accurate survey data obtained with GPS measurement should lead to appropriately express the amount of settlement and horizontal displacement. The authors hope to propose a quantitative safety management method based on these research results.

Use of these methods should enable us to ensure appropriate management and future prediction of dam body deformation. The authors intend to work on applicability of the proposed techniques and verify their practicality through analysis of measurement results at other dams.

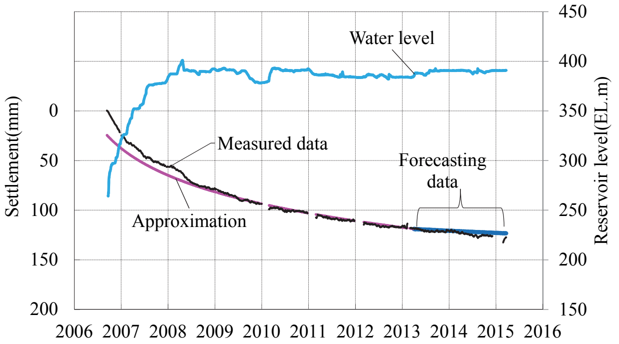

Figure 13. Measurement and approximation of settlement (GD-11)

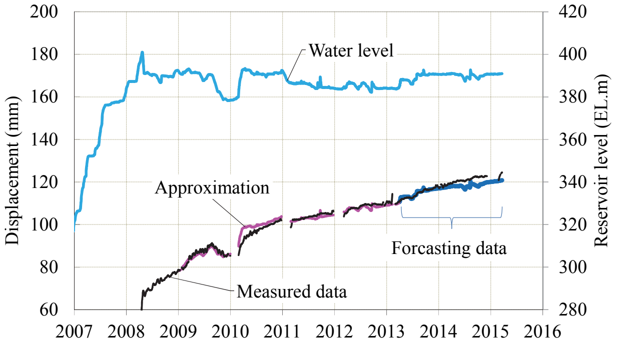

Figure 14. Measurement and approximation of the horizontal displacement (GD-11)

REFERENCES

Matsumoto, N., Yasuda, N. and Itoh. M. (1991): Analyses of behaviours of filldams (Part 1), Technical Memorandum of P.W.R.I, No. 3001 (In Japanese)

Marsal,R.J.(1967) : Large-Scale Testing of rockfill materials, Proc.ASCE, Vol.93, SM2, pp.27-43.

Yamaguchi, Y., Kobori, T., Yokomori, G., Ohno, M. and Iwasaki, T..(2005): Study of measurement of external deformation of fill dams using GPS, Dam Engineering, Vol.15, No.2, pp.120-136.(in Japanese).

Japan Society of Dam Engineers (J.S.D.E)(2014):Engineering Manual on External Displacement Measurement of Embankment Dams Using GPS, Japan Society of Dam Engineers.(in Japanese)

Shimizu, N., Nakashima, S. and Masunari, T.,(2014): ISRM suggested method for monitoring rock displacements using the Global Positioning System (GPS), Rock Mechanics and Rock Engineering, 47(1), pp.313-328.

Nakashima, S., Namba, T., Itagaki, S., Soda, H., Iwasaki, T., Shimizu, N. and Ono K., (2014): Tropospheric delay correction of GPS displacement measurements in the presense of large height differences using fixed-point observation, Journal of MMIJ, Vol.130, pp.479-487 (in Japanese).

4th APG Symposium and 9th EADC on

INNOVATIVE TECHNOLOGIES FOR DAMS AND RESERVOIRS TOWARD THE FUTURE GENERATIONS

GPS Precise Positioning Technology Applied in the Project Deformation Measurement of Xiaowan Hydropower Station

C.Hao, A.Yongping

Huaneng Lancang River Hydropower Co., Ltd., Kunming City, Yunnan Province 650214, China

C.Hao, B.Tengfei, Z.Zhiyong

Hohai University College of Water Conservancy and Hydropower Engineering, Nanjing City, Jiangsu Province 210098, China

Z.Zhiyong

PowerChina Kunming Engineering Co., Ltd, Kunming City, Yunnan Province 650051, China

ABSTRACT:
Xiaowan Hydropower Station built the largest engineering safety monitoring system in China for protecting the Power Plant safety construction and operation. The engineering deformation monitoring system based on GPS precise positioning technology which has been successfully applied in engineering slope, dam and coast in reservoir of Xiaowan Hydropower Project. The framework, technical features and monitoring results of GPS deformation monitoring system were introduced in detail, and it provides a reference and demonstration for the construction of GPS deformation monitoring system of the hydropower projects.

Keywords: Xiaowan Hydropower Station, GPS precise positioning technology, Deformation monitoring

1. FOREWORD

Xiaowan Hydropower Station is situated on the middle-reach section of Lancang River, Yunnan Province, China. It is the second one of the eight cascade power stations planned to be built on the middle to lower reach of the river. The power station primarily works for power generation and also provides other benefits such as flood control and irrigation. With the installed power of 4,200MW. All its major permanent hydraulic structures included the concrete double-curvature arch dam, the back cushion pool and subsidiary dam, the left-bank flood-discharging tunnel, and the right-bank underground diversion power system. The reservoir is designed with multi-year regulation capability. It and was first filled to the normal pool level in October 2012.

In view of the characteristics of the project, as well as its topographic and geological conditions, and construction and operation of hydraulic structures, Xiaowan Hydropoower Station is equipped with a monitoring system which has total 10,761 monitoring apparatuses installed or buried, and is connected to more than 6,500 automation systems. It mainly monitors deformation; seepage and seepage pressure; stress-strain and temperature; supporting effect; seismic response; and environmental variables. The system satisfies the monitoring requirements for engineering safety during the construction, filling, and operation periods of the power station.

Some new safety monitoring technologies that are leading in China were cautiously employed in Xiaowan Hydropower Station during its more than 10 years of construction.Among of these technologies,GPS precise positioning has been successively used for monitoring the deformation of the engineering slope in the hub area, the dam, and the destabilized bodies on the banks of the reservoir.

2. ADVANTAGES OF GPS PRECISE POSITIONING TECHNOLOGY APPLIED TO ENGINEERING DEFORMATION MEASUREMENT

Compared to the approaches adopting traditional technologies for the monitoring of external deformation, GPS precise positioning technology has the following advantages:

Using a monitoring system that is based on the GPS precise positioning technology can fully automate the data acquisition and storage, compilation, calculation, and safety analysis.

GPS monitoring systems are almost immune to external climate, and it can perform all-process online monitoring over buildings and structures on 7x24h basis.

GPS monitoring system can be tailored based on the task, and quickly calculate the measurement data from all monitoring points at a time point, thereby giving real-time feedback on the overall external deformation in engineering works.

3. GPS MULTI-ANTENNA SYSTEM FOR DEFORMATION MEASUREMENT ON ENGINEERING SLOPE IN HUB AREA

Ridge No. 2 is located upstream to the dam abutment on the left bank of the dam site in Xiaowan Hydropower

Station. Downstream to it is the accumulation body of diversion ditch. When excavation proceeded to EL.1,276m in December 2003, the slope deformed and appeared to be abnormal. When the accumulation-body slope were consolidating, including GPS multi-antenna system for deformation measurement, were put into use to provide early-warning on destabilization and guide the emergency response work.

3.1. System architecture and components

The GPS multi-antenna system for deformation easurement consists of three parts, namely, Data Acquisition, Monitoring Center, and Data Communication. Data Acquisition consists of 16 monitoring points and 2 monitoring stations, in addition to 14 monitoring points deployed on EL.1,250-EL.1,500m slope berms on Ridge No. 2. GPS receiver antennas are installed on concrete monitoring piers on which forced centering devices. Each of the two reference points, as well as the monitoring station No.1 and No.2 is equipped with a NovAtel's double-frequency receiver DL-MILLEN-RT2 respectively. Monitoring Center includes data servers and working devices, which receive monitoring data and perform calculation and analysis.

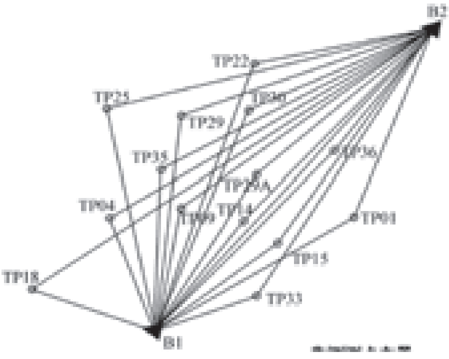

Figure 1. Schematic arrangement of monitoring points and appearance of reference points

3.2. Technical characteristics

(1)Multi-antenna technology is employed. All monitoring points other than the reference points are divided into individual units, each of which consist of 6 or 8 points that share a GPS receiver. The receiver is connected to the reception antenna of each monitoring point through a channel controller, which switches between different channels to connect to the GPS antennas of different monitoring points based on the tailored task and time. By doing so, the controller continuously and cyclically receives the GPS data from each point. See Fig. 2.

(2) A GPS positioning mode and a coordinate calculation approach suitable to the multi-antenna system and the monitoring of slope-surface deformation are selected. The static relative positioning mode is used, with the monitoring period of each monitoring point being 1-2h, the interval of data sampling being 5s. Information about the monitoring station corresponding to the antenna is appended during the acquisition process before data are sent back to Control Center. Data of the reference stations are directly sent back to Control Center. After data from the monitoring points are differentiated from each other and classified, station-center coordinates are calculated primarily through single-epoch resolution, whereby the WGS-84 3D coordinates obtained by each monitoring points through GPS precise positioning are transformed to those in the station-center horizontal coordinate system with reference point B1 as the origin.

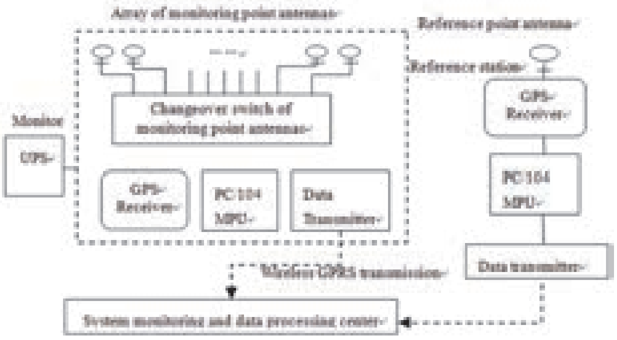
Array of monitoring point antennas
Reference point antenna
Reference station
Changeover switch of monitoring point antennas
Monitor
UPS
GPS Receiver
PC/104 MPU
Data Transmitter
GPS Receiver
PC/104 MPU
Wireless GPRS transmission
Data transmitter
System monitoring and data processing center

Figure 2. Components of GPS multi-antenna system

3.3. Comparison of monitoring results

The system had been operating for 5 years with the overall operating rate of more than 80%. The gross error is located using the robust iterative weighting method with Huber weight function, and the weight of detected gross error is reduced. Fig. 3 indicates that the monitoring result on horizontal resultant displacement obtained from a typical GPS monitoring point follows the same trend as that from its adjacent surface-deformation-monitoring (SDM) point. However, the GPS point does not completely coincide with the SDM point in terms of the plane position. Moreover, the error effect and monitoring time periods are different between the two measurement approaches. Therefore, the amount of deformation is somehow different.

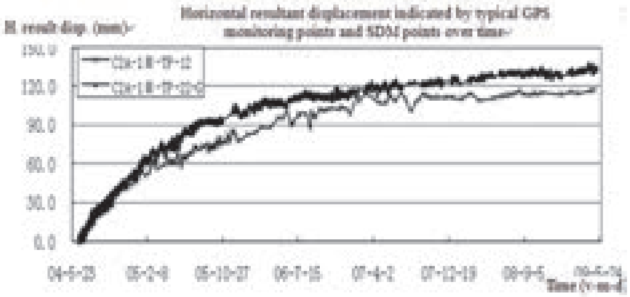

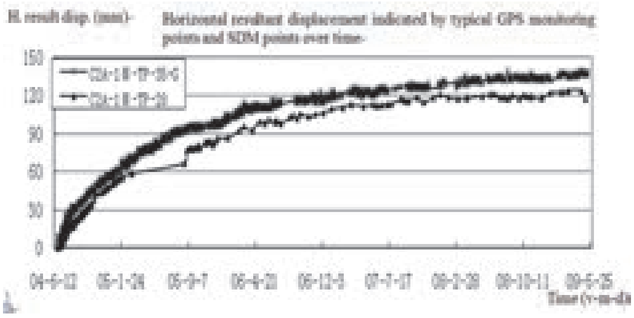

Figure 3. Comparing horizontal resultant displacement indicated by typical GPS monitoring points with that by SDM points on Ridge No. 2

4. GNSS DEFORMATION MEASUREMENT SYSTEM FOR TOP OF CONCRETE DOUBLE CURVATURE ARCH DAM

The concrete double-curvature arch dam of Xiaowan Hydropower Station is the first especially-high arch dam with the height of the 300m class that had ever been built in the world. In addition to these traditional deformation monitoring devices, GNSS monitoring points are set on the top of 15 selected sections to monitor the horizontal and vertical displacement of the dam top in real time.

4.1. System architecture and components

The dam-top GNSS deformation measurement system consists of five parts, namely, Data Acquisition, Data Transmission, Data Control and Analysis, Lightning Protection, and Power Supply. Data Acquisition includes 2 reference points, as well as 15 monitoring points, one on the top of each of the 15 key sections. The system is of single-antenna architecture composing of Leica's AR25 3D choke ring antenna and GMX902GG double-frequency, double-satellite receiver. The antenna and lightning rod are mounted on the top of a monitoring pier, while the receiver is arranged in a device casing at the bottom of the pier. Monitoring Center includes servers and workstations for data analysis and storage, and runs Leica's professional software Spider for data acquisition, management, and calculation, and GeoMos software for data analysis and system integration. Data Transmission is implemented with two systems - optical cable and microwave.

4.2. Technical characteristics

(1) The GNSS system is scalable to receive navigation and positioning signals from multiple satellite systems. A single-antenna GNSS deformation monitoring system was used instead according to the development of GPS monitoring technology and to satisfy the operating needs of the power station. The selected receiver is GMX902, the first high precision multi-frequency, multi-satellite GNSS receiver designed specifically for monitoring applications, which primarily receives American GPS signals in addition to Russian GLONASS signals. Channels are also reserved for EU's Galileo and China's BeiDou-2. Multi-satellite support means that the receiver can receive positioning signals from satellites that are twice or even four times as many as those available if only a single GPS system were used at any time point. This further improves the precision of positioning, and substantially shortens the time required for the calculation of carrier signals.

(2) Sophisticated mutual supplement and verification of deformation monitoring is designed. In order to mutually compensate for and verify the data results from different monitoring systems and ascertain the reliability of the GNSS monitoring system, the receiver antenna and a 360° omni-directional optical prism are arranged in different layers on the coaxial forced centering frame on the top of the monitoring pier. The omni-directional optical prism is manually measured with using the intersection method on a regular time basis and comparison and analysis.

(3) Influence of the multi-path effect resulting from vicinity to a large water body is eliminated. AR25 3D multi-frequency, multi-satellite choke ring antenna is used in order to substantially mitigate the influence caused by the multi-path effect of radio signals resulting from the large-area water body in front of the dam. The antenna provides submillimeter precision of phase center, suppressed radio signal interference. See Fig. 4.

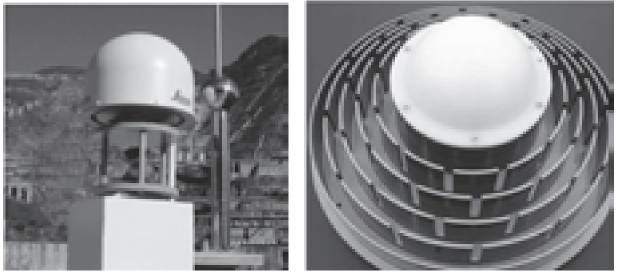

Figure 4.GNSS monitoring points on the top of the dam and AR25 3D choke ring antenna

(4) A GPS positioning mode and a coordinate calculation approach suitable for the monitoring of arch dam body deformation are selected. The system adopts the differential mode of static relative positioning with two base stations. It calculates each baseline from a reference point to a monitoring point using monitoring data in 12-24 hours. Then the coordinates of each monitoring point are obtained. Moreover, variations to dam-top monitoring points can be separately calculated from each reference point. This enables the mutual verification on the data of each monitoring point. The ultimate monitoring result is transformed into Xiaowan arch dam coordinate system; and converted to radial displacement and tangential displacement adapted to the axial direction of each dam section based on the azimuth between the axis and the center line of the arch dam.

4.3. Comparison of monitoring results

Since it was formally brought on-stream on October 27, 2011, the system has been well operating through three filling and depleting cycles of the reservoir. Nine of the dam sections equipped with monitoring points are furnished with pendulum wires for monitoring purpose. The monitoring points on other sections coincide with dam-top SDM points. Therefore, the monitoring data from the SDM points on dam top and the pendulum wires on dam body may be used as the reference for the comparison against GNSS monitoring result. The measurement values of the aforesaid three monitoring systems on November 9, 2011 are selected as the relative initial values and compared against each other. According to Fig.7 and Fig.8, GNSS monitoring result follows the same trend as those of SDM points and pendulum wires in radial and tangential directions under major characteristics water levels. Their measurement values are generally identical to and agree with each other. All these values comply with the deformation pattern of the arch dam in response to the variation of reservoir water load. In radial direction: when the reservoir water level rises, the load increases and the dam body deforms towards downstream; when the reservoir water level drops, the load decreases, and the dam body deforms towards upstream; the radial deformation gradually decreases from the dam section on the riverbed towards the section on the bank slope. In tangential direction: when the reservoir water level rises, all dam sections tend to change towards the slopes on the two banks; when the reservoir water level drops, the sections tend to change towards the riverbed; the tangential deformation is generally symmetrical.

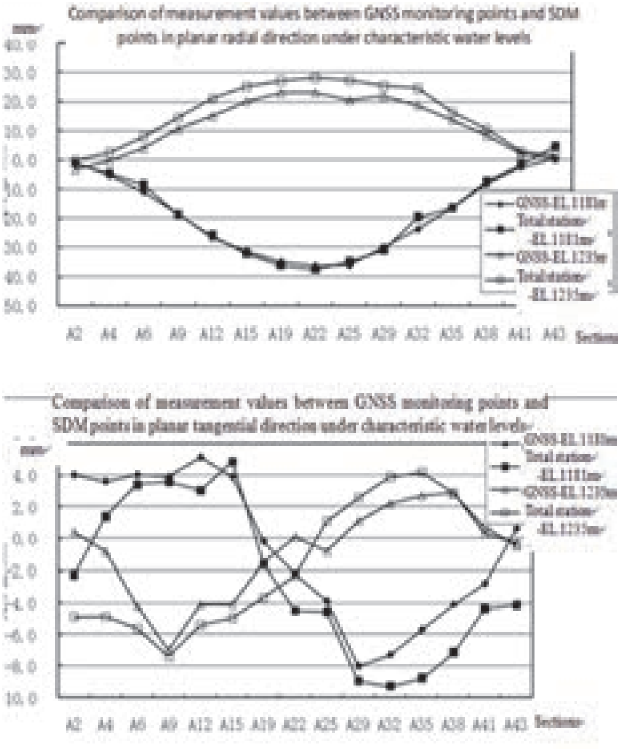

Figure 5. Comparison of measurement values between dam-top GNSS monitoring points and SDM points in planar radial and tangential directions under characteristic water levels

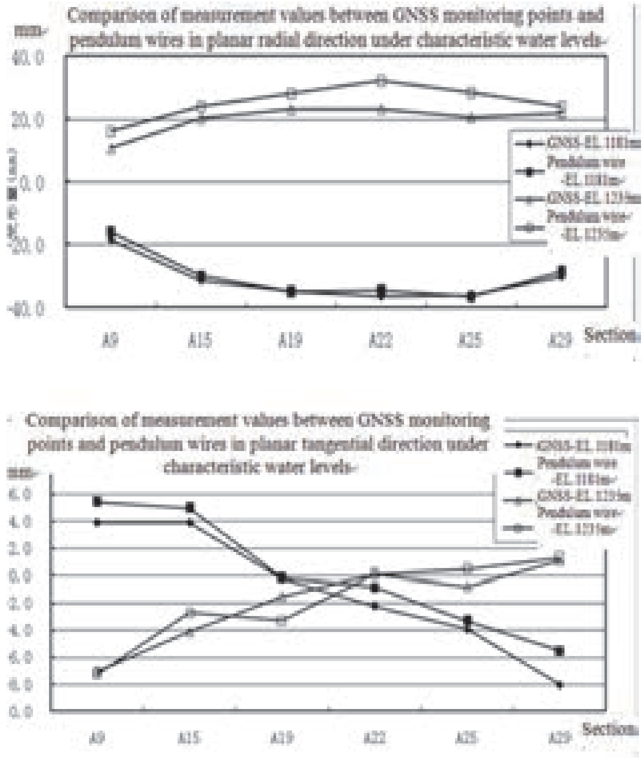

Figure 6. Comparison of measurement values between dam-top GNSS monitoring points and pendulum wires in planar radial and tangential directions under characteristic water levels

5. GNSS DEFORMATION MEASUREMENT SYSTEM FOR DESTABILIZED BODIES ON RESERVOIR BANK

Xiaowan Reservoir began filling water on December 19, 2008 and reached normal pool level for the first time in October 2012. By that time, two reservoirs had been formed, one on the main stream of Lancang River with the backwater length of 178km and the other on the tributary on Heihui River with the backwater length of 123km. During the filling period, destabilization tendency was found on the bank slope at two places in August 2009 and June 2010, respectively. One of the places was in the Bazierduo section as part of the branch reservoir of Heihui River, 3.2km away from the dam site; and the other was in the Xiaoshuijing section as part of the main reservoir of Lancang River, 2km away from the dam site. SDM points were arranged on the destabilized bodies, which were near the hub area, in June 2011 for monitoring on regular time basis. In April 2012, GNSS monitoring points were put into operation on the two destabilized bodies, which improved the real-time and early-warning monitoring.

5.1. System architecture and components

The GNSS system for destabilized bodies in the reservoir area has the same architecture as the dam-top GNSS system. Both systems share the reference point on the high-cable-crane platform on the left bank, as well as the Control Center in the Control Center Building on the right bank. Four GNSS monitoring points are arranged on the main monitoring profile of each of the two slide bodies. The selected receivers are Leica's cost-effective GMX901 integrated single-frequency model for monitoring applications. The model can meet the requirements for low-frequency GPS monitoring of the slide bodies. The antenna and receiver are integrated with each other and enclosed in a disc-shaped casing. Because the monitoring points are far away from Control Center and cabling on the slide bodies is difficult, the points are powered by solar energy. Data are wirelessly transmitted. Each monitoring point is equipped with a directional wireless bridge, which transmits monitoring data to Control Center via the wireless relay station on the right bank of Lancang River.

5.2. Technical characteristics

(1)The GNSS system that is scalable to receive navigation and positioning signals from multiple satellite systems is adopted. Similar to the dam-top GNSS system, the GNSS system for the monitoring of the slide bodies also supports multiple satellite systems, thereby improving its positioning precision and reliability in the region where high mountains and deep valleys exist.

(2) Each monitoring point is equipped with a standalone unit to accommodate for the deformation monitoring of slide bodies. Because the GNSS monitoring points are widely spread on the remote and unstable slide bodies, each of these points is equipped with a standalone unit consisting of an integrated GMX901 receiver, an outdoor solar power supply and storage device, a grounding arrestor, and a wireless communication device. By doing so, each point can independently collect data and will not be affected by any other point that may be damaged by local destabilization of the slide bodies. This effectively improves the viability of the entire data acquisition system. See Fig. 10.

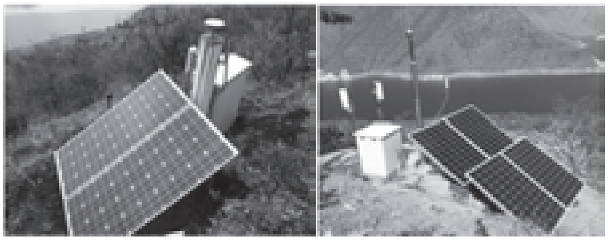

Figure 7. Standalone monitoring unit at a GNSS monitoring point for a slide body

5.3. Comparison of monitoring results

Both of the destabilized bodies on the bank of Bazierduo and Xiaoshuijing reservoir sections are approx. 3km away from the reference point on the cable crane platform on the left bank. With a baseline formed by each monitoring point and the reference point, high-precision 3D positioning coordinates of each monitoring point are obtained around the clock through post-processing, and then inputted into a GeoMoS workstation to analyze deformation of the slide bodies. In the practical monitoring process, the monitoring data from the GNSS monitoring points on the slide bodies were compared to those from adjacent SDM points observed with total stations using the intersection method. For Bazierduo body, the monitoring result of GNSS monitoring points followed the same trend as that of the SDM points. However, the two types of monitoring points do not completely coincide with each other in terms of the plane position, resulting in somehow different amount of deformation. In terms of the Xiaoshuijing body, the monitoring result of GNSS monitoring points gave the same trend and measurement values as the SDM points. See Fig. 11.

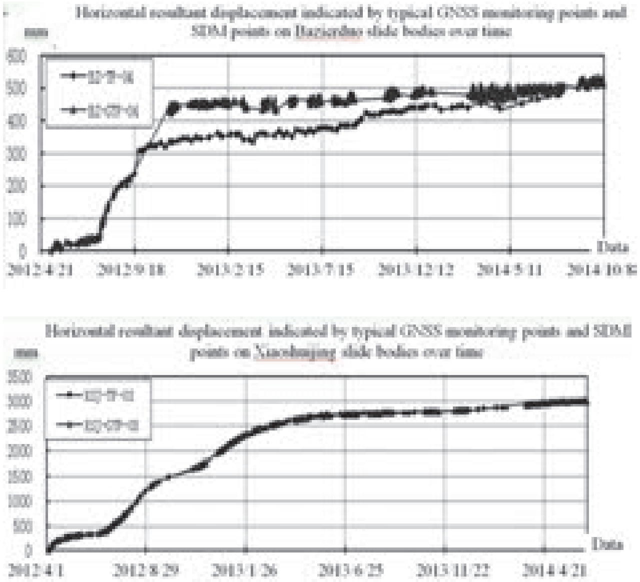

Figure 8. Comparing horizontal resultant displacement indicated by typical GNSS monitoring points with that by SDM points on slide bodies in reservoir area

6. CONCLUSION

GPS precise positioning technology has been successfully applied to the monitoring over external deformation of engineering slope, dam, and destabilized bodies in the reservoir area of Xiaowan Hydropower Station. As an effective means of supplement and verification for traditional monitoring of such deformation, the technology dependably ensures the engineering safety of the power station during its construction, filling, and operation periods.

Throughout its application, the GPS deformation monitoring system has been continuously optimized and improved from a multi-antenna design to the GNSS system for dam top and slide bodies in the reservoir area. As such, it becomes more suitable for the monitoring over the external deformation of different types of structures. Moreover, the quality of obtained data, the operational guarantee, and the cost-effectiveness of system construction have been continuously improved. Especially, the dam-top GNSS deformation measurement system has been the first of its type applied on non-linear dam profiles in a region where high mountains and deep valleys exist in China. The experience summarized and accumulated from the construction and operation of the system has provided a reference and demonstration for the GPS precise positioning technology to monitor dam deformation in later works, including the large-scaled hydropower stations of Nuozhadu, Jin'anqiao, and Guanyinyan etc..

ACKNOWLEDGEMENT

The authors gratefully appreciate the supports from the Foundation for National Key Technology R&D Program (2013BAB06B04) and Joint National Support Program of Yunnan Province (2014GA007).

REFERENCES

Xiao Shenchang, Wang Chong et al. (2014): Application of GPS Multi-antenna System for Real-time Monitoring in Xiaowan Hydropower Station,Water Power, 32(11), pp.22−27.

Dong Zerong et al. (2004):Review of Safety and Stability Monitoring of High Slopes in Xiaowan Hydropower Station. Water Power, Vol.30. (10), pp.74−78.

Wang Chuan, Yang Shanshan, Dong Zerong et al. (2013):Application of GNSS Monitoring System in Safety Monitoring of Xiaowan Arch Dam, Hydropower Automation and Dam Monitoring,Vol.37. (1), pp.63-67.

He Xiufeng et al. (2002): Application of GPS Technology in Hydropower Works and its Outlook,Hydropower Automation and Dam Monitoring, Vol.26. (4), pp.6-9.

4th APG Symposium and 9th EADC on

INNOVATIVE TECHNOLOGIES FOR DAMS AND RESERVOIRS TOWARD THE FUTURE GENERATIONS

Application of Global Positioning System for Dam Deformation Monitoring

H. Arizono, H. Okumura & H. Onishi
Electric Power Development Co., Ltd, Tokyo, Japan
hiroki_arizono@jpower.co.jp

N. Shimizu
Yamaguchi University, Ube, Japan

ABSTRACT:
Renovation of safety monitoring system of existing dams has been becoming one of main issues for dam owners. In this regard, Global Positioning System (GPS) has been applied for dam external deformation monitoring in considerable numbers of existing dams in Japan. Electric Power Development Co., Ltd. which is one of the electricity utility companies in Japan, and owns rather old dams for hydropower stations, has started to utilize GPS for dam deformation monitoring for some years, and it has been applied in five dams. Since GPS enables to obtain the data more frequently than those obtained by the conventional manual measurement, it is useful to figure out deformation characteristics and its long-term trends more precisely. In addition, since digital data can be obtained automatically and transmitted online, it is also useful to acquire the status in real time, even if personnel cannot access to dams. On the other hand, the accuracy of GPS data is prone to be affected by some external factors such as climate conditions, surrounding plants growth. This paper shows continuous monitoring data of dam deformation by GPS through case histories in five dams and their effectiveness as well as countermeasures actually provided to improve foresaid matters.

Keywords: GPS, dam deformation monitoring, renovation of dam safety monitoring

1. INTRODUCTION

Global Positioning System (GPS) has been actively applied to numbers of existing dams in Japan recently for observation of those external deformations. It is expected that monitoring works on dam safety will be highly automated and facilitated by applying GPS. Japan Society of Dam Engineers published guidelines on dam safety monitoring method by using GPS in 2014. The guidelines (Japan Society of Dam Engineers, 2014 ; Shimizu, N., et al. 2014) offered basic information and standards on the system and devices of GPS, selection of measure points, maintenance methods, etc. GPS is expected to prevail widely in Japan as an effective system for monitoring of behaviour and safety of dams.

J-Power (Electric Power Development Co., Ltd.) has conducted observation of deformations of dam bodies by applying GPS at its own five sites of which names are Numappara, Akiha, Funagira, Kuromatagawa No.2, and Miboro. Numappara and Miboro are rock fill type, Akiha and Funagira are concrete gravity type and Kuromatagawa No.2 is concrete arch type. Fig. 1 shows locations of the dams. All the dams were constructed by J-Power for hydropower generation purpose. The following sections present the result of observation by using GPS, its technical knowhow, improvement measures, and other information obtained through the works at each site. Some recommendations for further effective use of GPS are also given based on the experiences on use of the system during some years.

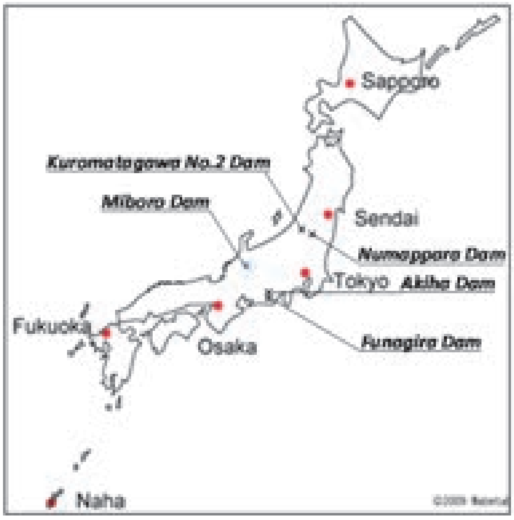

Figure 1. Locations of 5 dams where GPS applied

2. MONITORING WORK AT NUMAPPARA DAM

2.1. General Features of the Dam

Numappara dam is an Asphalt Facing Rockfill Dam and is located in Tochigi Prefecture. It was constructed in 1973 for the upper pond of 675 MW pumped storage hydropower station. The height, the crest length and the volume of dam body are 38 m, 1,597 m and 1,260,000 m^3 respectively. The upper pond provides 4,220,000 m^3 of effective capacity for generation with 40 m drawdown.

2.2. System and Equipment

As shown in Fig. 2, GPS survey unit at Numappara dam is composed of 3 measure points and 2 benchmarks at present. At the time of starting the observation, only K-1 benchmark was located on the northern slope adjacent to the dam, and K-2 benchmark was added on the southern side slope after the 2011 Off the Pacific Coast of Tohoku Earthquake which brought a certain movement of the K-1 benchmark. The dam is located about 280 km from the seismic center. This is the first case of application of GPS for survey of dam deformation among the five dams. The system has functioned and recorded the data for over 8 years since its installation in 2007.

Before introducing GPS, the survey works at Numappara dam was limited to only the period from spring to fall except for winter season due to its hard weather condition with frequent snowfalls and blizzards. The application of GPS changed the situation and enabled continuous survey works throughout the year including winter season by its functions of digital measurement and automatic data transmission.

A specific condition at Numappara site was revealed in the initial stage of the observation using the K-2 benchmark. Fig. 3 shows a upward half-sphere view from the K-2 benchmark. Usually, GPS signals from the direction near the ground surface, mostly in the area lower than 15 degrees of elevation angle, are omitted from the analysis to prevent negative influence to the data by noise or reflection at around the surface. However, growing trees on the east side of K-2 exceeds the standard omission area as shown in Fig. 3. It was serious concern that the signals through the trees were strongly disturbed or deteriorated by moisture in and around the trees. After check of the signals at the site, the data processing methods was improved to expand omission area as shown in Fig.3.
Fig. 4 shows a comparison of analysis results with and without the improved mask processing. The result indicates a clear difference of data dispersion between two groups and better convergence of the data in case of the improved mask processing (Hisano, A., et al. 2015).

2.3. Result of Observation

J-Power has conducted the deformation survey of the dam body by two methods; GPS and the conventional manual survey, in parallel so as to check and verify reliability of the data. Fig. 5 shows the observation results comparing two sorts of the data; surveyed by GPS and by conventional manual survey. Both the data show comparatively good conformity as shown in Fig. 5.
When the 2011 Off the Pacific Coast of Tohoku Earthquake occurred, the asphalt surface of the dam was damaged, and a considerable amount of leakage was caused accordingly. Not only the leakage data but the dam deformation data by GPS were continuously transmitted to the site administration office, even though the access road to the dam was closed due to the heavy snow, which was very useful to know the dam's state just after the earthquake.

Numappara dam was the first site where GPS was planned and employed for the survey of dam deformation in the company. Various technical knowhow on the proper survey method, the problems and measures, and the improvement technique obtained from the work at the site have been referred and reflected to succeeding cases of observation by using GPS at the other sites.

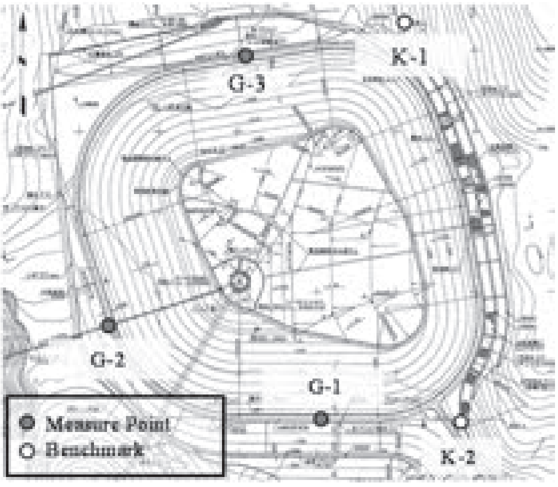

Figure 2. GPS Equipment Layout at Numappara dam

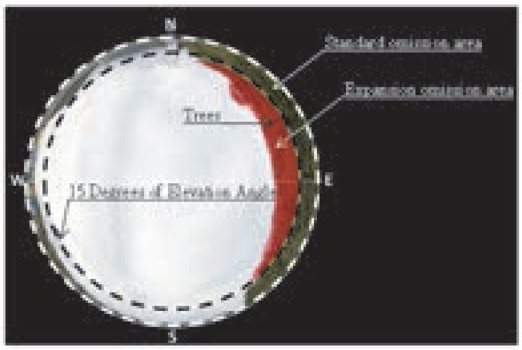

Figure 3. Upward Half-sphere View from K-2

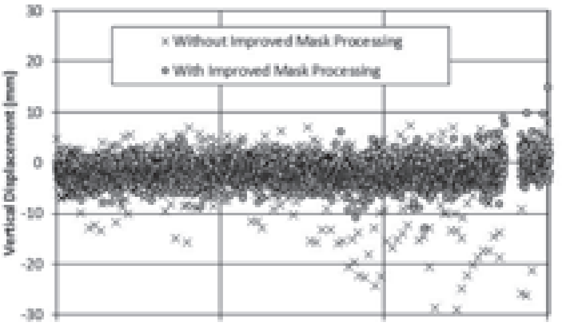

Figure 4. Comparison of Analysis Method

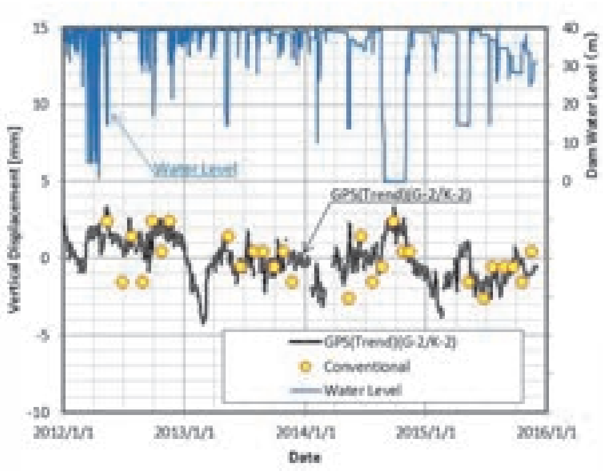

Figure 5. Comparison of GPS/Conventional Survey

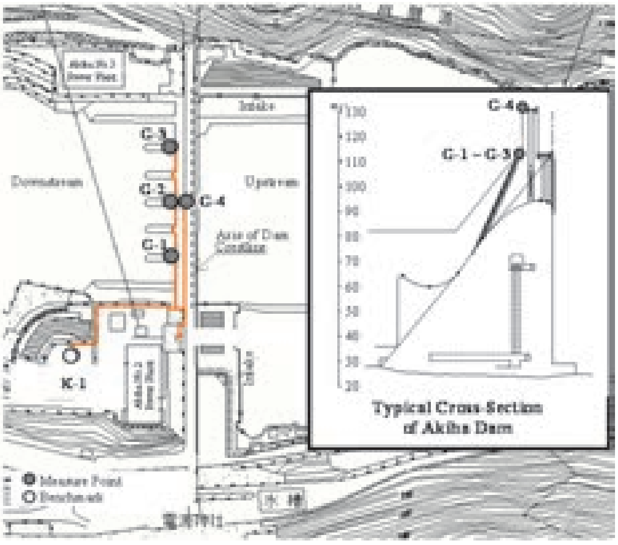

Figure 6. GPS Equipment Layout at Akiha dam

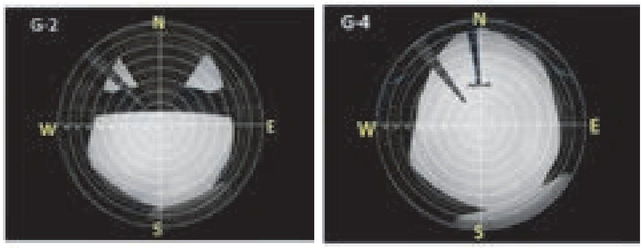

Figure 7. Upward Half-sphere Views from G-2 and G-4

3. MONITORING WORK AT AKIHA DAM

3.1. General Features of the Dam

Akiha dam is a Concrete Gravity Dam which is located at 47 km upstream from the Tenryu River mouth in Shizuoka Prefecture. It was constructed in 1955 for 127 MW hydropower stations. The height, the crest length and the volume of dam are 89.0 m, 273.4 m and 515,000 m^3 respectively. The reservoir provides 7,750,000 m^3 of effective capacity for daily regulation in the operation. Available drawdown is 5.0 m in depth.

3.2. System and Equipment

As shown in Fig. 6, GPS survey unit at Akiha dam is composed of 4 measure points and 1 benchmark.

There is a disadvantageous condition at three measure points (G-1, G-2 and G-3) among four. These 3 measure points are installed under the gates hoist bridges of the spillway structure which obstructed the upward visual areas. Fig. 7 shows the upward half-sphere views from G-2 and G-4 as examples. The condition of G-2 may adversely affect stable reception of GPS signals.

3.3. Result of Observation

Fig. 8 shows an observation result of upstream-downstream displacement at the measure points, G-2 and G-4. The long term trends of displacement are periodical and steady. The trend line at the point G-2 indicates approximate 5 mm of yearly displacement toward upstream side in summer and downstream side in winter. G-4 indicates a bit larger displacement than that of G-2 due to difference of their vertical locations. It seems to be a normal behaviour of concrete gravity dams because such seasonal displacements are caused by expansion and shrinkage of the downstream concrete face due to difference of the temperature. In this case, the obstruction of upward half-sphere view seems not to cause adverse effect for GPS signals reception. The reservoir is operated within 5.0 m drawdown depth, however, the displacement is hardly affected by the operational water level.

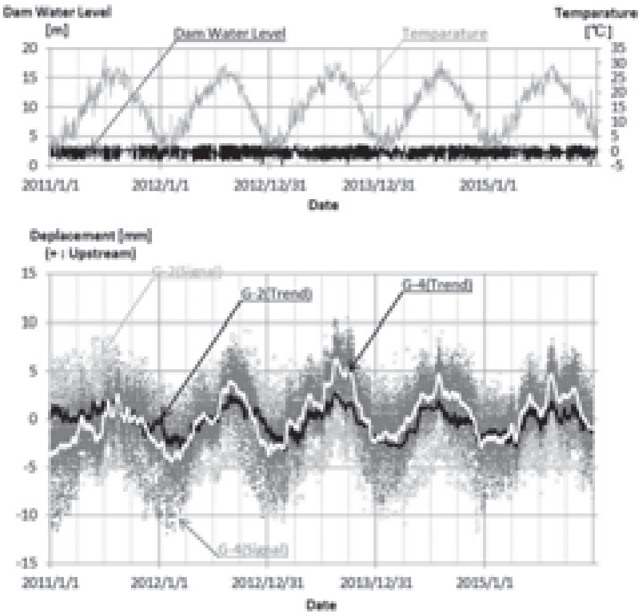

Figure 8. Observation Result at Akiha Dam

4. MONITORING WORK AT FUNAGIRA DAM

4.1. General Features of the Dam

Funagira dam is a concrete gravity dam which is located at 30 km upstream from the Tenryu River mouth and 17 km downstream of Akiha dam in Shizuoka Prefecture. It was constructed in 1977 for 32 MW hydropower generation, water supply and irrigation purposes. The height, the crest length and the volume of dam body are 24.5 m, 220 m and 54,000 m^3 respectively. The reservoir provides 3,600,000 m^3 of effective capacity for daily regulation, and available drawdown of 2.2 m in depth.

4.2. System and Equipment

GPS survey unit at Funagira dam is composed of 8 measure points and 3 benchmarks as shown in Figs. 9 and 10. All the measure points were set on the top of spillway piers but below the hoist bridges of spillway. They have a similar condition on upward views as that in Akiha dam accordingly.

There are three benchmarks named K-1, K-2 and K-3. K-1 is installed on the upstream right bank, K-2 is on the concrete structure at the right abutment, and K-3 is on the filling area just on the downstream left bank of the dam respectively. K-2 is the main benchmark for regular observation among them because of its high reliability of fixation. The concrete base of K-2 may generate a slight displacement due to change of the temperature, but it is negligible comparing with the long term behaviour of the dam body. K-1 on the natural rock had moved a little by the past rain washing and may have a possibility of further error. K-3 on the well compacted filled material has been stable so far but has some risk of unexpected movement in case of earthquake. K-1 and K-3 have been used for subsidiary purpose. The accumulated knowledge on the various foundations for benchmark at Funagira site will be very useful information for establishment of more reliable observation system in the future case.

4.3. Result of Observation

A survey result of the upstream-downstream displacement at the point G-5 is given in Fig. 11. The trend line shows around 8 mm of yearly periodical displacement. The amplitude and cycle of the movement are steady and constant throughout the observation period. The influence by water drawdown is assumed to be negligible because of its limited depth; 2.2m.

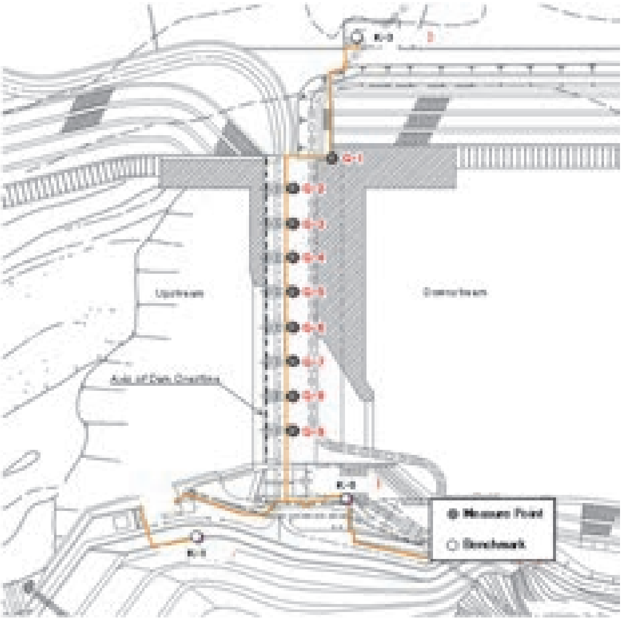

Figure 9. GPS Equipment layout at Funagira dam

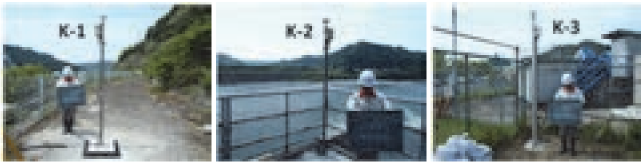

Figure 10. K-1 to K-3 Benchmarks

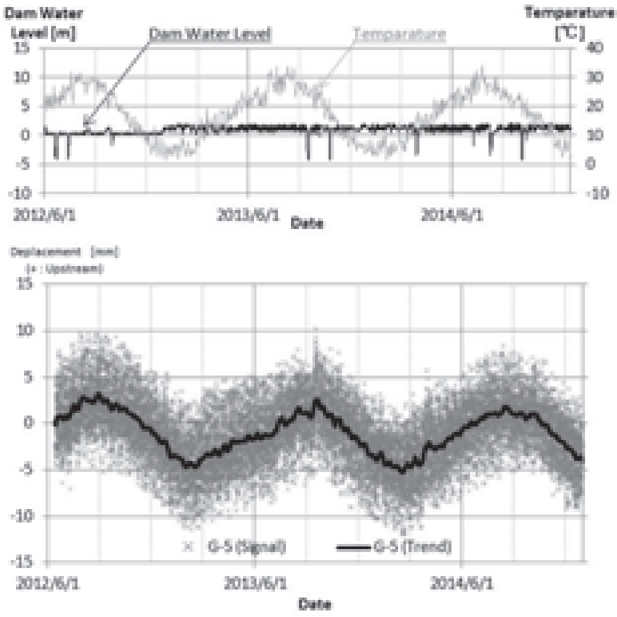

Figure 11. Observation Result at Funagira Dam

5. MONITORING WORK AT KUROMATAGAWA NO.2 DAM

5.1. General Features of the Dam

Kuromatagawa No.2 dam is a Concrete Arch Dam which is located at the upstream of the Kuromatagawa River in Niigata Prefecture. It was constructed in 1964 for 17 MW hydropower station. The height, the crest length and the volume of dam are 82.0 m, 235 m and 91,000 m^3 respectively. The reservoir provides 50,000,000 m^3 of effective capacity, and available drawdown is 37.0 m in depth.

5.2. System and Equipment

As shown in Fig. 12, GPS survey unit at Kuromatagawa No.2 dam is composed of 3 measure points and 2 benchmarks. The dam is located in the heavy snowfall mountainous area, therefore, the sensors for the measure points and the benchmarks were designed to be workable under the heavy snowfall and icy condition in winter. The sensor poles were also designed to be higher than the expected snow depth at the site. Standard height of the poles was 4.0 m.

5.3. Result of Observation

Application of GPS enabled the observation of the dam in all seasons including winter period in which the access and works at the site are difficult as same as that in Numappara dam due to heavy snow. Fig. 13 shows an observation result of the upstream-downstream displacement. The figure indicates three results of displacement based on the local benchmarks (K-1, K-2) and the national GPS-based Control Station named "Sumon" which is located around 10 km away from the dam site. The lines show high correlation with temperature and reservoir water level, like that the dam body moves to the upstream along with the temperature rising and moves to the downstream along with the water level rising. The results by GPS well conform to those data obserbed by the conventional manual survey.

The results obtained by the local benchmarks K-1 and K-2 in Fig. 13 show different trend in winter seasons of year 2013 and 2015 comparing with that in 2014. The reason is assumed that the local benchmarks were affected by heavy snow pressure during the winter and restored to the original condition along with snow melting. Both 2013 and 2015 are known as years having snowy winters.

The result suggests that the national GPS-based Control Station is useful for verification of availability and accuracy of the local benchmarks and measure points in heavy snowfall region.

6. MONITORING WORK AT MIBORO DAM

6.1. General Features of the Dam

Miboro dam is a Rockfill Dam with Center Impervious Core which is located at the upstream of the Shokawa River in Gifu Prefecture. It was constructed in 1961 for 215 MW hydropower generation. The height, the crest length and the volume of dam are 131.0 m, 405 m and 7,950,000 m^3 respectively. The reservoir provides 330,000,000 m^3 of effective capacity, and available drawdown is 65.0 m in depth.

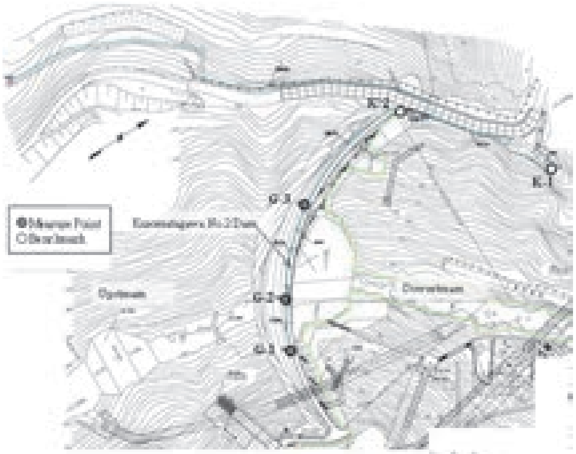

Figure 12. GPS Equipment Layout at Kuromatagawa No.2 dam

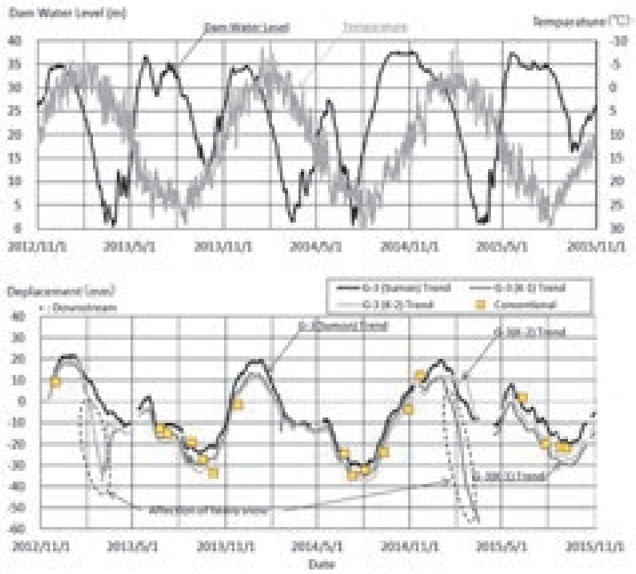

Figure 13. Observation Result at Kuromatagawa No.2 Dam

6.2. System and Equipment

GPS survey unit at Miboro dam is composed of 5 measure points and 3 benchmarks as shown in Fig. 14. Since the dam also is located in the heavy snowfall area similarly to Kuromatagawa No.2 dam, the sensors for the measure points and the benchmarks were designed to be workable under the heavy snowfall and icy condition as well. Height of the sensor poles was set as 3.5 m considering the expected snow depth at the site.

6.3. Result of Observation

Fig. 15 shows an observation result of upstream-downstream displacement. It shows a clear trend that the dam body moves to the upstream when the reservoir water level is lowering. The measured data by GPS basically conform to the data by the conventional manual survey.

Miboro dam is a typical annual operation resevoir among the five cases. The water level is lowered to around the lowest level by the end of winter for impounding snow melting water in spring season to utilize the river water effectively. On the contrary, the water level is kept comparatively stable high water level throughout the year except winter. A difficulty of the survey in winter season is a common problem at the sites located in deep snowfall region. Therefore, the dam behaviours during winter season were not been made cleared until GPS was adopted. The relationship between the dam behaviour and water level fluctuation throughout a year is understandable by GPS.

Two benchmarks, K-2 and K-3, of three are installed on the dam abutment at both right and left sides and another one, K-1, is on the spillway structure at the upstream rock foundation. Fig. 15 shows the displacement trends at G-6 point by three benchmarks and a considerable difference between K-2/K-3 and K-1. It is assumed that K-2 and K-3 were also affected by the movement of the dam body along with water level. K-1 kept its stable position independently with the firm foundation.

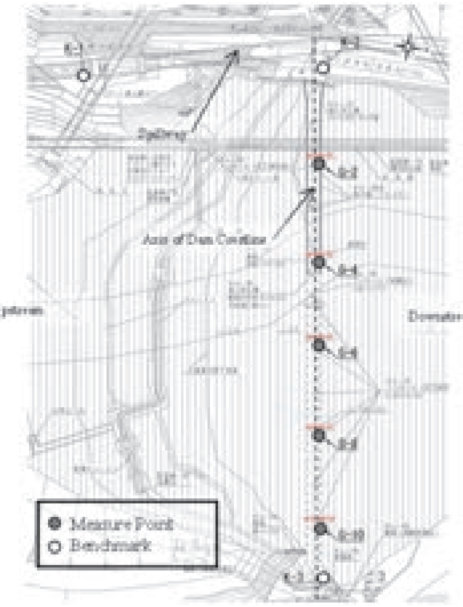

Figure 14. GPS Equipment Layout at Miboro dam

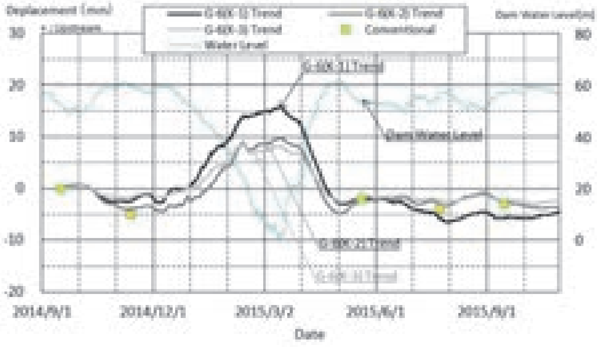

Figure 15. Observation Result at Miboro Dam

7. CONCLUSION

As the conclusion, the merits of GPS confirmed through the experiences of the abovementioned five instances are summarized as follows:

1) GPS enables always monitoring of dam behaviour throughout a year regardless weather conditions of the site.
2) GPS survey is useful for immediate check and monitoring of the dam safety in case of natural disasters such as earthquakes or sudden floods.

Also some recommendations for further effective use of GPS are given as follows:

1) The conventional manual survey should be continued in combination with GPS survey after its application. Comparison of two sorts of data is beneficial for verification and improvement of data reliability.
2) Accuracy of GPS is negatively affected by surrounding condition and visibility at the site, however, such influence can be mostly eliminated by proper measures such as the masking process described in Section 2.
3) Plural number of benchmarks should be provided to prevent sudden trouble or interruption of observation due to unexpected damage or movement of a benchmark.
4) GPS-based Control Station, if available near the site, is useful for verification of accuracy of local benchmarks.

REFERENCES

Japan Society of Dam Engineers (2014): GPS using manual concerning about measuring of fill dams, Japan Society of Dam Engineers. (in Japanese)

Shimizu, N., Nakashima, S. & Masunari T (2014): ISRM Suggested Method for Monitoring Rock Displacements Using the Global Positioning System (GPS), Rock Mech. Rock Eng., 47:313-328. DOI 10.1007/s00603-013-0521-5.

Hisano, A., Okumura, H., Koyama, K. (2015): Application of GPS to The Deformation Monitoring of Numappara Dam, Electric Power Civil Engineering, Vol. 378, pp. 66-70. (in Japanese)

4th APG Symposium and 9th EADC on

INNOVATIVE TECHNOLOGIES FOR DAMS AND RESERVOIRS TOWARD THE FUTURE GENERATIONS

Study on The Deformation Mechanism of an Ageing Dam Aiming at Future Deformation Prediction

H. Onishi & M. Kashiwayanagi
Chigasaki Research Institute, Electric Power Development Co. Ltd., Japan
hideaki_oonishi@jpower.co.jp

M. Yoda
JP Business Service Co. Ltd., Japan

ABSTRACT:
In evaluation of dam behaviour, deformation monitoring is essential. Although most dams show a stable deformation trend, it is highly important to confirm whether these trends will continue in the future assuming that the lifespan of a dam is more than 100 years. If a unique deformation behaviours have been encountered in a dam, such as monotonic increase toward the stream direction of the dam and variation in the deformation degree corresponding to reservoir water level or the ambient temperature, the current deformation mechanism, future dam behaviour, and also the necessity of correspondence should be addressed considering dam safety in the future.

In this report, we studied the deformation and related data of a 50-year-old concrete gravity dam and interpreted the deformation mechanism with the aid of numerical analysis, and conducted a simulation of dam behaviour in an elastic and steady manner considering the three parameters of reservoir water level, ambient temperature, and sediment depth. The results of the simulation show the consistent dam behaviour against these loads acting on the concrete gravity dam usually.

Keywords: concrete gravity dam, ageing dam, deformation mechanism, stability, measurement

1. OUTLINE

Dam deformation monitoring is essential in evaluation of dam safety because dam deformation shows the comprehensive behaviour of the dam and foundation rock. Recently, consecutive automatic measurement by GPS, in addition to collimation or levelling survey and plumb line measurement have been adopted for more detailed interpretation of dam behaviour.

Around 50 dams owned by J-power (Electric Power Development Co. Ltd.) which is one of the electricity utility companies in Japan, show a stable deformation trend. However, it is very important to confirm whether these trends will continue into the future assuming that these lifespans are more than 100 years. When the deformation behaviours are examined in detail, unique deformation behaviours have been encountered in some dams, such as monotonic increase, even though, slightly toward the upstream direction of the dam and variation in the deformation degree corresponding to the reservoir water level or the ambient temperature, which are cyclic loads on the dam surface. Although these are limited cases under the current condition, the deformation mechanism, future behaviour, and possible correspondence of the dam should be addressed of considering dam safety in the future.

We studied the deformation and related data of a 50-year-old concrete gravity dam and interpreted the deformation mechanism with the aid of numerical analysis. Factors affecting dam behaviour were examined for a prediction of future behaviour of the dam.

2. INTERPRETATION OF DAM DEFORMATION

2.1. Major characteristics of the dam

Monitored deformation of a 50-year-old concrete gravity dam as shown in Fig. 1 is studied. The major parameters and the monitoring schemes are shown in Table 1 and in Table 2 and Fig. 2, respectively.

Table 1. Parameters of the dam

Type	Concrete gravity
Height(m)	155.50
Crest length (m)	293.50
Width of crest (m)	8.10
Volume (m^3)	1,120,000
Crest elevation (EL. m)	270.00
Geology of foundation rock	Granite
Year of completion	1956

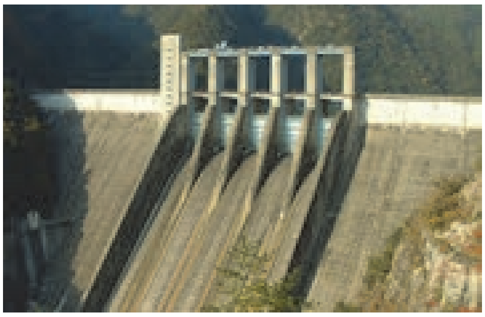

Figure 1. Downstream view of the dam

Table 2. Monitoring scheme

Type of monitoring	Frequency of monitorng	Notes
Deformation	1 time/month	Plumb line:1line
Seepage	2 times/month	
Uplift pressure	4 times/year	

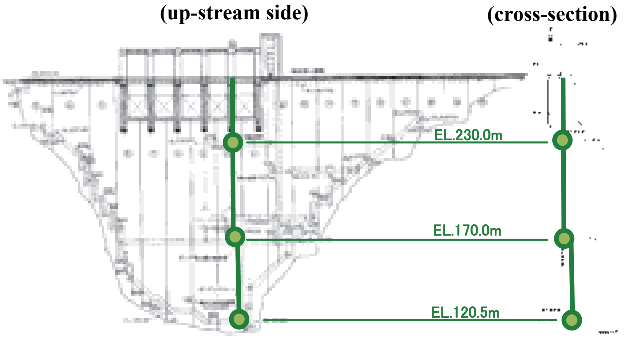

Figure 2. Position of the plumb line

2.2. Deformation of the dam

Deformation of the dam from completion in 1956 is shown in Fig. 3 with related data of the reservoir water level, ambient temperature around the dam, and rainfall. The following can be observed in these data.

1) The dam was deformed upstream at the beginning corresponding to reservoir impoundment at a maximum of 12 mm recorded in 1957. This was followed by downstream deformation up to approximately 30 mm until 1965.

2) After 1965, the dam was continuously deformed gradually upstream with yearly fluctuation. It has moved to almost zero deformation in respect to the initial position of the dam just after its completion in 1956 from the maximum downstream deformation of 18 mm in 1960.

3) In terms of yearly fluctuation, the dam is deformed elastically in the range of 5 mm, which is downstream in the winter season with lower ambient temperature and upstream in the summer season with higher ambient temperature.

The wide range of deformation fluctuation in the initial several years is not consistent with the elastic structural behaviour of concrete gravity dams against loads due to hydrostatic pressure and ambient temperature. It may be supposed that the interaction of the dam and the foundation affected by the initial infiltration into the dam foundation from the reservoir and temperature ageing in the dam body due to hydration of the concrete are the reasons. However, the behaviour after 1965 is the focus of this report to clarify the mechanism of elastic deformation of the concrete gravity dam due to the usual loads that are commonly loaded onto the dam.

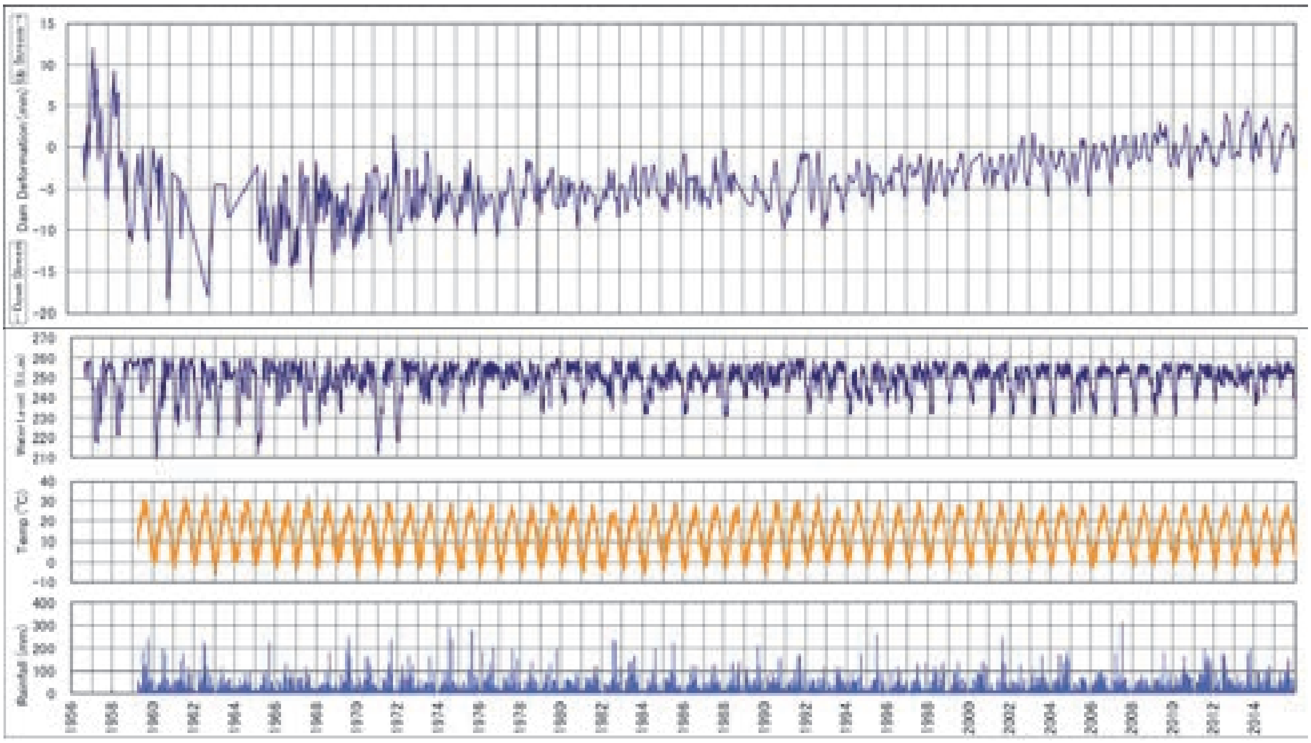

Figure 3. Charts of dam deformation, reservoir water level, temperature, and rainfall

2.3. Study on the factors on dam deformation

Variation in reservoir water level and temperature are major loads incurring the yearly periodical deformation behaviour of the concrete gravity dam. The correlations of dam deformation with reservoir water level and ambient temperature are shown in Fig. 4 and Fig. 5 respectively. Data period is 50 years when the dam is continuously deformed gradually upstream from 1966 through 2015. In these graphs, the influence of the elapsed days is subtracted because the dam was continuously deformed gradually upstream. The rise in reservoir water level causes downstream deformation of the dam when it is under the same temperature. This is reasonable behaviour for the concrete gravity dam subject to hydrostatic pressure. The deformation range is approximately 10 mm by the fluctuation of the 30-m-deep water level or the 0-30 degrees Celsius and the deformation degree corresponding to the reservoir water level or the ambient temperature is not change.

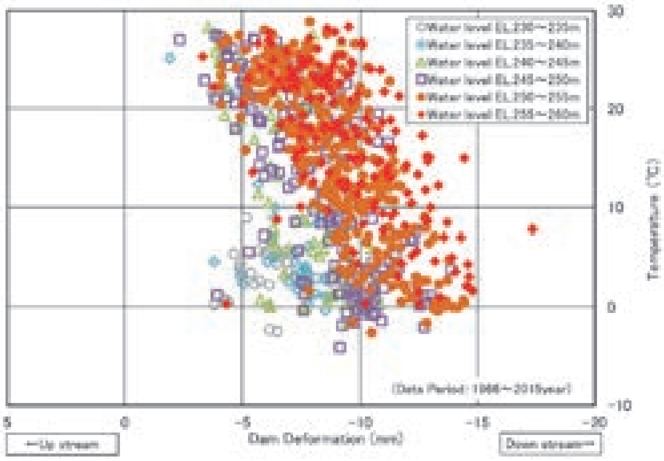

Figure 4. Correlation between dam deformation and water level

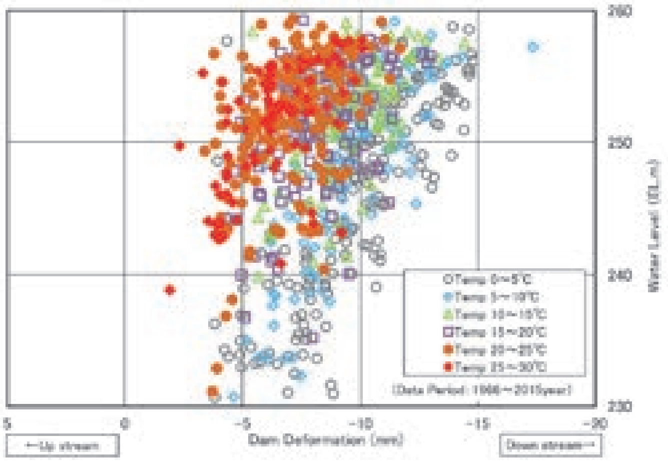

Figure 5. Correlation between dam deformation and temperature

To understand the long-term behaviour of the dam against the usual loads, the annual averaged values of dam deformation, sediment level in front of the dam, reservoir water level and ambient temperature are shown in Fig. 6. The dam shows a clear tendency to deform upstream after 1965, which is shown in Fig. 3, though the reservoir water level and the temperature show a roughly flat tendency. Though property variation of the dam body or the foundation rock might be suspected, the influence of sedimentation in front of dam is supposed to be a major factor in the long-term behaviour of the dam. The increase in sediment height seems to match the dam behaviour even though there is less data on sediment.

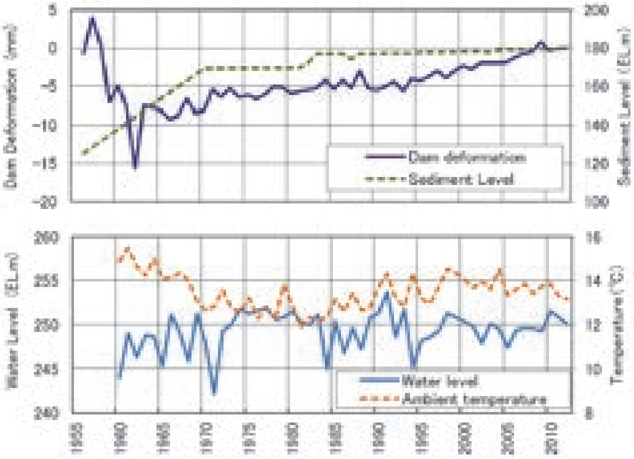

Figure 6. Annual average charts of dam deformation, water level, temperature, and sediment level

The multiple regression analysis on the dam deformation in terms of the reservoir water level, the ambient temperature, and the elapsed days of the operation from 1965 is conducted to examaine the dam behaviour during whole period and each decade of the monitoirng after 1966. The sediment depth is not incorporated in the analaysis due to the unsufficient data number comparing others. The elapsed days are adopted taking the development of the sedimentation into consideration.

The analysis prvides regression coefficient and each constant of $c0$, $c1$, $c2$, $c3$ as shown in Table 3. The dam deformation is fomulated as Eq. 1 usig these parameters.

$$D = c0 + c1 \times H + c2 \times T + c3 \times t \tag{1}$$

Where, D: dam deformation (mm), H: reservoir water level (m, 0m = EL.220m), T: ambient temperature (degrees Celsius), t: elapsed days (0 = 1965/1/1), $c0$: intercept coefficient, $c1$ to $c3$: coefficient of explanatory variables

The good relations are found in all periods of which regression coefficients are approximately 0.8 and more except the period from 1986 to 1995. It is illustrated in Fig.7. Overall both ones of monitoed and esitmated by Eq. 1 shows good correlation. The coefficient ($c1$) of the reservior water level and the coefficient ($c2$) of the temperature are almost consistent during whole monitoring period, showing that the deformation mechanism corresponding to these variables is consistent.

Table 3. Results of the multiple regression analysis

(1)	1966 -2015	1966 -1975	1976 -1985	1986 -1995	1996 -2005	2006 -2015
	50	10	10	10	10	10
(2)	809	356	116	108	110	119
(3)	0.90	0.88	0.78	0.67	0.80	0.89
*c*0	-4.143	-5.371	-1.097	1.776	-6.153	-7.905
*c*1	-0.237	-0.255	-0.222	-0.251	-0.215	-0.242
*c*2	0.192	0.221	0.181	0.136	0.170	0.227
*c*3	0.0005	0.0013	0.0000	-0.0001	0.0006	0.0007
*a*1	-0.47	-0.69	-0.65	-0.72	-0.78	-0.73
*a*2	0.45	0.61	0.82	0.53	0.79	1.04
*a*3	0.75	0.41	0.02	-0.05	0.34	0.41

(1) :data piriod (yaar)
(2): number of data
(3): regression coefficient
*c*0: intercept coefficient
*c*1 to *c*3: coefficient of water level, temperature, time
*a*1 to *a*3: standard partial regression coefficient of water level, temperature, elapsed days

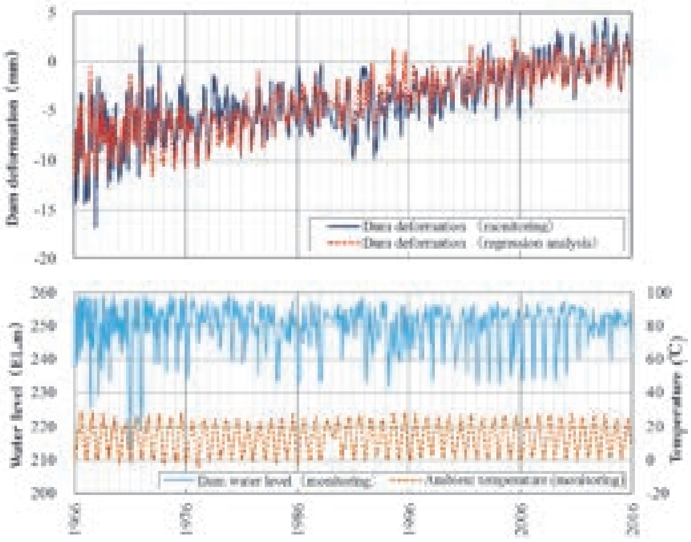

Figure 7. Multiple regression analysis of the dam deformation

The larger standard partial regression coefficients are interpreted that the contirbutions of those are predominant in the dam defromation. From this basis, the larger ones are found in the whole period of *a*3and in the decases periods of *a*1 and *a*2. In addition, *a*3 is estimated in lower and fluctuating figures in decades periods. These are considered that the reservoir water level and the temperature act majorly on the yeraly behavior of the dam. On the other hand, the elapsed days act major role on the longer term behavior of the dam. While the elapsed days does not directly relate to the sediment developement, both are approximately related to affect the dam deformation. It is considered that the unique upstream deformation of the dam is caused by the sediment development.

Therefore the study aided by the numarical simulation is conducted in the following section to quantify the influence of the reservoir water level, the abminet temperature and the sediment on the dam deformation.

3. NUMERICAL SIMULATION OF THE DAM BEHAVIOUR

Numerical simulation using elastic FEM is conducted to examine the dam behaviour against loads due to the reservoir water level, ambient temperature and sediment. The non-linearity of the dam and the foundation and the unsteady fluctuation of the temperature of the air and/or the reservoir are sometimes incorporated into the simulation of dam behaviour. There are difficulties in knowing these parameters and to conducting unsteady calculation.

In this report, we conducted a simulation of dam behaviour in an elastic and steady manner considering the three parameters of reservoir water level, ambient temperature, and sediment depth.

3.1. Conditions of simulation

The highest section of the dam where the plumb lines are arranged is selected for the simulation model. The model consists of the dam and the foundation, as shown in Fig. 8, with the properties shown in Table 4. The side boundary and the bottom boundary of the model are modelled as the roller boundary and the fixed boundary, respectively.

The simulation cases are corresponded to the abovementioned loads, shown in Table 5. Hydrostatic pressure is loaded on the upstream face perpendicularly on the dam surface, not on the foundation, corresponding to the reservoir water level. In terms of temperature loads, the ambient temperature around the dam and the water temperature of the reservoir water are considered. In preliminary examination, both temperatures are strongly related and the water temperature of the reservoir water shows a vertical uniform distribution from the water surface to the bottom of the reservoir. The water temperature is added to the submerged surface of the dam with the value correlated to the ambient temperature and the unique in the vertical direction. The ambient temperature is added to the exposed dam surface.

The sediment pressure is added perpendicularly to the surfaces of both the dam and the foundation. The specific weight and the horizontal earth pressure coefficient of the sediment are assumed to be 1.1 t/m^3 and 0.4 in reference to the design value. Loading images are shown in Fig. 9.

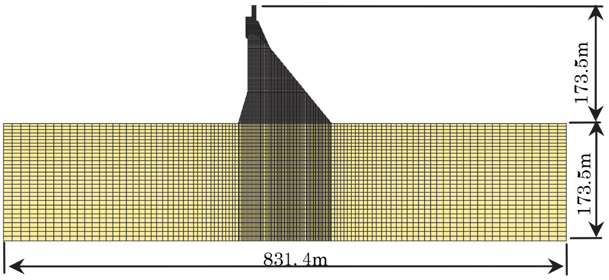

Figure 8. Simulation model

Table 4. Properties for simulation

Item	Dam	Foundation
Elastic coefficient (MPa)	32,000	20,000
Poisson ratio	0.2	0.25
Thermal conductivity (kj/mh°C)	9.2	5.0
Linear coefficient of expansion (1/°C)	1×10^{-5}	0

Table 5. Simulation cases

Case	Condition
Water level (EL. m)	180, 200, 220, 240, 260
Ambient temperature (°C)	0(4), 10(11), 20(18), 30(24) *
Sediment level (EL. m)	120, 140, 160, 180, 190, 200

* The number in the parenthesis is water temperature

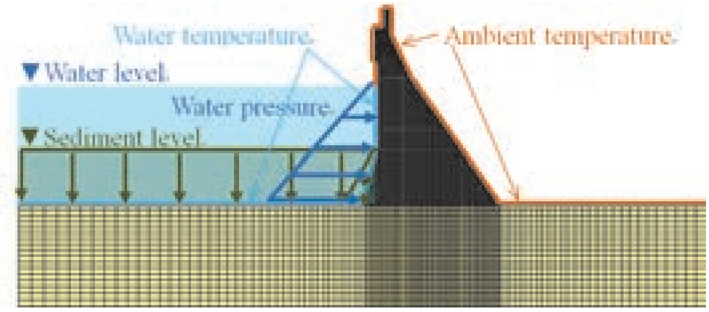

Figure 9. Loading image

3.2. Results of analysis

The relative displacement of the stream direction between each monitoring location respective to the lowest location along the plumb line in the dam is shown in Tables 6 to 8, and Figs. 10 to 12.

Table 6. Dam deformation against reservoir water level

No.	Water level (EL.m)	Dam deformation (mm)
1	180	-0.9
2	200	-2.5
3	220	-5.4
4	240	-10.4
5	260	-18.2

Table 7. Dam deformation against temperature

No.	Temperature (°C)		Dam Deformation (mm)
	Ambient	Water	
6	0	4	-9.9
7	10	11	-2.7
8	20	18	4.6
9	30	24	11.8

Table 8. Dam deformation against sediment depth

No.	Sediment Level(EL.m)	Dam Deformation (mm)
10	120	0.5
11	140	2.2
12	160	3.8
13	180	5.2
14	190	5.8
15	200	6.2

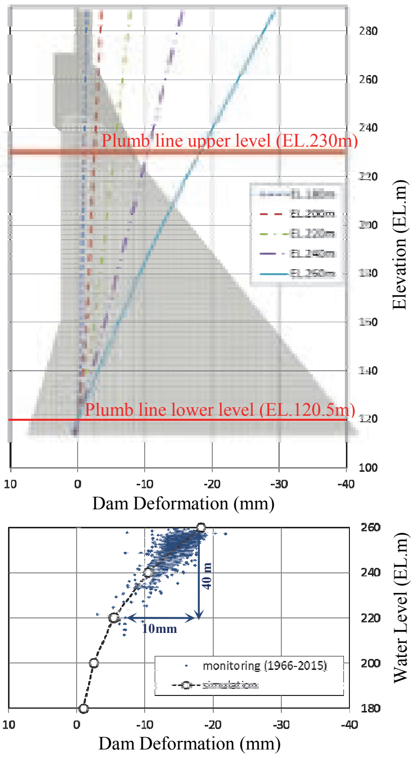

Figure 10. Correlation between dam deformation and water level

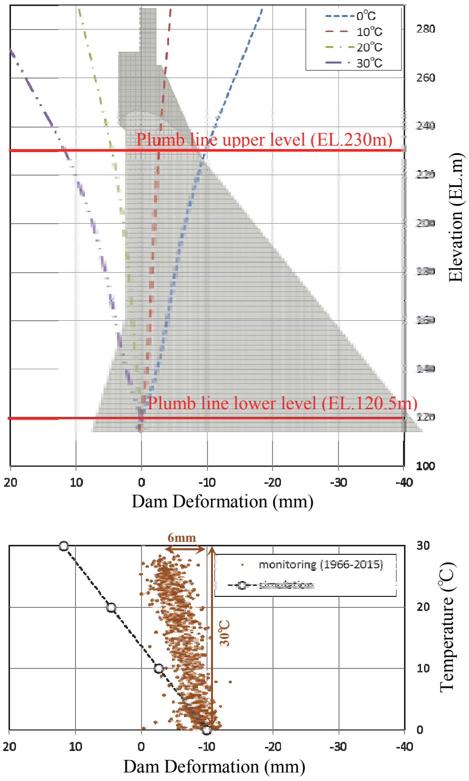

Figure 11. Correlation between dam deformation and temperature

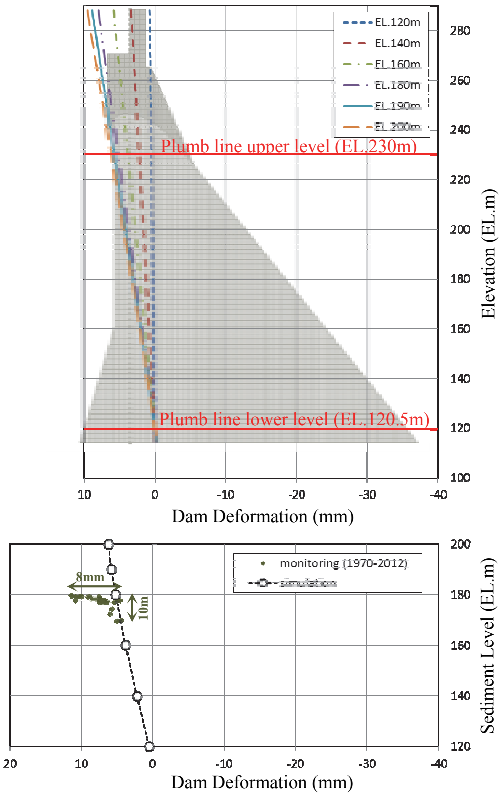

Figure 12. Correlation between dam deformation and sediment level

Each result of the simulation shows a similar tendency to the monitored results. A higher reservoir water level induces downstream deformation, while higher temperature and deeper sediment induce upstream deformation. The consistency between the monitoring and the simulation is preferable in the deformation due to the reservoir water level, while the deformation due to the temperature is simulated in approximately 3 times of the monitored ones. Assumed sediment effect in the simulation does not represent the monitored ones, even though it makes the upstream deformation of the dam, which is monitored as unique behaviour.

The simulated deformation of the dam due to reservoir water level is approximately 10 mm by 40-m-deep variation from a water level of EL. 220 m to EL. 260 m, which is quantitatively consistent with the monitored values as shown in Fig. 10.

When the ambient temperature rises from 0 to 30°C, the simulated dam deformation is approximately 20 mm, while the monitored one is approximately 6 mm as shown in Fig. 11. Due to the steady-state calculation method in the simulation, the dam temperature is considered to be uniform in the whole dam body. In reality, the ambient temperature around the dam fluctuates in certain periods such as day, season, and year. This causes temperature distribution inside the dam, which results in large inconsistency between the simulated and the monitored results.

The long-term behaviour of the dam from 1970 shows 8-mm upstream deformation and sediment level rises from EL. 170 m to EL. 180 m as shown in Fig. 12. The corresponding result of the simulation shows 1-mm upstream deformation by the 10-m-sediment level-variation. Because of the finite depth of the model, the sediment load does not impact deep enough and results in less deformation than monitored one. This should be addressed in the future. The study on the horizontal earth pressure coefficient shows a very slight influence on the simulated deformation. In addition, the simulation result shows that dam deformation converges so that the sediment level becomes higher. It is important to predict the future deformation of the dam.

The results of the abovementioned simulation show consistent dam behaviour against major loads acting on the dam usually. However, it is confirmed that further study is necessary to assess dam behaviour quantitatively. Dam behaviour is the consequence of combined factors including the abovementioned loads. Study of a combination of major loads, which is not considered in this paper, is an issue to be addressed in future.

4. CONCLUSIONS

The conclusions in this report are summarized below.

1) Three major factors on the deformation mechanism of the concrete gravity dam are identified, which are loads due to the reservoir water pressure, the ambient temperature change and the sediment.
2) Based on the multi regression analysis on those parameters, first two act a role on the yearly fluctuation of the dam deformation, while the last one acts a role on the long-term behaviour of the dam. These characteristics are consistently found during whole monitoring period of five decades.
3) The numerical simulation on the dam behaviour due to these loads provides following findings;
   (1) The deformation due to water pressure is quantitatively simulated consistent to the monitored one.
   (2) The deformation due to the temperature change is simulated qualitatively, not quantitatively by the steady state method. A time-dependent simulation is necessary for more preferable representation of the monitoring results.
   (3) The deformation due to the sediment pressure is simulated qualitatively, not quantitatively due to the defectiveness of the numerical model. It is clarified that the sediment pressure can cause the unique deformation of the dam developing upstream continuously.
4) The further study is necessary especially on the effect of the temperature change and the sediment pressure on the simulation of the dam deformation. It is essential to predict the future safety condition of the dam.

Gate Operation Support Table of Ohno Flood Control Dam against Excess Flood Inflow

J. KASHIWAI
Dam Engineering Center, Tokyo, Japan
kashiwai@jdec.or.jp

T. KUBOZONO &T. TAKADA
Kyoto Prefecture, Kyoto, Japan

ABSTRACT:
Flood control operation requires smaller discharge than inflow. This operation raises water level of a reservoir, and cannot be continued until reservoir water level reaches to the dam design flood stage. Flood control operation mode should be changed into overtopping prevention mode in an appropriate way at a certain inflow and water level condition during excess flood inflow. Mode changing timing and the gate operation ways for increasing discharge to prevent overtopping are one of the most serious matters for operation managers.

In above situation, MOPO (minimum outflow to prevent overtopping) table, which was developed by Public Works Research Institute Japan, was employed by Ohno dam for supporting the operation judgment. MOPO is obtained through the gate operation simulation in the large inflow condition which reaches to the design inflow. If the outflow at the time in the pair of inflow and water level condition is greater than MOPO, future water level must be controlled under the dam design flood stage without extreme outflow increase. This paper will show the simulation conditions for the Ohno dam's MOPO table. They consist of the inflow condition, gate movement restrictions and outflow increase limitations.

Keywords: gate operation, excess flood, over topping, risk management

1. INTRODUCTION

Gate operations for flood control and preventing overtopping are completely opposite. The former operation releases much smaller discharge than the inflow of a dam, but the latter operation increases the outflow to reach to the inflow.

There are many multi-purpose dams, including flood control purpose, in Japan. They have, of course, rules of flood control operation and preventing overtopping operation. For the effective use of a reservoir capacity, water level regions for flood control and preventing overtopping operation are usually overlapped at 20% of a flood control capacity (Fig. 1).

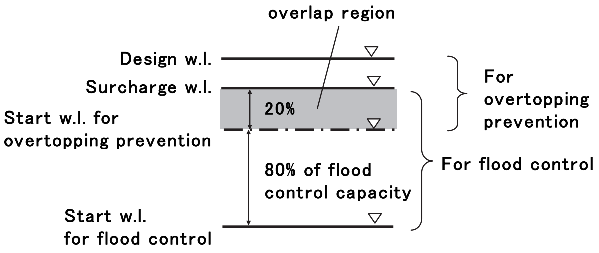

Figure 1. Overlap water level region of flood control and overtopping prevention

In the overlapping water level, flood control operation should be done if a flood is smaller than the flood control planning. On the other hand, overtopping prevention should be done in an excess flood condition. Therefore, if a water level is in the overlapping region and gate operation is in a flood control mode, flood magnitude should be predicted and the judgment of changing a operation mode from flood control to overtopping prevention should be done.

There are some responsible persons for the decision making of the judgment. Most influential and respectable judgment is given by a director of a dam management office. He is the best person to understand the situations of a dam, a reservoir, surrounding area of a dam and a reservoir, related facilities for a dam's management includes operation systems of gates, and so on.

Since the methods for flood dimension prediction and changing operation mode judgment have not been established, the decision of a director should be made using supports of his office staffs and his empirical knowledge. In this situation, a director may feel serious stress for the decision making of the judgment.

In the above situation, the method using the table of minimum outflow to prevent overtopping (MOPO) was proposed by Public Works Research Institute Japan and its prototype was employed by Ohno dam as a support method. Fundamental idea of MOPO and outline of the operation simulation were introduced together with the actual application of the prototype table at the excess flood in 2013 (Kashiwai et. al. 2015).

This paper will show the more details of the meaning of MOPO table and the simulation conditions for obtaining table based on the Ohno dam's revised one. They consist of the inflow condition, relationship between water level and reservoir storage capacity, gate movement restrictions and outflow increase limitations.

2. Outline of MOPO

Putting Qit is the inflow, Qot is the outflow and Wlt is the water level at the mode change time from flood control to overtopping prevention. From the operation conditions, Wlt is in an overlap region and Qot is smaller than Qit. If gates can immediately move to the target openings, which release the inflow at a time, the outflow will increase very rapidly and reach to the inflow in a moment. The water level will be kept near Wlt in this case and overtopping can be easily prevented. Rapid outflow increase, however, may increase the evacuation risk of residents and visiting people in a river and inundation areas. Also, that may cause damages to river structures such as intake structures including weirs, banks and flood storage facilities and so on. An outflow increase should be somewhat restricted.

A gate movement speed is also limited by some reasons such as operation error prevention matters, mechanical matters including power supply conditions. An outflow increase cannot be so immediate, so the storage capacity is necessary for getting the inflow (Fig 2). In the same Qit and Wlt condition, smaller Qot requires larger capacity and MOPO is defined as the minimum Qot that can reach to the inflow before the water level ups to a design water level in the Qit and Wlt condition.

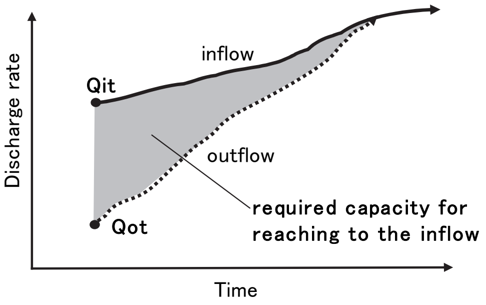

Figure 2. Required capacity for reaching to the inflow

From the above definition, it is clear that if Qot is greater than MOPO in the same Qit and Wlt condition, the outflow can reach to the inflow under the design water level. Gate operation has some options such as constant opening operation, constant discharge operation or reducing outflow operation to MOPO. On the other hand, if Qot is less than MOPO, outflow should be increased to MOPO. Images of time series of the outflow in the inflow increase condition are shown in Fig. 3,

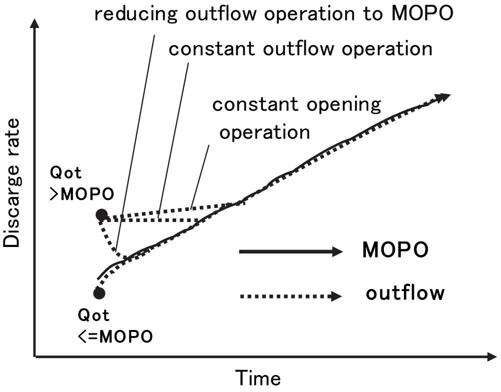
reducing outflow operation to MOPO
constant outflow operation
constant opening operation
Discharge rate
Qot >MOPO
MOPO
outflow
Qot <=MOPO
Time

Figure 3. Images of time history of outflow based on MOPO information

MOPO is obtained by a gate operation simulation including a reservoir storage calculation for each pair of Qit and Wlt. Conditions for the simulation are an inflow increase from Qit, relationship between storage capacity and water level and outflow increase restrictions. Setting methods of these conditions were executed through the MOPO table application for Ohno dam. So the methods introduced bellows strongly reflect the characteristics of Ohno dam's specific conditions.

3. CONDITION SETTING FOR MOPO SIMULATION THROUGH OHNO DAM CASE

3.1 Outline of Ohno dam

Ohno dam is a gravity concrete dam completed in 1957. Location of the dam is in the upstream are of Yura River system, Kyoto prefecture. Area of Yura River basin is 1882 km^2 and catchment area of the dam is 354 km^2.

The dam height is 61.4 m, and the flood control capacity is 21.32 million m^3. The flood control method of Ohno dam is constant ratio-constant discharge method. If the inflow will increase and beyond the start discharge of flood control, 500 m^3/s, flood control operation will start, where constant ratio of 58% of inflow will be released to the downstream area till inflow peak. After the inflow peak, outflow at the inflow peak will be kept till the inflow will be equal to the keeping outflow. Fig. 4 shows the flood control operation at the flood control planning flood of Ohno dam. Maximum inflow is 2400 m^3/s and the outflow at the inflow peak is 1400 m^3/s.

Ohno dam has three conduit gates for flood control. These gates are also used for overtopping prevention with three crest gates. Conduit gates will be firstly fully opened, and then crest gates will start to open at the operation.

Table 1 shows Ohno dam's water levels shown in Fig. 1. The design discharge at the design water level is 3510 m^3/s, about 1000 m^3/s larger than the peak inflow of flood control planning flood. This value, however, is obtained by the current rule, which was established after the completion of Ohno dam, the outflow with all gates fully opened condition is about 300 m^3/s less than the design discharge. Considering the shortage of this outflow capacity, both conditions of reaching to the inflow and obtaining fully opened condition of the crest gates under design water level are employed as the satisfactory condition for overtopping prevention at MOPO simulation.

Total outflow of the three conduits at the design water level is about 950 m^3/s, which is about a quarter of the design discharge.

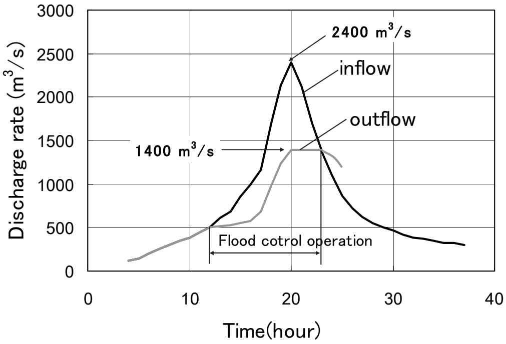

Figure 4. Flood control operation at planning flood

Table1. Ohno dam's water levels shown in Fig. 1

Design water level	EL. 175.9 m
Surcharge water level	EL. 175.0 m
Start water level for overtopping prevention	EL. 172.6 m
Start water level for flood control	EL. 155.0 m

3.2 Inflow condition

Inflow condition for MOPO simulation should be set as a probable maximum increase condition. The probable maximum increase of Ohno dam was obtained from hydrographs of all experienced floods. Peak discharges of floods were enlarged to the design discharge and the largest increase of all floods at each continuous time length was applied. It is important that the probable maximum increase is given as the function of continuous time length.

The probable maximum increase of shorter continuous time length was arranged from the start of the simulation, because this arrangement gave the largest MOPO. Inflow increase rate decreases along with the passage of time.

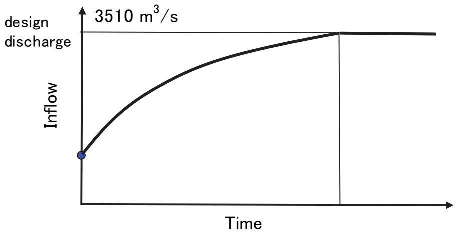

Figure 5. Ohno dam's inflow hydrograph for obtaining MOPO table

Fig. 5 shows Ohno dam's inflow hydrograph for obtaining the MOPO table. The design discharge is set as the maximum inflow. In Japan, a spillway is designed to outflow more than or equal to a design discharge at a design water level and it is considered at a spillway design that the outflow of a design discharge may continue some duration. Referring to above design idea, the inflow of the design discharge is set after reaching to that discharge.

3.3 Relationship between water level and storage capacity

A storage capacity of a reservoir is obtained by measurement, and future change of the capacity by sedimentation has to be considered for MOPO simulation. In order to keep the long term safety against overtopping, capacity reduction by sedimentation should be counted. Evaluation of future sedimentation in a region between start water level for overtopping prevention and design water level is required. This means, sediment distribution should be estimated as well as sedimentation volume. In the case of Ohno dam, measurement survey of the reservoir has been executed once in every year, and 100 years sedimentation or more was set based on the analyses of survey results.

3.4 Restrictions of outflow increase

3.4.1 Items to be set for operation error prevention and mechanical matters

As mentioned before, a gate movement is limited by operation error prevention matters and mechanical related matters. They may vary with dam and reservoir characteristics such as dam's purpose, reservoir dimension, principle of dam management and so on.

Table 2 shows actual setting items of Ohno dam's MOPO simulations. Since most of items have the both meaning of operation error prevention matters and mechanical related matters, they are not appropriate for classifying the actual items. In the table, data processing system related matters and gate control system related matters are applied for the classification from the other point of view.

Regarding a data processing system, a smoothing way of water level data should be set for MOPO simulations. A storage capacity change, which is used for estimating inflow, is obtained from a water level change in a decided time interval. Water level smoothing is necessary to obtain stable inflow outputs.

Table 2. Actual setting items of data processing system and gate control system related matters, considered in Ohno dam's MOPO simulations

1. Data processing system related matters.
   - (1) Water level smoothing
     - a. Number of firstly averaging data (measuring original data)
     - b. Number of secondary averaging data (firstly averaging data)
   - (2) Calculation methods to obtain inflow from smoothing water level
   - (3) Minimum time interval of the start of the same gate movement
   - (4) Time interval of indication of target outflow
2. Gate control system related matters
   - (1) Fundamental course of gate movement
     - a. Order of operation gate (classified by purpose)
     - b. Gate opening combination of the same purpose gates for releasing target outflow
   - (2) Gate movement
     - a. Staggered start time in plural gate condition
     - b. Opening/closing speed
     - c. Maximum opening distance in continuous gate movement
     - d. Minimum holding time to the next movement

Ohno dam's smoothing way is based on the past data averaging as shown in Table 2. Firstly, measuring data of every 2 seconds from the present to the past in decided time interval is averaged. Then secondary averaging is added using firstly averaged data. By this smoothing way, estimated inflow represents the averaged past inflow, so the gate operation based on this estimated inflow is always delayed compared with the operation based on the present inflow.

Target openings of gates are calculated and indicated by the system, which uses above estimated inflow, sum of released flow, flood control rule and overtopping prevention rule and so on. If the officer judges the indicated openings are appropriate, the officer orders the gates to move to target openings. If not, the officer can change the target. Final decision of the gate movement will be done by human beings.

The minimum time interval of the beginning of the same gate movement is also set. This time interval is required for the operational decision time including the handling time against unexpected incidents as well as the data processing. Ohno dam's gate control system has several rules for the gate movement. Since items of rules for the conduit and crest gates are almost same, Table 2 is applied to both gate types.

When gates are ordered to move to target openings, plural gates do not move at the same time to reduce power capacity of gate control facilities. Start time of each gate is staggered and each gate starts to move at the setting opening/closing speed. The gate speed should be fit with feelings of operators, ensuring braking accuracy and providing appropriate required power etc., and empirical value is commonly used.

The maximum opening distance in the continuous gate movement is set to prevent too much outflow increase. If the distance to the target opening is larger than the maximum distance, gate is once stopped in short duration to be checked to continue the gate movement. Gates will automatically restart to move if the target opening still lager than the maximum. Next movement to the target opening will be start after the all gates will have reached to the former target. In the case of Ohno dam, the same target openings are set for the three gates of conduit and crest. So, the three gate openings are always the same at the start of the gate movement.

Above items, which related with data processing system and gate control system, are organized in Table 2, and the actual values for each items should be decided for MOPO simulations.

3.4.2 Influences of outflow increase

Restrictions of outflow increase are ideally examined and decided by the influences on downstream areas. The examinations, however, may require analyses of various rainfall and run-off situations of floods at downstream area and a reservoir. Add to this, the evaluation of outflow increase should be discussed from the view point of disaster prevention plans, disaster reduction plans and damage reduction plans of downstream areas.

Recently, the importance of an operation considering the flood situation of downstream areas is getting recognized and examinations from some points of view have been executed. Areas and dams of the examinations, however, are limited and there are very few cases which try to exam the relation with overtopping prevention operation. It may be a long way to establish examination procedures and evaluation methods of decision making. Technical development of them should be expected, but more empirical or simple methods should be employed for the majority of flood control dams including Ohno dam.

For the simulation of Ohno's MOPO, the outflow restriction was decided referring to following three points of view.

(1) outflow increase that people in the river area can escape to the outside
(2) past records of inflow increase
(3) outflow increase based on the operation idea of overtopping prevention rule

The outflow increase restriction of (1) is already regulated in the operation rule by checking water level rise in the downstream area. This increase restriction is applied in the condition of inflow is 0 m$^{3/}$s to the flood control start discharge 500m^3/s.

Inflow increase records mean discharge increases at a dam site before a dam completion. The inflow condition of MOPO simulation is set as a probable maximum increase condition like Fig. 5, so the maximum increase during each flood, which was correlated with the maximum inflow increase, was picked up for Ohno dam. Fig. 6 shows the relationship between the maximum inflow increase and the inflow just before the maximum increase occurred. The linear approximate line and the envelope line are also shown in the figure. In order to use these relationships, 'inflow' should change 'outflow', of course.

Outflow increases of (1) and (2) are allowed without problems. Only these limitations, however, large amount of capacity for overtopping prevention will be required to cope with the probable maximum increase condition of the inflow. The restriction based on the idea of overtopping prevention rule ((3)) was introduced.

By an overtopping prevention rule, single relation between water level and gate opening is given to each gate. Fig. 7 shows the recommended relation for crest gate. The gate opening increase is zero at the start water level of overtopping prevention, and enlarged in the higher water level (parabola is usually employed). This relation may consider reducing the outflow increase near the start water level of overtopping prevention.

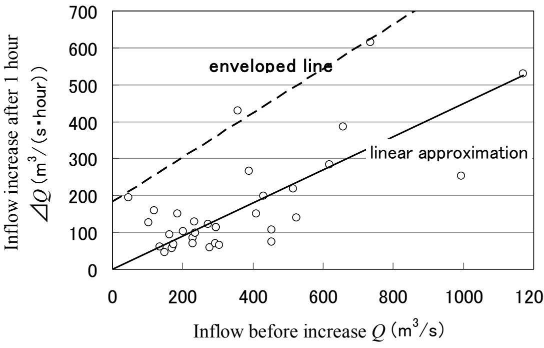

Figure 6. Relationship between inflow increase and inflow just before the increase

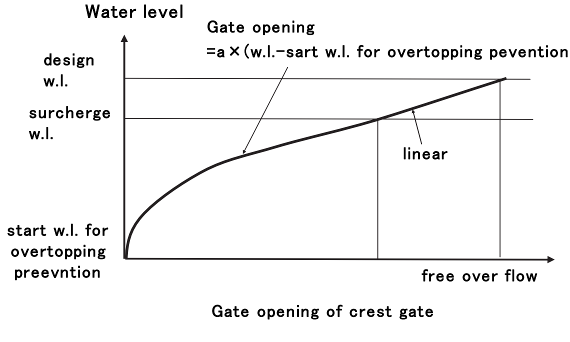

Water level
Gate opening
=a×(w.l.−sart w.l. for overtopping pevention)^2
design w.l.
surcherge w.l.
linear
start w.l. for overtopping preevntion
free over flow
Gate opening of crest gate

Figure 7. Recommended relation for overtopping prevention rule (crest gate)

Fig. 8 shows the example of the relationship between water level and outflow increase obtained by MOPO simulation, where the outflow increase restriction is based on the recommended relation and the increases of (1) and (2) conditions are allowed. The outflow increase relatively rapidly increases from the start water level of overtopping prevention, and has the peak. The greater initial inflow Qit condition brings the greater peak and the rapid increase.

Though variation characteristics shown in Fig.8 are fundamentally appreciable, there are following problems.

(a) outflow increase in the relatively larger initial inflow Qit condition is very large compared with inflow records (Fig. 6)

(b) in the probable maximum inflow condition, where inflow increases very rapidly and continue design discharge, it is more appropriate to enlarge the outflow increase in higher water level condition.

With regard to (a), the maximum outflow increase, an outflow increase cannot exceed that, was set for Ohno dam. From Wlt to the surcharge water level, that was set by substituting the design inflow for the linear approximation relation in Fig. 6 and the enveloped relation in Fig 6 was used at the design water level. The value of surcharge and design water level is connected by line. The maximum outflow increase mentioned above is also shown in Fig. 8. It is quite small in the relatively large initial inflow condition and greatly influence to MOPO.

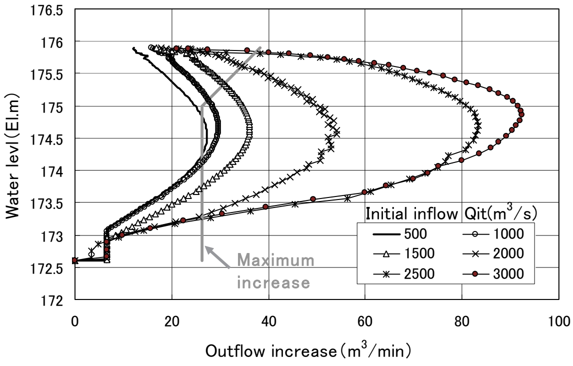

Figure 8. Example of relationship between outflow increase and water level at MOPO simulation (outflow increase restriction is based on the overtopping prevention rule)

For the problem (b), the simulation condition of 'if the outflow increase restriction obtained by the above explained way at the water level is smaller than that of the lower water level, the latter is employed' was introduced.

4. OHNO DAM'S MOPO TABLE AND EXAMPLE OF OPERATION SIMULATION BASED ON THE TABLE

Ohno dam's MOPO table obtained by above conditions is graphically shown in Fig. 9. Though, MOPO is given every 50m^3/s inflow for the table, the figure shows only every 250m^3/s.

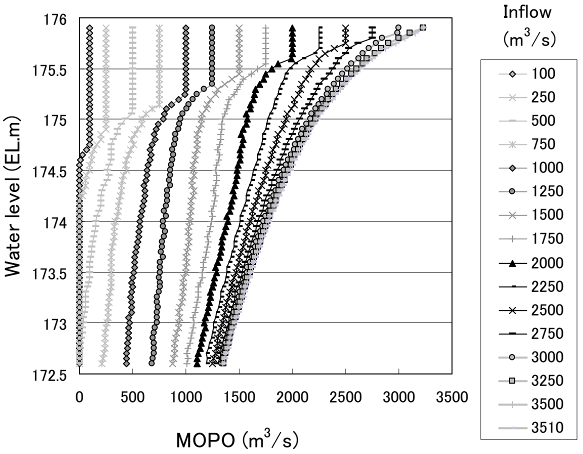

Figure 9. Graphic expression of Ohno dam's MOPO table

MOPO at the start water level of overtopping prevention is less than or equal to the outflow discharge of flood control operation, so the flood control operation is guaranteed at the start water level. Mode change from flood control to overtopping prevention operation will be introduced at higher than or equal to the start water level.

MOPO increases as the water level rises or the inflow increases. This character of discharge variation may follow the feeling of human being. Also, MOPO increasing rate increases at higher water level in the same inflow condition. Image of this is similar to the recommended curve of the gate opening and the water level relation shown in Fig. 7. Office staffs may easily get familiar with characteristics of MOPO variation.

Upper side of MOPO-water level curve in the same inflow condition has a vertical portion, where MOPO equals to the inflow. This means the outflow reaches to the inflow at a lower water level than the design water level in an actual operation. The lowest water level of the vertical portion is lower in the smaller inflow condition. One of the reasons of this may be the smaller allowable outflow increase in the smaller outflow situation.

Fig. 10 shows the example of operation simulation results using the MOPO table. The hydrograph of Ohno dam's flood control plan (Fig. 4) is used with changing peak discharge (maximum inflow peak is 3500m^3/s). The flood control operation is executed till the water level reaches to the start water level of overtopping prevention, then operation based on MOPO is executed, with constant gate opening operation if the outflow is greater than MOPO.

As the maximum water levels of all peak ratios are higher than the start water level of overtopping prevention, it is ascertained that the mode change from flood control to overtopping prevention is executed by the MOPO table without officer's judgment. Also, as the inflow peak increases, the maximum outflow increases and the highest water level rise. This indicates the operation is appropriately executed along with the flood magnitude. The highest water levels of all cases are controlled under or equal to the design water level.

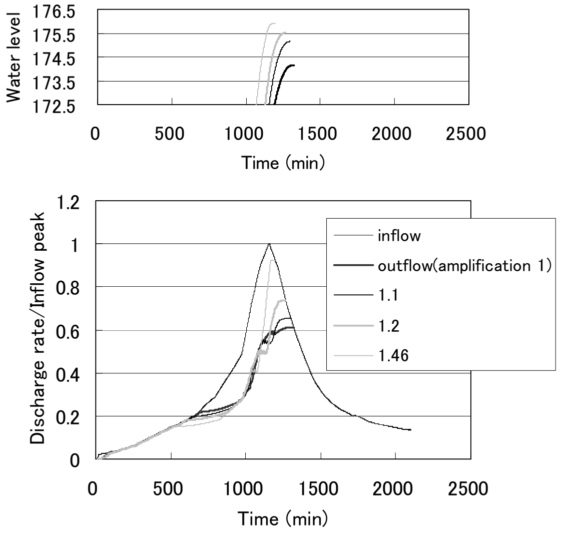

Figure 10. Examples of operation simulation results using the MOPO results (flood control planning flood)

5. CONCLUSIONS

MOPO (Minimum outflow to prevent overtopping) table was developed for supporting the mode change judgment from flood control to overtopping prevention and the decision making of the outflow increase way to get the inflow. This paper introduced the outline of MOPO and conditions for operation simulation to obtain MOPO table. Example of MOPO table and satisfactory gate operation results using the table were also shown.

Most of the introductions and explanations were done by Ohno dam's examination results. So the condition setting for MOPO simulations, especially outflow restrictions, were basically reflecting speciality of Ohno dam. Establishment of methods for the condition setting will be required for the future development of gate operation using MOPO table.

REFERENCES

Kashiwai, J., Kubozono, T. and Takada, T. (2015): Ohno dam's operation results for redusing innundation damage in excess inflow situation, Proceedings of Twenty-fifth congress of ICOLD

4th APG Symposium and 9th EADC on

INNOVATIVE TECHNOLOGIES FOR DAMS AND RESERVOIRS TOWARD THE FUTURE GENERATIONS

Safety Technology Application and Development of the Management of the Chaersen Reservoir Dam

Y. Fan
Chaersen Reservoir Management Bureau (CRMB), Songliao Water Resources Commission
Ulanhot, Inner Mongolia, China. Zip code 137400
fyy2699@126.com

ABSTRACT:
Safety management plays an important role in the secure operation of the dam and the whole reservoir project. Introducing and applying advanced automation technology is an important way to improve the safety management of reservoirs. Therefore, the development and application of 8 automation systems in the Chaersen Reservoir is introduced in this paper. They are the Dam Seepage Automatic Monitoring System; the Dam Automatic Monitoring System that uses double-satellite receiving equipment; the Real-Time Analysis and Evaluation System for dam safety monitoring; the Spillway Gate Automatic Monitoring System; the Automatic Telemetry System for Hydrological Data Acquisition; the Flood Dispatching System; the Video Transmission System and the Information Management System. In this paper, not only the important roles that these systems play in reservoir safety management is discussed, but also the future prospects for the application of automatic monitoring technologies is analyzed. Meanwhile, by reference to the rapid development globally of the application of automation technology, the significance of information management for reservoirs is elaborated. This paper can provide a good reference and guidance for the reservoirs in China, for those who want to adopt new technologies for automatic management and to improve the comprehensive level of reservoir safety management.

Keywords: Reservoir Dam, Automation System, Safety Management, Technology, Application

1. INTRODUCTION

Reservoir dam safety concerns people's lives and ensures that properties are safe downstream. Dam failure may cause devastating disasters downstream of the dam. There are very many previous cases of failure of earth-filled dams in China and the world. For example, in August 1975 a rainstorm swept Henan province, China and flood caused both the Banqiao reservoir and Shimantan reservoir to fail, which brought heavy losses. According to China’s statistics for earth-filled dam failure cases, 25% of dam failures were caused by overtopping; 10% by landslide; 32% by seepage; 21% by protective covering damage and dam face scouring; and 12% by vibration and cavitation damage of water conveyance structures within the dam （D.Liu 2006）. The above analysis shows that dam safety monitoring, safety dispatching and safety management are particularly important for dam safety. Furthermore, the safety of monitoring systems and intelligentized dispatching systems is essential for ensuring dam safety.

Reservoir dam safety management is not only an important guarantee for China's economic development, but also an important measure to ensure the safety of people's lives and properties. Therefore, the construction and application of eight systems for the Chaersen Reservoir Dam safety management are summarized and analyzed in this paper. The importance of applying automation technology on China’s dam safety management is also discussed.

2. BASIC SITUATION

2.1. The outline of the project

The Chaersen reservoir is located on the middle reaches of the Taoerhe River, a tributary of the Nenjiang River. The dam site is 1.7 km north of Chaersen town, Keyouqianqi County, Xing’an League, in the Inner Magnolia Autonomous Region. The length of the dam is 1,712 m, with a maximum dam height of 40 m. The drainage area above the dam is 7,780 km^2. The total reservoir capacity is 1.253 billion m^3. The reservoir is a large water conservancy project with many purposes, which are mainly flood control, irrigation, combined with power generation and fish farming. It is also a very important project in the Taoerhe River.

2.2. The situation for applying automation in dam safety management

The key technologies for establishing a Chaersen reservoir status information management system are several visualization technologies, such as RS, GPS and GIS. Through automatic monitoring, network technology and other measures, a series of comparatively perfect monitoring and transmission systems for the water regime has been established.

These monitoring systems can be used for monitoring the status of storage capacity, backwater areas, flooding areas, water quality, water environment and so forth. The spatial information database of the drainage area can be updated timely. These systems have played an important role in supporting the secure operating management of the reservoir.

Through the process of developing, installation and commissioning, automatic management has been realized step by step for the Chaersen reservoir. Eight systems have been established, which are: the Dam Seepage Automatic Monitoring System; the Dam Automatic Monitoring System that uses double-satellite receiving equipment; the Real-Time Analysis and Evaluation System for dam safety monitoring; the Spillway Gate Automatic Monitoring System; the Automatic Telemetry System for Hydrological Data Acquisition; the Flood Dispatching System; the Video Transmission System and the Information Management System. All the above systems constitute the core part of the Chaersen reservoir automation management. These systems, which are extremely accurate and high speed, provide a high-performance management method for reservoir dam safety monitoring, monitoring data compilation, medium and long-term flood prediction, and flood prevention and control.

3. THE DAM SEEPAGE AUTOMATIC MONITORING SYSTEM

Chaersen reservoir started its water impoundment in 1989. The main works of the project were completed in 1990. In early 1991, the hydraulic structure monitoring started to take place. Monitoring mainly has two categories: deformation monitoring and seepage monitoring. A total of 70 observation holes were set on 12 sections of the dam for monitoring seepage. Among them, 50 observation holes were set inside the dam body, 15 observation holes were set inside the dam foundation, and 5 observation holes were set around the dam. Meanwhile, monitoring of the reservoir water level, the downstream water level and the tail water level of the hydropower station was carried out.

A water pressure sensor was adopted in the early system for monitoring the seepage of the dam. In this system, the water level was converted into electrical signals through a water level sensor, and then the electrical signals were sent into the computer control system, which consisted of single board computers. In 1996, a set of J-type capacitive water level sensors were installed and fitted up with a PC data acquisition system. In July 2000, the CRMB and Nanjing Hydraulic Research Institute jointly developed a distributed automatic monitoring system with an integrated module. The system has the following three advantages: multi-functional, a friendly interface and easy to operate. The system can be adapted to safety monitoring for both earth dams and earth rock dams. This system adopts the vibration string pressure sensor that is produced by USA GeoKon Instrument Co. Ltd, and it operates with an analysis system. It is comprehensive, and runs an extremely effective automation monitoring system in real-time, which has multiple functions, including Data Acquisition, Data Storage, Data Transmission, Data Management, Data Analysis and Evaluation. In May 2010, by design and emulation debugging, a distributed automatic information acquisition system was built up. Its transformation means was changed from wired transmission to wireless transmission, and the power source was changed from electrical to solar energy. It is a system whose strong points are high reliability, good stability, and a high automation level. The measurement and control unit (MCU) of the system is the SWN-01 type intelligent distributed measurement and control unit. The MCU can eliminate problems with communication lines and power lines being frequently impacted by lightning, which used to be a common problem. Since the system was put in use, it has run stably and provided valid data for dam safety analysis. Therefore, the automation operation and management level have improved.

4. THE DAM AUTOMATIC MONITORING SYSTEM THAT USES DOUBLE-SATELLITE RECEIVING EQUIPMENT

In March 2009, by dint of Project No. 948 as an opportunity, through an investigation and research on dam monitoring systems and collaborating with Nanjing Hydraulic Research Institute and Leica Measuring Instruments (Beijing) Co., Ltd, CRMB set up a Dam Automatic Monitoring System that uses double-satellite receiving equipment.

The Dam Automatic Monitoring System uses double-satellite receiving equipment. The system uses US GPS technology, and receives GNSS satellite signals, which used to specifically for continually monitoring the structure, by using the latest equipment: a Switzerland Leica GRX1200 GG Pro and GMX902 GG, and it is fitted with an AT504 GG binary choke coil antenna, that is an antenna with the strongest anti-interference capacity and highest precision currently in the world. By using the system, the accuracy for plane location monitoring can reach 1 mm. In addition, the system not only uses a US GPS, but can also receive satellite signals from the Russian GLONASS. With the establishment and perfection of the Sino Beidou Satellite Navigation System, the EU Galileo and the Russian GLONASS system, the number of available satellites in the working time will greatly increase, and that has effectively improved the reliability and applicability of the system.

Since CRMB set up the dam monitoring system which is based on the highest precision GPS, the dam deform monitoring works in all weathers and monitors continuously in real-time. By applying the monitoring system, the dam condition can be known in good time, and it provides reliable information for the reservoir's operation. After the interface between the monitoring system and the reservoir information network platform, the higher level authorities can get monitoring data and relevant information in good time, which has improved the management level and efficiency of the project.

5. THE REAL-TIME ANALYSIS AND EVALUATION SYSTEM FOR DAM SAFETY MONITORING

Based on the situation of the Chaersen reservoir, with an eye to future water information development, the CRMB worked together with Nanjing Hydraulic Research Institute and developed the Real-Time Analysis and Evaluation System for dam safety monitoring. The system's functions include information management and analysis. The analysis function includes three sub functions, which are Real-time Analysis, Feedback Analysis and Comprehensive Evaluation. The Network and database technology used in the system is in line with international standards. The theory and method for data analysis is advanced and in full compliance with the relevant norms, rules and regulations on safety monitoring and software developing of hydraulic structures in China, that ensured the system's high-performance and reliability of the analysis results. Both the technology and method for building the system are ahead of other reservoirs or projects in China.

In 2005, the Real-Time Analysis and Evaluation System for dam safety monitoring was put into operation. The system integrates modules of engineering situation information acquisition, information processing and information reporting, and it is compatible with the existing Hydrological Regime Information Management System in the reservoir. The data produced was engineering and hydrological regime information with the advantages of timeliness, accuracy and being immediately readable without extra processing. The application of the system perfected the method of information acquisition for the reservoir project, improved the quality and efficiency of safety monitoring, and provided an important basis for decision making of flood control and optimal operation. The system plays an important role in many respects, such as ensuring the safety of the reservoir during flooding, conducting modern dynamic information management for flood control, using flood water resources wisely, and improving the capability of disaster prevention.

6. THE SPILLWAY RADIAL GATE AUTOMATIC MONITORING SYSTEM

Four submersible radial gates were set up at spillways in the reservoir, each of which has a size of 9.0*9.0 m and weight of 54.1 tons. The gate form is slab and girder, with a raking strut and articulated joint. The design head is 13.4 m. The headpiece of the gate is a movable breast wall, whose size is 9.9*4.8. The radius of the slab is 14.4 m. The height of the articulated joint is 8.29 m. Each gate has a fitted QRQ80t fixed winch as a lifting device. The gate is operated by lifting using 2 steel wire ropes, which is on the winch drum and connected with the gate through the guide pulley and fixed pulley of the pier, and a movable pulley at the suspension center.

In order to change the original gate lifting method, the CRMB commissioned the Nanjing Automation Institute of Water Conservation and Hydrology to develop the Spillway Radial Gate Automatic Monitoring System. The system can be controlled by either computer or executives. The lifting device can be remotely controlled at the administration office in the Chaersen reservoir and the control building in Ulan Hot. Reliable verification and a safety lockout mechanism were designed in the system, and different operators were empowered accordingly. Furthermore, timer programs were built into the system for monitoring the software and hardware, and the system automatically sounds the alarm when there is a fault in the operation（Q. Ding 2000）. After years of running, it has been shown that the error of gate lifting <20 cm, error of discharge <5%, and therefore the accuracy of the gate control meets the requirements. The system is easy to operate, is multi-functional and has good compatibility. The performance of the system meets the requirements in aspects of reliability, accuracy, preventing lightning and anti-interference.

7. THE AUTOMATIC TELEMETRY SYSTEM FOR HYDROLOGICAL DATA ACQUISITION

The Automatic Telemetry System for Hydrological Data Acquisition was designed by the Communication remote sensing centre of the Songliao Water Resources Commission, and installed by the CRMB. Based on the network design principles, after analysis and verification, 14 stations were designed as information sources for the system. These are: 10 telemetric rain gauge stations; 1 telemetric hydrologic station and 3 telemetric stage stations. The telemetric hydrologic station's survey items include water level, precipitation and flow rate. The three telemetric stage stations are deployed at upstream of the dam, downstream and at a hydrologic station near by Chaersen town respectively. The telemetric stage station upstream of the dam surveys items including telemetry rainfall besides water level measurement. For the telemetric stage stations combined with the hydrologic station nearby Chaersen town, its discharge record can be artificially uploaded through telemetering and telemetry relay. In addition to the 14 telemetric stations, a junction center for automatic telemetry was also set up in the CRMB.

The system was put into operation in June 1996 and has been running for 19 years. By being constantly upgraded during its use so far, the system has been gradually perfected. The hydrologic data are automatically collected by the system and transmitted to the junction center through a communication line. There in the junction center, the date are collated, stored into a database, and the hydrologic real-time monitoring, reporting and forecasting work are completed. The data acquisition and transmission can be stably and reliably completed by the system, even under bad weather conditions during flooding periods. In particular, the system played a decisive role during the 1998 Flood by providing timely and precise information.

8. THE FLOOD DISPATCHING SYSTEM

The Flood Dispatching System is a comprehensive information system for assistance in decision-making on flood dispatching, which is composed of 9 subsystems and 1 integrated database. The subsystems include 1. information receiving and processing; 2. application of meteorological products; 3. flood monitoring; 4. information service; 5. flood forecasting; 6. flood regulation; 7. flood control consultation; 8. flood management and; 9. flood disaster evaluation.

The flood dispatching system has the advantages of being multi-functional, user-friendly, adaptable and compatible, and it can be used in the fuzzy optimal operation of interactive flood forecasting. The system uses the most advanced computer technology, such as visualization, multimedia and databases and so on. It builds up the object model by using object technology. That made the system has the advantages of good generality and ease for system maintenance. The model for flood forecasting offers an open interface for future designing and is easy to be extended and modified to fit any future expansion in the system, and it is also easy to quickly generate a real-time flood control scheme. The flood regulation model adopts a multi-objective fuzzy optimization model for flood control decisions. The Four Order Runge Kuta method is adopted in the calculation of flood control of the reservoir. This method has the advantages of not needing drawings or trial calculations, and it is easy to develop a general module and get the calculation results very quickly and with high precision. The method is very suitable for reservoir cases with multiple water discharge equipment and changing open states, and changing calculation periods for flood regulating. （H. Zhou 1999） The Information Service model is a headwords hierarchical model; it is very easy to get wanted information by entering multiple headwords. The flood monitoring model has the inquiry function for comparing the real-time water regime with historical rainfall and its water regime at that time, and comparing the real-time flood to its forecast flood. This can enable the reservoir manager to make timely and correct decisions about the flood variation. The model also has a strong graphic output function.

According to the experience of flood dispatching, three targets were taken into account in the system for one process of a flood regulation: 1. the lower the maximum water level, the closer to the optimal storage capacity; 2. the maximum discharge flow of the reservoir or combined maximum river flow through a control points should be as small as possible; 3. apart from the above, for the reservoirs whose task is to generate electric power, it should be considered that the more the power, the far better it is. It is obvious that the first target reflects the safety of the reservoir itself, the second target is concerned with the safety of downstream and the third target is to consider increased water storage, meanwhile with an eye on flood superposition when conducting flood dispatching.

9. THE VIDEO TRANSMISSION SYSTEM (ENGINEERING REMOTE MONITORED SYSTEM)

Video screens for remotely monitoring the reservoir are available in the machine hall. The videos show a general survey of the project, the spillway outlet, the indoor scene of the headstock gear room, the downstream slope, the dam upstream slope, the inlet of the water conveyance tunnel and the outlet of the water conveyance tunnel. The videos are transmitted through optical fiber to the machine hall and output there.

The Chaersen reservoir engineering remote monitored system managed by three level authorities, which are the main control centre in Songliao Water Resources Commission, the sub control centre in the CRMB and the duty room at the dam. The system can realize the automatic collection of images, remote real-time display in the computer and remote control operation; support multiple workstation access to real-time monitoring videos at the same time; set aside a full interface for future use, and can share information with the existing flood control platform.

Before implementation of the remote video monitoring system, the reservoir staff had to inspect both the operating conditions of the dam and the water gate personally on the spot. This method had disadvantages in that the situation report to the Flood Control and Drought Relief Headquarter was not very accurate, which adversely affected the headquarters' ability to make the right decisions. Through the remote monitoring system, the operation situation about the dam, the water gate, and the water level at the upstream and downstream slopes can be acquired in good time. Also, real-time changes of the reservoir flood and all kinds of latent dangers can be known immediately. By using the system, the flood control and drought relief office can take the initiative in grasping the comprehensive data of reservoir flood in good time, and that is a great help to managers in making a proper flood control plan and giving orders for reservoir dispatching.

10. THE INFORMATION MANAGEMENT SYSTEM

The traditional water conservancy is now developing to modern water conservancy. One example of this development is that the reservoir management information system is in an important stage to its integrating and network upgrade. The establishment of the Chaersen reservoir information management platform is one of these innovative practices.

The keynote of the reservoir information is the dam. The previous information system of the reservoir was composed of subsystems of a hydrological telemetry system, a flood dispatching system, a dam monitoring system and a gate control system, and these systems mainly focused on the dam safety and reservoir operation. They were developed by different research departments respectively. There were large differences among the data structures, interface specifics, and a lack of integrity, compatibility and security which is a major prerequisite for large systems.

According to the principle of a rapid and accurate, friendly interface, high technology, safety and reliability, by solving all kinds of problems, the new generation of reservoir information platform in the Chaersen reservoir has been established. The large information system has building an integrated and networked system as the goal, adopting advanced system integration and GIS Web network technology, so that the reservoir information management have achieved a new level.

3S information technology is used in the information platform. Using modern means, such as RS, GIS and GPS to collect data, image, sound, video and other basic information, not only improves the accuracy of the data, but also enables the hydrologist to finally bid farewell to the traditional backward ways of data collection. By improving the digital degree of the data, the modernization level of the project is improved accordingly, and actualized comprehensive consideration of the overall situation of the project, as well as the efficiency and technical level of the Chaersen reservoir management, are improved.

11. CONCLUSIONS AND DISCUSSION

11.1. The technology in use in China for building automatic monitoring systems

11.1.1. The dam safety automatic monitoring system

The mission of dam safety automatic monitoring is to obtain the real-time working status of a dam, and to provide data for analysis of the dam's condition. That is needed to find out the weak part of the dam before the designing and planning of a safety monitoring system, and then setting up the monitoring device and apparatus in the right place. Meanwhile, the designer must make sure the monitoring facilities and installation works are highly reliable, the data from the designed system must accurate, and the safety automatic monitoring of the system must be in real time.

11.1.2. The automatic hydrometry monitoring and forecasting system

An automatic hydrometric monitoring and forecasting system is an advantageous tool used for flood forecast in river basins and reservoirs, flood control operation and the rational utilization of water resources, through real-time monitoring, transmitting and processing hydrologic information using modern science and technology. For dam safety, obtaining the water regimen is very important basic work for flood control and disaster reduction. Since the 1990s, especially after the Big Flood in 1998, China has attached great importance to the hydrological automatic measuring and reporting technology in the study, and therefore the hardware and software has been rapidly developed. China's national flood control headquarters carried out a key science and technology program on the reservoir flood dispatching system development, and accomplished key computer networks in the Ministry of Water Resources, the seven River Basin Organizations, 31 provinces respectively, and in four key projects. At present, China is at the forefront of the world in hydrological automatic measuring techniques and in hardware and software development. The large and medium-sized reservoirs around China have met the basic requirement of hydrological automation both in hardware and software aspects.

11.1.3. The water gate automatic monitoring and video transmission system

The water gate automatic monitoring and video transmission system usually consists of a remote monitoring system, a central control system, an on-the-spot control system and a decision support system. The whole system is formed by a backbone network. The key technology for building the whole system includes a sensor and transducer that are set at the gate, a programmable logic controller (PLC), configuration software and system fault tolerance technology. Furthermore, a C/S and B/S combination of the mixed mode are usually adopted for construction of the system. The mode has the advantages of being simple, practical, reliable, and easy to expand and to upgrade. By using the mode in the system, the gate can be accurately opened and closed according to the dispatching instructions, and it achieves rapid exchange and sharing of information.

11.1.4. The reservoir real-time safety dispatching technology and the automatic system

Engineering safety is the precondition for utilization of flood resources. The premise of safety is the only way to benefit from flood control and disaster reduction, and make full use of water resources. Therefore, it is necessary to know whether the project is safe and the gate is running normally before flood dispatching, and to constantly revise the flood dispatching scheme according to the actual situation. The precondition for making the separated data available for decision making is to achieve data sharing through integrating the engineering running condition monitoring system, hydrological monitoring and the gate monitoring system, and to establish a real-time safety dispatching system to provide timely technical support for decision-making concerning safety dispatching

The development and research into reservoir real-time safety dispatching technology starts with some key technologies, such as the integration of a subsystem, real-time evaluation of dam safety, optimization of the dispatching scheme and decision-making support.

11.2. The prospects for automation technology development

Italy's GPDAS system, the United States of America's 2380/3300 and the IDA distributed system are representative automatic monitoring systems that are currently being used in the world （Y. He 2005）. Communication methods for automatic monitoring systems for dam safety generally include a variety of ways, such as wired, wireless, satellite, telephone lines, optical fiber, GSM/GPRS and others. In recent years, most automatic safety monitoring systems for building dams have two or more ways of communication in order to facilitate forming a network. Many systems give priority to optical fiber communication, which not only improves the communication speed, but also improves the anti-EMI interference ability and the anti-lightning ability of the system. At present, in order to facilitate the dam safety, monitoring automatic systems can be used in different situations, most of them with a variety of power supply, e.g. alternating current, direct current, battery, solar power supply, etc. As the most basic unit of the water conservancy system, the information construction of the reservoir is the foundation of the whole water conservancy information construction. A reservoir information system is mainly composed of an automatic hydropower station monitoring system, an automatic dam safety monitoring system, a hydrological telemetry system, an automatic office system, a reservoir optimal scheduling system, a gate monitoring and control system, a video surveillance system and a comprehensive information publishing system through a website. Each subsystems is integrated through the computer network system to realize the data sharing and collaboration among the subsystems. To adopt database technology for processing information, and combined with a Web information publishing system that is developed based on the B/S model, the different users at all levels can easily and intuitively get information through the system.

Although the automation management level of the Chaersen reservoir has reached an advanced level globally and the leading level domestically, there is still a certain gap comparing to developed countries. In the risk management of the reservoir, China is in the initial stage of research. In comparison, developed countries have established a long-term alarm system and even carry out regular exercises. In order to avoid disaster and reduce losses, there is still a need to develop an alarm system in the Chaersen reservoir, and a need to put forward a set of feasible technical schemes of alarm criterion, classification, equipment and method, to institute the safety alarm standards and norms until there are suitable conditions. In respect of the dam dynamic monitoring system, the dam CT techniques are in the research stage. The technician will accelerate the pace of the research. It is expected that the new technology will serve the reservoir in the near future.

REFERENCES

D. Liu (2006): Chaersen reservoir project management, Jilin University Press

Q. Ding (2000): The design report of automatic monitoring and control system for piezometric tube and spillway gate in the Chaersen reservoir, Nanjing automation Institute of Water Conservation and Hydrology

H. Zhou (1999): Flood dispatching system technical report of Chaersen Reservoir, Dalian University of Technology

Y. He (2005): Development and research report of the Chaersen reservoir dam safety analysis and evaluation system, Nanjing Hydraulic Research Institute and Chaersen Reservoir Management Bureau

Study on the Seismic Safety of Foundation Gallery of High Rockfill Dam Located on Deep Alluvium Deposit

C.X.Xing
Huaneng Lancang River Hydropower Inc, China;. State Key Lab. of Water Resources and Hydropower Eng. Sci. ,
caoxxxing@163.com

H.Y.Long
State Key Lab. of Water Resources and Hydropower Eng. Sci. , Wuhan Univ. , China

X.Kun
Changjiang Institute of Survey, Planning, Design and Research, China

ABSTRACT:
The stress conditions are very complex of foundation gallery in the earth dam located on deep alluvium deposit, which is the weak link of seepage control system as well as the key part of seepage control and safety control. Three dimensional nonlinear finite element analysis was carried out to explore the stress and deformation as well as the seismic safety of the foundation gallery of 240m Changheba dam, based on the dynamic submodeling method. The filling materials of this dam and alluvium deposit were simulated by the Hardin-Drnevich constitutive model that could consider the effect of confining pressure. The results demonstrate that: the dynamic response of acceleration and dynamic displacement of the gallery is smaller as it located inside the dam. The stress of the gallery under dynamic condition is increased than it under static condition. The longitudinal maximum tensile stress increased 8% at the most. The stress state is not worse as the improvement of the dynamic strength of concrete. The maximum tension deformation of the joint on the left bank is 4.0 cm, increased 11.4% the under static condition.

Key words: foundation gallery, Changheba Dam, submodeling analysis method, dynamic response, stress and deformation

1. FOREWORD

If a high rockfill dam located on deep alluvium deposit contains a concrete diaphragm wall in its foundation, the connection between the wall and the core wall in dam body will be the weak link of the entire seepage control system of the dam, and also the key part to control seepage and the safety of the system (L.Jie,1992). If the connection were damaged, the dam might be ultimately destroyed, leading to severe loss of human life and property. The connection is commonly made through a grouting gallery on the top of the diaphragm wall, or by directly inserting the wall by a certain depth into the earth core wall at home and abroad. In the large-scaled Chinese Pubugou, Qiaoqi, and Shiziping projects, the amount of curtain grouting is considerable due to deep alluvium deposit on riverbed. In order to speed up construction, keep the bedrock curtain grouting at the bottom of the diaphragm wall from occupying the linear construction period, and facilitate safety monitoring over key parts of the dams and take immediate and effective remedies in case of abnormality during operating period, grouting galleries were provided on the top of the diaphragm walls for connection purpose.

In Changheba Hydropower Station, a 240m-high rockfill dam with gravel-earth core is built on a foundation of deep alluvium deposit that is 60m-70m deep. The dam uses two fully enclosed concrete diaphragm walls. A gate-arch-shaped reinforced concrete gallery is built on the top of the primary diaphragm wall to connect the wall to the core. The gallery has an internal dimension of 3 m×4 m, sidewall thickness of 2 m, and base plate thickness of 3 m. The primary diaphragm wall is connected to the gallery using a rigid junction. The connection between the wall and the gallery bottom is of reverse-trapezoid shape. The riverbed segment of the gallery is not equipped with any structural joint in the longitudinal direction. According to the original design, joints would be made at the boundary between the bedrock and alluvium deposit to connect to the grouting adits in both banks. However, the Qiaoqi and Pubugou projects with similar structures have both suffered gallery cracking and damage of water seal. Numerical calculation on the original design also suggested large deformation in case of joints at the boundary between the bedrock and alluvium deposit(X.Kun,2011). After profound study, the foundation gallery is changed to penetrate into the bedrock by 1m to create joint connection with the grouting adits in both banks.

Few study has been carried out on the stress and deformation state of galleries in foundation of deep alluvium deposit at home and abroad. Only

(X.Kun,2011) analyzed the stress and deformation characteristics of the foundation gallery with joints at the boundary between bedrock and alluvium deposit under static condition in Changheba Project. (Z.X.Xi,2012) evaluated the seismic safety of the foundation gallery in the 91.5m-high Jinping Rockfill Dam with an asphalt and concrete core. However, the Changheba Project, which is examined in this paper, has a seismic precautionary intensity of Degree 9 for its dam. Both the height and the seismic intensity of the dam are far more than any other similar works already built. Moreover, the foundation gallery is buried in the dam body. Its bottom is rigidly connected to the diaphragm wall and both ends are penetrated into bedrock and connected to the adits in both banks. As such, both the structure and stress condition of the gallery are extremely complex; and its stress condition will be more special in case of earthquake. In this paper, nonlinear 3D FEM based on the submodeling method is used to finely simulate the gallery in the foundation of deep alluvium deposit. Dynamic calculation during earthquake is successively carried out on the entire dam-foundation body and then on the foundation gallery. Next, the static and dynamic characteristics of the foundation gallery are analyzed to evaluate its seismic safety.

2. PRINCIPLE OF CALCULATION

2.1. Dynamic Submodeling

To simplify analysis modeling, shorten calculation time, and increase the calculation precision of interested parts, FEM submodels with finer calculation mesh are built using the submodeling technique for foundation gallery, as well as the foundation diaphragm wall and other anti-seepage systems in the foundation. Submodeling method is also referred to as the cut-boundary displacement method or the specified boundary displacement method. It is a new FEM technique developed from the traditional FEM method and has seen several applications in the static and dynamic analysis of detailed structures such as dam joints, anti-seepage systems, and dam openings (K.Kun,2011, Z.X.Xi,2012, Y.F.Hai,2010, W.Q.Jun,2006, L.X.Qing,2016). Based on the Saint Venant's principle, submodeling is preceded by the calculation and analysis on the overall FEM model of which the mesh is relatively coarse. Next, a zone of interest is cut out from the overall model to build a finer FEM mesh for re-calculation. In case of static calculation, boundary conditions for the zone are the displacements calculated for the corresponding position in the overall model. For the purpose of dynamic calculation, the node displacement, velocity, and acceleration of the cut boundary for the submodel are obtained by interpolation in the overall model and are applied to submodel boundary as the boundary conditions of dynamic time history used for submodel calculation.

2.2. Dynamic Constitutive Model of Earth and Rock Material

In static calculation, Duncan E-μ hyperbolic model is used for the materials in the dam body and the alluvium deposit, and the layered filling process of the dam and the water filling process are simulated. The static result is used as the initial state for the dynamic calculation. Dynamic calculation is performed using the modified Hardin-Drnevich model in which the confining pressure effect is considered (Hardin.B.O,1972, C.X.Xing,2010). The expression of shear MOE is as follows:

$$G/G_{\max}=1/(1+(\gamma_d/\gamma_r)^m) \qquad (1)$$

Wherein: m is the form coefficient of the dynamic shear MOE ratio curve, which is a fitting parameter related to material properties; γ_r is the reference amplitude of shear strain. γ_r and m are both related to confining pressure.The expression of damping ratio is as follows:

$$\lambda = a_3 + a_4(1-G/G_{\max})^{a_5} \qquad (2)$$

Wherein: λ is the equivalent damping ratio; a_3 is the basic damping ratio of material, which is related to earth properties and consolidation state; a_4 and a_5 are the form coefficients of the damping ratio curve, which are fitting parameters related to material properties.

2.3. Permanent Seismic Deformation

The permanent seismic deformation of dam is calculated using the softening modulus method. The following formulas that consider the confining pressure effect are used to calculate the residual volumetric strain and residual axial strain:

$$\varepsilon_v = K_v(\Delta\tau/\sigma_0^{'})^{n_v} \qquad (3)$$

$$\varepsilon_p = K_p(\Delta\tau/\sigma_0^{'})^{n_p} \qquad (4)$$

Wherein: K_v, n_v, K_p and n_p are coefficients and indexes related to earth properties, strain state, and shake frequency and are determined from experimental results. Set $K_v = a_1(\sigma_3)^{b_1}$, $n_v = a_2(\sigma_3)^{b_2}$, $K_p = a_3(\sigma_3)^{b_3}$, and $n_p = a_4(\sigma_3)^{b_4}$. Wherein, a_i and b_i (i =1, 2, 3, 4) are experimental fitting parameters.

3. FEM MODEL AND CALCULATION PARAMETERS

3.1. FEM Model

Fig.1 is the overall FEM model. The overall model consists of 23,418 nodes and 21,586 elements. The submodel includes the primary diaphragm wall, secondary diaphragm wall, foundation grouting gallery, high plastic clay, and the junction between the foundation gallery and the bedrock grouting galleries on bank slopes. It consists of 14,474 nodes and 13,176 elements. The submodel encloses the entire alluvium deposit and reaches the underlying bedrock. On both banks, it reaches the bedrock.

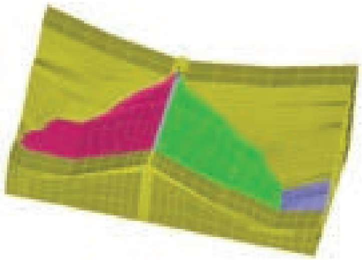

Figure 1. FEM Mesh Model

3.2. Material Parameters and Calculation Load

Refer to (X.Xun,2011) for the static parameters of earth and rock materials and the mechanic parameters of interface. In dynamic calculation, the aforesaid Hardin-Drnevich model considering the confining pressure effect is used for earth and rock materials. Refer to (C.X.Xing,2010),for the calculation parameters of the materials. Linear elastic models are used for bedrock and concrete. The concrete has the density of 2400 Kg/m^3, MOE of 30 GPa, and Poisson's ratio of 0.167. The bedrock has the MOE of 9 GPa, and Poisson's ratio of 0.28. The dynamic MOE is 30% higher than the static MOE. Dynamic calculation is performed using a massless bedrock model. The input for the dynamic calculation is the seismic wave for time-history analysis as fit with the field spectrum in seismic safety evaluation. After inversion with SHAKE91 program, the peak values of the horizontal and vertical seismic waves inputted from the bedrock surface into the foundation bedrock is 0.29 g and 0.193 g, respectively. In the calculation, the seismic duration is 30s, and time step is 0.02s. Fig.2 illustrates the accelerograms of the seismic waves in different directions.

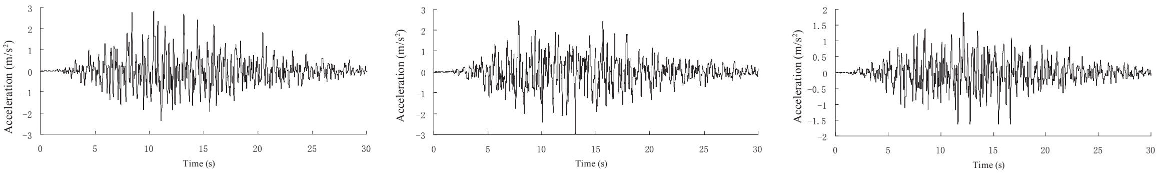

(a) Transverse (b) Longitudinal (c) Vertical

Figure 2. Accelerograms in Transverse, Longitudinal and Vertical Direction

4. STRESS AND DEFORMATION ANALYSIS OF FOUNDATION GALLERY UNDER STATIC CONDITION

The gallery flexibly deforms in the vertically downward direction due to its dead weight and the pressure from the dam-body earth over it; and in the downstream direction as pulled by the diaphragm wall below. The resultant effect of the two deformations creates significant stress in the gallery in the longitudinal direction. In the upstream face, it is compressed in the middle riverbed and stretched on both ends. In the downstream face, it is stretched in the middle riverbed and compressed on both ends. Because the gallery penetrates into the bedrock by a certain depth, it is constrained by the bedrock on the bedrock surface, resulting in considerable stress concentration at the position. Moreover, the compressive stress is large at the 1/4 span from the right and left banks on the upstream face; and the tensile stress is large at the 1/4 span from the right and left banks on the downstream face.

Tab.1 lists the max. values of deformation and normal stress of the gallery under the static condition in all directions. In the calculation results, the tensile stress is positive and compressive stress is negative; transverse deformation is positive if it is in the downstream direction; and settlement is positive if it is upwards.

Table 1. The Maximum Deformation and Stress of The Foundation Gallery

	Settlement /cm	Transverse displacement /cm	Longitudinal normal stress / MPa		Transverse normal stress / MPa		Vertical normal stress / MPa	
	Vertically downwards	Downstream	Tensile stress	Compressive stress	Tensile stress	Compressive stress	Tensile stress	Compressive stress
Value	16.5	40.7	26.5	-37.0	4.89	-35.9	6.0	-53.7
Position	Bottom of upstream face in mid-span profile	Gallery bottom in mid-span profile	Bottom of upstream face of right-bank bedrock	Bottom of downstream side of right-bank bedrock	Center of base plate in mid-span profile	Bottom of downstream side of right-bank bedrock	Bottom of upstream face near right-bank bedrock	Bottom of upstream face of right-bank bedrock surface

5. STRESS AND DEFORMATION ANALYSIS OF FOUNDATION GALLERY UNDER SEISMIC CONDITION

5.1. Response of Acceleration and Dynamic Displacement

Because the foundation gallery is buried in the dam body and foundation, its dynamic response of acceleration and dynamic displacement are not considerable. Fig.3 gives the distribution curves of the acceleration and dynamic displacement in three dam axis directions on gallery crown. The response in the transverse direction is apparently the most intense among the three directions. The transverse acceleration has a max. value of 6.0 m/s^2 and apparently larger at middle riverbed. The distribution of longitudinal and vertical acceleration is relatively even along the length of the gallery. The transverse dynamic displacement has a max. value of 2.7 cm and apparently larger at middle riverbed. The distribution of longitudinal and vertical dynamic displacement is relatively even along the length of the gallery.

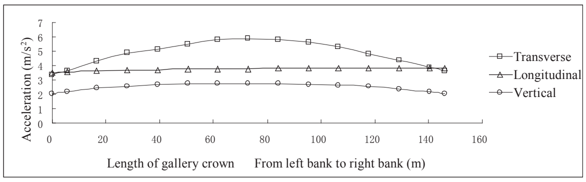

(a) Max. Acceleration

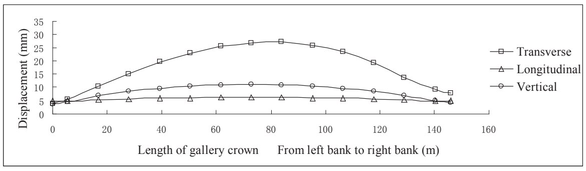

(b) Max. Dynamic Displacement

Figure 3. Dynamic Response on The Gallery Crown

5.2. Dynamic Stress Response

Fig.4 gives the max. longitudinal dynamic stress in the gallery. Fig.5 is the distribution chart of longitudinal normal stress in the gallery after static-dynamic superposition. Under seismic impact, the gallery is subjected to larger longitudinal dynamic stress at the bedrock surface on the right and left banks, 1/4 span from the left bank, and 1/4 span from the right bank; and especially, dynamic stress concentration is significant on the bedrock surface on both banks. During earthquake, the max. absolute value of longitudinal dynamic tensile stress occurs at the bottom of upstream gallery face on the right-bank bedrock surface, which is 2.14 MPa, the max. absolute value of longitudinal dynamic compressive stress occurs at the bottom of downstream gallery face on the right-bank bedrock surface, which is 2.23 MPa. The dynamic tensile and compressive stress in the upstream and downstream gallery face are higher than 1MPa in the zones of 1/4 span from the left bank and 1/4 span from the right bank.

The distribution pattern of gallery stress after the dynamic-static superposition is generally the same as that under the static condition. After the superposition, the max. tensile stress occurs at the upstream gallery bottom at the right-bank bedrock surface, which is 28.6MPa, 8% higher than that under the static condition; and the max. compressive stress occurs at the downstream gallery bottom at the right-bank bedrock surface, which is -39.2MPa, 6% higher than that under the static condition.

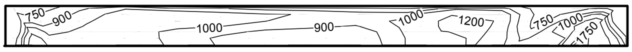

(a) Upstream Face

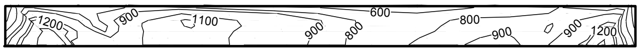

(b) Downstream Face

Figure 4. The Maximum Dynamic Tensile Stress of Gallery in Longitudinal/MPa

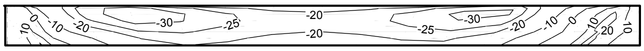

(a) Min. normal stress in upstream face

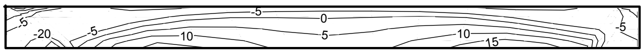

(b) Max. Normal Stress in Downstream Face

Figure 5. The Total Longitudinal Stress of The Gallery/MPa

6. ANALYSIS ON SEISMIC SAFETY OF FOUNDATION GALLERY

6.1. Possible Cracking Zones in Gallery

According to the Calculation results, the areas in excess of concrete tensile strength in each direction under the dynamic condition are generally the same as those under the static condition because the concrete strength is somehow higher under the dynamic condition and the dynamic stress is less than the static stress. Therefore, the strength requirements under seismic condition can be satisfied as long as the tensile areas under the static condition are controlled.

6.2. Deformation of Joints between Gallery and Bank Adits

In both of Pubugou and Qiaoqi projects, joints have been built between gallery and bank adits at the boundaries between bedrock and alluvial deposit. Because bank adits deform little while the gallery has little constraint, the joints have deformed relatively considerably. In Changheba Project, the gallery penetrates into the bedrock on each bank by 1m. As a result, the bedrock constraints somehow reduce the deformation of the joints between the gallery and bank adits, as well as the difficulty of water-seal design. Under seismic impact, the left-bank gallery joint has the max. tensile deformation in the normal direction of 4.0cm, which is 11.4% higher than that under the static condition.

6.3. Permanent Deformation of High Plastic Clay around Gallery

Because the clay is relatively soft, it is compressed towards the center and deforms downstream after earthquake. The interface between the upstream gallery face and the clay is tightly compressed. The interface between the downstream gallery face and the clay tends to get loose and deform under seismic impact. The interface between the downstream face of secondary diaphragm wall and the clay is tightly compressed. The interface between the upstream face of secondary diaphragm wall and the clay tends to get loose and deform under seismic impact. The clay at the gallery crown and near the core has a max. settlement deformation of 26 cm, max. upward compression of 6cm, and max. permanent deformation towards the upstream and downstream directions by about 15cm.

7. CONCLUSION

(1) The foundation gallery, which is buried in the dam body and foundation, has little dynamic response under seismic impact. Therefore, the distribution pattern of gallery stress after the dynamic-static superposition is generally the same as that under the static condition. However, the stress in the gallery of a high earth-rockfill dam is worse than that of a low dam under comparable conditions because the body and diaphragm wall of the high dam deform more significantly due to the higher water head they carry, leading to larger deformation in the gallery in the dam body as well as the joints between gallery and bank adits.

(2) After the dynamic-static superposition, the max. longitudinal tensile stress in the gallery is 28.6MPa, which is 8% higher than that under the static condition. The tensile strength in relatively large areas on both ends of the upstream gallery face and in middle riverbed of the downstream gallery face in the longitudinal direction has far exceeded that of concrete. The foundation gallery is designed to penetrate into the bank bedrock by 1m. The bedrock constraints somehow reduce the deformation of the joints between the gallery and bank adits. The left-bank gallery joint has the max. tensile deformation in the normal direction of 4.0cm, which is 11.4% higher than that under the static condition. After earthquake, the high plastic clay at the gallery crown and near the core has a max. settlement deformation of 26 cm, max. upward compression of 6cm, and max. permanent deformation towards the upstream and downstream directions by about 15cm.

(3) The gallery stress under seismic condition is still controlled by the static condition under seismic condition. Reference may be made to Manicouagan 3 dam, which is built on a foundation of deep alluvium deposit; that is, the gallery axis may be arranged to an arc that is convex towards upstream. This creates pre-tensioning on the upstream face and pre-compression on the downstream face, thereby reducing the longitudinal tensile stress. Moreover the gallery may be wrapped with steel plates of a certain depth at the bedrock surfaces on both left and right banks, provided that rebars are normally provided. For the joints between the gallery and both bank adits, it is suggested that water seals with double-U-structured expansion joints should be used and reserve should be made for phase-2 concrete works.

(4) In the calculation of the paper, concrete is analyzed as linear elastic bodies. The calculated max. tensile stress at the gallery bottom on the upstream side at the bedrock surface is 28.6MPa; the tensile strength in considerably large areas has far exceeded that of concrete. Therefore, a nonlinear model will be used to simulate the behavior of concrete cracking and damage on the next step. This will more truly reflect the actual work state of foundation galleries in high earth-rockfill dams located on deep alluvium deposit.

REFERENCES

L.Jie.(1992): Case Study of Seepage Control by Concrete Diaphragm Walls. Dam Observation and Geotechnical Tests, 5，pp. 39-43.

X.Kun, H.Y.Long, W.X.Yu et al.(2011): Research on Stress and Deformation Characteristics of Foundation Gallery in Changheba Dam. Chinese Journal of Geotechnical Engineering, 33:11, pp. 1767-1774.

Z.X.Xi, H.Y.Long, Z.Rong.(2012): Evaluation on Seismic Safety of Foundation Gallery in Rockfill Dam over Deep Alluvium Deposit. Engineering Journal of Wuhan University, 45:4, pp. 447-453.

Y.F.Hai.(2010): Discussion on Structural Model of Foundation Gallery in Earth-rockfill Dam over Deep Alluvium Deposit. Water Power,36:6, pp. 54-55, 59.

W.Q.Jun, F.S.Jun.(2006): Submodeling Research on Anti-seepage Structure in Pubugou Earth-rockfill Dam. Engineering Journal of Wuhan University,39:3, pp. 55-59.

L.X.Qing, L.T.Chun, Y.Y.Yuan et al.(2009): Dynamic Submodeling Method for Stress Analysis of Concrete Dam Opening under Seismic Impact. Journal of Hydroelectric Engineering, 28:5, pp. 88-91.

Hardin.B.O, Vincent.P.D.(1972) Shear Modulus and Damping in Soils Design Equations and Curves. Journal of Soil Mechanics and Foundations Division, 9006:SM7, pp. 667-691.

C.X.Xing, H.Y.Long, X.Kun.(2010): Confining pressure effect on dynamic response of high rockfill dam *Frontiers* of Architecture and Civil Engineering in China, 4:1, pp. 116-126

Determination of Dam Construction Schedule Robustness Metric Weight with Analytic Hierarchy Process

M.Q. Zhao, X.L. Wang & J. Yu
State Key Laboratory of Hydraulic Engineering Simulation and Safety of Tianjin University, Tianjin, China
iamfromtju@126.com

L. Bi
Water Transportation Planning and Design Institute Ltd, Beijing, China

ABSTRACT:
The measurement of robustness is the basis of robustness analysis of dam construction schedule. Because the reliable result of the robustness measurement plays a key role in the maintenance of security and stability for the dam construction. The Start Time Deviation Method has the ability to take different demands for float time from different procedures into consideration, which accords with the characteristics of the dam construction simulation model. Meanwhile, the corresponding robustness indices can refresh the evaluation of every procedure, so that scientific analysis methods can be provided for the robustness analysis of dam construction schedule based on the simulation analysis. Therefore, the disturbance of procedures during the construction is set as the value of weight and quantified in this paper. And then, the Analytic Hierarchy Process (AHP) is used to determine the value of robustness. The value of robustness gotten from this method is able to combine the quantitative and qualitative indices from the robustness question during the dam construction together, making the results more systematic. This method can also make the determination of dam construction schedule robustness more practical and effective.

Keywords: Dam construction schedule, Robustness metric, Weight, AHP

1. INTRODUCTION

Robustness metric is the basis for robustness analysis of the construction schedule. At present, many scholars have given some kinds of relevant definitions of robustness metric. Al-Fawzan & Haourai[1] defined summary of project activities' free relaxation time as a robustness index firstly. Abbasi et al.[2] followed Al-Fawzan's method. They defined summary of project activities' total free float as the robustness index and proposed a comprehensive evaluation function with liner weighted summary of duration and total free float. Kobylański & Kuchta[3] pointed out the shortcomings by most of the literatures whose authors defined different kind of summary of free float as the robustness index. They proposed the ratio of free float and activity duration as the robustness index. Van de Vonder et al.[4] presented the project activity starting time deviation as a robustness measure method. Lambrechts et al.[5] evaluated the defect that summary of project activities free float was defined as a scheduling project's robustness index. They proposed weighted summary of deviation between activities scheduled start time and actual execution time as the robustness index.

Above robust measure could be mainly divided into two kinds: difference measurement method and starting time deviation method. However, the feature that different processes have different requirements on float time deviation is not taken into account in the difference measurement method. So, starting time deviation method is the better method[6].

Starting time deviation method's formula includes the right to weight. Traditionally, researchers mainly used expertise method to give the weights assignment directly. It is a simple method, but it is also creates a not small error, which is misleading to the final robustness metric result. Therefore, in this paper, costs incurred through inference are used as the basement of weight determination and AHP is used to determine each process's final weight.

2. DETERMINATION OF ROBUSTNESS INDEX WEIGHT

2.1. Starting Time Deviation Method

Starting time deviation method is: the robustness index is the weighted summary of absolute deviation between the actual process starting time and the planned process starting time, which is shown in Formula 1.

$$r_s = \sum_{i=0}^{n} w_i \left(\left| S_i - s_i \right| \right) \qquad (1)$$

where i is process number; n is the total number of process; S_i is the actual process starting time, which is the starting time for process of the construction schedule by interference, and it is obtained based on uncertainty interference probability distribution curve and the dam construction schedule simulation model; s_i is planned process starting time, which is each process's starting time in the analysed dam construction schedule simulation program; w_i is each process's deviation weight.

The deviation weight of each process is determined by the cost resulting from the process disturbance. Greater cost comes with the greater weight. This kind of cost includes the increasing resources, the increasing storage space, costs arising from loss of working time, and so on. They are determined by the empirical method, as well. Typically, the impact of process on critical path to the total duration is greater than the impact of process on the non-critical path to the total duration. Namely, lag process on critical path will lead to a greater cost increasing. So, the weight of process on critical path is always larger than that on non- critical path.

2.2. Determination of Index Weight

The weight of the index is a subjective and objective response of the relative importance in the process of the index evaluation. The difference of the weight between the indexes is caused by the following three points:

1) The degree of attention of the reviewers is different, which reflects the subjective differences of the reviewers;

2) The function of each index in the process of evaluation is different, which reflects the objective differences between the indicators;

3) The reliability of each index is different, which reflects the reliability of the information provided by the indicators.

There are two methods for weighting:

1) Empirical weighting method: this method is al-so called the qualitative weighting method. It has the merit of the expert direct assessment, simple and easy.

2) Mathematics weighted method: this method is also called the quantitative method, which has the advantage of the background of the experience, the mathematics principle, the indirect generation, and has the strong science.

At present, experience judgment method via expert consultation is mainly adopted as the determination method of the weight. And the determination method of the basic energy of weight has transformed from personal experience to expert collective decisions.

When the dates are being processed, arithmetic mean is generally adopted to be on behalf of the judges focused comments. The formula is as followed:

$$a_j = \sum_{i=1}^{n} a_{ij} / n \quad j = 1, 2, 3, ..., m \tag{2}$$

where a_j is the average weight of indicator i; n is the number of judges; m is the total number of evaluation; a_{ij} is rate value the number i judge giving to the number j index weight. Then, the above results are normalized:

$$a_j' = \frac{a_j}{\sum_{j=1}^{m} a_j} \tag{3}$$

where a_j is value of the weight after normalization process.

In general, the above method is according to the expert's knowledge, experience and personal values. Those methods are assigned subjectively by the experts who analyse, judge and subjectively evaluate the index system. Therefore, the weight value determined in this way can reflect the importance of each indicator to a certain extent, and can ensure the accuracy of the evaluation results. However, the weight should be changed as the changing of different objective factors in different construction. Therefore, in order to improve the accuracy of the evaluation results, the adaptation of AHP to obtain a more accurate weight result could be regarded as a better method. The analysis of importance degree between each index can be more logical by using this method. More mathematical treatments have been coupled into this method. So, the credibility of this method is greater and the range of this method is wider.

3. ANALYTIC HIERARCHY PROCESS

Analytic hierarchy process (AHP) was formally pro-posed by Saaty[7,8] of the United States in the 20th century, mid-70s. It is a kind of analysis method which is a combination of qualitative and quantitative, systematic, hierarchical. Because of its usefulness and effectiveness in dealing with complex decision-making problems, it soon obtained attention in the worldwide.

3.1. Analytic Hierarchy Process

The steps that weight determination by AHP is as followed:

1) Judgment matrix

In the AHP, judgment matrix is necessarily needed to be built in order to represent the relative importance of each process to other processes in robustness index calculation. In order to quantify the relative importance of each step, scaling method is used in the analytic hierarchy process. The meanings of these values are listed in Table 1.

Table 1. Judgment Matrix Scale and Its Implications

Scale	Meaning
1	Two factors' comparison, having the same importance level
3	Two factors' comparison, one factor is a little important than the other one
5	Two factors' comparison, one factor is obviously important than the other one
7	Two factors' comparison, one factor is strongly important than the other one
9	Two factors' comparison, one factor is extremely important than the other one
Reciprocal	$X_i/x_j=a_{ij}$, so x_i/x_j should be judged as $a_{ji}=1/a_{ij}$
2/4/6/8	Median of adjacent said judgment

With these scales, we can give the judgment of the relative of each process's importance. Now, a judgment matrix has been constructed already, and it is named as A.

2) Importance sequence calculation

According to the judgment matrix, the maximum characteristic root is $\lambda_{\max}$. Feature vector's corresponding characteristic root is W, and:

$$W = W\left(\omega_1, \omega_2, ..., \omega_n\right) \tag{4}$$

where *n* is the numbers of the process and its equation is:

$$AW = \lambda_{\max} W \tag{5}$$

Then, it is normalized:

$$\omega_i' = \omega_i / \sum_{i=1}^{n} \omega_i \tag{6}$$

So,

$$W' = W\left(\omega_1', \omega_2', ..., \omega_n'\right) \tag{7}$$

where W' is each process's weight.

3.2. Conformance Test

In order to measure the consistency of the matrix A and guarantee the reliability of the matrix, it is necessary to test the consistency of the judgment matrix. Namely, it is necessary to calculate the consistency index:

$$CI = \frac{(\lambda_{\max} - n)}{(n-1)} \tag{8}$$

where *CI* is the consistency test index of judgment matrix; $\lambda_{\max}$ is the maximum characteristic root; *n* is the number of elements of the judgment matrix.

The average random consistency index of the judgment matrix is expressed by *RI*. For the 1-9 order determination matrixes, values of *RI* are shown in Table 2.

Table 2. Average Random Consensus Index of Judgment Matrix

Judgment matrix order	*RI*	Judgment matrix order	*RI*
1	0.00	6	1.24
2	0.00	7	1.32
3	0.58	8	1.41
4	0.90	9	1.45
5	1.12		

When the order of the judgment matrix is greater than 2, the ratio of the consistency index of judgment matrix and the same order average random consistency index is the rate of random consensus, which is denoted as *CR*:

$$CR = \frac{CI}{RI} \tag{9}$$

where *CR* is the rate of random consensus; *CI* is the consistency index of judgment matrix; *RI* is the same order average random consistency index.

Only when $CR<0.1$, the judgment matrix is considered to have good agreement. And the single sort is considered reasonable. Otherwise, the adjustment of the value of the judgment matrix is needed to be changed.

4. CASE STUDY

In this paper, a hydropower station dam project in southwest China is proposed as a case study. Five processes on plant system construction critical path are chosen as the underlying data source analysis.

The weight values determined by the traditional expertise law are shown in set 1, Fig. 1.And the weight values determined by AHP are shown in set 2, Fig. 1.

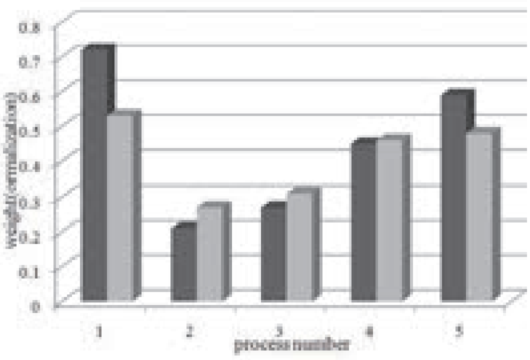

Figure 1. Weight construction histogram

From the histogram, we can see that: the weight of set 2 is more evenly than that of set 1, which means the weight determined by AHP can make the weight value homogenization.

The robustness indexes using the weight determined by the traditional expertise law are shown in set 1, Fig. 2. The robustness indexes using the weight determined by AHP are shown in set 2, Fig. 2. And the real robustness indexes provided from the construction logs are shown in set 3, Fig. 2.

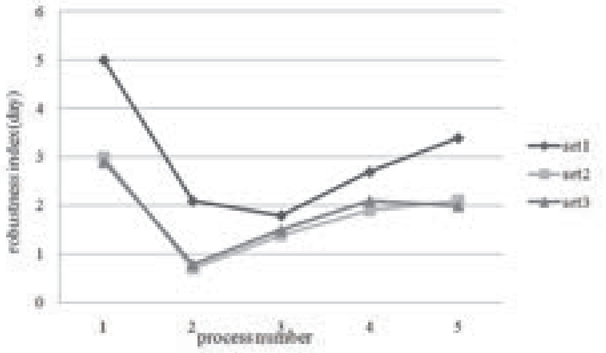

Figure 2. Robustness index contrast line chart

From the line chart, we can see that: the dates from set 1 are higher than that from set 3, meanwhile, the dates from set 2 are close to that from set 3. In other words, the robustness indexes using the weight determined by AHP are much closer to the real dates than the robustness indexes using the weight determined by the traditional expertise law. So, weight determined by AHP is more realistic.

5. CONCLUSION

This paper overcomes the traditional method's shortcoming in calculating the weight of the robustness index, by which the results are less accurate.

1) The necessity and superiority of the robustness analysis for the progress of construction projects has been demonstrated.

2) The advantages and disadvantages of each robustness index have been compared and starting time deviation is proposed as the suitable index.

3) Analytic hierarchy process (AHP) is presented to determine the weight values in the formula and its superiority in accuracy and practicality compared with the traditional method is shown.

4) The method is applied to a real construction.

The results explains the effectiveness of this method that it improves the accuracy of the robustness metric index and provide a scientific basis for the improvement of accuracy of robustness analysis for construction progress.

AKCNOWLEDGEMENT

The research was supported by the Innovative Research Groups of the National Natural Science Foundation of China (Grant no. 51021004), the Natural Science Foundation of China (Grant no. 51439005) and the Natural Science Foundation of China (Grant no. 91215301). The authors gratefully acknowledge the helpful comments of the editor and referees of this manuscript.

REFERENCES

Al-Fawzana, M.A. and Haouari, M. (2005): A bi-objective model for robust resource-constrained project scheduling, Produc-tion Economics, 96:2, pp. 175-187.

Abbasi, B., Shadrokh, S. and Arkat, J. (2006): Bi-objective re-source-constrained project scheduling with robustness and makespan criteria, Applied Mathematics and Computation, 180:1, pp. 146-152.

Kobylański, P. and Kuchta, D. (2007): A note on the paper by M. A. Al-Fawzan and M. Haouari about a bi-objective problem for robust resource-constrained project scheduling, Produc-tion Economics, 107:2, pp. 496-501.

Van de Vonder, S. et al. (2007): Heuristic procedures for reactive project scheduling, Computer & Industrial Engineering, 52:1, pp. 11-28.

Lambrechts, O., Demeulemeester, E. and Herroelen, W. (2008): A tabu search procedure for developing robust predictive project schedules, Production Economic, 111:2, pp. 493-508.

Herroelen, W. and Leus, R. (2004): Robust and reactive project scheduling: A review and classification of rocedures, Inter-national Journal of Production Research, 42:8, pp. 1599-1620.

Saaty, T.L. (1980): The analytic hierarchy process, New York: McGraw-Hill.

Saaty, T.L. and Wong, M.M. (2013): Projective average family size in rural India by the Analytic Hierarchy Process, Jour-nal of Mathematical Sociology, 9, pp. 181-209.

Numerical Simulation of Grouting for Dam Foundation

X.F. Ao, X.L. Wang, S.H. Deng & R.J. Li
State Key Laboratory of Hydraulic Engineering Simulation and Safety, Tianjin University, Tianjin, China
aoxuefei26@163.com

ABSTRACT:
Due to the specific requirements and complex rock mass structures of large-scale hydropower projects located in mountains and gorges, grouting for dam foundations has become an important issue for performance and safety operation. With the development of computer technology, numerical simulation is increasingly used for the grouting simulation. Computational Fluid Dynamics (CFD) has emerged as a viable option to reveal the flow characteristics and simulate diffusion process of grouting. Previous researches mainly focused on a seepage model for a single fracture or grouting hole, ignoring the interaction of dense grouting holes and the actual turbulent state of the flow. Based on a three-dimensional geological information model, a three-dimensional *k-ε* turbulence mathematical model considering Bingham fluid characteristic was presented in this paper. The grout concentration distribution was obtained. The filling rates of each zone under the grouting pressure of 0.5 MPa, 1.0 MPa and 1.5 MPa were illustrated. The simulated stem ash consumption was in a good agreement with the actual value. This research provides an important theoretical significance and practical value for the dam safety and stable long-term operation.

Keywords: grouting; computational fluid dynamics; k-ε turbulence model; Bingham fluid; dam safety

1. INTRODUCTION

Grouting is the most common strengthening action undertaken to improve the performance of concrete dams with cracks and leaking joints. The rock mass grouting is a major part of the construction process and must be given great attention in the planning and execution phases in order to obtain a satisfactory result. Due to the complex and volatile characteristics of rock mass and the hidden diffusion grouting process, it is difficult to monitor the diffusion process during the construction. Since empirical models lack extrapolation capabilities, they are not suitable for exploring newer designs. With the development of computation techniques, the numerical simulation methods were used to calculate the grouting process with the focus on the grouting technology. Computational tools based on computational fluid dynamics (CFD) can be utilized to simulate the diffusion process of cement grouting.

Previous grouting simulations mainly adopted a seepage model for a single fracture or grouting hole. Houlsby (1990) simulated the flow process of grout in a single fracture. Hao et al. (2001), Yang et al. (2001), and Luo et al. (2007) studied crack grouting in a single fracture and have developed the corresponding computer simulation procedure. Bouchelaghem (2009) employed the effective permeability identified to model successfully fluid flow and grout transport through a saturated fine sand in medium and large scale columns. Sun et al. (2007) established a finite element model for calculating the diffusion of permeation grouting. Based on the Darcy's law and the analysis on the grouting theory of post-grouting, grout diffusion in soil under bored piles is studied by Qiao (2014).

However, these researches placed their emphasis on laminar flow using the seepage model in a single fracture or a single grouting hole. In other words, they failed to consider the interaction of dense grouting holes and the actual state of the grout flow. A three-dimensional *k-ε* turbulence mathematical model considering Bingham fluid characteristic was presented in this paper on the basis of a three-dimensional geological information model. The grout concentration distribution of each layer in 1.0 MPa and the filling rates of each layer under different pressures were obtained. The simulated and the actual stem ash consumption showed a good agreement.

2. MATHEMATICAL MODEL

2.1. Constitutive Equation of Bingham Fluid

The constitutive equation of Bingham fluid can be expressed as

$$\mu = \eta_b + \tau_0 \Big/ \left(\frac{1}{2} A : A\right)^{1/2} \qquad (1)$$

where η_b and τ_0 were the plastic viscosity and yield stress of Bingham fluid respectively, Pa·s, Pa; A was the strain rate tensor, $A = \frac{\partial u_i}{\partial x_j} + \frac{\partial u_j}{\partial x_i}$, dimensionless.

The diffusion coefficient of each variable is as follows

$$\Gamma^{u,v,w} = \mu + \mu_t \qquad (2)$$

$$\Gamma^k = \mu + \frac{\mu_t}{\sigma_k} \qquad (3)$$

$$\Gamma^\varepsilon = \mu + \frac{\mu_t}{\sigma_\varepsilon} \qquad (4)$$

$$\mu = \eta_b + \tau_0 \Bigg/ \left\{ \begin{array}{l} 2\left[\left(\frac{\partial u}{\partial x}\right)^2 + \left(\frac{\partial v}{\partial r}\right)^2 + \left(\frac{\partial w}{r\partial\theta} + \frac{v}{r}\right)^2\right] + \\ \left(\frac{\partial u}{\partial r} + \frac{\partial v}{\partial x}\right)^2 + \left(\frac{\partial w}{\partial x} + \frac{\partial u}{r\partial\theta}\right)^2 \\ + \left(\frac{1}{r}\frac{\partial v}{\partial\theta} + \frac{\partial w}{\partial r} - \frac{w}{r}\right)^2 \end{array} \right\}^{\frac{1}{2}} \qquad (5)$$

where σ_k and σ_ε were the turbulent kinetic energy and Prandtl Number of turbulent kinetic energy dissipation respectively, dimensionless; μ was the apparent viscosity, Pa·s; μ_t was the turbulent viscosity of Bingham fluid, dimensionless.

2.2. Governing Equation

Assuming that the Bingham fluid and particles were the well-mixed continuum. The flow model is a hybrid model, which is closed by standard turbulence model. In the cylindrical symmetric coordinate, the governing equation of fluid flow can be expressed as.

$$\begin{aligned} &\frac{\partial\rho}{\partial t} + \frac{\partial}{\partial z}(\rho w\varphi) + \frac{1}{r}\frac{\partial}{\partial r}(r\rho u\varphi) + \frac{1}{r}\frac{\partial}{\partial\theta}(r\rho v\varphi) = \\ &\frac{\partial}{\partial z}\left(\Gamma\frac{\partial\varphi}{\partial z}\right) + \frac{1}{r}\frac{\partial}{\partial r}\left(\Gamma r\frac{\partial\varphi}{\partial r}\right) + \frac{1}{r}\frac{\partial}{\partial\theta}\left(\frac{\Gamma}{r}\frac{\partial\varphi}{\partial\theta}\right) + S \end{aligned} \qquad (6)$$

where Γ is the generalized diffusion coefficient, cm^2/s; ϕ is variable of transport, which represents 1, Y_m, u, v, w and ε, respectively; Y_m is the mass fraction of m component, dimensionless; u, v, w are the velocities, m/s; k is turbulent kinetic energy, m^2/s^2; ε is turbulence dissipation rate, m^2/s^2; S is the source term.

$$\text{mixing density: } \rho_m = \sum_{i=1}^{N} \alpha_i \rho_i \qquad (7)$$

$$\text{mixing speed: } \vec{v}_m = \frac{\sum_{i=1}^{N} \alpha_i \rho_i \vec{v}_i}{\sum_{i=1}^{N} \alpha_i \rho_i} \qquad (8)$$

where α is volume fraction, dimensionless; $\vec{v}$ is velocity vector, m/s; the subscript i means phase. The constants in equations above is the same in standard k-ε model, $C_{1\varepsilon}$=1.44, $C_{2\varepsilon}$=1.92, C_μ=0.99, C_k=1.0, C_ε=1.3.

The solution is based on the finite volume method. A third–order quadratic upstream interpolation of convective kinematics (QUICK) scheme is used for discretization, and the pressure implicit with splitting of operator (PISO) algorithm is adopted.

2.3. Boundary Conditions

(1) Inlet condition: According to the engineering, the pressure and volume fraction of Bingham fluid for inlet were imposed and adopted as uniform distributions. Two kinds of inlet conditions were defined for sub-sequence grouting.
(2) Outlet condition: The outlet condition was specified as pressure boundary and was disposed as local unilateralization.
(3) Boundary condition: According to the solid wall law, the no-slip boundary condition was applied (Wang, 2013).

3. CASE STUDY

3.1. Grid Model

Based on the three-dimensional unified model coupled with various geological information models, the CFD mesh model was established combining the real data from the geological model. Body-fitted grid technology and local refinement techniques were applied for the mesh generation. Curvilinear grids were generated to match the computational domain boundaries. Different porosities were applied according to the different geological parameters of the strata (fault zones, collapsed zones, goaf, coal floor, etc.). There were 260,550 units in the 3D grid model, as shown in Fig. 1. The thicknesses of the fault zone, collapsed zone I, goaf #1, collapsed zone II, goaf #2 and the coal floor were 13.5m, 3.46m, 0.86m, 5m, 0.86m and 5m, respectively. The distance between rows and holes are all 18 meters. The water cement ratio is 1:1.

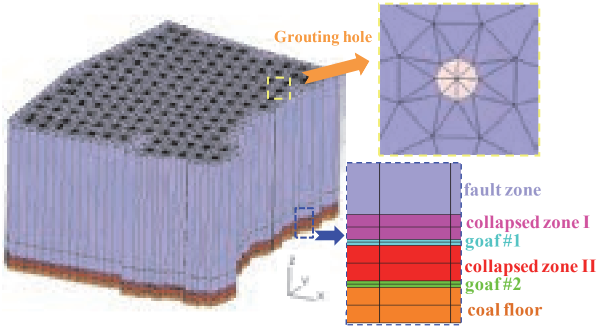

Figure 1. The 3D grid model

3.2. Grout Concentration Distribution

Numerical simulations of the grouting processes were carried out using the grouting pressure standards of 0.5 MPa, 1.0 MPa and 1.5 MPa, combing with the grouting technical requirements in the research area. The grout diffusion results of the collapsed zone I, goaf #1, collapsed zone II, goaf #2 and the coal floor in 1.0 MPa were illustrated (shown in Fig. 2).

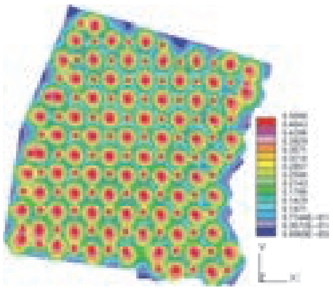

(a) collapsed zone I

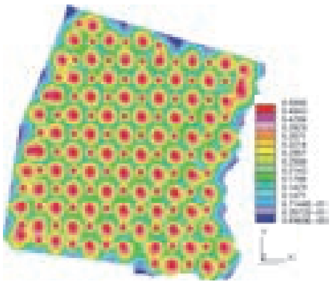

(b) goaf #1

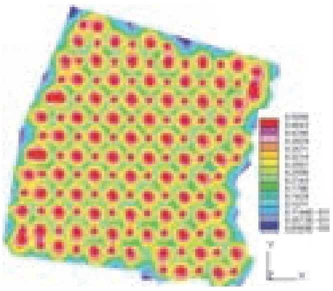

(c) collapsed zone II

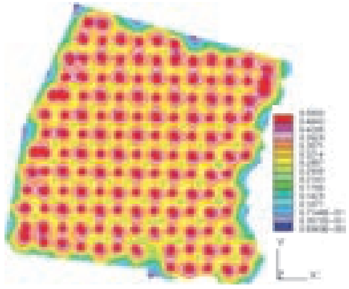

(d) goaf #2

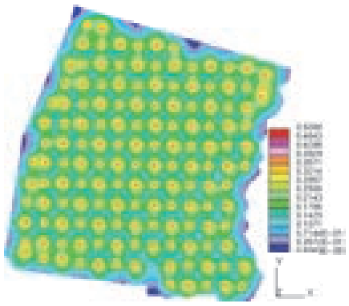

(e) coal floor

Figure 2. Grout concentration distribution of goaf #2

The grout concentration gradually decreased from the grouting hole toward all directions. The outer margin of grout diffusion was overlapped. The grout concentration in each layer was shown in Table 1.

Table 1. Grout concentration in each layer

layer	grout concentration
collapsed zone I	42.6%
goaf #1	43.8%
collapsed zone II	44.3%
goaf #2	45.5%
coal floor	16.4%

Due to the effect of the gravity, the grout concentration increased from 42.6% to 45.5% as the depth increased. The coal floor has the small porosity and good structure, so the grout concentration was the lowest. The same distribution law demonstrated that the grout was mainly concentrated around the grouting hole.

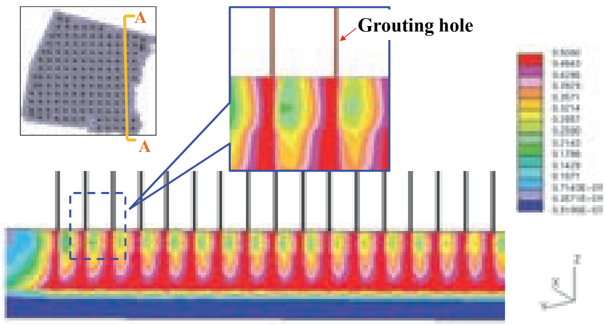

Figure 3. Grout distribution on section A-A

Section A-A was selected as the typical section. The grout diffusion distribution on section A-A was illustrated in Fig. 3. Under the action of both gravity and grouting pressure, the grout diffused at the bottom with the change in time. The grout distribution was approximately an inverted funnel shape.

3.3. Filling Rate

The filling rates of each zone under the grouting pressure of 0.5 MPa, 1.0 MPa and 1.5 MPa were illustrated in Fig.4. The filling rates of the grouting zones (i.e., the fault zone, collapsed zone I, goaf #1, collapsed zone II and goaf #2) increased as the depth increased. Because of the reduction of porosity and pore resistance of the coal floor, the grout concentration was low and the filling rate was also small. The filling rates under each grouting pressure were consistent and increased gradually with increasing grouting pressure. The markedly increases were in the coal floor and the fault zone.

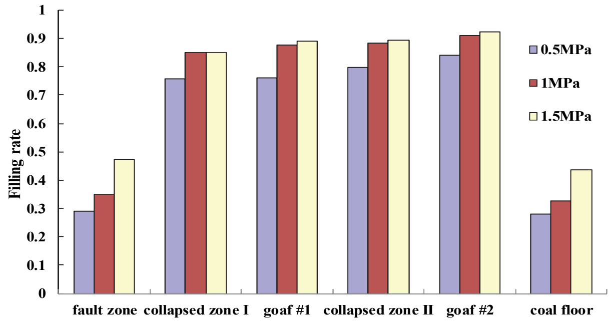

Figure 4. Filling rates of each layer under three pressures

The simulated data of the stem ash consumption were shown in Table 2. The actual stem ash consumption under 1.0 MPa was 24,914,173.1kg. The relative error between the simulated data and the experimental value under 1.0 MPa was 10.3%, which was in good agreement.

Table 2. Simulation result and actual value of stem ash consumption (10^6 kg)

Pressure(Mpa)	0.5	1.0	1.5
Simulated data	17.43	22.35	24.81
experimental value		24.91	

4. CONCLUSIONS

The objective of the grouting is mainly to reduce the hydraulic conductivity but also to improve the stiffness of the ground under the dam or foundation. Computational fluid dynamics (CFD) provided a solution to simulate the diffusion process of grouting. Previous researches placed their emphasis on laminar flow using the seepage model in a single fracture or a single grouting hole. A three-dimensional k-ε turbulence mathematical model considering Bingham fluid characteristic was presented in this paper. The results showed that the grout concentration gradually decreased from the grouting hole toward all directions. Due to the effect of the gravity and the porosity, the grout concentration of goaf #2 was the largest. The filling rates under each grouting pressure were consistent and increased gradually as the grouting pressure increased. The simulated data of the stem ash consumption under 1.0 MPa have been compared to the actual ones, and the relative error was 10.3%.

These results provide an important theoretical basis and a wide application prospect for rock mass grouting and other underground projects. The numerical models will be still improved and elaborated in next stage of the research project.

ACKNOWLEDGEMENT

The research was supported by the Innovative Research Groups of the National Natural Science Foundation of China (Grant no. 51021004), the Natural Science Foundation of China (Grant no. 51439005) and the Specialized Research Fund for the Doctoral Program of Higher Education of China (Grant no. 20120032110045). The authors gratefully acknowledge the helpful comments of the editor and referees of this manuscript.

REFERENCES

Houslby, A.C. (1990): Construction and design of cement grouting. New York: A Wiley Interscience Publication, John Wiley&Sons.

Hao, Z., Wang, J.Q., Liu, B. (2001): Theoretical study of osmotic grouting in rock mass, Chinese Journal of Rock Mechanics and Engineering 20:4, pp. 492-496.

Yang, M.J., He, Y.N., Chen, M.X. (2001): Law of grouting penetrating through fracture network of rock mass, Journal of Hydraulic Engineering 7:pp. 41-46.

Luo, P.P., Chen, L., Zou, Z.S. (2007): Numerical simulation of grouting in space fracture network of rock mass, Chinese Journal of Geotechnical Engineering 29:12, pp. 1844-1848.

Bouchelaghem, F. (2009): Multi-scale modelling of the permeability evolution of fine sands during cement suspension grouting with filtration, Computers and Geotechnics 36:pp. 1058–1071.

Sun, B.T., Ling X.Z., Ling C., Zhu G.R. (2007): Numerical simulation for diffusion and pressure distribution of permeation grouting, Journal of Hydraulic Engineering 37:11, pp. 1402-1407.

Qiao, D.Y. (2014): Study on Numerical Simulation of Post-Grouting of Bored Piles, Master's thesis, Jilin University, China.

Wang, X.L., Wang, Q.S., Zhou, ZY., Ao, X.F. (2013): Three-dimensional Turbulent Numerical Simulation of Bingham Fluid in the Goaf Grouting of the South-to-North Water Transfer Project, Journal of Hydraulic Engineering 44:11, pp. 1295-1302.

Technical Feasibility Evaluation and Optimized Selection of Discharging and Energy Dissipation Scheme of High Dams

B.Pang[1,2]
1.Tianjin University, China; 2. Huaneng Lancang River Hydropower Co., Ltd., China
1098848736@qq.com

G.Wang
State Key Laboratory of Water Resources and Hydropower Engineering Science，Wuhan University，China

ABSTRACT:

Technical feasibility evaluation and optimization optimized selection of for discharging and energy dissipation scheme are the key and difficult points for the design of high dams. In this paper, discharge of high dams is simulated efficiently and accurately with numerical simulation methods based on TruVOF free surface tracer technology, FAVOR technology and multi-grid block establishing technology in consideration of the discharging and energy dissipation characteristics of high dams, and the technical feasibility of discharging and energy dissipation scheme of high dams is raised to be evaluated from the aspects of safety, discharging capacity and energy dissipation effects to determine the index weight with interval analytic hierarchy process. The discharging and energy dissipation scheme of a certain large-scale gravity dam is evaluated. According to the results, the joint energy dissipation scheme adopting three surface outlet discharge, narrow gap and diffusion flip bucket and plunge pool is optimal.

Keywords: discharging and energy dissipation, feasibility evaluation, numerical simulation

1. GENERAL INTRODUCTION

Discharging and energy dissipation problem of high dams is the key factor affecting project safety, investment benefit and operation and management, so sufficient research shall be given. The technical difficulty for large flow flood discharging and energy dissipation of 200 m level and 300 m level super-high dams under construction and planned for construction in recent years is much greater than the experience level of the projects constructed over the world. Can the discharging and energy dissipation scheme be finally determined only after going through hydraulic model test, numerical simulation analysis, special-subject consultancy and feasibility evaluation. Evaluation for feasibility of discharging and energy dissipation scheme involves technology, economy, layout, construction, operation and management, environment and other multiple factors, which is quite difficult and complex. The technical feasibility is the most fundamental requirement to be met for judging if the scheme is feasible. It will be of no practical significance for evaluating the economy, layout, construction, operation and management, environment and other aspects when the technology is infeasible, so research on technical feasibility of discharging and energy dissipation scheme is crucial.

Influenced by terrain, geology and other aspects, hydraulic structure shows obvious "characters", together with the complexity of flow pattern caused by all kinds of boundary conditions, application of experience formula has certain limitations. At present, hydraulic model test methods are applied mainly for evaluation of the technical feasibility for discharging and energy dissipation scheme. Wang Junxing et al. (2008) put forth the optimal hub layout scheme and discharge building structural type by analyzing the energy dissipation effects, current connection problem, scouring condition and water level fluctuation situation at tailrace outlet; Li Jing et al. (2010) compare and optimize the scheme by analyzing the discharge capacity, flow velocity and flow regime, pressure distribution and other hydraulics problems of layout plan for discharge buildings of Misong Hydropower Station; Wu Xiaohong et al. (2005) evaluate the discharging and energy dissipation design scheme of Pengshui Dam by analyzing the discharge capacity, pressure on dam surface, downstream flow velocity and flow regime and scour at rear apron of the dam; Zhang Yingke et al. (2005) evaluate the discharging and energy dissipation scheme of Furong River Yutang Hydroelectric Power Station by analyzing the flow regime of spillway inlet, discharge capacity, the flow regime, flow velocity and water surface profile of plunge pool and energy dissipation and anti-scour capacity. Feasibility of discharging and energy dissipation scheme of dams is evaluated via hydraulic model test, which features waste of time and vigour, high cost and low efficiency during frequent scheme modification or comparison and selection of multiple schemes. Furthermore, there are some problems in evaluation process at present, such as the basic evaluation indexes are non-standard, and the evaluation results will be affected in case of omission of certain index; moreover, unified evaluation standards are lacked for some indexes such as energy dissipation effect. Though Tian Jinghuan et al. (2005) adopt efficient numerical analysis methods, discusses the determination of the energy dissipation and anti-scour type by taking merely the scouring pit and pressure on weir surface of downstream riverbed as the objective function.

To improve the design efficiency and level of discharging and energy dissipation structures of high dams, in this paper, the numerical simulation methods based on *TruVOF* free surface tracer technique, *FAVOR* technology and multi-grid block establishing technology are adopted. The technical feasibility of discharging and energy dissipation scheme is raised to be evaluated comprehensively from the aspects of safety, discharge capacity and energy dissipation effects, making preliminary exploration for standardizing the evaluation on discharging and energy dissipation scheme and providing theoretical basis for comprehensive evaluation on the feasibility of the discharging and energy dissipation scheme.

2. RESEARCH ON INDEXES AND METHODS OF EVALUATION ON TECHNICAL EASIBILITY

In consideration of the basic requirements and functions of discharging and energy dissipation structures of high dams and by summarizing the evaluation on technical feasibility of discharging and energy dissipation schemes made previously, this paper proposes to evaluate the technical feasibility of discharging and energy dissipation scheme from the aspects of safety, discharge capacity and energy dissipation effects. Due to diversified category and type of discharging and energy dissipation structures and complex energy dissipation combination mode, the specific evaluation index differs greatly. In this paper, research on evaluation of technical feasibility is made first for the most common discharging and energy dissipation combination: spillway dam discharge and plunge pool energy dissipation.

For technical feasibility evaluation on discharging and energy dissipation scheme, A is the objective; safety B_1, discharge capacity B_2 and energy dissipation effect B_3 are primary indexes.

2.1. Safety valuation indexes for discharging and energy dissipation scheme

Safety B_1 refers to the anti-scour and cavitation resistance capacity of discharging and energy dissipation structures, which is the basic index for feasibility of the discharging and energy dissipation scheme. It is mainly divided into 5 sub-indexes: (1) Negative pressure on weir crest C_{11}; (2) Pressure of flip bucket C_{12}; (3) Flow velocity of dam toe C_{13}; (4) Safety of plunge pool C_{14}; (5) Safety of bank slope C_{15}.

(1)Negative pressure on weir crest C_{11} is mainly applied for evaluating the cavitation condition on weir crest based on the standard as: there shall be small negative pressure for overflow curve section (refer to *Design Specification for Concrete Gravity Dams* for the specific provisions), ensuring relatively great discharge capacity on the premise of not resulting in cavitation erosion. If the negative pressure on weir crest is failed to meet the standard, weir surface curve shall be modified.

(2)Pressure of flip bucket C_{12} is mainly applied for evaluating the safety of flip bucket based on the standards as: no cavitation erosion, and the centrifugal pressure intensity is less than the compressive capacity of structures. In case of unideal pressure distribution for flip bucket, radius of flip bucket and other dimensions should be adjusted.

(3)Flow velocity of dam toe C13 is mainly applied for evaluating the safety of dam toe based on the standards as: the main stream will not smash and strike the dam toe directly, and the flow velocity near dam toe shall be less than the allowed anti-scour flow velocity of dam toe material. If the flow velocity at dam toe is failed to meet the requirement, measures like adjusting the size of spillway dam outlet shall be taken to increase the horizontal length of nappe.

(4)Safety of plunge pool C_{14} is mainly in relation to the flow regime, underflow velocity, impact hydrodynamic pressure in the pool, etc. The evaluation standard is: the water flow shall dissipate energy sufficiently in plunge pool; the underflow impact velocity shall be less than the limit of underflow impact velocity; the impact hydrodynamic pressure generally shall not be greater than 100-150 kPa; the impact hydrodynamic pressure = maximum hydrodynamic pressure - hydrostatic pressure. If the underflow and hydrodynamic pressure of plunge pool are failed to meet the standard, measures like excavating the plunge pool, adjusting the size of spillway dam outlet and protecting the pool bottom shall be taken.

(5)Safety of bank slope C_{15} is mainly related to the nappe width in water, flow velocity and pressure. The evaluation standard is: the slope shall not be impacted directly by nappe; the nappe width in water is controlled to approach to the width of low flow surface since the batholith below low water level has relatively strong anti-scour capacity after being impacted by water flow for a long time; the flow velocity on slope shall be less than the anti-scour flow velocity of slope material; the hydrodynamic pressure on slope shall not be greater than the pressure on central line of plunge pool. If safety of bank slope is failed to meet the standard, measures like modifying the size of outlet, protecting slope or excavating bank slope shall be taken.

2.2. Indexes of evaluation on discharge capacity of discharging and energy dissipation scheme

According to statistics made on the 14th International Dam Meeting in 1982, more than 65% dam accidents were caused by scarce discharge capacity of middle- and small-sized discharge structures. For some large-sized structures, reservoirs at upstream were always failed to be fully filled with water due to high design standards and big design flood, which is a great waste. So discharge capacity B_2 is one of the important functional indexes of discharging and energy dissipation structures, which is measured by calculating the discharge flows under various working conditions.

The calculation formula and experimental flow coefficient of discharge capacity can both be found in design manual. Practices have proven that some testing results are quite different with the design. Numerical simulation method can truly simulate the discharge relatively, without involving flow coefficient and other experience coefficient or model scale, etc., which is simple, rapid and reliable. The specific steps are: carry out hydraulic numerical simulation for design scheme; calculate the flow velocity v of measured points evenly distributed on flow measurement control section; calculate the volume fraction f of water body at different measured points; work out the discharge Q according to formula (1).

Selection of flow measurement control section: select the starting section at straight line section on weir surface with stable flow, relatively low flow velocity and with no negative pressure as the flow measurement control section (as shown in Fig. 1).

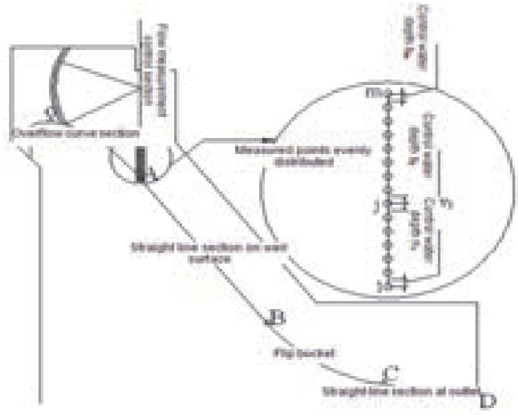
Overflow curve section
A
Measured points evenly distributed
m
j
1
Straight line section on weir surface
B
Flip bucket
C
Straight line section at outlet
D

Figure 1. Layout of Flow Measurement Control Sections and Measured Points

The discharge shall be calculated with numerical simulation method via formula below:

$$Q = \sum_{i=1}^{n} \sum_{j=1}^{m} v_{xij} h_{ij} b_{ij} f_{vij} \tag{1}$$

In the formula, Q: discharge (m^3/s); n: No. of overflow surface outlets; m: No. of flow velocity measured point; v_{xij}: flow velocity (m/s) in horizontal direction (X-direction) of the j^{th} measured point on the i^{th} surface outlet flow measurement control section; h_{ij} and b_{ij}: control water depth of the j^{th} measured point on the i^{th} surface outlet flow measurement control section and width (m) of corresponding water surface; f_{ij}: volume fraction of water body at the j^{th} measured point on the i^{th} surface outlet flow measurement control section.

The evaluation standard for discharge capacity is: The discharge capacity shall be greater than the designed discharge capacity appropriately. The discharge capacity is affected by flow regime at water inlet, flow regime and pressure on weir surface, size of outlet, etc. If the indexes are failed to meet the standard, measures below can be taken: ① Improve the flow regime at water inlet to enable stable flow regime, small detour flowing impact and stable water surface; ② Adjust the weir surface curve so that the water flow on weir surface is smooth, and the negative pressure on weir crest meets relevant requirement, maximizing the discharge capacity based on safety; ③ Improve the size of outlet; ④If the discharge capacity is much greater than the design value, reduce the number or sizes of outlets.

2.3. Indexes of evaluation on energy dissipation effect of discharging and energy dissipation scheme

The released flow of high dams has huge kinetic energy. Besides ensuring the engineering safety and enough discharge capacity as required, the discharge energy shall be dissipated within limited scope, or severe flow regime will be caused during flooding, impacting the shape of riverway and public security downstream. So energy dissipation effect B_3 is another important functional index for evaluating the discharging and energy dissipation scheme.

The energy dissipation effect B_3includes mainly 3 sub-indexes: (1) energy dissipation effect in the air C_{31}: the lost energy of water-jet nappe flow due to diffusion, aeration, collision and air friction in the air; (2) Energy dissipation effect in plunge pool C_{32}: the energy consumed due to turbulent shear after water-jet nappe flow dropping into water-pillow at downstream; (3) Energy dissipation efficiency in plunge pool C_{33}.

(1)Aerial energy dissipation effect C_{31} is mainly related to the flow regime of nappe. The qualitative evaluation standard is: ① nappe is pulled open longitudinally and is appropriately diffused transversely, with staggered dropping points but no radial concentration; ② Too small or large jet trajectory length is not allowed to avoid scouring the dam-toe and dissipating the energy by making the best of water body downstream; ③ Too large or small angle of nappe in water is not allowed to avoid excessive impacting pressure for riverbed or dissipating the energy insufficiently; ④ The nappe shall be thick and wide, with maximum contact area with water surface, thus the energy will be dissipated sufficiently.

(2)Energy dissipation effect of plunge pool C_{32} is mainly related to the flow regime therein. The qualitative evaluation standard is: ① With no centripetal concentration, and the main stream shall fully fill the plunge pool as much as possible; all the water body shall be involved in energy dissipation; ② With adequate water body in plunge pool for energy dissipation, so that the riverbed will not bear excessive impact; ③ The water flow in plunge pool shall be steady and connected smoothly with water flow in riverway downstream.

(3)Energy dissipation effect of plunge pool C_{33} is a quantitative index for evaluating the energy dissipation effect: $\Delta p_m \leq 15.0\times 9.81$kPa is recommended for design and protection standard for plunge pool at downstream of high dams, with $\varphi \geq 0.0077$.

$$\varphi = \frac{\Delta p_m}{\gamma H_1}\frac{QH}{V_w\sqrt{gH}} \tag{2}$$

In the formula, φ refers to comprehensive evaluation index for energy dissipation efficiency of plunge pool, without dimension; Δp_m refers to impulse dynamic water pressure, viz. $p_{max} - \gamma H_1$; γ refers to unit weight of water; H_1refers to depth of water-pillow at downstream of dams; Q refers to total discharge; H refers to water level difference between upstream and downstream; V_w refers to volume of water body involved in energy dissipation; g refers to gravity acceleration.

2.4. Technical feasibility evaluation and optimization method for discharging and energy dissipation scheme

In case any index of a scheme is failed to meet the evaluation standard, the scheme is infeasible and shall be modified, or new scheme shall be designed. During optimized selection of multiple feasible schemes, analytic hierarchy process can be applied, which is a better scientific decision-making method integrating qualitative analysis with quantitative analysis organically. Hierarchy structure chart for technical feasibility evaluation on discharging and energy dissipation scheme is established in this paper, as shown in Fig. 2.

Different concern may be attached to indexes for different projects, and the weight of indexes may be different; however, weight of all indexes can be worked out via Interval Analytic Hierarchy Process.

To eliminate the impact of different physical dimensions on the calculation results, the schemes to be evaluated and indexes in evaluation standards shall be normalized during actual evaluation.

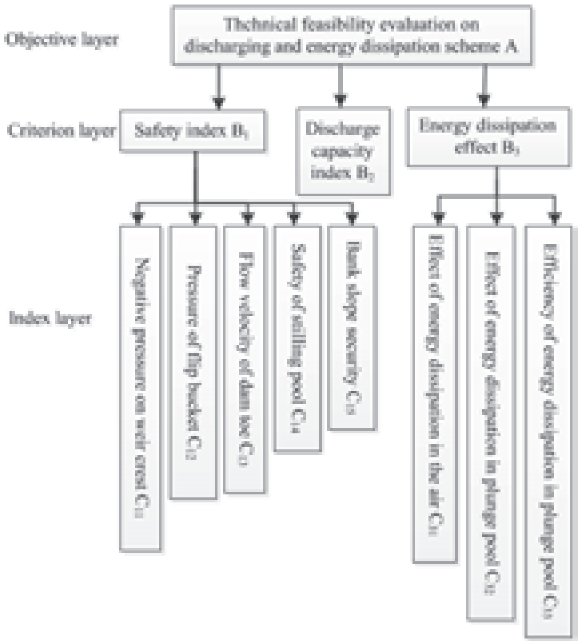
Objective layer
Thchnical feasibility evaluation on discharging and energy dissipation scheme A
Criterion layer
Safety index B1
Discharge capacity index B2
Energy dissipation effect B3
Index layer
Negative pressure on weir crest C11
Pressure of flip bucket C12
Flow velocity of dam toe C13
Safety of stilling pool C14
Bank slope security C15
Effect of energy dissipation in the air C31
Effect of energy dissipation in plunge pool C32
Efficiency of energy dissipation in plunge pool C33

Figure 2. Hierarchy Structure Chart for Technical Feasibility Evaluation on Discharging and Energy Dissipation Scheme

For the index "the greater the better", such as energy dissipation efficiency C_{33}:

$$x_i = \frac{x_i' - \min\{x_i'\}}{\max\{x_i'\} - \min\{x_i'\}} \qquad i = 1,2,\ldots,n \tag{3}$$

For the index "the less the better", such as negative pressure on weir crest C_{11}, pressure of flip bucket C_{12} and flow velocity of dam toe C_{13}:

$$x_i = \frac{\max\{x_i'\} - x_i'}{\max\{x_i'\} - \min\{x_i'\}} \qquad i = 1,2,\ldots,n \tag{4}$$

For fixed indexes, such as discharge capacity B_2, formula below can be applied:

$$x_i = 1 - \frac{x_i' - a}{\max\limits_i \left|x_i' - a\right|} \qquad i = 1,2,\ldots,n \tag{5}$$

In the formula, a is fixed value.

As the safety of plunge pool C_{14} and safety of bank slope C_{15} need to be evaluated qualitatively and quantitatively, which are similar to qualitative indexes as energy dissipation effect in the air C_{31} and energy dissipation effect in plunge pool C_{32}, therefore they can be evaluated based on the comment set that is composed of 7 comments after subjective analysis by the designer, viz. $V=(V_1, V_2, \ldots, V_7)$= (extremely bad, very bad, bad, ordinary, good, very good and extremely good). For the corresponding scale of discrete language value, please refer to Table 1.

Table 1. Scale of Discrete Language Value

Rating scale	Extremely bad	Very bad	Bad	Ordinary
Points	0.1	0.2	0.3	0.5
Rating scale	Good	Very good	Extremely good	
Points	0.7	0.85	0.95	

The evaluation model for technical feasibility of discharging and energy dissipation scheme is:

$$F=W\times X \tag{6}$$

In the formula: F $(f_1,f_2,\ldots,f_n)$ represents the technical feasibility evaluation result vector of n scheme(s); $W(W_1,W_2,\ldots,W_m)$ represents the weight vector of m evaluation index(es); X $(x_{ij})_m\times_n$ represents the non-dimensionalized data matrix of all indexes of n scheme(s).

During optimized selection of n feasible scheme(s), the scheme will be better with greater f.

3. TECHNICAL FEASIBILITY EVALUATION AND OPTIMIZED SELECTION OF DISCHARGING AND ENERGY DISSIPATION SCHEMES FOR HIGH DAMS

According to topographic and geologic conditions, design specifications and design experience, overflow dam section discharging and downstream plunge pool energy dissipation are adopted for a large (1) hydropower station. As water-pillow is thick, measures of slope protection without bottom protection is adopted for plunge pool. 5 schemes are designed for outlet flip bucket type and bucket angle of overflow dam, as shown in table 2.

Table 2. Discharging and Energy Dissipation Scheme for A Large Hydropower Station

Scheme	Side hole			Middle hole		
	Quantity (dimension m × m)	Type	Bucket angel (°)	Quantity (dimension)	Type	Bucket angel (°)
Scheme 1	2 (13×20)	Non-symmetrical narrow slit	-20	2 (13×20)	Microdiffusion	-20
Scheme 2	2 (13×20)	Symmetrical narrow slit	-20	2 (13×20)	Diffusion	-30
Scheme 3	2 (13×20)	Symmetrical narrow slit	-20	2 (13×20)	Diffusion	-25
Scheme 4	2 (15×21)	diffusion	-25	1 (15×21)	Narrow slit	-20
Scheme 5	2 (15×21)	Diffusion	-22	1 (15×21)	Narrow slit	-20

Numerical simulation method can be adopted to make simulated analysis on 5 discharging and energy dissipation schemes. Flow regimes of each scheme are shown in Fig. 3.

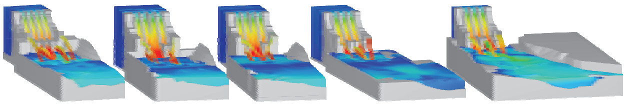

Figure 3. Simulated Flow regime Values of 5 Design Schemes (respectively scheme 1, 2, 3, 4 and 5 from left to right)

According to above evaluation indexes and evaluation criterion, analyze technical feasibility of the 5 discharging and energy dissipation schemes. For scheme 1, asymmetrical narrow slit leads to uneven water flow distribution in plunge pool, and small bucket angel of the middle outlet leads to insufficient use of plunge pool energy dissipation along water surface, and thus this scheme is not practical. Other schemes are practical.

Select optimal scheme among the 4 schemes, and determine their weights through section analytical hierarchy process. Interval judgment matrix by experts for importance of indexes of discharging and energy dissipation schemes is s shown below.

Interval judgment matrix for substructure of criterion hierarchy:

$$A=\begin{bmatrix} [1,1] & [1,2] & [1,3] \\ [0.5,1] & [1,1] & [1,2] \\ [0.33,1] & [0.5,1] & [1,1] \end{bmatrix} \tag{7}$$

Interval judgment matrix for substructure of index hierarchy:

$$B_1=\begin{bmatrix} [1,1] & [1,3] & [0.33,0.5] & [0.5,1] & [1,2] \\ [0.33,1] & [1,1] & [0.33,0.5] & [0.25,0.33] & [0.5,1] \\ [2,3] & [2,3] & [1,1] & [1,2] & [1,3] \\ [1,2] & [3,4] & [0.5,1] & [1,1] & [1,2] \\ [0.5,1] & [1,2] & [0.33,1] & [0.5,1] & [1,1] \end{bmatrix} \tag{8}$$

$$B_3=\begin{bmatrix} [1,1] & [0.2,0.33] & [0.33,0.5] \\ [3,5] & [1,1] & [1,2] \\ [2,3] & [0.5,1] & [1,1] \end{bmatrix} \tag{9}$$

Consistency checks of judgement matrix conform to requirements.

Weight of each index calculated by particle swarm optimization method:

$(a_1, a_2, a_3) = (0.4499, 0.3393, 0.2108)$, weight of criterion hierarchy indexes relative to objective hierarchy

b_1=(0.0732, 0.0408, 0.1393, 0.1238, 0.0728), weight of security sub-indexes relative to objective hierarchy

b_3=(0.0248, 0.1116, 0.0744), weight of energy dissipation effect sub-indexes relative to objective hierarchy

In conclusion, weights of C_{11}, C_{12}, C_{13}, C_{14}, C_{15}, C_{31}, C_{32}, C_{33} and B_2 relative to target A are respectively 0.0732, 0.0408, 0.1393, 0.1238, 0.0728, 0.0248, 0.1116, 0.0744 and 0.3393.

In addition, write down actual value of each index of each scheme, as shown in Table 3; and make normalization treatment for actual values according to formula (3), formula (4), formula (5) and table 1, as shown in table 4; finally, get technical feasibility evaluation results of the 4 schemes according to formula (6): value *f* of scheme 2, scheme 3, scheme 4 and scheme 5 is respectively 0.359, 0.672, 0.807 and 0.880. It can be seen that scheme 5 is the optimal one for joint energy dissipation adopting3 surface holes discharging, narrow gap and diffusion flip bucket and plunge pool. The evaluated result is as same as that obtained from hydraulic model test.

Table 3. Actual Values of Indexes

Indexes		Weights	Actual value			
			Scheme 2	Scheme 3	Scheme 4	Scheme 5
Security B_1	Negative pressure on weir crest C_{11}	0.0732	-40968 Pa	-18957 Pa	-24841 Pa	-26761 Pa
	Pressure of flip bucket C_{12}	0.0408	23m water column	32.6m water column	25m water column	36.6m water column
	Flow velocity of dam-toe C_{13}	0.1393	8m/s	2.1m/s	2.3m/s	1.9m/s
	Plunge pool security C_{14}	0.1238	0.2	0.3	0.5	0.7
	Bank slope security C_{15}	0.0728	0.5	0.7	0.85	0.95
Discharge capacity B_2		0.3393	9460m^3/s	9460m^3/s	9351m^3/s	9351m^3/s
Effect of energy dissipation B_3	Effect of energy dissipation in the air C_{31}	0.0248	0.7	0.7	0.85	0.85
	Effect of energy dissipation in plunge pool C_{32}	0.1116	0.5	0.5	0.7	0.95
	Efficiency of energy dissipation in plunge pool C_{33}	0.0744	0.0081	0.0083	0.0089	0.0092

Table 4. Normalization Data of Indexes

Indexes		Weights	Normalization data			
			Scheme 2	Scheme 3	Scheme 4	Scheme 5
Security B_1	Negative pressure on weir crest C_{11}	0.0732	0.303	0.678	0.578	0.545
	Pressure of flip bucket C_{12}	0.0408	0.981	0.888	0.962	0.850
	Flow velocity of dam-toe C_{13}	0.1393	0.200	0.790	0.770	0.810
	Plunge pool security C_{14}	0.1238	0.200	0.300	0.500	0.700
	Bank slope security C_{15}	0.0728	0.500	0.700	0.850	0.950
Discharge capacity B_2		0.3393	0.3393	0.840	0.989	0.989
Effect of energy dissipation B_3	Effect of energy dissipation in the air C_{31}	0.0248	0.700	0.700	0.850	0.850
	Effect of energy dissipation in plunge pool C_{32}	0.1116	0.500	0.500	0.700	0.950
	Efficiency of energy dissipation in plunge pool C_{33}	0.0744	0.267	0.400	0.800	1.000

4. CONCLUSIONS

As the process of evaluation on technical feasibility of discharging and energy dissipation scheme has not been specified, this paper comprehensively evaluates technical feasibility of discharging and energy dissipation scheme in terms of security, discharge capacity and energy dissipation effect. With regard to time consuming, manpower consuming, high cost and other problems of hydraulic model test method, it simulates high dam discharging through numerical simulation method based on TruVOF free surface tracer technology, FAVOR technology and multi-grid block establishing technology. Main conclusions include:

(1)In consideration of the basic requirement and functions of discharging and energy dissipation structures of high dams, this paper proposes to evaluate the technical feasibility of discharging and energy dissipation scheme from three aspects, i.e. security B_1, discharge capacity B_2 and energy dissipation effects B_3, and index weight is determined by interval analytic hierarchy process .

(2) Evaluate the design scheme for overflow dams of a large hydropower station by evaluation on technical feasibility of high dam discharging energy dissipation scheme suggested in the paper. According to the results, the scheme with joint energy dissipation with three surface outlet discharge, narrow gap and diffusion flip bucket and plunge pool is optimal. The result is as same as that obtained from hydraulic model test.

As the evaluation on technical feasibility of discharge energy dissipation scheme is of great significance, which is also difficult and complicated, thus further study is required based on this paper, such as building one set of evaluation index system suitable for all dams and all discharging and energy dissipation groups; researching comprehensive evaluation method involving technology, cost effectiveness, arrangement, construction, operation management and environment etc.

AKCNOWLEDGEMENT

The authors gratefully appreciate the supports from the Foundation for National Key Technology R&D Program (2013BAB06B04) and Joint National Support Program of Yunnan Province (2014GA007).

REFERENCES

Wang Junxing, Yin Hao and Liu Jinxiu et al .(2008): Energy Dissipation and Scour Prevention of Longkaikou Hydropower Station , Journal of Wuhan University (Engineering and Technology Edition) , 41:1, pp. 27-34.

Li Jing and Jiang Bole.(2010): Model Test Study on the Flood Discharging and Energy Dissipation for Hydropwer Station, Innovation in Science and Technology,2, pp. 32-36.

Wu Xiaohong and Cheng Dehu.(2005): Study on the Design of Flood-releasing Energy Dissipation for Pengshui Dam, Hydro Power,31:12, pp. 39-41.

Zhang Yingke, Wang Jibao and Chen Hechun.(2005) : Model Test Study on the Scheme of Flood Discharging and Energy Dissipation of Furong River Yutang Hydropower Station, China Three Gorges University Journal(Natural Science Edition),27:1, pp. 20-23.

Tian Jinghuan and Zhai Wenhang.(2005) : Numerical Method of Selection of Downstream Energy Dissipation and Scour Protection Scheme for High Arch Dam, Guangdong Water Conservancy and Hydro Power,6, pp. 1-3.

Rockfill Dam Construction Simulation based on CYCLONE and Stochastic Petri

J.Zhang,X.Wang&J.Yu
Tianjin University, China
zhangjun12138@126.com

ABSTRACT:
Schedule control is quite important in rockfill dam construction management. Construction simulation technology provides a promising alternative solution for dynamic project schedule analysis, optimization and control. For present study of rockfill dam construction simulation, simulation model was mainly built up with queuing theory and discrete simulation technology, which were not capable of visually indicating logic or resource constraint relation between each subsystem. Given the graphical format for model design, Stochastic Petri nets (SPNs) can intuitively describe the construction activities and relationships therein. Moreover, the SPNs is capable of simulating construction system with taking concurrent activities, uncertain time parameters and simultaneous resource possessing into account. Considering the complex construction organization structure and inherent uncertainty in construction processes, based on integrating CYCLONE and Stochastic Petri nets methods, this research establishes an improved rockfill dam construction simulation modelling method, with use of hierarchical modelling concept. Through simulation, reasonable resource allocation scheme can be provided, and corresponding schedule risk analysis can be carried out, which help making strategic decision evaluation and improving the project management level in rock fill dam project.

Keywords: Rockfill dam, Schedule optimization, Construction simulation, Stochastic Petri nets, CYCLONE.

1. INTRODUCTION

With the advantages of convenient access to materials, good adaptability to foundation geological conditions and lower cost, rockfill dam has become an increasingly popular dam type in China, especially in high dam projects.

Schedule control is a major concern in rockfill dam construction planning and management, and how to formulate a reasonable construction plan in design stage is the problem to be solved. Traditional schedule network method, such as CPM, cannot effectively simulate the dynamic nature of construction process. The application of construction simulation technology provides an effective way for dynamic project schedule analysis and resource usage optimization of rockfill dam project. However, generally among the existing simulation methods for rockfill dam construction process, simulation model was mainly built up based on CYCLONE(Cyclic Operations Network) and discrete simulation technology, which were not capable of visually indicating logic or resource constraint relation between each subsystem.

The objective of this research described in this paper is the establishment of an improved rockfill dam construction simulation method that can intuitive considers logic and resource constraints between each construction subsystem and each dam zone. Here the hierarchical modelling concept is utilized to achieve effective decomposition of a complex construction simulation model. Generally the established Stochastic Petri net represents overall construction process with lower levels incorporating more details based on CYCLONE. The CYCLONE method was adopted to simplify the simulation process of repetitive earthwork transportation operations, with considering the queuing problem of different types of vehicles before the forks. The process interdependence between two construction subsystems and detailed resource sharing between different zones are simulated in the project level with Stochastic Petri nets. Given the complex construction organization structure and inherent uncertainty in construction processes, by taking the advantages of the two methods, an improved hierarchical simulation model for rockfill dam can be established.

The proposed method can be used as a project simulation tool with both rapid and reusable merits. The obtained optimized equipment configuration scheme and relevant statistical parameters can real help making strategic decision evaluation and improving the project management level in rock fill dam project.

The structure of this article is as follows. First, a detailed relevant literature background review will be given to illustrate the benefits of this study. Then, the concrete methodology of proposed simulation method for rockfill dam project will be detailed interpretation. For better understanding, the construction process of rockfill dam will be briefly described. Finally the schedule study of an practical rockfill dam project in China will be used as an example to demonstrate the benefits and significance of this study.

2. BACKGROUND

Construction simulation has been demonstrated to be an effective tool for planning and improving the performance of a construction process. Cyclic Operations Network (CYCLONE) developed by Halpin has become the basis of a number of construction simulation systems (Halpin D W, 1979) (Sawhney A et al, 1998). In the CYCLONE system, six simple modelling elements with certain defined functions are used to structure a wide variety of construction activities and processes. CYCLONE can simplified the simulation modeling process and made it accessible to construction practitioners with limited simulation background (AbouRizk et al, 1992). Besides, adopting the CYCLONE approach can efficiently facilitate modeling of repetitive processes.

Existing construction simulation research is mostly concentrated in the building engineering, road construction and underground engineering construction management field (Simaan AbouRizk, 2010) (Al-Bataineh et al, 2013)(Sze-Chun Lau et al, 2014)(Vargas et al, 2014). Studies in rockfill dam construction simulation are rarely reported. John W.Leonard first put forward using computer simulation technology to simulate the concrete gravity dam construction process, and suggested using different machinery matching schemes in different periods of construction, which is the earliest study of dam construction simulation (Leonard, 1973). Zhong Denghua proposed a construction simulation method of high rockfill dam (CSHRD), CYCLONE and Discrete Event Simulation were adopted to effectively model repetitive activities which can reflect the specific construction process (Zhong Denghua et al, 2007). However, in this model, instead of visual expression, logic or resource constraint relations among construction subsystems were converted to corresponding programming language, and were embedded into the discrete simulation program. For construction engineers who are not familiar with the software-specific terminology, during the modeling process, revising the constraints with combination of practical situation can be difficult, heavy workload and inefficient.

In view of the above problems, here the Stochastic Petri nets(SPNs) are introduced. Petri nets was proposed by Carl Adam Petri in his PhD thesis (Carl Adam Petri, 1962). Given the graphical representation and mathematical formalism, Stochastic Petri nets (SPNs) can intuitively describe the construction activities and relationships therein and take concurrent activities, uncertain time parameters and simultaneous resource possessing into account, which are an effective tool for modelling discrete event systems. Due to these advantages, Petri nets have been proposed as a tool for modelling and analyzing complex discrete event dynamic systems in project management. Structural properties of the Petri net model were detailedly described and could be seen in Murata's study (Murata, 1989). Ron R. Wakefield demonstrated how Petri net approach could be effectively used for modeling construction systems, two illustrative examples including the concrete placement operation and an earthmoving construction system were presented (Ron R. Wakefield et al, 1997). Bruno de Athayde Prata adopted Stochastic Colored Petri Nets to represent the operational dynamics of earth moving work, and provide an important instrument for economic assessment of the identified operational scenarios(Bruno de Athayde Prata et al, 2008). Cheng F proposed an extended Petri net model for virtual construction of earthmoving operations, with considering the constraint relationship between various operational equipment and construction restrictions (Cheng F F et al, 2011).

In order to establish a visual general modeling template and component for rockfill dam construct simulation, a more effective intuitive simulation modeling method combining both the merits of CYCLONE and SPNs was proposed. Accordingly, the modeling difficulty can be reduced while the universal applicability and transplantability of model can be obviously improved. With the given dam volume parameters and assumed mechanical configuration, the proposed method can be adopted to predict the construct duration and equipment utilization rates, thus to provide guidance for the construction organization and design. Specific methodology of the method will be explained in detail.

3. METHODOLOGY

The methodology of proposed method in this study is introduced here. Following the concepts and modeling elements of Stochastic Petri nets are introduced in the first section.

The second section presents the proposed hierarchical simulation modeling framework. Logic and resource constraints between each construction subsystem and each dam zone are considered during the modelling process.

3.1. Stochastic Petri Nets

As Fig. 1 shows, graphical representation of a Stochastic Petri net comprises four basic components: arcs, tokens, places and transitions. Places represent start of an activity when conditions including completion pf preceding activities and resources availability are satisfied. Transitions represent activities, which may spend time and change the state of system. It is worthwhile to note that two places or transitions cannot be collected. Each arc connects either a transition and a place or a place and a transition. Besides, arcs can be labelled with integer numbers representing their weights, thus to indicate the number of tokens that are transferred to or from a place on the firing of a transition. The tokens drawn as dots reside on the places and can flow in a Petri network as mobile entity. During the simulation modelling process, the tokens can be used to represent the main machinery in rockfill dam project while the occurrence of transitions represents arrival of machinery.

The Stochastic Petri net can be defined as $SPN=(P,T,F,\Lambda,M)$ where:

- $P=\{p_1,p_2,\cdots,p_m\}$ and $T=\{t_1,t_2,\cdots,t_n\}$ are finite, non-null sets of places and transitions respectively.
- $P\cap T=\varnothing$ means that places and transitions are mutually disjoint sets.
- $F\subseteq(P\times T)\cup(T\times P)$ -a set of edges, defined as a subset of the set of all possible connections.
- $\Lambda:T\to R^{+}$ - firing rates of exponentially distributed timed transtions.
- $M:P\to N$ is marking of SPN. It shows current number of tokens present in each place.

A transition $t\in T$ is enabled to fire within marking M, if all of its input places contain at least as many tokens as the weight of the corresponding input arc and all of its inhibitor places contain less tokens than the weight of the corresponding inhibitor arc.

Firing enabled transition will result in a new marking and remove a number of tokens from each input place and adds a number of tokens to output places. To include a timing concept into the SPNs formalism, two different classes of transitions, immediate transitions and timed transitions, are used to model the discrete event system. The Statistic Petri Nets (SPNs) count the occurrence of transitions as a stochastic process, activity duration follows a designated probability distribution. Therefore, the enabled immediate transitions fire in zero time while enabled timed transitions fire after a deterministic or random distribution of time. A net structure can be created with four basic modelling elements. A typical Stochastic Petri net is shown in Fig. 1.

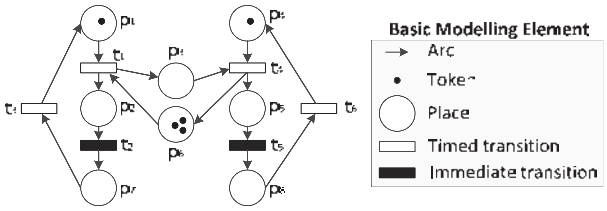

Figure 1. A typical Stochastic Petri net

3.2. Integrated Modelling Framework

Rockfill dam is often structurally divided into several zones with multiple stages of construction. In order to facilitate the modeling, a brief description of the construction process is first given. The construction process generally includes two important parts: material haulage subsystem and material placement subsystem. Trucks are loaded in the material yard first, then run along the specified road segments and intersections until reaching the corresponding filling area. After finishing unloading, the trucks return to the previous metrical yard and wait for reloading. The transportation process repeats until sufficient quantity of filling materials are delivered. For a single construction layer, when enough material is unloaded and lifting constraints are met, paving and rolling activities will successively occur. Hence, the core activities in rockfill dam project involve five works which are earthwork load, haul, unload, pave and compact.

During the rockfill dam construction process, in terms of operation characteristics, many repetitive activities are involved, especially in filling material transportation process. If CPM methods are adopted for analyzing, a very large network will be generated while too much repetitive activity cycles existing, and will not legibly show the project details. In addition, the transport route schemes are complex and change along with the advance of construction in rockfill dam project. The queuing problem caused by large transport volume is also common. Therefore, for reducing the model scale, CYCLONE is adopted for transportation process simulation.

Note that how to intuitively and effectively simulate the constraint conditions between each zone construction and each activity subsystem are important issues to be handled. Here the hierarchical modelling concept is introduced to simplify model and consider more construction features. Generally the established Stochastic Petri net represents overall construction process with lower levels incorporating more details regarding the specific transportation process based on CYCLONE. Mutual influence between different construction activities are mainly caused by process interdependence and resource sharing, such as the simultaneous resource possessing of different dam zone construction and the elevation lifting constraints between adjacent dam zones. The two aspects are both represented in the project level. Therefore, for the project level, during the specific modelling process, places indicate the starting state of construction activities. Different kinds of construction equipment are regarded as floating entity and are represented as tokens. Transitions present occurrence of each activity, and the arcs present the moving directions of machinery and the execution order of the activities. Given the uncertainties in construction process, time parameters including working time and waiting time are considered as obeying certain distributions. Hence, if the constraint conditions are demanded to be changed according to the requirement of engineering construction, or different equipment configuration are assigned for the task, the simulation model can be changed quickly. The overall framework of proposed integrated model is shown in Fig. 2.

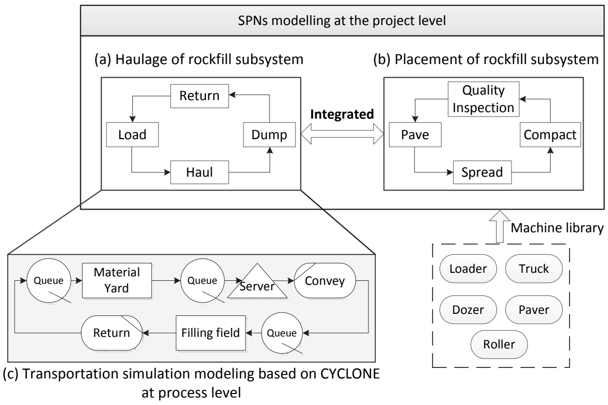
SPNs modelling at the project level
(a) Haulage of rockfill subsystem
(b) Placement of rockfill subsystem
Return
Load
Dump
Haul
Integrated
Quality Inspection
Pave
Compact
Spread
Machine library
Queue
Material Yard
Queue
Server
Convey
Return
Filling field
Queue
Loader
Truck
Dozer
Paver
Roller
(c) Transportation simulation modeling based on CYCLONE at process level

Figure 2. Conceptual Breakdown Structure of proposed integrated model

4. CASE STUDY

In this study, a rockfill dam project situated in China was adopted as demonstration. Data including specified construction scheme and mechanical parameters are obtained from provided construction organization design report. The involved construction equipment types are listed in Table 1.

Table 1. Selected Construction Equipment Types

Construction Zone	Construction equipment type			
	Loader capacity(m^3)	Dump Truck	Dozer	Roller
Core material	N(10,0.5)	25t	T180	20t
Filter material				
Transitional material	N(15,0.9)	32t		
Rockfill material	N(20,1)	45t	T320	25t

As mentioned above, the primary operations during the rockfill dam construction process considered here are earthwork load, haul, unload, pave and compact. According to provided traffic planning scheme, the detailed dam earthwork transportation simulation model of different zones and construction periods were established. Here the transportation of core material in first construction period is taken as example, which is shown in Fig. 3. In the rockfill dam project, resource sharing situations exist between different dam zone construction. Here for illustration the significance of proposed method, the simulation model at the project level of upstream rockfill zone and upstream transition zone based on Stochastic Petri net are given in Fig. 4, sharing of pavers and rollers are taking into consideration.

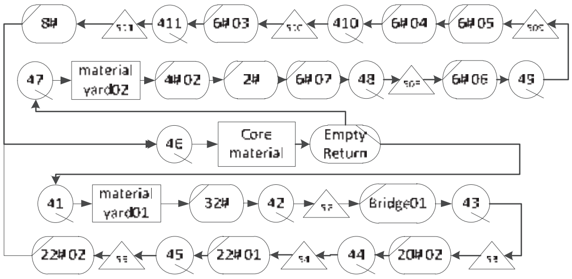
8#
411
6#03
410
6#04
6#05
47
material yard02
4#02
2#
6#07
48
6#06
49
46
Core material
Empty Return
41
material yard01
32#
42
Bridge01
43
22#02
45
22#01
44
20#02

Figure 3. Transportation simulation model based on CYCLONE for core zone at first period

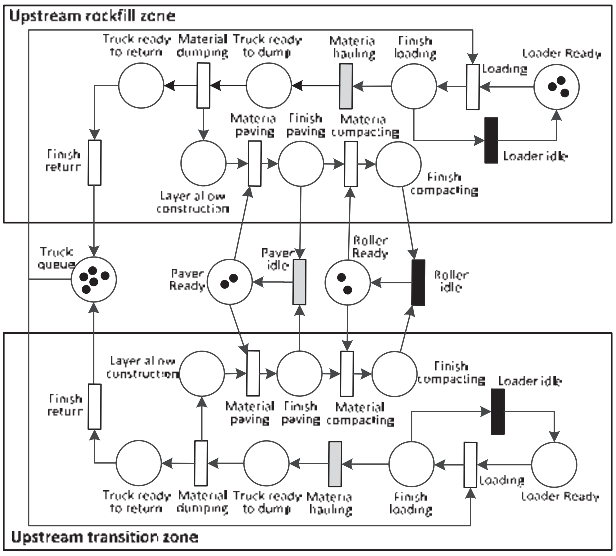
Upstream rockfill zone
Truck ready to return
Material dumping
Truck ready to dump
Materia hauling
Finish loading
Loading
Loader Ready
Loader idle
Materia paving
Finish paving
Materia compacting
Finish return
Layer al ow construction
Finish compacting
Truck queue
Paver Ready
Paver idle
Roller Ready
Roller idle
Layer al ow construction
Finish compacting
Loader idle
Finish return
Material paving
Finish paving
Material compacting
Loading
Truck ready to return
Material dumping
Truck ready to dump
Materia hauling
Finish loading
Loader Ready
Upstream transition zone

Figure 4. Schematic diagram of partial simulation model at project level

After running the established overall simulation model, relevant results can be obtained through sorting and statistics, such as construct schedule, equipment utilization rates and maximum road traffic density. Here the monthly complete filling voulume of each dam zone, an index of project completion situation, are show in Fig. 5. Combined with the actual construction progress, the proposed method can help to develop a more reasonable schedule plan for better construction management.

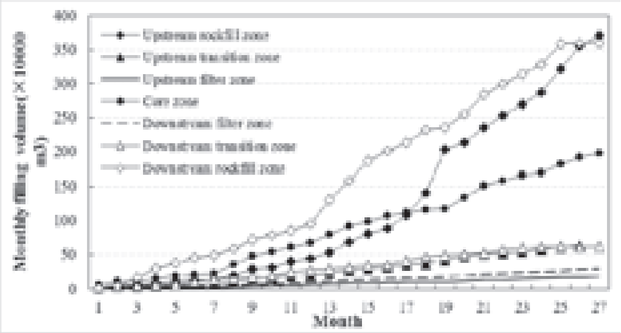

Figure 5. Simulation results: monthly filling volume of each dam zone

5. CONCLUSION

Construction simulation technology has provided an effective way for dynamic project schedule analysis and resource usage optimization. However, existing simulation modelling methods for rockfill dam construction were mainly based on CYCLONE and discrete simulation technology, logic or resource constraint relations were embedded into the programme, which is not easy to modify with poor readability. This paper presented work in establishing an intuitive construction simulation modeling method combining both the merits of CYCLONE and SPNs for rockfill dam project. To achieve this goal, hierarchical modelling concept is utilized, repetitive earthwork transportation operations are simulated based on CYCLONE while overall construction process is represented by Stochastic Petri nets with intuitive considering logic and resource constraints between activities. The proposed method could provide a visual general modeling template and component for rockfill dam construct simulation, and made it possible to rapidly build up reusable project simulation model. The application of the proposed method is demonstrated through a practical example, simulation results such as optimized mechanical configuration and equipment utilization rates can help making strategic decision evaluation and improving the project management level in rock fill dam project.

REFERENCES

Halpin D W.(1979): An investigation of the use of simulation networks for modeling construction operations, University Microfilms.

Sawhney A, AbouRizk S M, Halpin D W.(1998): Construction project simulation using CYCLONE, Canadian Journal of Civil Engineering, 25:2, pp.16-25.

AbouRizk, S.M., Halpin, D.W., and Lutz, J.(1992): State of the art in construction simulation, Proceedings of the Winter Simulation Conference, pp. 1271-1277.

AbouRizk S. (2010):Role of simulation in construction engineering and management, Journal of construction engineering and management, 136:10, pp.1140-1153.

Al-Bataineh M, AbouRizk S, Parkis H.(2013): Using simulation to plan tunnel construction, Journal of Construction Engineering and Management,139:5,pp. 564-571.

Lau S C, Lu M, Poon C S. (2014): Formalized Approach to Discretize a Continuous Plant in Construction Simulations, Journal of Construction Engineering and Management, 140:8, pp. 04014032.

Vargas J P, Koppe J C, Pérez S.(2014): Monte Carlo simulation as a tool for tunneling planning, Tunnelling and Underground Space Technology,40, pp.203-209.

Leonard, J. W. (1973). Plant and procedure concepts for rapid construction of concrete dam. Eleventh International Congress on Large Dams.

Zhong, D. H., Zhang, P., and Wu, K. X. (2007): Theory and practice of construction simulation for high rockfill dam, Sci. China Ser. E:Technol. Sci., 50(Supp. I),pp. 51–61.

Petri, C.A. (1962): Kommunikation mit automaten, Rhein.-Westfäl. Inst. f. Instrumentelle Mathematik an der Univ.Bonn, Germany.

Murata T. (1989): Petri nets: Properties, analysis and applications, Proceedings of the IEEE, 77:4, pp.541-580.

Wakefield R R, Sears G A.(1997): Petri nets for simulation and modeling of construction systems, Journal of construction engineering and management, 123:2, pp.105-112.

de Athayde Prata B, Ferreira Nobre E, Cordeiro Barroso G. (2008): A stochastic colored petri net model to allocate equipments for earth moving operations, ITcon,13, pp.476-490.

Cheng F F, Wang Y W, Ling X Z, et al.(2011): A Petri net simulation model for virtual construction of earthmoving operations, Automation in Construction, 20:2, pp.181-188.

Schedule Risk Analysis of Roller Compacted Concrete Dam Based on Risk Driver Theory

J. Yu, B. Wu, X. Wang & M. Zhao
State Key Laboratory of Hydraulic Engineering Simulation and Safety, Tianjin University, China
yj1592533724@126.com

ABSTRACT:
Construction of RCC (Roller Compacted Concrete) dam is quite complicated, and is affected by various uncertain factors. Schedule Risk Analysis is of vital importance for project schedule management. Current research mainly adopts probability distribution to reflect the uncertainty of activity duration, and does not analyze schedule risk from the angle that risk driver is the source leading to construction uncertainty. In light of this, this paper proposes a schedule risk analysis method of RCC dam based on risk driver theory. From the perspective of risk driver, this method identifies risk factors affecting the schedule of RCC dam and makes analysis of corresponding occurrence probability and consequence. In addition, Monte Carlo method is utilized to analyze construction schedule risk with consideration of risk factors, and completion probability of planned construction period can be obtained. Furthermore, sensitivity analysis is conducted to identify critical risk factor, which provides scientific guidance for construction risk control.

Keywords: RCC dam construction, Schedule risk analysis, Risk driver theory, Monte Carlo, Sensitivity analysis

1. GENERAL INTRODUCTION

Construction of RCC (Roller Compacted Concrete) dam is affected by weather condition, concrete production capacity, transport efficiency, dam surface rolling condition, management level and other risk factors. These factors will lead to construction delay and cause schedule risk. Scholars at home and abroad have started to analyze schedule risk. Maleplm D G, Roseboom C E, Clark C E, et al (1958) proposed Program Evaluation and Review Technique (PERT), which assumed that activity duration obeyed to β distribution. This method adopted three-point estimate (namely, optimistic duration a, most likely duration m and pessimistic duration b) to calculate mean and variance of activity duration, then changed PERT network to CPM network so as to obtained critical path and completion probability. Li Z M, Ge W, Wang J, et al (2015) believed that β distribution determined with four parameters was able to describe well the uncertainty of activity duration. Through analyzing engineering data, Chou J S (2011) thought Normal or Weibull distribution was more suitable distribution to reflect construction uncertainty. Špačková O, Šejnoha J, Straub D (2013) proposed that joint probability distribution could be used to reflect the impact of risk factors. Based on theory and experience, Trietsch D, Mazmanyan L, Gevorgyan L, et al (2012) put forward using logarithmic normal distribution to fitting duration probability distribution. Hajdu M, Bokor O (2014) proved that accurate estimation of three-point was more important than determination of distribution type. Ye Y Q, Yin F C (2014) introduced t distribution and Fisher Z distribution to PERT network, and found out when activity duration obeyed to t distribution, schedule risk was larger.

Researches mentioned above all adopt distribution probability to reflect construction uncertainty, but aren't able to analyze schedule risk from the angle that risk driver affects activity duration. In light of this, this paper proposes schedule risk analysis method of roller compacted concrete dam based on risk driver theory. This method focuses on risk factors, analyzes their occurrence probability as well as impact on construction schedule. In addition, sensitivity analysis is conducted to identify critical risk factors, and provide scientific guidance for construction process risk control.

2. RISK DRIVER METHOD

Risk driver method refers to approach that pays attention to risk factors, quantitatively analyzes occurrence probability and consequence so as to reveal the nature of schedule risk, and provide theoretical basis and technical support for control risk from the source.

3. QUANTITATIVE ANALYSIS OF RISK FACTORS

Risk factors have two important attributes-occurrence probability and consequence. Quantization of the two attributes can utilize historical materials, expert judgement, probability distribution theory, etc., to reasonably determine occurrence probability and consequence probability distribution of each risk factor.

Risk probability P refers to the occurrence probability of risk factor in each iteration. Risk factors during RCC dam construction can be divided into two types. One refers to factor that is inevitable to happen (P=1), such as construction efficiency is not in line with design value; the other refers to one that is likely to occur ($0<P<1$), such as reduction of management level. Since risk occurrence probability is affected by project feature and construction environment to a large extent, this paper combines historical material and expert experience to determine the occurrence probability of each factor.

Risk consequence I means risk's impact on activity when it happens. Since risk influence degree is also uncertain, it assumes that risk consequence I ($I>0$) is a random variable following a certain probability distribution D_i. $I<1$ means risk factor has a positive impact on duration; $I=1$ means risk exerts no impact on duration; $I>1$ means risk factor has a negative impact on duration. Since influence degrees that the same risk factor exerts on diverse projects may be different, this paper fully considers the characteristic of RCC dam, and determines probability distribution of risk consequence. Then random sampling is conducted in each iteration to stochastically determine risk consequence. Calculation of activity duration with the consideration of risk factor is shown in Equation (1).

$$T = T_p \cdot \prod_{i=1}^{n} I_i \tag{1}$$

$$I_i = \begin{cases} 1, risk\ \ factor\ i\ does\ not\ happen \\ sampling\ of\ \ distribution\ D_i, risk\ \ factor\ i\ happens \end{cases}$$

Where, n represents the number of risk factors; T_p represents planned duration; T is the calculated duration with consideration of risk factors.

4. SCHEDULE RISK ANALYSIS BASED ON MONTE CARLO SIMULATION

Monte Carlo method is also called statistical simulation method, random sampling technique and is a stochastic simulation method on the basis of probability and statistical theory. Monte Carlo method is adopted to randomly judge whether risk happens determine influence degree that risk factors exert on activity. Schedule risk analysis steps based on Monte Carlo simulation is presented as follows:

(1) Draw schedule network diagram. Logical relationship between activities and plan duration T_p are determined according to construction organization design.
(2) Analyze construction risk factors. Risk occurrence probability P_i and its influence probability distribution D_i (i=1, 2,…n) are analyzed, where n represents the number of risk factors.
(3) Determine activity duration in each iteration considering risk factors. For risk factor i, random number w_i following uniform distribution is first generated, then the number's relation with occurrence probability P_i is judged. When $w_i>P_i$, risk factor i does not occur, and construction is not affected; when $w_i<P_i$, risk i happens, and its influence on activity can be determined through random sampling. The calculation of activity duration is shown in Equation (1).
(4) After calculating the duration of all activity, CPM forward and backward pass calculation is conducted to obtain total construction duration.
(5) The simulation is repeated N times, and the simulation results are analyzed to obtain completion probability and other risk index.

5. SCHEDULE RISK ANALYSIS BASED ON MONTE CARLO SIMULATION SENSITIVITY ANALYSIS OF RISK FACTORS

Sensitivity analysis is an uncertainty analysis method, which can be used to evaluate influence degree that change of one or more factors exerts on target. There exist various risk factors during RCC dam construction. Identification of critical risk factors is of vital importance to assist in controlling construction risk. Sensitivity analysis steps in this paper is presented as follows:

(1) Determine common change range of occurrence probability that all the risk factors can reach;
(2) In common variation range, change the occurrence probability of a certain risk factor gradually, while the occurrence probability of other factors are keep the same. Then schedule schemes with the same risk factors in diverse occurrence probability can be obtained.
(3) Use Monte Carlo method to analyze schemes gained in step (2), and obtain corresponding completion probability. "completion probability-risk factors" sensitivity curve is utilized to determine uncertainty of each risk factor and critical risk factor can be identified.

6. CASE STUDY

RCC dam can be determined into 14 divisional works. Logical relationship between each divisional work and planned duration are shown in Figure 1.

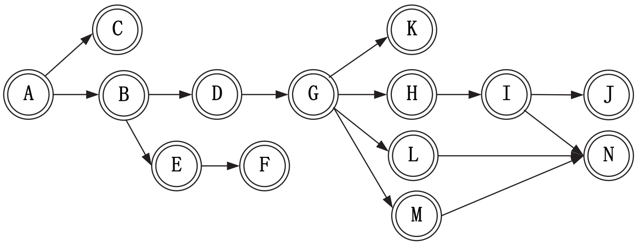

A : Normal concrete construction, dam foundation consolidation grouting, roller compacted concrete construction of the lower part
B : Construction of roller compacted concrete block
C : Casting with cable crane in advance
D : ……

Figure 1. Schedule network diagram of a RCC dam

5 important risk factors, which can be seen in Table 1, are selected from main construction links such as concrete production, transportation and surface construction. It is

assumed in this paper that risk consequences all obey to triangular distribution. Due to space limitation, Table 1 only lists risk factors in diversional work A, where p, a, b, c represent occurrence probability, optimistic impact, most likely impact and pessimistic impact, respectively.

Table 1. Parameter of risk factors in diversional work A

Activity	Risk	p	a	b	c
A	poor weather condition	0.30	1	1.05	1.15
	change of concrete production efficiency	1.00	0.85	1.00	1.25
	change of transport efficiency	1.00	0.83	1.00	1.30
	change of surface rolling efficiency	1.00	0.80	1.00	1.35
	reduction of management level	0.25	1.00	1.10	1.30

Monte Carlo method is adopted to conduct simulation for 10000 times, and the simulation results are analyzed, as is shown in Fig. 2. The completion probability of planned duration (1302days) is 0.728, and the mean value and standard deviation of total duration are respectively 1259 days and 84.73.

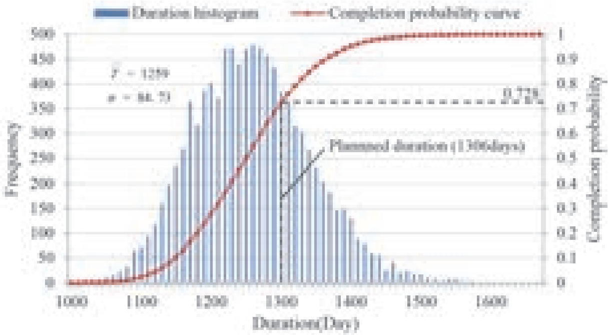

Figure 2. Completion probability curves

Sensitivity analysis is carried out on risk factors and the "completion probability-risk factors" curve is obtained, as shown in Fig. 3. It can be seen from this figure that completion probability is most sensitive to change of surface efficiency and secondly to change of transport efficiency. Poor weather condition is the factor exerting least influence on completion. Therefore, the analysis results provide scientific supports for managers to control risk factors according to their importance and ensure construction schedule.

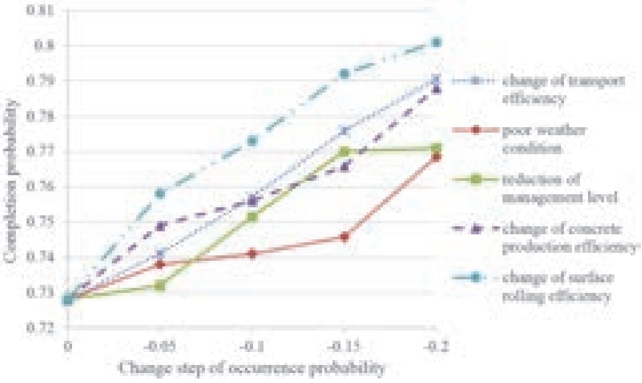

Figure 3. Sensitivity curves of each risk factor

4. CONCLUSION

This paper proposes a schedule risk analysis method of RCC dam based on risk driver theory. The approach pays attention to construction risk factors, analyzes their occurrence probability as well as consequences, and adopts Monte Carlo method to realize schedule risk analysis. In addition, sensitivity analysis is conducted on risk factors, and critical risk factor can be identified. The method proposed in this paper can overcome the defect that current risk analysis mainly adopts distribution probability to reflect uncertainty and does not analyze schedule risk from the angle of risk factor, and provide scientific basis for risk management during construction process.

REFERENCES

Maleolm D G, Roseboom C E, Clark C E, et al. (1958): Application of a technique for research and development program evaluation, Operations Research, 7:5, pp. 646-669.

Li Z M, Ge W, Wang J, et al. (2015): Risk analysis of overtopping during the construction period of earth-rock dam, Journal of Hydroelectric Engineering, 34: 3, pp. 145-149.

Chou J S. (2011): Cost simulation in an item-based project involving construction engineering and management, International Journal of Project Management, 29: 6, pp. 706-717.

Špačková O, Šejnoha J, Straub D. (2013): Probabilistic assessment of tunnel construction performance based on data, Tunnelling and Underground Space Technology, 37, pp. 62-78.

Trietsch D, Mazmanyan L, Gevorgyan L, et al. (2012): Probabilistic assessment of tunnel construction performance based on data, European Journal of Operational Research Technology, 216: 2, pp. 386–396.

Hajdu M, Bokor O. (2014): The effects of different activity distributions on project duration in PERT networks, Procedia - Social and Behavioral Sciences, 119: 19, pp. 766–775.

Ye Y Q, Yin F C. (2014): Construction schedule risk analysis of hydraulic engineering, Guangdong Hydropower, 8, pp. 119-121.

Study on Safety Assessment of Earth and Rock-fill Dam Based on Multi-level Fuzzy Evaluation

C.Hongjie
Huaneng Lancang River Hydropower Inc., Kunming, Yunnan, China, 650214
chj_1018@163.com

L.Ji
Huaneng Lancang River Hydropower Inc., Kunming, Yunnan, China, 650214

ABSTRACT:
This paper presents the analytic hierarchy process and fuzzy mathematical methods applied in assessment, then proposes multi-level blurry based assessment methods after making comprehensive consideration of those two methods. From safety and cost perspective, taking various factors and indexes that may influence dam safety operation into account, this paper gives out safety index, assessment rule and method, concept of safety indicator weight vector and its solutions. This paper， indeed, draws the degree of membership for the rock and soil dam to different security level. Finally, the improvement and the potentiality of this method were analysed.

Keywords: earth and rock dam, safety evaluation, analytic hierarchy process (AHP), fuzzy mathematic method

1. RESEARCH SITUATION OF EARTH-ROCK FILL DAMS' SECURITY COMPREHENSIVE ASSESSMENTS

Numerous dams have been built in China (Huo Yucheng, 2005), most of them have running for four or five decades or even longer. On the basis of current running situations, especially, the aging phenomenon, it is an urgent task in security management to assign risk ratings to dangerous dams. With years studying and groping, abundant achievements have obtained on this task, nevertheless, there are many influential factors still existed, which are random and could not be predicted. Earth-rock-fill dam is the most common type in China. In spite of its small scale, earth-rock-fill dam playing an irreplaceable role in local industrial and agricultural production and economical construction. With years running, a multitude of dangerous and defective dams will appear

China usually have preferred to re-check safety factors of engineering structure in the past (Hu Yunhe, 2011;Peng Xuhui,2003; Huo Yucheng, 2005), while the west have adopted SEED and value-at-risk ways. Li Junchun and his co-workers in Nanjing Hydraulic Research Institute adopts integral dam safety degree as evaluation criteria (Hu Yunhe, 2011; Peng Xuhui, 2003; Zhang Xiaofei, 2009; Peng Xuehui, 2003). Taking safety of dam structure and its impacts on economical into accounts, this theory shunned one-sidedness of emphasizing on structural reliability merely and gained great achievements. In addition, seeking possible cause is an important channel to improve dams' security by the means of field-based test and observation. Currently, ways to evaluate dam security emerges endlessly. The principal methods are dam structure form mathematical method and AHP. With rapid development and extensive use of fuzzy mathematics, combining those two methods and putting it use do have great research value as a newly subject.

2. EARTH-ROCK FILL DAM'S MULTI HIERARCHY EVALUATION APPROACH MODEL OF SECURITY COMPREHENSIVE JUDGMENT

Various factors affects the safety of earth-rock-fill dam (Li Lei, 1999; Li Zhongkun, 2003). Each factor could be represented by a sign. Assuming that there are signs, and those signs could constitute a sign domain:

$$U=\{u_1,u_2,\cdots,u_j,\cdots u_m\} \qquad j=1,2,\cdots,m \tag{1}$$

To distinguish the superior from inferior, every sign should be subdivided into several grades. Assuming each sign could be divided into n degrees, then it will form a degree domain V :

$$V=\{v_1,v_2,\cdots,v_i,\cdots v_n\} \qquad i=1,2,\cdots,n \tag{2}$$

Each sign u_j （$j=1,2,\cdots,m$） has its corresponding grade membership v_i （$i=1,2,\cdots,n$）. Namely, u_j corresponds with v_i , and those mutual relevance relationship could be denoted as r_{ij} . All degree membership of one sign could constructed one fuzzy vector Y. The Fuzzy vector of number j could be expressed as:

$$Y=\left\{r_{1j},r_{2j},\cdots,r_{ij},\cdots r_{nj}\right\} \tag{3}$$

All Fuzzy vector of signs constitute fuzzy relation, recording as fuzzy transformation matrix:

$$R=\begin{bmatrix} r_{11} & r_{21} & \cdots & r_{n1} \\ r_{12} & r_{22} & \cdots & r_{n2} \\ \vdots & \vdots & \vdots & \vdots \\ r_{1m} & r_{2m} & \cdots & r_{nm} \end{bmatrix} \tag{4}$$

Among m numbers factors, each have different affections on dam safety. It is necessary to attach every weighting factor to every sign. Those weighting factors form an weight vector A:

$$A'=\left\{a_1,a_2,\cdots,a_j,\cdots a_m\right\} \tag{5}$$

Fuzzy matrix times weight vector A', then get an compound fuzzy transition:

$$Y=A'\cdot R=\left\{a_1,a_2,\cdots,a_j,\cdots a_m\right\}\begin{bmatrix} r_{11} & r_{21} & \cdots & r_{n1} \\ r_{12} & r_{22} & \cdots & r_{n2} \\ \vdots & \vdots & \vdots & \vdots \\ r_{1m} & r_{2m} & \cdots & r_{nm} \end{bmatrix}$$

$$=\{y_1,y_2,\cdots,y_i,\cdots y_n\} \tag{6}$$

Then the fuzzy vector Y:

$$Y=\left\{y_1,y_2,\cdots,y_i,\cdots y_n\right\} \tag{7}$$

Finally, comprehensive evaluation results were obtained. y_i represents the number i grade membership of the total dam security. It is observed from above derivation that different factors have different impacts on dam security, in spite of blurry consequence.

3. ENGINEERING PRACTICE ANALYSIS

3.1. Project Overview of Shizi Gou Dam Reservoir

Shizigou reservoir located in Nanya Village, Fenxiang Town, Yiling district, Yichang city, Hubei province, and be about 40 km apart from north of Yiling city. Shizigou reservoir intercepts west branch of Huangbaihe River at the north shore of Yangtze River. It was started building in June, 1973 and completed in December, 1974.

3.2. Subject Problems and Reasons

Safety appraisal shows dam barrage, spillway, and outlet tunnel and management facility have problems as following:

(1) Dam barrage: Based on achievements deduced from field test and exploration test, subject problems and cause could be deduced as following: Substitute materials filled in core-wall and dam shell are poor quality. Main filling materials in core-wall are clayey sand, compactness of which is about 0.83 to 0.90, the coefficient K of permeability of which was between 1.05×10-4 and 9.57×10-4. Those specifications are not standard. Filling materials in dam shell are weathering shale, most of which are breccia states. Filling body is a little loose, therefore, it is randomness when backfilling. Both graduation and grinding effects are poor; Bank slope of dam foundation is fault fracture zone, which have the trait of strong water permeability. Filling materials in bank slope are moderately weathered rock, while bed are silky weathered rock. Foundation clearing is not completely and seepage channel existing; Dimension blocks in upstream batter were crushed and badly weathered. Part of it has collapsed; Drainage system in downstream slope is not perfect. It was eroded badly, therefore, surface is not smooth, and gully appeared.

(2) Spillway: The sector from open flooding canal to downstream stilling basin do not have regular shape and is not smooth. The whole line do not built lining and, moreover, has been weathered and destroyed by rush of water severely. All existing problems pose threats on left jetty head’s security; downstream water in discharge chute cannot link up with downstream catch-drain smoothly. It is as well as adjacent to left dam slope. Both of those factors could endanger dam security.

(3) Water delivery tunnel: Entrance gate hoist room is located in the centre of water delivery tunnel, which exerts bad influences on flood discharge and management application during flood season; the lining of flank wall and top arch were both built with concrete-slurry. The lining for baseboard is not built. After checking, tensile stress of inside top arch and flank wall is more than standard, which cannot satisfy code demand; Cast-iron gate had rusted and leaked severely; it is hard to open gate hoist for it and diagonal bar had rusted, and the bar is out of shape.

(4) Engineering supervision: Simplicity of facilities for engineering supervision, for instance, without monitoring, flood prevention road is not clear, impacts bad effects on flood prevention.

3.3. Solving Steps

3.3.1 Selecting safety evaluation indexes

According to current national testing specification and social economic development, following security evaluation indexes (signs) (As is shown in Figure 1.) could be preliminary confirmed for further study on feasibility of fuzzy comprehensive evaluation.

3.3.2 Figure up weight sets A

In model, each index weight was confirmed by Delphi and Analytic Hierarchy Process (Liu Chengdong, 2004; Peng Hui, Chen Cheng, 2006; Liu Yalian, 2010). In other words, to avoid logical mistakes, weight depends on scores marked by a group of experts.

(1) Constructs judgment matrix: Judgment matrices could be constructed by each grade index showed in Table 1. and its interrelation. Judgment matrices constructs according to hierarchy. For example: two indicators in factor level B and its related target level A could constructs a judgment matrix; four indicators in sub-factors level C and its related factor level B could constructs a judgment matrix. Natural number 1, 2, ~9 and reciprocal 1/2, 1/3, ~1/9could be used to show degree of relative importance. Sub-factor level C1 corresponding index level D1、D2、D3、D4 showed in Table 2.:

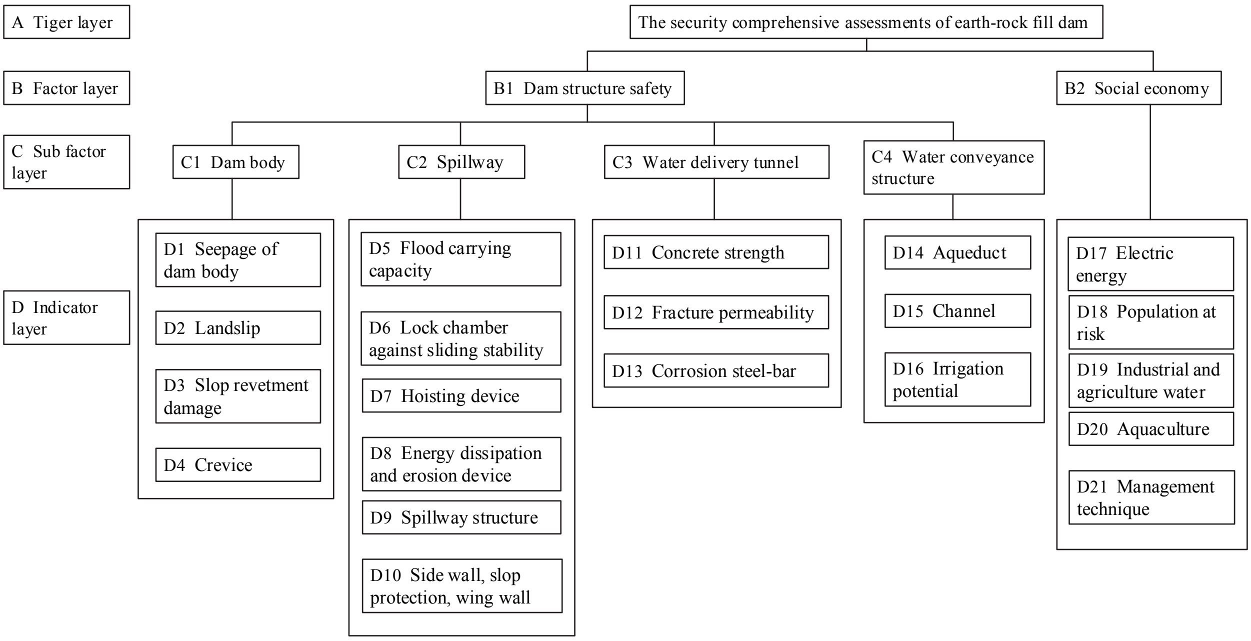
A Tiger layer
B Factor layer
C Sub factor layer
D Indicator layer
The security comprehensive assessments of earth-rock fill dam
B1 Dam structure safety
B2 Social economy
C1 Dam body
C2 Spillway
C3 Water delivery tunnel
C4 Water conveyance structure
D1 Seepage of dam body
D2 Landslip
D3 Slop revetment damage
D4 Crevice
D5 Flood carrying capacity
D6 Lock chamber against sliding stability
D7 Hoisting device
D8 Energy dissipation and erosion device
D9 Spillway structure
D10 Side wall, slop protection, wing wall
D11 Concrete strength
D12 Fracture permeability
D13 Corrosion steel-bar
D14 Aqueduct
D15 Channel
D16 Irrigation potential
D17 Electric energy
D18 Population at risk
D19 Industrial and agriculture water
D20 Aquaculture
D21 Management technique

Figure 1. multi-hierarchy fuzzy judgment index system diagram of earth-rock dam safety comprehensive evaluation

$\lambda_{\max} = 4.074$, CI= 0.024, CR= 0.028 Eigenvector $\omega = \{0.868 \;\; 0.345 \;\; 0.085 \;\; 0.345\}$ CR= 0.028<0.1, the consistency of the judgment matrix is consistent with the requirement, and the feature vector is normalized as below. $\omega_1 = \{0.528 \;\; 0.210 \;\; 0.052 \;\; 0.210\}$. ω_1 is a weight vector of D1,D2,D3 and D4 to C1.

Similarly $\omega_2 = \{0.280 \;\; 0.280 \;\; 0.280 \;\; 0.064 \;\; 0.064 \;\; 0.032\}$. ω_2 is a weight vector of index level D5,D6,D7,D8,D9 and D10 to C2. $\omega_3 = \{0.2 \;\; 0.6 \;\; 0.2\}$. ω_3 is a weight vector of index level D11, D12 and D13 to sub-factors levelC3. $\omega_4 = \{0.2 \;\; 0.2 \;\; 0.6\}$. ω_4 is a weight vector of index level D14, D15 and D16 to sub-factors levelC4.

$\omega_5 = \{0.560 \;\; 0.250 \;\; 0.095 \;\; 0.095\}$. ω_5 is a weight vector of index level C1, C2, C3 and C4 to sub-factors level B1.

$\omega_6 = \{0.282 \;\; 0.282 \;\; 0.282 \;\; 0.107 \;\; 0.048\}$. ω_6 is a weight vector of index level D17, D18, D19, D20 and D21 to factor level B2. Weight vector of index level from D1 to D16 correspond to factor level B1 as following table: Factors layer B2, B1 are consistent with each other, for the Shizi Gou project can be assumed that the factor layer B1, B2 on the weight of the target layer A. $\omega_7 = \{0.65 \;\; 0.35\}$

(2) Figure up weight sets A: As previously mentioned, different signs have different affection on dam security. In addition, under different operation condition, one sign will exert several influences on dam body. Therefore, it is necessary to add appropriate weight to each sign, in spite of tough working. We acquired abundant first-hand data from on-site detecting 24 large, medium, small dams. A number of experts and technicists from local water conservancy department giving opinions and making decisions of different affections on dam body that above-mentioned 21 indexes made. On the basis of judgment matrices of different grades, eigenvalue of maximum, hierarchy and synthetic weight, combining opinions from experts and technicists, correspondent weight sets to index were obtained. Substituting above calculated data into the follow formula.

$$A' = \begin{bmatrix} \omega_1^T & & & & \\ & \omega_2^T & & & \\ & & \omega_3^T & & \\ & & & \omega_4^T & \\ & & & & \omega_6^T \end{bmatrix}_{21\times5} \times \begin{bmatrix} \omega_5^T & 0 \\ 0 & 1 \end{bmatrix}_{5\times2} \times (\omega_7^T)_{2\times1} = \begin{bmatrix} a_1 \\ a_2 \\ \vdots \\ \vdots \\ a_{21} \end{bmatrix}$$

Weight sets obtained. Specific data as following Table 4.:

3.3.3 Figure up membership

Sign u_j for the grate v_i ,and the degree of membership r_{ij} determined by the following formula:

$$r_{ij} = \frac{u_j \in v_i times}{N} \tag{8}$$

N represents the total number of samples. Obviously, the lager the N is, the more representative the r_{ij} have.

Considering subjective assessments from different experts and technicists and Fig. 1., membership r_{ij} was obtained after conducting an investigation to Shizi Gou reservoir located in Yiling District, Yichang City. It could be seen as following Table 5.:

Table 1. Signs degree instruction

Evaluation index(sign)	Excellent	Fine	Average	Slightly poorer	Poor
Seepage of dam body	No-leakage	No obvious	Obvious	Relatively serious	Serious
Landslip	No	No obvious	Obvious	Relatively serious	Serious
Slop revetment damage	No	No obvious	Obvious	Relatively serious	Serious
Crevice	No	No obvious	Obvious	Relatively serious	Serious
Flood carrying capacity	Standard	Relatively standard	Common	Relatively poor	Poor
Lock chamber against sliding stability	Quite stable	Fairly stable	General	Lower stability	Instability
Hoisting device	Standard	Relatively standard	Common	Relatively poor	Poor
Energy dissipation and erosion device	Standard	Relatively standard	Common	Relatively poor	Poor
Spillway structure	Excellent	Fine	Common	Relatively poor	Poor
Side wall, slop protection, wing wall	Excellent	Fine	Common	Relatively poor	Poor
Concrete strength	Excellent	Fine	Common	Relatively poor	Poor
Fracture permeability	No	No obvious	Obvious	Relatively serious	Serious
Corrosion steel-bar	No	No obvious	Obvious	Relatively serious	Serious
Aqueduct	Excellent	Fine	Common	Relatively poor	Poor
Channel	Excellent	Fine	Common	Relatively poor	Poor
Irrigation potential	Excellent	Fine	Common	Relatively poor	Poor
Electric energy	Excellent	Fine	Common	Relatively poor	Poor
Population at risk	No	Few	Common	Many	A lot of
Industrial and agriculture water	Standard	Relatively standard	Common	Relatively poor	Poor
Aquaculture	Great benefit	High benefit	Common	Lit benefit	No benefit
Management technique	Very advanced	Advanced	Common	Backward	More backward

Table 2. Judgment matrix of C1

C1	D1	D2	D3	D4
D1	1	3	7	3
D2	1/3	1	5	1
D3	1/7	1/5	1	1/5
D4	1/3	1	5	1

Table 3. Weight vector of index level from D1 to D16

D1	D2	D3	D4	D5	D6	D7	D8
0.296	0.118	0.029	0.118	0.070	0.070	0.070	0.016
D9	D10	D11	D12	D13	D14	D15	D16
0.016	0.008	0.019	0.057	0.019	0.019	0.019	0.057

Table 4. Weight Sets $A^{'}$

index	D1	D2	D3	D4	D5	D6	D7
weight	0.072	0.029	0.007	0.029	0.017	0.017	0.017
index	D8	D9	D10	D11	D12	D13	D14
weight	0.004	0.004	0.002	0.005	0.014	0.005	0.005
index	D15	D16	D17	D18	D19	D20	D21
weight	0.005	0.014	0.213	0.213	0.213	0.080	0.036

Table 5. Degree membership to its related signs in Shizi Gou reservoir dam

Membership	Excellent	Fine	Average	Relatively poor	Poor
Seepage of dam body	0.10	0.30	0.10	0.30	0.20
landslip	0.03	0.14	0.08	0.46	0.29

Destruction of protection slop	0.03	0.05	0.12	0.31	0.49
Crevice	0.35	0.40	0.17	0.05	0.03
Flood carrying capacity	0.10	0.15	0.40	0.20	0.15
Stability of lock chamber against sliding	0.03	0.04	0.50	0.24	0.20
Lifting facilities	0.08	0.10	0.12	0.50	0.20
Energy dissipation and erosion device	0.01	0.10	0.24	0.40	0.25
Spillway structure	0.05	0.07	0.13	0.45	0.30
Side wall, slope protection, wing wall	0.01	0.04	0.10	0.35	0.50
Concrete strength	0.01	0.02	0.27	0.45	0.25
Crack leakage	0.01	0.14	0.20	0.35	0.30
Corrosion of reinforcement	0.10	0.20	0.40	0.25	0.05
Flume	0.10	0.20	0.25	0.30	0.15
channel	0.20	0.25	0.15	0.30	0.10
Irrigation capacity	0.35	0.22	0.18	0.15	0.10
Electricity generation	0.20	0.25	0.20	0.25	0.10
Population at risk	0.01	0.02	0.20	0.40	0.37
Industrial and agriculture water	0.02	0.08	0.10	0.30	0.5
aquaculture	0.10	0.30	0.10	0.30	0.20
Management technique	0.10	0.30	0.10	0.30	0.20

4. CONCLUSION

Earth-rock fill dam is the most common but most complicated dam type. Despite it was constructed by common earth and rock, earth-rock fill dam contains unfathomable science. On account of age-old, immaturity technique, unscientific management and aging, most earth-rock dams have been insecure. That make comprehensive assessments to dam security degree is necessary.

The evaluation methodology studied in this paper have considered various factors that may influence earth-rock-fill dams' security comprehensively. On the basis of fundamental states of dams, with modern mathematical methods, assessment process is more scientific. Evaluation theory as well as the obtained conclusion is unassailable.

REFERENCES

Huo Yucheng. (2005): Study of the theory and method of health diagnose for earth-rock-fill dam, Dissertation of Hohai University

Hu Yunhe. (2011): Research on earth-rock-fill dam safety assessment method and system development, Dissertation of Zhengzhou University

Peng Xuehui. (2003): Application of risk analysis in China dam safety, Dissertation of Nanjing hydraulic research institute.

Huo Yucheng. (2005): Study of the theory and method of health diagnose for earth-rock-fill dam, Dissertation of Hohai University

Hu Yunhe. (2011): Research on earth-rock-fill dam safety assessment method and system development, Dissertation of Zhengzhou University

Peng Xuehui. (2003): Application of risk analysis in China dam safety, Dissertation of Nanjing hydraulic research institute.

Zhang Xiaofei, Su Guoshao and Wu Zhangdun. (2009): A new safety evaluation method on dams based on analytic hierarchy process and fuzzing mathematics theory, Journal of Guangxi Univ ersity :Nat Sci Ed, 12:3, pp. 321-325.

Peng Xunhui, Lilei and Wang Renzhong. (2004): Dam risk analysis and its application to shaheji dam, Journal of hydro-science and engineering, 12:4, pp. 21-25.

Lilei and Shen Jinbao. (1999): Primary research on comprehensive evaluation method of earth-rockfill dam safety, Journal of dam observation and geotechnical tests, 12:4, pp. 24-26+30.

Li Zongkun, Zhou Jing and Zheng Jingxing. (2003): Multi-pole fuzzy pattern recognition method for behavior evaluation of earth-rock dam, Journal of Hydraulic Engineering, 12:9, pp. 83-87.

Liu Chengdong. (2004): Analysis method of multi-factor weighting of dam safety evaluation and its application, Dissertation of Hohai University

Peng Hui, Peng Huiming and Cheng Shengguo. (2006): Research on safety comprehensive evaluation of earth rock dam with multi layer fuzzy evaluation, Journal of disasters and prevention and control engineering, 12:1, pp. 5-11.

Chen Cheng and Hua Jianlan. (2010): Application of improved analytic hierarchy process method in safety assessment of earth-rockfill dams, Advances in Science and Technology of Water Resources, 12:2, pp. 58-62.

Liu Yalian and Zhou Cuiying. (2010): Application of Fuzzy Multi-level Comprehensive Evaluation on Earth-rock Dam Safety, Hydropower, 12:5, pp. 38-40+87.

Effects of the Hydropower Station Operation on the Water Temperature in the Downstream

H. Xiang,Y. Fuhai & L.Sihua
Da Du River Hydropower Development CO.,LTD, China.
huangxiang125125@163.com

ABSTRACT:
The annually averaged discharged water temperature of the reservoir is in different low degree from March to May and July to August based on the discharged water temperature observation. The temperature is lower than the natural water temperature of 1.8℃ significant in April. And it is higher than the natural of 3.3℃ in December obviously. The discharged water temperature was delayed for 14 days compared with the natural water temperature such as 16℃. The minimum temperature of discharged water appears in February and it is 9.0℃ higher 2.1℃ than the reservoir construction. The maximum temperature appears in August same as becoming the reservoir. Analyzing the daily variation of temperature of discharged water in mid April to mid November 2013, the phenomenon of low temperature water is present in the mid April to mid June, and the high temperature water is present in the later mid Jun to mid November. Studying the daily variation of discharged water temperature during the fish spawning period, which is able to advise several methods for optimized reservoir operation to ease negative impacts on eco-environment.

Keywords: Effects, Hydropower station, Operation, water temperature,

1. INTRODUCTION

There have been more than 760 large reservoirs in China by 2016(Sun *et al*.,2013). Temperature stratification phenomenon usually occurs when the formation of the reservoir. The discharged water temperature lower than natural, which lead to fish spawning period delay and coastal crops suffer chilling injury(Wang *et al*.,2005;Li,1982;Ban and Li,2007;Zhang,1987) .In early 1930s, United States, Soviet Union, and Japan had carried out a lot of observation on temperature of the reservoir(Zhang,1987). China began researching on reservoir water temperatures at 1950s, but mostly observation paid attention on vertical water temperature in front of the dam(Zhang,1984;Zhu,1985). Late 1990s, The water temperature problem was increasingly active. However, the observations mainly focused on the model parameter calibration(Deng *et al*.,2001;Liu *et al*.,2007). The researches were lack of continuity observation for day changes on discharged water temperature. Especially, there were less results and engineering applications on the reduction of low temperature water harm to downstream.

The hydropower station is located in DaDu river. It is a main control project on the middle reaches of the river. The dam operated in December 2010, and the maximum backwater high is 173m. It is impact on spatial and temporal distribution of natural river water temperature after the reservoir formation. Carry out monitoring the discharged water temperature to research the effect of reservoir operation on the discharged water temperature and provide technical basis on the temperature recovery.

2. ONLINE OBSERVATION SCHEME OF DISCHARGED WATER TEMPERATURE

2.1. The observation section arrangement

There are two observation sections. The one is at tail water of the Power station and the other one is downstream of dam at 3.7km.

2.2. Observation method, apparatus, and frequency

Put in one water temperature sensor at 0.5m below the surface, which is in tail water place as there is not water temperature stratification. Put in four water temperature sensors at the downstream of the dam 3.7km according to elevation as the water level amplitude is 12m.One of the four sensors layout at 0.5m below the surface also.

ZDR recording temperature instrument is made by ZeDa instrument equipment factory. A resolution of 0.1℃, accuracy of +/-0.2℃, range -40~100℃. Observe the discharged water temperature continuously and record automatically from middle of April to November 2013.

3. ANALYSIS OF OBSERVATION DATA

3.1. Water temperature variation calculate in ten days

From mid April to mid November of 2013, The change process of water temperature in the two sections was consistent. It is rise after falling. The water temperature was 13.6℃ and 13.2℃ respectively in mid-April, and reached the maximum 19.5℃ in mid-August, and then reduced to 13.9℃ in mid-November. It is shown in Table 1.

Table 1. Water temperature variation calculate in ten days

Time/Site	Tail water	At 3.7km
Mid April	13.6*	13.2
Late April	14.7	14.7
Early May	15.9	15.9
Mid May	15.8	15.8
Late May	16.2	16.3
Early June	16.8	16.9
Mid June	17.2	17.3
Late June	18.4	18.5
Early July	18.7	18.7
Mid July	18.9	19.2
Late July	18.7	19.1
Early August	18.7	18.7
Mid August	19.1	19.1
Late August	19.5	19.5
Early September	19.4*	19.1
Mid September	17.6	17.6
Late September	17.4	17.4
Early October	16.9	17.1
Mid October	16.1	17.0
Late October	15.4	15.6
Mid November	14.4	14.4
Late November	13.9	13.9

Note: "*" error was excluded

3.2. Water temperature variation along the river channel

The water temperature at the section, which is downstream of dam at 3.7km, is higher than tail water temperature. The maximum increase is 0.9℃, and the minimum is 0.1℃. The maximum rate of temperature increase is 0.3℃/km, and the minimum is 0.067℃/km along the river channel. It is shown in Table 1.

3.3. Characteristics of water temperature changes every hour in typical days

The tail water temperature at difference a day per hour is not significant as shown in Fig.1. The maximum temperature difference respectively is 0.2℃,0.2℃,0.3℃,0.1℃,0.1℃ corresponding to the day, which is on May 15, June 15, July15, August 15 and September 15.

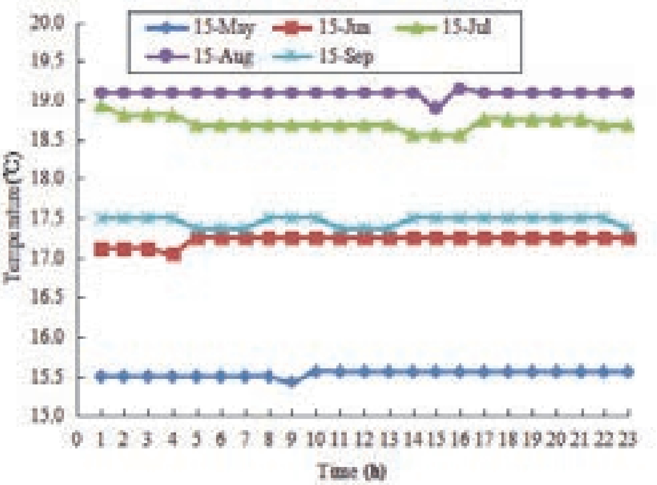

Figure 1. Characteristics of water temperature changes every hour in typical days of tail water

4. EFFECT ON RIVER WATER TEMPERATURE OF POWER STATION OPERATION

Table 2-1. Compare with the measured water temperature and the natural water temperature

Items/Month	1	2	3	4	5	6
Natural water temperature	6.9	8.3	11.9	15.2	16.9	16.8
Measured in 2012				13.2	15.9	16.1
Measured in 2013	9.5*	9.0*	10.9	13.5	16.0	17.5
Average on 2012 and 2013	9.5	9.0	10.9	13.4	16.0	16.8

Note: some observation data was lost, "*" was calculate by the upstream and downstream relationship

Table 2-2. Compare with the measured water temperature and the natural water temperature

Items/Month	7	8	9	10	11	12
Natural water temperature	18.3	18.6	17.0	14.2	10.9	7.8
Measured in 2012	16.7	17.6	17.4	15.2	13.9	
Measured in 2013	18.8	19.1	18.1	16.3	14.2	11.1*
Average on 2012 and 2013	17.8	18.4	17.8	15.8	14.1	

Note: some observation data was lost, "*" was calculate by the upstream and downstream relationship

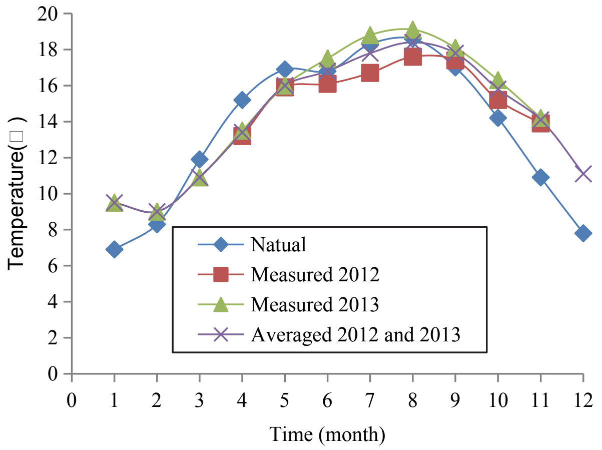

Figure 2. Comparison the discharged water temperature and natural water temperature

4.1. Comparison the discharged water temperature and natural water temperature (It is shown in Table 2 and Fig. 2)

Compare with the measured average water temperature and the natural water temperature, the measured water temperature is lower than natural from March to May and July to August. The maximum lower is 1.8℃ in April, and the minimum lower is 0.2℃ in August. However, the water temperature is significantly higher than natural water temperature from September to next February, and increase from 0.4℃ to 3.3℃. The maximum higher is 3.3℃ in December, and the minimum higher is 0.4℃ in September. The average higher temperature is 3.0℃ from November to next January. What's more, the discharged water temperature and the natural water temperature are consistent in June.

The temperature changes in tail water during one year get smaller than natural water. The natural water temperature changes from 6.9℃ to 18.6℃, and the changes is 11.7℃ in the year. The discharged water temperature changes from 9.0℃ to 18.4℃ during one year, and the changes is 9.4℃ in the year, which decrease 2.3℃ than natural water changes. Both the maximum temperature appears in August, and the measured value is lower 0.2℃ than the natural. The minimum value of natural water temperature is in January, and the minimum measured value is in February, which increased 2.1℃ than natural water temperature.

In conclusion, there are different levels of low-temperature water effect in March to May and July to August. The lower than natural water temperature is 1.8℃ in April. And discharged water temperature is higher than natural water temperature from January to February and September to December. and is significantly higher than natural water temperature of 3.3℃ in December.

4.2. The effect of water temperature variation on the downstream river (It is shown in Fig. 3)

4.2.1. Delay time

The spawning, feeding and other activities of the fish or other aquatic should have been in specific water temperature in the seasons. If the discharged water temperature missed the time, which is required for the biological activity, even if other habitats meet the requirements, it will cause the inhibition of normal activity. What is more, the delay time is too long to bring harm to aquatic organisms. For example, the reservoir water temperature was delayed for 14 days compared with the natural water temperature at 16℃.

4.2.2. Extreme value

The extreme value of discharged water temperature is the maximum and the minimum value. The minimum water temperature is 9.0℃ higher 2.1℃than the reservoir construction. The minimum temperature of discharged water appears in February after building the dam, when it appears in January before. The maximum temperature appears in August the same as becoming the reservoir. Changes in extreme value of water temperature will affect the cold water fish or warm water fish habitat directly.

4.2.3. Daily variation

The daily average tail water temperature of measuring is lower than the natural water temperature obviously from the middle of April to early of June. On the contrary, it is from later middle of June to middle November. The phenomenon of low temperature water is present from the middle of April to middle of June, and the phenomenon of high temperature water is present from the later middle of Jun to middle of November.

The discharged water temperature is averaged by month. It is lower than natural water temperature in April and May, and lower range is 0.9~1.7℃. It is higher than natural water temperature from June to November, and higher range is 0.5~3.3℃.

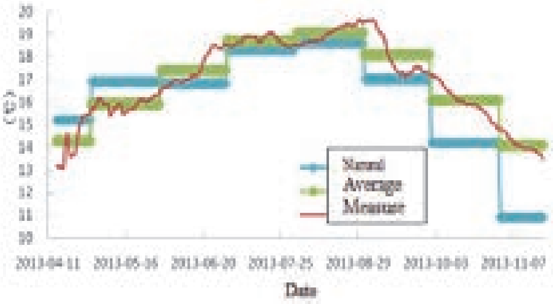

Figure 3. The daily average tail water temperature of measuring

5. CONCLUSION AND DISCUSSION

The annually averaged discharged water temperature of the reservoir is in low degree from March to May and July to August significant in April. However, the annually averaged discharged water temperature is higher than the natural from January to February and from September to December. The reservoir water temperature was delayed for 14 days compared with the natural at 16℃, and the water temperature will cause the inhibition of normal activity. Changes in extreme value of water temperature will affect the cold water fish or warm water fish habitat directly. Studying the daily variation of discharged water temperature during the fish spawning period, which is able to advise several methods for optimizing reservoir operation to ease negative impacts on eco-environment.

There is much more difference in temperature changes during a year, though every day or every meadow is changed in the same month. The measured data sequence has a great influence on the accuracy, therefore it should have carried on the long-term water temperature monitoring to understand the effect of power station operation on river water temperature accurately.

Study on the distribution and the demand for water temperature of the rare fish in the downstream further to guide the operation scheduling under the premise of hydropower station operation. Make the discharged water temperature as far as possible consistent with the natural water temperature when the fish spawning and other sensitive period.

ACKNOWLEDGEMENT

This research was supported by the National Science and Technology support plan (Grant No. 2012BAC06B00).

REFERENCES

SUN Zhengang, ZHANG Lan,DUAN Zhongde. (2013) :The number and distribution of reservoirs in China. China Water Resources, 7,pp.10-11.

WANG Yunchun, ZHU Jun, MA Mei, et al.(2005) :Thermal stratification and paroxysmal deterioration of water quality in acanyon-reservoir, southwestern China. Journal of Lake Sciences, 17:1,:pp.54-60.

LI Yongsheng.(1982):Water temperature in reservoir and rice irrigation. China Rural Water and Hydropower, 1: pp.7-9.

BAN Xuan, LI Damei.(2007) :Ecological hydrological influence of large water conservancy projects on Acipenser Sinensis in Yangtze River. Engineering Journal of Wuhan University, 40(3): pp.10-13.

ZHANG Dafa. (1987):A review of foreign and domestic research on water temperature in reservoirs. Water Resources & Hydropower of Northeast China,3:pp.21-27.

ZHANG Dafa. (1984):Analysis and estimation of water temperature in reservoirs. Hydrology, 1:pp. 19-27.

ZHU Bofang.(1985): Prediction of water temperature in reservoirs.Journal of Hydraulic Engineering, 2: pp.12-21.

DENG Yun, ZHAO Wenqian, LI Jia, et al.(2001) Simulation on thermal stratification of the huge-cubage and deep reservoirs. Proceedings of the Congress-international Association for Hydraulic Research.pp584-592.

LIU Lanfen, ZHANG Shijie, LIU Chang, et al. (2007):Study on the water temperature structure of the Manwan Reservoir. Journal of China Institute of Water Resources and Hydropower Research, 5(2):pp. 87-94.

4th APG Symposium and 9th EADC on

INNOVATIVE TECHNOLOGIES FOR DAMS AND RESERVOIRS TOWARD THE FUTURE GENERATIONS

Seepage Safety Assessment of Fill Dam using Safety Evaluation Chart

D. Shin, K. Kim & J. Lee
K-water Institute Infrastructure Research Center, Daejeon, South Korea
Cute_lion@daum.net

ABSTRACT:

This study proposes a safety evaluation chart (SEC) for seepage to assess the seepage safety of a fill dam as reservoir's water level changes. The SEC for seepage is developed as a tool which can indicate the safety of fill dam in real-time through the safety based on both the monitoring by instruments and the fragility analysis by numerical method. For seepage safety assessment of embankment dam, it is common to check each effect of seepage quantity, pore water pressure, hydraulic gradient and seepage velocity according to changes of water level, which mainly affect the failure probability. In the present study, however, the probability of failure due to seepage velocity and hydraulic gradient is mainly examined. For probabilistic seepage analysis, data obtained from the statistical analysis on the design values of 24 fill dams are used. The SEC for seepage is constructed based on the fragility curve derived from the probabilistic seepage analysis. And also using the SEC for seepage, it is expected that the results of this study will be very useful to evaluate the safety of water resources facilities such as dams as well as levees.

Keywords: Safety assessment, Fill dam, Probability of failure, Seepage safety evaluation chart

1. INTRODUCTION

Seepage safety is one of the most important elements in safety management of dams. Especially, in case of embankment type dams, if unpredicted or excessive seepage is observed, then emergency inspection should be urgently carried out to know what's happening at the downstream slope of the dam or at other spots, and consequently, if required, urgent measures should be applied to prevent unwanted further progress of excessive seepage, i.e., leakage.

Many examples of dam collapses in the literature are giving us valuable lessons that unpredicted, uncontrolled and/or excessive seepage behaviours of fill type dam inevitably lead to catastrophic failure.

Moreover, recently threats of climate change on the river flood risk have been deepened much more and more. In relation to this, Arnell, N.W. et al. (2014) warns that:

> *In 2050 the current 100-year flood would occur at least twice as frequently across 40 % of the globe, approximately 450 million flood-prone people and 430 thousand km^2 of flood-prone cropland would be exposed to a doubling of flood frequency, and global flood risk would increase by approximately 187 % over the risk in 2050 in the absence of climate change. There is strong regional variability (most adverse impacts would be in Asia).*

The necessity of flood early warning system equipped with sensors installed in dams, dikes and levees exists here. If the system monitors sensing networks of dams or levee, detects sensor signal abnormalities, calculates dam failure probability, and simulates possible scenarios of dam breaching and flood propagation, it will be very helpful to improve the flood-related disaster prevention systems.

This study proposes a safety evaluation chart (SEC) for seepage to assess the seepage safety of a fill dam as reservoir's water level changes. The SEC for seepage is developed as a tool which can indicate the safety of fill dam in real-time through the safety based on the measurement by instruments and the fragility analysis by numerical method. For seepage safety assessment of fill dam, it is common to check the effects of seepage quantity, pore water pressure, hydraulic gradient and seepage velocity according to changes of water level, which mainly affect the failure probability. In the present study, however, the probability of failure due to seepage velocity and hydraulic gradient is mainly examined.

2. SEEPAGE BEHAVIOUR OF THE STUDY DAM

Imha multipurpose dam, the study dam, was built on the Banbyenoncheon River, a tributary of the Nakdong River in South Korea (see Fig. 1). The main purpose of Imha dam is to reduce the flood damage at the middle and downstream area of the Nakdong River, and to supply municipal and industrial water to the cities including Gumi, Daegu, Masan, Changwon, Jinhae, Woolsan, and Busan cities. Table 1 shows the key data of Imha dam.

Figure 1. Aerial view of Imha dam

Table 1. Imha multipurpose dam data

Items	Data
Type	Center-core rockfill dam
Height	73.0m
Crest length	515.0m
Crest elevation	EL.168.0m
Gates	W12.0mxH13.8mx4Gates (Radial gate)
Basin area	1,361km^2
Total storage capacity	595 million m^2
Eff. reservoir capacity	424 million m^2
Design flood level	EL.164.7m
Normal pool level	EL.163.0m
Flood restriction level	EL.161.7m
Low-water level	EL.137.0m
Overflow level	EL.151.4m
Flood control capacity	80 million m^2
Design flood capacity	4,600m^3/sec (year 200 frequency x 1.2)
Power plant capacity	50,000kW (25,000kW x 2)

Fig. 2 shows the instruments for monitoring leakage and crest settlements over time after its completion in December, 1991. The records of leakage water incorporated with rainfall and change in reservoir water levels are shown in Fig. 3. In Fig. 3, the second leakage measurement gauge (LW2) looks to be affected mainly by rainfall rather than main dam body. The average leakage water is about 385 l/min at EL.158.84m of reservoir water level.

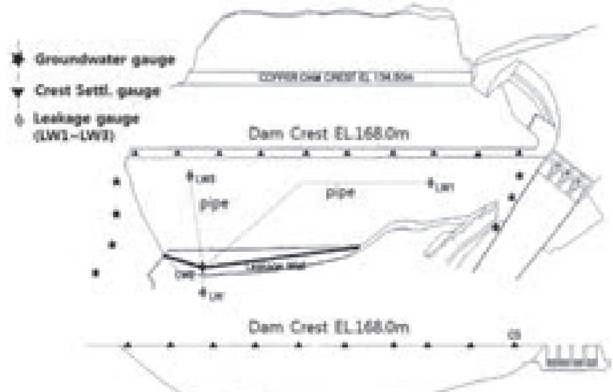

Figure 2. Instruments for leakage, groundwater and crest settlement installed at Imha dam

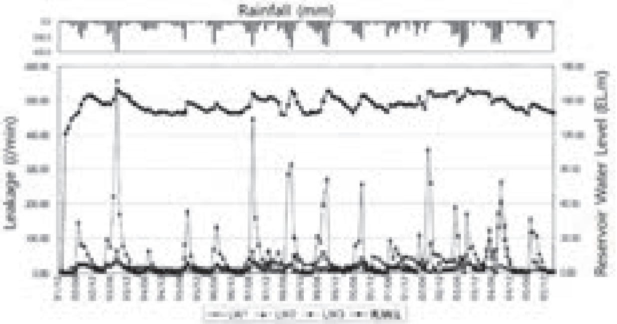

Figure 3. Records of leakage water measurement

To date, Imha dam has not experienced yet any serious seepage-related phenomena since its completion, hence no provisions are required.

However, considering the uncertainty in safety management of dams to be seriously affected by extreme precipitation due to unpredictable climate change, and also by deterioration of dam materials over time, it is recommended to improve the existing seepage safety management system by introducing pseudo-real time safety evaluation technique, in which the probability of failure by expected or unexpected seepage behaviours is evaluated and used to warn the public about the risk if required.

3. THEORY OF RELIABILITY ANALYSIS

3.1. The basic concepts

For more effective safety management of dams, it is valuable to take account into variability and uncertainty in performance of dam arising from a number of sources such as loadings, parameter values, and analytical models.

Reliability analysis is a good framework that may handle those variability and uncertainty in performance of dam.

In reliability analysis, the First-Order Second-Moment Reliability Method (FOSM method) is the primary approach in geotechnical engineering. In this approach, uncertainty in performance is taken to be a function of uncertainty in model parameters or in the model itself. The expected values and standard deviations of the random variables (and sometimes model accuracy) are used to estimate the expected value and standard deviation of a performance function, such as the factor of safety against slope instability.

For reliability evaluation of most geotechnical structures, in particular existing dams or levees, their reliabilities are calculated using the capacity-demand model and quantified by the reliability index β, which is a measure of the reliability of a dam or levee that reflects both the mechanics of the problem and the uncertainty in the input variables. The reliability index is defined in terms of the expected value and standard deviation of the performance function, and permits comparison of reliability among different structures or mode of performance.

Usually, in the capacity-demand model, the expected value and standard deviation of the random variables such as exit hydraulic gradient, *i* and the factor of safety, FS, can be calculated by using the expected value and standard deviation of those random variables in conjunction with the Taylor's series method.

In the capacity-demand model, uncertainty in the performance of dam or levee is taken to be a function of the uncertainty of various parameters used for calculating some measure of their performances.

3.2. The steps of reliability analysis

The followings are the steps illustrating reliability analysis for seepage and slope stability according to the USACE method (USACE, 1999).

a. Selection and Characterization of Random Variables: Important variables considered to have sufficient inherent uncertainty are taken as random variables and characterized by their expected values, standard deviations, and correlation coefficients. For the analyses of dams or levees, random variables typically include material strengths, soil permeability or permeability ratio.
b. Identification of a Performance Function and Limit State
c. Calculation of the Expected Value and Standard Deviation of the Performance Function: In concept, this involves integrating the performance function over the probability density functions of the random variables.
d. The reliability index β is calculated from the expected and standard deviation of the performance function. The reliability index, a measure of the distance between the expected value and the limit state.
e. If a probability of failure value is considered, a distribution such as normal distribution or lognormal distribution is assumed and the failure probability is calculated.

3.3. The moments of random variables

To model random variables in the Taylor's series, one must provide their expected values and standard deviations, which are of two of several probabilistic moments of a random variable such as mean value, expected value, variance, standard deviation, and coefficient of variation.

In particular, when a random variable X is lognormally distributed, then the random variable Y=ln X is normally distributed with parameters $\mathrm{E[Y]} = \mathrm{E}[ln\,X]$ and $\sigma_Y = \sigma_{lnX}$. In this context, the coefficient of variance of X is calculated:

$$V_X = \frac{\sigma_X}{E[X]} \quad (1)$$

The standard deviation of Y is then calculated as:

$$\sigma_Y = \sigma_{lnX} = \sqrt{\ln(1 + V_X^2)} \quad (2)$$

The expected value of Y is calculated using the standard deviation σ_Y.

$$\mathrm{E[Y]} = E[\ln X] = \ln E[X] - \frac{\sigma_Y^2}{2} \quad (3)$$

The density function of the lognormal variable X is:

$$\mathrm{f(X)} = \frac{1}{X\sigma_Y\sqrt{2\pi}} exp\left[-\frac{1}{2}\left(\frac{lnX - E[Y]}{\sigma_Y}\right)^2\right] \quad (4)$$

The reliability index β is:

$$\beta = \frac{E[lnX]}{\sigma_{lnX}} = \frac{ln\left[\frac{E[X]}{\sqrt{1+V_X^2}}\right]}{\sqrt{\ln(1+V_X^2)}} \quad (5)$$

The probability of failure can be calculated as:

$$P_r(f) = \Psi(-\beta) = \Psi(-z) \quad (6)$$

where Ψ(-z) is the cumulative distribution function of the standard normal distribution evaluated at –z.

4. SAFETY EVALUATION CHART (SEC) FOR REAL-TIME SAFETY ASSESSMENT AGAINST SEEPAGE

If the probability of failure of dam subject to unexpected changes in reservoir water level due to extreme rainfall can be known, then safety management will become much easier than the past. In addition, when the safety information supported by the instrumental data that are transferred to the entire safety monitoring system of the dam are available in real-time, then decision-making on what- to-do at an emergency situation can be easily made with convince.

This study proposes a safety evaluation chart by which overall safety information of the dam can be strengthened by the real-time measurements and by the quantified safety level.

Fig. 4 shows the flow diagram illustrating the safety evaluation chart for real-time safety assessment against seepage.

In Fig. 4, if conditions of initial reservoir water level and design rainfall intensity should be given first, then hydrological scenarios are developed. At the same time, real-time monitoring system works to record the seepage behaviour with change of reservoir water level. Thirdly, using SEEP/W, a finite element program for seepage analysis by Geo-Slope Ltd., steady-state and transient analyses are carried out to check if the dam is safe or not against seepage in terms of hydraulic gradient and flow velocity.

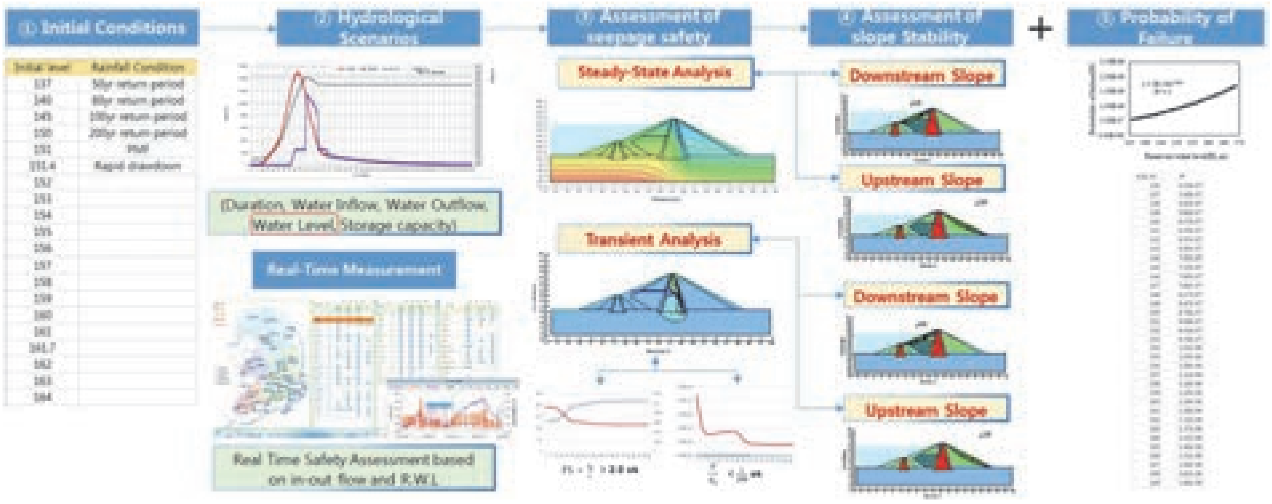
① Initial Conditions
② Hydrological Scenarios
③ Assessment of seepage safety
④ Assessment of slope Stability
+
⑤ Probability of Failure
Steady-State Analysis
Transient Analysis
Downstream Slope
Upstream Slope
Downstream Slope
Upstream Slope
(Duration, Water Inflow, Water Outflow, Water Level, Storage capacity)
Real-Time Measurement
Real Time Safety Assessment based on in-out flow and R.W.L

Figure 4. Concept of safety evaluation chart

Fourthly, slope stability will be checked based on the results of seepage analyses. Finally, based on the reliability analysis described above, the probability of failure is calculated.

5. RESULTS OF CASE STUDY ON IMHA DAM

To calculate the failure probability, P_f depending on hydraulic gradient, flow velocity and factor of safety, seepage and slope stability analyses by using SEEP/W and SLOPE/W.

Fig. 5 shows the typical cross section of Imha dam including foundation and material properties are shown in Table 2.

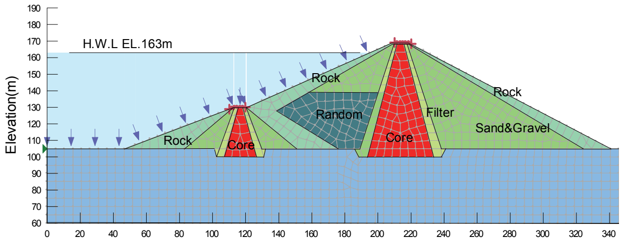
H.W.L EL.163m
Rock
Rock
Rock
Random
Core
Core
Filter
Sand&Gravel
Elevation(m)
190
180
170
160
150
140
130
120
110
100
90
80
70
60
0
20
40
60
80
100
120
140
160
180
200
220
240
260
280
300
320
340

Figure 5. Typical cross section of Imha dam

Table 2. Material properties of Imha multipurpose dam

Zone	r_t (kN/m^3)	c (kPa)	Φ (˚)	k_{sat} (cm/s)	Θ, Fn	$Θ_{sat}$ (m^3/m^3)	k
Core	19.9	50.0	31.2	$1.36\text{x}10^{-6}$	sample clay	0.5	Fredlund & Xing
Filter	19.3	-	37.0	$2.0\text{x}10^{-3}$	sample silt	0.43	Fredlund & Xing
Sand & gravel	20.8	-	38.0	$3.0\text{x}10^{-3}$	sample sand	0.35	Fredlund & Xing
Rock zone	18.8	-	42	$1.0\text{x}10^{-1}$	sample gravel	0.25	Fredlund & Xing
Random zone	20.8	-	37		sample sand	0.35	Fredlund & Xing
Found-ation	21.0	-	-	$1.0\text{x}10^{-6}$	-	0.25	Fredlund & Xing

The parts of calculation results of failure probability given in Figs. 5 and 6 imply that Imha dam is sufficiently safe against seepage in terms of hydraulic gradient and slope stability.

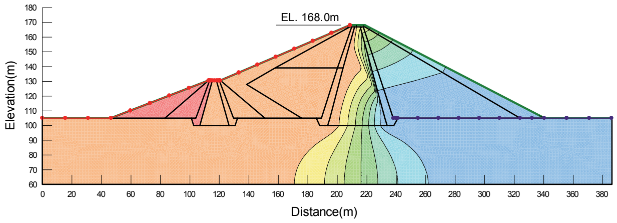
EL. 168.0m
Elevation(m)
180
170
160
150
140
130
120
110
100
90
80
70
60
0
20
40
60
80
100
120
140
160
180
200
220
240
260
280
300
320
340
360
380
Distance(m)

Figure 5. Results of transient seepage analysis

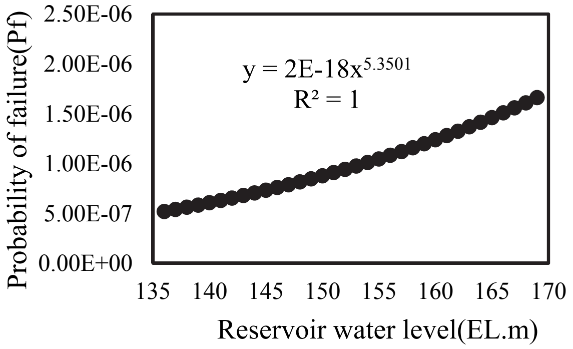

Figure 6. Probability of failure against seepage

6. CONCLUSION

(1) Using reliability analysis based on the First-Order Second-Moment Reliability Method (FOSM method) and Taylor's series method, the probability of failure due to seepage velocity and hydraulic gradient was successfully examined.

(2) The results of reliability analysis imply that Imha dam is sufficiently safe against seepage in terms of hydraulic gradient and slope stability.

(3) When the real-time monitoring of seepage is incorporated into the reliability analysis, and in addition, a safety evaluation chart is applied to the monitoring system, then safety management of existing dams can be effectively improved.

ACKNOWLEDGEMENT

This research was supported by a grant (15SCIP-B065985-03) from Smart Civil Infrastructure Research Program funded by Ministry of Land, Infrastructure and Transport (MOLIT) of Korea government and Korea Agency for Infrastructure Technology Advancement (KAIA).

REFERENCES

Arnell, N.W. and (2014), “The impacts of climate change on river flood risk at the global scale,” Climate Change, Volume 134, Issue 3, pp 387-401.

USACE (1999), “Risk-based analysis in geotechnical engineering for support of planning studies,” ETL 1110-2-556, 28 May 1999.

GEO-SLOPE International Ltd. (2010), SEEP/W 2007: An engineering methodology..

GEO-SLOPE International Ltd. (2010), SLOPE/W 2007: An engineering methodology.

4th APG Symposium and 9th EDADC on

INNOVATIVE TECHNOLOGIES FOR DAMS AND RESERVIORS TOWARD THE FUTURE GENERATIONS

Study on Water Resources Security of Three Gorges Reservoir from the Non-traditional Security Perspective

X.H. Wen
School of Hydropower and Information Engineering, Huazhong University of Science and Technology, Hubei, China
China Three Gorges Corporation, Beijing, China
wen_xiaohao@ctg.com.cn

J.Z. Zhou
School of Hydropower and Information Engineering, Huazhong University of Science and Technology, Hubei, China

X.E. Hu
China Three Gorges Corporation, Beijing, China

ABSTRACT:
In the View of Nontraditional Security, water resources security is an important part of national security and social economic security. The Three Gorges Reservoir, as the backbone in the Yangtze River, plays an important role in regulating spatial and temporal distribution of the rainfall, reducing flood and drought disasters, supplying fresh water reliably and protecting water resources security. In recent years, the major challenges of water resources security of Three Gorges reservoir are cited such as the reduced incoming flow, the uneven rainfall distribution over a year, fresh water supply pressure, water environment problems, the underdeveloped water resources potential and the lack of the necessary social environment guarantees. Water resources security problems of the Three Gorges Reservoir are social, crossover and diffuse. It has vital practical significance for the optimal scheduling of the Three Gorges Reservoir and efficient utilization of the Yangtze River Basin to conduct a comprehensive security system of water resources from the aspects of specification, scheduling innovation, market orientation, material guarantees, technical support and society coordination.

Key Words: Non-traditional, Water Resources, Three Gorges Reservoir, Strategies

1. INTRODUCTION

Nontraditional security is a new concept of security and a new security research field that caused by non-political and non-military factors, while affecting the development, stability and security of the country and region and even the world （Z.Y. Li, 2009）. With the economy recovering and developing, the global water use rose sharply. And The World Water Resources Comprehensive Assessment published by the United Nations in 1997 pointed out that the water problem will seriously affect the twenty-first century global economic and social development, and becoming an important part of nontraditional security. Shortage in per capita water resources, water supply pressure, hostile hydrographic environmental problems and the lack of imperative social atmosphere are the major dilemmas of water resources security of China. The Three Gorges Reservoir, as the backbone in the Yangtze River, plays an important role in regulating spatial and temporal distribution of the rainfall, reducing flood and drought disasters, supplying fresh water reliably and protecting water resources security （J.Q. Li, 2011）. Researches on the water resource security of Three Gorges Reservoir in recent years, have been regarded as water supply security study its essence is the national strength contest in the energy field, which still belongs to traditional security problems. Therefore, it is necessary to develop an objective understanding for the water resource security of the Three Gorges reservoir from perspective of nontraditional security, constructing a strong water resources security system.

2. THREE GORGES RESERVOIR AND ITS WATER RESOURCES SECURITY IMPLICATION

2.1. Three Gorges reservoir

The Yangtze River Basin, rich in water resources, across three major economic zones of China, is the world's third largest basin, with a total area of 1,800,000 square kilometers, accounting for 18.8% of the territory of China. The Three Gorges Reservoir as a mainstay type reservoirs in the Yangtze Basin, controlled drainage area 1084 square kilometers with the total designed capacity of 39.3 billion cubic meters and flood control capacity of 22.15 billion cubic meters is a multi-purpose reservoir servicing for flood control, drought resistance, water supply, shipping and power generation. It has aroused extensive attention amid its immense flood control capacity, wide adjustable range, flexible scheduling methods and the comprehensive benefits.

2.2. Water resources security Implication of the Three Gorges reservoir

Water resource security closely connected with the nation’s water security. Presently thinking, the water resource has been popularized as one kind of resource security in a certain sense referring to water safety. In the nontraditional security view, water resources security is part of the national security, which refers to that, under the existing economic and technical conditions, the water supply can meet the demands of economic construction and social development citizens enjoy the right of water resources free from pollution and damage, and the government implement public power to ensure that the natural circulation water system the resources are not damaged or threatened, and undertake an obligation of realizing the sustainable utilization of water resources.

From the aspect of water resources security properties the Three Gorges reservoir is one of the national security related to people's production and life safety in the middle lower Yangtze area. At the form level, the Three Gorges reservoir water resources security related to the coordinated development of social economy, as one of the basic natural resources and strategic economic resources, becoming a major strategic resources on the basis of economic and social development. From the perspective of value, the safety of water resources in the Three Gorges reservoir is the basic premise to realize the sustainable utilization of water resources. No security, no sustainable utilization of water resources. From the target aspect, the final destination of water resources security in the Three Gorges reservoir is to guarantee the rights of people’s survival and development. From non-traditional security perspective, people is the main security and objective realization of security. Water is the lifeblood of human existence, constituting the material basis for human ecological system. From the perspective of practice, the security of water resources in Three Gorges reservoir is the exercise of rights and obligations. Water resource is a kind of public product, competitive and exclusive. Public Service Department should create appropriate institutional environment to maintain the water resources security and guarantee that citizens can enjoy the security of water resources.

3. THREE GORGES RESERVOIR WATER RESOURCES SECURITY SITUATION

3.1. Reduction of the total inflow

From 2008 to 2015, the average annual inflow of Three Gorges reservoir is 402.276 billion cubic meters, the average storage capacity of 12800 cubic meters per second, 10.8% lower than long-time average annual value of 14300 cubic meters, as is shown in Table 1.

Table 1. Total inflow of a year from 2008 to 2015

Year	Total Inflow （Billion cubic meters）	Average Flow （m^3/s）	Mean Comparison （%）
2008	428.9	13600	-4.9
2009	388.1	12300	-14.0
2010	406.6	12900	-9.8
2011	339.5	10800	-24.5
2012	448.0	14200	-0.7
2013	367.8	11600	-18.4%
2014	438.0	13900	-2.8%
2015	377.7	12000	-16.3%

3.2. Uneven distribution over a year

Since 2003, the average monthly inflow in a year of Three Gorges reservoir are shown in Table 2.Obviously, the distribution of water inflow during the year is rich in month January to April, dry in May to December, and especially dry in June, September, October, compared with the year mean, drier 17.3%, 15.2% and 27.3% respectively （X.H. Wen）.

Table 2. Average Monthly Inflow (2003-2015)

month	1	2	3	4	5	6
Year （2003-2015） m^3/s	4860	4350	5090	7000	10500	16300
Mean Comparison （%）	11.7	8.8	13.1	4.2	-12.5	-12.4
month	7	8	9	10	11	12
Year （2003-2015） m^3/s	27500	23400	23300	14400	9190	5810
Mean Comparison （%）	-8.3	-17.0	-12.4	-27.3	-14.1	-3.6

3.3. Water supply pressure

With the rapid development of social economy, and the influence of extreme weather, the demand for water resource and security in the lower reaches of the Yangtze River Basin is increasing. In 2009 October, in order to ease the worst drought of the Dongting Lake and Poyang Lake in middle and lower reaches of the Yangtze River, we carried out the security delay of Three Gorges Reservoir test impoundment and enlarged the outflow for the downstream, guarantying downstream water supply and navigation safety. In 2011 May, Hubei province suffered rare winter and spring drought in 50 years, therefore starting the emergency scheduling of Three

Gorges Reservoir. The flow from reservoir remained at 7000 cubic meters per second, 1500 cubic meters per second higher than those of the upstream, which alleviate the drought area water supply pressure. In 2014 February, to solve the saltwater intrusion at Shanghai Yangtze River Estuary with the longest duration in the history, the Three Gorges reservoir implemented saltwater pressure reduction scheduling for a period of 11 days, 960,000,000 cubic meters water replenishment larger than the standard of 6000 cubic meters per second. Meanwhile, to guarantee the safety of Yangtze River and aquatic healthy breeding, we carried out the sedimentation reduction scheduling and ecological scheduling test, during which the flow increased and, in certain sense the water supply pressure increased as well.

3.4. The worse water environment

In recent years, the class of water quality in main sections of Three Gorges Reservoir falls into group II - III; Water quality differs in different periods, the abundant water period (June ~ September) water quality obviously inferior to normal water period (April ~ May and October ~ November) and dry season (from January to March and December), water quality in dry season is relatively good. The main tributaries of water quality in reservoir area are inferior to class III mainly. Year 2009 ~ 2012, up to or exceeding class III water quality were 4.8%, 6%, 6% and 7.2% respectively; class III water quality frequency of occurrence was basically stable, while the frequency of occurrence of the IV water quality gradually reduced. V grade occurrence increased.

3.5. Not-fully developed water resources potential

Yangtze River is an important base for hydropower clean energy development in China. The Three Gorges Reservoir plays an important role in fully taking advantage of the Yangtze River, controlling floods in Yangtze River Basin and safeguard the security of water supply. At present, Xiluodu and Xiangjiaba and other large reservoir upstream tributaries have completed been the upper reaches of the Yangtze River flood control capacity is further expanded leading extreme changes in the external condition of Three Gorges Reservoir Operation Giving full play to backbone project and its strategic position, it is necessary to further optimization of the Three Gorges reservoir water resource management concept, through overall planning, promoting the comprehensive dispatching of reservoir groups, from research to practice to develop the Three Gorges Reservoir water resources potential and ensure the Three Gorges Reservoir water resources security. In 2014, comprehensive consideration on flood control, ecology protection, water supply, navigation and power generation and the further study on the Three Gorges Reservoir basis joint scheduling have been listed in On Relaying the Golden waterway to promote the Yangtze River Economic Belt Announced by the State Council as the important construction content for Yangtze Green Economic Belt.

3.6. Unsupported social environment

At present, China has faced the not yet formed safe social environment for national water resources, the not strong citizen’s water saving awareness, the serious water waste phenomenon and the deteriorated water environment. We are lack of water resources security incentive policy and the safeguard law system in water resources of the Three Gorges Reservoir has not been formed yet. The security accountability supervision mechanism should be perfected. Besides, the integrated management of water resources is relatively weak with the insufficient people’s water livelihood investment and the scanty water business capital and technology. In addition, in some foreign countries, the cascade reservoir has been built and the capacity accounts for 70.37% of the annual average runoff; however, in China, the planned adjustment capacity of Jinsha is relative lower than those in overseas. Even fully completed, according to the plan, the capacity of reservoirs are only 20% of the annual average runoff. There is a large room for developing the potential of rivers in our country.

4. CONSTRUCT THE THREE GORGES RESERVOIR WATER RESOURCES SECURITY SYSTEM

4.1. Standard system

Form the Three Gorges Reservoir water resources security law system as soon as possible. Formulate the Three Gorges Reservoir Water Resource Security Management Regulations and other relevant laws and regulations. Construct the water resources security guarantee system. Strengthen the comprehensive management of Three Gorges Reservoir and regional water resources allocation. Establish the strictest water resources management and supervision, inspection and accountability system in the aspect of demand planning, pollution control, water saving, environmental protection. Explore water resources reserve mechanism to improve the ability to resolve the water resources risk resistance and the crisis through the ground, underground reserves （X.P. MA, 2009）.

4.2. Operation innovation

The key to solve the security problems of water resources in the Three Gorges reservoir is to optimize its scheduling mode, giving full play to the great advantage of science and technology in the field of water resources security, through the optimization of scheduling to solve the problem of the average annual reduction of inflow, mal-annual-distribution and water environment governance. The first is to put successful experience into the normal operation period of scheduling rules, such as the beginning of the impounding water in advance, medium and small flood dispatching, ecological regulation, sediment reduction. Under the premise, without increasing the flood control risk, continuously explore the small and medium-sized flood dispatching scope delayed-fluctuation or expansion. The second is to analyze the running of Three Gorges reservoir boundary conditions, combined with the present system of hydrological telemetry covering of the Yangtze River Basin and continue to carry out the study and practice of real time joint dispatching of cascade reservoirs in the Yangtze basin. In addition, we should actively promote the water system linkage of rivers and lakes to constantly improve water allocation capacity. From national level, based on vital rivers and lakes, on vital controlling reservoirs and on the major inter-basin water diversion projects such as South-to-North Water Diversion Project, we will gradually form the Four-vertical and Three Horizontal, South-North Allocation and East-West Support overall river and lake linkage format. From regional dimension, we will accelerate the rivers and lakes linkage construction of reasonable structure and perfected functions, flood impounding and discharging, properly leding-out, the complementary water resources, reasonable wet-dry season scheduling, unobstructed water system and beautiful environment. From project level, we will deepen the connective operation management and scheduling optimization of rivers and lakes to full play the comprehensive role of rivers and lakes water linkage project.

4.3. Market orientation

We will continue to deepen reform in water field, to make efforts to improve the water harnessing system, to innovate water financing and investment system, to stabilize and increase public financial investment, to actively seek financial support policies, to encourage investment in social capital conservancy construction, to constantly improve water infrastructure and to strengthen the Three Gorges Reservoir cooperated water supply. We fully play a decisive role of the market in allocating water resources, and actively play the role of price lever to ease the contradiction between supply and demand of water resources in Three Gorges reservoir; and encourage social capital to participate in the market in the allocation of water resources. The insurance industry should timely start against sudden water crisis and water shortage for the insufficient water supply in the Yangtze River Basin and a wide range of drought occurs. The banking industry must actively provide credit support to the water resource security technology research and development.

4.4. Material guarantee

Through the promotion of inter basin and inter regional water conservancy project construction, the formation of water resources security system combined with the Three Gorges reservoir, is strengthening the regulation of water resource and water level of flood control and disaster mitigation system support capabilities; the comprehensive management of water environment in the Yangtze Basin, to advance comprehensive management of river, lake is improved; Establishing Three gorge reservoir water resources security network system, strengthen the detection and prediction on the security of water resources, drought relief materials preparation work; increase investment in policy and funding of water resources security in the Three Gorges Reservoir area.

4.5. Social coordination

Taking the national strategy of the Yangtze River Economic Zone as an opportunity to adjust the Yangtze River Economic Belt industrial structure to change the mode of economic development and develop economic structure and industrial layout compatible with the Three Gorges Reservoir. Enlarge propaganda and actively guide. Strengthen the water saving awareness. Promote water saving culture to create a good atmosphere of water saving among the whole society, improving the water civilization of the whole society. Encourage public participation of water protection. Strengthen the supervision of public opinion, preventing pollution behavior of breeding fish in cages. Strengthen water environmental protection and the management of the sewage outfall and remediation. Explore the Three Gorges Reservoir water ecological protection zone.

5. CONCLUSION

From the non-traditional security, water resources security is an important part of national security and social economic security. In recent years, the major challenges of water resources security of Three Gorges reservoir are cited such as the reduced incoming flow, the uneven rainfall distribution over a year, fresh water supply pressure, water environment problems, the underdeveloped water resources potential and the lack of the necessary social environment guarantees. Water resources security problems of the Three Gorges Reservoir are social, crossover and diffuse. It has vital practical significance for the optimal scheduling of the Three Gorges Reservoir and efficient utilization of the Yangtze River Basin to conduct a comprehensive security system of water resources from the aspects of specification, scheduling innovation, market orientation, material guarantees, technical support and society coordination.

REFERENCES

Z.Y. Li, 2009. Analyses of the Definition of Non-traditional Safety. Journal of Tarim University. 21（3）:44-49

J.Q. Li, 2011.Current situation of water security and analysis of major problem in China. CHINA WATER RESOURCES.（1）42-51

X.H. Wen, 2013. Flood resources practice and its prospect of the Three Gorges reservoir. The seventeenth cross strait exchange Seminar on water science and technology.（1）:126-135

X.P. MA, 2009. Main Threats of Environmental Safety in China and Countermeasures in the View of Nontraditional Security. Safety and Environmental Engineering. 17（3）:111-116.

4th APG Symposium and 9th EADC on

INNOVATIVE TECHNOLOGIES FOR DAMS AND RESERVOIRS TOWARD THE FUTURE GENERATIONS

Structure Design of Dam Section in Riverbed Parts for a Hydropower Station

Y. Xu, J. Wang & L. Yang
Technology Center of State Grid Xinyuan Company LTD., Beijing, China
yaowu-xu@sgxy.sgcc.com.cn

ABSTRACT:
The hydropower station mentioned in this paper is a project mainly utilized for electricity generation. Concrete gravity dam is set as barrage of this hydropower station and surface outlets section as well as spillway bottom outlets section is located in riverbed parts of the dam. More specifically, surface outlets section is free overflow section without sluice control and there are a sand duct and a sand-flushing hole set in spillway bottom outlets section. The main flood discharge outlets is spillway bottom outlets and surface outlets serve as auxiliary flood discharge outlets. In this paper, we adopt material mechanics method to conduct stress calculation of surface outlets section and spillway bottom outlets section. Based on the results of this stress calculation, we investigate the stress state of dam body and foundation of this hydroelectric station, and then, identify the most dangerous part of the dam possible sliding surface and the most effective part of material resistance according to the partial coefficient limit state formula. Furthermore, the carrying capacity of dam stability against sliding is determined, which is helpful for the dam body strength and stability evaluation of surface outlets and spillway bottom outlets of this hydropower station.

Keywords: Concrete gravity dam , Stress , Carrying capacity , Anti-sliding stability analysis

1. PROJECT PROFILE AND THE INTRODUCTION OF DAM SECTION ARRANGEMENT

The hydropower station mentioned in this paper is a project mainly for power generation, and it consists of head works, diversion tunnels, surge tank, high-pressure pipelines and ground powerhouse. The normal water level of reservoir is 3132.00 m, and the dead water level, design flood level, check flood level are 3123.00 m, 3134.20 m and 3136.10 m respectively. In addition, the total storage capacity of reservoir and the regulating storage for daily regulating of the reservoir are 2.5192 and 1.0909 million m^3 respectively. Impulse units with unit capacity of 60MW are adopted in this hydropower plant and the total installed capacity of this plant is 120MW. The average annual generating capacity is 5.628 million kW•h, and the annual utilization hours reaches 4690h. The rated head of this hydropower station is 485.00m. The flow of single unit generation is 14.37m^3/s. Diversion type is adopted in this plant and the length of water diversion system is 15.58km.

Concrete gravity dam is set as barrage of this hydropower station. The crest elevation and total length of the dam are 3137 and 78.55 m respectively. The dam is divided into five sections with the maximum dam height of 36.2m (surface outlets section). The upstream dam surface is vertical and the ratio of downstream dam slope is 1:0.75. From the right bank to the left bank along with the axis of the dam, the dam is divided as follow: the right bank of non-overflow dam section, surface outlets overflow dam section, spillway bottom outlets dam section, the left bank of non-overflow dam section, the left bank of the connecting section.

Surface outlets and spillway bottom outlets dam sections are located in riverbed parts. Note that surface outlets section is free overflow section without sluice control and there are a 3m×4.5m sand duct and a 1m×1.5m sand-flushing hole set in spillway bottom outlets section. The main flood discharge outlets is spillway bottom outlets and surface outlets serve as auxiliary flood discharge outlets.

2. BASIC INFORMATION FOR CALCULATION

2.1. Building Grade and Structural Safety Level

The hydropower project is a level-Ⅲ medium-size engineering, and its discharge structures is a level-3 buildings(State economic and trade commission of the PRC,2003), which has a level-Ⅱ structure security level(State economic and trade commission of the PRC,2003). Secondary structures such as aprons and revetments are designed according to level-4 standard (Ministry of housing and urban-rural development of the PRC,2014) and the structure security level of secondary structures is Ⅲ-level (State economic and trade commission of the PRC,2003).

2.2. Flood Standards and Water Levels for Calculation

Fifty year return period is employed as the flood standard for design flood (Ministry of housing and urban-rural development of the PRC,2014) and the corresponding peak discharge is 321m^3/s. Five hundred years return period is adopted as the flood standard for check flood (Ministry of housing and urban-rural development of the PRC,2014) and the corresponding peak discharge is 508m^3/s.

Characteristic water levels of the hydropower plant and corresponding discharge amount are shown in Table 1.

Table 1. Characteristic water level and corresponding discharge

calculation situation	reservoir water level m	downstream discharge m^3/s	downstream water level in dam site m
normal water level	3132.00	321	3115.67
design water level	3133.53	321	3115.67
check flood level	3136.10	508	3116.58

2.3. Seismic Intensity Parameters

The degree of basic seismic intensity and seismic design intensity are Ⅷ and 8 respectively, and the engineering anti-seismic classification is C class (National energy administration of the PRC,2015).

Note that, the design of anti-seismic of this engineering only involves horizontal seismic effect in the river flow direction, and normal high water level is set as upstream water level. Pseudo-static method is utilized to calculate effect of seismic action.

2.4. Standard Values of Materials Performance

Standard values of shear strength for different lithology are listed in Table 2. Note that in Table 2 WWL, SWL, C/WWL and C/SWL are short for weak weathered limestone, slightly weathered limestone, concrete/ weak weathered limestone and concrete/ slightly weathered limestone respectively. The notation CS, SS, EM, BD, Sat. and Dry. are short for compressive strength, shear strength, elastic modulus, bulk density, saturation state and dry state respectively in Table 2.

Table 2. Standard values of shear strength

lithology		WWL	SWL	C/WWL	C/SWL
CS MPa	Sat.	70	100	-	-
	Dry.	100	120	-	-
SS MPa	C'	1.2	1.8	0.8	0.9
	f'	0.8	1.2	1.1	1.1
EM GPa		10-15	15-20	-	-
BD kN/m^3	Sat.	27.2	27.4	-	-
	Dry.	27	27.3	-	-

Table 3 exhibits the standard values of concentric axial compression of dam normal concrete under various strength standard values. Note that in Table 3 CAC and sym. is short for concentric axial compression and symbol respectively.

Table 3. Standard values of compressive strength

type	sym.	standard strength values of dam normal concrete					
		C7.5	C10	C15	C20	C25	C30
CAC	f_{ck}	7.6	9.8	14.3	18.5	22.4	26.2

The strength standard of dam normal concrete of this dam is C15 and the age strength and guarantee rate are 90d and 80% respectively.

3. PRINCIPLES AND ASSUMPTIONS OF CALCULATION

3.1. Principles of Calculation

Dam strength checking includes checking of dam strength limit state and checking of upstream and downstream dam surface tensile stress serviceability limit state. Checking of dam strength limit state consists of compressive strength bearing capacity limit state of dam toe and compressive strength affordability limit state of downstream endpoint in selected dam cross section. Checking of serviceability limit state includes the calculation of upstream and downstream dam surface tensile stress limit state in serviceability (National energy administration of the PRC,2014).

The main purpose of stability analysis is to check the stability safety degree of gravity dam under all possible loads (National energy administration of the PRC,2014). In this paper, we calculated two instability damages under loads: dipping fractures which are induced by the suffering of tension of rock masses below the upstream dam heel and toppling failures which are caused by crushed zone resulting from the suffering of stress of downstream dam site rock masses. The calculation and checking is based on the bearing capacity limit state and serviceability limit state respectively.

The proposed section size of dam will satisfy stability requirements if it meets stability against sliding requirement and bearing capacity requirement after the above calculation.

3.2. Assumptions of Calculation

1) The dam concrete materials are homogeneous, continuous and isotropic elastic materials;
2) The dam section is considered as cantilever beam consolidated on the foundation. The effect of foundation deformation on dam stress is neglected. Each dam section is supposed to work independently and transverse joints do not transfer force;
3) Vertical normal stress of the dam horizontal section is supposed to distribute linearly and the influence of corridors on dam stress is neglected.

4. CALCULATION CASES

In the following context of this paper, A, B, C, D, E, F, G and H represent dead weight, hydrostatic pressure in normal water level, hydrostatic pressure in seismic events, hydrostatic pressure in check flood level, uplift pressure in normal water level, uplift pressure in seismic events, uplift pressure in check flood level, silt pressure, wave pressure under lasting condition, wave pressure under accidental situation and seismic load respectively. Load combinations(Ministry of electric power industry of the PRC,1997) and cases in the calculation(National energy administration of the PRC,2009) are shown in Table 4. Note that in Table 4 LS and AS are short for lasting status and accidental status.

Table 4. Load combinations and calculation cases

case	combination	condition	loads					
LS	basic	normal water level	A	B	D	F	G	-
AS	accidental 1	check flood level	A	C	E	F	H	-
	accidental 2	seismic	A	B	D	F	H	I

Fig. 1 to Fig. 3 illustrate the calculation diagram of load combinations in surface outlets dam section under various working conditions and Fig. 4 to Fig. 6 show the calculation diagram of load combinations in bottom outlets dam section under various working conditions.

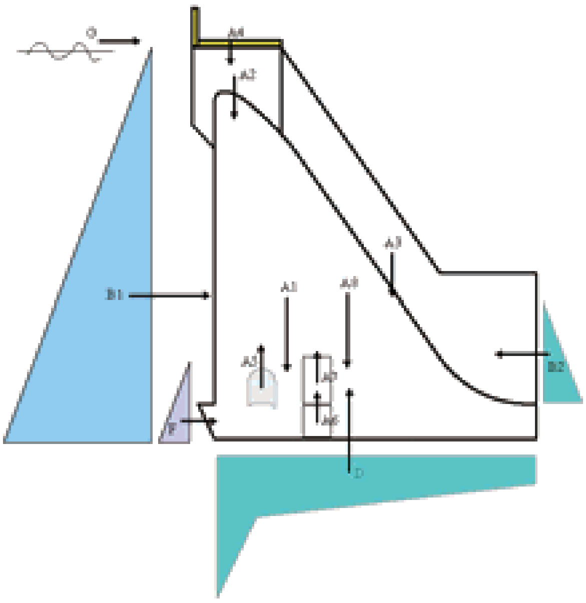

Figure 1. Calculation diagram of load combinations for dam surface outlets section at normal storage water level

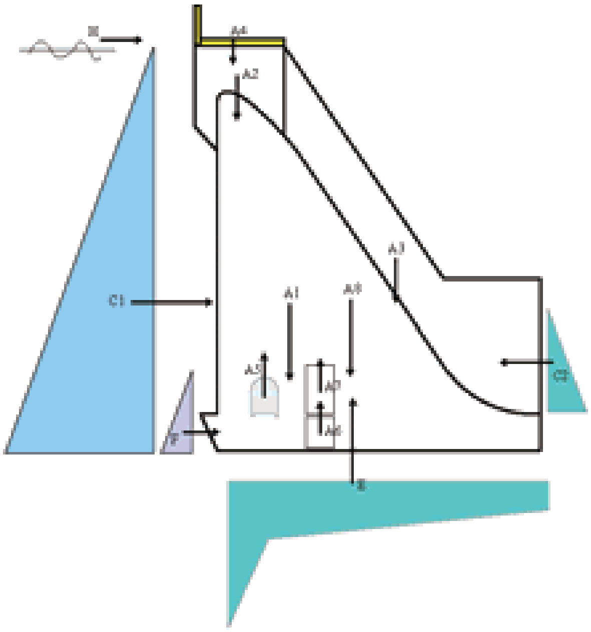

Figure 2. Calculation diagram of load combinations for dam surface outlets section at check flood stage

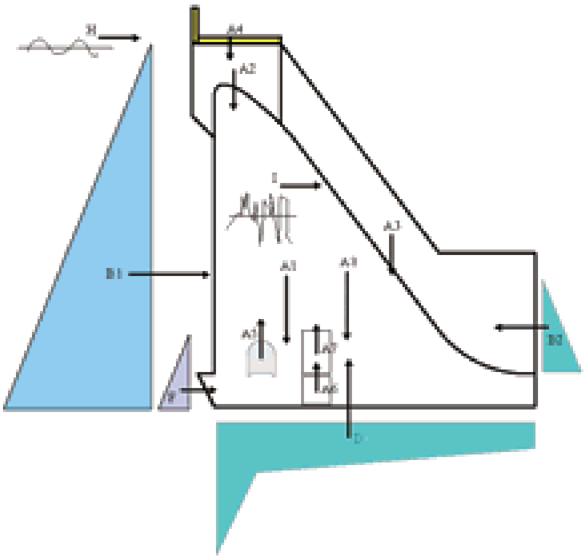
H
A4
A2
I
A3
B1
A1
A3
A7
A6
B2
F
D

Figure 3. Calculation diagram of load combinations for dam surface outlets section at earthquake affairs

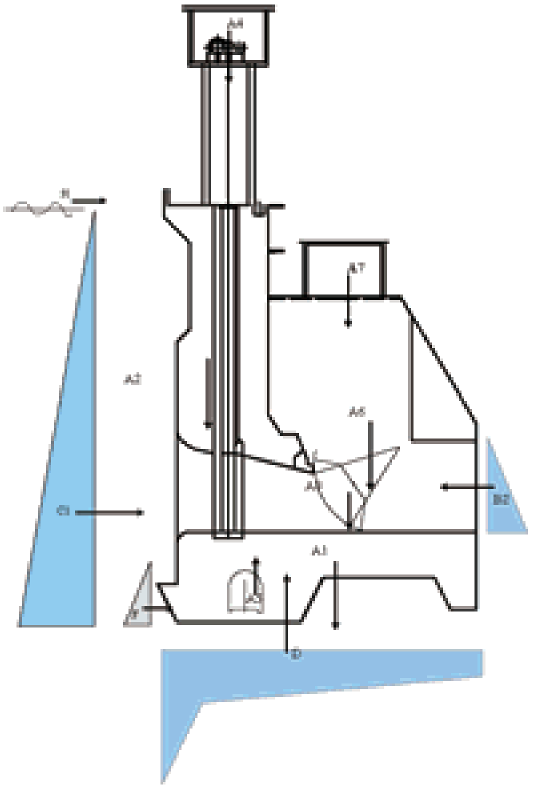
A4
H
A7
A2
A6
A5
C1
B2
A1
F
D

Figure 4. Calculation diagram of load combinations for dam bottom outlets section at normal storage water level

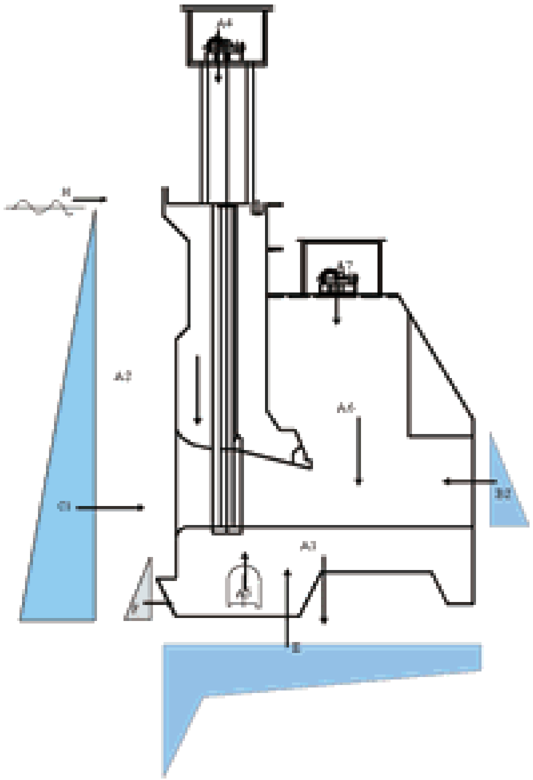
A4
H
A7
A2
A6
C1
B2
A1
A5
F
E

Figure 5. Calculation diagram of load combinations for dam bottom outlets section at check flood stage

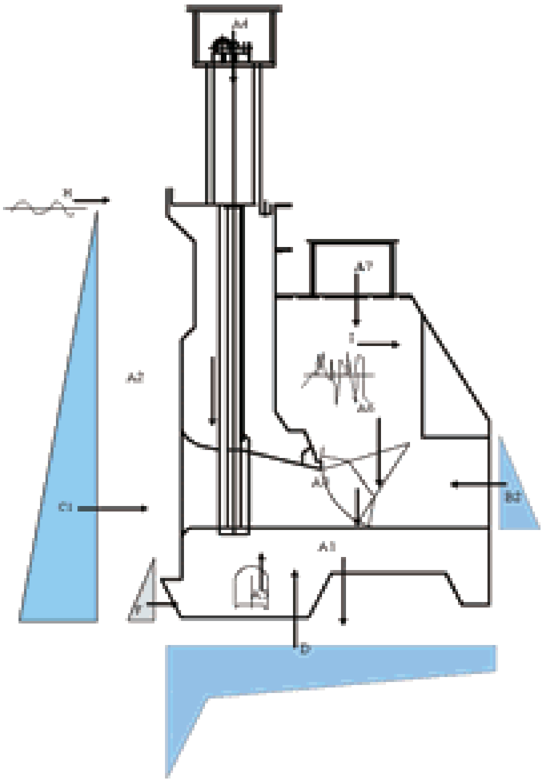
A4
H
A7
I
A2
A6
A5
C1
B2
A1
F
D

Figure 6. Calculation diagram of load combinations for dam bottom outlets section at earthquake affairs

5. CALCULATION RESULTS

The results of dam foundation stability and stress calculation of the surface outlets dam section and bottom outlets dam section are listed in Table 5 and Table 6 respectively. Note that in Table 5 and Table 6 combination 1, 2, 3 and 4 stand for basic combination(in normal water level), accidental combination(in check flood level), accidental combination(in seismic events) and long-term combination respectively. CCLS, SLS, SAS, DSS and DHS in Table 5 and Table 6 are short for carrying capacity limit state, serviceability limit state, stability against sliding, dam site stress and dam heel stress respectively. Furthermore, the notation ①, ②, ③, ④, ⑤and req. stand for $R(\cdot)/\gamma_{d1}$kN,$\gamma_0\psi S(\cdot)$kN,$R(\cdot)/\gamma_{d1}$MPa,$\gamma_0\psi S(\cdot)$MPa, S(·)MPa and requirement respectively. The notation ^{a} and ^{b} represent concrete and bedrock respectively.

Table 5. Results of foundation stability and stress calculation for dam surface outlets section

combination			1	2	3	4
CCLS	SAS	①	217445.4	212452.1	217445.4	
		②	102112.9	93943.84	87464.92	
	DSS	③	5.3^{a} 25.9^{b}	5.3^{a} 25.9^{b}	3.405^{a} 16.6^{b}	
		④	0.387	0.349	0.298	
SLS	DHS	⑤				0.32
		req.				>0

Table 6. Results of foundation stability and stress calculation for dam bottom outlets section

combination			1	2	3	4
CCLS	SAS	①	107477	105623	107477	
		②	34841.67	38856.92	36750.05	
	DSS	③	5.3^{a} 25.9^{b}	5.3^{a} 25.9^{b}	3.405^{a} 16.67^{b}	
		④	0.675	0.563	0.583	
SLS	DHS	⑤				0.41
		req.				>0

6. CONCLUSIONS

In this paper, we perform strength and stability calculations of surface outlets and bottom outlets dam section for a certain hydropower station. Our calculations are designed according to carrying capacity limit state and takes basic combination and accidental combination into account. Furthermore, we check our calculations in serviceability limit state and take short-term combination and long-term combination into consideration. According to the results of our calculation, under different working conditions, the values of carrying capacity limit state of stability against sliding effect function of dam concrete and bedrock interface are smaller than the values of stability against sliding function, which satisfies the requirements of standards. Under different working conditions, the values of carrying capacity limit state of dam toe compressive strength effect function is smaller than the values of resistance function of compressive strength of concrete and bedrock, which meets the requirements of standards. The vertical stress value of dam heel is greater than zero, therefore, there is no tensile stress, which fulfil the requirements of standards.

In conclusion, the stability against sliding of surface outlets and bottom outlets dam section can fulfil the requirements of standards under various working conditions, the dam is stable. The dam stress and dam foundation stress can meet the requirements of standards under various working conditions, structural strength of dam and dam foundation is safe and reliable.

The hydropower station has operated stably about eight years since it began to generate power in the year 2008. During this period, the dam of this station services in good condition, instable events have not appeared in surface outlets and bottom outlets of dam section, which makes contribution to the safety and stable operation of the hydropower station.

REFERENCES

State economic and trade commission of the PRC. (2003): Classification and design safety standard of hydropower projects, China electric power press.

Ministry of housing and urban-rural development of the PRC. (2014): Standard for flood control, China planning press.

National energy administration of the PRC. (2015): Code for seismic design of hydraulic structures of hydropower project, China electric power press.

National energy administration of the PRC. (2014): Design code for concrete gravity dams, China electric power press.

Ministry of electric power industry of the PRC. (1997): Specifications for load design of hydraulic structures project, China electric power press.

National energy administration of the PRC. (2009): Design specification for hydraulic concrete structures, China electric power press.

4th APG Symposium and 9th EADC on

INNOVATIVE TECHNOLOGIES FOR DAMS AND RESERVOIRS TOWARD THE FUTURE GENERATIONS

Numerical Investigation of Upper Gotvand Rockfill Dam's Settlement During Construction Stage and First Impounding Reservoir

A. K. Tooseh
Master of Science in Geotechnical Engineering, Department of Civil Engineering,
K.N Toosi University of Technology, Tehran, Iran.
amir.kazemitoose@yahoo.com

H. Akbari
M.Sc. Student of Geotechnical engineering, Amirkabir University of Technology,
Taban Water Development Engineering Company, Tehran, Iran.

ABSTRACT:
Upper Gotvand dam and hydroelectric power plant project is located 380 Km from Karun river and 10 Km in north-east Gotvand city in Khuzestan province in Iran. The Gotvand dam is a 246 m high Rock-fill with clay core, serves power generation, flood control and irrigation needs. Accurate and comprehensive information about the project is needed to achieve proper monitoring. In order to measure parameters needed in monitoring such as stress, pore pressure and deformation, instrumentation facilities are installed in sensitive areas of the structure. The deformation process of rock fill dam starts at construction stage and continues years after construction therefore, with increasing embankment level during construction, inclinometer pipes and magnetic settlement cells are installed around the pipes at the desired levels and in various sections of the structure's body. The process of body deformation is controlled by periodic reading of the vertical and horizontal deformation.

In this paper, vertical and horizontal deformation of dam's body is processed and analyzed using the data recorded by the instrumentation installed in the upper Gotvand dam. In order to evaluate the result of instrumentation measurements, a three-dimensional numerical model is performed by Midas GTS software that uses the finite element method for numerical solution.

Keywords: Upper Gotvand rock-fill dam, Instrumentation, Finite element method, Midas gts.

1. INTRODUCTION

Except unexpected factors such as earthquakes, floods and etc., failure of earthen dams is always accompanied by worrying warnings such as the increase of pore pressure, deformations, subsidence, cracking and strain discontinuity. In order to investigate the process of these variations (deformation), possible causes and events, considering the following steps during the construction and operation of dams is of major importance:

- Instrumentation in dams in order to investigate the process of deformation, pore pressure, etc.
- Recording instruments information periodically appropriate to the relevant instrument
- Investigation of variations, specially unexpected variations, recognizing its causes.

Since the behavior of the dam during construction and first impounding can offer a clear image of its behavior during operation, thus the behavior assessment in these critical sections of the dam life can provide a true image of its future behavior.

In this study the deformation behavior of a rockfill dam during construction and first impounding reservoir was investigated and as a case study Upper Gotvand rockfill dam was studied.

2. DAM SPECIFICATION

The upper Gotvand dam and powerhouse site is located in geographical coordinates of 48 degrees 56 minutes 10 seconds east along latitude 32 degrees 16 minutes and 8 seconds and 380 Km from Karoon river and 10 Km in northeast Gotvand city in Khuzestan province. Gotvand dam is a rock-fill dam with a vertical core, side slopes of core are 1 vertical to 0.25 horizontal. Major part of the upper body is formed by merger coffer dam. . The upstream slope of …..Core is 1 to 2.25 and its downstream slope is 1 to 2. The upstream slope of … is 1 to 2.75 and the downstream slope is 1 to 1.4. Main slopes in upstream and downstream of the rockfill are 1 to 2.2 and the width of berm embankment is considered 10 meters. A brief specification of the dam is given in Table1.

Table 1. Dam Specification

Parameter	Value	Parameter	Value
1075 m	Width in foundation	ECRD	Dam type
285 *105 m3	Dam volume	181 m	Height from foundation
15 m	Crest width	760 m	Crest length

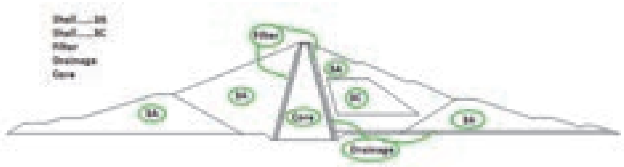

Figure 1. Dam's zone

7 main section and 4 sub-section instrumentation are designed in the body of Gotvand dam. The location of the instrumentation sections is illustrated in Fig. 2.

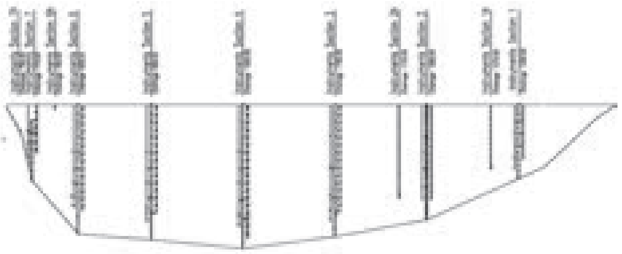

Figure 2. Cross section of the main instrumentation sections

3. DEVELOPMENT OF NUMERICAL MODEL

Midas GTS software is used in dam modeling. It is a professional geotechnical software and is employed for analysis of soil structures. The numerical analysis used in this software is finite element method (FEM) and is capable of simultaneous analysis of water flow and soil deformation using linear and nonlinear behavioral model. Creating initial dam geometry, applying boundary and initial conditions are the steps in this program. In order to model the dam, elastic and elastic-plastic models are used respectively in bedrock and body of the dam. Fig. 3 shows Large-scale triaxial test and axial symmetry numerical model for dam shell material.

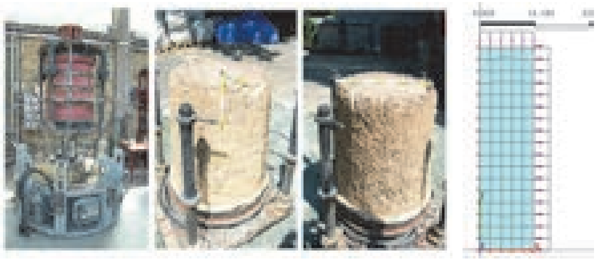

Figure 3. Large-scale triaxial apparatus and the sample

Table 2. Model parameters

K (m/sec)	ψ	E (kN/m^2)	C (kN/m^2)	ν	n	Material
1e-9	–	35000	100	0.35	0.3	Core
1e-9	–	32000	60	0.35	0.3	Core
1e-9	–	28000	40	٠,٣٥	0.3	Core
1e-9	–	15000	10	.35	0.3	Contact clay
1e-5	6	160000	0	0.25	0.33	Shell 3A
1e-5	4	120000	0	.28	0.33	Shell 3A
1e-5	1	70000	0	0.32	0.33	Shell 3A
1e-5	2	100000	0	0.3	0.33	Shell 3C
1e-6	–	40000	0	0.25	0.23	Filter
1e-3	–	60000	0	0.25	0.23	Drainage
1e-10	–	260000	–	0.25	–	Aghajari bedrock
1e-7	–	170000	–	0.25	–	Bakhtiari bedrock
1e-3	–	500000	–	0.25	–	Relocaited zone(formation)

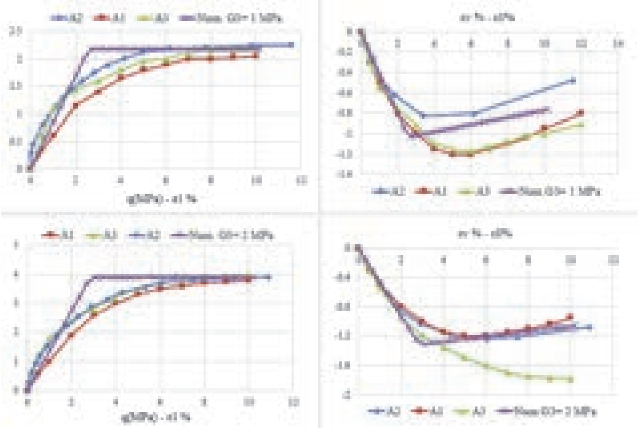

Figure 4. Calibration results of the shells materials

4. SPECIFICATIONS FINITE ELEMENT MODEL OF THE UPPER GOTVAND DAM

In order to simulate FEM analysis of Upper Gotvand dam a three-dimensional model is used. The model geometry was created based on the type section of the dam. Dam site is modeled to a depth of 350 meters, upstream and downstream to distances up to 600 meters and abutment to 300 meters away from the dam. The final finite element model of the dam has 12,633 nodes and 64,859 members**.** The four nodal tetrahedron members with twelve degrees of freedom is used in grids network of three-dimensional components.

Analysis of the construction of a dam includes: coffer dam in 4 layers, downstream in 4 layers and central part in 10 layers are modeled. Construction timing coincides with dam construction timing obtained from field reports. Analysis in effective stress space is done by solving coupled water flow and core consolidation in order to estimate the amount of pore pressure inside the core during construction and stress path inside the core get close to reality.

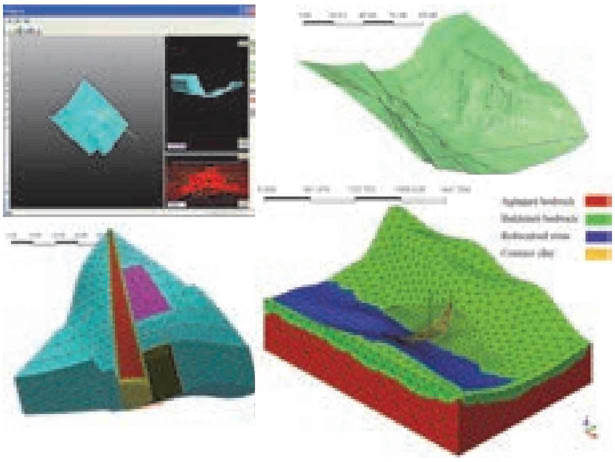

Figure 5. Finite element model of the dam

Boundary conditions used in the analysis of the dam during construction of the dam, include the followings:

- Model displacement perpendicular to the boundaries is closed.
- Gravel materials are presented as an unconsolidated material so as to prevent any water pressure in these materials.
- Drainage zones are supposed to have a free drainage boundary conditions. Pore water pressure is zero at the boundary of the core and the core pore water pressure dissipates through the drain by time.
- In the analysis of initial stress, the initial displacement of the abutment is considered to be zero.
- Displacement caused by the construction of coffer dam and downstream are zero at the end of construction, because the settlement of any amount during construction can be filled by embankment to the required level continues.

5. RESULTS OF BACK-ANALYSIS

5.1. CONCLUSIONS DERIVED BY NUMERICAL MODEL:

The maximum settlement resulted from numerical model is in the middle of the dam in instrumentation section 4-4 and its amount is 249 cm and is located in level/alignment 148 m.

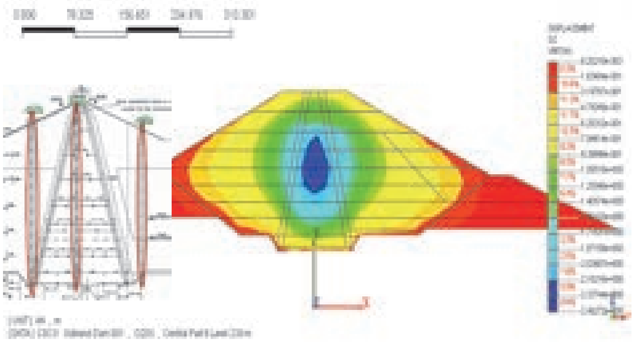

Figure 6. Vertical displacement during construction

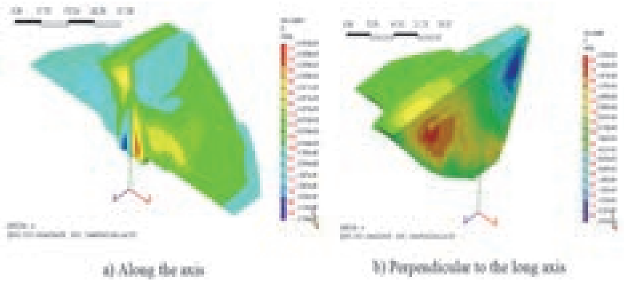

a) Along the axis

b) Perpendicular to the long axis

Figure 7. Horizontal displacement of dam

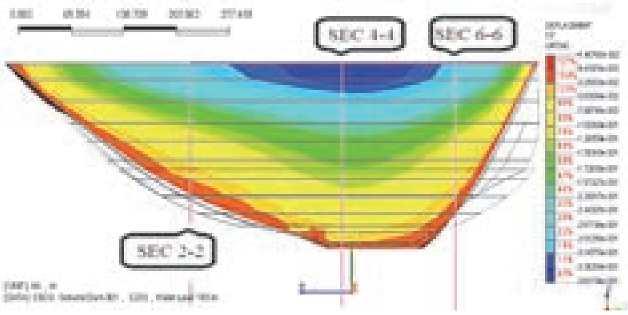

Figure 8. Vertical displacement during first impounding reservoir

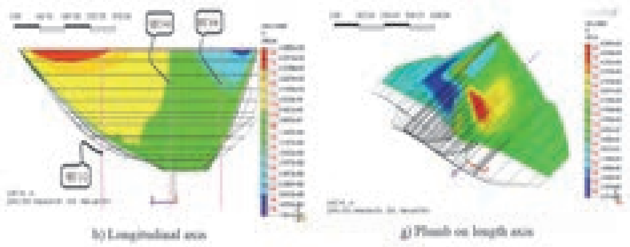

h) Longitudinal axis

g) Plumb on length axis

Figure 9. Horizontal displacement during first impounding reservoir

In reality the dam embankment to reach a certain level/alignment, the amount of settlement is filled by extra embankment. But it is not applicable in numerical model, thus the amount of the extra embankments should be specified in each level and subtract from its settlement in order to determine the pure settlement of each level for comparing with instrumentation measurements. For example, in table (3) the modified values of the settlement made by extra embankment in axis I-4-3 (the core of the instrumentation section4-4) is given and the pure/Absolute settlement of each level is calculated to compare with instrumentation result.

Table 3. Modified displacement – Axis I-4-3

Embankment level	Total settlement (cm)	Extra settlement (cm)	Absolute/pore settlement (cm)
Level one	85	9	76
Level two	148	16	132
Level three	191	19	172
Level four	223	21	202
Level five	249	31	218
Level six	222	36	186
Level seven	202	49	153
Level eight	127	47	80
Level nine	74	74	0

The values of settlement during construction are matched well with the values recorded by instrumentation. It may be due to:

- ❖ Appropriate construction timing according to dam construction stage. Because during construction stage, appropriate timing has major effects on settlements,
- ❖ Applying three groups of parameters for dam layers.

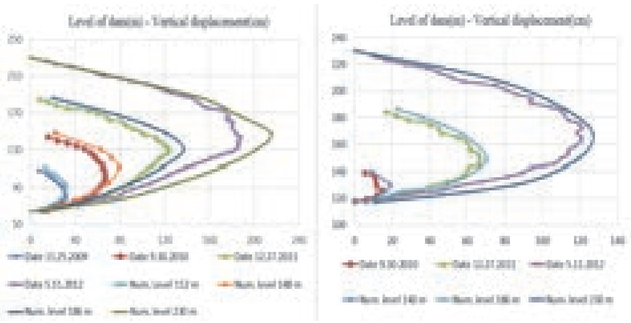

Figure 10. Comparison of displacement of the construction stages between instrumentation and numerical model

Impounding reservoir during construction was begun in level 230 m. In order to model impounding reservoir more precisely, the displacements in the model are adjusted to zero after reaching level 230 m and the displacements due to impounding reservoir and resumption of construction to 246 m are determined separately.

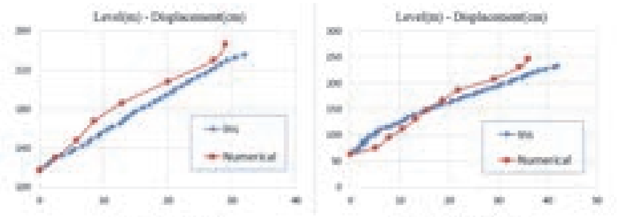

a) Section 2-2. Core   b) Section 4-4. Core

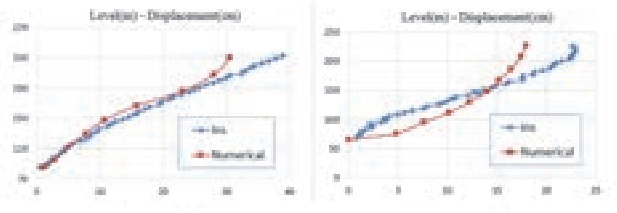

c) Section 6-6. Core   d) Section 4-4. Shell

Figure 11. Comparison of displacement of first impounding reservoir between instrumentation and numerical model

According to settlement curve after impounding reservoir in upstream and downstream the following results are derived:

- ❖ After impounding reservoir the upstream shell gets wet and settles more than the downstream shell
- ❖ The difference between numerical model and recorded settlements in upstream is due to wetness and settlement of upstream shell due to water accumulation in upstream (about 30 m) between coffer dam's core and dam's core by means of water leakage from reservoir and rain. Piezometeric level in upstream filter approves this conclusion**.**

According to dam horizontal deformation curve after impounding reservoir following results are derived:

- ❖ The dam's reservoir moves down stream due to hydrostatic pressure but due to wetness of rock-fill, the upstream shell moves toward reservoir
- ❖ In instrumentation results some jumps are recorded which is due to piecemeal impounding reservoir. There is a tendency to swell and move downward in a newly saturated level due to impounding reservoir and hydrostatic pressure. Gradually by water level rise due to hydrostatic pressure of the reservoir there is a tendency to settle in bottom layers which reflects deformation and makes jumps.
- ❖ Deformations are relative and are measured relative to a datum level therefore the amount of settlement below the level is subtracted from the total height and compared with inclinometer results.

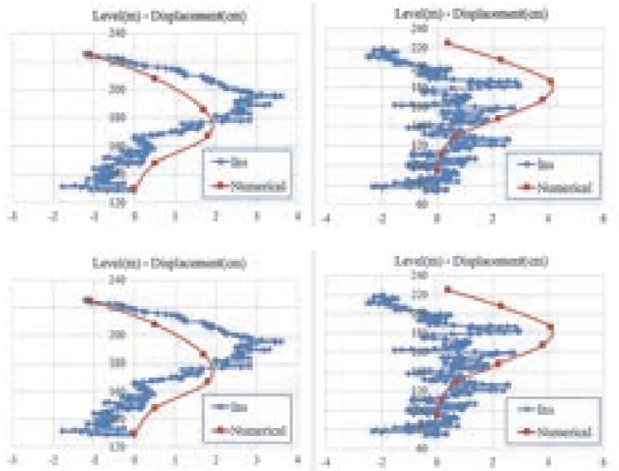

Figure 12. Comparison of horizontal displacement of first impounding reservoir between instrumentation and numerical model

It is expected the downstream shell moves laterally downward after water impounding. It is approved in most of the incline-metric axes installed in the downstream of the dam but in instrumentation section in dam's left base the inclinometers shows the shell tendency to move upward. This is due to a large outcrop in left (Fig. 13) base of the downstream shell. In fact after impounding reservoir due to hydrostatic pressure on upstream shell/face of the core, the downstream shell tends to move downward but the outcrop prevents horizontal displacement of the downstream shell downward the instrumentation sections in left base also due to large dimensions and the degree of permeation into the dam the downstream shell is forced to move toward negative direction or upward.

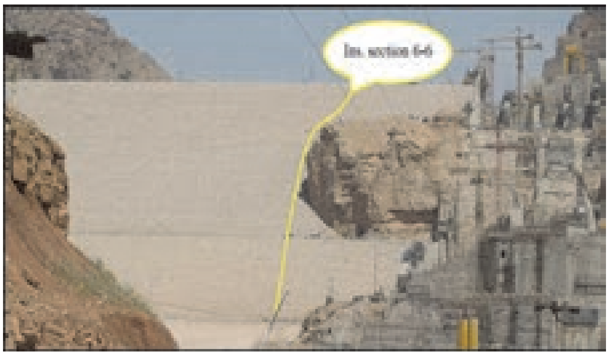

Figure 13. Upper Gotvand rockfill dam

ACKNOWLEDGEMENT

The maximum vertical displacement during construction occurred in core center in the level 148 m near section 4-4 and the net settlement is 218 cm equivalent to 1.2% of dam height that results from subtraction of 31 cm extra embankment from the overall displacement (249 cm) predicted by numerical model. According to USBR studies, settlement of rockfill dam body is between 0 to 1 percent and varies between 2 and 4 percent of height maximal. Gotvand dam's displacement of 1.2% is acceptable.

The horizontal displacements during construction of the dam along longitudinal axis (B-B) are a maximum of 24 cm on the left and 22.5 cm on the right abutment**.** In the direction perpendicular to the longitudinal axis of the dam (A-A) are 42 cm to the downstream and 32 cm to the upstream side.

The values of the horizontal displacements of the dam in both longitudinal and perpendicular to the longitudinal axis after impounding are also in a good agreement with instrumentation measurements but there are differences in some directions.

REFERENCES

Miidas GTS, (2013): Manual, Version 1.1.

Jafarzadeh. F. and Talebi. M., (2002): Behavior of Zoned Rockfill Dams During Construction and First Impounding, Proceeding of the 3rd International Conference on Dam Engineering, Vol. I: pp. 137-144.

Soroush, A. and Aghaei, A., (2005): Uncertainties in Mechanical Behavior of Rockfills During First Impounding of Rockfill Dams, 73rd Annual Meeting of ICOLD, Vol. II: pp. 186-S5.

Maleki, M. and Alavifar, A., (2005): Safety Evaluation of Masjed I Soleyman Rockfill Dam During Construction and First Stage Impounding, 73rd Annual Meeting of ICOLD, Vol. II: pp. 101-S5.

Dunncliff, J. and Green, G.E., (1993): Geotechnical Instrumentation for Monitoring Field Performance, John Wiley & Sons Inc.

Naylor, D.J., (1991): Finite Element Methods for Fills and Embankment Dams, Springer.

Investigation and Rehabilitation of Abnormal Seepage Monitoring System of Rockfill Dam

J. Lee
Korea Water Resources Corporation, Daejeon, Korea
geoljw@Kwater.or.kr

ABSTRACT:
Inflow into the seepage measuring house of Sueo dam was increased from April 2012. The V-notch weir was flooded by the increased flow rate exceeding the capacity of drainage pump. If the increased flow had resulted from the flow through the core zone, the possibility of severe problem on the dam stability such as internal erosion and piping of core zone could be considered but these were not questioned because the turbidity of incoming water was almost clear with maximum 2.2 NTU. Another cause could be expected was the inflow of the downstream river water through the seepage collecting system. In this study, correlations among the measured seepage flow rate, the reservoir water level and the released water supply rate for agricultural are analysed and the temperature, turbidity and pH of the inflow water also measured and analysed to investigate the possibility of inflow of the river water. CCTV surveys and field investigations were carried out to find out inflow path of the river water. Repair and Rehabilitation work for the collecting pipe and the foundation under the collecting wall, had possibility of inflow of the river water, was started on Mar. 2013, and completed in Jun. 2013.

Keywords: Monitoring, Seepage, Seepage Rate, Water Quality

1. INTRODUCTION

Sueo dam is a central core type rockfill dam with 67m high and 437m long as shown in Fig. 1. Construction of the dam began in August 1974 and completed in May 1978. The Crest elevation is EL.69.2m, the lowest excavation elevation of core zone is EL.1.95m, the basin-area is 49km^2, the total water storage capacity is 27.5million m^3 and the effective water storage capacity is 22.2 million m^3.

Sueo dam release the stored water of average 22,000m^3/day into the downstream river through the outlet pipe to supply an agricultural water. The downstream water level can be controlled by the water barrage built in the downstream river. The crest elevation of the barrage is EL.11.85m. Fig. 2 shows the aerial photo of Sueo dam.

Inflow into the seepage measuring house was increased from April 2012. The V-notch weir was flooded by the increased flow rate exceeding the capacity of drainage pump. The capacity of drainage pump was 60m3/hr. If the increased flow had resulted from the flow through the core zone, the possibility of severe problem on the dam stability such as internal erosion and piping of core zone could be considered but these were not questioned because the turbidity of incoming water was almost clear with maximum 2.2 NTU (Nepthelometric Turbidity Unit). Another cause could be expected was the inflow of the downstream river water through the seepage collecting system

In this study, correlations among the measured seepage flow rate, the reservoir water level and the released water supply rate for agricultural are analysed and the temperature, turbidity and pH of the inflow water also measured and analysed to investigate the possibility of inflow of the river water. CCTV (closed circuit television) surveys and field investigations for the collecting pipe and seepage collecting wall and the foundation of it were carried out to find out inflow path of the river water

2. EXISTING SEEPAGE MEASURING SYSTEM

Initially seepage measuring system was not built in Sueo dam during construction and the simple seepage measuring device installed in the river bed of downstream of the dam to measure seepage rate through the dam and the foundation roughly. It loose its function when it was flooded during flooding and the release of water through the spillway, because it was installed without any extra facilities at EL.11.5m. Also, it could not measure the seepage flow through the foundation of the dam because

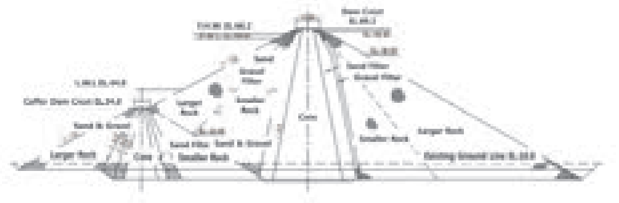

Figure 1. Maximum cross section of Sueo dam

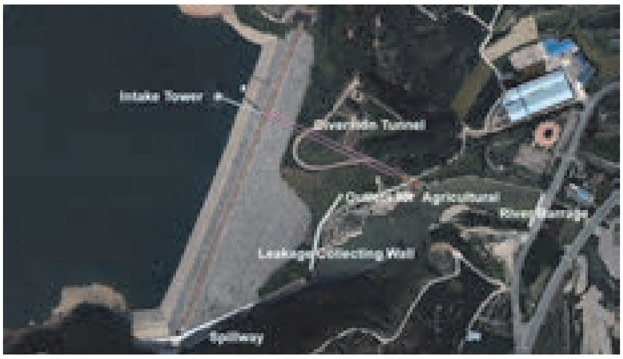

Figure 2. Aerial photo of Sueo dam

it was installed above the lowest excavation elevation of core zone (EL.1.95m). So new seepage measuring system was installed in July 2005 (KISTEC, 2008).

Drilling survey was carried out with focused on the seepage collecting wall location as shown on Fig 3. The results were as shown on Table 1. Boulder layer was filled layer with rock after excavation of the bedrock.

The seepage collecting wall was 67m long, the right side was 1.5m high semi-gravity type retaining wall and the left side was 3.5m high cantilever retaining wall type as shown on Fig.4. The crest elevation was EL.12.5m considering the normal river water elevation EL.11.0m. The right side was excavated to EL.11.0m and the left side was excavated EL.9.0m. Curtain grouting with 1.5m hole spacing in 1 line for the rock layer from the bottom of the foundation to EL.4.0m and grouting with 0.75m hole spacing in 1 line for the boulder layer were carried out.

New seepage measuring system was composed of the seepage collecting pipe transporting collected water to the seepage measuring house and the measuring devices of the collected water as shown in Fig. 5. For convenience of maintenance, the seepage measuring house was built behind the seepage collecting wall with closed to existing paved road. The seepage collecting pipe was 15m long and it was installed with d300mm PVC pipe covered by a d600mm hume pipe (K-water, 2004)

3. INVESTIGATION FOR THE INCREASED SEEPAGE RATE

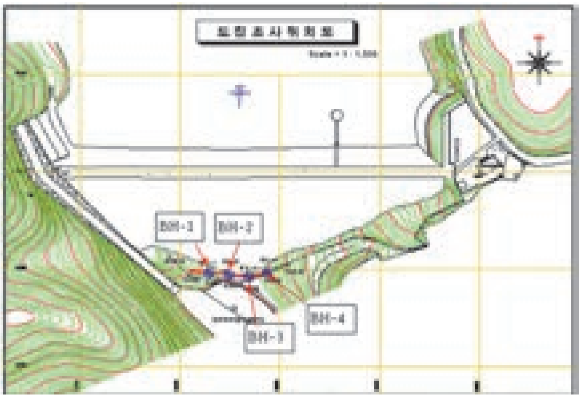

Figure 3. Drilling survey locations for the new seepage collecting wall

Table 1. Boring log and ground water table

Hole No.	Ground (EL.m)	Layer thickness		Bedrock (EL.m)	Ground water (EL.m)
		Boulder	Alluvium soil		
BH-1	17.8	6.4	-	11.4	13.4
BH-2	15.2	8.5	-	6.7	12.4
BH-3	15.5	6.3	0.4	8.8	12.2
BH-4	18.5	4.9	-	13.6	15.6

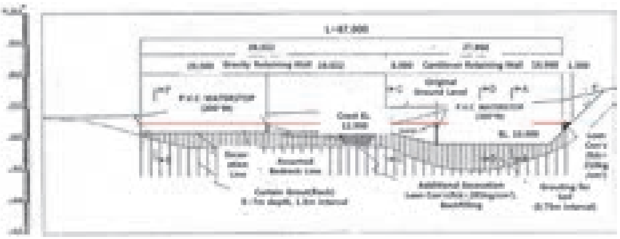

Figure 4. Profile of new seepage collecting wall

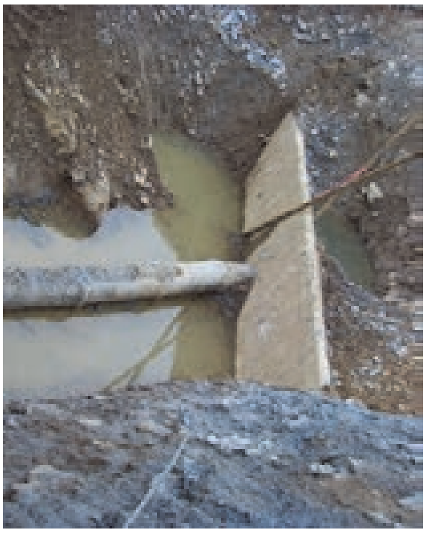

Figure 5. Photo of connection of the seepage measuring house and the collecting wall (after excavation for replacement)

Correlation of seepage rate, reservoir water elevation and the released water rate for agricultural was analysed and temperature, turbidity and pH of the seepage water were measured and analysed. CCTV (closed circuit television) surveys and field investigations for the collecting pipe and seepage collecting wall and the foundation of it were carried out to find out inflow path of the river water.

3.1. Analysis of seepage rate and water quality

The seepage rate, rainfall, the released water rate, reservoir water elevation of Sueo dam from 2006 to 2012 were shown in Fig. 6. The measurement of seepage rate was missed in 2 times (from Aug. 2008 to Dec. 2008, from Jun 2009 to Sep. 2009) and the flooding of weir by the increased water was very often (from Jun to Sep. in 2007, Jun 2008, Mar. 2010, from July to Sep. 2010, from May to Dec. in 2011, from Jan. to July in 2012). The measured seepage rate showed the tendency of rise and fall in according to rainfall and reservoir water elevation and especially the released water rate affected to it in severe as shown in Fig. 7.

From 20, July to 1, Aug. in 2012 when the rain did not come, the measured temperature, turbidity and pH of the collected water were shown in Fig. 8. On 24, July, after the released water rate increased from 100m^3/hr to 500m^3/hr, the turbidity increased form average 0.8NTU to 2.2NTU, pH increased from average 7.2 to 7.5 and the temperature increased from average 13.2℃ to 18.3℃.

Sueo dam release the stored water of average 22,000m^3/day into the downstream river through the outlet pipe to supply an agricultural water. The river water surface elevation increased in according to increasing the released water rate for agricultural. Thorough these analysis, the cause of increasing inflow into the measuring house was anticipated with that the downstream river water with high water elevation by the release of water for agricultural, flowed into the measuring house.

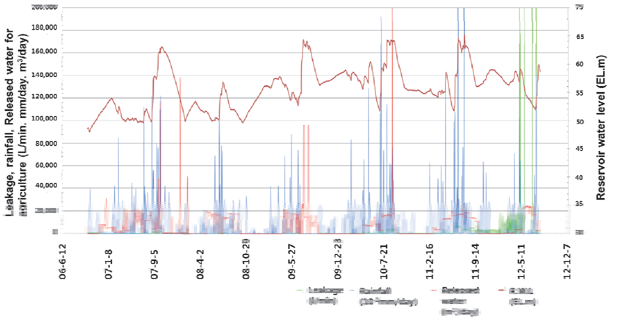

Figure 6. Time series graph of the seepage rate, rainfall, the released water rate and reservoir water elevation

3.2. Field Investigation

The anticipated inflow paths of the river water were the collecting pipe between the collecting wall and the measuring house, the collecting wall and the foundation under the collecting wall. CCTV survey on the collecting pipe to check out whether it was damaged or not, on 25, July 2012. Inside and outside of the collecting wall investigated by trenching to find out the inflow paths of the river water into the measuring house over 2 times (21, Aug. 2012, from 3, Sep. to 4, Sep. in 2012)

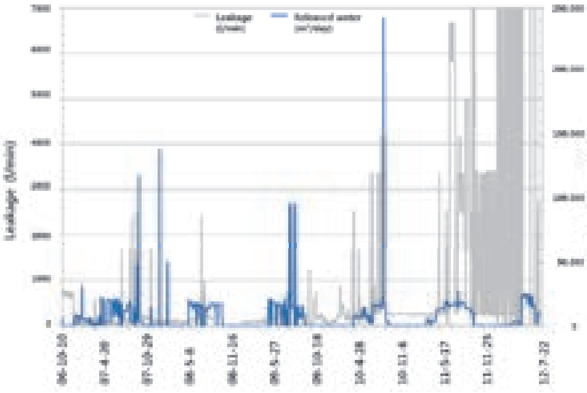

Figure 7. Time series graph of the seepage rate and the released water rate

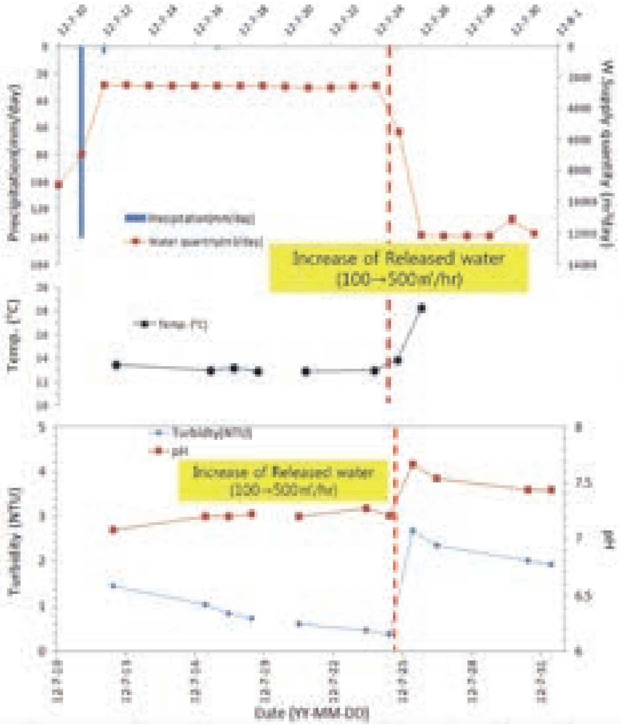

Figure 8. The temperature, turbidity and pH values of the collected water (from 20, July to 1, Aug. in 2012)

Through the CCTV survey, the breakage of the collecting pipe was revealed at the location about 5m away from the measuring house toward the collecting wall as shown in Fig. 9. The water surface elevation of the collecting wall inside lowered by 2.47m from EL.11.85 to EL.9.38m as shown in Fig. 10 from 13:00 to 17:00 4, Sep. in 2012. It was anticipated that there was no inflow from the collecting wall to the measuring house because the elevation of bottom of the collecting pipe was EL.10.29, but the measured seepage rate was 250liter/min. This revealed the possibility of inflow of the river water to the measuring house through the collecting pipe.

From 18:00, 4, Sep. to 15:00, 5, Sep. in 2012, the downstream river barrage opened with shut down the release of water for agricultural. Because of this, the water surface of the river lowered by 0.3m from EL.11.85m to EL.11.54m and the water surface of inside of the collecting wall lowered by 4cm from EL.11.85m to EL.11.81m while the river water surface elevation had been maintaining as EL.11.54m. It was found that pressurized water flowed out at the 4 point of river bed by this head difference 0.27m as shown in Fig. 11. From this, the possibility of inflow of the river water to the collecting wall through the boulder layer treated with grouting also could be considered.

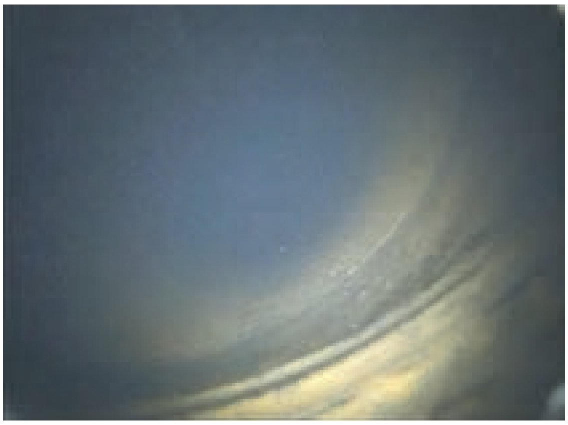

Figure 9. Inside of the seepage collecting pipe by CCTV Survey

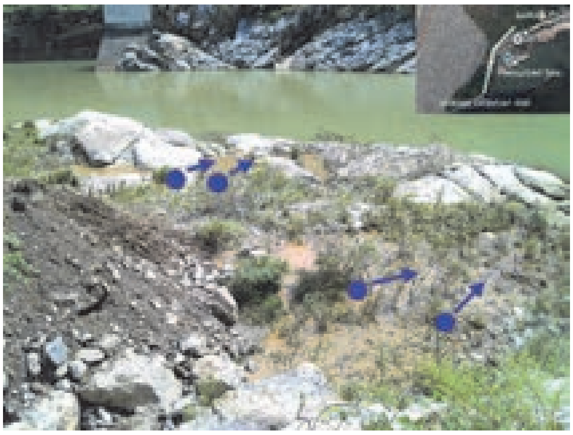

Figure 10. Flow out of pressurized water from the river bed

4. REPAIR AND REHABILITATION OF THE SEEPAGE MEASURING SYSTEM

Repair and Rehabilitation work for the collecting pipe and the foundation under the collecting wall, had possibility of inflow of the river water, was started on Mar. 2013, and completed in Jun. 2013. The collecting pipe was replaced with D300mm high density polyethylene pipe (PEM) covered with d500mm steel pipe and the inside between them grouted with mortar as shown in Fig. 11.

Grouting with 2 line were carried out inside of the existing grouting line for the boulder layer treated with grouting under the collecting wall, had the possibility of inflow path of the river water. Drilling survey was carried out as shown in Fig. 12 to determine the depth of grouting. From the drilling survey, soft rock line was deeper in the middle part of the collecting wall than the left and right side of it.

Grouting was carried out with 2 line and 1m hole spacing, to the bedrock from minimum 1.9m to maximum 11m after the cap concrete with 3m wide and 0.5m thick inside of existing collecting wall as shown in Fig. 12. The maximum grouting depth of the middle part of the collecting wall was EL.0.0m. This was 4m deeper than the original one.

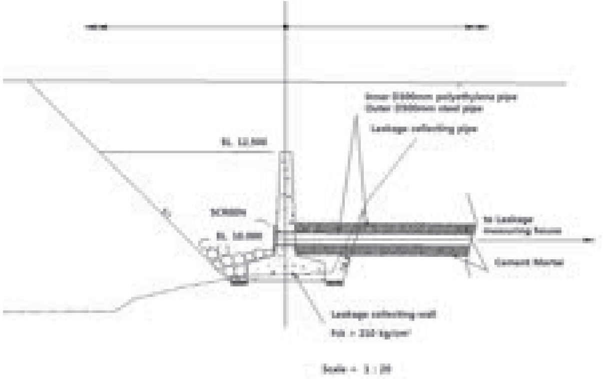

(a) Cross section of new collecting pipe

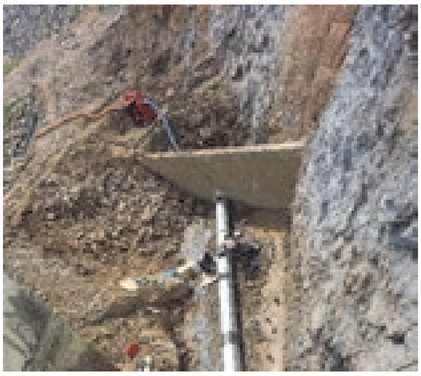

(b) photo of replacement

Figure 11. Replace of the collecting pipe

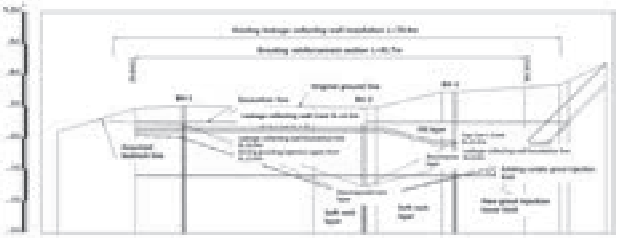

Figure 12. Rehabilitation of the foundation under the collecting wall by grouting

5. CONCLUSION

In this study, for investigation of cause of increased seepage rate of Sueo dam, correlation of seepage rate, reservoir water elevation and the released water rate for agricultural was analysed and temperature, turbidity and pH of the seepage water were measured and analysed. CCTV surveys and field investigations for the collecting pipe and seepage collecting wall and the foundation of it were carried out to find out inflow path of the river water. The results are as below.

1) From the measured values analysis, change of seepage rate, temperature, turbidity and pH were big in according to the released water rate for agricultural. It showed that the cause of the increased inflow was anticipated as the river water increased in water surface elevation by the released water for agricultural.

2) Through the CCTV Survey, the breakage of the collecting pipe was revealed at the location about 5m away from the measuring house toward the collecting wall. The water surface elevation of the collecting wall inside lowered to make no inflow from the collecting wall to the measuring house but the inflow was continuing. This revealed the possibility of inflow of the river water to the measuring house through the collecting pipe.

3) In the condition of the river water surface lower than the one of inside of the collecting wall by the downstream river barrage opened with shut down the release of water for agricultural, It was found that pressurized water flowed out at the 4 point of river bed, so, the possibility of inflow of the river water to the collecting wall through the boulder layer treated with grouting also could be considered.

4) Blocking the Inflow path of the collecting pipe and the foundation under the collecting wall, the damaged collecting pipe was replaced with D300mm high density polyethylene pipe (PEM) covered with d500mm steel pipe and the inside between them grouted with mortar and grouting was carried out with 2 line and 1m hole spacing, to the bedrock from minimum 1.9m to maximum 11m after the cap concrete with 3m wide and 0.5m thick inside of existing collecting wall.

ACKNOWLEDGEMENT

The Author thank the Korea Water Resources Corporation for permission to publish this paper. The author would also like to thank the colleagues at Yeosu Office of the Korea Water Resources Corporation.

REFERENCES

KISTEC (2008): 3rd Comprehensive Facility Review on Sueo dam, Korea Infrastructure Safety Corporation, pp 29-35.

K-water (2004): Detailed design report for Sueo dam seepage measuring system installation, Korea Water Resources Corporation

A Study on the Multi-criteria Decision Making Using Hydrological Safety Evaluation Result

J.Y. Park & J.H. Kwon
Infrastructure Safety & Technology Corporation(KISTEC), Korea
jeeyun87@naver.com

T.H. Kim
Nakdong River Flood Control Office(MOLIT), Korea

ABSTRACT:
In this study, hydrological safety vulnerability assessment on dam facilities was estimated using dams' hydrological safety evaluation result and in-depth inspection condition assessment score and grade. In-depth inspection condition assessment score and grade. In-depth inspection result was performed in Korea Infrastructure Safety & Technology Corporation(KISTEC) in Korea. Multi-Criteria Decision Making was used for vulnerability ranking decision on dams', and assessment scores of hydrological safety evaluation were applied as payoff matrix. It can be available for calculating dams' vulnerability ranking considered dams' hydrological safety.

Keywords: Dam hydrological safety, in-depth inspection, Multi-Criteria Decision Making (MCDM)

1. INTRODUCTION

Korea facilities are classified by 1 type and 2type depending on the size and social importance by Special Act on the safety management of facilities. 1 type and 2 type facility are periodically graded comprehensive by according to the in-depth inspection. In depth in inspection is composed of condition assessment and safety assessment. Hydrological safety evaluation is belonged to safety assessment. Hydrological safety evaluation has been carried out 3 step assessment that is dam freeboard and dam Structural stability during overtopping for the PMF and dam downstream risk. It can be estimated the dam hydrological safety vulnerability ranking using the existing dam hydrological safety assessment results.

2. ANALYSIS METHOD

Dam Hydrological safety vulnerability ranking is calculated using hydrological safety 3 step assessment results of the existing 6 dams and 4 type method of Multi-Criteria Decision Making (MCDM). Location of six target dams was shown in Fig. 1 Five dams belong to the Han river, and one dam belongs to the Geum river and the 6 target dam type was concrete dam.

2.1. Hydrological safety assessment

Hydrological dam safety has been currently evaluated depending on freeboard allowance, overflow and downstream hazard without any consideration of types, material and structural conditions. Hydrological safety assessment is made in three steps (MOLTL, 2011), The first step for safety evaluation is to check overflow possibility and freeboard allowance under the consideration of structural type and physical condition obtained from dam inspection results. Fill dam and CFRD(Concrete Faced Rock fill Dam) was applied to a more stable basis than concrete dam because of dam body safety difference when overflow.

If the first step is not satisfied, structural safety evaluation for overflow condition should be carried out as a second step. The evaluation of downstream hazard including human and economical factors is the final step. The final step is assessed to downstream risk with reference to the EAP on the assumption that PMF occurs.

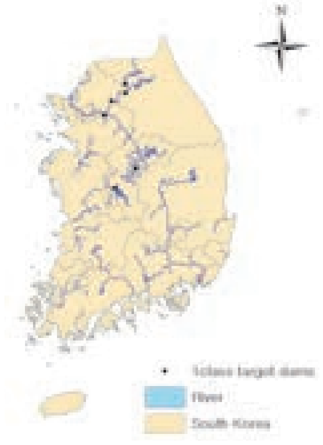

Figure 1. Target dams location

Table 1. Hydrological safety evaluation 3 step

Evaluation step	Evaluation contents	Evaluation standard
1^{st}	Evaluation for freeboard allowance and overflow	Whether or not to secure dam freeboard
2^{nd}	Evaluation of structural safety for overflow(PMF)	Dam structural stability during overtopping for the PMF
3^{rd}	Evaluation for downstream hazard(PMF)	Assessment downstream for PMF

2.2. Multi-Criteria Decision Making(MCDM)

Multiple-criteria decision-making is a sub-discipline of operations research that explicitly considers multiple criteria in decision-making environments (Triantaphyllou, 2000). Pareto optimal solution is a concept in multi-criteria optimization that allows for the optimization of multiple criteria. MCDM is the process of finding such a Pareto optimal solution (Alternative) on a variety of criteria (Criteria) and shown in Fig. 3(Kim, 2013).

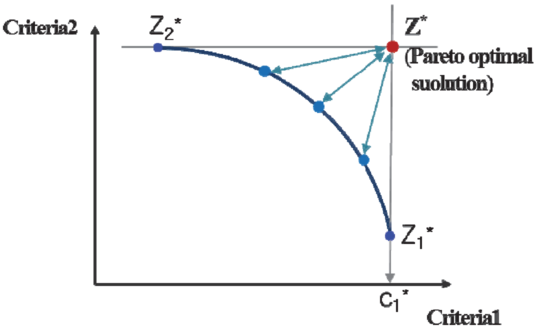

Figure 2. Pareto Optical Solution of MCDM

In this study, MCDM was used for vulnerability ranking decision on dams, and assessment scores of each step of the hydrological safety evaluation results which was applied as payoff. It can be available for calculating dams' vulnerability ranking considered dams' hydrological safety.

Compromise Programming(CP), PROME-THEE, VIKOR and TOPSIS, generally used as MCDM technique, were applied to determine the hydrological vulnerability ranking of dams According to each technique, the dam ranking was calculated. In conclusion, the most vulnerable dam and the most safety dam was selected.

3. ANALYSIS RESULTS

In this study, It was ranked using various techniques of MCDM that hydrological safety assessment vulnerability ranking. Criteria of MCDM payoff matrix was shown in Table 2.

Table 2. MCDM criteria

Evaluation contents	Criteria	Evaluation Criteria
Condition assessment grade of Dam In-Depth safety diagnosis	Criteria1	Lower the vulnerable
Assessment of freeboard for dam type and condition assessment	Criteria2	Lower the vulnerable
Assessment of dam Structural stability during overtopping for the PMF	Criteria3	Lower the vulnerable
Assessment of dam downstream risk	Criteria4	Lower the vulnerable

The target dams were ranked by 4 criteria. The score range of 4 criteria is between 1 and 5. And the vulnerability has been evaluated as vulnerable if indicating a lower score for 4 criteria. If dam has high hydrological safety vulnerability, that ranking is low value (ex: 1 ranking). Table 3 was shown by MCDM payoff matrix. The payoff matrix score in 4 criteria was used as hydrological safety assessment value of recently performed the in-depth inspection.

Table 3. MCDM Payoff Matrix

	Payoff Matrix			
	Criteria1	Criteria2	Criteria3	Criteria4
Dam1	5	5	5	3.70
Dam2	1	4	1	2.87
Dam3	1	5	4	3.17
Dam4	1	5	4	2.95
Dam5	5	5	5	3.32
Dam6	1	5	4	2.90

MCDM result values and ranking were shown in Table 4. MCDM result values were calculated according to various methods. The dams' hydrological safety vulnerability ranking was calculated by using the average value of the ranking to each result values.

Table 4. MCDM values and vulnerability ranking hydrological safety

	CP	VIKOR	TOSIS	PROME-THEE	Ranking
Dam1	0.0650	0	0	-2.867	6
Dam2	0.6815	1	1	3.1322	1
Dam3	0.5165	0.8662	0.7895	0.4485	4
Dam4	0.5275	0.8751	0.7913	0.7666	3
Dam5	0.0840	0.0438	0.0433	-2.318	5
Dam6	0.5300	0.8771	0.7915	0.8389	2

The Vulnerability ranking of hydrological safety in existing dams was shown in Fig. 3. Dam 2 estimates the highest priority for all techniques, it showed the most vulnerable on hydrological safety. Dam 1, 5 estimate the lowest priority for all techniques, hydrological appeared to be safe.

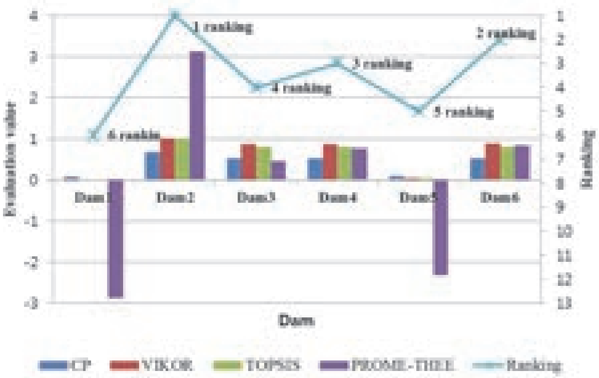

Figure 3. Vulnerability Ranking of hydrological safety in existing dams

4. CONCLUSION

In this study, Vulnerability Ranking of hydrological safety was ranked using MCDM method in the current hydro meteorological conditions. MCDM technique is difficult the choice of one way due to the differences in the advantages and disadvantages of each method (Min and Song, 2003), However using the results of the various MCDM methods, it is considered to be able to take advantage of prioritization on Vulnerability Ranking for dam hydrological safety. Next, it is expected to be calculated hydrological vulnerability considering climate change including climate change criteria (ex: rainfall intensity or annual precipitation). And I plan to conduct such research.

ACKNOWLEDGEMENT

This research was supported by a grant (14AWMP-B082564-01) from Advanced Water Management Research Program funded by Ministry of Land, Infrastructure and Transport of Korean government.

REFERENCES

Kim, T.H.(2013):Flood Risk Mapping Based on the Fuzzy MCDM by considering Inland River Inundations with Basin Runoff. Ph. D. dissertation, Kyungpook National University, Korea, pp.17-20.

Min, J.H., and Song, Y.M. (2003): A Comparison of MAUT, AHP and PROMETHEE for Multicriteria Decisions, Proceedings of the Korean Operations and Management Science Society Conference, Nov., pp. 229-232.

MOLIT, KISTEC(2011).:Specific Guide for In-depth Inspection on dams.

Triantaphyllou, E. (2000): Multi-Criteria Decision Making: A Comparative Study. Dordrecht, The Netherlands: Kluwer Academic Publishers (now Springer). ISBN 0-7923-6607-7.

Dam Management Strategies to Tackle Climate Change

A. Chantanumate & W. Kumnerdpet
Royal Irrigation Department, Bangkok, Thailand
atpongc@hotmail.com

ABSTRACT:
Climate change has resulted in drought and fluctuation of rain pattern. Generally, dams are designed for domestic and agricultural purposes which make the size of reservoir too small to handle climate variability. Four approaches derived from lessons learned of Thailand are: first, forest rehabilitation and check dam construction at upstream areas should be implemented to increase humidity and to slow down water flow. Second, mid-stream areas demand suitable location to build dams as a means of water management. New dams should be laid conceptual design to store water more than average annual runoff to be able to deal with flood or dry spell. Third, at downstream areas, drainage system in flood plain requires improvement to bear more rainfall from isolate rain. Further, dikes are essential in lowland. Fourth, modification of public behavior is done by educating the public to survive water hazards and to realize the necessity of dam construction. City planning, moreover, needs to be relocated not to block waterway. As a result, each basin should have dam and watergate to manage water. Systematic development helps lessen loss of life, assets, and economic. Forest restoration is needed to enhance balance of water cycle thus alleviating climate change effects.

Keywords: Dam management strategies, Dam strategies, Climate change

1. BACKGROUND

Climate change has resulted in higher temperature. Moreover, the anthropogenic contribution to natural resources depletion leads to climatic impacts all over the world. The impacts comprise higher temperature in dry seasons, shorter period and higher temperature in cold seasons, and fluctuation of rain pattern in rainy seasons. The fluctuation pattern includes unseasonal rainfall that only rains in one area without distribution. Furthermore, the rain pattern has shifted to rain heavily in a short period with fewer numbers of rainy days. This effects water cycle which later remains to be runoff in rivers and tributaries. It makes water flow rapidly and inundate lowland in rainy seasons. In dry seasons, there is a small amount of water flow from upstream areas, and thus rivers run dry and drought occurred in many countries see Fig. 1. The climate change has significant effects to upstream areas, mid-stream areas, downstream areas, and public's behavior modification to cope with water-related problems (IPCC, 2014).

Figure 1. Effects from climate change

2. PROBLEM ANALYSIS

2.1. Upstream areas

Upstream areas of Thailand have been deteriorated from careless use of natural resources, lack of conservation, and agricultural area expansion into forest. The climate change keeps temperature rising continuously which accelerates evaporation of forest moisture. Furthermore, forest deterioration makes nature imbalanced quickly. In

1961, Thailand had forest areas of approximately 274,000 sq.km. or 53% of the country's areas. The deforestation has been continually increased from anthropogenic activities, for example, house building, logging, and farming. The forest areas of Thailand then remained 173,000 sq.km. and 163,000 sq.km. in the year 2012 and 2015, respectively (Royal Irrigation Department, 2016).

The climate change affects biodiversity and forest fertility (IPCC, 2014). In rainy seasons, water flows rapidly and washes away top soil, seeds, and seedlings which sometimes cause landslide and directly effect on forest abundance see Fig. 2. The decrease of forest moisture influences trees to be dry and eventually die. The dry trees not only act as hot spots that can ignite forest fire see Fig. 3, but also lose their capability to absorb water that can be a source of water for mid-stream areas.

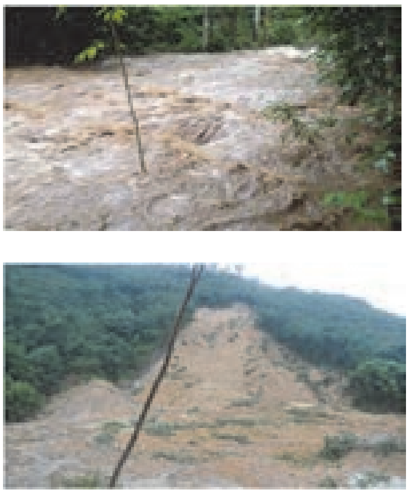

Figure 2. Flash flood and landslide

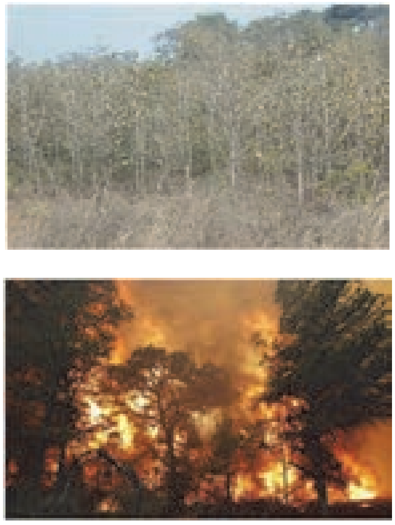

Figure 3. Dry trees and forest fire

2.2. Mid-stream areas

Deforestation, decrease of rain distribution, and heavy rain in a short period cause flash flood in rainy seasons, but dry rivers in dry seasons. The difficulties then occur throughout mid-stream areas.

Most mid-stream areas are rural communities and agricultural areas. In the past, farmers used water from natural water courses or seeping water for their living and farming. At present, upstream deterioration, agricultural areas expansion, rural community expansion, and water demand for domestic use, ecological maintenance, and industry have been increased. The government has solved these difficulties by developing weirs, reservoirs for supporting domestic use, ecological maintenance, and agriculture. The reservoirs generally store water only 30-70% of average annual runoff. However, the effects of climate change and rural community expansion make stored water insufficient for water demand from every sector. The climate change also puts impacts on reservoirs by having minimal inflow into reservoirs in dry seasons and excessive inflow from prolonged heavy rainfall, which are the cause of drought and flood, respectively see Fig. 4.

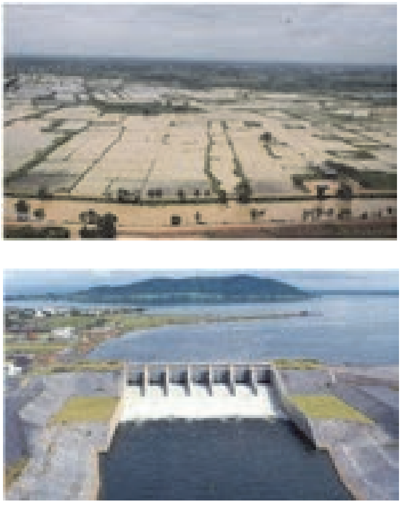

Figure 4. Flood occurred from excessive inflow more than storage capacity

2.3. Downstream areas

Downstream areas are mainly urban communities that accommodate dense population, factories, and economic zone. Majority of areas are lowland which have drainage system connected to a main water channel and dikes surrounded urban spaces. In rainy seasons, a great amount of water from deteriorated upstream areas together with dike construction in some areas that narrow water channels make water level higher and quicker flow over embankments into lowland. Heavy rainfall occasionally induces flood in the areas which leads to economic damage see Fig. 5. In dry seasons, freshwater shortage for domestic use, ecological maintenance, industry, and tourism is frequent because a vast number of water is drawn before reaching downstream areas as well as freshwater is needed to prevent saltwater intrusion from the Gulf of Thailand. The government have to announce a campaign of unavailable water for dry-season crop in order to provide water for domestic use and economic zone.

Figure 5. Flood in urban areas

2.4. Public's behavior modification

Climate change is a new phenomenon that affects every person. People, however, lack of knowledge and understanding to cope with emerging natural disasters, for example, drought, flood, storm, etc. see Fig. 6. Inappropriate city planning and no early warning system stimulates loss of life and assets.

Figure 6. Emerging natural disasters e.g. flood, drought, and storm

3. SOLUTION APPROACHES

The solution approaches need to be systematically deliberated over upstream areas, mid-stream areas, downstream areas, and public's behavior modification. Besides, irrigation structures are able to help rehabilitate depleted nature to meet water demand of every sectors. The approaches are detailed as the followings.

3.1. Upstream areas

An approach to cope with climate change is to rehabilitate upstream forest in order to be a source of moisture trap and air purifier or CO_2 collector. Deteriorated forest can be restored by building check dams and sabo dams at upstream areas see Fig. 7 and Fig. 8. These dams serve as water and moisture storage as well as suspended sediment catcher. The dams, built by semi-permanent structures, should be first constructed along tributaries near hilltop to help reduce water harshness from upstream areas and decelerate suspended sediment to sink into upstream areas. Check dams therefore assist in increasing soil and plant moisture which is a key component to regenerate deteriorated forest. In addition, forest rehabilitation without reforestation is needed. The forest can be self-revived if it is refrained from human disturbance for a certain period (Office of Royal Development Projects Board, 2016).

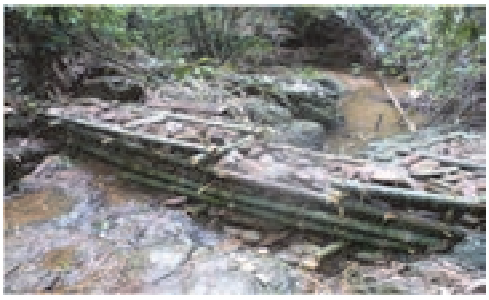

Figure 7. Check dams

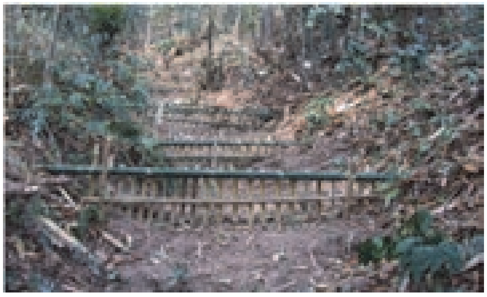

Figure 8. Sabo dams

3.2. Mid-stream areas

Due to climate change, using available tools, e.g. reservoirs or diversion dams, is necessary to plan carefully to handle overflow in rainy seasons or drought in dry seasons. The approaches for each specific case are as follows:

3.2.1. Having an existing reservoir case

An existing reservoir in each area needs to be conducted a potential study. In the past, Thailand did build a reservoir that stored water only 30-70% of average annual runoff because of limited budget. A potential study of an existing reservoir therefore has to be done by analyzing statistical data of repeated flood and drought, including damage incurred. In case of water overflow every 1-2 years, a reservoir is too small and should be expanded its storage capacity based on potential of topography and condition of dam structure. If the storage capacity cannot be increased, a water management plan may be adjusted to cope with emerging flood and drought by adjusting an operation rule curve. In case modified water management plan cannot solve a problem, methods to mitigate economic loss, e.g. constructing the system of dike, retention area, or farm pond, need to be implemented to reduce incurred damage from flood and drought.

In case of storage capacity expansion, a consideration of an original dam's detailed design, average annual runoff, and site topography and contour is necessary to identify storage capacity. However, flooding areas from dam improvement should be minimal to have least impacts on local residents. Spillway improvement is also needed.

If an existing spillway is a weir that is as high as normal water level, weir's height has to be decreased about 2-3 meters as well as installing a radial gate in order to control water to reach maximum water level in case of a large-scale dam. This is to enhance a chance to manage water for damage reduction and to be able to increase storage capacity. However, this method requires a control staff see Fig. 9.

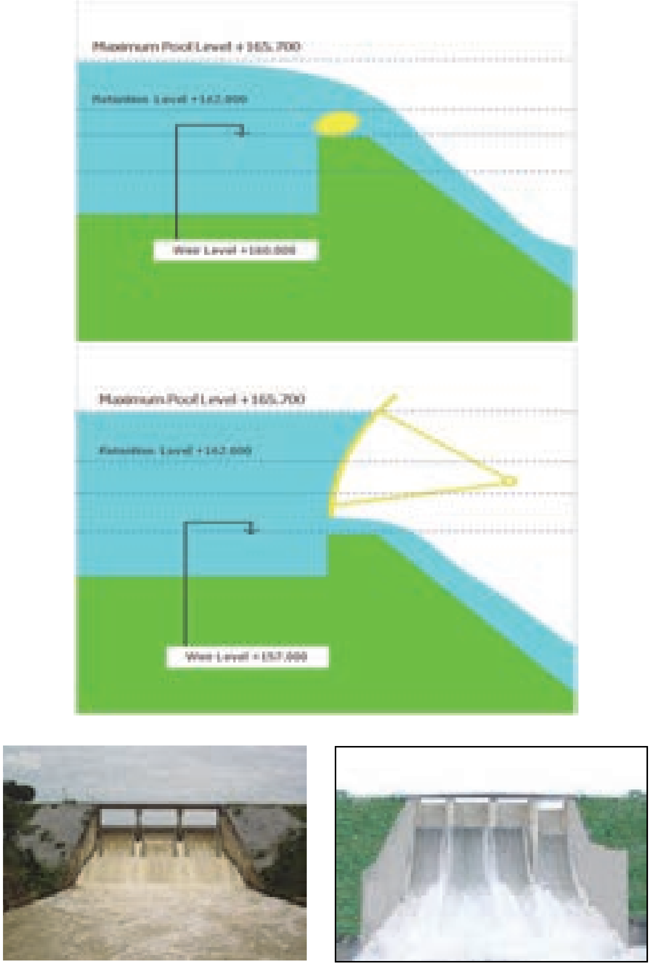

Figure 9. Spillway design and dam's height increase

If an existing spillway is an open channel, available data including annual runoff, percentage of water storage per average annual runoff, overflow frequency, and appropriate topography need to be considered to specify an alternative of storage capacity increase by heightening an earthen dam. In case of spillway improvement, establishing a watergate or weir is important to expand storage capacity see Fig. 10.

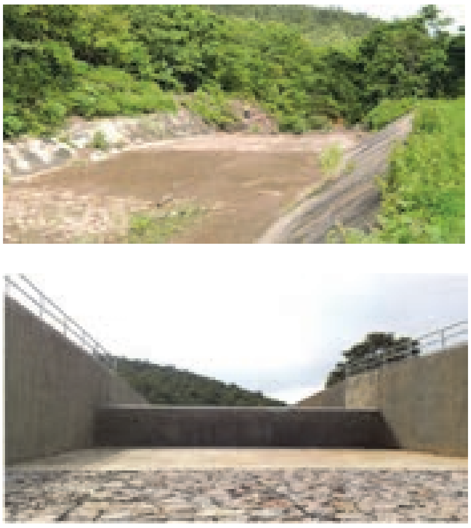

Figure 10. Storage capacity increase by building a weir at spillway

However, storage capacity expansion depends upon original dam structure, suitable topography, budget, personnel constraints on control and management, and drainage system from dam. In case of a medium-scale or small-scale dam, applying a weir to increase water level may be feasible due to limited staff to monitoring and managing a watergate.

3.2.2. Constructing a new reservoir case

Feasibility study of a proposed reservoir must be aimed to store water at least 90% of average annual runoff. Besides, dam design covering a 10-year return period of flood is needed to identify storage capacity built upon a concept of multi-purpose dam, i.e. storage, drainage, and flood mitigation. The dam may be designed to store water at two levels such as normal water level and maximum water level so as to handle flash flood, to manage a dam to prevent flood, and to supply sufficient water for every sector in dry seasons and thus for future development. Moreover, the dam must be able to drain more water through river outlet. The river outlet should also be designed to allow suspended sediment drained out with water as much as possible. The more suspended sediment is drained out, the longer dam's life will be extended. In addition, a new reservoir should have a tool to control and manage water level in accordance with climate change. If there are, for instance, consecutive storms, dam will be capable to drain water in case of emergency. Or if it is necessary to drain water for the upcoming flash flood, dam will be able to do so. However, a constraint regarding water management should be taken into account. Especially, a staff is needed to control a watergate in case of gate installment at spillway see Fig. 11.

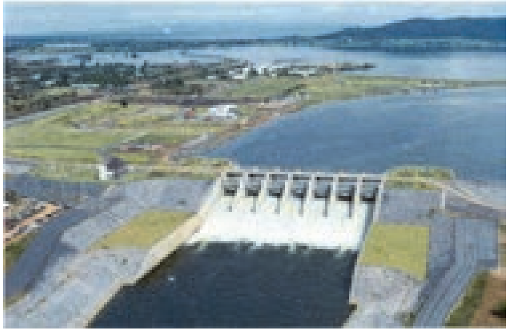

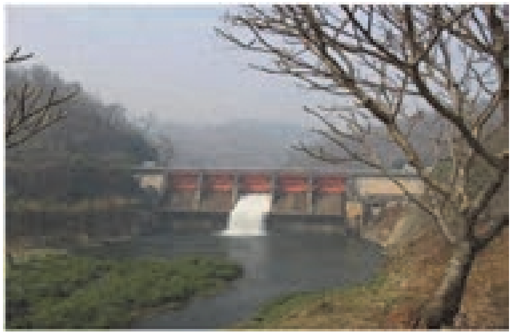

Figure 11. A large-scale dam uses watergates to control water at spillway

3.2.3. Having no suitable site to construct a new reservoir case

In case of no suitable site to construct a new reservoir, we may consider to build a structure to control and retain water in a water channel, e.g. diversion dam or weir. These structures help raise water level and then distribute water into an irrigation system or store water in lagoons or ponds to use in a dry season. Diversion dam and weir have both advantages and disadvantages depending upon topography appropriateness and mode of control. Diversion dam is generally applied for a large water channel and required cautious control see Fig. 12. While weir is suitable to build over a small water channel in order to raise water level in dry seasons but water level may be higher than usual in rainy seasons and lead to flood in an upstream area. In case of no suitable site to construct a diversion structure, we may consider about retention areas to divert water when excessive water and to gradually use in dry seasons see Fig. 13. The retention areas can mitigate the intensity of flood and drought in a certain level.

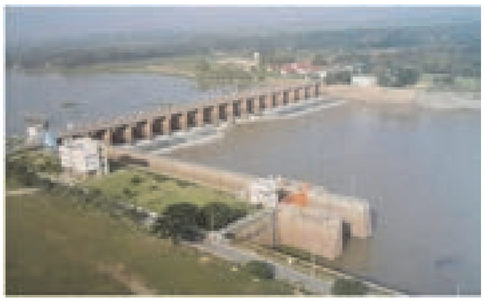

Figure 12. Diversion dam

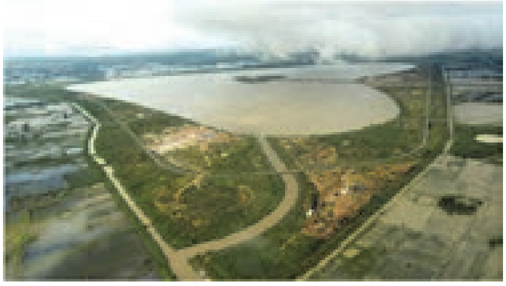

Figure 13. Retention area

3.3. Downstream areas

Most downstream areas are lowland where will be at highest risk to get impacts from climate change if water management at upstream and mid-stream areas appears not good enough. Downstream areas, which are mostly economic zone, therefore need to be determined the amount of water flowing through the areas by collecting statistical data of rainfall and runoff at a main river. Furthermore, locating dikes and drainage system is necessary to be planned carefully see Fig. 14 and Fig. 15.

In case of drainage efficiency improvement, statistical data of rainfall in the areas must be considered because rainfall is currently intense in a short period. If an old drainage system is proceeded, inundation will surely be occurred. Drainage improvement, including drainage pipe enlargement, flap valve installment at the conjunction of drainage system and a main river to prevent backwater into drainage system, and establishing a pumping system from a sump to accelerate drainage, should also take into consideration.

An area near a main river has to study the river flow passing through the area and to identify repeated flood areas. The embankment in lowland needs to be designed to cover maximum flash flood. There was, for example, dike improvement from channel capacity of 2,000 cms to be 3,500 cms in Bangkok because of higher water level. The higher water level was caused by a number of dike development throughout mid-stream areas based on variation between water quantity and areas.

Freshwater shortage in urban communities must be solved by reservoir or pond development. Diverting water from other basins may be another option to supply water for domestic use, industry, and tourism within urban communities see Fig. 16.

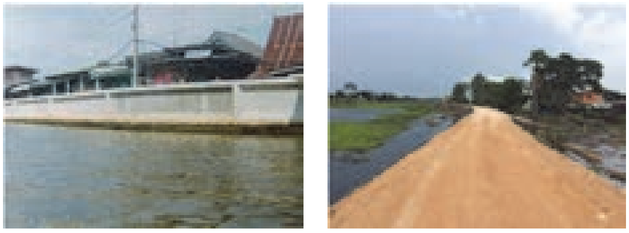

Figure 14. Embankment or dike at an urban community

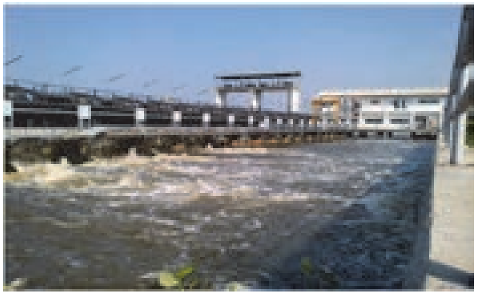

Figure 15. Drainage system from an urban community

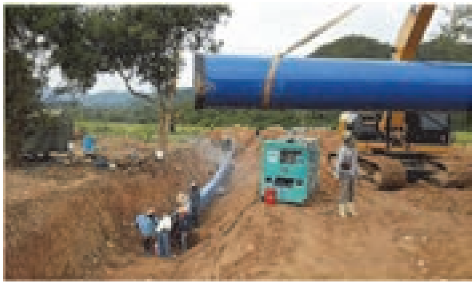

Figure 16. Water diversion system for using at different sectors

3.4. Public's behavior modification

According to climate change, the public and relevant sectors must have a mutual learning to jointly solve problems. The public's behavior at each area needs to be modified as the followings.

3.4.1. Upstream areas

A mutual learning of forest conservation needs to be promoted. The forest conservation involves no logging, no forest encroaching for agriculture, no forest burning for mushroom collection, and forest fire precaution. Forest rehabilitation, moreover, has to be done by building check dams and sabo dams in order to retain water and increase moisture for the forest. Eventually the abundance of forest ecosystem at upstream areas will be gradually revived. Furthermore, education of upstream people about sharing natural resources with downstream people is imperative.

3.4.2. Mid-stream areas

Mid-stream areas are rural communities and agricultural areas. Therefore, a shared learning of maximized use from natural resources, e.g. surface runoff, is vital. Construction of reservoirs, diversion dams, or weir is a key to sufficiently supply water for domestic use, ecological maintenance, agriculture, industry, and others. Water stored at mid-stream areas is used not only for alleviating water shortage in dry seasons, but also for mitigating flood in rainy seasons. Water management is another key to help decrease damage from flood and drought at mid-stream and downstream areas. An understanding of dam necessity for local residents is then critical to relieve an opposition trend of water resource development. Meanwhile, the government needs to immediately improve the remedial approaches, both monetary and non-monetary aids, for impacted persons from the water resource development and specify to be laws accordingly. In addition, related environmental laws should be revised to certify development and systematically protect the use of natural resources.

3.4.3. Downstream areas

Public education regarding living with climate change is necessary. The required education includes the quantity of rainfall and runoff, weather, warning system, and downstream effects. Mass media communication plays an important role to deliver information and knowledge for early warning and dealing with water hazards to the public. The government, moreover, must pay close attention to: city planning; setting the drainage system and infrastructure; educating the public to locate houses properly and to use a suitable house type in each area see Fig. 17; and, establishing warning system in risk areas. Law enforcement should also be implemented to fulfill accomplishment.

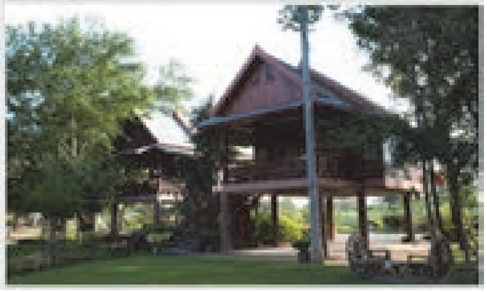

Figure 17. Thai-styled house that is raised the first floor is suitable to be built at flood plain

4. BENEFITS FROM IMPLEMENTATION

Direct and indirect benefits from implementation of dam management strategies to tackle climate change are as follows:

1) To rehabilitate and conserve upstream areas
2) To enhance water stored at upstream areas
3) To maximize the use of water resources
4) To prevent and mitigate flood and drought in different areas
5) To support water security for every sector
6) To strengthen economic stability
7) To serve as a fundamental factor to investors regarding confidence of water security

REFERENCES

IPCC. (2014): Summary for policymakers. In: Climate Change 2014: Impacts, Adaptation, and Vulnerability, Cambridge, U.K. and New York, USA.

Office of Royal Development Projects Board. (2016): http://km.rdpb.go.th/Knowledge/View/21.

Royal Irrigation Department. (2016): http://www.rid.go.th.

Geophysics Interpretation Unveil Cause of Dam Imperfection for Dam Improvement and Dam Safety Management
: Bang Niao Dum Dam, Phuket, Thailand

C.Pedugsorn
Head of Design, Engineering Branch, Royal Irrigation Office Region 1, Chiangmai, Thailand
Chatpongnoi@hotmail.com

N.Poomviset
Director of Geophysics Branch, Geological and Survey Office, Royal Irrigation Department, Bangkok, Thailand

ABSTRACT:
Bang Niao Dum dam stands on deep pervious foundation composed of three main layers, first layer, black soft soil (N-value = 4-6) about 30.00m beneath ground surface, second layer highly weathered to completely weathered granite around 30.00-60.00m, and third layer moderately to highly weathered granite about 60.00-90.00 m, respectively. Foundation was designed as combination impervious partial cutoff trench with partial cutoff wall. Complete construction in 2008, first impound in 2009, excessive seepage was found at rock-fill toe, closed to left abutment at cutting slope of appurtenant structures. In 2015, resistivity dipole-dipole was accomplished along dam axis following with Multichannel Analysis Surface Wave (MASW) at the same position. Resistivity profile displays various anomalies under impervious curtain whereas MASW shows high shear wave velocity 180-450 m/s. Three sets of rock fracture are beneath reservoir and immense at left abutment. Positions of opened cracks adjacent anomalous body around rock-fill toe at left abutment exhibited of leakage path. Geophysics unveils cause of excessive seepage. Dam improvement is by drainage design response watershed deep seepage. Geophysical interpretation shows overview seepage interaction of dam-foundation system apart from dam instrument. The Benefit of geophysics can extend to dam design, dam improvement and dam safety management.

Keywords: MASW, Resistivity dipole-dipole, dam imperfection

1. GENERAL INFORMATION

Phuket province locates in southern region of Thailand (Fig. 1). Phuket Island, named as pearl of Andaman Sea, is the most famous destination among tourist around the world. Instantaneous economic growth concurrent with water usages come out lack of water supply. Sustainable economic growth will not attain in case of fresh water shortage crisis. RID (Royal Irrigation Department) untangle water resources problem by structural measures of Bang Niao Dum reservoir project as following project summary.

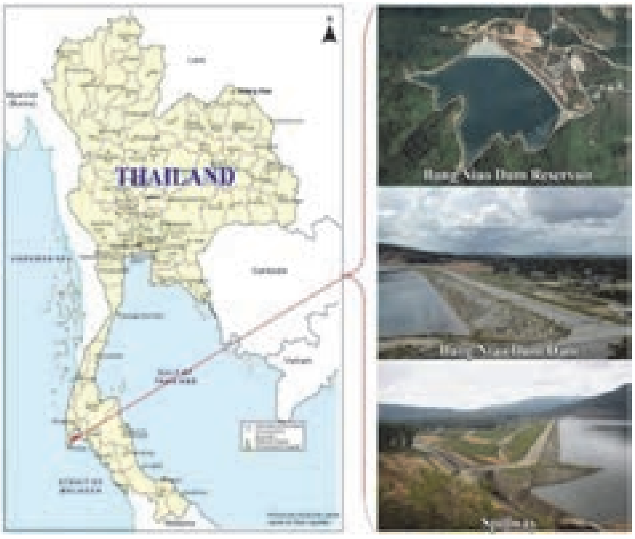

Figure 1. Location map of Bang Niao Dum Reservoir, Phuket, Thailand

Normal storage retention 7.20 million-cubic meter
Average annual rainfall 2400 millimeter
Average annual inflow 8.10 million-cubic meter
Embankment Zone type dam
Dam height 32.00 meters (from N.G.L.)
Crest width 8.00 meters
Crest length 861.45 meters
Spillway capacity 200.00 cubic meter / second
Outlet structure
    River outlet (left abutment)
    Water supply outlet (right abutment)

2. COMPLICATED DAM AND FOUNDATION DESIGN

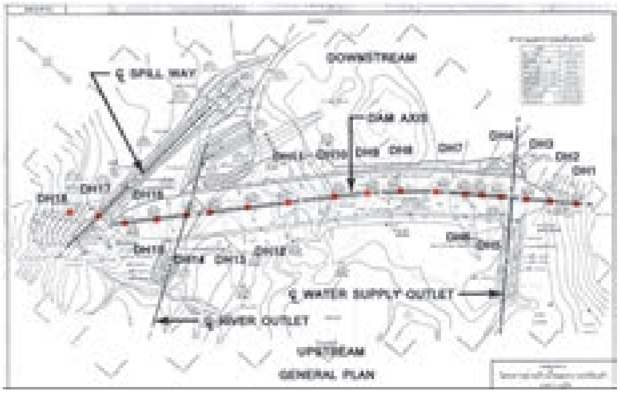
℄ SPILL WAY
DOWNSTREAM
DAM AXIS
DH18
DH17
DH16
DH11
DH10
DH9
DH8
DH7
DH6
DH5
DH4
DH3
DH2
DH1
DH13
DH14
DH15
DH12
℄ WATER SUPPLY OUTLET
℄ RIVER OUTLET
UPSTREAM
GENERAL PLAN

Figure 2. Geological investigation Plan

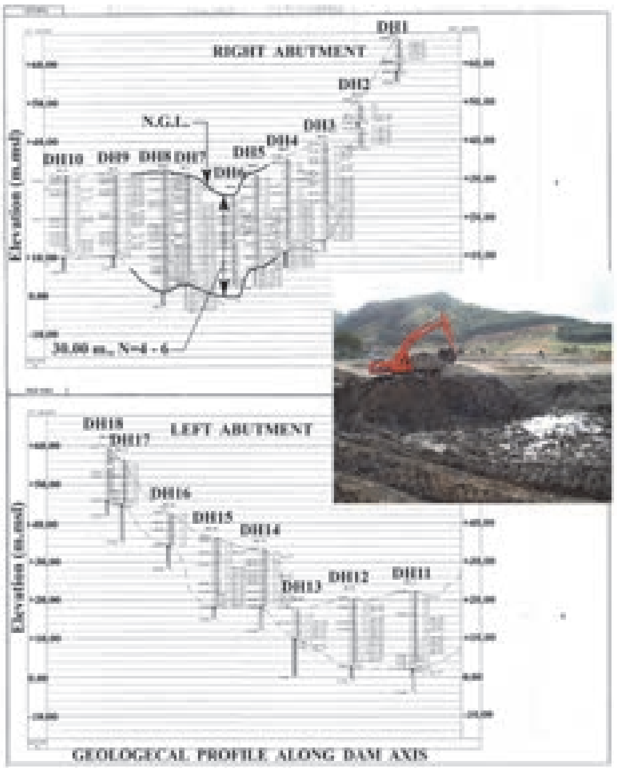
RIGHT ABUTMENT
DH1
DH2
DH3
DH4
DH5
DH6
DH7
DH8
DH9
DH10
N.G.L.
30.00 m., N=4 - 6
Elevation (m.msl)
LEFT ABUTMENT
DH18
DH17
DH16
DH15
DH14
DH13
DH12
DH11
GEOLOGICAL PROFILE ALONG DAM AXIS

Figure 3. Geological Profile along dam axis

After general layout was designed (Fig. 2), 18 boring logs has been investigated by geological process ASTM D 1586. Geological profile along dam axis is shown in Fig. 3. Geological data from DH.6, DH.7 and DH.8 are depicted top of weathering granite rock below natural ground surface about 30.00 meters. Permeability test of soil layer is less than 5x10^{-5} centimeter/second. Bearing capacity of loose black foundation soil from geological survey DH.11 and DH.12 by SPT (Standard Penetration Test) N = 0 - 6 are about 0 – 13 meter from ground surface. For over view of dam foundation, embankment dam stand on foundation difficulties. Deep foundation alignment compose of, first layer black soft soil (N=4-6) about 30.00 meter beneath ground surface, second layer weathering to completely weathering granite around 30.00-60.00 meter , third layer moderately to weathering granite about 60.00-90.00 meter respectively. In order to control annual seepage loss within 5 percent of reservoir capacity, foundation is designed combination partial cutoff trench with partial cutoff wall. Below bottom of cutoff trench is impervious diaphragm wall by jet grouting to extend seepage path to rock foundation. Foundation areas which bearing capacity less than 25 ton/square meter is improved by soil cement column. Poor engineering properties and limitation of fill material are constrained for dam designer. Most of borrow area compost of intermediate soil, semi-impervious property. Volume of core zone (Zone1) has to match with impervious soil from left and right abutments borrow areas. Dam instrumentation such as piezometer are installed at maximum depth section Sta.0+640 to observe pore pressure of dam and foundation, to analyse seepage characteristic. Dam design and dam instrumentation design are in Fig. 4.

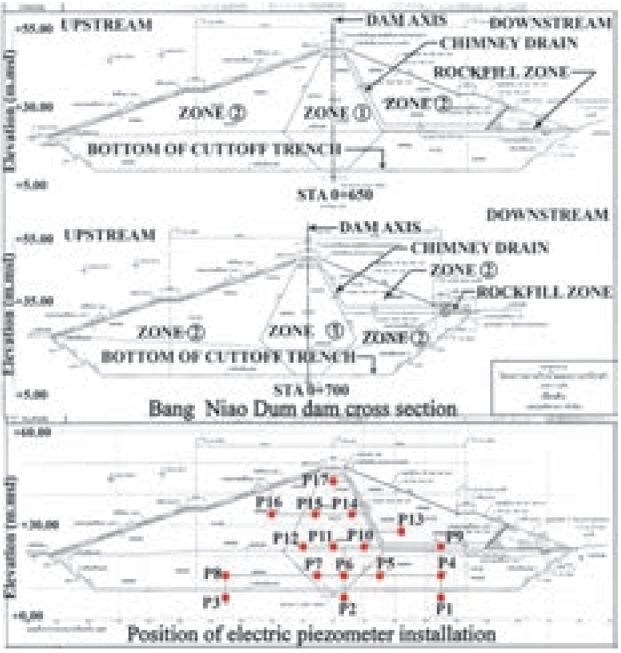
UPSTREAM
DAM AXIS
DOWNSTREAM
CHIMNEY DRAIN
ROCKFILL ZONE
ZONE ②
ZONE ①
ZONE ②
BOTTOM OF CUTTOFF TRENCH
STA 0+650
Elevation (m.msl)
UPSTREAM
DAM AXIS
DOWNSTREAM
CHIMNEY DRAIN
ZONE ②
ROCKFILL ZONE
ZONE ②
ZONE ①
ZONE ②
BOTTOM OF CUTTOFF TRENCH
STA 0+700
Bang Niao Dum dam cross section
P17
P16
P15
P14
P13
P12
P11
P10
P9
P8
P7
P6
P5
P4
P3
P2
P1
Position of electric piezometer installation

Figure 4. Cross section of Bang Niao Dum dam

3. SEEPAGE PROBLEM OF BANG NIAO DUM DAM

Construction period of Bang Niao Dum dam take 4 years, 2005 to 2008, complete construction in 2008, first impound in 2009. Excessive seepage was found at rock-fill toe closed to left abutment cutting slope of appurtenant structures (spillway, control house of river outlet). Leakage exit appear at toe drain, gutter drain and slope of rock-fill toe up to one third height. Location of excessive seepage is shown in Fig. 5. Measured data from piezometer installation of dam cross-section Sta. 0+640 apart from excessive seepage zone about 160.00 meter exhibit in range of design criteria. Dam instrument data are not representing cause of seepage problem. Bang Niao Dum dam seepage problem can be established 4 assumptions as following.

First assumption: Seepage through impervious diaphragm wall in case of intersection between jet grouting column are not overlap around dam body grounded on left abutment.

Second assumption: Reservoir rim leakage pass left abutment through rock-fill toe and cutting slope of appurtenant structures.

Third assumption: Leakage from deep seepage through aquifer system of left abutment watershed exit around rock-fill toe and cutting slope of appurtenant structures.

Fourth assumption: Others unexpected seepage pattern apart from First assumption to Third assumption.

From 2010 to 2014, designer are accompanied with Geophysics branch, Office of Engineering Topographical Geotechnical Survey, Royal Irrigation Department in seepage behaviour observation and investigation plan, finally geophysics investigation are accomplish in 2015. Resistivity dipole-dipole accomplish along dam axis following with Multichannel Analysis Surface Wave (MASW) at same position to prove assumption

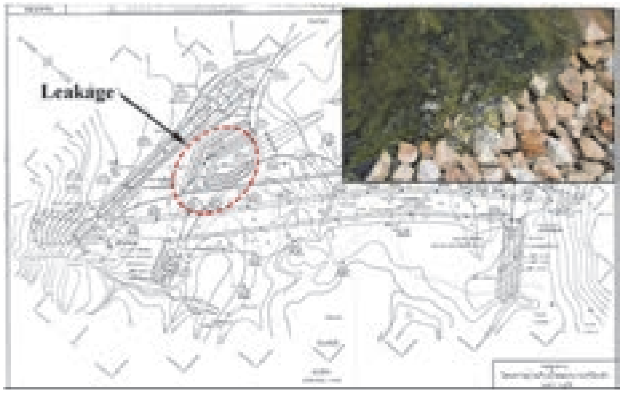

Figure 5. Location of excessive Seepage

4. GEOPHYSICS INVESTIGATION AND INTERPRETATION

In 2015, resistivity dipole-dipole accomplish along dam axis following with Multichannel Analysis Surface Wave (MASW) at same position. Resistivity profile displays various anomalies as seepage path under impervious curtain and MASW shows high shear wave velocity 180-450 meter/second. Three sets of rock fracture are beneath reservoir and immense at left abutment. Position of open cracks adjacent anomalous around rock-fill toe with cutting slope of outlet structure at left abutment exhibited of leakage path through left abutment. Geophysics unveils cause of excessive seepage as shown in Figs. 6 to 9.

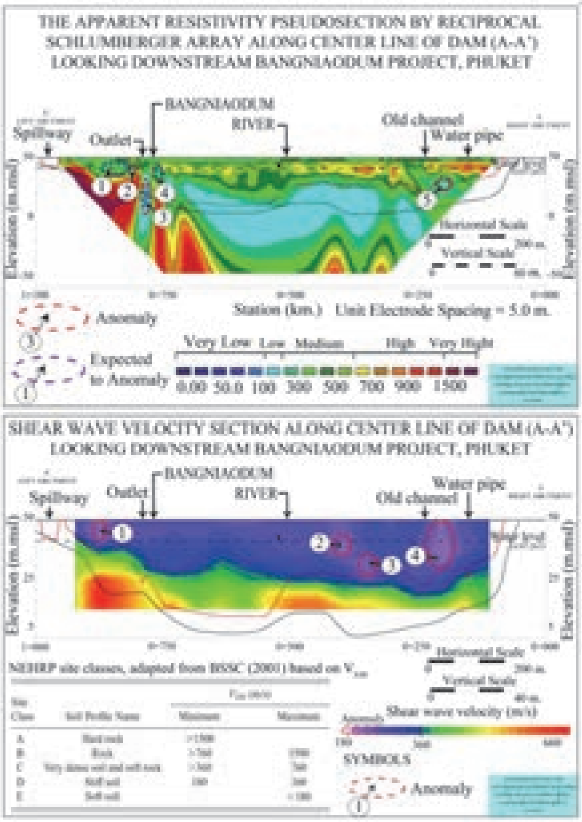

Figure 6. Geophysics investigation
(Resistivity A-A' and Shear wave velocity A-A')

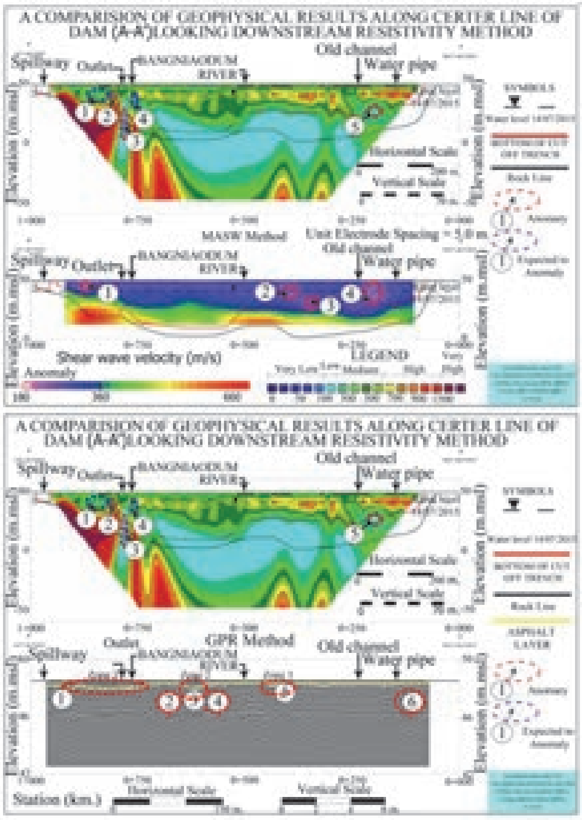

Figure 7. Geophysics investigation
(MASW A-A' and GPR A-A')

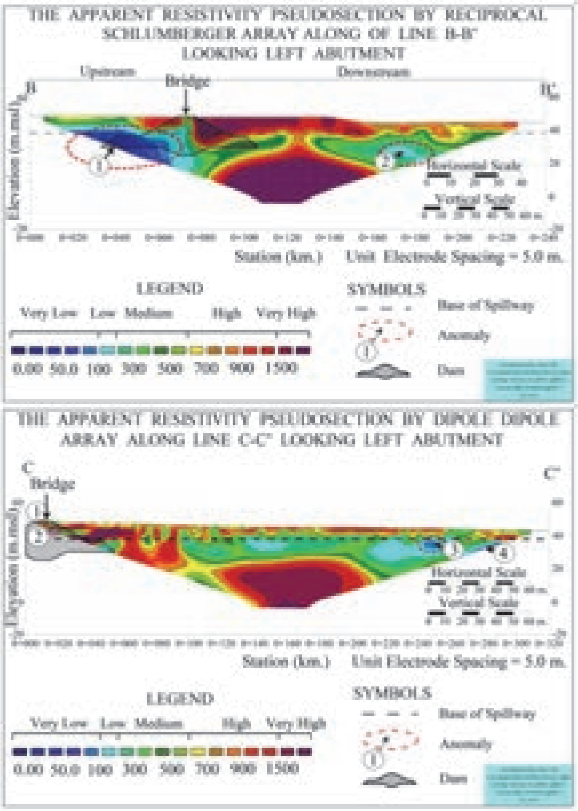

Figure 8. Geophysics investigation
(Resistivity B-B' and Resistivity dipol-dipol B-B')

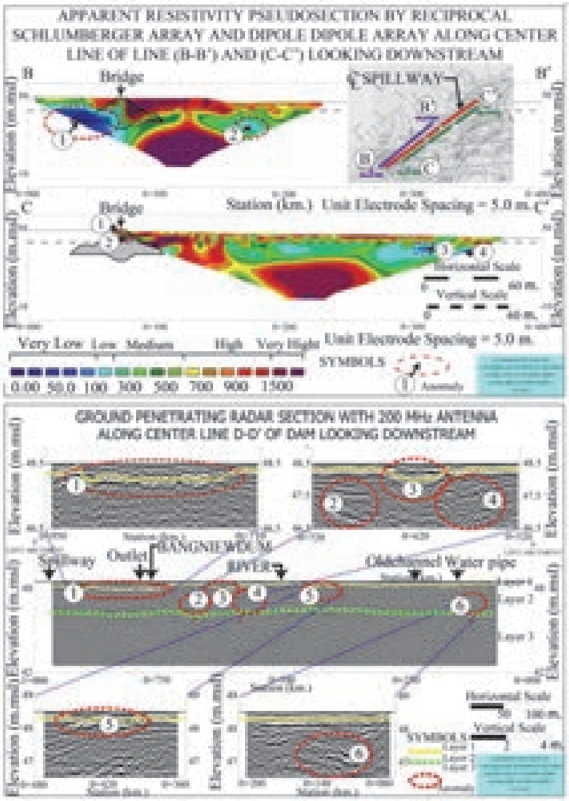

Figure 9. Geophysics investigation
(Resistivity B-B' and C-C' and GPR D-D')

5. ENGINEERING JUDGEMENT AND SOLUTION

Engineering judgement and proposed dam improvement solution for several assumptions are as following.

First assumption solution: dam improvement by vertical cutoff design from Core Zone (Zone1) to impervious rock foundation.

Second assumption solution: dam and left abutment improvement by vertical cutoff design from Core Zone (Zone1) to left abutment impervious bed rock. Vertical cutoff overlap embankment with left abutment to impervious rock foundation as wing wall.

Third assumption solution: improvement downstream rock-fill slope and cutting slope of appurtenant structures response watershed deep seepage.

In case of miss assumption, consequential improvement technique effect high construction cost and cannot solve excessive seepage problem. Geophysics investigation show leakage comes from left abutment watershed deep seepage corresponding as third assumption. Since leakage path come from left abutment outside reservoir, excessive seepage is not effect water loss from reservoir. Regardless of anomalous improvement is not effect reservoir retention. Improvement concepts are sufficient drainage and filter preventing particle migration. Incline filter drain and toe drain at rock-fill toe and gutter drain (Fig. 10) together with appurtenant structure cutting slope are proposed sufficiently to prevent piping and convey to seepage flow meter. Third assumption solution is cheapest compared with first and second solution.

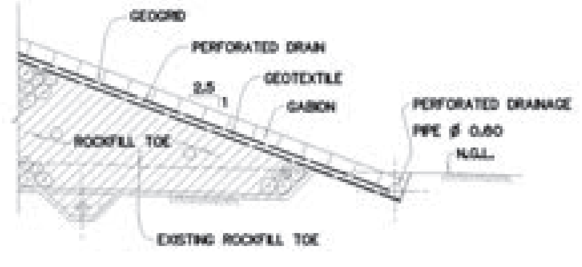
GEOGRID
PERFORATED DRAIN
GEOTEXTILE
2.5
1
GABION
PERFORATED DRAINAGE PIPE Ø 0.80
N.G.L.
ROCKFILL TOE
EXISTING ROCKFILL TOE

Downstream rock-fill toe slope improvement

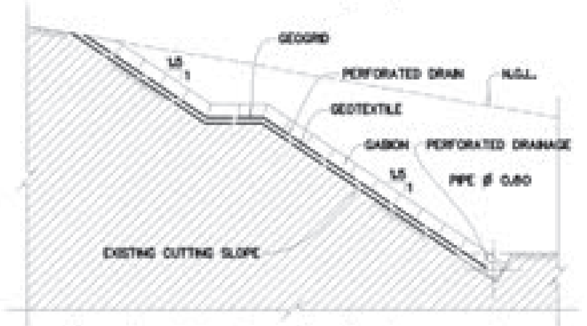
GEOGRID
1.5
1
PERFORATED DRAIN
N.G.L.
GEOTEXTILE
GABION
PERFORATED DRAINAGE PIPE Ø 0.80
1.5
1
EXISTING CUTTING SLOPE

Appurtenant structure cutting slope improvement

Figure 10. Improvement for sufficient drainage and preventing particle migration.

6. ADVENTAGE OF GEOPHYSICS INTERPRETATION TO DAM SAFETY MANAGEMENT

RID use CI (Condition Index) as tool for dam safety management. Since CI is derived from visual inspection as outside dam body investigation for rating dam component. Cause of dam imperfection inside dam body cannot be detected. Geological investigation is focus around observe area with certain destructive measure and cannot exhibited overview cause of problem. Dam instrument data cannot represent overview cause of imperfection problem. Geophysics interpretation is non-destructive measure and cheaper than geological investigation while cause of dam imperfection can be depicted for overview. Case study of Bang Niao Dum dam is impact to RID dam safety management policy to use geophysics investigation with visual inspection.

$$\mathrm{CI} = \sum_{i=1}^{n}(\mathrm{WFi} * \mathrm{SCi}) \tag{1}$$

Where
CI = Condition Index of dam, between 0% to 100%
WFi = Weight factor of dam component i
SCi = Score of dam component i

Level1. (0%-20%), very poor condition,
Extensive deterioration: barely function
Level2. (>20%-40%), poor condition,
Serious deterioration: function inadequate
Level3. (>40%-60%), fair condition,
Moderate deterioration: function still adequate
Level4. (>60%-80%), good condition,
Minor deterioration
Level5. (>80%-100%), excellent condition,
No noticeable defects

Condition Index represents physical deterioration of dam. RID use CI as tool to set priority ranking of dam maintenance. Since Bang Niao Dum dam CI=78.45 is in good condition, immediate action is not require but downstream community panic accelerate priority ranking of dam maintenance and rehabilitation.

7. CONCLUSION

From geophysics interpretation, three sets of rock fracture are founded beneath reservoir and immense at left abutment. Geophysics investigation show leakage comes from left abutment watershed apart from reservoir. Geophysics unveils cause of excessive seepage, bring confidence to dam designer, as leakage from deep seepage through aquifer system of left abutment watershed and exit around rock-fill toe and cutting slope.

Geophysics interpretation shows overview seepage interaction of dam-foundation system aside from dam instrument data. Benefit of geophysics can extend to dam design, dam improvement and dam safety management as engineer eyes to expose dam imperfection.

Since leakage path come from left abutment outside reservoir, addition incline filter drain and toe drain at rock-fill toe together with appurtenant structure cutting slope are proposed sufficiently to prevent piping and convey to seepage flow meter.

8. RECOMMENDATION

For dam design, after dam designer set general layout and boring log, geological investigation should go together with geophysics investigation for small, medium and large scale dam.

For dam improvement, cause of dam imperfection should be investigated by dam instrument data and geophysics interpretation to solve seepage problem.

For dam safety management, Geophysics investigation should be used with visual inspection in case of fair to very poor condition index to search for cause of dam deterioration.

ACKNOWLEDGEMENTS

The authors are deeply thankful to Mr Thongprew Krongjun, Deputy Director of Royal Irrigation Department, Mr Phemporn Sopanangkoon, Director of Dam Safety Management and JCOLD in giving opportunities to present this paper, thanks to Miss Rungthip Suriya in arranging figures.

REFERENCES

Geophysics Report 10/2558, (2015): Office of Engineering Topographical Geotechnical Survey, Royal Irrigation Department

Park, C.B., R.D. Miller, and J Xia, (1999), Multi-channel analysis of surface waves: Geophysics, 64, 3, pp. 800-808.

Standard Test Method for Standard Penetration Test (SPT) and Split-Barrel Sampling of Soils, ASTM D1586-11

Increasing the Safety of Rock Fill Dams by reducing the Possibility Of Hydraulic Fracturing

D. Djarwadi
Engineering Division, PT Pamapersada Nusantara, Jakarta, Indonesia
didiek.djarwadi@pamapersada.com

K.B. Suryolelono, B. Suhendro & H.C. Hardiyatmo
Civil & Environmental Engineering Department, Gadjah Mada University, Yogyakarta, Indonesia

ABSTRACT:
Hydraulic fracturing becomes one of the major problems in rock fill dams for its significant role in the initiation and extension of cracks in the clay core, a probable factor in dam's leakage and internal erosion. Hydraulic fracturing may occur in the upstream face of clay core of a rock fill dam whenever the vertical effective stress in it reduced to a level small enough to allow tension fracture to occur. This situation is related to arching effect due to stiffness difference between the embankment materials, steepness of the slope of foundation abutments, and clay core configuration.

This paper reported the study of the hydraulic fracturing in the laboratory and numerical analysis using finite element method in order to understand the mechanism of hydraulic fracturing and the method to reduce the hydraulic fracturing in the rock fill dams. The effects of clay core configurations, base width of the upstream filter, and the clay core materials are investigated. The clay core materials used in this study was obtained from 5 major dams in Indonesia; there are Batubulan, Batutegi, Pelaparado, Sermo and Wonorejo dams. Numerical analysis of hydraulic fracturing was carried out using finite element method. Couple analysis between deformation & stress, and seepage was adopted the final stresses obtained from construction period will be used as initial stresses during impounding period. The results indicated that the dam which have which have higher fine contents (ϕ<0.075mm) in the clay core materials, and wider base of upstream filter will have more resistant against hydraulic fracturing.

Keywords: One hydraulic fracturing, arching effects, dam safety, laboratory tests, numerical analysis

1. INTRODUCTION

Hydraulic fracturing may occur in the upstream face clay core of the rock fill dam in case the vertical effective stress in the core is reduced to levels that are small enough to allow tension fracture to occur. Pore water pressure in the core will also increase during impounding, and this will further reduce the effective stresses in the core. Wedging due to water pressure may crack the upstream face of the clay core. The vertical effective stresses in the clay core was reduce below the overburden pressure was mainly due to arching effect. Arching effect on the clay core of the dam occurred due to the slope of the abutment foundations, stiffness of the embankment materials, and configuration of the clay core. Zhang & Du (1997) reported that abutment with slope of 1V: 0.5H indicated that the total stress measured was only 52% of their overburden pressure, while on the abutment slope of 1V: 0.85H, the total stress was only 74%. Loftquist (1951) also reported that Holle and Harspranget dams in Norwegia that the total stress in only 50% of their overburden pressure. The possibility of hydraulic fracturing on the rock fill dams due to load transfer between embankment zones has been analyzed and reported by Kulhawy & Gurtowski (1976). Widening of base width of the upstream filter may reduce the arching effect and reduce the risk of hydraulic fracturing on the rock fill dams as reported by Djarwadi et al (2011). Lo & Kaniaru (1990) analyses on the dams experiencing hydraulic fracturing indicated that the dams with longer time in construction period which allow the greater consolidation comparing to the shorter period, and also slower in impounding rate which allow the wetting and development of the flow-net compare to the faster impounding rates which did not affect to the occurring the hydraulic fracturing. Zhu & Wang (2004) analyzed the influence of arching effect to the hydraulic fracturing of rock fill dams, and found that the increasing of the stiffness in the filter or clay core and widening the base width of the clay core will reduce the arching effect. Statistical analysis on rock fill dams with central core by Fell et al (2004) concluded that the dams with ratio of height of the dam (H) against base width of the clay core (W) more than 2 (H/W >2) were much more likely will experiencing with hydraulic fracturing, while if (1 < H/W < 2) were more likely will experiencing with hydraulic fracturing. All the studies mentioned above leads to the conclusion that the main cause of hydraulic fracturing in the rock fill dams was due to the arching effect. Analyses of hydraulic fracturing using numerical analyses were carried out using finite element method. Couple analysis between deformation & stress, and seepage was adopted. The similar method has been successfully used by Cavounidis & Hoeg (1977), Naylor et al (1988), Alonso et al (1988) and Ng & Small (1999). This method was adopted considering that the hydraulic fracturing recorded mostly occurred on the first reservoir filling. The selection of soil model on the stress and deformation analyses is very important, since its represent the actual condition and control the accuracy of calculation results. In the dam construction, the embankment materials were compacted layer by layer to form the final dam configuration. In this case the non linear elastic hyperbolic soil model suits the embankment process, where the elastic modulus was formulated as function of the confining pressure, so at every loading step the magnitude of the elastic modulus will be increased accordingly. The high order elements which consist of 8 nodal points of quadrilateral and 6 nodal points of triangular were used in the element discretization. The final effective stresses resulting from the couple analyses then will be used to evaluate whether the hydraulic fracturing was occurred. The evaluation steps described as follows;

- The vertical effective stresses along upstream face of the clay core obtained from couple analysis (σ_y') compared to the hydraulic pressure due to the maximum water level in the reservoir (σ_w),
- In case the vertical effective stress at certain point less than the hydraulic pressure ($\sigma_y' < \sigma_w$), the tension stress was occurred at those points,
- In the case the tension stress at certain point less than the tensile stress at failure obtained from the hydraulic fracturing test at the laboratory, there were no hydraulic fracturing may occurred,
- In the case the tension stress at certain point along the upstream face of clay core greater than tensile stress at failure obtained from the hydraulic fracturing test at the laboratory, the hydraulic fracturing was occurred on that point (Djarwadi, 2010).

2. LABORATORY TEST OF HYDRAULIC FRACTURING

The soil samples for hydraulic fracturing test in the laboratory were taken from the borrow pits of the 5 major rock fill dam in Indonesia; they are Batubulan, Batutegi, Pelaparado, Sermo and Wonorejo dams. The soil samples were then modeled into six (6) different fine contents, there are the fraction passing sieve no. 200 at approximately 30%, 40%, 50%, 60%, 70% and 80%, in order to investigate the effects of fine contents to the hydraulic fracturing. The soil specimens were compacted hollow cylinder, compacted inside a Proctor mould measuring 100 mm in diameter and 120 mm high. The inner diameter of the borehole was 18 mm, based on the borehole fracturing research results (Widjaja et al. 1984). Fig. 1 show the typical soil specimen used in the hydraulic fracturing tests.

Mode of failure of the clay core of a rock fill dam due to hydraulic fracturing has been justified as a tension failure. The development of hydraulic fracturing test apparatus in the laboratory has limitations where not all the conditions of the dams can be modelled in such a way in the laboratory.

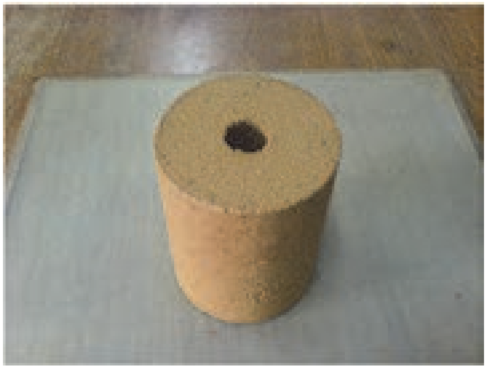

Figure 1. Soil specimen for hydraulic fracturing test

The reduction of the overburden stress due to arching effect can be modeled in the laboratory by applying the initial stress states to the specimens. The preliminary hydraulic fracturing tests (Djarwadi et al. 2009) indicated that the tension failure is only found on the soil specimen if the initial stress state given to the soil specimens prior the test started falls in the envelope of $\frac{1}{2}(\sigma_y - \sigma_x) < c$, where the σ_y and σ_x are the initial vertical and horizontal stresses which are applied to the soil specimens, which reflecting the vertical and horizontal stresses on the upstream face of clay core before impounding was take place and c is the cohesion of the soil specimen. In the preliminary test, the soil specimens were compacted clay with low plasticity obtained from Batubulan borrow pit. The geotechnical parameters are; $\gamma_{d\ max}$ = 15.32 kN/m^3, w_{opt} = 20%, ϕ (internal angle of friction) = 18.15°, and cohesion (c) = 78.20 kPa. The preliminary tests were carried out on the five (5) variations of the initial stresses. Table 1 show the variation of the initial stresses applied to the soil specimens.

Table 1. The variations of the initial stresses

Test	σ_x (kPa)	σ_y(kPa)	½ (σ_y-σ_x) (kPa)
1st	100	160	30
2nd	140	240	50
3rd	180	320	70
4th	200	380	90
5th	240	460	110

The preliminary test results on five (5) different initial stresses are summarized in the Table 2, while the fractured specimens after tests are presented on Fig.2. The preliminary test results indicated when the initial stresses applied fell within $\frac{1}{2}(\sigma_y - \sigma_x) < c$, the stress at failure were negative or tension failure was occurred, while when initial stresses fell within $\frac{1}{2}(\sigma_y - \sigma_x) > c$, the stress at failure were positive, and no tension failure occurred even the specimen was fractured.

The mechanisms of the above tests are mentioned as follows; the stress on the soil specimen during the hydraulic fracturing test is assumed to be the same, and the stress equilibrium on the soil specimen at the end of the test is shown in Fig. 3.

Table 2. The preliminary hydraulic fracturing test results

Test	$\Delta\sigma'$	u_f	σ_1'	σ_t	Remark
1st	43	170	142	-28	Fig. 2a
2nd	44	205	183	-22	Fig. 2b
3rd	53	240	233	-7	Fig. 2c
4th	66	255	266	11	Fig. 2d
5th	54	270	295	25	Fig. 2e

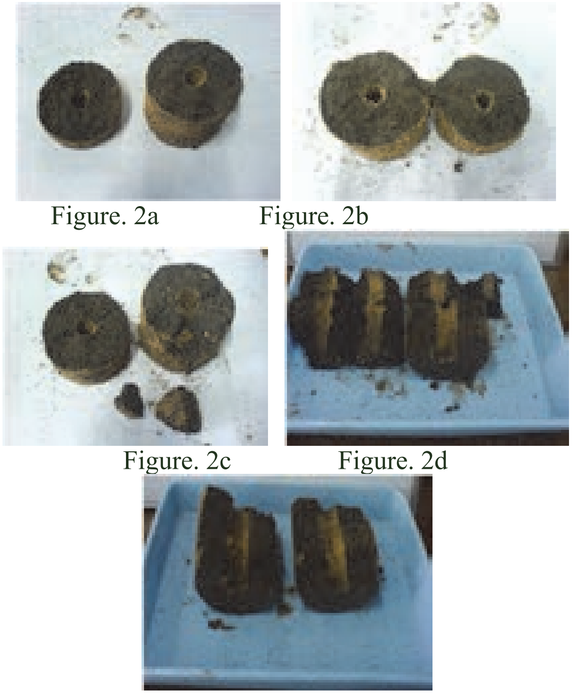
Figure. 2a Figure. 2b

Figure. 2c Figure. 2d

Figure. 2e

Figure 2. Fracture directions of the soil specimens at the end of hydraulic fracturing tests

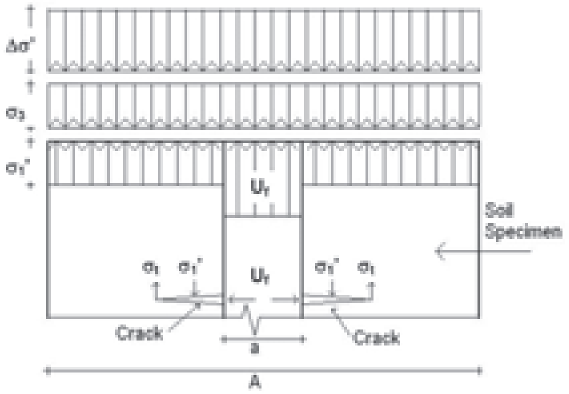

Figure 3. The stress equilibrium on the specimen and crack tip after hydraulic fracturing occurred

Two (2) stress equilibriums on the specimen after fracturing occurred consist of stress equilibrium on the specimen and surroundings crack on the inner borehole wall. The equilibrium of the stresses on the specimen after crack occurred is as follows;

$$\sigma_1' = \frac{A^2\left(\Delta\sigma' + \sigma_3\right) - a^2 u_f}{\left(A^2 - a^2\right)} \tag{1}$$

$$\sigma_t = \sigma_1' - u_f \tag{2}$$

where σ_1' is the vertical effective stress in the specimen, $\Delta\sigma'$ is the apparent vertical effective stress, σ_3 is the confining pressure, u_f is the hydraulic fracturing pressure, A and a were the outer diameter and inner borehole diameter of the specimen, and σ_t is tension stress at failure.

Based on the preliminary test result, the three (3) initial stress states were applied to the soil specimens in order to study the effect of arching on the upstream face of clay core to the hydraulic fracturing. Table 3 show the initial stresses applied to the soil specimens. All the cohesion of the soil samples have been checked and compared to the initial stresses will be applied prior the hydraulic fracturing tests in the laboratory, to ensure that the conditions of $\frac{1}{2}(\sigma_y - \sigma_x) < c$ are valid for all soil samples.

Table 3. Initial stresses applied to the specimens

Initial stresses	σ_x (kPa)	σ_y(kPa)	$\frac{1}{2}(\sigma_y-\sigma_x)$ (kPa)
A	140	200	30
B	200	280	40
C	260	360	50

The hydraulic fracturing tests in the laboratory of the soil samples obtained from five (5) borrow pits of major dams in Indonesia there are; Batubulan, Batutegi, Pelaparado, Sermo and Wonorejo dams with variations in six (6) fine contents ($\phi < 0.0074$ mm) at around 30%, 40%, 50%, 60%, 70% and 80%, and 3 variation in stress states are presented in Table 4. The total hydraulic fracturing tests in the laboratory with all variations above will be 90 tests.

3. EFFECT OF CLAY CORE CONFIGURATION

The effect of clay core configuration to the hydraulic fracturing was studied on the unusual configuration of the Hyttejuvet dam which hydraulic fracturing was occurred (Kjaernsli & Torblaa, 1968). Fig.4 shows the typical cross section of the Hyttejuvet dam. The clay core of the Hyttejuvet dam was moraine till, and the downstream slope of the clay core was vertical, while in the upstream the slope approximately was 2V : 1H. Hyttejuvet dam was constructed within 2 consecutive years. In the first year construction had reached elevation +700 m, and it's found that the pore water pressure dissipation in the clay was very slow. In order to accelerate the pore water pressure dissipation, the configuration of the upstream slope clay core was revising to be thinner and steeper. Hydraulic fracturing was occurred in the first reservoir filling, when the water level of the reservoir has reached their normal elevation.

Table 4. Hydraulic fracturing test results in the laboratory

Dam	Fine content (%)	Tension failure (kPa)		
		Initial stress A	Initial Stress B	Initial stress C
Batubulan	30.14	-20.60	-16.60	-14.60
	40.12	-21.60	-19.70	-16.60
	50.24	-23.70	-21.90	-17.80
	60.21	-24.80	-23.90	-19.80
	70.27	-26.90	-26.00	-21.90
	81.00	-28.00	-27.20	-23.00
Batutegi	30.54	-18.70	-16.50	-13.10
	40.37	-23.70	-21.50	-18.00
	50.25	-28.70	-25.60	-22.00
	59.24	-31.60	-29.40	-24.90
	72.37	-36.60	-31.40	-26.00
	79.60	-41.60	-34.40	-29.90
Pelaparado	30.84	-20.90	-13.50	-8.10
	40.71	-22.80	-17.50	-11.10
	50.60	-25.90	-20.60	-16.10
	60.28	-30.90	-24.60	-22.30
	70.40	-34.80	-28.50	-26.20
	79.44	-36.80	-31.40	-29.20
Sermo	30.17	-18.90	-15.70	-10.30
	40.71	-20.00	-16.60	-12.30
	47.68	-23.90	-18.50	-16.40
	60.38	-32.40	-24.60	-22.30
	69.95	-37.40	-33.70	-26.20
	80.50	-44.50	-36.80	-30.20
Wonorejo	30.26	-23.70	-15.30	-14.40
	40.23	-25.70	-16.50	-15.50
	50.14	-26.90	-20.70	-18.70
	61.68	-31.00	-24.80	-21.90
	70.26	-32.20	-28.00	-25.10
	80.50	-36.30	-30.10	-27.20

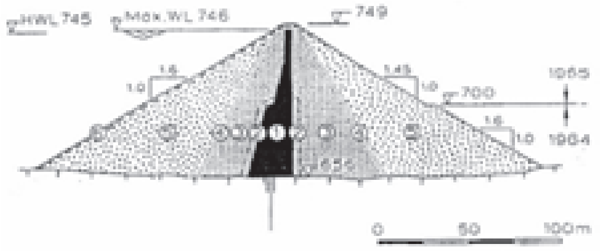

Figure 4. Typical cross section of the Hyttejuvet dam (Kjaernsli & Torblaa, 1968)

The investigation by boring confirmed that the erosion was occurred in the clay core at the elevation between +717m up to +740m at the point where hydraulic fracturing occurred.

In this paper, the focus was drawn in the investigation the effect of clay core configuration against hydraulic fracturing. In case the clay core of the Hyttejuvet dam replaces with soil materials which have different engineering properties, did the hydraulic fracturing were still occurred. In case the hydraulic fracturing was not occurred, it can be concluded that the clay core configuration was not sensitive to the hydraulic fracturing. But if the hydraulic fracturing still occurred even the engineering properties of the clay core were change, the clay core configuration was sensitive to the hydraulic fracturing. It was not possible to obtain the original materials used in the embankment of the Hyttejuvet dam. In order to obtain the geotechnical parameters required in the analyses, the clay core will be change with the clay core obtained from 5 major rock fill dams in Indonesia with variations in fine contents, while the filter was a local sand-gravel which the gradation was modeled using the gradation curve of the Hyttejuvet dam. The hyperbolic and shear strength parameters of the clay core and filter were obtained from triaxial unconsolidated-undrained test results using calculation method developed by Duncan et al (1980). The soil model for rock fill embankment materials was linear-elastic follow the works of Covarrubias (1969). The embankment of the Hyttejuvet dam were modeled in 14 step loadings to represent the construction time which reported in 520 days within 2 consecutive years. Fig. 5 shows the element discretization of the Hyttejuvet dam.

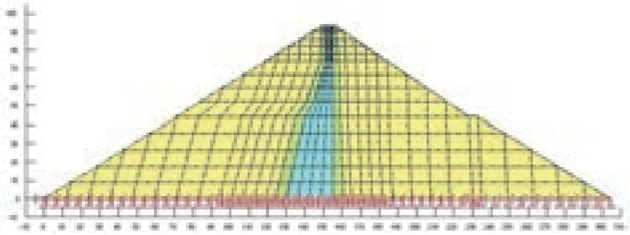

Figure 5. Element discretization of the Hyttejuvet dam

The total number of analyses was 30, variations of 5 clay core materials used in major rock fill dams in Indonesia, and 6 variations of fine contents at approximately 30%, 40%, 50%, 60%, 70% and 80%. The variations in hyperbolic and shear strength parameters, and unit weight enhanced the interpretation of the analyses results. The analyses results of Hyttejuvet dam model with clay core materials from Batubulan dams was shown in Fig. 6. All the analyses results from Batutegi, Pelaparado, Sermo and Wonorejo dams with their variations in fine contents indicated the similar results. Hydraulic fracturing occurs at mostly same locations, there are from elevation +718m up to +740m. It can be concluded that the clay core configuration was sensitive to the hydraulic fracturing in the rock fill dam.

4. EFFECT OF BASE OF UPTREAM FILTER

The effect of base of upstream filter to the hydraulic fracturing on the rock fill dams has been studied by Djarwadi et al (2011). The upstream filter has been known as an embankment zones with designed gradation to fill the crack on the upstream face of the clay core if occurred, but also will act as a bridging layer between the rock fill and clay core embankment materials which have big different in stiffness. A wider base of the upstream filter may reduce the arching effects on the upstream face of the clay core of the rock fill dams.

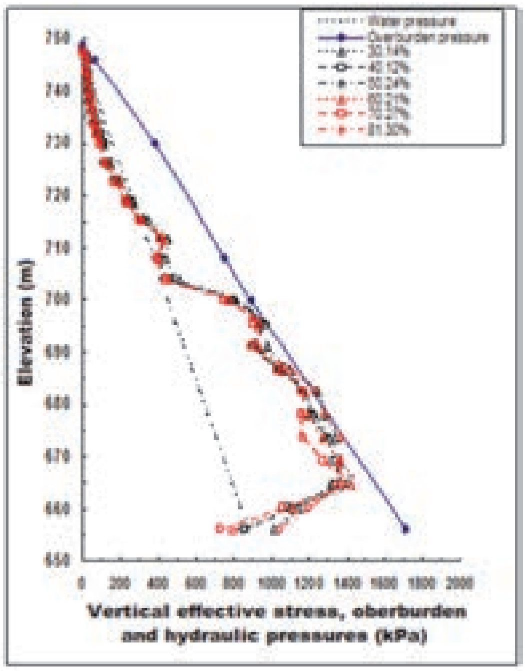

Figure 6. Position of hydraulic fracturing on Hyttejuvet model dam with clay core materials from Batubulan dam

The investigation on the effects of the base of upstream filter of the rock fill dams against hydraulic fracturing was carried on the Hyttejuvet dam which reported experiencing hydraulic fracturing. The base of the upstream filter were modeled in 2.00 m, 4.00 m, 6.00 m, 8.00 m, and 10.00 m, while the top width of the upstream filter all were kept in 2.00 m. The numerical analyses were carried out in a similar way with the analyses of the effect of the clay core configuration. The analysis results for the base width of upstream filter of 2.00 m, 4.00 m and 6.00 m was presented on Fig. 7, while the analysis results for the base width of upstream filter of 8.00 m, and 10.00 m was presented on Fig. 8.

Fig.7 indicated that the increasing of the base of the upstream filter reduced the area of hydraulic fracturing, and on the 6.00 m base of filter, the area of the upstream filter which experiencing hydraulic fracturing was similar to the actual location reported by Kjaernsli & Torblaa (1968). Fig. 8 indicated there were no hydraulic fracturing occurred on the clay core when the base width of the upstream filter was 8.00 m and 10.00 m. The analyses results strongly indicated that the wider base width of the upstream filter will reduce the arching effects, and load transfer between rock fill to the clay core embankment materials.

5. EFFECT OF COHESION OF THE CLAY CORE

The modus of failure of the clay core of the rock fill dam due to hydraulic fracturing has been justified as a tension failure, and in assumption that the cohesion of the soils as part of soil strength contributed a resistant against tension failure.

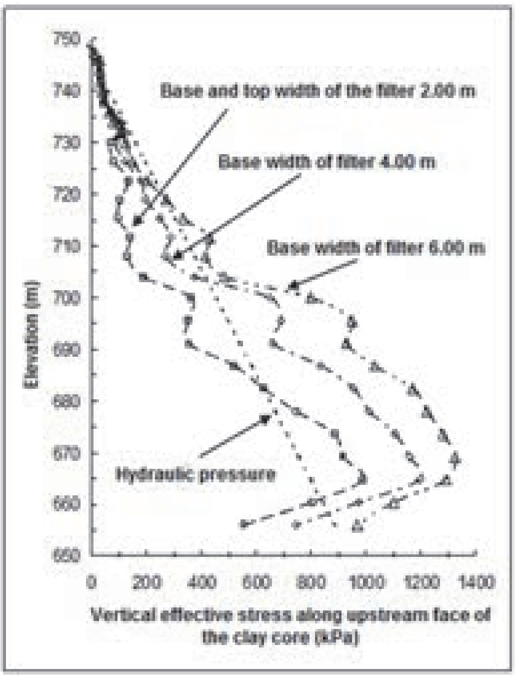

Figure 7. Position of the hydraulic fracturing of the clay core with base width of upstream filter at 2.00 m, 4.00 m and 6.00 m

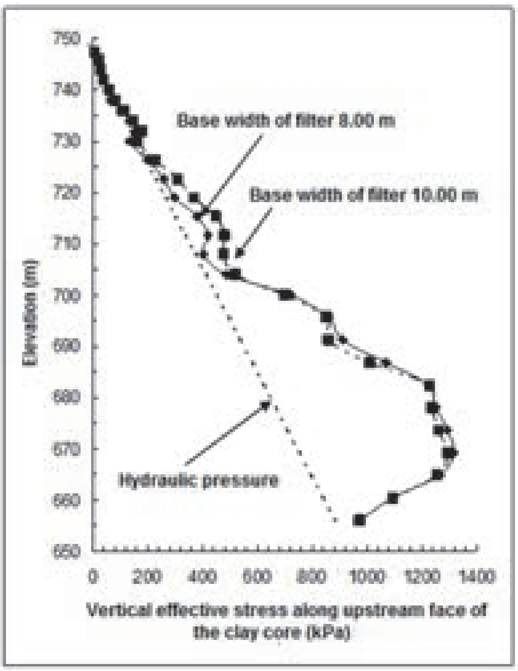

Figure 8. No hydraulic fracturing of the clay core with base width of upstream filter at 8.00 m, and 10.00 m

The effect of the cohesion of the clay core materials to the hydraulic fracturing has been studied and reported by Djarwadi et al (2014). The study were carried out by performing the relationship between the cohesion of the clay core materials obtained from unconsolidated undrained triaxial tests and the tension stress at failure of the same materials from hydraulic fracturing tests in the laboratory. Fig. 9 indicated strong and constant relations that when the cohesion increased, the tension stresses at failure were also increased.

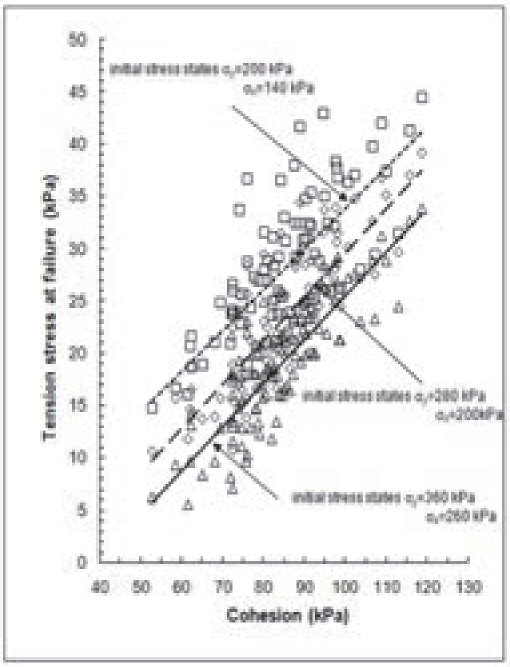

Figure 9. Relationship between cohesion and tension stress at failure of the clay core materials.

6. CONCLUSION

The effects of clay core configuration, base of the upstream filter and cohesion of the clay core materials to the hydraulic fracturing has been presented, and the following conclusions can be drawn from this study:

- The clay core configuration of the rock fill dams are sensitive to the hydraulic fracturing due to the arching,
- The base of the upstream filter influenced to the hydraulic fracturing on the rock fill dams, where the wider base may reduce the risk of hydraulic fracturing,
- The cohesion of the clay core materials may control the occurrence of the hydraulic fracturing, where the higher cohesion have greater resistance against hydraulic fracturing,

REFERENCES

Zhang, L., and Du, J., 1997: Effects of abutment slopes on the performance of high rockfill dams. Canadian Geotechnical Journal. Vol.34. no. 4. pp 489-497.

Loftquist, B. 1951: Earth Pressure in a Thin Impervious Core, Transaction of 4th International Congress on Large Dams, New Delhi, Vol 1, pp.99-109.

Kulhawy, F.H., and Gurtowski. T.M. 1976: Load transfer and hydraulic fracturing in zoned dams. Journal Soil Mechanics and Foundation Engineering, ASCE, Vol.102, No.GT9, pp 963-974.

Djarwadi, D., Suryolelono, K.B., Suhendro, B., and Hardiyatmo, H.C. 2011: Dimension effects of upstream filter of the rockfill dams against hydraulic fracturing. Proceedings of the 3rd Intl Conference of the European Asian Civil Engineering Forum. Atma Jaya University. pp.G35-G40.

Lo, K. Y., and Kaniaru, K. 1990: Hydraulic Fracture in earth and rockfill dams. Canadian Geotechnical Journal. Vol 27. No 4. pp 496-506.

Zhu, J.G., and Wang, J.J. 2004: Investigation to arch action and hydraulic fracturing of core rockfill dam. New Development in Dam Engineering. Proc 4th Intl Conf on Dam Engineering. Taylor & Francis Group. London, pp 1171-1180.

Fell, R., Wan, C. F. and Foster, M. 2004: Methods for Estimating the Probability of Failure of Embankment Dams by Internal Erosion and Piping through the Embankment. Uniciv Report R-428. May 2004. University of New South Wales. Australia. ISBN: 85841 395.7.

Cavounidis, S., and Hoeg, K. 1977: Consolidation during construction of earth dams. Journal of Geotechnical Engineering. ASCE. Vol. 103. No. 10. pp1055-1067.

Naylor, D. J., Knight, D. J., and Ding, D. 1988: Coupled consolidation analysis of construction and subsequent performance of Monasavu dam. Journal Computers and Geotechnics. No.6. pp95-129.

Alonso, E. E., Battle, F., Gens, A., and Lloret, A. 1988: Consolidation analysis of partially saturated soils, application to earth dams construction. Proceedings 6th International Conference on Numerical Methods in Geomechanics. Innsbruck. Vol.2. pp 1303-1308.

Ng, K.L.A., and Small, J.C., 1999: A Case Study of Hydraulic Fracturing using finite element. Canadian Geotechnical Journal, Vol 36, pp 861 –875.

Djarwadi, D. 2010: Analyses of hydraulic frcaturing of the clay core of the rock fill dams on the variation of fine contents. Doctorate dissertation. Gadjah Mada University. Yogyakarta. Indonesia (in Indonesian).

Widjaja, H., Duncan, J. M., and Seed, H. B. 1984: Scale and Time effects in hydraulic fracturing. Miscellaneous Paper GL-84-10. US Army Engineers Waterways Experiment Station. Vicksburg, MS.

Djarwadi, D., Suryolelono, K.B., Suhendro, B., and Hardiyatmo, H.C. 2009: Failure Criterion of Soils during Hydraulic Fracturing Test. Proceedings 1st International Conference on Sustainable Infrastructure and Build Environment in Developing Country. Bandung 2-3 Nov 2009. pp: G.30-G.35.

Kjaernsli, B., and Torblaa, I. 1968: Leakage through horizontal cracks in the core of Hyttejuvet Dam, Norwegian Geotechnical Institute. Publication no. 80, pp 39-47.

Duncan, J. M.,Byrne, P., Wong, K. S., and Mabry, P. 1980: Strength, stress strain and bulk modulus parameters for finite element analysis of stress and movements in soil masses. Report no. UCB/GT/ 80-01. Dept of Civil Engineering. University of California. Berkeley. USA.

Covarrubias, S. W. 1969: Cracking of earth and rock fill dams. PhD thesis. Harvard University. Cambridge. Massachuset.

Djarwadi, D., Suryolelono, K.B., Suhendro, B., and Hardiyatmo, H.C. 2014: Selection of soils as clay core embankment materials for rock fill dams to resist hydraulic fracturing. Procedia Engineering vol 95. pp. 489-497. Elsevier. New York.

Impact of Climate Change to Safety of Pasak Jolasid Dam

E.Nanudorn
Dam safety Division, Office of Water Management and Hydrology, Royal Irrigation Department (RID), Thailand
ekkapong59@gmail.com

S.Sopanangkool
Director of dam safety Division, Office of Water Management and Hydrology, Royal Irrigation Department (RID), Thailand

ABSTRACT:
Pasak jolasid dam is the one of large earth-fill dam which located in central part of Thailand, some longitudinal cracks were found on the road of dam crest which probably affect to safety of the dam. This paper presents a study to find the solution of this problem. The cause of longitudinal cracks was investigated by field test, laboratory test and geotechnical model. Two test pits were done between Sta.4+000 to Sta.4+860 where the crack is approximately 1.0–10.0 centimetres width and 65–75 centimetres depth. Longitudinal crack was caused by swelling soil. The 4-meter-thick of soil beneath pavements has a swelling pressure higher than the overburden stress. Moreover, it is found that the change in moisture content of swelling soil in shoulder area is the one cause of longitudinal crack. The change in moisture content is related to evaporation from dam surface, rainfall and groundwater table which is accelerate by climate change. Furthermore, the material specification and conceptual improvement design were done.

Keywords: Longitudinal Crack, Swelling Soil, Earth-fill Dam, Extreme Weather Change

1. INTRODUCTION

Pasak Jolasid (PJ) dam Located in the district settlement. Lopburi and Saraburi Province Wang Muang district. Construction began in 1994 and launched in September 1999, the dam design as zone type embankment dam with a total length of 4860 meters and a height of 31.5 m (Fig. 1) pavement on the dam crest consists of Asphaltic and Prime coat 0.05 meters thick, sub grade 0.20 meters thick, sub base 0.20 meters thick and selected materials "A" and "B" 0.30 meters thick.

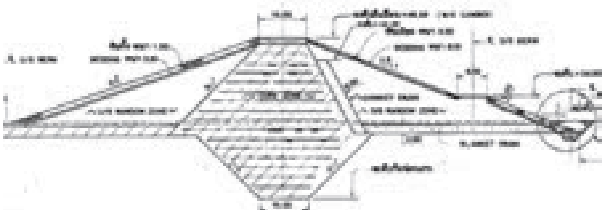

Figure 1. General Section of PJ Dam.
(Office of Engineering and Architectural Design, 2009)

Royal Irrigation Department (Office of Water Management and Hydrology, 2013) survey found cracks longitudinal cracks on the dam crest. Both upstream and downstream side km 3 + 500 to km 860 + 4 (Fig. 2 and Fig. 3), although pavement has repaired with new compacted and asphaltic, but the survey by sight. It still found a crack lengthwise. The more so for safety of the dam. Determination of the cause of such problems have to be done.

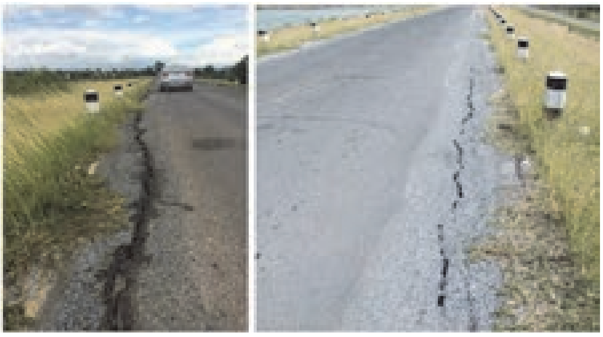

Figure 2. Longitudinal cracks were found on dam crest.
(Office of Water Management and Hydrology, 2013)

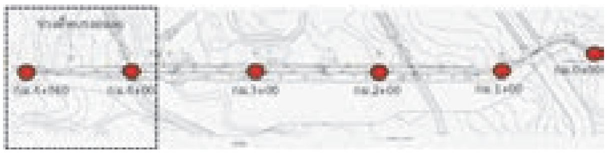

Figure 3. Longitudinal cracks found from km 3 + 500 to km 4 + 860.

The preliminary results of Resistivity survey (Fig. 4) found the area has a high electrical resistance and is similar to a bulb. Consistent with the position of the longitudinal cracks. The survey conducted during dry season. The area has cracks. Electrical resistance is lower Therefore, as long as the present condition crack spread has not continued.

Shear wave velocity test results (Fig. 5) on the longitudinal cracks (from km 4+ 000 to left abutment) were done. Shear wave velocity is less than 180 meters per second in upper part of embankment, so the soil in this area is stronger than areas where no longitudinal cracks**.**

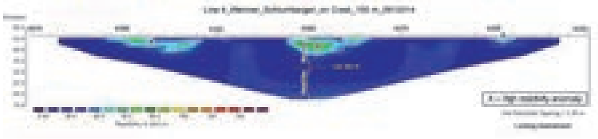

Figure 4. The results of the survey Resistivity Survey at km 4 + 300. (Dam Safety Research Unit, 2014)

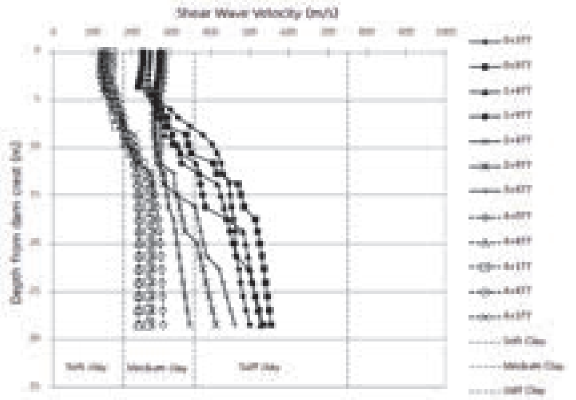

Figure 5. Shear wave velocity test method MASW. (Office of Engineering Topographical and Geotechnical Engineering, 2013)

USBR (1988) and Bureau of Land Management (2006) summarize common reasons of the longitudinal cracks on the dam. For example

- Differential settlement between clay-core dam shells.
- The dam foundation settlement.
- Loss of slope stability.
- Subsidence due to the earthquake.
- The type of soil as Collapsible Soil, Swelling Soil or Dispersive soil, etc.

Yongyutt et al. (2004) The main reasons that cause cracks along the top. The features beneath the road surface is soft clay which is low bearing capacity or hi shrinkage/swelling potentials. It may due to local condition as inappropriate height or slope of embankment.

F.H. Chen (1988) found that the volume of soil that can swell and shrink. It will have much effect to road damage. Which is T. Manosuthikij (2008) described the nature of the swelling soil. A montmorillonite is the one of soil mineral. The soil will absorb water and swell during rainy season. When the water evaporates soil will cause shrinkage and a gap.

Puppala et al. (2011) found that cracks as long as soil swelling. Often in the dry season between 1.0 to 4.5 meters and a depth. This humidity change is simple cycles of swelling and shrinking. This factor will be encouraging the cracks caused more serious.

Kodikara et al. (2004) found that the process of swelling soil consolidation. The soil will buckle caused by bending (Curling behaviour).

Puppala et al. (2011) said that the edge of the pavement shoulder. The point is easy to change humidity when swelling soil moisture evaporates. Apply to soil shrinkage and pressure (Shrinkage induced pressure, SIP). This is one cause of longitudinal cracks in the pavement.

Gupta et al. (2008) found that the shrinking and expansion behaviour of the swelling soil will result in shear and bending at the edge of the pavement. Figure 7

T. Manosuthikij (2008) said that when there are cracks on the pavement. Humidity will be channelled into the soil and swell up. Lead to the cracking of shoulder which likely spread to the other location.

2. METHODS

From the collection of the above information. The study assesses the cause of cracks on the dam crest into two types of cracks. Caused by mechanical engineering such as subsidence moving or losing the stability of the slope, etc., and cracks caused of soil properties such as soil reclamation. These are how to analyse and determine the cause of the crack lengthwise. The methodology is follow such principles.

3. THE SURVEY

Dug open pit exploration depth of 1.5 meters at the crack by the digging out a layer of 0.20 meters, then to measure the magnitude and direction of the crack (Fig. 6) Dam Safety Research Unit (2014). To dig 3 open pits in position that found the longitudinal cracks TP-1 (north side of I Sta.4 + 300) and TP-2 (the end of my Sta.4 + 789) as well as the position that have no longitudinal cracks TP-3 (the side. Na's Sta.2 + 942). The appearance of cracks can be summarized as follows.

- The formation of cracks, Vertical crack No tilting toward central axis of the dam.
- A crack width not exceeding 10 cm, depth not exceeding 80 cm (in the pavement).
- The soil beneath the pavement is typically black-grey clay (CH) conditions soft to very soft clay.
- The soil beneath the dam, the TP-3 is a brown clay. Gravel and sand mixed with granules soil conditions are stiff, clearly different from the cracking area.

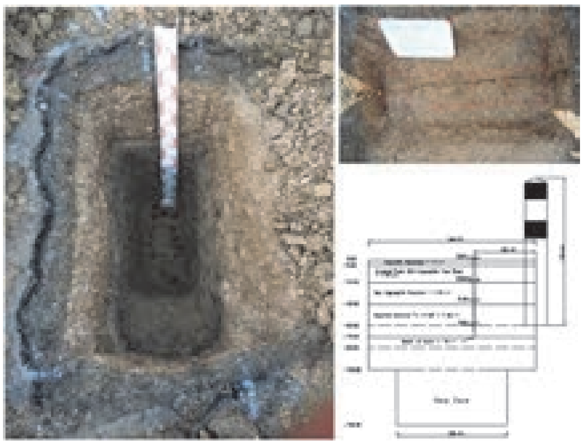

Figure 6. Test pit and Mapping the cracks.
(Dam Safety Research Unit, 2014)

4. THE CAUSE OF LONGITUDINAL CRACK

4.1 Slope stability analysis of the dam.

Such cracks may be due to loss of stability of the slope. Therefore, it is necessary to analyse. The analysis using the Slope / W 2007 with limit equilibrium theory. The soil property of embankment dam gains from laboratory testing (Triaxial Test). Results in overall slope stability (Fig. 7) both upstream and downstream slope of the dam are higher safety factor than the design threshold. The stability analysis of upper part of the dam (Local slope stability) which is insufficient support from dumped rock (hypothesis) higher than the threshold as well.

The survey results, the slope of the dam with a high resolution camera, GPS. The steep embankment has not changed from the original design. Also visual inspection of the dam was done, there is no unusual condition. Therefore, it was concluded that the longitudinal cracks on the dam are not caused by the slope instability and insufficient support from dumped rock.

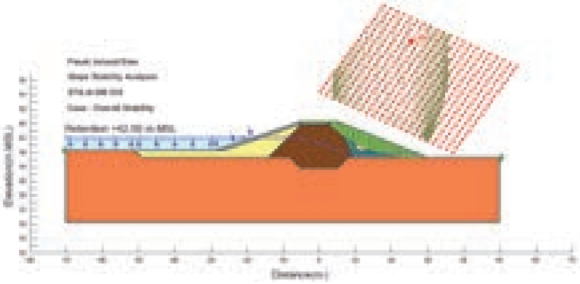

Figure 7. The slope stability analysis of the dam.
(Dam Safety Research Unit, 2014)

4.2 Bearing capacity of the soil under the pavement (Bearing Capacity).

The cracks can be caused by the bearing capacity of the clay core dam insufficient to the road edge. Therefore, it will analyse the bearing capacity by means of Meyerhof (1957) and soil properties of the embankment under the pavement are perform by laboratory tests (Direct shear test). The results found that safety factor was calculated as the upstream and downstream are higher than acceptable criteria despite in saturated condition due to water trapped in the cracks or the embankment below. Thus, the embankment strength is enough to resist the movement of the embankment top slope and unlikely the main cause of the longitudinal crack.

4.3 Dam instrumentation.

The analysis of dam safety instruments. There are no abnormal behaviour of the movement from Inclinometer and the seepage behaviour both from the piezo-meter and seepage flow meter. Found that the pore water pressure is normal and the low rate of leakage. Thus, in the current conditions. The stability of the dam slope and the water seepage problem are not an issue to worry.

4.4 Soil properties analysis of the embankment dam.

Soil test results of the PJ dam. The basic properties, Swelling Soil Test and Collapsible Soil Test found that a soil swell. But soils at foundation and pavement are not swell (Mekhao et al., 2015). However, even swell though the compacted clay, but the swelling is caused only in part on an overburden pressure less than swelling pressure. In Fig. 8 shows the results of the comparison of them. The conclusion that the embankment under the thick layer 3.0 meters (depth from 1.0 to 4.0 meters from dam crest). Swelling pressure is higher than the weight above. This behaviour, the top layer of soil has a higher pressure to cause a longitudinal crack. At the levels 6.0 meters deep, although swelling pressure is high but also the overburden pressure is heavy too, the more so swelling pressure is impossible to spread the load. So the pressure could not reach the top.

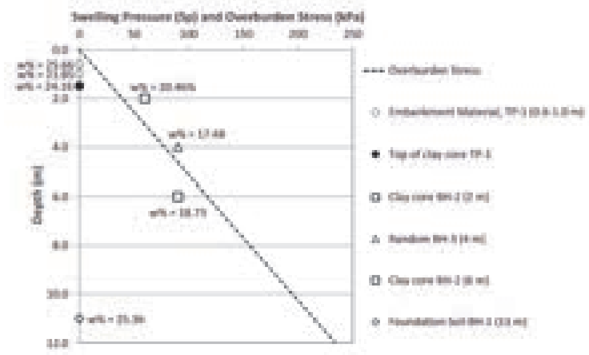

Figure 8. Comparisons the swelling pressure and overburden pressure with depth. (Dam Safety Research Unit, 2014)

4.5 Soil moisture content, volume change and the characteristic curve.

The Shrinkage Volume Change test results (Fig. 9) found that compacted soil which swelling. The change of water amount in soil from 10.92 to 71.75%, and can shrink and swell from 31-52%.

The amount of water in the soil from the test in the field found. Between 15-30%, with values close to the Plastic Limit. During the test Soil reclamation is a semi-solid state. This could be caused Consistent as possible is usually the left abutment area of dams is dry. However, if the soil in dry conditions or get moisture. Rain water will cause swelling and expanding high volume. And impact to the structure of pavement above, as Fig. 10 shows that the soil in upper part of embankment can absorb or lose water in the soil more easily than lower due to the soil has more void ratio in mass over. The other words that different soils that swell in the depth of 4-6 meters, which makes the void ratio is higher, which is consistent with past results.

Considering the suction force of the water in the soil from 0.1-100 kPa follow the tested depth. The embankment dam with a relatively constant amount of water when suction force increase that means the embankment has potential to hold the water.

The test results also show that the earth dam has Hysteresis behaviour. Which is the range that water evaporates from the soil. Soil water content will decrease but when soil absorb moisture then the water content will be returned. The test confirm that the swelling soil Influenced by absorb and loss of moisture.

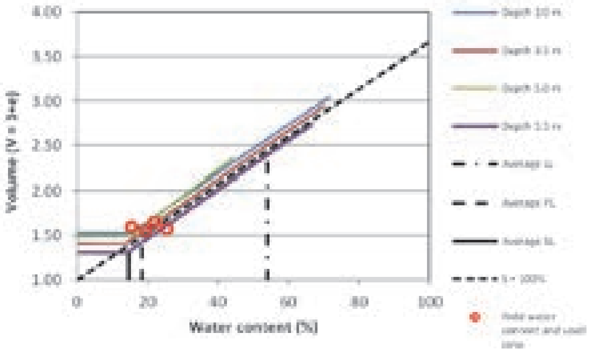

Figure 9. The water content and volume changing in soil. (Dam Safety Research Unit, 2014)

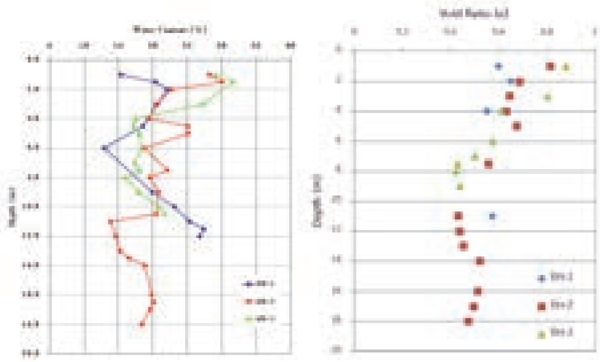

Figure 10. Soils water content and void ratio in the field. (Dam Safety Research Unit, 2014)

5. ANALYSIS OF THE COLLAPSE MODEL

To determine the cause of longitudinal cracks on the dam crest. Due to swelling soil beneath the pavement. To perform stress and strain model, the soil properties at the current dam was conducted. Compared with the original testing of the design and construction. The limitations is not a simulation of the impact of the change in humidity to swelling property. This is a following study of the authors.

Model analysis of the dam using SIGMA / W 2007. Total Stress Analysis with Elastic Plastic Model separate by 2 cases. The first case, the same soil properties at the upper and lower of the dam. The second, the properties of the clay core, shell and lower part of embankment are different. As shown in Table 1.

Table 1. Soil Properties summarizes the PJ dam.

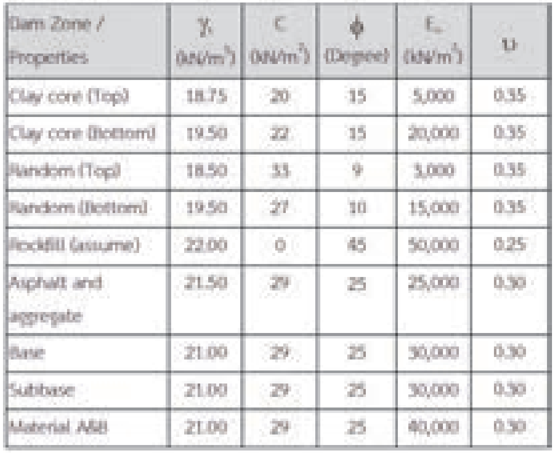

Dam Zone / Properties	γ_t (kN/m³)	c (kN/m²)	ϕ (Degree)	E_s (kN/m²)	υ
Clay core (Top)	18.75	20	15	5,000	0.35
Clay core (Bottom)	19.50	22	15	20,000	0.35
Random (Top)	18.50	33	9	3,000	0.35
Random (Bottom)	19.50	27	10	15,000	0.35
Rockfill (assume)	22.00	0	45	50,000	0.25
Asphalt and aggregate	21.50	29	25	25,000	0.30
Base	21.00	29	25	30,000	0.30
Subbase	21.00	29	25	30,000	0.30
Material A&B	21.00	29	25	40,000	0.30

(Dam Safety Research Unit, 2014)

The results showed that the subsidence in the first case equal to 0.035 meters in the second case is equal to 0.045 meters, so though the upper embankment dam that swelling pressure more than the overburden, it will not affect the settlement that will lead to disaster in the overflow cross the dam since the settlement of the two cases is less than the designed for subsidence (Camber), which is about 1% of normal high, or about 0.1 meters (considering that cross the left bank of the dam).

The XY shear strain (Fig. 11) at the top of the dam embankment. The first case is equal to 0.0005, the second is equal to 0.002. Analysis showed that the upper part of embankment is swelling soil (case 2), X-Y shear strain and yielding point are more than case 1. So the swelling soil (on clay core) with less strength, it will has more displacement on more and cyclic load.

Analysis of bending on pavement due to the actions of the swelling soil. Assume that soils are continuously under the pavement (Fig. 12) shows that on the two edge of pavement will act as a point of more stress than the other points. Bending and shear are in this area as well.

The bending occurs not higher than the strength of pavement. Not immediately crack. But it is a gradually accumulate. When this cycle been accumulated for a long time. To show the cracks agreed with the PJ dam. The dam used to be 10-15 years. The longitudinal cracks shown.

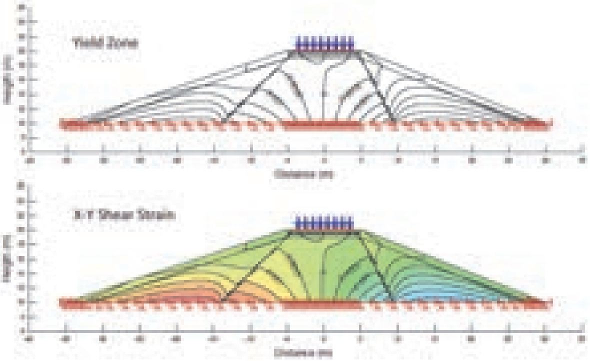

(A) Case 1

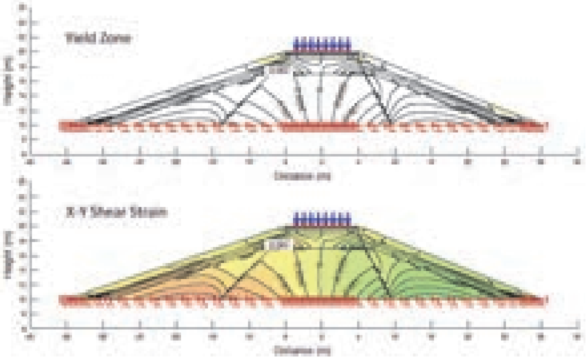

(B) Case 2

Figure 11. Analysis of XY Shear Strain and Yield zone. (Dam Safety Research Unit, 2014)

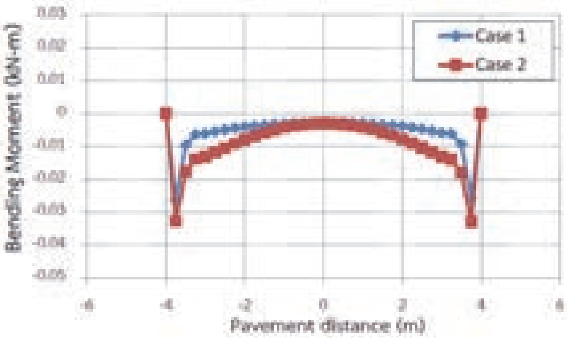

Figure 12. Bending moment on top of the ground swell. (Dam Safety Research Unit, 2014)

6. CONCLUSION

1. The cause of cracks along the PJ dam. Not due to Subsidence or deformation of the steep embankment. However, the embankment below the pavement is the swelling soil. Due to the Swelling pressure more than the weight pressure Influence of soil swelling at 4 meters' depth up to the dam crest.

2. Changes in soil moisture or water content are a factor. Cause longitudinal cracks. The ground swell will behave accordingly the season. The soil will swell when exposed to moisture and shrink in dry seasons (Shrink-Swell behaviour). As this behaviour. The pressure build-up to the pavement when the time passed, by 10-15 years. The old dam will show longitudinal cracks accordingly.

3. Longitudinal cracks formed on the PJ dam as shallow cracks in the pavement only. So it will not affect the safety of the dam. Especially in terms of slope instability leading to overflow over the dam, however, it is necessary to improve. The cracks may have spread to cause unsafety in others. Because of moisture or rain water enter to the dam body from longitudinal cracks.

4. The longitudinal crack repair. It may proceed in several ways. For example, dredging soil swelling out new compacted, reinforcement to the pavement using Geo-grid and protection of humidity changes, such as paving impervious layer.

5. The design or construction of roads in the future. Either by road or the road on the dam should avoid using a soils swell potential. If not. The soil should have a better improvement to reduce the swelling down.

ACKNOWLEDGEMENTS

This study is belonging to Dam Safety Division, Office of water management and hydrology, Royal Irrigation Department which employ Dam Safety Research Unit, Geotechnical and Foundations Research and Development Center (GERD), Faculty of Engineering, Kasetsart University, Thailand

REFERENCES

Office of Engineering and Architectural Design (2009): The dam stability over maximum water level. Case Study: Pasak Jolasid Dam, Royal Irrigation Department, Thailand.

Office of Water Management and Hydrology (2013): Analysis of Dam Safety of Pasak dam by Visual inspect and Condition Index 30 July to 2 August 2556 and 5-9 October, Royal Irrigation Department, Thailand.

Dam Safety Research Unit (2014): Final Report: Analysis and design of repair work Pasak Jolasid Dam Project, Geotechnical and Foundations Research and Development Center, Faculty of Engineering, Kasetsart University, Thailand.

Office of Engineering Topographical and Geotechnical Engineering (2013): The investigation of embankment dam by geophysical methods of Pasak Jolasid Dam Prasae Dam, Royal Irrigation Department, Thailand.

USBR (1988): Training Aids for Dam Safety Module: Inspection of Embankment Dams, US Department of Interior Bureau of Reclamation.

Bureau of Land Management (2006): Dam Condition Assessment Guidelines for Embankment Dams, BLM Manual Handbook H-9177-1. Denver, Colorado.

Yongyutt et al. (2004): Edit damaged pavement areas, seminar at you thick Research Office of Research and Development of the Department of Highways.

F.H. Chen (1988): Foundation on expansive soils, American Elsevier Science Public., New York.

T. Manosuthikij (2008): Studies on Volume Change Movements in High PI Clays for Better Design of Low Volume Pavements, Doctor of Philosophy Dissertation.

Puppala et al. (2011): Shrinkage induced pressure measurements in unsaturated expansive clays, Preceding of the 5th asia pacific conference on unsaturated soils, Pattaya, Thailand, 14-16 NOVEMBER, pp.93-102.

Kodikara et al. (2004): Modelling of curling in desiccating clay, Canadian Geotechnical Journal, 41 (3): 560-566. doi: 10.1139 / t04-01.

Gupta et al. (2008): Moisture Migration in Geogrid Reinforced Expansive Subgrades, The First Pan American Geosynthetics Conference & Exhibition 2-5 March 2, Cancun, Mexico.

Mekhao et al. (2015): Evaluating potential swelling of the Embankment dam. Study Pa Sak dam lakes, National Convention on Civil Engineering at 20 on 8-10 July, Chonburi.

ASIA-PACIFIC GROUP
ICOLD

Secretariat, APG & EADC 2016 Sapporo

(Japan Commission on Large Dams)
Address : Ningyo-cho Sun City Bldg. 2F., 1-2-7, Nihonbashi-Ningyo-cho,
Chuo-ku, Tokyo 103-0013 Japan
Tel : +81-3-5614-0968 Fax : +81-3-5614-0969
E-Mail : secretariat@jcold.or.jp URL : http://jcold.or.jp/e/apg-eadc/